Flow Science Incorporated
48 S Chester Ave, Suite 200, Pasadena, CA 91106
(626) 304-1134 • Fax (626) 304-9427

Climate Change Impacts on Water Quality and Internal Nutrient Cycling in Lake Mead

Prepared for

Bureau of Reclamation

WaterSMART Grant Agreement #R13AP80034

Reviewed By
Todd Tietjen, Ph.D.
(Southern Nevada Water Authority)
Peggy Roefer
(Southern Nevada Water Authority)

Reviewed By
E. John List, Ph.D., P.E. (NV)
(Flow Science Incorporated)
Li Ding, Ph.D., P.E. (VA)
(Flow Science Incorporated)

Prepared By
Ben Martin, P.E. (VA)
(Flow Science Incorporated)
Al Preston, Ph.D., P.E. (CA)
(Flow Science Incorporated)

FSI 134063
December 17, 2015

Table of Contents

ACKNOWLEDGEMENTS ..... **I**

1 INTRODUCTION **2**

1.1 Lake Mead 3
1.2 Goals of this Project 4
1.3 Report Organization 5

2 METHOD OF ANALYSIS **6**

2.1 Description of ELCOM and CAEDYM 6
2.2 Whole Lake Model 6
2.3 Previous Climate Change Modeling 7
2.3.1 Climate change Projections 8
2.3.1.1 CMIP3 Ensemble Projections 8
2.3.1.2 Inflow Water Quality 9
2.3.1.3 Projected SNWA and Effluent Flows and Water Quality 9
2.3.1.4 Volume/WSEL 9
2.3.1.5 Algal Adaptation and Shifts in Species 10
2.3.1.6 Summary 10
2.3.2 Previous Climate Change Simulations 11
2.3.3 Climate Change Conclusions (Previous Modeling) 13
2.4 Current Climate Change Modeling 13

3 SEDIMENT PHOSPHORUS FLUX IN LAKE MEAD **14**

3.1 Literature review 14
3.2 Data Analyses 17
3.3 Implementation into Model and Verification 19

4 DESCRIPTION OF ELCOM/CAEDYM SIMULATIONS **22**

4.1 "Baseline" Simulation with Phosphorus Flux (Run 11) 22
4.2 "High Warming" sIMULATION WITH Phosphorus Flux (Run 12) 24
4.3 Other Simulations (Runs 13, 14, and 15) 24
4.4 "2014" Simulation (Run 16) 25

5 RESULTS **27**

5.1 Visualization of Phosphorus release 27
5.2 Analysis of sediment Phosphrus flux 29
5.2.1 Temperature and Conductivity 29
5.2.2 Dissolved Oxygen 31
5.2.3 Phosphorus 33
5.2.4 Chlorophyll *a* 35
5.3 "2014" Simulation 37
5.3.1 Description of "2014"Simulation and Data Collection 37
5.3.2 Results 38
5.4 Animations 41

6 CONCLUSIONS **42**

6.1 Water Temperature 43
6.2 Dissolved Oxygen 43
6.3 Phosphorus Concentrations and loading 44
6.4 chlorophyll *a* 45

7 REFERENCES **47**

APPENDIX A: Time-Series Plots
APPENDIX B: Year 2014
APPENDIX C: Animations

ACKNOWLEDGEMENTS

This project was funded by the U.S. Bureau of Reclamation through WaterSMART Grant Agreement Number R13AP80034. The grant was awarded under Funding Opportunity Announcement Number R13AS80009, “Applied Science Grants for the Desert Landscape Conservation Cooperative”.

This project builds on previous grant work (WaterSMART Agreement Number R11AP81452) that was conducted by Flow Science Incorporated with the Southern Nevada Water Authority (SNWA), San Diego Public Utilities Department, and Metropolitan Water District of Southern California. That previous work made use of the publicly available World Climate Research Programme's (WCRP's) Coupled Model Intercomparison Project Phase 3 (CMIP3) multi-model dataset to provide information on future climate conditions, and these same data are also used in the present work. We acknowledge the modeling groups, the Program for Climate Model Diagnosis and Intercomparison (PCMDI) and the WCRP's Working Group on Coupled Modelling (WGCM) for their roles in making available the WCRP CMIP3 multi-model dataset. Support of this dataset is provided by the Office of Science, U.S. Department of Energy.

The project used the three-dimensional (3-D) hydrodynamic and water quality model of Lake Mead previously developed by Flow Science Incorporated. The development of this model was primarily sponsored by the Clean Water Coalition (comprising Clark County Water Reclamation District, City of Henderson, City of Las Vegas and City of North Las Vegas) and the SNWA, with additional support from the National Park Service (NPS). Extensive measured field data provided by U.S. Bureau of Reclamation, U.S. Geological Survey, Clark County Water Reclamation District, City of Las Vegas, and SNWA were pivotal in the development and calibration of the model.

1 INTRODUCTION

Previous modeling work, performed by Flow Science Incorporated (Flow Science) as a subcontractor to the SNWA as part of a U.S. Bureau of Reclamation (Reclamation) WaterSMART grant (Funding Announcement No. R11SF80344), identified that warmer water temperatures arising from climate change will lead to lower dissolved oxygen (DO) levels in Lake Mead, Arizona-Nevada, through increased rates of oxygen consuming metabolic processes, extended periods of reservoir stratification, and potentially less direct oxygen replenishment from inflows.

The broad goal of the previous modeling work (Flow Science, 2013) was to address critical issues, such as those identified by past studies (USACE, 2011, Rosen *et al*., 2012), through water quality modeling of Lake Mead under future climate change. A previously developed 3-D hydrodynamic and water quality model for Lake Mead (Preston *et al*., 2013, Flow Science, 2007, 2010a, 2010b) was used to perform simulations under a range of future climate conditions. The parameters included in the model were water velocities (*i.e.*, circulation patterns), temperature, salinity, conductivity, pH, and concentrations of bromide, chlorophyll *a*, phosphorus (various species), nitrate, ammonium, total organic carbon (TOC), DO, suspended-solids, and a generic effluent tracer. The model was used in order to evaluate reservoir stratification and water quality impacts of warmer climatic conditions, possible changes in algal productivity (blooms), and possible decreases in DO concentrations resulting from such changes. Additionally, the modeling evaluated the impacts of lower reservoir water volumes and lower inflow and outflow volumes on hydrodynamics and water quality. Several locations, including municipal water intakes, were examined specifically with regard to water qualities that may affect water treatment processes, such as increased temperature, increased TOC and/or bromide concentrations (potentially leading to increased concentrations of disinfection byproducts). Attention was also directed at the quality of water released from Hoover Dam that may affect downstream users (*e.g.*, phosphorus concentrations that may affect productivity in downstream reservoirs).

Previous modeling (Flow Science, 2013, Preston *et al*., 2013) did not address the increase in internal nutrient recycling (*i.e*., increase in release of nutrients from the sediments) that would occur as a result of lower DO concentrations. Increased internal nutrient recycling will likely lead to increased nutrient concentrations in the water column and increased productivity (*i.e*., algal growth). This in turn may lead to further decreases in DO concentrations, resulting in additional releases of nutrients from the sediments. This potential "feed-back" effect may ultimately have serious and significant impacts on the water quality and trophic status of Lake Mead and downstream Colorado River stakeholders, and on other lakes within the Desert Landscape Conservation Cooperative (LCC) geographic area. The research reported here extended previous modeling efforts by including and examining the effects of internal nutrient recycling (*i.e*., sediment nutrient fluxes) through the incorporation of these mechanisms into the 3-D hydrodynamic and water quality model previously developed for Lake Mead. The study provided an understanding of how water quality characteristics and internal nutrient

recycling in Lake Mead may change under future warmer conditions resulting from a changing climate. Algal growth in Lake Mead is phosphorus limited (Lieberman, 1995) therefore the analysis of internal nutrient recycling focused on phosphorus.

1.1 LAKE MEAD

Lake Mead is the largest-volume constructed reservoir in the U.S. and was formed in 1935 by the erection of Hoover Dam on the Colorado River. It supplies irrigation and drinking water for more than 25 million people in Nevada, Arizona and California. The lake comprises four large basins: Boulder, Virgin, Temple, and Gregg (**Figure 1.1**) and extends approximately 70 miles along the Colorado River between the States of Nevada and Arizona. At full capacity the lake has a maximum depth of 490 feet, a volume of 26 million acre-feet, and a residence time of approximately three years. The principal outflow is through Hoover Dam to the lower Colorado River. The SNWA withdraws drinking water via Intakes 1 and 2, located on the east side of Saddle Island in Boulder Basin (**Figure 1.1**) at 992 feet elevation. Construction of Intake 3 is presently underway at a deeper location (860 feet elevation) in Boulder Basin and is expected to be completed in 2015.

The inflows to Lake Mead are dominated by the Colorado River at the upstream (eastern) end, which on average supplies more than 97 % of the inflow (Holdren and Turner, 2010). There are smaller inflows from the Muddy River and Virgin River in the Overton Arm (northern boundary) and from the Las Vegas Wash (LVW) in the northwestern corner of Boulder Basin (**Figure 1.1**). Historically, LVW was an ephemeral stream that reached the Colorado River system only as a result of storm runoff. However, since the 1950s effluent from wastewater treatment plants in the Las Vegas Valley has been discharged into Boulder Basin via the LVW. This effluent now dominates the flow volume in the LVW and provides year-round discharge to Lake Mead.

Lake Mead is typically described as mesotrophic (LaBounty and Burns, 2005), with productivity primarily phosphorus-limited (Lieberman, 1995). The supply of phosphorus contributed by the ortho-phosphate concentration of the effluent in the LVW has a direct effect on the trophic status and clarity of Boulder Basin. Within Boulder Basin chlorophyll *a* concentrations are higher near the LVW and in the Las Vegas Bay and lower in the open water of Boulder Basin.

During the spring and summer months Lake Mead is thermally stratified (Fischer and Smith, 1983, LaBounty and Horn, 1997). This stratification, combined with inflows of differing water quality and the large spatial extent of the reservoir, results in complex 3-D distributions of constituents within the lake. The fate of each of the inflows and the resulting distribution of constituents in Lake Mead are subtle functions of the density of each inflow relative to the receiving water and vertical mixing through wind action, horizontal advection, and dilution (Fischer and Smith, 1983, Preston *et al*., 2013). Lake Mead is best described as monomictic (LaBounty and Burns, 2005). However, field data

(LaBounty and Horn, 1997, LaBounty and Burns, 2005) and modeling (Preston *et al*., 2013) indicate that a deep, weak thermocline persists in some years throughout the winter in the deepest portions of Boulder Basin.

The complex hydrodynamic processes (*i.e*., stratification, mixing and circulation) of Lake Mead may be altered by future climate change (*e.g*., warmer temperatures leading to increased stratification). These changes, coupled with potentially different inflow regimes, and could lead to changes in productivity and water quality within Lake Mead that may have far-reaching consequences in the U.S. Southwest.

1.2 GOALS OF THIS PROJECT

The goal of this project was to evaluate the potential for productivity increase in Lake Mead through increased nutrient release from sediments due to climate and other changes. It addressed gaps in current knowledge regarding climate change impacts on lake and reservoir water quality and how beneficial uses are likely to be impacted. More specifically, it identified changes in water quality and trophic status of Lake Mead due to increased internal nutrient recycling that may result from warmer water temperatures and lower DO concentrations. This project:

- Evaluated and quantified nutrient release rates from the sediments under present and historical conditions so that release rates could be implemented in the previously developed 3-D model.

- Determined how sediment nutrient release flux rates vary with other parameters such as DO concentrations and temperature to provide better calibration of the release rates for implementation in the model. The potential for warmer climatic conditions could increase internal nutrient recycling due to lower DO concentrations.

- Implemented sediment nutrient flux rates into the Lake Mead model to evaluate the effect of increased internal nutrient recycling on general water quality and trophic status of Lake Mead. In particular, the potential for increased internal nutrient recycling and productivity to lead to further decreases in DO concentrations and additional nutrient release through "feed-back" mechanisms.

- Used the model to evaluate nutrient loads from sediments under a range of scenarios, including climate and other changes, to determine the sensitivity of water quality within Lake Mead to various potential climate change parameters.

1.3 REPORT ORGANIZATION

The methodology used in the analysis is described in Section 2, including details of the Lake Mead model development. Section 2 also includes a summary of the previous climate change modeling. Section 3 presents the implementation of phosphorus sediment flux into the 3-D hydrodynamic and water quality model of Lake Mead. A literature review of release rates for relevant reservoirs is presented along with the data analysis used to estimate flux rates. Implementation of the flux rates in the model is discussed along with results of the validation simulation. Section 4 describes the simulations performed to investigate the effects of climate change on the water quality of Lake Mead, including baseline simulations without phosphorus flux, phosphorus flux simulations, and a simulation of lake conditions from Year 2014 that showed a decrease in DO concentrations. Results of the simulations are presented and discussed in Section 5, and conclusions are drawn in Section 6.

2 METHOD OF ANALYSIS

The Whole Lake Model (WLM) that was developed by Flow Science under contracts with Clean Water Coalition (comprising Clark County Water Reclamation District, City of Henderson, City of Las Vegas and City of North Las Vegas), SNWA and the NPS was used to simulate water quality in Lake Mead with various climate change scenarios. The WLM is a 3-D hydrodynamic and water quality model developed using the ELCOM and CAEDYM computational programs. This section provides brief descriptions of the ELCOM and CAEDYM programs, the development of the WLM and a brief overview of how climate change projections are used to modify WLM inputs to enable assessment of Lake Mead under climate change.

2.1 DESCRIPTION OF ELCOM AND CAEDYM

The Center for Water Research at the University of Western Australia has developed a modeling system for aquatic ecosystems that combines a 3-D hydrodynamic simulation method with a suite of water quality modules that compute interactions between biological organisms and the chemistry of their nutrient cycles. This integrated approach allows for the feedback and coupling between biogeochemical and hydrodynamic systems so that a complete representation of all appropriate processes can be included in an analysis. The hydrodynamic simulation code is the Estuary, Lake, and Coastal Ocean Model (ELCOM), and the biogeochemical model is the Computational Aquatic Ecosystem DYnamics Model (CAEDYM).

ELCOM allows the user to define boundary conditions, physical inputs, and bathymetry in a grid structure to simulate a body of water. It is used to predict variations in water velocity, temperature, salinity, and the concentration of conservative tracers in space and time within the body of water. This is accomplished by numerically solving the unsteady Reynolds-averaged Navier-Stokes equations and scalar transport equations.

CAEDYM can be linked to ELCOM (or any another appropriate hydrodynamic model) to predict aquatic ecological behavior within the same body of water. CAEDYM uses parameter-specific algorithms to calculate the variations in aquatic ecology. Detailed information concerning the history, methodology, and validation of ELCOM and CAEDYM, as well as technical descriptions of each, are available in previous reports (Flow Science, 2007, 2010a, 2010b, 2013) and papers (Preston *et al*., 2013).

The simulations documented in this report were performed using ELCOM v2.1.1 and CAEDYM v2.2.1.

2.2 WHOLE LAKE MODEL

Flow Science developed the WLM in 2006 and 2007 under contract to and on behalf of the Clean Water Coalition (CWC) and SNWA (Flow Science, 2007). The domain of the WLM extends from the Hoover Dam to the mouths of the Muddy, Virgin and Colorado Rivers and is divided into 300×300×2 meter computational cells (**Figure 2.1**).

The original WLM was calibrated and validated for a six year period, spanning years 2000 through 2005, for the following parameters: temperature, conductivity, perchlorate, bromide, chlorophyll *a*, phosphorus (various species), nitrate, ammonium, TOC, pH, and DO (Flow Science, 2007). The calibration/validation simulations were generally completed as separate single year simulations. That is, at the beginning of each calendar year the simulation was re-initialized. The exception was year 2003, which was run as a continuation of the 2002 simulation, so that the incomplete destratification that occurred in that winter could be captured by the model (Flow Science, 2007).

In 2008 and 2009, Flow Science extended the calibration and validation period to include years 2006 and 2007, under contract with the CWC, SNWA and the NPS (Flow Science, 2010a). Additional enhancements were added to the model, including the use of wind data from multiple on-lake locations, the implementation of spatially-variable sediment oxygen demand, and the continuous simulation of years 2005 through 2007. In addition the model benefited from the more recent phosphorus field data obtained with lower detection limits. These data resulted in a better understanding of the phosphorus and algae processes in Lake Mead and a subsequent re-calibration of the relevant bio-geochemical model (CAEDYM) parameters (Flow Science, 2010a).

In 2010, Flow Science further extended the calibration and validation period to include year 2008 (Flow Science, 2010b). Thus, the entire model calibration period spans nine years (2000 through 2008), with the last four years (2005 through 2008) being simulated in one continuum.

As detailed in the calibration and validation reports (Flow Science, 2007, 2010a, 2010b), the WLM is able to accurately replicate the hydrodynamic and biogeochemical processes in Lake Mead for the complete 2000 through 2008 calibration period, and thus provides a powerful tool that can be used for analysis of many different future scenarios. The WLM has subsequently been used to analyze Lake Mead at different effluent nutrient loadings, and with suspended-solids in various inflows, at water surface elevations (WSEL) ranging from 925 feet to 1100 feet (Flow Science, 2011a, 2011b).

2.3 PREVIOUS CLIMATE CHANGE MODELING

The current climate change study was built upon the previous climate change work as part of a prior U.S. Bureau of Reclamation WaterSMART grant (Fund Agreement Number R11AP81452). The previous climate change work used the WLM to assess the water quality of Lake Mead under different climate change scenarios. The inputs for the WLM were modified to reflect anticipated changes in climate, for several different climate change projections. The climate change projections were based upon the WCRP's CMIP3 multi-model dataset. A brief summary of the previous modeling work is presented here As noted the previous work did not address the increase in internal nutrient recycling (*i.e.*, increase in release of nutrients from the sediments) that would occur as a result of lower DO concentrations, which the current study focused on.

2.3.1 Climate change Projections

To investigate the effect of climate change on the water quality of Lake Mead, suitable climate change projections were required to determine appropriate changes to the WLM inputs in order to simulate changes in the water quality. The WLM inputs that were considered for adjustment to represent climate change, and other future projected changes, were:

- meteorology (air temperature, rainfall, wind-speed, solar radiation, and relative humidity)
- flow rates of inflows
- inflow water quality (water temperatures, DO concentrations, and other water quality parameters)
- Hoover Dam releases
- SNWA withdrawals
- effluent flow rates and water quality
- lake storage volume/WSEL
- physiological parameters to reflect algal adaptation and shifts in dominant algal species.

The following sections briefly describe some of the research results and considerations made in determining appropriate changes to WLM inputs to reflect climate change.

2.3.1.1 CMIP3 Ensemble Projections

The WCRP's CMIP3 multi-model dataset was utilized to obtain an ensemble of 112 projections for changes in meteorology and flow rates (*i.e.*, run-off). Specifically, the methodology used in Reclamation's 2011 reports (Reclamation, 2011a and 2011b) was specialized to Lake Mead, including obtaining projections for run-off in the Colorado River immediately upstream of Lake Mead, and extended to also include run-off changes in the LVW, Virgin and Muddy Rivers, and projections for the 2090s.

Climate and hydrologic projections for the Lake Mead area and its tributaries were obtained from the Bias Corrected and Downscaled WCRP CMIP3 Climate Projections archive[1]. Monthly projections through year 2099 were obtained for a total of 112 projections, comprising of three different emission scenarios ("higher" (SRES A2), "middle" (SRES A1B) and "lower" (SRES B1)), and using 16 different CMIP3 models each with between one and seven unique initial conditions[2].

[1] **http://gdo-dcp.ucllnl.org/downscaled_cmip3_projections/**

[2] **http://gdo-dcp.ucllnl.org/downscaled_cmip3_projections/#About**

Following Reclamation's approach (2011a and 2011b), differences in climate projections for three decadal periods (2020s, 2050s, and 2070s) relative to the baseline 1990s period were initially computed for 112 realizations. The methodology was then extended to compute differences for a fourth decadal period (2090s). Differences were computed on both an annual and monthly basis.

These CMIP3 ensemble projections provided readily available projections at any location of interest (*i.e.*, Lake Mead and its tributaries) for any time period through 2099. The uncertainties of the climate projections were accounted for to a certain extent by considering the *ensemble* of all 112 CMIP3 projections. That is, both centrally tended values (*e.g.*, medians) and extreme values (*e.g.*, 10th and 90th percentiles) were considered in the analyses where appropriate.

2.3.1.2 Inflow Water Quality

Climate change is anticipated to alter the water quality of the inflows to Lake Mead (*i.e.*, the Colorado, Virgin and Muddy Rivers, and the LVW), which in turn will directly affect the water quality of Lake Mead. In particular, projected increased air temperatures are anticipated to lead to increased inflow water temperatures and corresponding decreases in DO concentrations (due to lower solubility). Other water quality changes may also be possible.

2.3.1.3 Projected SNWA and Effluent Flows and Water Quality

Future changes in the SNWA withdrawals and the return effluent flows are primarily correlated with population growth rather than climate change. Estimated SNWA and effluent flows will generally follow these population trends, although there may be other changes due to use differences (*e.g.*, increased water conservation measures and/or increased recycling and re-use of effluent). The water quality of the SNWA withdrawals will depend upon changes within Lake Mead, and will be predicted as an output of the WLM, rather than specified as an input. The water quality of the effluent inflows will primarily depend upon the level of treatment and nutrient (*i.e.*, phosphorus and nitrogen) removal at the waste-water treatment plants.

2.3.1.4 Volume/WSEL

Approximately 97 % of the inflow to Lake Mead is from the Colorado River (Holdren and Turner, 2010). The median climate-change projections indicate decreased run-off in the Colorado River of approximately 8 % in the 2050s, 2070s and 2090s. Whether these potentially decreased inflows ultimately lead to periods of lower lake WSEL depends upon a myriad of other factors, including adaptation in management strategies, water conservation measures, and other potential supplies of water.

Various studies (Barnett and Pierce, 2008, 2009, Rajagopalan *et al.*, 2009, Reclamation, 2012a, 2012b) suggest that the Colorado River Basin will face increased

stress from a combination of reduced future inflows and increased future demands, and that the WSEL of Lake Mead is more likely to decrease than increase. In addition, the water quality in Lake Mead is more likely to deteriorate with lower WSEL than with higher WSEL. Furthermore, the USGS recently identified a need to evaluate "the potential effects of chronically lower water levels in Lake Mead on lake configurations, hydrology and water quality" (Rosen *et al*., 2012). Thus, the examination of water quality in Lake Mead at lower WSELs is important.

2.3.1.5 Algal Adaptation and Shifts in Species

Warmer water temperatures are expected to result in adaptations within algal species as well as shifts in dominant species. Algal adaptations and shifts in algal species may have important effects on chlorophyll *a* concentrations, which in Lake Mead are subject to water quality standards.

2.3.1.6 Summary

Of the potential climate-change induced changes identified only the changes that were deemed most important were implemented into the future scenario simulations. These important changes are summarized as:

- increased air temperatures, also leading to,
    - increased inflow water temperatures
    - decreased inflow DO concentrations
- extreme variations in the Colorado River inflow volumes
    - low flows
    - high flows
- lower lake volumes (*i.e*., lower WSEL)
- algal adaptation and shifts in dominant algal species.

Other potential changes that were identified, but not implemented into the simulations included, changes to the water quality (*e.g*., conductivity, constituent concentrations) of the inflows, potential decreased annual run-off, seasonal changes in run-off, and increased storm flow frequency in the Virgin and Muddy Rivers, and potential increased average run-off and storm flow frequency in the LVW. These potential changes were deemed as less important than the implemented changes noted above.

2.3.2 Previous Climate Change Simulations

Ten WLM simulations that were used to explore the above changes are summarized in **Table 2.1**. Run 1 was a "baseline" simulation representing present conditions, and was used to compare with the future scenario simulation results. Runs 2, 3 and 4 explored the effect of differing amounts of projected air temperature increase. Extreme low and high flows in the Colorado River were simulated in Runs 5 and 6, respectively, while Runs 7 and 8 explored the effect of lower WSEL. Potential adaptation of algae to warmer water temperatures was explored in Runs 9 and 10. Runs 5 through 9 all assume a 2090s median air temperature, while Run 10 assumes a 2090s 90th percentile air temperature.

It is noted that the Colorado River inflow rates are not modified from the baseline simulation for the majority of the future scenario simulations (*i.e.*, except for Runs 5 and 6). This is due to the relatively moderate median projected decrease in run-off coupled with the large degree of uncertainty in the run-off projections (Section 3.1.4.1.1). Rather than implement the relatively moderate median projected decrease of less than 8 % in all the future case scenarios, Runs 5 and 6 are used to examine the extremes. This approach also has the advantage of enabling more direct comparison to the "baseline" simulation, to enable water quality changes due to other effects (*e.g.*, different increases in air temperature) to be examined in isolation. Similarly, the Virgin and Muddy River flow rates are not modified for any of the simulations.

All simulations are carried out over a two-year period and include temperature, conductivity, pH, and concentrations of bromide, chlorophyll *a* (*i.e.*, algae), nutrients, TOC, DO and suspended-solids.

Table 2.1: Lake Mead WLM Simulations for Previous Climate Change Modeling

Run #	Purpose	Initial WSEL[1] (feet)	Air Temperature	Colorado River (CR) Inflow	Las Vegas Wash (LVW) Inflow[2]	SNWA withdrawal
1	Baseline	1100	2006-07	2006-07 (9.23 MAF/yr)	200 MGD effluent	389 MGD
2	Moderate warming	1100	2050s median	2006-07 (9.23 MAF/yr)	298 MGD effluent	671 MGD
3	High warming	1100	2090s median	2006-07 (9.23 MAF/yr)	441 MGD effluent	823 MGD
4	Extreme warming	1100	2090s 90th percentile	2006-07 (9.23 MAF/yr)	441 MGD effluent	823 MGD
5	Low CR inflow	1100	2090s median	2006-07 scaled to 7.00 MAF/yr	441 MGD effluent	823 MGD
6	High CR inflow	1100	2090s median	2011 (both years) (14.78 MAF/yr)	441 MGD effluent	823 MGD
7	Low WSEL	1040	2090s median	2006-07 (9.23 MAF/yr)	441 MGD effluent	823 MGD
8	Extreme low WSEL	925	2090s median	2006-07 (9.23 MAF/yr)	441 MGD effluent	823 MGD
9	Second algae group (high warming)	1100	2090s median	2006-07 (9.23 MAF/yr)	441 MGD effluent	823 MGD
10	Second algae group (extreme warming)	1100	2090s 90th percentile	2006-07 (9.23 MAF/yr)	441 MGD effluent	823 MGD

1. The WSEL is fixed for the baseline simulation (*i.e.*, Run 1) by adjusting the Hoover Dam outflow. The Hoover Dam outflow rates are kept the same as Run 1 for the future case scenarios (*i.e.*, Runs 2 – 10) and due to other flow rate and evaporation differences the WSEL for Runs 2 – 10 may vary.

2. The LVW inflow comprises 20 MGD baseflow flow-weighted with 200 MGD to 441 MGD of effluent.

2.3.3 Climate Change Conclusions (Previous Modeling)

The ten WLM simulations (Runs 1 – 10) predicted that the primary changes in the lake water quality were: increased water temperature, longer duration of algae growth and in particular growth beginning earlier in the year, generally similar annual average chlorophyll *a* concentrations (although chlorophyll *a* concentrations in Boulder Basin increased at extreme low WSEL and at lower Colorado River inflow volumes), decreased DO concentrations (particularly in the hypolimnion), and increased suspended-solids concentrations at lower WSEL and higher Colorado River inflow rates. Climate change was generally predicted to have less effect on the overall nutrient and TOC concentrations and pH.

In addition the operation of the Hoover Dam, and in particular the depth to the uppermost open outlets, was found to alter the concentrations of constituents from the LVW (*e.g.*, effluent tracer, conductivity, and bromide concentrations) within the epilimnion of Boulder Basin. While water quality at the Hoover Dam outlets and SNWA intakes were somewhat effected by warmer air temperatures and different Colorado River inflow rates, changes in the depths of these outflows due to varying WSEL (*i.e.*, changes in the position of the hypolimnion/epilimnion relative to the outlets) were generally found to have the greatest effect on water quality at these locations. In addition to simulated changes in water quality, increased temperatures were predicted to result in evaporation increasing by as much as 17 % by the 2090s.

As previously stated, these WLM simulations (Runs 1 – 10) it did not account for internal nutrient recycling. The conclusions reached, specifically decreased DO concentrations, make understanding and accounting for sediment nutrient flux critical for projecting future water quality changes. Coupled with warmer temperatures and increased algae growth duration, increased nutrient concentrations due to sediment flux have the potential to increase productivity in Lake Mead. Understanding and quantifying the potential effect on water quality from increased productivity and internal nutrient recycling is the motivation for implementing sediment phosphorus flux into the WLM in the current study.

2.4 CURRENT CLIMATE CHANGE MODELING

The goal of the present work is to include sediment phosphorus flux in the WLM to assess the water quality of Lake Mead under various climate change scenarios. Estimates for the phosphorus flux rates are discussed in Sections 3. Six simulations were modeled to evaluate the effects of sediment phosphorus flux on water quality. Only some of the climate change scenarios deemed to be most important by the previous modeling were evaluated. Descriptions of the six simulations are presented in Section 4.

3 SEDIMENT PHOSPHORUS FLUX IN LAKE MEAD

In the development of the Lake Mead ELCOM/CAEDYM model, the sediment nutrient fluxes (*i.e.*, the internal nutrient recycling) were not included on the premise that Lake Mead generally has DO concentrations high enough to prevent substantial nutrient release from the sediments. However, the previous work conducted for WaterSMART illustrates that under warmer conditions driven by climate change, substantial volumes of the hypolimnion may have DO concentrations less than 2 mg/L. DO concentrations below 2 mg/L typically result in high sediment nutrient release rates, particularly for phosphorus, where sediment release rates exceed diagenesis rates (DiToro, 2001). This additional supply of phosphorus to the lake may increase productivity (*i.e.*, algae concentrations), lead to further decreases in DO concentrations, and lead to decreased water quality in and downstream of Lake Mead.

The first step in realizing the goal of evaluating the potential for productivity increases of Lake Mead through increased nutrient release from sediments is to obtain estimates of appropriate rates for sediment fluxes of filterable reactive phosphorus (FRP[3]), nitrate, and ammonia. However, the primary effort in the analysis and modeling will target the FRP flux, since phosphorus is the limiting nutrient in Lake Mead.

This was a two-pronged approach consisting of a literature search and additional in-reservoir data collection and analysis. The literature search investigated appropriate flux rates for Lake Mead and other similar lakes as well as approaches to modeling sediment nutrient fluxes. The data collection was conducted by SNWA within Lake Mead through 2014 and involved sampling and subsequent laboratory analysis to determine nutrient concentrations. The 2014 data were analyzed and used to evaluate the Year 2014 simulation.

3.1 LITERATURE REVIEW

Sediment nutrient flux in Lake Mead has not been a widely studied phenomenon. Therefore the literature search included lakes from the same geographical area, mainly the southwest United States. The results of the literature review are summarized in **Table 3.1,** which includes the relevant lake, location, trophic status, documented phosphorus flux rate, and the reference from which the information was obtained. Flux rates are varied for lakes even when they are in close proximity (Lakes Skinner, Mathews, Perris, Elsinore, and Canyon are within approximately 35 miles of each other in Riverside County, CA). Trophic status is also varied even when comparing lakes with similar flux rates. Generally, reservoirs with higher phosphorus flux rates have increased productivity; however, there is not always a linear correlation.

[3] FRP refers to phosphorus that is readily available for uptake by algae (*i.e.*, biologically available phosphorus). It is also often referred to as ortho-phosphorus or soluble reactive phosphorus.

Table 3.1: Sediment Phosphorus Flux Values from Literature Review

Name	Location	Trophic Status	Phosphorus Flux (mg P/m^2/day	Reference
Mead: Las Vegas Bay	NV	mesotrophic	2.5 – 3.9[1]	Murray *et al*., 1981
Mead: Bonelli Bay (Virgin Basin)	AZ	oligotrophic	0.12 – 0.36[1]	Murray *et al*., 1981
"most mesotrophic lakes"	World-wide	mesotrophic	2 – 10	Nurnberg, 1988
"most mesotrophic lakes"	CA	mesotrophic	5 – 10	Beutel, 2006
Skinner	CA		0.5	Anderson *et al*., 2007
Mathews	CA	oligo-mesotrophic	3.4 ± 0.8	Beutel *et al*., 2008
Bard	CA		6 – 8	Debroux *et al*., 2012
Perris	CA	eutrophic	6 – 12	Beutel, 2006
Elsinore	CA	eutrophic	9.4	Anderson *et al*., 2007
Canyon	CA	hyper-eutrophic	6.3 – 15.1	Anderson *et al*., 2007
San Vicente	CA	eutrophic	10 – 29	Beutel *et al*., 2007
Los Vaqueros	CA		≤ 26	Martin *et al*., 2013

1. Flux rates corrected to 20°C assuming Flux(20°C) = Flux(T)/[$1.05^{(T - 20°C)}$]

The most relevant research to Lake Mead is a study by Murray *et al.* performed in 1981 on sediment flux rates in Las Vegas Bay and Bonelli Bay of Lake Mead. The study was concerned with quantifying nutrient exchange with the sediments to establish a nutrient budget for Lake Mead in order to help address the impact the LVW has on water quality in Las Vegas Bay and Boulder Basin. Samples of sediment cores and interstitial water were collected from four stations in Las Vegas Bay, as well as two stations in Bonelli Bay, to assess regional variability. The study focused on different forms of phosphorus and nitrogen since those elements had been previously identified as possible nutrients that control phytoplankton growth [phosphorus is now known to be the limiting nutrient in Lake Mead (Lieberman, 1995)].

The study found that large gradients of sediment nutrient flux did exist across the sediment-water interface in Lake Mead. Dioxygen (O_2) and nitrate (NO_3) were being consumed by the sediment (flux into the sediment) at rapid rates. As a result, chemicals such as phosphate (PO_4) were being released from the sediments with concentrations increasing sharply at the sediment-water interface. The fluxes were described by Fick's first law of diffusion (Berner, 1980). Flux rates determined by the study for Las Vegas Bay ranged between 2.5 and 3.9 mg P/m^2/day (corrected to 20 °C, see **Table 3.1**) while rates for Bonelli Bay ranged between 0.12 and 0.36 mg P/m^2/day (corrected to 20 °C, see **Table 3.1**). The study noted that sediment fluxes are strongly influenced by the overlying water quality. When DO concentrations are low, flux into the sediments is low and flux out of the sediment is high. It also noted that fluxes likely vary seasonally and spatially.

A report by the United States Department of Interior Bureau of Reclamation in 2002 (USBR, 2002) analyzed sediments from Las Vegas Bay that were exposed due to a WSEL drop of 30 feet in 2001. The study analyzed the composition of the sediments to better determine the effect of sediments in the delta on water quality within Lake Mead. Note that the analysis was performed on exposed sediments that had dried.

Samples were collected from 36 sites and analyzed for nutrients, metals, and perchlorate concentrations as well as leachate from sediment equilibriums from exposure to water from Lake Mead, LVW, and pore water. The study did not determine flux rates, but it did provide some relevant conclusions on sediment flux in Las Vegas Bay. It was determined that due to the composition of sediments, which have low organic content, there is a limited capacity to absorb or release nutrients. The study also confirmed that sediments have the potential to release phosphorus, the limiting nutrient in Lake Mead. However, sediments release phosphorus when mixed with water from Lake Mead, but absorb phosphorus when mixed with water from LVW. Therefore, sediment phosphorus flux is not a significant source of phosphorus to Las Vegas Bay.

In the study of phosphorus release rates for California lakes by Nurnberg in 1998, a literature review of lakes worldwide was performed. The lakes were categorized by trophic status as well. Trophic status refers to the biological productivity of a lake and can be categorized as one of the following in descending order of productivity, hypertrophic, eutrophic, mesotrophic, and oligotrophic. Data from the review shows that sediment phosphorus flux rates in mesotrophic lakes are typically 2 – 10 mg P/m^2/day and that oligotrophic lakes are typically less than 2 mg P/m^2/day.

Another pertinent finding in some studies was the spatial and temporal variation of sediment phosphorus flux rates. In a study of Canyon Lake (Anderson, *et. al.*, 2007) large spatial differences in flux rates were found between two sites, speculated to be due to geochemical differences. In a study of Lake Perris (Beutel, *et. al.*, 2006), which also showed spatial differences in sediment phosphorus flux, a more detailed explanation was provided. Sediment quality was likely responsible for different rates with deeper stations having more organic material leading to higher flux rates. In contrast, shallower stations

had sandier sediments and reduced flux rates. Temporal changes are typically related to the overlaying water quality, particularly the changes in dissolved O_2 status (Moore, *et. al.*, 1998). Anaerobic conditions result in higher sediment phosphorus flux rates. When conditions become anaerobic can be effected by meteorology conditions, inflows, and depth. Spatial and temporal variations are particularly relevant to a large lake such as Lake Mead, which has several different regions creating a variety of conditions.

3.2 DATA ANALYSES

In-reservoir sampling of FRP was performed from 2000 through 2013 to aid in the estimation of phosphorus flux. Concentrations of FRP collected by SNWA at Station CR346.4 are show in **Figure 3.1.** The majority of the data available are from grab samples, as opposed to profiles, which limits the vertical resolution of the data. There is a noticeable difference in FRP concentrations beginning in Year 2008 for all elevations, except near the bottom. This difference is likely caused by a change in sample analysis, possibly increasing the detection limit of FRP concentration.

Concentrations of DO within approximately 10 feet of the bottom (*i.e.*, below elev. 735 feet) at Station CR346.4 are plotted in **Figure 3.2**. Plotted data are a combination of sets collected by SNWA and the United States Bureau of Reclamation (USBR). The data show a defined pattern of decreasing DO in the stratified period of each year with minimum DO concentrations typically occurring in November and December and ranging from 0 to 5 mg/L, depending on the year,. Concentrations increase in January and February after destratification and mixing allows for re-oxygenation of the hypolimnion. After re-oxygenation concentrations can range from 7 to 10 mg/L depending on year.

Near bottom FRP concentrations are also plotted in **Figure 3.2**, with the SNWA and USBR data sets defined. Data sets show disagreement during the 2006 and 2007 years, but tend to agree on concentrations levels during years 2008 – 2012. Increases in FRP concentrations show a correlation with decreases in DO concentrations. The highest measured FRP concentrations (between 0.02 and 0.03 mg P/L) occur during two years, 2003 and 2005, in which DO concentrations are particularly low (< 3 mg/L). In general, FRP concentrations near the bottom increase when DO concentrations decrease. USBR data were chosen to estimate sediment flux rates due to readily available FRP measurements and DO profiles.

The following equation (EQ-1) was used here to derive the relationship between sediment FRP flux (F_{FRP}) and DO based on in-reservoir data. This is a simplified version of the original equation used in CAEDYM to calculate the sediment FRP flux. The effect of pH on the sediment FRP flux was ignored here.

$$F_{FRP} = S_P \left[1 - \left(\frac{K_{DO}}{K_{DOS}} \right) \right] \qquad \text{EQ-1}$$

where F_{FRP} is the actual sediment FRP flux in mg P/m^2/day, S_p is the maximum potential flux in mg P/m^2/day, K_{DO} is the actual concentration of DO in mg/L at the sediment-water interface, and K_{DOS} is the maximum concentration of DO in mg/L at which flux will occur. When K_{DO} is greater than K_{DOS} the flux rate is zero. Data analysis of the USBR DO and FRP data was used to estimate both S_p and K_{DOS}. As shown in the literature review (Murray *et al*., 1981) flux rates for Boulder Basin and the Upper Basins can be different. Therefore an estimation of the flux was performed at Station CR380.0 as well as a Station CR346.4.

Bottom concentrations of FRP and DO at Stations CR346.4 and CR380.0 are compared in **Figures 3.3** and **3.4**, respectively, for years 2006 – 2012 when both FRP and DO data from USBR are available. However, Year 2012 data sets were incomplete so they were not used as part of the analysis. Both stations show good correlation between changing DO and FRP concentrations. Note that only those data showing obvious rising FRP concentrations with decreasing DO were used in the calculation and they are marked with black loops in **Figures 3.3** and **3.4**. Using these data, the rate of change in FRP concentration during periods of decreases in DO (dFRP/dt) were calculated for each year.

The rate of change in FRP (dFRP/dt) can be related to the sediment FRP flux through a mixing length theory, which assumes that the sediment flux would change the concentration of FRP in the water column up to the height of the mixing length. Since the FRP data are not vertically resolved, DO profiles were used to estimate the mixing length. An example from Station CR346.4 is shown in **Figure 3.5**. The mixing length (L) was estimated based on the elevation above the bottom below which there exist obvious DO increases with rising elevation and thus non-negligible vertical mixing near the bottom of the lake. In the example, L is approximately 20 meters (~ 66 feet). For Station CR346.4, L typically ranges between 17 to 22 meters (56 to 72 feet). The mixing length for CR380.0 was much smaller ranging from 3.2 to 5.9 meters (10.5 to 19 feet). Assuming a linear variation of FRP concentration up through the mixing length, a mass balance can yield the relationship between the rate of change in FRP (dFRP/dt) and the sediment FRP flux (F_{FRP}) as follows:

$$F_{FRP} = \left(\frac{dFRP}{dt}\right) \times \left(\frac{0.5L}{1{,}000}\right) \qquad \text{EQ-2}$$

where F_{FRP} is in mg P/m^2/day, dFRP/dt is in mg P/L/day, L is in meters, and multiplying by 1,000 is the conversion factor between cubic meters and liters. Note that dFRP/dt was derived from data shown in **Figure 3.3** and **3.4**. This method was used to estimate flux rates for applicable periods during the years 2006 – 2011 at both stations. Estimated flux rates at Station CR346.4, plotted against corresponding DO concentrations in **Figure 3.6** (calculated as the average of DO during the period), can range up to 2.2 mg P/m^2/day with an average rate of 1.2 mg P/m^2/day. The upper end of the range is on the order of rates calculated in Murray *et al*. 1981 for Las Vegas Bay. Flux rates were adjusted to a temperature of 20 °C. Error bars were estimated due to the resolution of FRP

measurements (0.3 mg P/m^2/day) and the estimation of L based on DO concentrations (10 %).

Figure 3.7 shows the estimated flux rates at Station CR380.0. Estimated flux rates are lower at Station CR380.0, only ranging up to 0.32 mg P/m^2/day. The average flux rate is 0.14 mg P/m^2/day, which is approximately 9 times lower than Station CR346.4. The upper end of the flux estimation range at Station CR380.0 is on the order of rates calculated in Murray *et al*. 1981 for the Virgin Basin. Errors bars estimated due to FRP measurement resolution (0.08 mg P/m^2/day) decreased compared to errors bars for CR346.4. The decrease is likely due to the general decrease in magnitude of FRP concentrations. However, error bars due to the estimation of L increased (23 %) likely because of increased magnitude of DO concentrations.

3.3 IMPLEMENTATION INTO MODEL AND VERIFICATION

The WLM was updated to implement the sediment phosphorus flux. This involved revising the original CAEDYM function for phosphorus flux as well as changing the default coefficients of EQ-1. Maximum flux rates (S_p) and maximum DO concentration at which flux occurs (K_{DOS}) were varied spatially between Boulder Basin and the Upper Basins. To test the sediment phosphorus flux function and validate the flux relationships a previous calibration for the WLM for years 2005 – 2008 was re-run (Flow Science, 2007, 2010a, 2010b). Initial estimates for the coefficients S_p and K_{DOS} in EQ-1 were based on the data analysis at Stations CR346.4 and CR380.0 and the values of the coefficients were revised through an iterative process to arrive at the final equations.

Based on the analysis for Station CR346.4 the flux-DO relationship implemented in the model for Boulder Basin assumes a maximum flux of 5 mg P/m^2/day when DO is equal to 0 mg/L with a maximum DO concentration of 5 mg/L at which flux will occur. The actual sediment FRP flux was governed by equation 3 (EQ-3)

$$F_{FRP} = 5\,mgP/m^2/day\left[1-\left(\frac{K_{DO}}{5mg/L}\right)\right] \qquad \text{EQ-3}$$

where F_{FRP} is in mg P/m^2/day, S_p (the maximum potential flux) is set to 5 mg P/m^2/day, K_{DO} is the actual concentration of DO in mg/L at the sediment-water interface, and K_{DOS} (the maximum concentration of DO at which flux will occur) is set to 5 mg/L. The relationship is shown on **Figure 3.6**. Based on the analysis for Station CR380.0, the flux-DO relationship for the Upper Basins assumes a maximum flux of 1 mg P/m^2/day when DO is equal to 0 mg/L with a maximum DO concentration of 5 mg/L at which flux will occur. For the Upper Basins, flux rates were based on analysis of data from Station CR380.0 and the actual sediment FRP flux was governed by equation 4 (EQ-4)

$$F_{\mathrm{FRP}} = 1\,mgP/m^2/day\left[1-\left(\frac{K_{DO}}{5mg/L}\right)\right] \qquad \text{EQ-4}$$

where F_{FRP} is in mg P/m^2/day, S_p (the maximum potential flux) is set to 1 mg P/m^2/day, K_{DO} is the actual concentration of DO in mg/L at the sediment-water interface, and K_{DOS} (the maximum concentration of DO at which flux will occur) is set to 5 mg/L. The relationship is shown on **Figure 3.7**.

Phosphorus flux rates calculated using EQ-3 (Station CR346.4) and EQ-4 (Station CR380.0) are shown in **Tables 3.2** and **3.3**, respectively. Flux rates estimated from the data are included for comparison. The mean error (ME) for Station CR346.4 was -1.02 mg P/m^2/day and the root mean square error (RMSE) was 1.38 mg P/m^2/day. The RMSE was approximately 28 % of the estimated maximum flux rate (5 mg P/m^2/day). The ME for Station CR380.0 was -0.23 mg P/m^2/day and the RMSE was -0.10 mg P/m^2/day, which is approximately 30 % of the estimated maximum flux rate (1 mg P/m^2/day).

Table 3.2: Comparison of Phosphorus Flux Rates for Station CR346.4

Year	DO (mg/L)	Estimated Phosphorus Flux from Data (mg P/m^2/day)	Estimated Phosphorus Flux from EQ-3 (mg P/m^2/day	Error (EQ-3 – Data)
2006	4.5	0.69	0.52	-0.17
2006	3.7	1.94	1.33	-0.61
2007	5.5	1.97	-0.46	-2.43
2008	6.6	-	-	-
2008	5.6	0.40	-0.55	-0.95
2008	5.3	1.15	-0.28	-1.43
2009	4.6	0.51	0.36	-0.15
2009	4.1	1.44	0.88	-0.56
2009	3.6	1.92	1.42	-0.50
2010	4.7	1.05	0.31	-0.74
2010	3.9	0.77	1.11	0.34
2010	4.8	1.05	0.16	-0.89
2011	6.5	0.59	-1.48	-2.07
2011	5.8	2.20	-0.85	-3.05

Results of the final iteration of the WLM with sediment phosphorus flux implemented are shown for Stations CR346.4 and CR380.0 in **Figures 3.8** and **3.9**, respectively. The figures compare measured DO and FRP concentrations near the bottom of the lake to predicted model results with (revised simulation) and without (original simulation) sediment phosphorus flux. DO concentrations are similar for the original and revised simulations. Release of FRP from sediment flux will produce slightly more algae and slightly lower the DO concentrations, however, effects are negligible.

Table 3.3: Comparison of Phosphorus Flux Rates for Station CR380.0

Year	DO (mg/L)	Estimated Phosphorus Flux from Data (mg P/m^2/day)	Estimated Phosphorus Flux from EQ-3 (mg P/m^2/day	Error (EQ-4 – Data)
2006	7.8	-	-	-
2006	7.6	0.03	-0.52	-0.55
2006	6.5	0.20	-0.31	-0.51
2006	4.8	-	-	-
2007	5.8	0.10	-0.16	-0.26
2007	5.1	0.11	-0.02	-0.13
2007	3.8	0.23	0.24	0.01
2008	5.7	0.17	-0.14	-0.31
2008	5.2	0.21	-0.04	-0.25
2008	4.6	0.32	0.09	-0.23
2009	5.8	0.24	-0.17	-0.41
2009	4.8	0.01	0.05	0.04
2009	3.9	0.14	0.22	0.08
2010	5.9	0.10	-0.18	-0.28
2010	5.5	0.05	-0.09	-0.14
2011	7.1	0.02	-0.41	-0.43
2011	3.9	0.31	0.21	-0.10

Results from the original simulation show no increase in FRP at the bottom of the lake that can be attributable to the decrease in DO. Due to this predicted FRP concentrations typically deviate from measured data during the end of each year. The revised simulation manages to capture increases in FRP concentrations during the end of the year when DO concentrations are low. The most noticeable improvement of the revised simulation is at Station CR346.4 (**Figure 3.8**) at the end of Year 2005 when there is a significant increase in FRP concentration due to low levels of DO. The WLM is able to accurately capture the magnitude of the increase in FRP with only a slight delay in the timing. The remaining years show an improvement in the timing of the model prediction for the increase in FRP at the bottom. Results of the revised simulation at CR380.0 (**Figure 3.9**) also show the model accurately capturing the magnitude and timing of the increase in bottom FRP concentrations. Increases are smaller than at CR346.4 due to lower phosphorus flux rate, but this is confirmed by the measured data.

4 DESCRIPTION OF ELCOM/CAEDYM SIMULATIONS

This section provides a description of the six simulations using the WLM with phosphorus flux implemented that were performed to investigate the effects of climate change on the water quality of Lake Mead. It is noted that not all *combinations* of climate change parameters were modeled. Only some of the climate change scenarios deemed to be most important by the previous modeling were evaluated.

All simulations are carried out over a two-year period and include temperature, conductivity, pH, and concentrations of bromide, chlorophyll *a* (*i.e.*, algae), nutrients, TOC, DO and suspended-solids. Details of the simulations, and in particular how the WLM inputs were modified to simulate the different effects of climate change, are provided in the following sections.

4.1 "BASELINE" SIMULATION WITH PHOSPHORUS FLUX (RUN 11)

The "baseline" simulation Run 11 is essentially the same as the "baseline" simulation from previous climate change modeling (Run 1 in Table 2.1) but with phosphorus flux implemented. It represents present conditions and is used to compare with projected climate change scenario simulations. The phosphorus flux rate used is described in Section 3.3. Full details of the "baseline" model inputs are provided in the report *ELCOM-CAEDYM Modeling with Climate Change Part 1: Lake Mead* (Flow Science, 2013), with a general summary provided here.

Run 11 used 2006–2007 meteorology and inflow rates for the Colorado, Virgin and Muddy Rivers. The LVW assumed a constant 20 MGD of baseflow and a monthly varying *total* annual average effluent flow rate of 200 MGD. The effluent flow rate had some reuse flows removed from it such that the *net* annual average flow to the LVW was 178 MGD (Flow Science, 2013). The water quality of the LVW inflow was generally determined by flow-weighting the constituent concentrations (Flow Science, 2013). The nominal effluent total phosphorus load was 225 lbs/day, which refers to the maximum monthly load. The annual average total phosphorus load was 215 lbs/day (Flow Science, 2013).

The SNWA withdrawal rate through Intake #3 varied monthly with an annual average withdrawal rate of 389 MGD (Flow Science, 2013). The flow through the Hoover Dam was assumed to be equally split between the lower (elevation 895 feet) and upper (elevation 1,045 feet) outlets, and the total flow rate was adjusted in order to maintain a constant WSEL of 1100 ft. The resulting average total outflow rate was 8.36 MAF/year. The adjustment was made on a daily basis while still maintaining the diurnal variation of dam operations (Flow Science, 2013). It is noted that the WSEL of 1100 feet is representative of recent conditions at Lake Mead.

Run 11 did not use the second algae group adapted to warmer temperatures that was used in previous modeling Runs 9 and 10 (Flow Science, 2013). The inclusion of a second algae group to represent algal adaptation to warmer temperatures resulted in forced algal succession in the summer and increased the growing season and summer average concentrations. However, the numeric values depend directly on the parameter choice for the second algae group. For example a species with lower phosphorus to chlorophyll *a* ratios (i.e., a species that uses phosphorus more efficiently) would be expected to result in higher predicted chlorophyll *a* concentrations. Additional research and experiments are required to properly parameterize the different algal groups that are present in Lake Mead, in order to more robustly account for algal adaptation and species succession. Therefore, only one algae group was modeled and results were compared to Run 1 which used the same algae group parameters. Two suspended solids sizes were simulated, with diameters of 1.2 μm and 2.0 μm and respective settling velocities of approximately 0.125 m/day and 0.35 m/day. These were assumed to enter in the Colorado River inflow only (Flow Science, 2013).

Run 11 used revised initial conditions based on end-of-year conditions of initial 2-year simulations. This is similar to running back-to-back Run 11 simulations in one continuum with the end of first Run 11 simulation (that was initialized based on the method adopted by Run 1 from the previous climate change modeling) serving as initial conditions for the Run 11 that was presented here. This minimized the effects of the initial conditions and allowed for the long-term effects of sediment phosphorus release to be manifested. The "baseline" simulation (Run 1 in Table 2.1) from the previous climate change modeling (Flow Science, 2013) is included with the present work to compare simulations with and without phosphorus flux and to aid in the visualization of nutrient release. It uses the same parameters as Run 11 aside from the initial conditions; however, it does not include phosphorus flux.

The method of initialization for Run 1 was from the previous climate change modeling (Flow Science, 2013). The initial temperature, pH and DO concentration throughout the lake were set as constant values (based upon Reclamation measurements in the hypolimnion of Station CR346.4 on 1/11/2006). The initial salinity, bromide concentrations, TOC concentrations, nutrient concentrations and effluent tracer concentrations in the upper basins were set equal to the average of the values of the Colorado River inflow (neglecting the effect of the smaller Virgin River and Muddy River inflows), while the flow-weighted averages of the Colorado River and LVW inflows were used to set values in Boulder Basin (Flow Science, 2013). The initial suspended-solids concentrations were set equal to the fully-mixed steady-state values, which depend on lake residence times and particle settling times (Flow Science, 2013). The flow-weighting and steady-state methodologies are preferable to using historical field data, since they are able to account for the flow rates and concentrations in the inflows being different from historical values.

As mentioned before, Run 11 used a different initialization method from Run 1. This is because the phosphorus load from sediment release is unknown prior to the completion

of the simulation and the flow-weighting and steady-state methodologies used by Run 1 cannot be applied.

4.2 "HIGH WARMING" SIMULATION WITH PHOSPHORUS FLUX (RUN 12)

The simulation Run 12 is similar to Run 11, however, increases were made to air temperatures to reflect "high warming" based on the median of 2090's CMIP3 projections. The annual increase in air temperature is approximately 3.3 °C. This annual increase varied depending on the month applied with the smallest increases during winter months and largest increases during summer months. Details of the "high warming" projections can be found in the previous modeling report (Flow Science, 2013).

In addition to air temperature increases, there are the associated effects of increases in the inflow water temperatures and decreases in the DO concentrations of the inflows. Inflow water temperatures for each of the four inflows (*i.e.*, the Colorado, Virgin and Muddy Rivers, and the LVW) were adjusted on a monthly basis using linear correlations (Flow Science, 2013). Inflow DO concentrations for each of the inflows were also adjusted on a monthly basis to account for lower oxygen solubility at the higher inflow water temperatures (Flow Science, 2013). Finally, the different projection period resulted in different effluent flow rates and SNWA withdrawal rates. The initial conditions for Run 12 followed the same method as were used for Run 11.

The "high warming" simulation (Run 3 from Table 2.1) from the previous climate change modeling (Flow Science, 2013) is included with the present work to provide a comparison for Run 12. It uses the same parameters as Run 12 aside from the initial conditions and no sediment phosphorus flux.

The same methodologies used to set the initial conditions for Run 1 were used for Run 3 except the initial temperatures were increased to account for the warmer air temperatures. This was based upon the assumption that the hypolimnion temperature of Lake Mead depends strongly on the inflow temperature of the Colorado River in the winter. It is noted that the higher effluent flow rates in Run 3 resulted in higher initial effluent concentrations in Boulder Basin.

4.3 OTHER SIMULATIONS (RUNS 13, 14, AND 15)

Runs 13, 14, and 15 also model the "high warming" conditions applied to Run 12. The "high warming" conditions, resulted in lower DO concentrations due to lower oxygen solubility, higher metabolic rates and longer duration of stratification (Flow Science, 2013). Therefore, this condition was applied to all subsequent simulations. In addition each simulation applies a second climate change based parameter to evaluate the sensitivity of conditions in Lake Mead to change.

Run 13 added "low wind" conditions, wind speeds were decreased by 20 %, to the "high warming" conditions of Run 12. In general less wind tends to decrease mixing of a lake, which can increase surface temperatures, decrease the thermocline depth, strengthen

stratification, and delay destratification. The combination of these effects can cause decreased DO concentrations, which can in turn affect internal nutrient recycling.

A higher WSEL was modeled for Run 14 along with the "high warming" conditions. The initial WSEL was increased from 1,100 feet (all other simulations) to 1,220 feet. An increased WSEL, with other parameters unchanged, will increase the volume of the hypolimnion, delay destratification, and likely decrease DO concentrations at the lake bottom.

An increase to the phosphorus flux rate was added to the "high warming" conditions for Run 15. The maximum flux rate was increased from 5 to 6 mg P/m^2/day, an increase of 20 %. The higher flux rate will cause increased sediment release when conditions are conducive to release (*i.e.* low DO).

Runs 13 – 15 also used revised initial conditions based on end-of-year results of an initial 2-year simulation, the same method used by Runs 11 and 12.

The five WLM simulations used to explore the above changes are summarized in **Table 4.1**. It is re-iterated that not all *combinations* of the above climate change parameters were modeled. Rather, the "corners" of the parameter-space are explored in order to identify important changes, and provide guidance for future research efforts.

Table 4.1: Lake Mead WLM Simulations with Phosphorus Flux

Run #	Purpose	Initial WSEL (feet)	Air Temperature	Wind Speeds	Maximum Phosphorus Flux Rate (mg P/m^2/day
11	Baseline	1,100	2006 - 2007	2006 - 2007	5
12	High Warming	1,100	2090s median	2006 - 2007	5
13	High Warming, Low Wind	1,100	2090s median	20 % reduction of 2006 - 2007	5
14	High Warming, High WSEL	1,220	2090s median	2006 - 2007	5
15	High Warming, High Flux	1,100	2090s median	2006 - 2007	6

4.4 "2014" SIMULATION (RUN 16)

In-reservoir data collected in Lake Mead during the Year 2014 showed low levels of DO particularly in Gregg Basin. The observed levels of DO would have likely caused nutrient release from sediments at the bottom of the lake. This provided a unique

opportunity to evaluate the phosphorus flux rates of the WLM that were derived from both literature review and analysis of in-reservoir data prior to 2013 against more recent in-reservoir data that potentially showed internal nutrient recycling. A simulation of the Year 2014 was performed as an experiment to gauge the accuracy of the WLM and the estimated phosphorus flux rates.

Run 16 used 2014 meteorology and inflow rates for the Colorado, Virgin and Muddy Rivers, and LVW. Inflow water quality was determined by using the nearest available upstream monitoring station for each inflow. Hourly outflow rates were obtained for both the Hoover Dam and SNWA withdrawals through Intake #3.

Two suspended solids sizes were simulated, with diameters of 1.2 µm and 2.0 µm and respective settling velocities of approximately 0.125 m/day and 0.35 m/day. These were assumed to enter in the Colorado River inflow only (Flow Science, 2013).

The initial conditions were spatially non-uniform (*i.e.*, used measured data at multiple locations in the lake) for several variables [temperature, conductivity, salinity (derived from conductivity), and DO]. The initial conditions were horizontally-uniform for other variables (chlorophyll *a*, bromide, TOC and pH), with the measured field data at Station CR346.4 being used to initialize the variables throughout the lake. Spatially variable initial conditions for phosphorus and nitrogen were implemented. For each parameter, a simple binary spatial distribution was used, with one concentration defined for all locations downstream of the Narrows (*i.e.*, Boulder Basin and the Las Vegas Bay), and a second concentration defined for all locations upstream of the Narrows. The downstream concentrations were determined from data measured at Station CR346.4, while the upstream concentrations were based on an aggregate of observed field data at Stations CR360.7, VR2.0 and VR12.9/13.0.

5 RESULTS

The results of the six simulations with phosphorus flux are presented in this section. First a brief discussion of the simulations with phosphorus flux [Runs 11 and 12] compared to similar simulations without phosphorus flux [Runs 1 and 3 from previous modeling (Flow Science, 2013)] is provided. The comparison aids with visualization of phosphorus release.

Following the discussion of Runs 11 and 12 are comparisons of five hypothetical phosphorus flux simulations (Runs 11 – 15) that model baseline, high warming, low wind, high WSEL, and high flux conditions. Comparisons for temperature, conductivity, DO, phosphorus, and chlorophyll *a* are discussed. Finally, results of the simulation modeling Year 2014 Lake Mead conditions (Run 16) are discussed. Only salient results are presented here, with full suites of time-series plots being available in Appendix A.

5.1 VISUALIZATION OF PHOSPHORUS RELEASE

To highlight the use of the phosphorus flux implementation Run 11 is compared to Run 1, both "baseline" simulations, and Run 12 is compared to Run 3, both "high warming" simulations. Time-series results of temperature for simulations with and without flux are compared at Stations CR394.0 and CR346.4 in **Figures 5.1** and **5.2**, respectively. Note that these two pairs of simulations use different initial conditions (see Section 4), which is apparent when looking at the first few months of the simulation period presented. However, after approximately 4 months differences in temperature at both locations are negligible, both at the surface and near the bottom.

DO concentrations are compared for simulations with and without flux in **Figures 5.3** and **5.4**, respectively. The largest differences are again seen at the beginning of the modeling period due to differences in initial conditions. Run 3 predicts slightly less DO near the bottom at CR346.4 at the beginning of the second year of simulation. The differences could be related to slight differences in the timing of destratification. Note that periods of low DO concentrations occur at different times depending on how far downstream a station is located relative to where the Colorado River enters Lake Mead (*i.e.* Gregg Basin) and the depth of water at that station. At CR394.0 (Gregg Basin), DO concentrations begin to decrease in April and remain low until the lake mixes in October. At CR346.4 (Boulder Basin), DO concentrations also start to decrease in April (albeit more gradually), but do not increase until January. These differences will influence the timing of sediment release in the different Basins.

The small differences in temperature and DO concentrations between the two pairs of simulations can be attributed to the relatively high DO concentrations at the lake bottom during the simulation period, which limits the release of phosphorus from sediments. Neither station shows the anoxic conditions that would increase sediment phosphorus flux. Small quantities of phosphorus released from the sediments are likely to only have

minor effects on areas other than near the bottom when mixed vertically across the entire water column during destratification.

The release of phosphorus can be seen clearly when comparing simulations with and without flux. Concentrations of FRP are compared with both contours and time-series at stations along the Colorado River thalweg. Differences in FRP concentrations seen at the beginning of the presented simulation period are not discussed since these are due to differences in initial conditions. The following discussion will focus on the differences created by implementation of phosphorus flux. FRP at Station CR394.0 is presented in **Figures 5.5** through **5.7**. Differences in FRP concentrations are restricted to below an elevation of 1,000 feet (to approximately 50 feet above the bottom). Concentrations predicted by Runs 11 and 12 are similar to Runs 1 and 3 until DO concentrations (**Figure 5.3**) fall below 5 mg/L (July - October). The low DO concentrations trigger sediment phosphorus release and raise the levels of FRP. Concentrations of FRP at the bottom increase approximately 150 % (from 0.002 to 0.005 mg P/L) for baseline conditions and approximately 200 % (from 0.002 to 0.006 mg P/L) for high warming conditions.

As the depth of Lake Mead increases, DO depletion along the bottom of the lake increases, this in turn increases sediment phosphorus release. Predicted concentrations of FRP at Station CR390.0 are show in **Figures 5.8** through **5.10**. Differences in FRP between the simulation with and without phosphorus flux are restricted to the bottom 50 feet of the lake. Note that peak concentrations of FRP at the bottom for the flux simulations are later in the year compared to CR394.0 since peak oxygen depletion also occurs later. During the periods when DO stimulates sediment release, FRP concentrations at the bottom can be increased by as much as 350 % (baseline) to 425% due to sediment release. However, FRP concentrations at the surface remain similar for all runs at the beginning of the second year after lake destratification. Since phosphorus is the limiting nutrient for algae growth in Lake Mead any available phosphorus at the surface is rapidly consumed. Therefore, similar FRP concentrations at the surface for all runs indicate minor effects on algal productivity by sediment phosphorus release in this part of lake.

In Boulder Basin, the deepest part of Lake Mead, minimum DO concentrations do not occur until approximately mid-January, which extends the period of sediment release and raises the FRP peak concentrations at the bottom compared to the upper Basins. Concentrations of FRP are typically higher in Boulder Basin relative to the Upper Basins due to phosphorus loading from LVW. Comparisons of FRP at Station CR346.4 are shown in **Figures 5.11** through **5.13**. The implementation of phosphorus flux can increase FRP concentration near the bottom to approximately 0.011 mg P/L (120 %) for baseline conditions and approximately 0.02 mg P/L (300 %) for high warming conditions. In contrast to results from the upper basins, in Boulder Basin the increase in FRP concentrations near the bottom for simulations with phosphorus flux implemented, raises surface FRP concentrations at the beginning of the second year after the lake destratifies. This provides additional nutrient for more algal increase in Boulder Basin for the simulations with phosphorus. The more significant effects of sediment

phosphorus release on overall phosphorus concentrations in Boulder Basin compared to the upper basins are believed to be the result of a much larger and deeper basin with long residence time.

Chlorophyll *a* concentrations are compared for simulations with and without flux in **Figures 5.14** and **5.15** at Stations CR394.0 and CR346.4, respectively. The concentrations are averages of chlorophyll *a* across the top five meters of the water column. Since phosphorus flux does not significantly increase surface concentrations of FRP at Station CR394.0 concentrations of chlorophyll *a* are similar for simulations with and without flux. At Station CR346.4, where phosphorus flux does raise surface FRP concentrations, specifically at the beginning of the second year, chlorophyll *a* concentrations increase due to the additional nutrients.

The following sections will describe the effects that sediment release of phosphorus has on the water quality within Lake Mead.

5.2 ANALYSIS OF SEDIMENT PHOSPHRUS FLUX

The following sections discuss the effects of sediment phosphorus flux on temperature, conductivity, DO, FRP, and chlorophyll *a*.

5.2.1 Temperature and Conductivity

The baseline simulation (Run 11) represents typical present day conditions (Section 4.1), and is primarily used for comparison with other simulation scenarios. Runs 12 - 15 explore the effect of warmer future air temperatures by considering a high warming scenario. Additionally, Runs 13 – 15 explore decreased wind, a higher WSEL, and increased phosphorus flux, respectively (**Table 4.1**). Results of these simulations are compared with each other and the baseline simulation (Run 11). Predicted temperatures for each scenario are shown at Station CR390.0 (Gregg Basin) in **Figures 5.16** through **5.18** and at Station CR346.4 (Boulder Basin) in **Figures 5.19** through **5.21**

In general, the figures provide clear visualization of the thermal stratification in Lake Mead in spring and summer and vertical mixing in the fall. Different mechanisms control thermal stratification in the Upper Basins and Boulder Basin. In the Upper Basins temperature profiles are mainly affected by the insertion level of the Colorado River flow. At Station CR390.0 in the Upper Basins (**Figures 5.16** through **5.18**), high warming conditions almost always produces higher temperatures at the surface and throughout the depth of the water column. Increases in temperature can range from a couple of degrees near the bottom of the lake to as much as 5 °C near the surface.

In Boulder Basin the depth of water above the upper Hoover Dam outlets influences temperatures by affecting the depth of the thermocline and drawing warmer water from the epilimnion in later summer and early fall. At Station CR346.4 in Boulder Basin

(**Figures 5.19** through **5.21**) high warming conditions also produce higher temperatures throughout the water column.

In both the Upper Basins and Boulder Basin decreased wind (Run 13) tends to produce warmer surface temperatures compared to just high warming conditions (Run 12) due to less evaporation and cooler temperatures at depth due to less mixing. Also as a result of decreased wind Boulder Basin appears to not fully destratify during the winter (**Figure 5.19**). Increased sediment nutrient flux (Run 15) has a negligible effect on temperatures.

A higher WSEL combined with high warming conditions changes the dynamics in the lake. In the Upper Basins (**Figures 5.16** through **5.18**) an increased WSEL (Run 14) can cause cooler temperatures at depth than shallower WSELs (Runs 12, 13, and 15) throughout the summer. However, during the late fall and winter the higher WSEL, which prolongs stratification of the lake, causes warmer temperatures at depth. For the shallower simulations with high warming (Runs 12, 13, and 15) the Colorado River inflow inserts between depths of 30 and 100 feet. For Run 14 with a high WSEL the Colorado River inflow is spread more vertically.

In Boulder Basin (**Figures 5.17** through **5.19**), the high WSEL condition (Run 14) shows warmer temperatures at depth due to the greater water cover over the upper Hoover outlets, which deepens the thermocline. Specifically, for the simulations at lower WSELS (Runs 12, 13, and 15) the depth to the upper Hoover Dam outlets is typically less than 50 feet and the depth of the epilimnion is restricted by the removal of warm water through the upper Hoover Dam outlets. In contrast, for the simulation at the high WSEL (Run 14) the depth to the upper Hoover Dam outlets can be greater than 100 feet. This "Hoover Dam effect" enables the epilimnion to deepen to a greater depth than when the WSEL is lower. Increases in temperature at depth can be approximately 5 °C, as large as near the surface.

The differences in temperature throughout the water column for the various simulated lake conditions will influence constituent values, such as conductivity, due to differences in stratification and mixing.

Conductivity is largely dependent on the water quality of the inflows. This is apparent when comparing relative concentrations at Station CR390.0 (**Figures 5.22** through **5.24**) and Station CR346.4 (**Figures 5.25** through **5.27**). The high conductivity inflow of the LVW raises the overall levels of conductivity in Boulder Basin (CR346.4) compared to the Upper Basins (CR390.0). In Boulder Basin conductivity levels are generally between 1,000 and 1,300 µS/cm at the surface and between 900 and 1,200 µS/cm near the bottom. In Gregg Basin, which receives the lower conductivity inflow of the Colorado River, conductivity levels are 900 and 1,050 µS/cm at the surface and between 850 and 1,000 µS/cm near the bottom.

Conductivity throughout the water column at a particularly location is influenced by temperatures, which determines at what depth an inflow will insert into the receiving water. Density will vary with temperature and inflows will insert into the water column when a level of neutral buoyancy has been reached. The conductivity of the inflow will influence conductivity in the lake at the insertion level.

In Gregg Basin (**Figures 5.20** through **5.22**), with its small volume, low residence time and closeness to the Colorado River inflow, conductivity is greatly affected by the Colorado River and differences are directly related to the insertion of the Colorado River inflow. From **Figure 5.20**, it is clear that the low conductivity Colorado River inflow enters the lake close to the bottom in the winter. In summer, Colorado River inflow enters the lake as an inter-flow and vertical mixing by wind and thermal convection mixes the Colorado River flow to the surface and lowers the surface conductivity (**Figure 5.21**). In Boulder Basin (**Figures 5.23** through **5.25**) LVW inflow resides in the epilimnion in the summer and raises conductivity in the epilimnion. The flow through the Narrows enters below the thermocline and lowers conductivity in the hypolimnion.

Compared to the baseline conditions, high warming conditions have little effect on conductivity concentrations in the Upper Basins. However, in Boulder Basin high warming can increase the concentration of conductivity in the epilimnion of by trapping more of the warm LVW inflow and by increasing evaporation.

In the shallower Upper Basins less wind (Run 13) does not change conductivity, however, in the deeper Boulder Basin it can increase epilimnion concentrations, while lower concentrations in the hypolimnion due to less vertical mixing of the lake. Higher concentrations in the epilimnion of Boulder Basin during the year then produce a spike in concentrations near the bottom when the lake destratifies and mixes. This spike can be seen in **Figure 5.26** for every simulation except Run 13, which does not fully destratify (see **Figure 5.27)**.

An increased WSEL (Run14) will increase conductivity in the Upper Basins by changing the thermal structure and altering the insertion level of the CR. The Colorado River inflow inserts slightly deeper in the summer and has smaller influence on the surface and bottom conductivity.

In Boulder Basin a higher WSEL (Run 14) enables the epilimnion to deepen to a greater depth. The Hoover Dam outflow draws less water from the epilimnion (and high conductivity water from the LVW) due to the depth of Hoover Dam outlet, which leaves more conductivity in the lake increasing concentrations in both the epilimnion and hypolimnion.

5.2.2 Dissolved Oxygen

The simulated DO concentrations in Gregg Basin (Station CR390.0) are shown in **Figures 5.28** through **5.30**. Warmer temperatures (Runs 12 – 15) cause decreased DO

concentrations throughout the water column compared to the baseline simulation (Run 11). The decreased DO concentrations are due to lower oxygen solubility of water in the lake, the warmer Colorado River inflows and stronger thermal stratification. The amount of decrease in DO concentrations is summarized in **Table 5.1**.

Table 5.1: Simulated Annual Average[1] and Change[2] in Annual Average DO Concentrations (mg/L)

Station	Location	Run 11	Run 12	Run 13	Run 14	Run 15
		Baseline	High Warming	High Warming, Low Wind	High Warming, High WSEL	High Warming, High Flux
CR390.0	Surface	8.9 (0)	8.5 (-0.4)	8.2 (-0.7)	8.3 (-0.6)	8.5 (-0.4)
	Near Bottom	6.3 (0)	5.7 (-0.6)	5.4 (-0.9)	5.1 (-1.2)	5.7 (-0.6)
CR346.4	Surface	8.9 (0)	8.5 (-0.4)	8.2 (-0.7)	8.4 (-0.5)	8.5 (-0.4)
	Near Bottom	6.4 (0)	5.4 (-1.0)	4.2 (-2.2)	5.5 (-0.9)	5.4 (-1.0)

1. Annual averages are for the second simulation year
2. Change is averages are in parenthesis and are relative to Run 11 (Baseline)

In the hypolimnion the DO concentrations begin to decrease during the winter and continue to decrease until the reservoir destratifies and mixes. The decreases in DO concentrations in the hypolimnion are likely caused by a combination of sediment oxygen demand (SOD) and the decreased advective supply of oxygen from the Colorado River inflow. The decrease in hypolimnetic DO concentrations is predicted to increase with warmer temperatures due to higher rates of metabolic processes, stronger thermal stratification, and longer stratified periods. In the epilimnion, warmer temperatures lower DO concentrations mainly due to lower oxygen solubility in warmer water.

Other simulated conditions mostly exacerbate the low DO conditions near the bottom in Gregg Basin. Low wind (Run 13) decreases the mixing to the bottom, which further lowers DO concentrations. A higher WSEL (Run 14) delays destratification and re-oxygenation at the bottom of the lake. Higher flux (Run 15) has little to no effect on DO concentrations.

The simulated DO concentrations in Boulder Basin (Station CR346.4) are shown in **Figures 5.31** through **5.33**. Trends for DO concentrations in Boulder Basin are similar to those in the Upper Basins. However, a major difference is that due to increased depth in Boulder Basin a decrease in wind (Run 13) causes the largest decrease in DO (**Table**

5.1). With lower wind the lake does not destratify during the winter of Run 13 and re-oxygenation in Boulder Basin is delayed until approximately February.

Contours showing the percent of time DO concentrations below 3 mg/L are plotted in **Figure 5.34**. Times of low DO increase particularly in deeper area along the river thalweg when water temperatures increase. A decrease in wind creates the worst conditions for the deeper areas such as Boulder and Virgin Basin. A higher WSEL increases the area affected by low DO concentrations.

5.2.3 Phosphorus

The discussion of sediment flux will focus on phosphorus since it is the limiting nutrient in Lake Mead. Phosphorus fluxes from the sediments typically depend upon the DO concentrations at the sediment-water interface. Low concentrations of DO will trigger phosphorus release.

Predicted concentrations of FRP in Gregg Basin (CR390.0) are shown in **Figures 5.35** and **5.36**. Phosphorus levels increase near the bottom when DO levels decrease to sufficient levels (5 mg/L and below) to trigger sufficient sediment release. This occurs during the summer and into the fall. Phosphorus levels near the surface show an increase in concentration during the winter after destratification, which mixes the phosphorus-rich hypolimnion to the surface. As discussed previously high warming (Runs 12 -15), low wind (Run 13), and high WSEL (Run 14) all contribute to decreasing DO concentration in the lake, particularly along the bottom, due to a longer and stronger stratification period. The low DO concentrations serve to increase the amount of phosphorus flux and raise the concentration of phosphorus. In addition, increasing the rate of sediment phosphorus flux (Run 15) increases the phosphorus concentration in the water column as well.

In Boulder Basin, which is deeper than Gregg Basin, phosphorus flux is predicted to increase due to longer periods of low DO concentration and a higher phosphorus release rate. This leads to increased concentrations of phosphorus at both the surface and near the bottom (**Figures 5.37** and **5.38**). The second peak in the mid-summer is caused by the decay of algae in the surface in the mid-summer due to high temperature. Phosphorus in the algae will convert to dissolved and particulate organic phosphorus, which will be converted to FRP through mineralization. Concentration increases due to low wind, high WSEL, and high flux are higher in Boulder Basin than in the Upper Basins.

The predicted total daily sediment phosphorus release to Lake Mead and Boulder Basin for the five flux simulations are shown in **Figures 5.39** and **5.40**, respectively. Warmer water temperatures by themselves will increase sediment phosphorus loads into the lake. Less mixing due to lower winds, higher WSELs, and increased flux rates exacerbate the sediment phosphorus release and increase the loading.

Boulder Basin accounts for the majority of the sediment phosphorus loading to Lake Mead. Average and maximum sediment phosphorus daily loads are shown in **Figures 5.41** and **5.42**, respectively. Averages and maxima were calculated from July 1, Year 1 to June 30, Year 2 to eliminate initial conditions from the calculations. Loading is divided between Gregg Basin, the combined Virgin and Temple Basins, and Boulder Basin. The loading contributions of each basin (or combination) along with the respective percentages are summarized in **Table 5.2**. On average a higher WSEL combined with warmer temperatures causes the greatest sediment phosphorus loading (of the scenarios simulated).

Table 5.2: Simulated Average[1] Sediment Phosphorus Loading (lbs/day) to Lake Mead with Percentages[2]

Location	Run 11	Run 12	Run 13	Run 14	Run 15
	Baseline	**High Warming**	**High Warming, Low Wind**	**High Warming, High WSEL**	**High Warming, High Flux**
Boulder Basin	33 (69%)	72 (70%)	129 (73%)	139 (63%)	124 (70%)
Virgin + Temple Basins	11 (24%)	26 (25%)	42 (24%)	71 (32%)	46 (26%)
Gregg Basin	3 (7%)	5 (5%)	6 (3%)	12 (5%)	7 (4%)
Total	48	103	177	221	177

1. Average is calculated from July 1, Year 1 to June 30, Year 2 to eliminate initial conditions from calculations.
2. Percentages contributed by each basin are in parenthesis.

Boulder Basin contributes the majority of sediment phosphorus loading for each of the five flux simulations. Sediment phosphorus loading in Boulder Basin is typically 2 to 3 times higher than in the Upper Basins due to higher sediment flux rates and larger areas that experience low DO. Average phosphorus loads to Boulder Basin by source are shown in **Figure 5.43** and listed in **Table 5.3**. The three sources are the LVW inflow, phosphorus carried from the Upper Basins through the Narrows, and from sediment release. For present conditions (Run11, Baseline) the LVW is the main source of phosphorus and sediment loading is similar to loading through the Narrows. Warmer temperatures, which lower DO concentrations leading to increased phosphorus flux, cause the sediment loading to approximately double. Combining warmer temperatures with either lower wind, higher WESL, or increased sediment flux causes the sediment loading to quadruple and be approximately equal to the current loading of the LVW. For

the scenario that causes the most loading (high warming, high WSEL) total phosphorus loading could increase by 50 %.

Table 5.3: Simulated Average[1] Phosphorus Loading (lbs/day) to Boulder Basin with Percentages[2]

Location	Run 11	Run 12	Run 13	Run 14	Run 15
	Baseline	**High Warming**	**High Warming, Low Wind**	**High Warming, High WSEL**	**High Warming, High Flux**
LVW[3]	132 (66%)	132 (55%)	132 (44%)	132 (43%)	132 (45%)
Narrows[3]	36 (18%)	36 (15%)	36 (12%)	36 (12%)	36 (12%)
Sediments	33 (17%)	72 (30%)	129 (43%)	139 (45%)	124 (43%)
Total	201	240	297	307	292

1. Average is calculated from July 1, Year 1 to June 30, Year 2 to eliminate initial conditions from calculations.
2. Percentages contributed by each basin are in parenthesis.
3. Loads are average of 2007 and 2008 phosphorus budget (Ding *et al*., 2014).

5.2.4 Chlorophyll a

Chlorophyll *a* is a surrogate for algae and is modeled as such. The average concentration of chlorophyll *a* in the top five meters of the water column is plotted in **Figures 5.44** and **5.45** for Stations CR390.0 and CR346.4, respectively. Increases in concentrations at CR390.0 are negligible. Most high warming simulations show equal or lower concentrations of chlorophyll *a* compared to the Baseline simulation. Modeled algae growth is limited at higher temperatures, so despite higher phosphorus concentrations, chlorophyll *a* concentrations do not increase. At Station CR346.4, concentrations of chlorophyll *a* increase and decrease depending on the time of year when compared to the Baseline simulation. Annual average chlorophyll *a* concentrations at CR346.4 for the first and second years of simulation are summarized in **Figure 5.46** and **Table 5.4**. Top five meter averages of chlorophyll *a* of the entire lake for the first and second simulations years are shown in **Figures 5.47** and **5.48**, respectively.

Table 5.4: Average Annual Chlorophyll *a* Concentrations at Station CR346.4

Run #	Purpose	Sediment Phosphorus Flux	Year 1	Year 2
1	Baseline	No	1.38	1.46
3	High Warming	No	1.37	1.48
11	Baseline	Yes	1.38	1.60
12	High Warming	Yes	1.41	1.77
13	High Warming, Low Wind	Yes	1.41	1.65
14	High Warming, High WSEL	Yes	1.14	1.78
15	High Warming, High Flux	Yes	1.51	1.95

While algae concentrations will remain low (**Table 5.4**), increased phosphorus loading to Lake Mead, specifically Boulder Basin, will likely cause increased algae growth compared to present growth at current phosphors loading. For Baseline conditions (Runs 1 and 11), productivity in chlorophyll *a* due to sediment phosphorus flux increases by approximately 10% during Year 2. For high warming conditions the productivity is increased by approximately 20% during Year 2. The "worst case" in regards to algae production is high warming with high flux (Run 15). Compared to the baseline simulation with flux (Run 11), high warming with high flux increases productivity by 22% during Year 2.

The relatively small increase in chlorophyll *a*, compared to the increase in phosphorus loading, is due to several factors. The sediment phosphorus loading is mostly in the hypolimnion, at these elevations this water is released through Hoover Dam, which will reduce the percentage of sediment loading that is used for algae production. In addition, sediment phosphorus loading can only be used for algae production after it has been mixed vertically to the surface. Therefore, sediment phosphorus loading has to increase phosphorus concentrations throughout the entire water column to effect algae production. The other major source of loadings, the LVW, is a surface inflow, which

increases phosphorus concentrations at the surface, thus making it more efficient at increasing algae production in Lake Mead.

5.3 "2014" SIMULATION

During the spring and summer of 2014 Gregg Basin in Lake Mead developed hypoxic and anoxic conditions that were atypical. A likely contributing factor was the increase in temperature of water entering lake through the Colorado River due to increases in temperature in water released from Lake Powell. Colorado River temperatures measured upstream of Lake Mead were 1.37 °C warmer per month on average during 2014 than the previous five years (2009 – 2013). Monthly average temperatures and the average difference to Year 2014 temperature are plotted in **Figure 5.49**. Lake Powell has been affected by the drought in the Colorado River Basin, resulting in lower lake levels and warmer releases to the Colorado River.

Effects of increasing Colorado River temperatures has been studied (Flow Science, 2013, 2015a, 2015b) and shown to influence the insertion level into Lake Mead of the Colorado River inflow, and the water temperatures and DO concentrations, particularly in Gregg Basin. The combined effect is to decrease DO concentrations in Gregg Basin. Areas of low DO are at the bottom near the confluence of the Colorado River and Lake Mead, but shift to higher in the water column as distance from the confluence increases due to higher insertion of Colorado River inflow.

Patterns observed during 2014 could be indicative of potential changes in water quality due to climate change, specifically warming of water temperatures in the Colorado River and Lake Mead. Therefore, a simulation of Year 2014 was performed using the WLM with sediment phosphorus flux. A calibration of the model for 2014 was not performed, merely a simulation using data from 2014 as described in the following section. A comparison of the model results to measured data is then presented.

5.3.1 Description of "2014"Simulation and Data Collection

To simulate Year 2014 all relevant meteorology, inflow and outflow, and water quality data were collected and applied to the model. Other model parameters, such as sediment phosphorus flux rates, remained the same as described for the Baseline simulation Run 11. ELCOM parameters (temperature and conductivity) were simulated using a 300 meter horizontal grid, while CAEDYM parameters (DO, nitrogen, phosphorus, and chlorophyll *a*) were simulated on a 600 meter horizontal grid to balance accuracy and computation time. A vertical grid of 2 meters was used for ELCOM and CAEDYM.

Previous modeling had used weather data from multiple meteorological stations from the various basins in Lake Mead; however, most of those stations have been discontinued as of 2014. Therefore, an active station in Boulder Basin was used to supply weather data for the entire lake including solar radiation, air temperature, relative humidity, wind

speed, and wind direction. A 15 % increase was applied to wind speeds based on previous calibrations of the WLM (Flow Science, 2007, 2010a, 201b). Precipitation data were obtained from McCarron International Airport in Las Vegas, NV.

Inflow data were obtained for the Colorado Virgin, and Muddy Rivers as well as the LVW. All fours sources use 15 minute frequency flow rate data. Water quality data including temperature, conductivity, DO, nitrogen, phosphorus, carbon, and pH were collected from the closest available upstream monitoring station for each inflow.

Outflows are through Hoover Dam and the SNWA intakes. Hourly outflow rates were obtained for both outflows. Outflows through the Hoover Dam were split evenly between the upper (elev. 1,045 feet) and lower outlets (895 feet). SNWA withdrawals were through SNWA Intakes #1 and #2 at an elevation of 992 feet. Outflows do not require defined water quality parameters as these are determined by the model.

In-reservoir data were collected for stations throughout the Lake Mead. Data included temperature, conductivity, DO, nitrate, ammonium, FRP, and total phosphorus. Initial conditions were defined using in-reservoir data from the beginning of 2014.

5.3.2 Results

Selected results of the "2014" Simulation are presented here. A full suite of results are available in Appendix B

A comparison of measured and simulated WSELs is shown in **Figure 5.50**. Both the 300 and 600 meter grid captured the changing WSEL during 2014. The average difference between the measured and simulated WSEL for the 300 meter grid is approximately 1.5 feet for the 300 meter grid and 2 feet for the 600 meter grid, less than 1% of average water depth in the lake.

The WLM was able to accurately capture temperature for the year 2014. Temperatures at Station CR390.0 in Gregg Basin are presented in **Figure 5.51**. The model captures the development of the thermocline including the timing and depth as well as destratification. **Figure 5.52** shows temperatures at Station CR346.4 in Boulder Basin. Temperatures are accurately captured at this deeper location as well. Contour profiles along the thalweg of the Colorado River are plotted in **Figures 5.53** and **5.54** for August and October, respectively. Temperatures and thermal stratification are accurately captured along the entire lake.

Conductivity for Station CR390.0 and CR346.4 are presented in **Figures 5.55** and **5.56**, respectively. Variations in concentrations throughout the year and across the depth of water column are accurately captured at both stations. At Station CR390.0, conductivity increases between March and July corresponding to a period low Colorado River inflow, which also causes a decrease in WSEL. After July, Colorado River inflows increase lowering conductivity (and stabilizing the WSEL). At Station CR346.4,

conductivity at the surface increased throughout the year due to inflows from LVW. Conductivity profiles, **Figures 5.57** and **5.58**, show good agreement between the measured and simulated data throughout the lake.

At Station CR394.0 (**Figure 5.59**) DO concentrations start to decrease near the bottom beginning in April and reach anoxic conditions by July. However, due to being relatively shallow, or possibly being close to the confluence of the Colorado River and Lake Mead, the location appears to mix and re-oxygenate by October. The timing of the changes in DO near the bottom in the WLM are off as DO depletion begins too early and lingers after the measured data show that re-oxygenation has occurred. In addition, the WLM does not capture the vertical extent of the hypoxic zone. Farther downstream in Gregg Basin at Station CR394.0 (**Figure 5.60**) the anoxic area increases according to measured data. Low levels of DO concentrations are observed at higher elevations and persist later in the year, until re-oxygenation occurs in November. Again the WLM prematurely predicts DO depletion and fails to capture the magnitude of depletion higher in the hypolimnion.

Station CR380.0 (**Figure 5.61**), located in Temple Basin, does not show the extreme anoxic conditions observed in Gregg Basin. Low DO concentrations do not appear until later in the year, approximately June, and are observed higher in the water column, between 900 and 950 feet, not near the bottom. However, hypoxic conditions persist through the end of 2014. The hypoxic zone observed here likely originates farther upstream and is simple traveling downstream. The WLM was unable to fully capture this migration as the lowest DO concentrations predicted at Station CR380.0 are near the bottom due to sediment oxygen demand.

Measured DO concentrations at Station CR346.4 (**Figure 5.62**) do not fall to the levels observed in either Gregg Basin or Temple Basin, however, a decline is still observed near the end of the year. Beginning in July concentrations decline and remain low through the end of the year, which could affect DO concentrations the following year. The WLM prediction for DO concentrations appear better at CR346.4, possibly since measured levels are not as low as observed in Temple and Gregg Basins. However, the model gives a slight under estimation of DO concentrations in the hypolimnion.

Measured DO concentration profiles along the Colorado River thalweg during August and October are plotted in **Figures 5.63** and **5.64**, respectively. By August the anoxic zone has migrated away for the confluence of the Colorado River and Lake Mead and stretches from Gregg Basin into Temple Basin. Also note that by the time it reaches Temple Basin it has lifted off the bottom of the lake and appears between 900 and 975 feet. Virgin Basin and Boulder Basin remain well oxygenated throughout the water column. By October the anoxic area has been reduced and however it still remains in Gregg and Temple Basin. DO levels below the thermocline in Virgin and Boulder Basins have declined.

Agreement between the measured DO data and WLM predictions for DO are fair, however, it is apparent that more refinement of the WLM sediment oxygen demand function is needed. Improved predictions of the timing and magnitude of DO depletion in areas that show anoxic conditions, such as in Gregg Basin, are needed since this then effects water quality in areas downstream. More data on sediment oxygen demand would allow for improved calibration of this behavior in Lake Mead.

The extremely low DO concentrations observed in Gregg and Temple Basins would likely have triggered sediment nutrient release. However, measured FRP concentrations do not support increased phosphorus concentrations due to flux. Measured and predicted concentrations of FRP at Stations CR394.0 and CR390.0 are compared in **Figures 5.65** and **5.66**. Surface concentrations are low (< 0.005 mg P/L) for both the measured and simulation data. Measured data at the bottom show minimal increase while the simulation data increase to approximately 0.08 mg P/L at Station CR394.0 and approximately 0.12 mg P/L at Station CR390.0. The increase in predicted FRP concentrations correlates with the decrease in DO concentrations near the bottom. The lack of increase in FRP concentrations in the measure data given the extremely low levels of DO suggests that these is a need for additional study since sediment phosphorus flux would be expected.

At Station CR380.0 (**Figure 5.67**) in Temple Basin there is also an increase in predicted FRP concentrations correlating with lower DO concentrations. However, because the low DO concentrations are less extreme at CR380.0, and observed above the bottom, increases in predicted FRP concentrations are smaller with peak concentrations being approximately 0.035 mg P/L. Note again that measured data only show a minimal increase during the same period as the simulation data show an increase. Neither the measured nor simulated data show appreciable increase in FRP concentrations at Station CR346.4 (**Figure 5.68**). DO depletion in Boulder Basin was limited during 2014, thus likely limiting phosphorus flux.

The WLM was able to accurately capture the thermal stratification and in Lake Mead during Year 2014. Some parameters dependent on the thermal stratification (e.g., conductivity) were accurately simulated. The WLM struggled to capture the hypoxic and anoxic conditions observed in the measured data, particularly in Gregg Basin, in both magnitude and timing. More data measuring sediment oxygen demand would be beneficial for the modeling.

Measured FRP data did not indicate increased phosphorus concentrations. However, incorporating sediment phosphorus flux in the model caused an increase in predicted FRP concentrations. Since a complete calibration of the WLM for 2014 was not performed, including calibration of phosphorus flux rates, it is possible that the model is over-predicting the increase in phosphorus concentrations. However, the lack of increase in phosphorus concentrations shown by the measured data, given the low measured DO concentrations, suggests a need for further study as a certain amount of sediment phosphorus release is to be expected with the low DO concentrations measured.

Regardless, the WLM could benefit from a complete Year 2014 calibration, which would allow for a more accurate prediction of phosphorus flux and resulting concentrations. More sediment nutrient release data would aid in a full calibration. In addition, improved quality control of the measured data would perhaps allow for better calibration and validation of the WLM.

5.4 ANIMATIONS

Appendix C includes animations for 5 simulations (Runs 11 – 15) for temperature, conductivity, salinity, effluent tracer[4], bromide concentration, Virgin River/Muddy River tracer[5], and concentrations of total phosphorus (TP), FRP, nitrate (NO3), TOC, chlorophyll *a*, DO, and suspended-solids (SS1 and SS2). Each animation includes a plan view of the lake, as well as profiles through the lake enabling the variation with depth (*i.e.*, stratification) and the effects of the inflows (*i.e.*, LVW, Colorado River and Virgin River/Muddy River) to be visualized. The animations provide daily output over the entire two-year simulation period.

The single run animations provide clear visualization of the thermal stratification in Lake Mead in spring and summer and vertical mixing in the fall, and the effect of this stratification and mixing as well as the different inflows on the constituent values (*e.g.*, conductivity, salinity, and effluent tracer) throughout the lake. The animations illustrate the 3-D variation of constituents throughout the lake, including the different insertion elevations of the LVW and other inflows, the spatial and temporal variation in chlorophyll *a* concentrations, including the sometimes rapid advection of algae (*i.e.*, chlorophyll *a*) on the lake surface, and the development of lower DO concentrations in the hypolimnion and subsequent re-oxygenation. These various limnological phenomena have been well described elsewhere (*e.g.*, Fischer and Smith, 1983, LaBounty and Burns, 2005, 2007, Holdren and Turner, 2010, and Preston *et al*., 2013) and are not further discussed here.

.

[4] Effluent tracer is a hypothetical tracer used to track the effluent portion of the LVW inflow throughout Lake Mead. For example, an effluent tracer concentration of 10 % at a specific location and time in the lake indicates that 10 % (i.e., one part in ten) of the water originated from effluent.

[5] Virgin River/Muddy River tracer is a hypothetical tracer used to track the Virgin and Muddy River inflows throughout Lake Mead. For example, a Virgin River/Muddy River tracer concentration of 10 % at a specific location and time in the lake indicates that 10 % (i.e., one part in ten) of the water originated from the Virgin or Muddy Rivers.

6 CONCLUSIONS

The WLM was used to extend previous modeling efforts by including and examining the effects of internal nutrient recycling (*i.e.*, sediment nutrient fluxes) through the incorporation of these mechanisms into the 3-D hydrodynamic and water quality model previously developed for Lake Mead. The study provided an understanding of how water quality characteristics and internal nutrient recycling in Lake Mead may change under future warmer conditions resulting from a changing climate. Other parameters were varied in conjunction with the warmer temperatures, including less wind, higher WSELs, and higher flux rates. In addition, a simulation of the Year 2014 was performed, since observed levels of DO would have likely caused nutrient release from the sediments, as an experiment to gauge the accuracy of the WLM and the estimated phosphorus flux rates. Algal growth in Lake Mead is phosphorus limited (Lieberman, 1995) therefore the analysis of internal nutrient recycling focused on phosphorus.

The simulations predicted that climate change (and other modeled parameters) mostly exacerbates conditions that can stimulate sediment phosphorus flux. Warmer temperatures increase water surface temperatures, strengthen thermal stratification, and increase stratified periods. Hypolimnetic DO concentrations are predicted to decrease with warmer temperatures due to higher rates of metabolic processes, stronger thermal stratification, and longer stratified periods. In the epilimnion, warmer temperatures lower DO concentrations mainly due to lower oxygen solubility in warmer water. Warmer water temperatures by themselves will increase sediment phosphorus loads into the lake due to the decrease in hypolimnetic DO. Less mixing due to lower winds, higher WSELs, and increased flux rates further decrease in hypolimnetic DO and increase the loading from the sediment phosphorus release.

Results of the Year 2014 simulation were mixed. The WLM was able to accurately capture the thermal stratification in Lake Mead during Year 2014. Some parameters dependent on the thermal stratification (*e.g.*, conductivity) were accurately simulated as well. The WLM struggled to capture the hypoxic and anoxic conditions observed in the measured data, particularly in Gregg Basin, in both magnitude and timing. While the measured FRP data did not indicate increased sediment nutrient release, FRP concentrations predicted by the WLM did. More data measuring sediment oxygen demand and sediment nutrient release would aid in a full calibration and benefit the model. In addition, improved quality control of the measured to data would allow for better calibration and validation of the WLM. A complete Year 2014 calibration would allow for a more accurate prediction of phosphorus flux and resulting concentrations.

The predicted general changes in water temperature, DO, phosphorus concentrations and loading, and chlorophyll *a* are summarized below.

6.1 WATER TEMPERATURE

Warmer future air temperatures will cause warmer water temperatures (high warming conditions). Different mechanisms control thermal stratification in the Upper Basins and Boulder Basin.

- In the Upper Basins temperature profiles are mainly affected by the insertion level of the CR, which can be altered by higher warming conditions.
    - This causes higher temperatures at the surface and throughout the depth of the water column. Increases in temperature can range from a couple of degrees near the bottom of the lake to as much as 5 °C near the surface.
- In Boulder Basin the water depth above the upper Hoover Dam outlets influences temperatures by affecting the depth of the thermocline and drawing warmer water from the epilimnion in later summer and early fall.
    - However, high warming conditions also produce higher temperatures throughout the water column in Boulder Basin despite the influence of the Hoover Dam.
- In both the Upper Basins and Boulder Basin decreased wind tends to produce warmer surface temperatures as compared to just high warming conditions due to less evaporation and cooler temperatures at depth from less mixing.
- A higher WSEL combined with high warming conditions changes the dynamics in the lake.
    - In the Upper Basins an increased WSEL can cause cooler temperatures at depth throughout the summer, however, stratification is prolonged causing warmer temperatures at depth during the late fall and winter.
    - In Boulder Basin an increased WSEL causes warmer temperatures at depth due to the greater depth of the upper Hoover Dam outlets, which deepens the thermocline.

6.2 DISSOLVED OXYGEN

In general warmer water temperatures cause decreased DO concentrations throughout the lake.

- In the Upper Basins the decreased DO concentrations are due to lower oxygen solubility of water in the lake, the warmer Colorado River inflows, and stronger thermal stratification.

- Low wind decreases the mixing to the bottom, which further lowers DO concentrations.

- A higher WSEL delays destraification and re-oxygenation at the bottom of the lake.

- Trends for DO concentrations in Boulder Basin are similar to those in the Upper Basins.

  - However, due to the increased depth in Boulder Basin a decrease in wind prevents the lake from destratifying during the winter and re-oxygenation in Boulder Basin is delayed until approximately February. This causes DO depletion near the bottom to be greater than for the higher WSEL conditions.

6.3 PHOSPHORUS CONCENTRATIONS AND LOADING

High warming, low wind, and high WSEL all contribute to decreasing DO concentration in the lake, particularly along the bottom, due to stronger stratification and longer stratification period. The low DO concentrations serve to increase the amount of phosphorus flux and raise the concentrations of phosphorus. In addition, increasing the rate of sediment phosphorus flux increases the phosphorus concentrations in the water column.

- Warmer water temperatures by themselves will increase sediment phosphorus loads into the lake.

  - The high warming conditions modeled are predicted to increase sediment phosphorus loading to Lake Mead by 114 % as compared to baseline temperatures.

- Less mixing due to lower winds, higher WSELs, and increased flux rates exacerbate the sediment phosphorus release and increase the loading.

  - Combining less wind with the high warming condition could increase sediment phosphorus loading by 72% compared to just warmer temperatures.

  - An increased WSEL produced the most phosphorus loading from sediment phosphorus flux of the conditions modeled. A high WSEL combined with the high warming conditions could increase sediment phosphorus loading by 118% compared to just warmer temperatures.

- An increased flux rate combined with the high warming conditions could increase sediment phosphorus loading by 72% compared to just warmer temperatures.

- The three sources of phosphorus loading to Boulder Basin are the LVW inflow, phosphorus carried from the Upper Basins through the Narrows, and from sediment release.
    - Sediment phosphorus loading in Boulder Basin is typically 2 to 3 times higher than in the Upper Basins due to higher sediment flux rates and larger areas that experience low DO.
    - Warmer temperatures cause the sediment loading to approximately double and overall loading to increase by 19%.
    - Combining warmer temperatures with either lower wind, higher WESL, or increased sediment flux causes sediment loading to quadruple and be approximately equal to the loading of the LVW.
        - For the scenario that causes the most loading (high warming, high WSEL) total phosphorus loading could increase by 50%.

6.4 CHLOROPHYLL *A*

While algae concentrations are predicted to remain low, increased phosphorus loading to Lake Mead, specifically Boulder Basin, will likely cause increased algae growth.

- For baseline conditions productivity in chlorophyll *a* due to sediment phosphorus flux increases by approximately 10 % during Year 2.

- For high warming conditions the productivity is increased by approximately 20 % during Year 2.

- The "worst case" in regards to algae production is high warming with high flux which, compared to the baseline simulation with flux, increases productivity by 22% during Year 2.

- The relatively small increase in chlorophyll *a*, compared to the increase in phosphorus loading, is due to several factors.
    - The sediment phosphorus loading is mostly in the hypolimnion below the thermocline where most of the Hoover Dam withdrawal is taken from,

which will reduce the percentage of sediment loading that is used for algae production.

- In addition, sediment phosphorus loading can only be used for algae production after it has been mixed vertically to the surface. Therefore, sediment phosphorus loading has to increase phosphorus concentrations throughout the entire water column to effect algae production.

7 REFERENCES

Anderson, M. A., Paez, C., and Men, S., (2007) Sediment Nutrient Flux and Oxygen Demand Study for Canyon Lake with Assessment of In-Lake Alternatives. Report to San Jacinto River Watershed Council.

Barnett, T. P., and Pierce, D. W. (2008) When will Lake Mead go dry? *Water Resour. Res., 44*.

Barnett, T. P., and Pierce, D. W. (2009) Sustainable water deliveries from the Colorado River in a changing climate. *PNAS, 106(18).*

Berner, R. A. (1980), Early Diagenesis: A Theoretical Approach. Princeton. 241 pp.

Beutel, M. W., (2006), Lake Perris Sediment-Water Interface Study. Report to Montgomery Watson Harza Americas, Inc. and the Metropolitan Water District of Southern California.

Beutel, M., Hannoun, I., Pasek, J., and Kavanagh, K. B., (2007) Evaluation of Hypolimnetic Oxygen Demand in a Large Eutrophic Raw Water Reservoir, San Vicente Reservoir, *Calif. Journal of Environmental Engineering-Asce, 133(2), 130-138.*

Beutel, M. W., Horne, A. J., Taylor, W.D., Losee, R.F. and Whitney, R.D., (2008) Effects of Oxygen and Nitrate on Nutrient Release from Profundal Sediments of a Large, Oligo-Mesotrophic Reservoir, Lake Mathews, California. *Lake Reserv. Manage. 24:18–29.*

Debroux, J. F., Beutel, M. W., Thompson, C. M., and Mulligan, S., (2012) Design and Testing of a Novel Hypolimnetic Oxygenation System to Improve Water Quality in Lake Bard, California. *Lake Reserv. Manage. 28:245–254.*

Ding, L., Hannoun, I. A., List, E. J., and Tietjen, T. (2014) Development of Phosphorus Budget for Lake Mead. *Lake Reserv. Manage. 30:2, 143 - 156.*

DiToro, D.M. (2001) "Sediment Flux Modeling", John Wiley & Sons, New York, NY.

Fischer, H. B. and Smith, R. D., (1983) Observations of Transport to Surface Waters from a Plunging Inflow to Lake Mead. *Limnol. Oceanogr. 28(2):258-272.*

Flow Science (2006) Lake Mead ELCOM/CAEDYM Joint Modeling Study: Alternative SNWA Intake Locations, February 7, 2006.

Flow Science (2007) Lake Mead ELCOM-CAEDYM Model, Extension to Entire Lake, November 30, 2007.

Flow Science (2010a) Whole Lake Mead ELCOM-CAEDYM Model: Addition of Years 2006 and 2007, December 9, 2010.

Flow Science (2010b) Whole Lake Mead ELCOM-CAEDYM Model: Addition of Year 2008, December 10, 2010.

Flow Science (2011a) ELCOM-CAEDYM Modeling and Statistical Analysis of Water Quality in Lake Mead, March 3, 2011.

Flow Science (2011b) ELCOM-CAEDYM Modeling of Lake Mead at Low Lake Levels and with Suspended-Solids, Draft Report, November 14, 2011.

Flow Science (2013) ELCOM-CAEDYM Modeling with Climate Change Part 1: Lake Mead¸ September 28, 2013.

Flow Science (2015a) Long Term Experimental and Management Plan (LTEMP) Screening Simulations of Lake Mead, Draft Report, January 9, 2015

Flow Science (2015b) Long Term Experimental and Management Plan (LTEMP) Modeling of Lake Mead, March 11, 2015

Holdren, G. C., and Turner, K., (2010) Characteristics of Lake Mead, Arizona-Nevada. *Lake Reserv. Manage. 26(4):230-239*.

LaBounty, J. F. and Burns, N. M., (2005) Characterization of Boulder Basin, Lake Mead, Nevada-Arizona, USA – Based on analysis of 34 limnological parameters. *Lake Reserv. Manage. 21(3):277-307*.

LaBounty, J. F. and Horn, M. J., (1997) The Influence of Drainage from the Las Vegas Valley on the Limnology of Boulder Basin, Lake Mead, Arizona-Nevada. *Lake Reserv. Manage. 13(2):95-108*.

Lieberman, D. M., (1995) Nutrient Limitation in a Southwestern Desert Reservoir: Eutrophication of Las Vegas Bay, Lake Mead, Nevada, Publications (WR). Paper 29.

Martin, B., Ding, L., Hannoun, I. A., and List, E. J., (2013) Predicting Effects of Reservoir Expansion with Three-Dimensional Modeling: Case study of Los Vaqueros Reservoir. *Lake Reserv. Manage. 29:4, 217–232.*

Moore, P. A., Reddy, K. R., and Fisher, M. M., (1998) Phosphorus Flux between Sediment and Overlying Water in Lake Okeechobee, Florida: Spatial and Temporal Variations. J. Environ. Qual. 27:1428-1439.

Murray, J. W., Jones, C. J., Kuivila, K., and Sawlan, J., (1981) Diagenesis of Organic Matter in Las Vegas Bay and Bonelli Bay, Lake Mead. Department of Oceanography Special Report No. 96, University of Washington, Seattle, WA.

Nürnberg, G. K., (1988) Prediction of Phosphorus Release Rates from Total and Reductant-Soluble Phosphorus in Anoxic Lake Sediments. Can. J. Fish. Aquat. Sci. 45:453-462.

Preston, A., Hannoun, I. A., List, E. J., Rackley, I., Tietjen, T. (2013), Three-dimensional Management Model for Lake Mead, Nevada, Part 1: Model calibration and validation. *Submitted to Lake Reserv Manage*.

Rajagopalan, B., Nowak, K., Prairie, J., Hoerling, M., Harding, B., Barsugli, J., Ray, A., and Udall, B. (2009) Water supply risk on the Colorado River: Can management mitigate? *Water Resour. Res., 45*.

Reclamation (2011a) West-Wide Climate Risk Assessments: Bias-Corrected and Spatially Downscaled Surface Water Projections, Technical Memorandum No. 86-68210-2011-01, prepared by the U.S. Department of the Interior, Bureau of Reclamation, Technical Services Center, Denver, Colorado, March 2011.

Reclamation (2011b) SECURE Water Act Section 9503c, Reclamation Climate Change and Water, Report to Congress, April 2011.

Reclamation (2012a) Colorado River Basin Water Supply and Demand Study, Study Report, prepared by the U.S. Department of the Interior, Bureau of Reclamation, December 2012.

Reclamation (2012b) Colorado River Basin Water Supply and Demand Study, Technical Report G – System Reliability Analysis and Evaluation of Options and Strategies, prepared by the U.S. Department of the Interior, Bureau of Reclamation, December 2012.

Rosen, M.R., Turner, K., Goodbred, S.L., and Miller, J.M., eds., (2012) A Synthesis of Aquatic Science for Management of Lakes Mead and Mohave: U.S. Geological Survey Circular 1381, 162 p.

USACE (2011) Addressing Climate Change in Long-Term Water Resources Planning and Management User Needs for Improving Tools and Information, prepared by the U.S. Army Corps of Engineers, January 2011.

USBR (2002) Analysis of Sediments from Las Vegas Bay Delta, Lake Mead, Technical Memorandum No. 8220-10-02, July 2002.

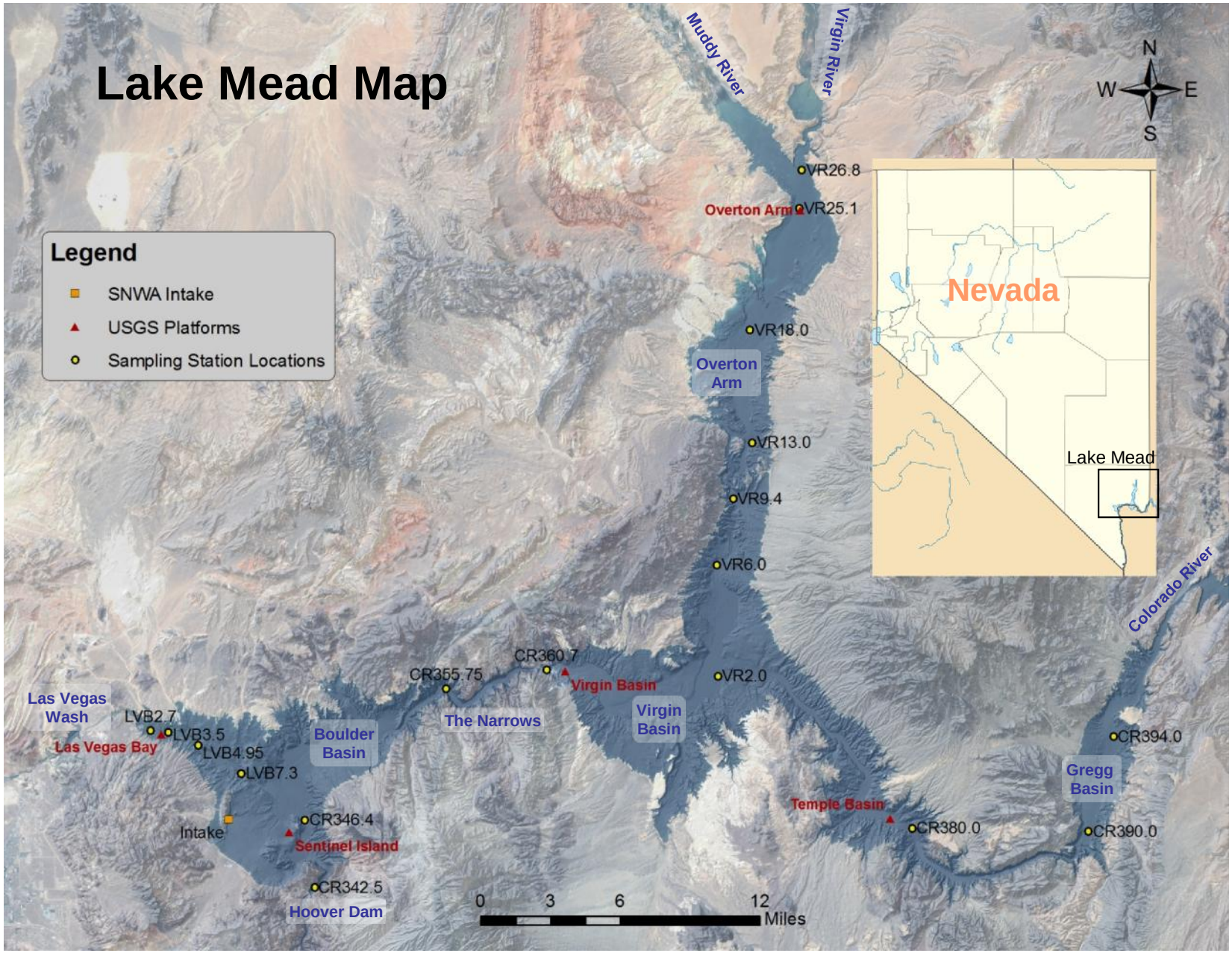
Lake Mead Map
Legend
SNWA Intake
USGS Platforms
Sampling Station Locations
Muddy River
Virgin River
N
W
E
S
VR26.8
Overton Arm
VR25.1
VR18.0
Overton Arm
VR13.0
VR9.4
VR6.0
Nevada
Lake Mead
Colorado River
CR360.7
CR355.75
Virgin Basin
VR2.0
Virgin Basin
The Narrows
Las Vegas Wash
LVB2.7
LVB3.5
Las Vegas Bay
LVB4.95
LVB7.3
Boulder Basin
CR394.0
Gregg Basin
Temple Basin
CR380.0
CR390.0
Intake
CR346.4
Sentinel Island
CR342.5
Hoover Dam
0
3
6
12
Miles

Figure 1.1

Computation Grid for Whole Lake Model

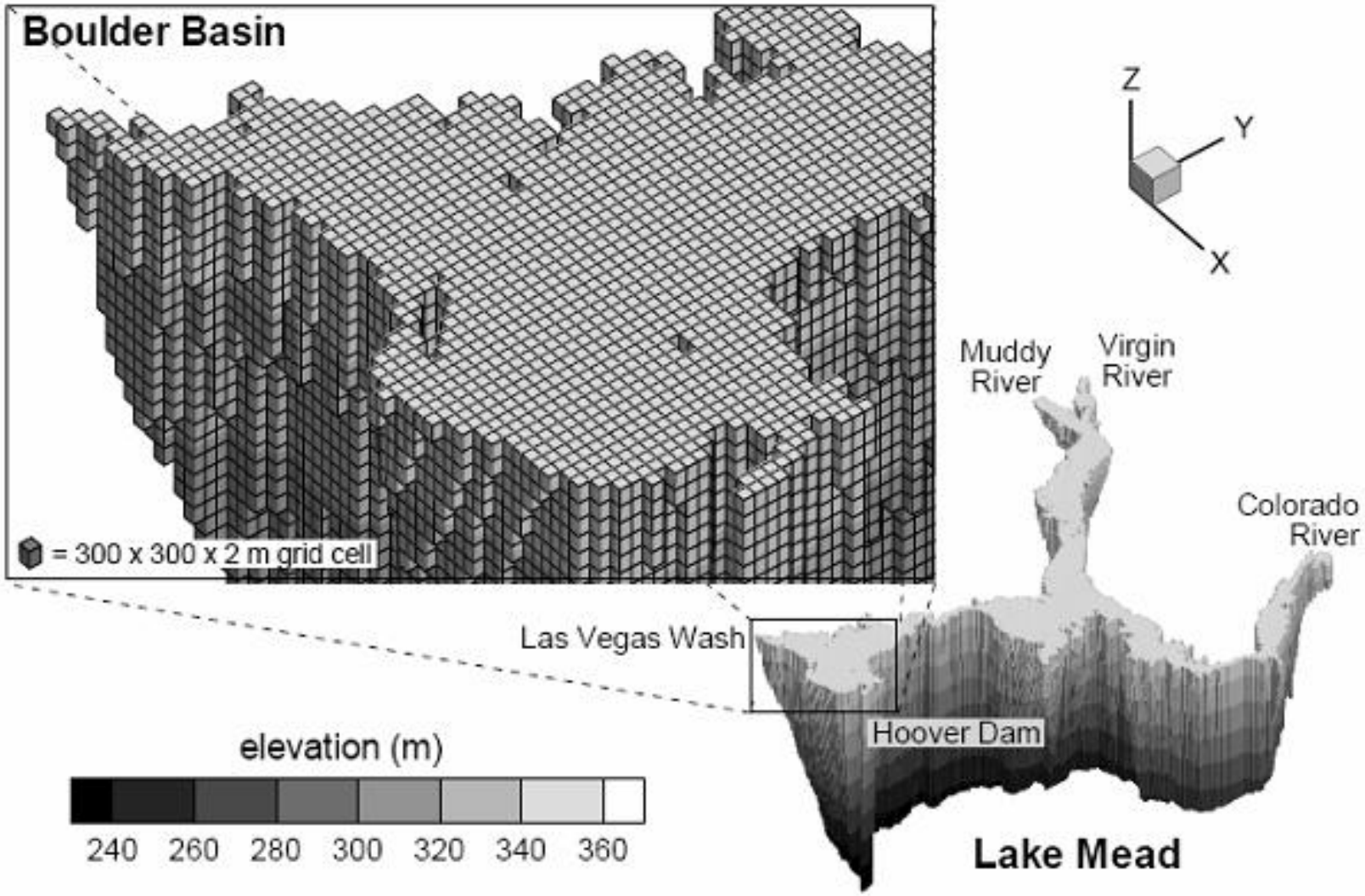

Figure 2.1

FLOW SCIENCE

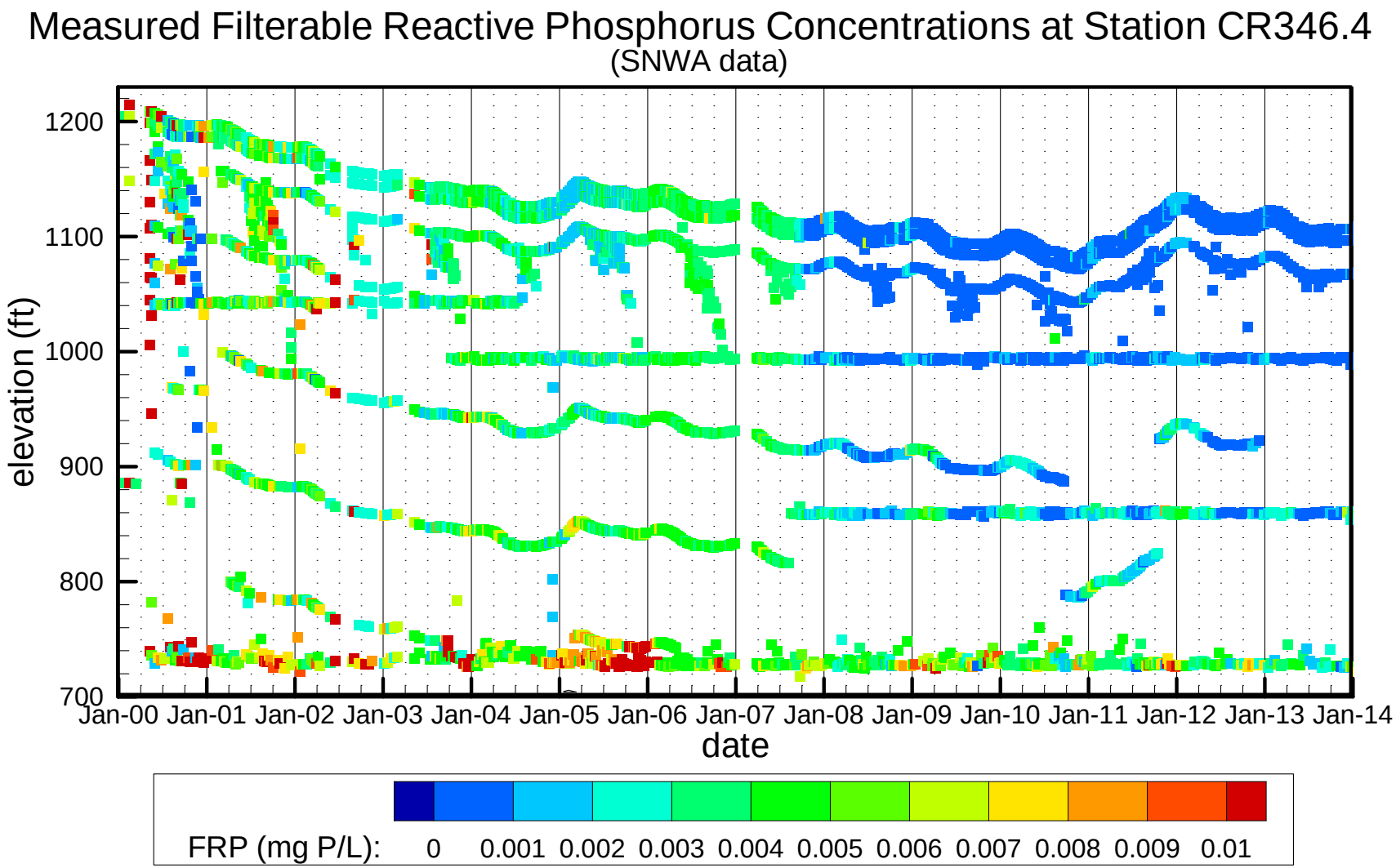
Measured Filterable Reactive Phosphorus Concentrations at Station CR346.4
(SNWA data)
elevation (ft)
1200
1100
1000
900
800
700
Jan-00 Jan-01 Jan-02 Jan-03 Jan-04 Jan-05 Jan-06 Jan-07 Jan-08 Jan-09 Jan-10 Jan-11 Jan-12 Jan-13 Jan-14
date
FRP (mg P/L): 0 0.001 0.002 0.003 0.004 0.005 0.006 0.007 0.008 0.009 0.01

Figure 3.1

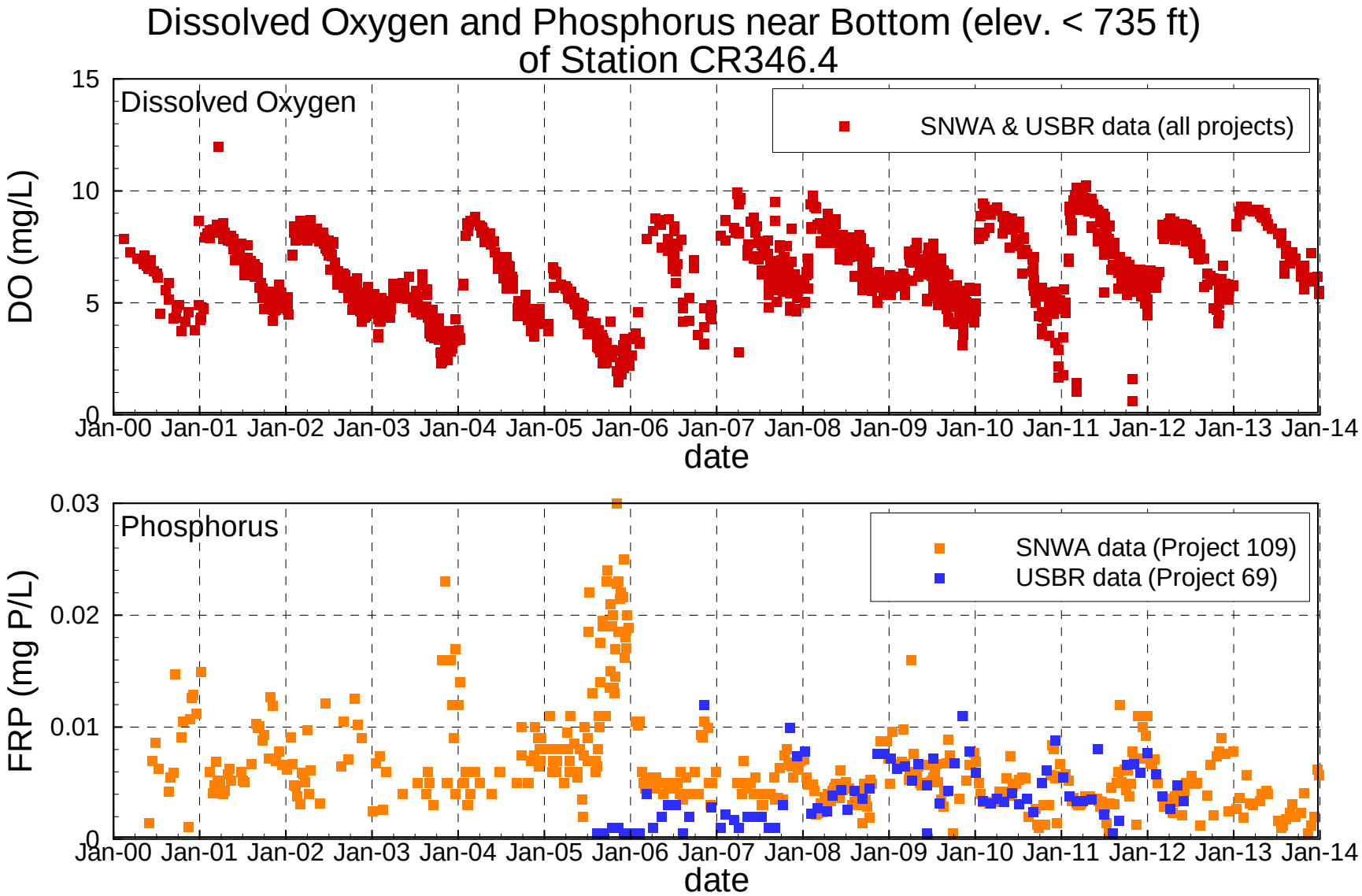
Dissolved Oxygen and Phosphorus near Bottom (elev. < 735 ft)
of Station CR346.4
Dissolved Oxygen
SNWA & USBR data (all projects)
DO (mg/L)
15
10
5
0
Jan-00 Jan-01 Jan-02 Jan-03 Jan-04 Jan-05 Jan-06 Jan-07 Jan-08 Jan-09 Jan-10 Jan-11 Jan-12 Jan-13 Jan-14
date
Phosphorus
SNWA data (Project 109)
USBR data (Project 69)
FRP (mg P/L)
0.03
0.02
0.01
0
Jan-00 Jan-01 Jan-02 Jan-03 Jan-04 Jan-05 Jan-06 Jan-07 Jan-08 Jan-09 Jan-10 Jan-11 Jan-12 Jan-13 Jan-14
date

Figure 3.2

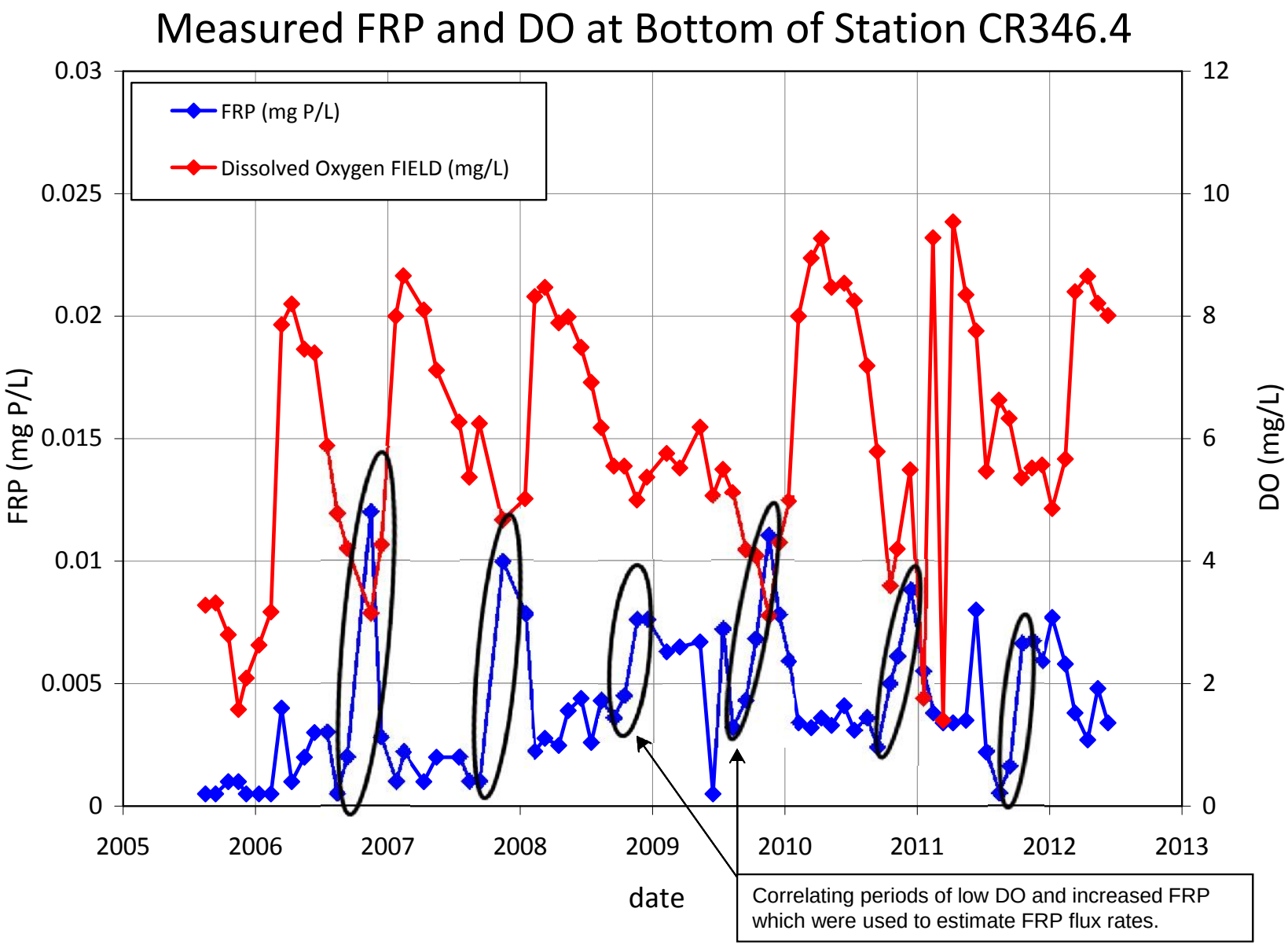

Figure 3.3

FLOW SCIENCE

Measured FRP and DO at Bottom of Station CR380.0

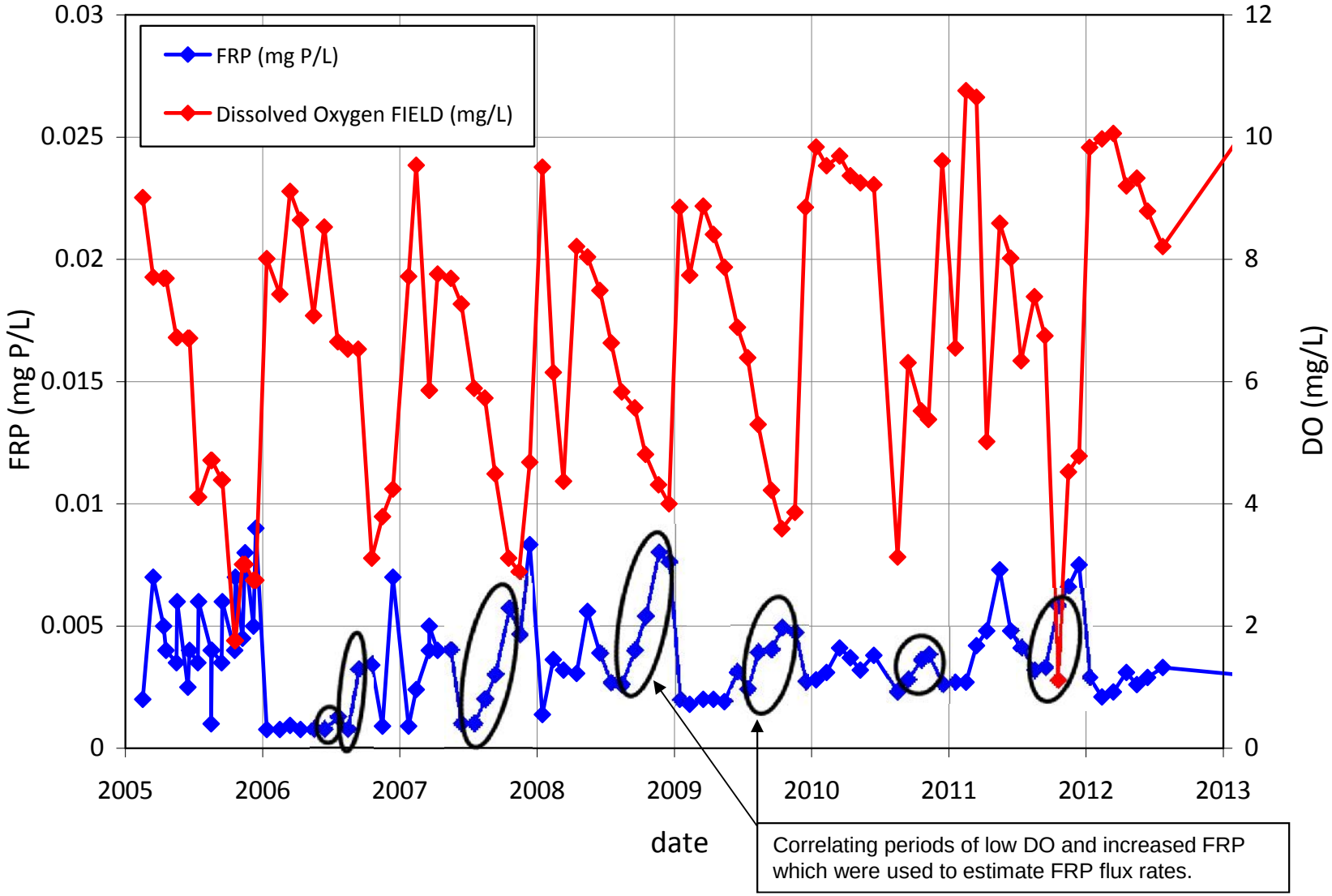

Figure 3.4

FLOW SCIENCE

DO Profile at Station CR346.4

8/15/2006

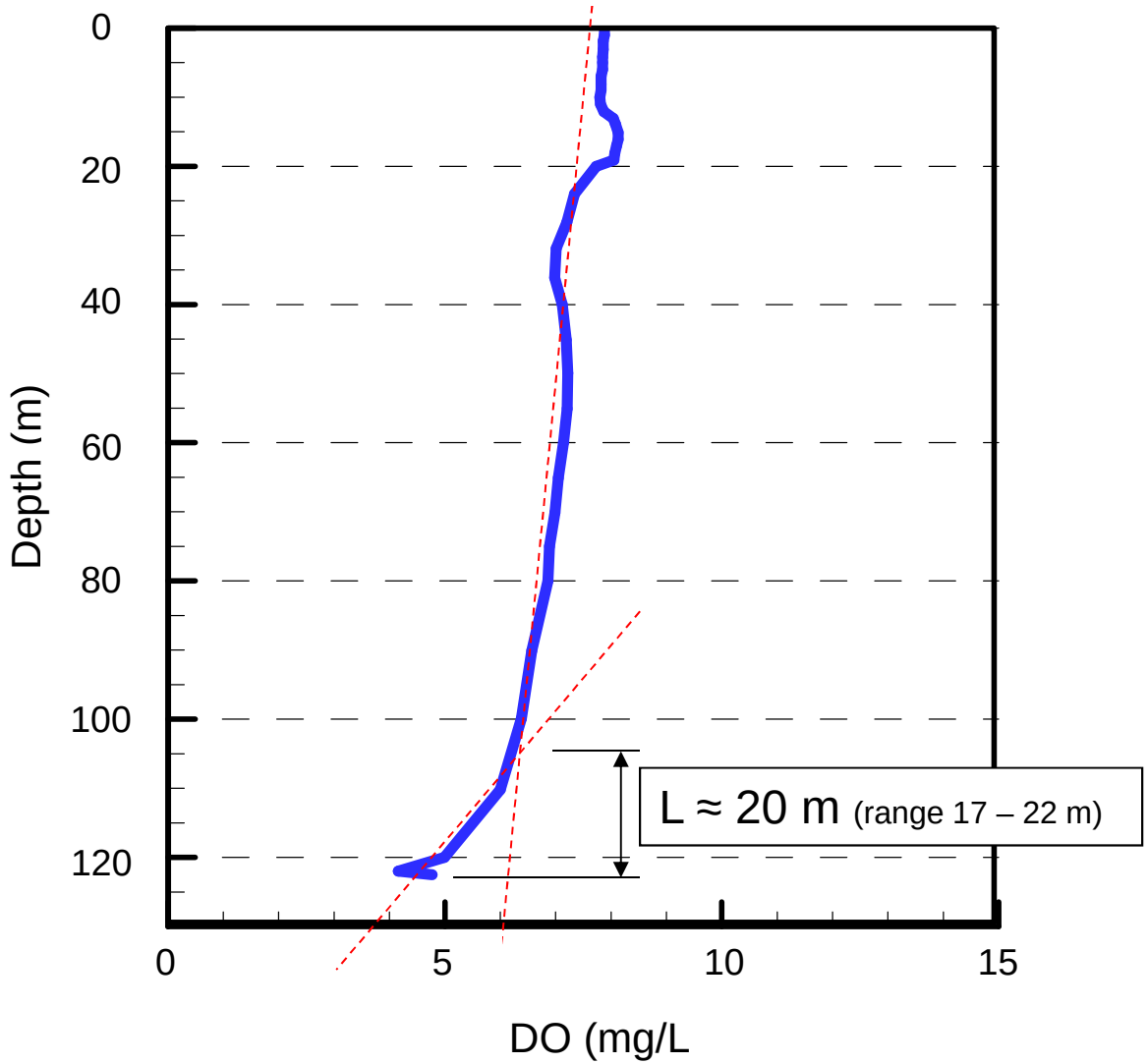

Figure 3.5

FLOW SCIENCE

Dissolved Phosphorus Sediment Flux at Station CR346.4

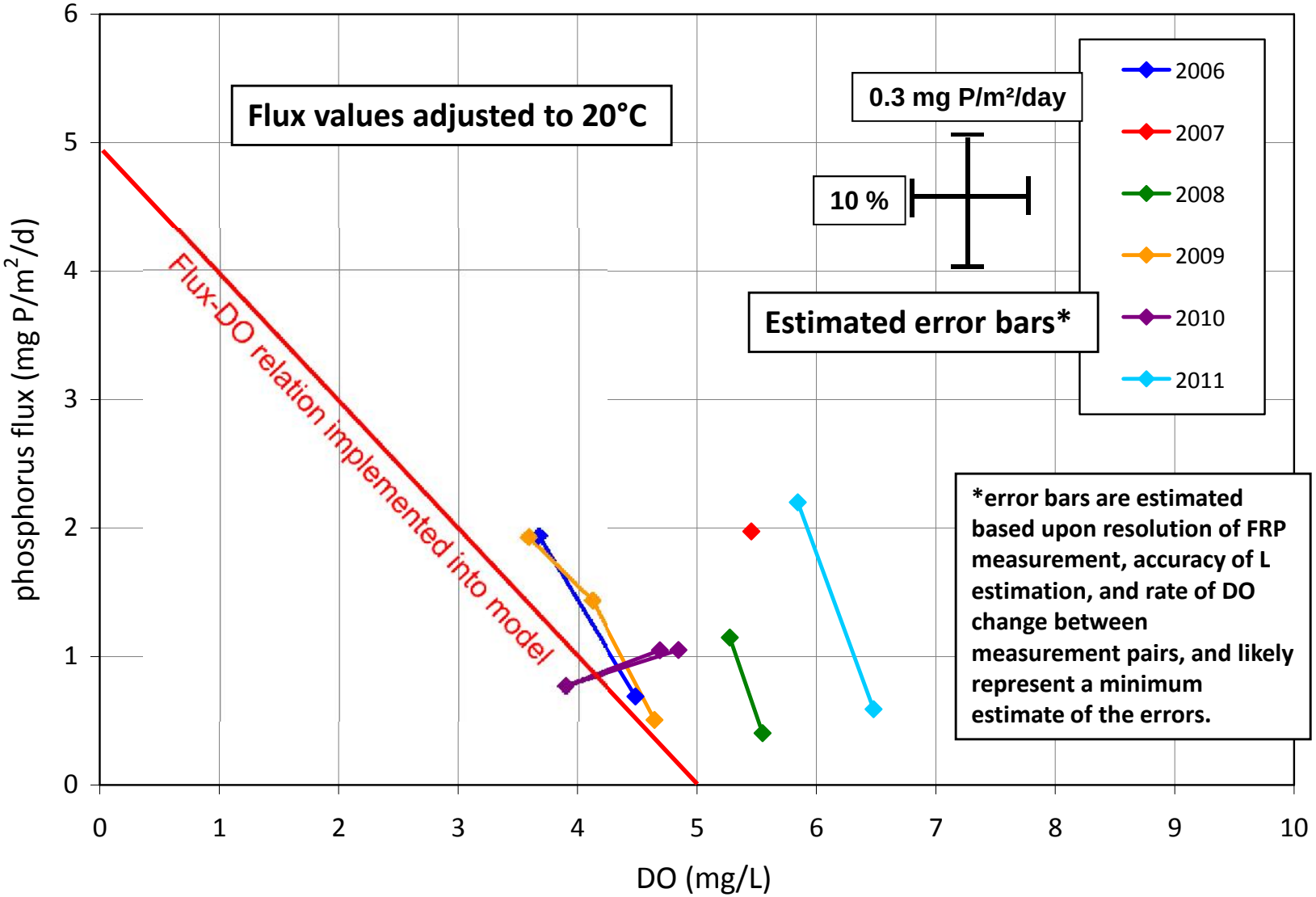

Figure 3.6

FLOW SCIENCE

Dissolved Phosphorus Sediment Flux at Station CR380.0

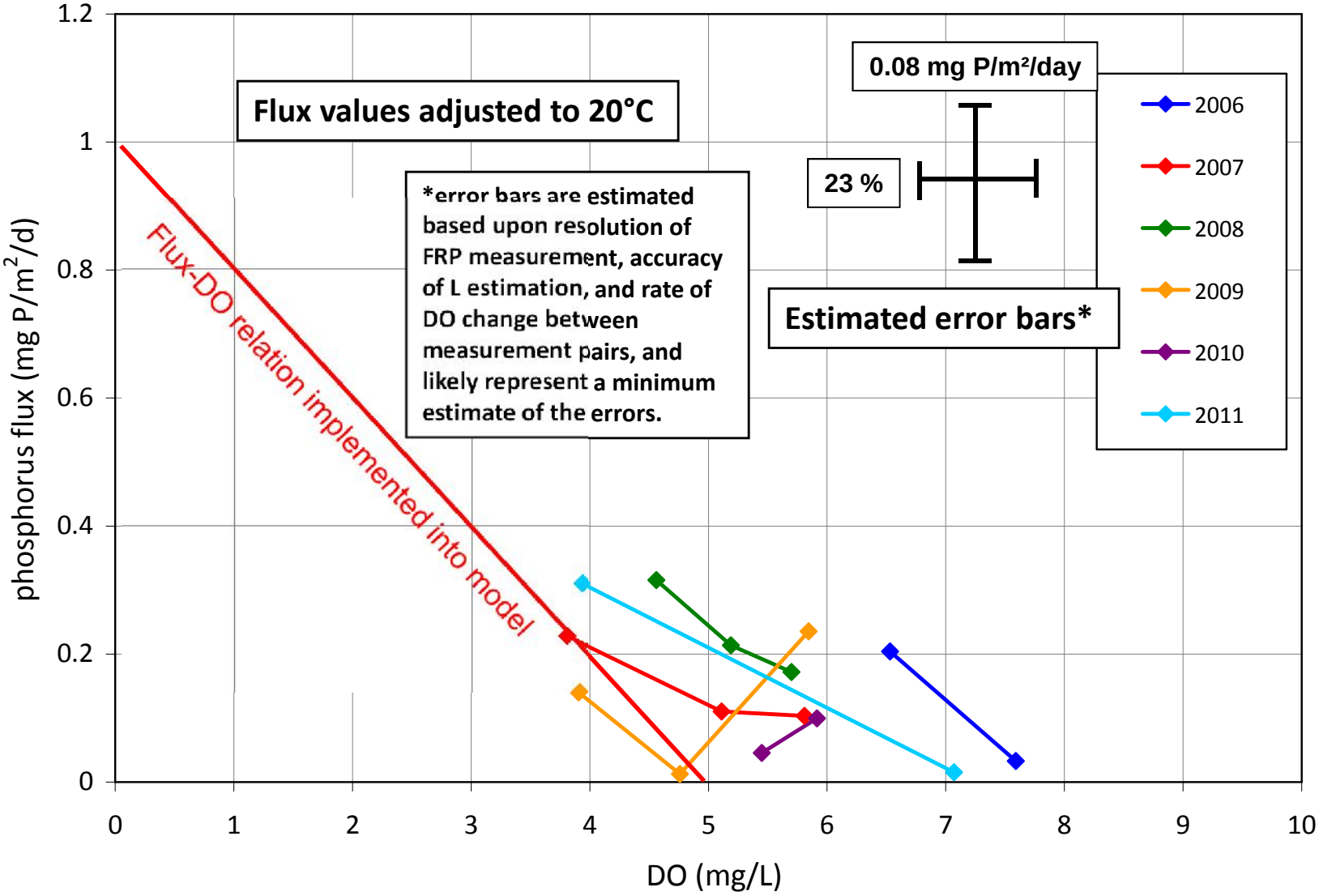

Figure 3.7

FLOW SCIENCE

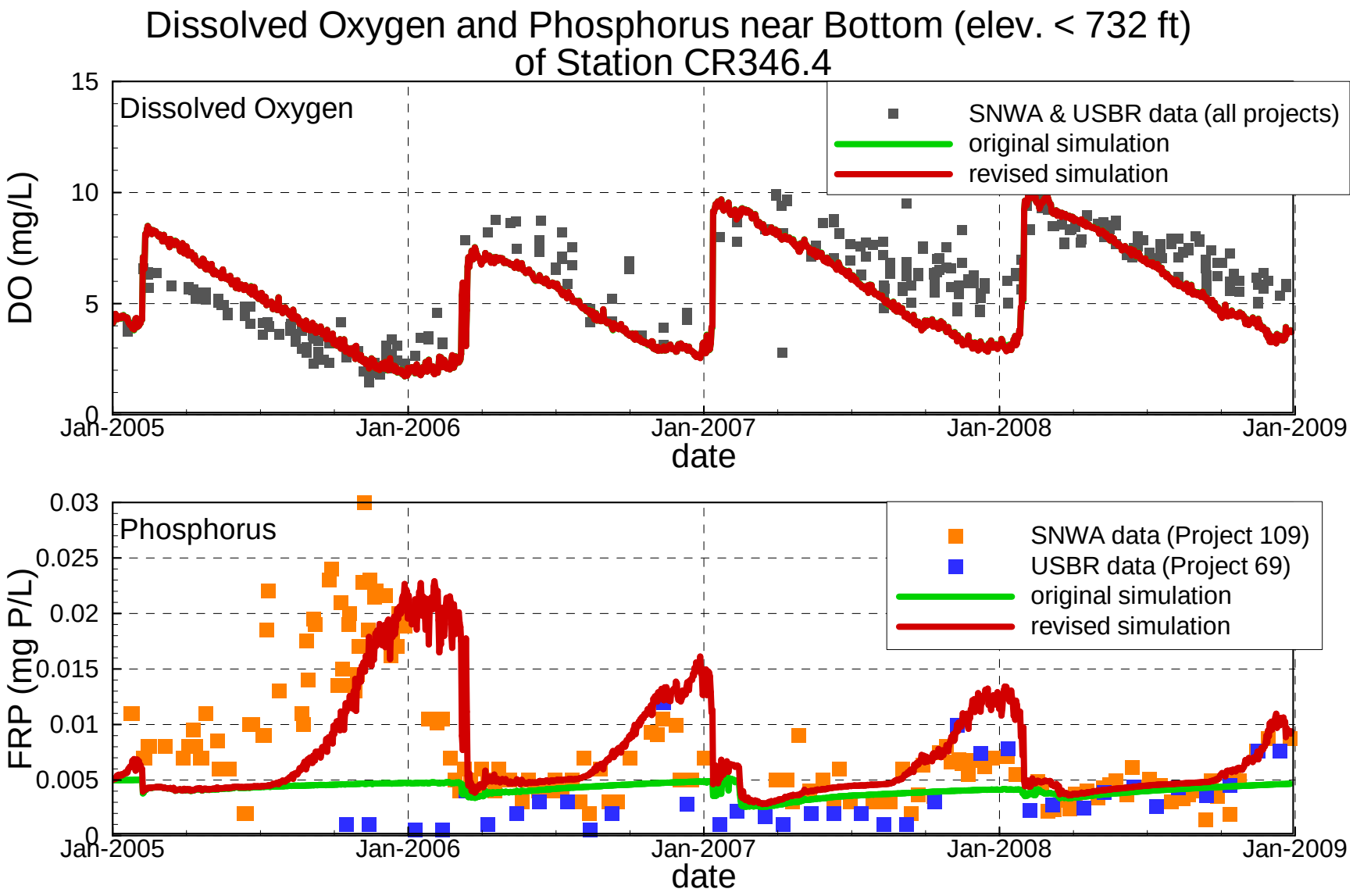

Figure 3.8

FLOW SCIENCE

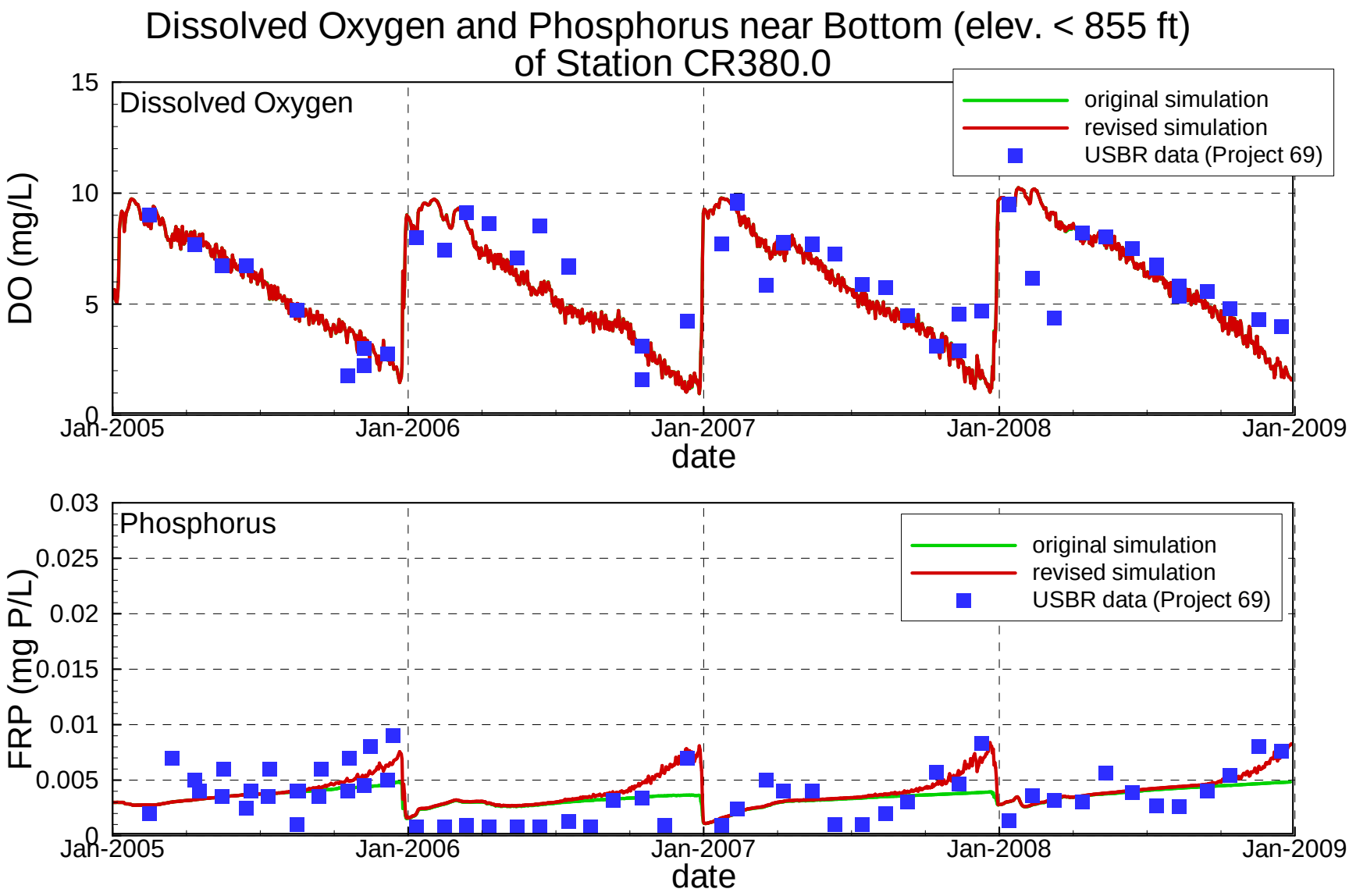

Figure 3.9

FLOW SCIENCE

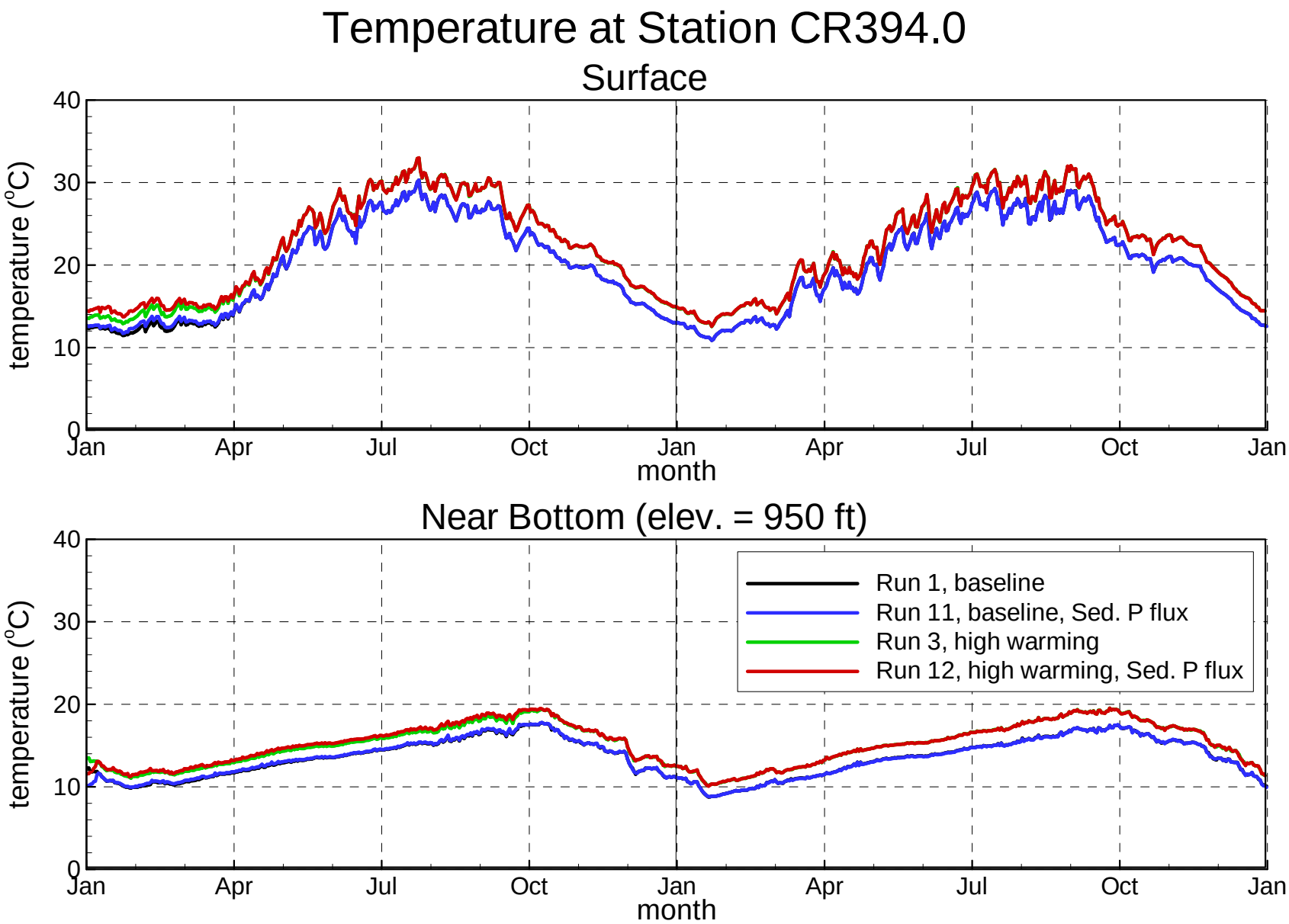
Temperature at Station CR394.0
Surface
temperature (°C)
40
30
20
10
0
Jan
Apr
Jul
Oct
Jan
Apr
Jul
Oct
Jan
month
Near Bottom (elev. = 950 ft)
temperature (°C)
40
30
20
10
0
Jan
Apr
Jul
Oct
Jan
Apr
Jul
Oct
Jan
month
Run 1, baseline
Run 11, baseline, Sed. P flux
Run 3, high warming
Run 12, high warming, Sed. P flux

Figure 5.1

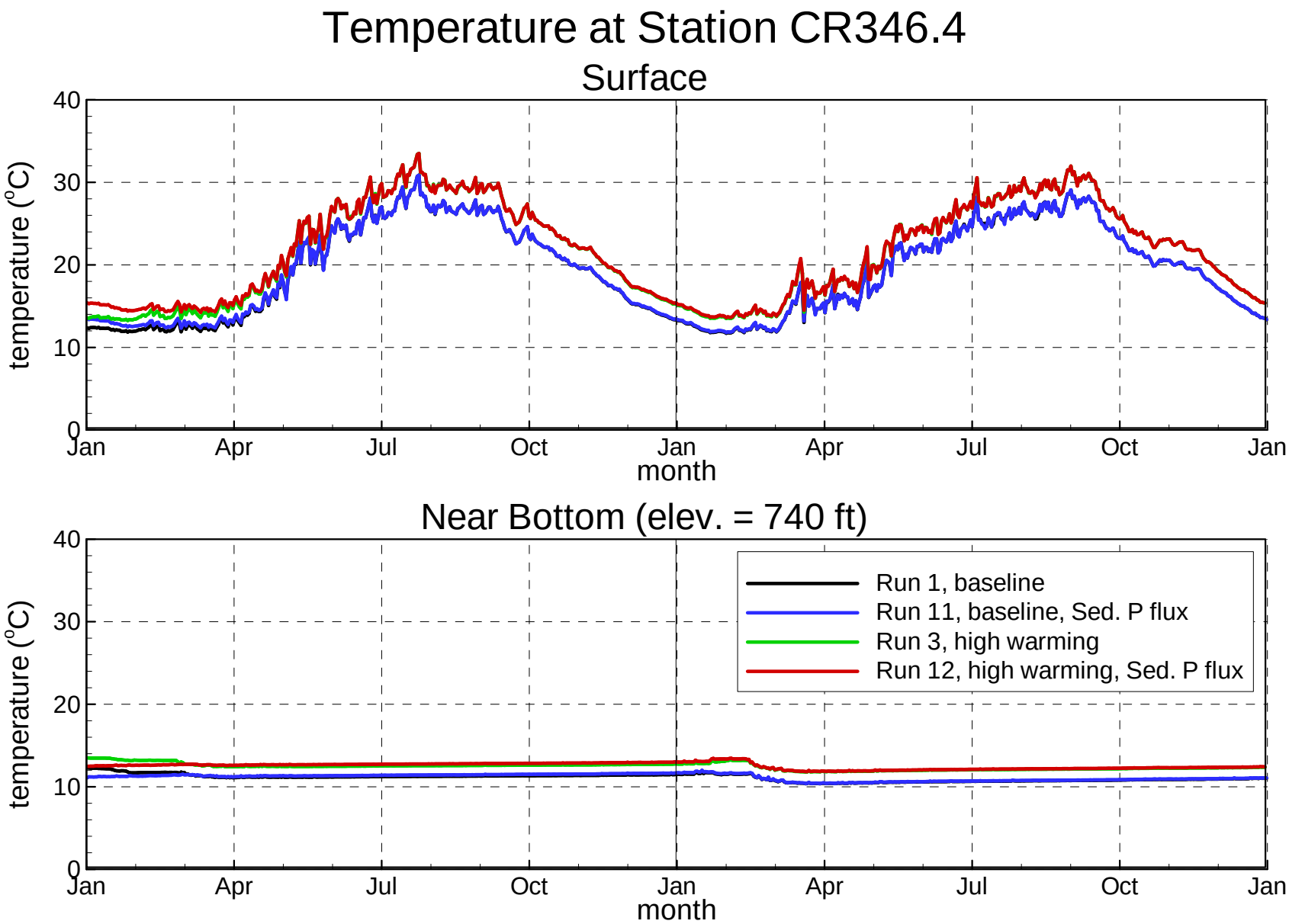
Temperature at Station CR346.4
Surface
temperature (°C)
40
30
20
10
0
Jan
Apr
Jul
Oct
Jan
Apr
Jul
Oct
Jan
month
Near Bottom (elev. = 740 ft)
temperature (°C)
40
30
20
10
0
Jan
Apr
Jul
Oct
Jan
Apr
Jul
Oct
Jan
month
Run 1, baseline
Run 11, baseline, Sed. P flux
Run 3, high warming
Run 12, high warming, Sed. P flux

Figure 5.2

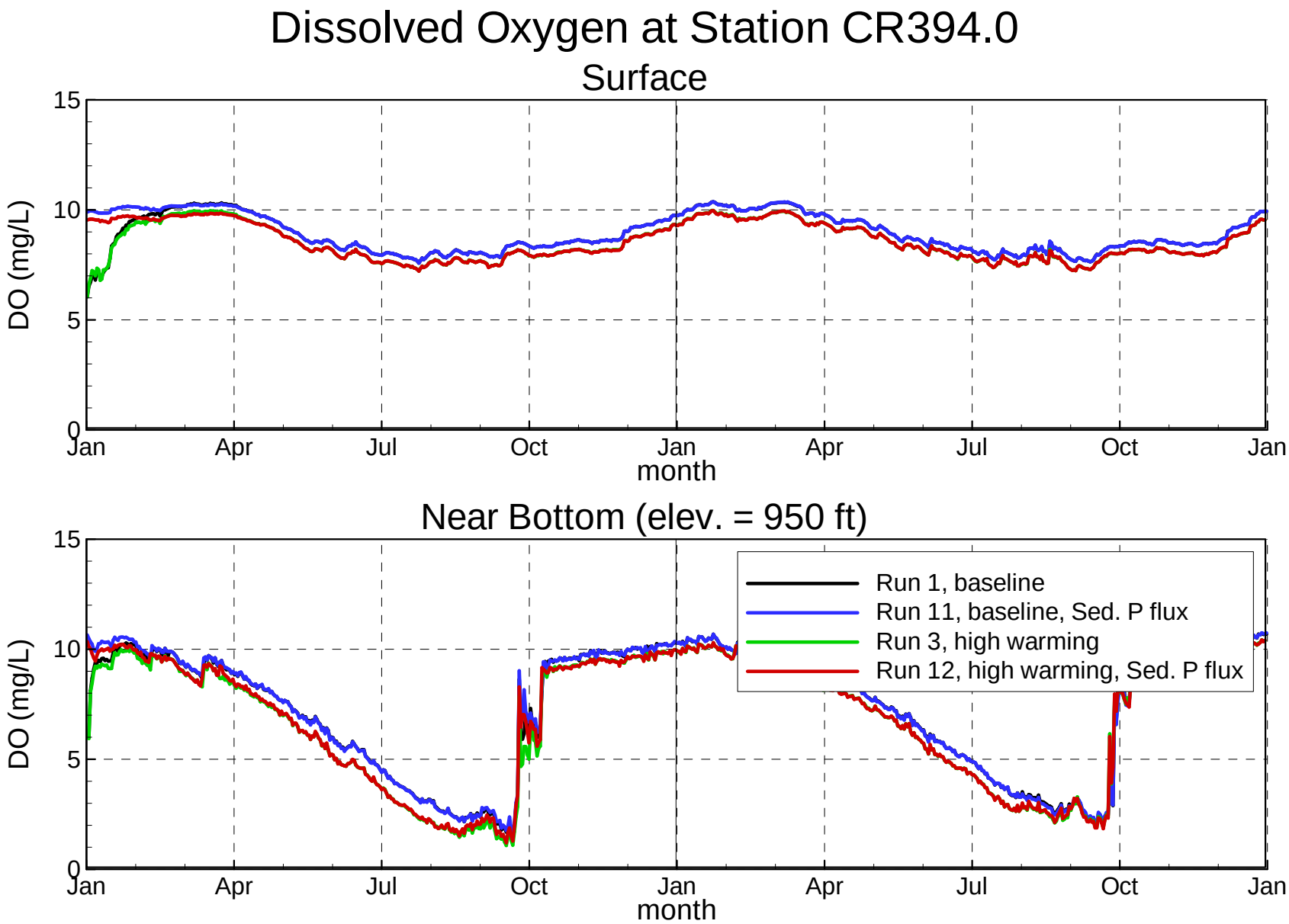

Figure 5.3

FLOW SCIENCE

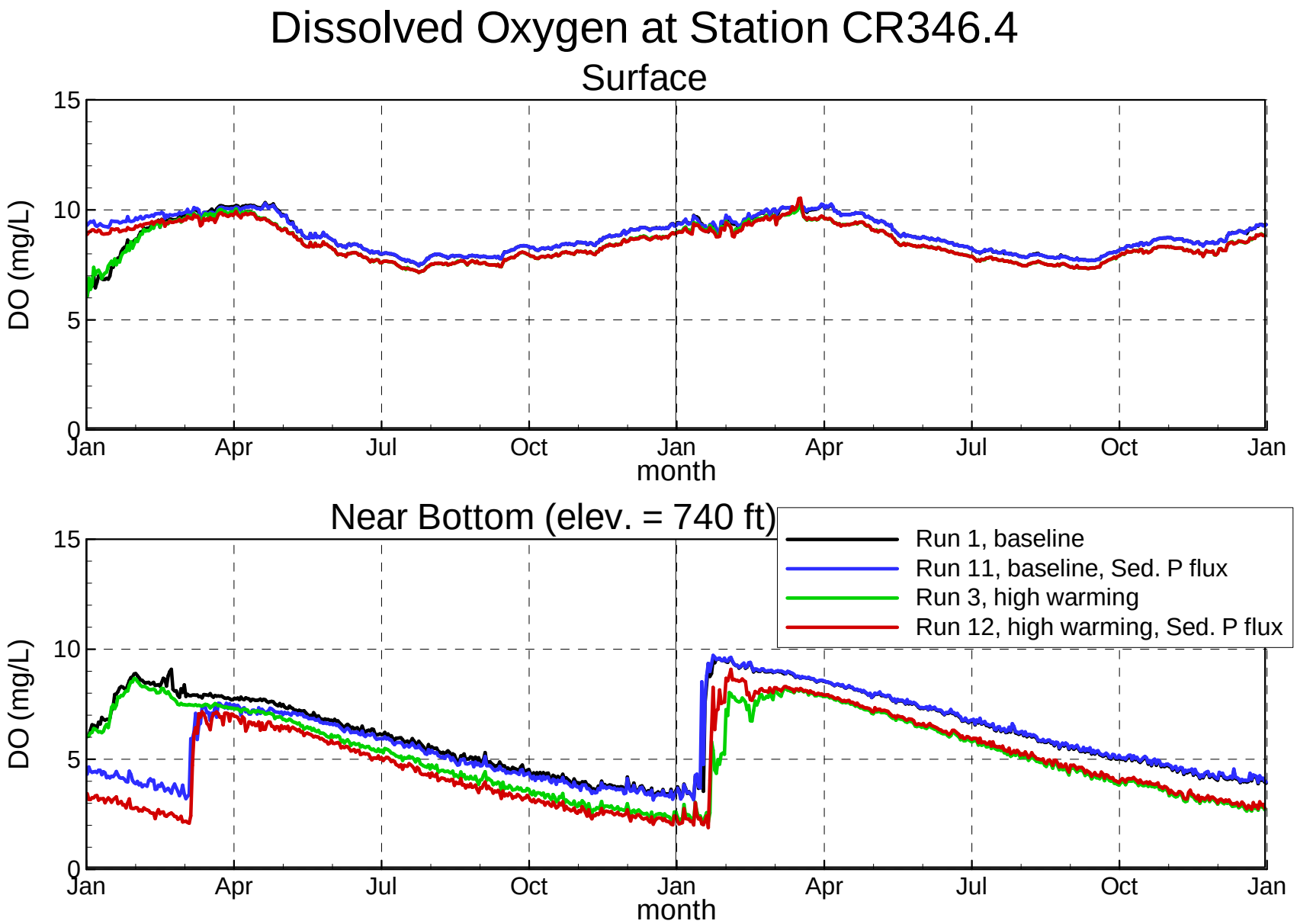
Dissolved Oxygen at Station CR346.4
Surface
DO (mg/L)
15
10
5
0
Jan
Apr
Jul
Oct
Jan
Apr
Jul
Oct
Jan
month
Near Bottom (elev. = 740 ft)
Run 1, baseline
Run 11, baseline, Sed. P flux
Run 3, high warming
Run 12, high warming, Sed. P flux

Figure 5.4

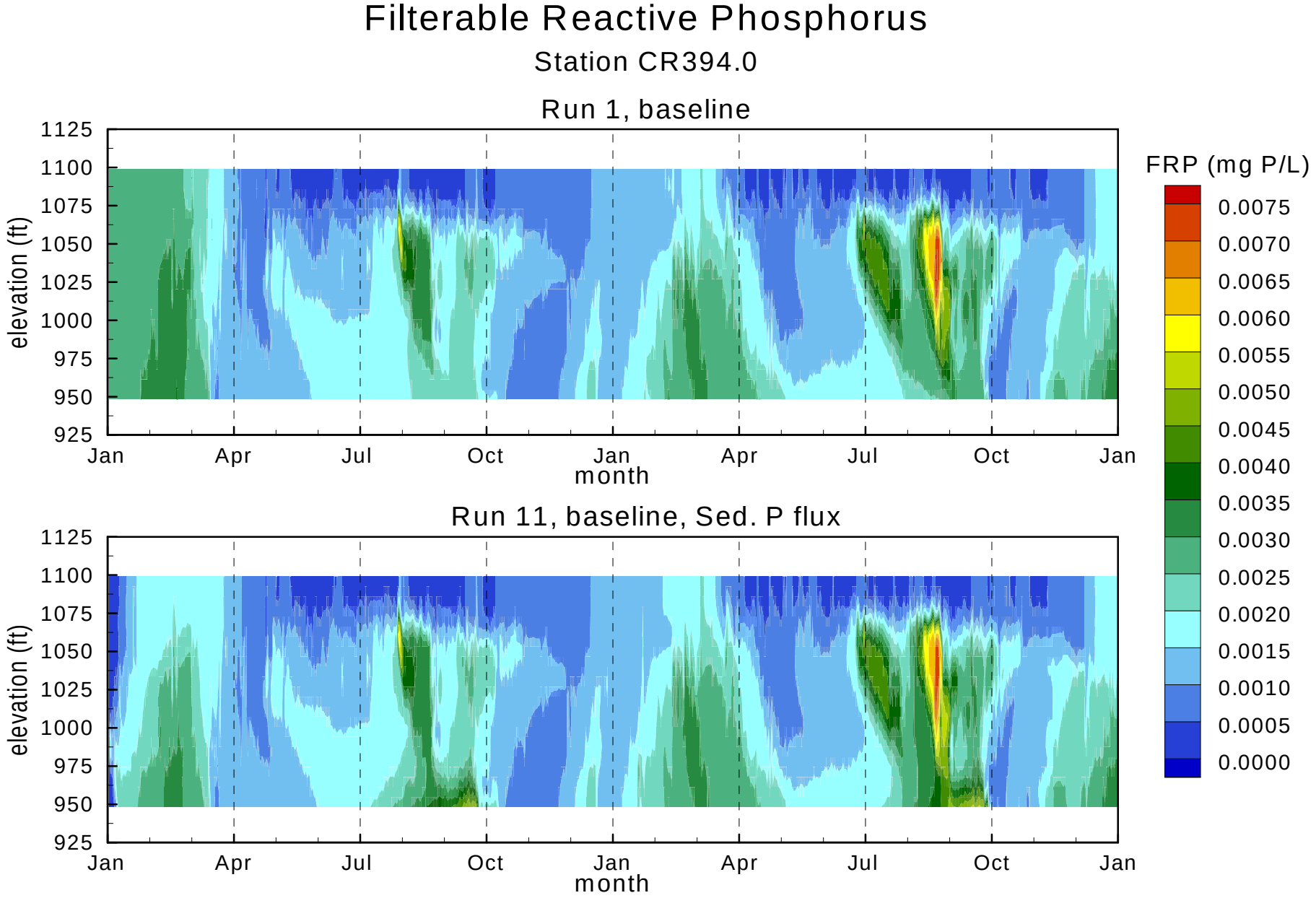
Filterable Reactive Phosphorus
Station CR394.0
Run 1, baseline
Run 11, baseline, Sed. P flux
elevation (ft)
1125
1100
1075
1050
1025
1000
975
950
925
Jan
Apr
Jul
Oct
Jan
month
FRP (mg P/L)
0.0075
0.0070
0.0065
0.0060
0.0055
0.0050
0.0045
0.0040
0.0035
0.0030
0.0025
0.0020
0.0015
0.0010
0.0005
0.0000

Figure 5.5

Filterable Reactive Phosphorus

Station CR394.0

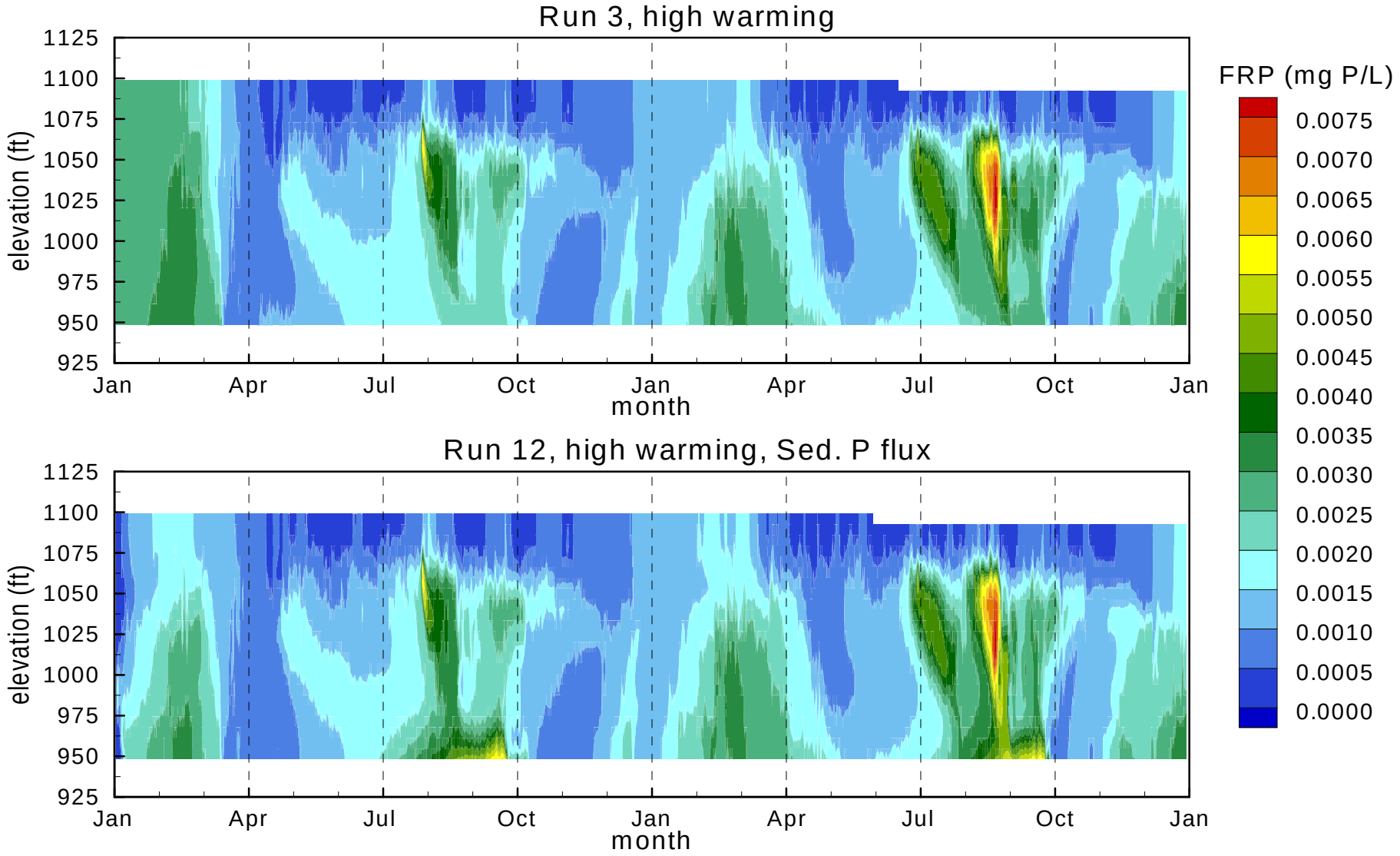

Figure 5.6

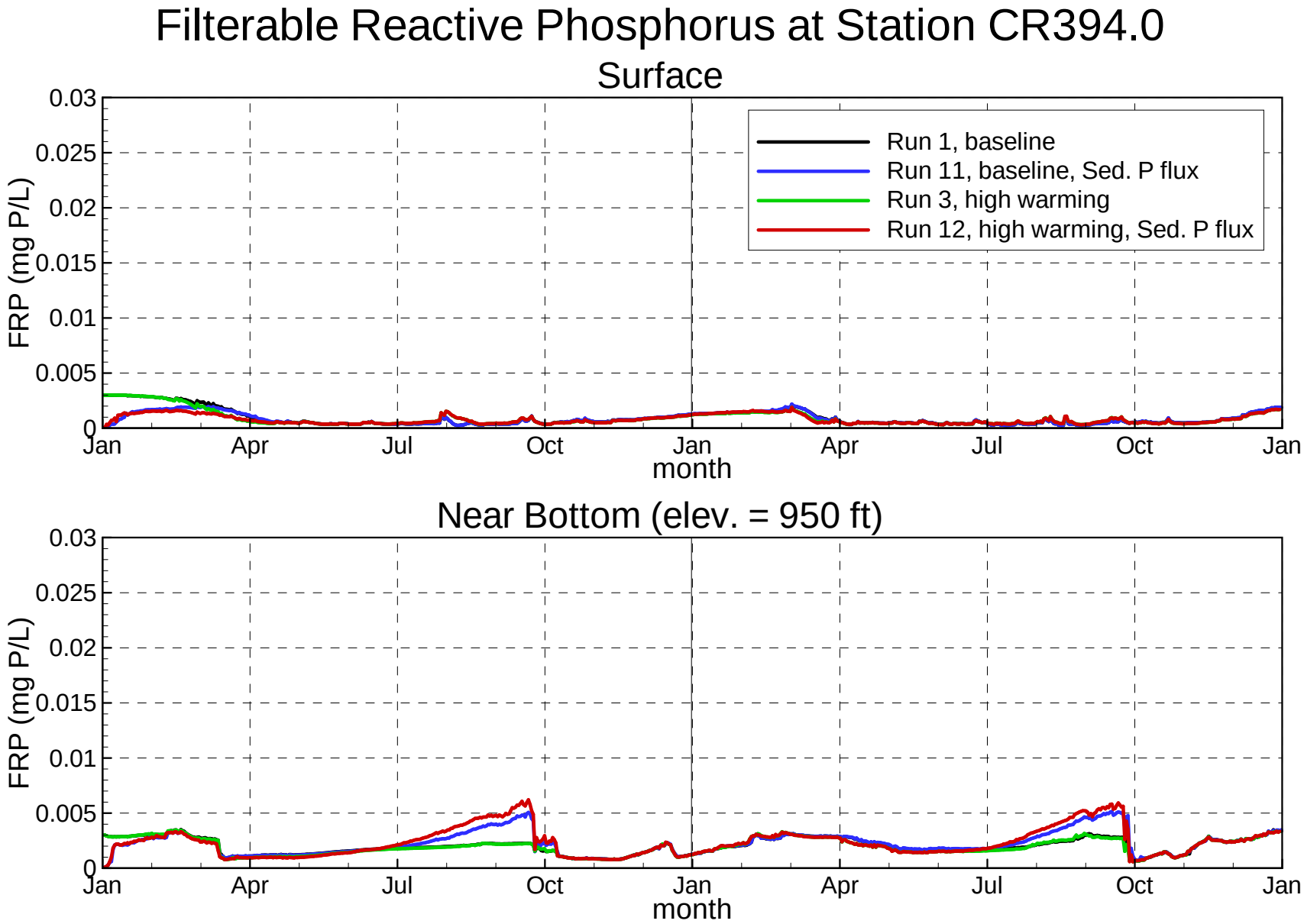
Filterable Reactive Phosphorus at Station CR394.0
Surface
Run 1, baseline
Run 11, baseline, Sed. P flux
Run 3, high warming
Run 12, high warming, Sed. P flux
FRP (mg P/L)
0.03
0.025
0.02
0.015
0.01
0.005
0
Jan
Apr
Jul
Oct
Jan
Apr
Jul
Oct
Jan
month
Near Bottom (elev. = 950 ft)
FRP (mg P/L)
0.03
0.025
0.02
0.015
0.01
0.005
0
Jan
Apr
Jul
Oct
Jan
Apr
Jul
Oct
Jan
month

Figure 5.7

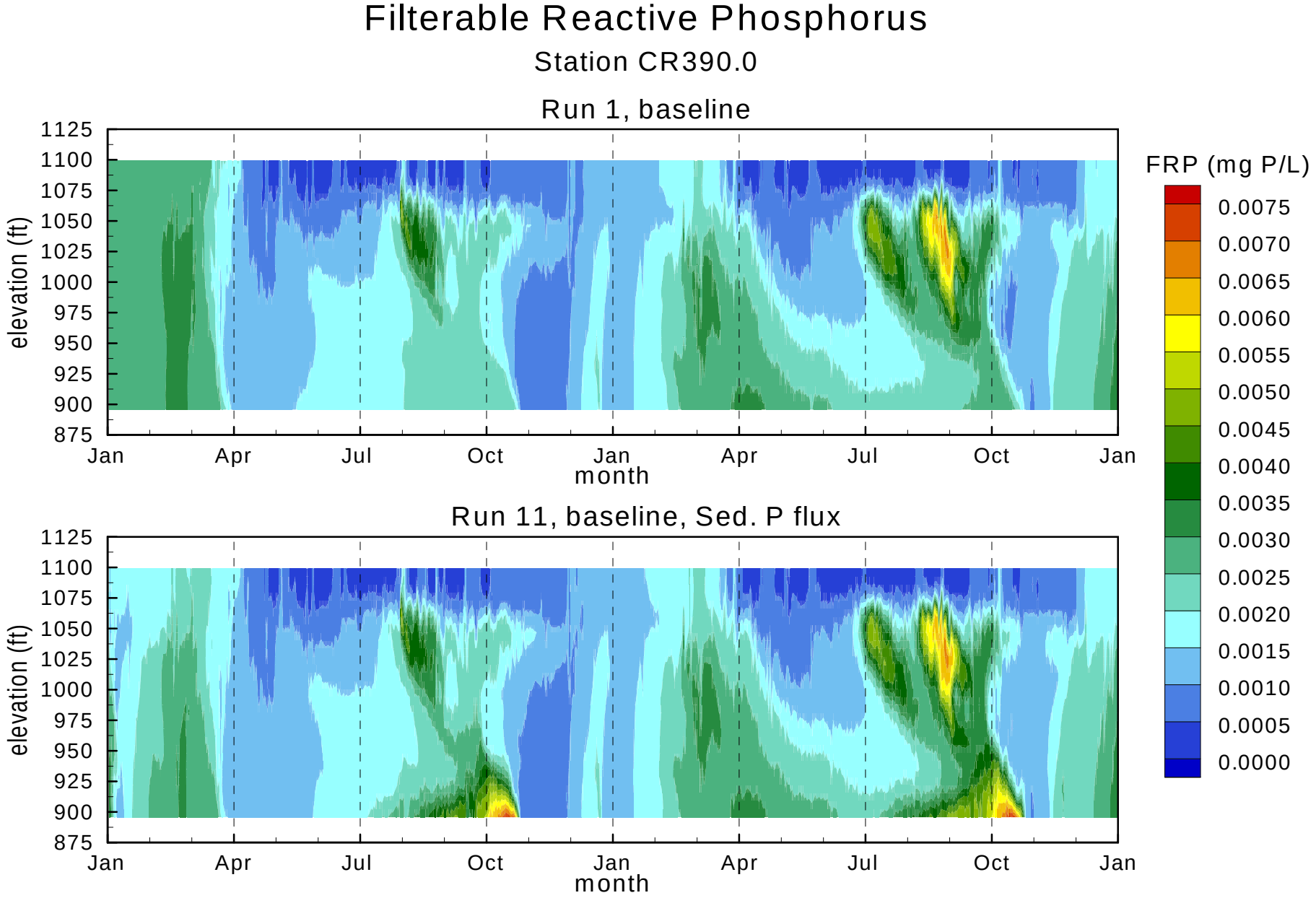

Figure 5.8

FLOW SCIENCE

Filterable Reactive Phosphorus

Station CR390.0

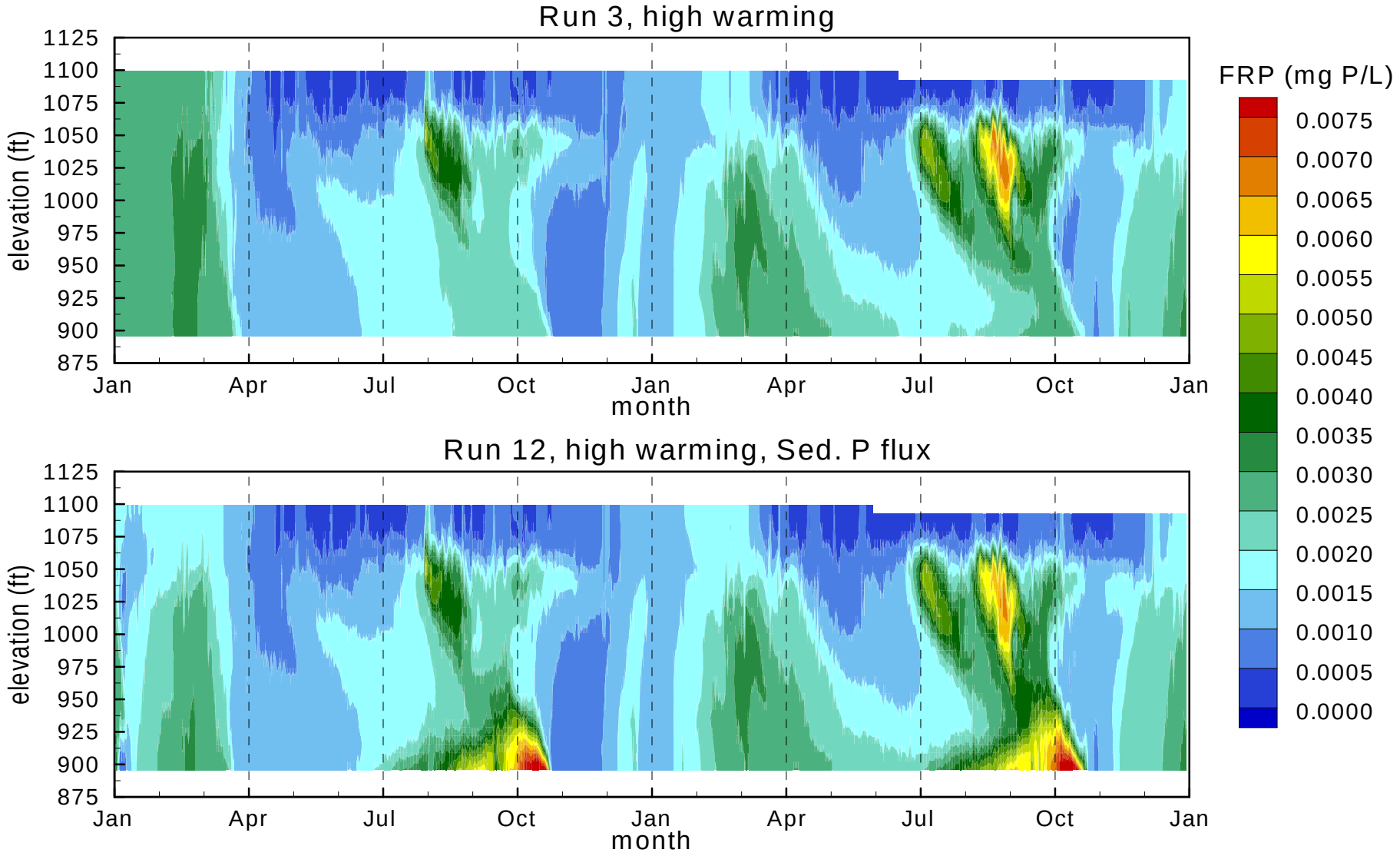

Figure 5.9

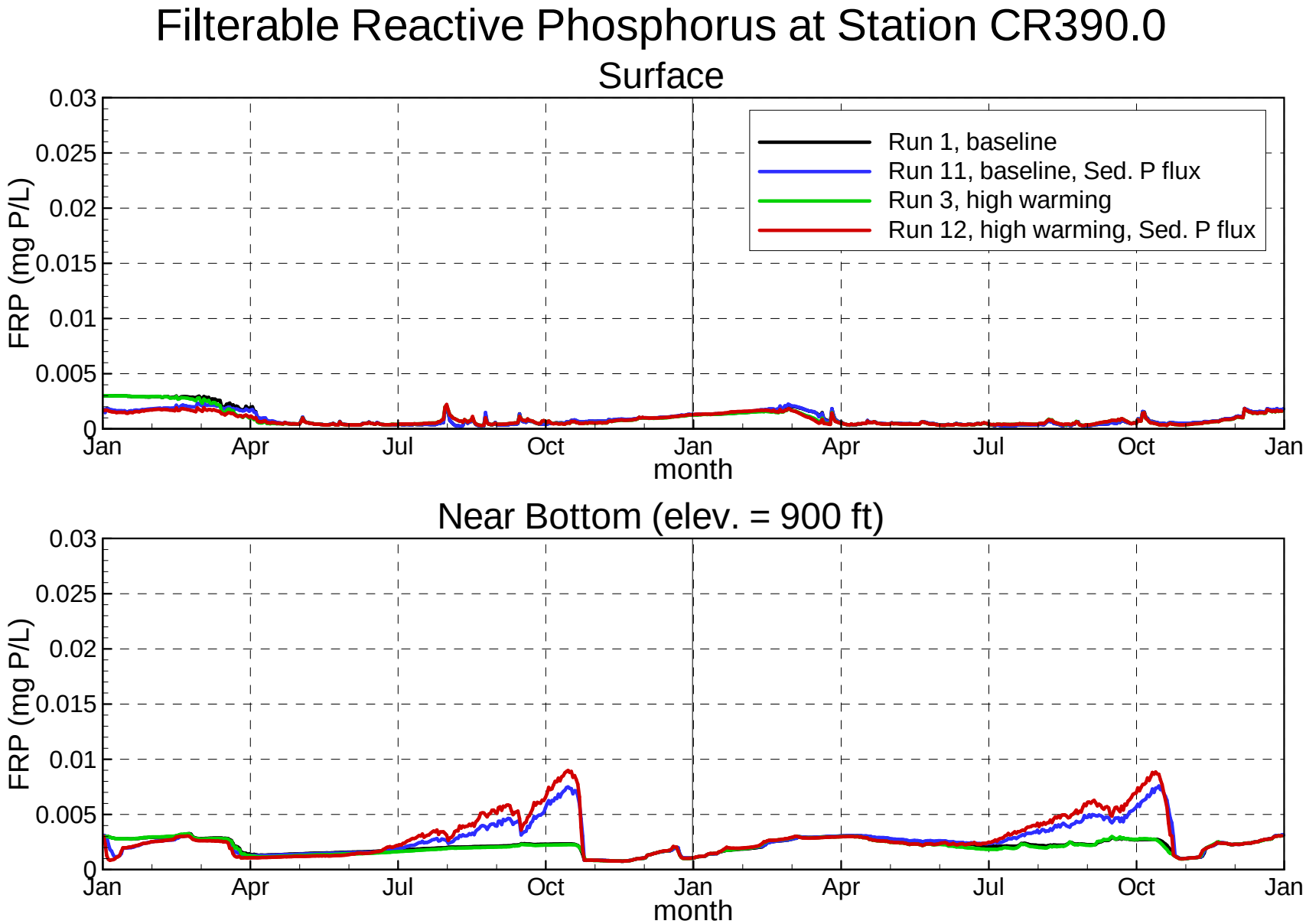

Figure 5.10

FLOW SCIENCE

Filterable Reactive Phosphorus

Station CR346.4

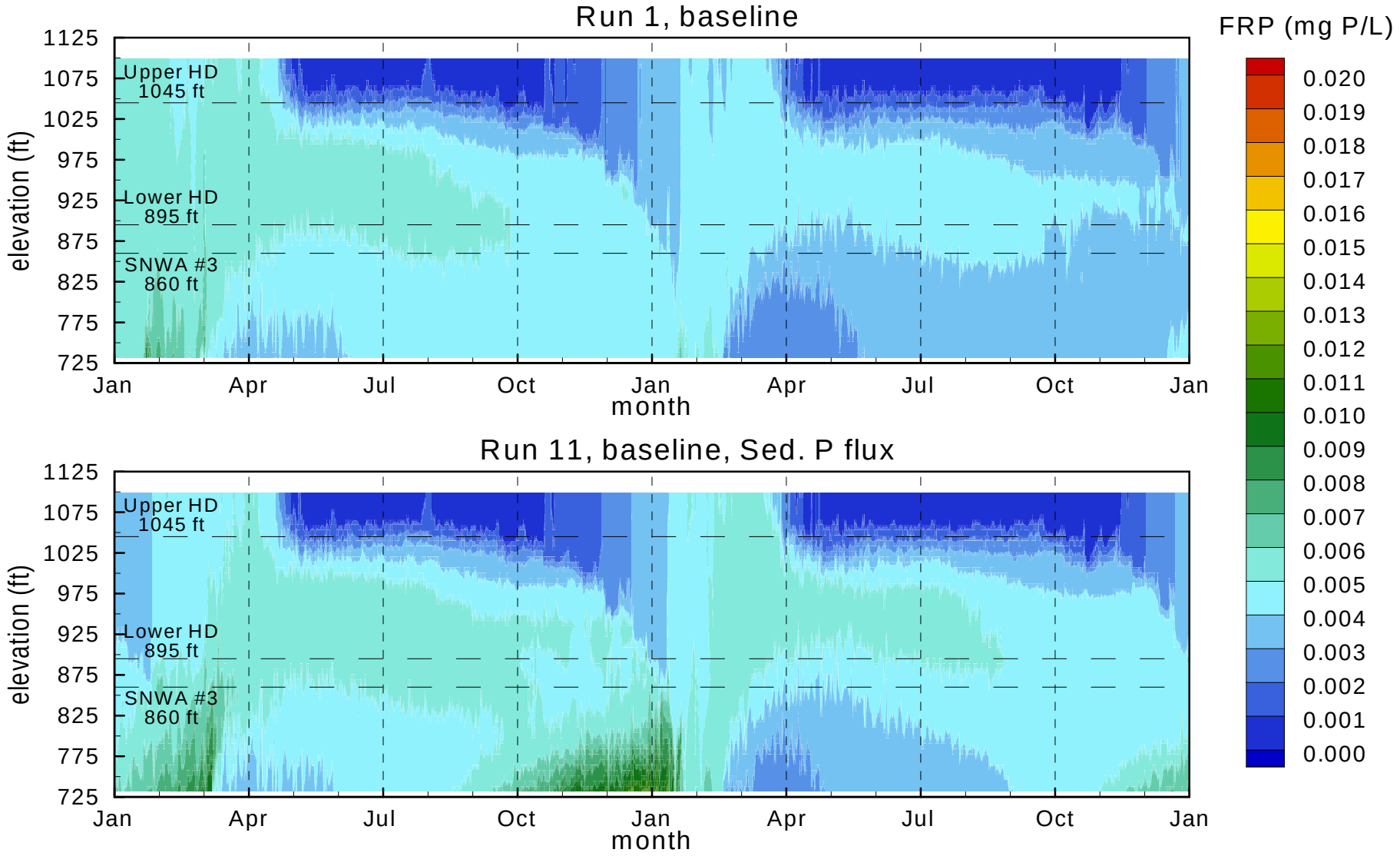

Figure 5.11

FLOW SCIENCE

Filterable Reactive Phosphorus

Station CR346.4

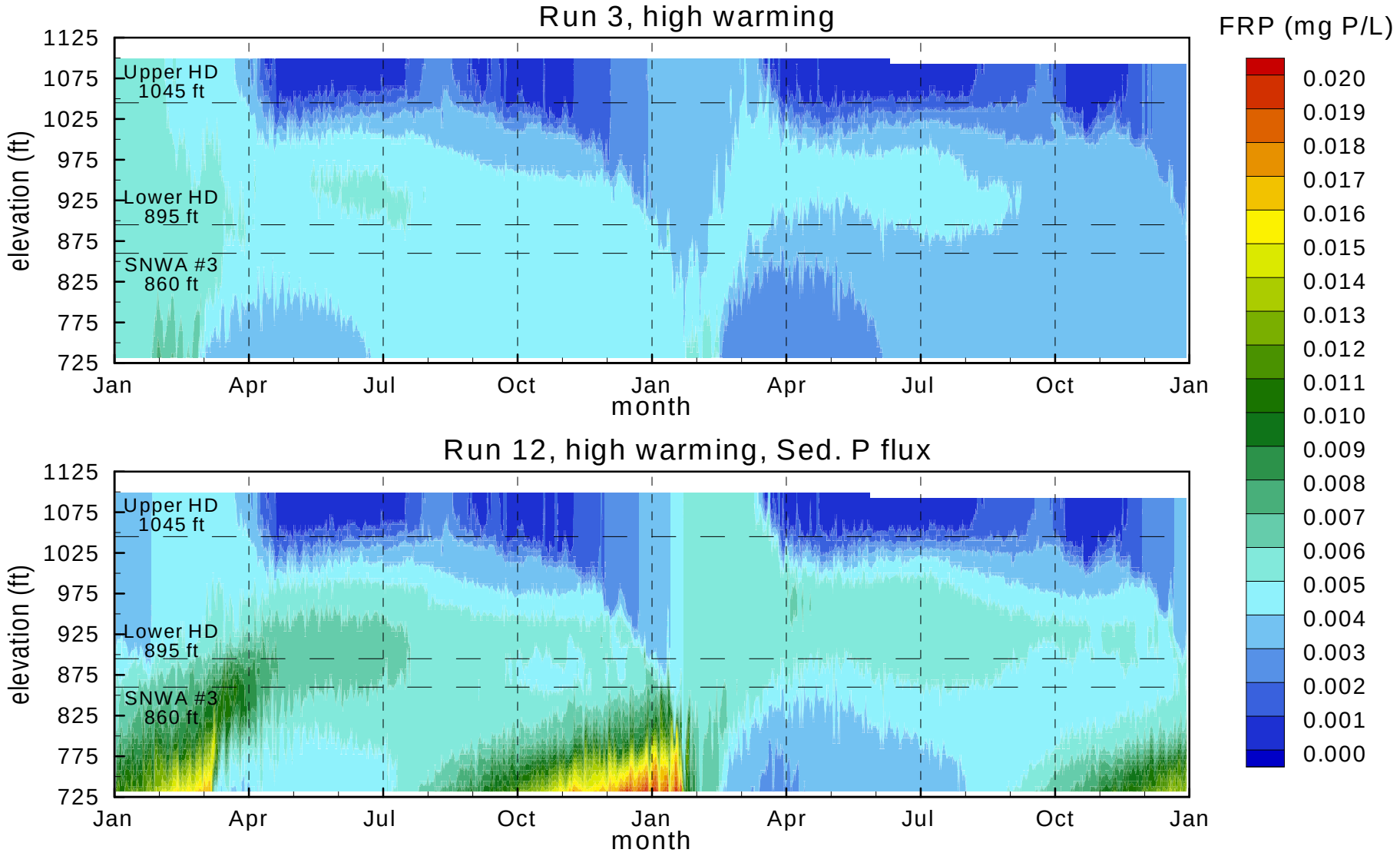

Figure 5.12

FLOW SCIENCE

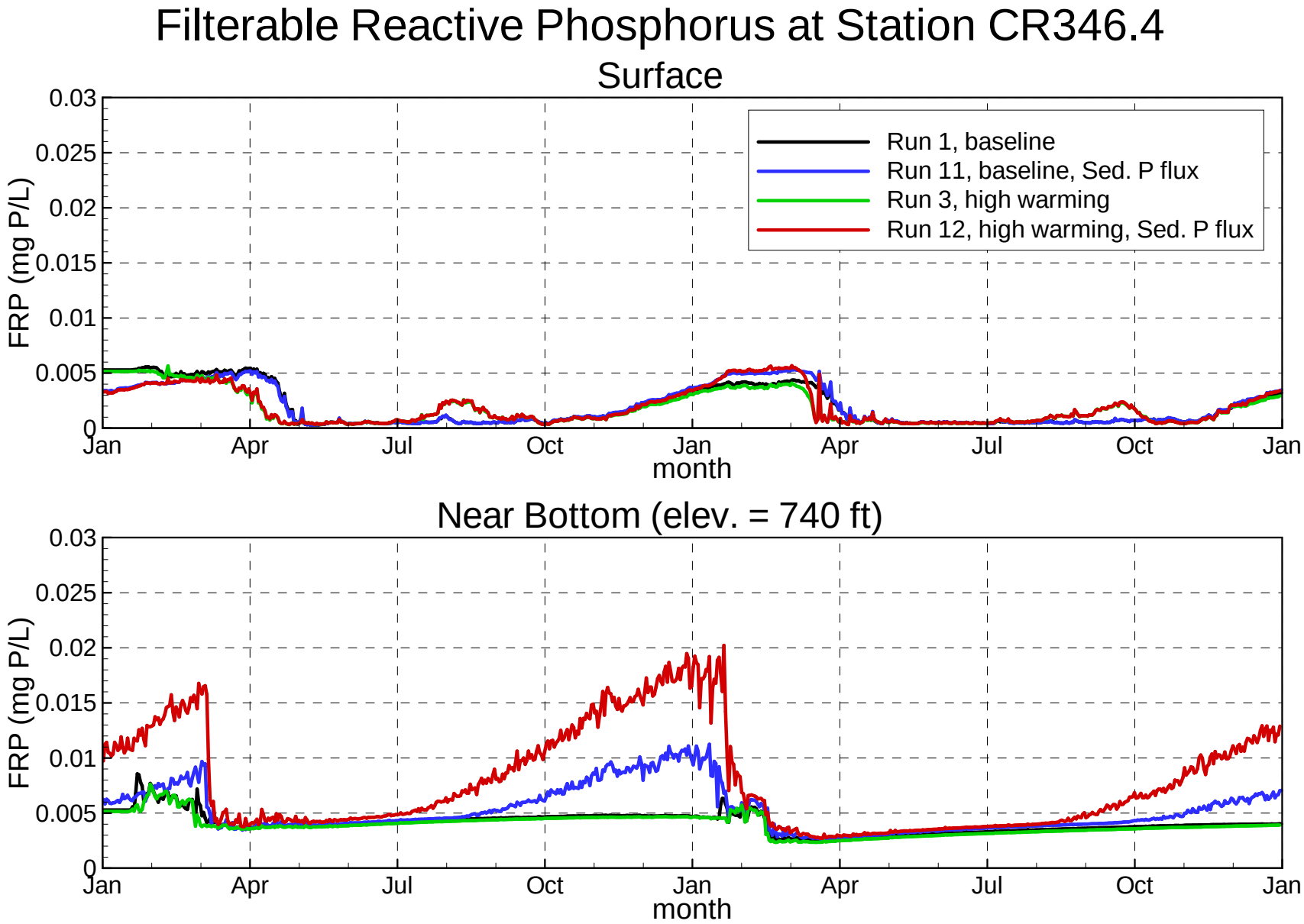

Figure 5.13

FLOW SCIENCE

Chlorophyll a at Station CR394.0

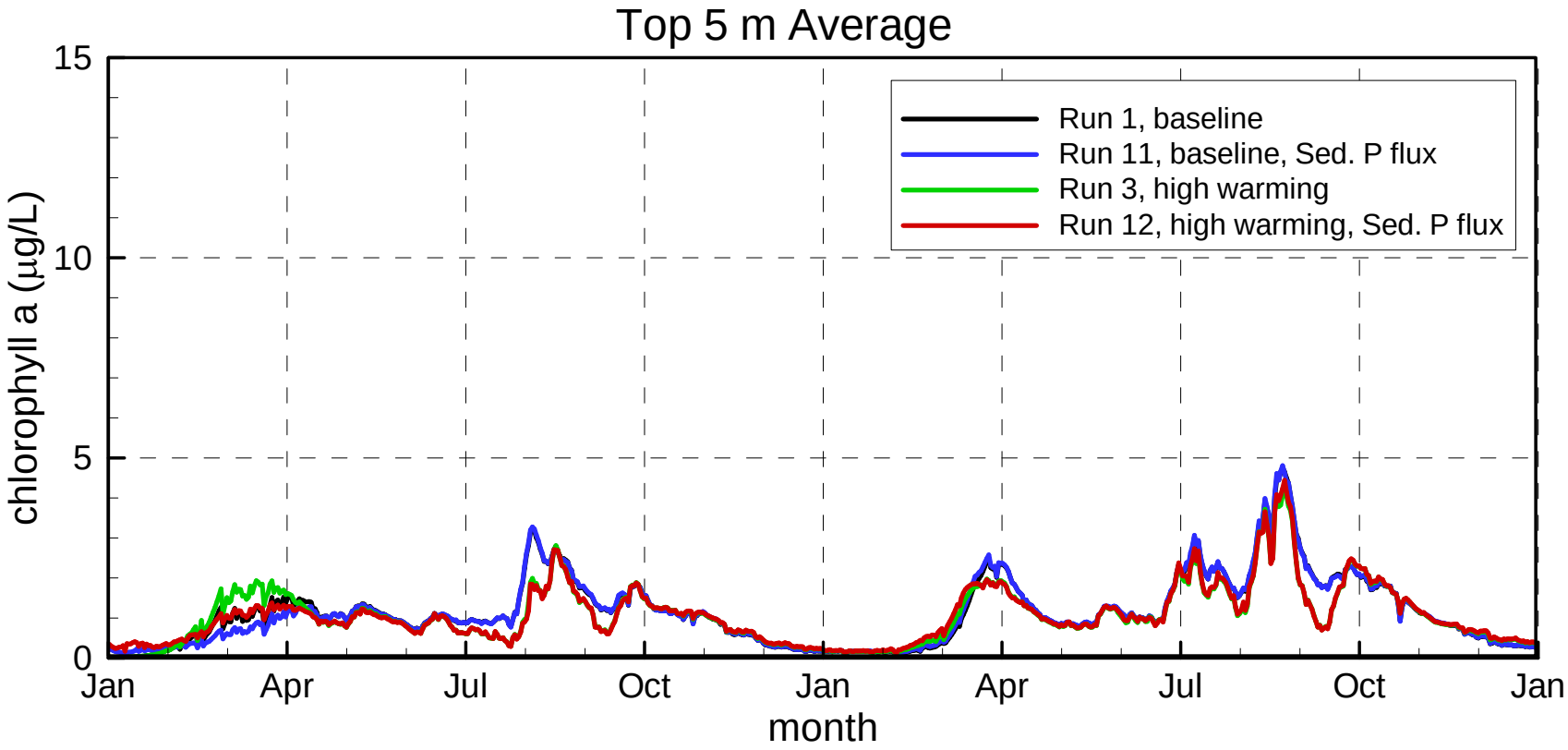

Figure 5.14

Chlorophyll a at Station CR346.4

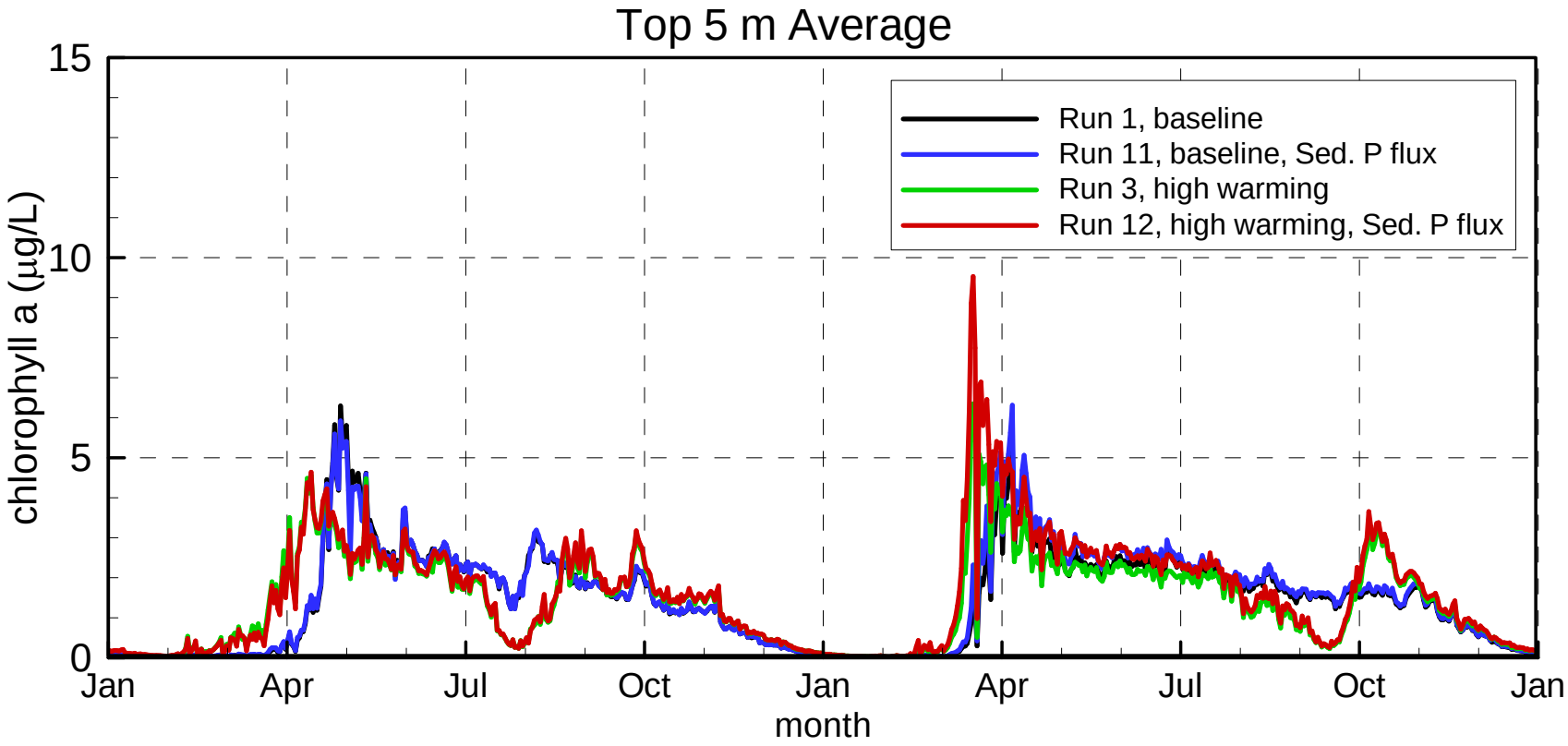

Figure 5.15

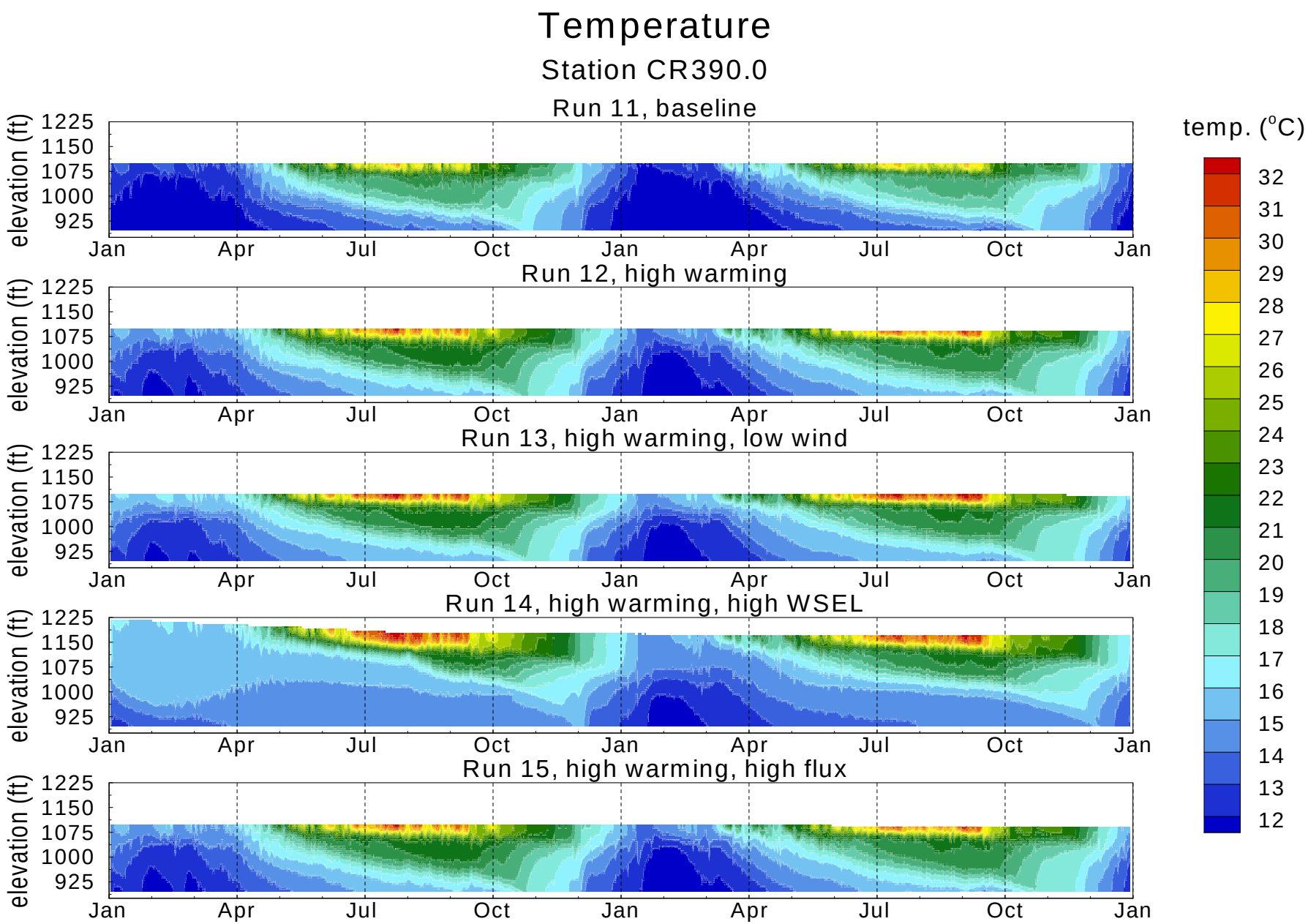

Figure 5.16

FLOW SCIENCE

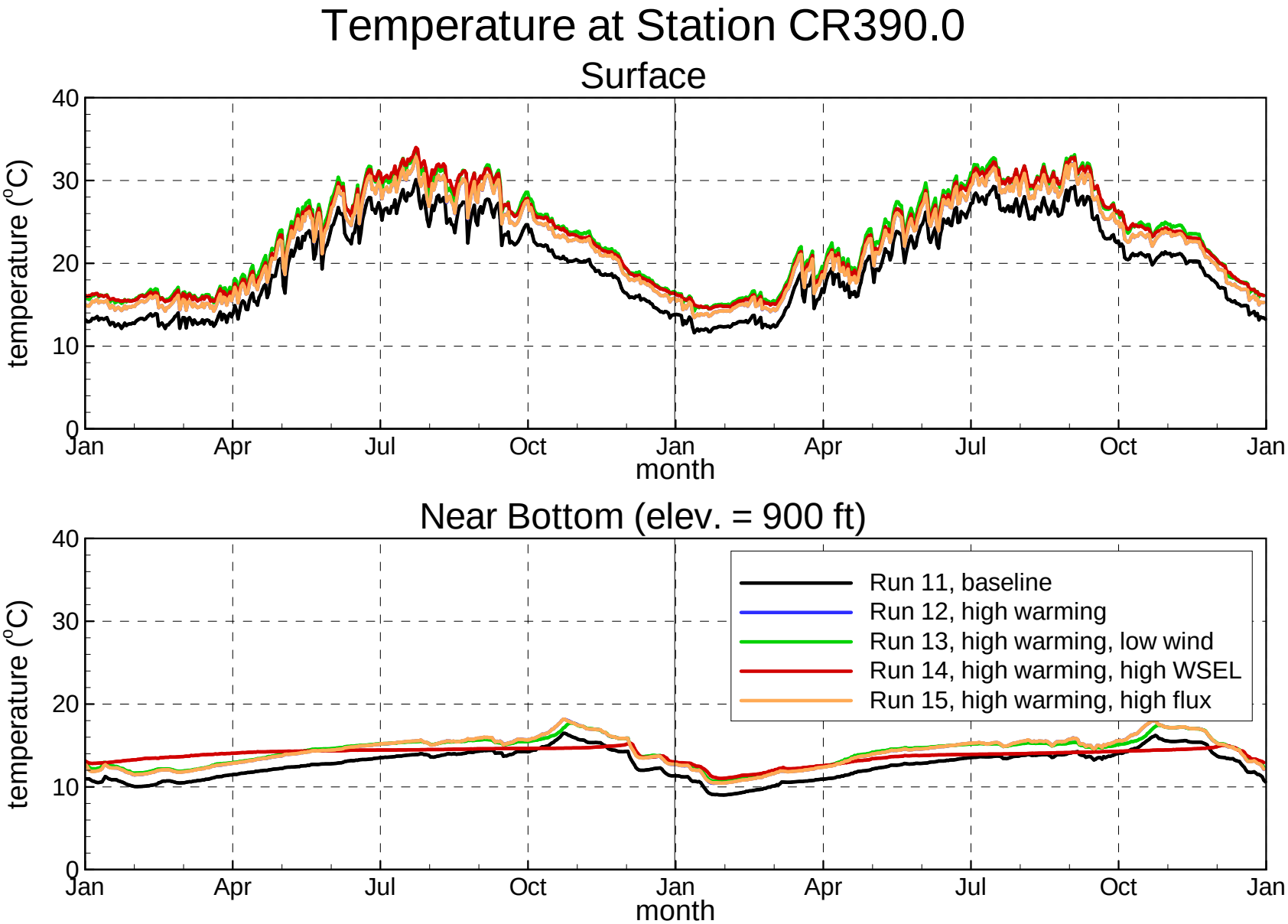
Temperature at Station CR390.0
Surface
temperature (°C)
40
30
20
10
0
Jan
Apr
Jul
Oct
Jan
Apr
Jul
Oct
Jan
month
Near Bottom (elev. = 900 ft)
temperature (°C)
40
30
20
10
0
Jan
Apr
Jul
Oct
Jan
Apr
Jul
Oct
Jan
month
Run 11, baseline
Run 12, high warming
Run 13, high warming, low wind
Run 14, high warming, high WSEL
Run 15, high warming, high flux

Figure 5.17

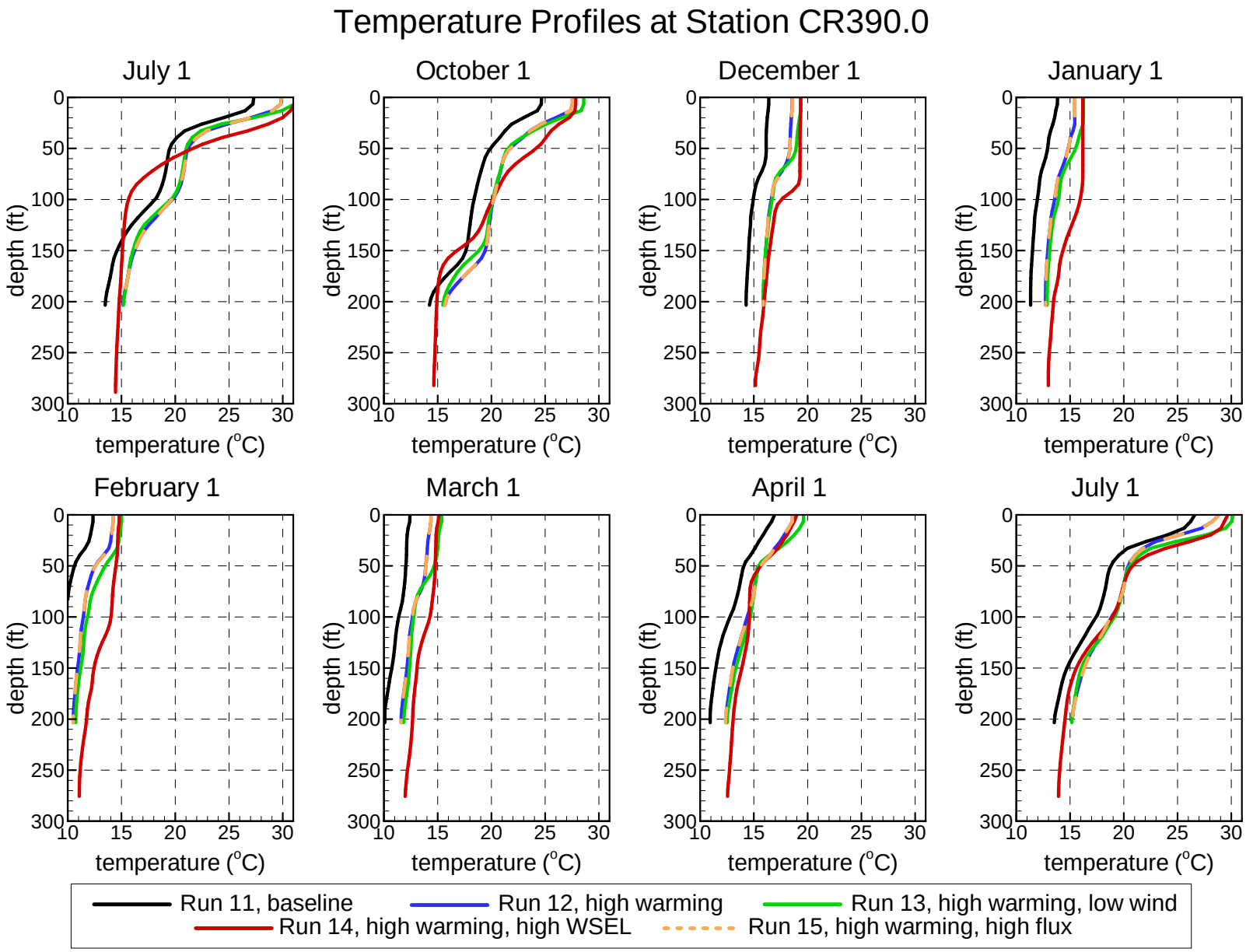

Figure 5.18

FLOW SCIENCE

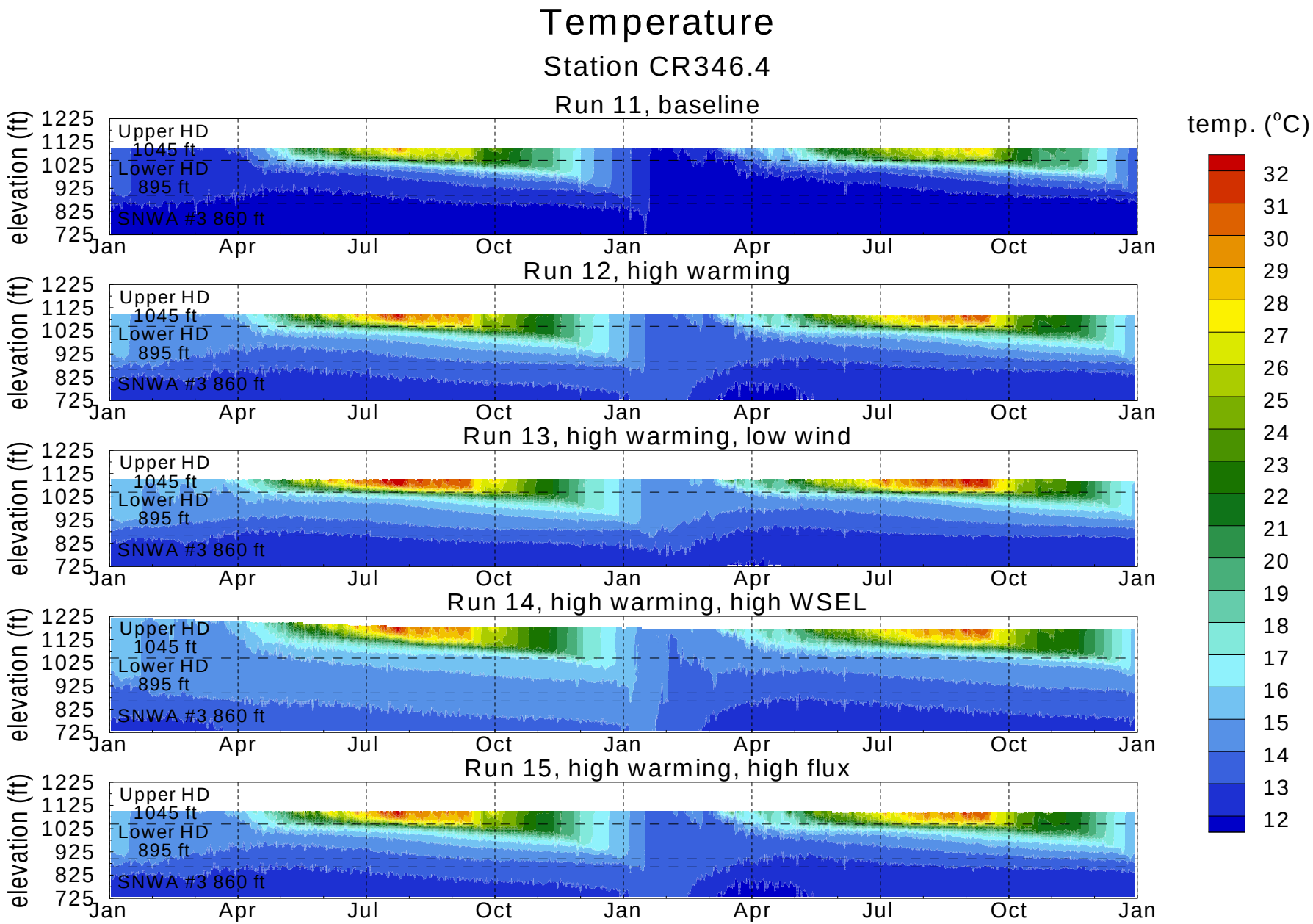
Temperature
Station CR346.4
Run 11, baseline
Run 12, high warming
Run 13, high warming, low wind
Run 14, high warming, high WSEL
Run 15, high warming, high flux
elevation (ft)
1225
1125
1025
925
825
725
Upper HD
1045 ft
Lower HD
895 ft
SNWA #3 860 ft
Jan
Apr
Jul
Oct
Jan
Apr
Jul
Oct
Jan
temp. (°C)
32
31
30
29
28
27
26
25
24
23
22
21
20
19
18
17
16
15
14
13
12

Figure 5.19

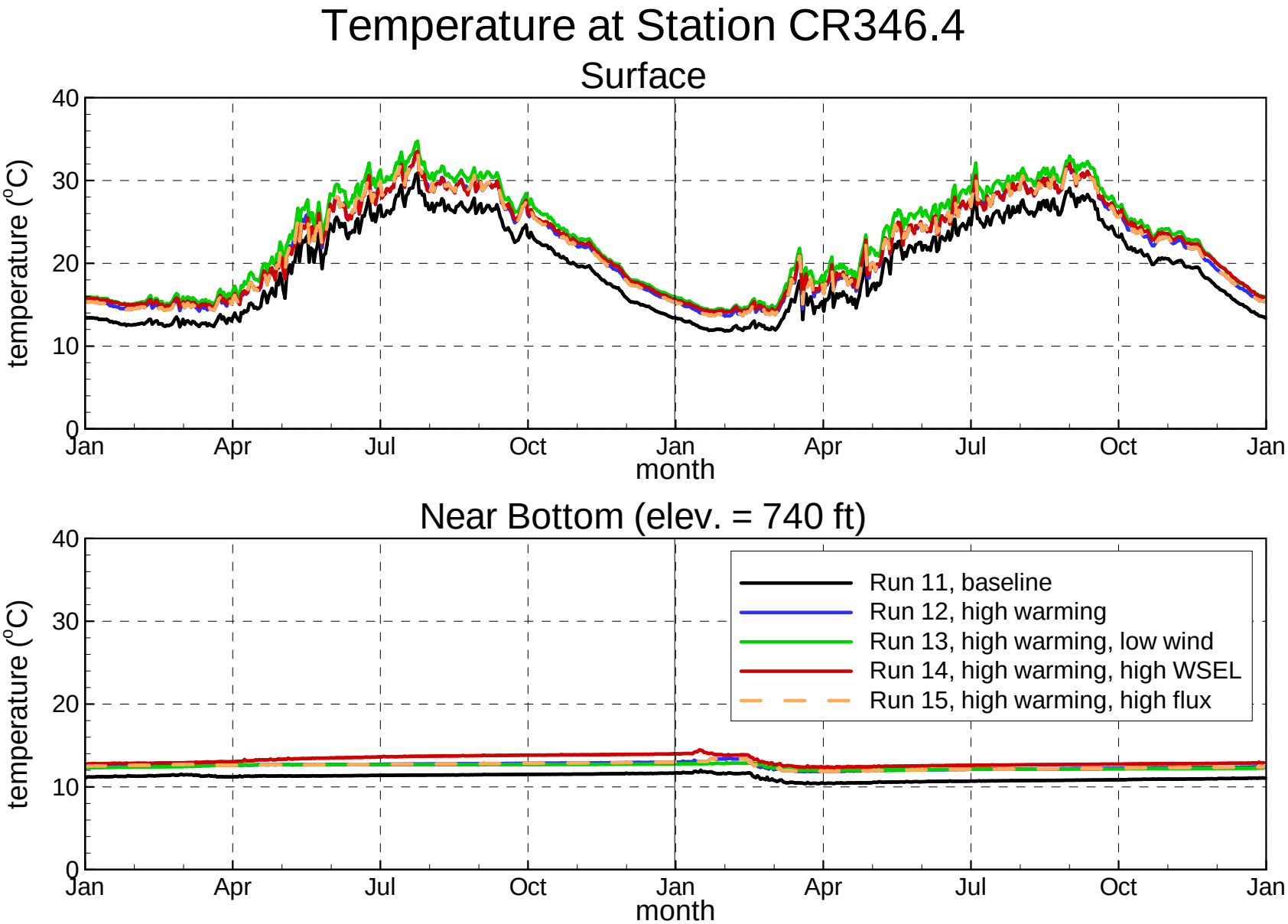
Temperature at Station CR346.4
Surface
temperature (°C)
40
30
20
10
0
Jan
Apr
Jul
Oct
Jan
Apr
Jul
Oct
Jan
month
Near Bottom (elev. = 740 ft)
temperature (°C)
40
30
20
10
0
Jan
Apr
Jul
Oct
Jan
Apr
Jul
Oct
Jan
month
Run 11, baseline
Run 12, high warming
Run 13, high warming, low wind
Run 14, high warming, high WSEL
Run 15, high warming, high flux

Figure 5.20

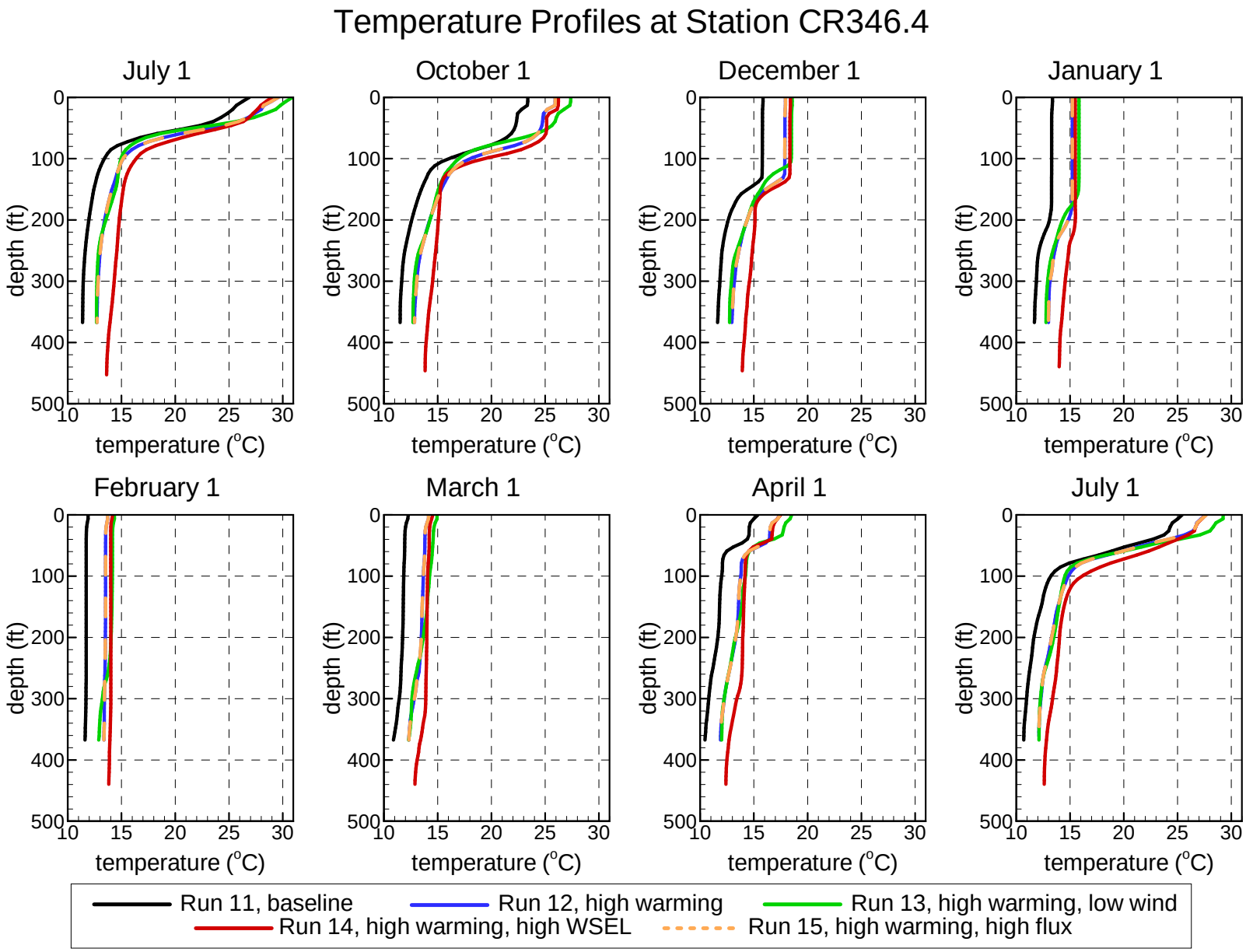

Figure 5.21

FLOW SCIENCE

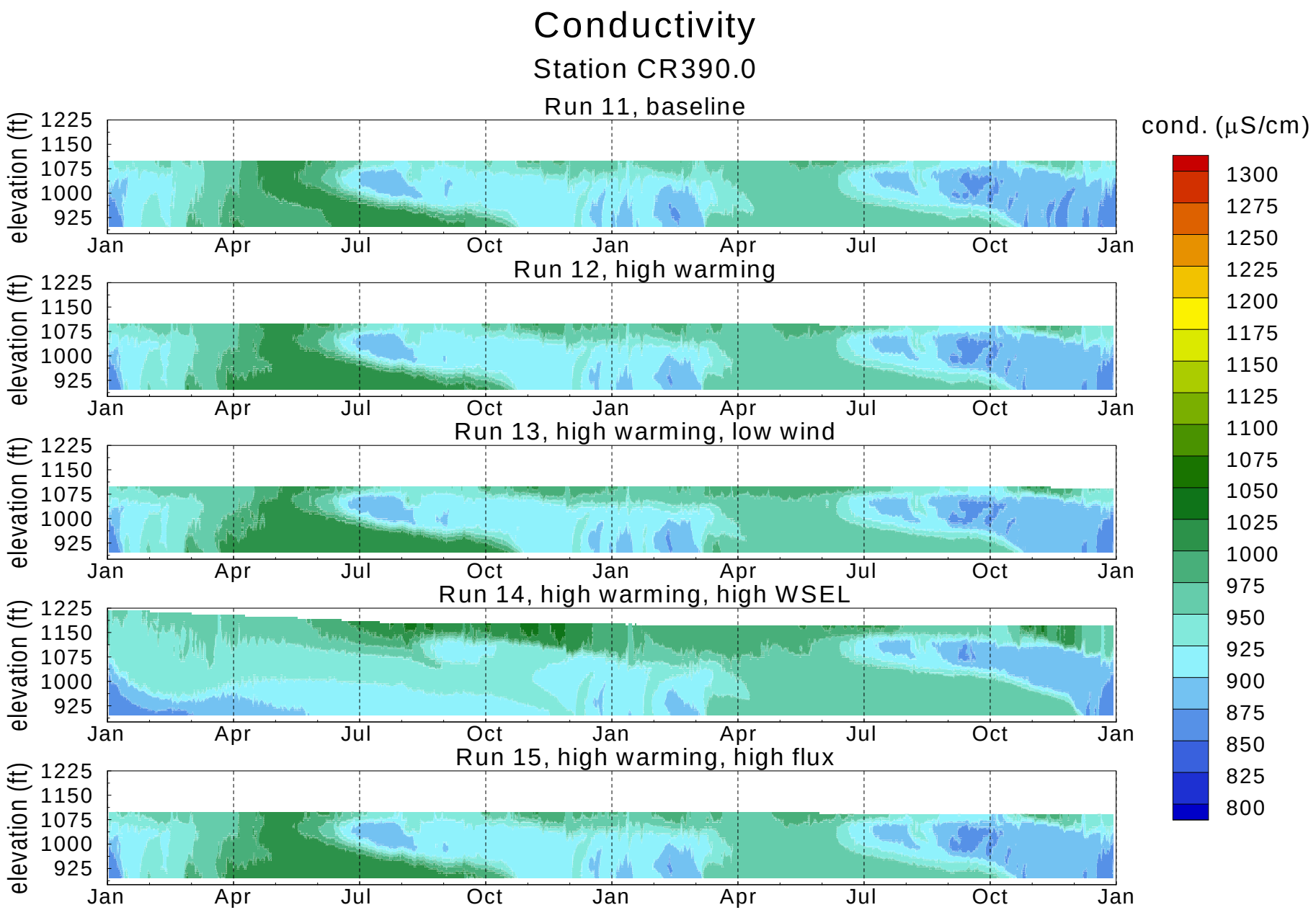
Conductivity
Station CR390.0
Run 11, baseline
Run 12, high warming
Run 13, high warming, low wind
Run 14, high warming, high WSEL
Run 15, high warming, high flux
elevation (ft)
1225
1150
1075
1000
925
Jan
Apr
Jul
Oct
Jan
Apr
Jul
Oct
Jan
cond. (µS/cm)
1300
1275
1250
1225
1200
1175
1150
1125
1100
1075
1050
1025
1000
975
950
925
900
875
850
825
800

Figure 5.22

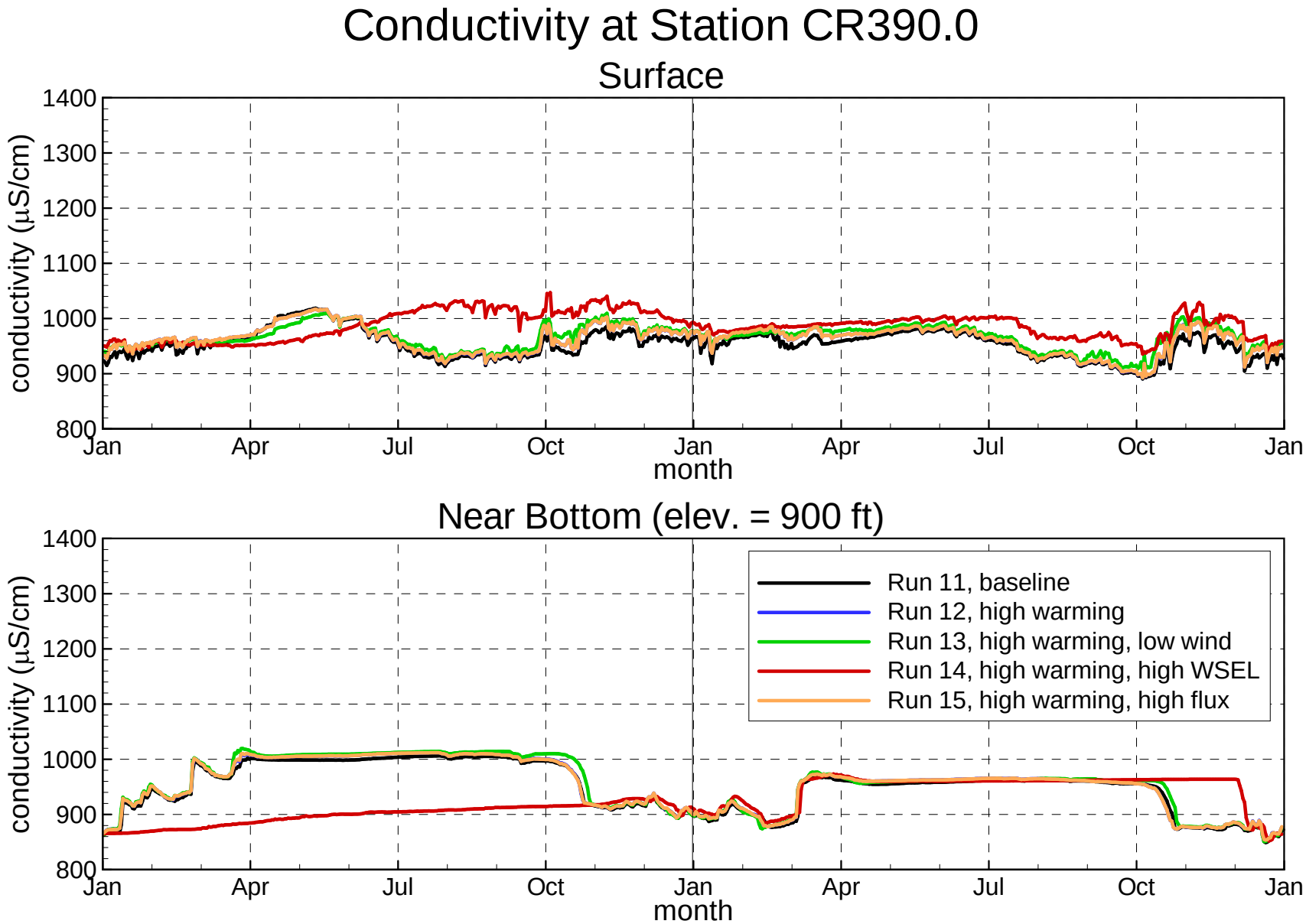

Figure 5.23

FLOW SCIENCE

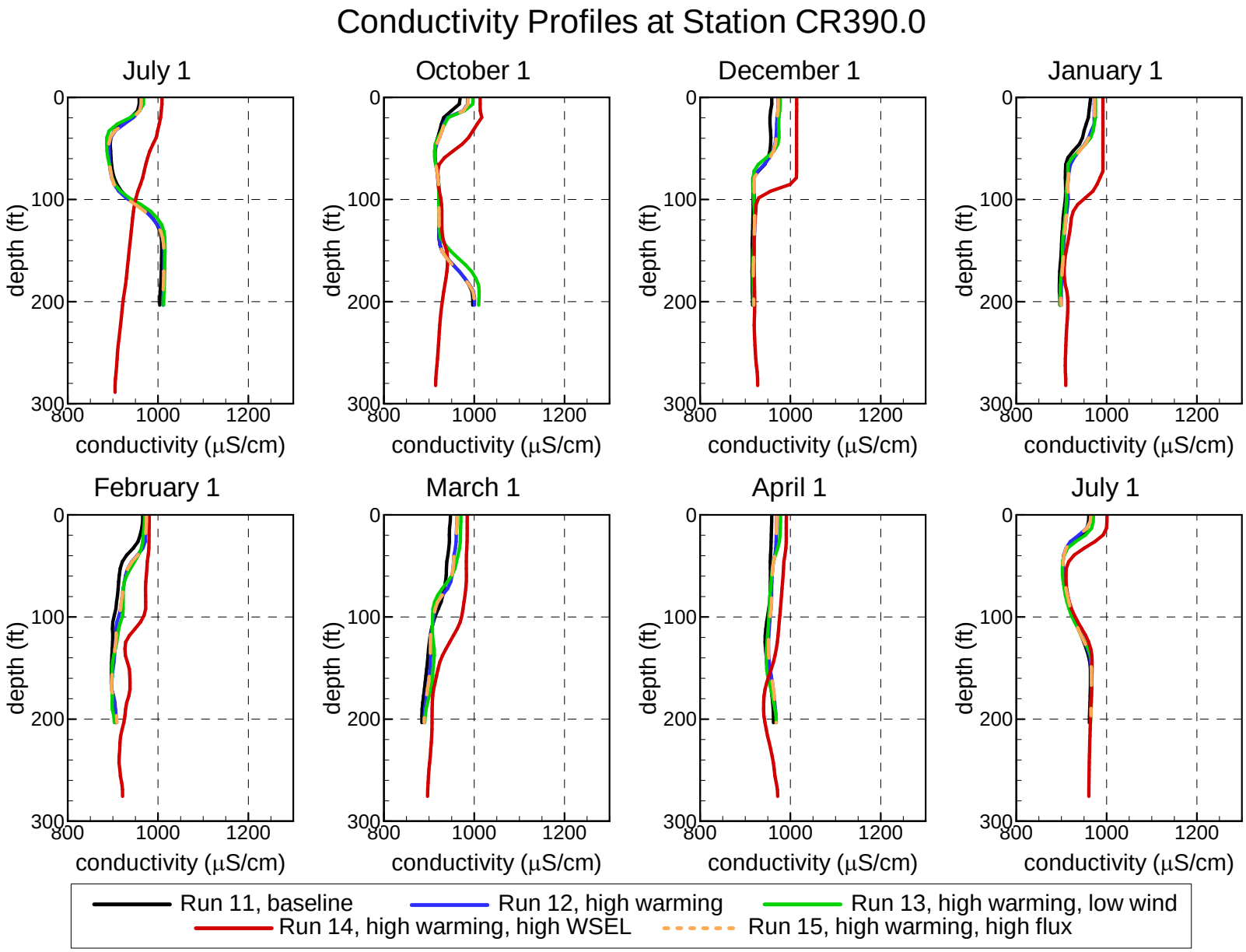

Figure 5.24

FLOW SCIENCE

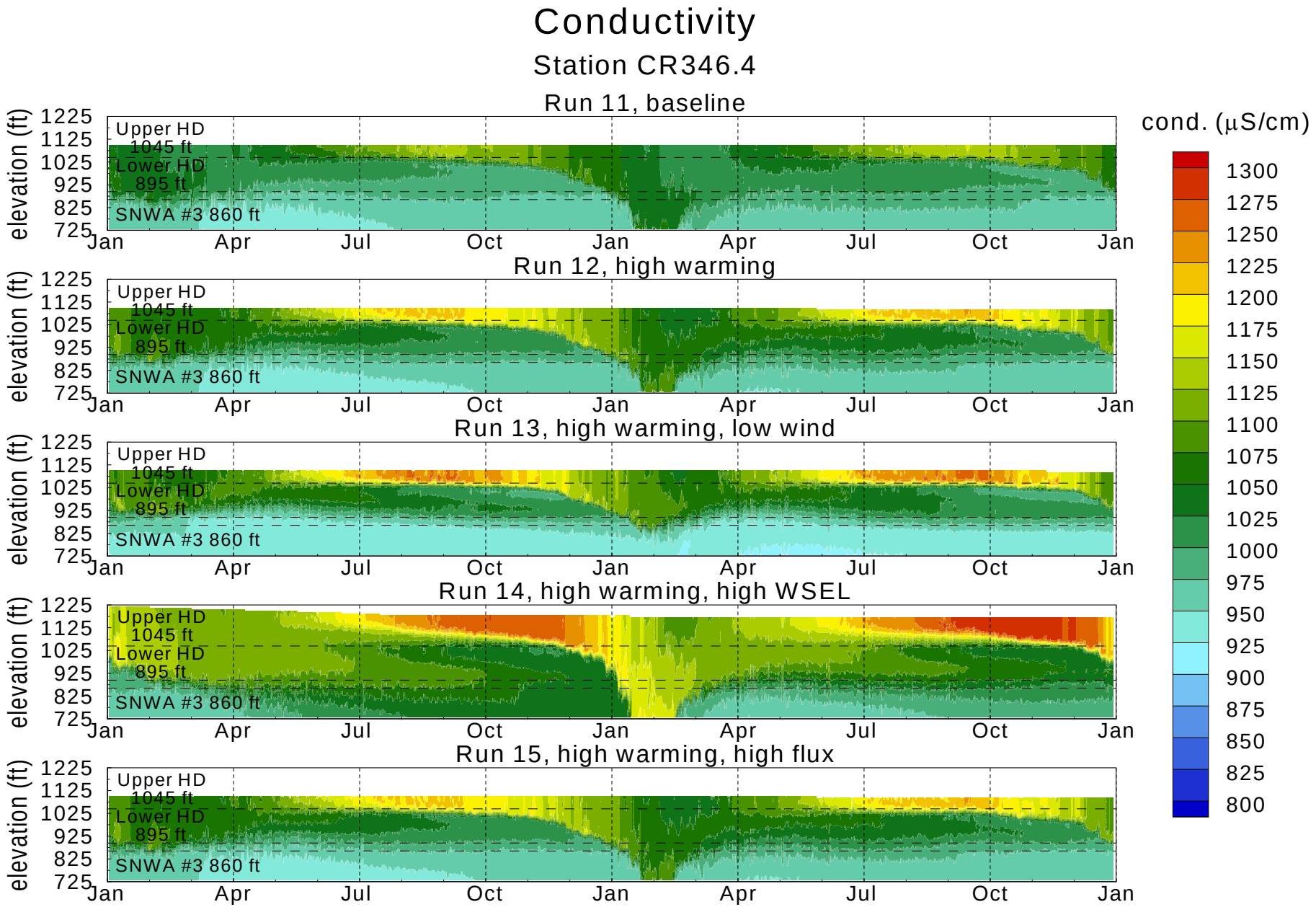

Figure 5.25

FLOW SCIENCE

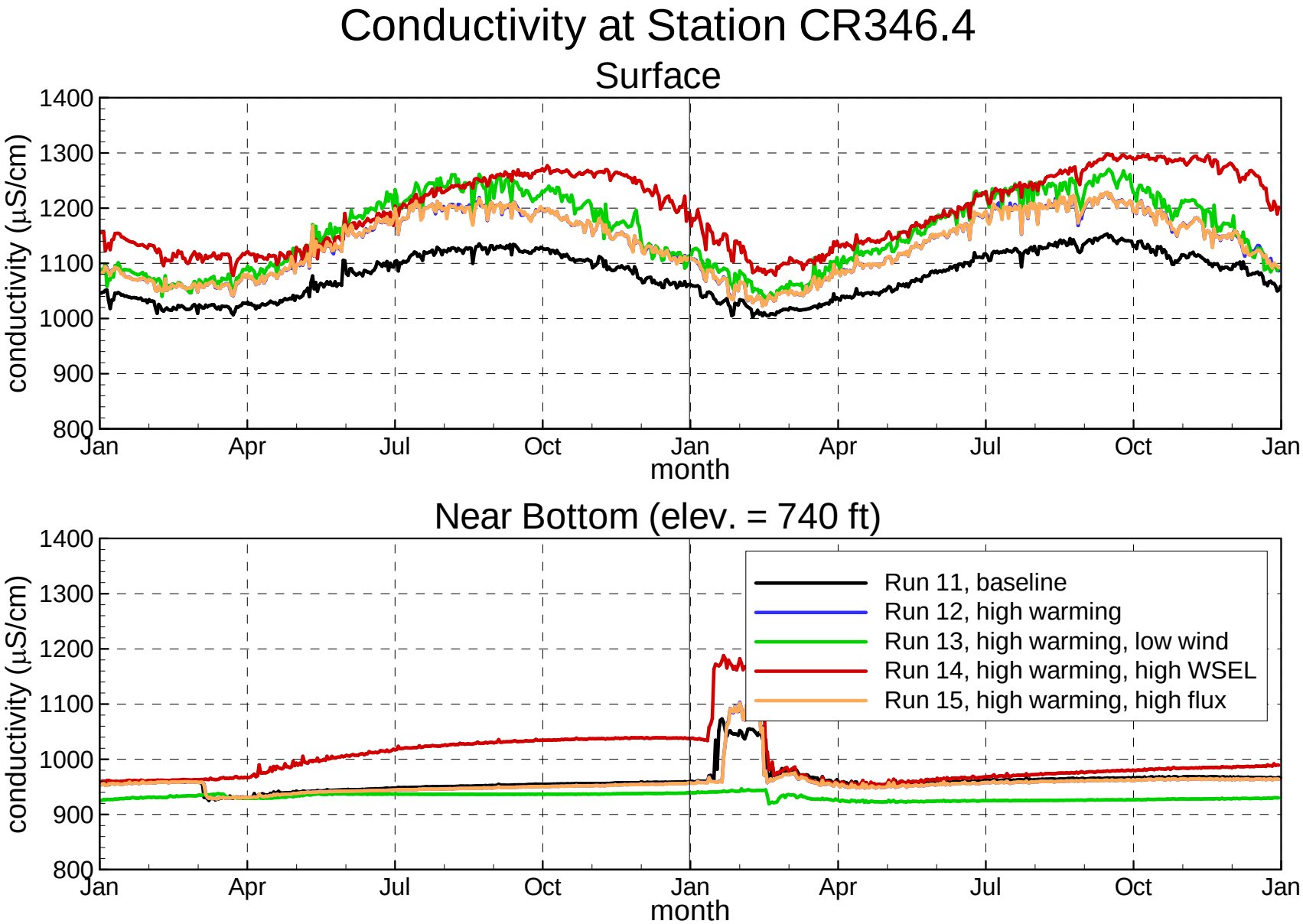

Figure 5.26

FLOW SCIENCE

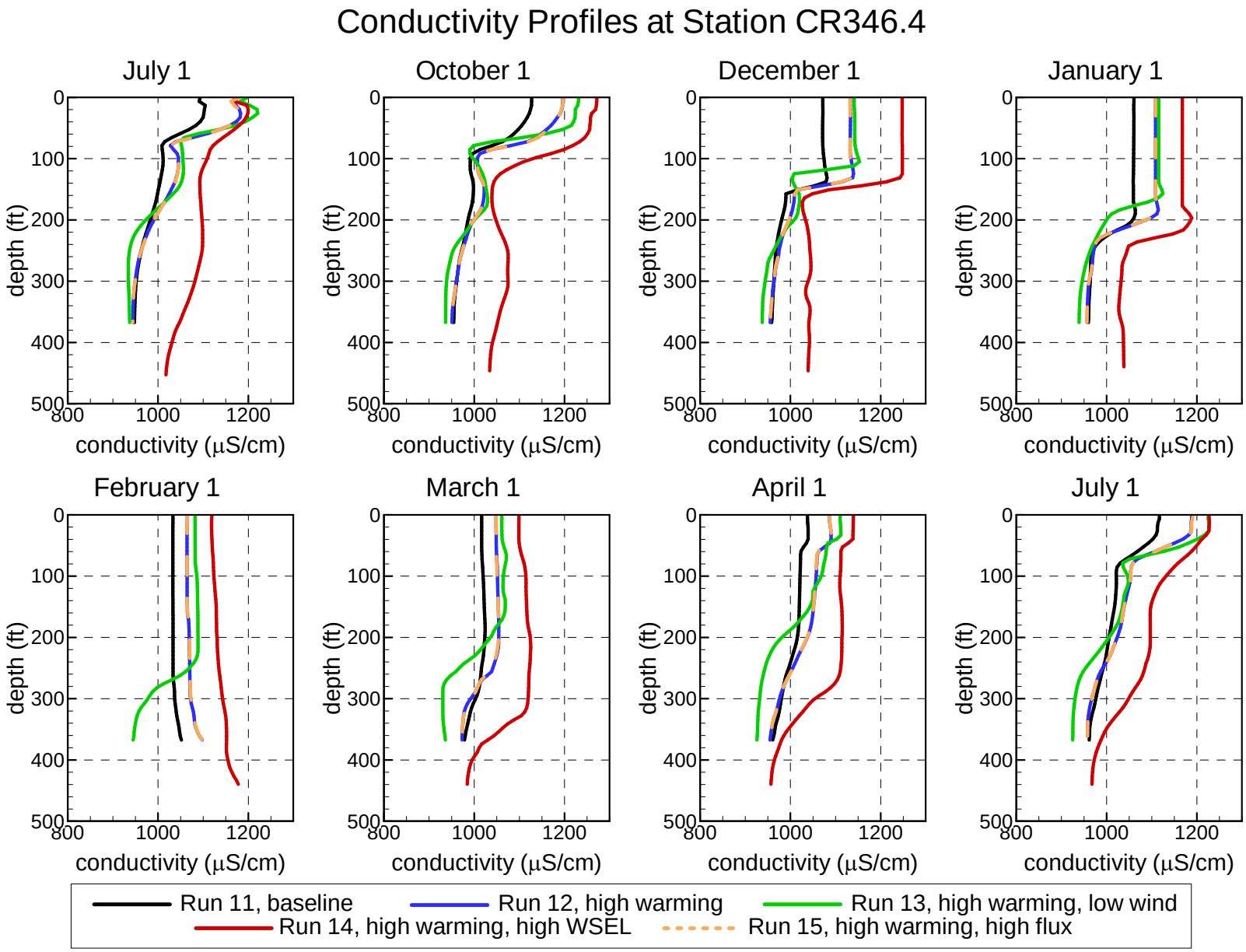

Figure 5.27

FLOW SCIENCE

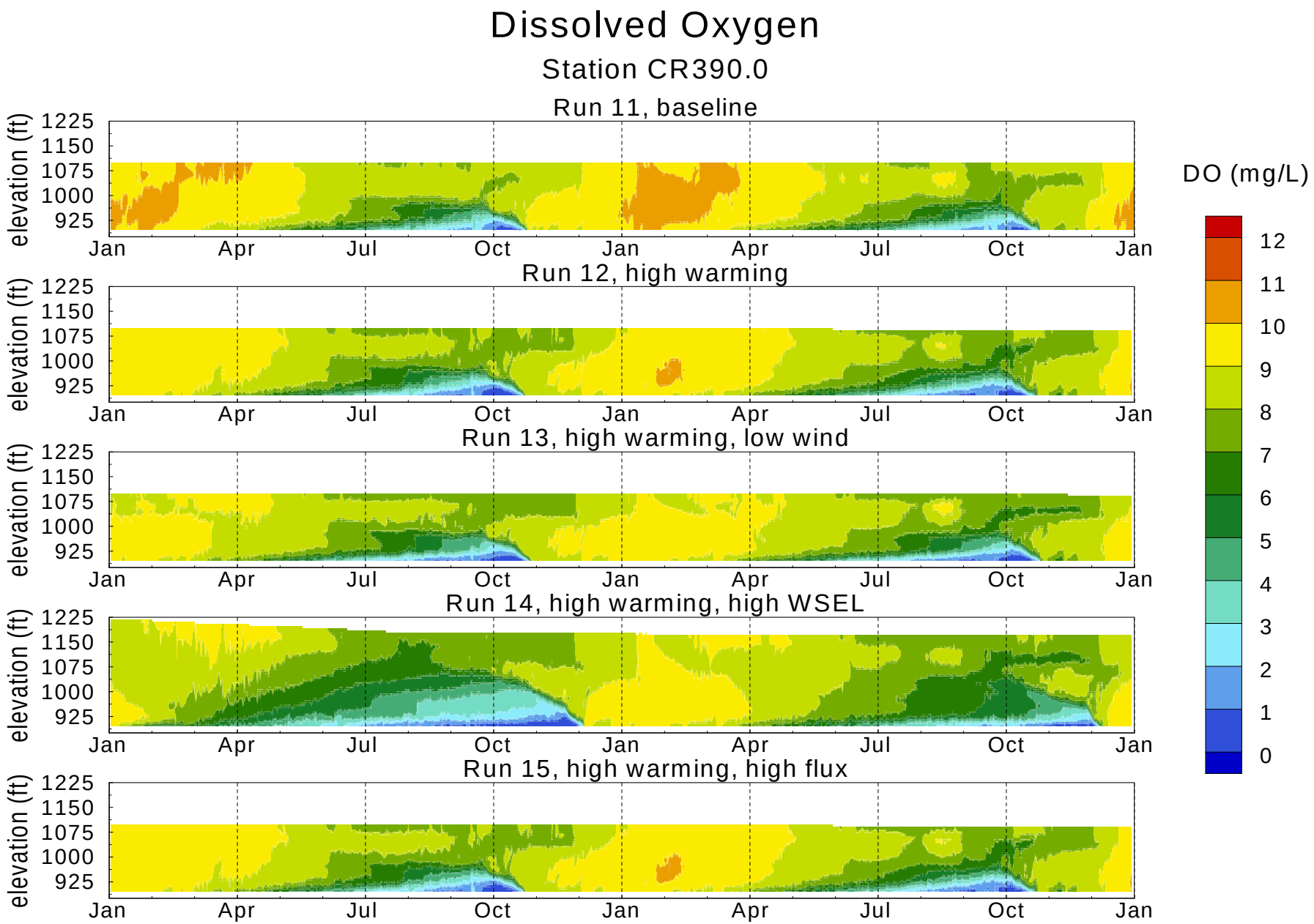

Figure 5.28

FLOW SCIENCE

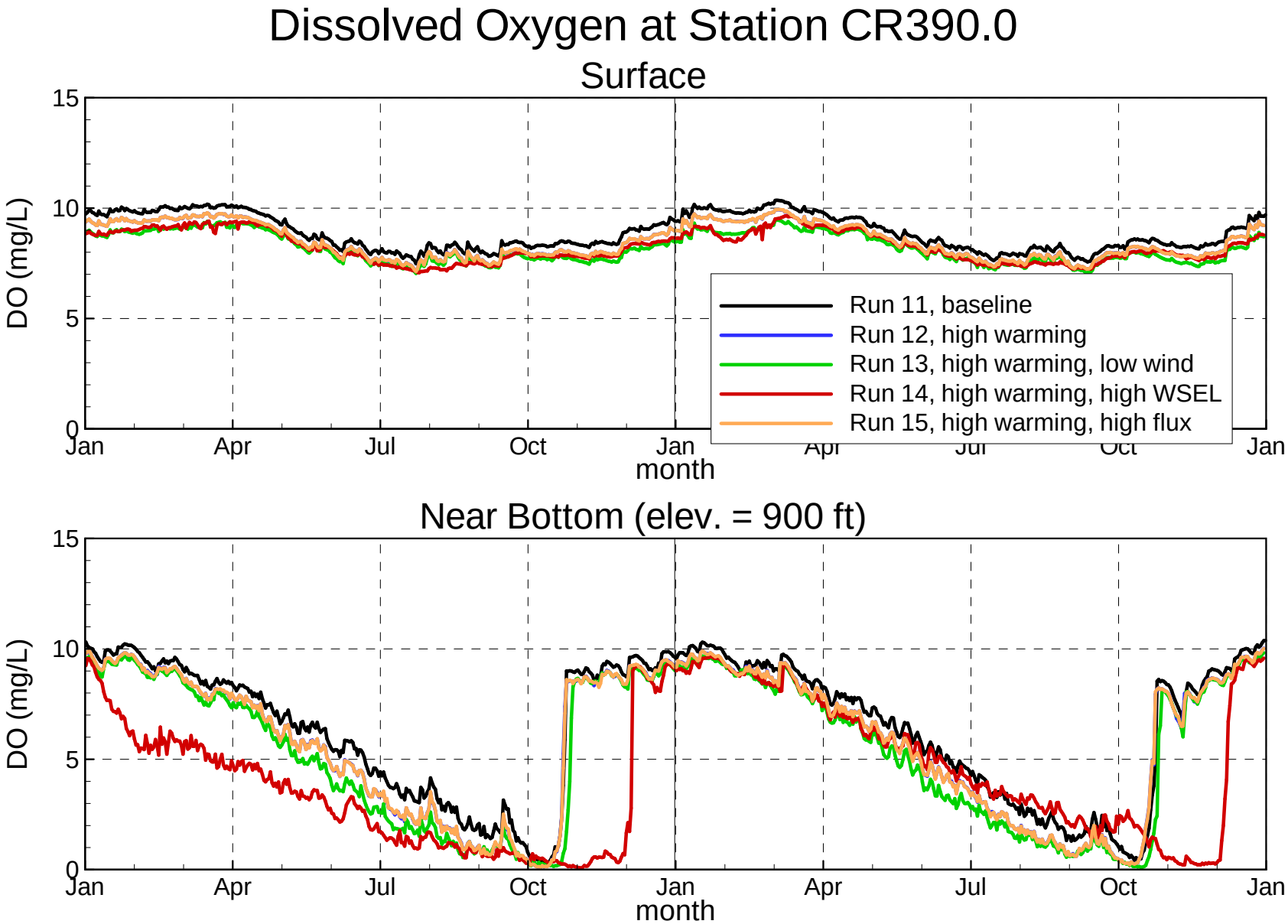
Dissolved Oxygen at Station CR390.0
Surface
DO (mg/L)
15
10
5
0
Jan
Apr
Jul
Oct
Jan
month
Run 11, baseline
Run 12, high warming
Run 13, high warming, low wind
Run 14, high warming, high WSEL
Run 15, high warming, high flux
Near Bottom (elev. = 900 ft)
DO (mg/L)
15
10
5
0
Jan
Apr
Jul
Oct
Jan
month
Apr
Jul
Oct
Jan

Figure 5.29

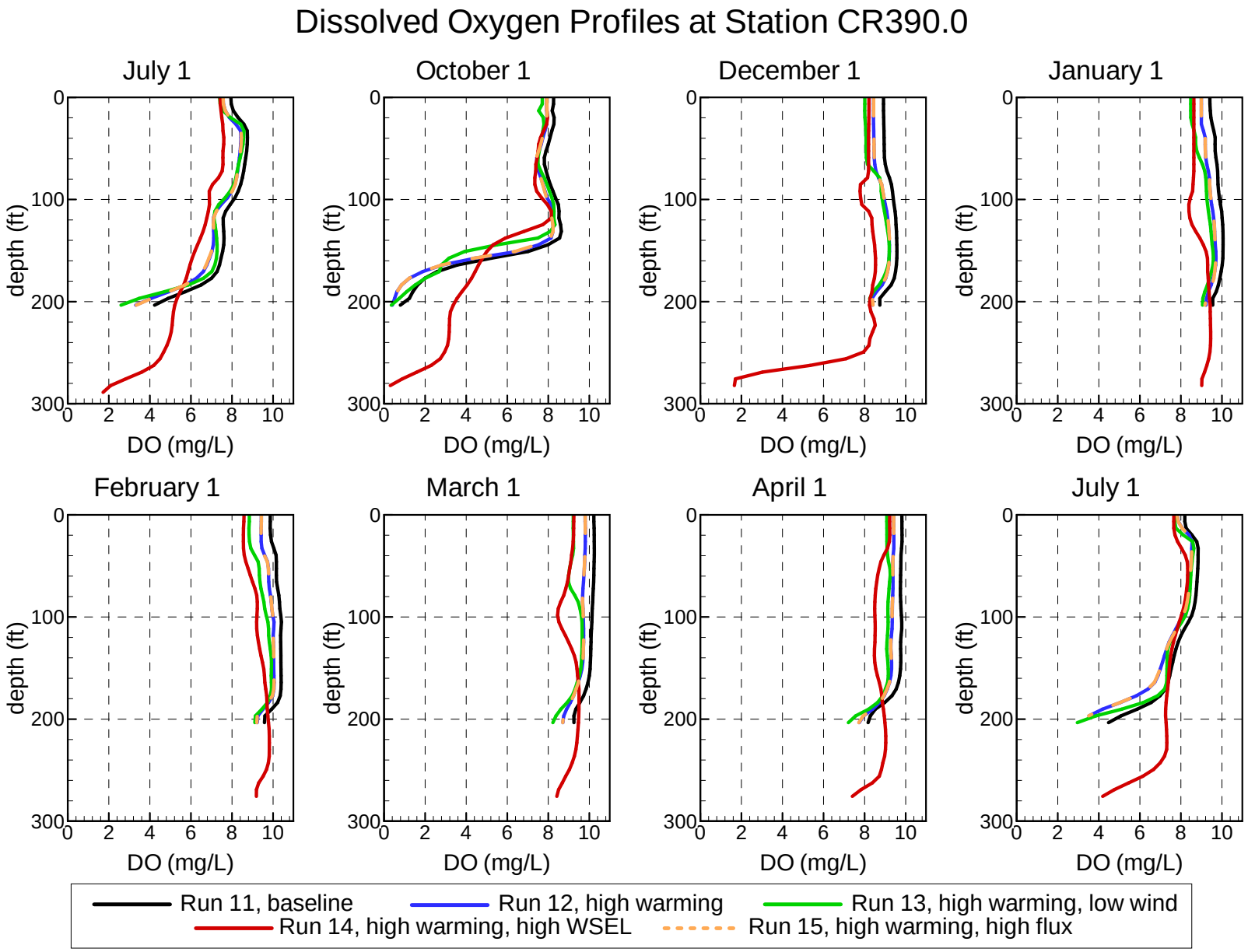

Figure 5.30

FLOW SCIENCE

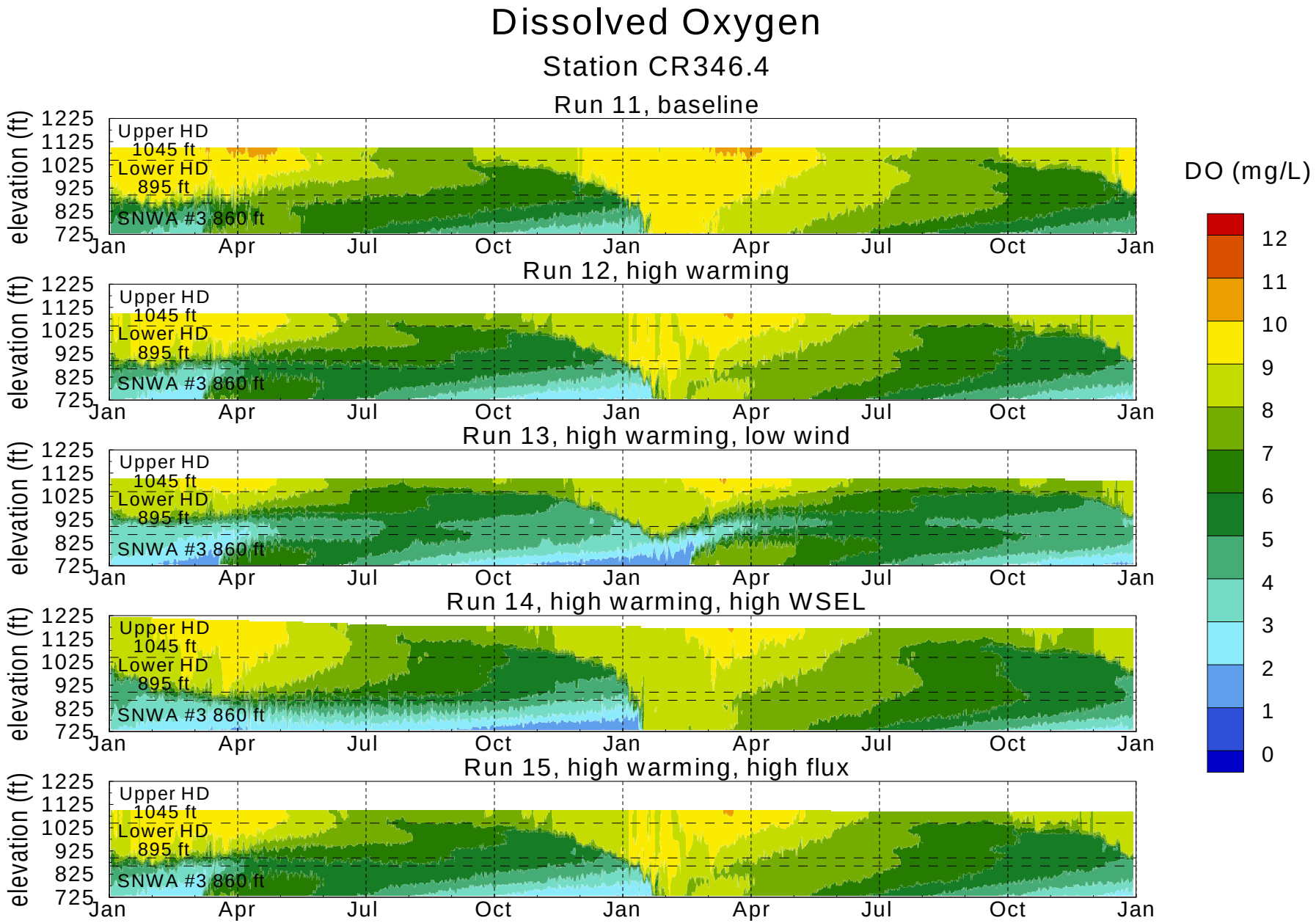

Figure 5.31

FLOW SCIENCE

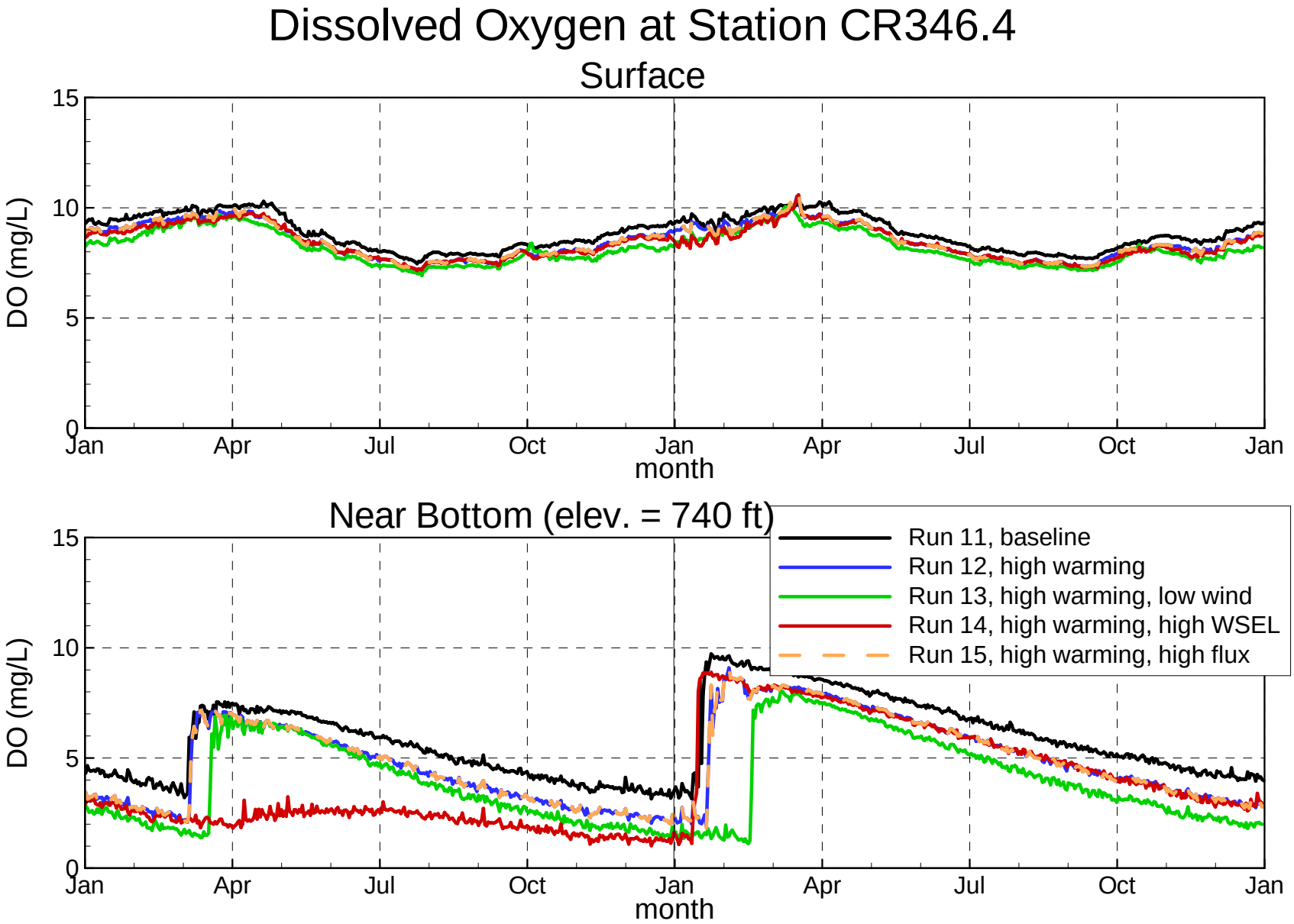

Figure 5.32

FLOW SCIENCE

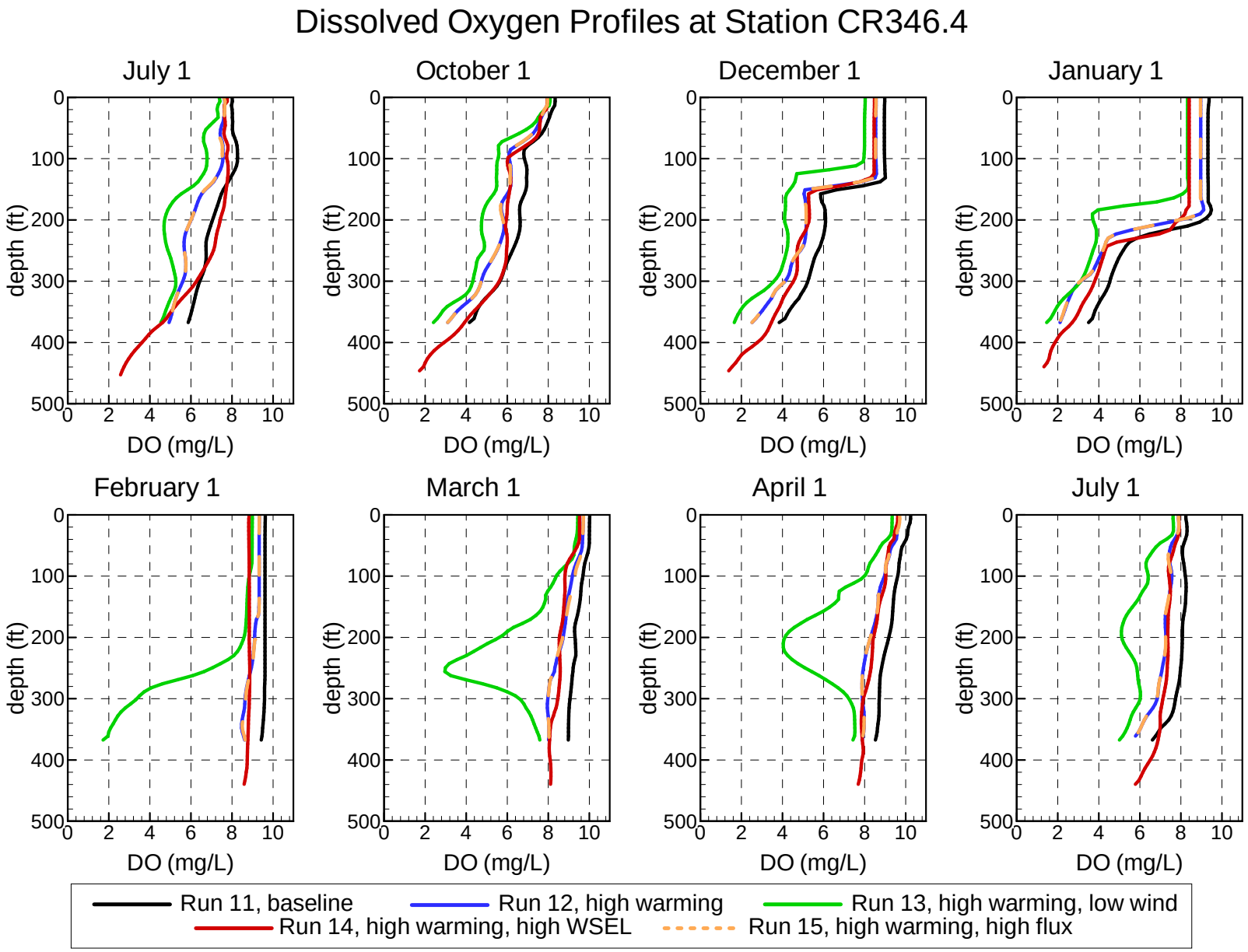

Figure 5.33

FLOW SCIENCE

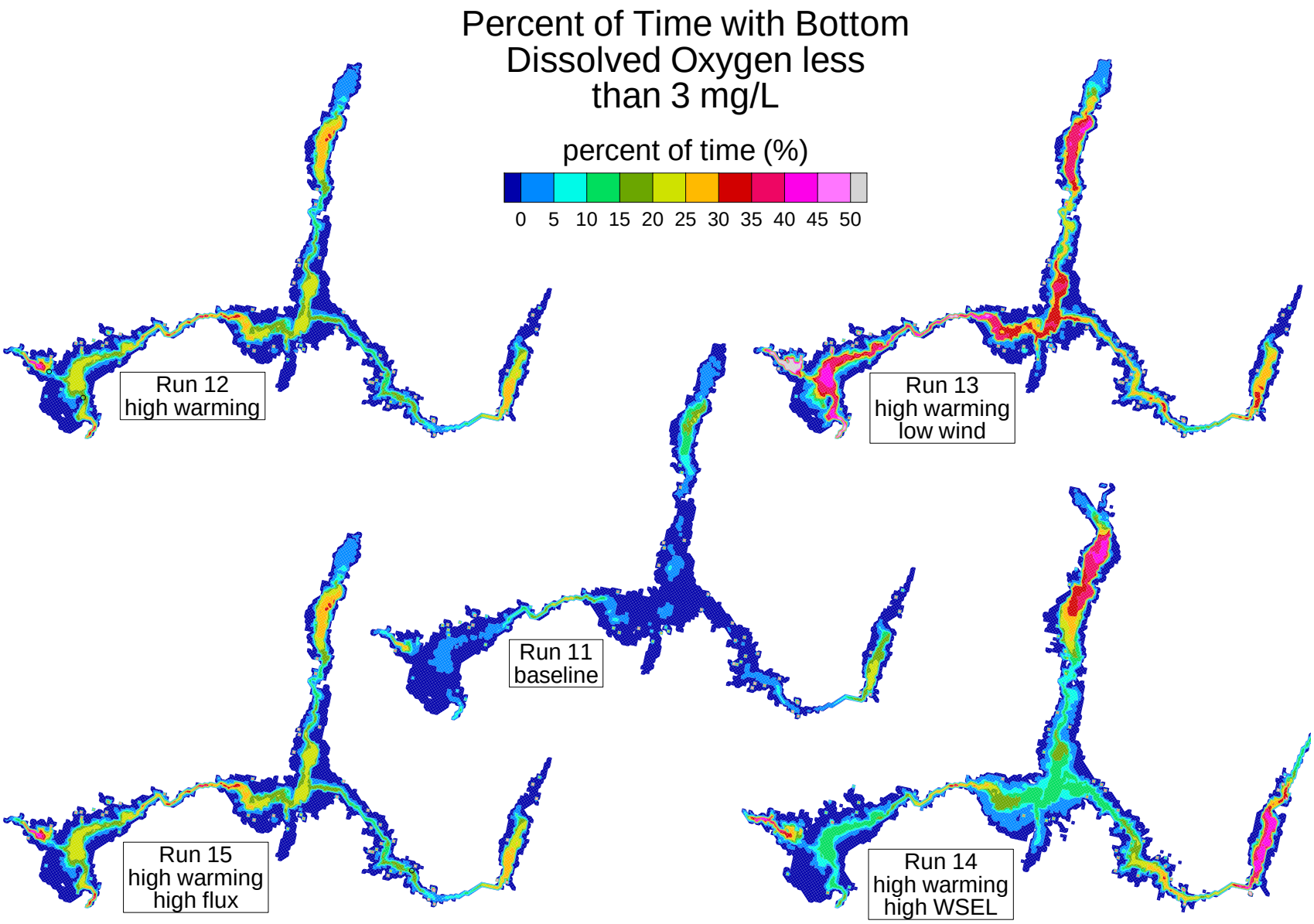
Percent of Time with Bottom Dissolved Oxygen less than 3 mg/L
percent of time (%)
0 5 10 15 20 25 30 35 40 45 50
Run 12
high warming
Run 13
high warming
low wind
Run 11
baseline
Run 15
high warming
high flux
Run 14
high warming
high WSEL

Figure 5.34

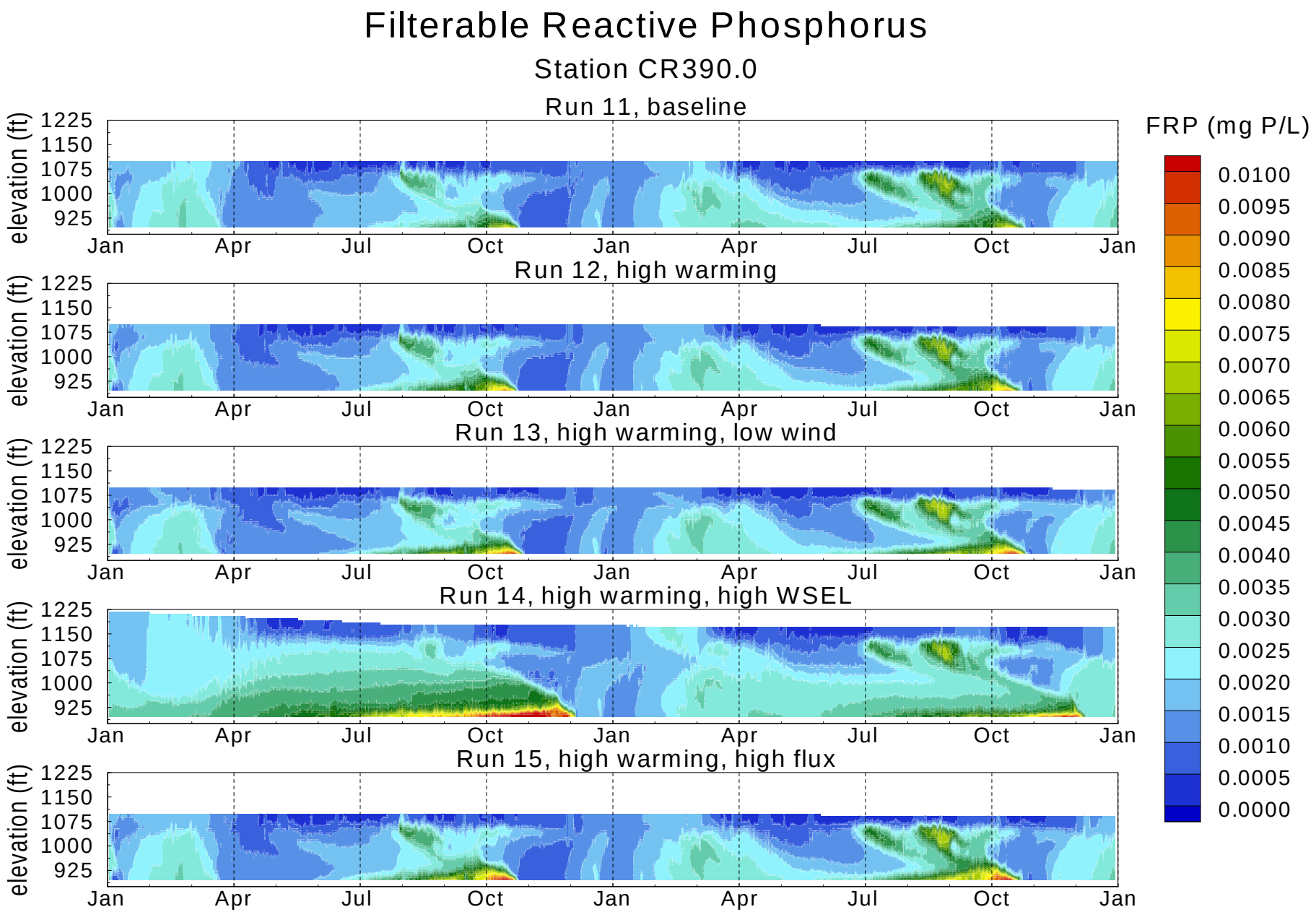
Filterable Reactive Phosphorus
Station CR390.0
Run 11, baseline
Run 12, high warming
Run 13, high warming, low wind
Run 14, high warming, high WSEL
Run 15, high warming, high flux
elevation (ft)
1225
1150
1075
1000
925
Jan
Apr
Jul
Oct
Jan
Apr
Jul
Oct
Jan
FRP (mg P/L)
0.0100
0.0095
0.0090
0.0085
0.0080
0.0075
0.0070
0.0065
0.0060
0.0055
0.0050
0.0045
0.0040
0.0035
0.0030
0.0025
0.0020
0.0015
0.0010
0.0005
0.0000

Figure 5.35

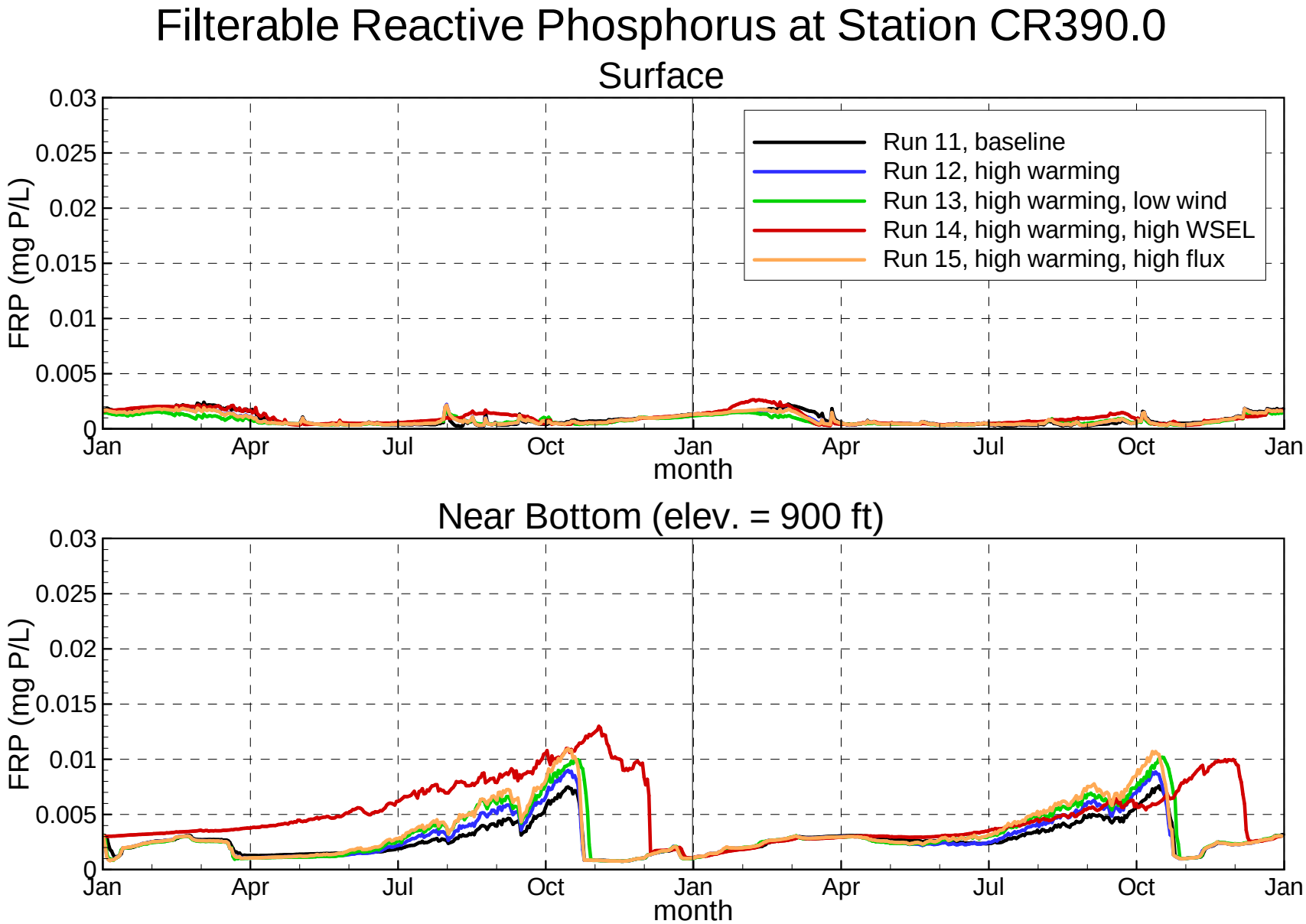

Figure 5.36

FLOW SCIENCE

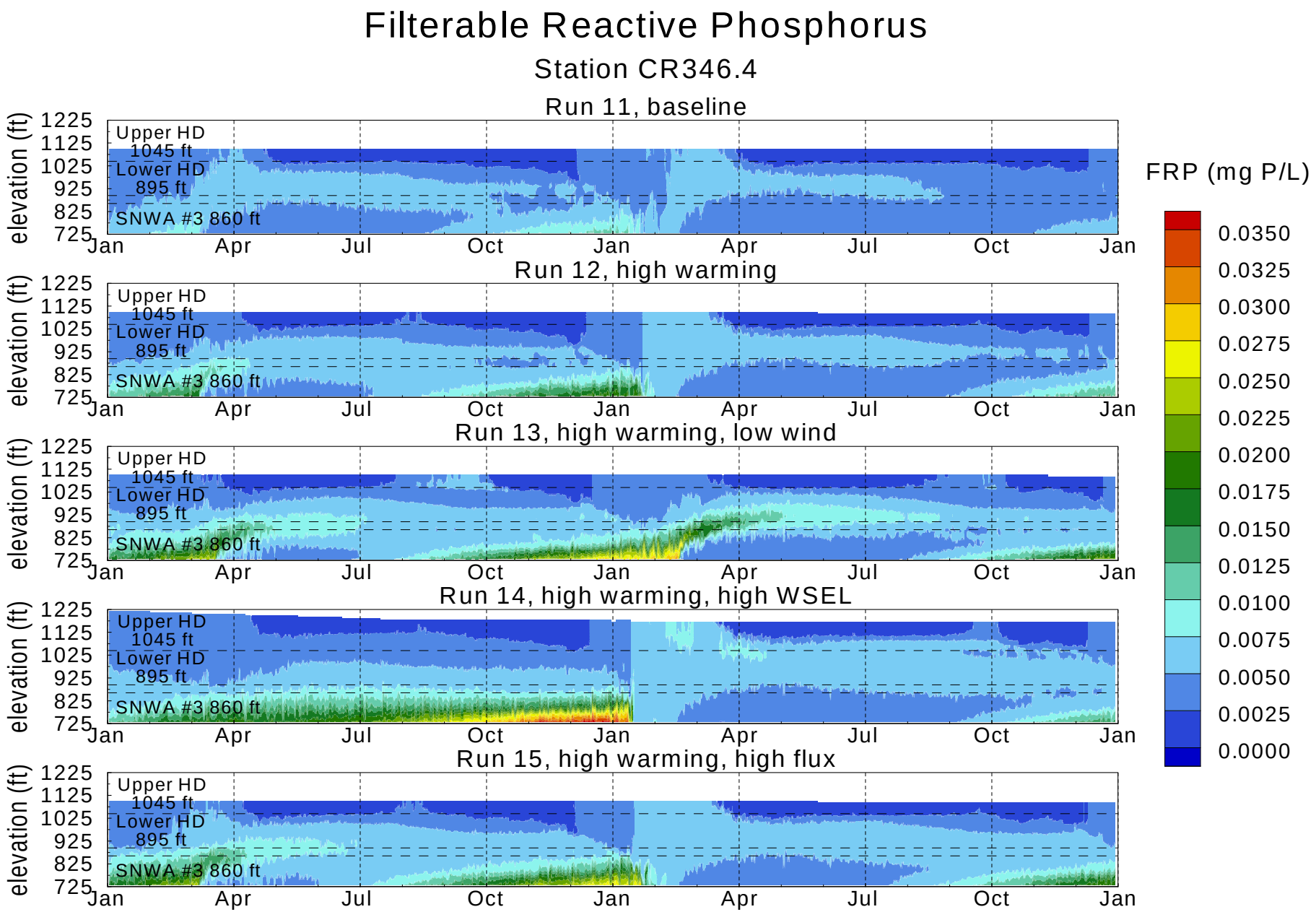

Figure 5.37

FLOW SCIENCE

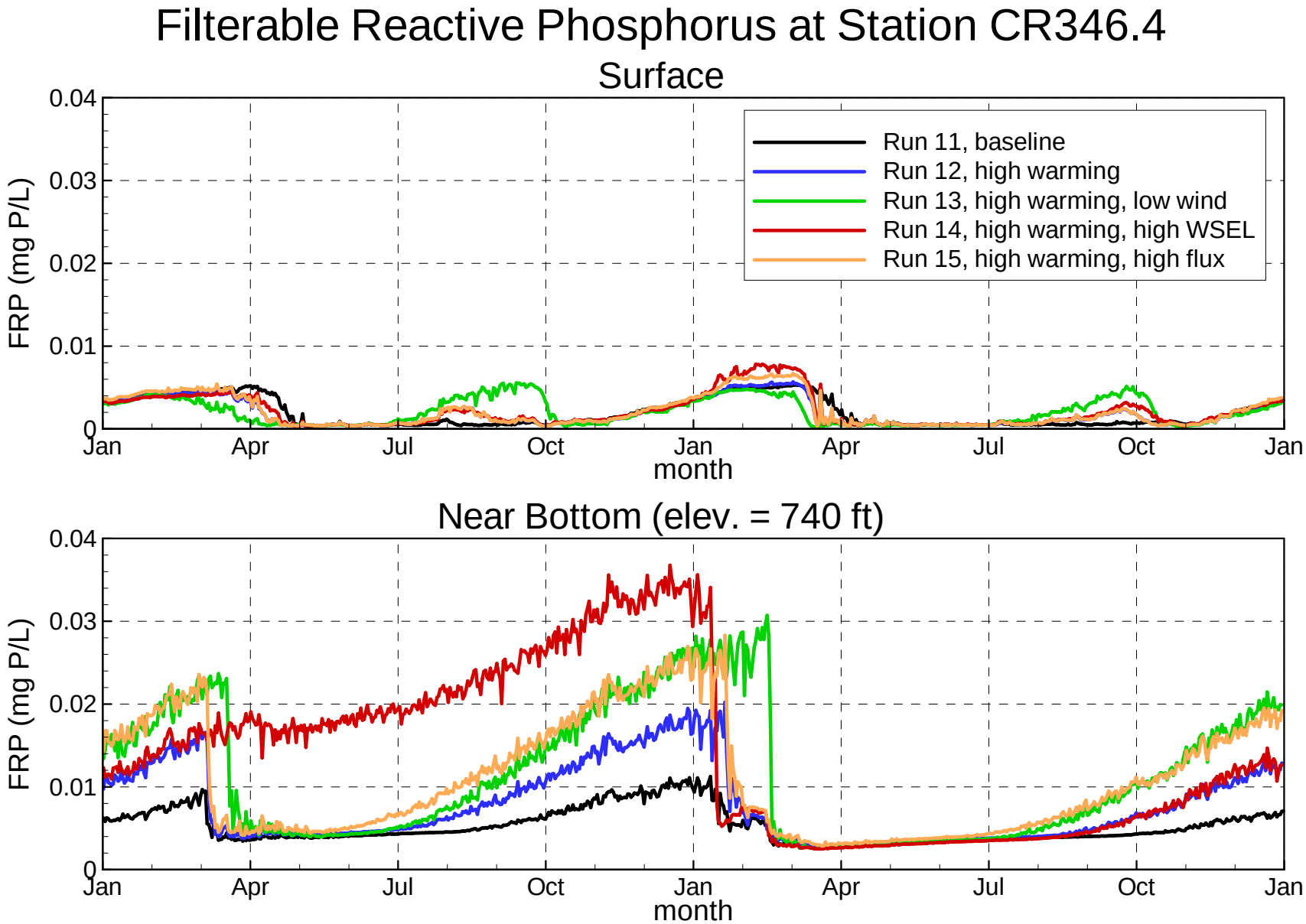
Filterable Reactive Phosphorus at Station CR346.4
Surface
Run 11, baseline
Run 12, high warming
Run 13, high warming, low wind
Run 14, high warming, high WSEL
Run 15, high warming, high flux
FRP (mg P/L)
0.04
0.03
0.02
0.01
0
Jan
Apr
Jul
Oct
Jan
Apr
Jul
Oct
Jan
month
Near Bottom (elev. = 740 ft)
FRP (mg P/L)
0.04
0.03
0.02
0.01
0
Jan
Apr
Jul
Oct
Jan
Apr
Jul
Oct
Jan
month

Figure 5.38

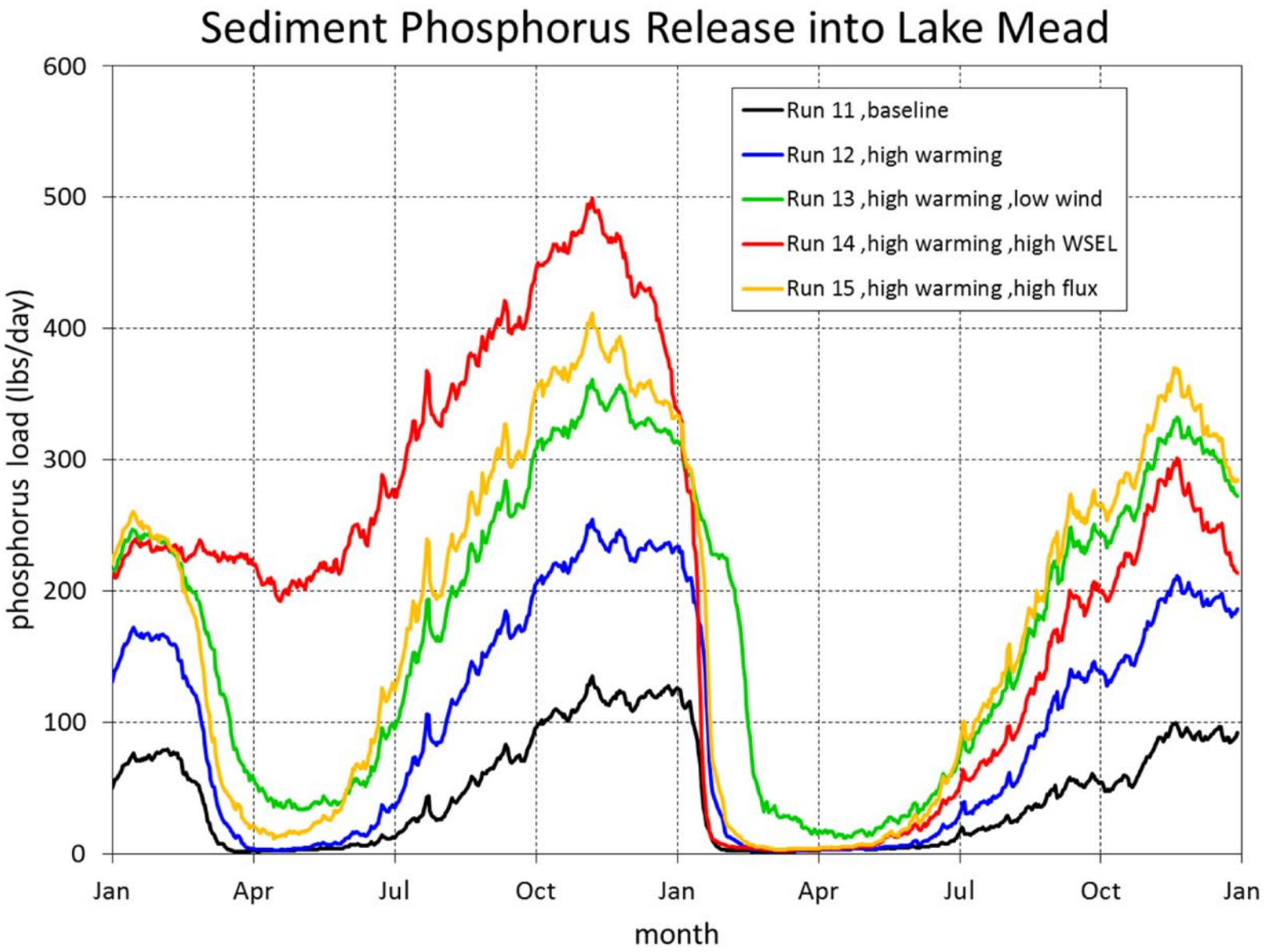
Sediment Phosphorus Release into Lake Mead
phosphorus load (lbs/day)
600
500
400
300
200
100
0
Jan
Apr
Jul
Oct
Jan
Apr
Jul
Oct
Jan
month
Run 11 ,baseline
Run 12 ,high warming
Run 13 ,high warming ,low wind
Run 14 ,high warming ,high WSEL
Run 15 ,high warming ,high flux

Figure 5.39

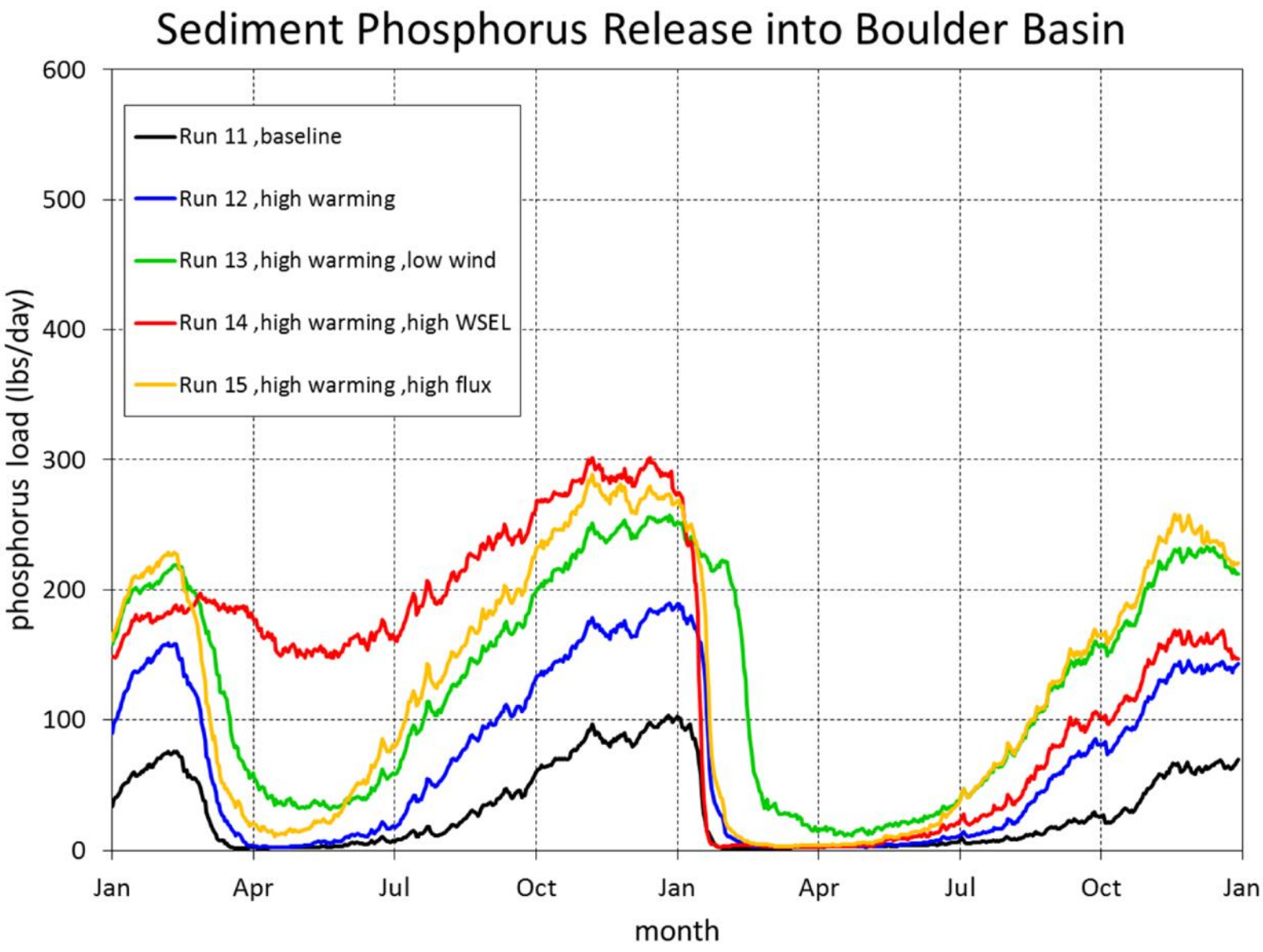
Sediment Phosphorus Release into Boulder Basin
Run 11 ,baseline
Run 12 ,high warming
Run 13 ,high warming ,low wind
Run 14 ,high warming ,high WSEL
Run 15 ,high warming ,high flux
phosphorus load (lbs/day)
600
500
400
300
200
100
0
Jan
Apr
Jul
Oct
Jan
Apr
Jul
Oct
Jan
month

Figure 5.40

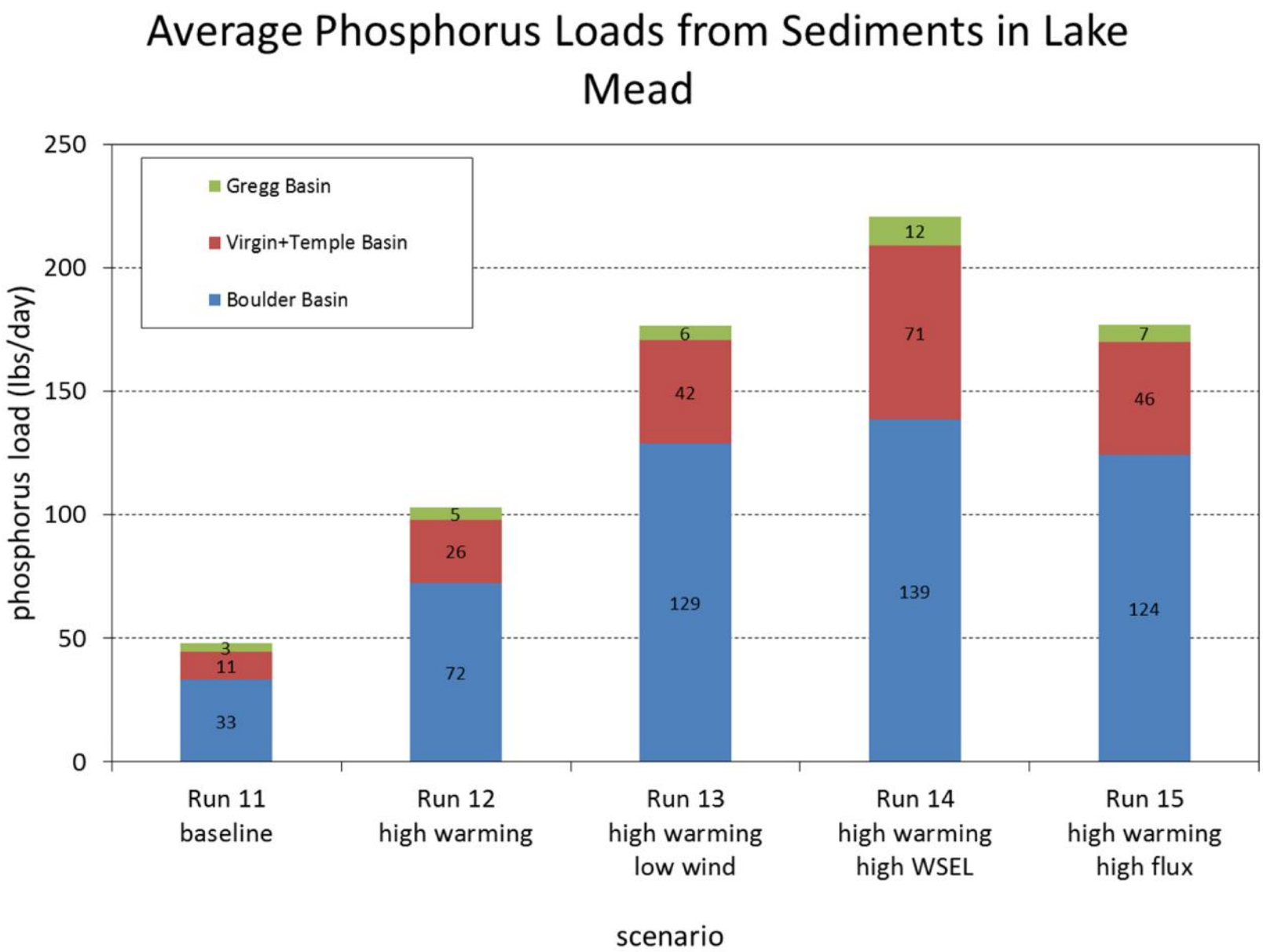
Average Phosphorus Loads from Sediments in Lake Mead
Gregg Basin
Virgin+Temple Basin
Boulder Basin
phosphorus load (lbs/day)
250
200
150
100
50
0
3
11
33
5
26
72
6
42
129
12
71
139
7
46
124
Run 11 baseline
Run 12 high warming
Run 13 high warming low wind
Run 14 high warming high WSEL
Run 15 high warming high flux
scenario

Figure 5.41

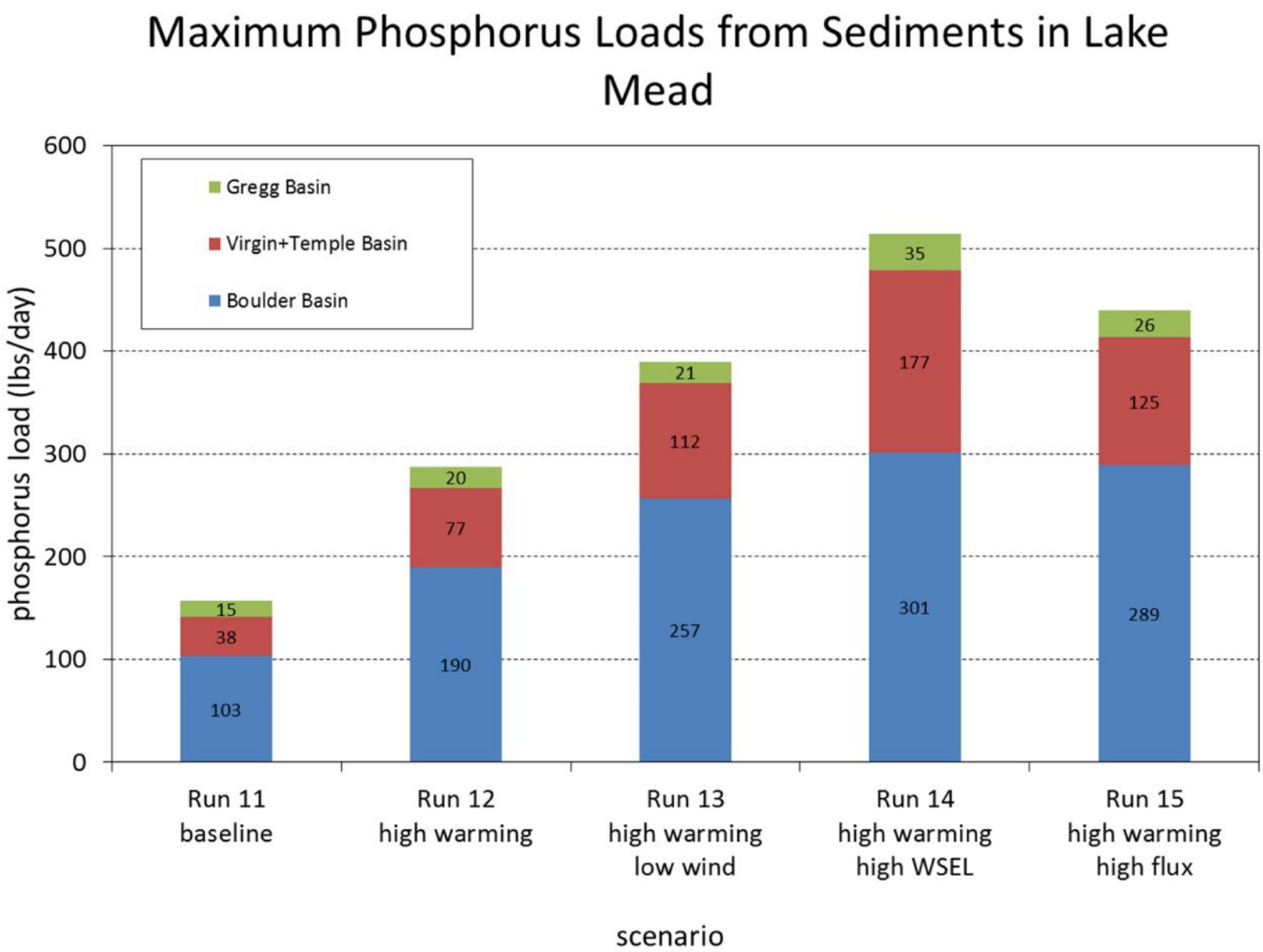
Maximum Phosphorus Loads from Sediments in Lake Mead
Gregg Basin
Virgin+Temple Basin
Boulder Basin
phosphorus load (lbs/day)
600
500
400
300
200
100
0
15
38
103
20
77
190
21
112
257
35
177
301
26
125
289
Run 11 baseline
Run 12 high warming
Run 13 high warming low wind
Run 14 high warming high WSEL
Run 15 high warming high flux
scenario

Figure 5.42

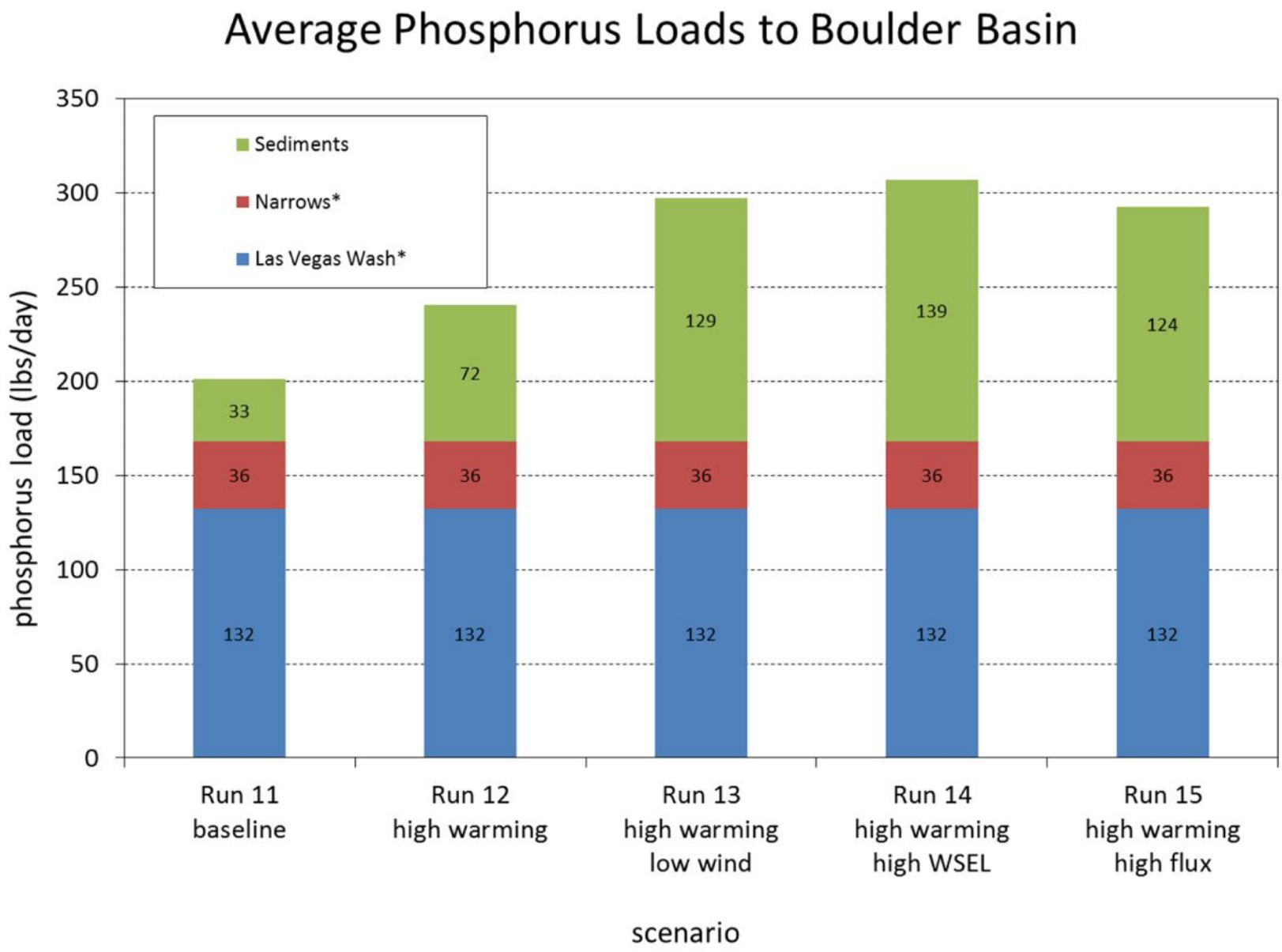

* Loads are average of 2007 and 2008 phosphorus budget (Ding et al., 2014)

Figure 5.43

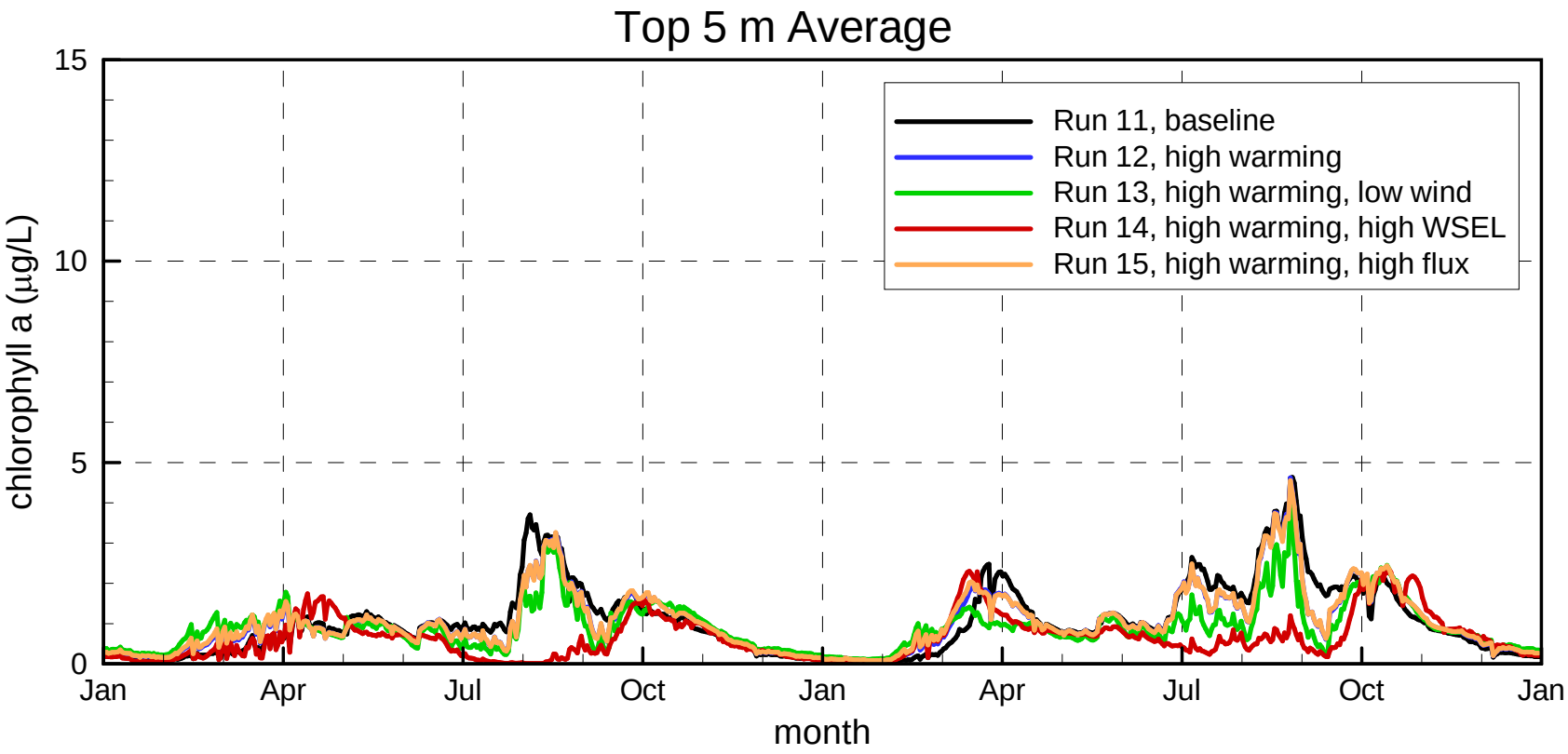
Chlorophyll a at Station CR390.0
Top 5 m Average
chlorophyll a (µg/L)
15
10
5
0
Jan
Apr
Jul
Oct
Jan
Apr
Jul
Oct
Jan
month
Run 11, baseline
Run 12, high warming
Run 13, high warming, low wind
Run 14, high warming, high WSEL
Run 15, high warming, high flux

Figure 5.44

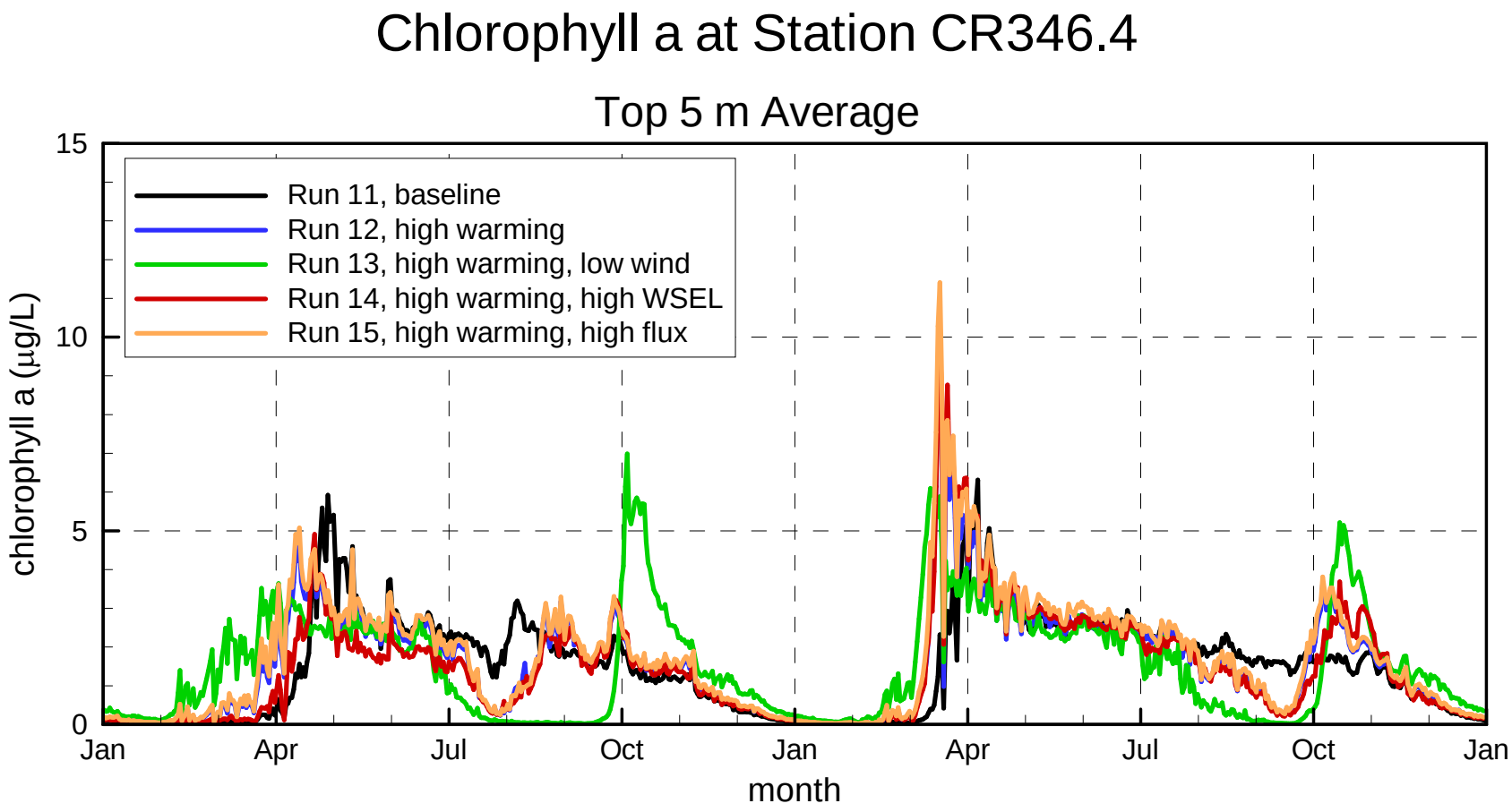
Chlorophyll a at Station CR346.4
Top 5 m Average
Run 11, baseline
Run 12, high warming
Run 13, high warming, low wind
Run 14, high warming, high WSEL
Run 15, high warming, high flux
chlorophyll a (µg/L)
15
10
5
0
Jan
Apr
Jul
Oct
Jan
Apr
Jul
Oct
Jan
month

Figure 5.45

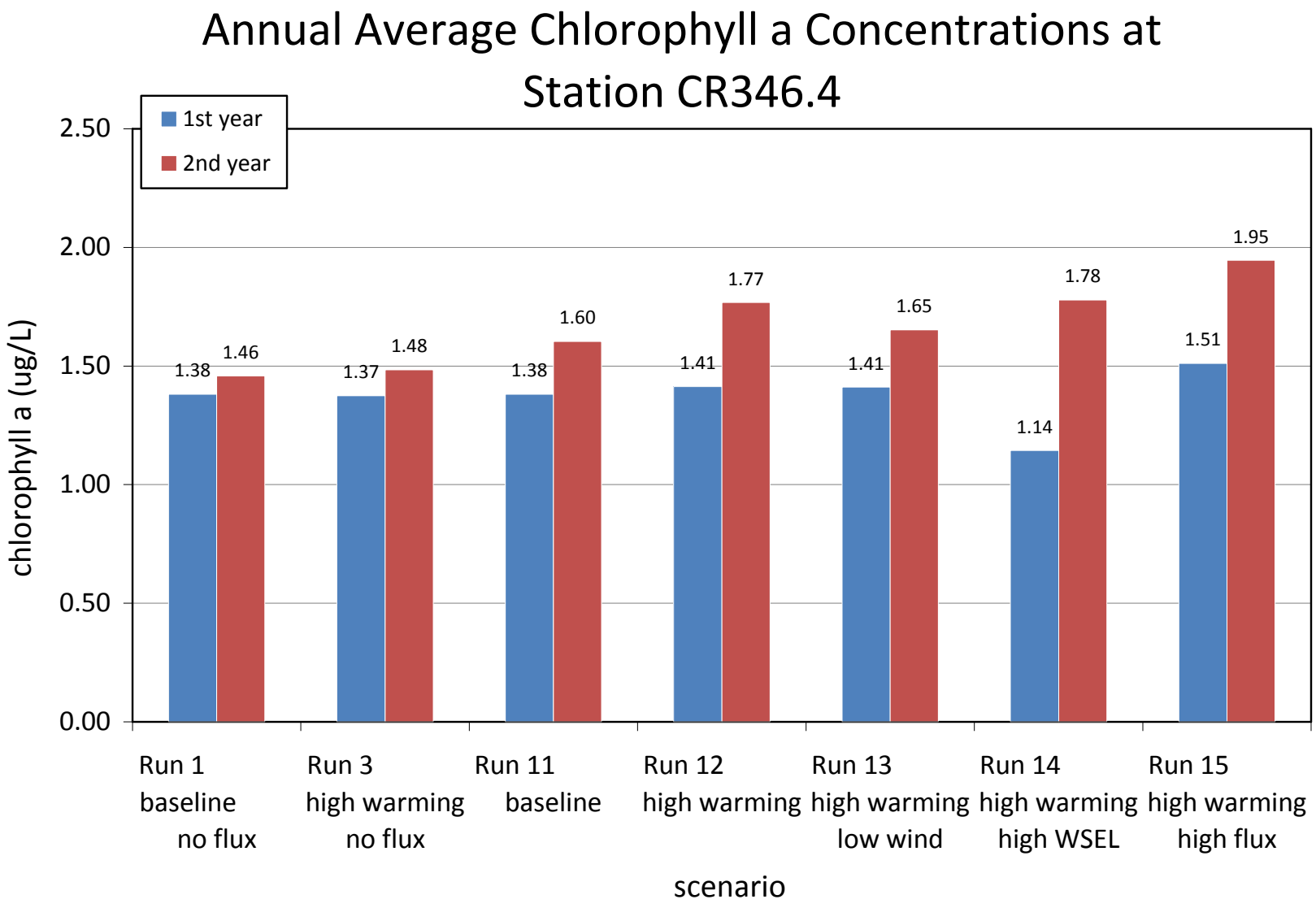
Annual Average Chlorophyll a Concentrations at Station CR346.4
1st year
2nd year
chlorophyll a (ug/L)
2.50
2.00
1.50
1.00
0.50
0.00
1.38
1.46
1.37
1.48
1.38
1.60
1.41
1.77
1.41
1.65
1.14
1.78
1.51
1.95
Run 1 baseline no flux
Run 3 high warming no flux
Run 11 baseline
Run 12 high warming
Run 13 high warming low wind
Run 14 high warming high WSEL
Run 15 high warming high flux
scenario

Figure 5.46

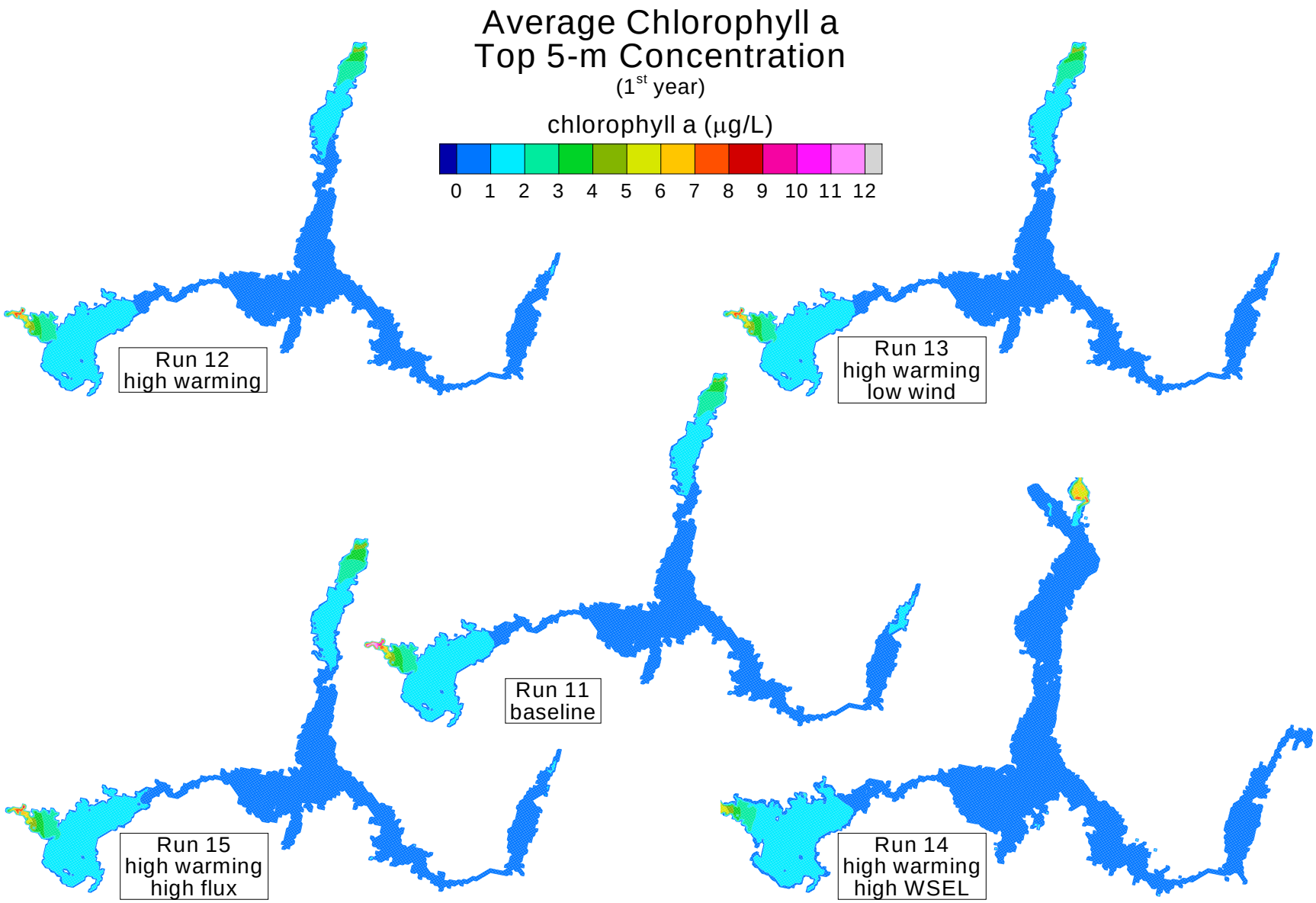
Average Chlorophyll a
Top 5-m Concentration
(1st year)
chlorophyll a (μg/L)
0 1 2 3 4 5 6 7 8 9 10 11 12
Run 12
high warming
Run 13
high warming
low wind
Run 11
baseline
Run 15
high warming
high flux
Run 14
high warming
high WSEL

Figure 5.47

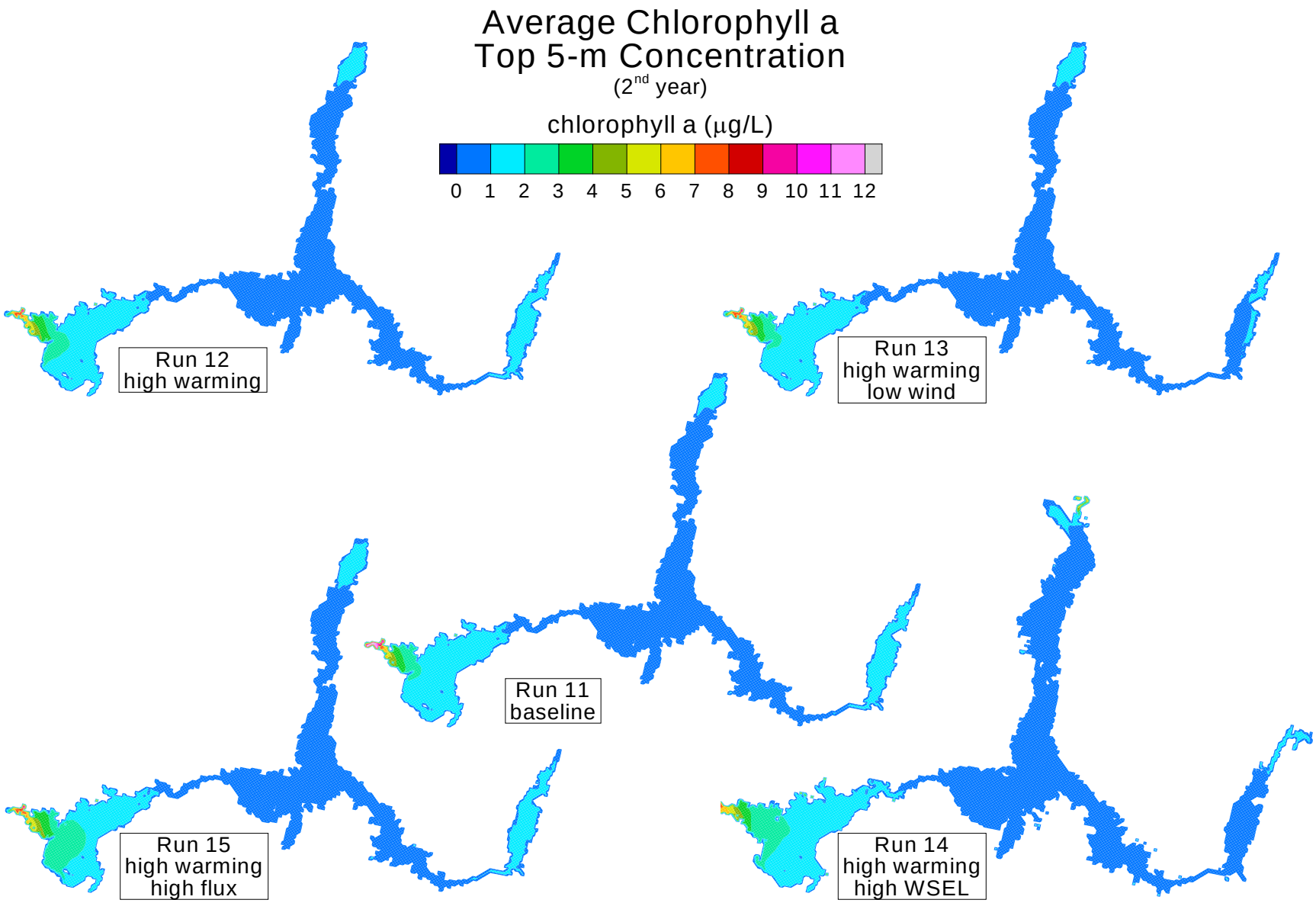
Average Chlorophyll a
Top 5-m Concentration
(2nd year)
chlorophyll a (μg/L)
0 1 2 3 4 5 6 7 8 9 10 11 12
Run 12
high warming
Run 13
high warming
low wind
Run 11
baseline
Run 15
high warming
high flux
Run 14
high warming
high WSEL

Figure 5.48

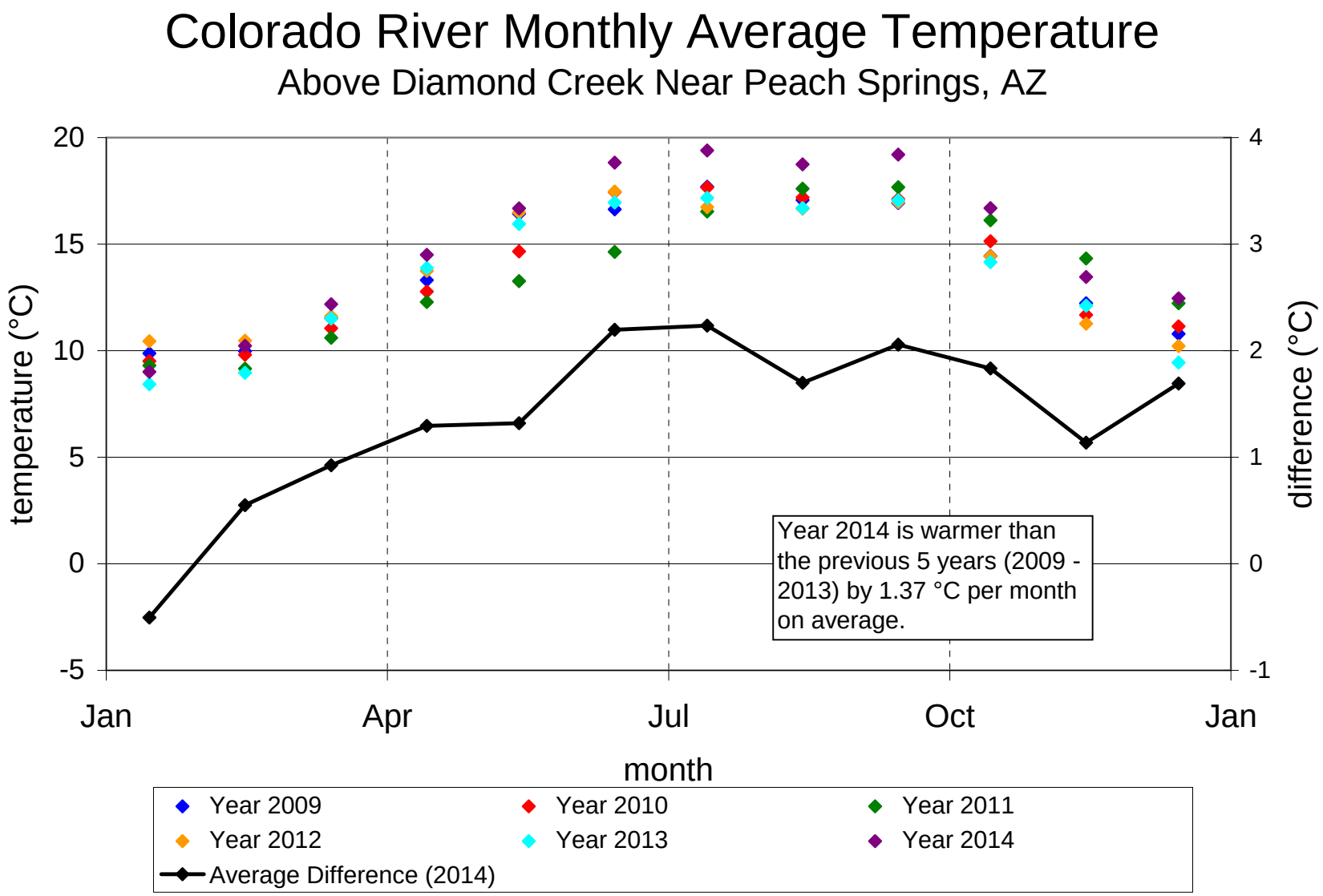
Colorado River Monthly Average Temperature
Above Diamond Creek Near Peach Springs, AZ
temperature (°C)
difference (°C)
20
15
10
5
0
-5
4
3
2
1
0
-1
Jan
Apr
Jul
Oct
Jan
month
Year 2014 is warmer than the previous 5 years (2009 - 2013) by 1.37 °C per month on average.
Year 2009
Year 2010
Year 2011
Year 2012
Year 2013
Year 2014
Average Difference (2014)

Figure 5.49

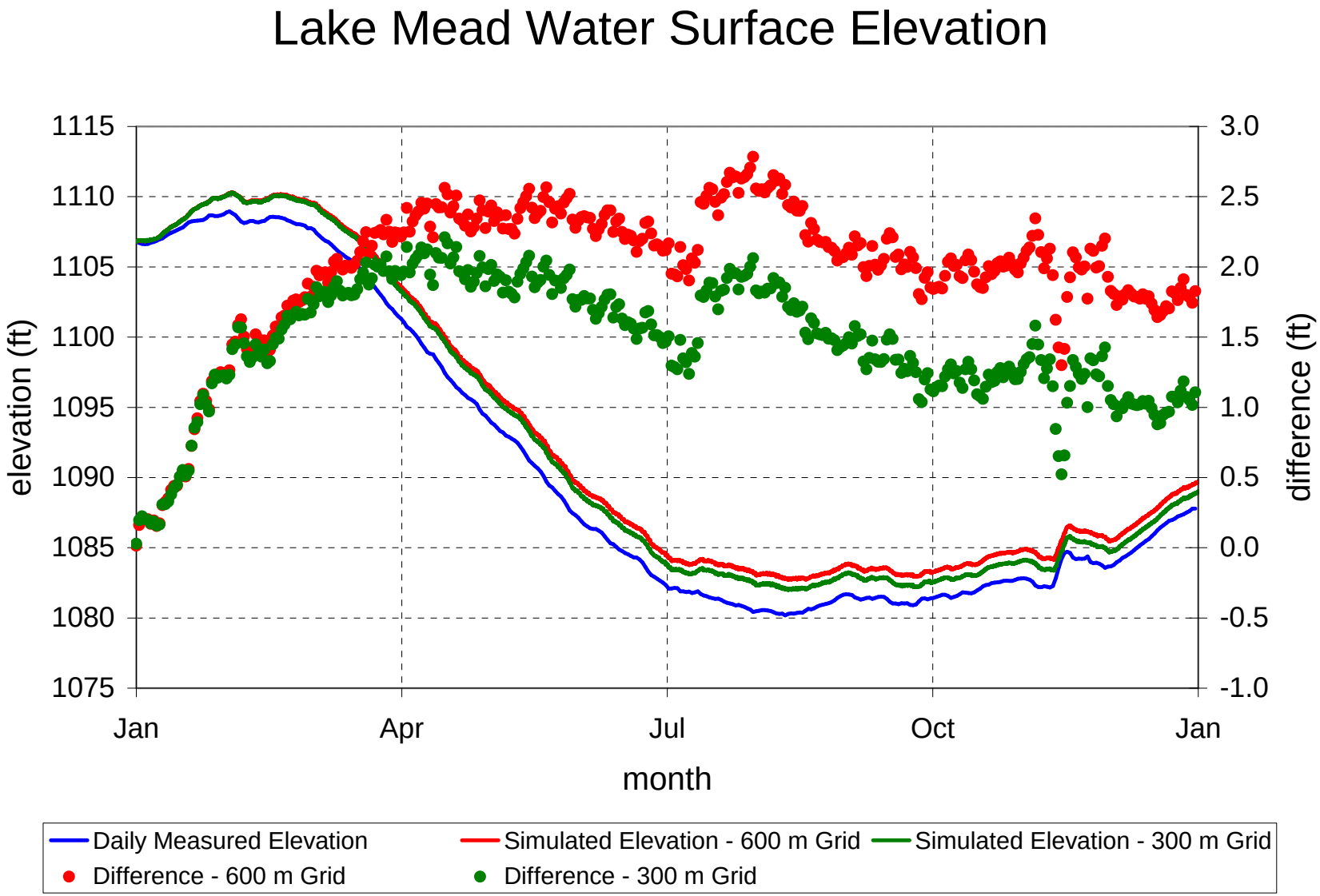

Figure 5.50

FLOW SCIENCE

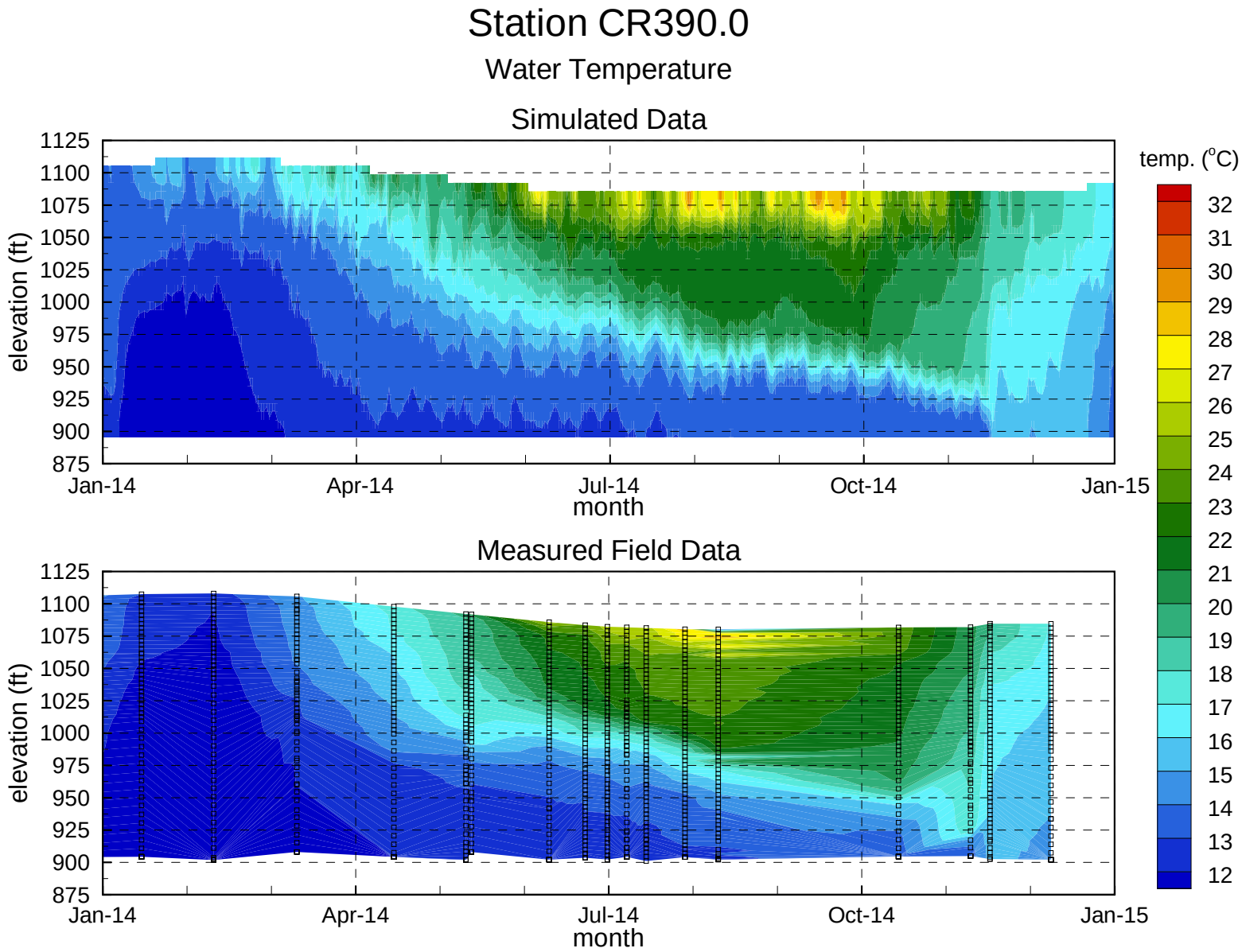

Figure 5.51

FLOW SCIENCE

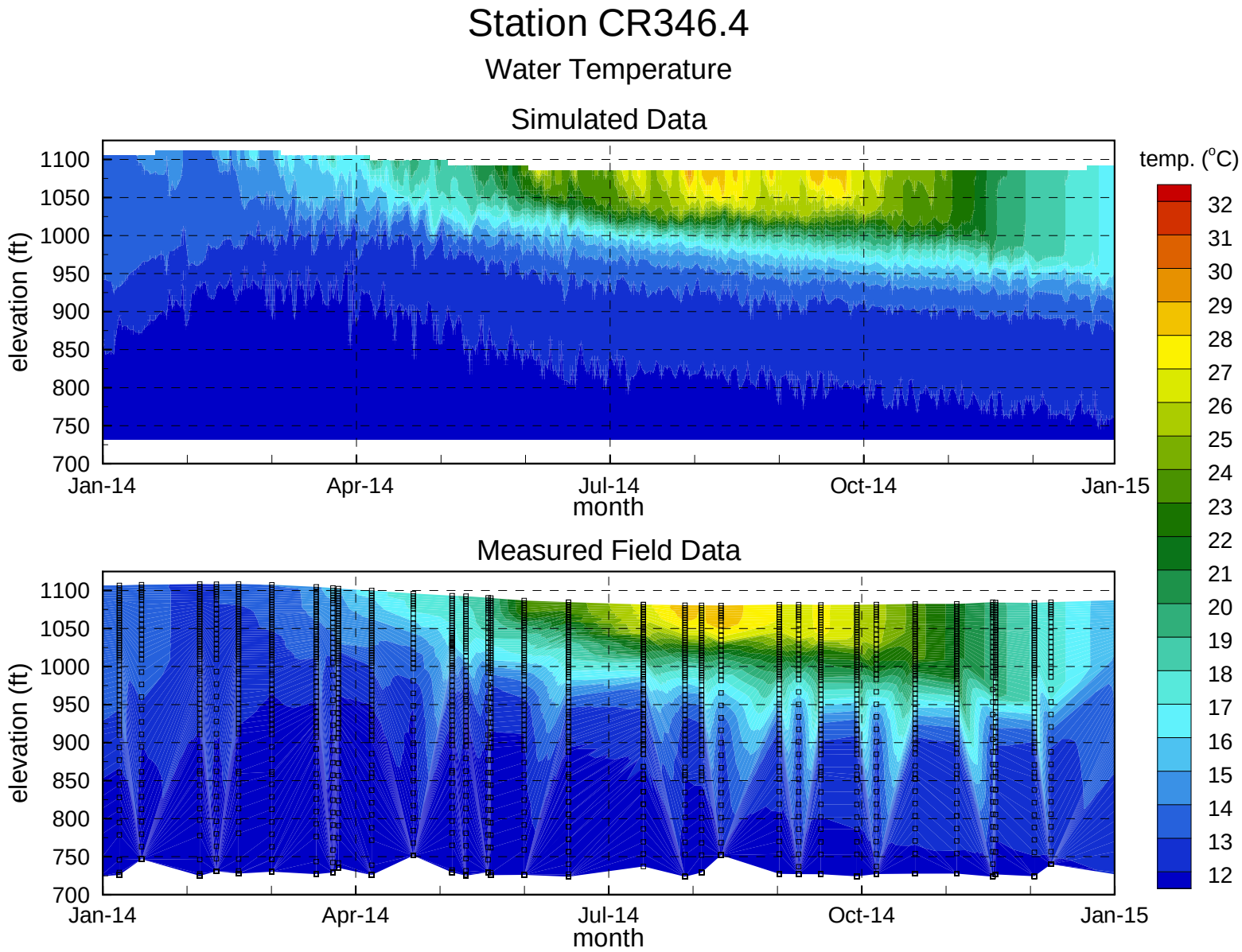
Station CR346.4
Water Temperature
Simulated Data
Measured Field Data
elevation (ft)
1100
1050
1000
950
900
850
800
750
700
Jan-14
Apr-14
Jul-14
Oct-14
Jan-15
month
temp. (°C)
32
31
30
29
28
27
26
25
24
23
22
21
20
19
18
17
16
15
14
13
12

Figure 5.52

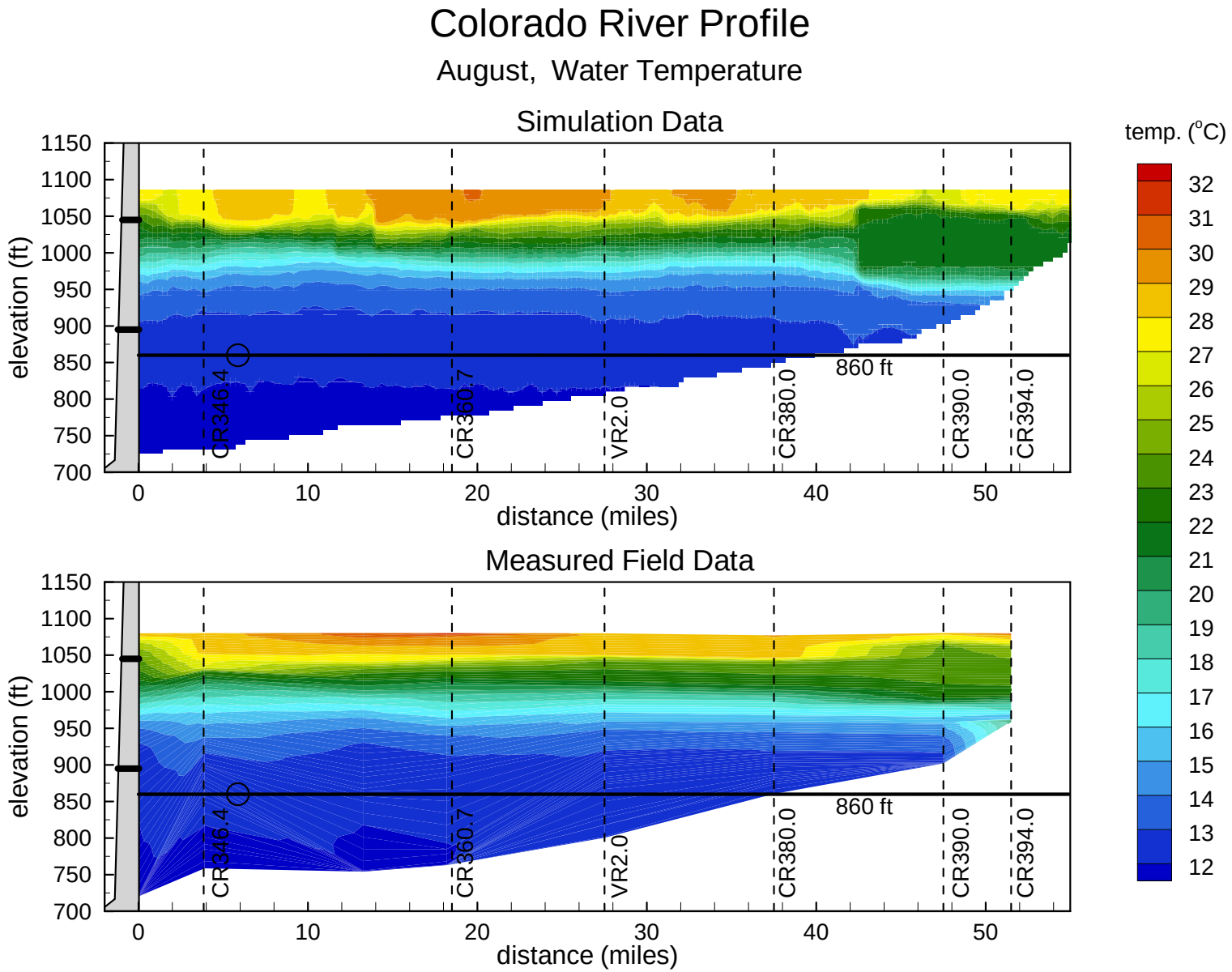

Figure 5.53

FLOW SCIENCE

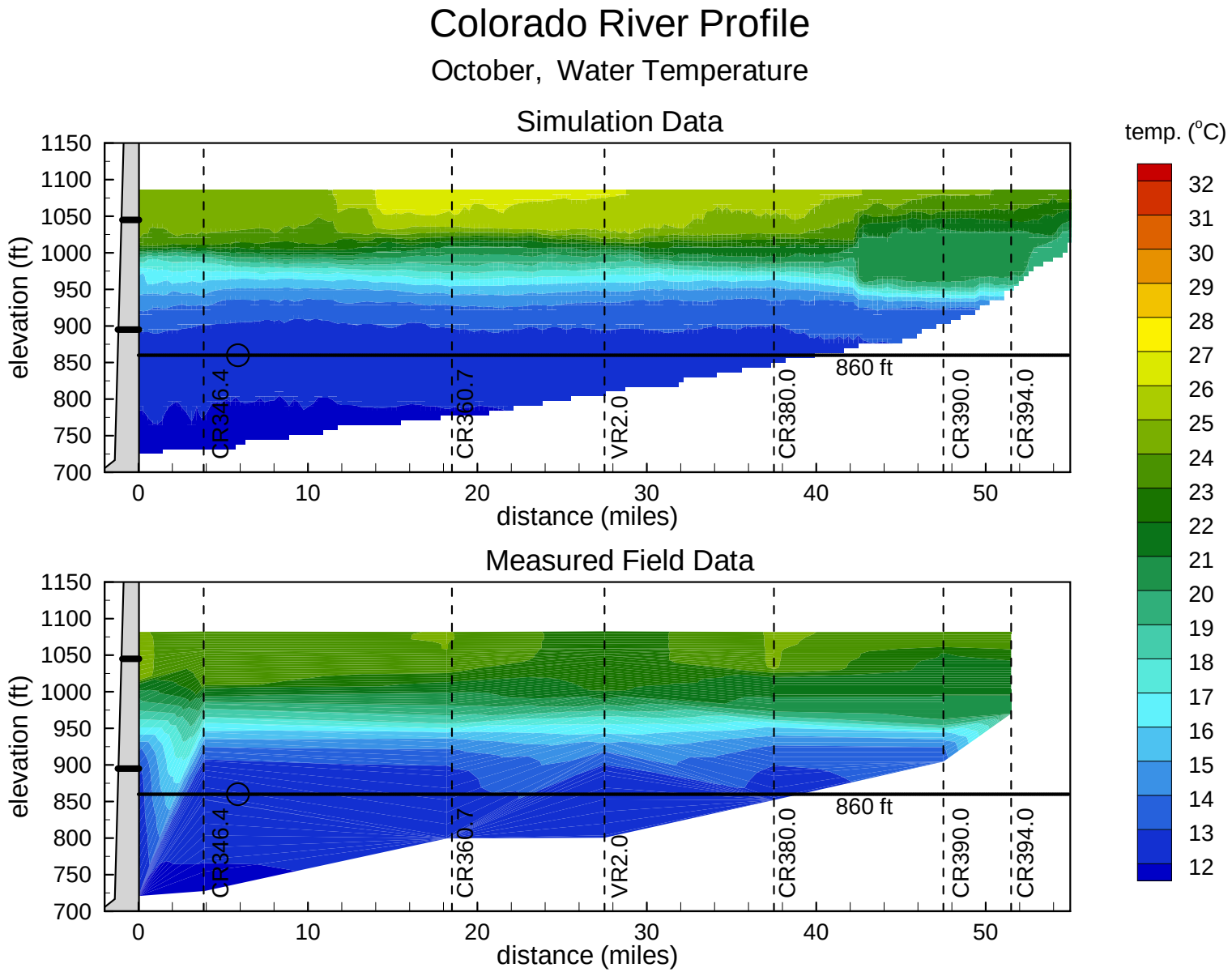

Figure 5.54

FLOW SCIENCE

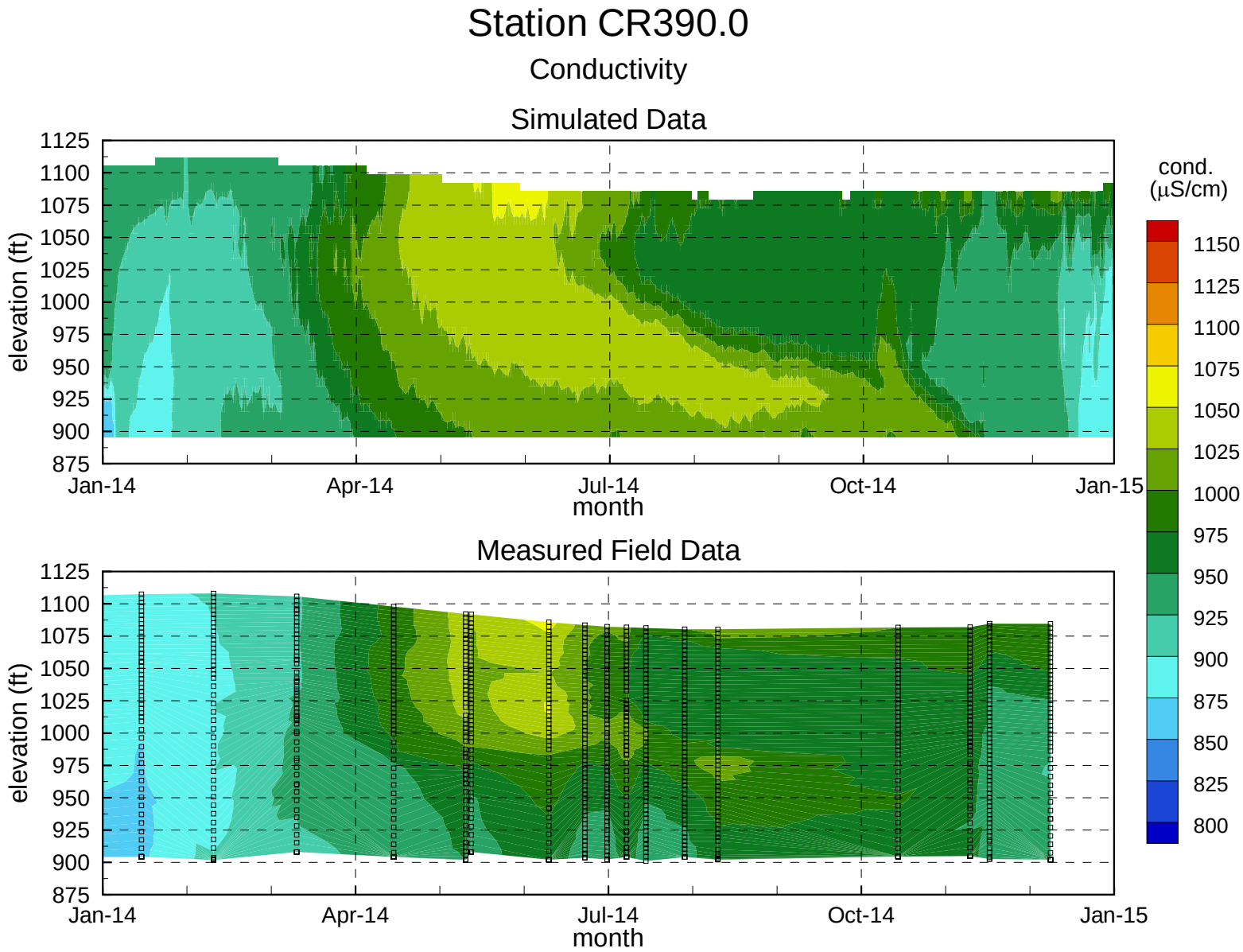
Station CR390.0
Conductivity
Simulated Data
Measured Field Data
elevation (ft)
1125
1100
1075
1050
1025
1000
975
950
925
900
875
Jan-14
Apr-14
Jul-14
Oct-14
Jan-15
month
cond.
(µS/cm)
1150
1125
1100
1075
1050
1025
1000
975
950
925
900
875
850
825
800

Figure 5.55

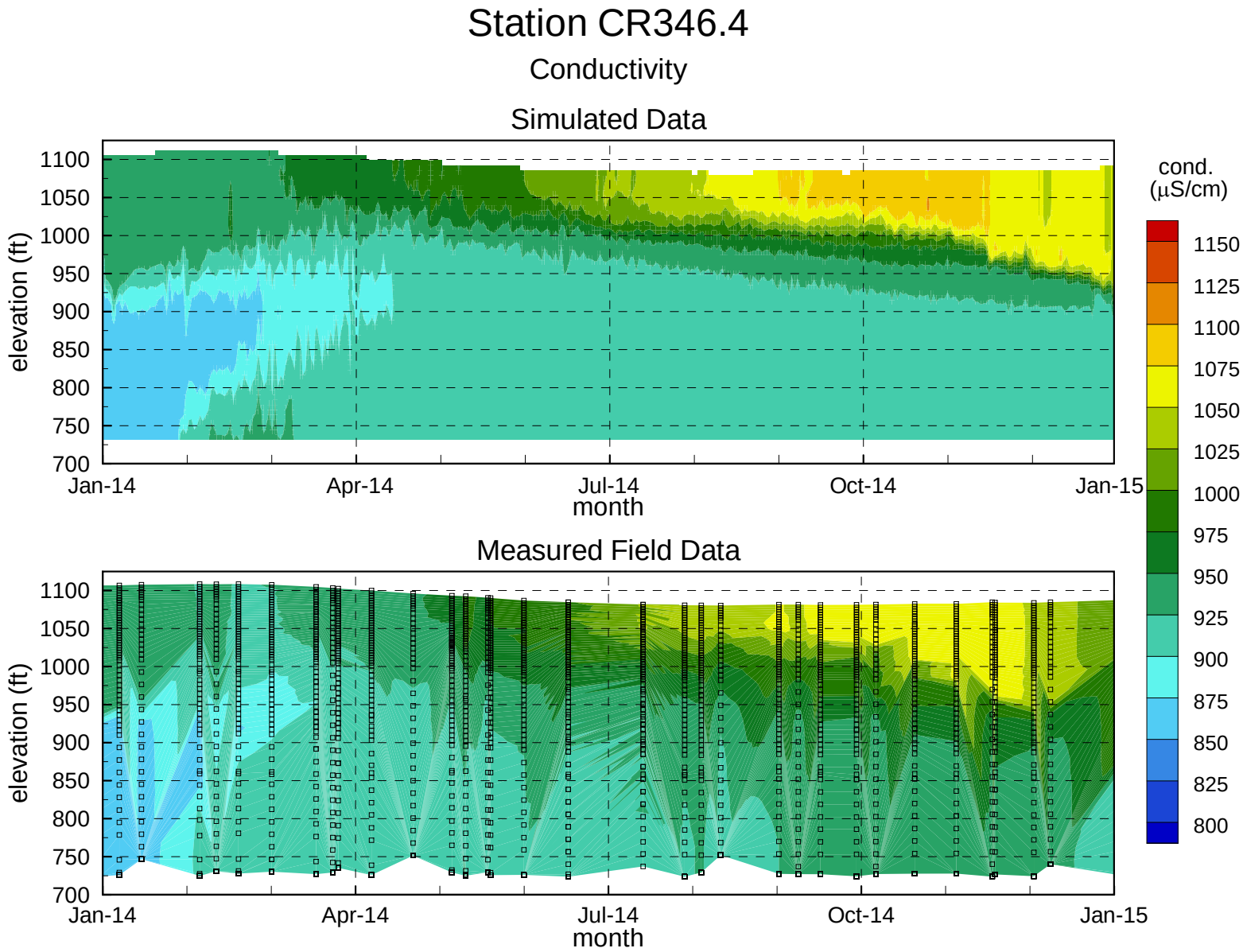
Station CR346.4
Conductivity
Simulated Data
Measured Field Data
elevation (ft)
1100
1050
1000
950
900
850
800
750
700
Jan-14
Apr-14
Jul-14
Oct-14
Jan-15
month
cond.
(µS/cm)
1150
1125
1100
1075
1050
1025
1000
975
950
925
900
875
850
825
800

Figure 5.56

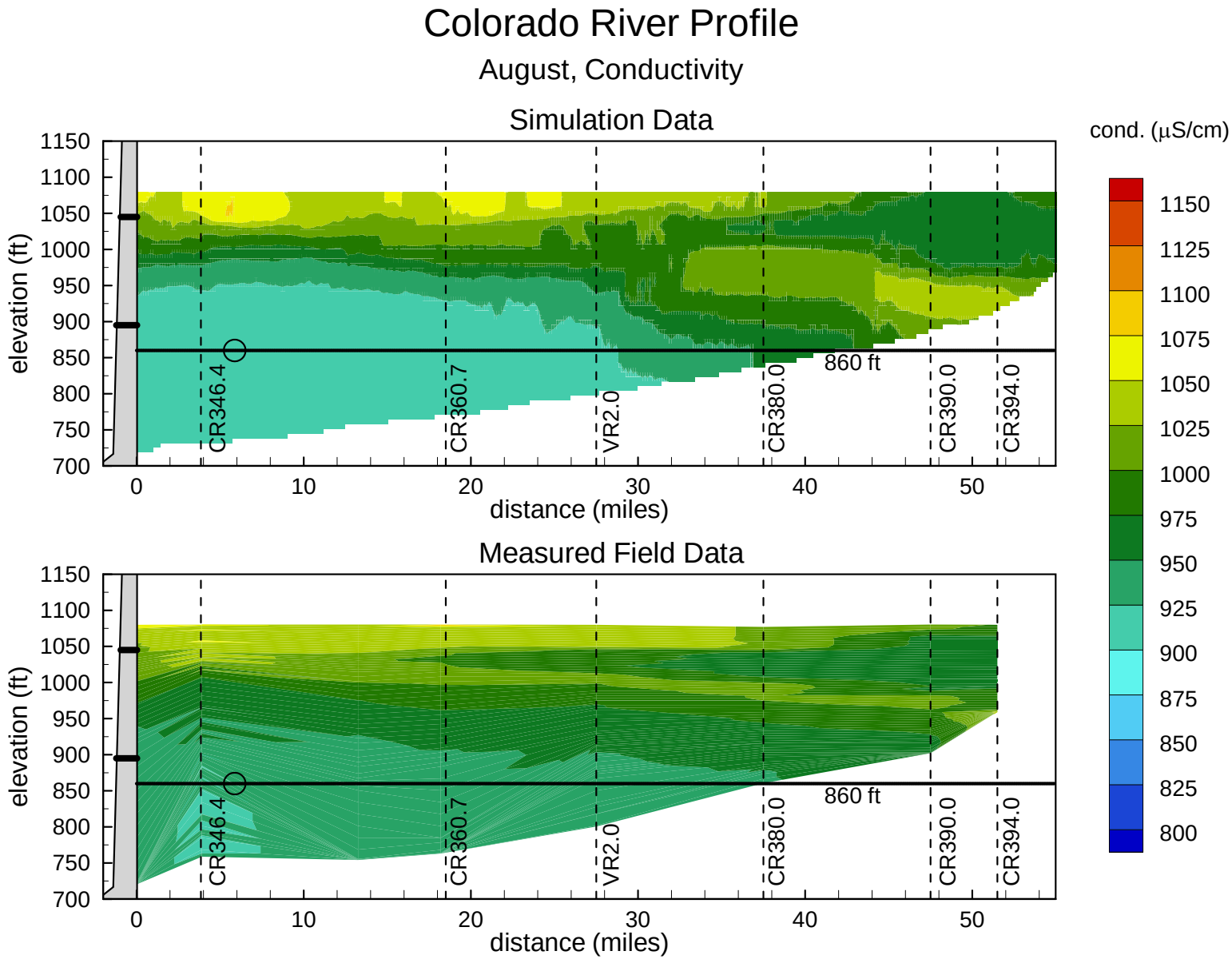
Colorado River Profile
August, Conductivity
Simulation Data
Measured Field Data
elevation (ft)
distance (miles)
860 ft
CR346.4
CR360.7
VR2.0
CR380.0
CR390.0
CR394.0
cond. (µS/cm)
1150
1125
1100
1075
1050
1025
1000
975
950
925
900
875
850
825
800

Figure 5.57

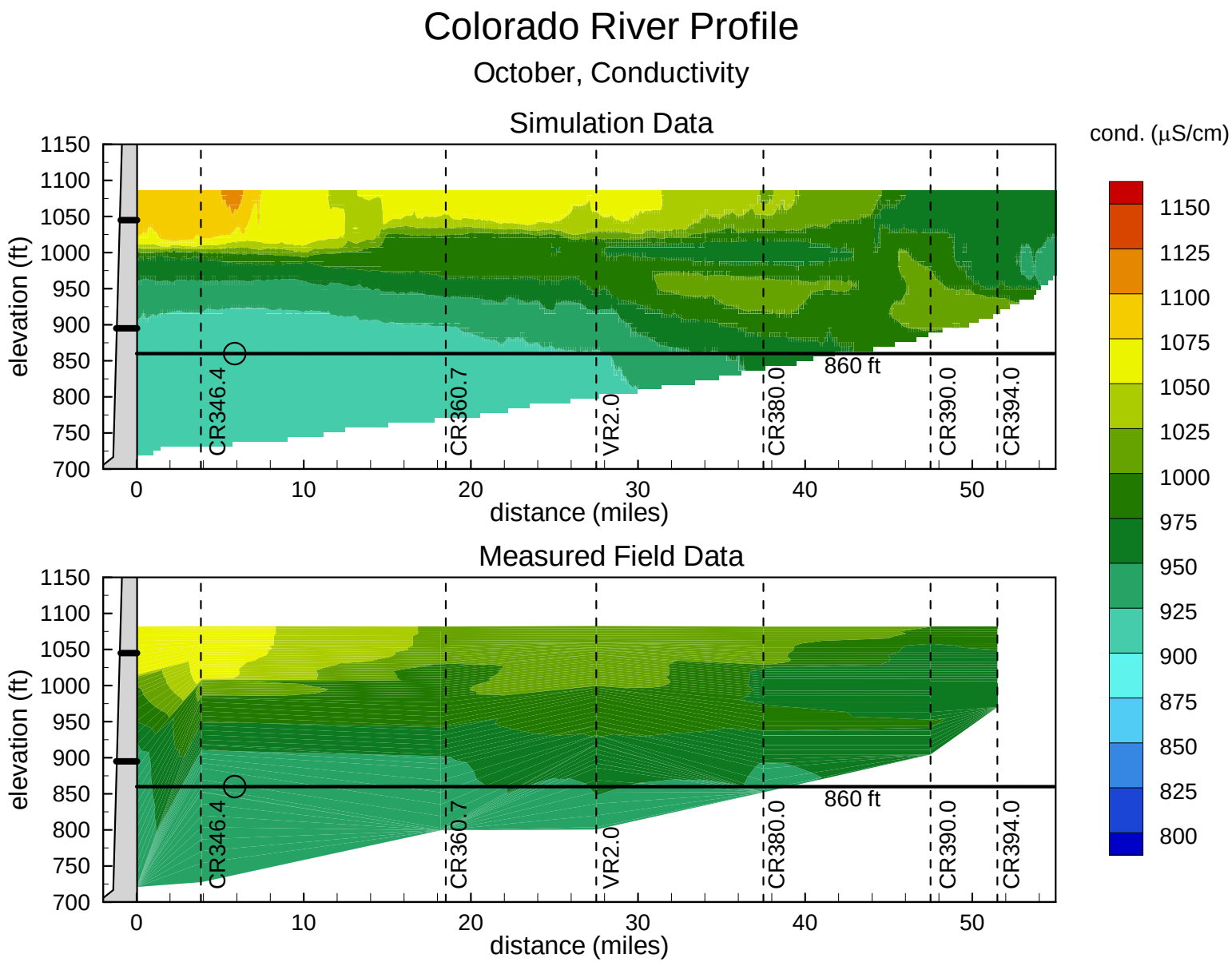
Colorado River Profile
October, Conductivity
Simulation Data
Measured Field Data
elevation (ft)
distance (miles)
860 ft
CR346.4
CR360.7
VR2.0
CR380.0
CR390.0
CR394.0
cond. (µS/cm)
1150
1125
1100
1075
1050
1025
1000
975
950
925
900
875
850
825
800

Figure 5.58

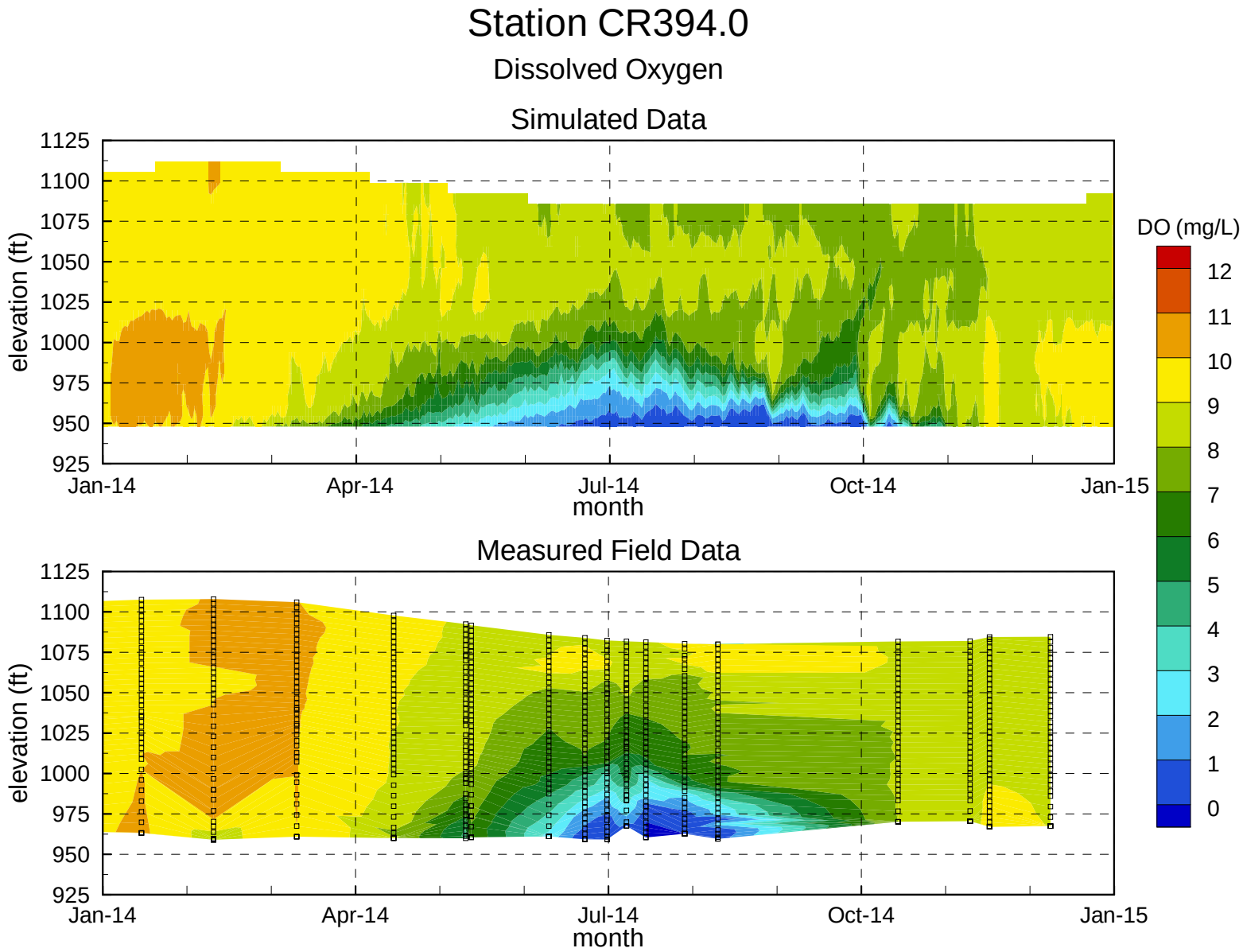

Figure 5.59

FLOW SCIENCE

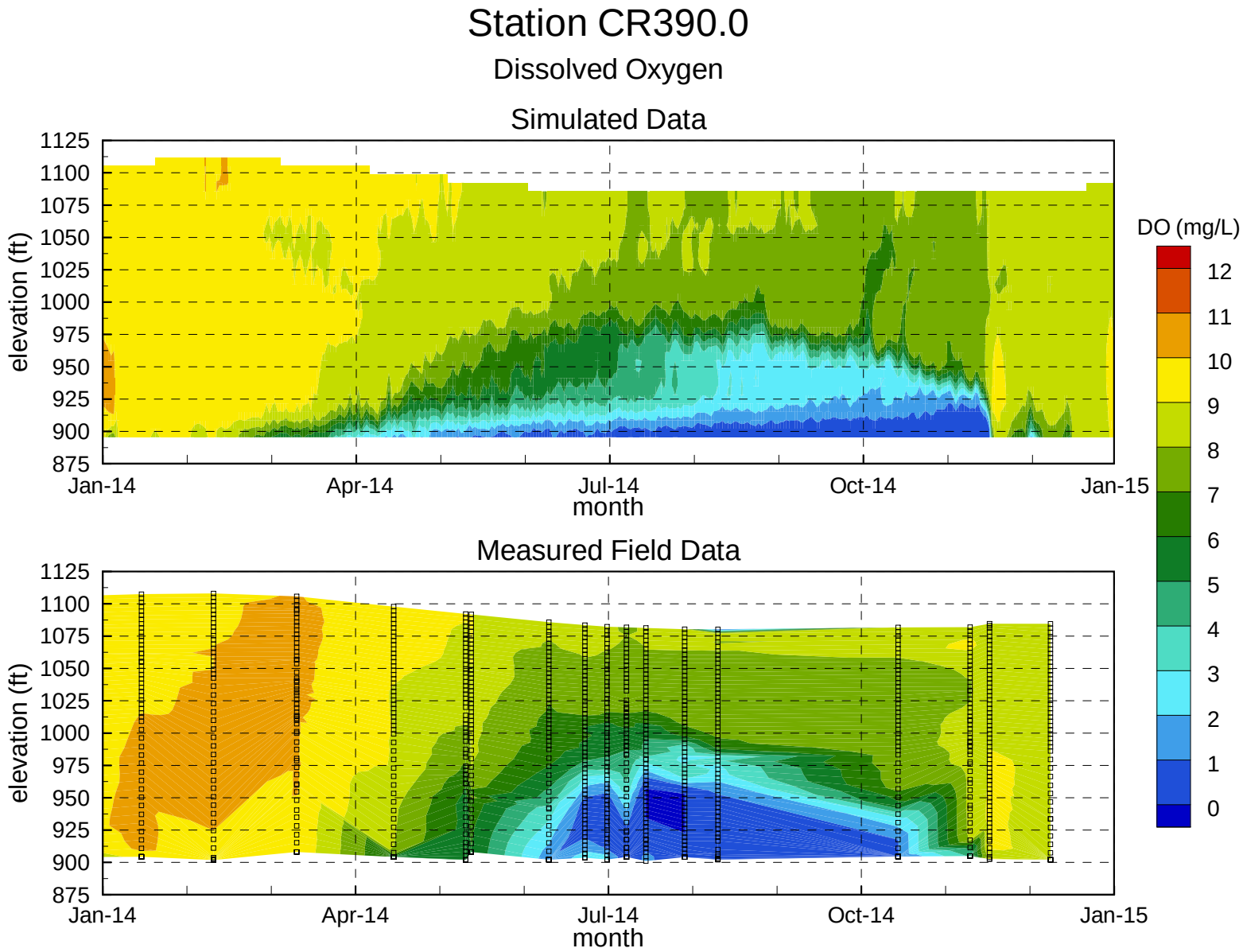
Station CR390.0
Dissolved Oxygen
Simulated Data
Measured Field Data
elevation (ft)
1125
1100
1075
1050
1025
1000
975
950
925
900
875
Jan-14
Apr-14
Jul-14
Oct-14
Jan-15
month
DO (mg/L)
12
11
10
9
8
7
6
5
4
3
2
1
0

Figure 5.60

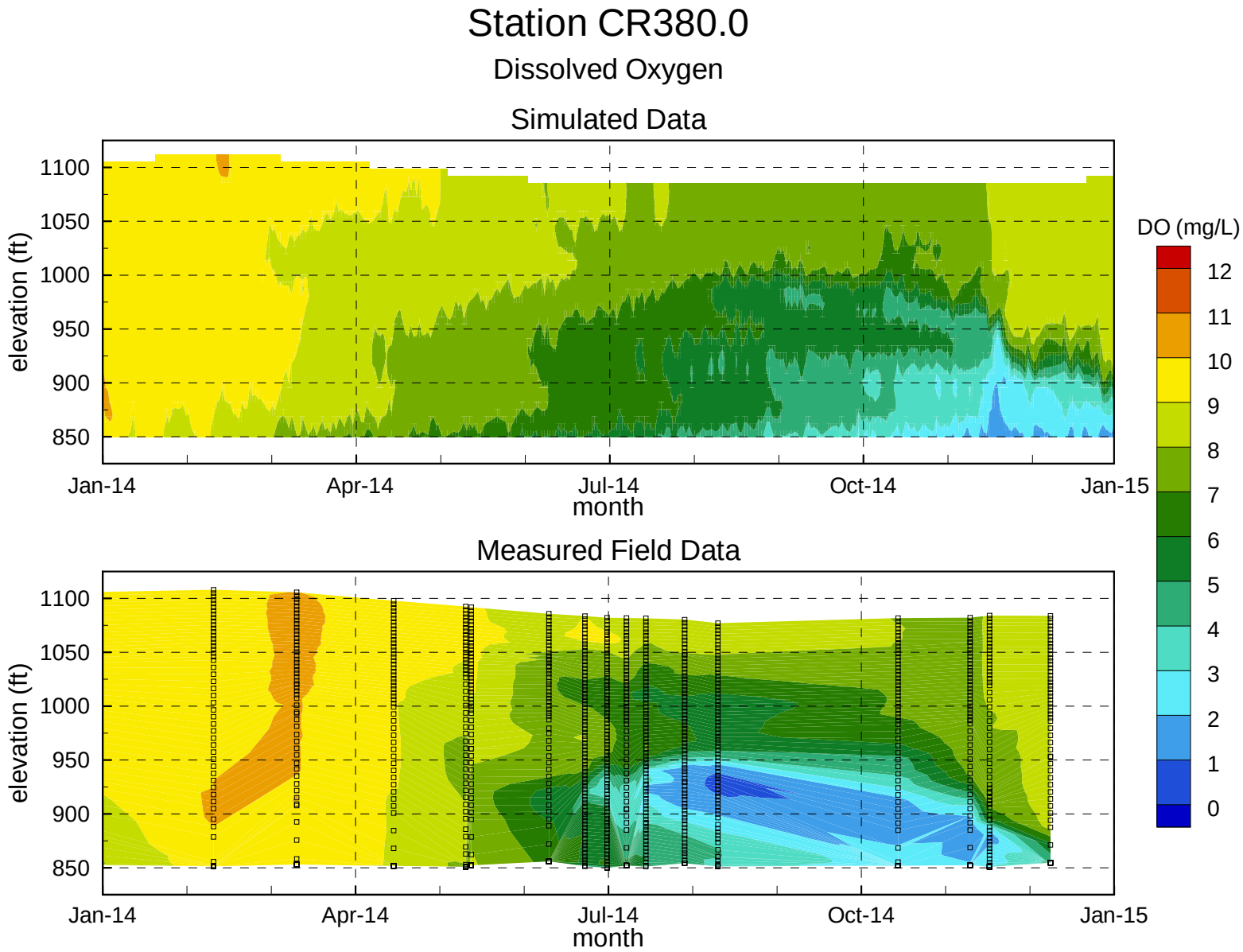
Station CR380.0
Dissolved Oxygen
Simulated Data
elevation (ft)
1100
1050
1000
950
900
850
Jan-14
Apr-14
Jul-14
Oct-14
Jan-15
month
Measured Field Data
elevation (ft)
1100
1050
1000
950
900
850
Jan-14
Apr-14
Jul-14
Oct-14
Jan-15
month
DO (mg/L)
12
11
10
9
8
7
6
5
4
3
2
1
0

Figure 5.61

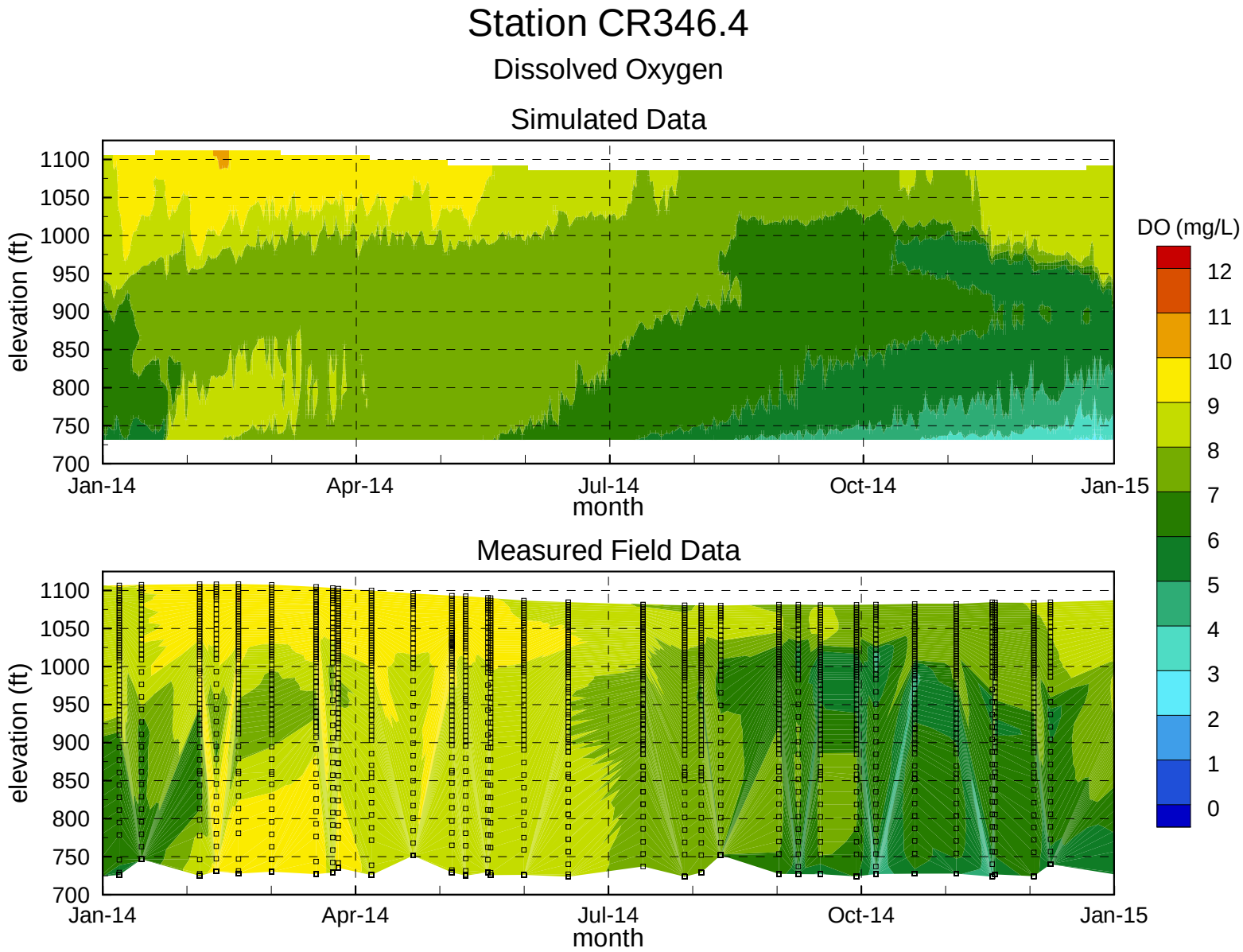
Station CR346.4
Dissolved Oxygen
Simulated Data
elevation (ft)
1100
1050
1000
950
900
850
800
750
700
Jan-14
Apr-14
Jul-14
Oct-14
Jan-15
month
Measured Field Data
elevation (ft)
1100
1050
1000
950
900
850
800
750
700
Jan-14
Apr-14
Jul-14
Oct-14
Jan-15
month
DO (mg/L)
12
11
10
9
8
7
6
5
4
3
2
1
0

Figure 5.62

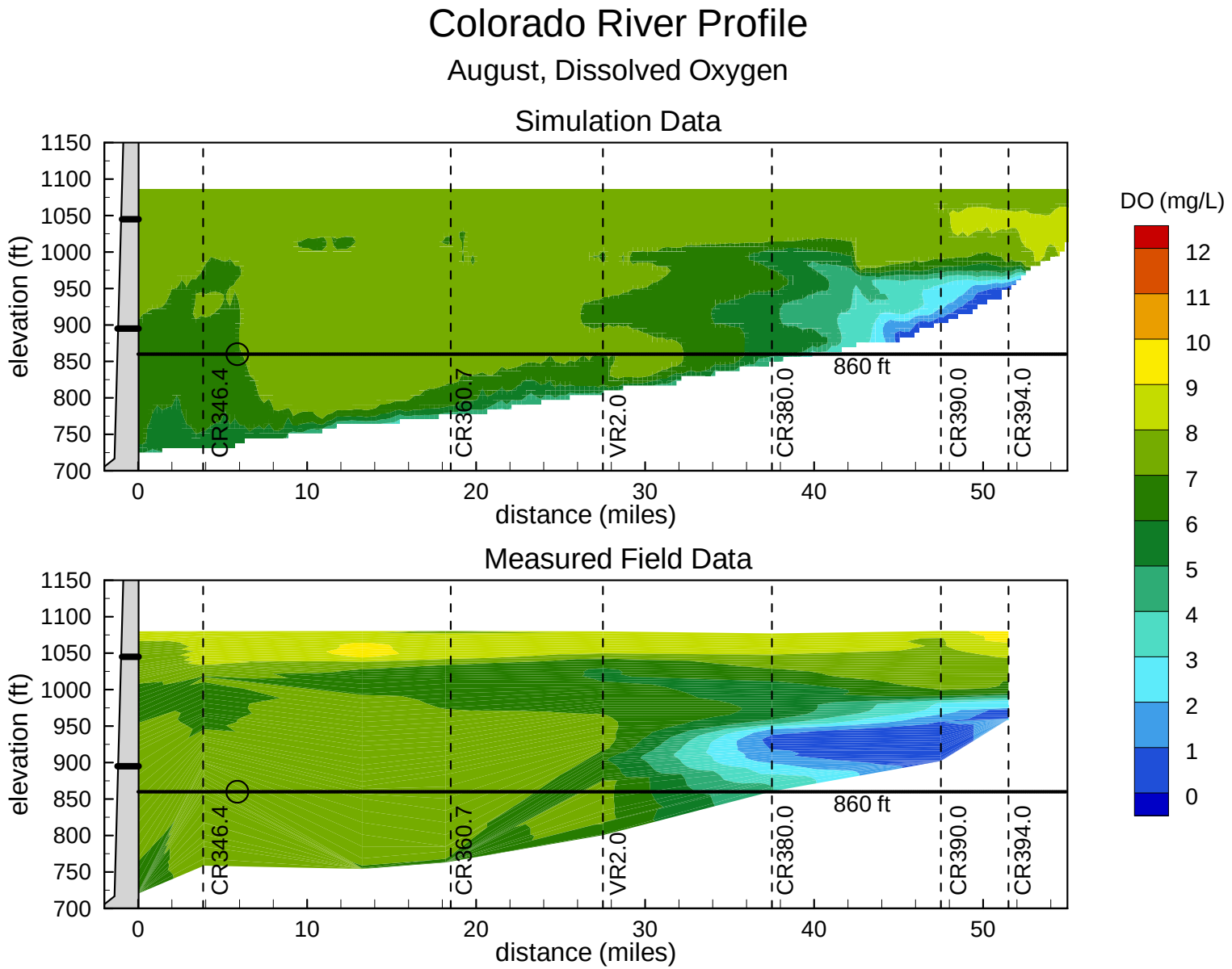

Figure 5.63

FLOW SCIENCE

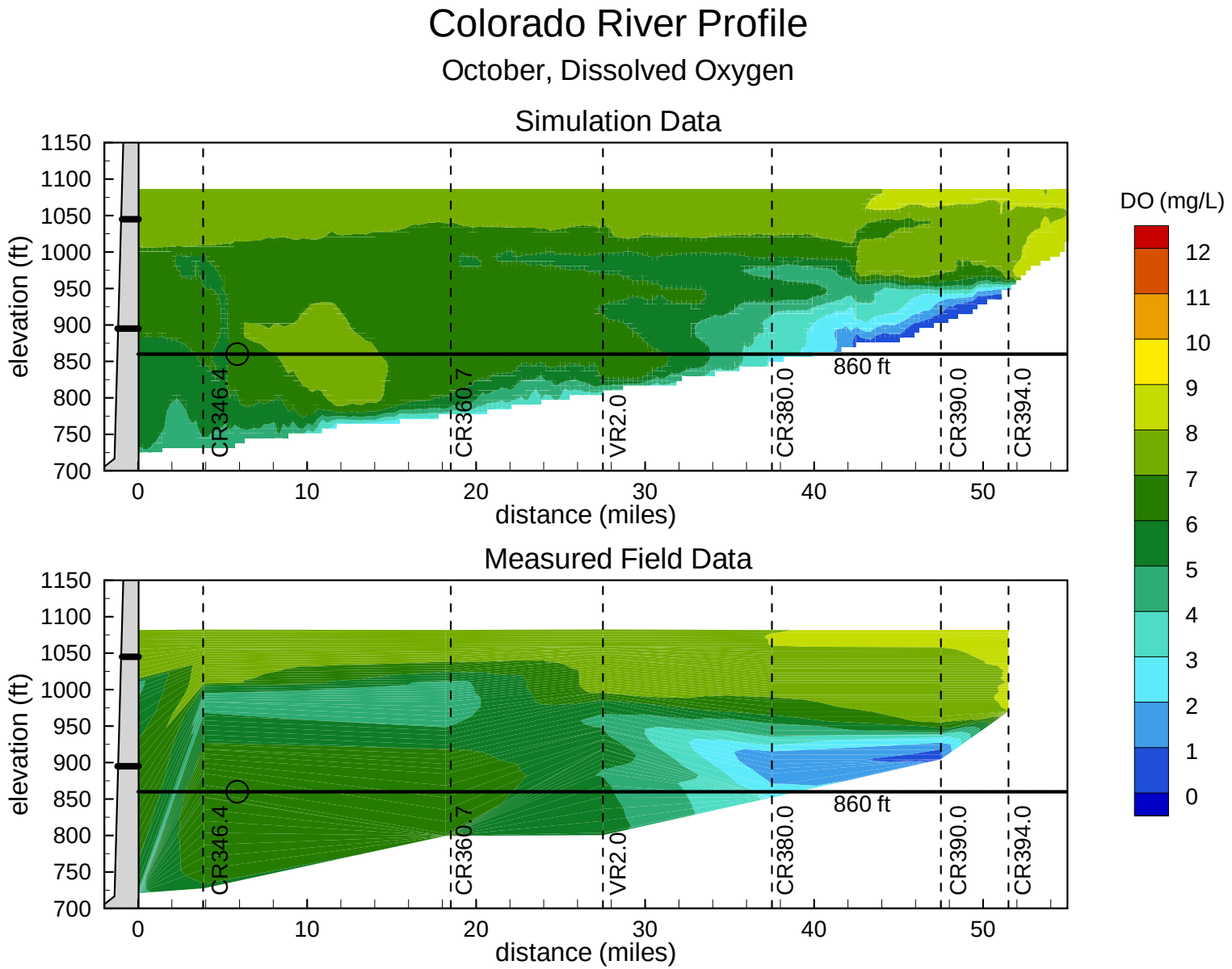

Figure 5.64

FLOW SCIENCE

Filterable Reactive Phosphorus at Station CR394.0

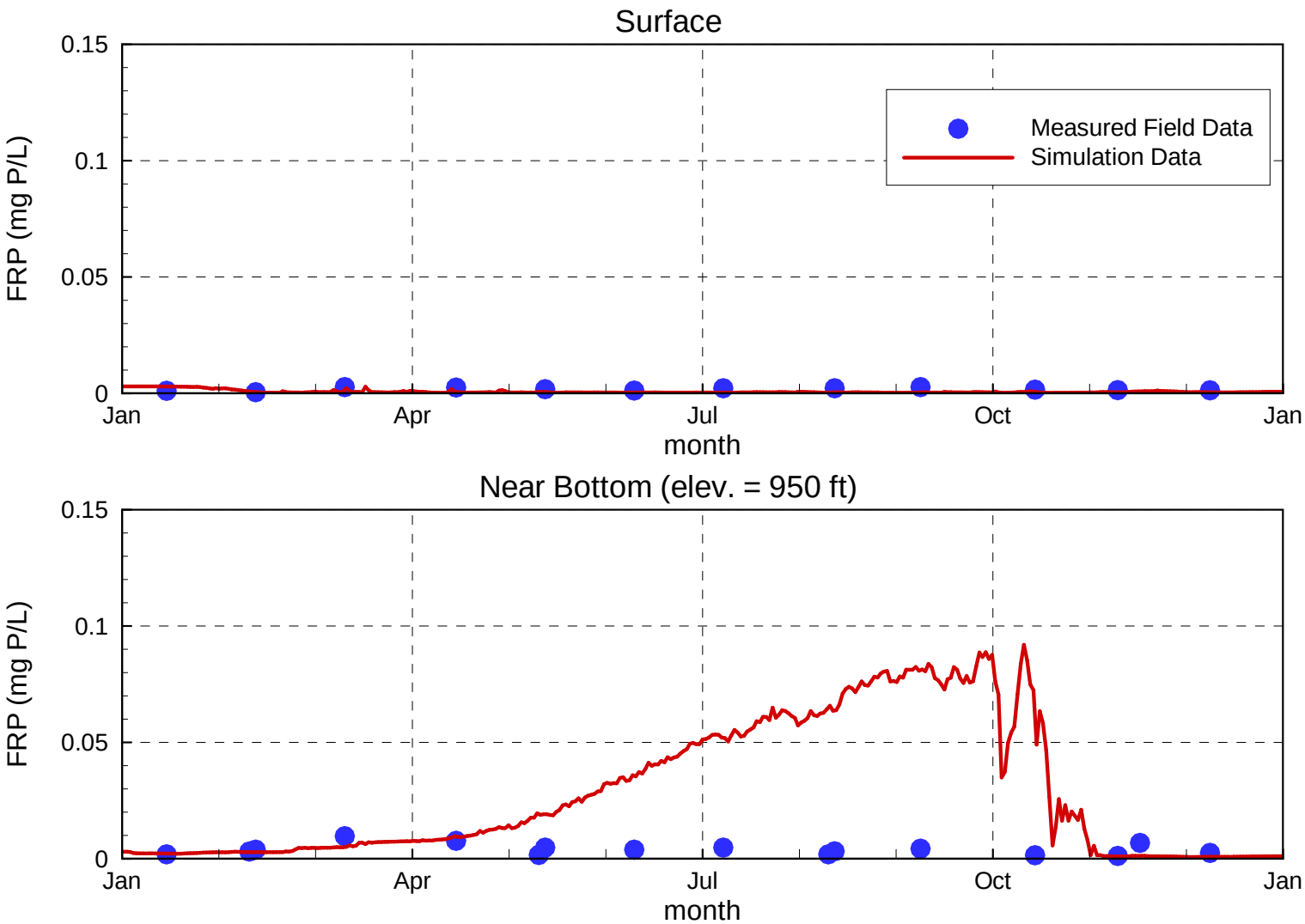

Figure 5.65

Filterable Reactive Phosphorus at Station CR390.0

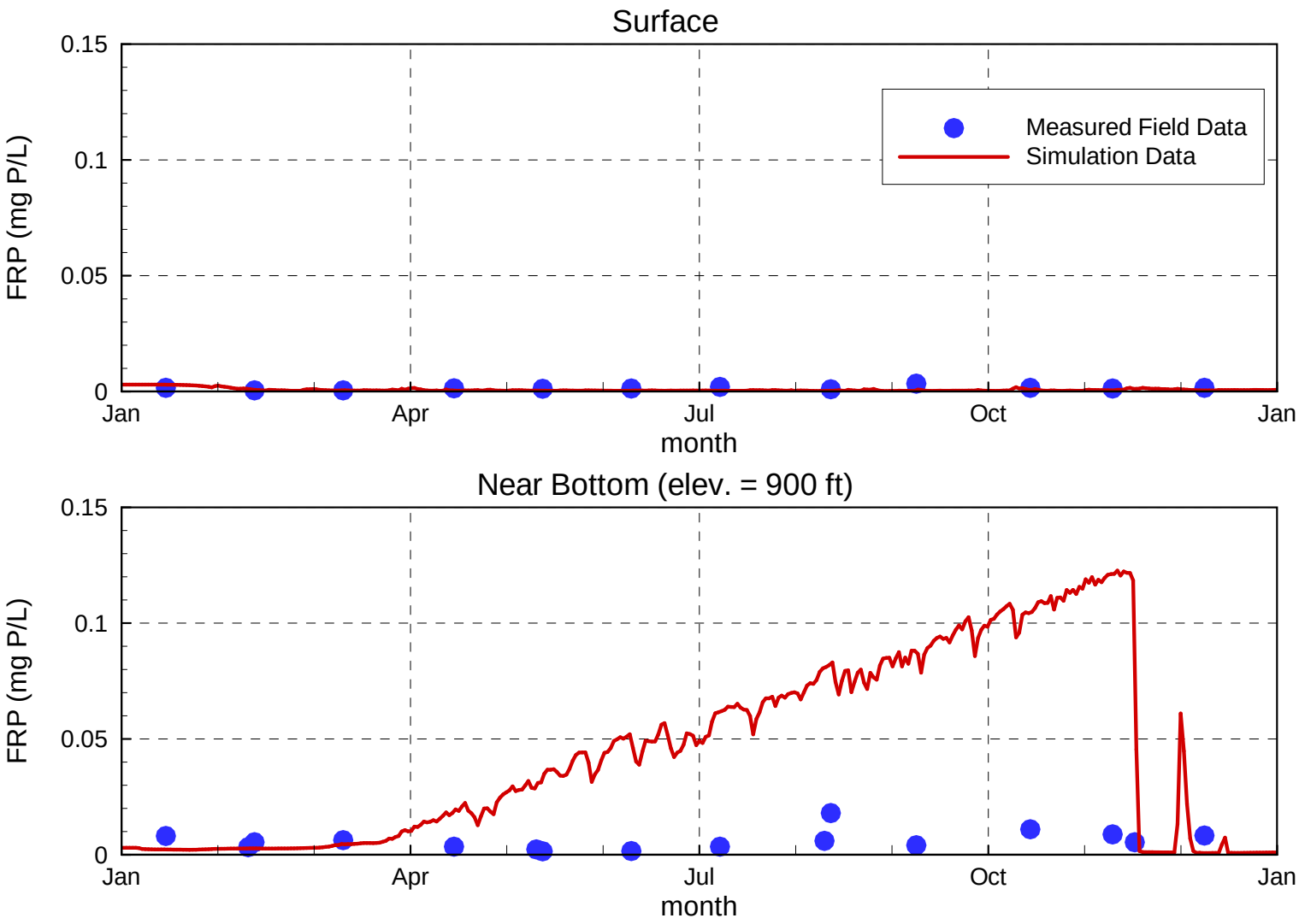

Figure 5.66

Filterable Reactive Phosphorus at Station CR380.0

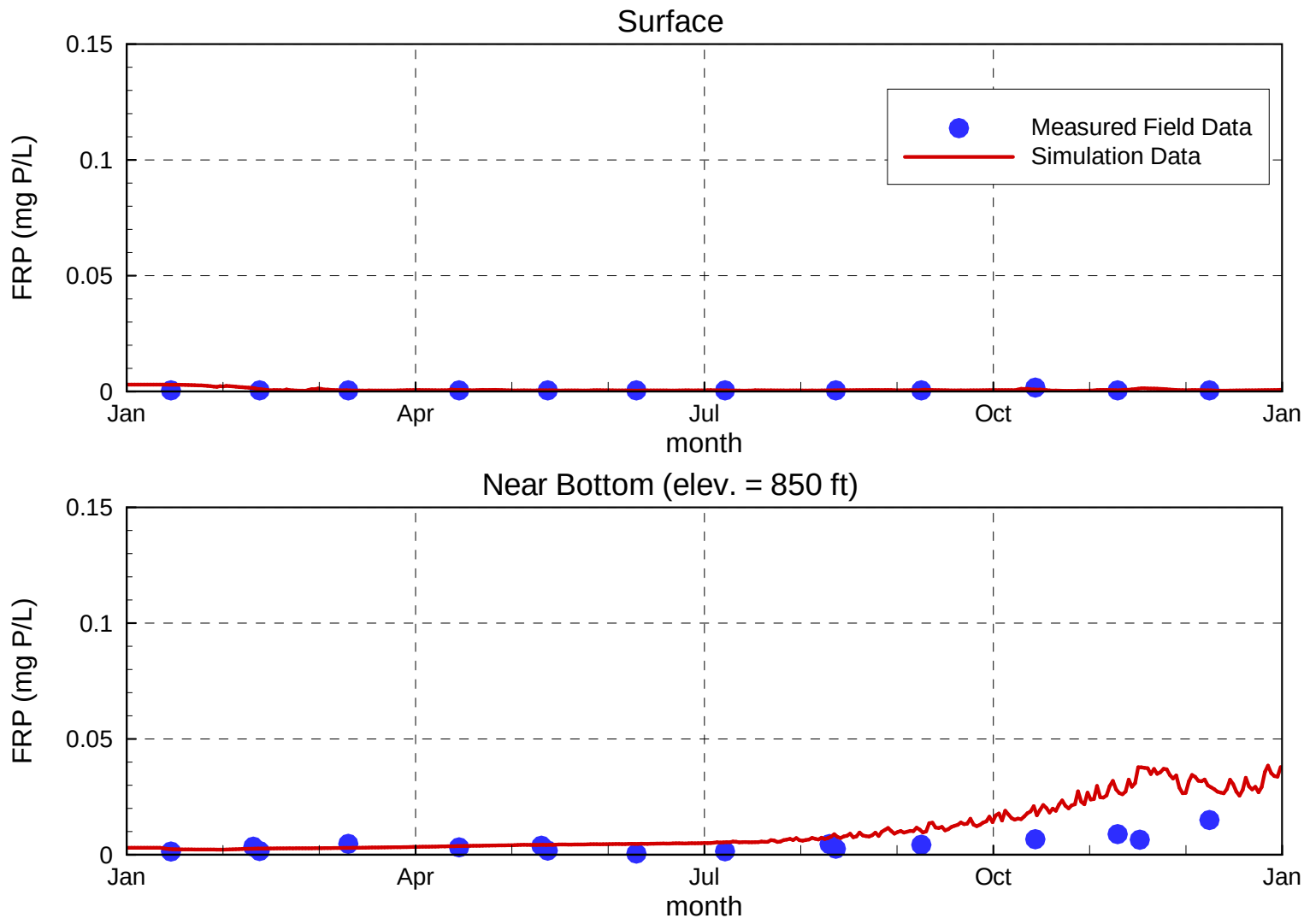

Figure 5.67

Filterable Reactive Phosphorus at Station CR346.4

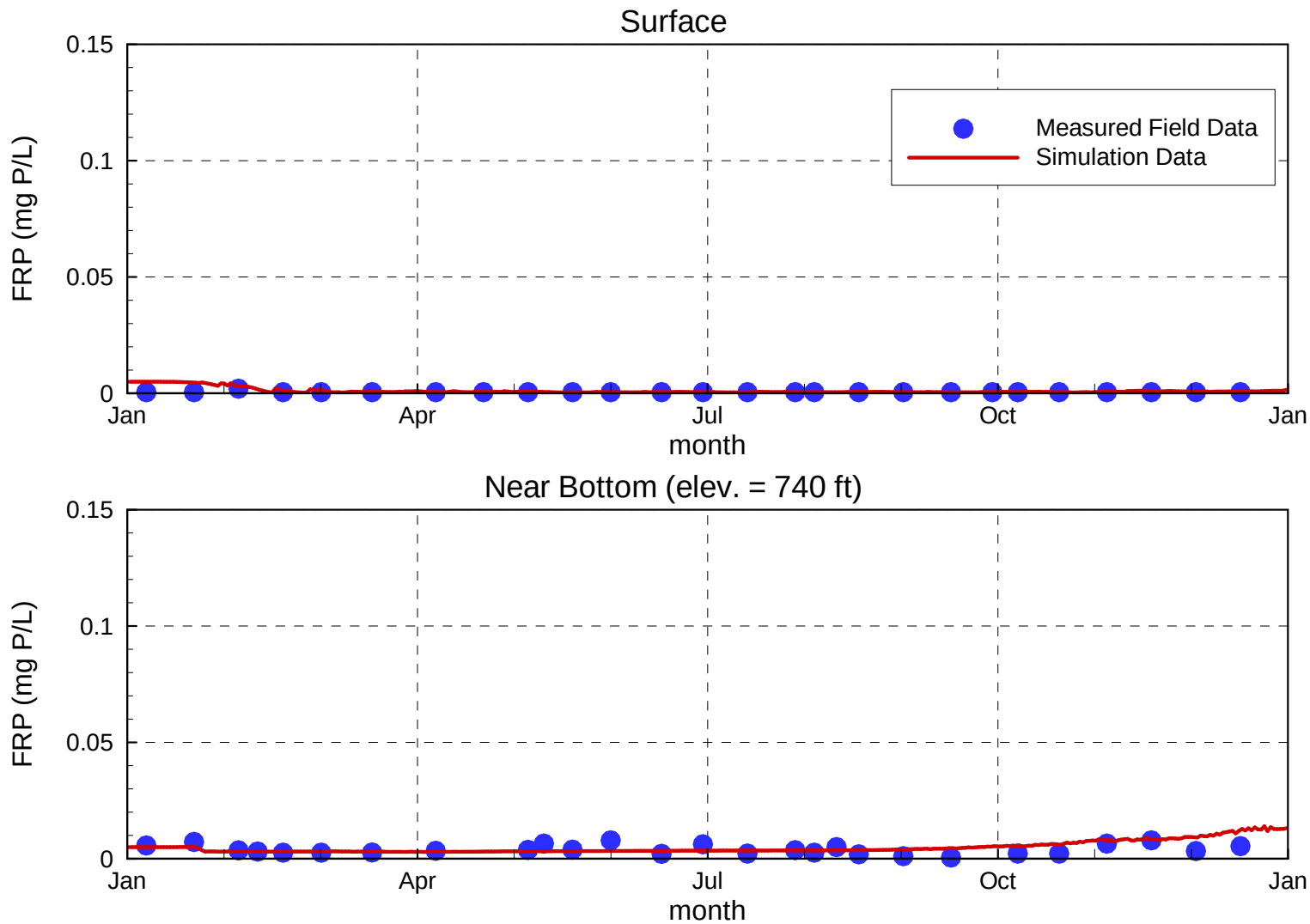

Figure 5.68

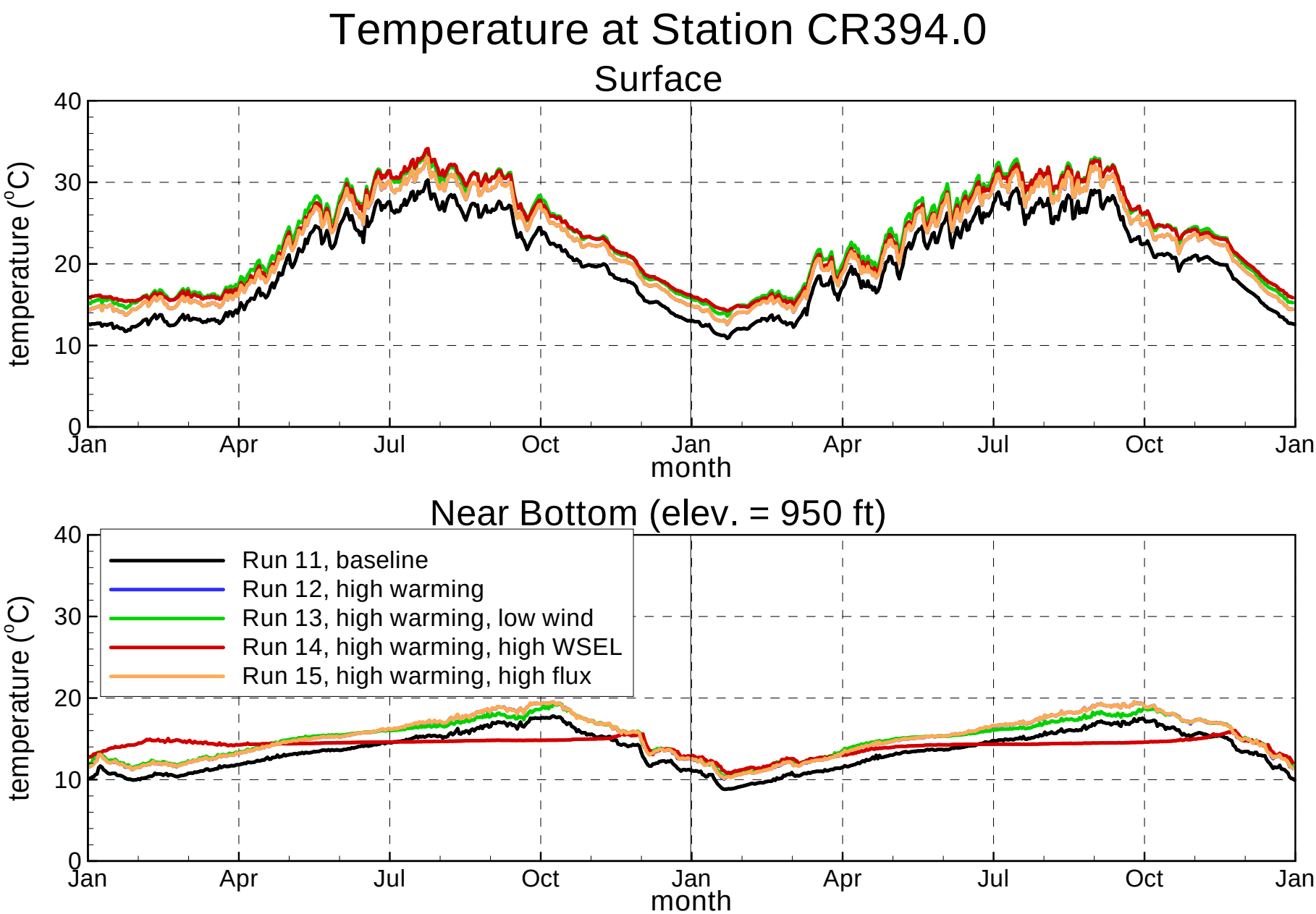
Temperature at Station CR394.0
Surface
temperature (°C)
40
30
20
10
0
Jan
Apr
Jul
Oct
Jan
Apr
Jul
Oct
Jan
month
Near Bottom (elev. = 950 ft)
Run 11, baseline
Run 12, high warming
Run 13, high warming, low wind
Run 14, high warming, high WSEL
Run 15, high warming, high flux
temperature (°C)
40
30
20
10
0
Jan
Apr
Jul
Oct
Jan
Apr
Jul
Oct
Jan
month

Figure A.1

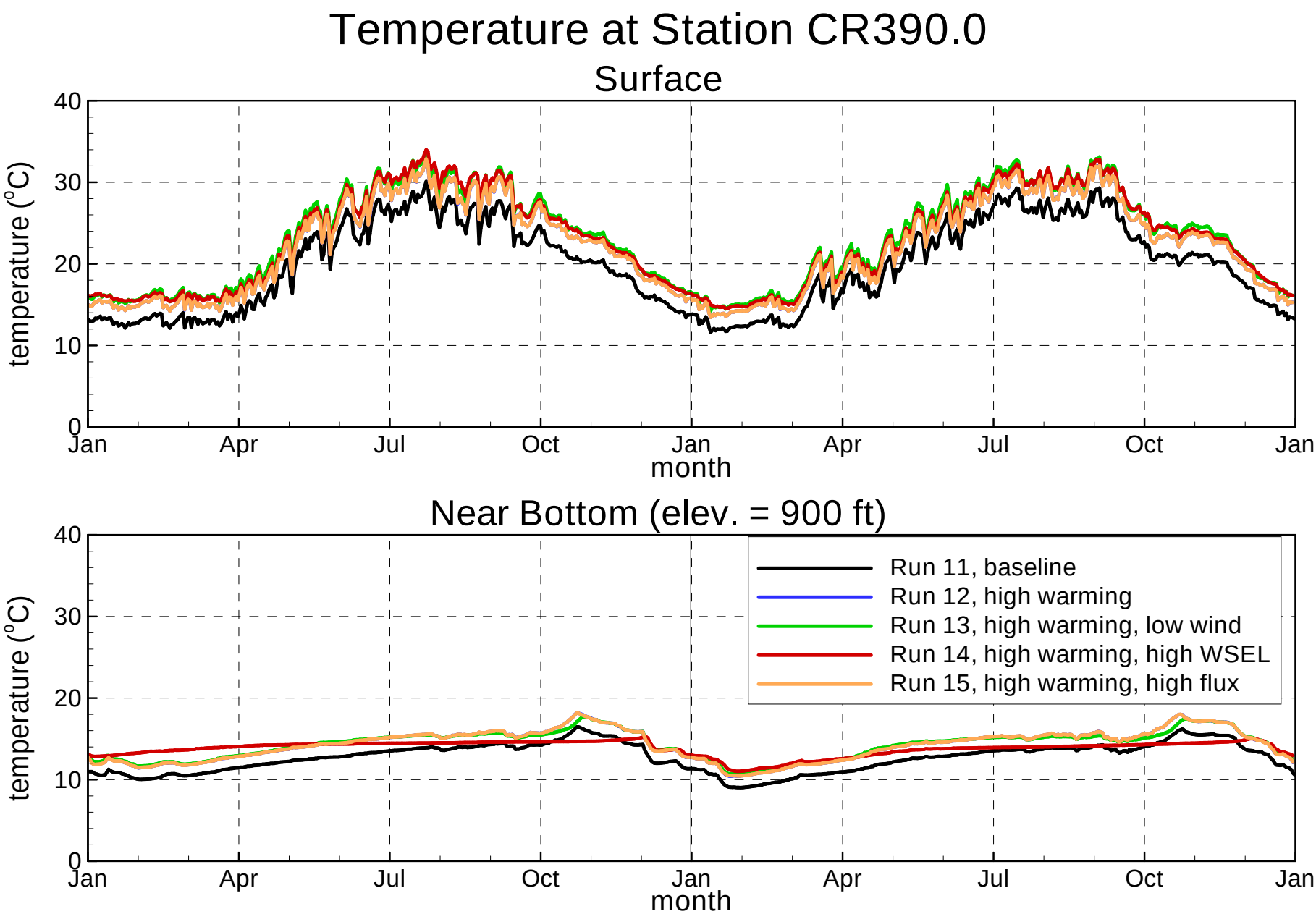
Temperature at Station CR390.0
Surface
temperature (°C)
40
30
20
10
0
Jan
Apr
Jul
Oct
Jan
Apr
Jul
Oct
Jan
month
Near Bottom (elev. = 900 ft)
temperature (°C)
40
30
20
10
0
Jan
Apr
Jul
Oct
Jan
Apr
Jul
Oct
Jan
month
Run 11, baseline
Run 12, high warming
Run 13, high warming, low wind
Run 14, high warming, high WSEL
Run 15, high warming, high flux

Figure A.2

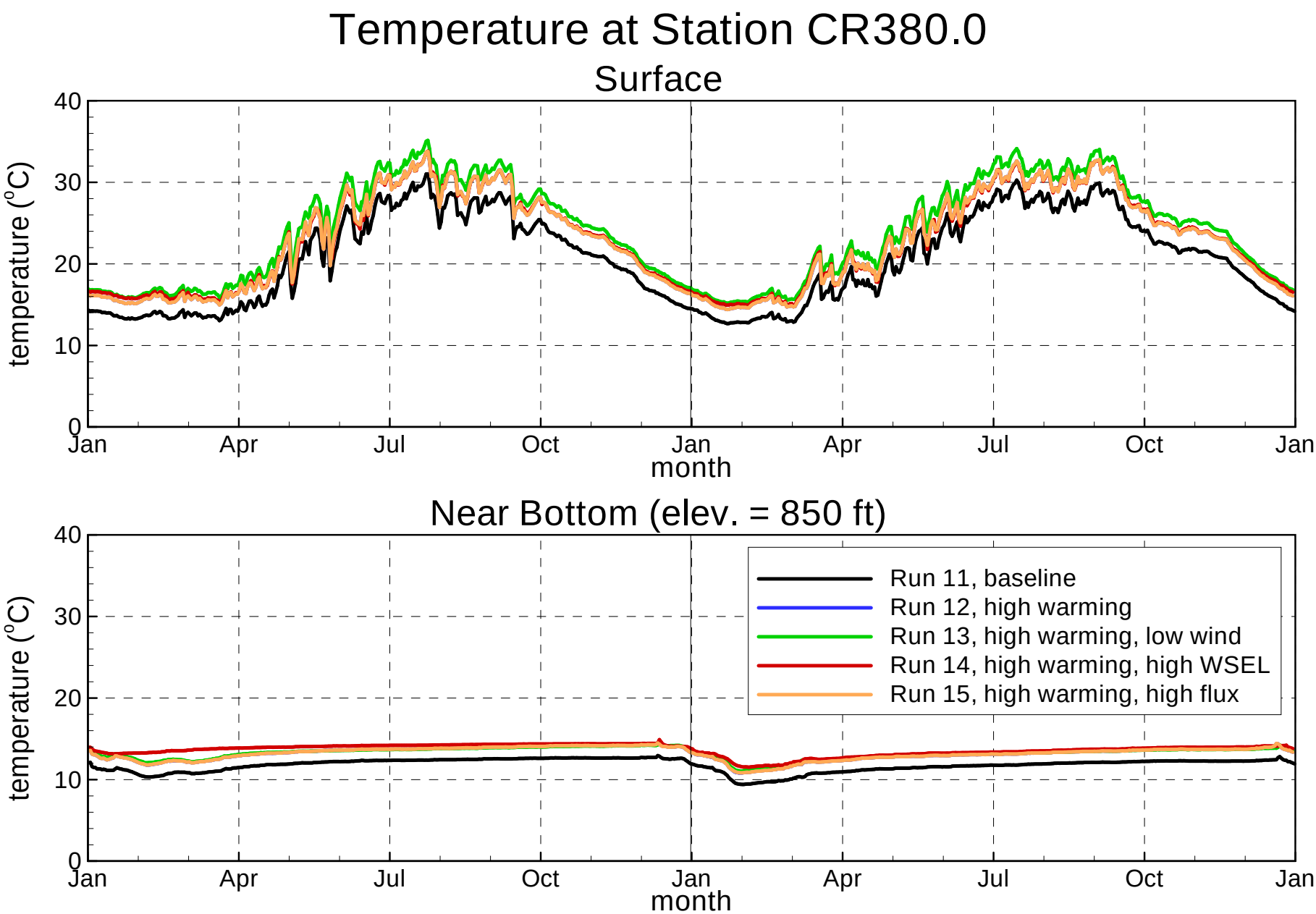
Temperature at Station CR380.0
Surface
temperature (°C)
40
30
20
10
0
Jan
Apr
Jul
Oct
Jan
Apr
Jul
Oct
Jan
month
Near Bottom (elev. = 850 ft)
temperature (°C)
40
30
20
10
0
Jan
Apr
Jul
Oct
Jan
Apr
Jul
Oct
Jan
month
Run 11, baseline
Run 12, high warming
Run 13, high warming, low wind
Run 14, high warming, high WSEL
Run 15, high warming, high flux

Figure A.3

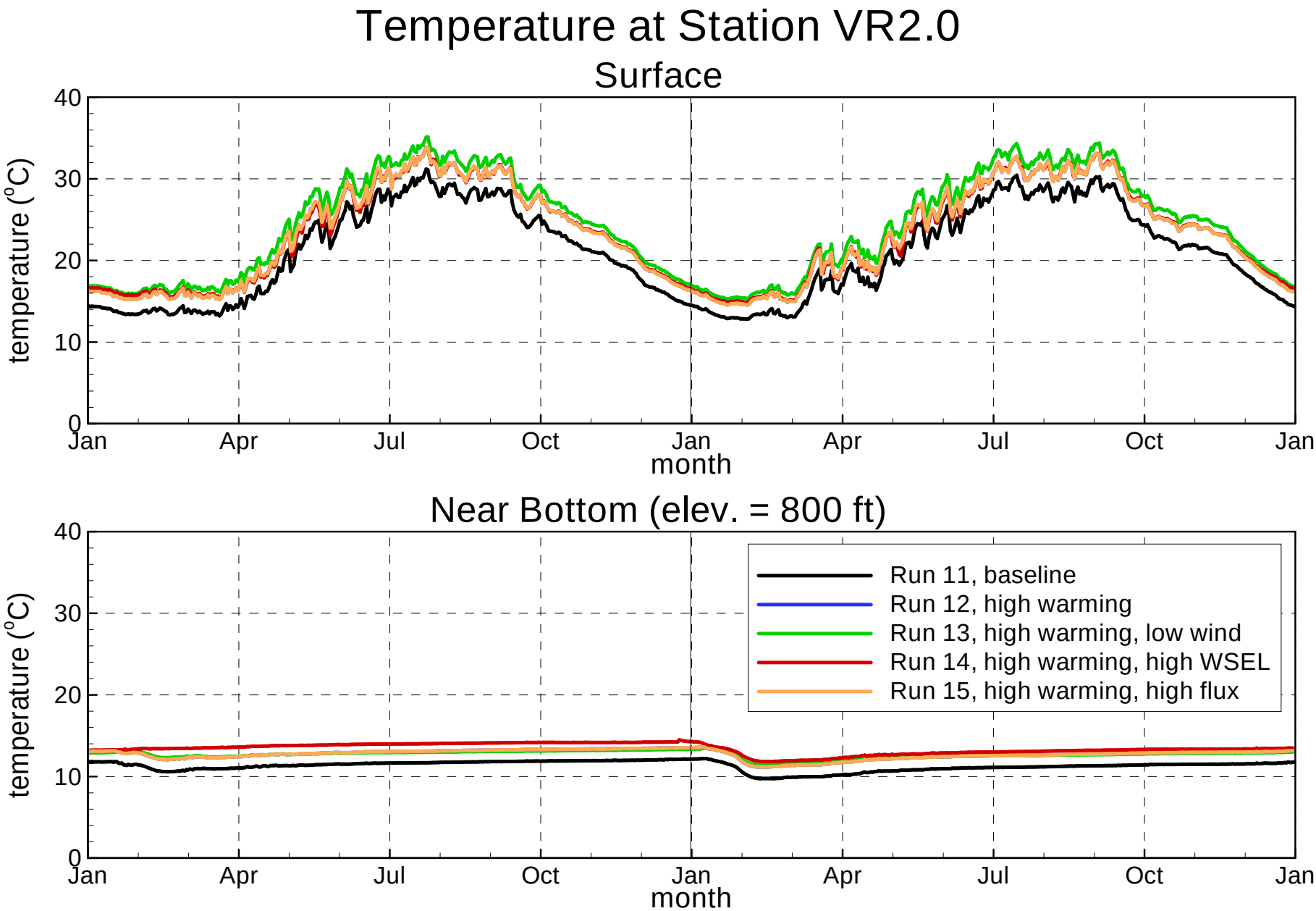
Temperature at Station VR2.0
Surface
temperature (°C)
40
30
20
10
0
Jan
Apr
Jul
Oct
Jan
Apr
Jul
Oct
Jan
month
Near Bottom (elev. = 800 ft)
temperature (°C)
40
30
20
10
0
Jan
Apr
Jul
Oct
Jan
Apr
Jul
Oct
Jan
month
Run 11, baseline
Run 12, high warming
Run 13, high warming, low wind
Run 14, high warming, high WSEL
Run 15, high warming, high flux

Figure A.4

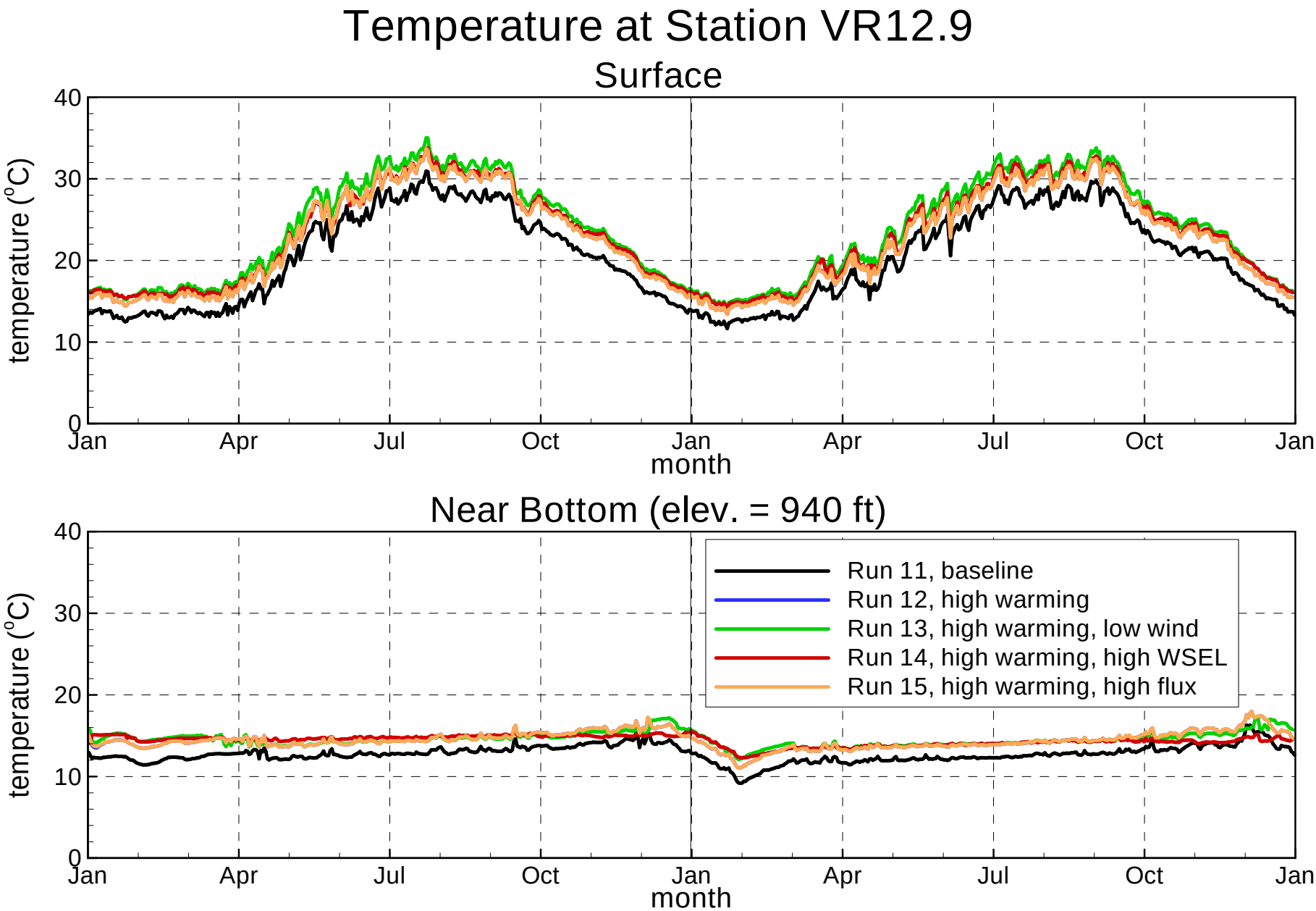

Figure A.5

FLOW SCIENCE

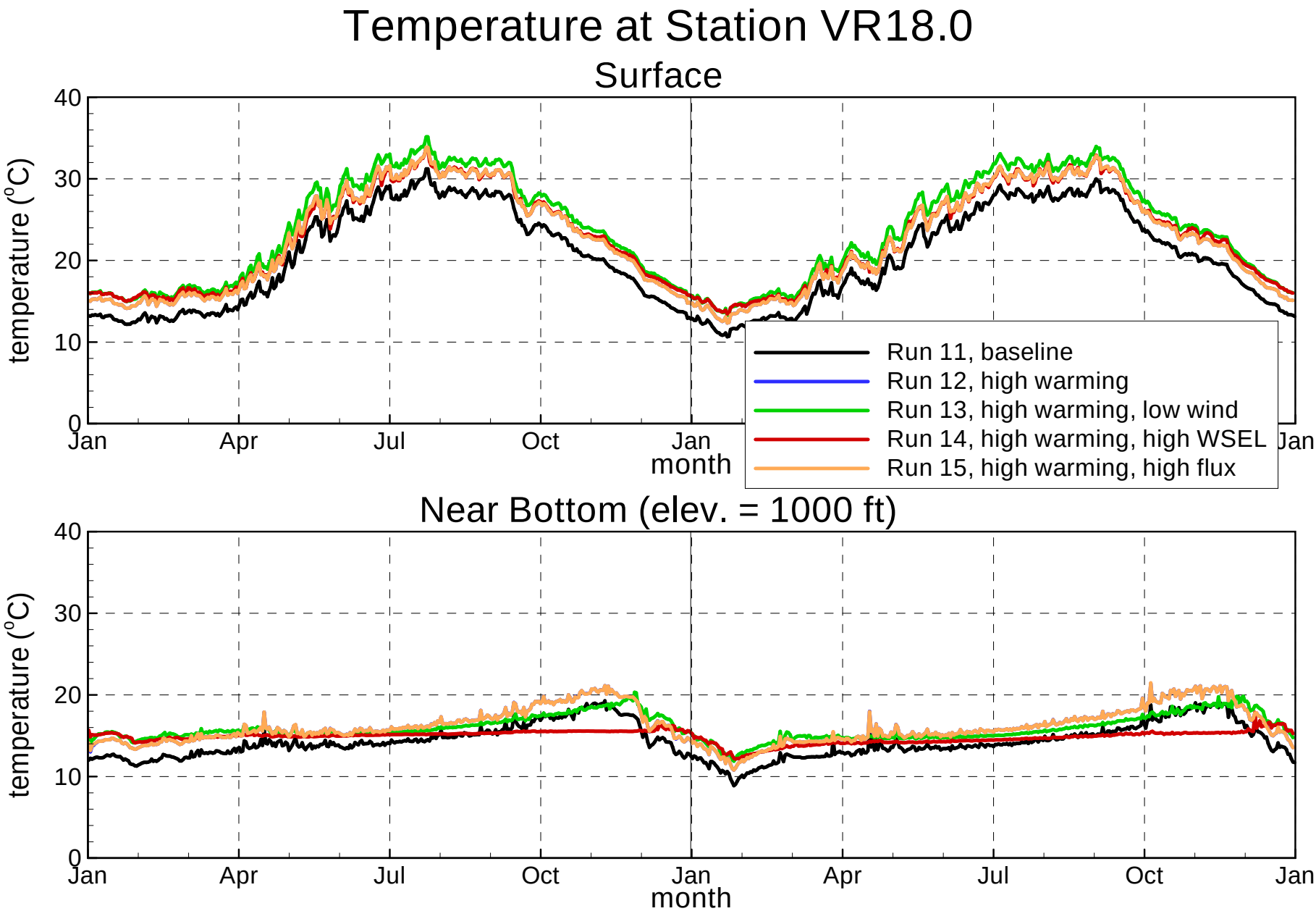

Figure A.6

FLOW SCIENCE

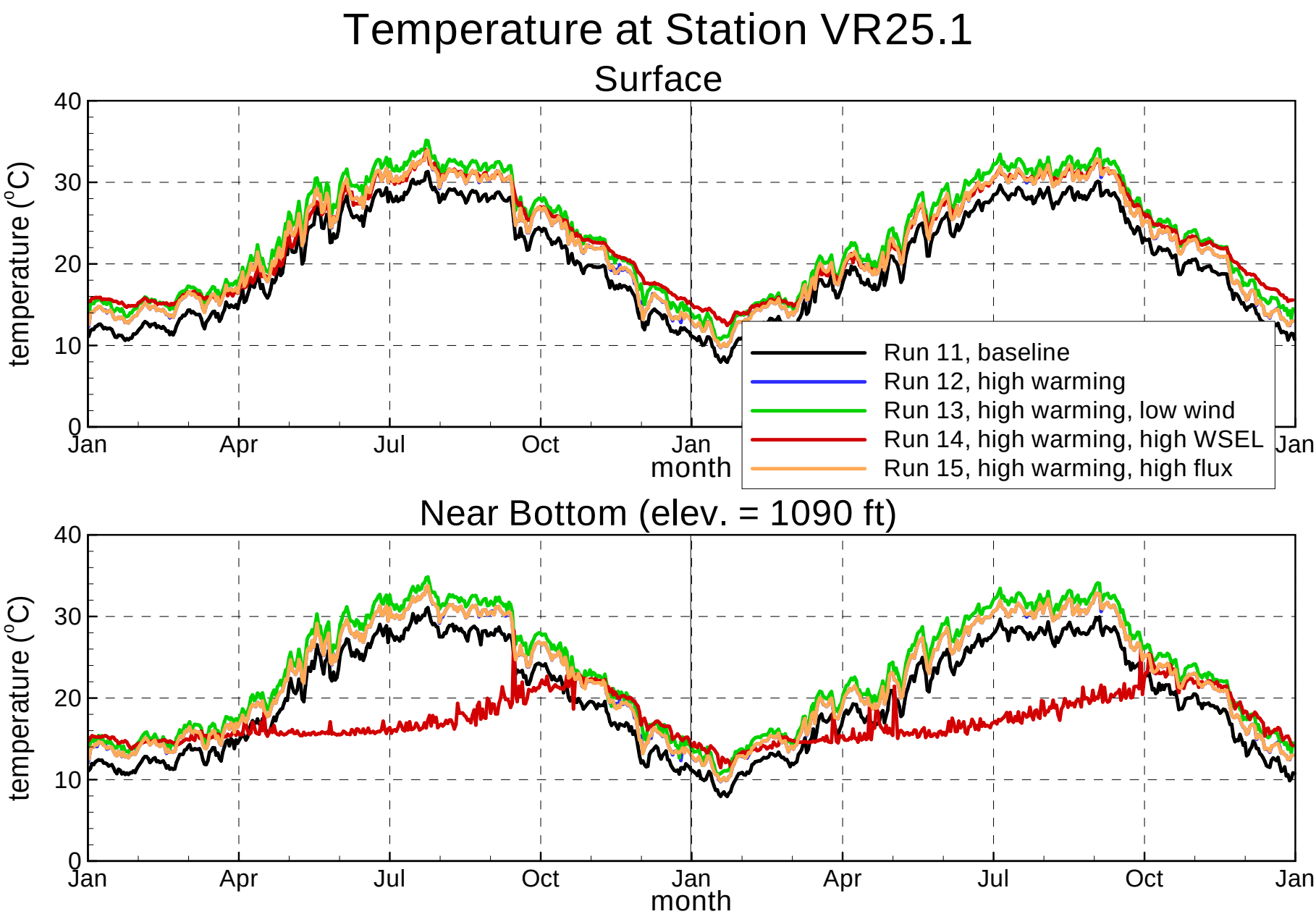
Temperature at Station VR25.1
Surface
temperature (°C)
40
30
20
10
0
Jan
Apr
Jul
Oct
Jan
month
Jan
Run 11, baseline
Run 12, high warming
Run 13, high warming, low wind
Run 14, high warming, high WSEL
Run 15, high warming, high flux
Near Bottom (elev. = 1090 ft)
temperature (°C)
40
30
20
10
0
Jan
Apr
Jul
Oct
Jan
month
Apr
Jul
Oct
Jan

Figure A.7

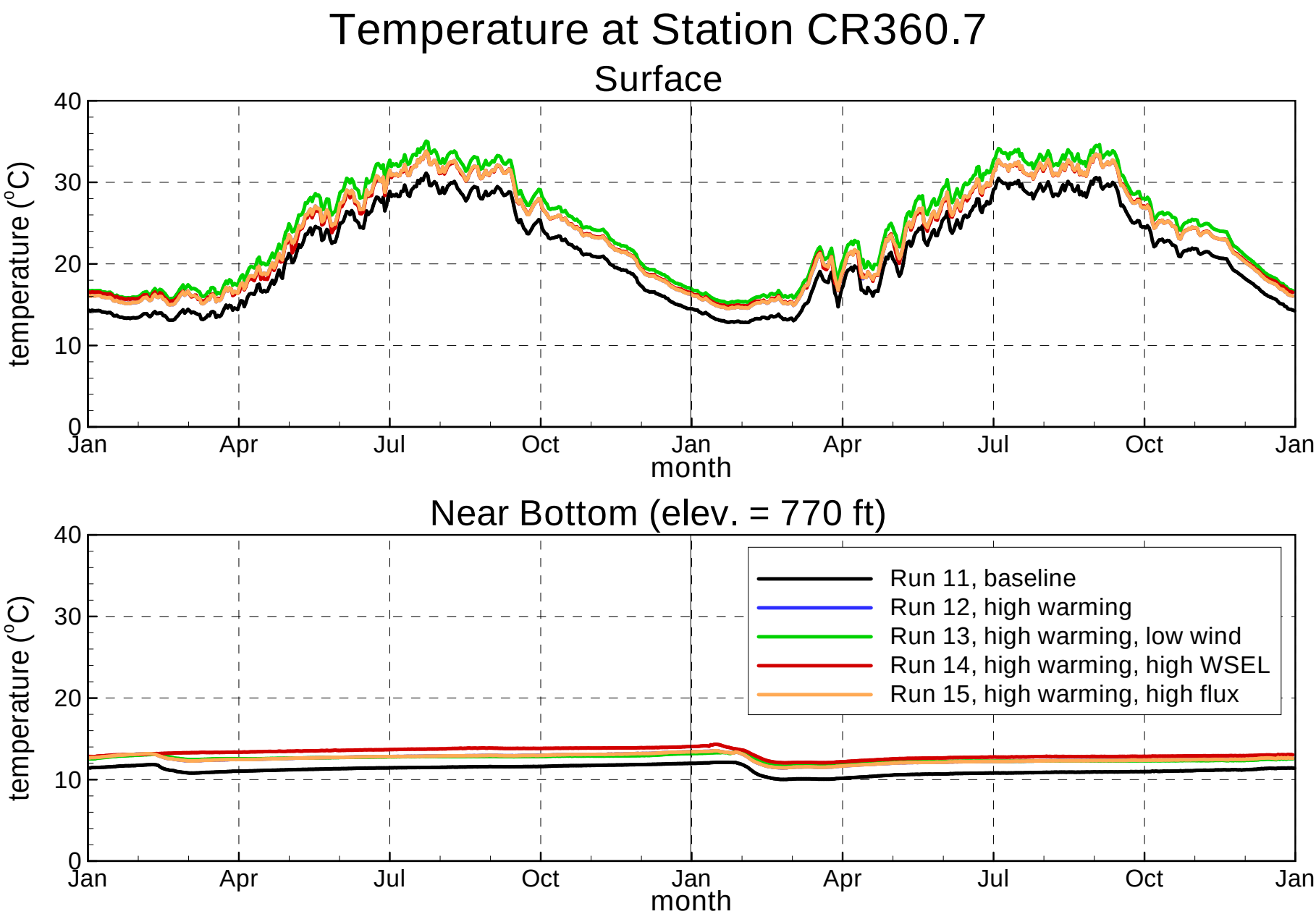
Temperature at Station CR360.7
Surface
temperature (°C)
40
30
20
10
0
Jan
Apr
Jul
Oct
Jan
Apr
Jul
Oct
Jan
month
Near Bottom (elev. = 770 ft)
temperature (°C)
40
30
20
10
0
Jan
Apr
Jul
Oct
Jan
Apr
Jul
Oct
Jan
month
Run 11, baseline
Run 12, high warming
Run 13, high warming, low wind
Run 14, high warming, high WSEL
Run 15, high warming, high flux

Figure A.8

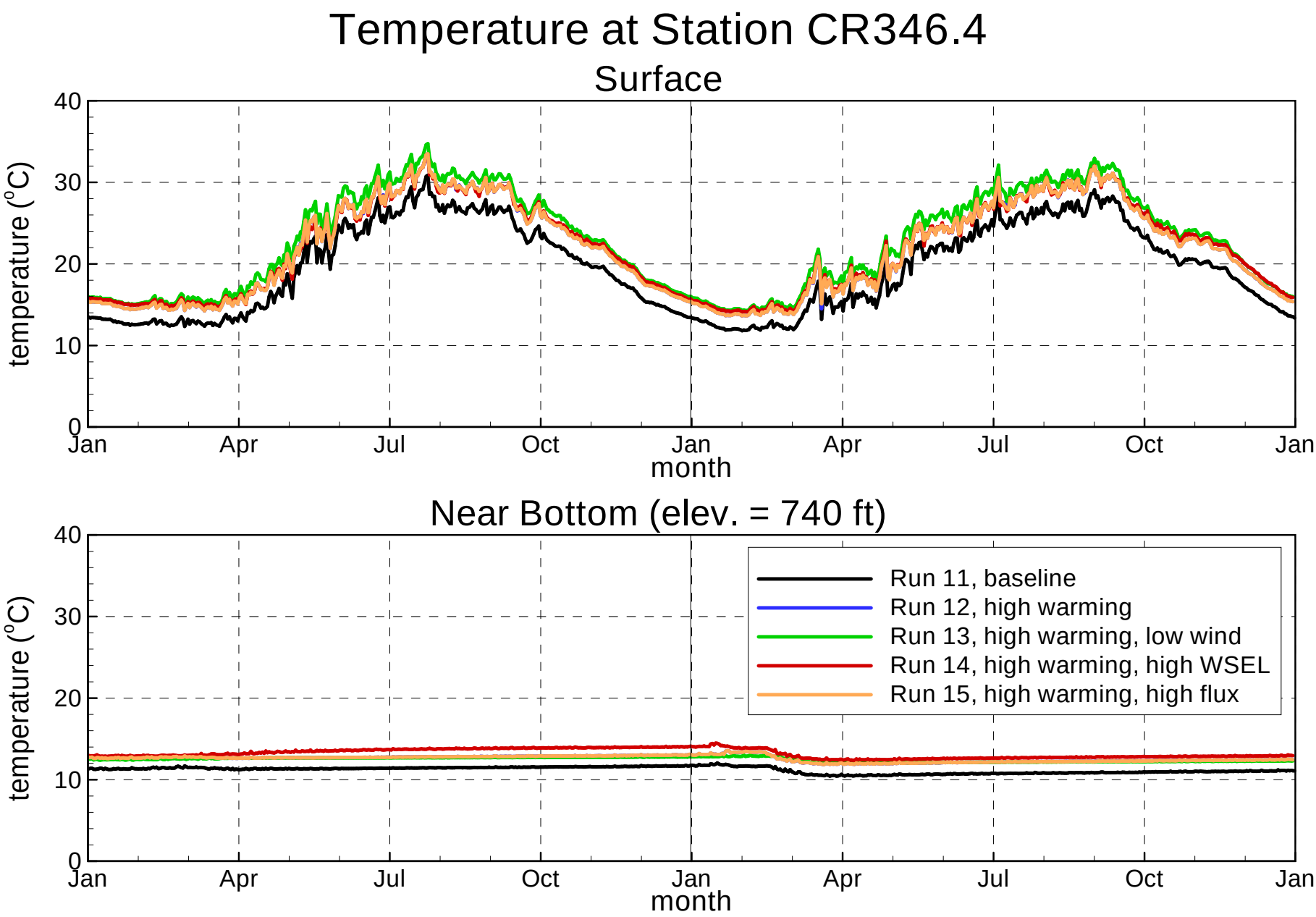
Temperature at Station CR346.4
Surface
temperature (°C)
40
30
20
10
0
Jan
Apr
Jul
Oct
Jan
Apr
Jul
Oct
Jan
month
Near Bottom (elev. = 740 ft)
temperature (°C)
40
30
20
10
0
Jan
Apr
Jul
Oct
Jan
Apr
Jul
Oct
Jan
month
Run 11, baseline
Run 12, high warming
Run 13, high warming, low wind
Run 14, high warming, high WSEL
Run 15, high warming, high flux

Figure A.9

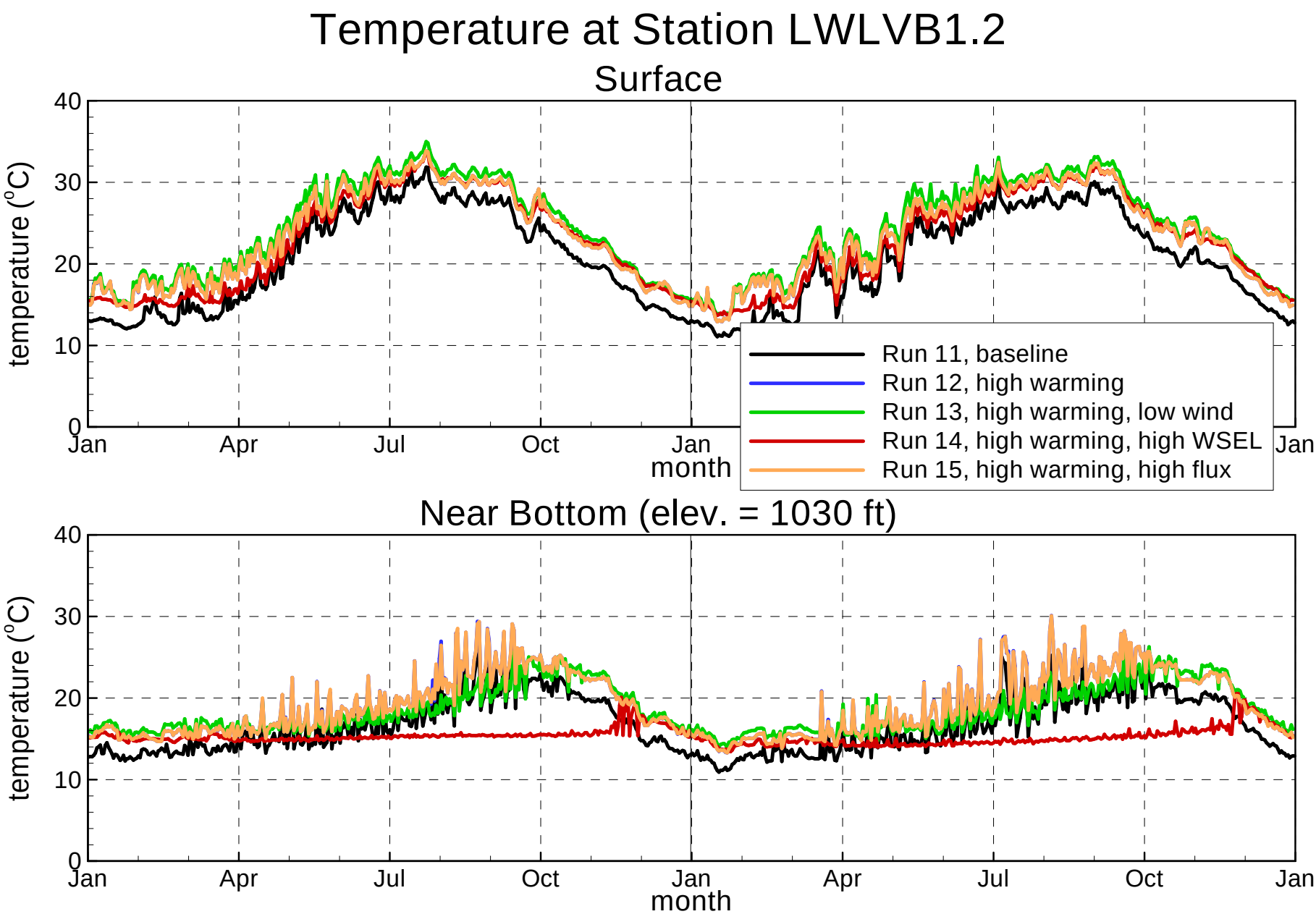
Temperature at Station LWLVB1.2
Surface
temperature (°C)
40
30
20
10
0
Jan
Apr
Jul
Oct
Jan
month
Jan
Run 11, baseline
Run 12, high warming
Run 13, high warming, low wind
Run 14, high warming, high WSEL
Run 15, high warming, high flux
Near Bottom (elev. = 1030 ft)
temperature (°C)
40
30
20
10
0
Jan
Apr
Jul
Oct
Jan
month
Apr
Jul
Oct
Jan

Figure A.10

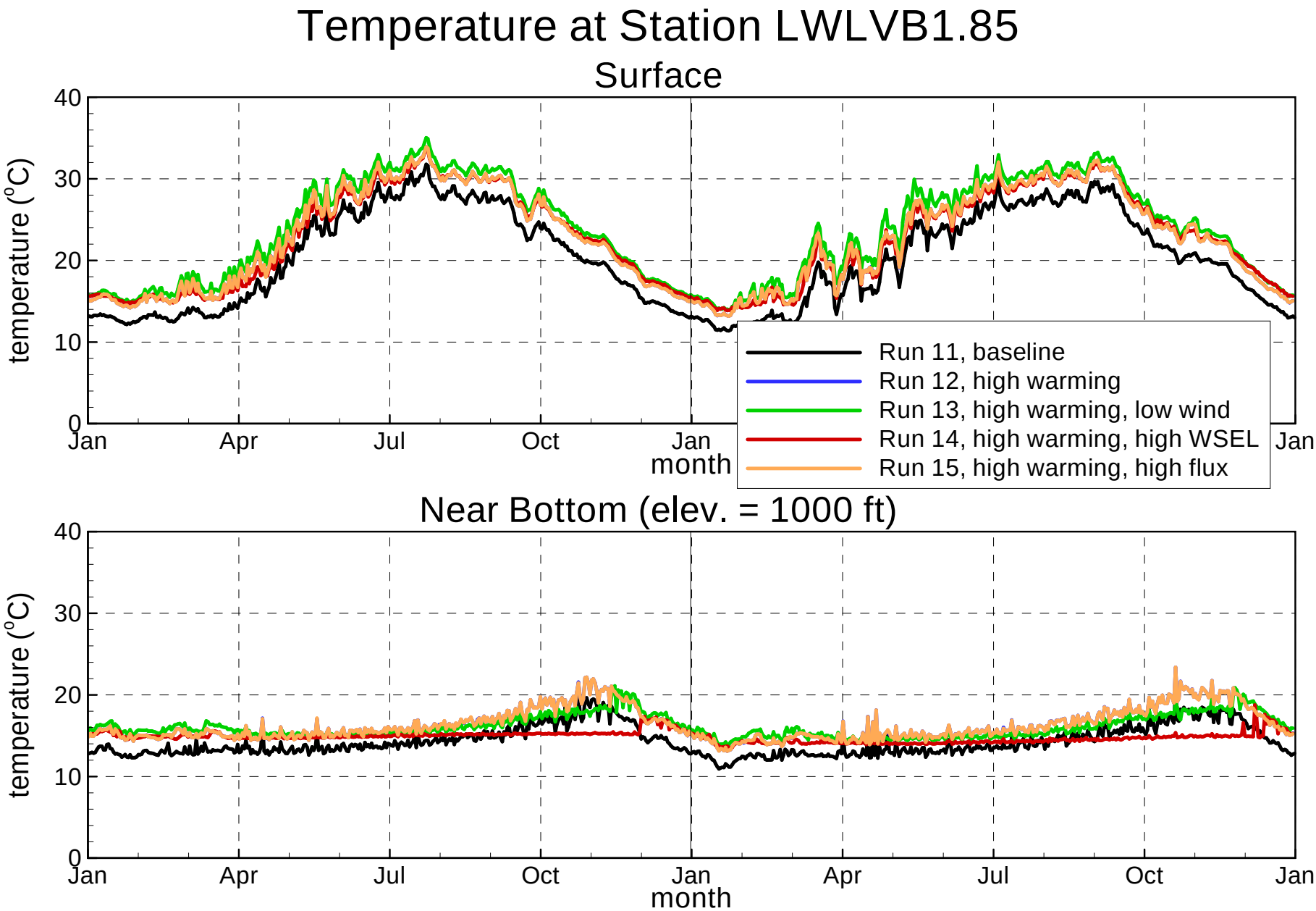
Temperature at Station LWLVB1.85
Surface
temperature (°C)
40
30
20
10
0
Jan
Apr
Jul
Oct
Jan
month
Jan
Run 11, baseline
Run 12, high warming
Run 13, high warming, low wind
Run 14, high warming, high WSEL
Run 15, high warming, high flux
Near Bottom (elev. = 1000 ft)
temperature (°C)
40
30
20
10
0
Jan
Apr
Jul
Oct
Jan
month
Apr
Jul
Oct
Jan

Figure A.11

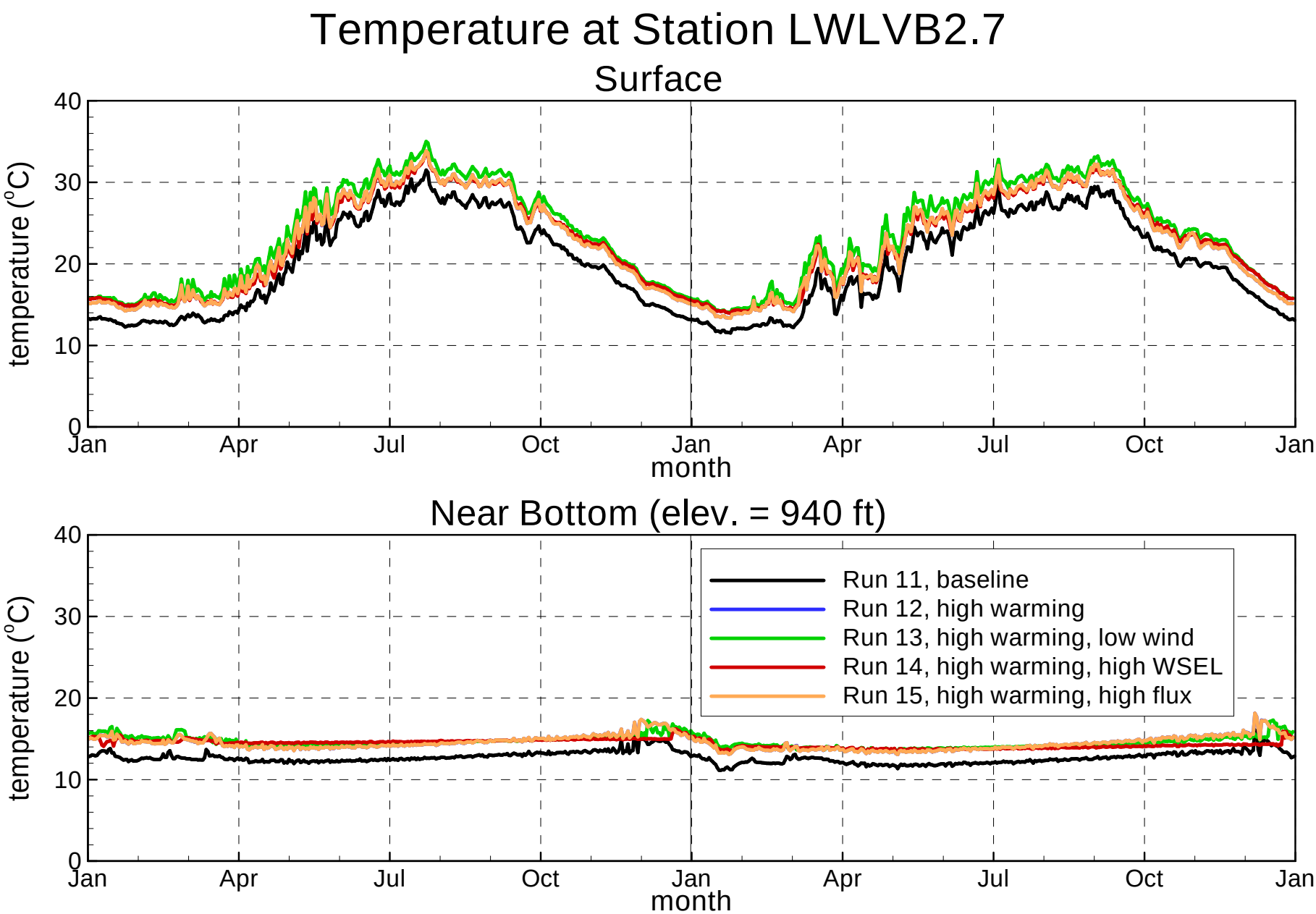

Figure A.12

FLOW SCIENCE

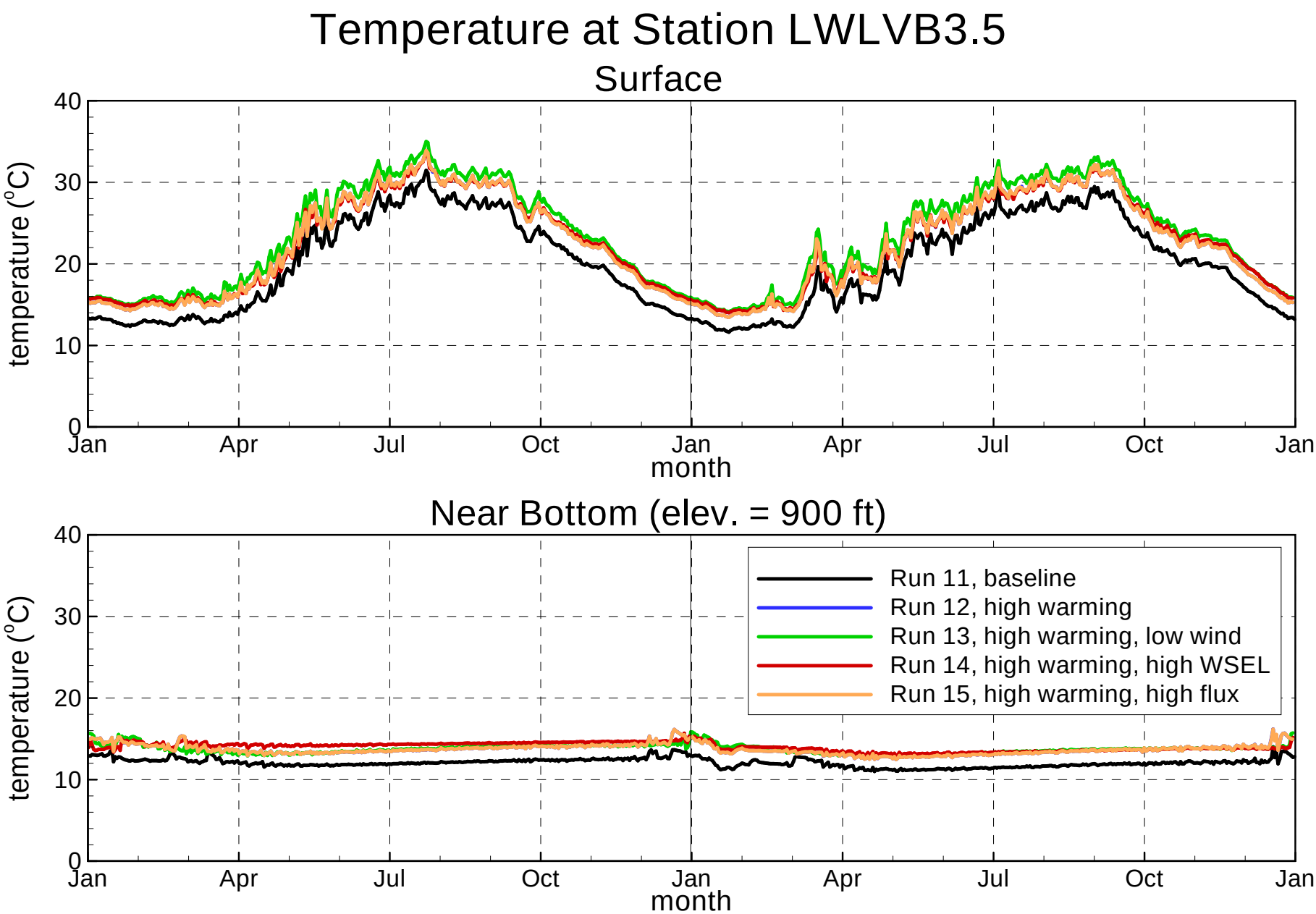

Figure A.13

FLOW SCIENCE

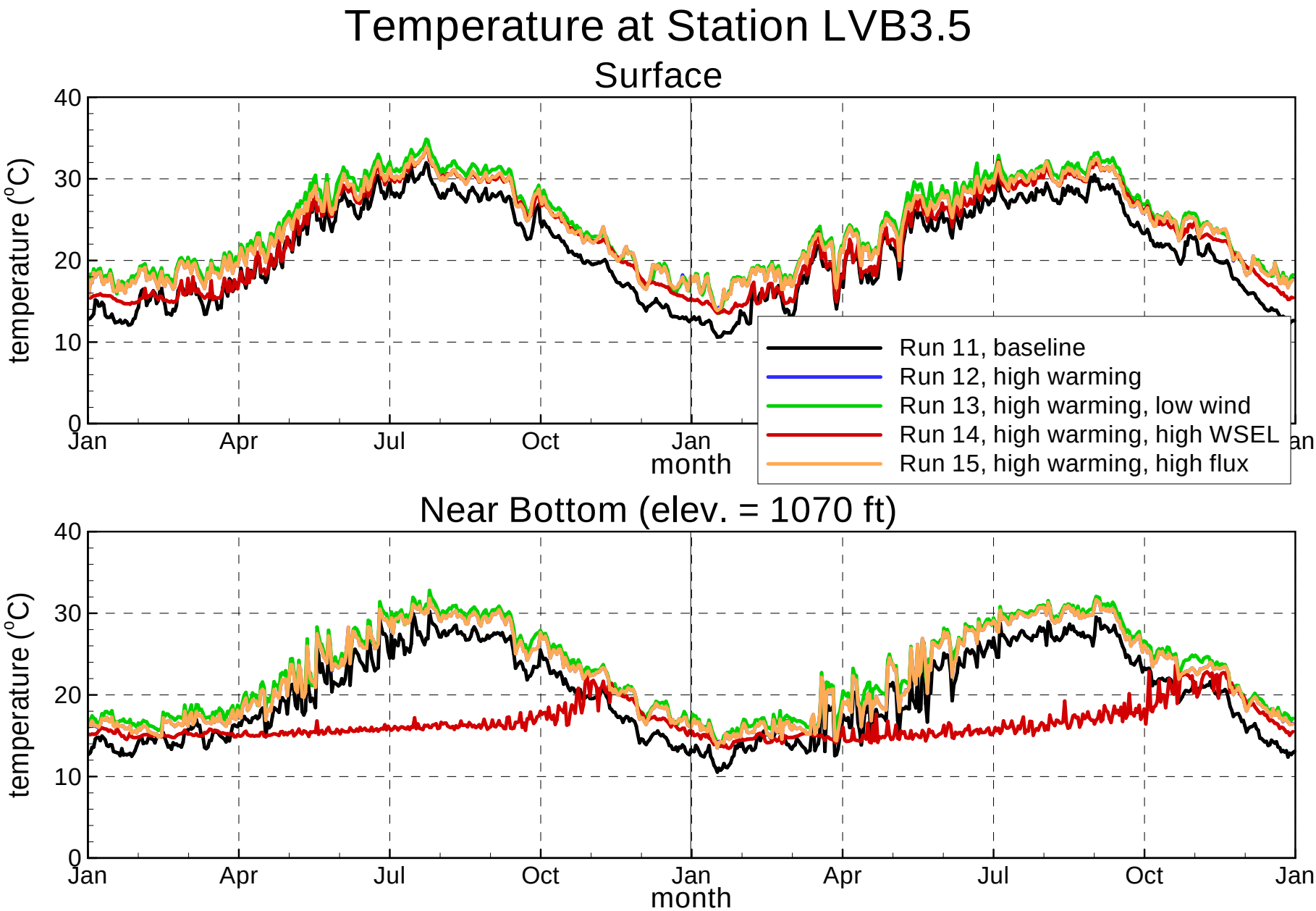
Temperature at Station LVB3.5
Surface
temperature (°C)
40
30
20
10
0
Jan
Apr
Jul
Oct
Jan
month
Run 11, baseline
Run 12, high warming
Run 13, high warming, low wind
Run 14, high warming, high WSEL
Run 15, high warming, high flux
Near Bottom (elev. = 1070 ft)
temperature (°C)
40
30
20
10
0
Jan
Apr
Jul
Oct
Jan
month
Apr
Jul
Oct
Jan

Figure A.14

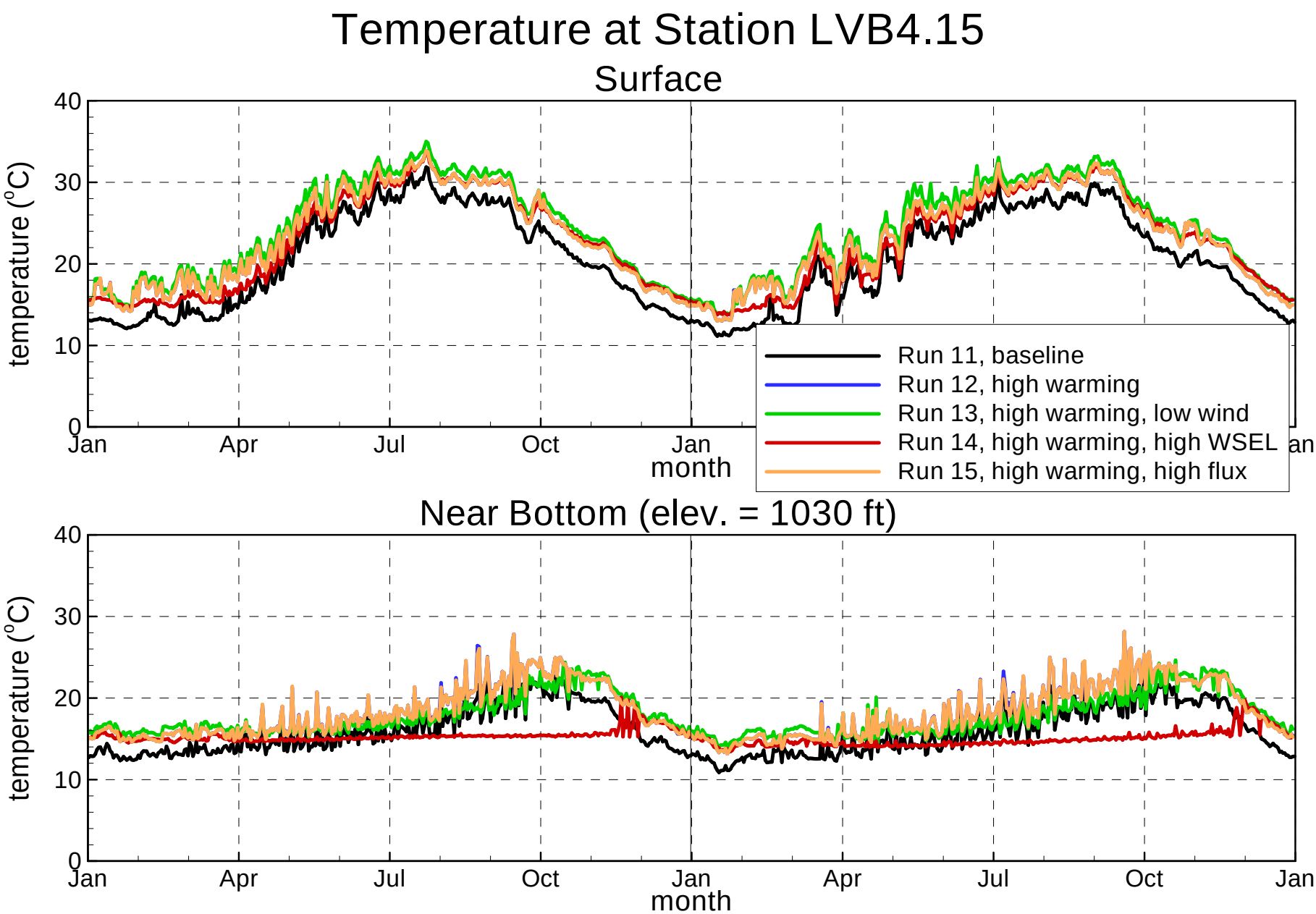
Temperature at Station LVB4.15
Surface
temperature (°C)
40
30
20
10
0
Jan
Apr
Jul
Oct
Jan
month
Run 11, baseline
Run 12, high warming
Run 13, high warming, low wind
Run 14, high warming, high WSEL
Run 15, high warming, high flux
Near Bottom (elev. = 1030 ft)
temperature (°C)
40
30
20
10
0
Jan
Apr
Jul
Oct
Jan
month
Apr
Jul
Oct
Jan

Figure A.15

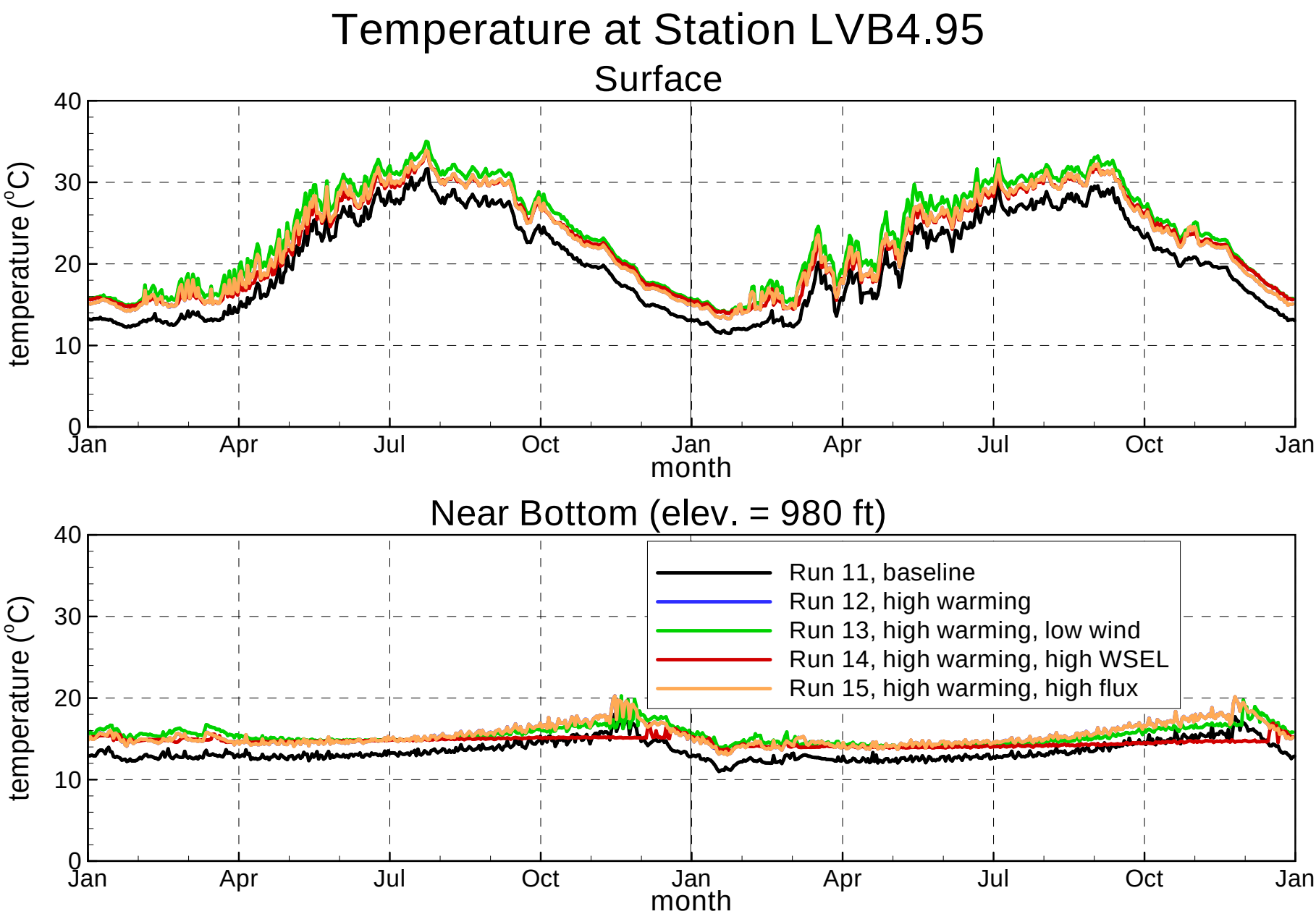

Figure A.16

FLOW SCIENCE

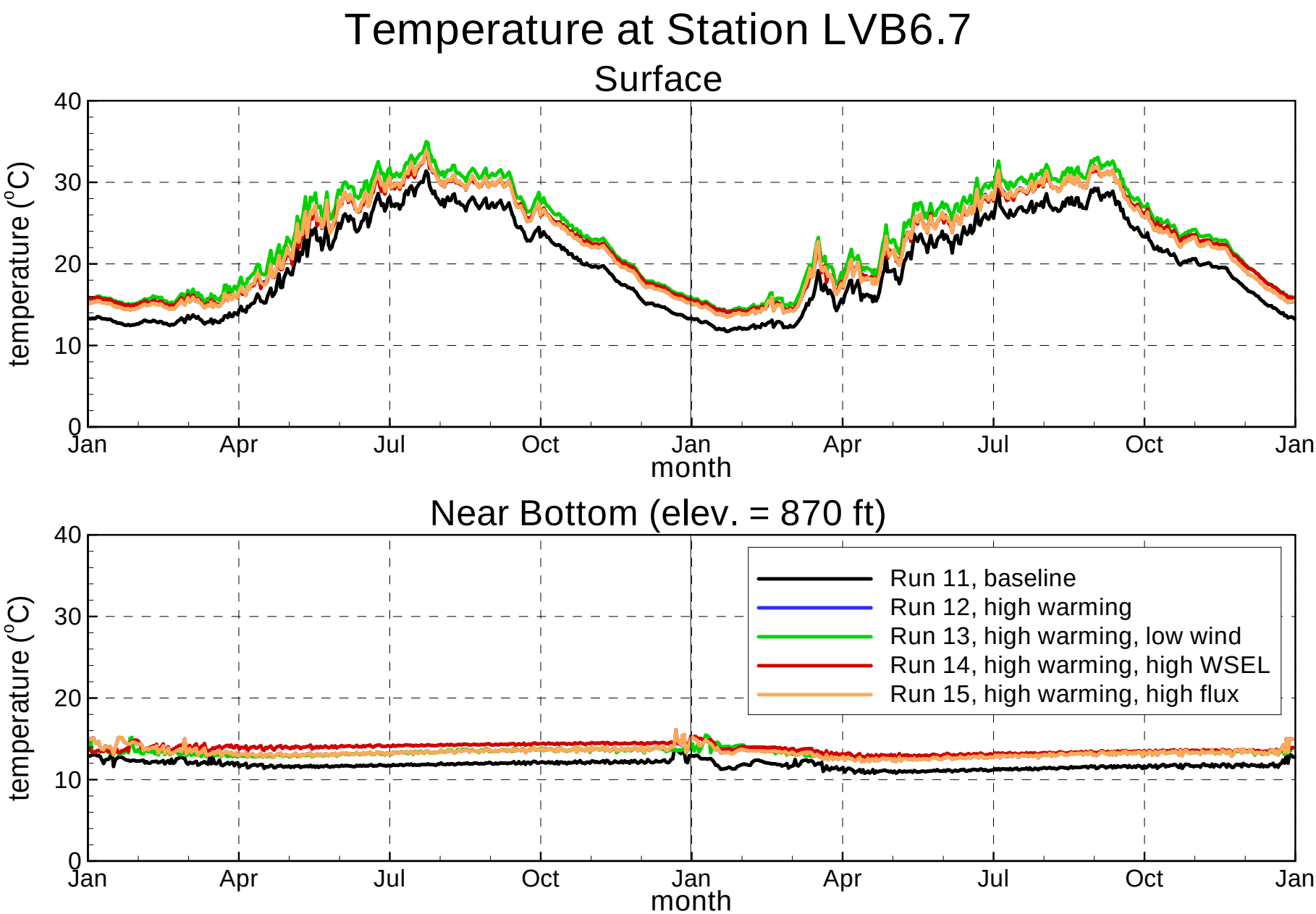
Temperature at Station LVB6.7
Surface
temperature (°C)
40
30
20
10
0
Jan
Apr
Jul
Oct
Jan
Apr
Jul
Oct
Jan
month
Near Bottom (elev. = 870 ft)
temperature (°C)
40
30
20
10
0
Jan
Apr
Jul
Oct
Jan
Apr
Jul
Oct
Jan
month
Run 11, baseline
Run 12, high warming
Run 13, high warming, low wind
Run 14, high warming, high WSEL
Run 15, high warming, high flux

Figure A.17

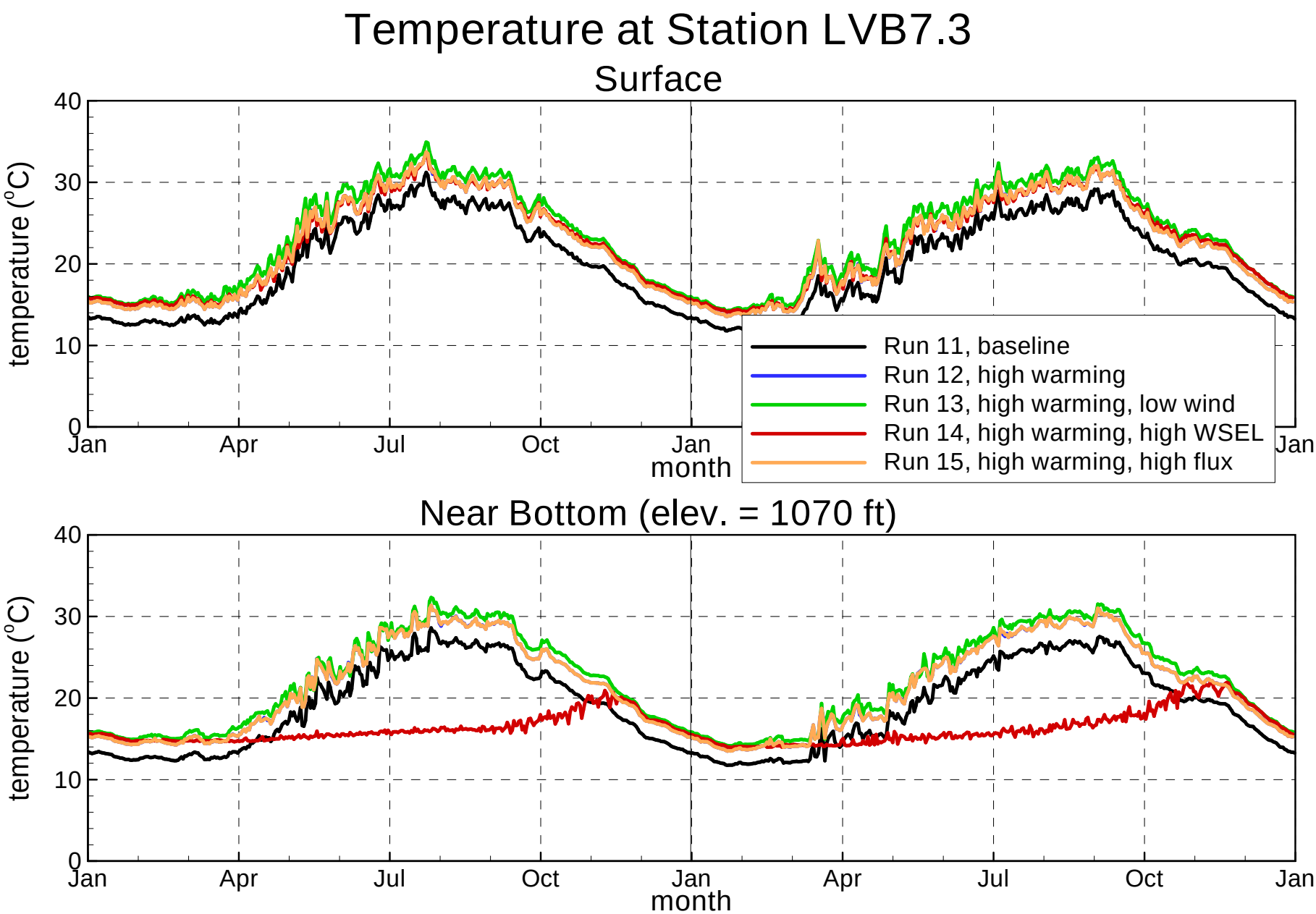
Temperature at Station LVB7.3
Surface
temperature (°C)
40
30
20
10
0
Jan
Apr
Jul
Oct
Jan
month
Jan
Run 11, baseline
Run 12, high warming
Run 13, high warming, low wind
Run 14, high warming, high WSEL
Run 15, high warming, high flux
Near Bottom (elev. = 1070 ft)
temperature (°C)
40
30
20
10
0
Jan
Apr
Jul
Oct
Jan
month
Apr
Jul
Oct
Jan

Figure A.18

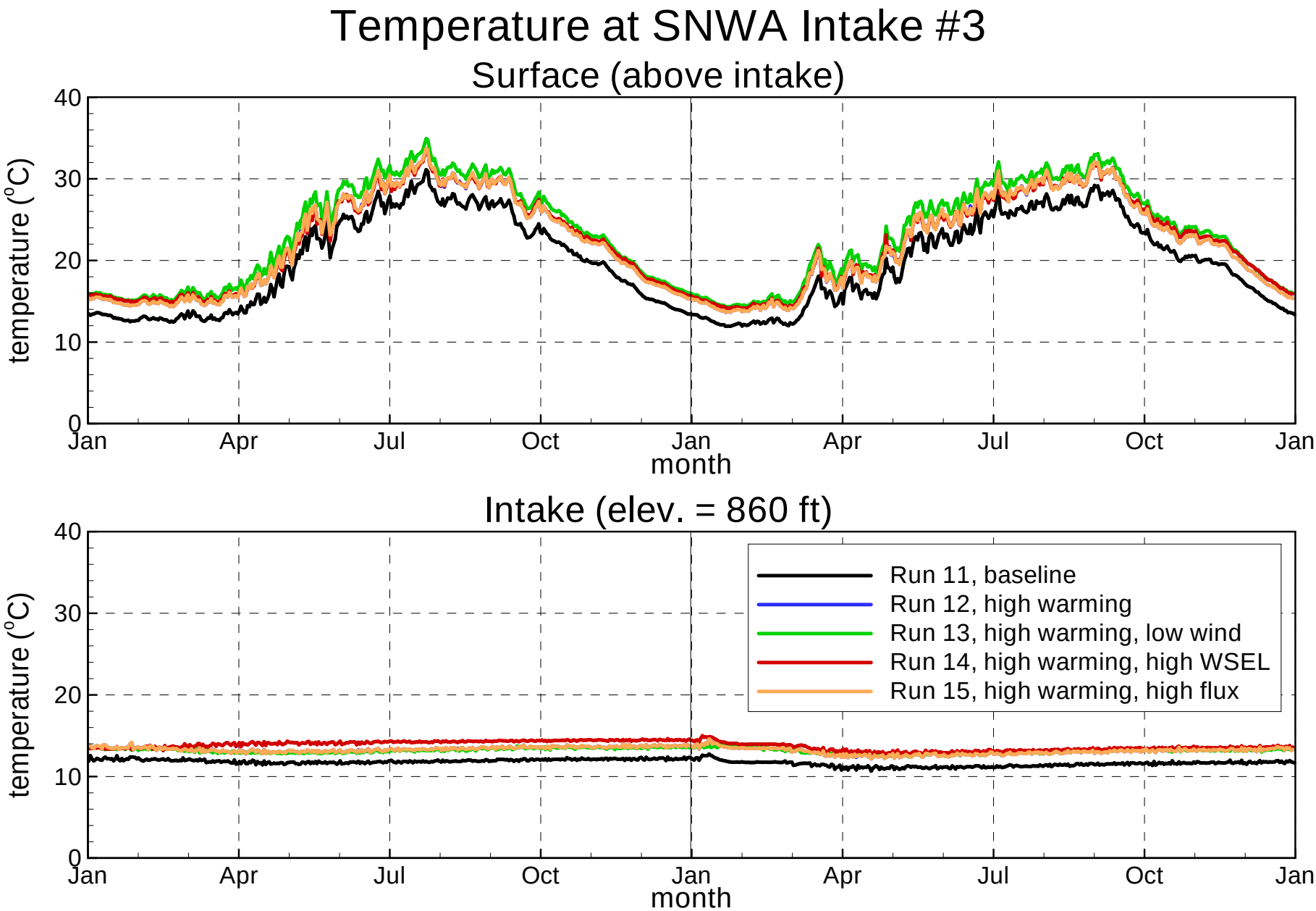

Figure A.19

FLOW SCIENCE

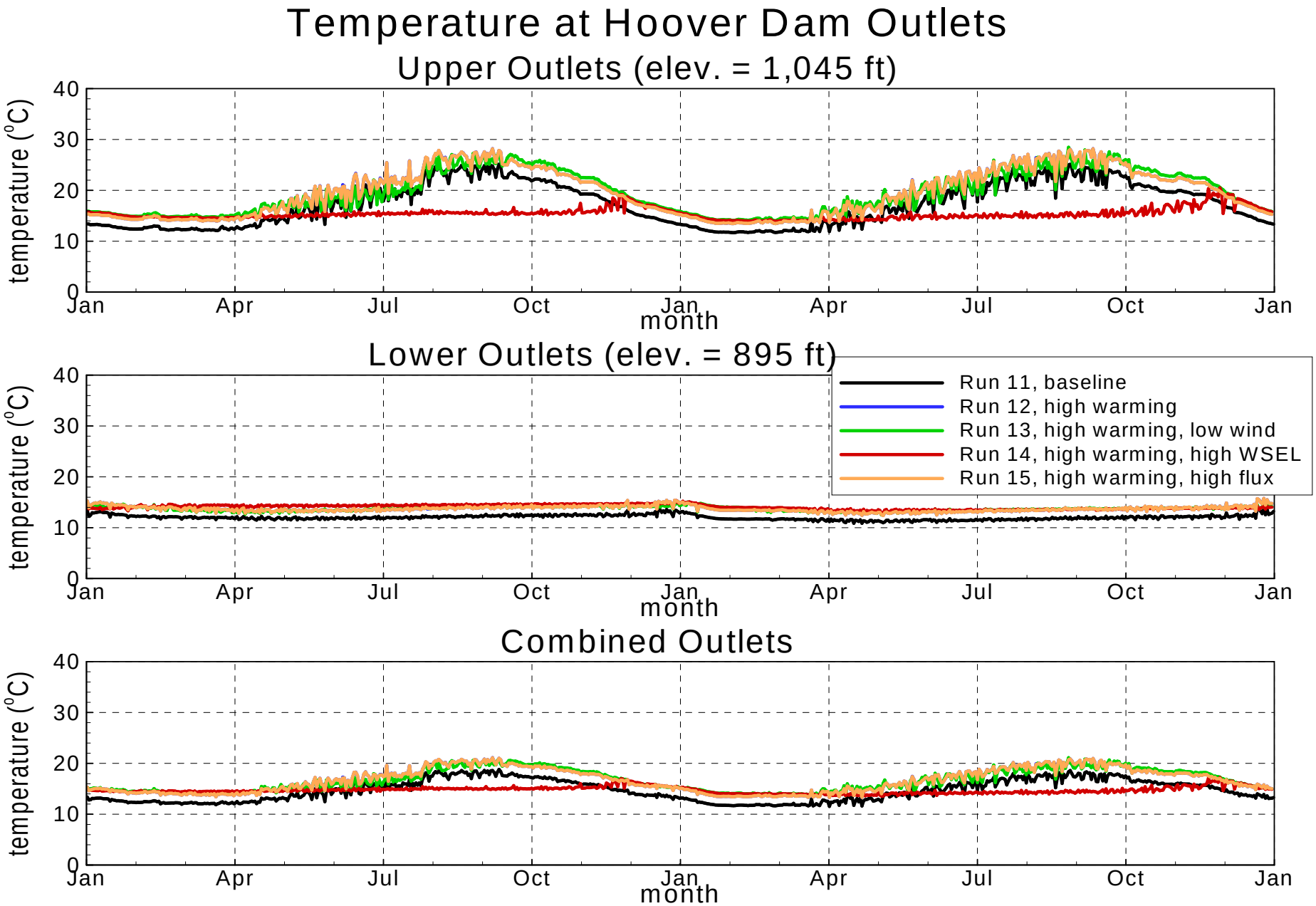
Temperature at Hoover Dam Outlets
Upper Outlets (elev. = 1,045 ft)
Lower Outlets (elev. = 895 ft)
Combined Outlets
temperature (°C)
month
Jan
Apr
Jul
Oct
Run 11, baseline
Run 12, high warming
Run 13, high warming, low wind
Run 14, high warming, high WSEL
Run 15, high warming, high flux

Figure A.20

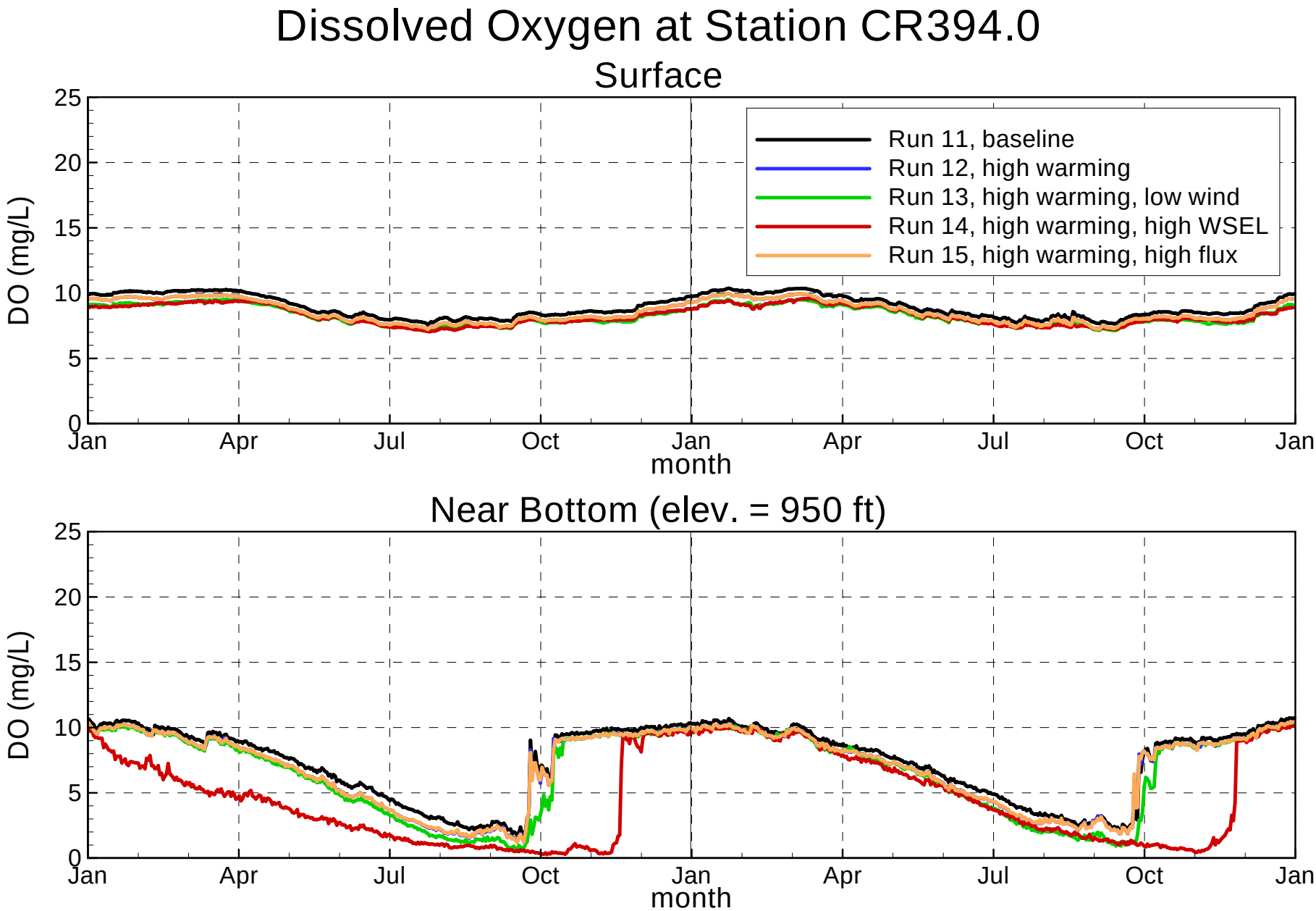
Dissolved Oxygen at Station CR394.0
Surface
Run 11, baseline
Run 12, high warming
Run 13, high warming, low wind
Run 14, high warming, high WSEL
Run 15, high warming, high flux
DO (mg/L)
25
20
15
10
5
0
Jan
Apr
Jul
Oct
Jan
Apr
Jul
Oct
Jan
month
Near Bottom (elev. = 950 ft)
DO (mg/L)
25
20
15
10
5
0
Jan
Apr
Jul
Oct
Jan
Apr
Jul
Oct
Jan
month

Figure A.21

Dissolved Oxygen at Station CR390.0

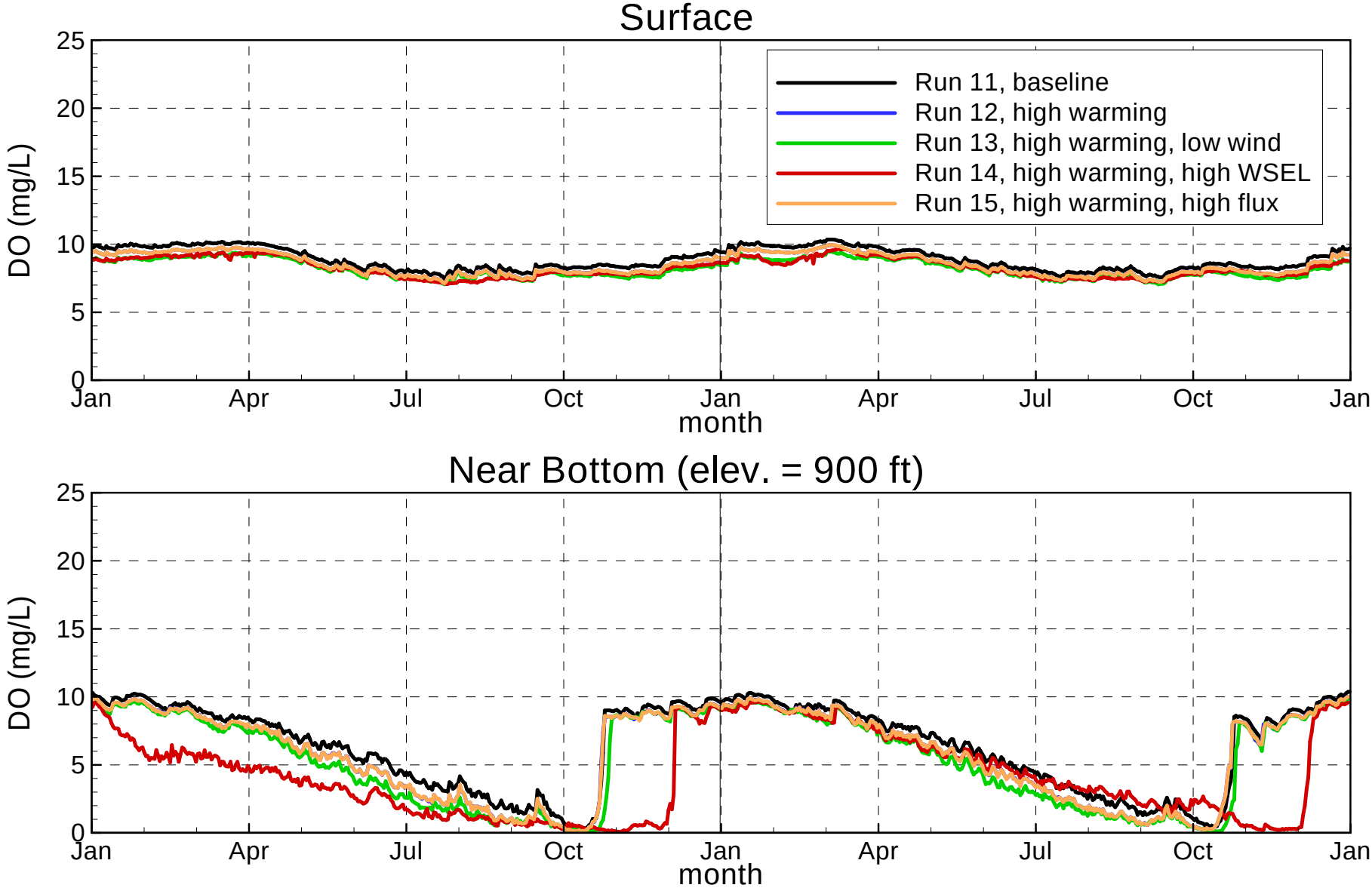

Figure A.22

Dissolved Oxygen at Station CR380.0

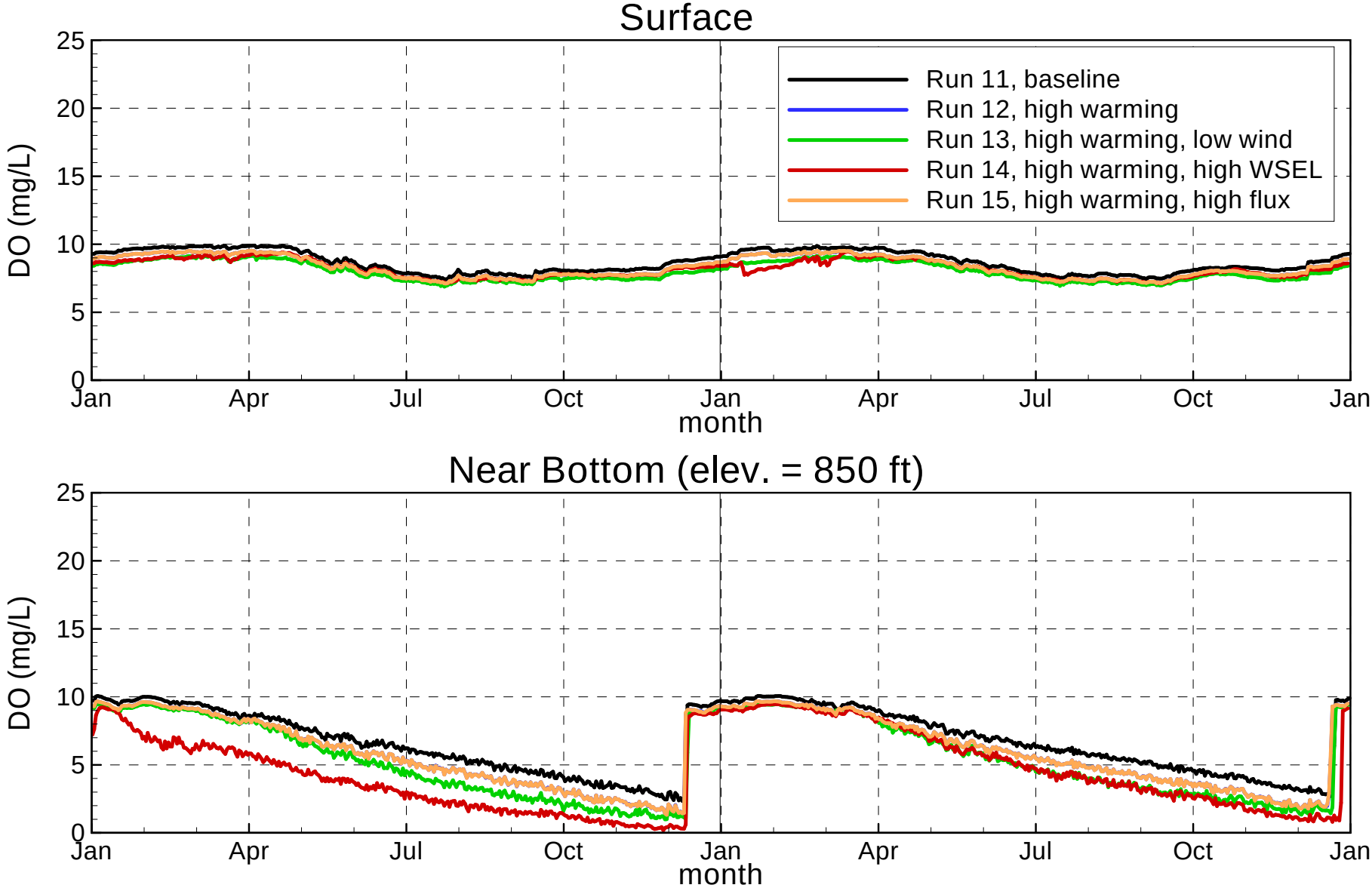

Figure A.23

FLOW SCIENCE

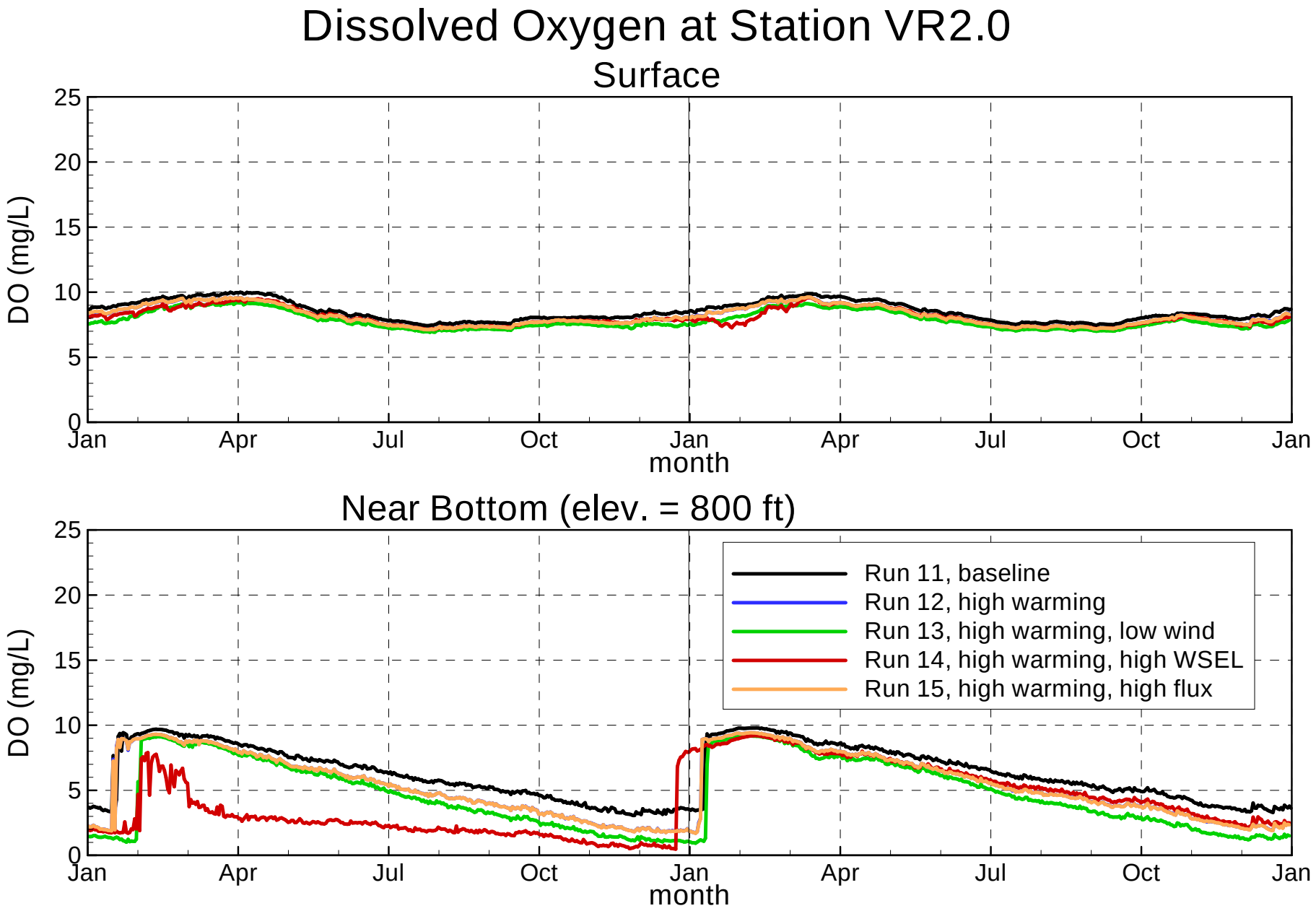
Dissolved Oxygen at Station VR2.0
Surface
DO (mg/L)
25
20
15
10
5
0
Jan
Apr
Jul
Oct
Jan
Apr
Jul
Oct
Jan
month
Near Bottom (elev. = 800 ft)
DO (mg/L)
Run 11, baseline
Run 12, high warming
Run 13, high warming, low wind
Run 14, high warming, high WSEL
Run 15, high warming, high flux
month

Figure A.24

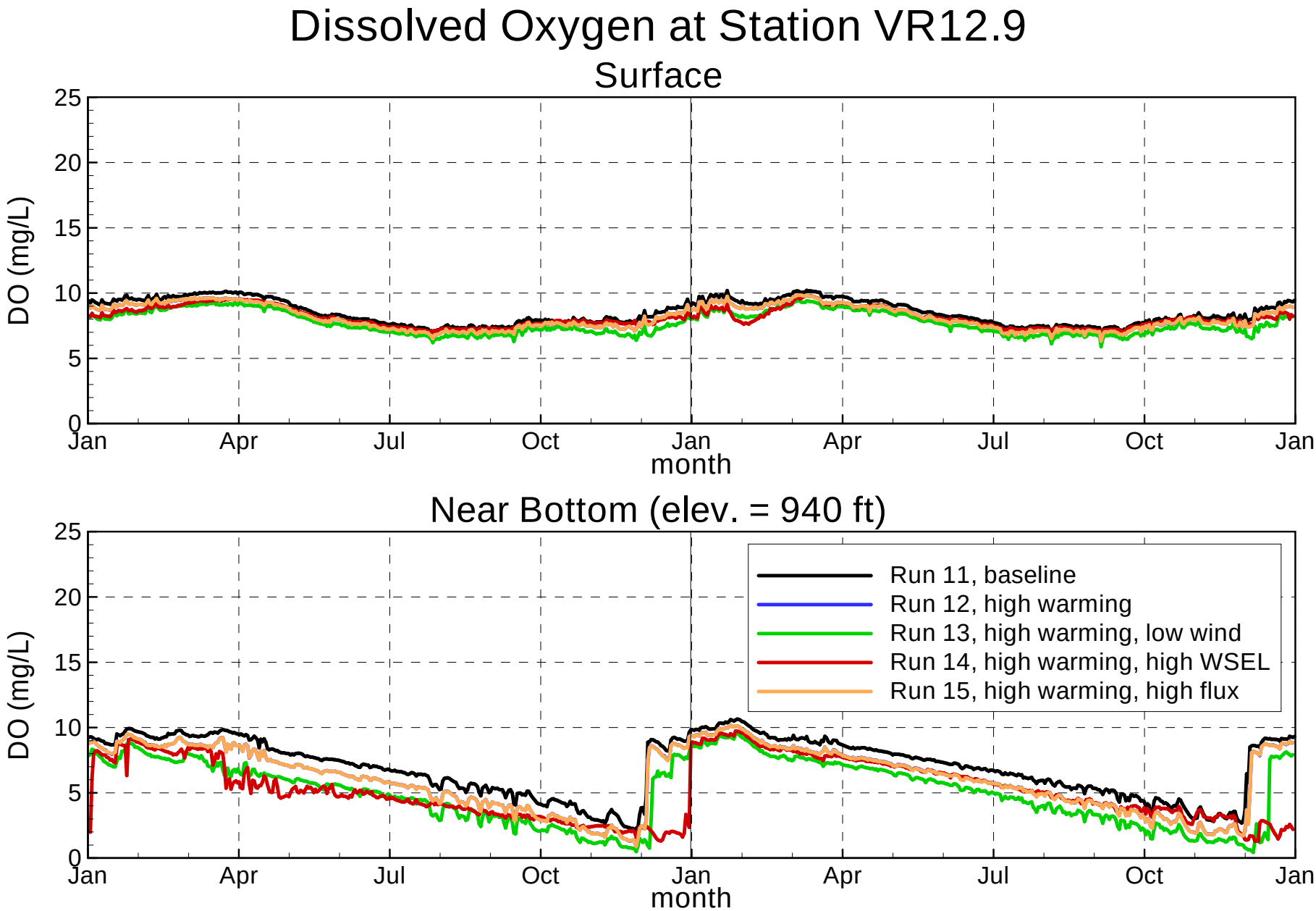

Figure A.25

FLOW SCIENCE

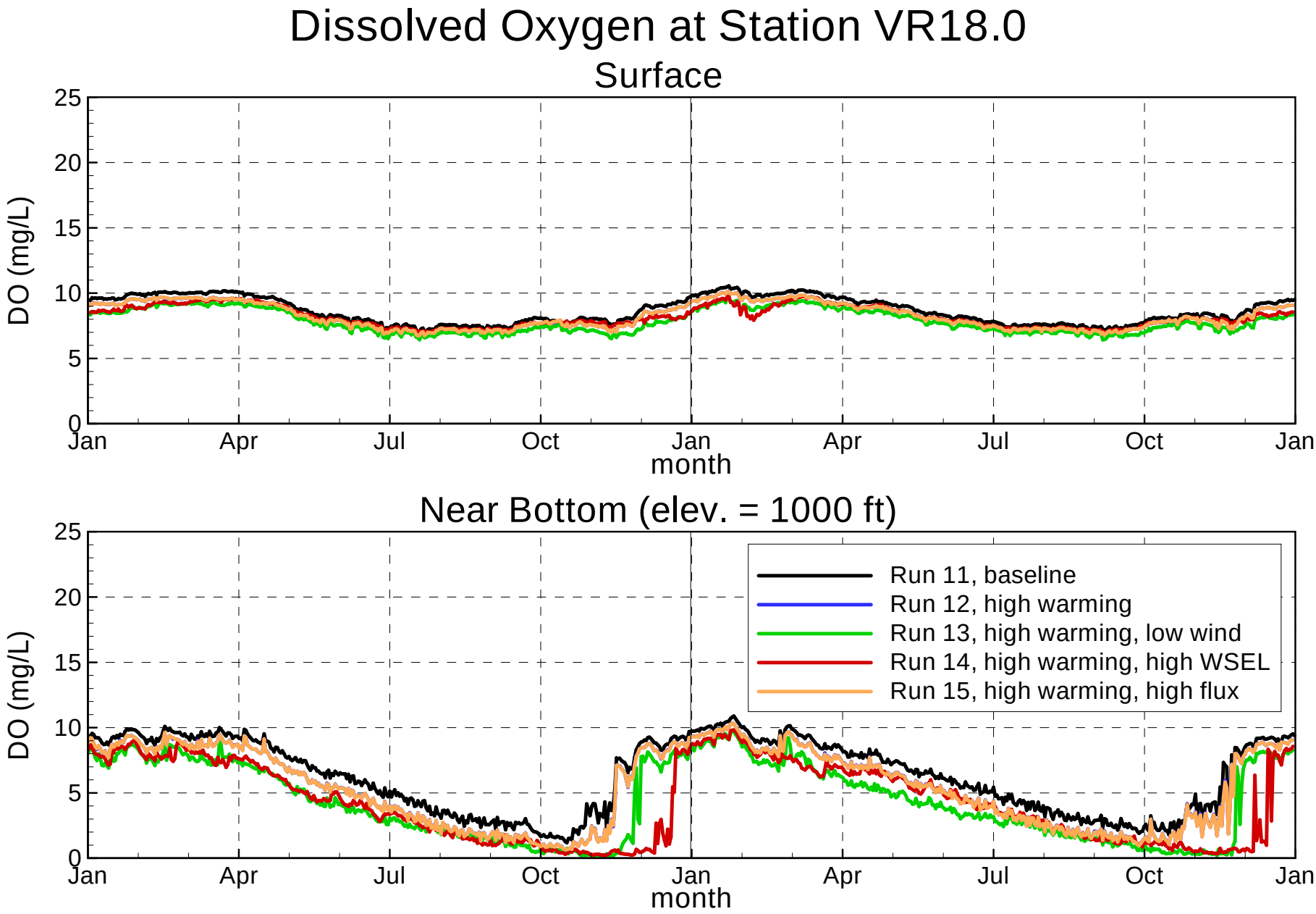
Dissolved Oxygen at Station VR18.0
Surface
DO (mg/L)
25
20
15
10
5
0
Jan
Apr
Jul
Oct
Jan
Apr
Jul
Oct
Jan
month
Near Bottom (elev. = 1000 ft)
DO (mg/L)
Run 11, baseline
Run 12, high warming
Run 13, high warming, low wind
Run 14, high warming, high WSEL
Run 15, high warming, high flux
month

Figure A.26

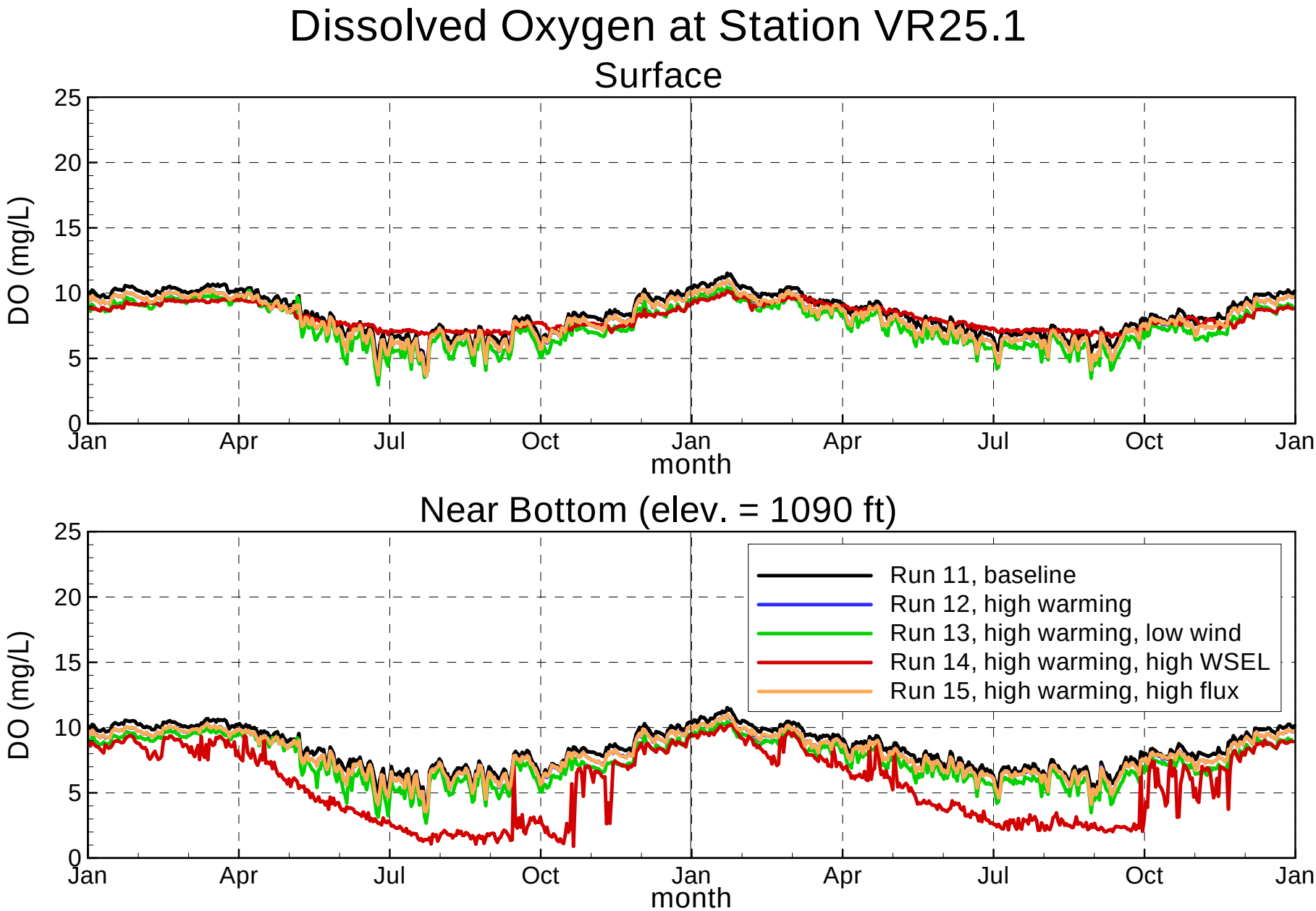

Figure A.27

FLOW SCIENCE

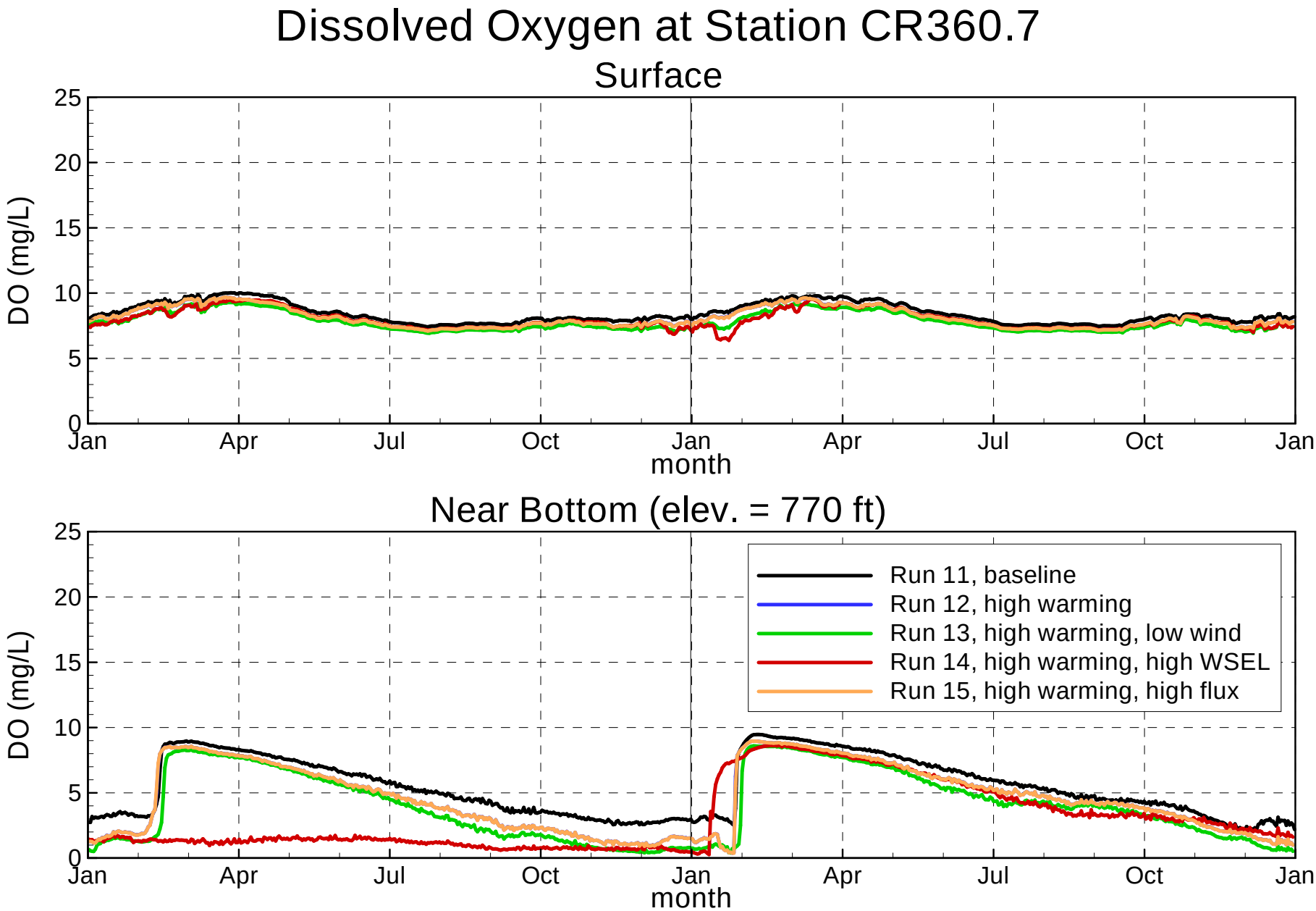
Dissolved Oxygen at Station CR360.7
Surface
DO (mg/L)
25
20
15
10
5
0
Jan
Apr
Jul
Oct
Jan
Apr
Jul
Oct
Jan
month
Near Bottom (elev. = 770 ft)
DO (mg/L)
Run 11, baseline
Run 12, high warming
Run 13, high warming, low wind
Run 14, high warming, high WSEL
Run 15, high warming, high flux
month

Figure A.28

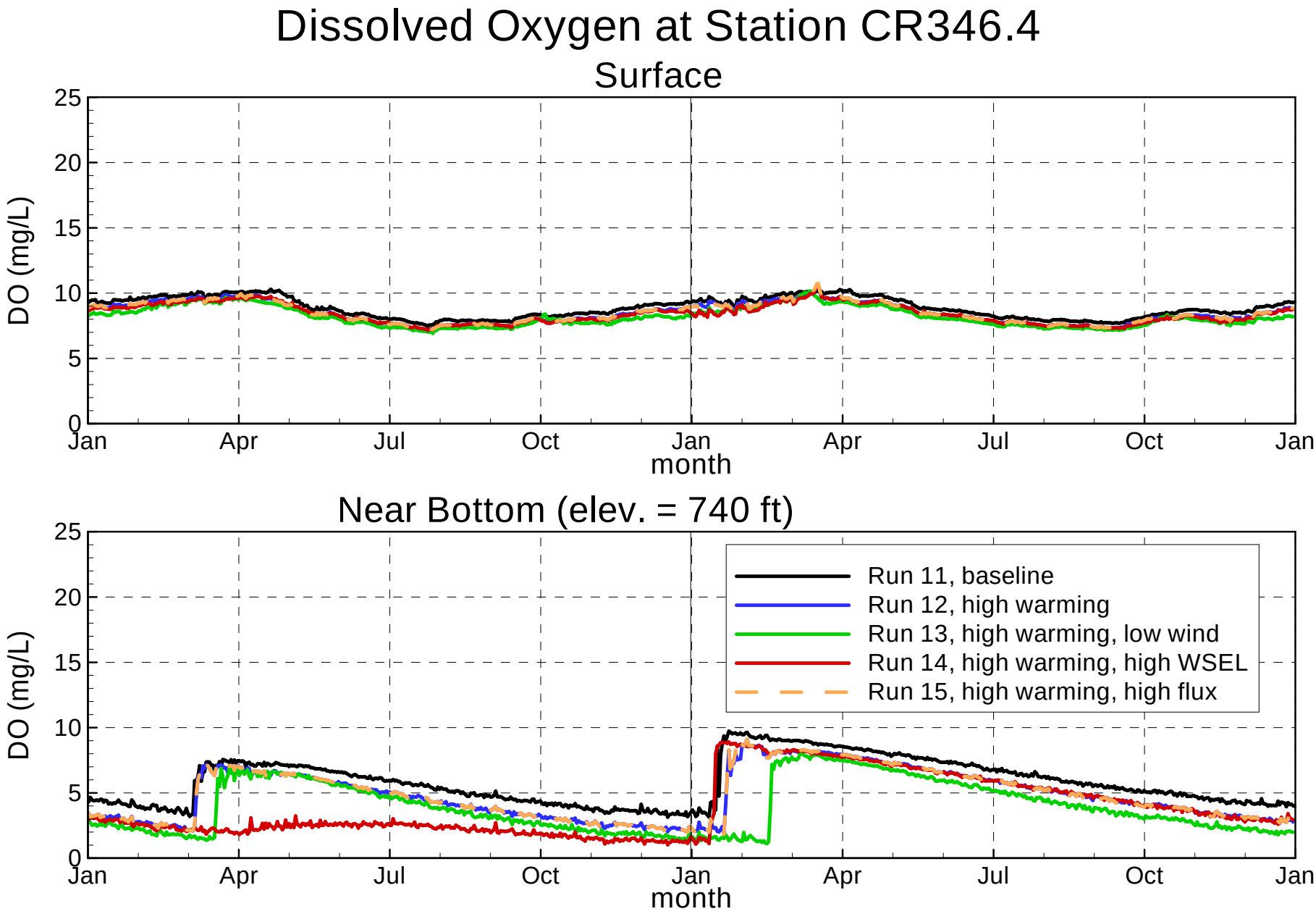
Dissolved Oxygen at Station CR346.4
Surface
DO (mg/L)
25
20
15
10
5
0
Jan
Apr
Jul
Oct
Jan
Apr
Jul
Oct
Jan
month
Near Bottom (elev. = 740 ft)
DO (mg/L)
Run 11, baseline
Run 12, high warming
Run 13, high warming, low wind
Run 14, high warming, high WSEL
Run 15, high warming, high flux
month

Figure A.29

Dissolved Oxygen at Station LWLVB1.2

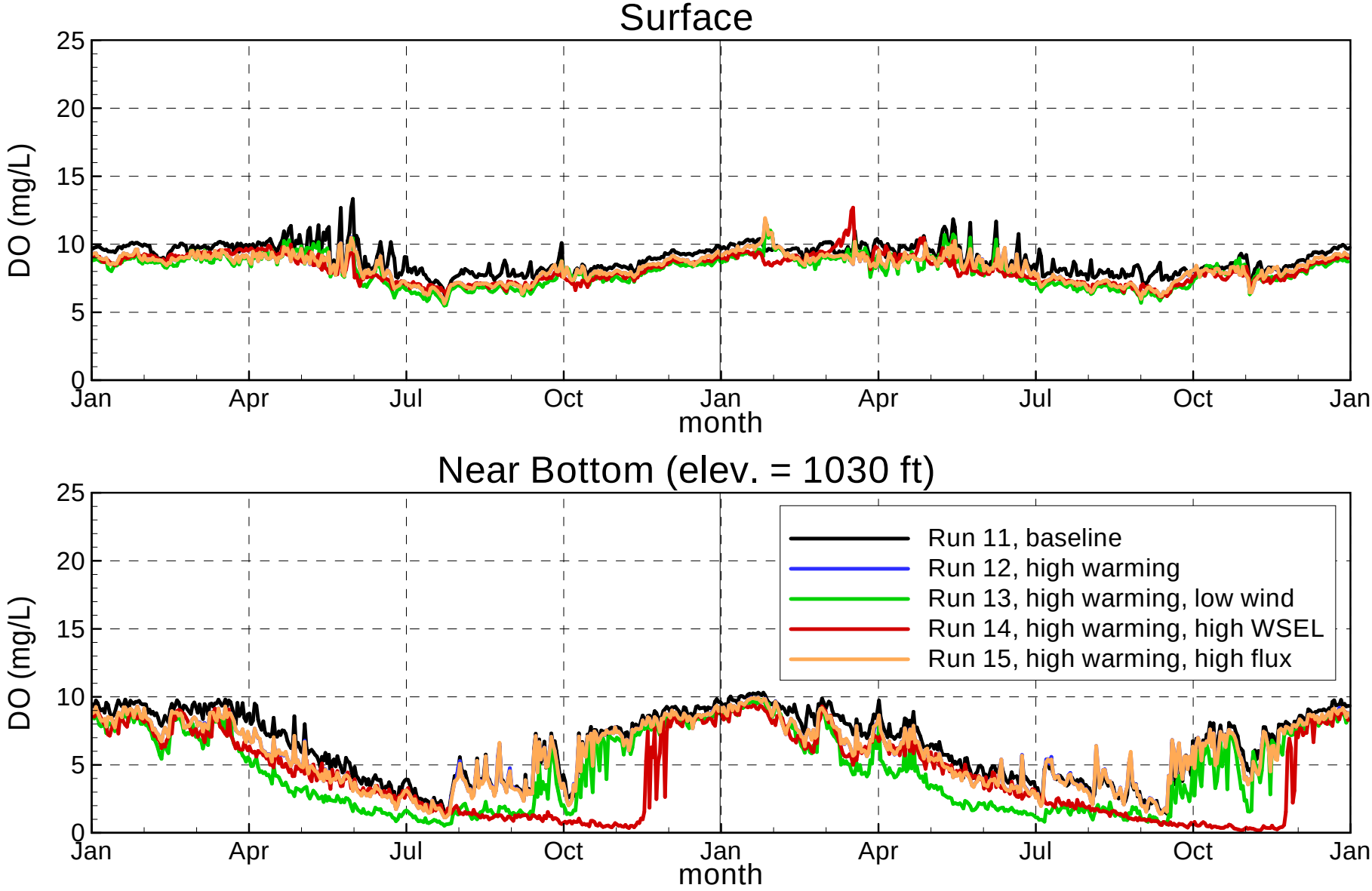

Figure A.30

FLOW SCIENCE

Dissolved Oxygen at Station LWLVB1.85

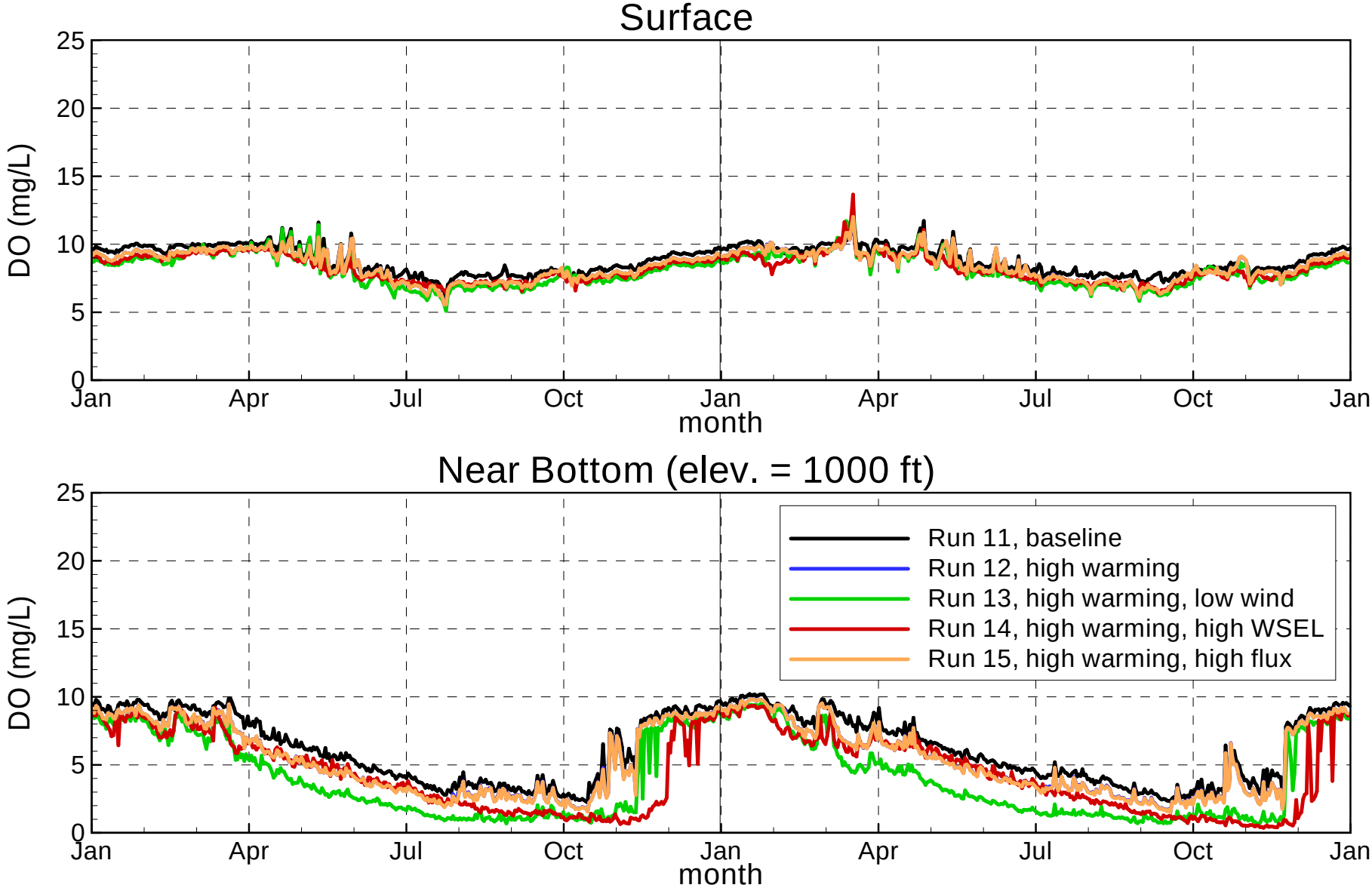

Figure A.31

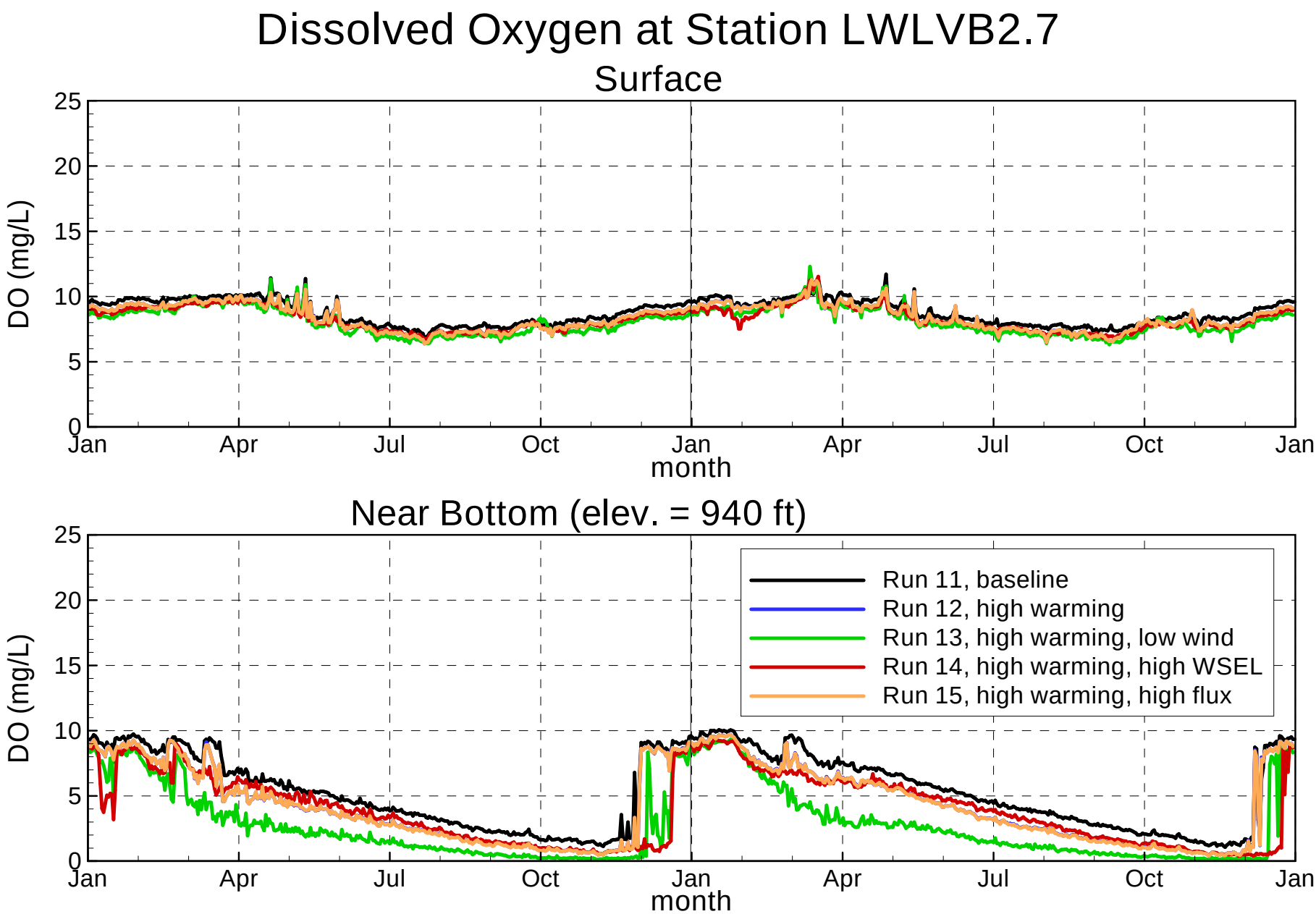

Figure A.32

FLOW SCIENCE

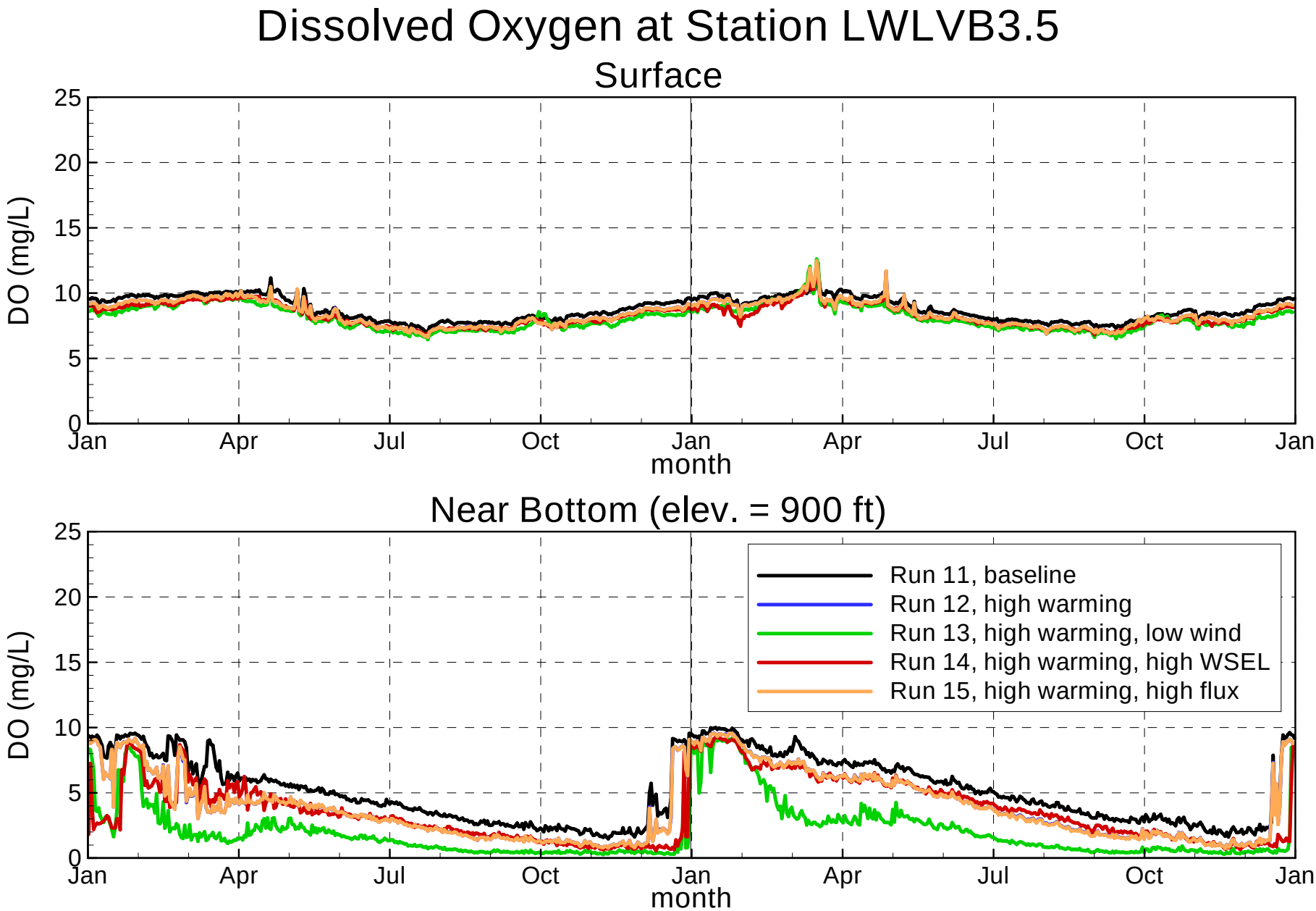
Dissolved Oxygen at Station LWLVB3.5
Surface
DO (mg/L)
25
20
15
10
5
0
Jan
Apr
Jul
Oct
Jan
Apr
Jul
Oct
Jan
month
Near Bottom (elev. = 900 ft)
DO (mg/L)
Run 11, baseline
Run 12, high warming
Run 13, high warming, low wind
Run 14, high warming, high WSEL
Run 15, high warming, high flux
month

Figure A.33

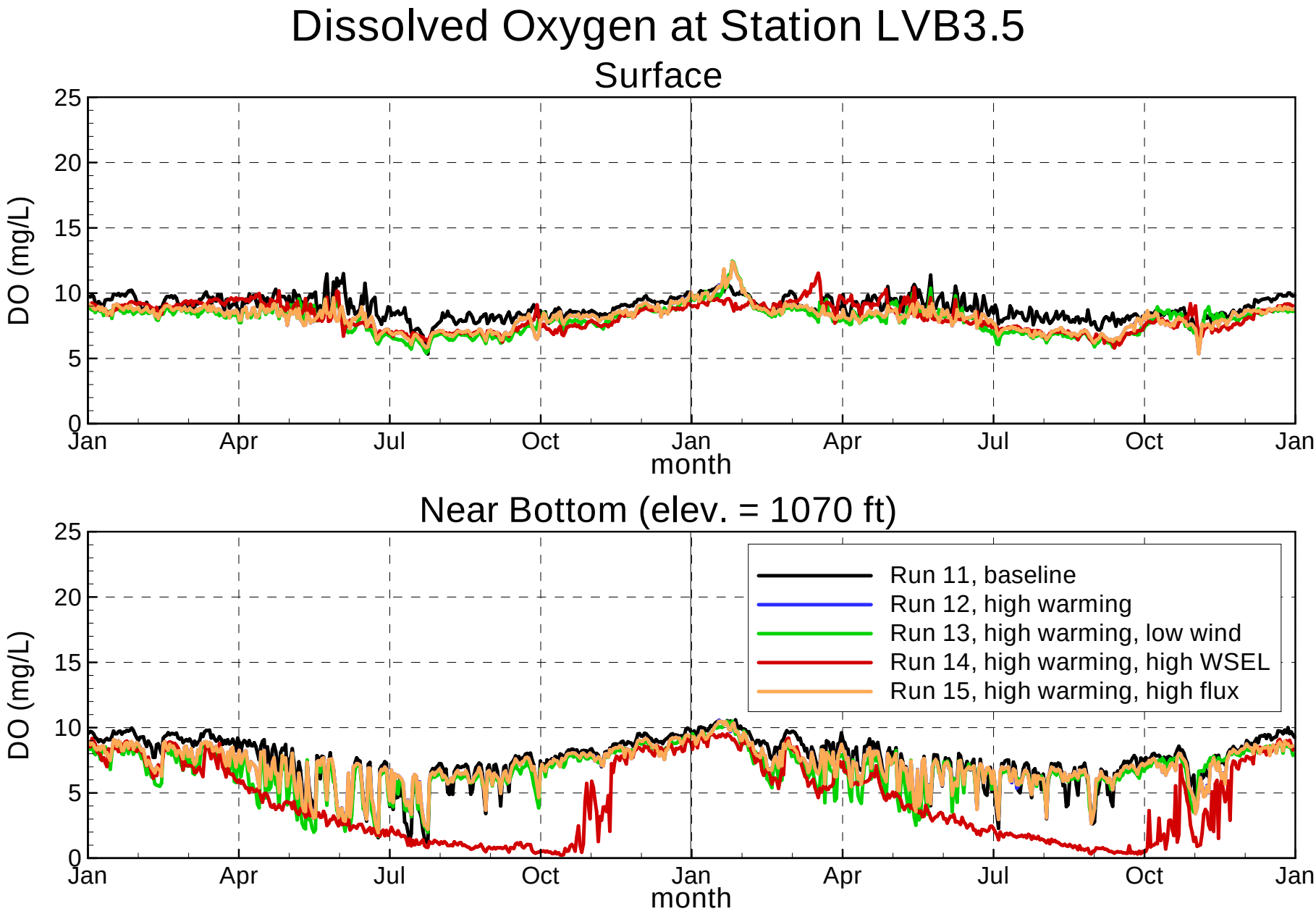

Figure A.34

FLOW SCIENCE

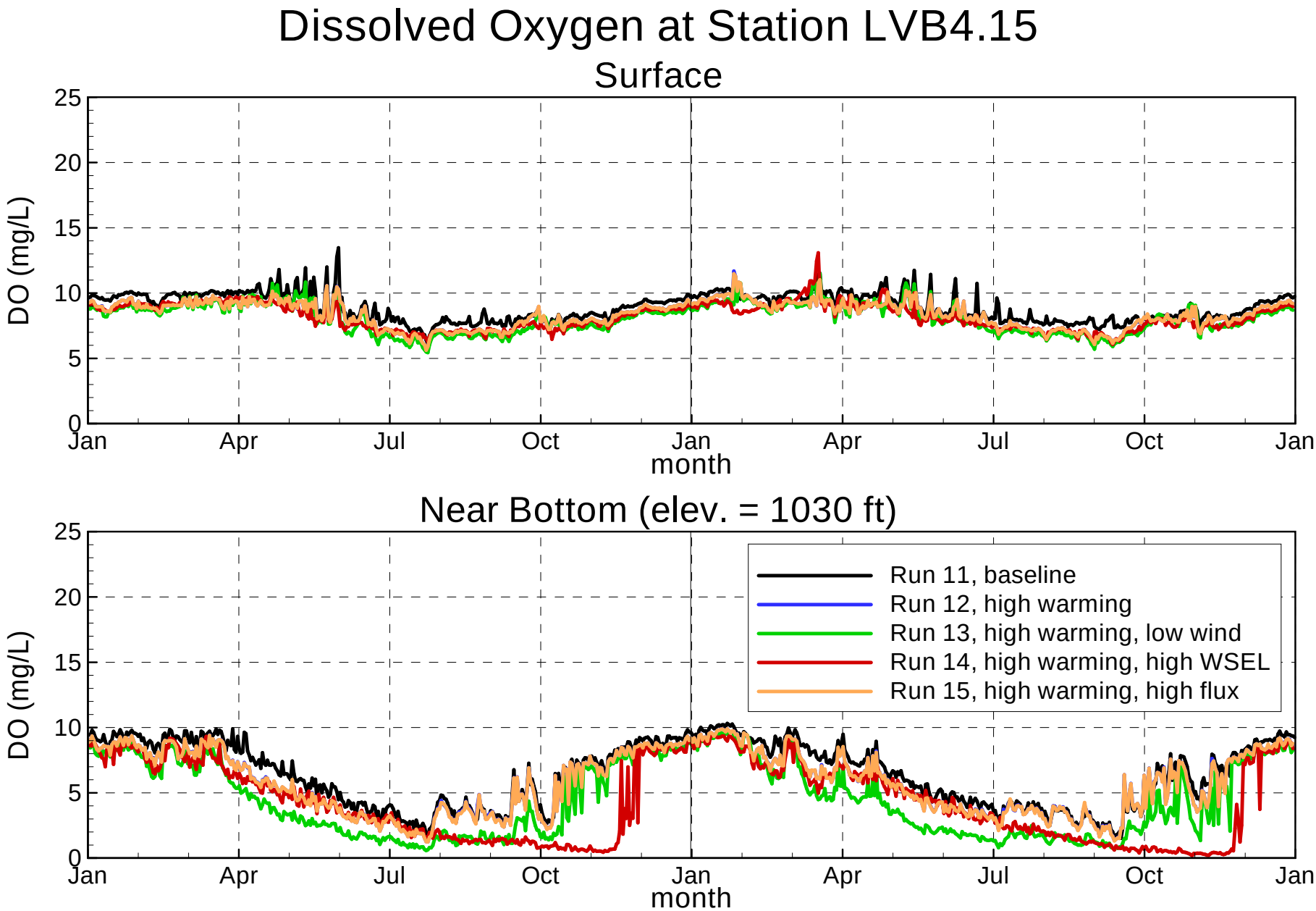
Dissolved Oxygen at Station LVB4.15
Surface
DO (mg/L)
25
20
15
10
5
0
Jan
Apr
Jul
Oct
Jan
Apr
Jul
Oct
Jan
month
Near Bottom (elev. = 1030 ft)
DO (mg/L)
Run 11, baseline
Run 12, high warming
Run 13, high warming, low wind
Run 14, high warming, high WSEL
Run 15, high warming, high flux
month

Figure A.35

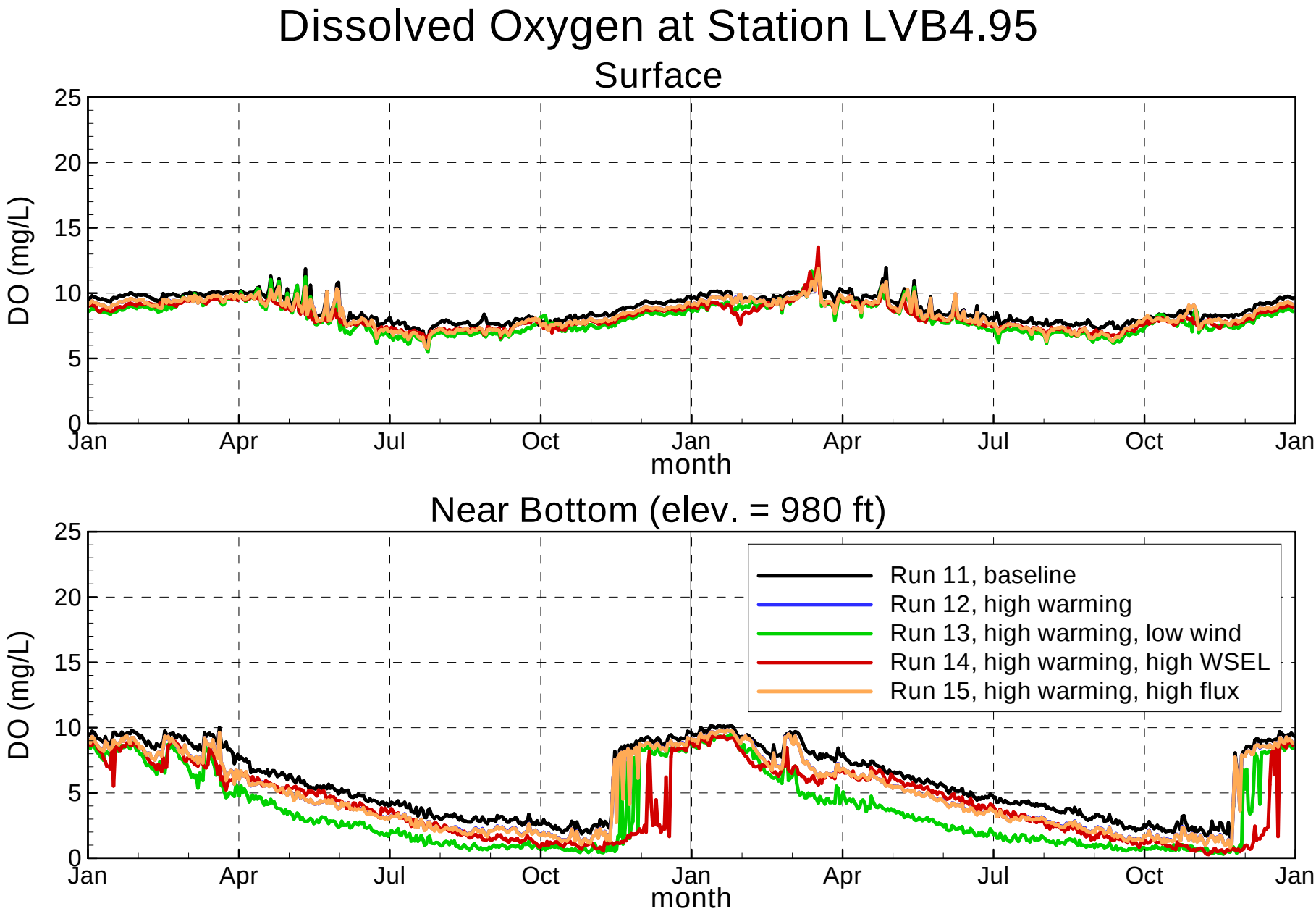
Dissolved Oxygen at Station LVB4.95
Surface
DO (mg/L)
25
20
15
10
5
0
Jan
Apr
Jul
Oct
Jan
Apr
Jul
Oct
Jan
month
Near Bottom (elev. = 980 ft)
DO (mg/L)
Run 11, baseline
Run 12, high warming
Run 13, high warming, low wind
Run 14, high warming, high WSEL
Run 15, high warming, high flux
month

Figure A.36

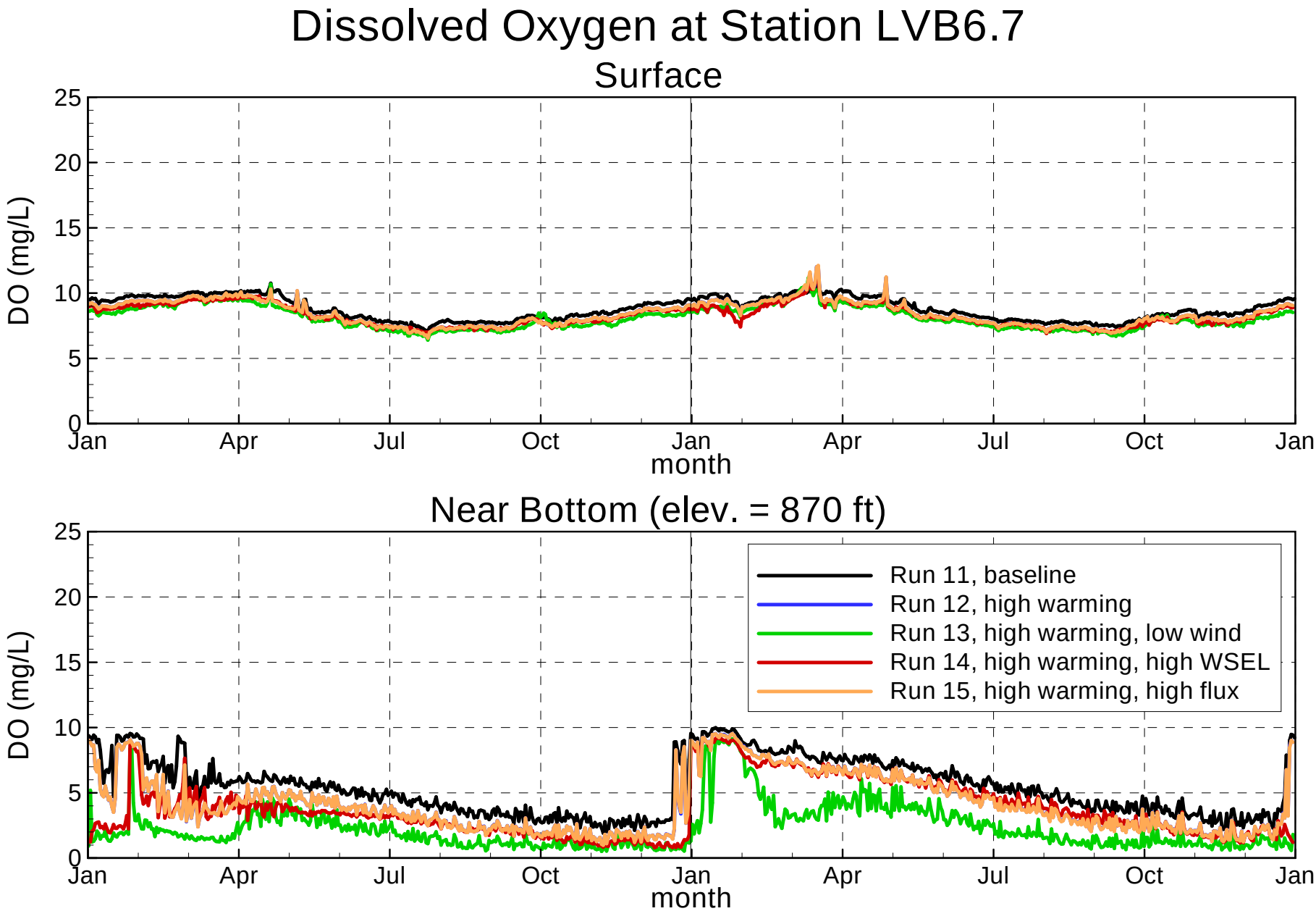

Figure A.37

FLOW SCIENCE

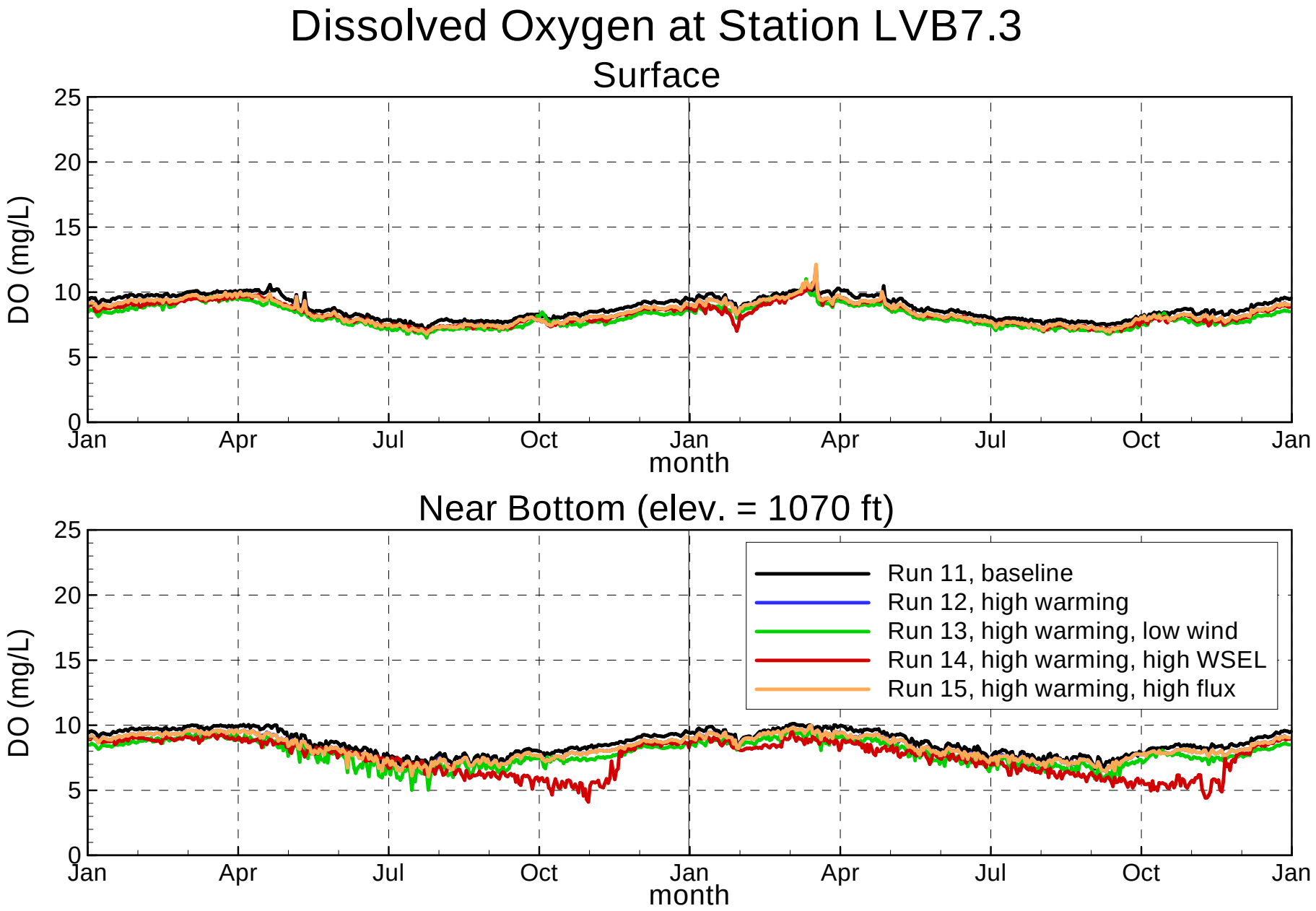

Figure A.38

FLOW SCIENCE

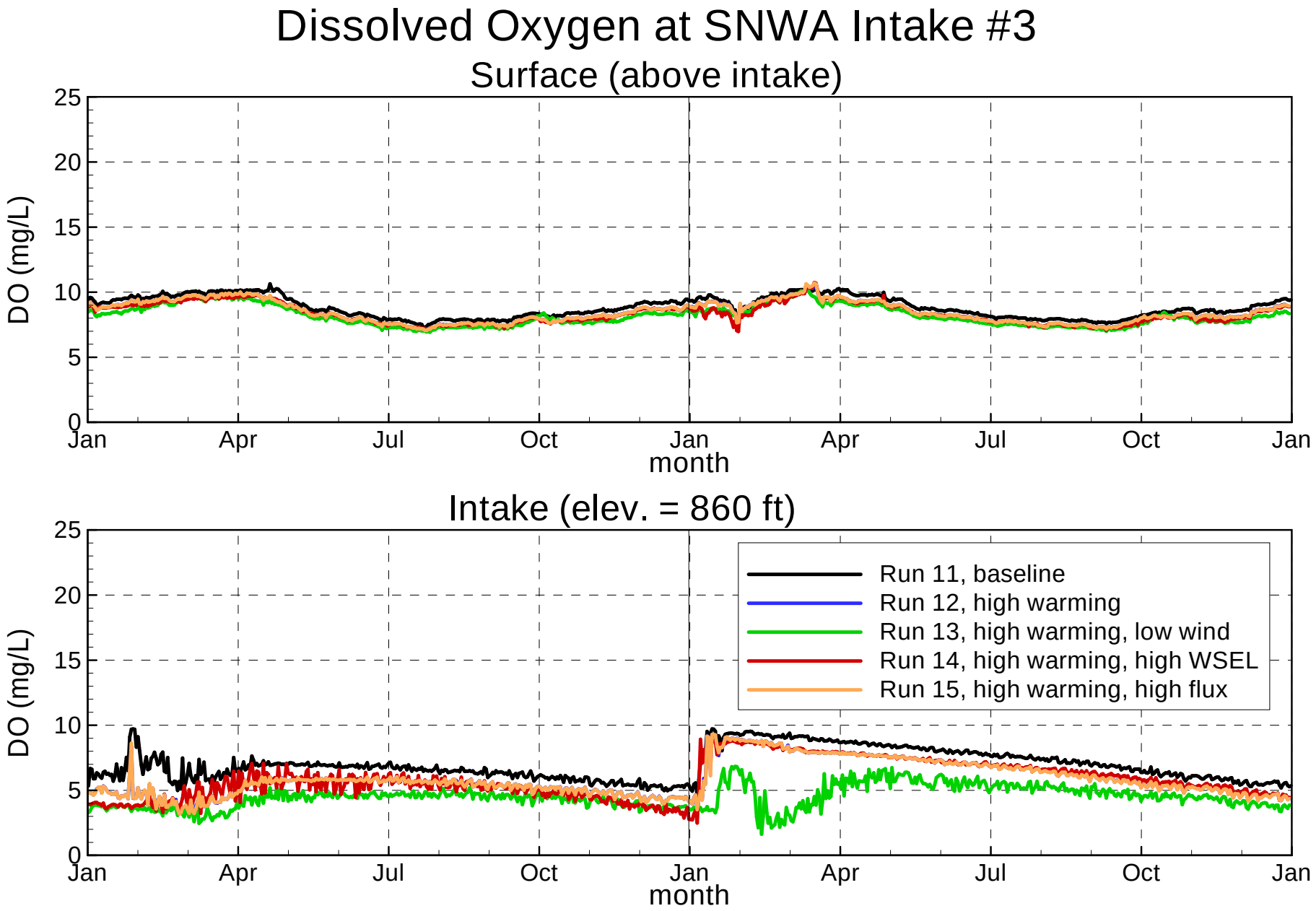

Figure A.39

FLOW SCIENCE

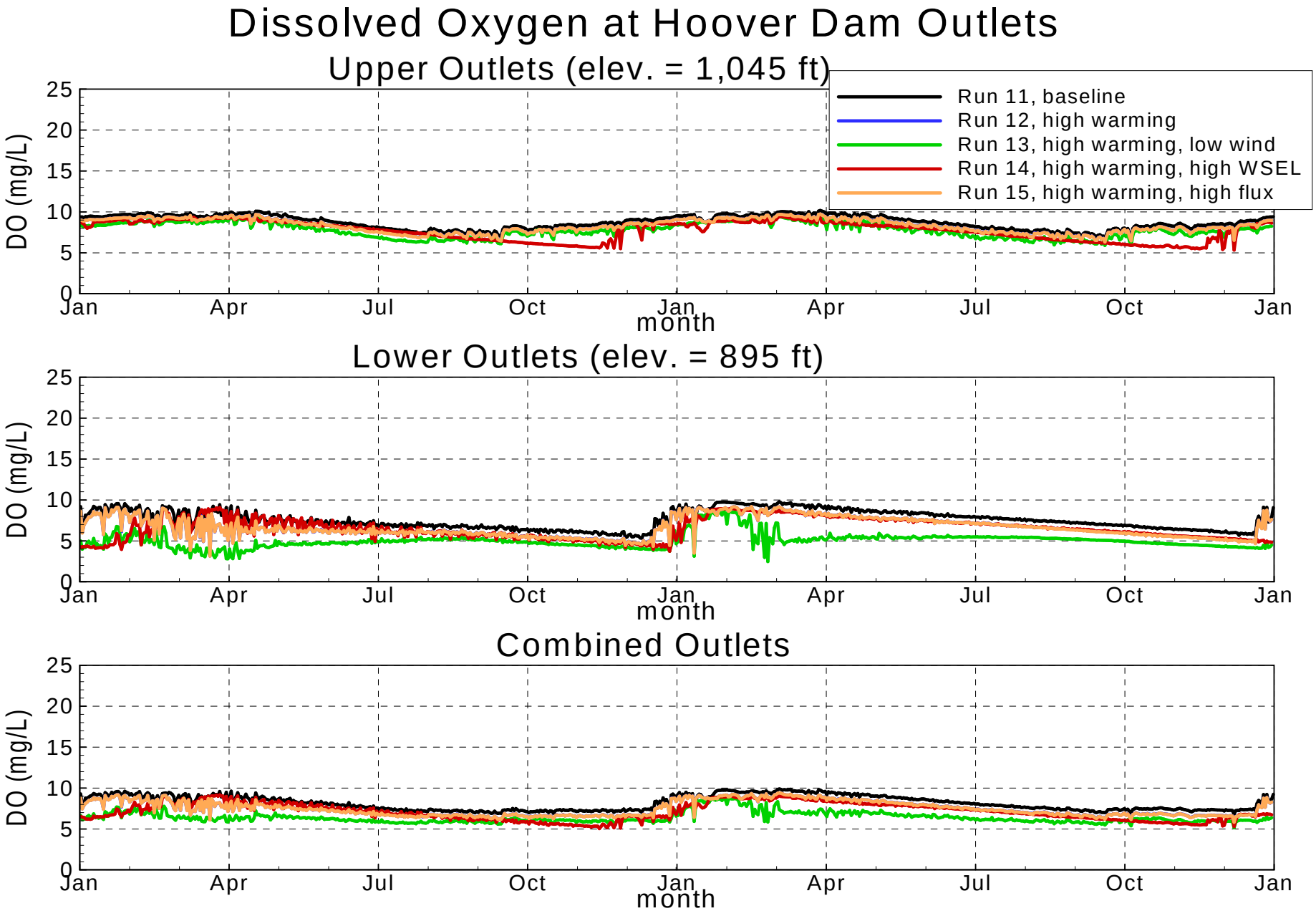

Figure A.40

FLOW SCIENCE

Effluent Tracer at Station CR394.0

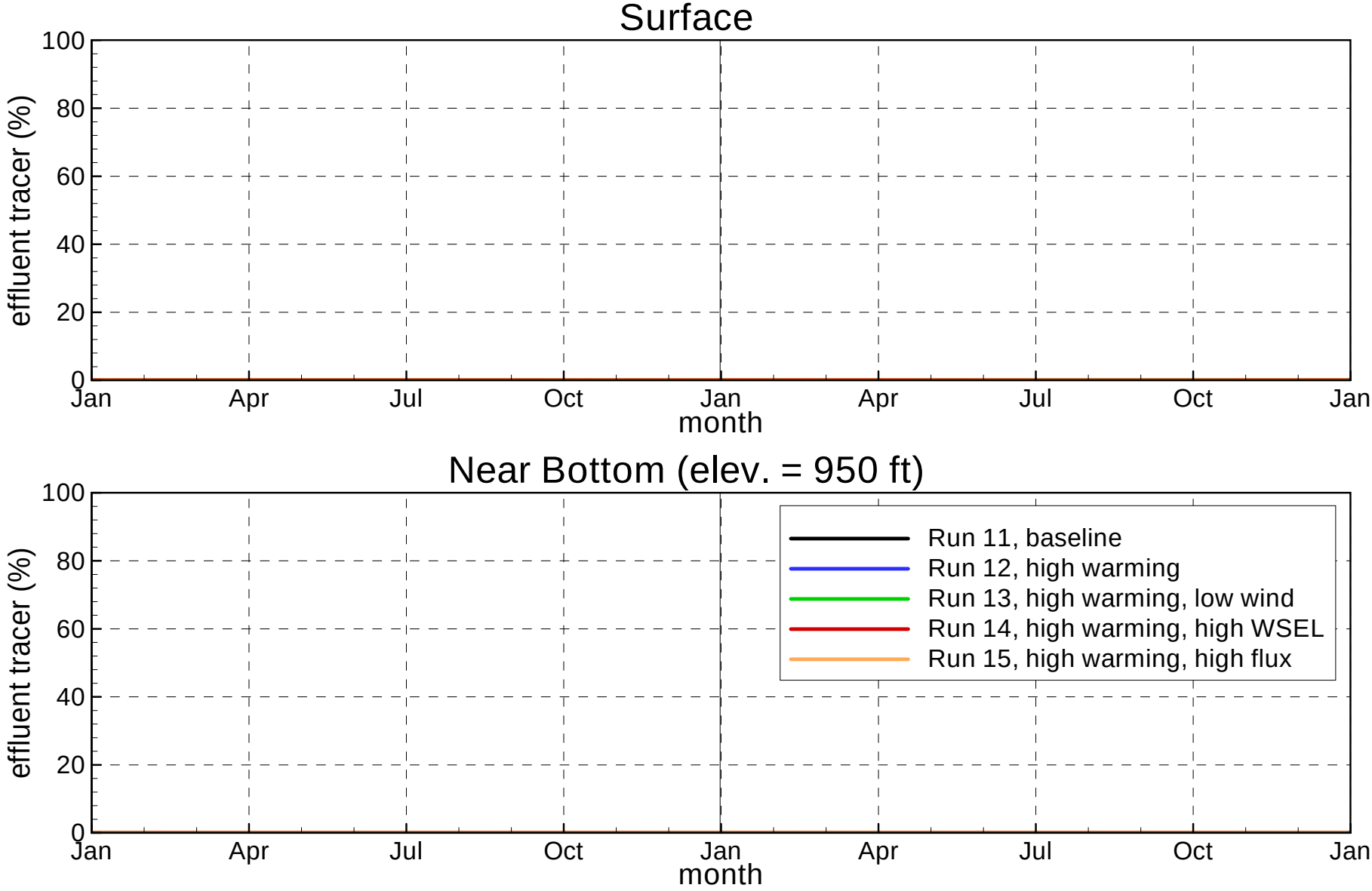

Figure A.41

Effluent Tracer at Station CR390.0

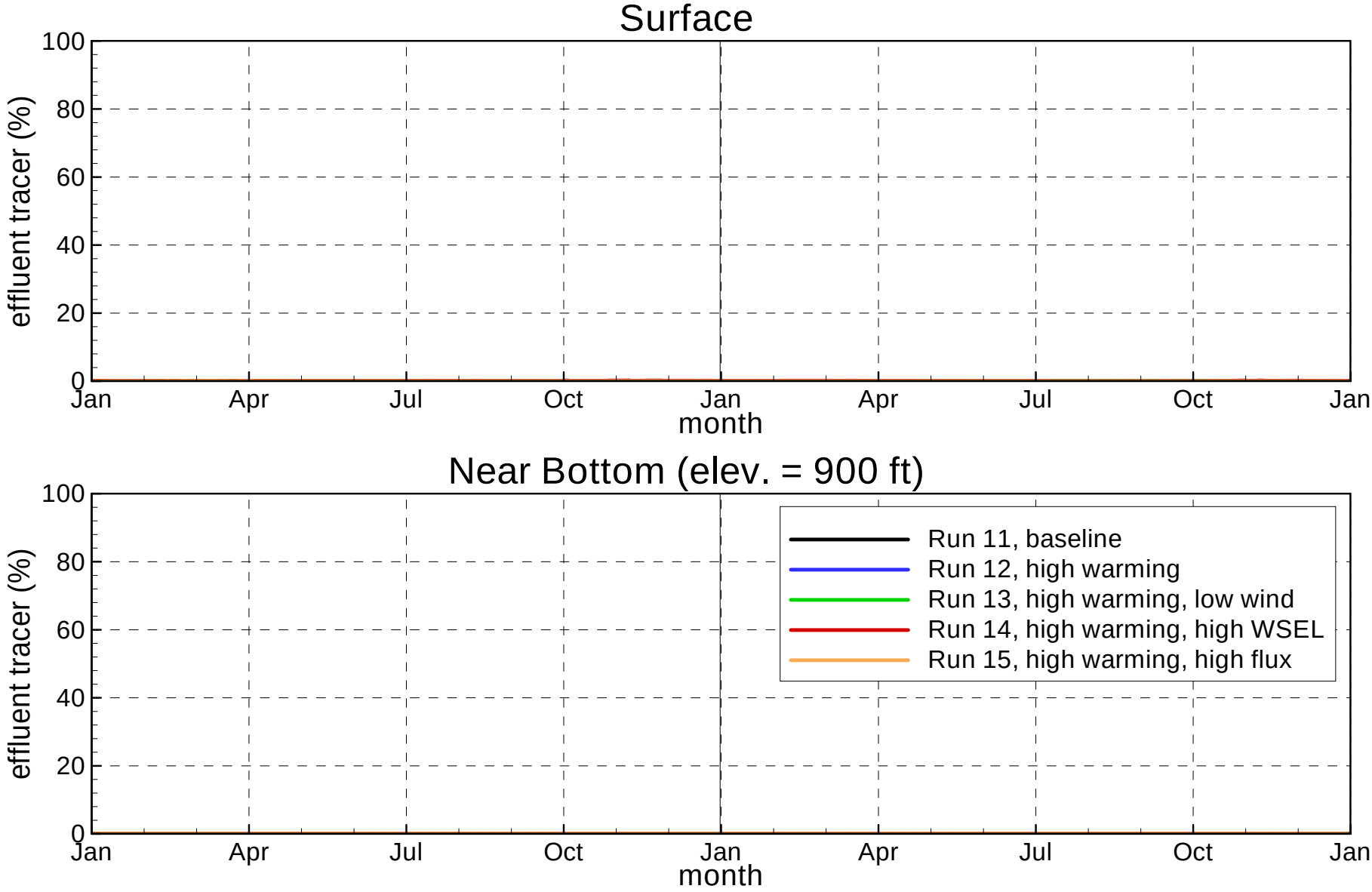

Figure A.42

Effluent Tracer at Station CR380.0

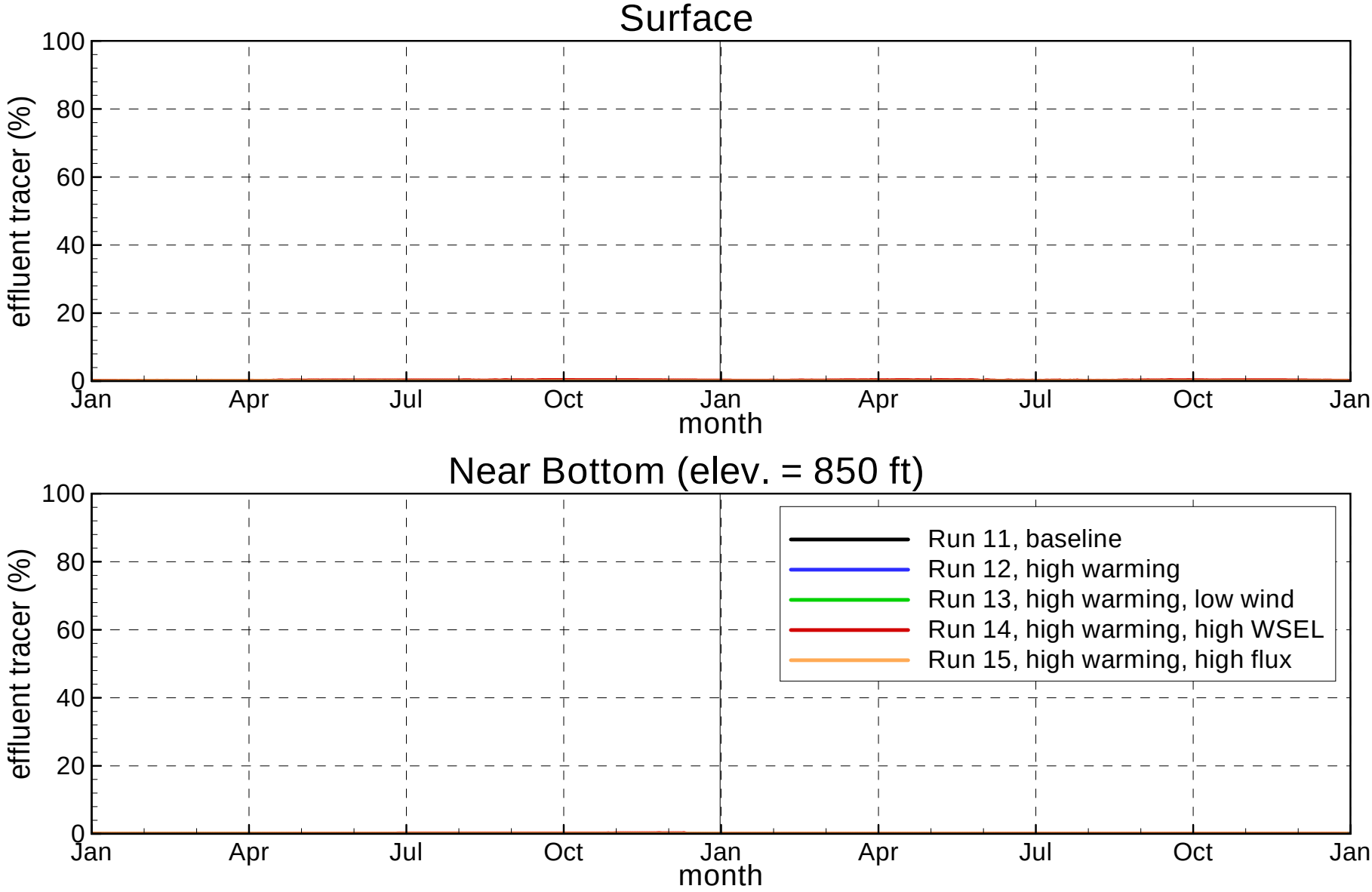

Figure A.43

Effluent Tracer at Station VR2.0

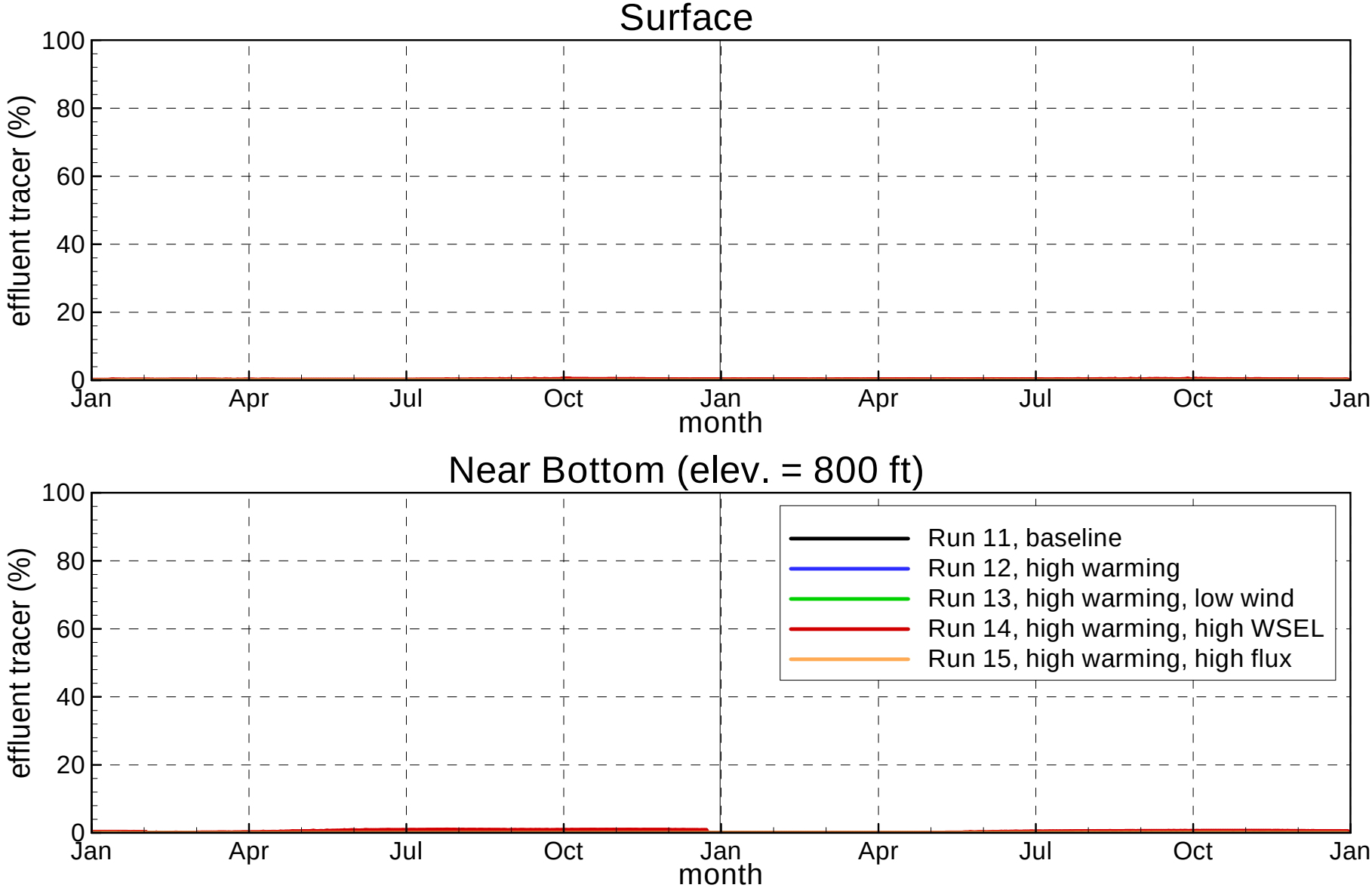

Figure A.44

Effluent Tracer at Station VR12.9

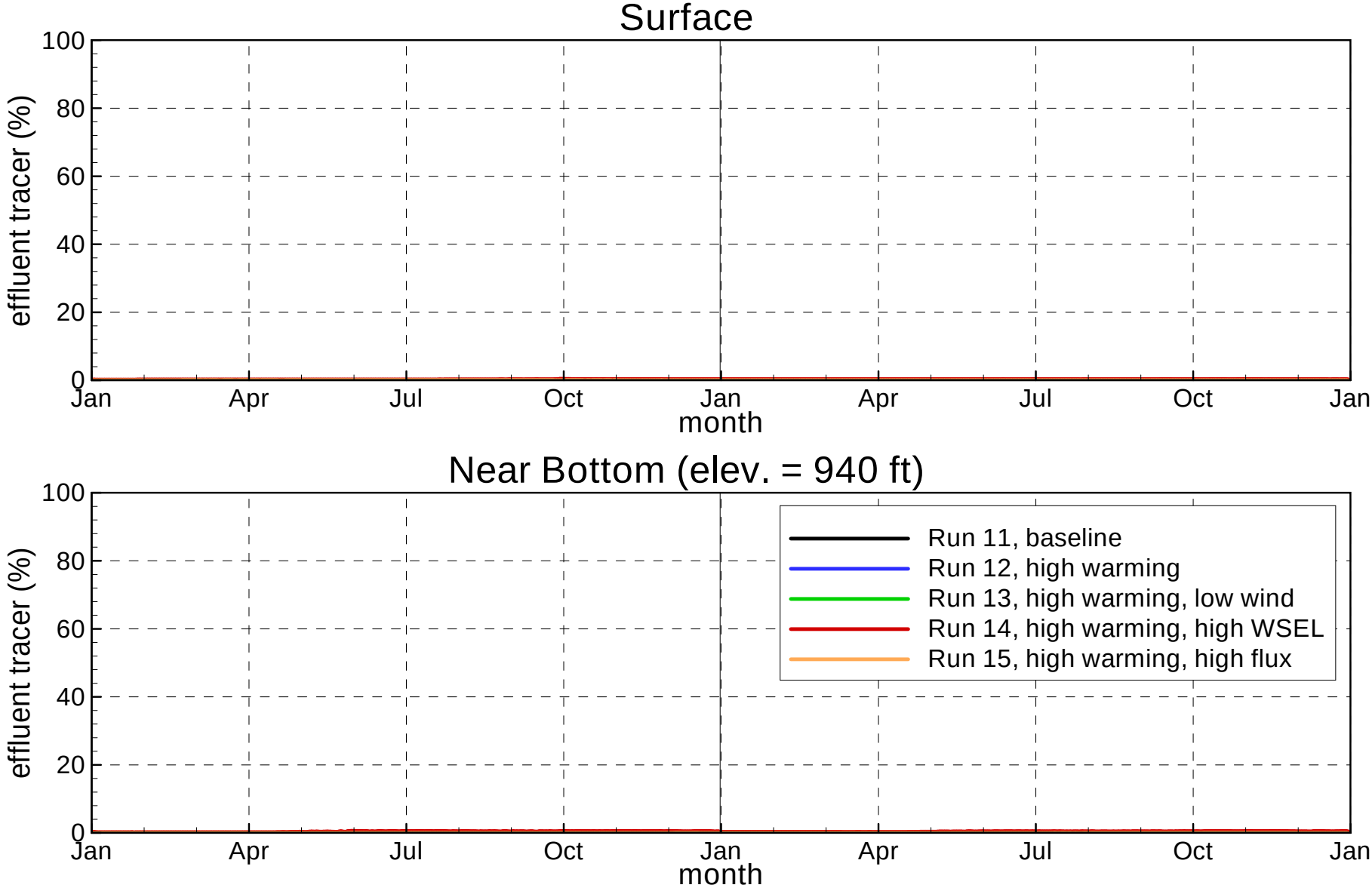

Figure A.45

Effluent Tracer at Station VR18.0

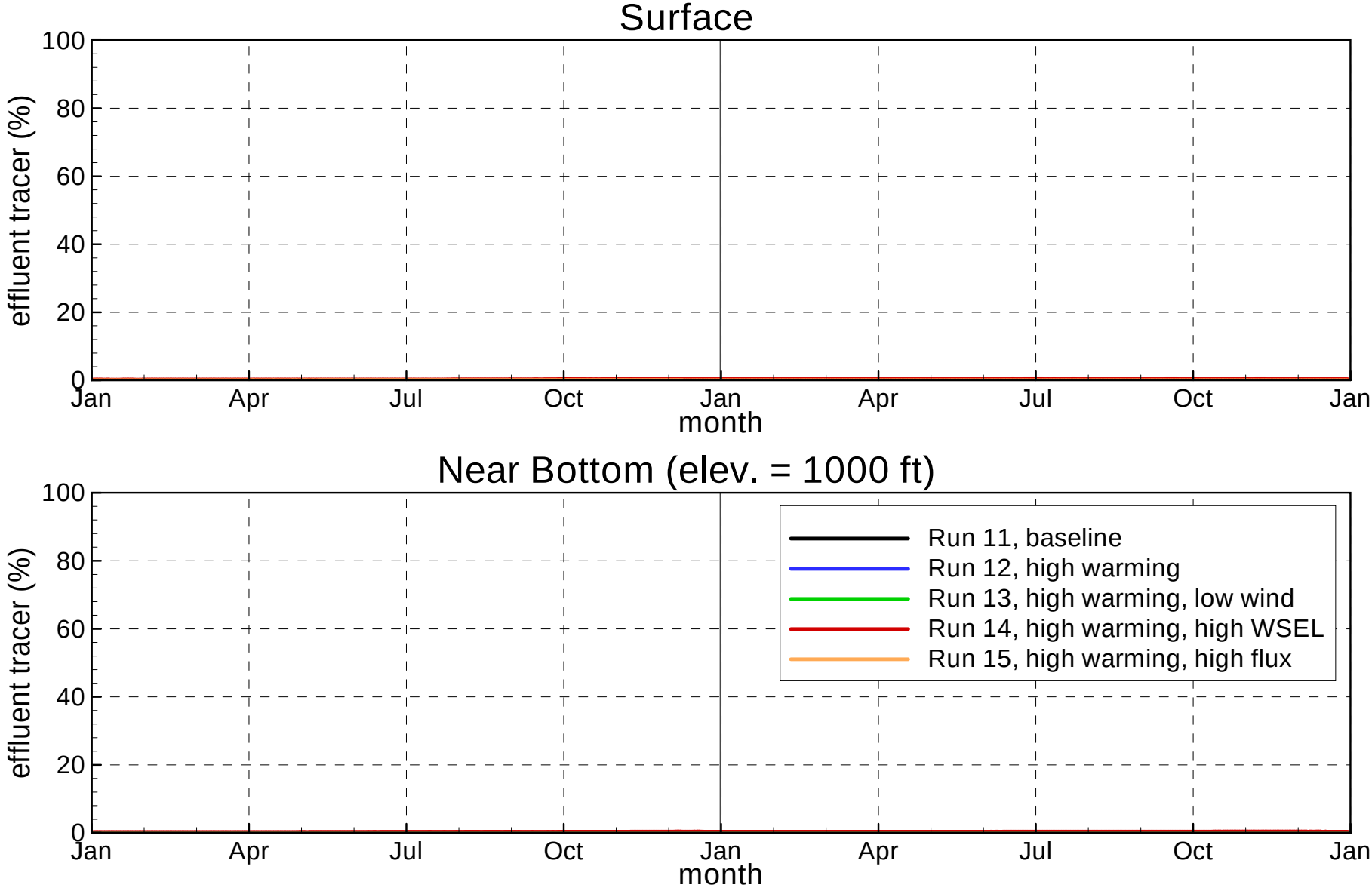

Figure A.46

Effluent Tracer at Station VR25.1

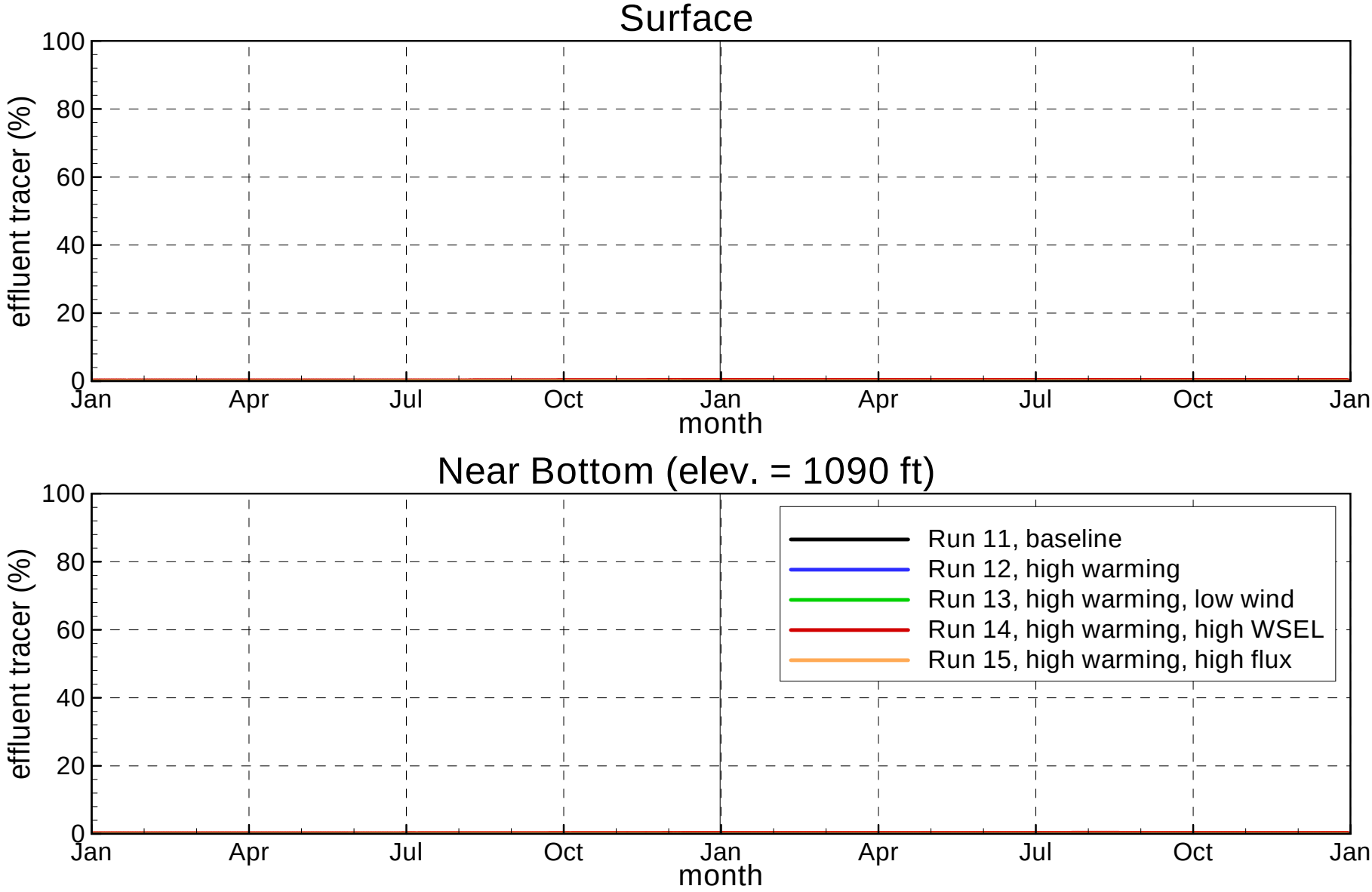

Figure A.47

Effluent Tracer at Station CR360.7

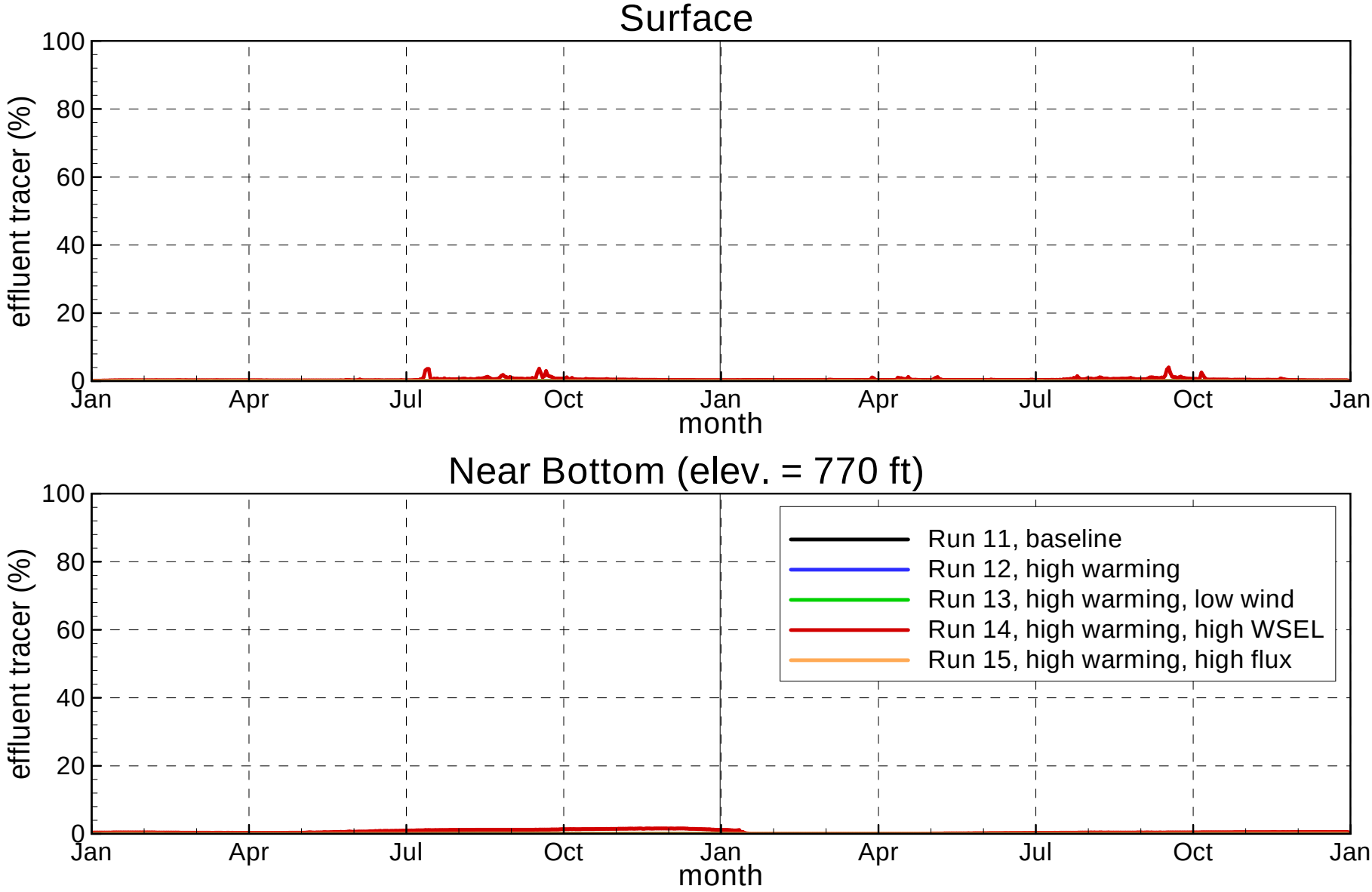

Figure A.48

Effluent Tracer at Station CR346.4

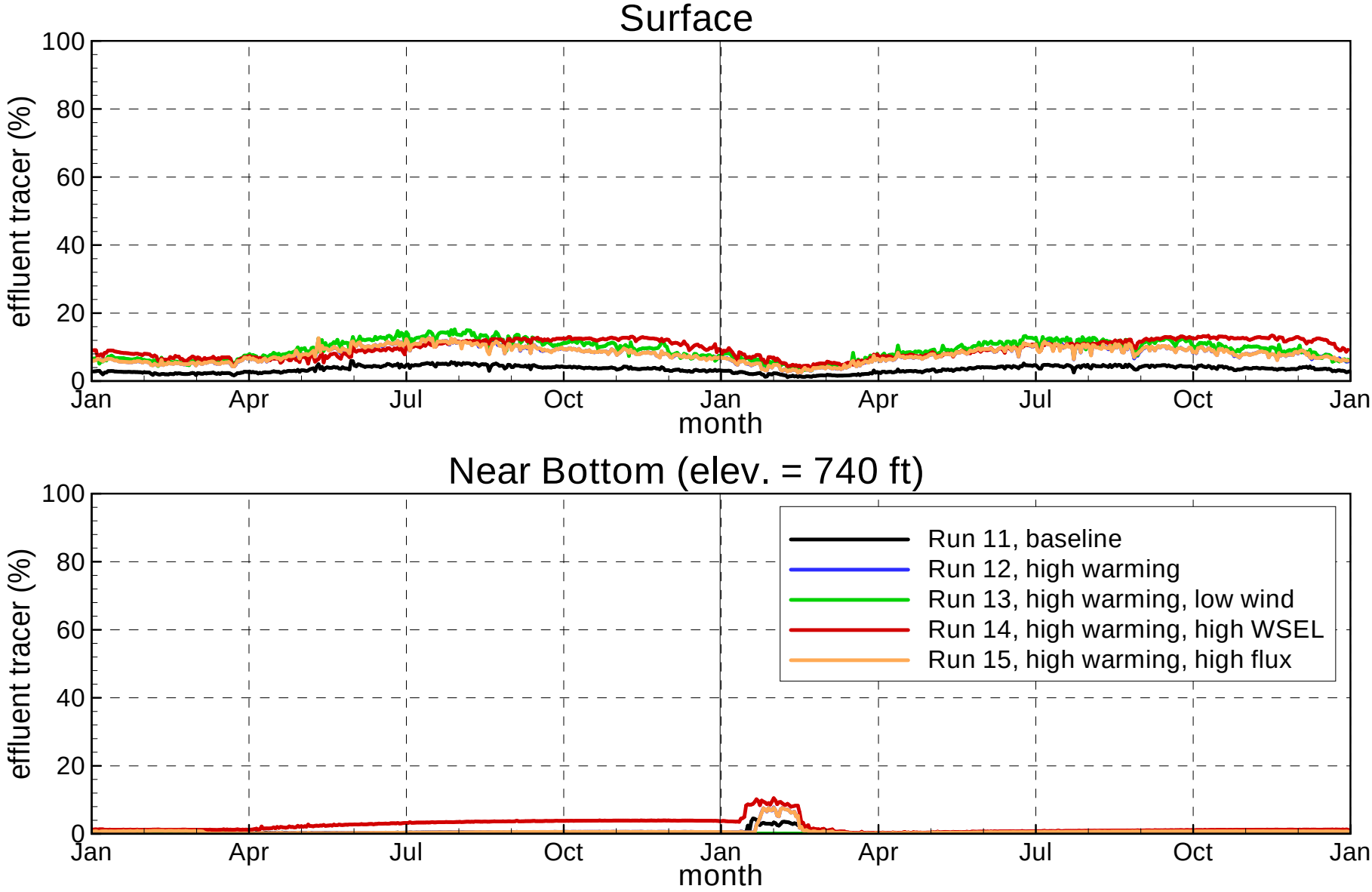

Figure A.49

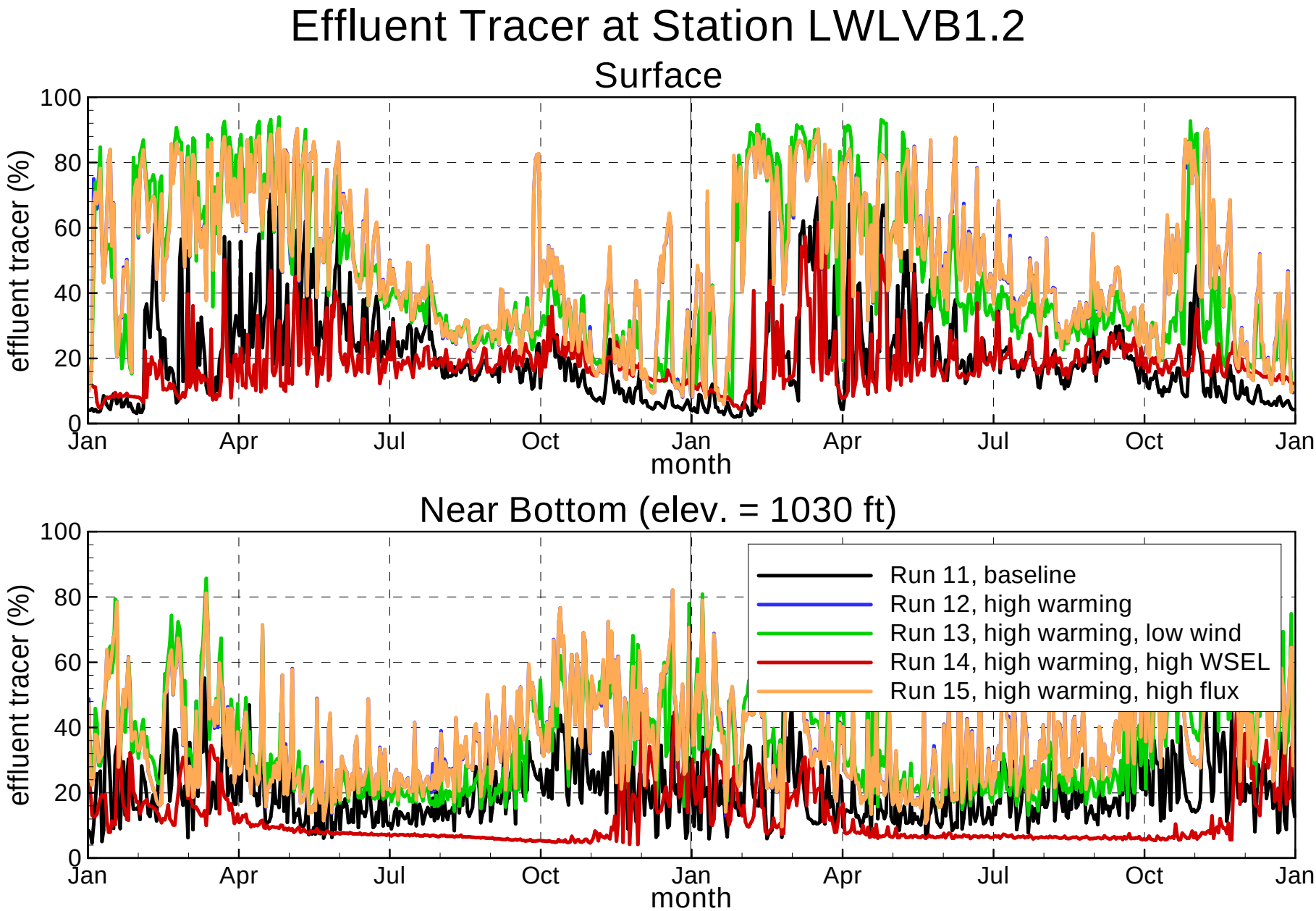

Figure A.50

FLOW SCIENCE

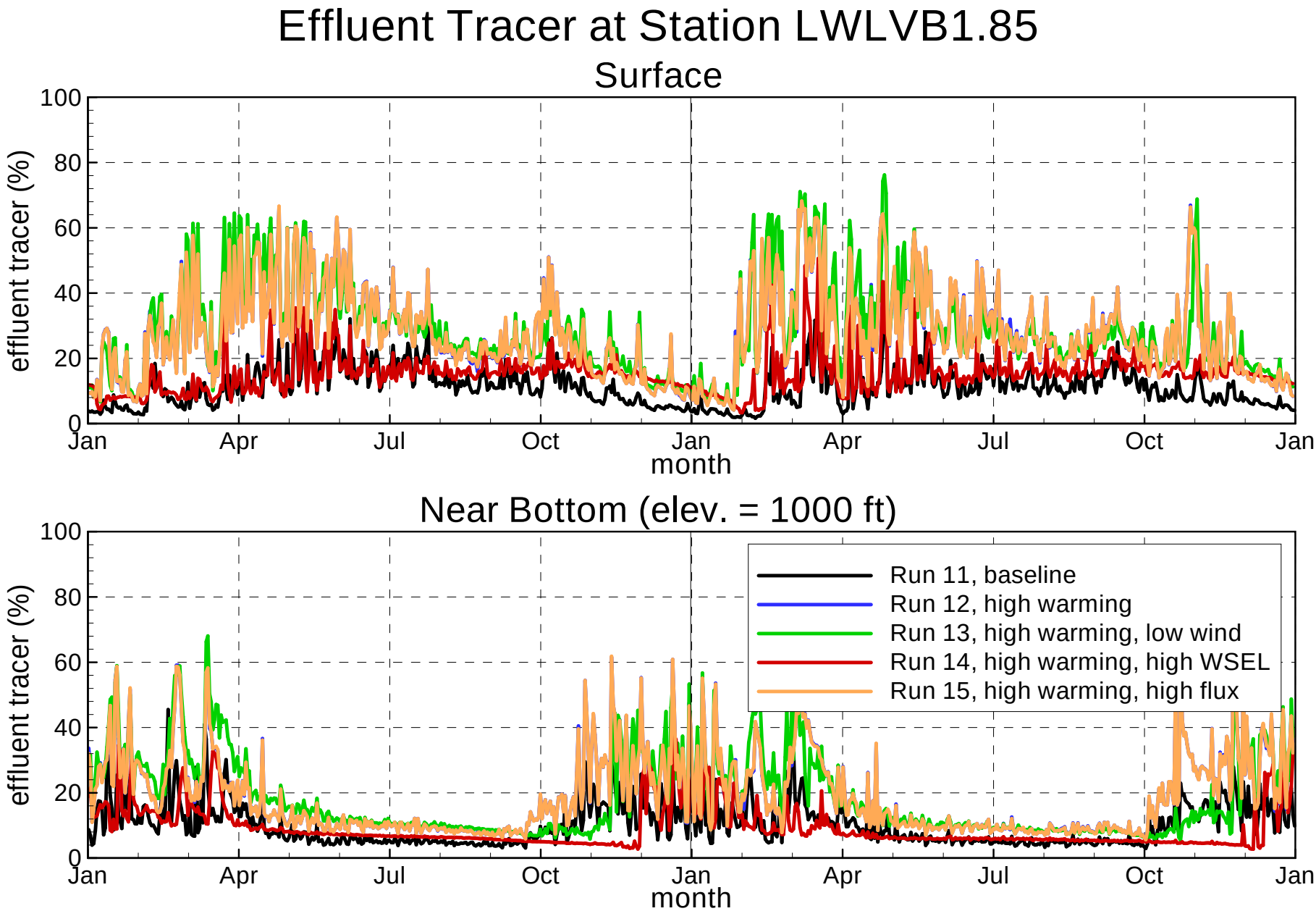
Effluent Tracer at Station LWLVB1.85
Surface
effluent tracer (%)
100
80
60
40
20
0
Jan
Apr
Jul
Oct
Jan
Apr
Jul
Oct
Jan
month
Near Bottom (elev. = 1000 ft)
effluent tracer (%)
Run 11, baseline
Run 12, high warming
Run 13, high warming, low wind
Run 14, high warming, high WSEL
Run 15, high warming, high flux
month

Figure A.51

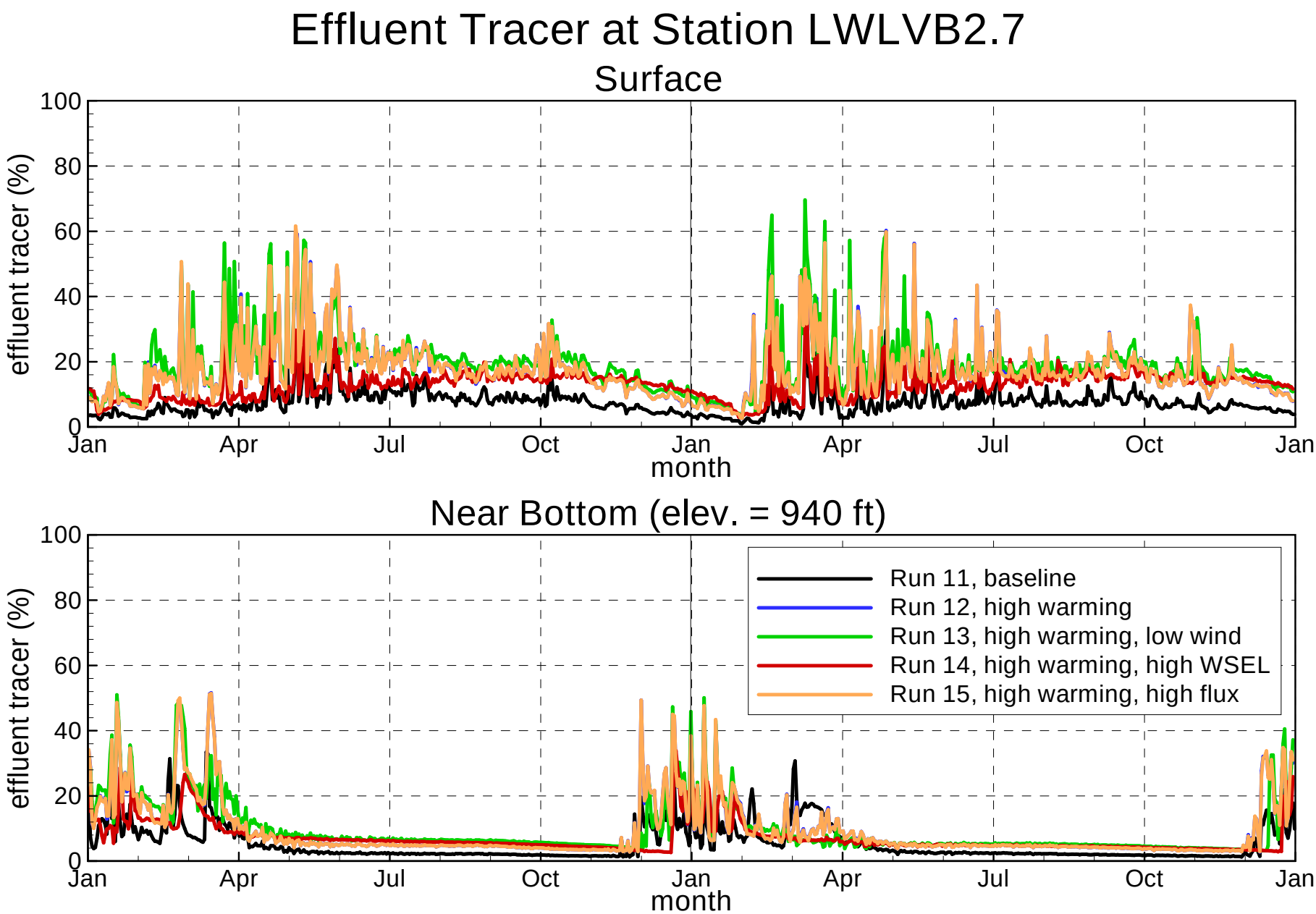

Figure A.52

FLOW SCIENCE

Effluent Tracer at Station LWLVB3.5

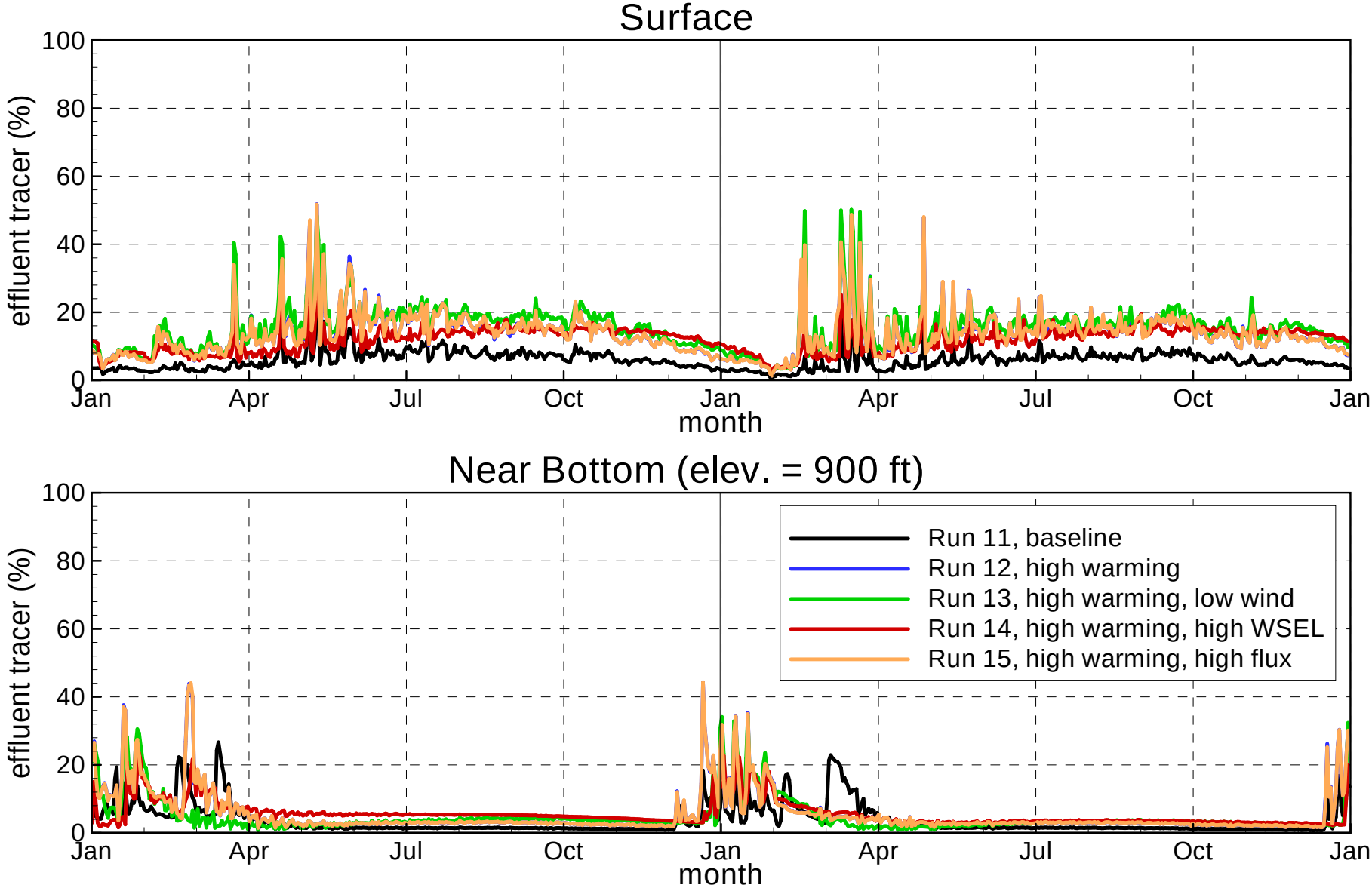

Figure A.53

FLOW SCIENCE

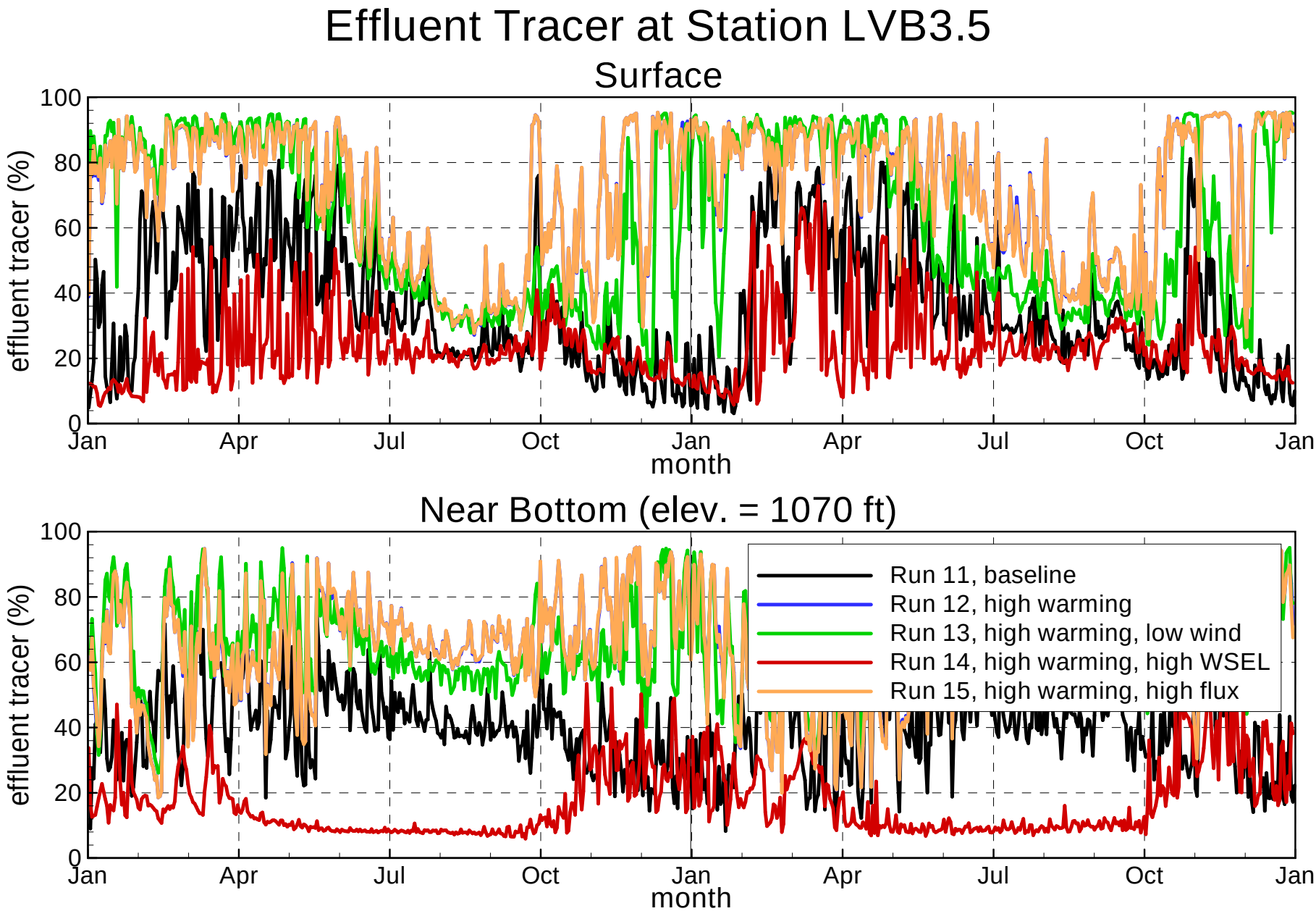
Effluent Tracer at Station LVB3.5
Surface
effluent tracer (%)
100
80
60
40
20
0
Jan
Apr
Jul
Oct
Jan
Apr
Jul
Oct
Jan
month
Near Bottom (elev. = 1070 ft)
effluent tracer (%)
Run 11, baseline
Run 12, high warming
Run 13, high warming, low wind
Run 14, high warming, high WSEL
Run 15, high warming, high flux
month

Figure A.54

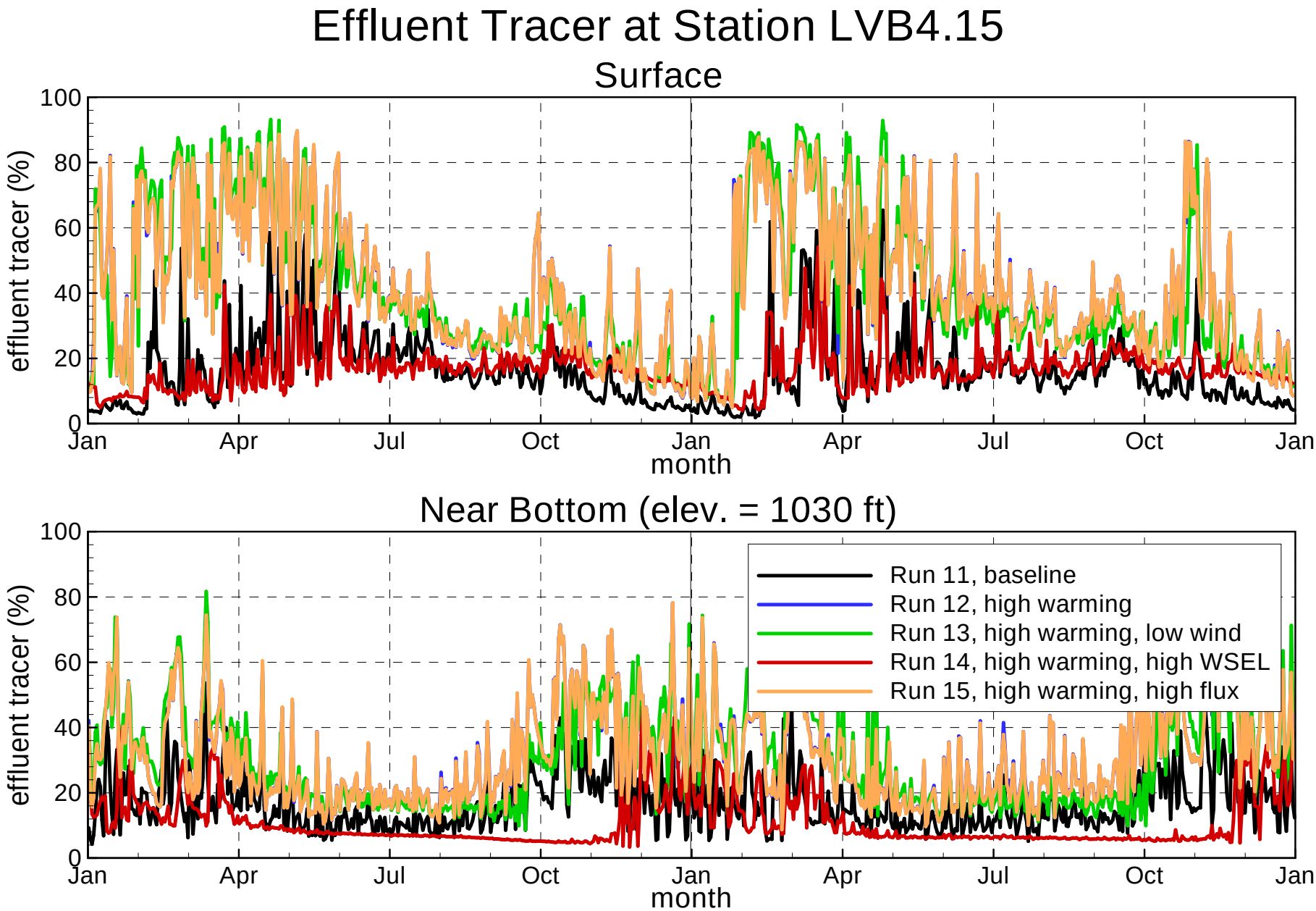
Effluent Tracer at Station LVB4.15
Surface
effluent tracer (%)
100
80
60
40
20
0
Jan
Apr
Jul
Oct
Jan
Apr
Jul
Oct
Jan
month
Near Bottom (elev. = 1030 ft)
effluent tracer (%)
Run 11, baseline
Run 12, high warming
Run 13, high warming, low wind
Run 14, high warming, high WSEL
Run 15, high warming, high flux
month

Figure A.55

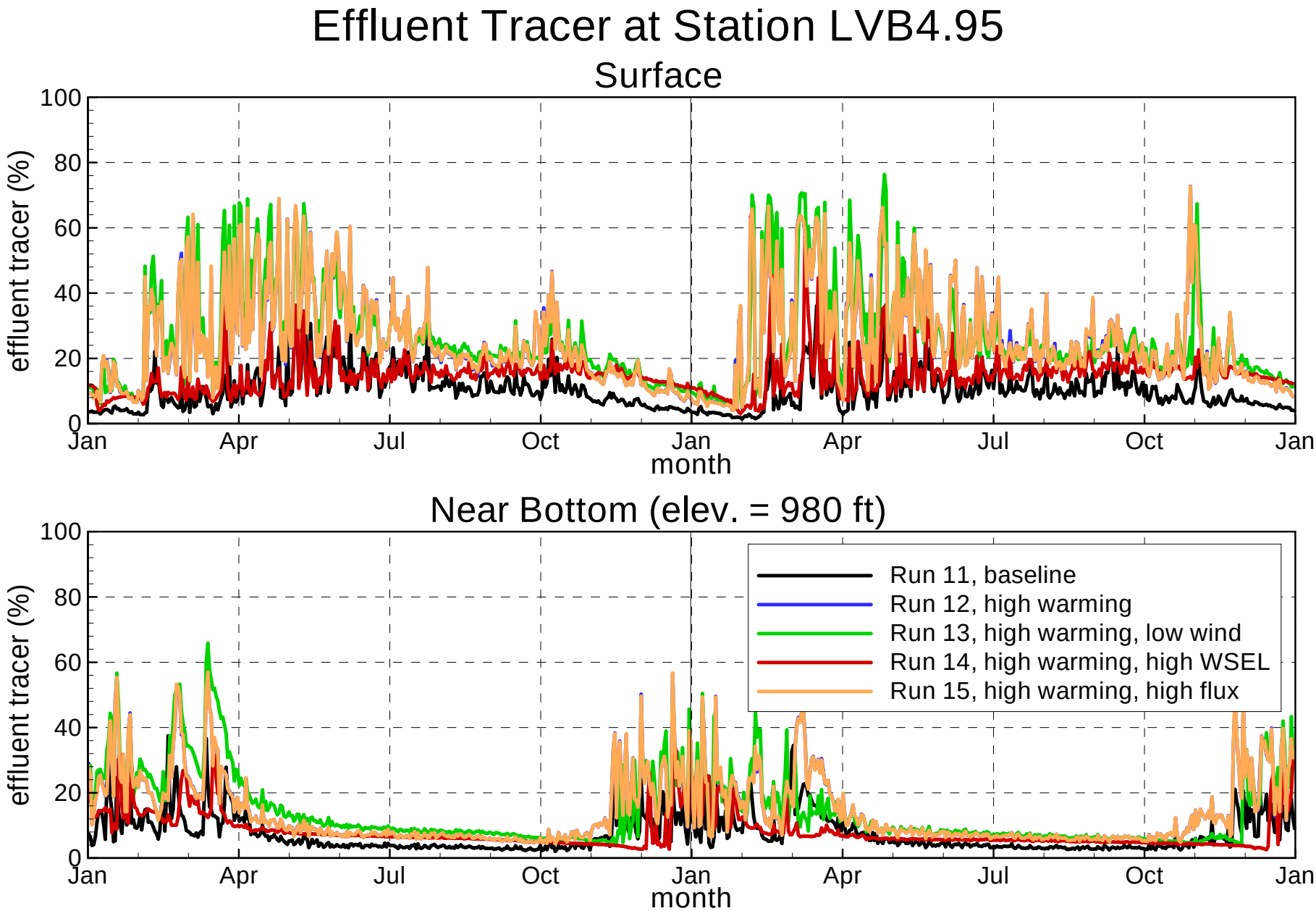
Effluent Tracer at Station LVB4.95
Surface
effluent tracer (%)
100
80
60
40
20
0
Jan
Apr
Jul
Oct
Jan
Apr
Jul
Oct
Jan
month
Near Bottom (elev. = 980 ft)
effluent tracer (%)
Run 11, baseline
Run 12, high warming
Run 13, high warming, low wind
Run 14, high warming, high WSEL
Run 15, high warming, high flux
month

Figure A.56

Effluent Tracer at Station LVB6.7

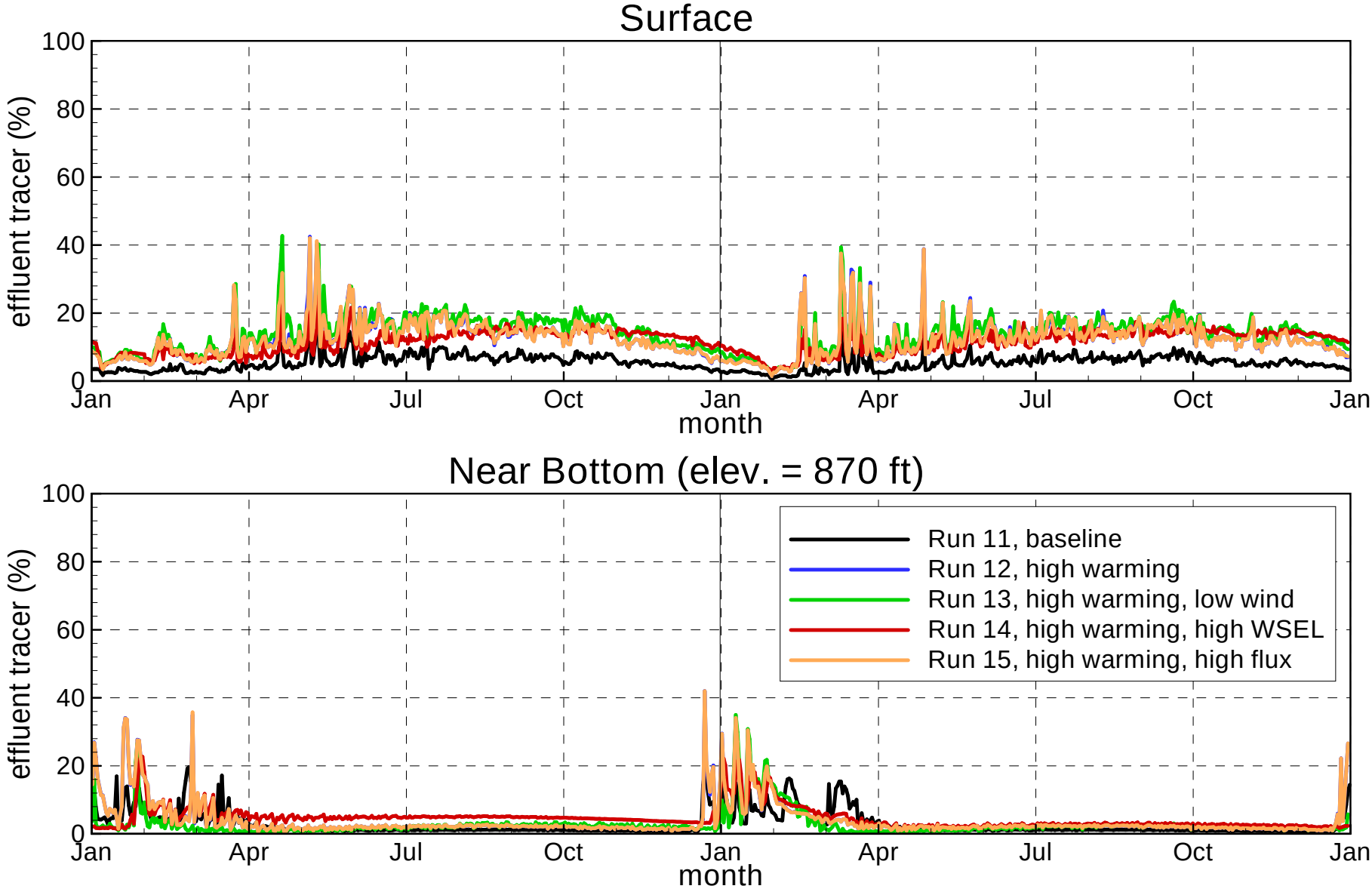

Figure A.57

FLOW SCIENCE

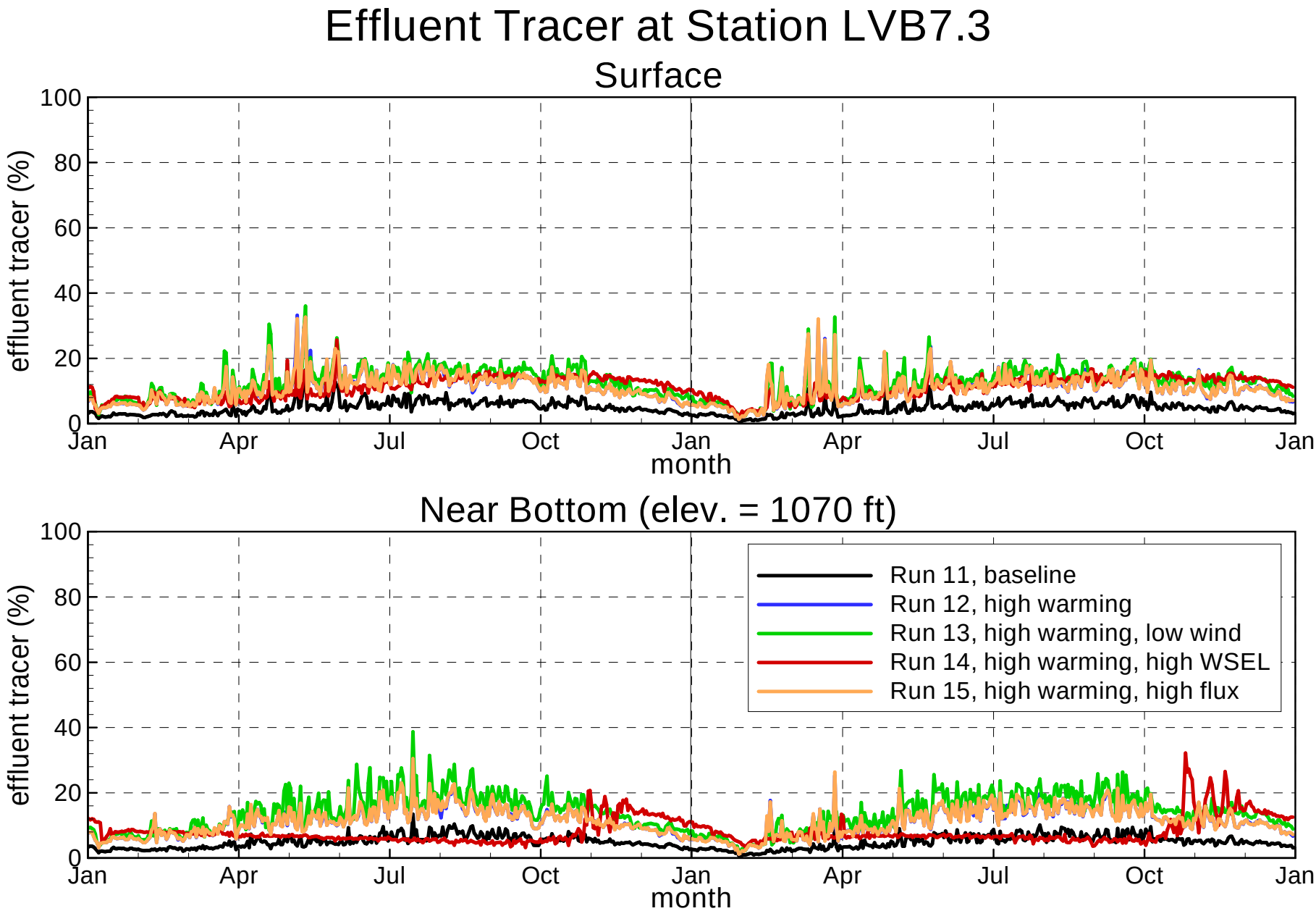
Effluent Tracer at Station LVB7.3
Surface
effluent tracer (%)
100
80
60
40
20
0
Jan
Apr
Jul
Oct
Jan
Apr
Jul
Oct
Jan
month
Near Bottom (elev. = 1070 ft)
effluent tracer (%)
100
80
60
40
20
0
Jan
Apr
Jul
Oct
Jan
Apr
Jul
Oct
Jan
month
Run 11, baseline
Run 12, high warming
Run 13, high warming, low wind
Run 14, high warming, high WSEL
Run 15, high warming, high flux

Figure A.58

Effluent Tracer at SNWA Intake #3

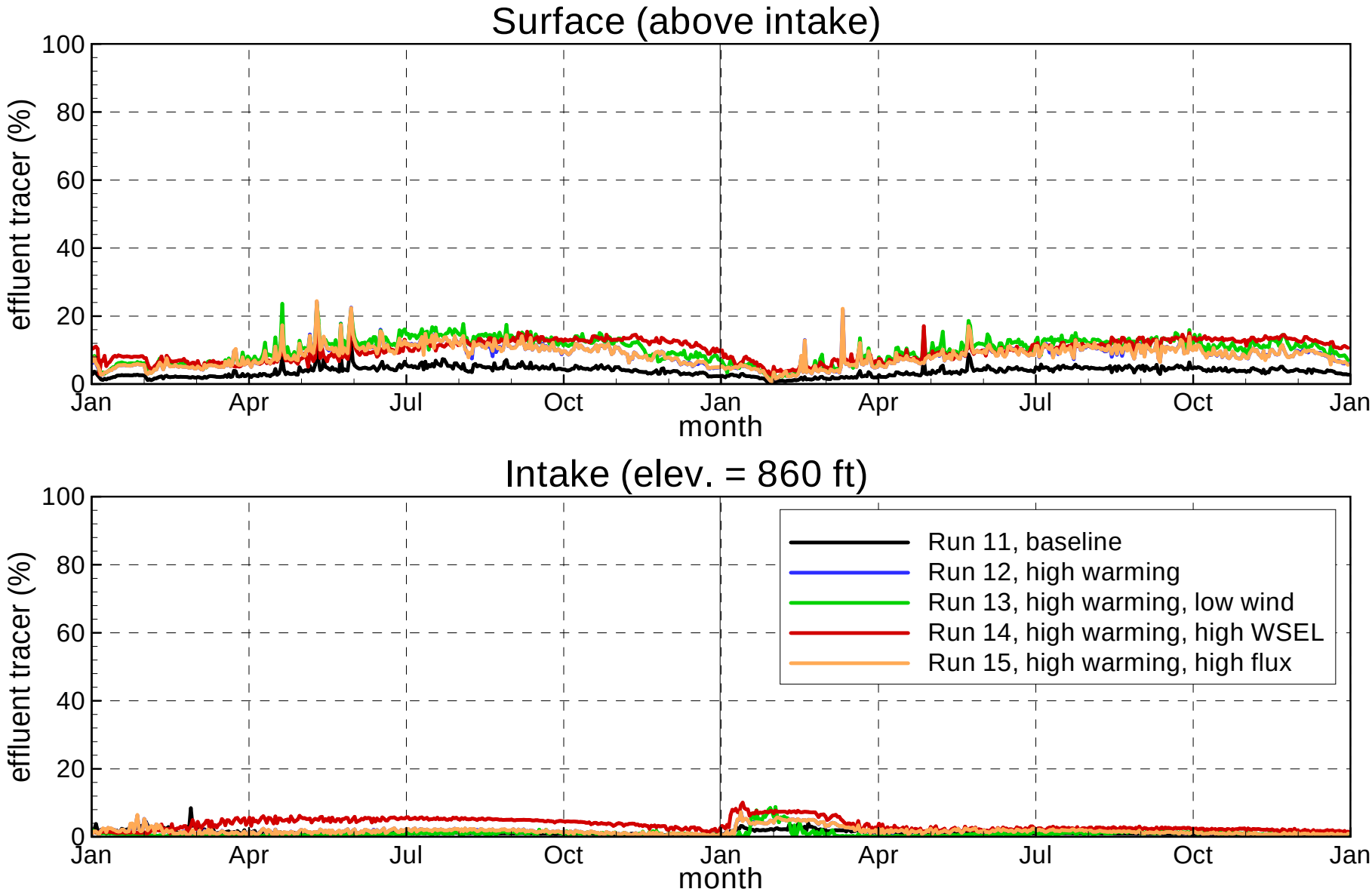

Figure A.59

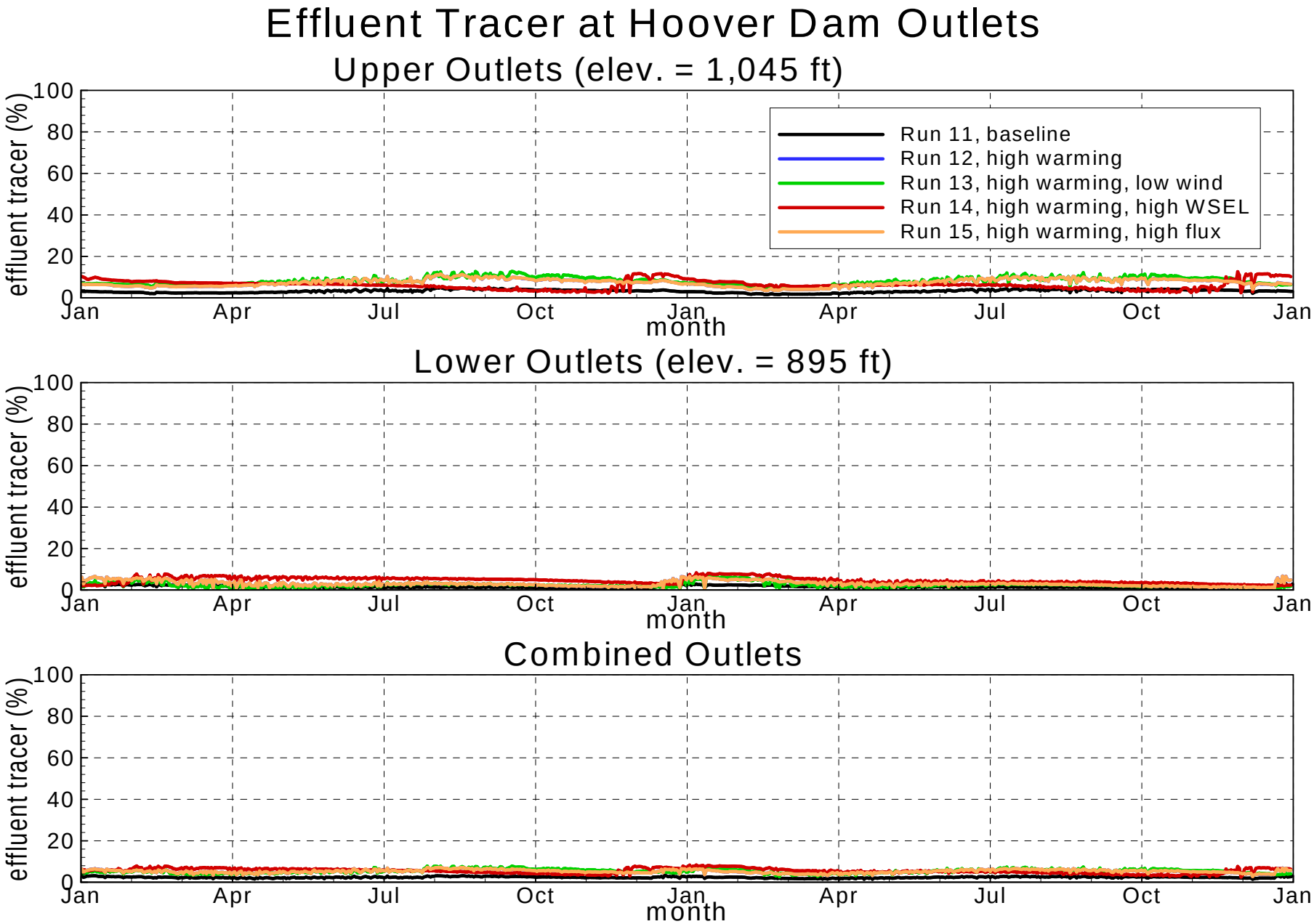

Figure A.60

FLOW SCIENCE

Filterable Reactive Phosphorus at Station CR394.0

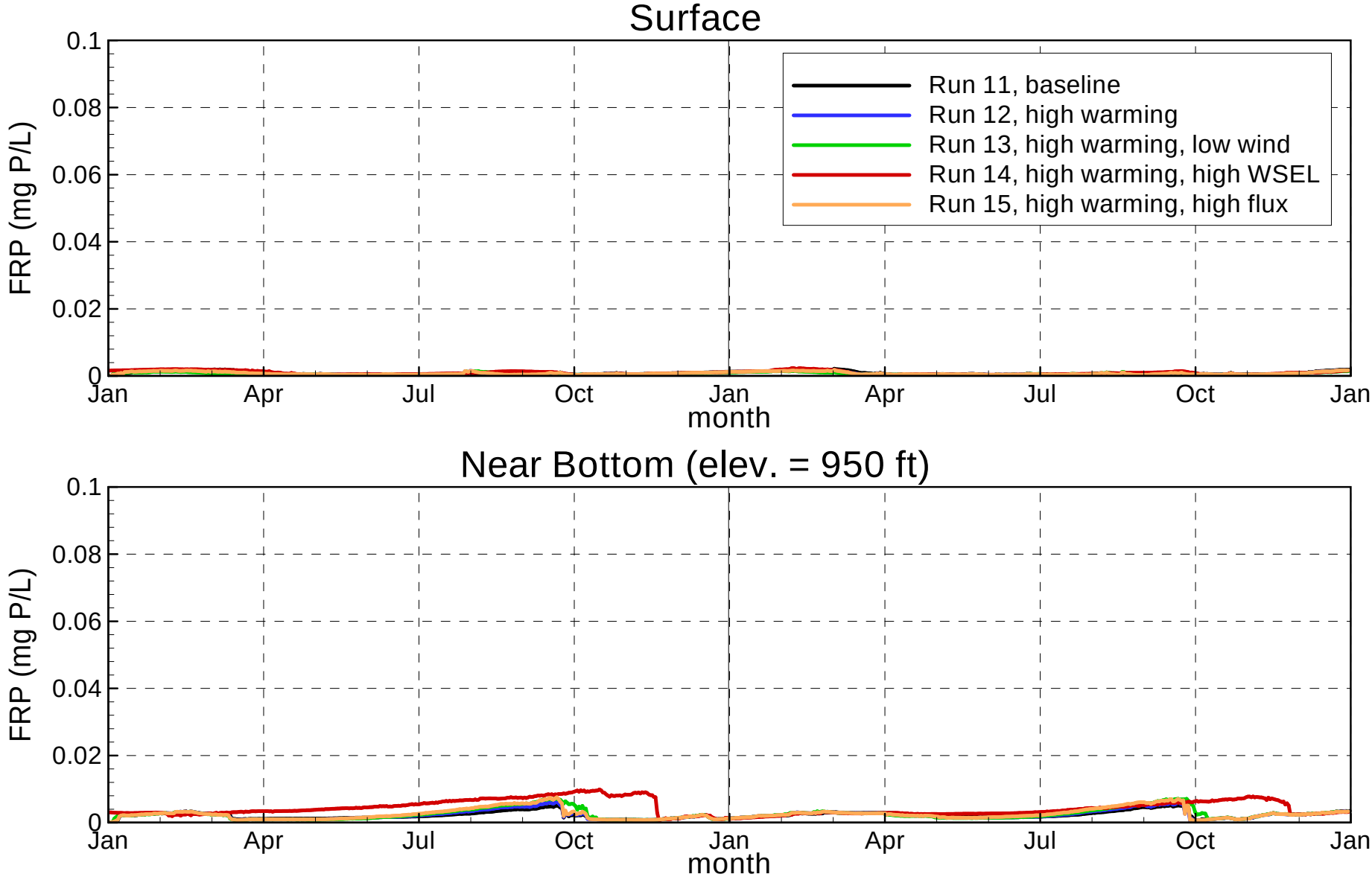

Figure A.61

FLOW SCIENCE

Filterable Reactive Phosphorus at Station CR390.0

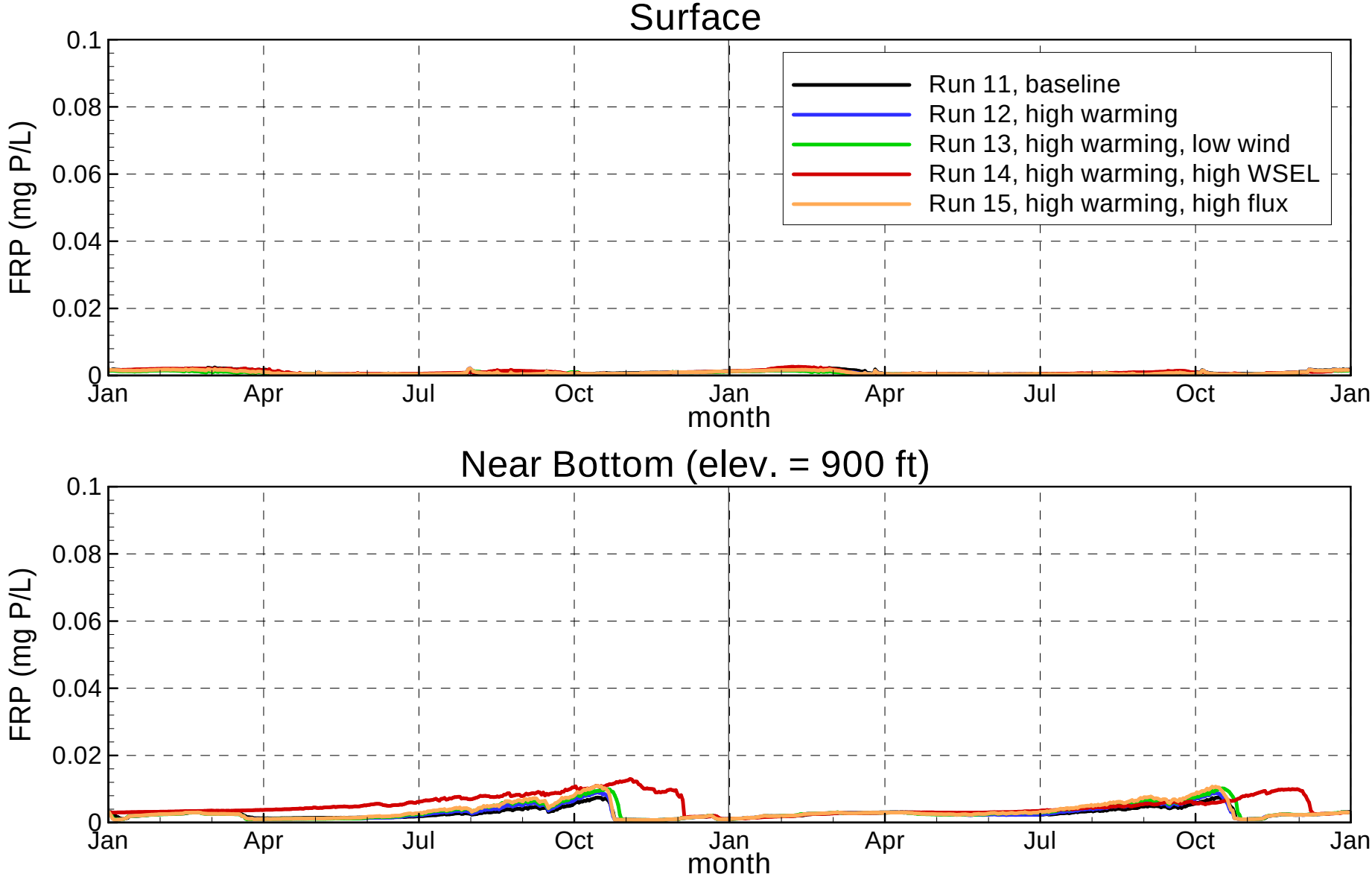

Figure A.62

FLOW SCIENCE

Filterable Reactive Phosphorus at Station CR380.0

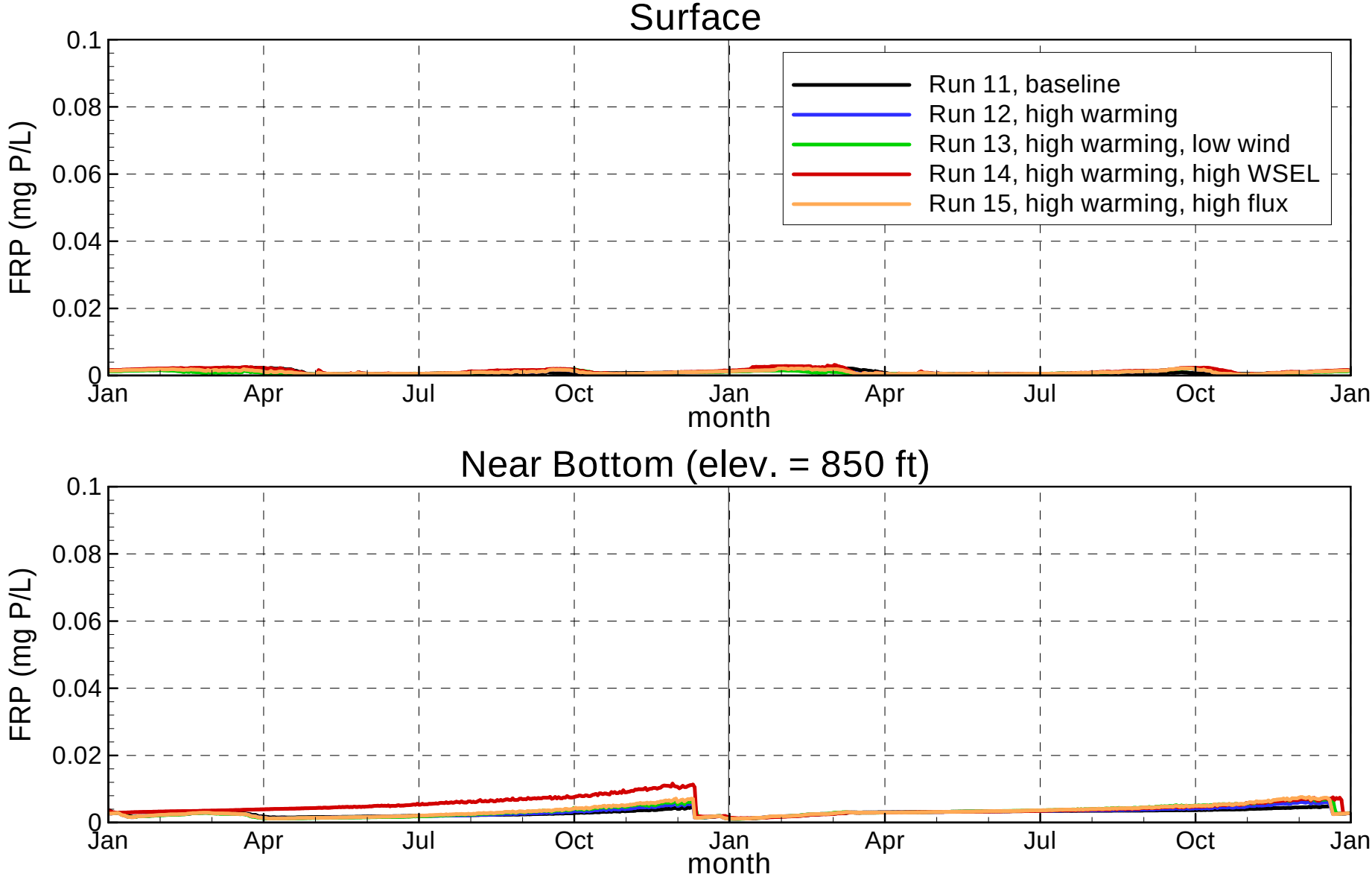

Figure A.63

Filterable Reactive Phosphorus at Station VR2.0

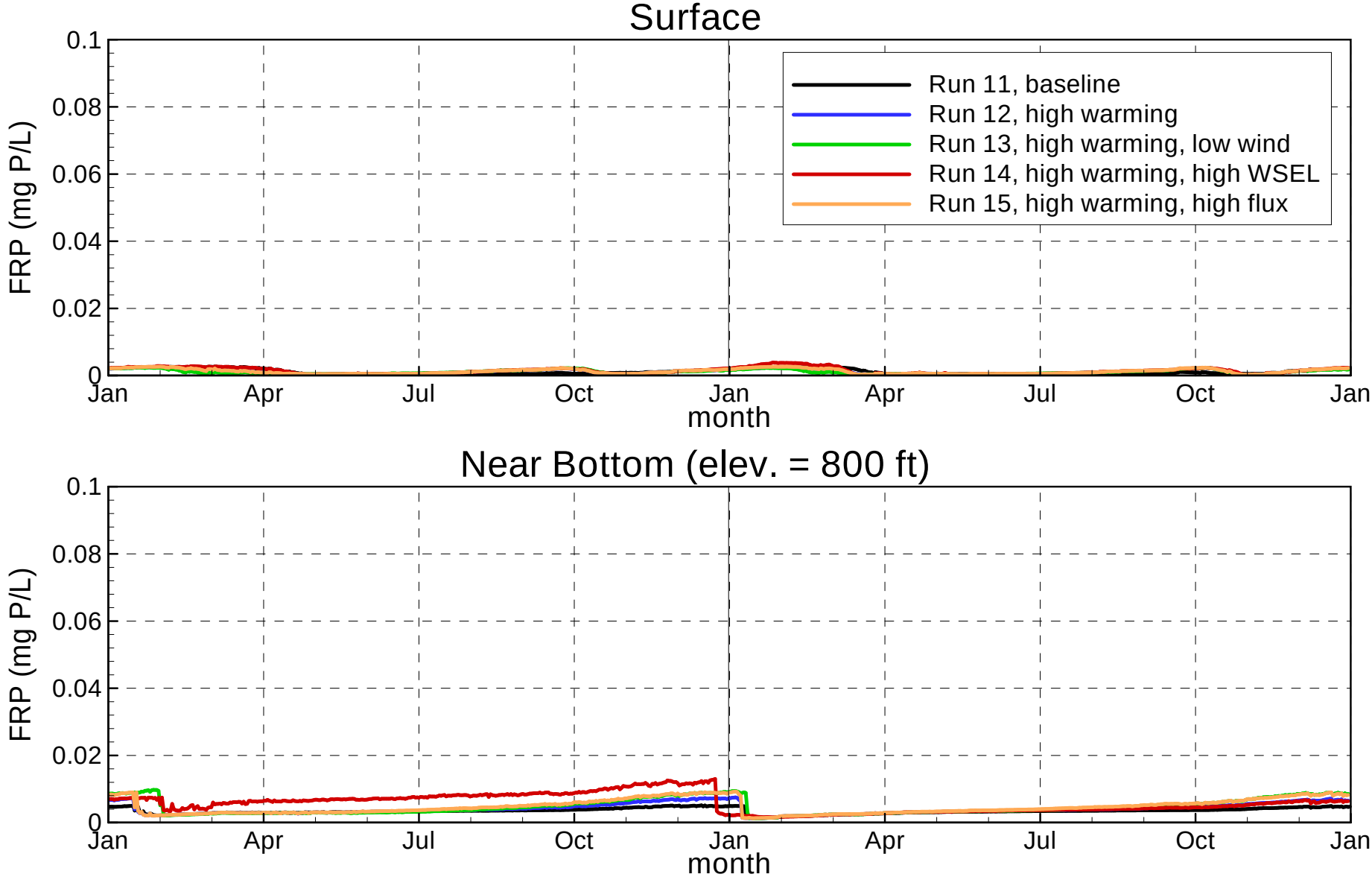

Figure A.64

FLOW SCIENCE

Filterable Reactive Phosphorus at Station VR12.9

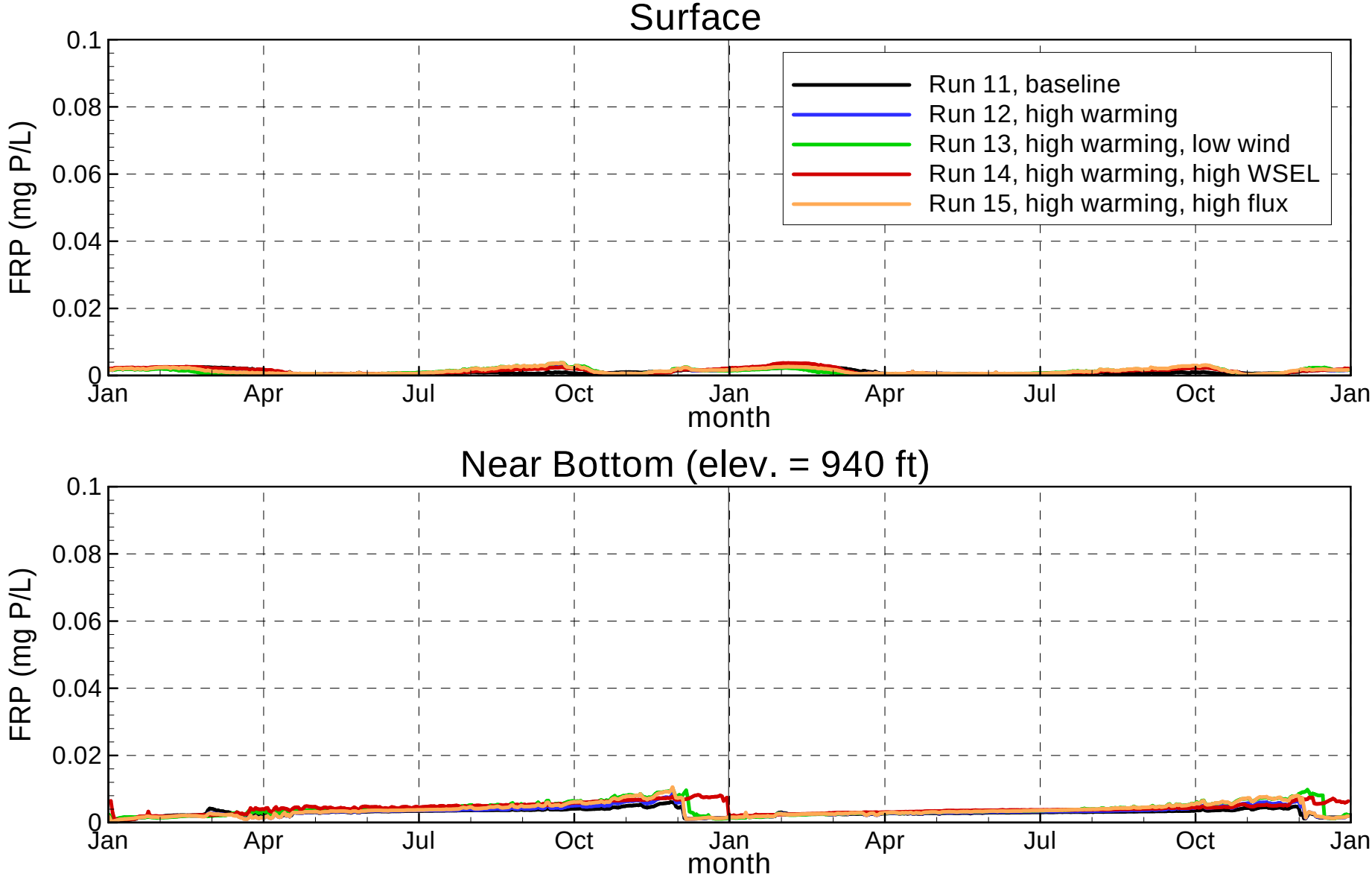

Figure A.65

Filterable Reactive Phosphorus at Station VR18.0

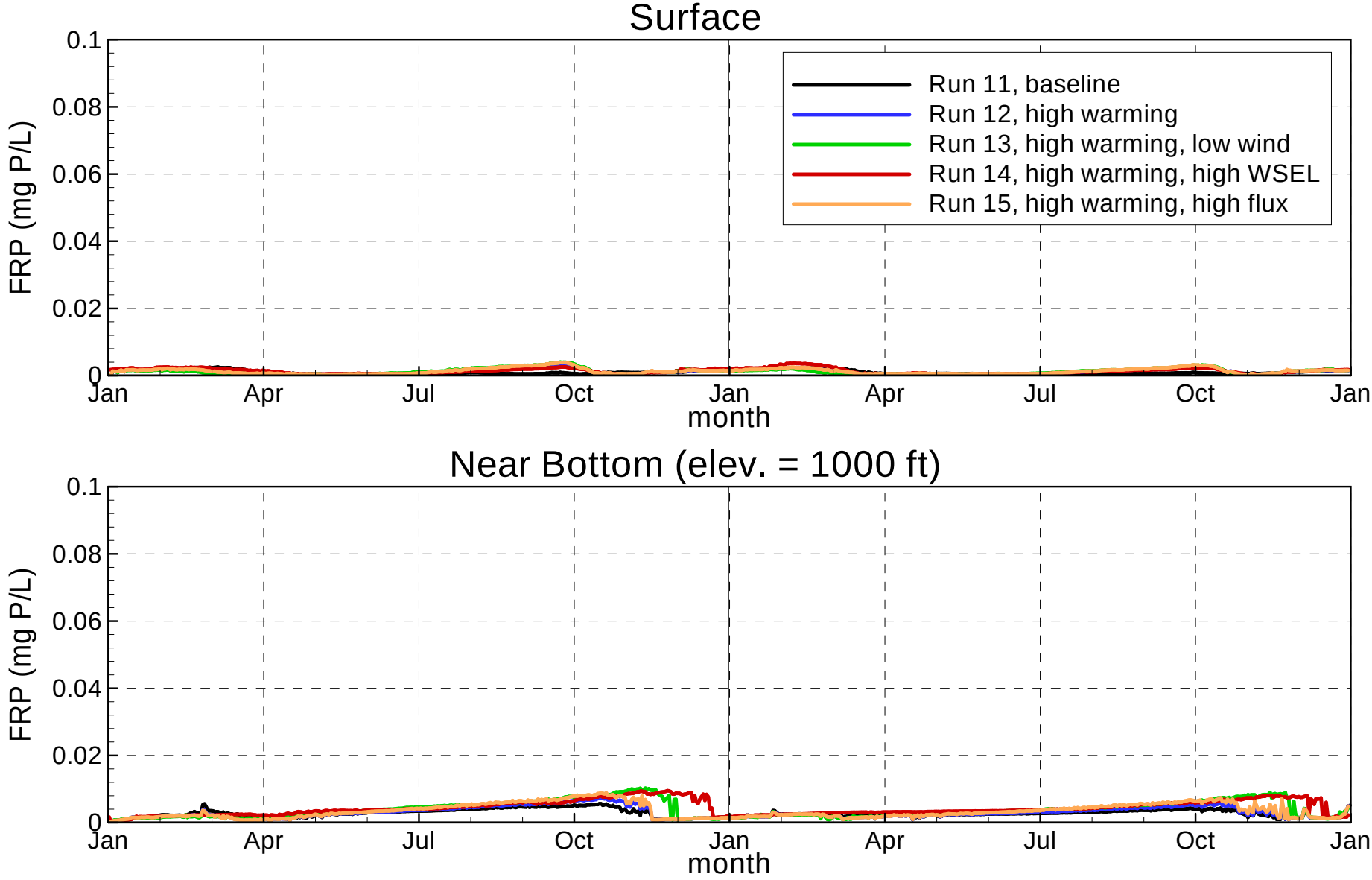

Figure A.66

Filterable Reactive Phosphorus at Station VR25.1

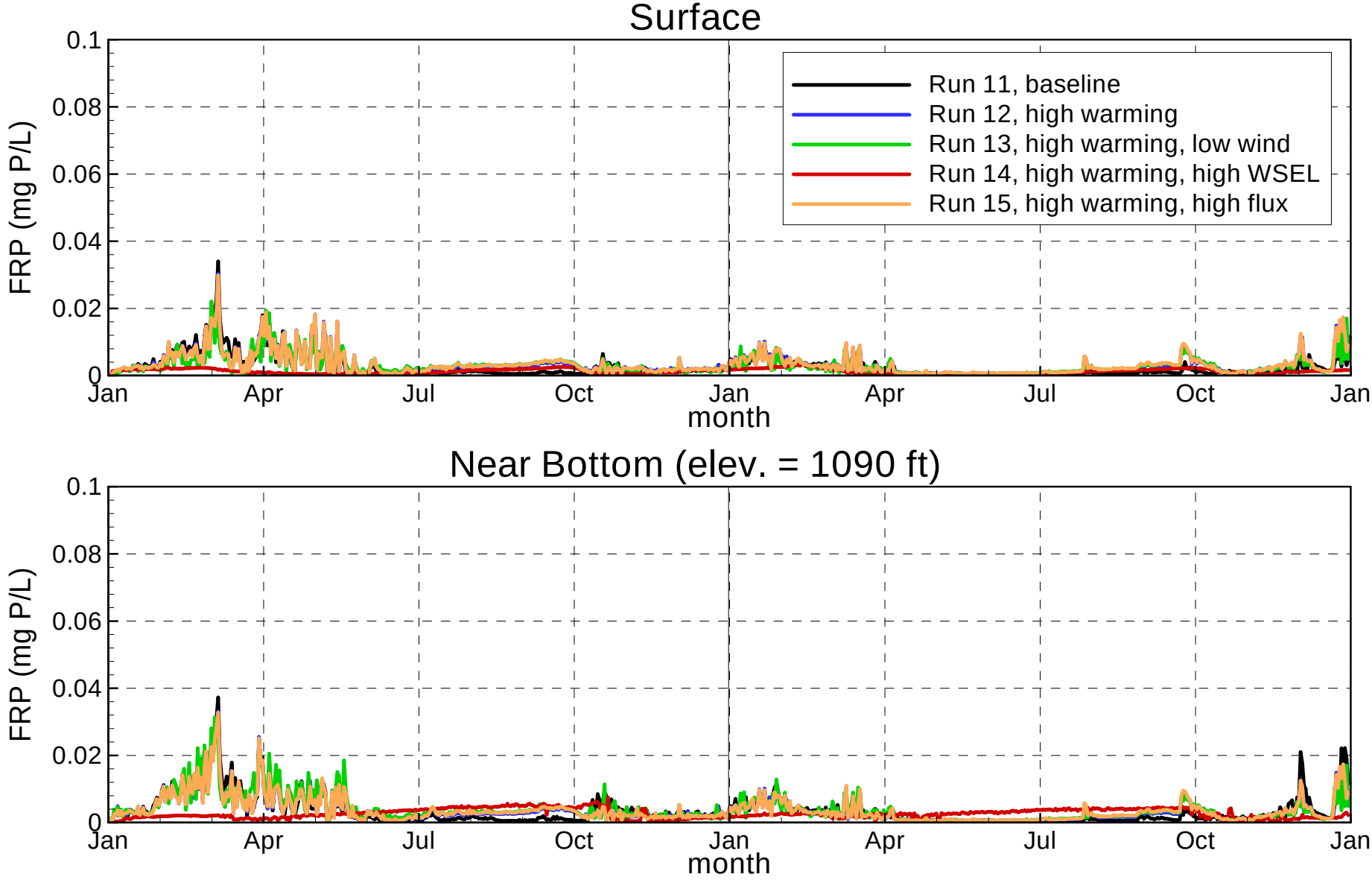

Figure A.67

FLOW SCIENCE

Filterable Reactive Phosphorus at Station CR360.7

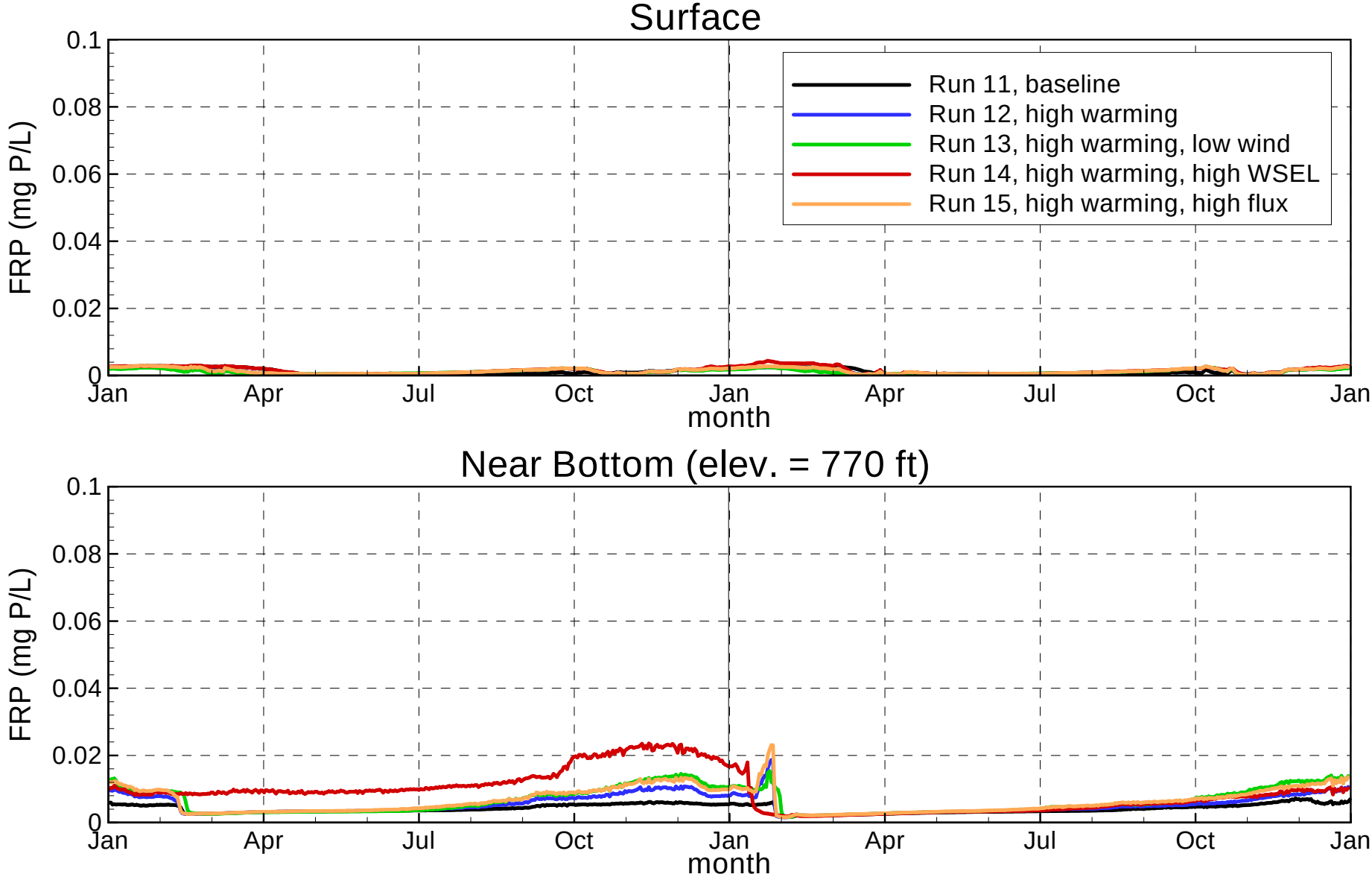

Figure A.68

FLOW SCIENCE

Filterable Reactive Phosphorus at Station CR346.4

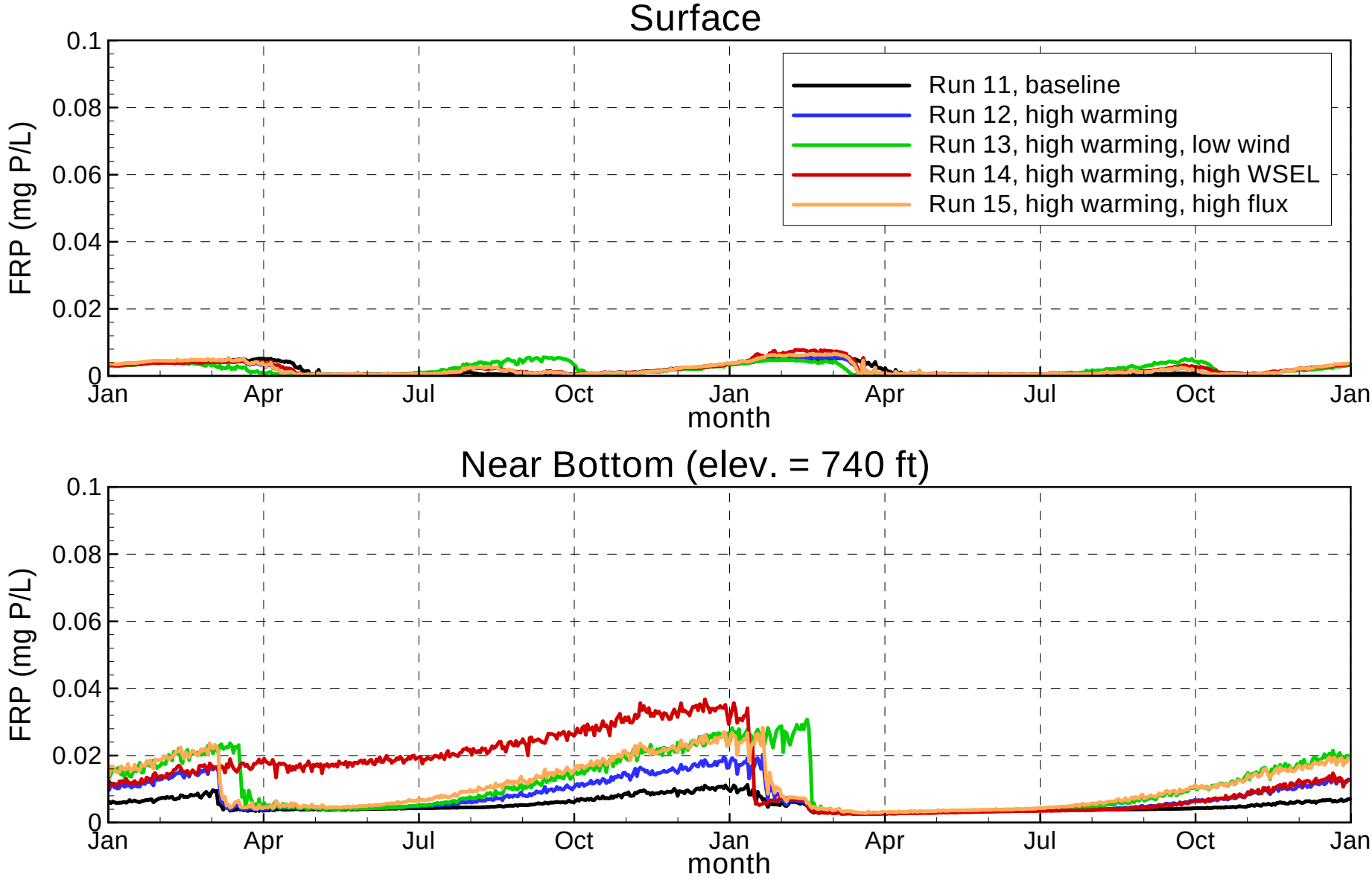

Figure A.69

FLOW SCIENCE

Filterable Reactive Phosphorus at Station LWLVB1.2

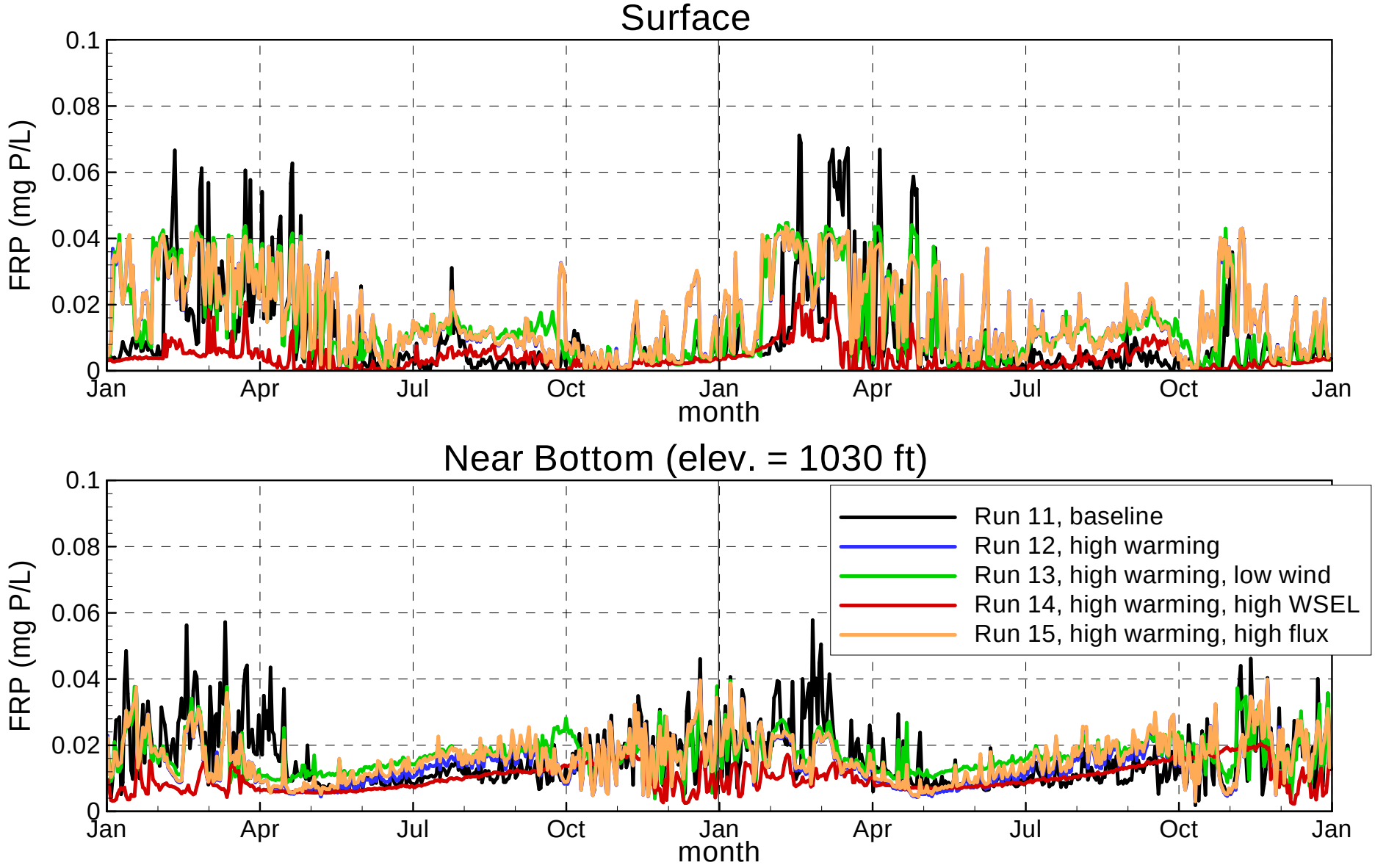

Figure A.70

Filterable Reactive Phosphorus at Station LWLVB1.85

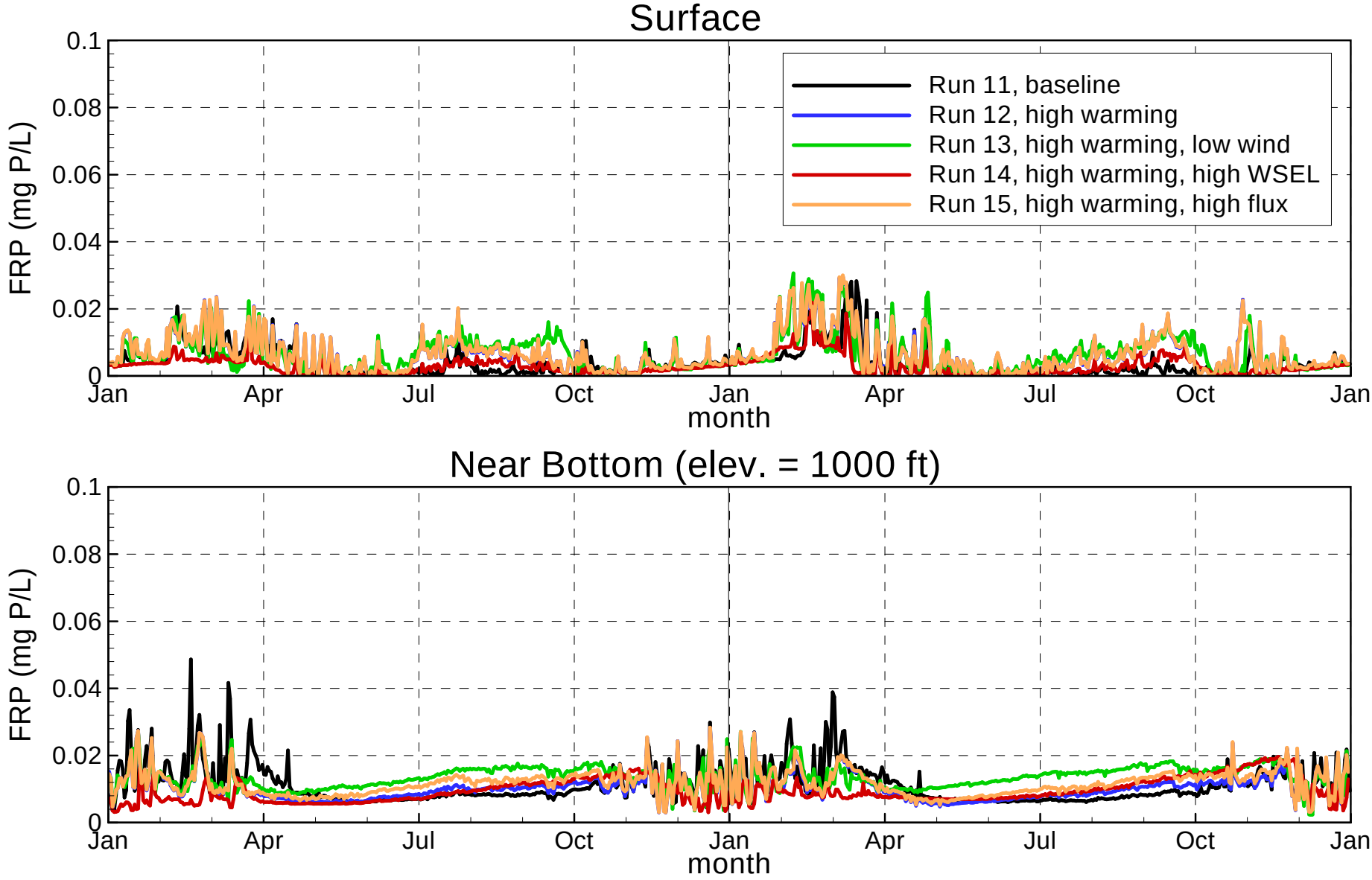

Figure A.71

Filterable Reactive Phosphorus at Station LWLVB2.7

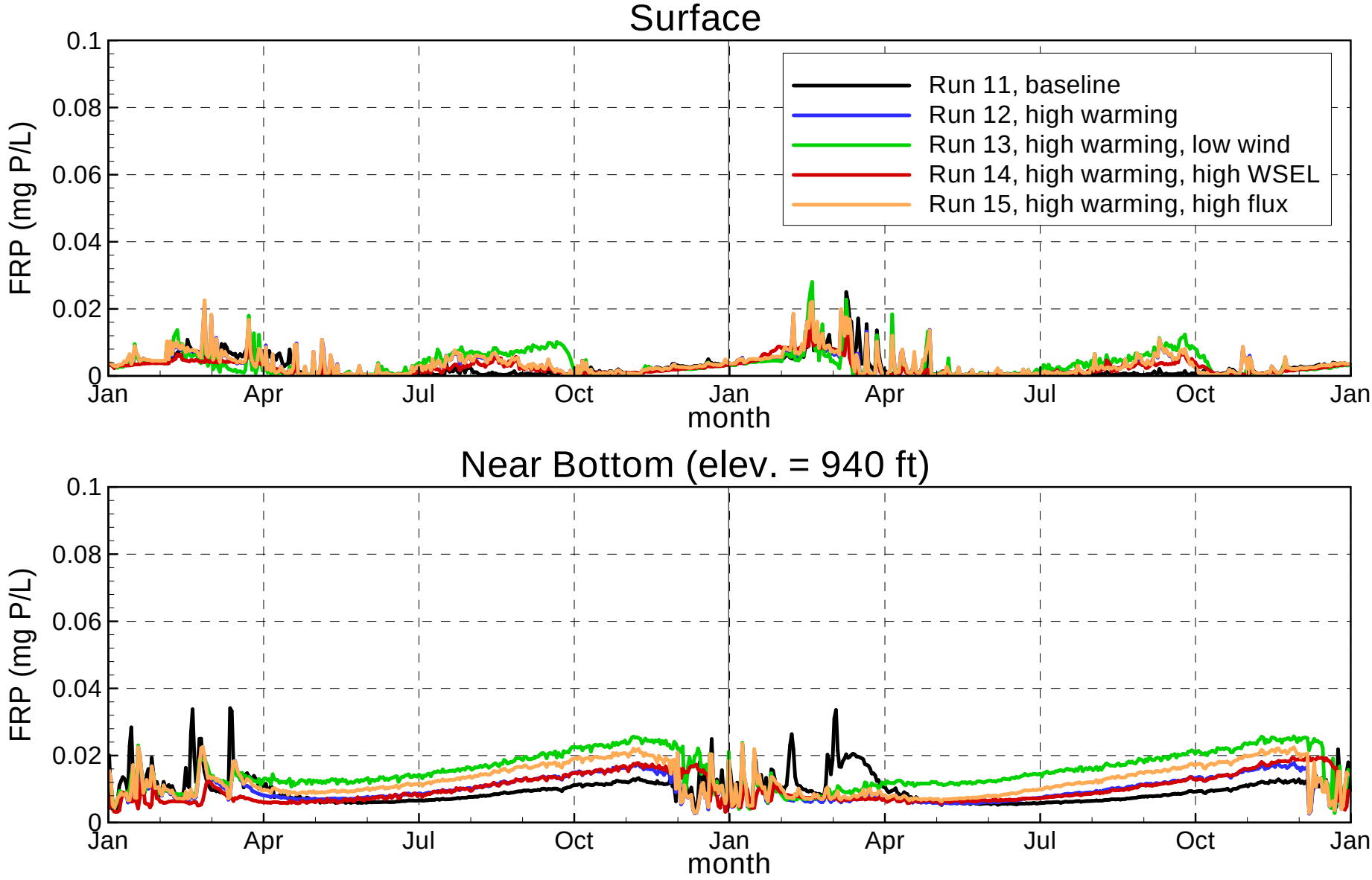

Figure A.72

FLOW SCIENCE

Filterable Reactive Phosphorus at Station LWLVB3.5

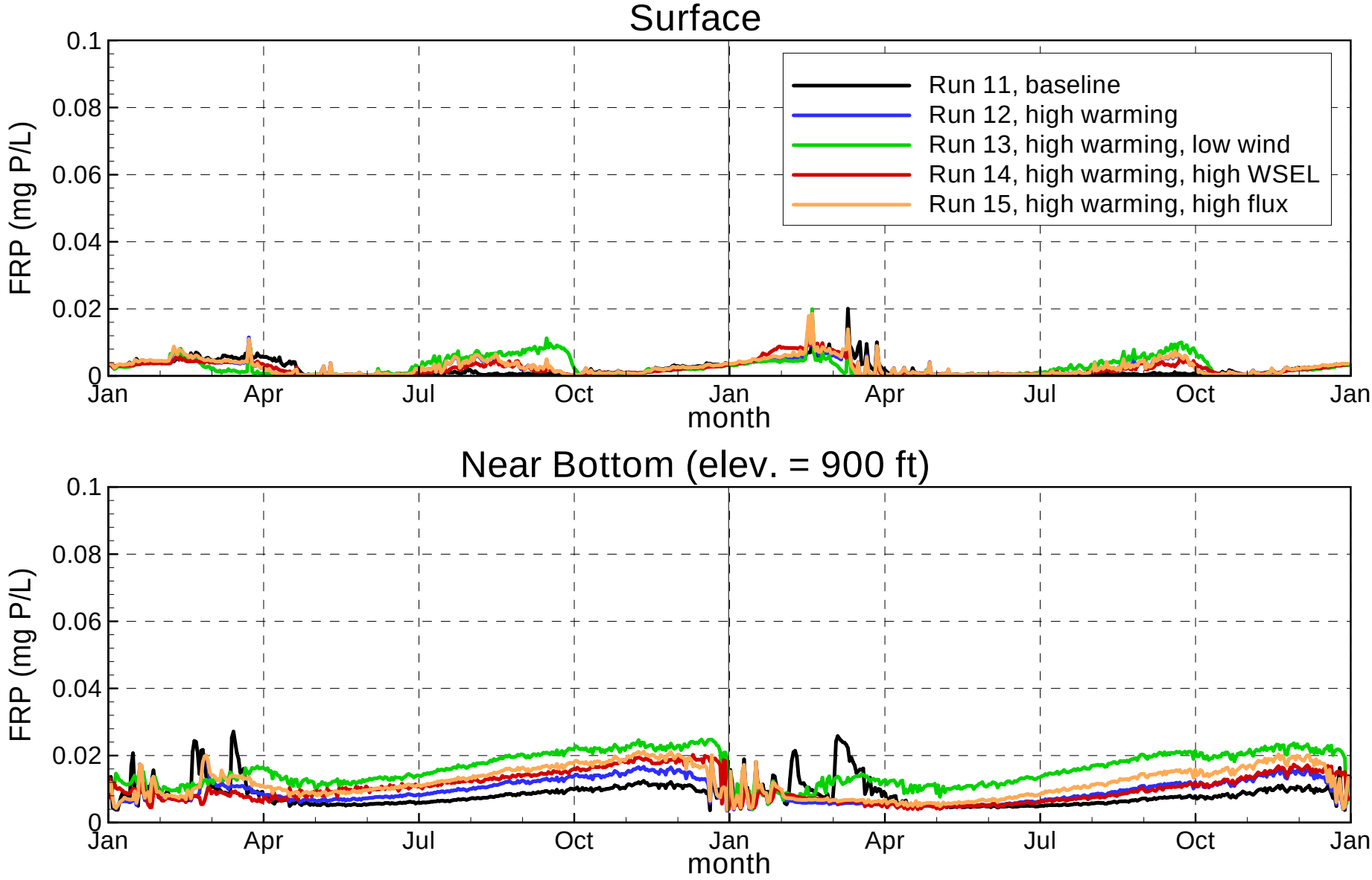

Figure A.73

Filterable Reactive Phosphorus at Station LVB3.5

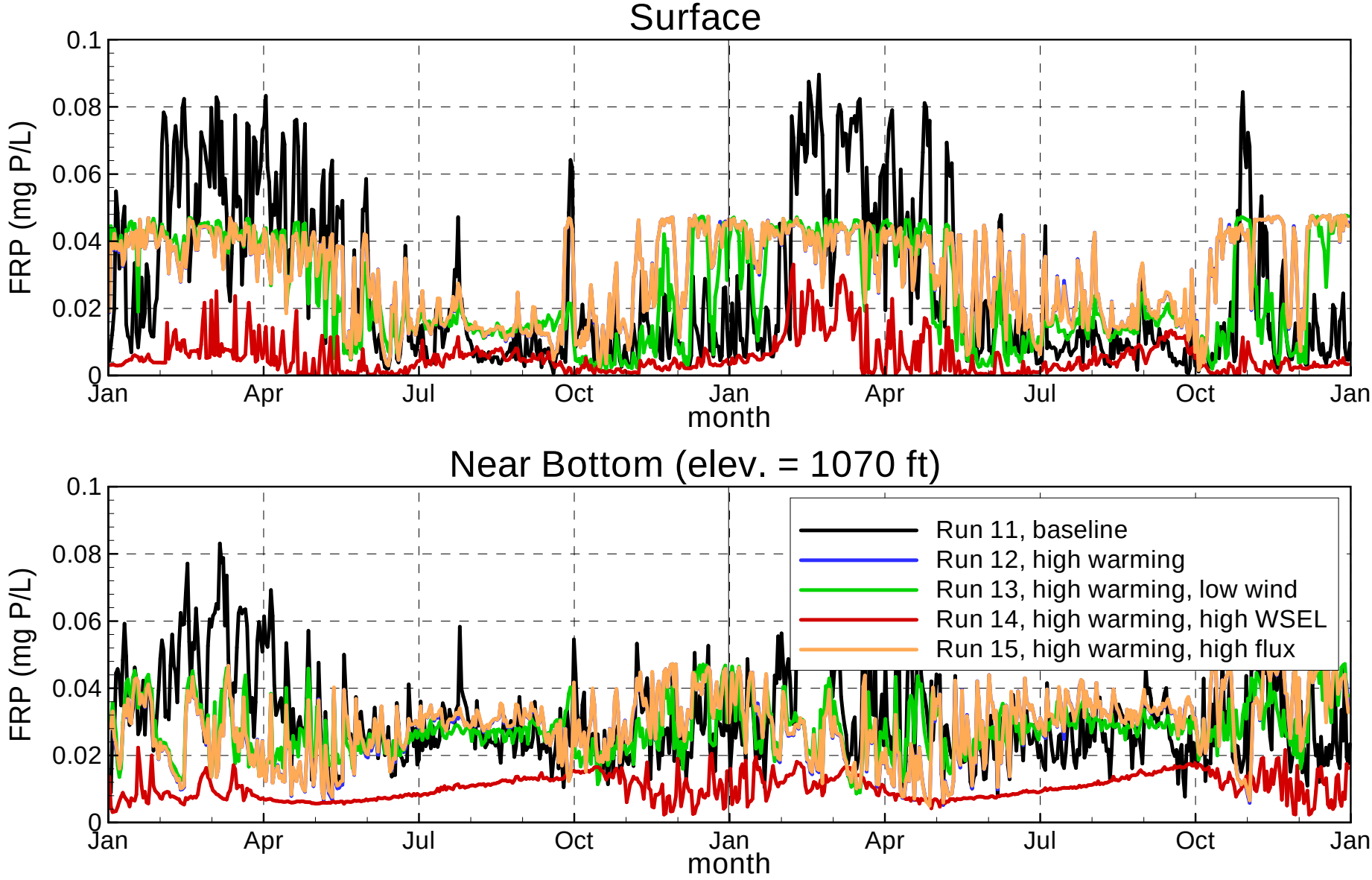

Figure A.74

FLOW SCIENCE

Filterable Reactive Phosphorus at Station LVB4.15

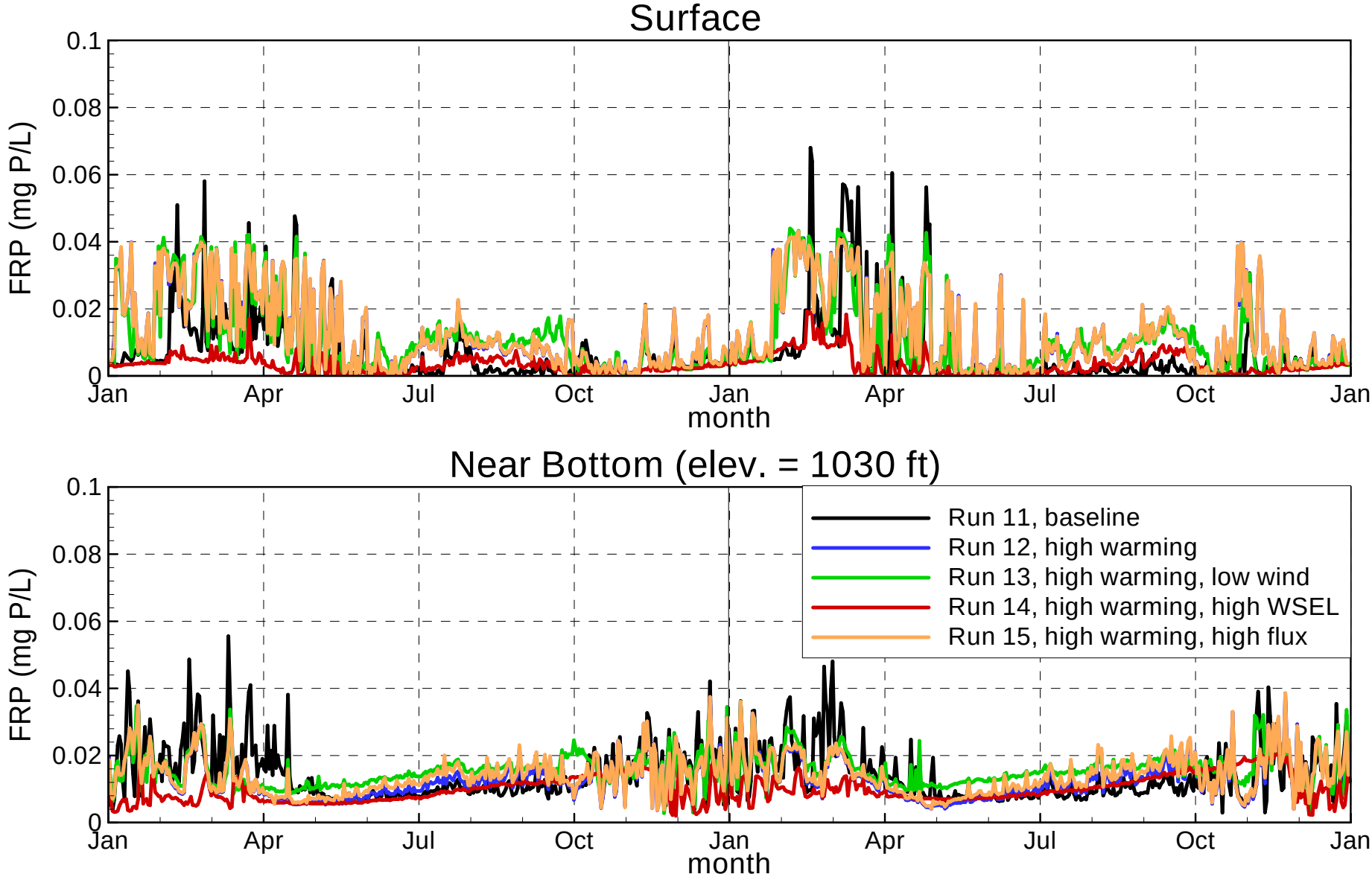

Figure A.75

FLOW SCIENCE

Filterable Reactive Phosphorus at Station LVB4.95

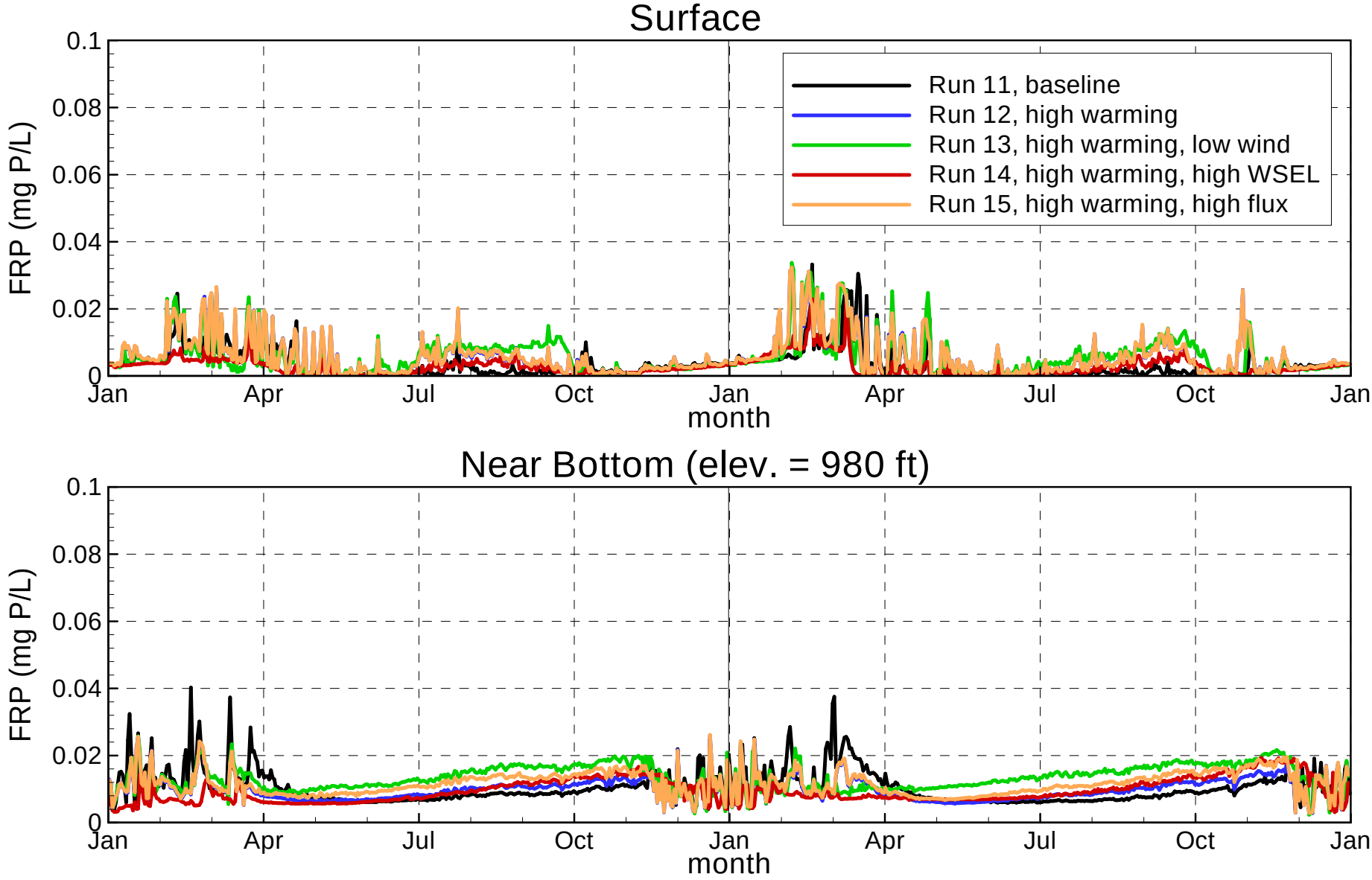

Figure A.76

FLOW SCIENCE

Filterable Reactive Phosphorus at Station LVB6.7

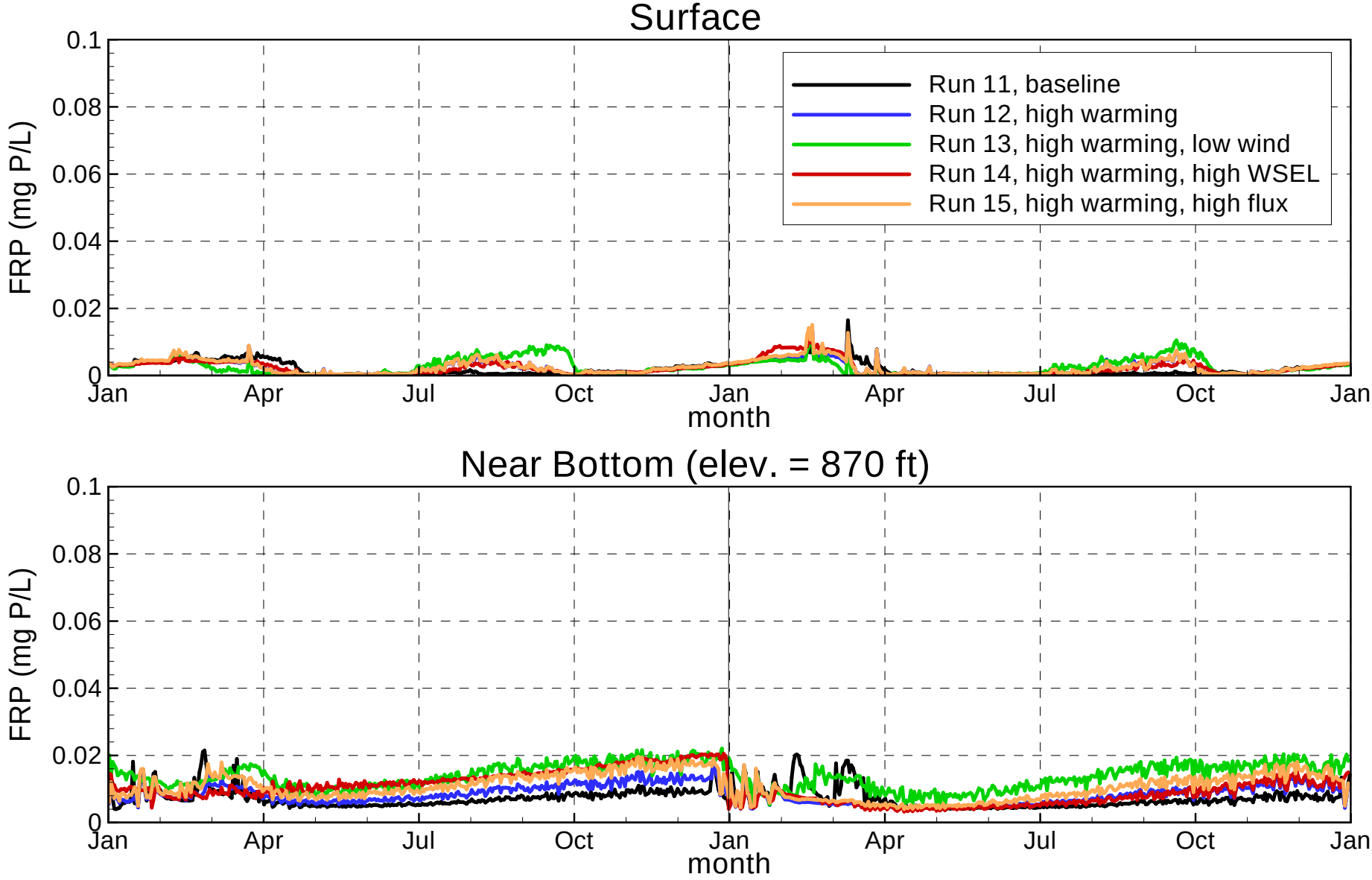

Figure A.77

FLOW SCIENCE

Filterable Reactive Phosphorus at Station LVB7.3

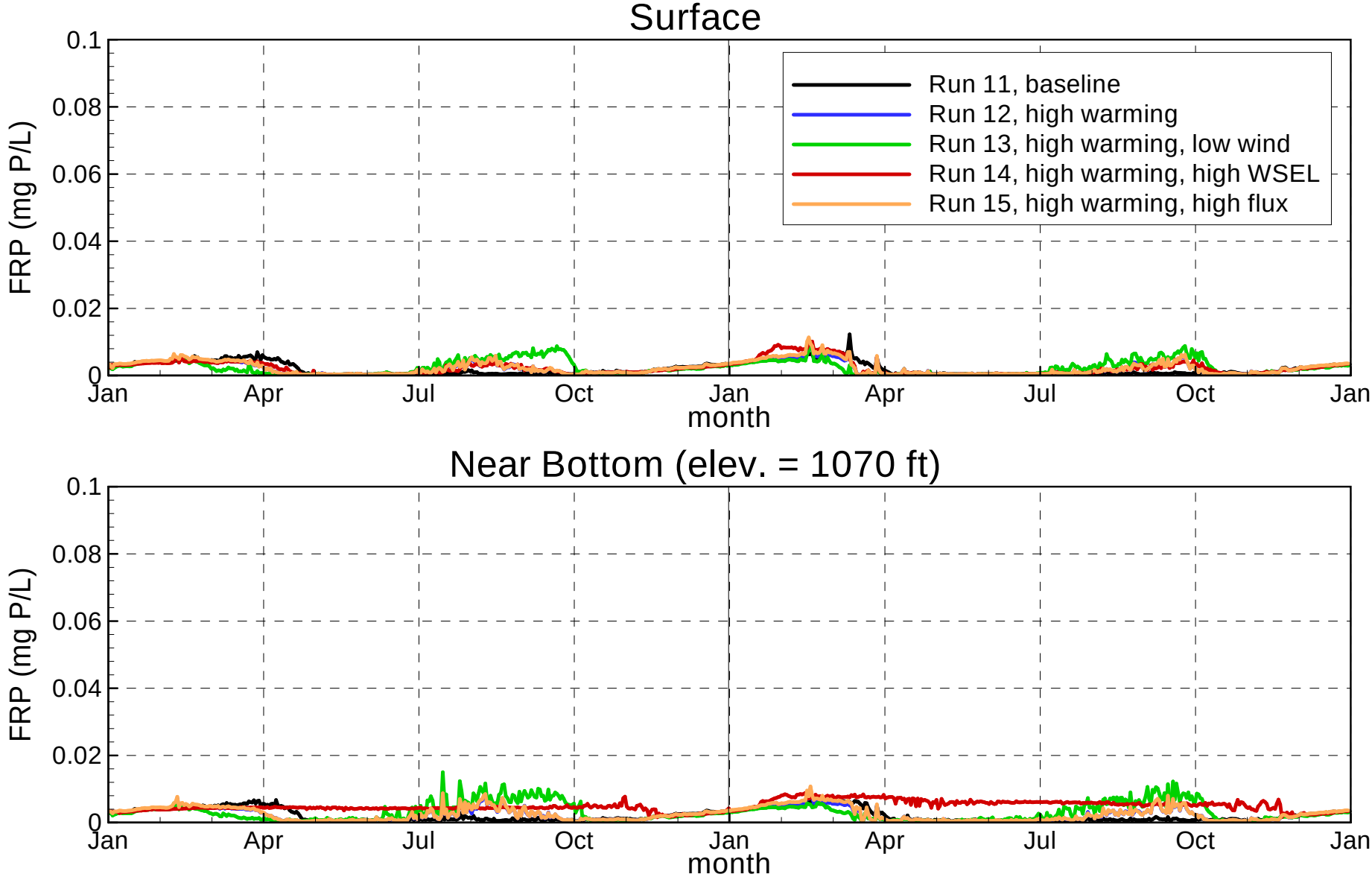

Figure A.78

FLOW SCIENCE

Filterable Reactive Phosphorus at SNWA Intake #3

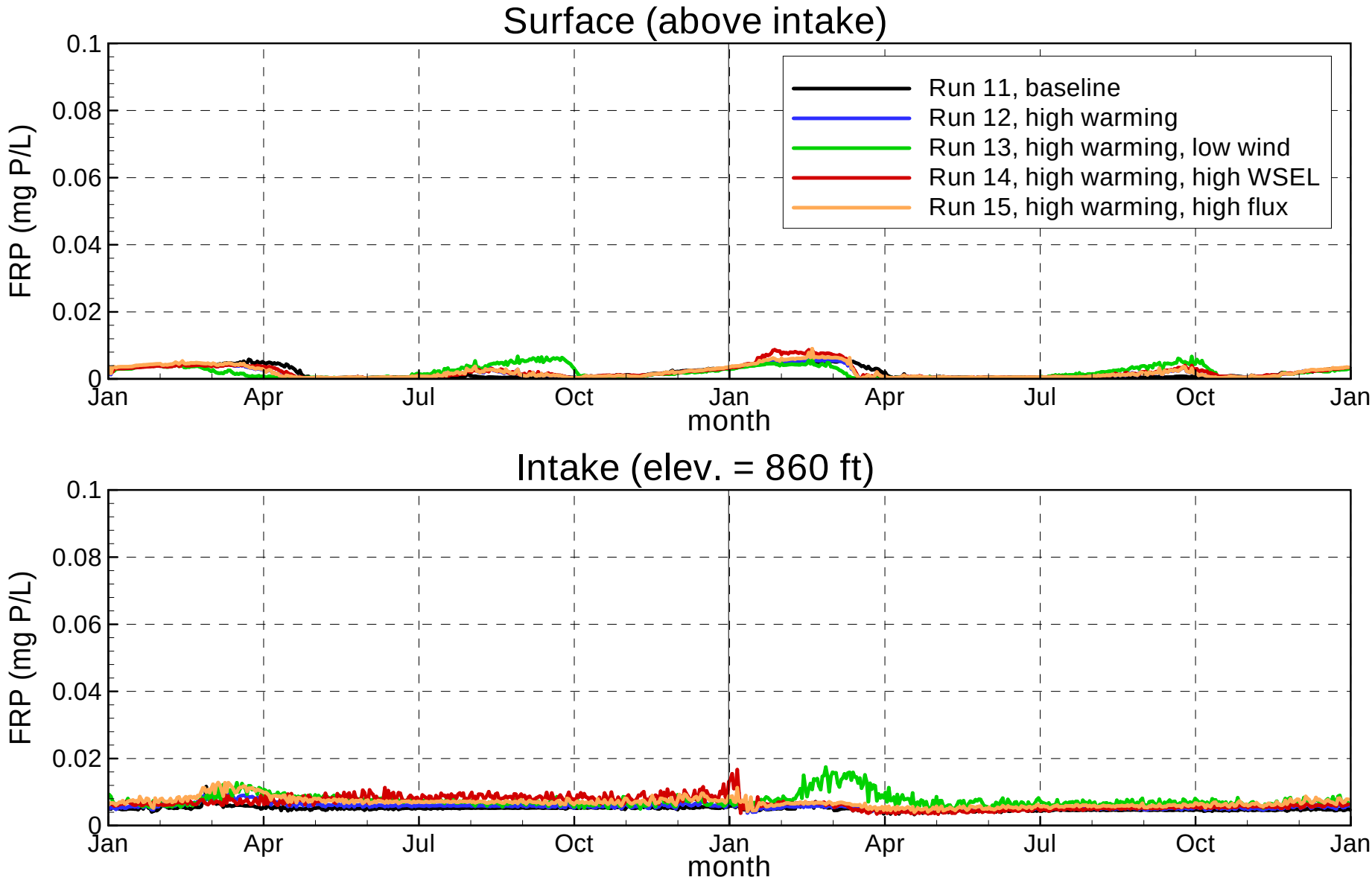

Figure A.79

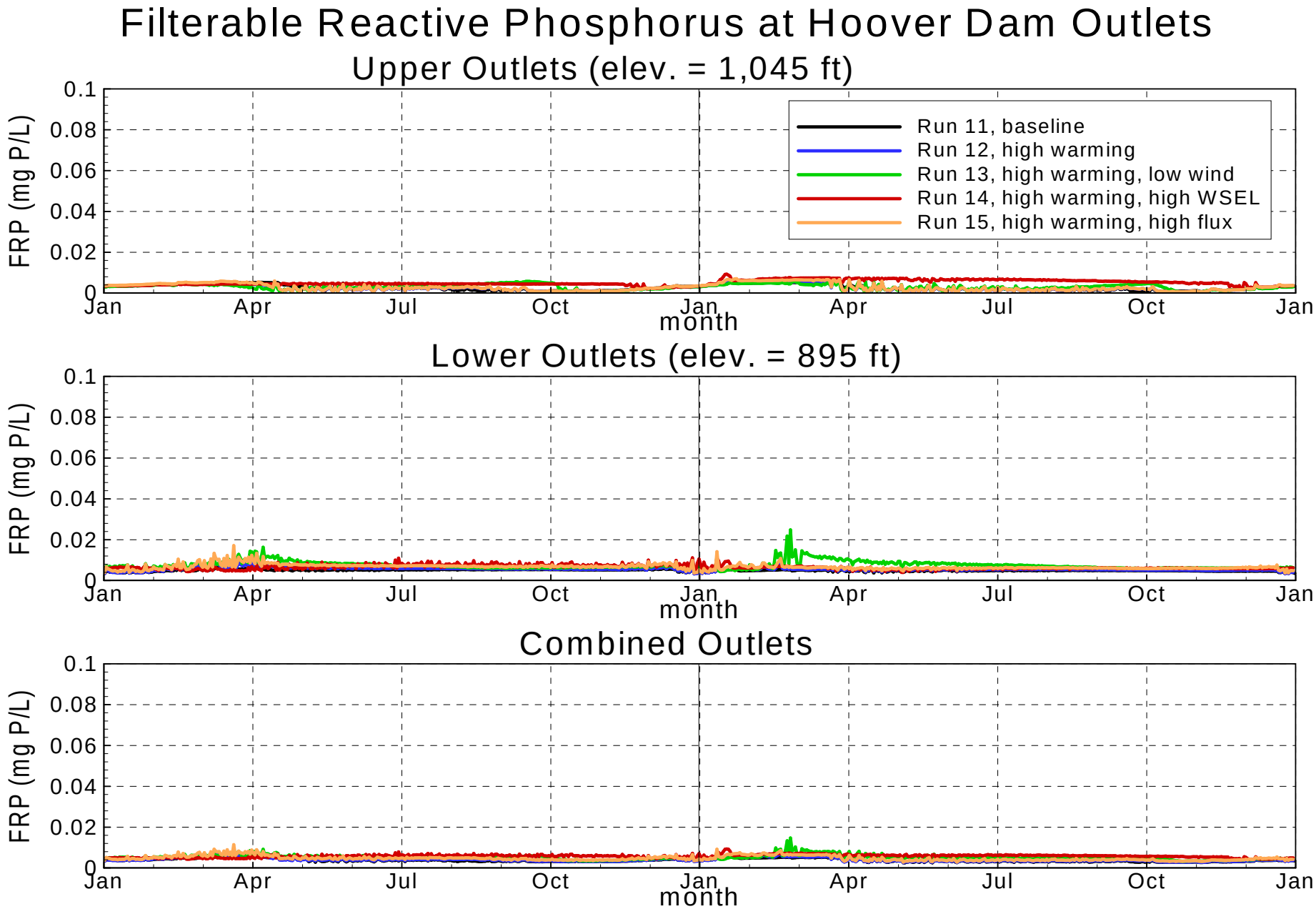

Figure A.80

FLOW SCIENCE

Total Phosphorus at Station CR394.0

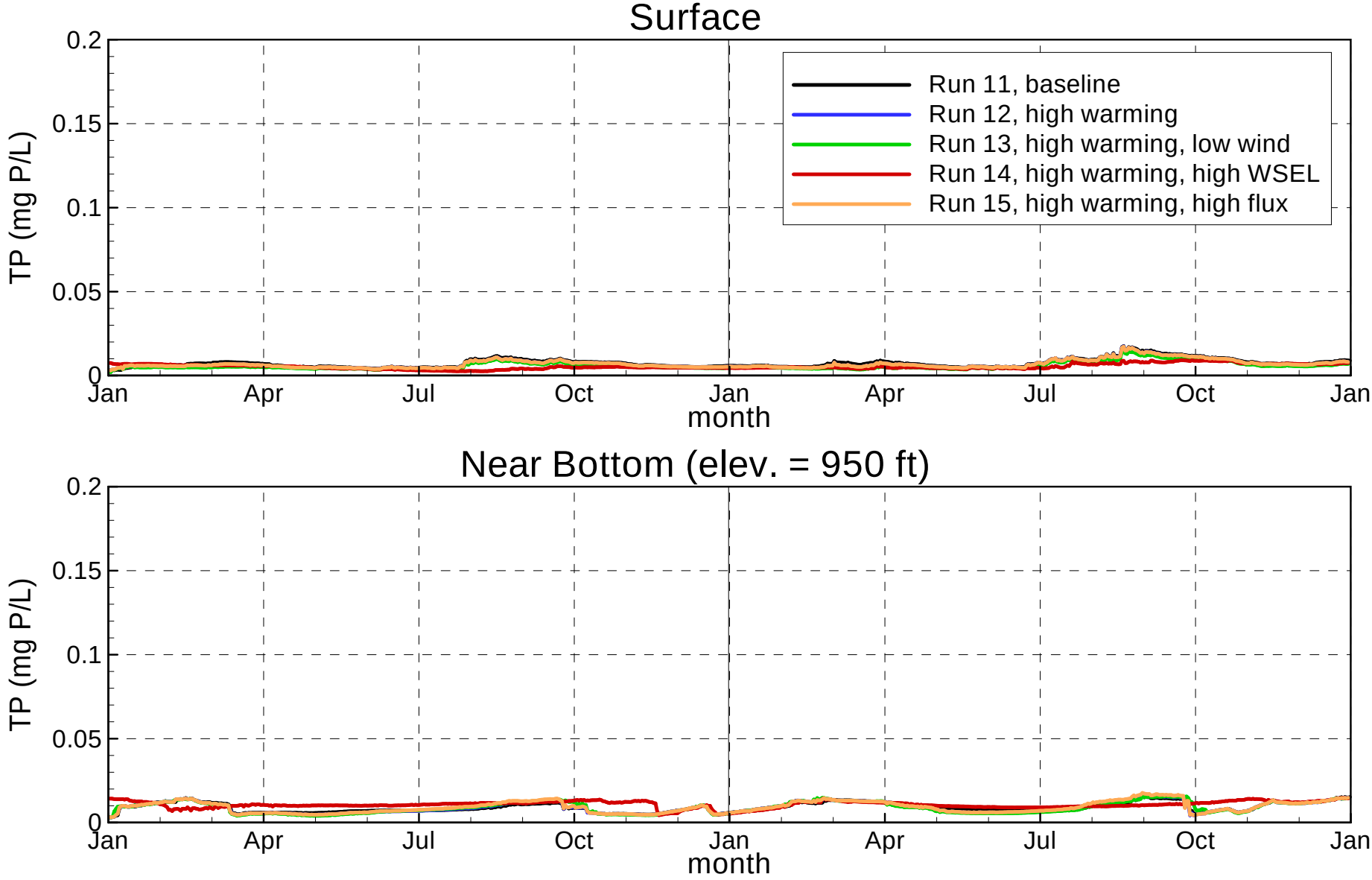

Figure A.81

FLOW SCIENCE

Total Phosphorus at Station CR390.0

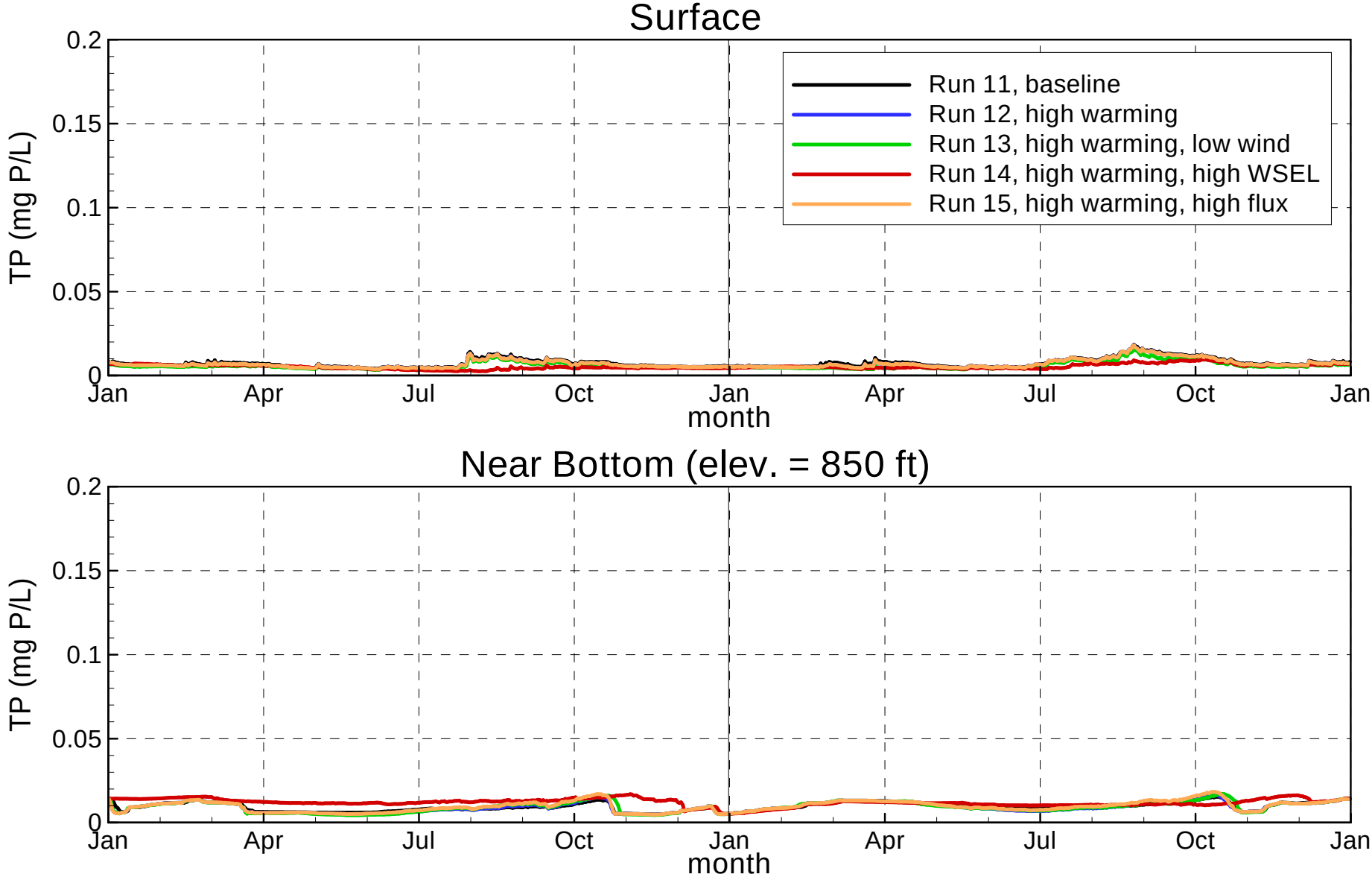

Figure A.82

FLOW SCIENCE

Total Phosphorus at Station CR380.0

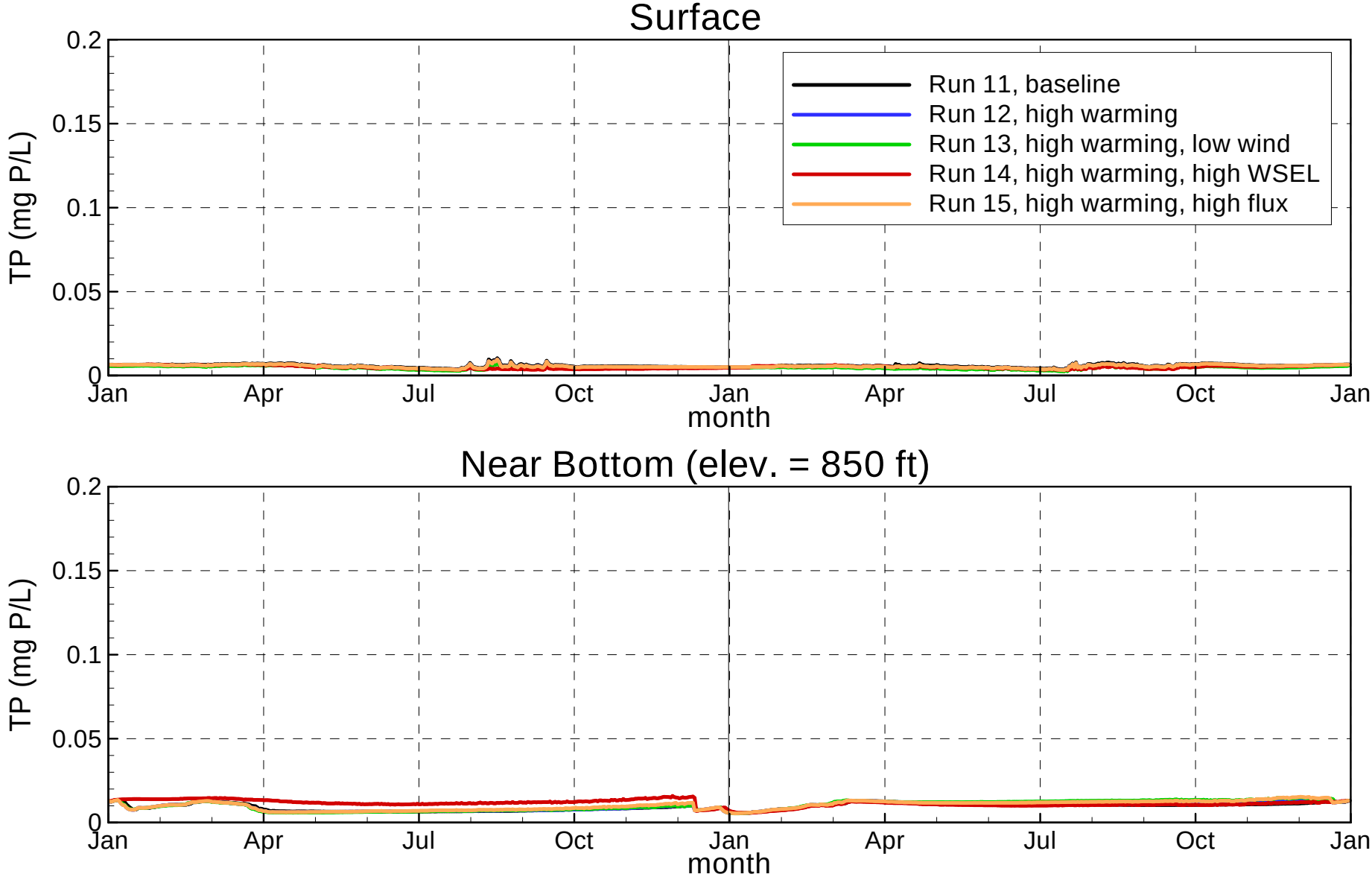

Figure A.83

Total Phosphorus at Station VR2.0

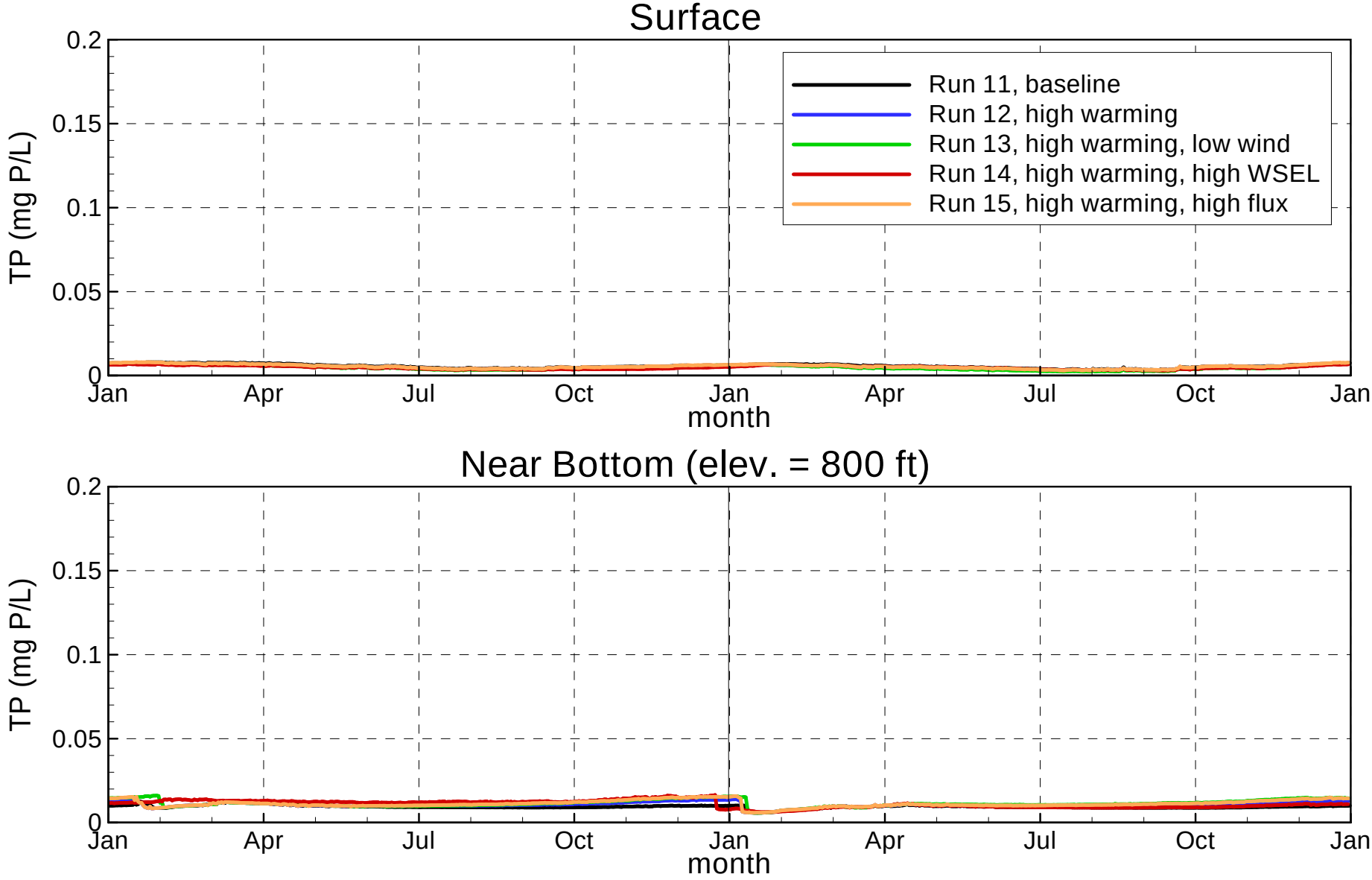

Figure A.84

Total Phosphorus at Station VR12.9

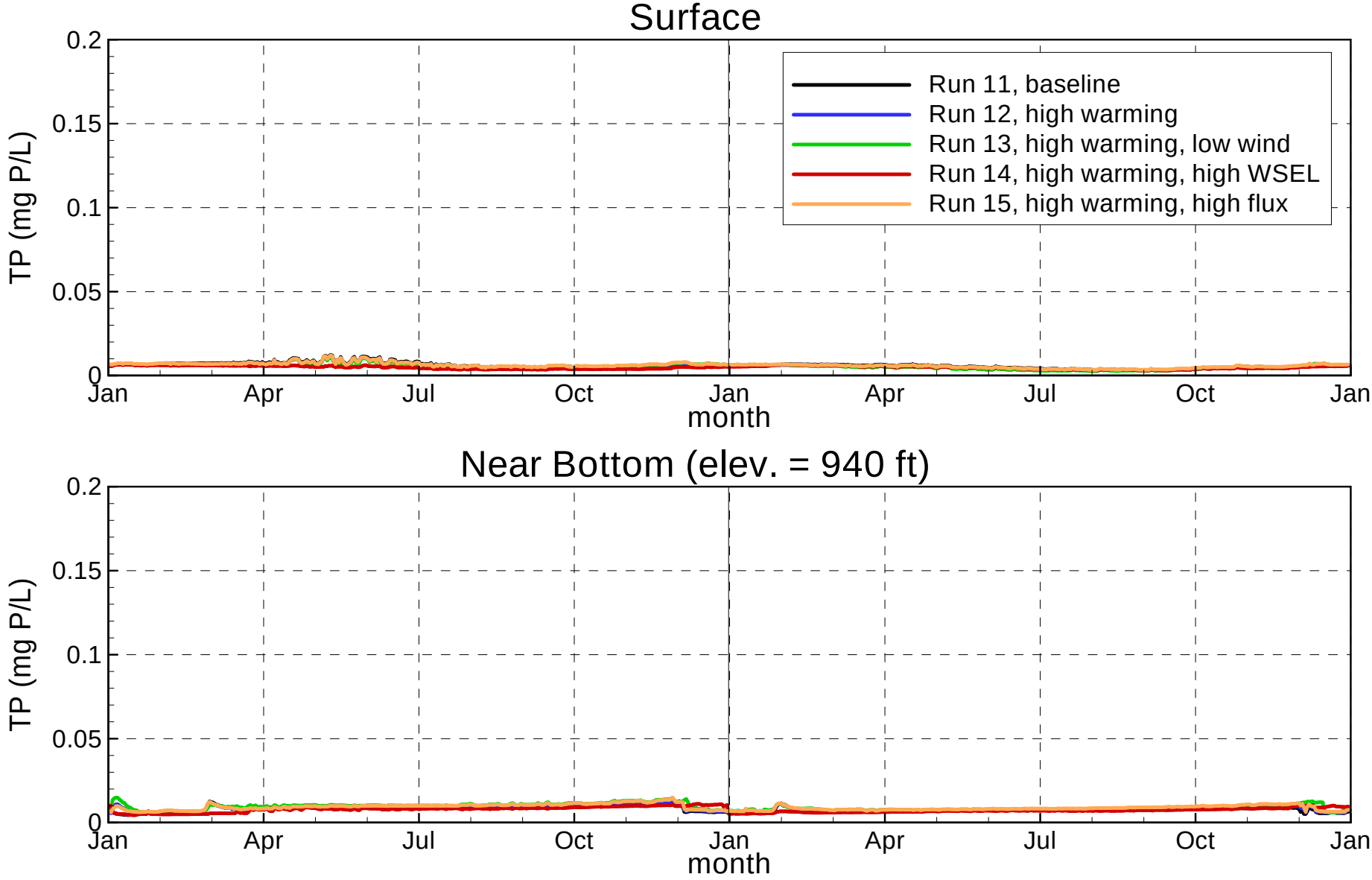

Figure A.85

FLOW SCIENCE

Total Phosphorus at Station VR18.0

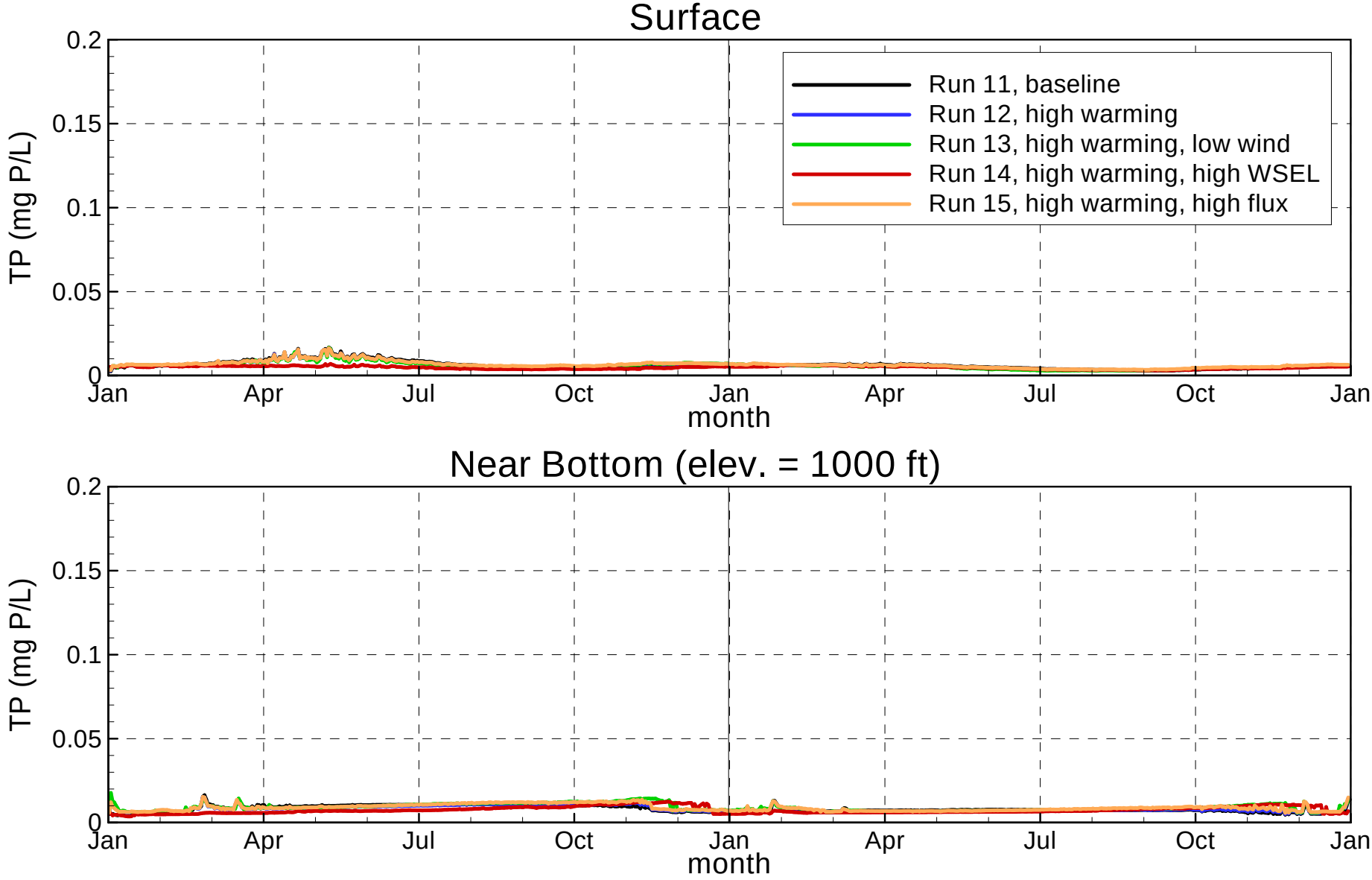

Figure A.86

FLOW SCIENCE

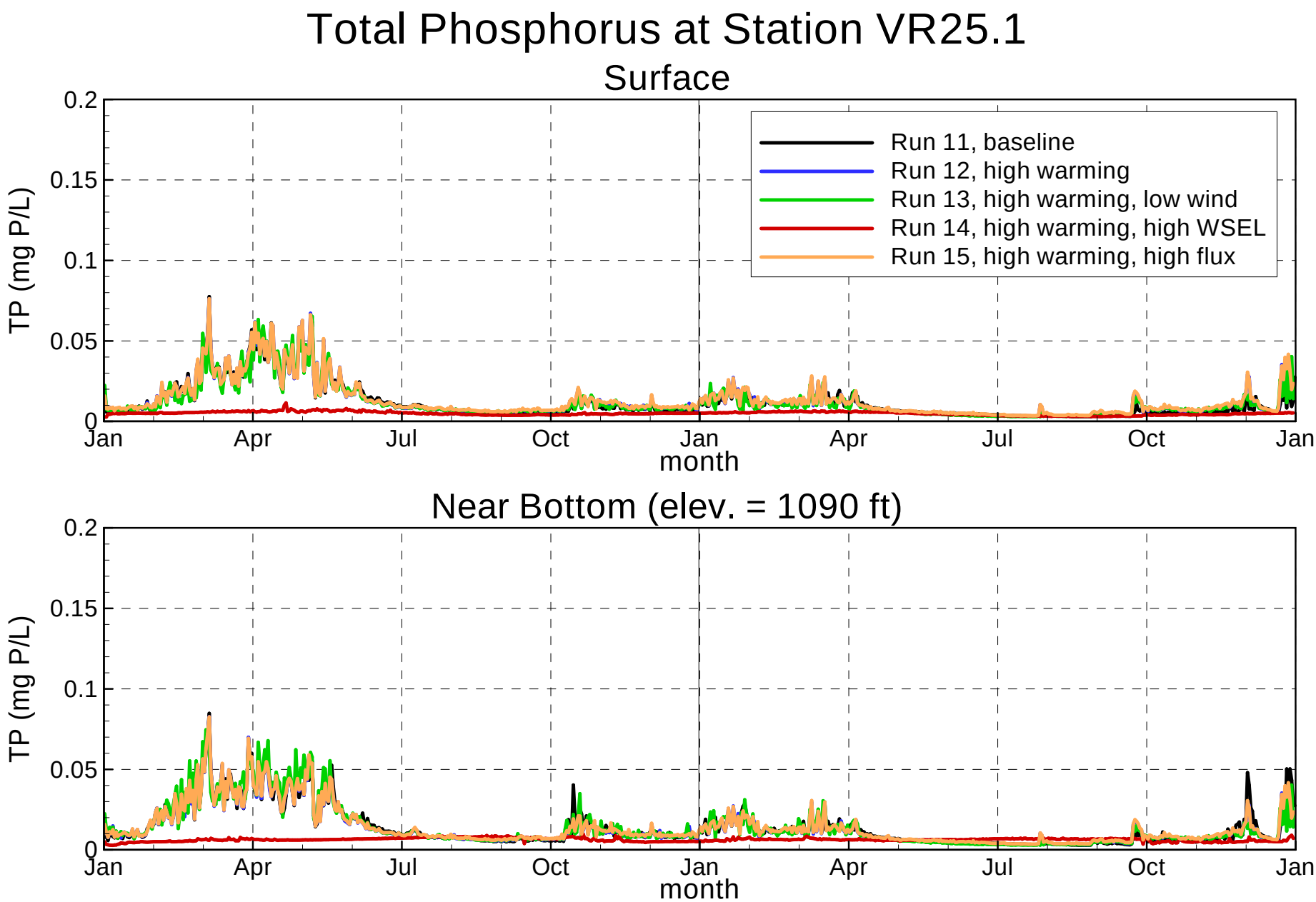
Total Phosphorus at Station VR25.1
Surface
Run 11, baseline
Run 12, high warming
Run 13, high warming, low wind
Run 14, high warming, high WSEL
Run 15, high warming, high flux
TP (mg P/L)
0.2
0.15
0.1
0.05
0
Jan
Apr
Jul
Oct
Jan
Apr
Jul
Oct
Jan
month
Near Bottom (elev. = 1090 ft)
TP (mg P/L)
0.2
0.15
0.1
0.05
0
Jan
Apr
Jul
Oct
Jan
Apr
Jul
Oct
Jan
month

Figure A.87

Total Phosphorus at Station CR360.7

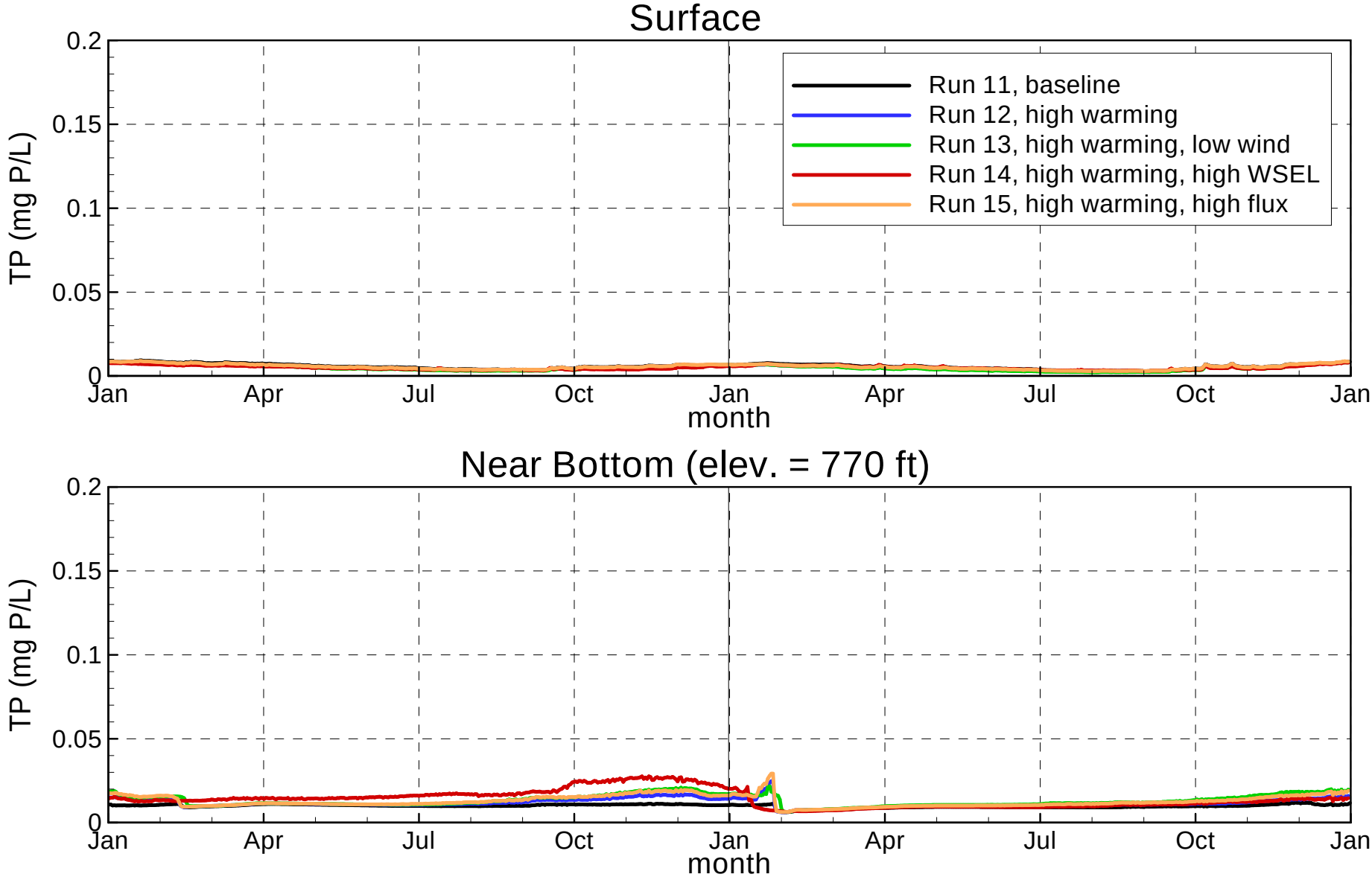

Figure A.88

FLOW SCIENCE

Total Phosphorus at Station CR346.4

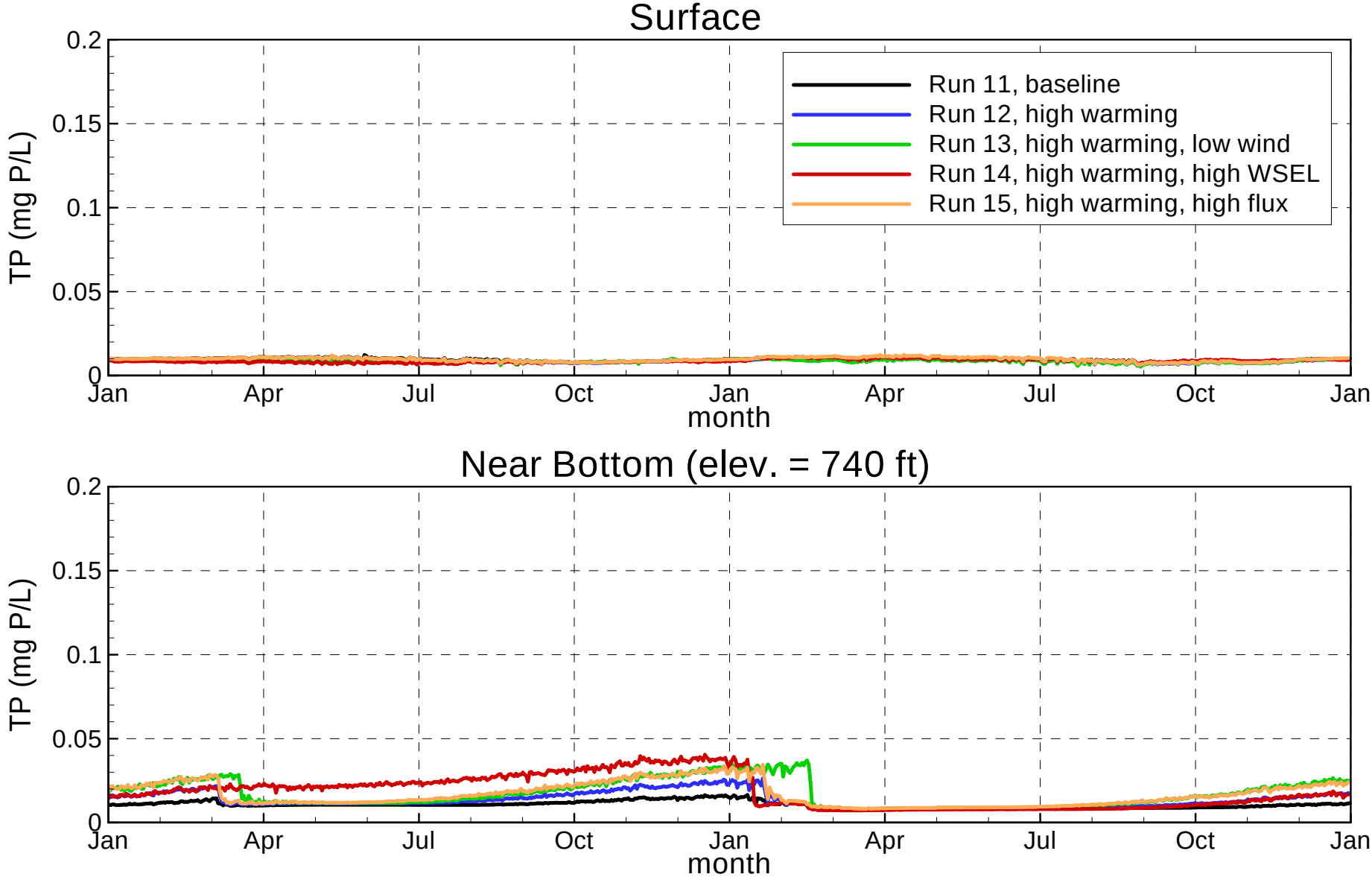

Figure A.89

FLOW SCIENCE

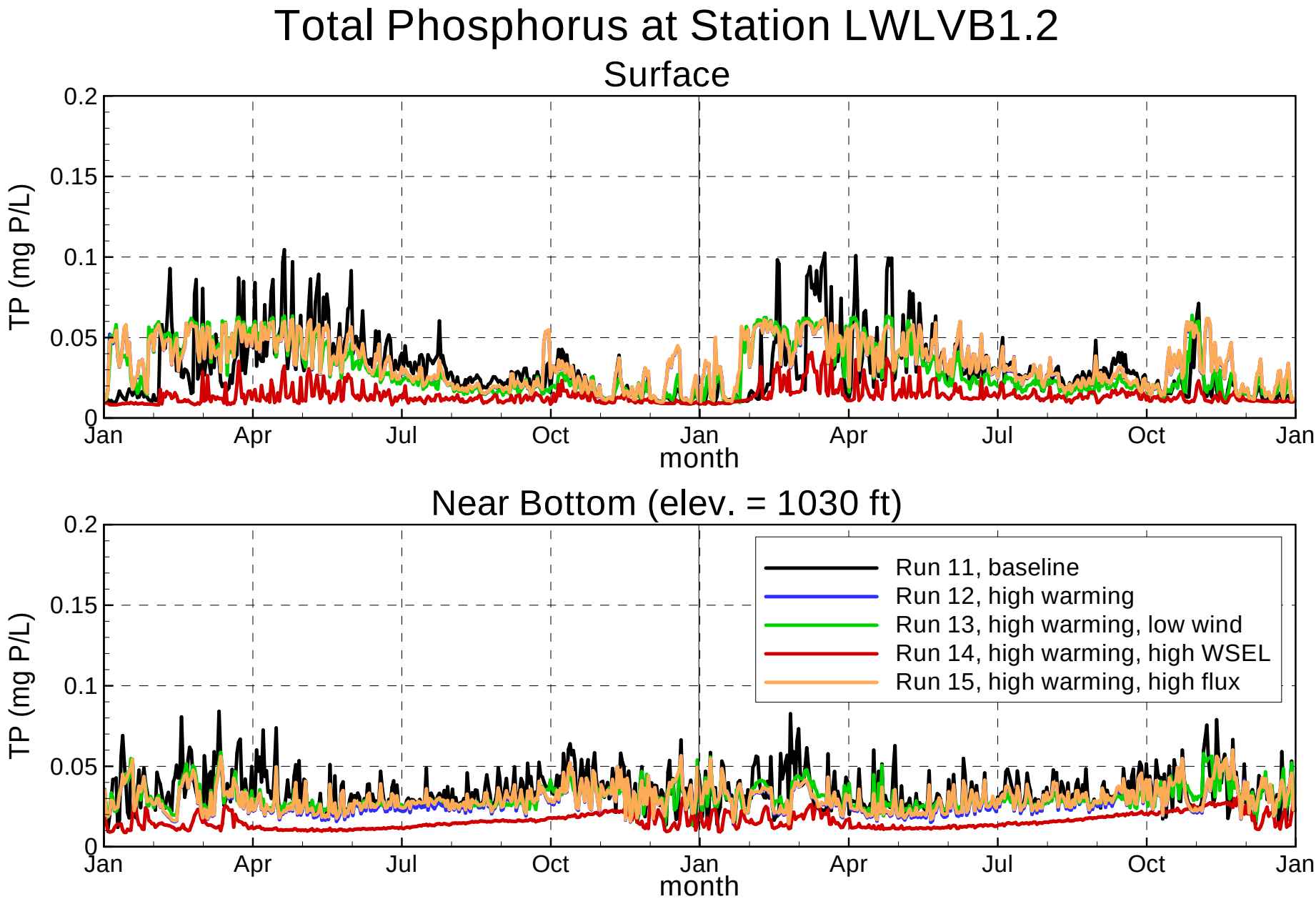
Total Phosphorus at Station LWLVB1.2
Surface
TP (mg P/L)
0.2
0.15
0.1
0.05
0
Jan
Apr
Jul
Oct
Jan
Apr
Jul
Oct
Jan
month
Near Bottom (elev. = 1030 ft)
Run 11, baseline
Run 12, high warming
Run 13, high warming, low wind
Run 14, high warming, high WSEL
Run 15, high warming, high flux

Figure A.90

Total Phosphorus at Station LWLVB1.85

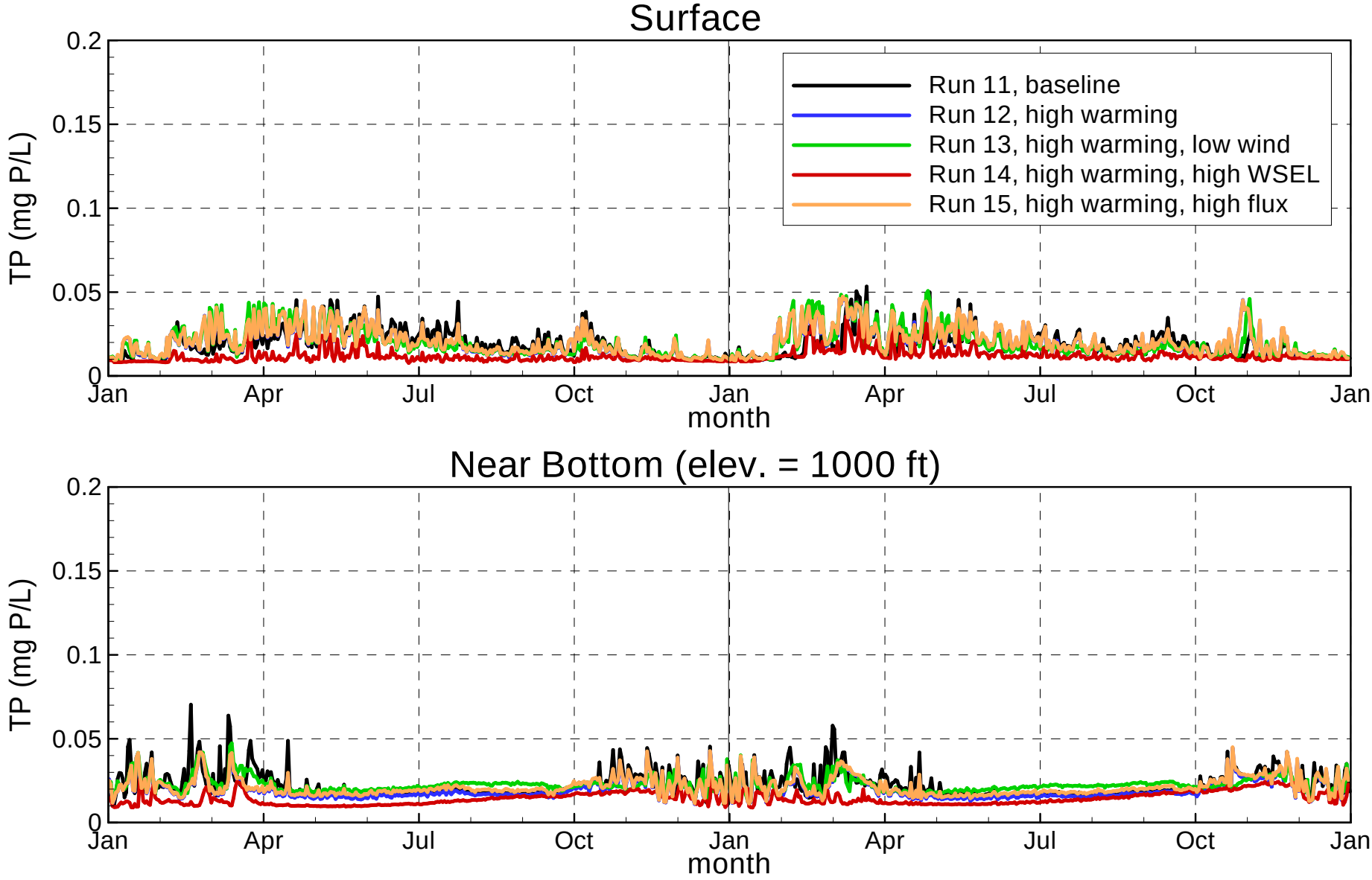

Figure A.91

Total Phosphorus at Station LWLVB2.7

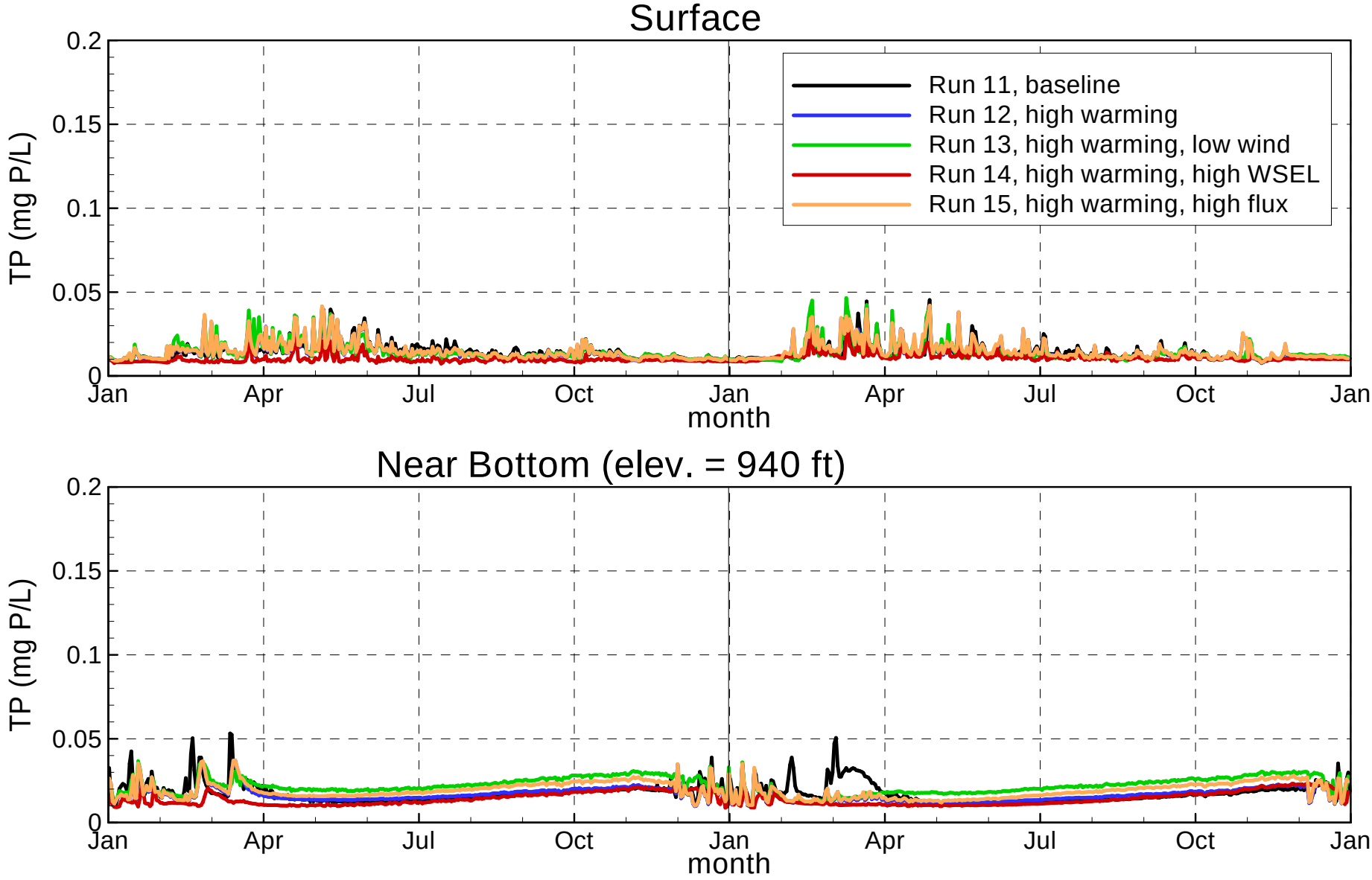

Figure A.92

Total Phosphorus at Station LWLVB3.5

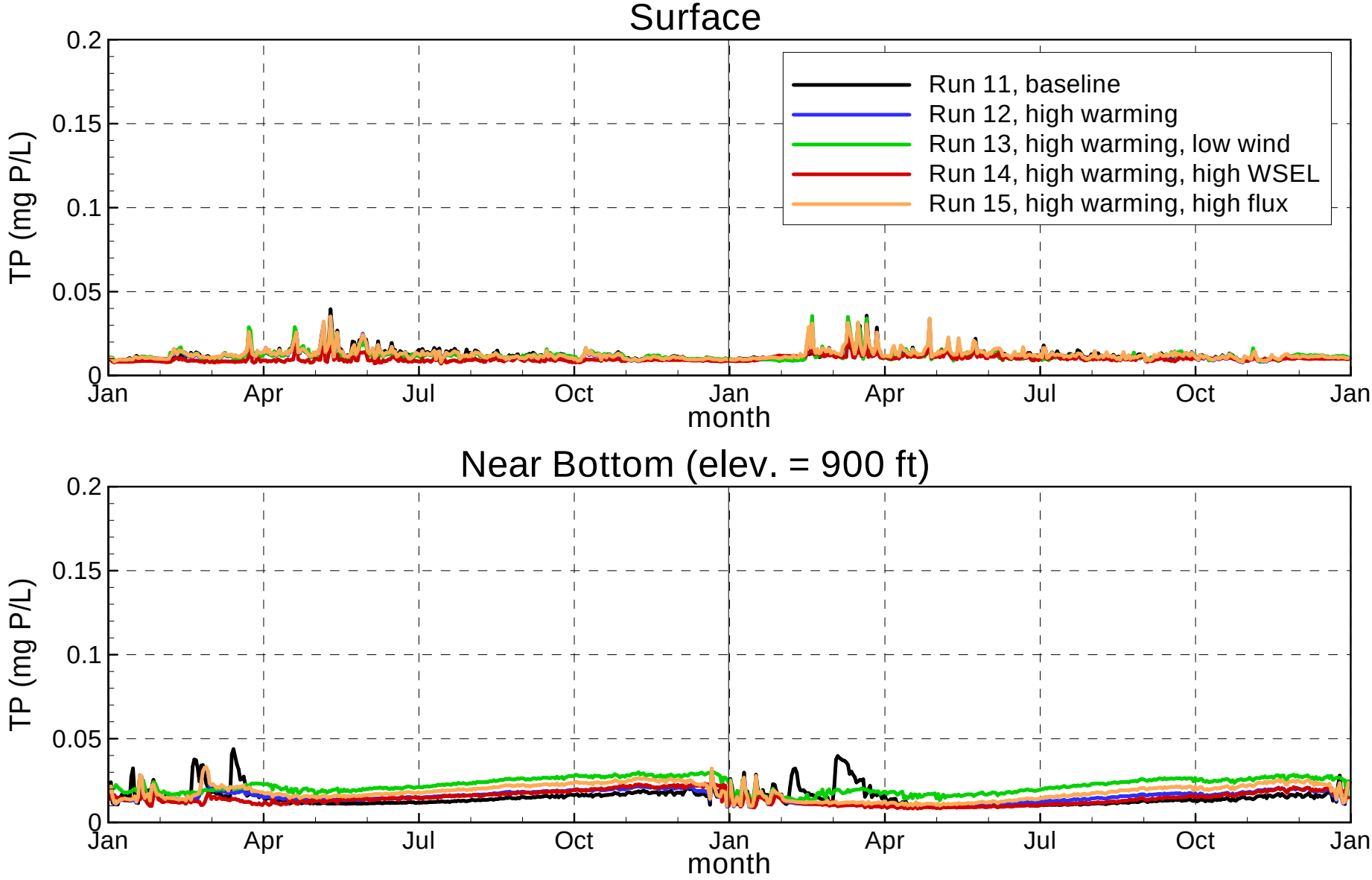

Figure A.93

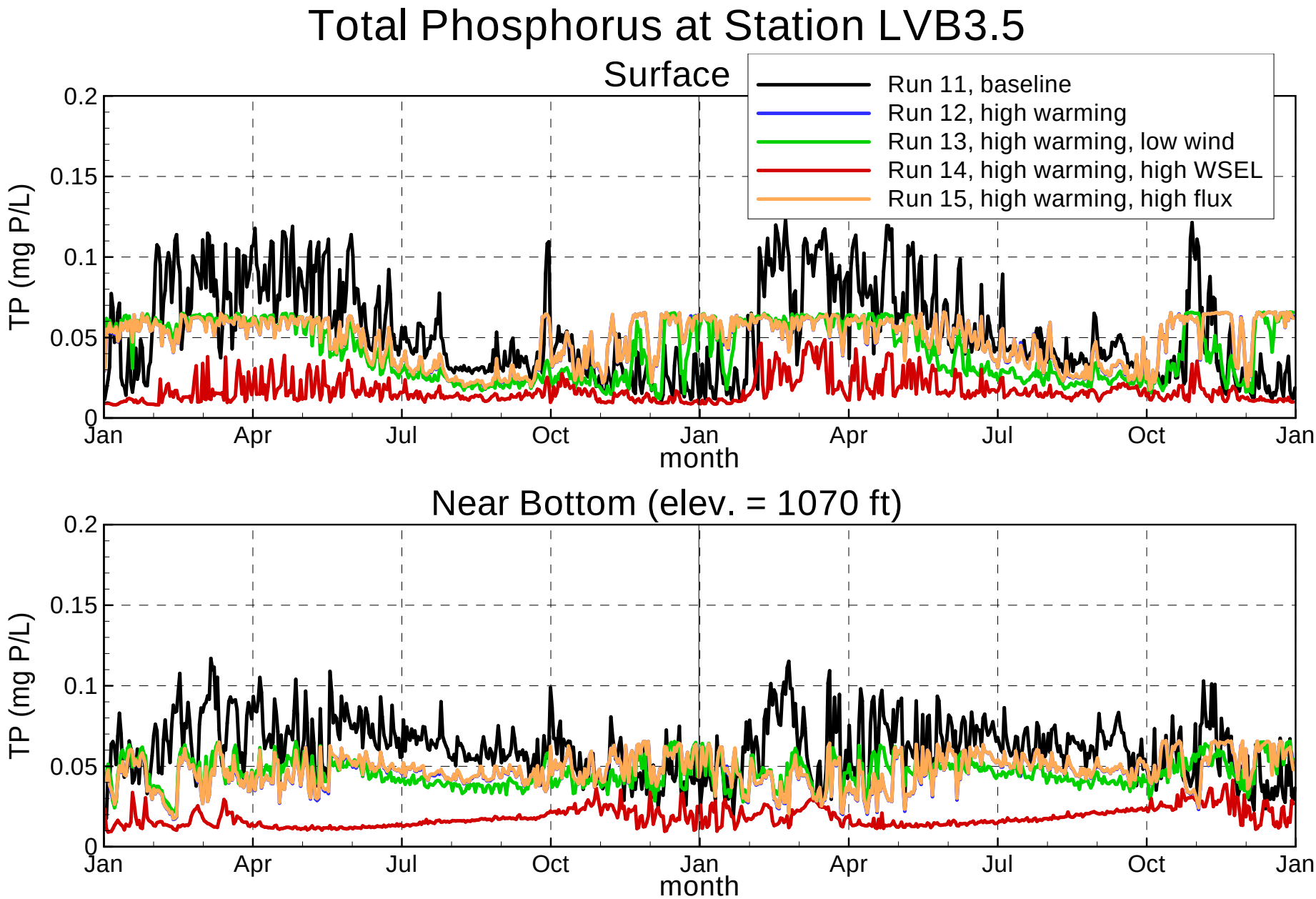
Total Phosphorus at Station LVB3.5
Surface
Run 11, baseline
Run 12, high warming
Run 13, high warming, low wind
Run 14, high warming, high WSEL
Run 15, high warming, high flux
TP (mg P/L)
0.2
0.15
0.1
0.05
0
Jan
Apr
Jul
Oct
Jan
Apr
Jul
Oct
Jan
month
Near Bottom (elev. = 1070 ft)
TP (mg P/L)
0.2
0.15
0.1
0.05
0
Jan
Apr
Jul
Oct
Jan
Apr
Jul
Oct
Jan
month

Figure A.94

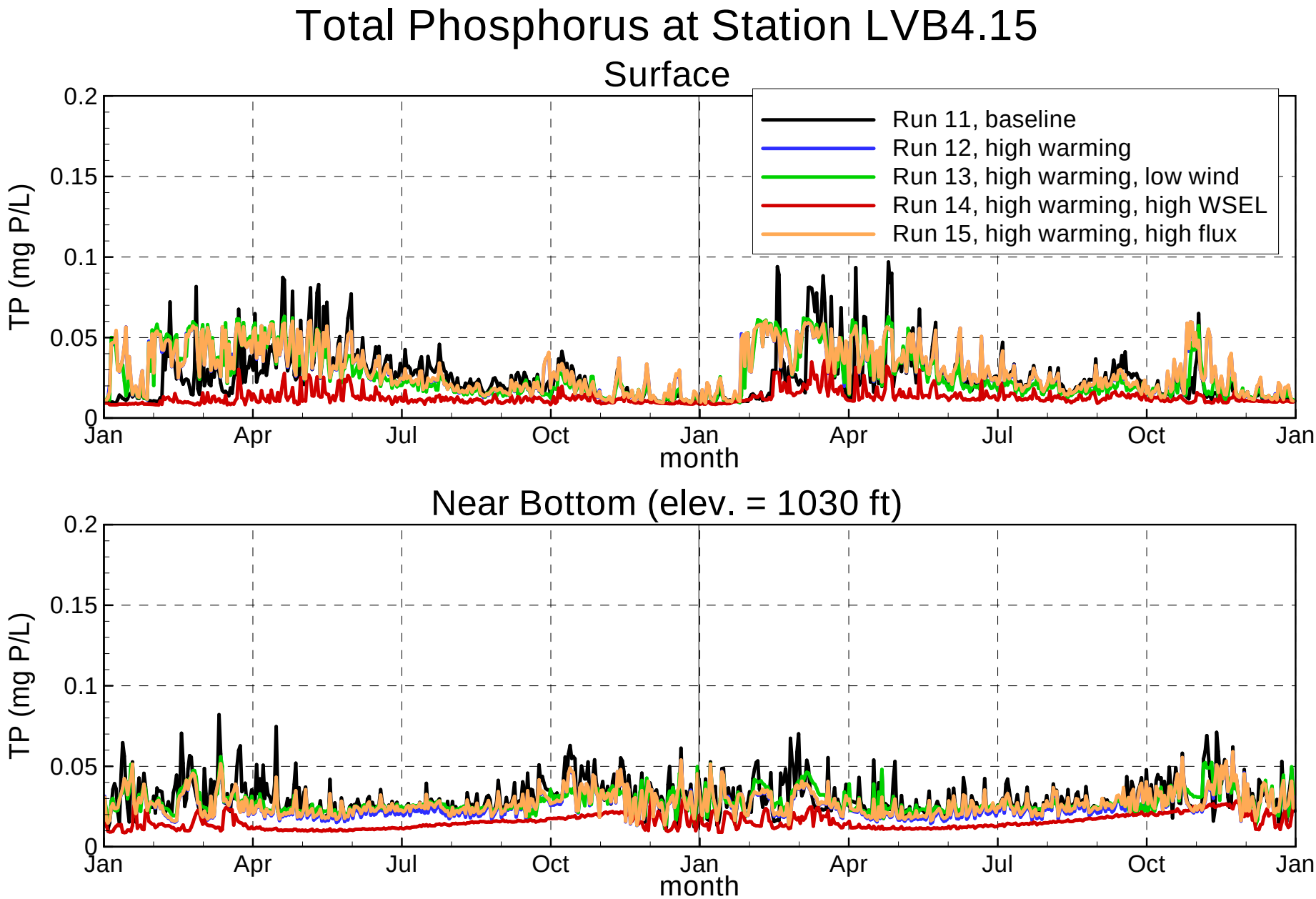
Total Phosphorus at Station LVB4.15
Surface
Run 11, baseline
Run 12, high warming
Run 13, high warming, low wind
Run 14, high warming, high WSEL
Run 15, high warming, high flux
TP (mg P/L)
0.2
0.15
0.1
0.05
0
Jan
Apr
Jul
Oct
Jan
Apr
Jul
Oct
Jan
month
Near Bottom (elev. = 1030 ft)
TP (mg P/L)
0.2
0.15
0.1
0.05
0
Jan
Apr
Jul
Oct
Jan
Apr
Jul
Oct
Jan
month

Figure A.95

Total Phosphorus at Station LVB4.95

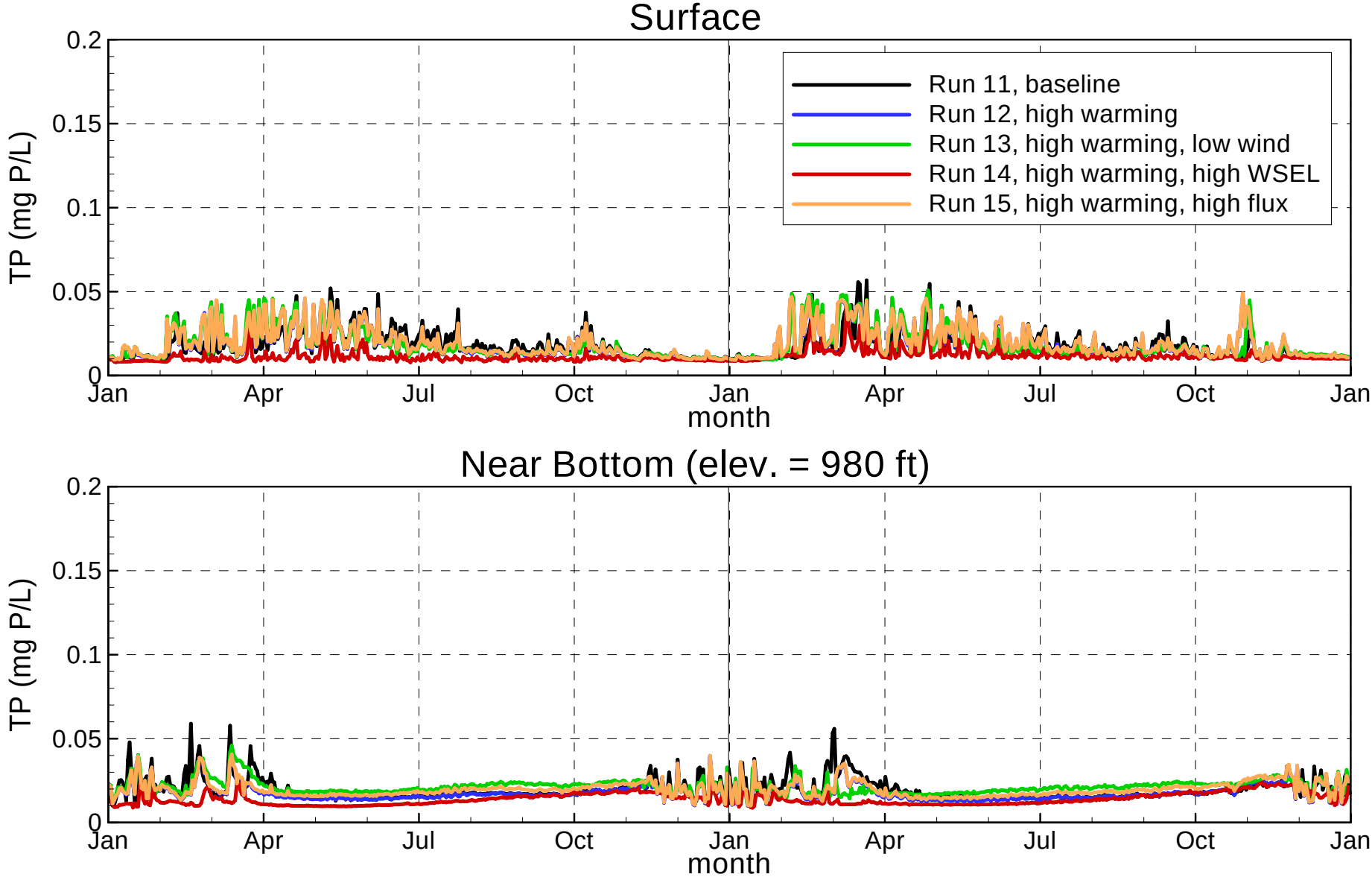

Figure A.96

Total Phosphorus at Station LVB6.7

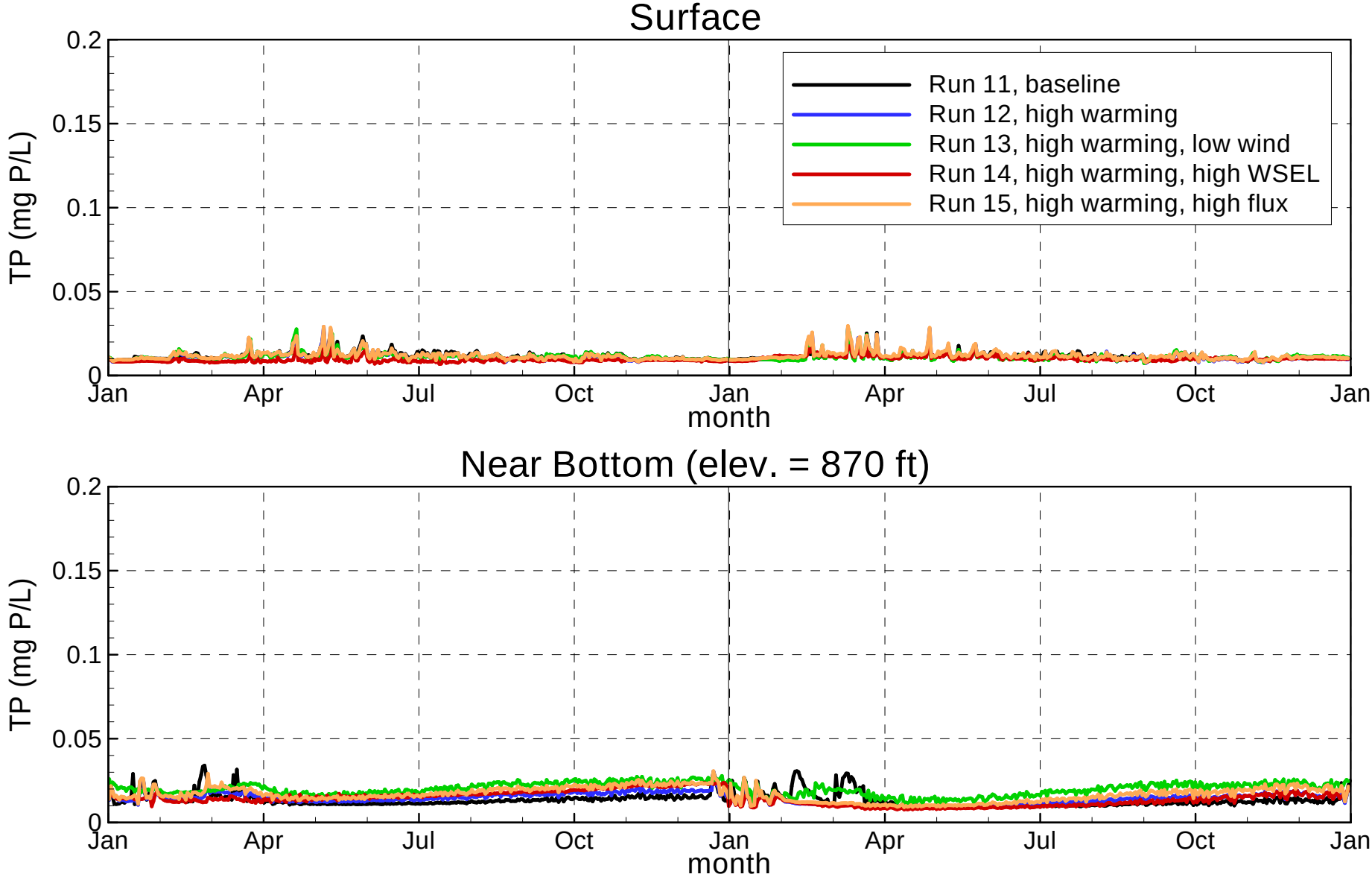

Figure A.97

FLOW SCIENCE

Total Phosphorus at Station LVB7.3

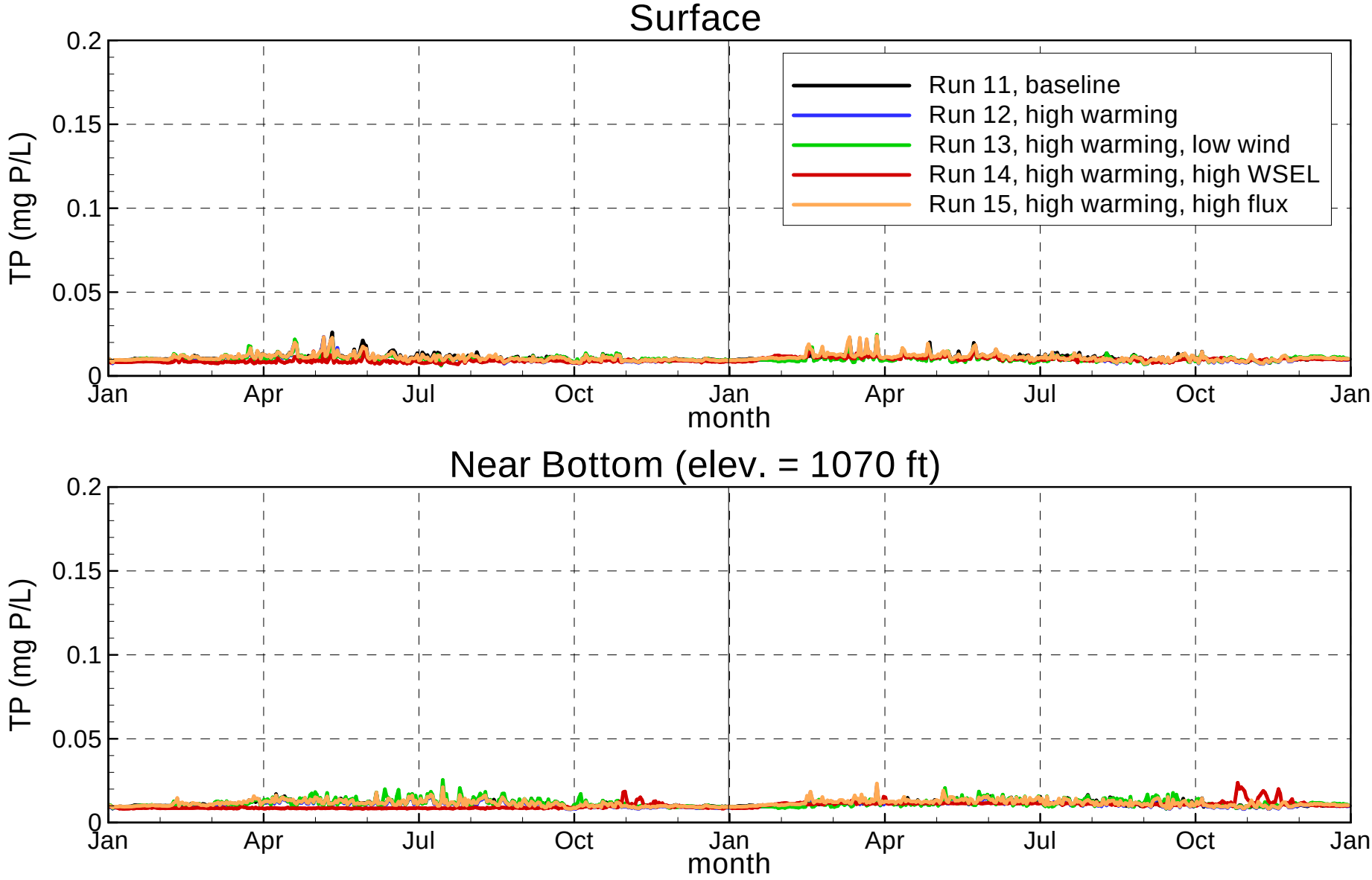

Figure A.98

Total Phosphorus at SNWA Intake #3

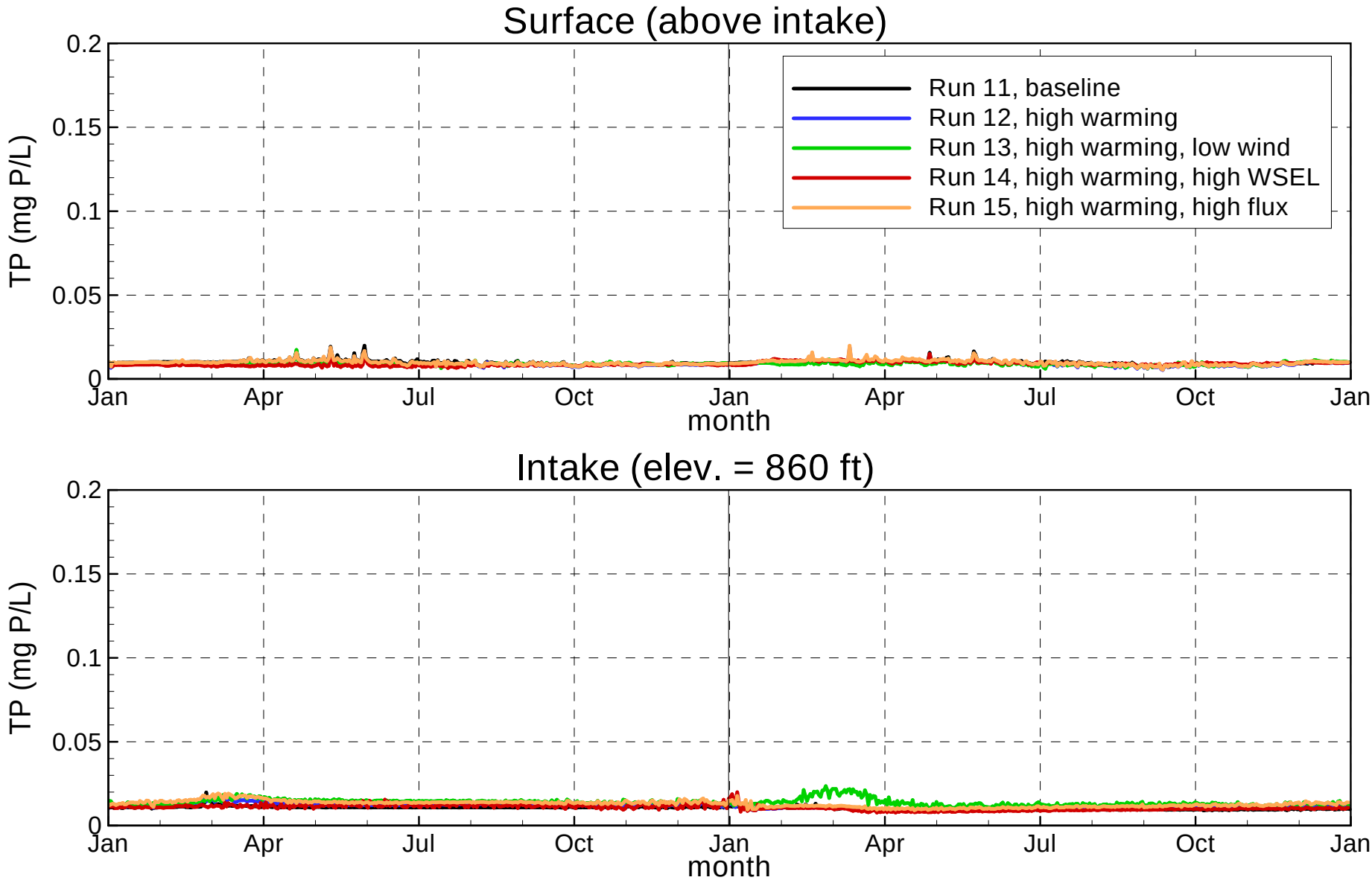

Figure A.99

FLOW SCIENCE

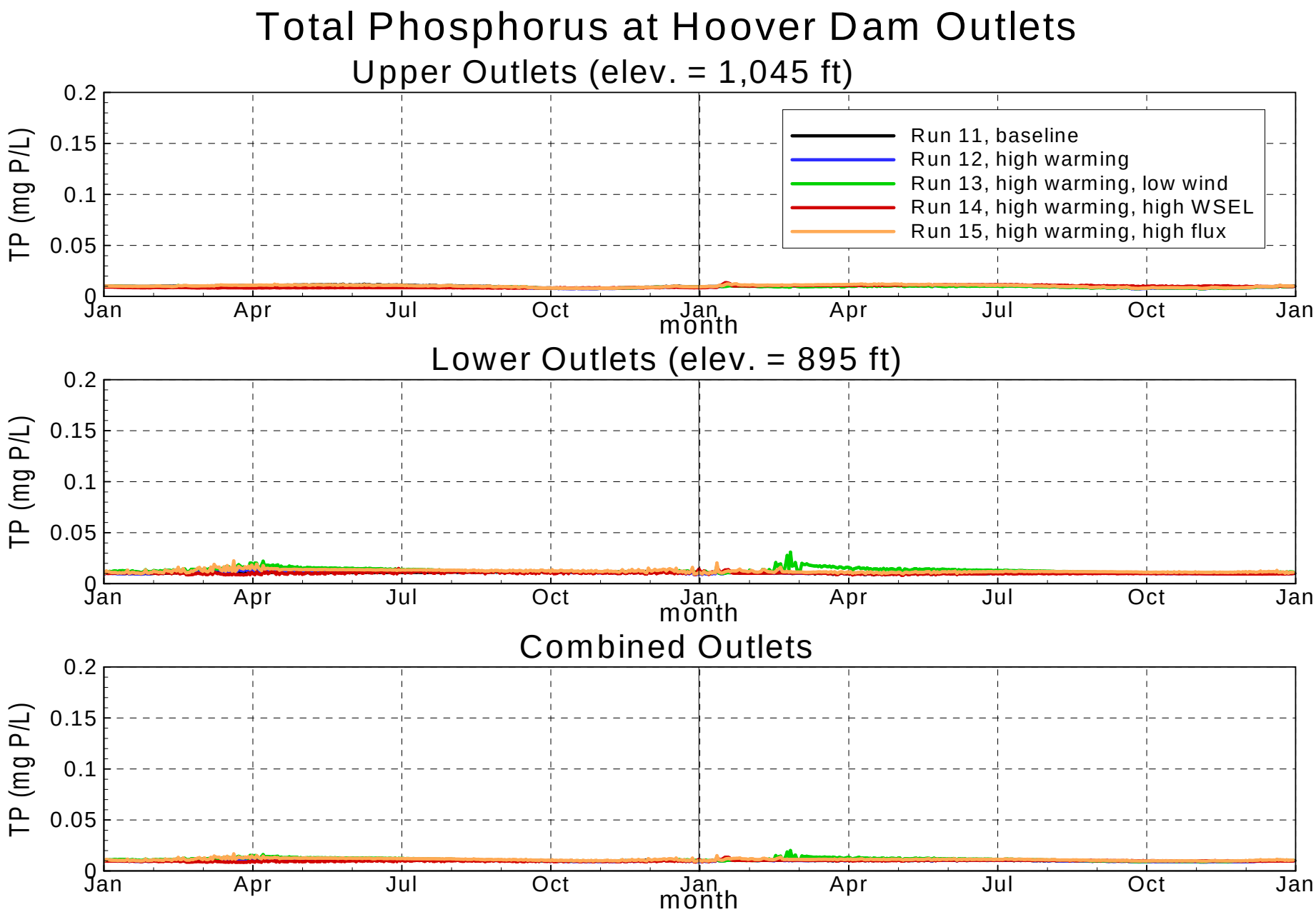

Figure A.100

FLOW SCIENCE

Chlorophyll a at Station CR394.0

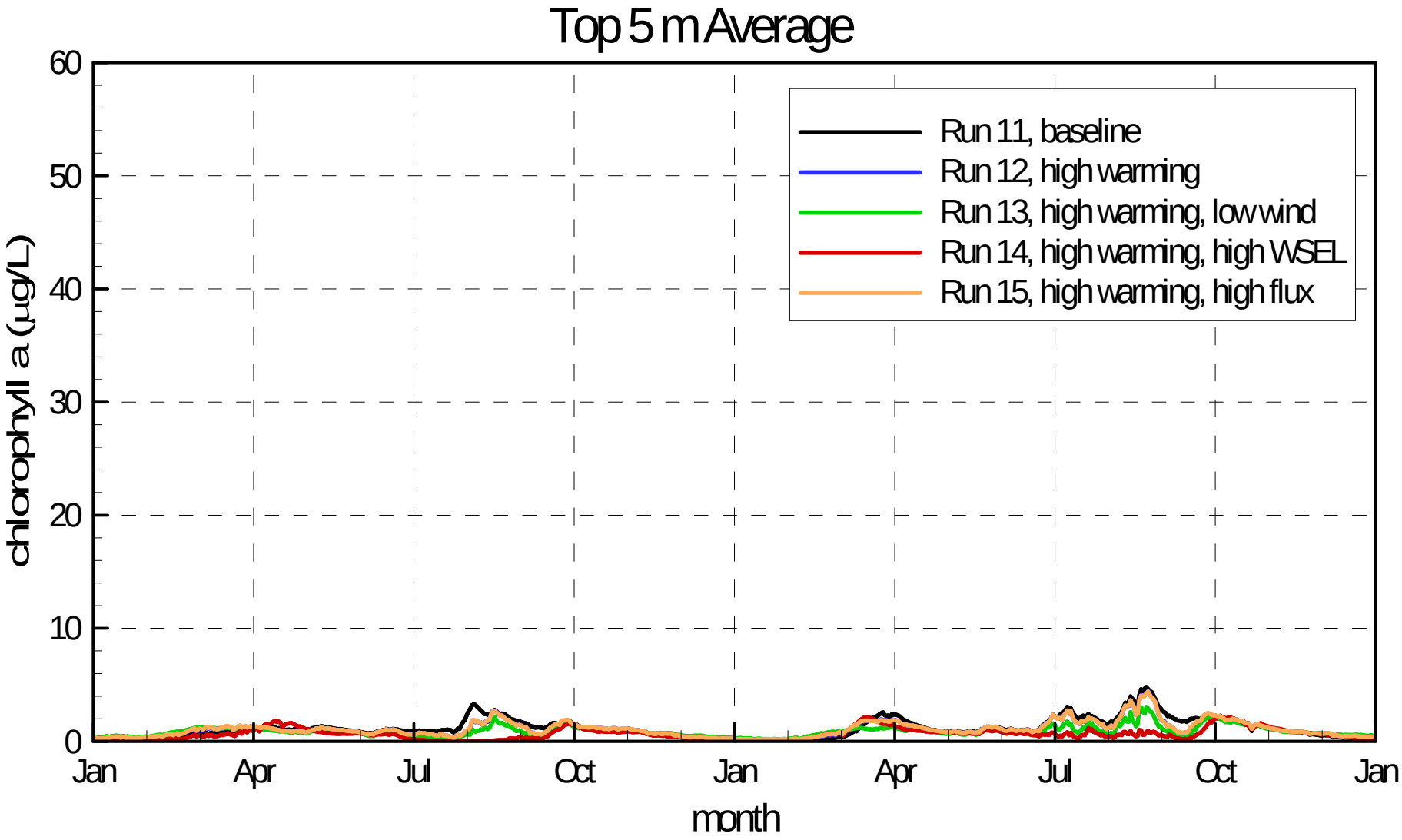

Figure A.101

Chlorophyll a at Station CR390.0

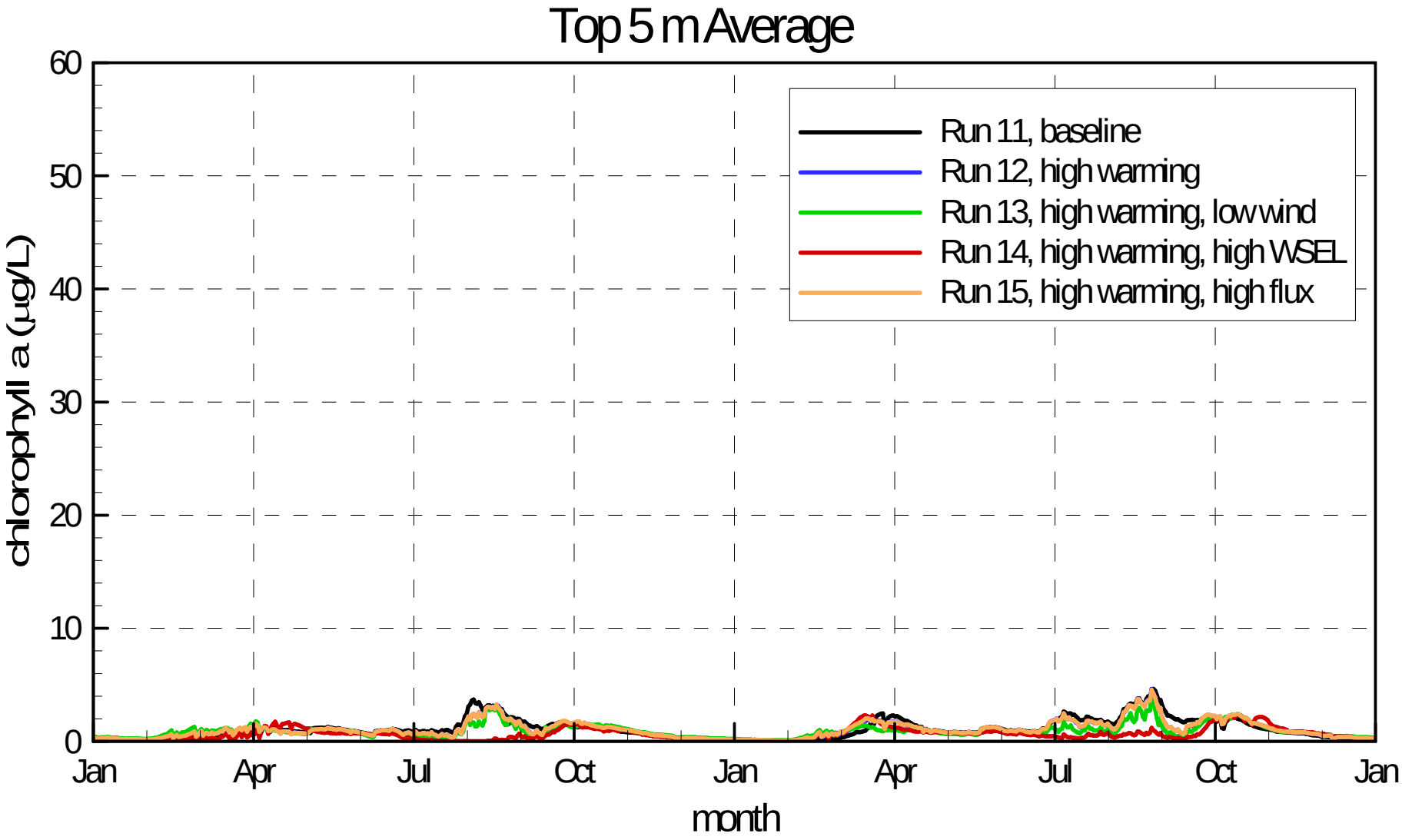

Figure A.102

Chlorophyll a at Station CR380.0

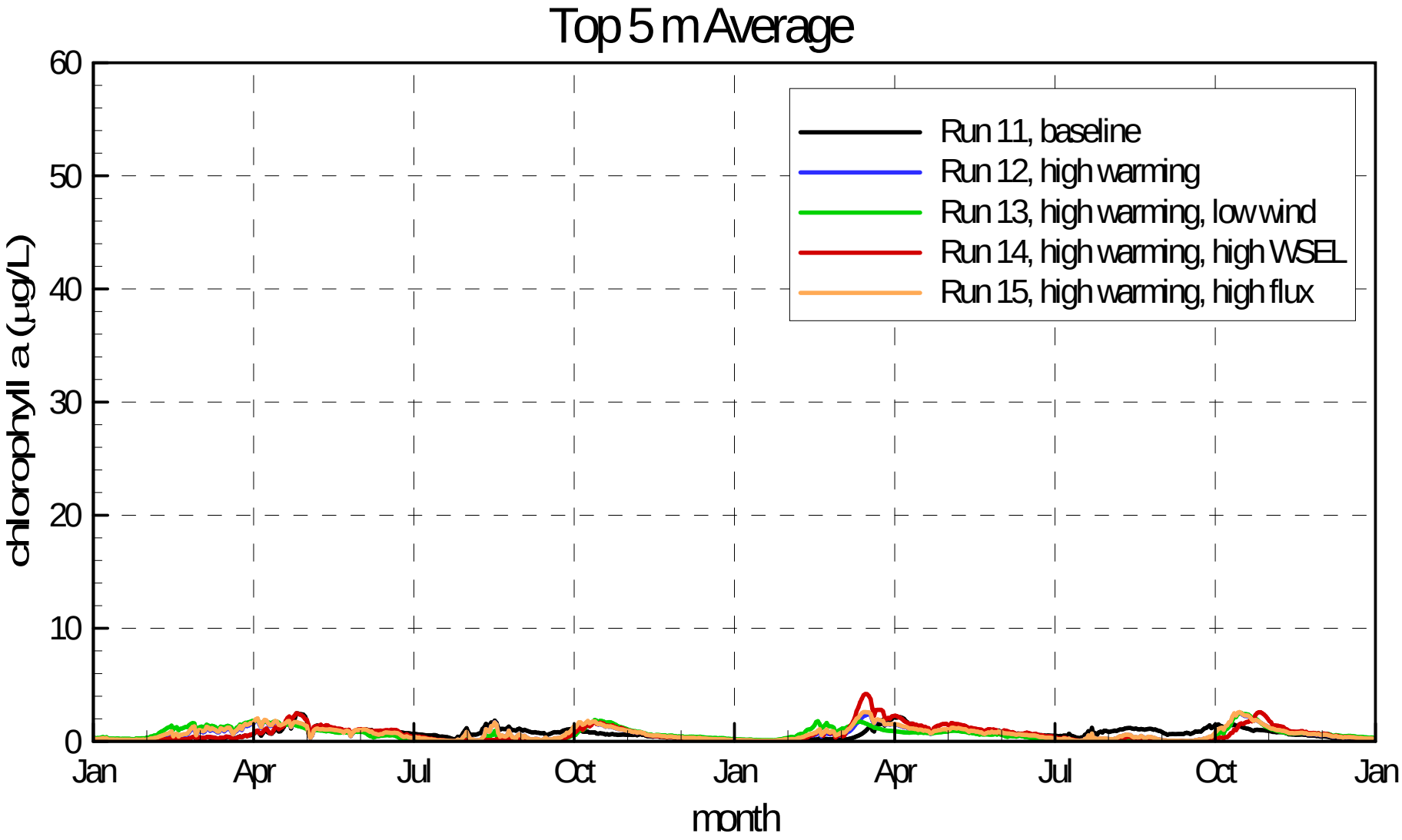

Figure A.103

Chlorophyll a at Station VR2.0

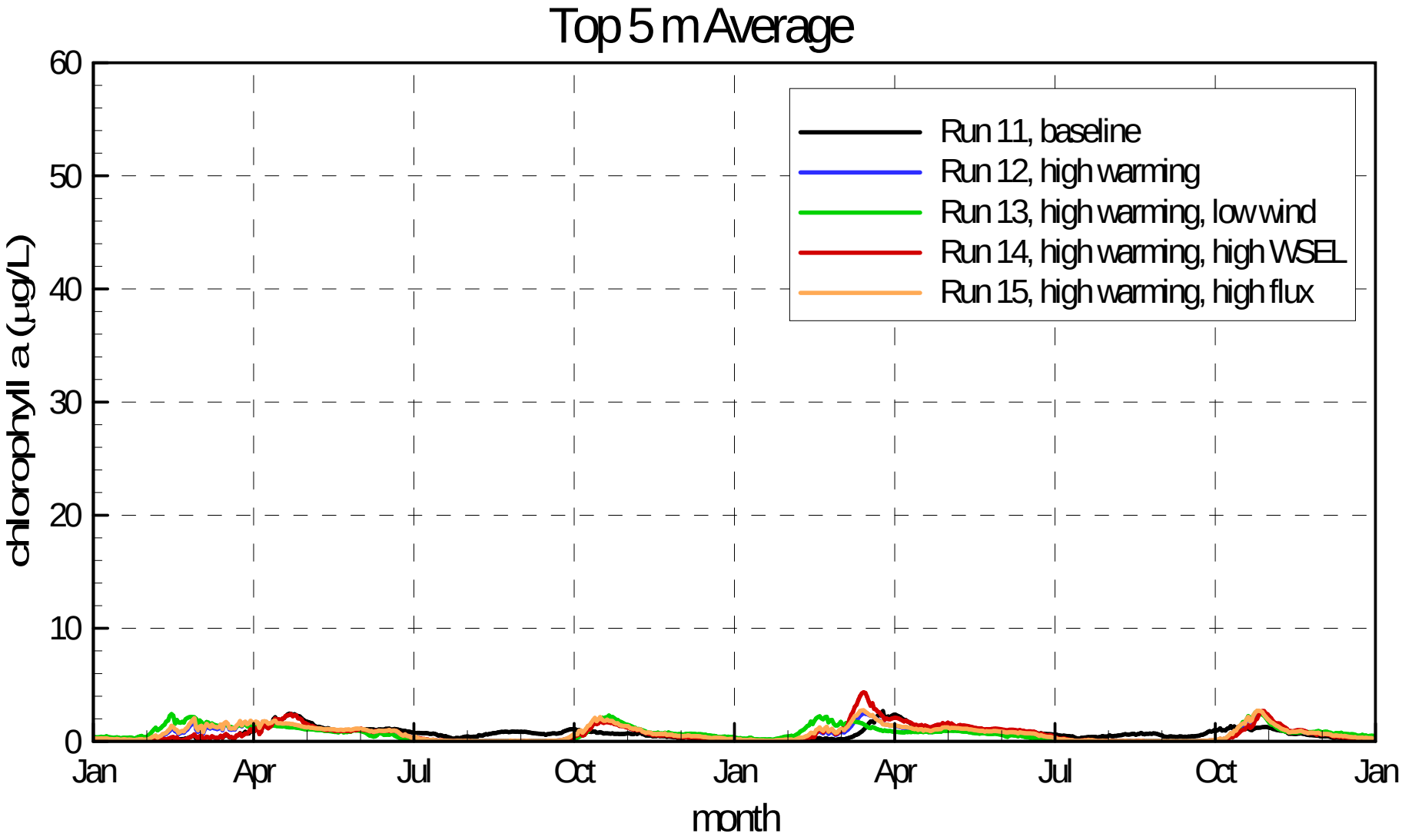

Figure A.104

Chlorophyll a at Station VR12.9

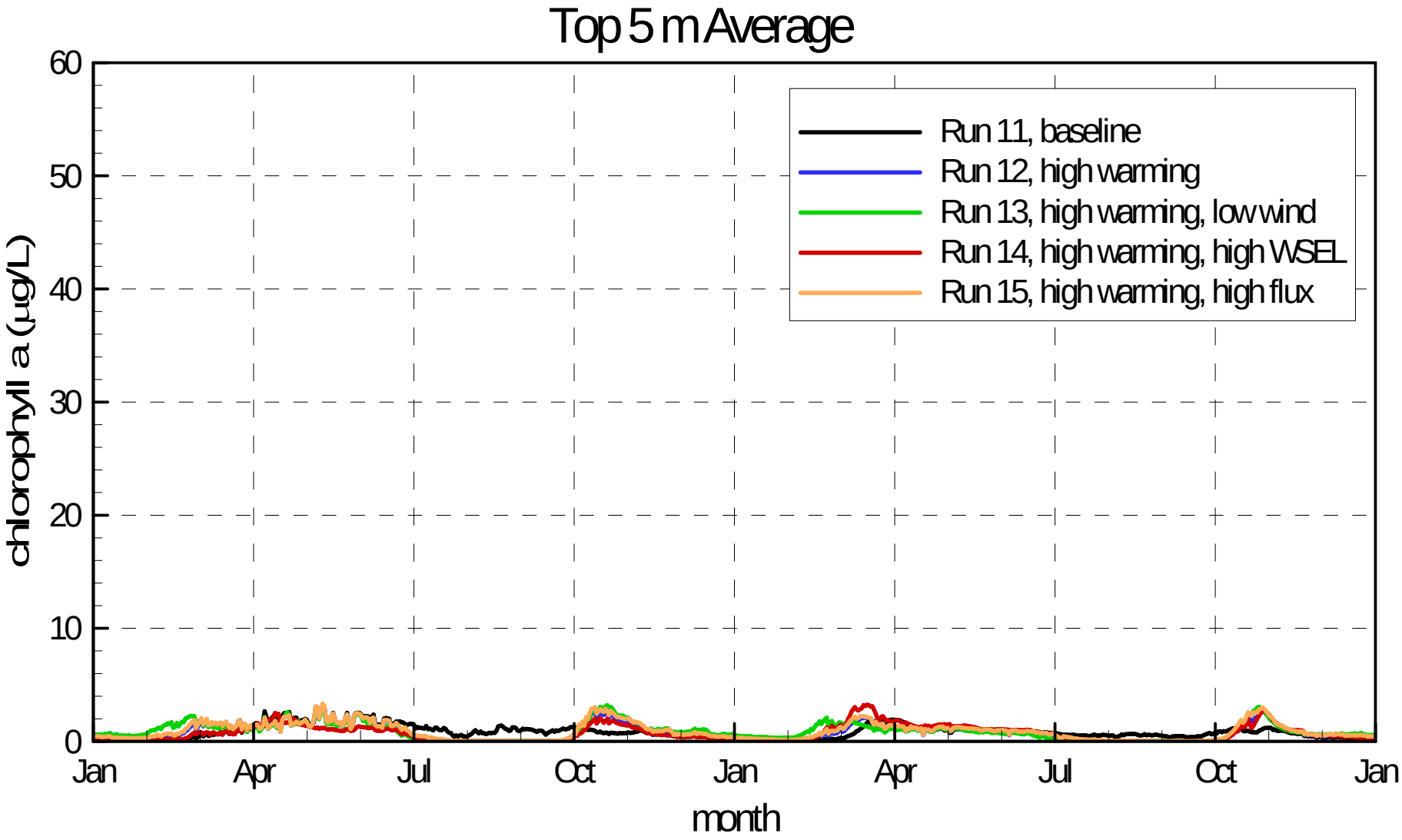

Figure A.105

Chlorophyll a at Station VR18.0

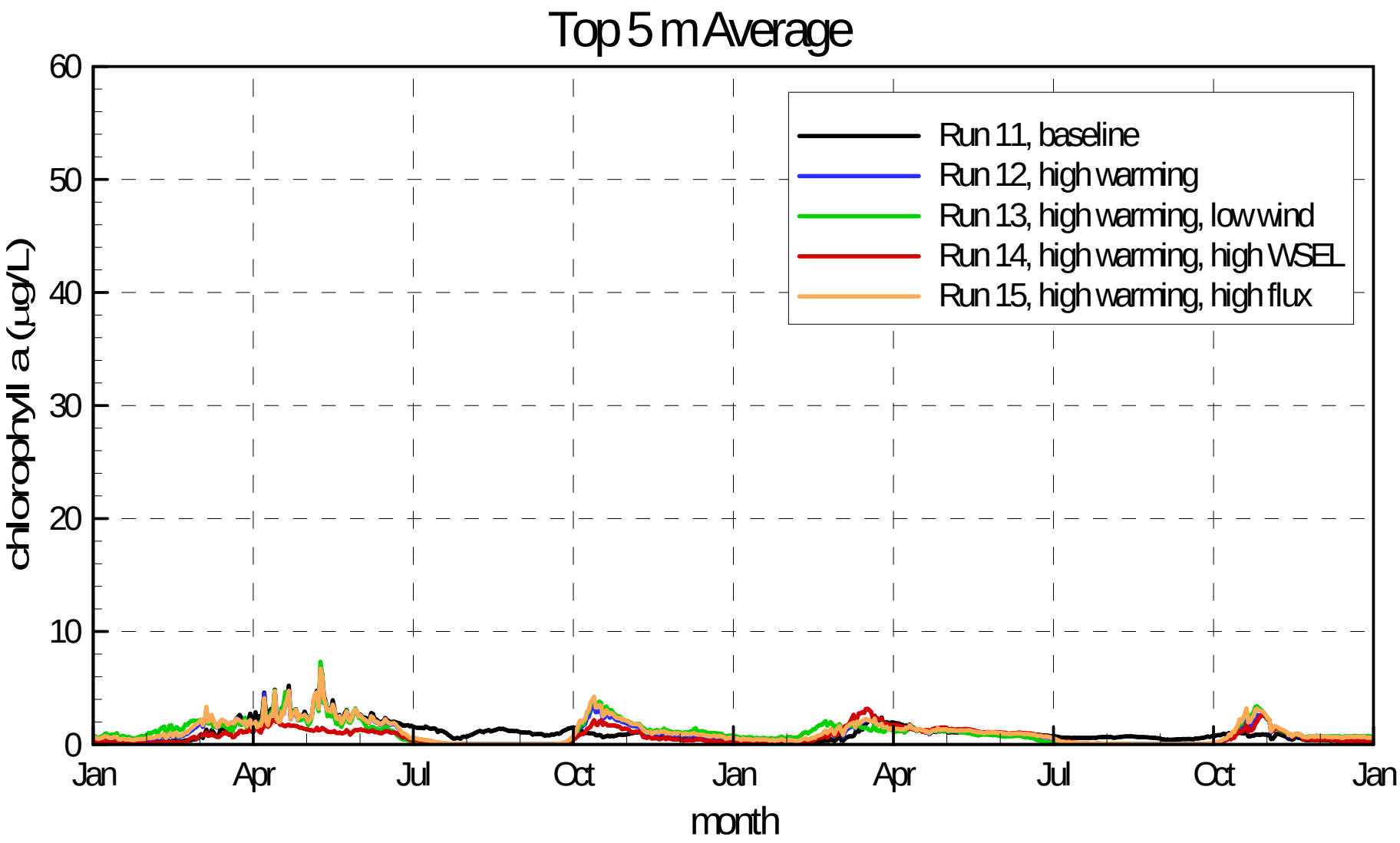

Figure A.106

Chlorophyll a at Station VR25.1

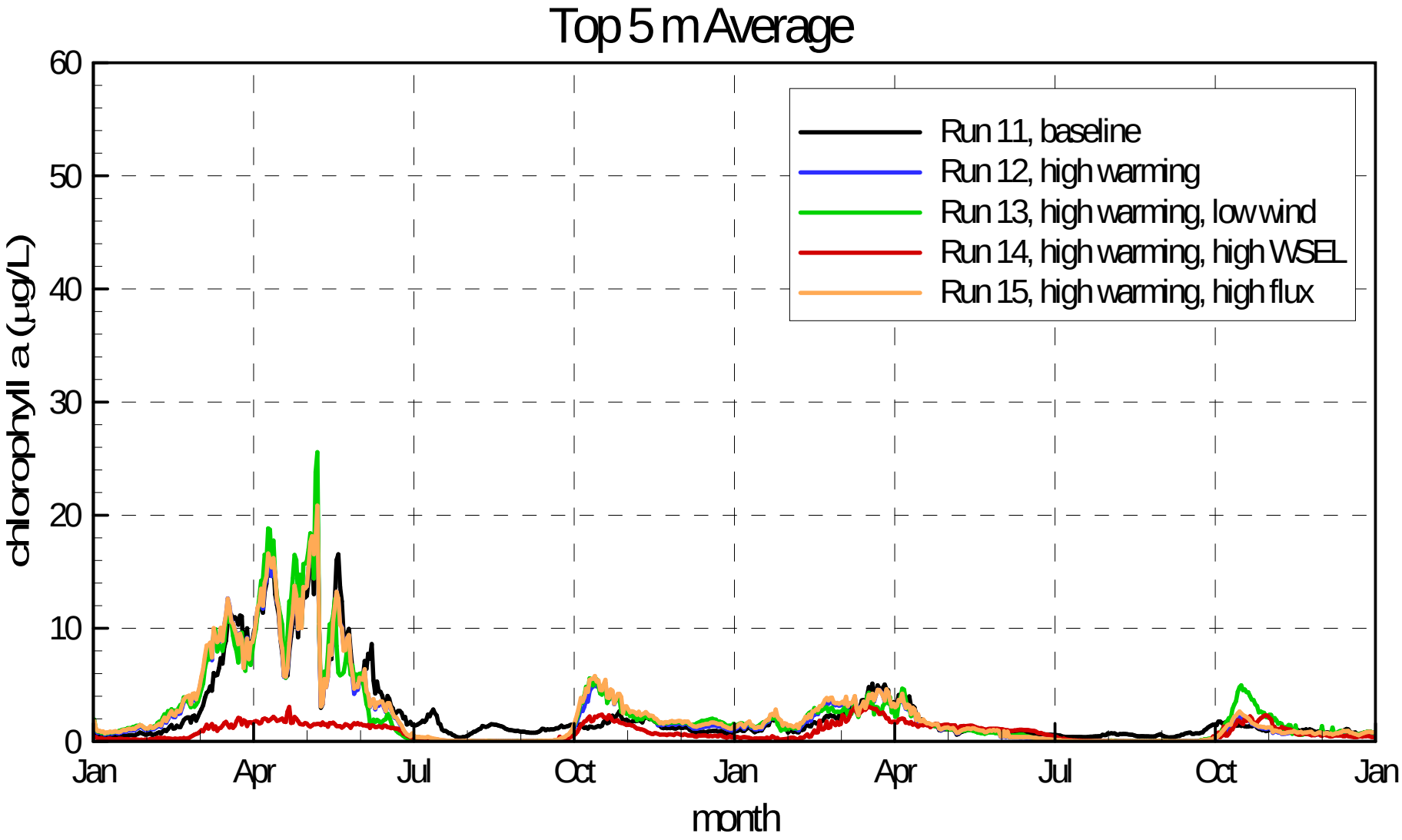

Figure A.107

Chlorophyll a at Station CR360.7

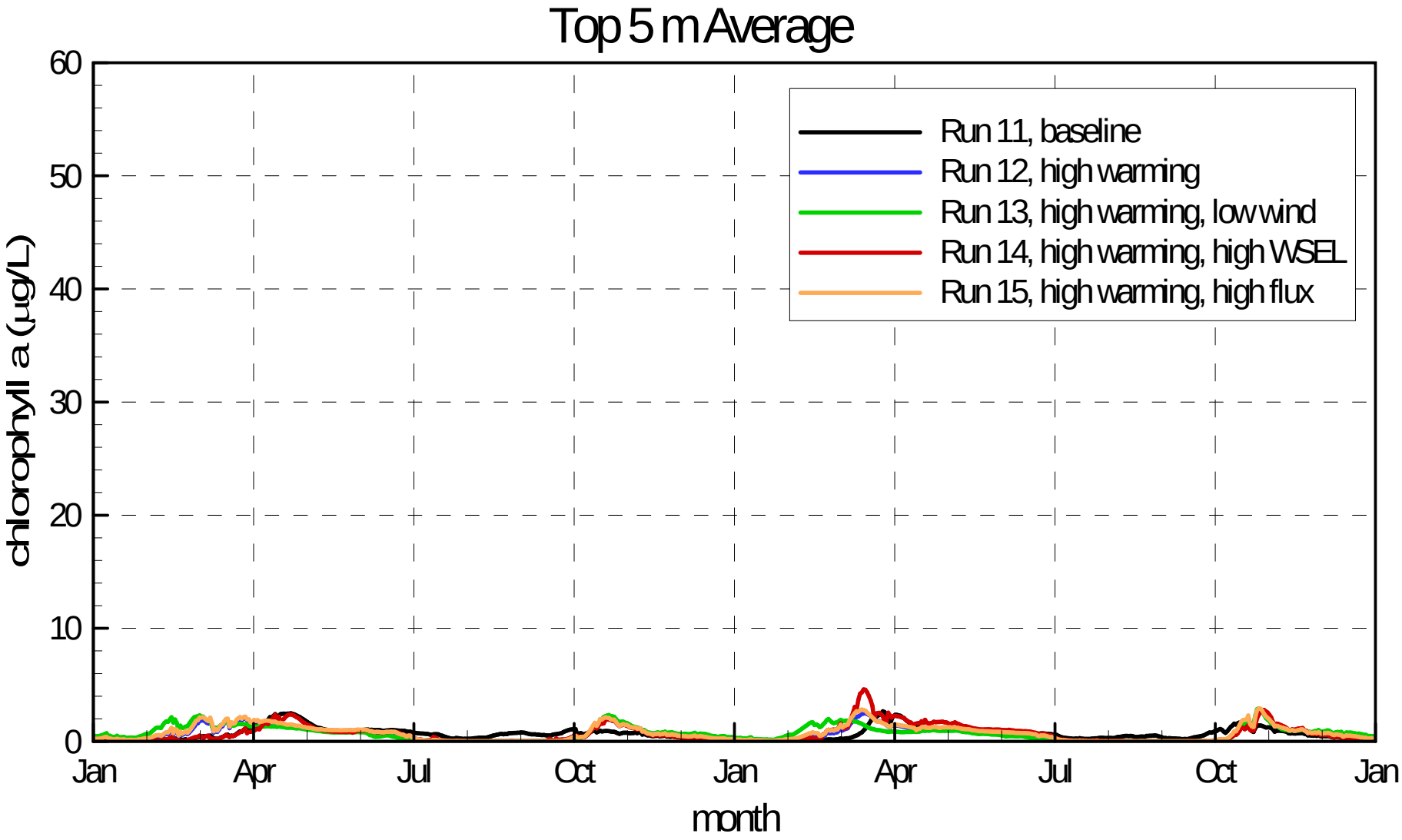

Figure A.108

Chlorophyll a at Station CR346.4

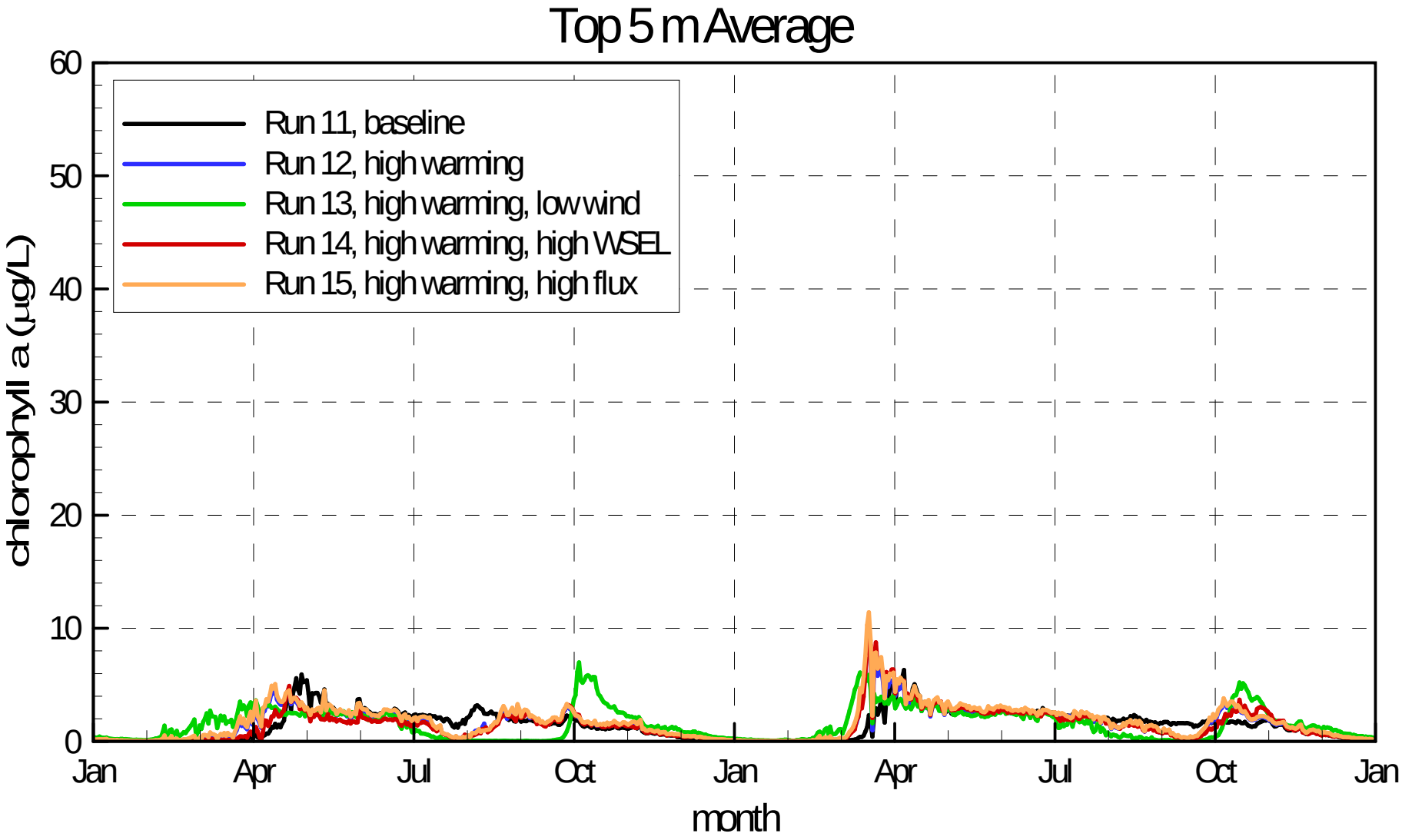

Figure A.109

Chlorophyll a at Station LWLVB1.2

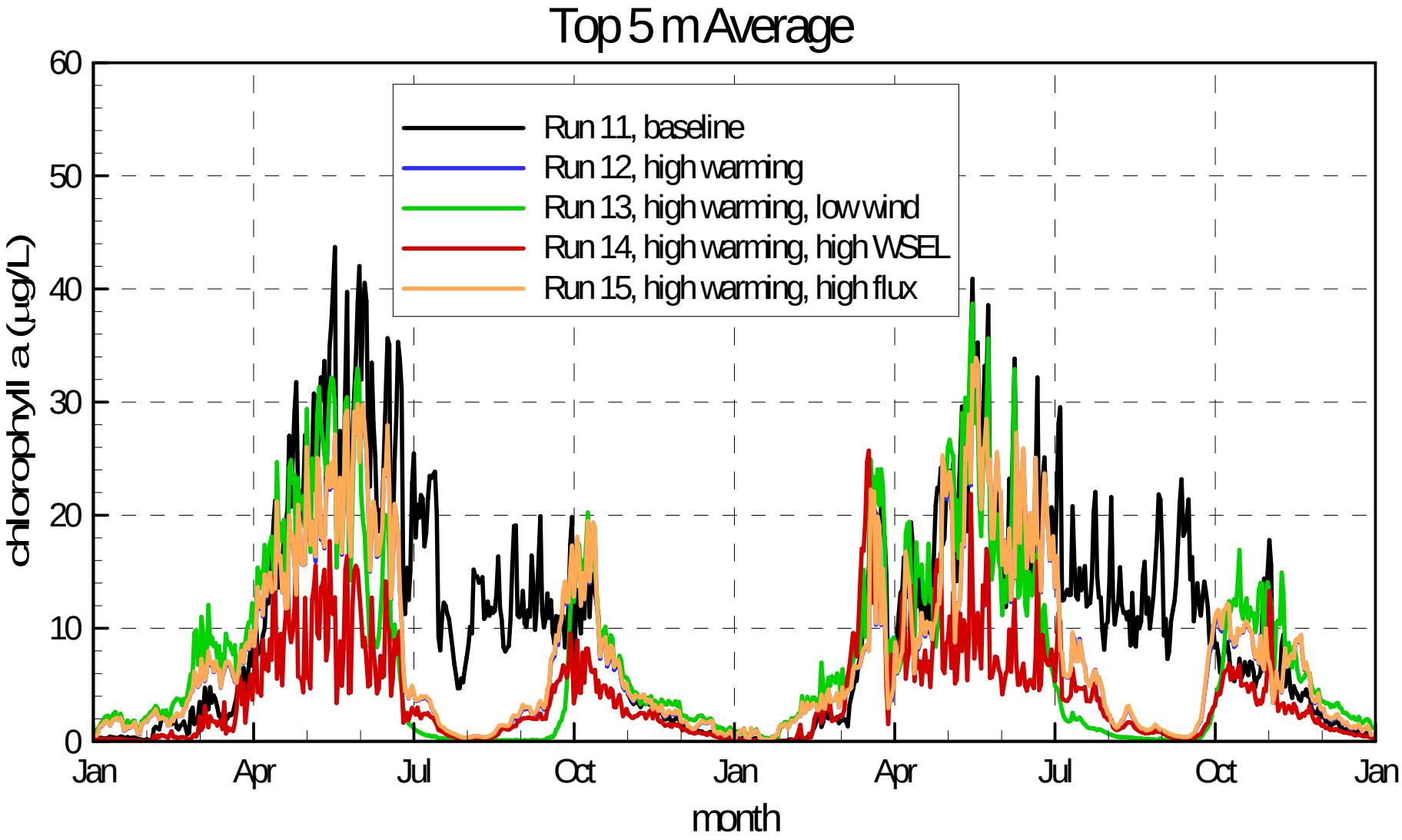

Figure A.110

Chlorophyll a at Station LWLVB1.85

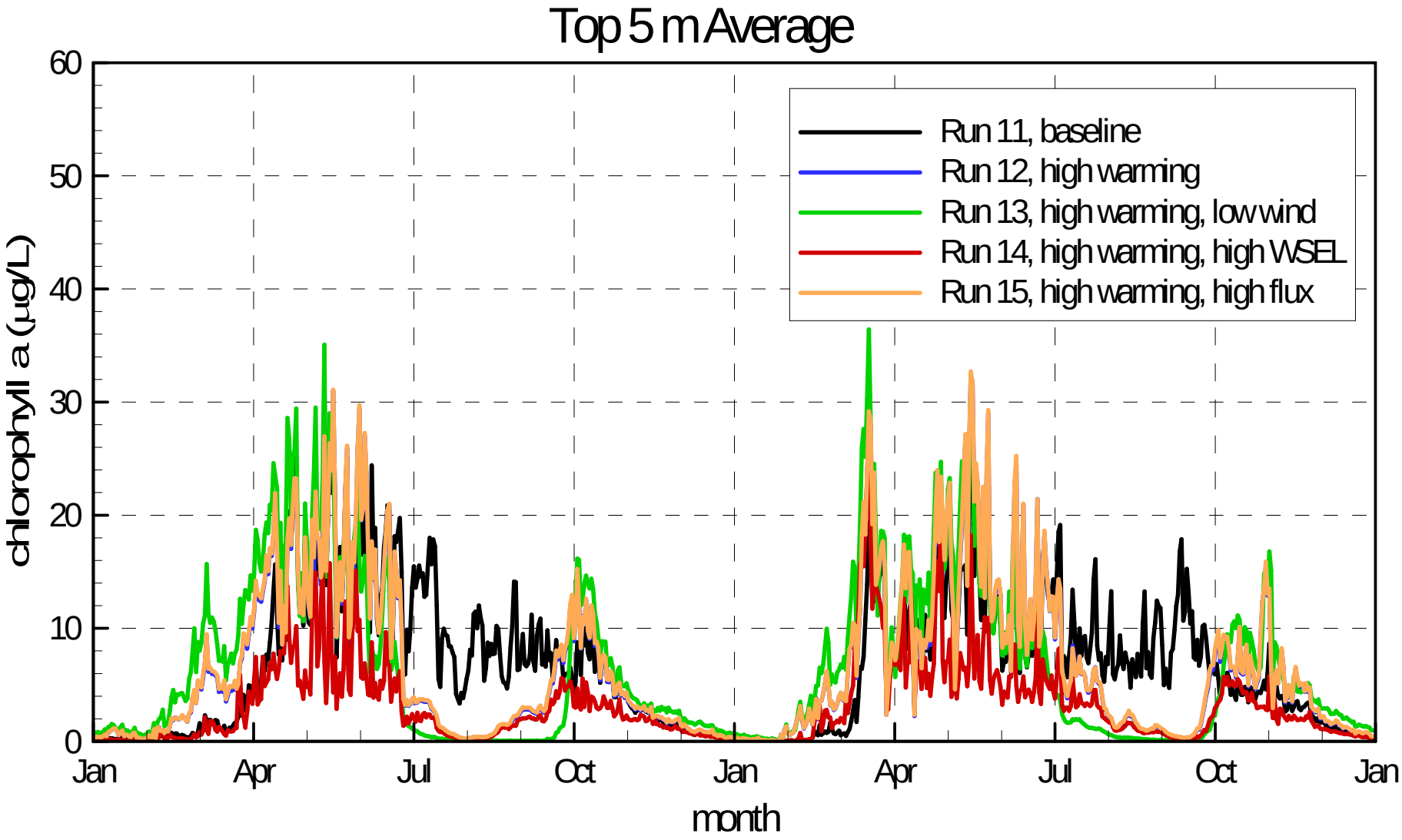

Figure A.111

Chlorophyll a at Station LWLVB2.7

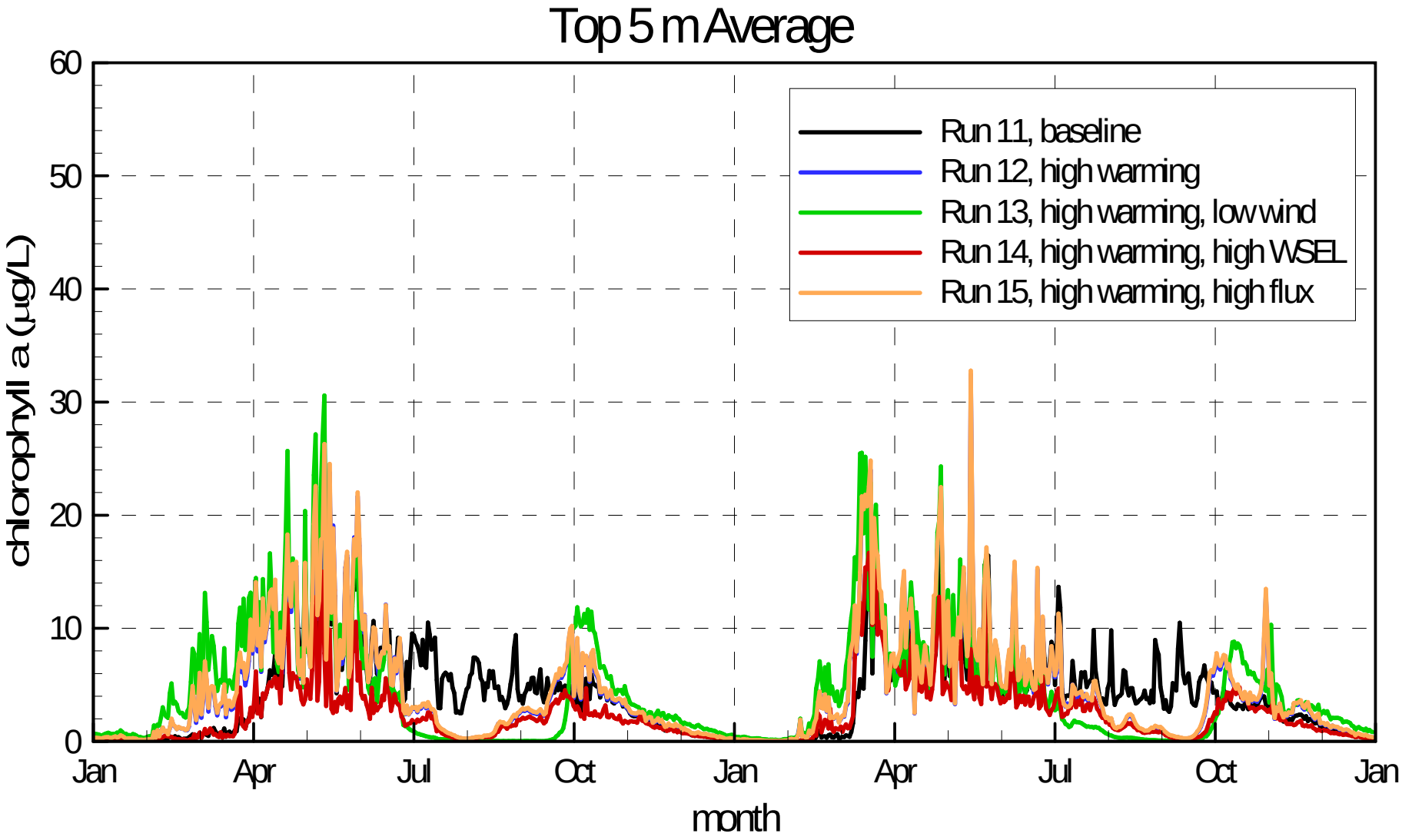

Figure A.112

FLOW SCIENCE

Chlorophyll a at Station LWLVB3.5

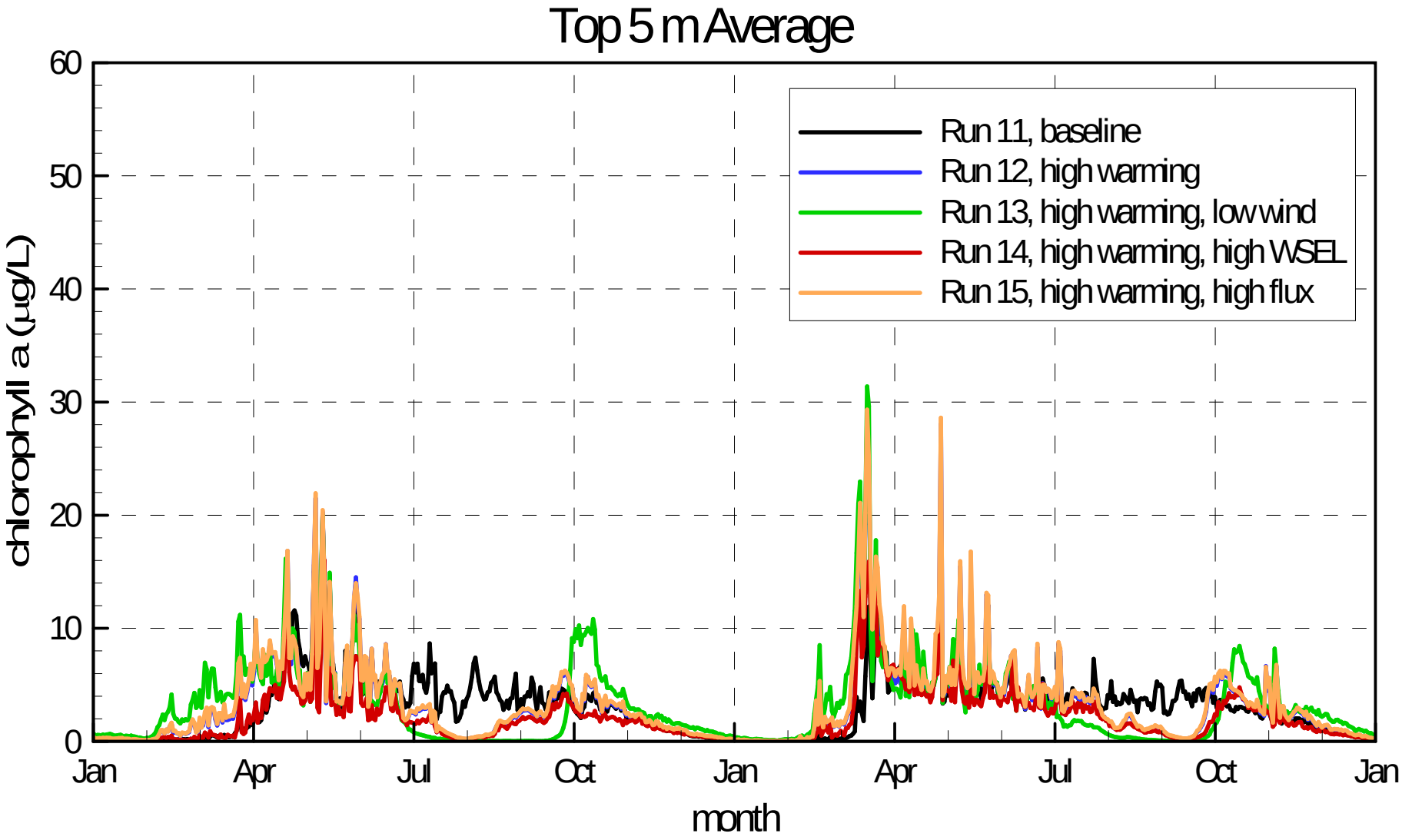

Figure A.113

Chlorophyll a at Station LVB3.5

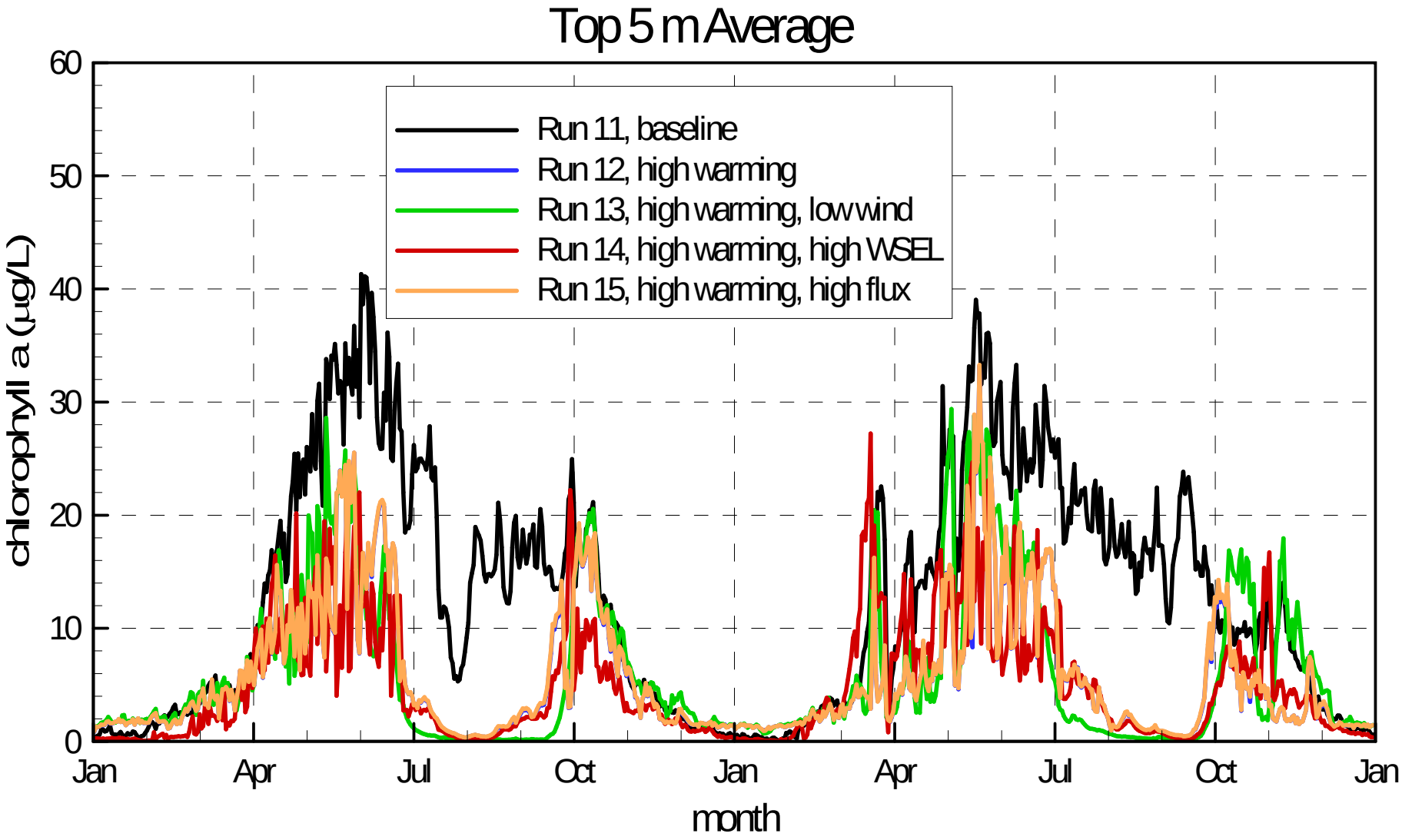

Figure A.114

FLOW SCIENCE

Chlorophyll a at Station LVB4.15

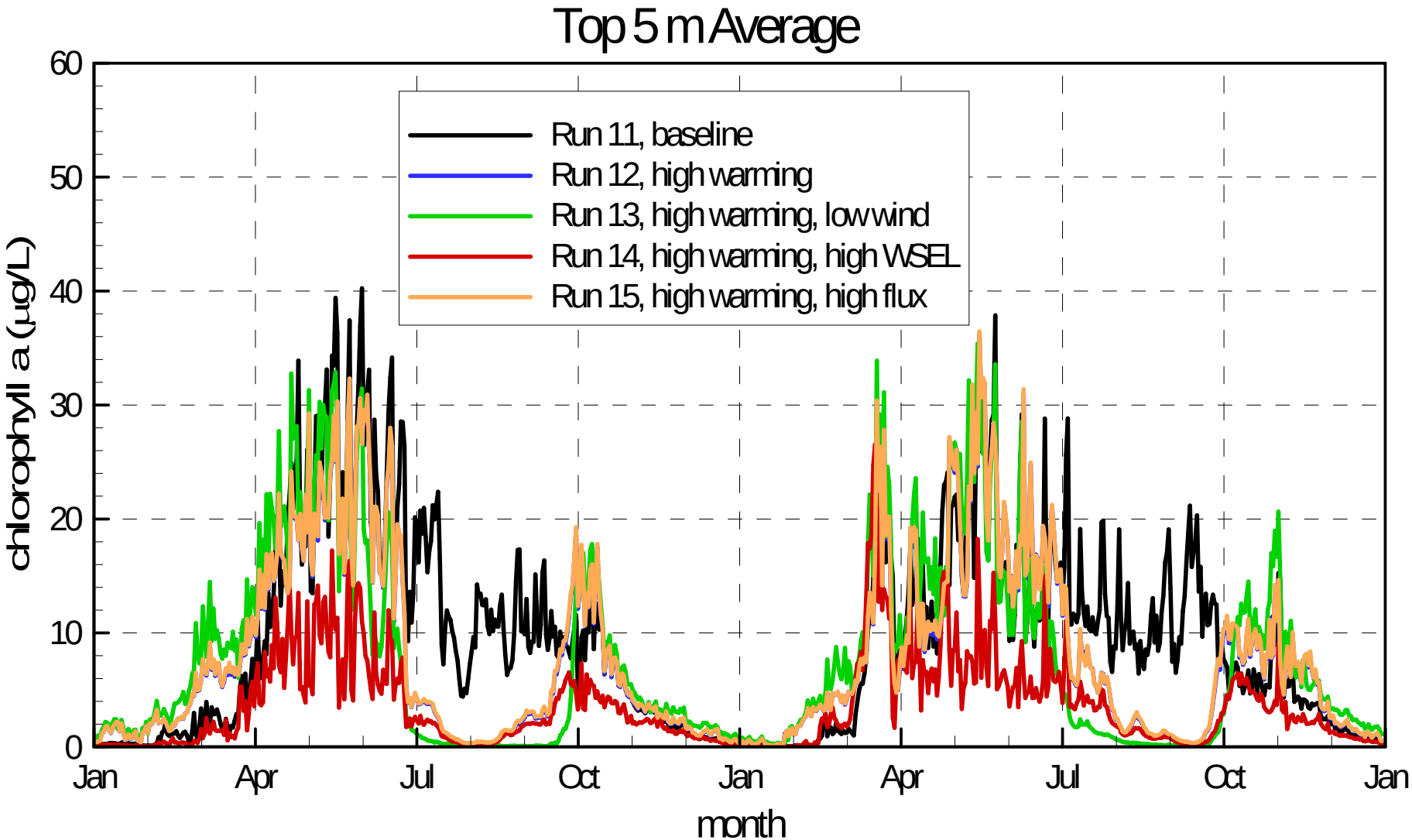

Figure A.115

FLOW SCIENCE

Chlorophyll a at Station LVB4.95

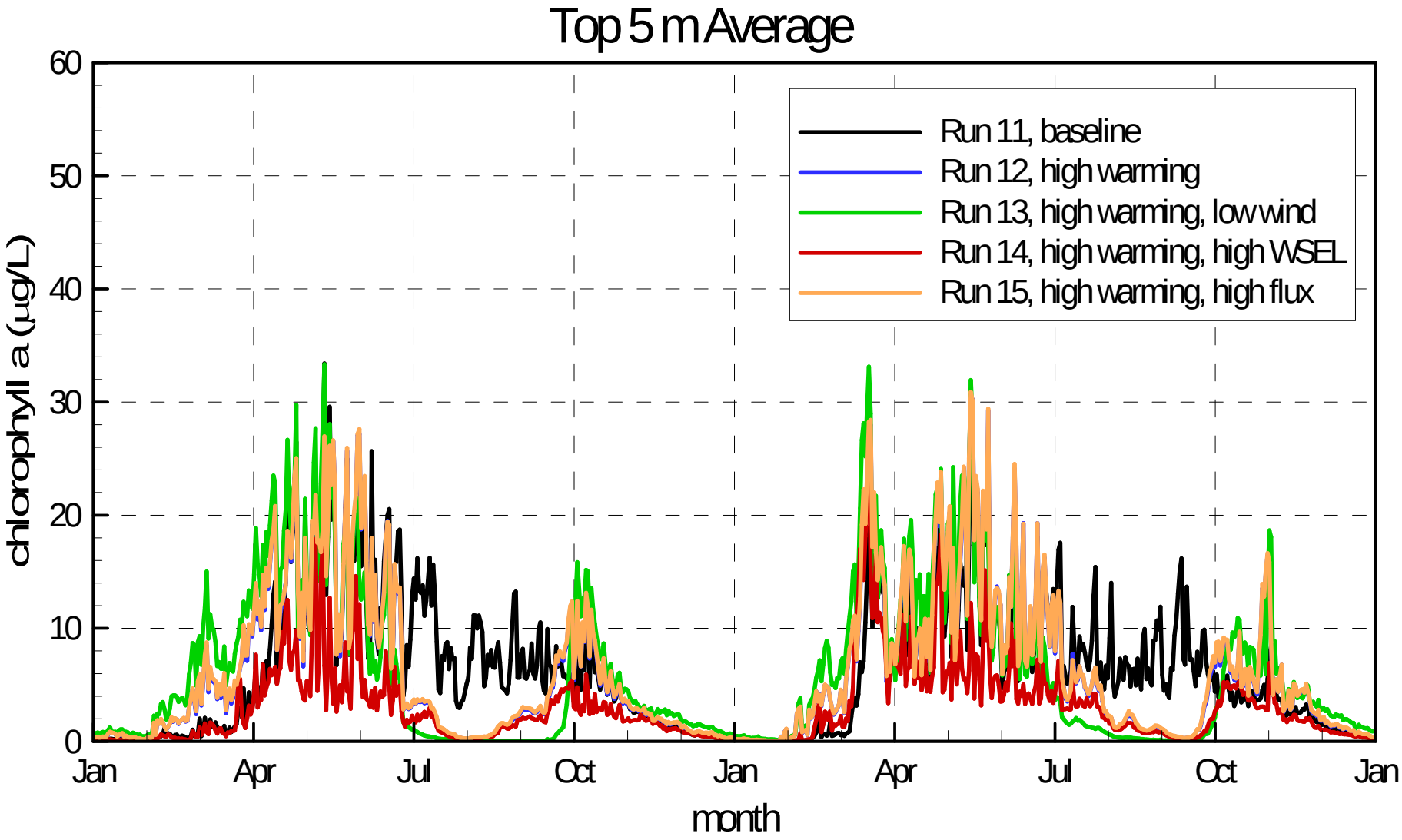

Figure A.116

Chlorophyll a at Station LVB6.7

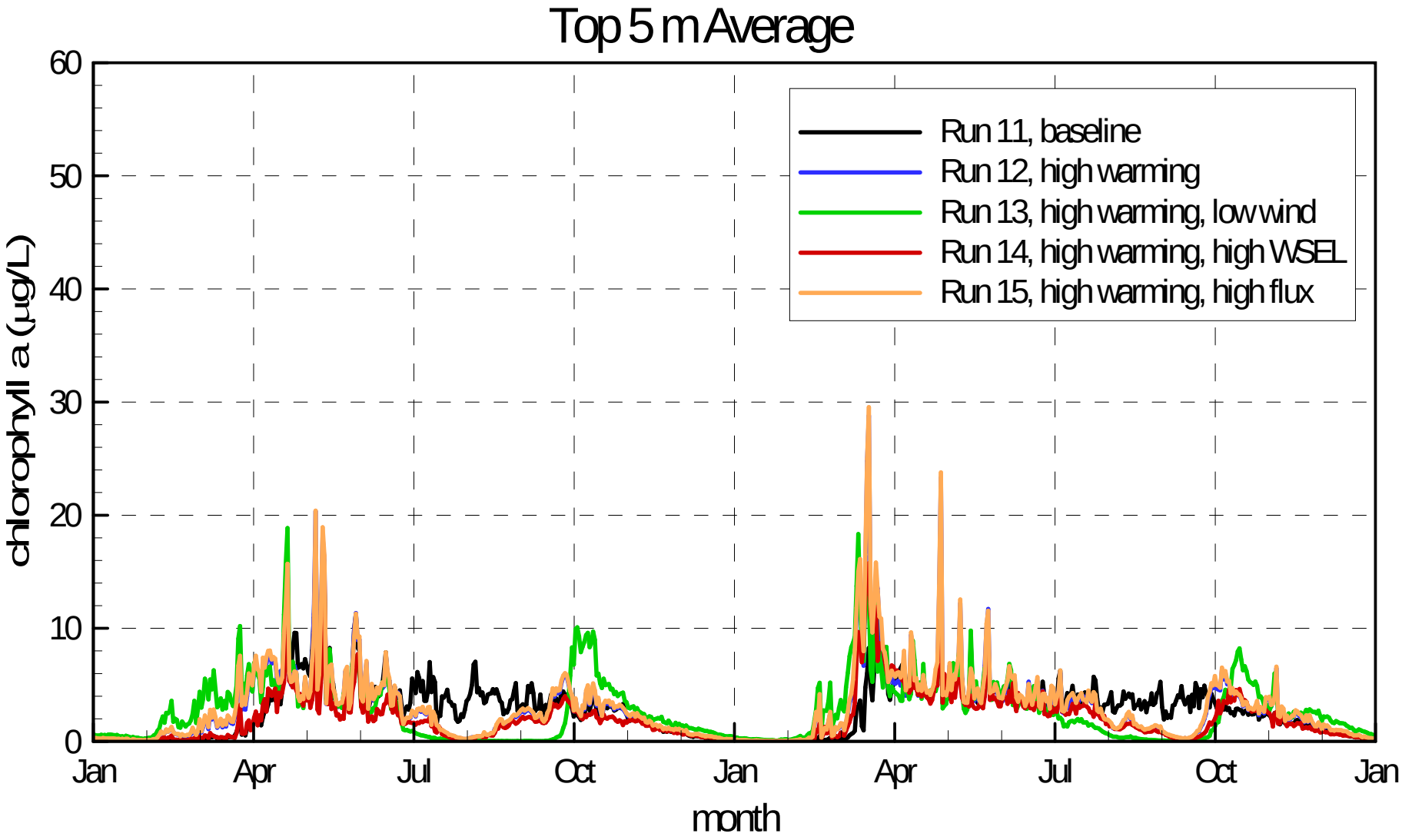

Figure A.117

Chlorophyll a at Station LVB7.3

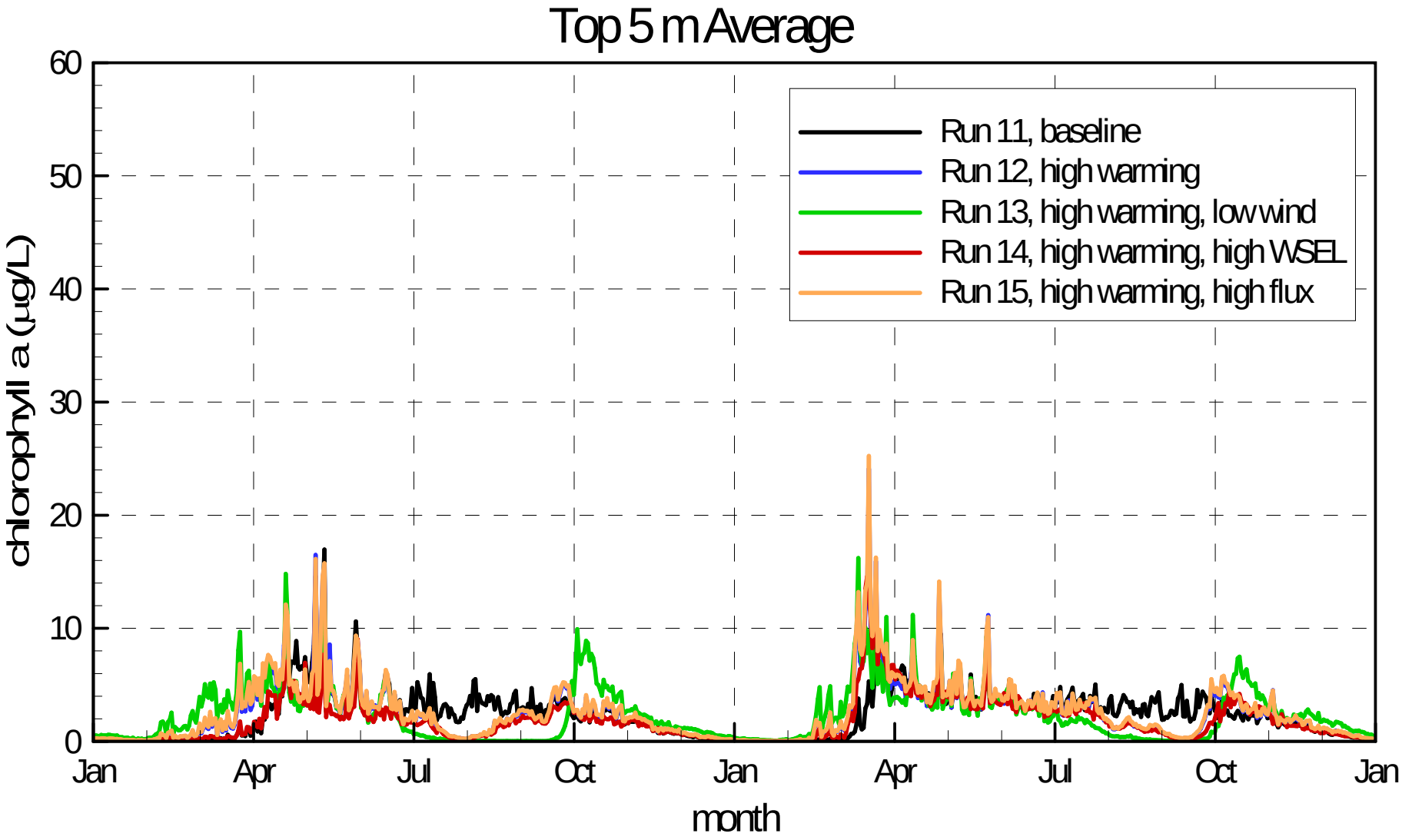

Figure A.118

Chlorophyll a at Surface Above SNWA Intake #3

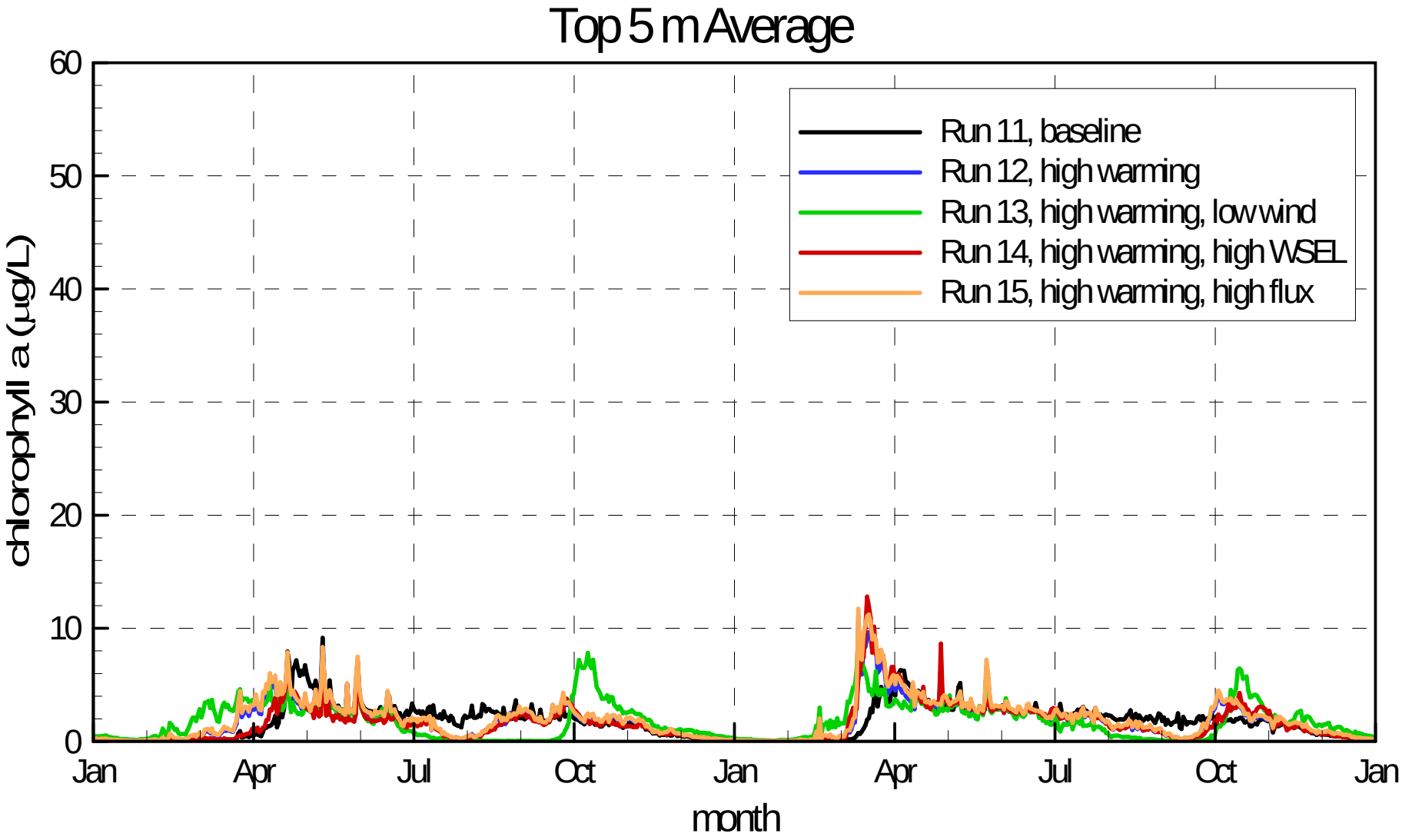

Figure A.119

Chlorophyll a at Surface at Hoover Dam

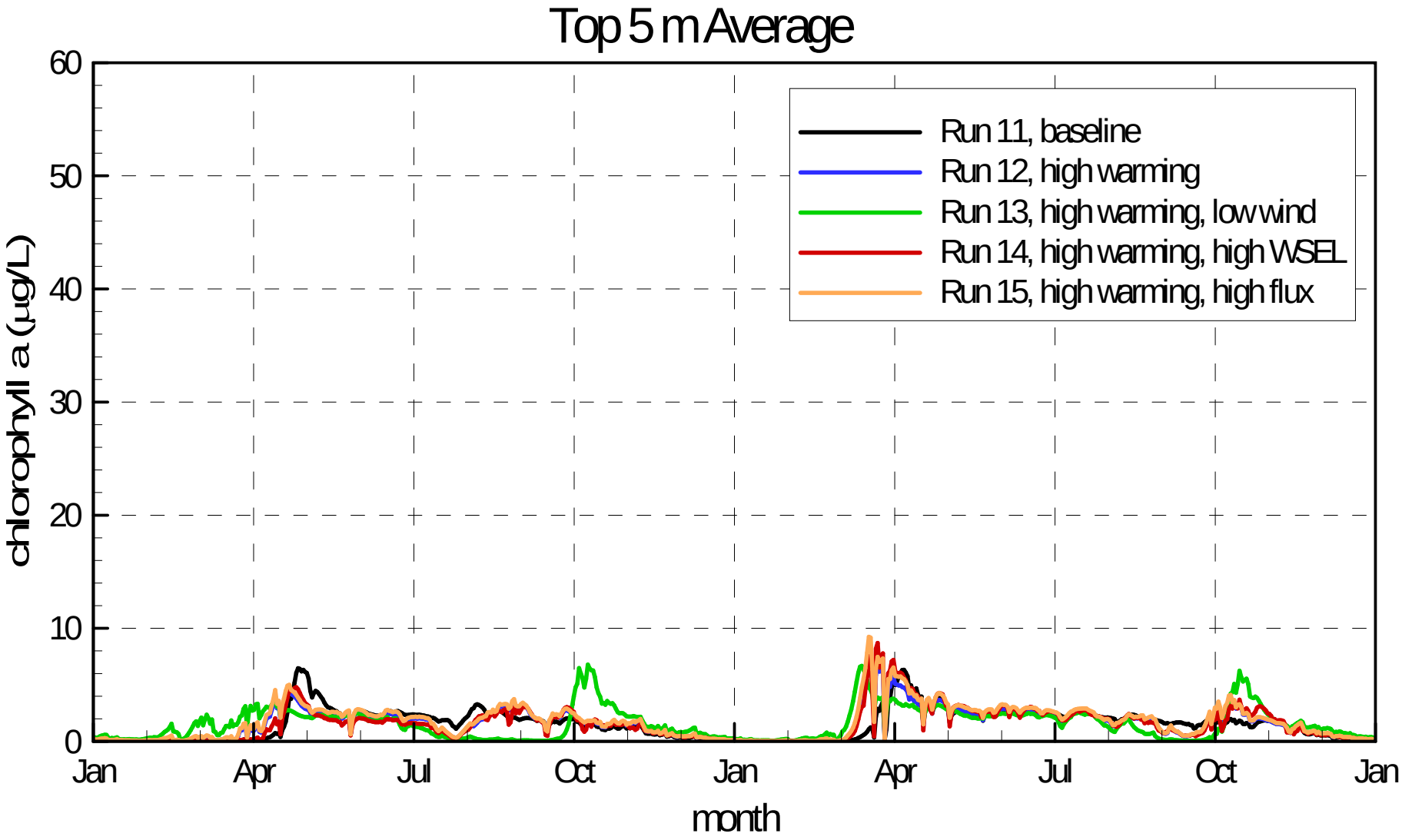

Figure A.120

Ammonium at Station CR394.0

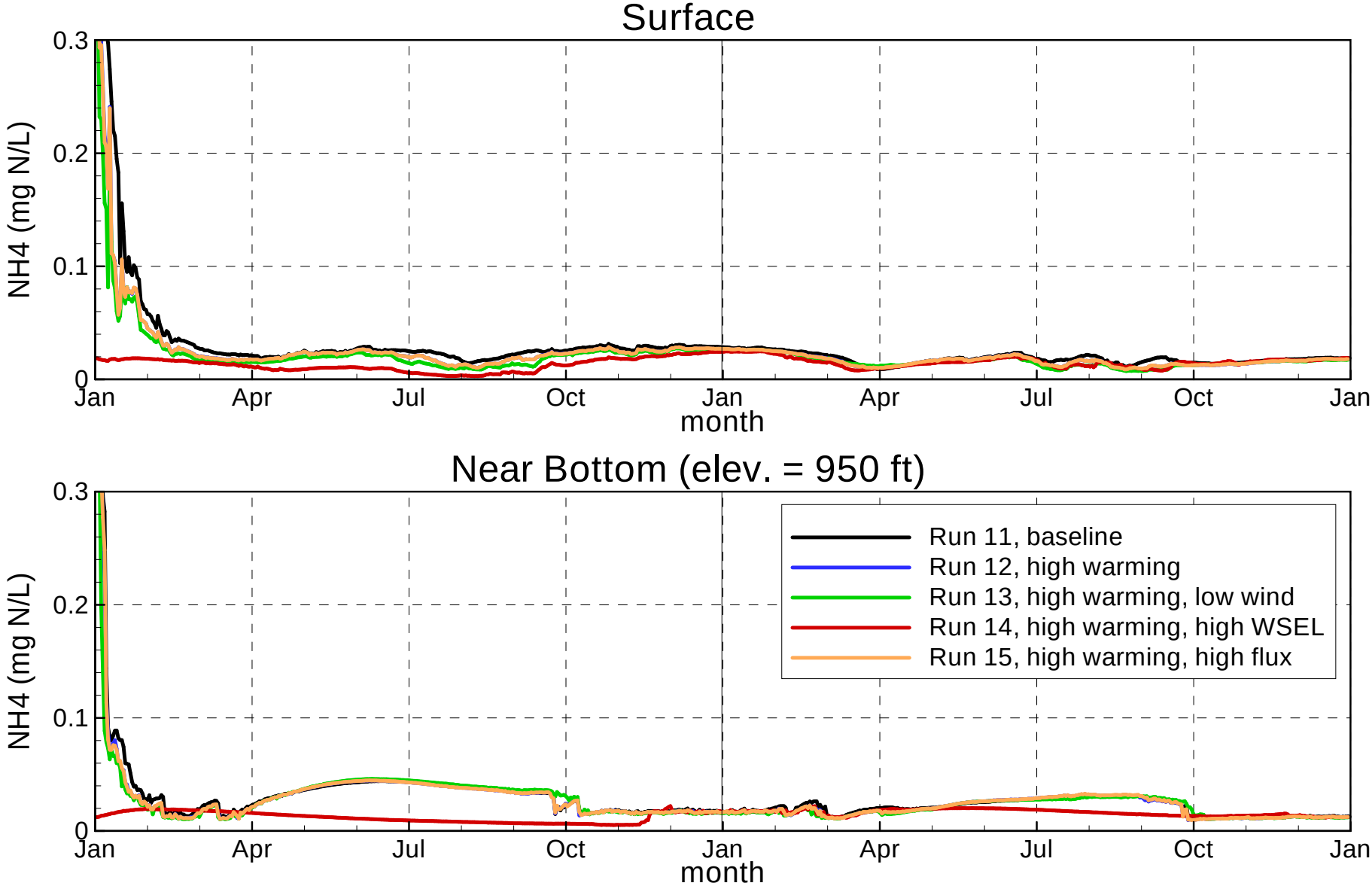

Figure A.121

Ammonium at Station CR390.0

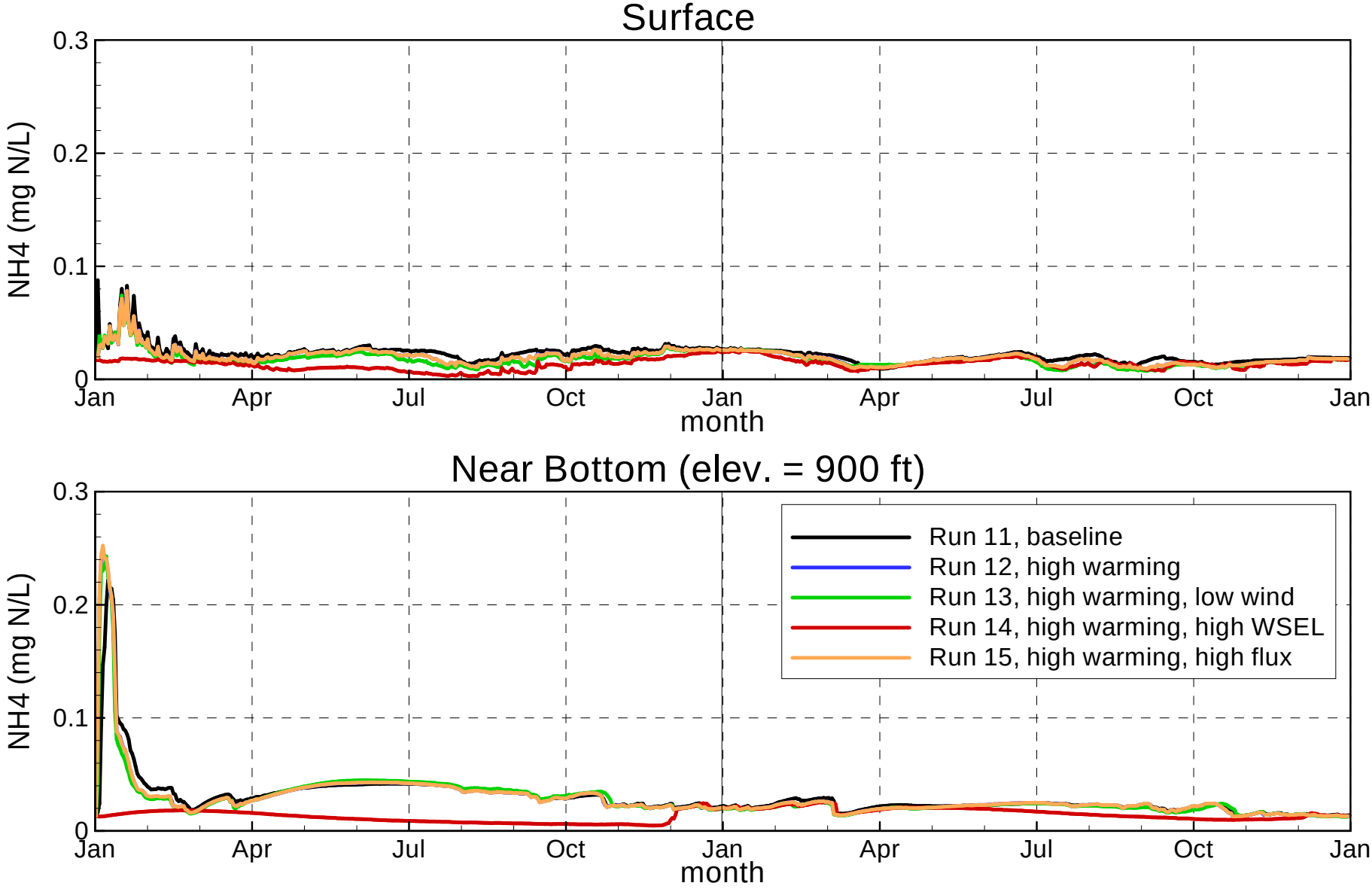

Figure A.122

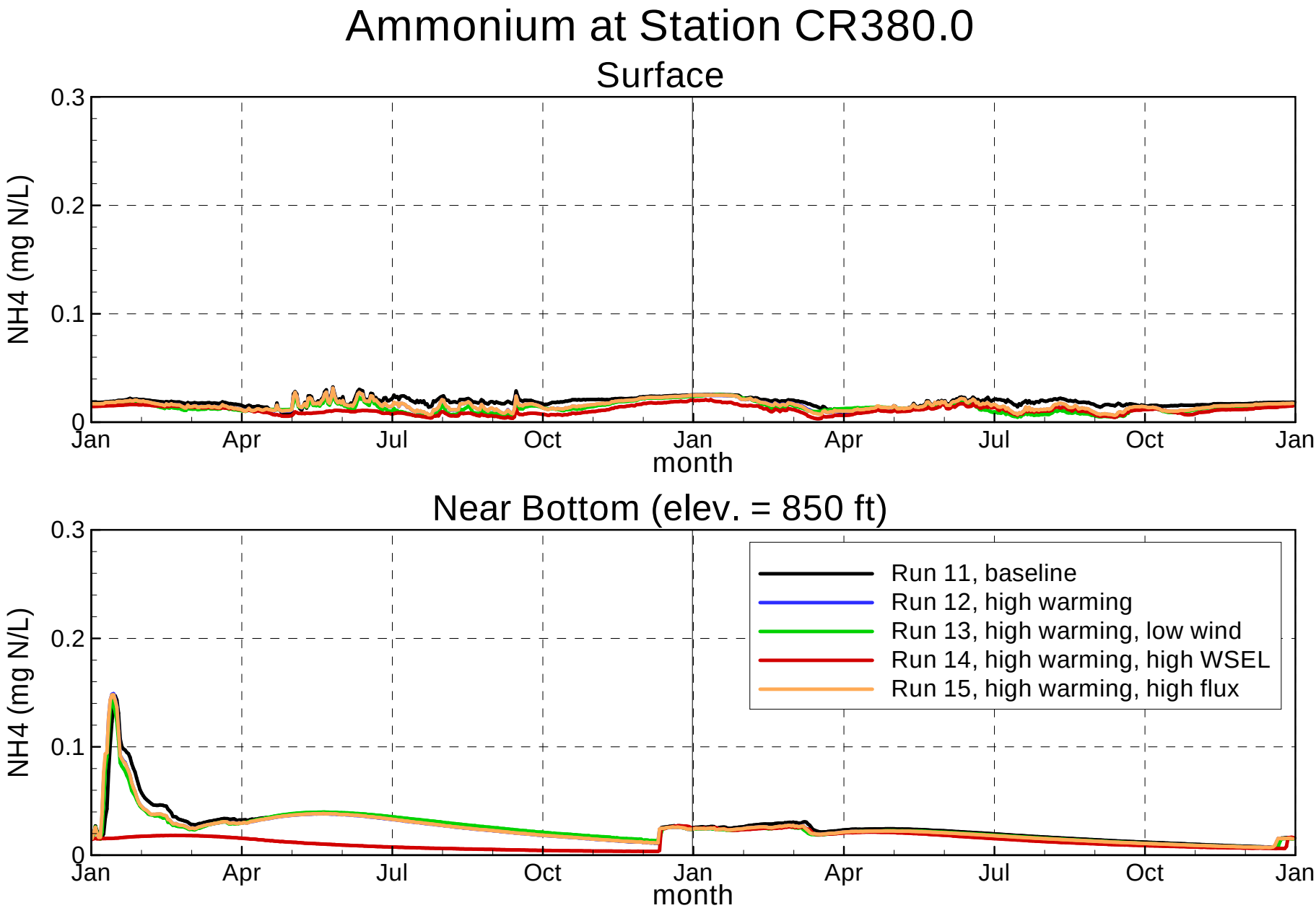
Ammonium at Station CR380.0
Surface
NH4 (mg N/L)
0.3
0.2
0.1
0
Jan
Apr
Jul
Oct
Jan
Apr
Jul
Oct
Jan
month
Near Bottom (elev. = 850 ft)
NH4 (mg N/L)
0.3
0.2
0.1
0
Jan
Apr
Jul
Oct
Jan
Apr
Jul
Oct
Jan
month
Run 11, baseline
Run 12, high warming
Run 13, high warming, low wind
Run 14, high warming, high WSEL
Run 15, high warming, high flux

Figure A.123

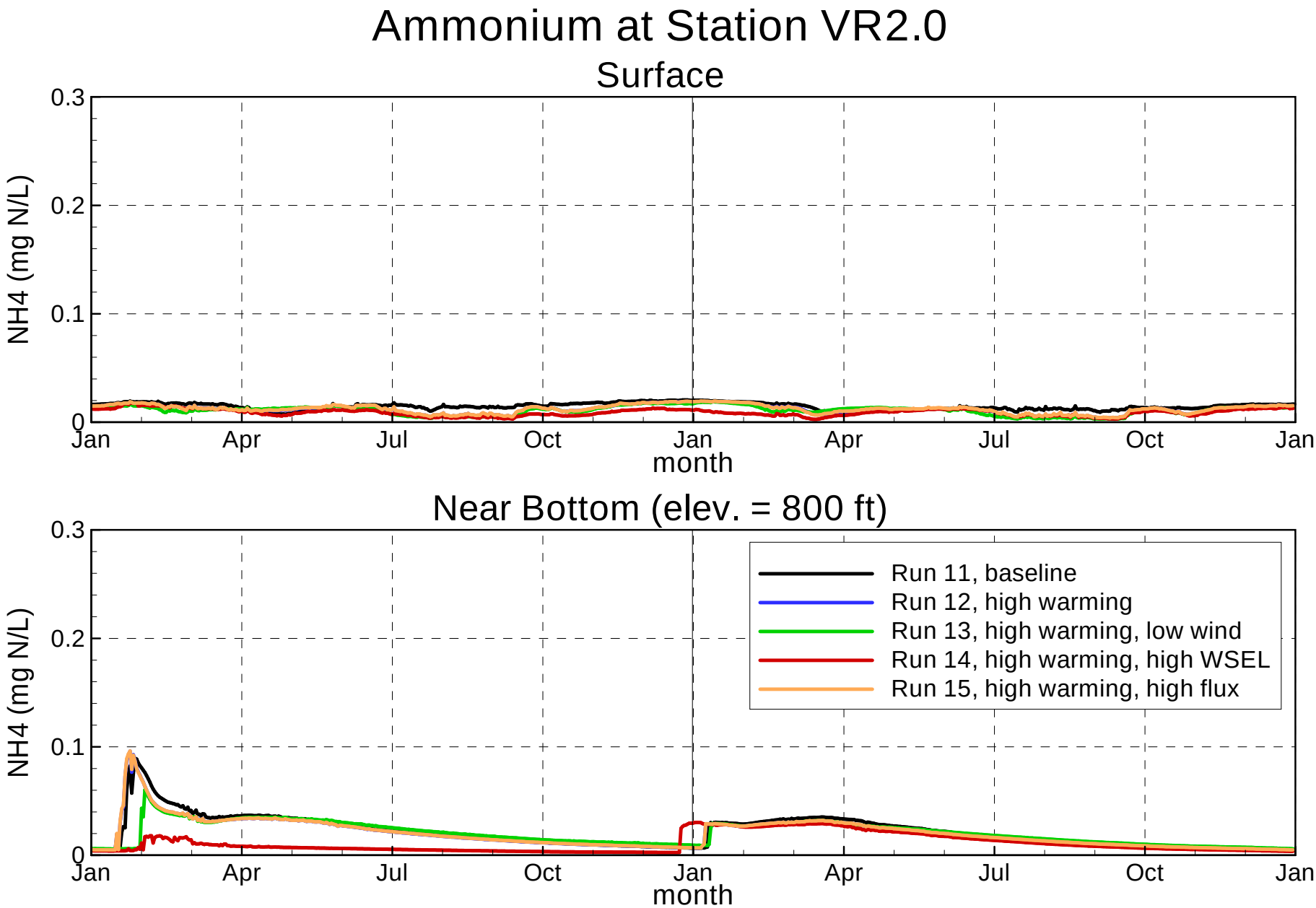
Ammonium at Station VR2.0
Surface
NH4 (mg N/L)
0.3
0.2
0.1
0
Jan
Apr
Jul
Oct
Jan
Apr
Jul
Oct
Jan
month
Near Bottom (elev. = 800 ft)
NH4 (mg N/L)
0.3
0.2
0.1
0
Jan
Apr
Jul
Oct
Jan
Apr
Jul
Oct
Jan
month
Run 11, baseline
Run 12, high warming
Run 13, high warming, low wind
Run 14, high warming, high WSEL
Run 15, high warming, high flux

Figure A.124

Ammonium at Station VR12.9

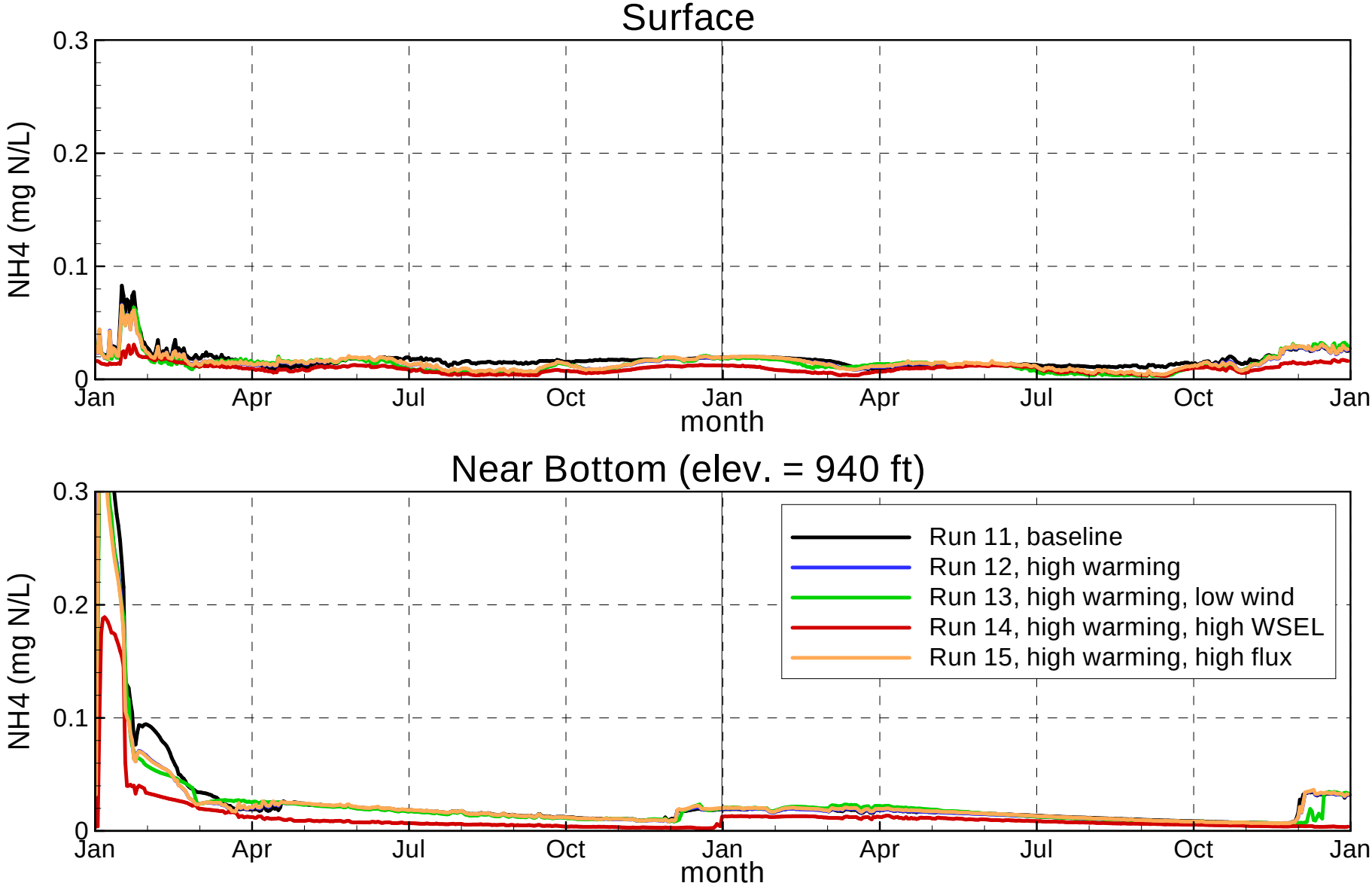

Figure A.125

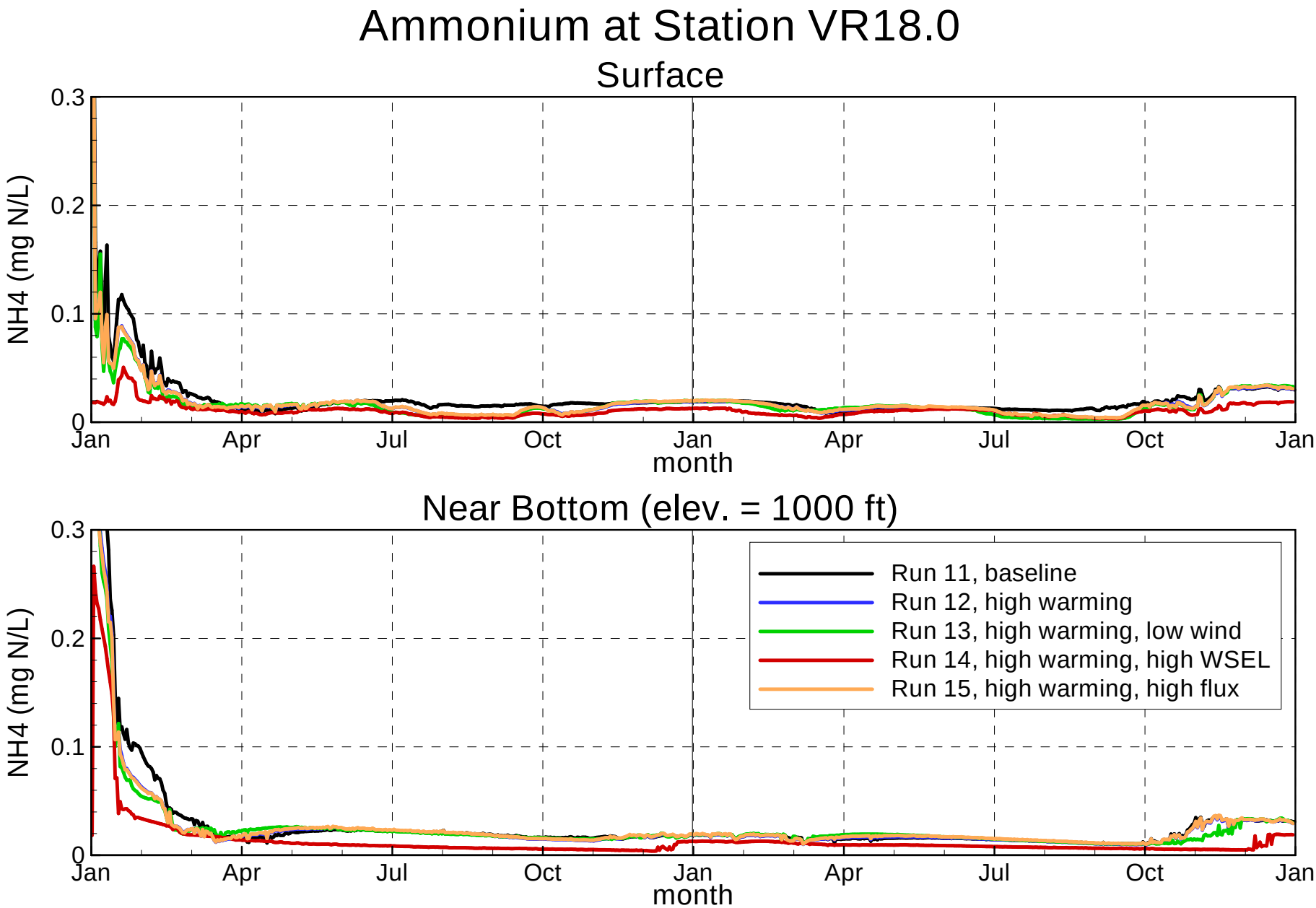
Ammonium at Station VR18.0
Surface
NH4 (mg N/L)
0.3
0.2
0.1
0
Jan
Apr
Jul
Oct
Jan
Apr
Jul
Oct
Jan
month
Near Bottom (elev. = 1000 ft)
NH4 (mg N/L)
0.3
0.2
0.1
0
Jan
Apr
Jul
Oct
Jan
Apr
Jul
Oct
Jan
month
Run 11, baseline
Run 12, high warming
Run 13, high warming, low wind
Run 14, high warming, high WSEL
Run 15, high warming, high flux

Figure A.126

Ammonium at Station VR25.1

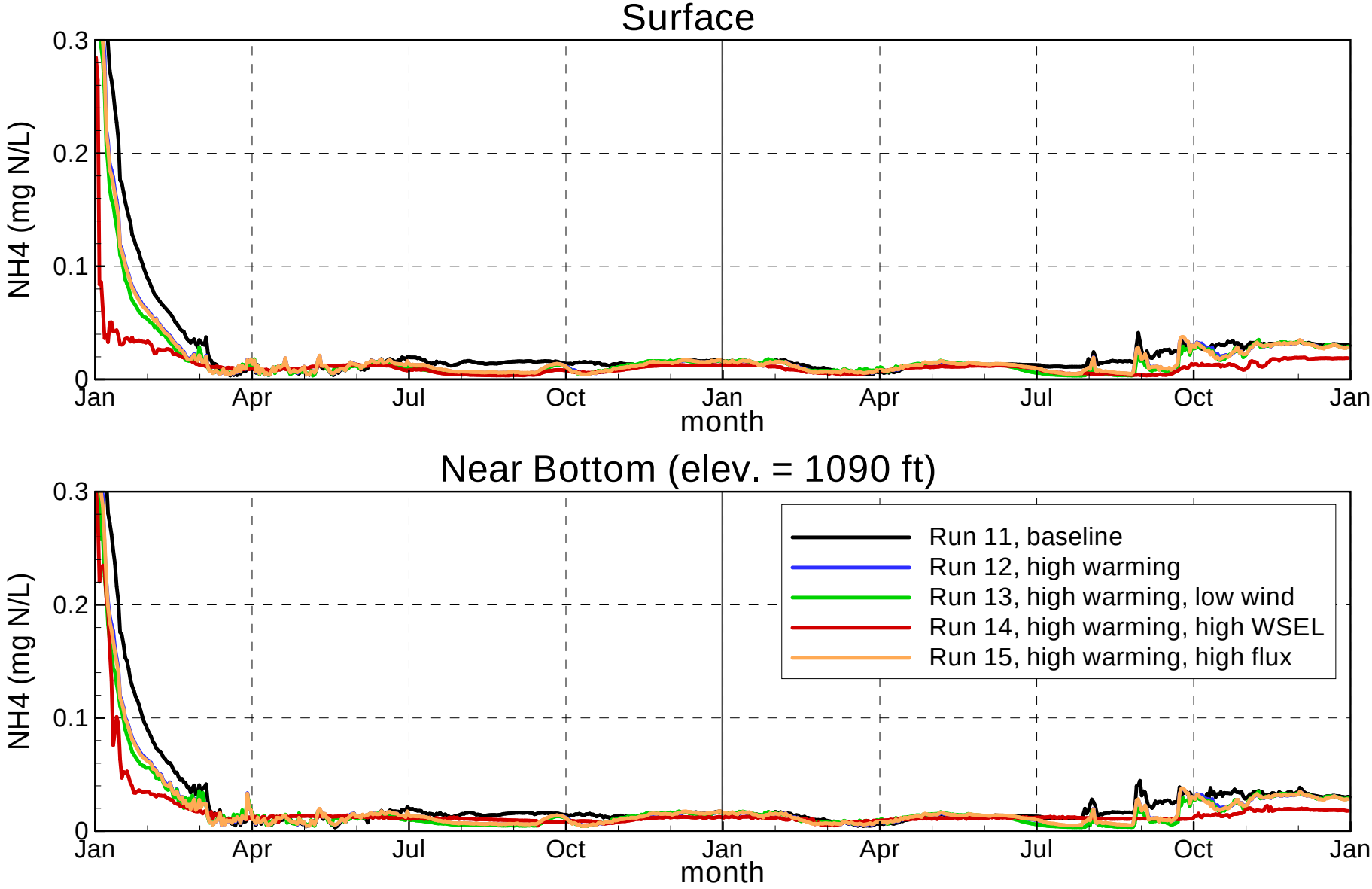

Figure A.127

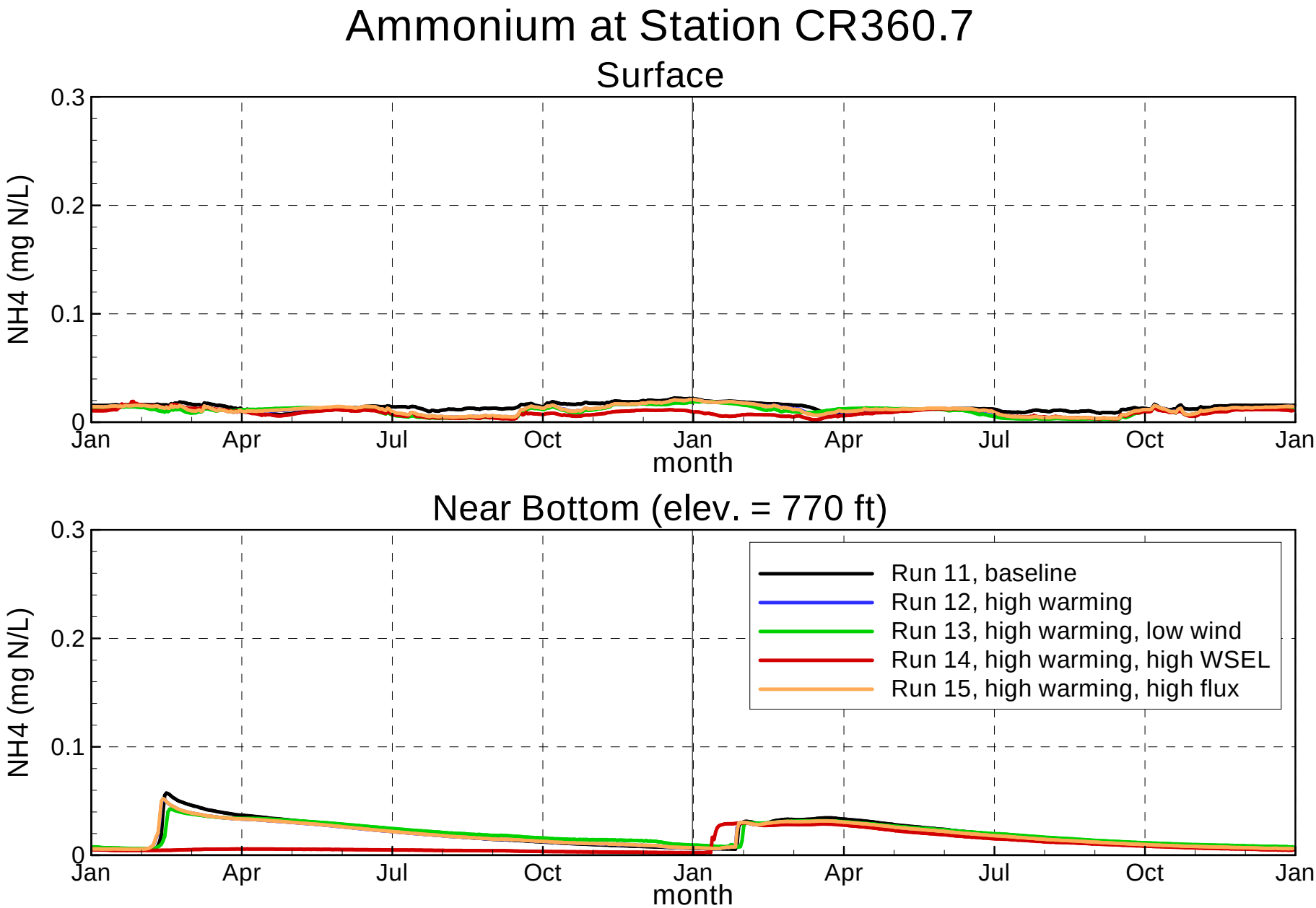
Ammonium at Station CR360.7
Surface
NH4 (mg N/L)
0.3
0.2
0.1
0
Jan
Apr
Jul
Oct
Jan
Apr
Jul
Oct
Jan
month
Near Bottom (elev. = 770 ft)
NH4 (mg N/L)
0.3
0.2
0.1
0
Jan
Apr
Jul
Oct
Jan
Apr
Jul
Oct
Jan
month
Run 11, baseline
Run 12, high warming
Run 13, high warming, low wind
Run 14, high warming, high WSEL
Run 15, high warming, high flux

Figure A.128

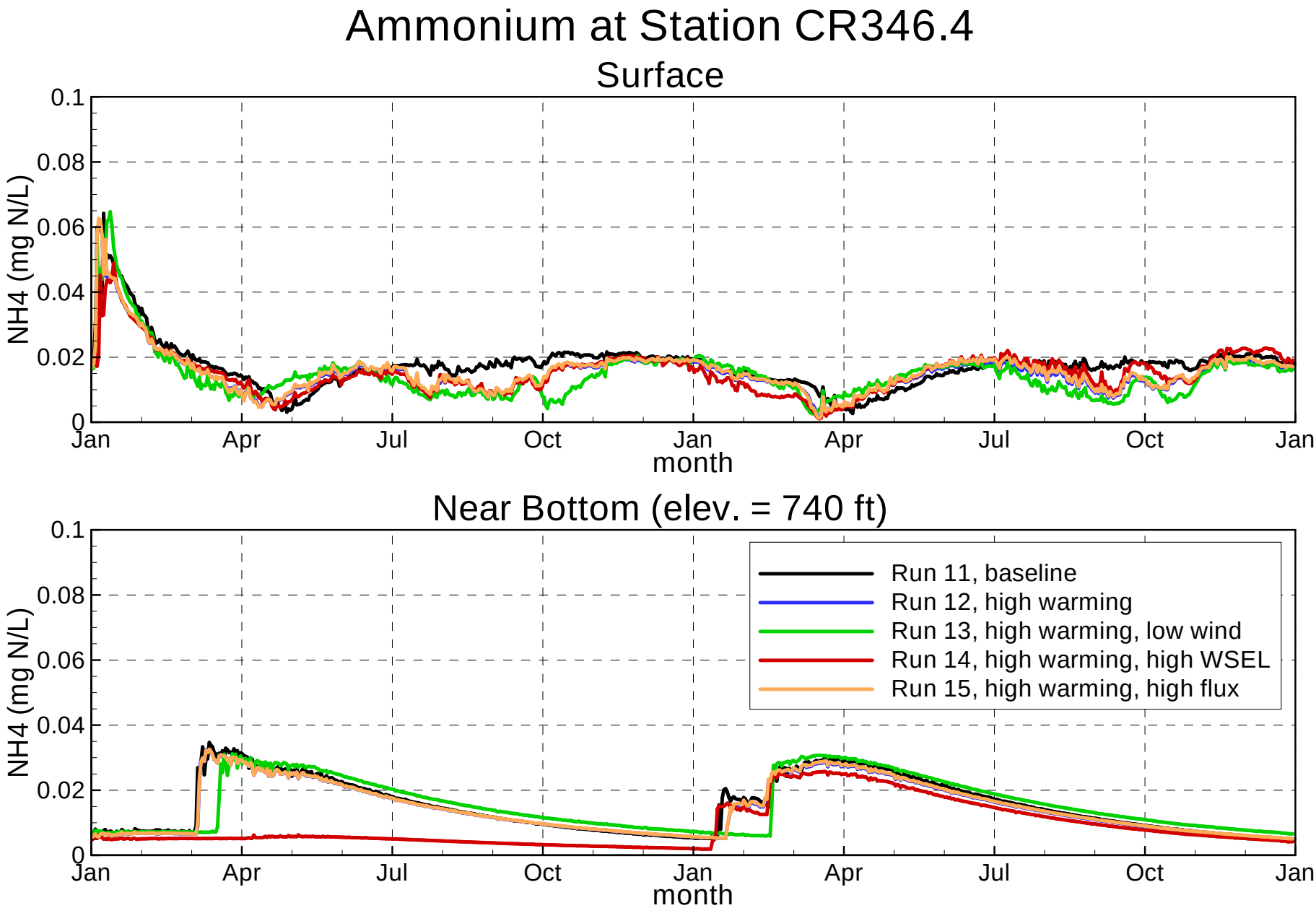
Ammonium at Station CR346.4
Surface
NH4 (mg N/L)
0.1
0.08
0.06
0.04
0.02
0
Jan
Apr
Jul
Oct
Jan
Apr
Jul
Oct
Jan
month
Near Bottom (elev. = 740 ft)
Run 11, baseline
Run 12, high warming
Run 13, high warming, low wind
Run 14, high warming, high WSEL
Run 15, high warming, high flux

Figure A.129

Ammonium at Station LWLVB1.2

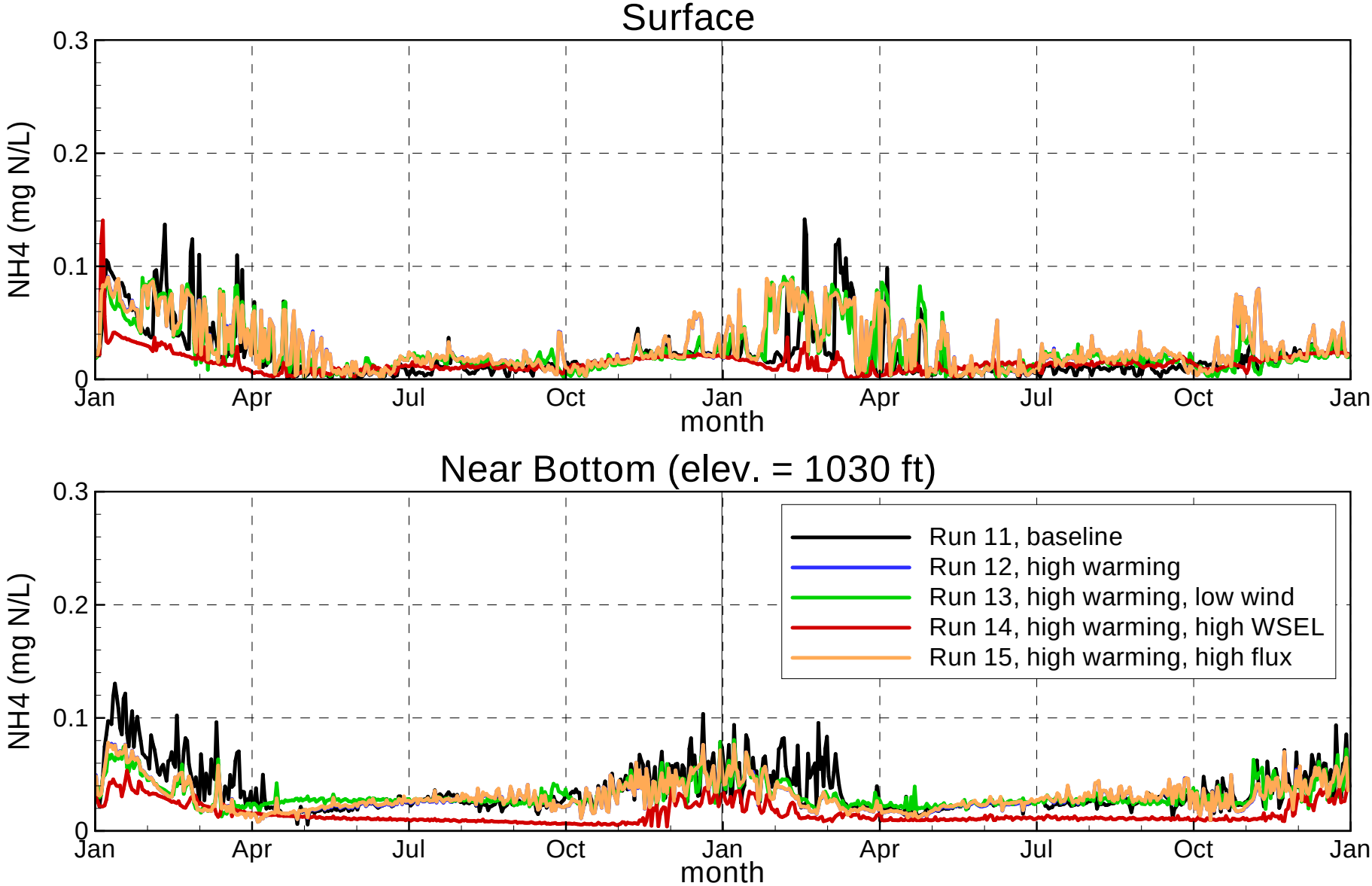

Figure A.130

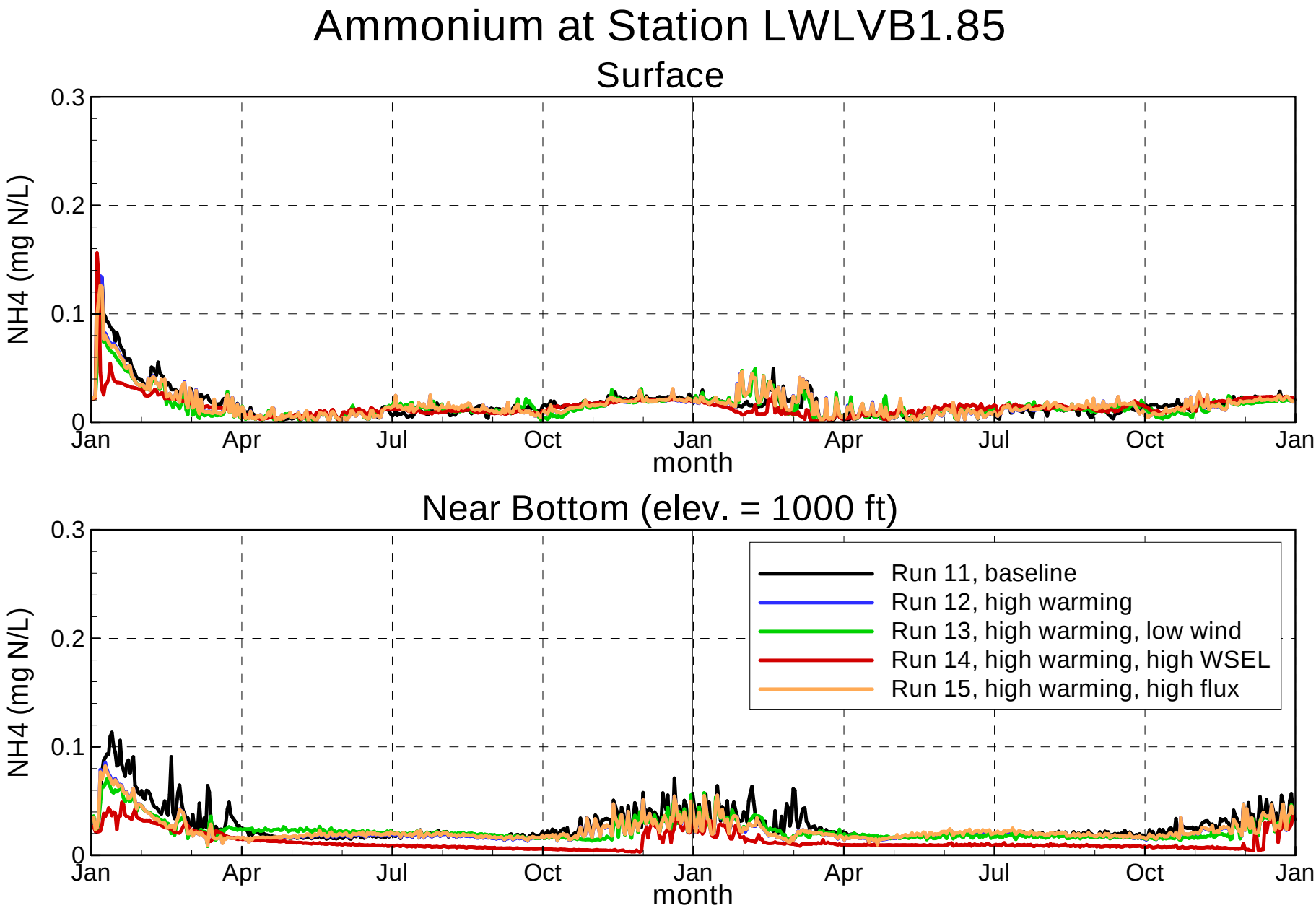
Ammonium at Station LWLVB1.85
Surface
NH4 (mg N/L)
0.3
0.2
0.1
0
Jan
Apr
Jul
Oct
Jan
Apr
Jul
Oct
Jan
month
Near Bottom (elev. = 1000 ft)
NH4 (mg N/L)
0.3
0.2
0.1
0
Jan
Apr
Jul
Oct
Jan
Apr
Jul
Oct
Jan
month
Run 11, baseline
Run 12, high warming
Run 13, high warming, low wind
Run 14, high warming, high WSEL
Run 15, high warming, high flux

Figure A.131

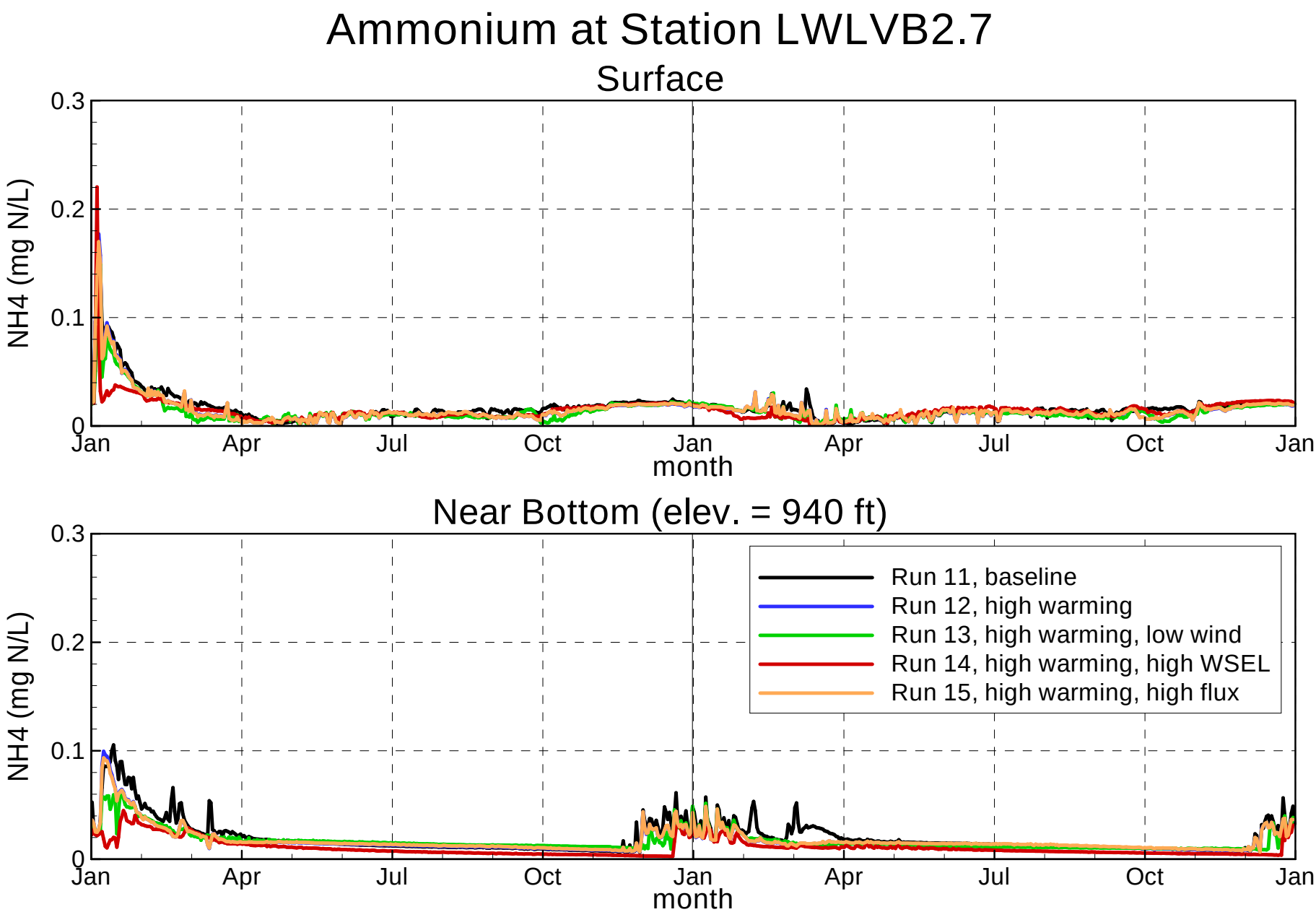
Ammonium at Station LWLVB2.7
Surface
NH4 (mg N/L)
0.3
0.2
0.1
0
Jan
Apr
Jul
Oct
Jan
Apr
Jul
Oct
Jan
month
Near Bottom (elev. = 940 ft)
NH4 (mg N/L)
0.3
0.2
0.1
0
Jan
Apr
Jul
Oct
Jan
Apr
Jul
Oct
Jan
month
Run 11, baseline
Run 12, high warming
Run 13, high warming, low wind
Run 14, high warming, high WSEL
Run 15, high warming, high flux

Figure A.132

Ammonium at Station LWLVB3.5

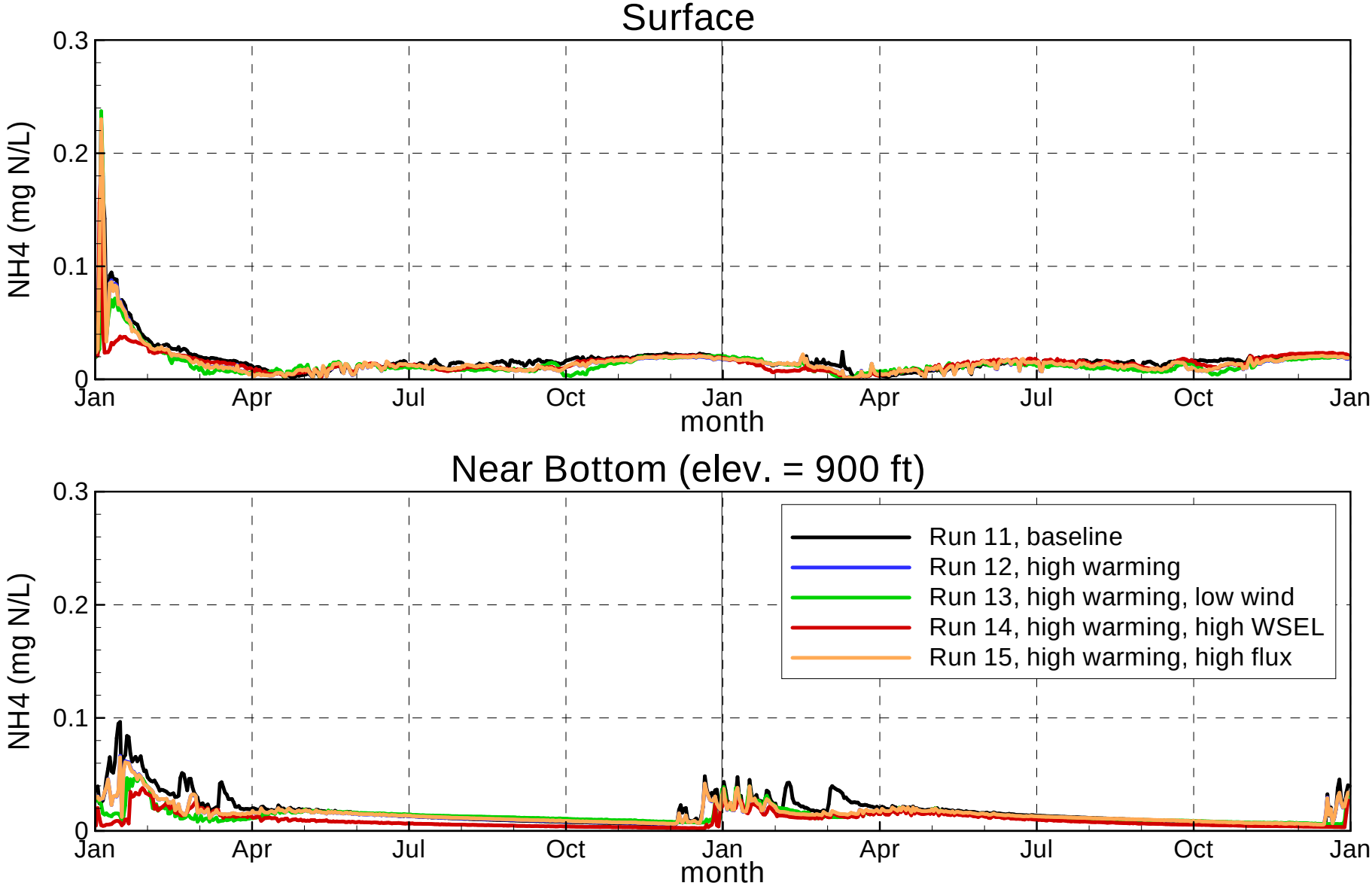

Figure A.133

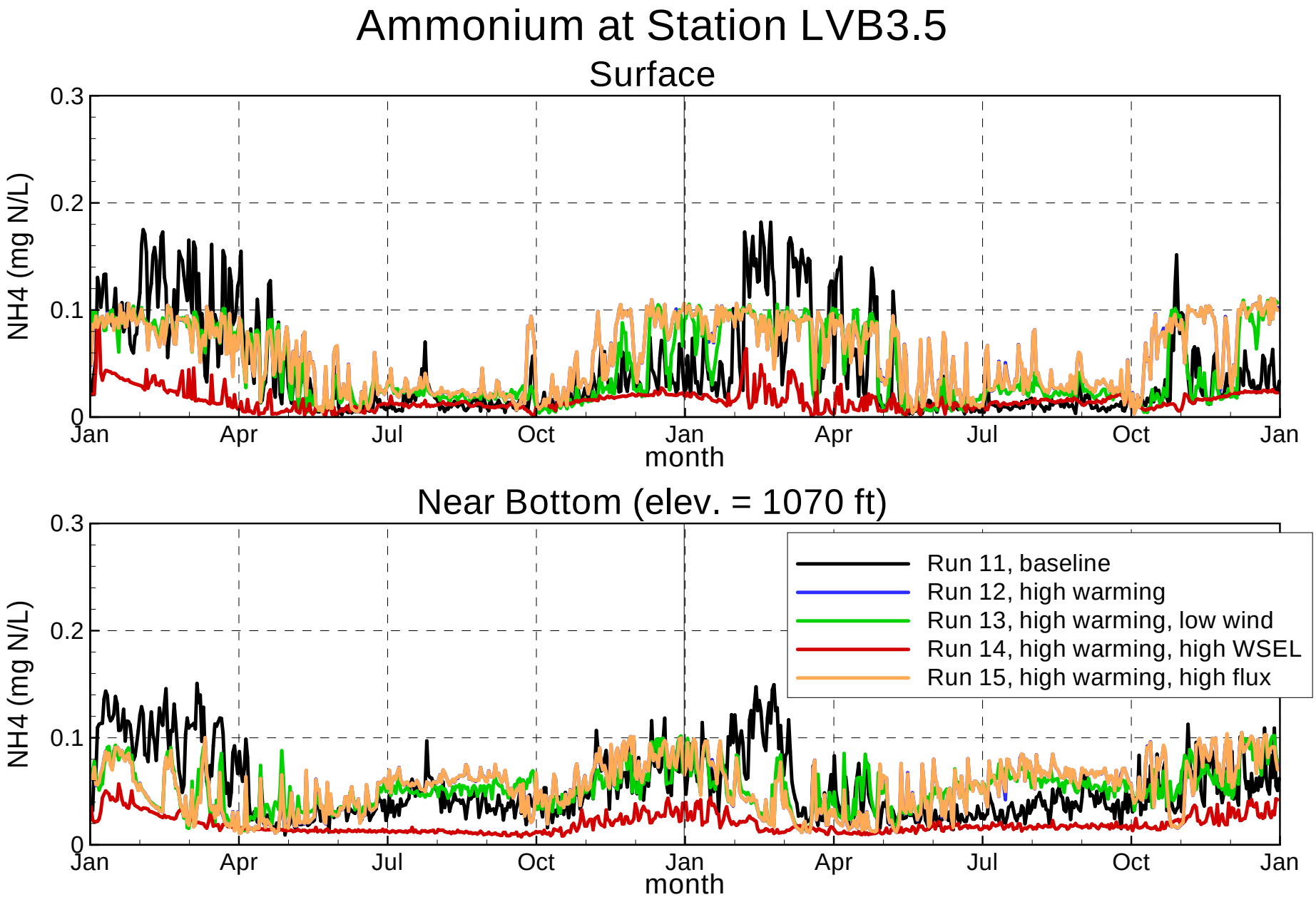
Ammonium at Station LVB3.5
Surface
NH4 (mg N/L)
0.3
0.2
0.1
0
Jan
Apr
Jul
Oct
Jan
Apr
Jul
Oct
Jan
month
Near Bottom (elev. = 1070 ft)
NH4 (mg N/L)
0.3
0.2
0.1
0
Jan
Apr
Jul
Oct
Jan
Apr
Jul
Oct
Jan
month
Run 11, baseline
Run 12, high warming
Run 13, high warming, low wind
Run 14, high warming, high WSEL
Run 15, high warming, high flux

Figure A.134

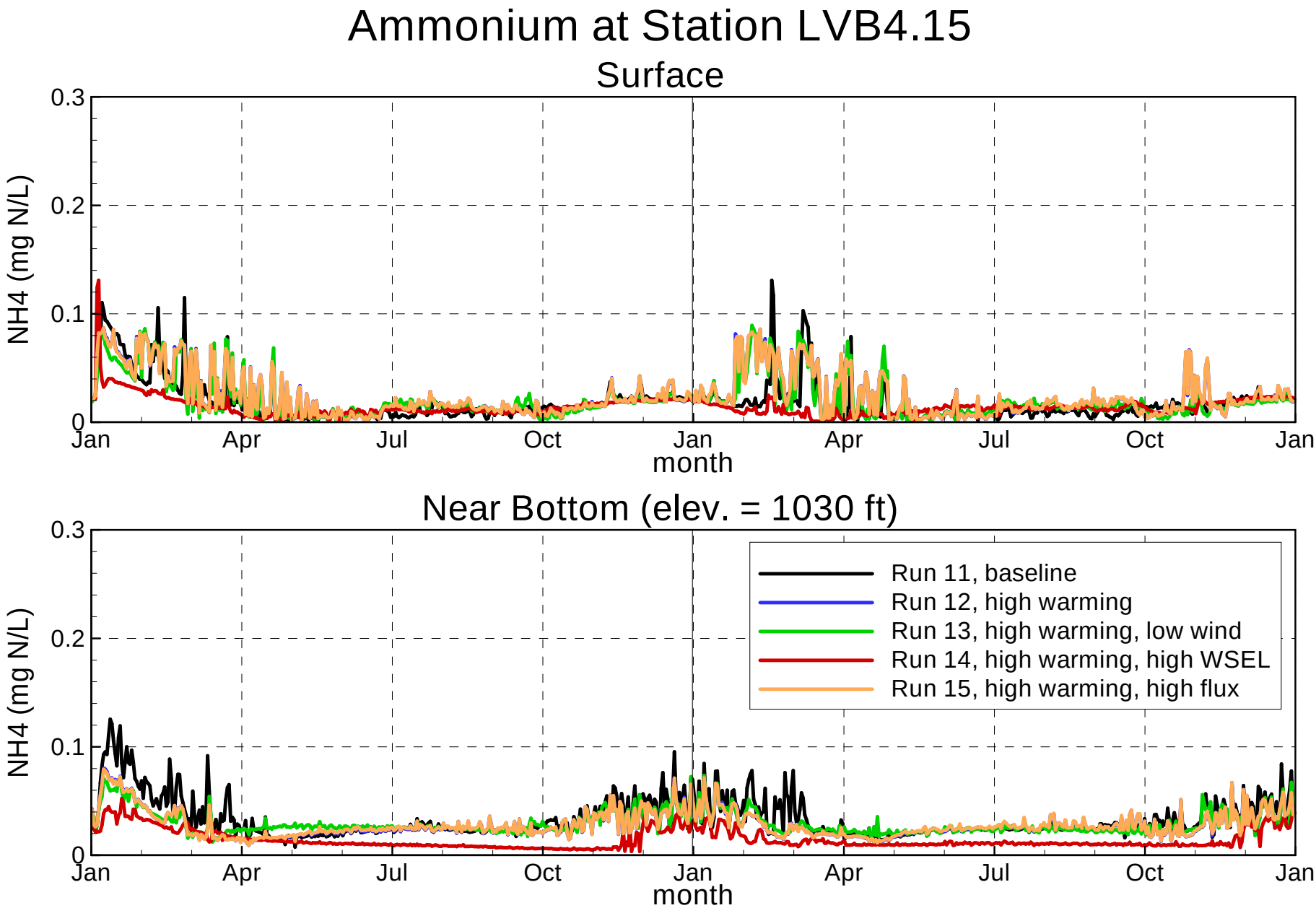
Ammonium at Station LVB4.15
Surface
NH4 (mg N/L)
0.3
0.2
0.1
0
Jan
Apr
Jul
Oct
Jan
Apr
Jul
Oct
Jan
month
Near Bottom (elev. = 1030 ft)
NH4 (mg N/L)
0.3
0.2
0.1
0
Jan
Apr
Jul
Oct
Jan
Apr
Jul
Oct
Jan
month
Run 11, baseline
Run 12, high warming
Run 13, high warming, low wind
Run 14, high warming, high WSEL
Run 15, high warming, high flux

Figure A.135

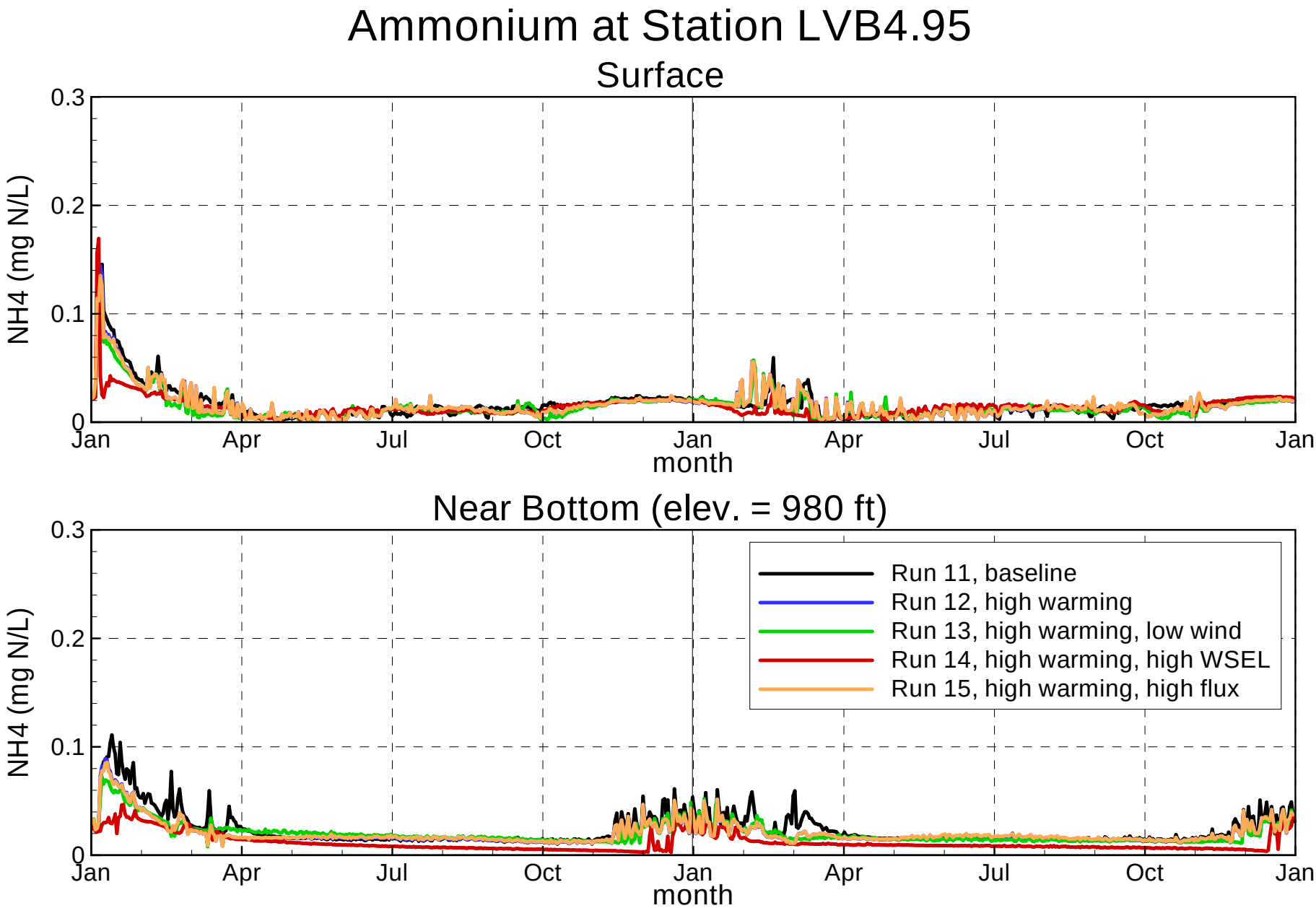
Ammonium at Station LVB4.95
Surface
NH4 (mg N/L)
0.3
0.2
0.1
0
Jan
Apr
Jul
Oct
Jan
Apr
Jul
Oct
Jan
month
Near Bottom (elev. = 980 ft)
NH4 (mg N/L)
0.3
0.2
0.1
0
Jan
Apr
Jul
Oct
Jan
Apr
Jul
Oct
Jan
month
Run 11, baseline
Run 12, high warming
Run 13, high warming, low wind
Run 14, high warming, high WSEL
Run 15, high warming, high flux

Figure A.136

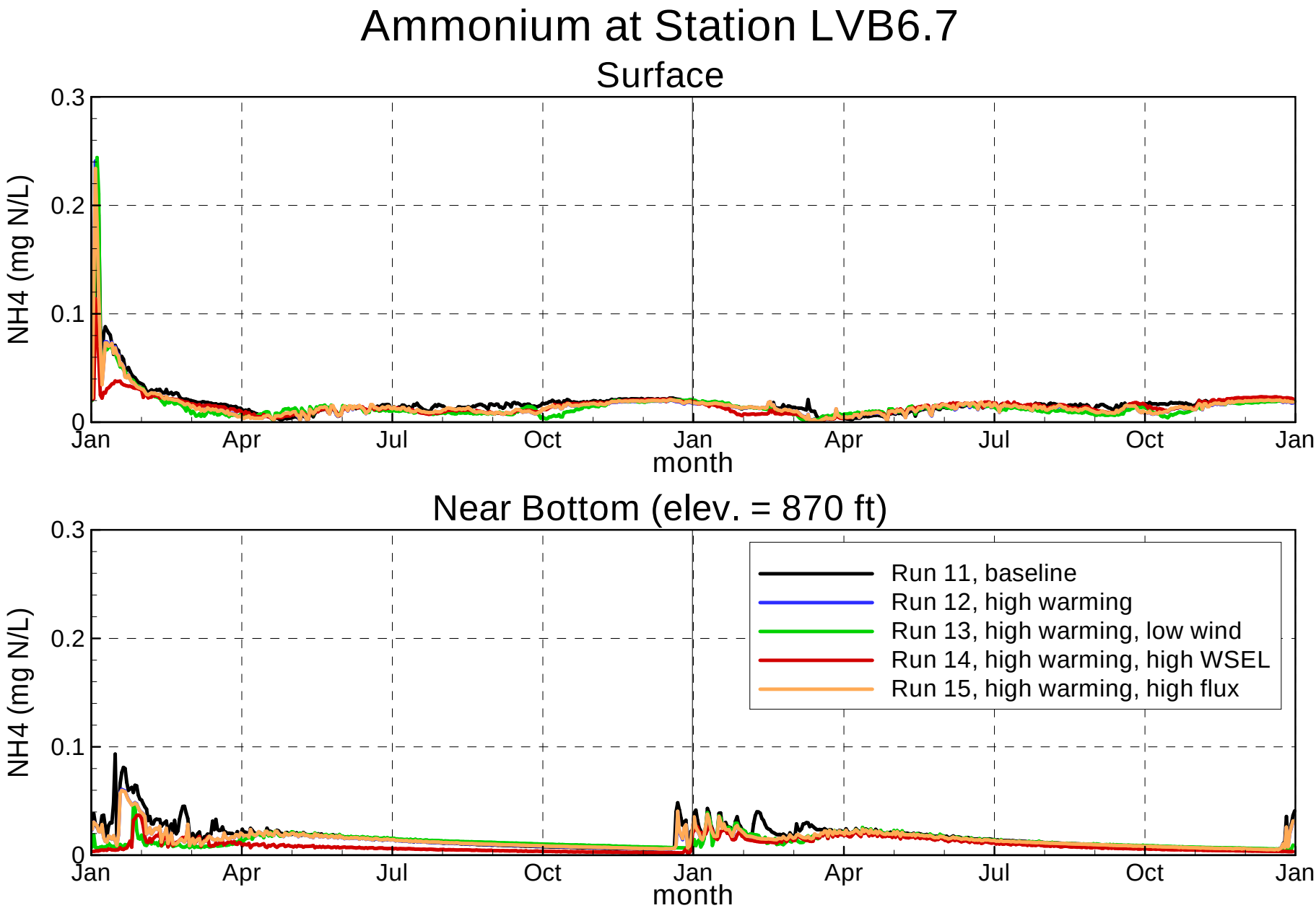
Ammonium at Station LVB6.7
Surface
NH4 (mg N/L)
0.3
0.2
0.1
0
Jan
Apr
Jul
Oct
Jan
Apr
Jul
Oct
Jan
month
Near Bottom (elev. = 870 ft)
NH4 (mg N/L)
0.3
0.2
0.1
0
Jan
Apr
Jul
Oct
Jan
Apr
Jul
Oct
Jan
month
Run 11, baseline
Run 12, high warming
Run 13, high warming, low wind
Run 14, high warming, high WSEL
Run 15, high warming, high flux

Figure A.137

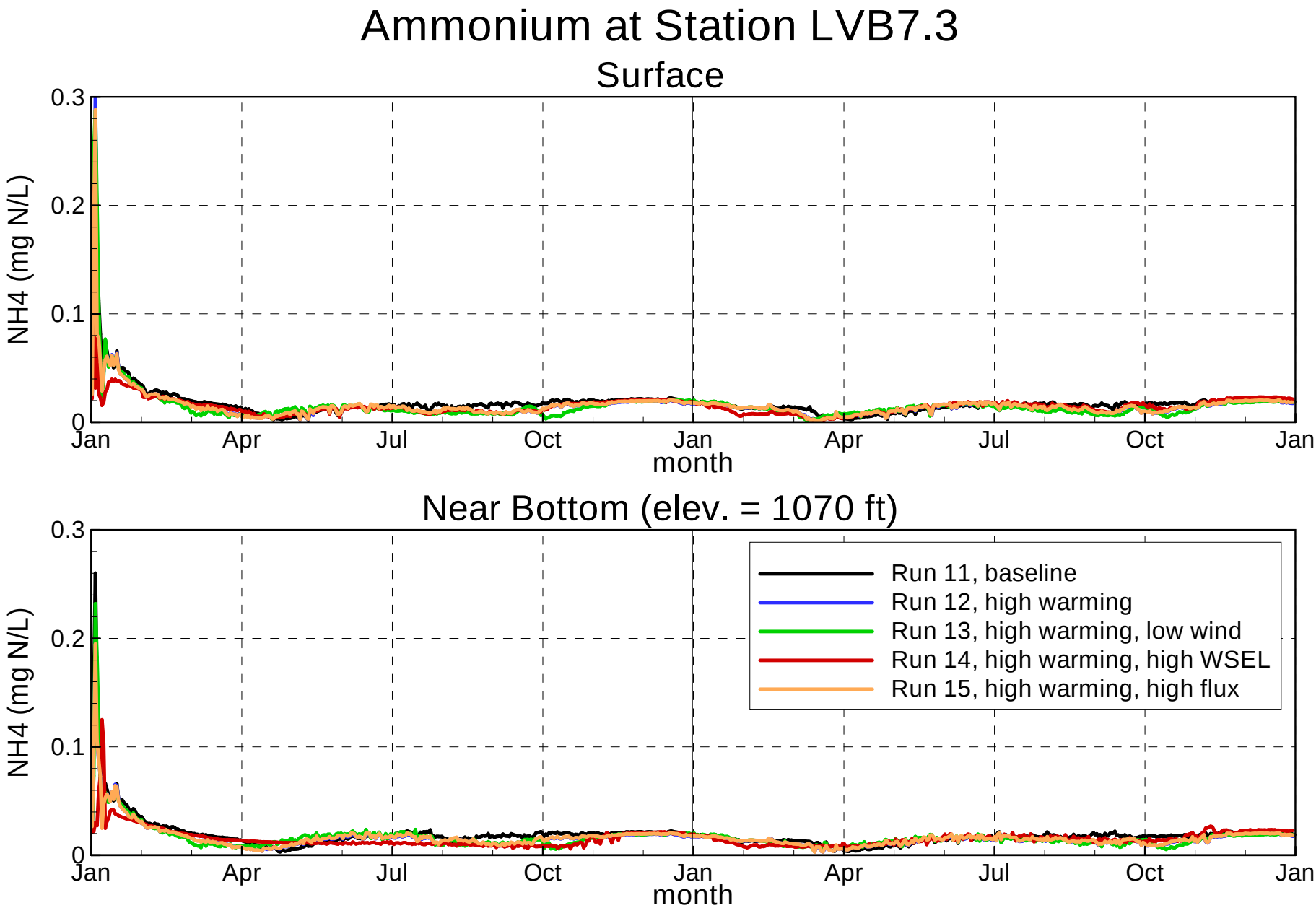
Ammonium at Station LVB7.3
Surface
NH4 (mg N/L)
0.3
0.2
0.1
0
Jan
Apr
Jul
Oct
Jan
Apr
Jul
Oct
Jan
month
Near Bottom (elev. = 1070 ft)
NH4 (mg N/L)
0.3
0.2
0.1
0
Jan
Apr
Jul
Oct
Jan
Apr
Jul
Oct
Jan
month
Run 11, baseline
Run 12, high warming
Run 13, high warming, low wind
Run 14, high warming, high WSEL
Run 15, high warming, high flux

Figure A.138

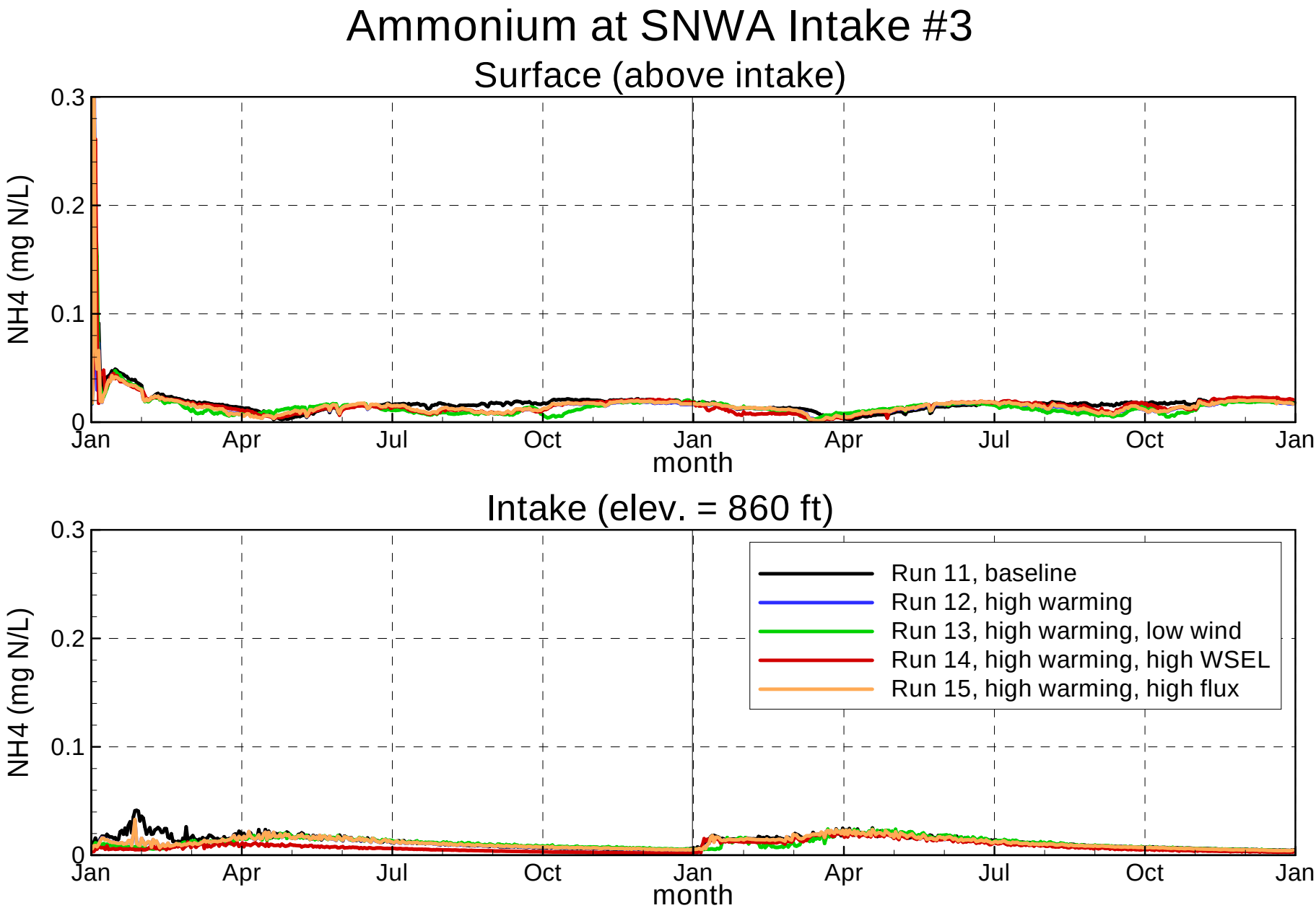
Ammonium at SNWA Intake #3
Surface (above intake)
NH4 (mg N/L)
0.3
0.2
0.1
0
Jan
Apr
Jul
Oct
Jan
Apr
Jul
Oct
Jan
month
Intake (elev. = 860 ft)
NH4 (mg N/L)
0.3
0.2
0.1
0
Jan
Apr
Jul
Oct
Jan
Apr
Jul
Oct
Jan
month
Run 11, baseline
Run 12, high warming
Run 13, high warming, low wind
Run 14, high warming, high WSEL
Run 15, high warming, high flux

Figure A.139

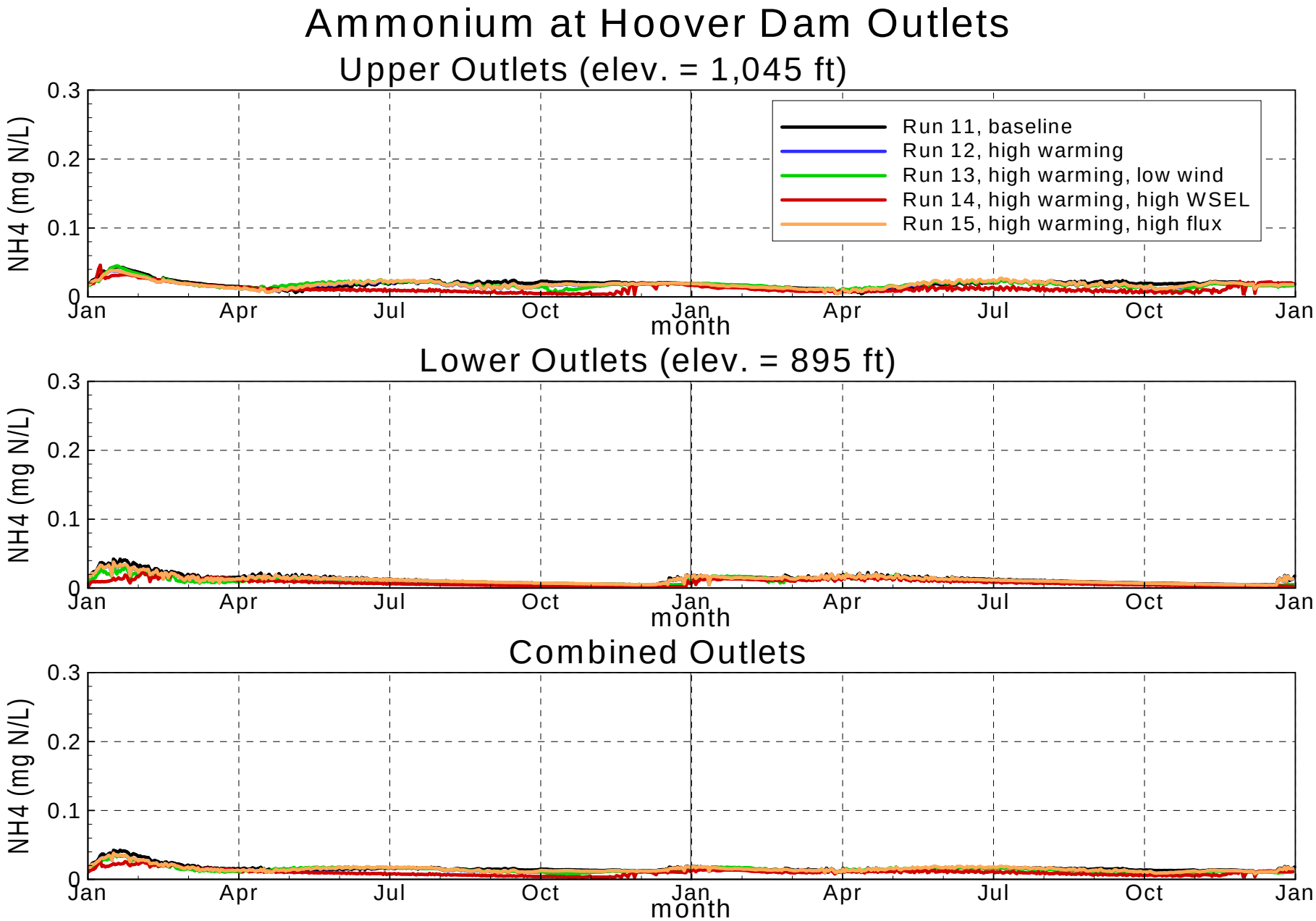

Figure A.140

FLOW SCIENCE

Nitrate at Station CR394.0

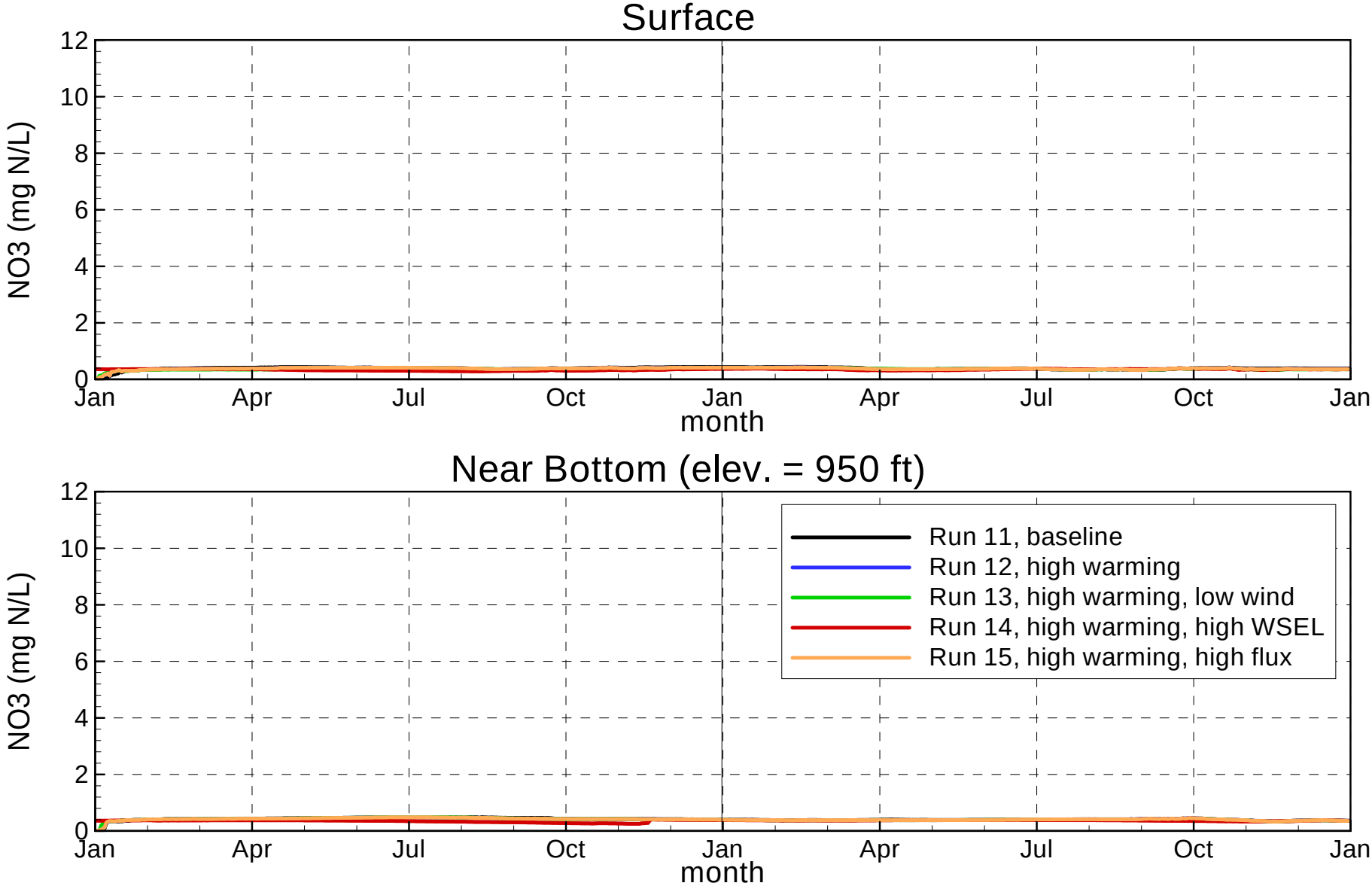

Figure A.141

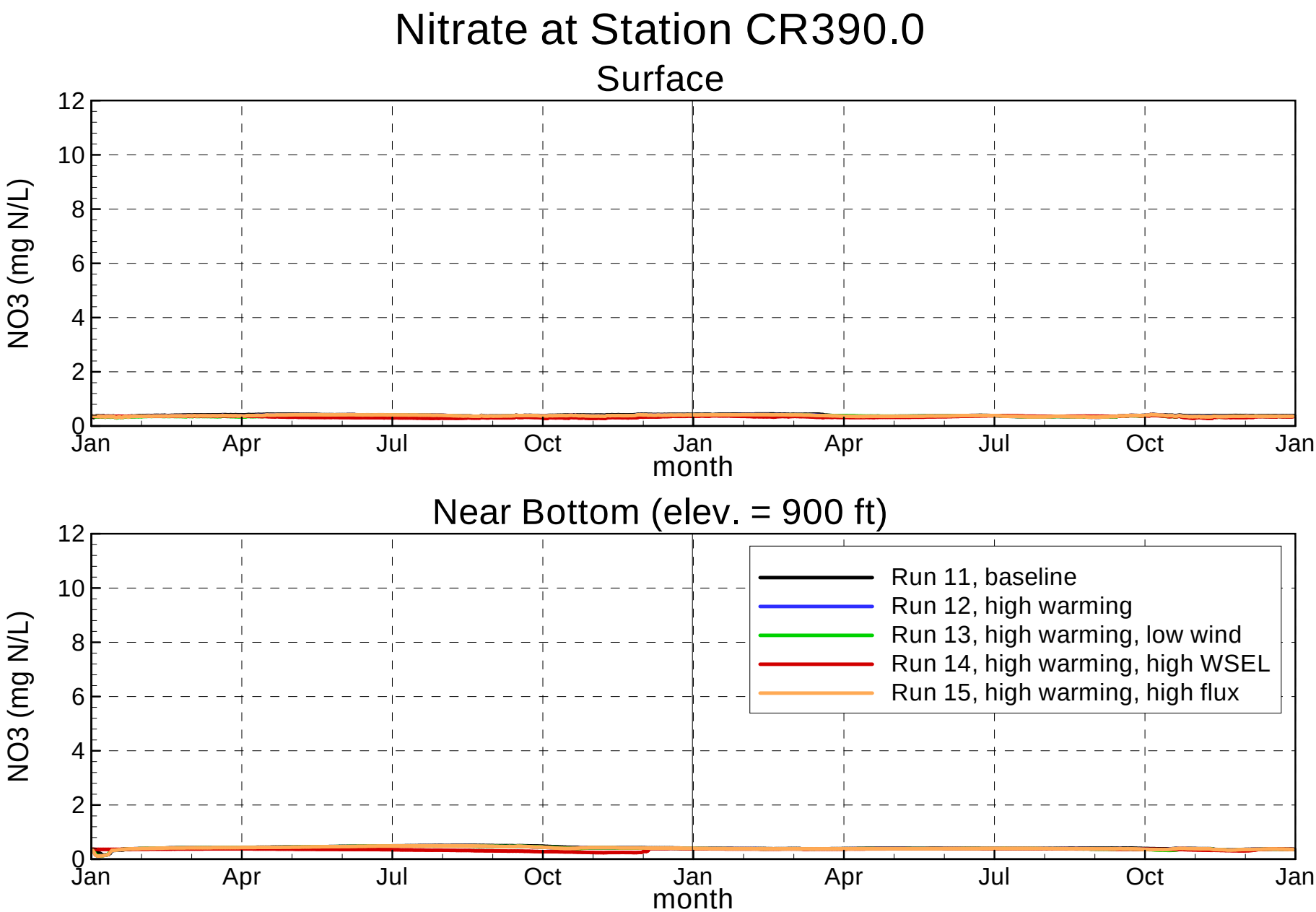
Nitrate at Station CR390.0
Surface
NO3 (mg N/L)
12
10
8
6
4
2
0
Jan
Apr
Jul
Oct
Jan
Apr
Jul
Oct
Jan
month
Near Bottom (elev. = 900 ft)
NO3 (mg N/L)
Run 11, baseline
Run 12, high warming
Run 13, high warming, low wind
Run 14, high warming, high WSEL
Run 15, high warming, high flux
month

Figure A.142

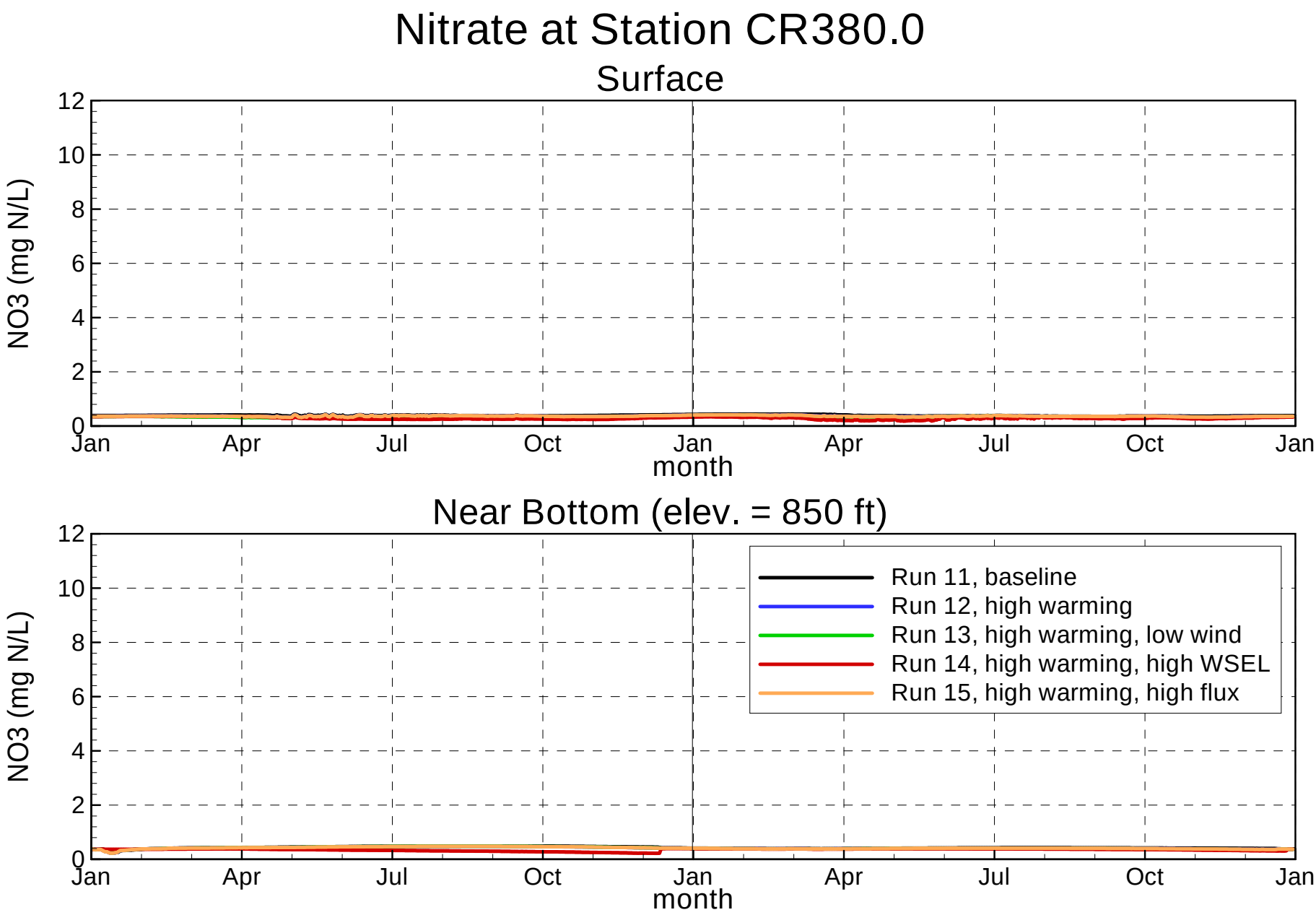
Nitrate at Station CR380.0
Surface
NO3 (mg N/L)
12
10
8
6
4
2
0
Jan
Apr
Jul
Oct
Jan
Apr
Jul
Oct
Jan
month
Near Bottom (elev. = 850 ft)
NO3 (mg N/L)
Run 11, baseline
Run 12, high warming
Run 13, high warming, low wind
Run 14, high warming, high WSEL
Run 15, high warming, high flux
month

Figure A.143

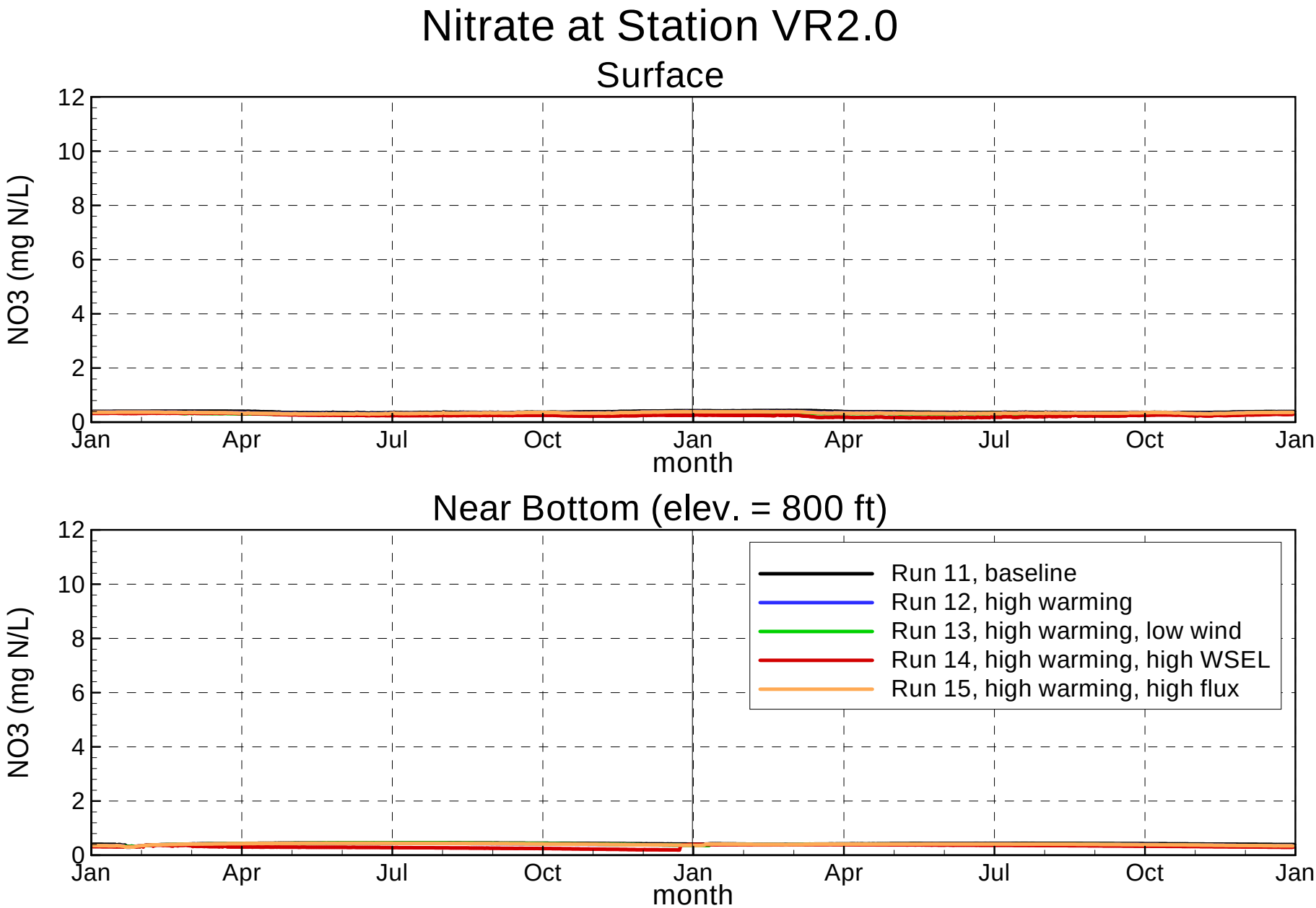
Nitrate at Station VR2.0
Surface
NO3 (mg N/L)
12
10
8
6
4
2
0
Jan
Apr
Jul
Oct
Jan
Apr
Jul
Oct
Jan
month
Near Bottom (elev. = 800 ft)
NO3 (mg N/L)
Run 11, baseline
Run 12, high warming
Run 13, high warming, low wind
Run 14, high warming, high WSEL
Run 15, high warming, high flux
month

Figure A.144

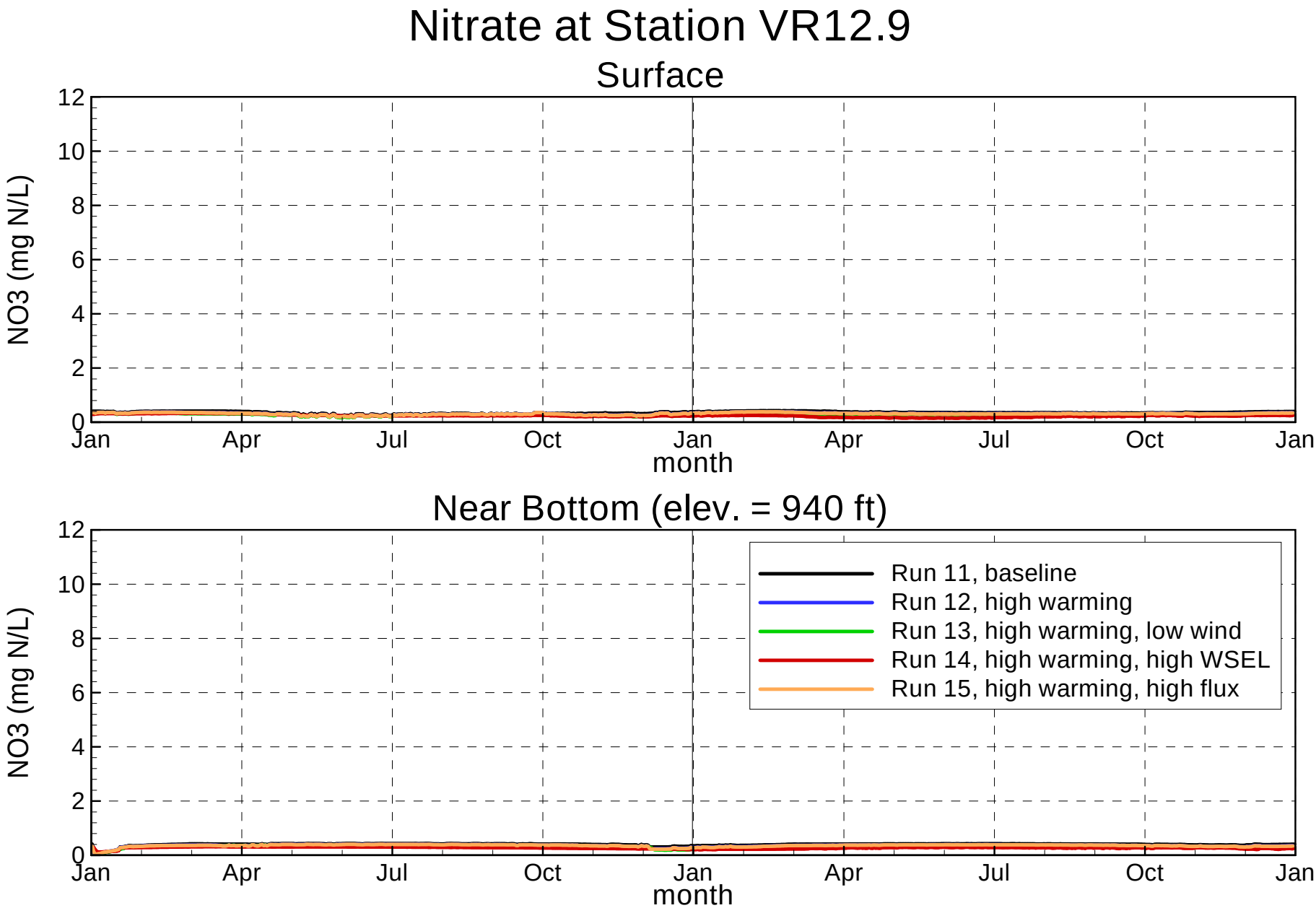
Nitrate at Station VR12.9
Surface
NO3 (mg N/L)
12
10
8
6
4
2
0
Jan
Apr
Jul
Oct
Jan
Apr
Jul
Oct
Jan
month
Near Bottom (elev. = 940 ft)
NO3 (mg N/L)
Run 11, baseline
Run 12, high warming
Run 13, high warming, low wind
Run 14, high warming, high WSEL
Run 15, high warming, high flux
month

Figure A.145

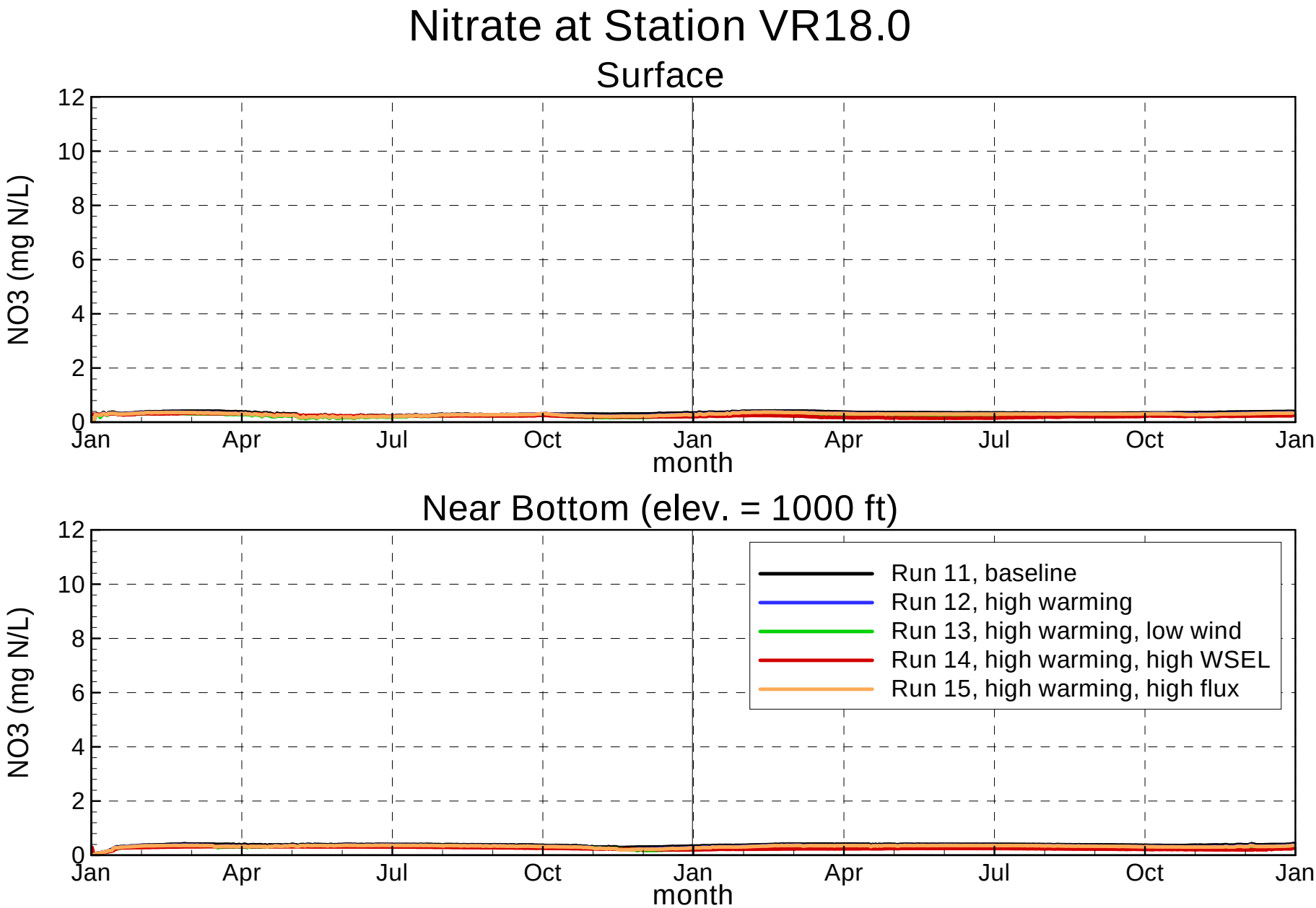
Nitrate at Station VR18.0
Surface
NO3 (mg N/L)
12
10
8
6
4
2
0
Jan
Apr
Jul
Oct
Jan
Apr
Jul
Oct
Jan
month
Near Bottom (elev. = 1000 ft)
NO3 (mg N/L)
Run 11, baseline
Run 12, high warming
Run 13, high warming, low wind
Run 14, high warming, high WSEL
Run 15, high warming, high flux
month

Figure A.146

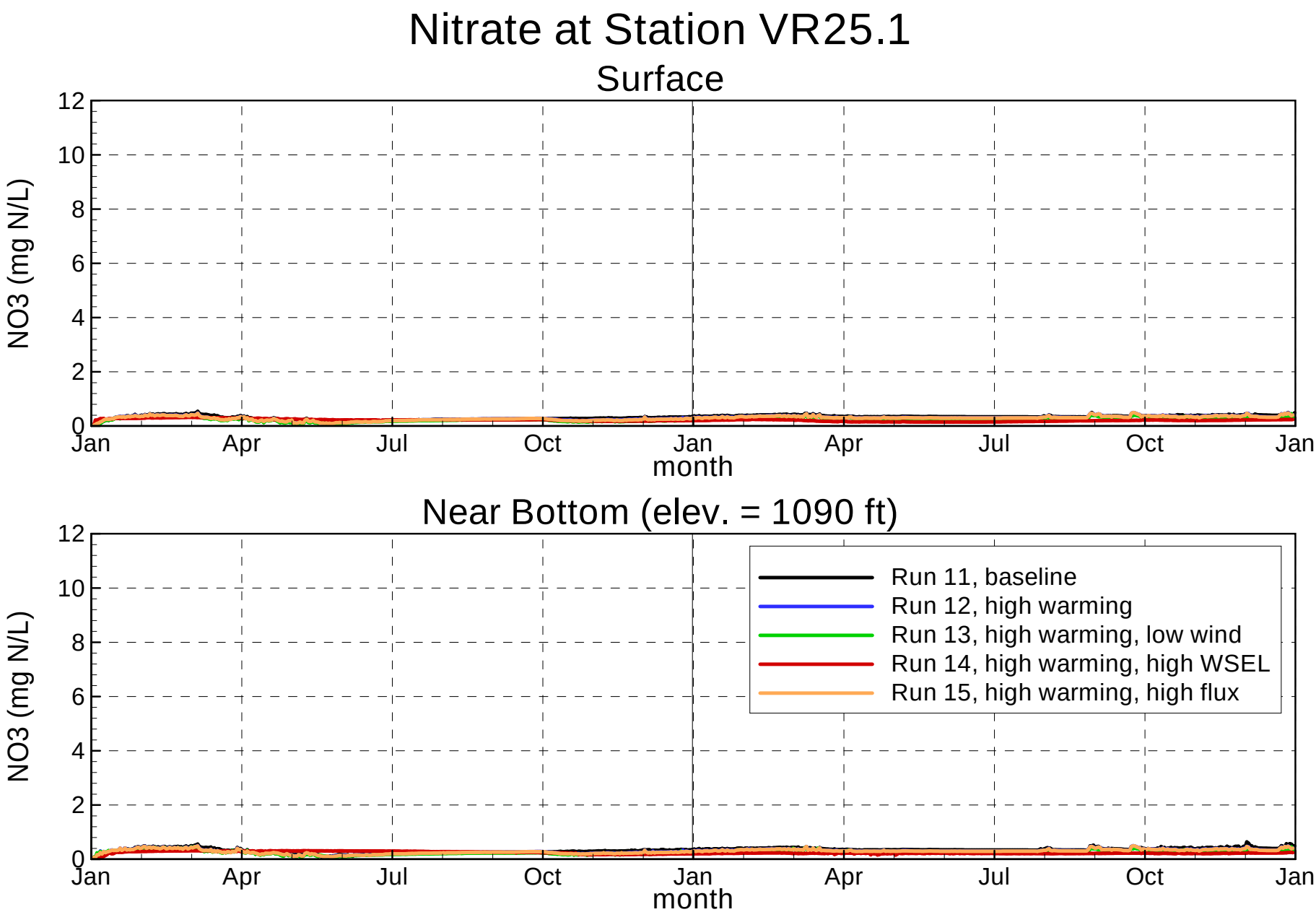
Nitrate at Station VR25.1
Surface
NO3 (mg N/L)
12
10
8
6
4
2
0
Jan
Apr
Jul
Oct
Jan
Apr
Jul
Oct
Jan
month
Near Bottom (elev. = 1090 ft)
NO3 (mg N/L)
Run 11, baseline
Run 12, high warming
Run 13, high warming, low wind
Run 14, high warming, high WSEL
Run 15, high warming, high flux
month

Figure A.147

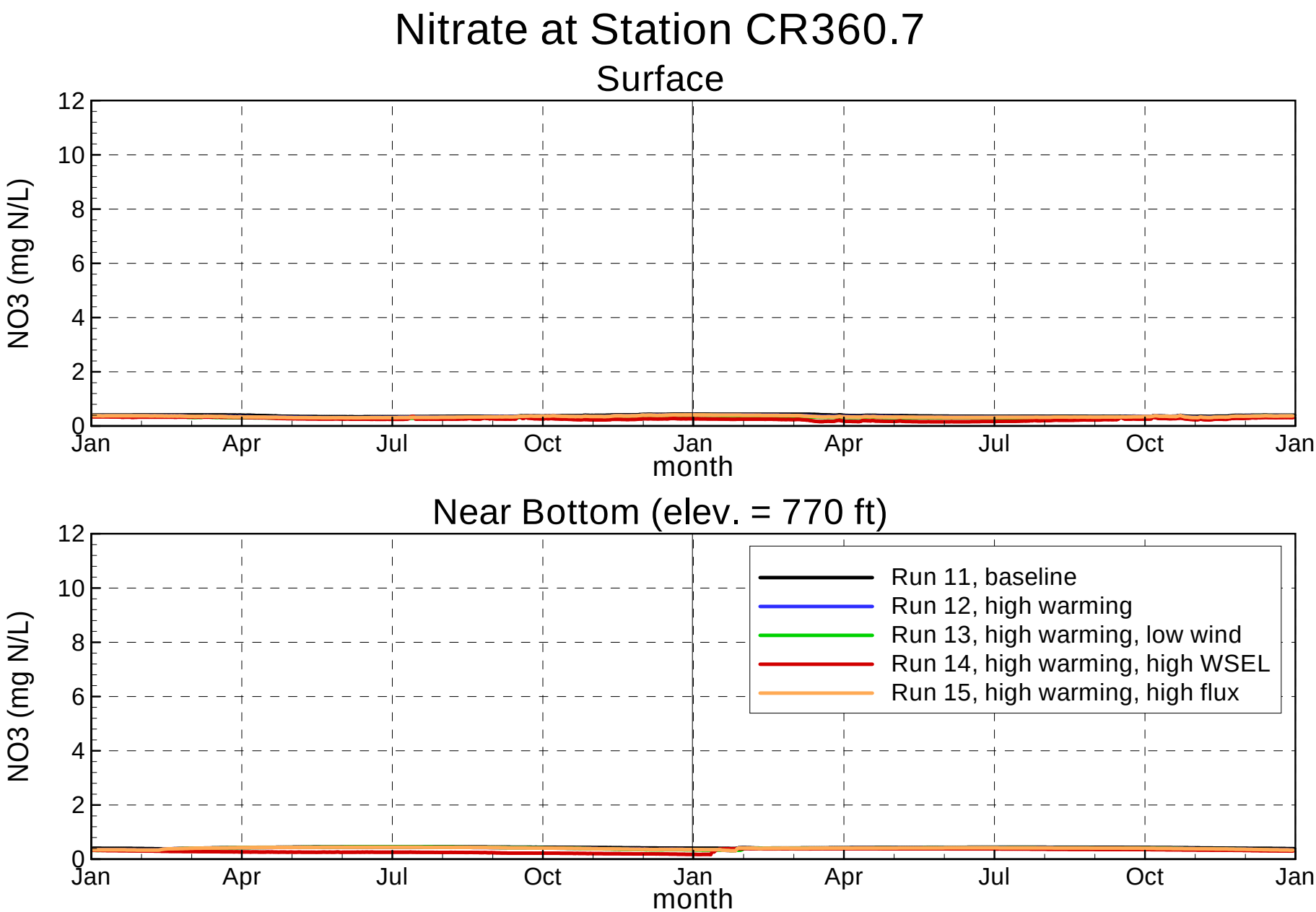
Nitrate at Station CR360.7
Surface
NO3 (mg N/L)
12
10
8
6
4
2
0
Jan
Apr
Jul
Oct
Jan
Apr
Jul
Oct
Jan
month
Near Bottom (elev. = 770 ft)
NO3 (mg N/L)
Run 11, baseline
Run 12, high warming
Run 13, high warming, low wind
Run 14, high warming, high WSEL
Run 15, high warming, high flux
month

Figure A.148

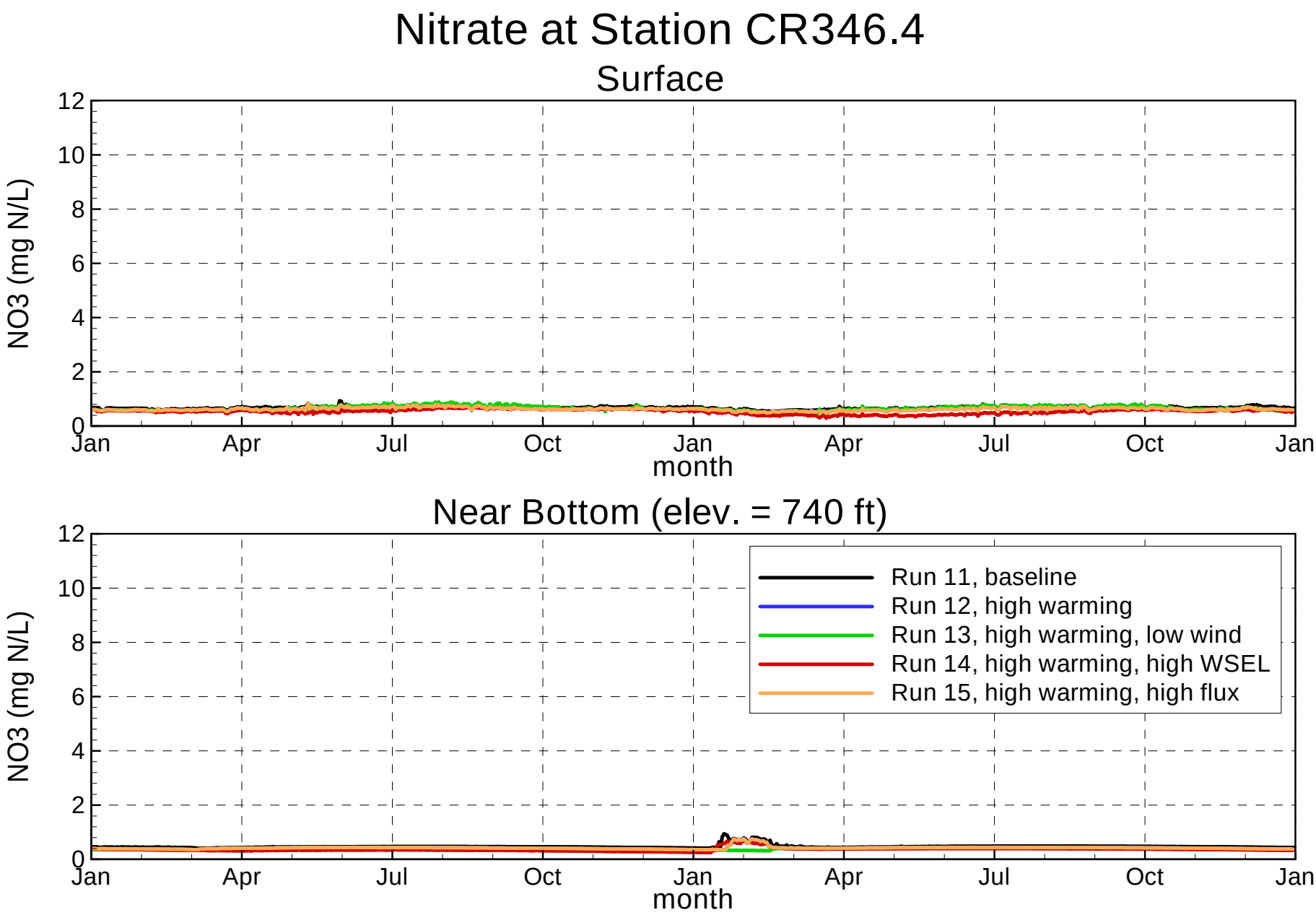
Nitrate at Station CR346.4
Surface
NO3 (mg N/L)
12
10
8
6
4
2
0
Jan
Apr
Jul
Oct
Jan
Apr
Jul
Oct
Jan
month
Near Bottom (elev. = 740 ft)
NO3 (mg N/L)
Run 11, baseline
Run 12, high warming
Run 13, high warming, low wind
Run 14, high warming, high WSEL
Run 15, high warming, high flux
month

Figure A.149

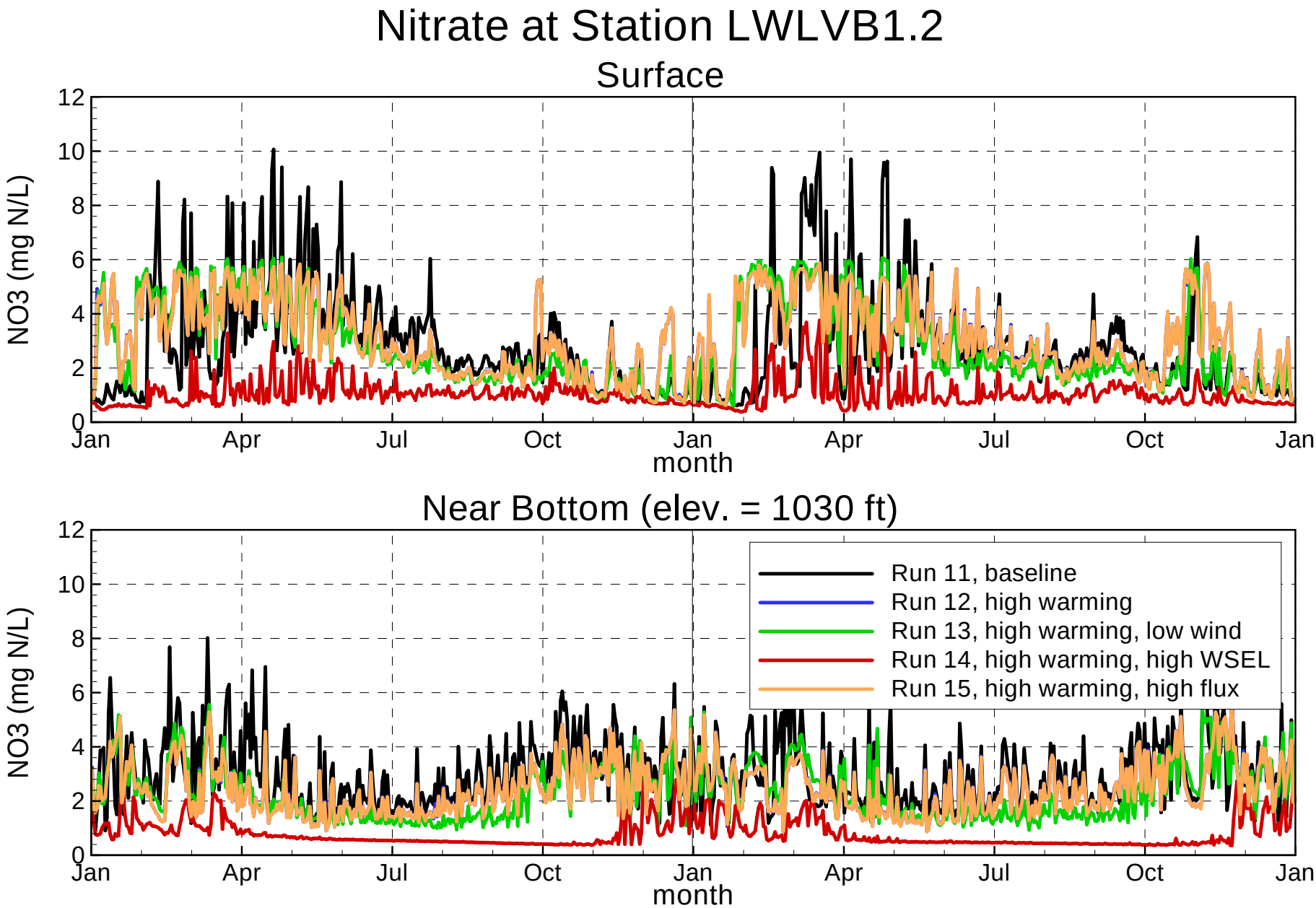
Nitrate at Station LWLVB1.2
Surface
NO3 (mg N/L)
0
2
4
6
8
10
12
Jan
Apr
Jul
Oct
Jan
Apr
Jul
Oct
Jan
month
Near Bottom (elev. = 1030 ft)
NO3 (mg N/L)
Run 11, baseline
Run 12, high warming
Run 13, high warming, low wind
Run 14, high warming, high WSEL
Run 15, high warming, high flux
month

Figure A.150

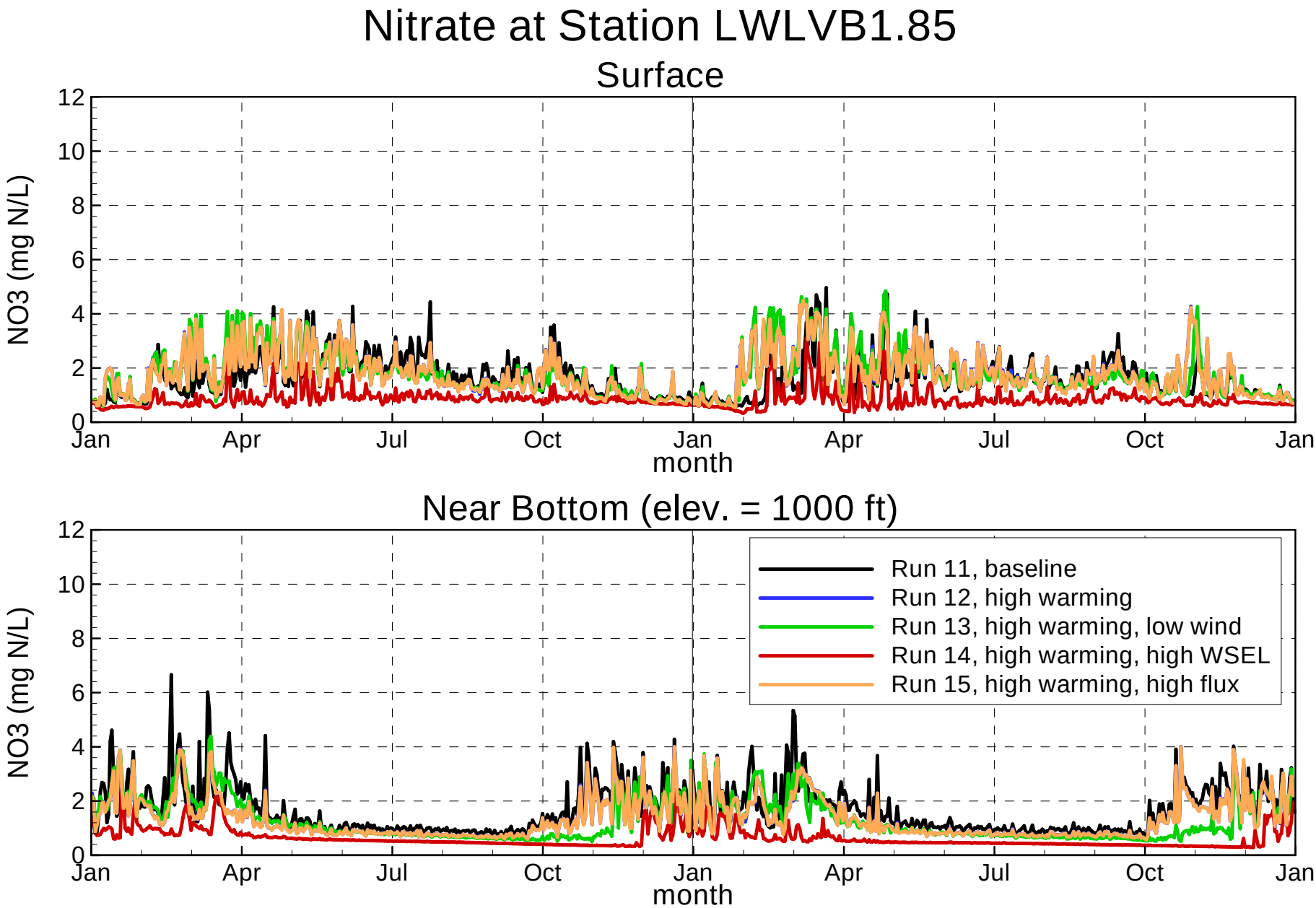
Nitrate at Station LWLVB1.85
Surface
NO3 (mg N/L)
12
10
8
6
4
2
0
Jan
Apr
Jul
Oct
Jan
Apr
Jul
Oct
Jan
month
Near Bottom (elev. = 1000 ft)
NO3 (mg N/L)
Run 11, baseline
Run 12, high warming
Run 13, high warming, low wind
Run 14, high warming, high WSEL
Run 15, high warming, high flux
month

Figure A.151

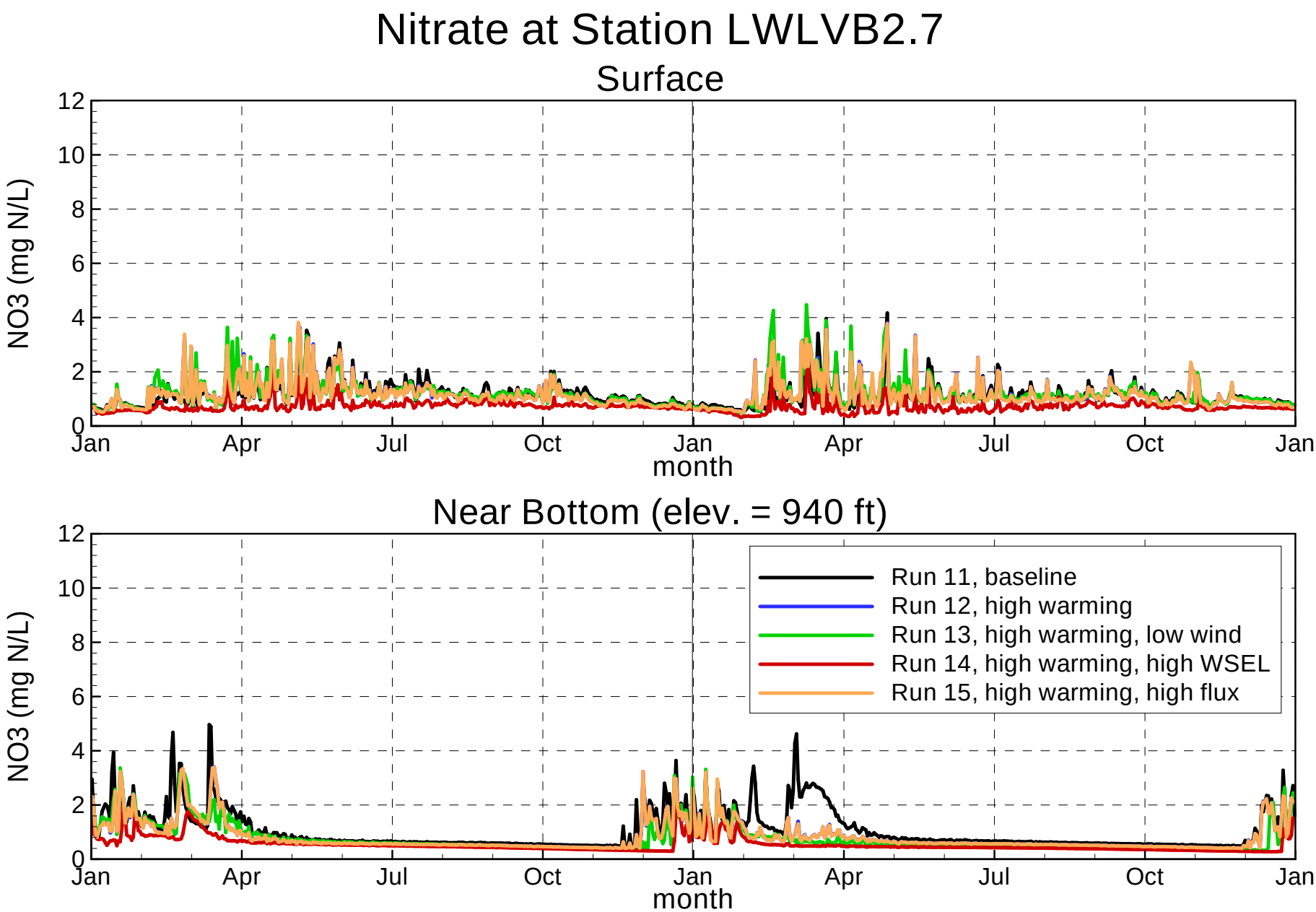
Nitrate at Station LWLVB2.7
Surface
NO3 (mg N/L)
12
10
8
6
4
2
0
Jan
Apr
Jul
Oct
Jan
Apr
Jul
Oct
Jan
month
Near Bottom (elev. = 940 ft)
NO3 (mg N/L)
Run 11, baseline
Run 12, high warming
Run 13, high warming, low wind
Run 14, high warming, high WSEL
Run 15, high warming, high flux
month

Figure A.152

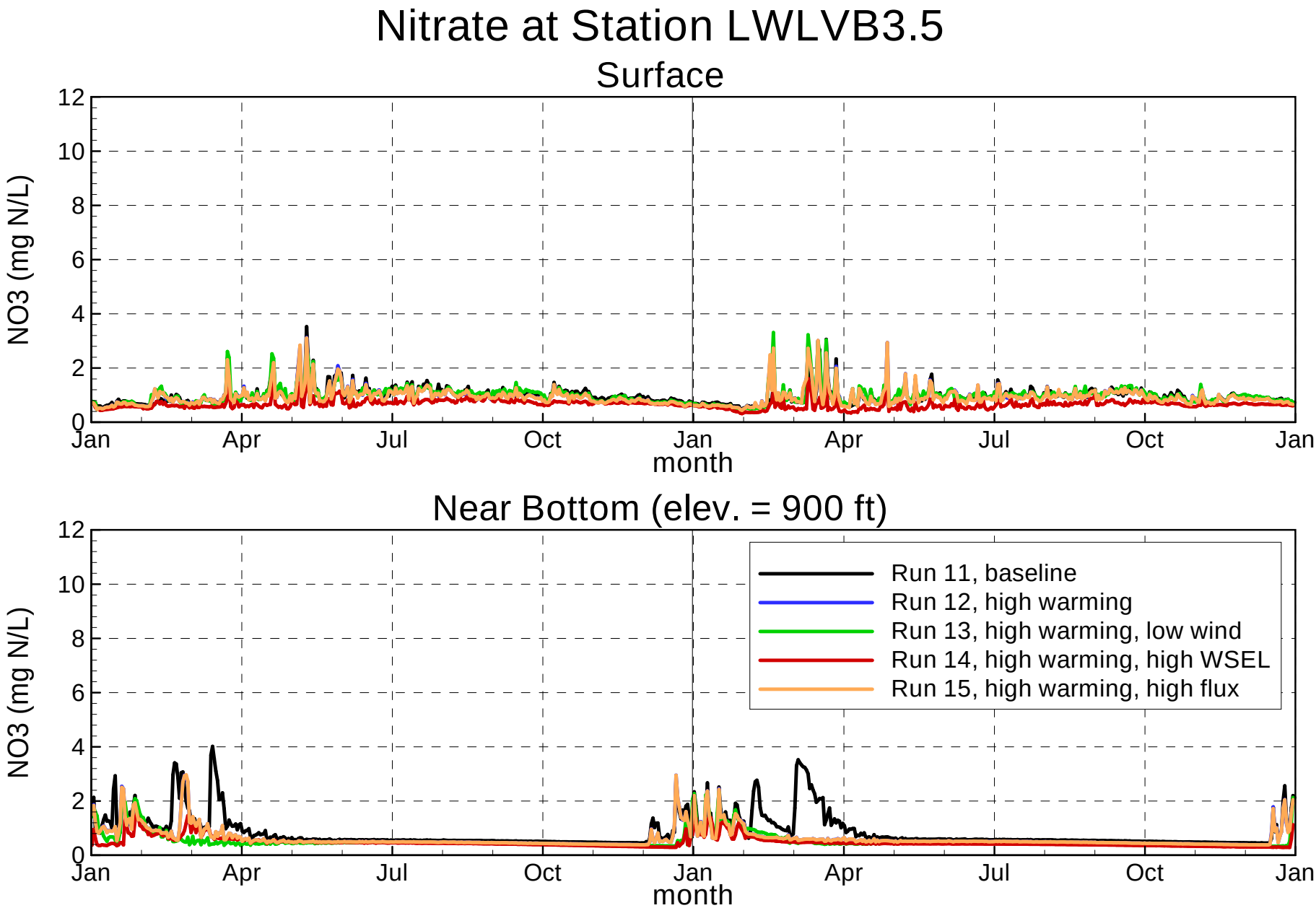
Nitrate at Station LWLVB3.5
Surface
NO3 (mg N/L)
12
10
8
6
4
2
0
Jan
Apr
Jul
Oct
Jan
Apr
Jul
Oct
Jan
month
Near Bottom (elev. = 900 ft)
NO3 (mg N/L)
Run 11, baseline
Run 12, high warming
Run 13, high warming, low wind
Run 14, high warming, high WSEL
Run 15, high warming, high flux
month

Figure A.153

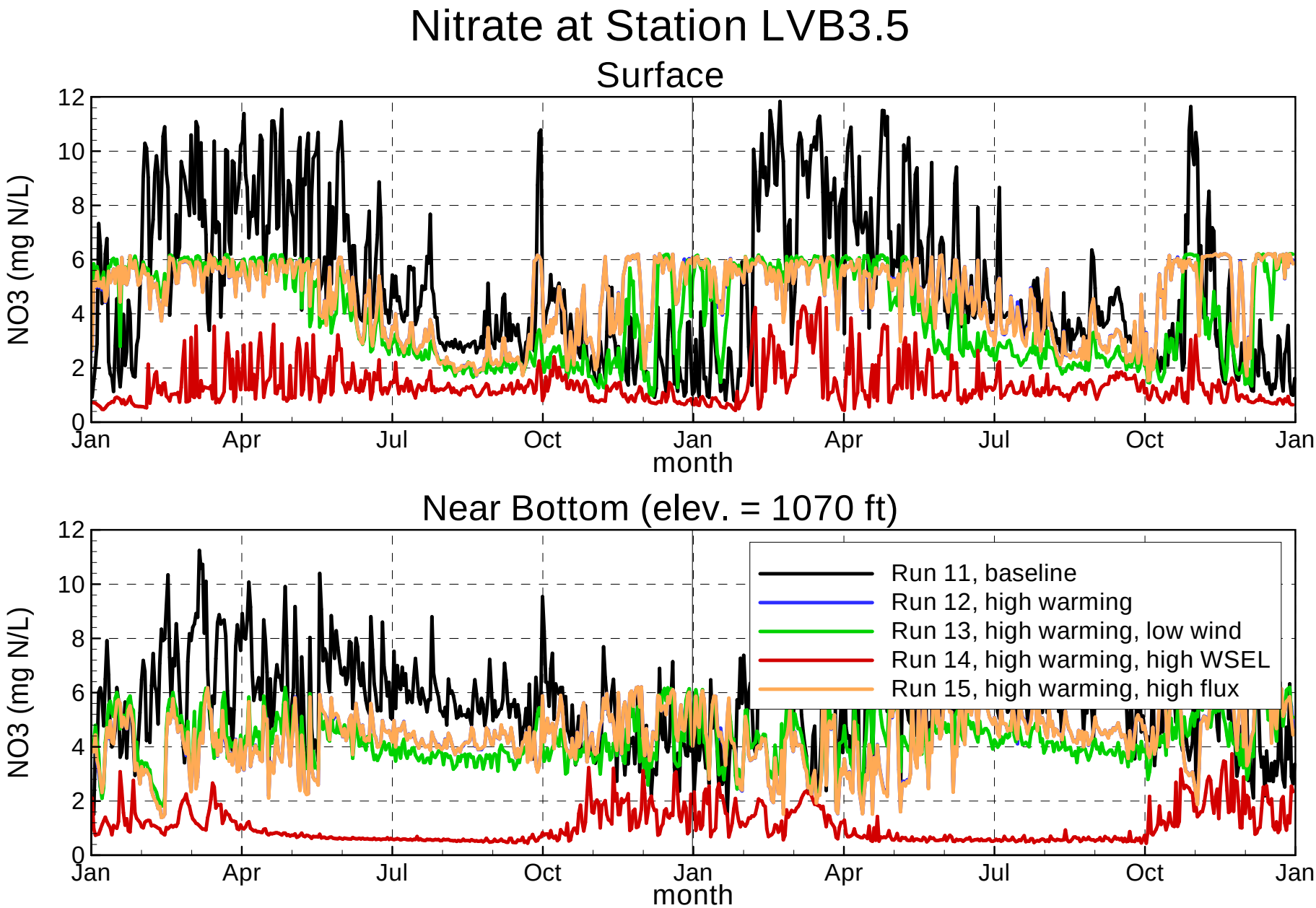
Nitrate at Station LVB3.5
Surface
NO3 (mg N/L)
12
10
8
6
4
2
0
Jan
Apr
Jul
Oct
Jan
Apr
Jul
Oct
Jan
month
Near Bottom (elev. = 1070 ft)
NO3 (mg N/L)
Run 11, baseline
Run 12, high warming
Run 13, high warming, low wind
Run 14, high warming, high WSEL
Run 15, high warming, high flux
month

Figure A.154

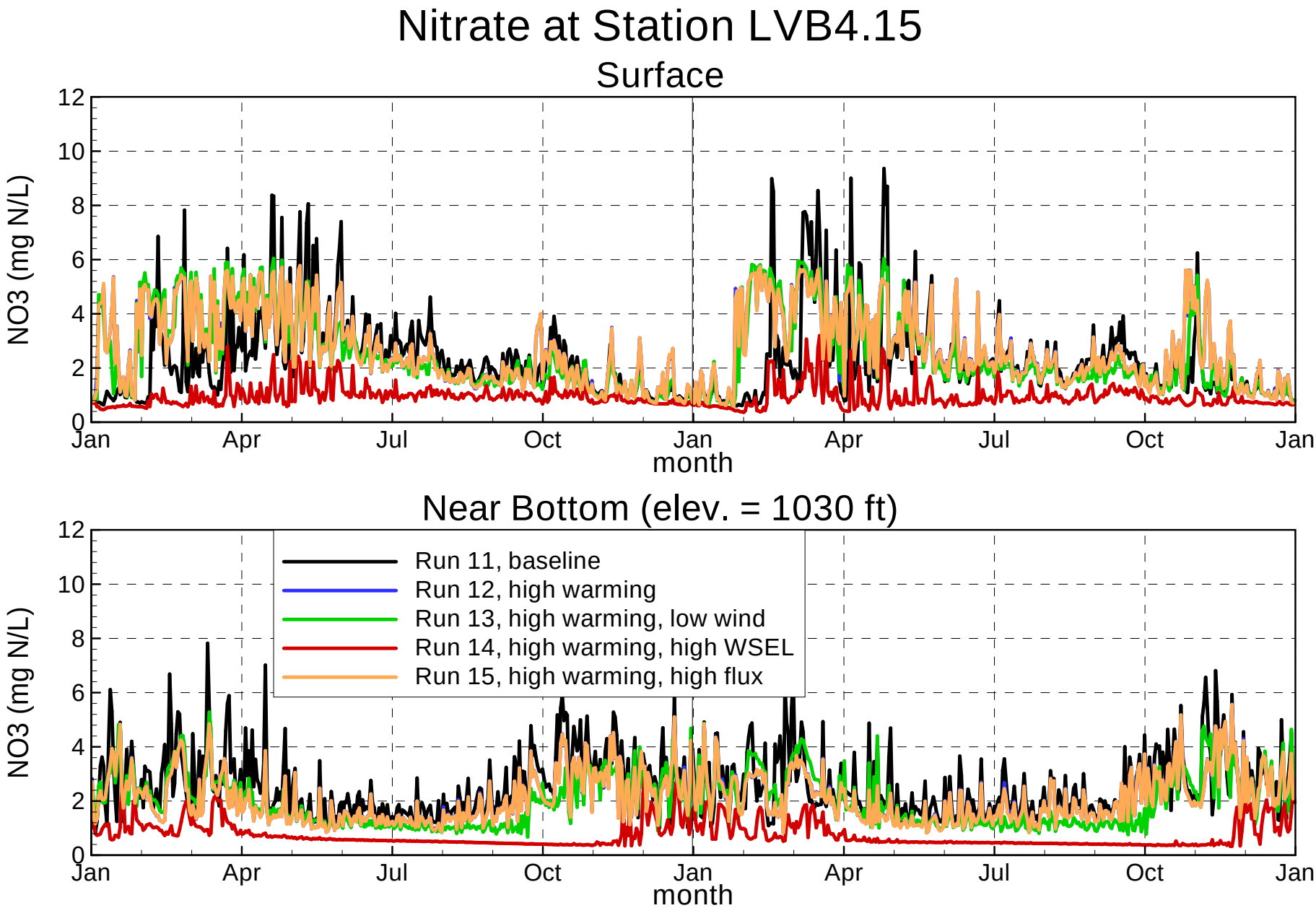
Nitrate at Station LVB4.15
Surface
NO3 (mg N/L)
0
2
4
6
8
10
12
Jan
Apr
Jul
Oct
Jan
Apr
Jul
Oct
Jan
month
Near Bottom (elev. = 1030 ft)
Run 11, baseline
Run 12, high warming
Run 13, high warming, low wind
Run 14, high warming, high WSEL
Run 15, high warming, high flux

Figure A.155

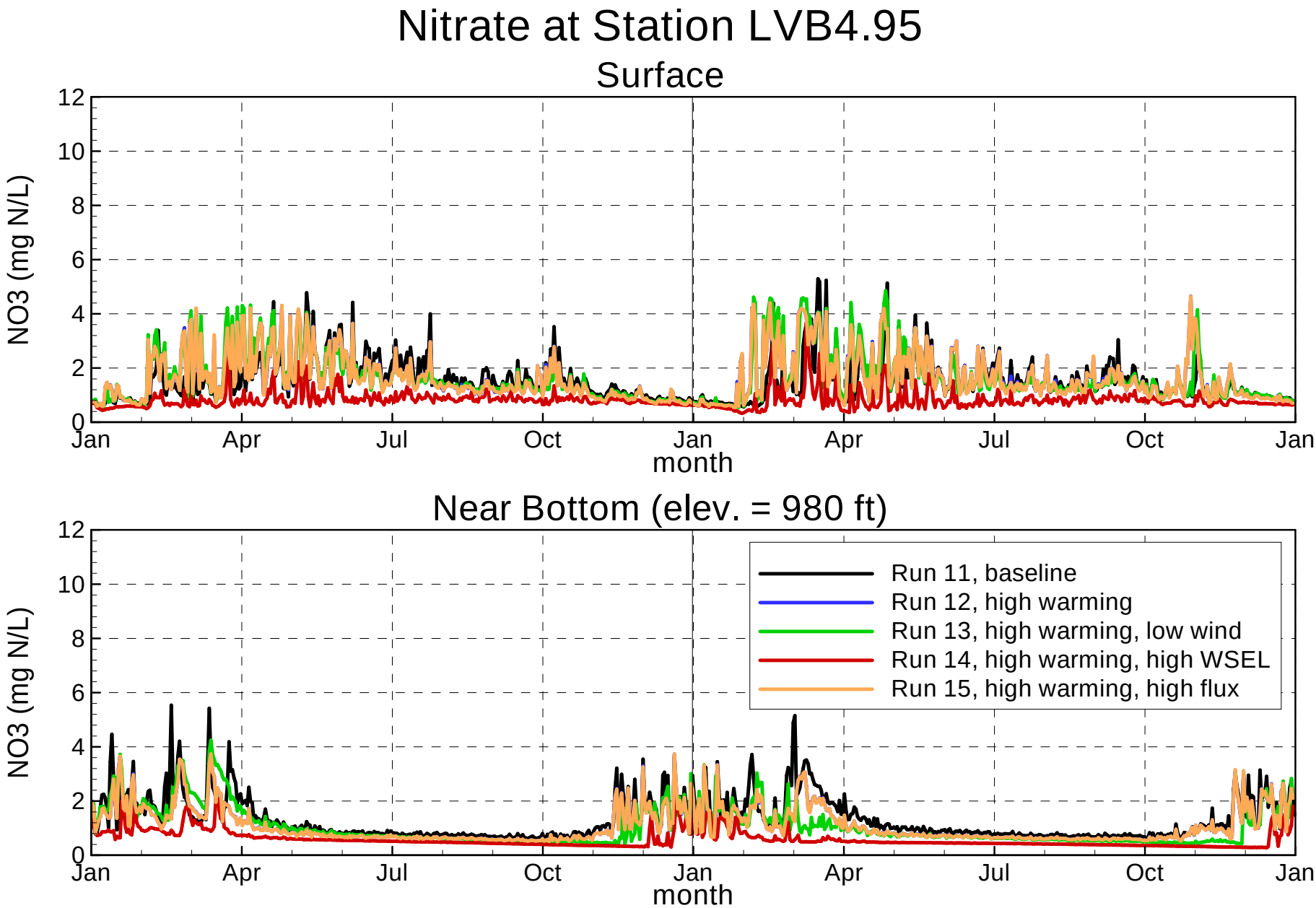
Nitrate at Station LVB4.95
Surface
NO3 (mg N/L)
0
2
4
6
8
10
12
Jan
Apr
Jul
Oct
Jan
Apr
Jul
Oct
Jan
month
Near Bottom (elev. = 980 ft)
NO3 (mg N/L)
Run 11, baseline
Run 12, high warming
Run 13, high warming, low wind
Run 14, high warming, high WSEL
Run 15, high warming, high flux
month

Figure A.156

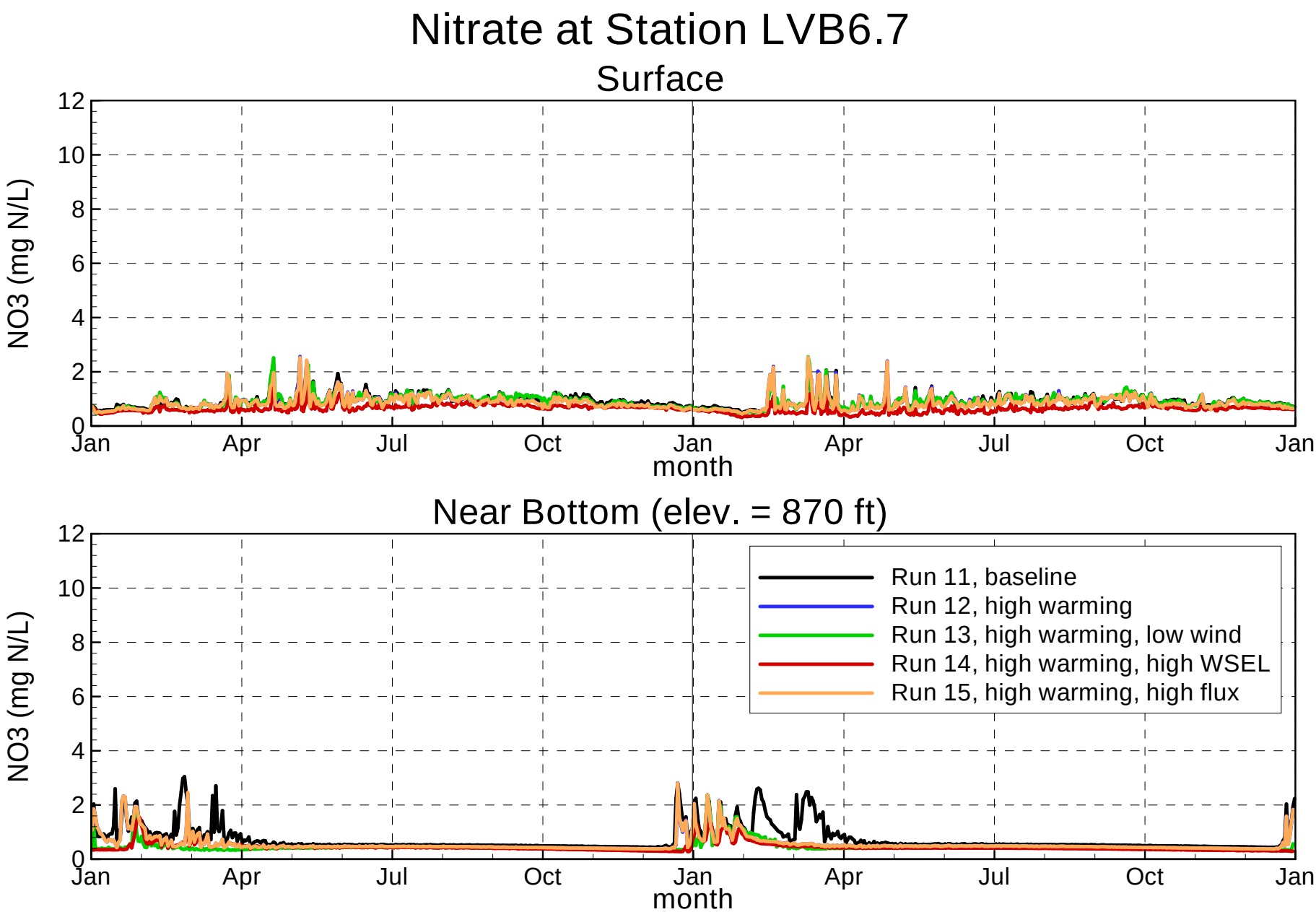
Nitrate at Station LVB6.7
Surface
NO3 (mg N/L)
12
10
8
6
4
2
0
Jan
Apr
Jul
Oct
Jan
Apr
Jul
Oct
Jan
month
Near Bottom (elev. = 870 ft)
NO3 (mg N/L)
Run 11, baseline
Run 12, high warming
Run 13, high warming, low wind
Run 14, high warming, high WSEL
Run 15, high warming, high flux
month

Figure A.157

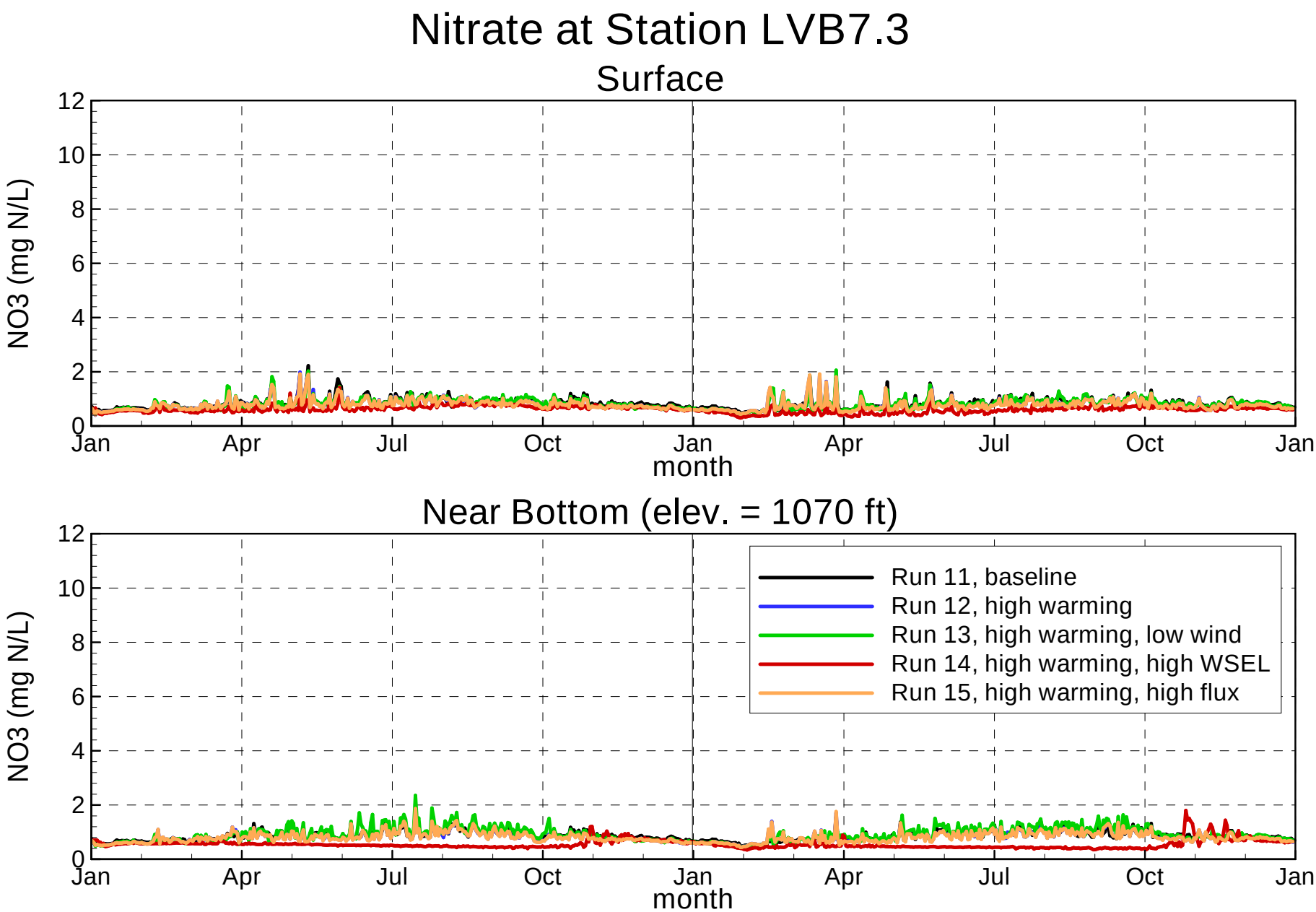
Nitrate at Station LVB7.3
Surface
NO3 (mg N/L)
12
10
8
6
4
2
0
Jan
Apr
Jul
Oct
Jan
Apr
Jul
Oct
Jan
month
Near Bottom (elev. = 1070 ft)
NO3 (mg N/L)
Run 11, baseline
Run 12, high warming
Run 13, high warming, low wind
Run 14, high warming, high WSEL
Run 15, high warming, high flux
month

Figure A.158

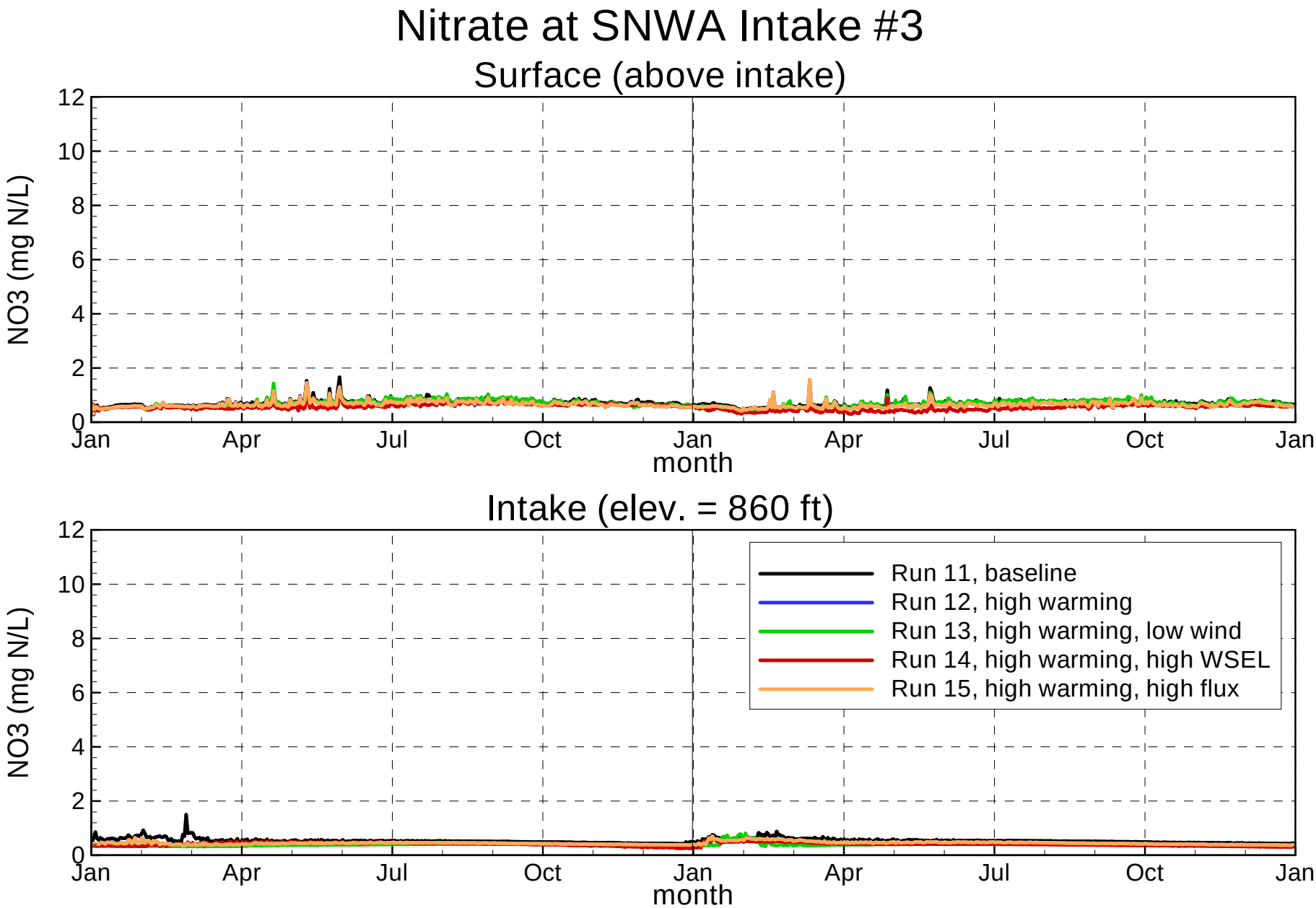
Nitrate at SNWA Intake #3
Surface (above intake)
NO3 (mg N/L)
12
10
8
6
4
2
0
Jan
Apr
Jul
Oct
Jan
Apr
Jul
Oct
Jan
month
Intake (elev. = 860 ft)
NO3 (mg N/L)
Run 11, baseline
Run 12, high warming
Run 13, high warming, low wind
Run 14, high warming, high WSEL
Run 15, high warming, high flux
month

Figure A.159

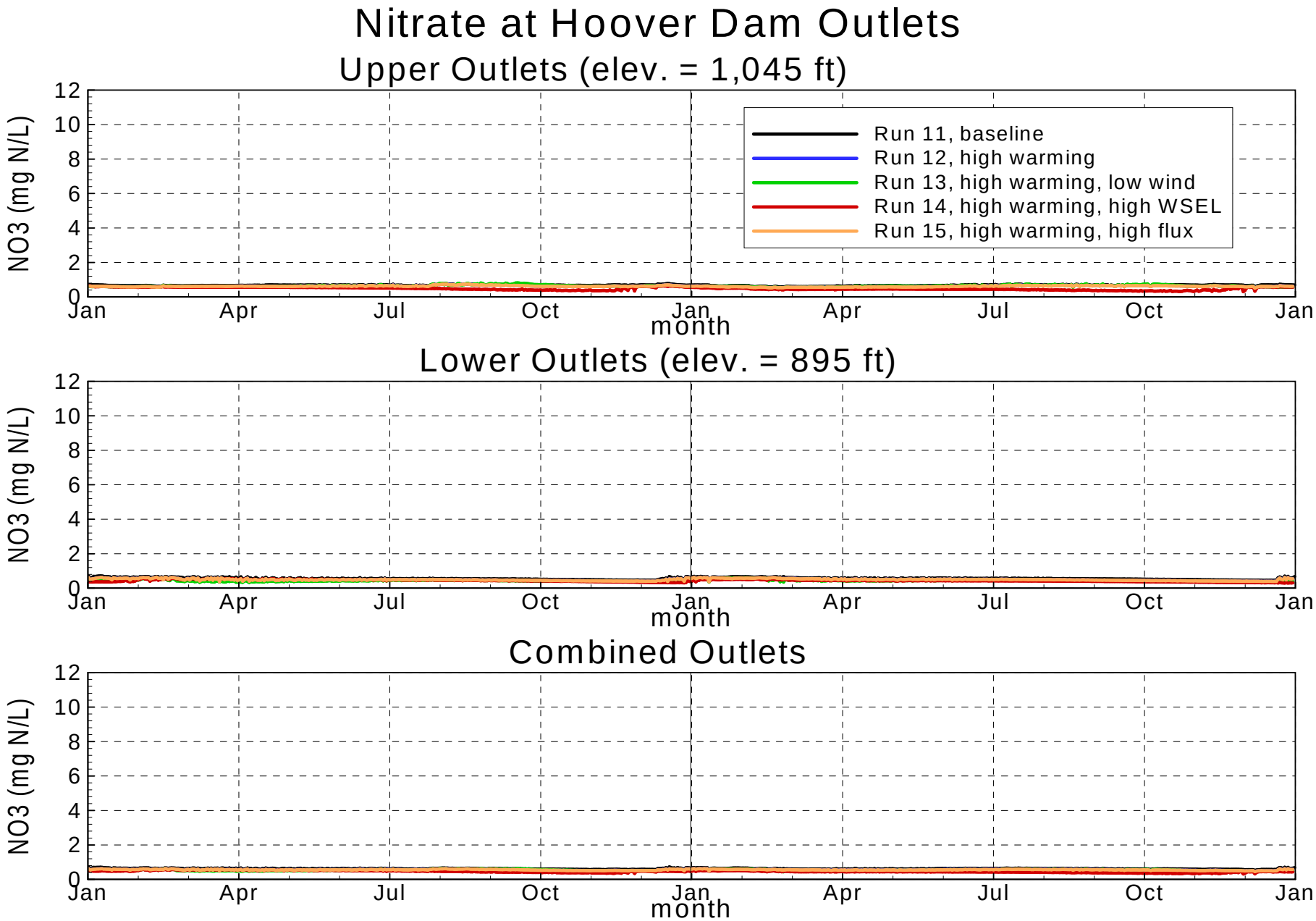

Figure A.160

FLOW SCIENCE

Total Inorganic Nitrogen at Station CR394.0

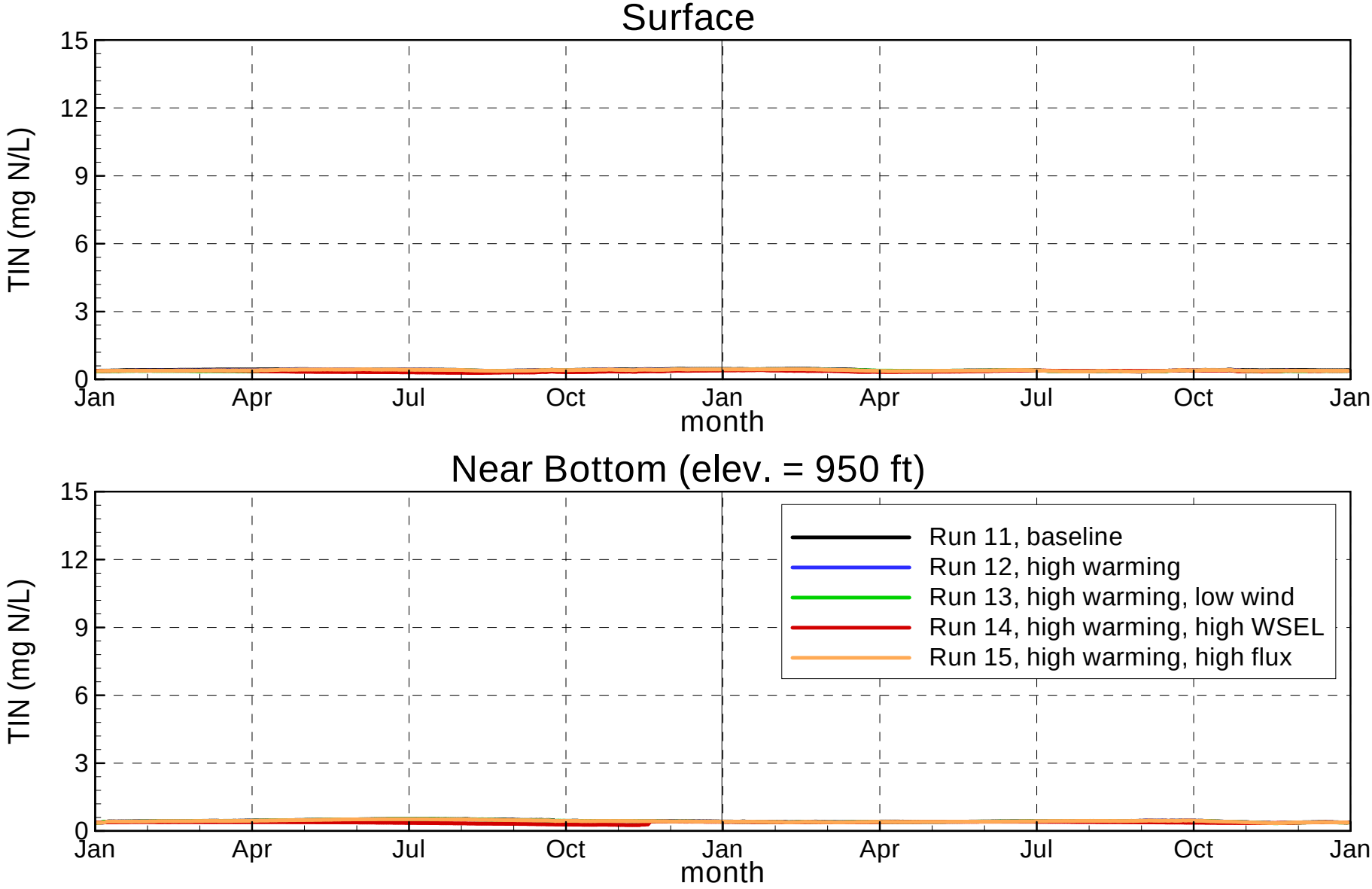

Figure A.161

Total Inorganic Nitrogen at Station CR390.0

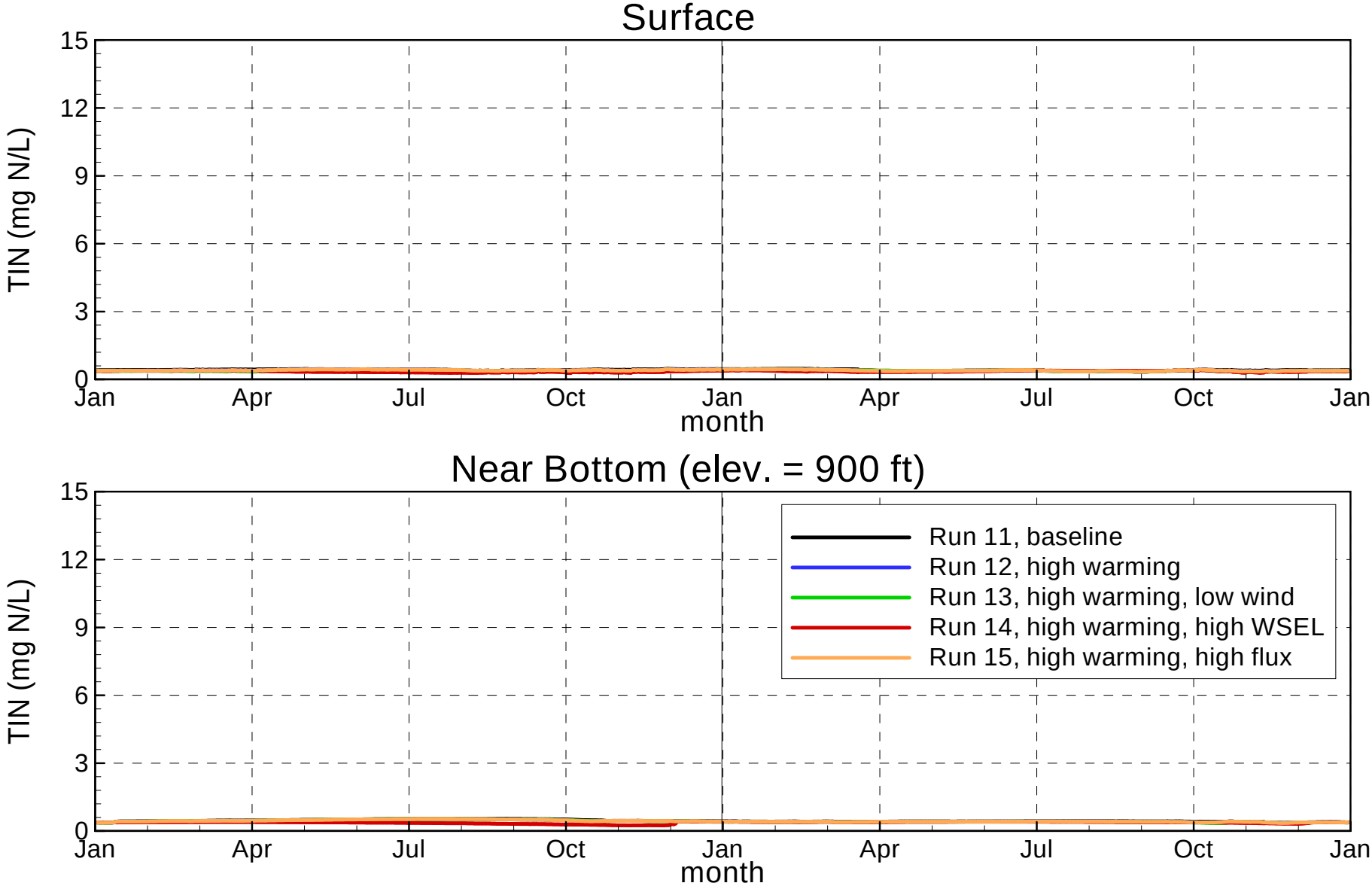

Figure A.162

Total Inorganic Nitrogen at Station CR380.0

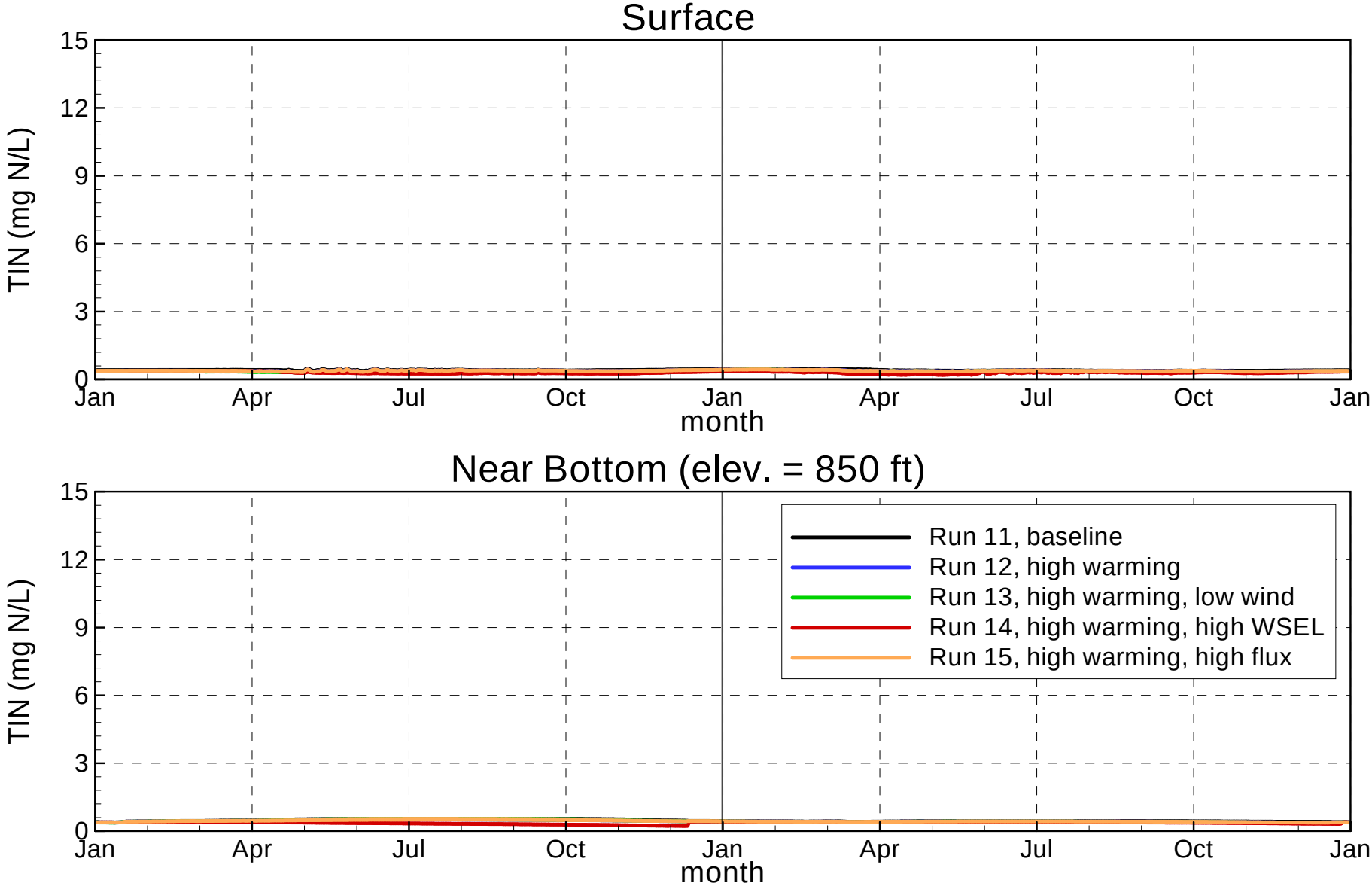

Figure A.163

Total Inorganic Nitrogen at Station VR2.0

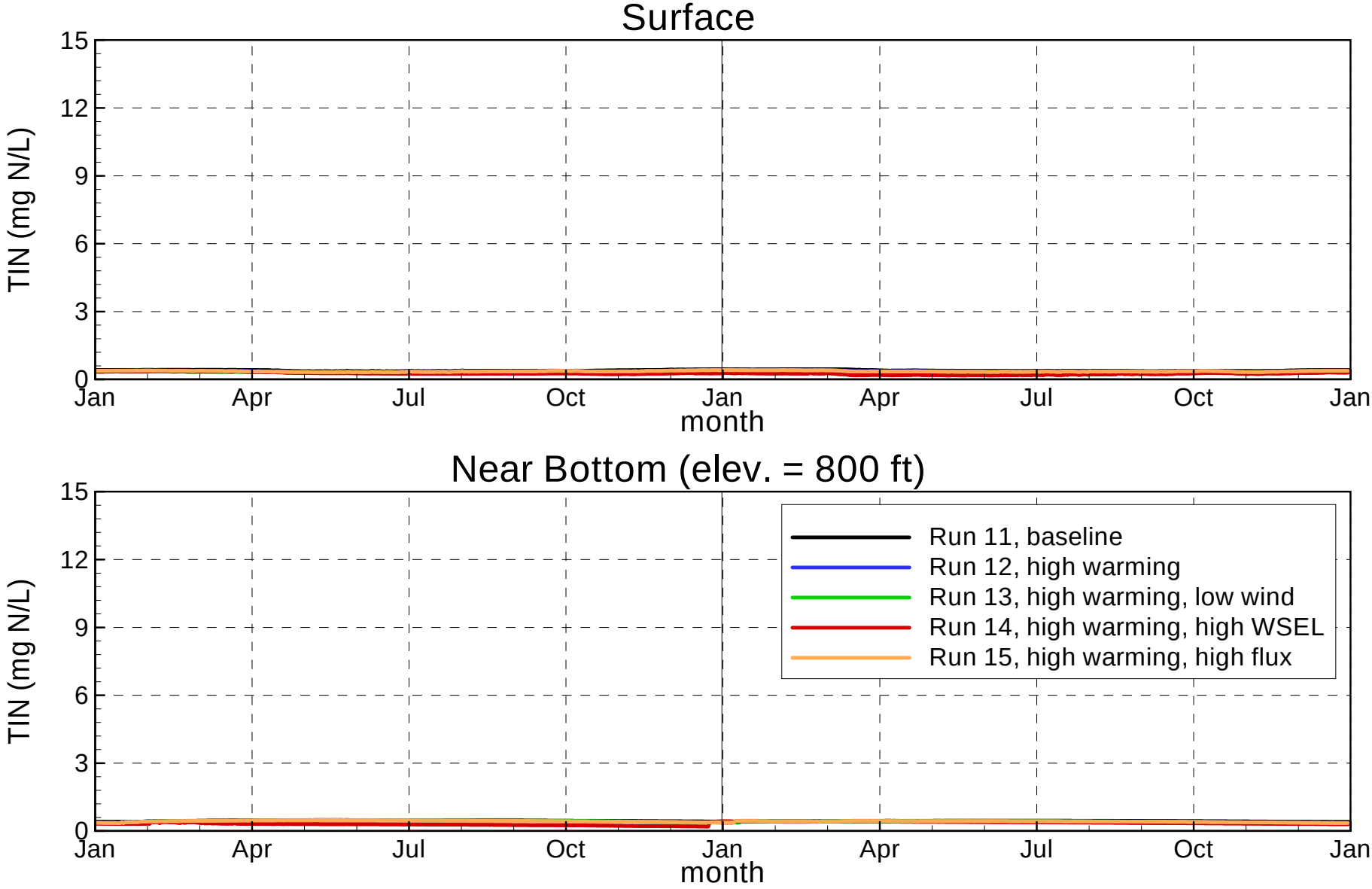

Figure A.164

Total Inorganic Nitrogen at Station VR12.9

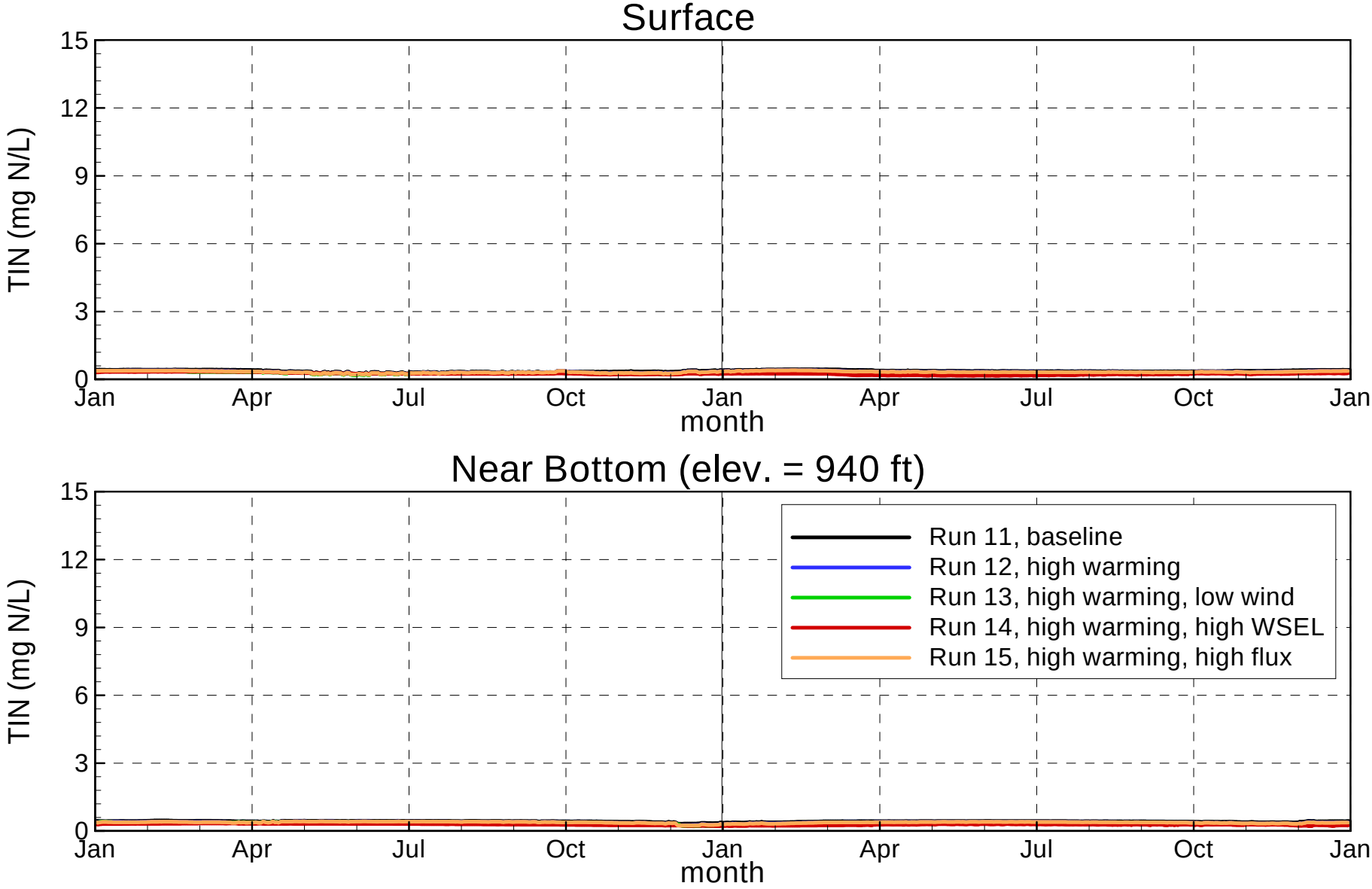

Figure A.165

Total Inorganic Nitrogen at Station VR18.0

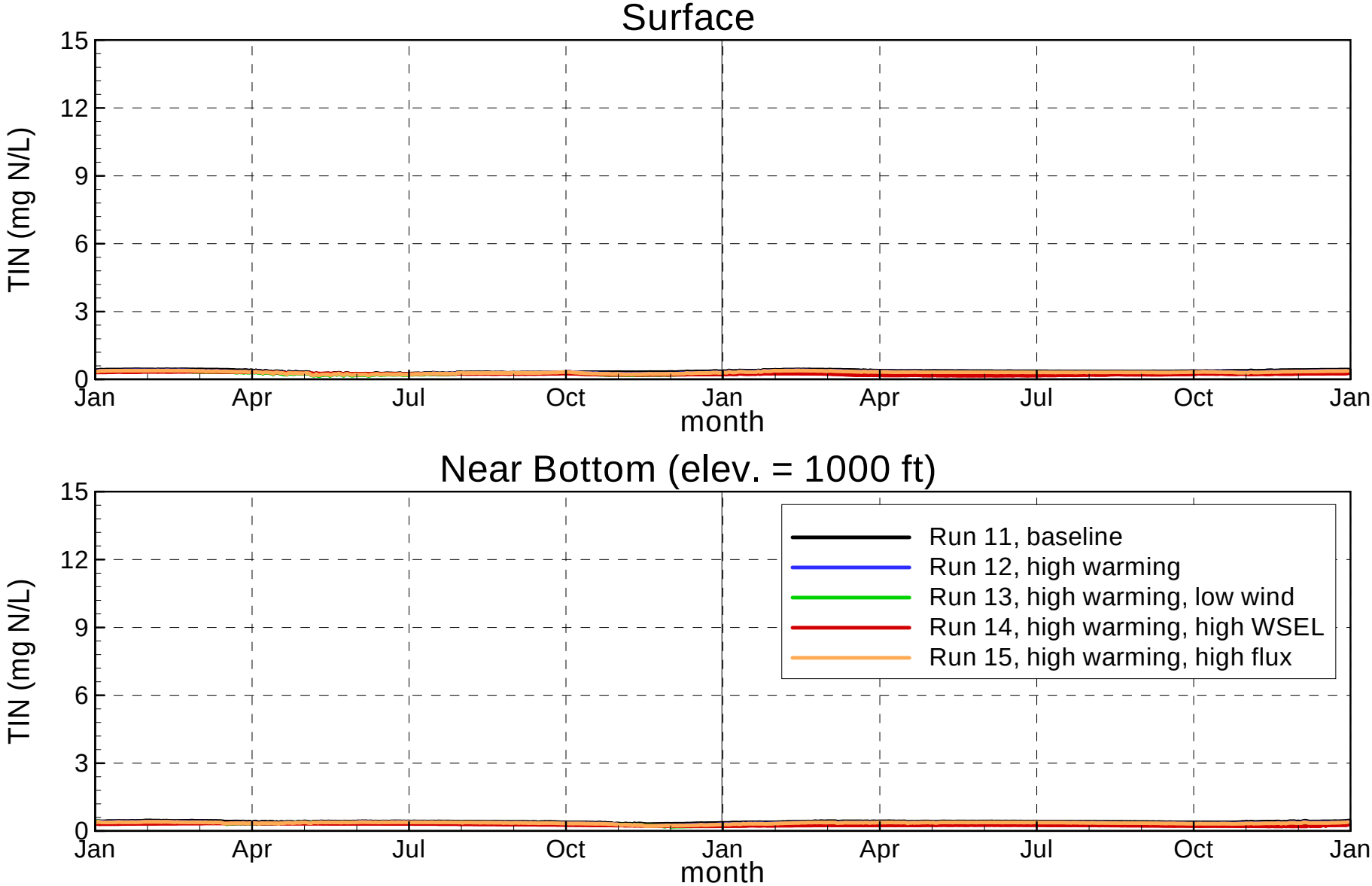

Figure A.166

Total Inorganic Nitrogen at Station VR25.1

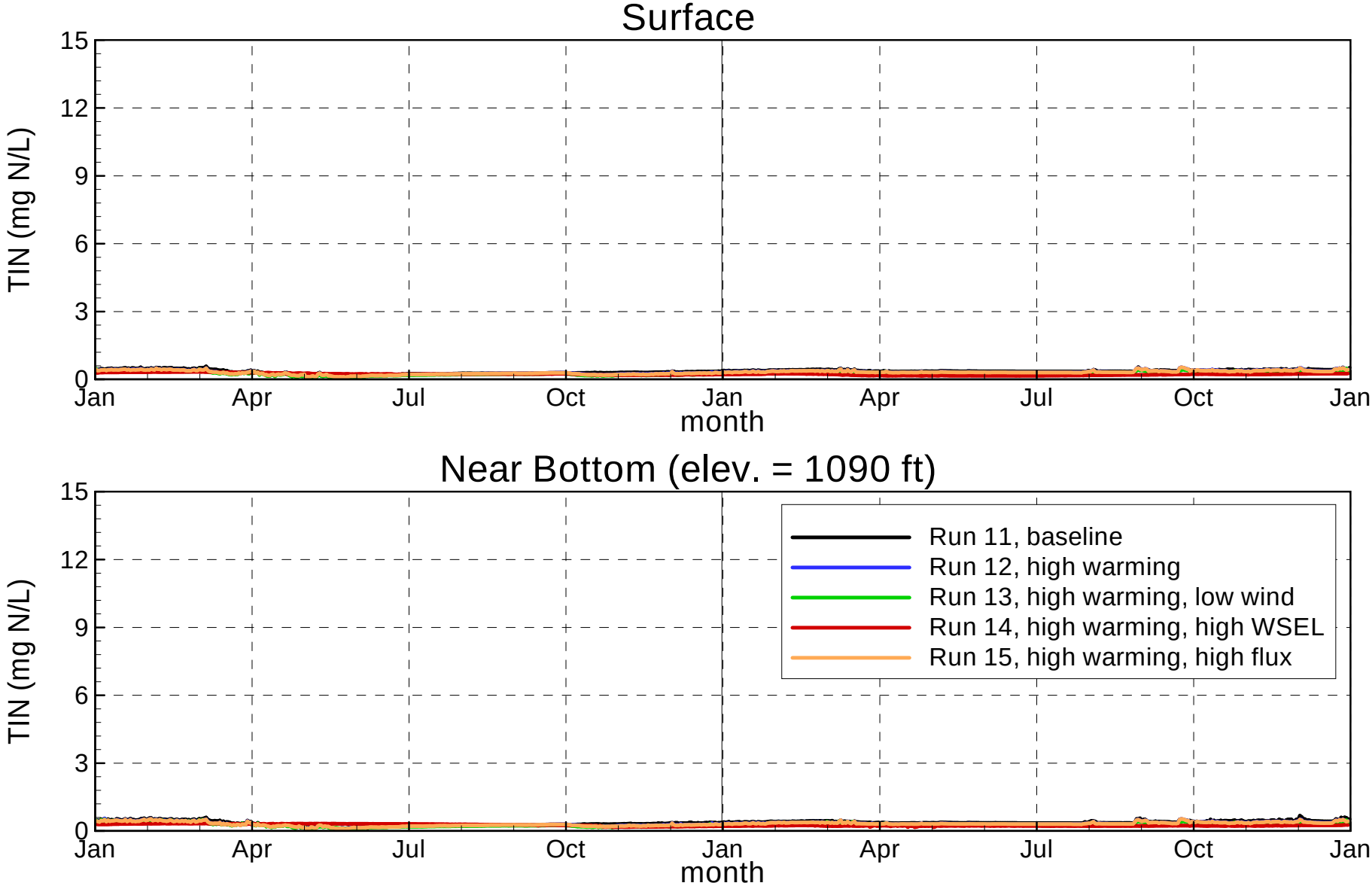

Figure A.167

Total Inorganic Nitrogen at Station CR360.7

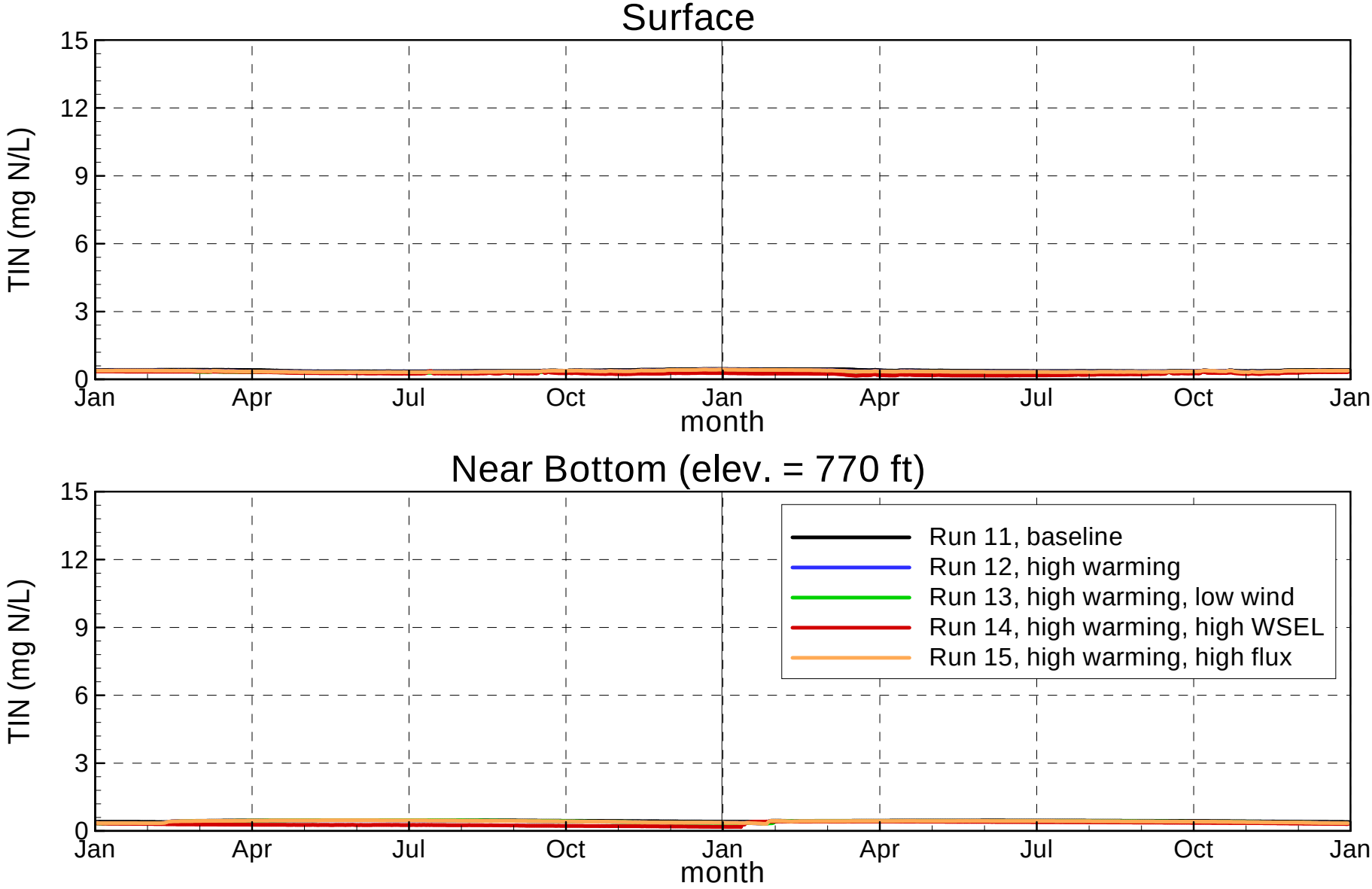

Figure A.168

Total Inorganic Nitrogen at Station CR346.4

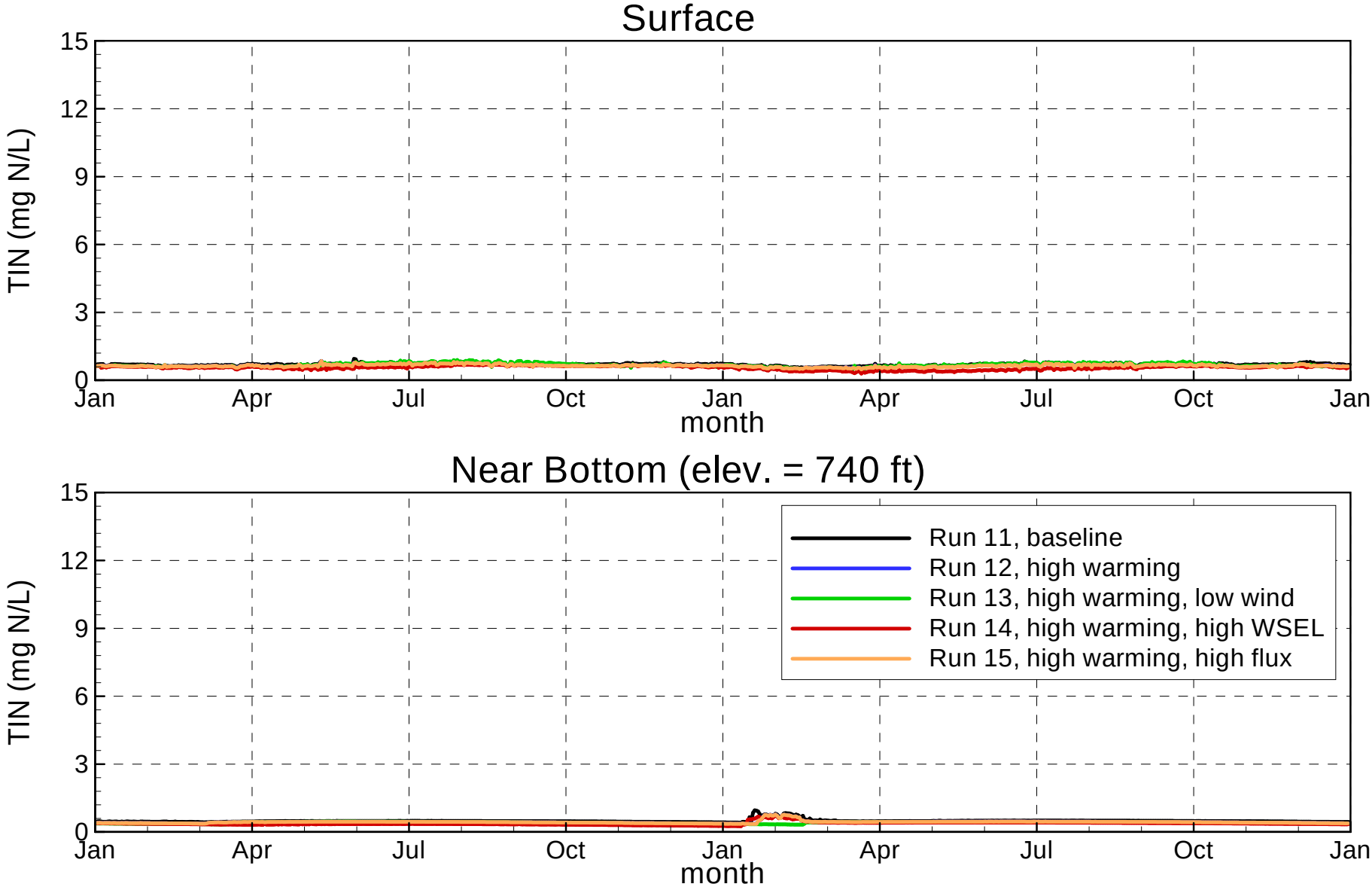

Figure A.169

Total Inorganic Nitrogen at Station LWLVB1.2

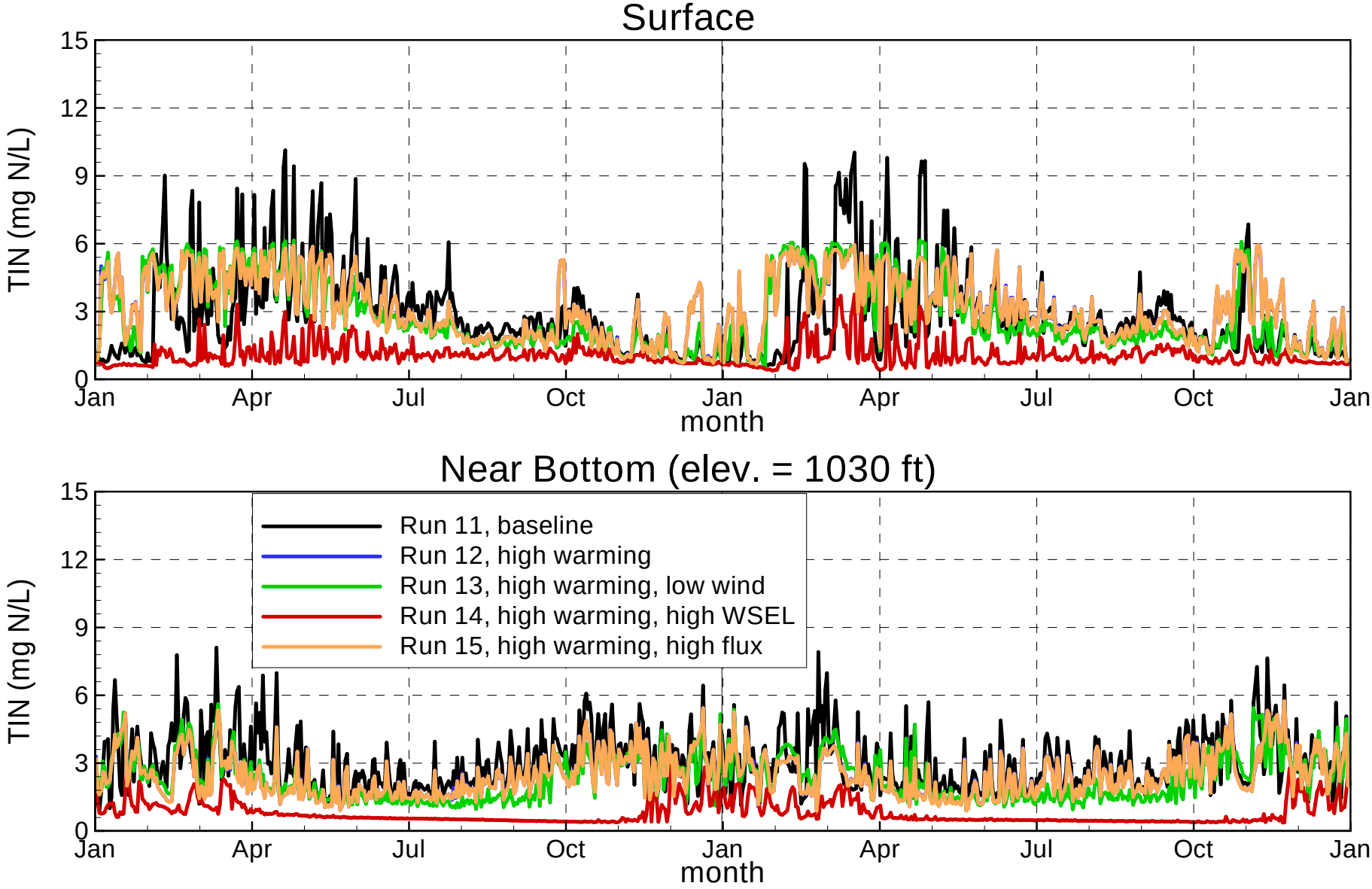

Figure A.170

FLOW SCIENCE

Total Inorganic Nitrogen at Station LWLVB1.85

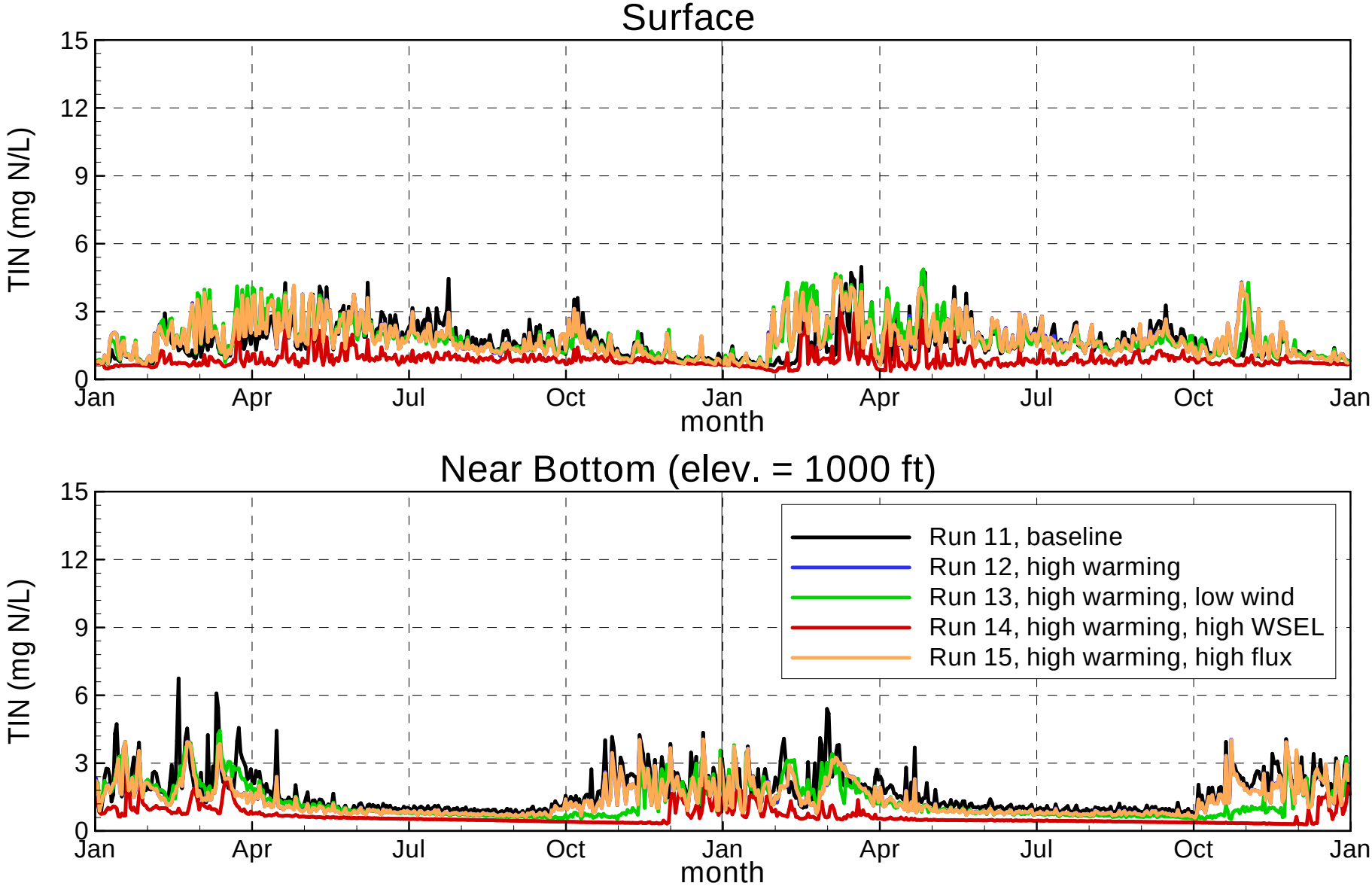

Figure A.171

Total Inorganic Nitrogen at Station LWLVB2.7

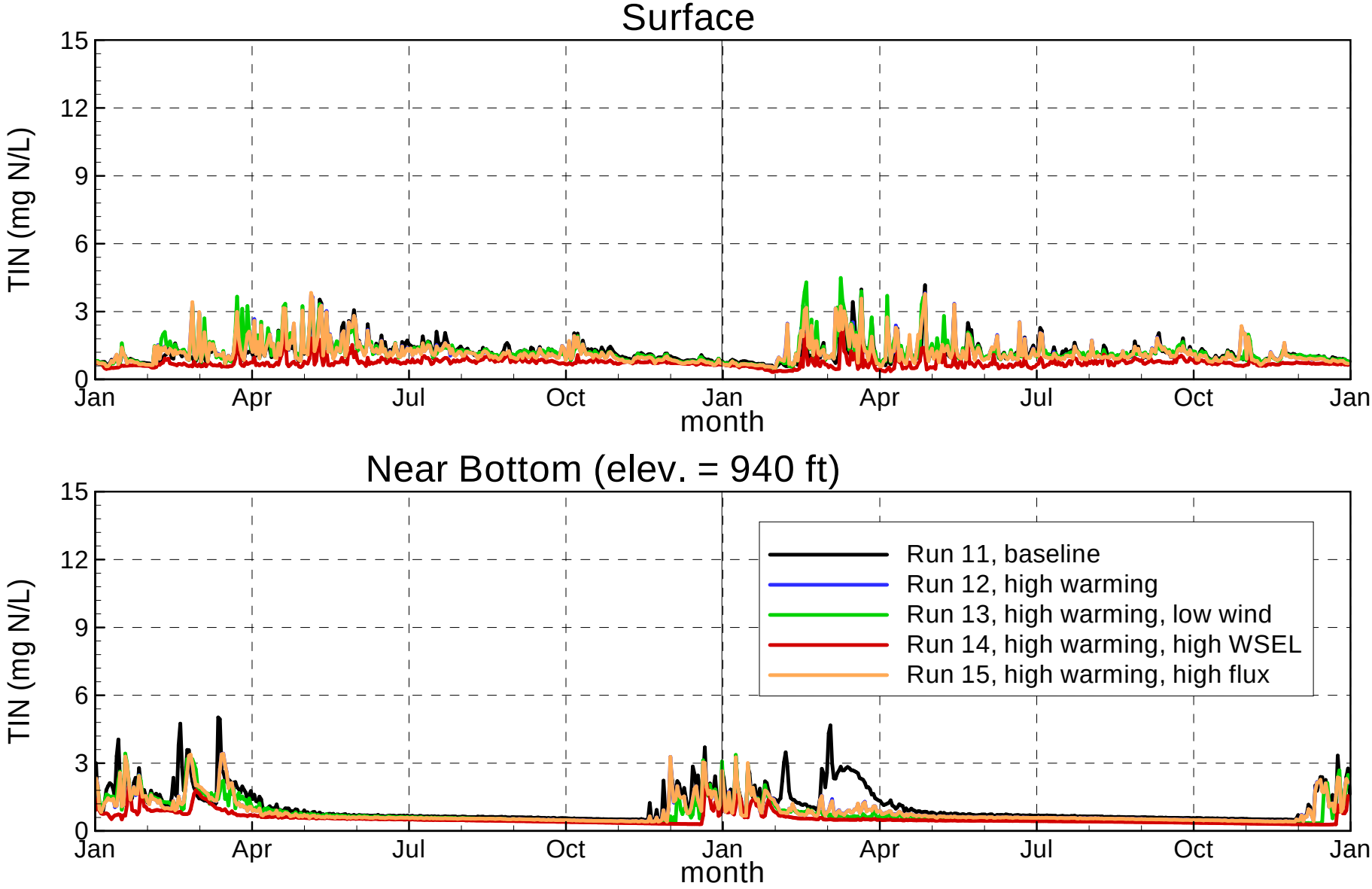

Figure A.172

Total Inorganic Nitrogen at Station LWLVB3.5

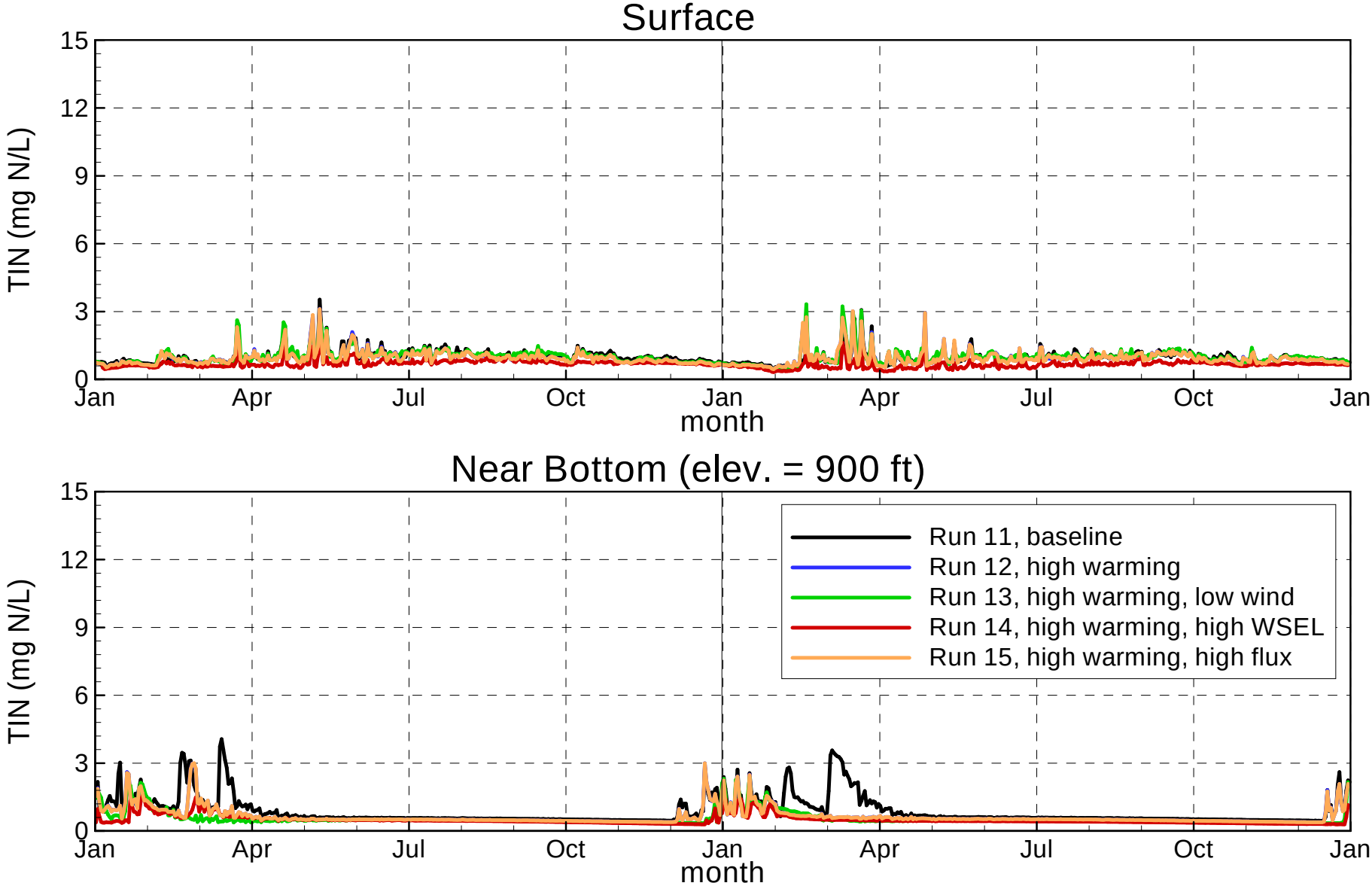

Figure A.173

Total Inorganic Nitrogen at Station LVB3.5

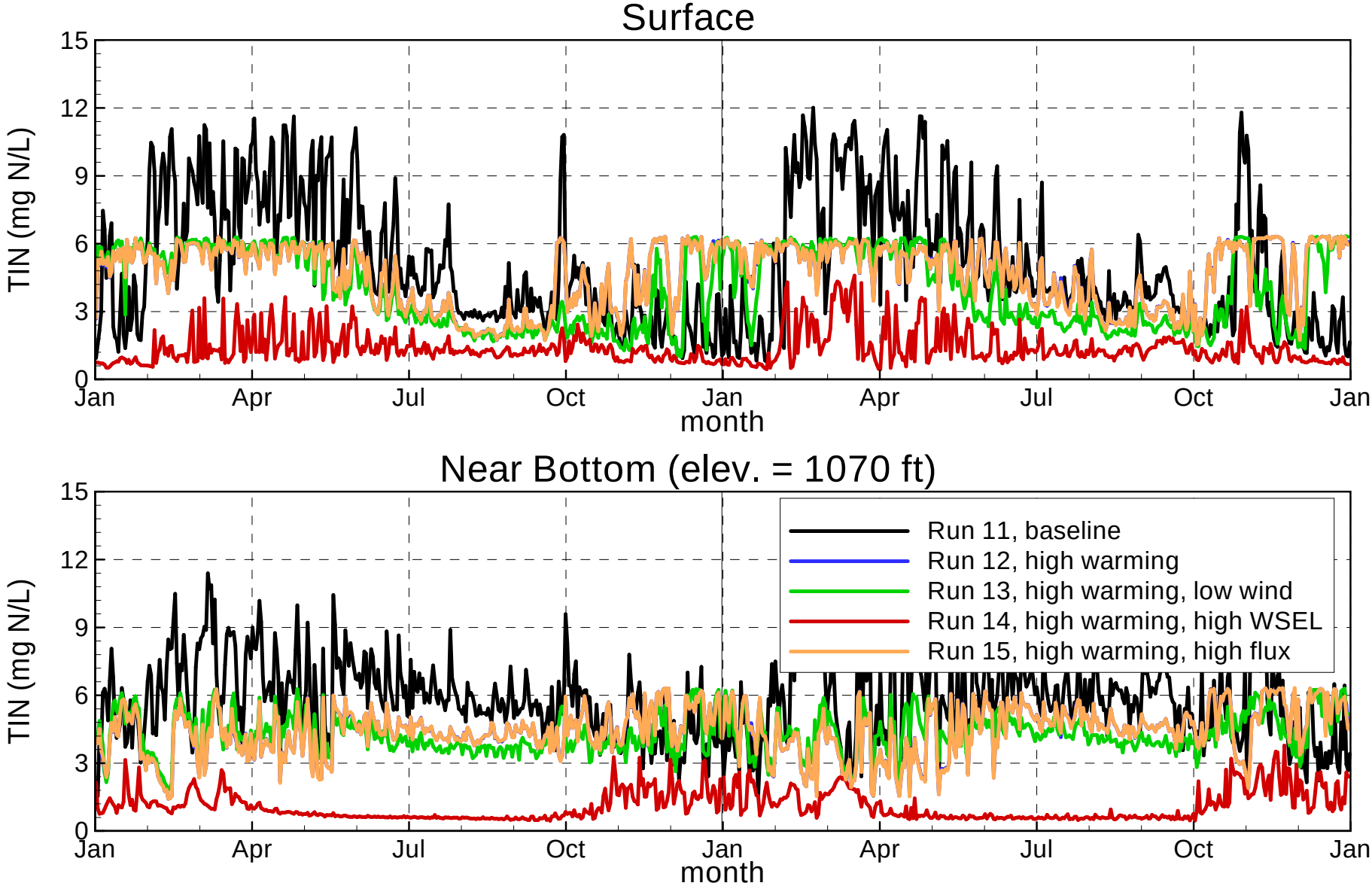

Figure A.174

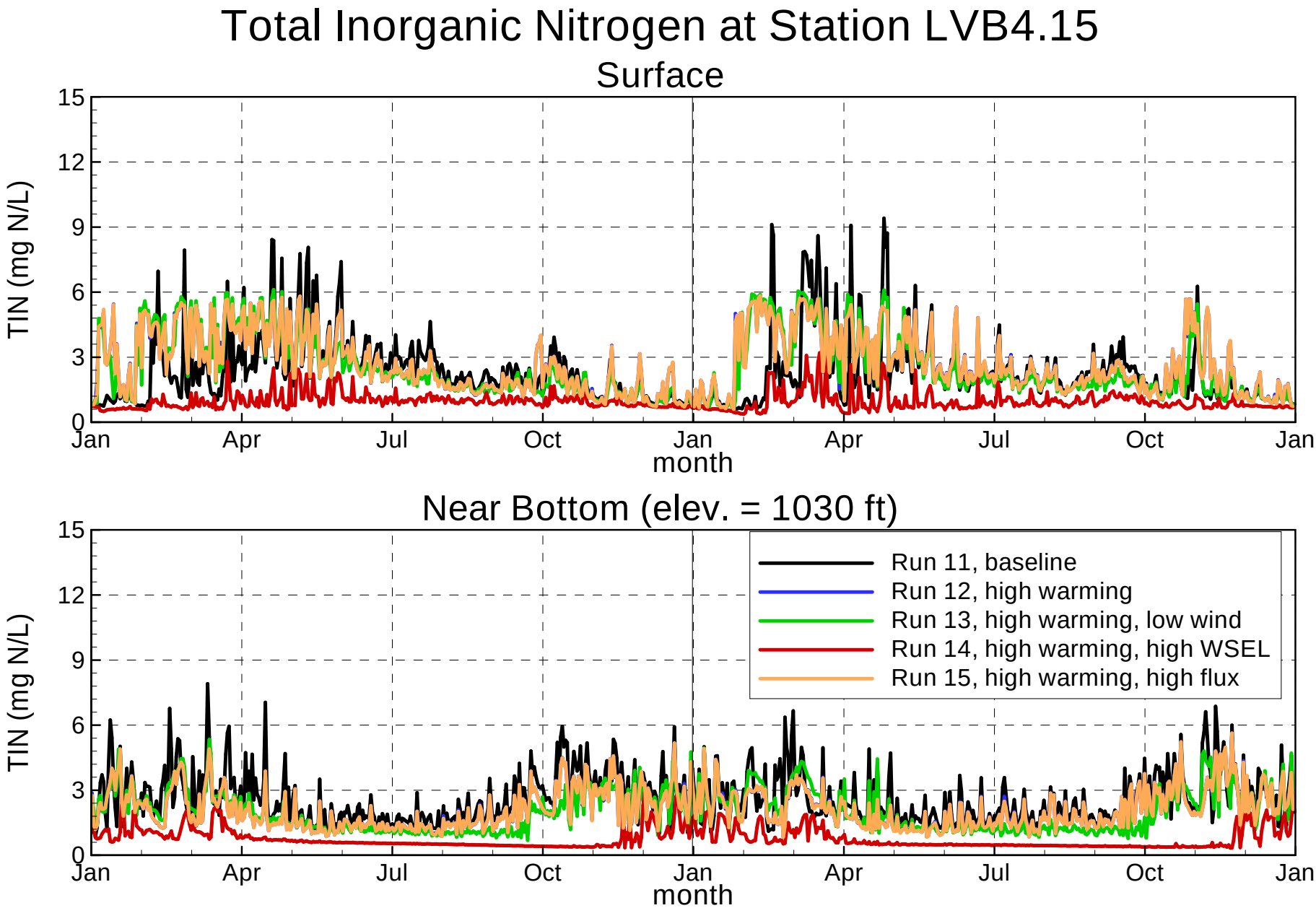
Total Inorganic Nitrogen at Station LVB4.15
Surface
TIN (mg N/L)
15
12
9
6
3
0
Jan
Apr
Jul
Oct
Jan
Apr
Jul
Oct
Jan
month
Near Bottom (elev. = 1030 ft)
TIN (mg N/L)
Run 11, baseline
Run 12, high warming
Run 13, high warming, low wind
Run 14, high warming, high WSEL
Run 15, high warming, high flux
month

Figure A.175

Total Inorganic Nitrogen at Station LVB4.95

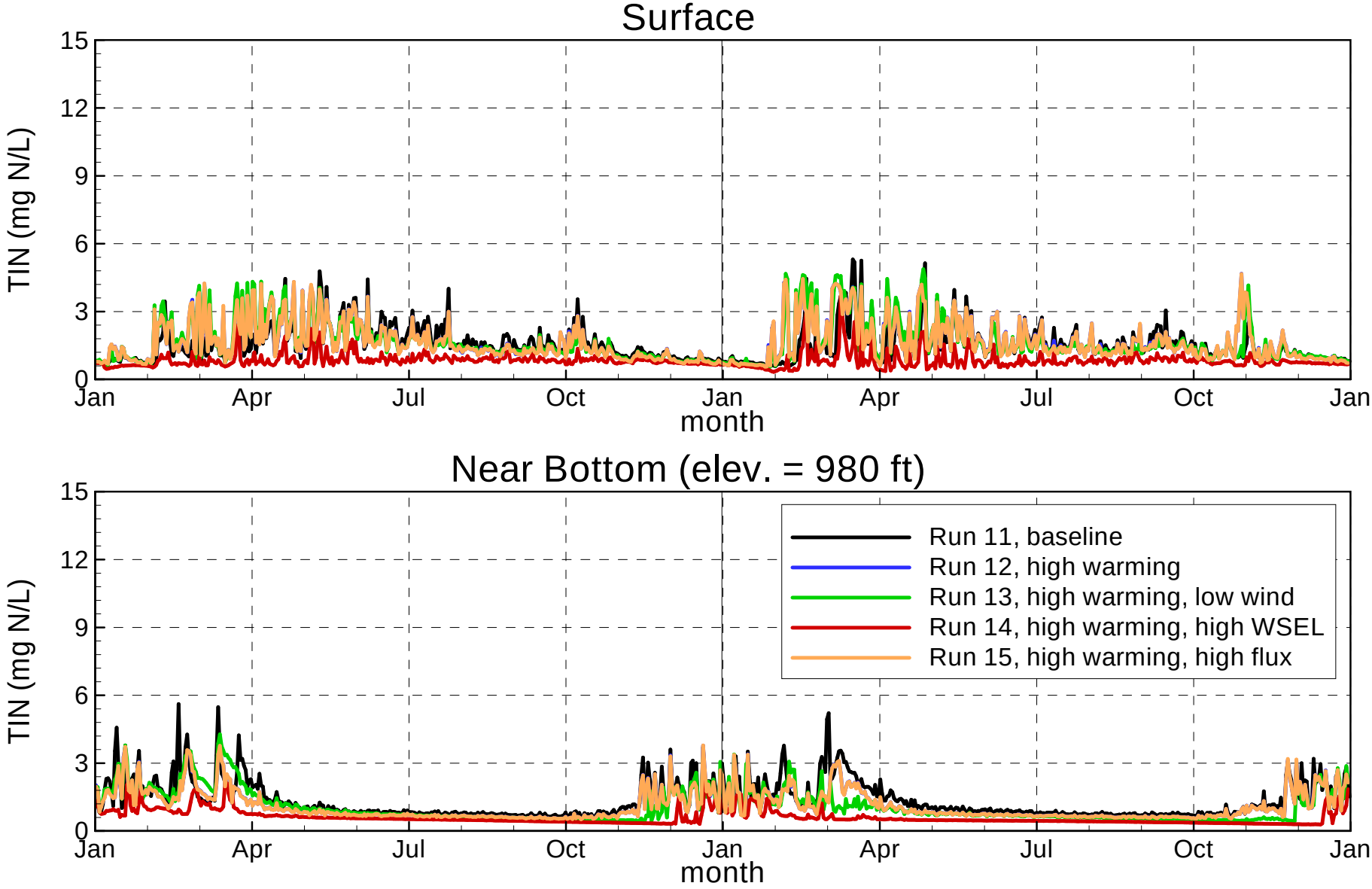

Figure A.176

Total Inorganic Nitrogen at Station LVB6.7

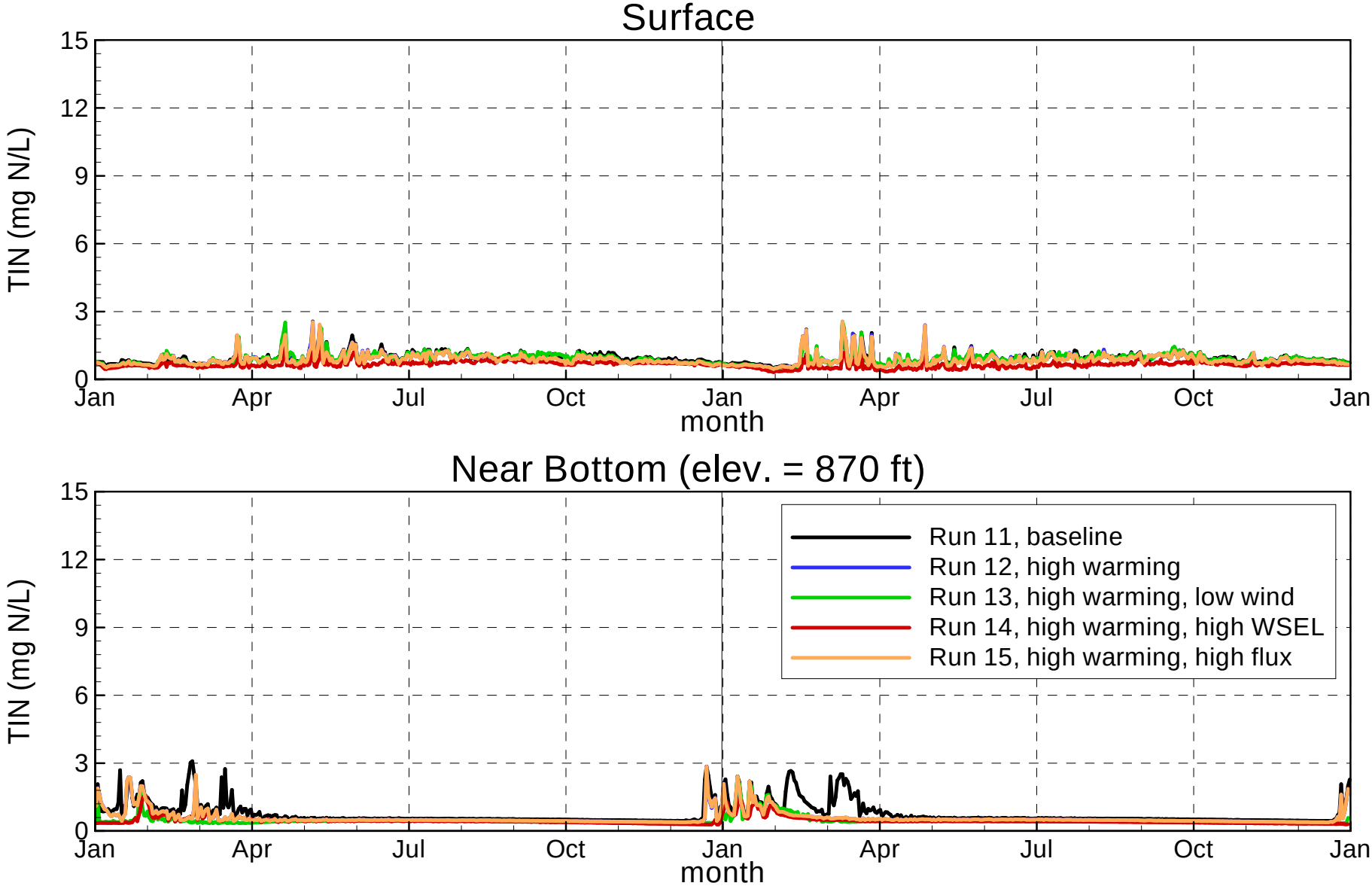

Figure A.177

Total Inorganic Nitrogen at Station LVB7.3

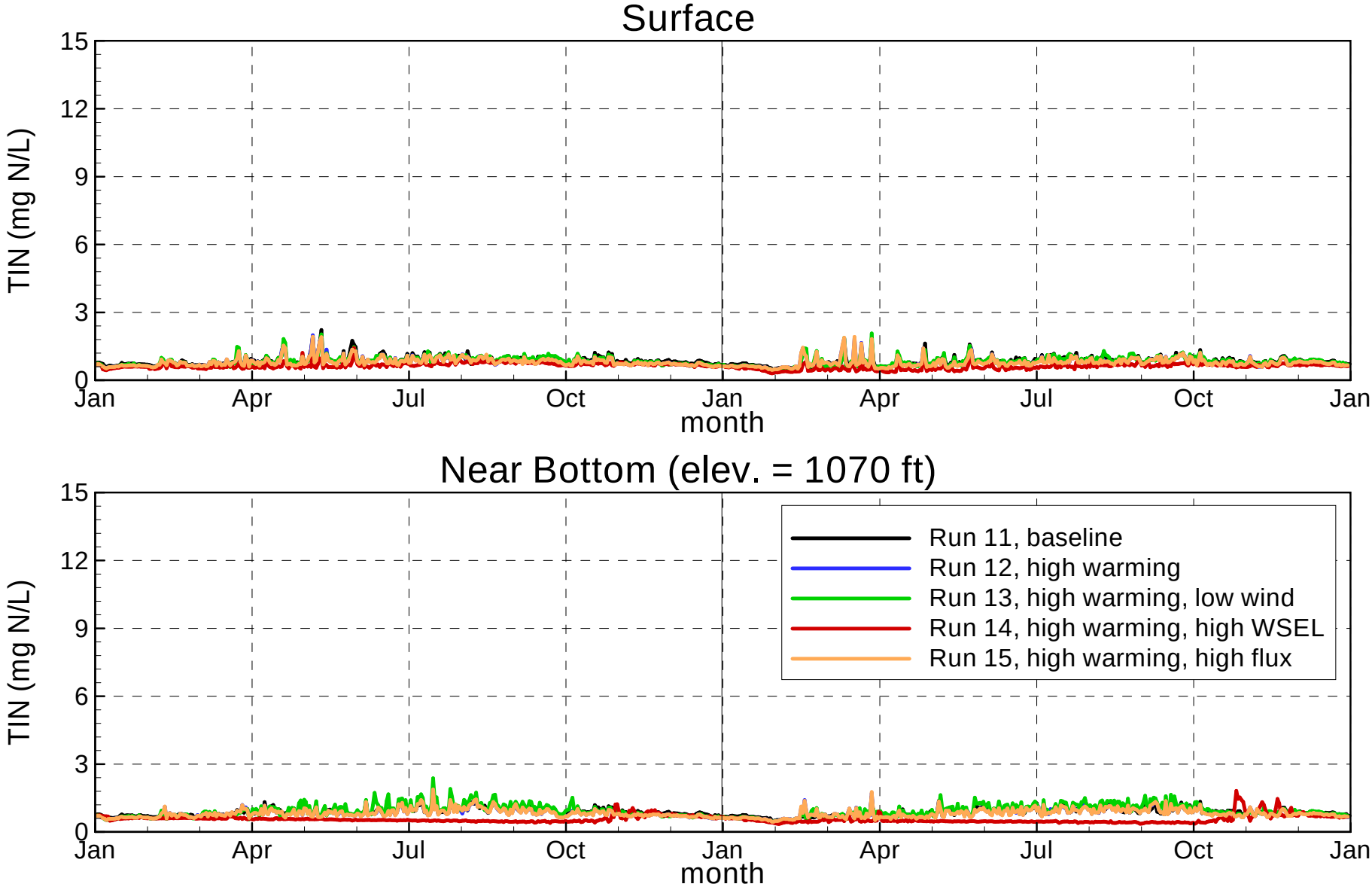

Figure A.178

Total Inorganic Nitrogen at SNWA Intake #3

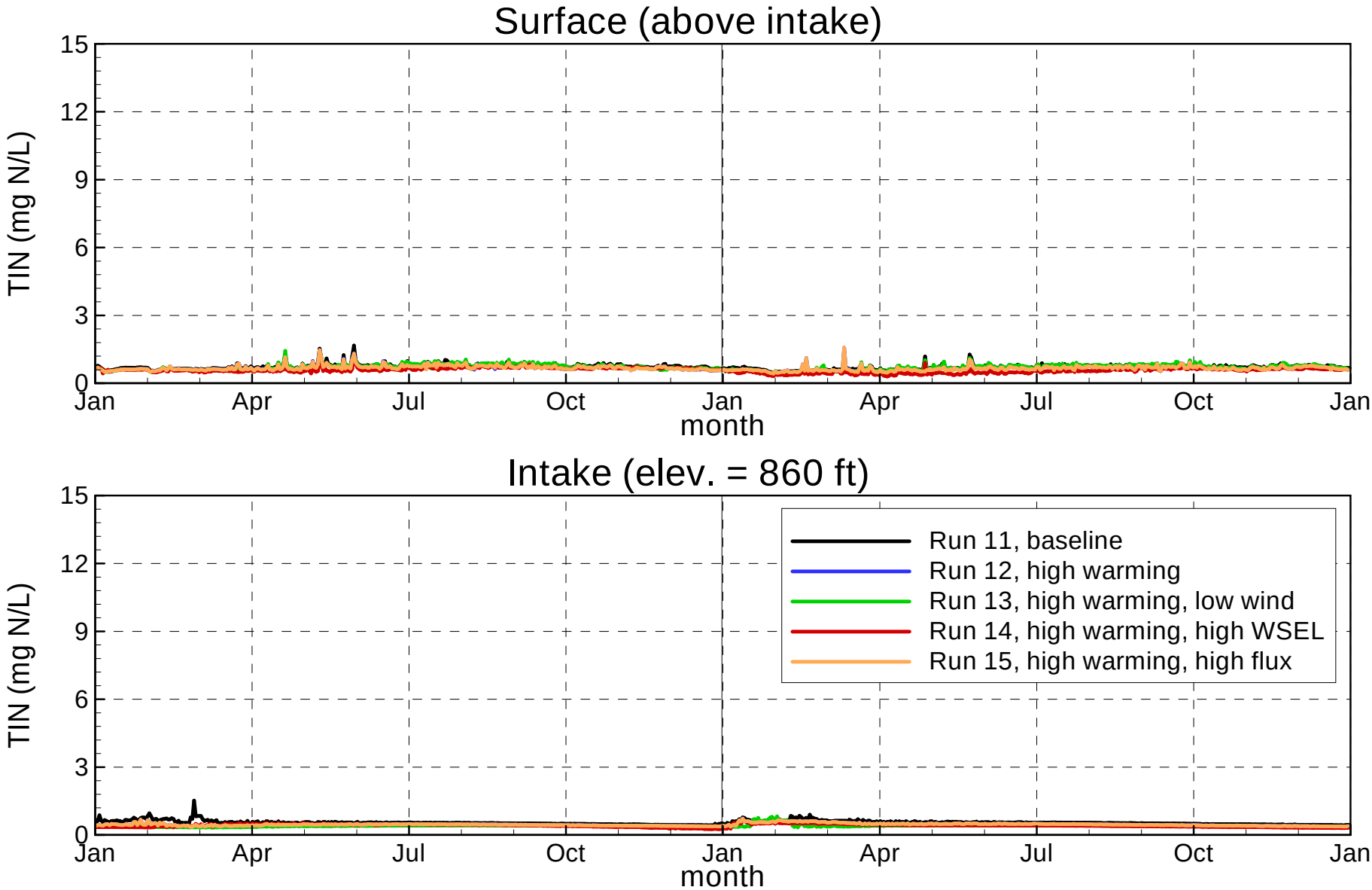

Figure A.179

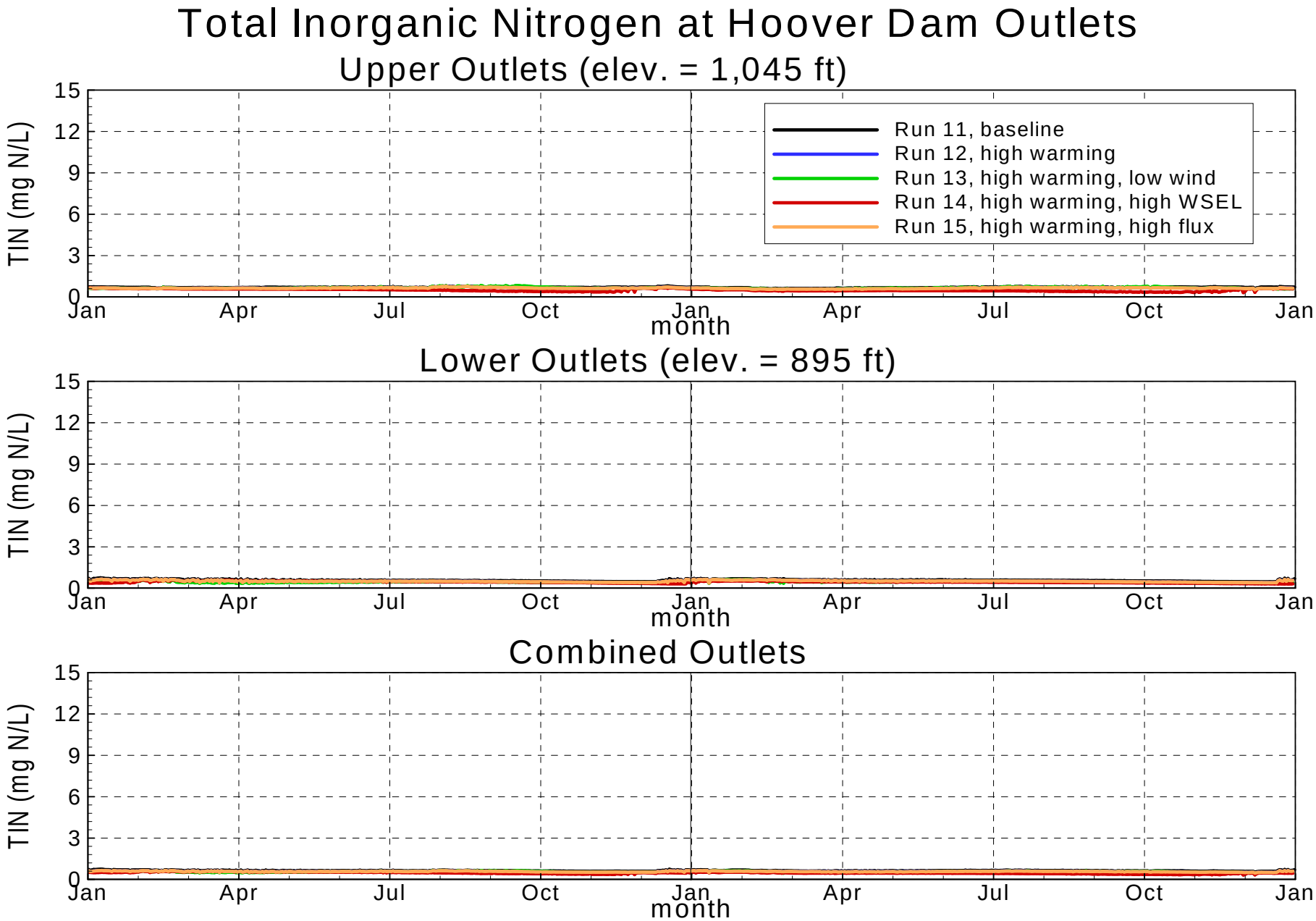

Figure A.180

FLOW SCIENCE

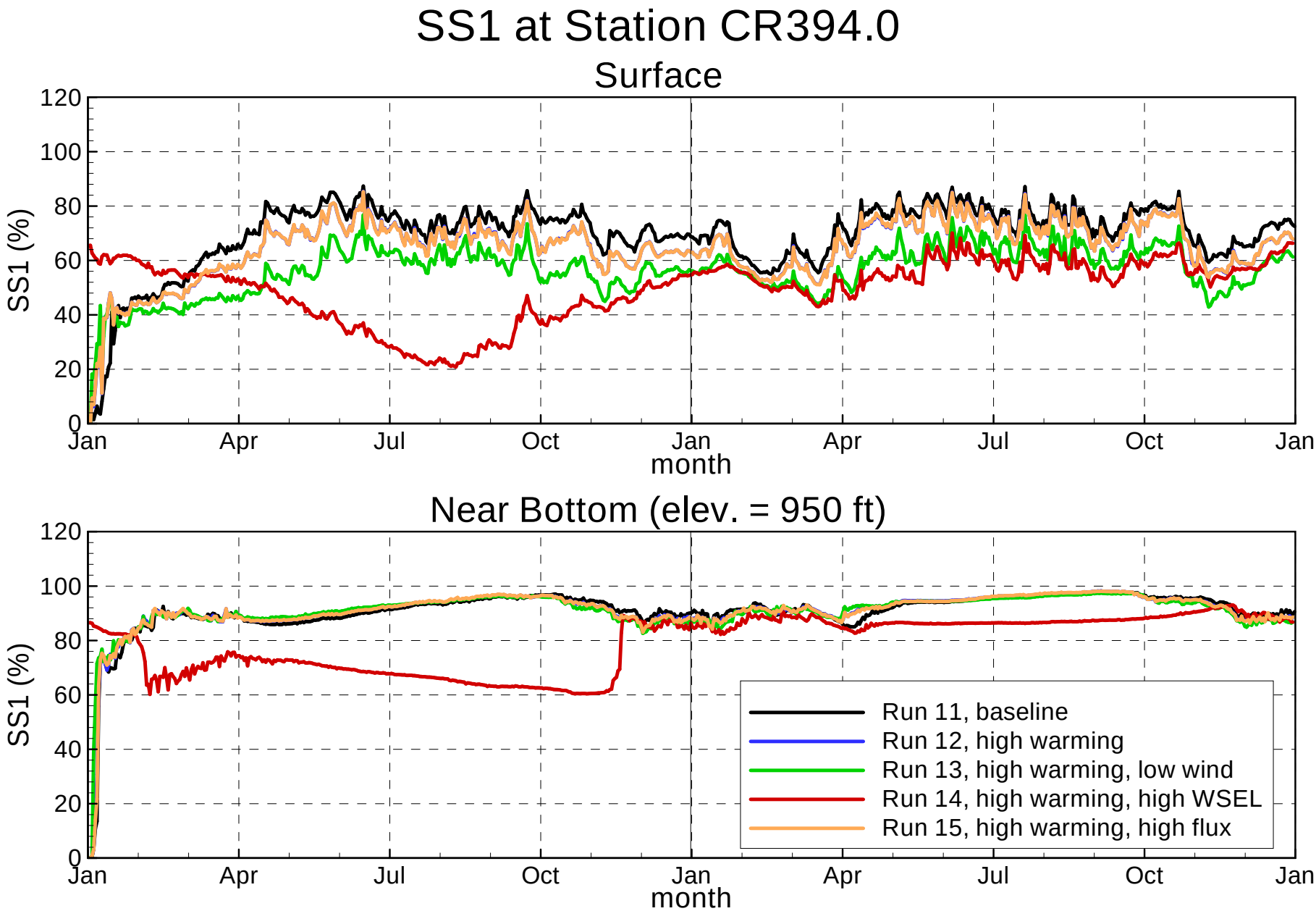
SS1 at Station CR394.0
Surface
SS1 (%)
120
100
80
60
40
20
0
Jan
Apr
Jul
Oct
Jan
Apr
Jul
Oct
Jan
month
Near Bottom (elev. = 950 ft)
SS1 (%)
Run 11, baseline
Run 12, high warming
Run 13, high warming, low wind
Run 14, high warming, high WSEL
Run 15, high warming, high flux

Figure A.181

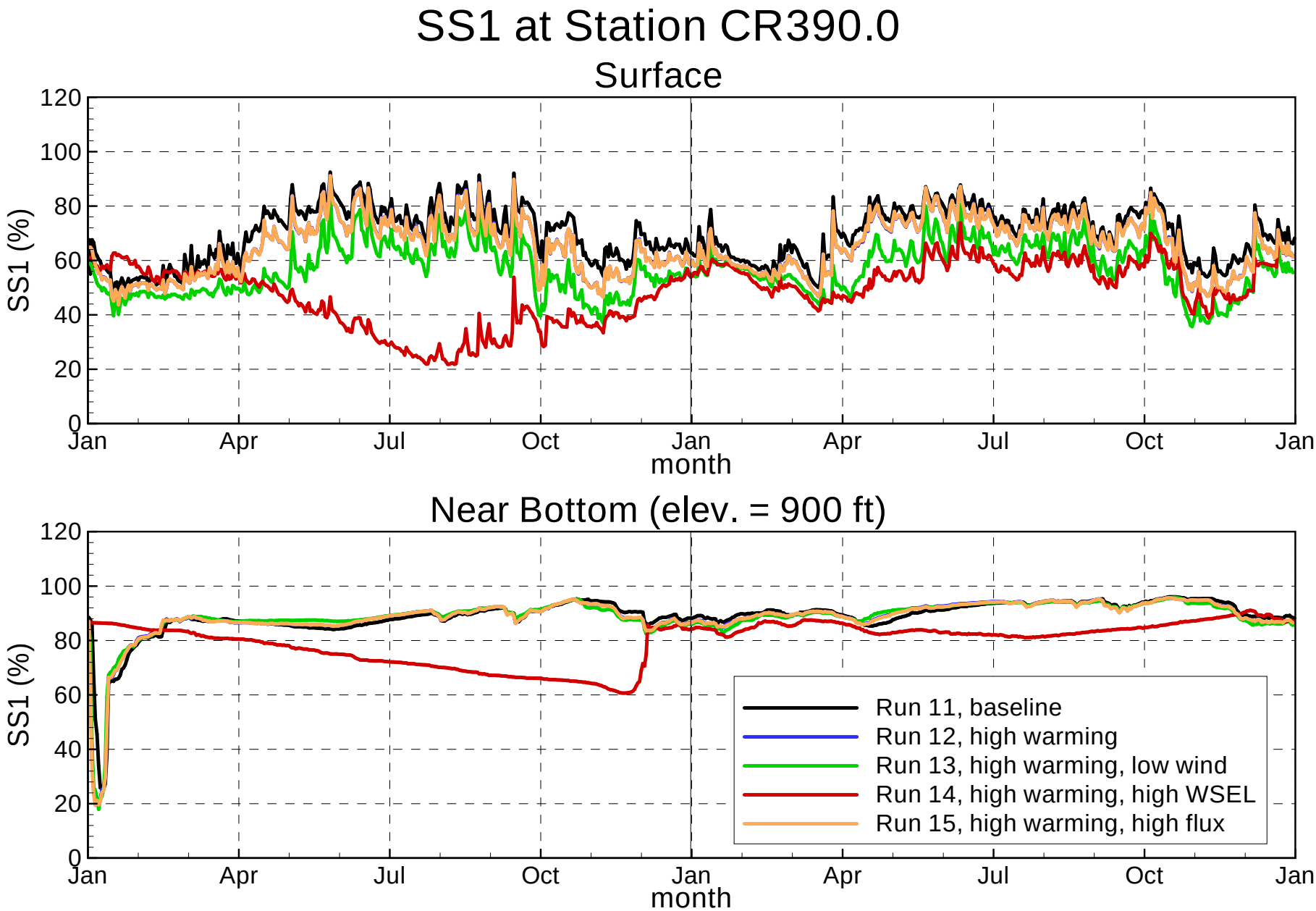
SS1 at Station CR390.0
Surface
SS1 (%)
120
100
80
60
40
20
0
Jan
Apr
Jul
Oct
Jan
Apr
Jul
Oct
Jan
month
Near Bottom (elev. = 900 ft)
SS1 (%)
Run 11, baseline
Run 12, high warming
Run 13, high warming, low wind
Run 14, high warming, high WSEL
Run 15, high warming, high flux

Figure A.182

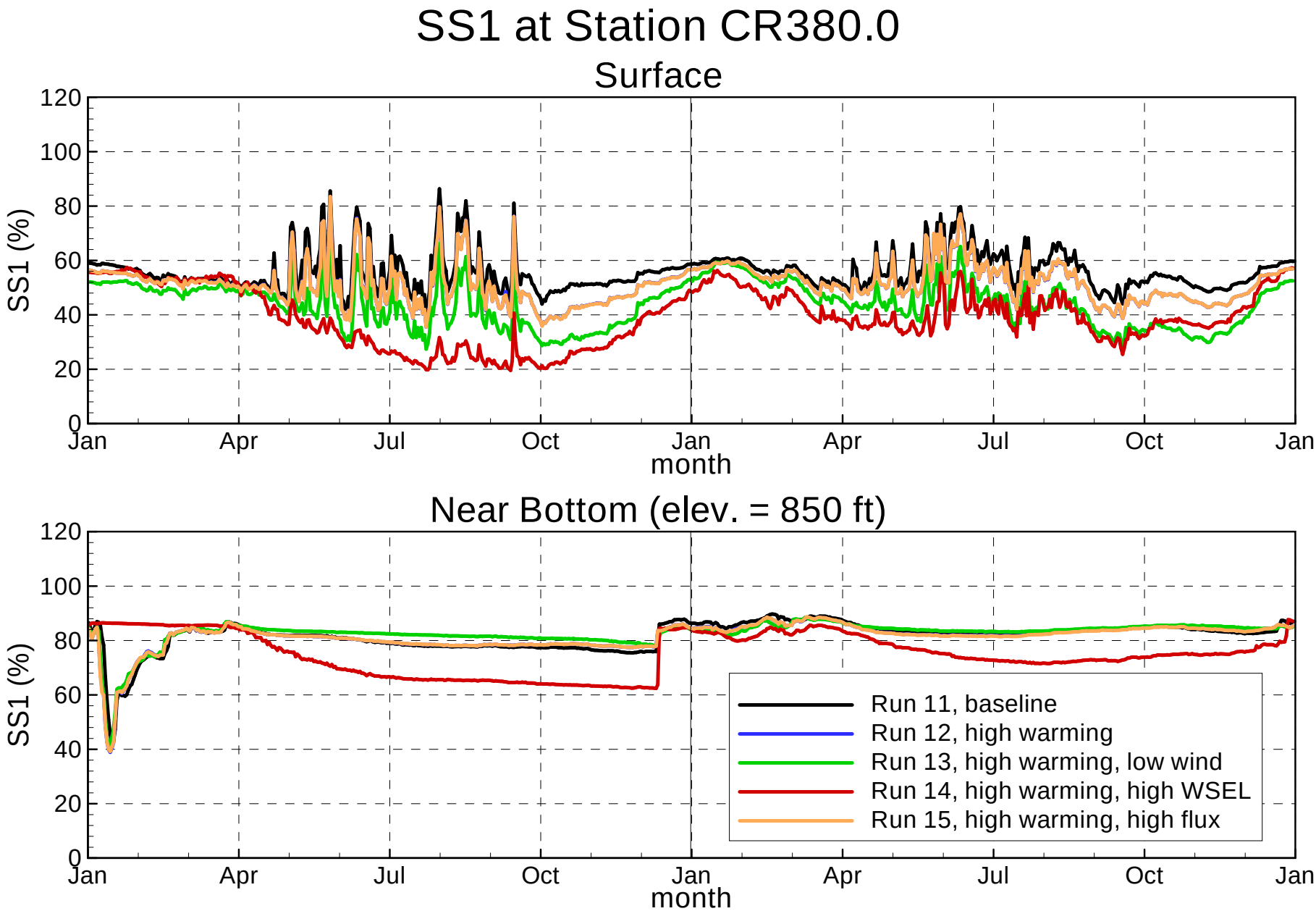
SS1 at Station CR380.0
Surface
SS1 (%)
120
100
80
60
40
20
0
Jan
Apr
Jul
Oct
Jan
Apr
Jul
Oct
Jan
month
Near Bottom (elev. = 850 ft)
SS1 (%)
Run 11, baseline
Run 12, high warming
Run 13, high warming, low wind
Run 14, high warming, high WSEL
Run 15, high warming, high flux

Figure A.183

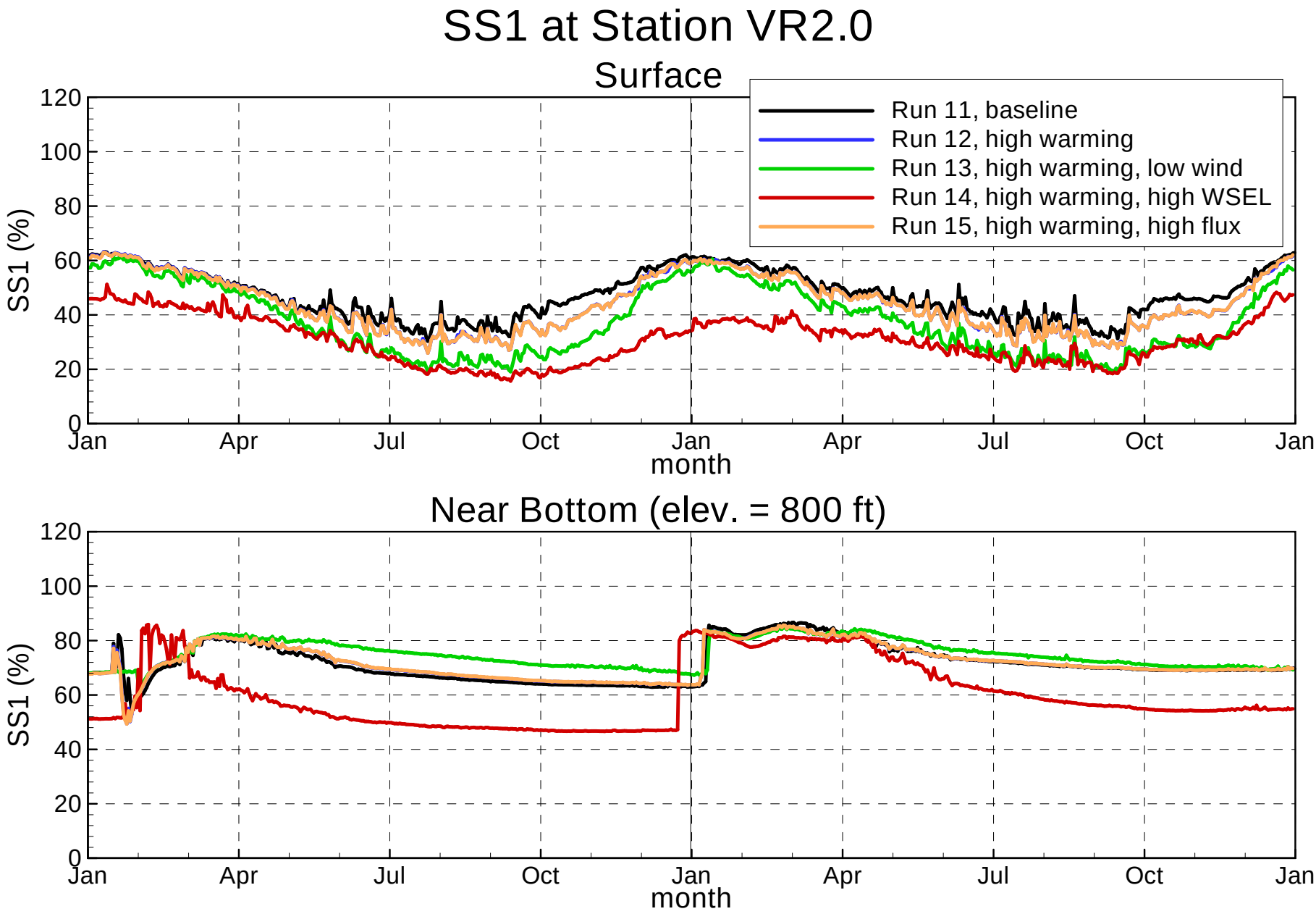
SS1 at Station VR2.0
Surface
Run 11, baseline
Run 12, high warming
Run 13, high warming, low wind
Run 14, high warming, high WSEL
Run 15, high warming, high flux
SS1 (%)
120
100
80
60
40
20
0
Jan
Apr
Jul
Oct
Jan
Apr
Jul
Oct
Jan
month
Near Bottom (elev. = 800 ft)
SS1 (%)
120
100
80
60
40
20
0
Jan
Apr
Jul
Oct
Jan
Apr
Jul
Oct
Jan
month

Figure A.184

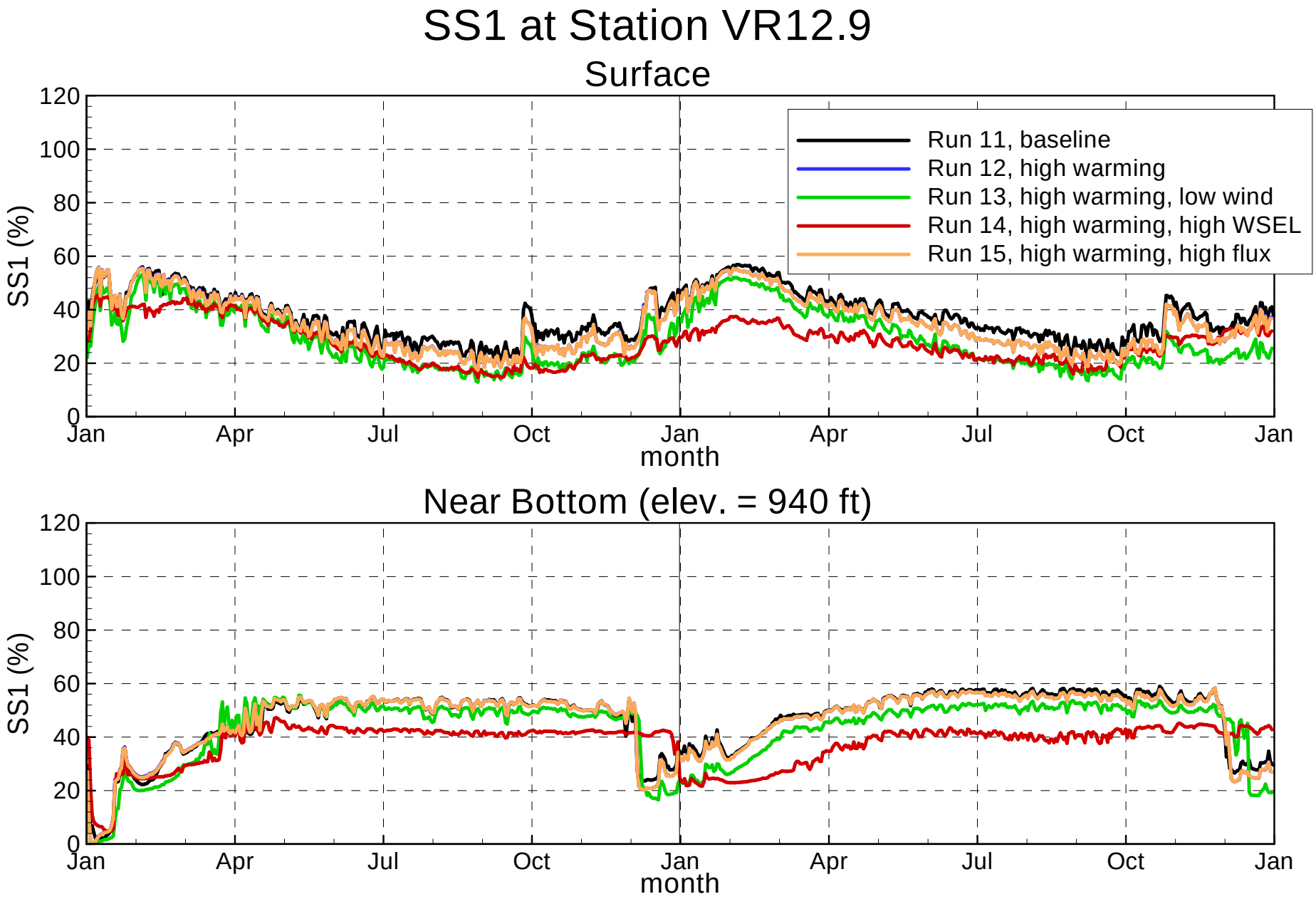
SS1 at Station VR12.9
Surface
Run 11, baseline
Run 12, high warming
Run 13, high warming, low wind
Run 14, high warming, high WSEL
Run 15, high warming, high flux
SS1 (%)
120
100
80
60
40
20
0
Jan
Apr
Jul
Oct
Jan
Apr
Jul
Oct
Jan
month
Near Bottom (elev. = 940 ft)
SS1 (%)
120
100
80
60
40
20
0
Jan
Apr
Jul
Oct
Jan
Apr
Jul
Oct
Jan
month

Figure A.185

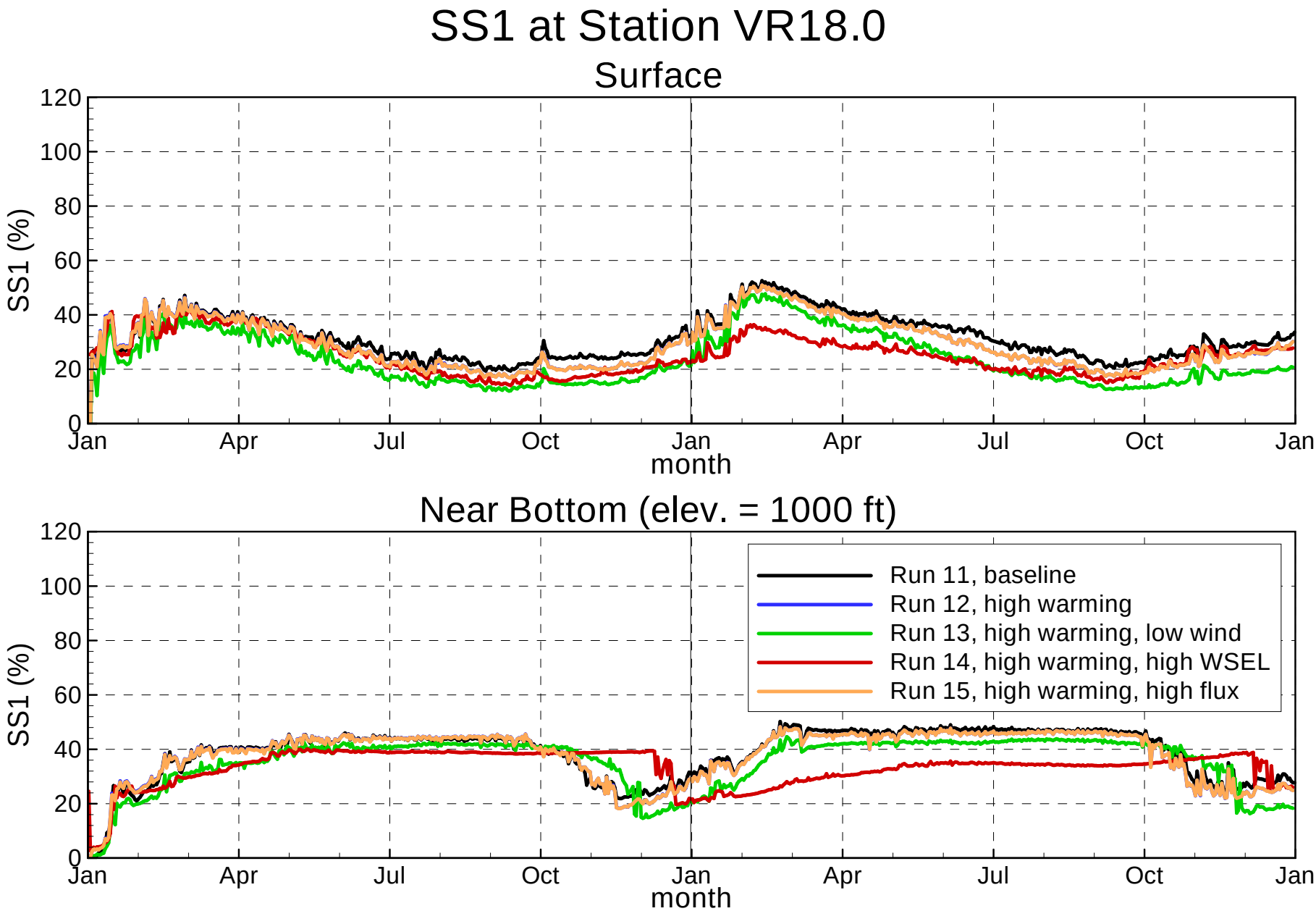
SS1 at Station VR18.0
Surface
SS1 (%)
120
100
80
60
40
20
0
Jan
Apr
Jul
Oct
Jan
Apr
Jul
Oct
Jan
month
Near Bottom (elev. = 1000 ft)
SS1 (%)
Run 11, baseline
Run 12, high warming
Run 13, high warming, low wind
Run 14, high warming, high WSEL
Run 15, high warming, high flux
month

Figure A.186

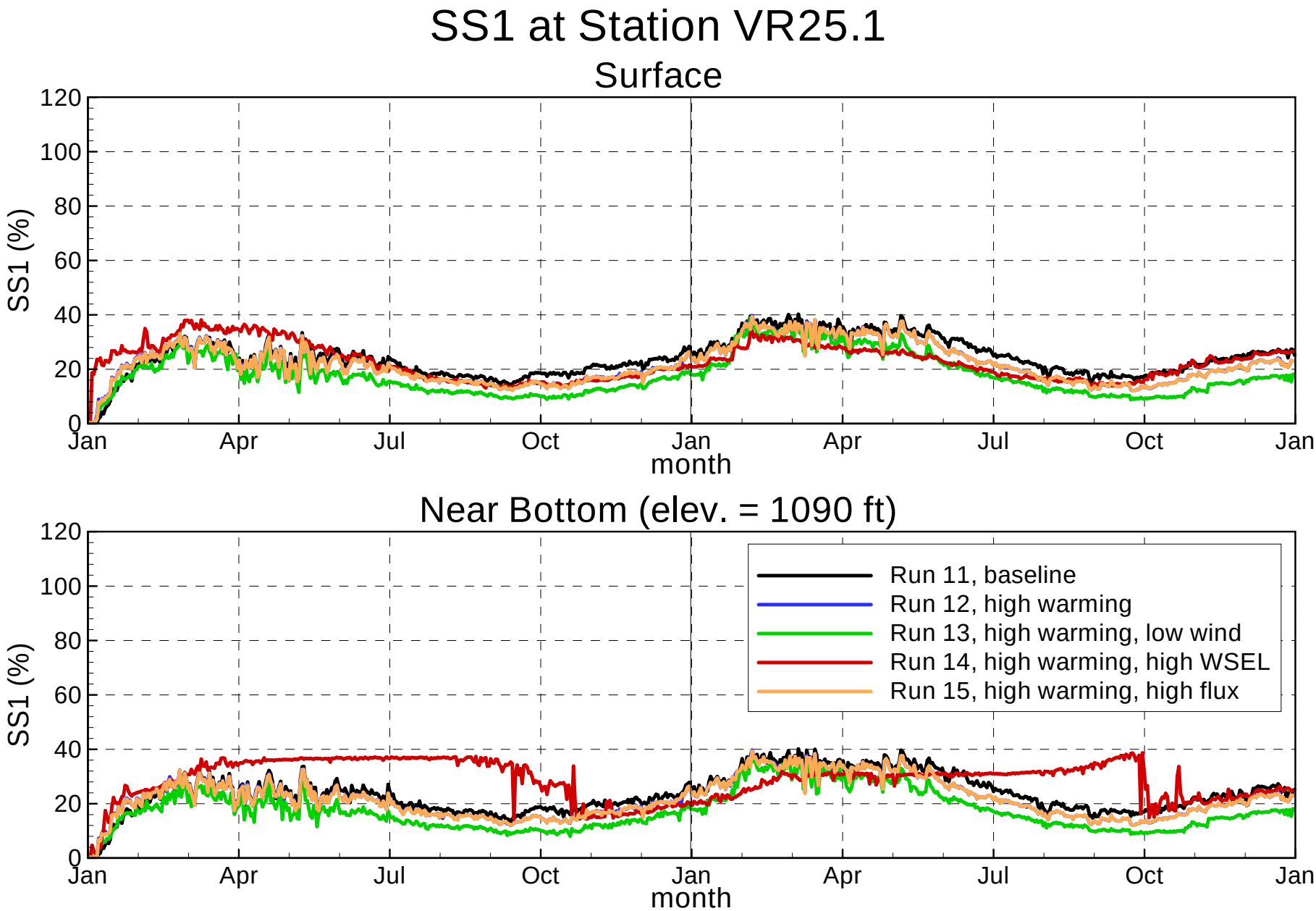
SS1 at Station VR25.1
Surface
SS1 (%)
120
100
80
60
40
20
0
Jan
Apr
Jul
Oct
Jan
Apr
Jul
Oct
Jan
month
Near Bottom (elev. = 1090 ft)
SS1 (%)
Run 11, baseline
Run 12, high warming
Run 13, high warming, low wind
Run 14, high warming, high WSEL
Run 15, high warming, high flux
month

Figure A.187

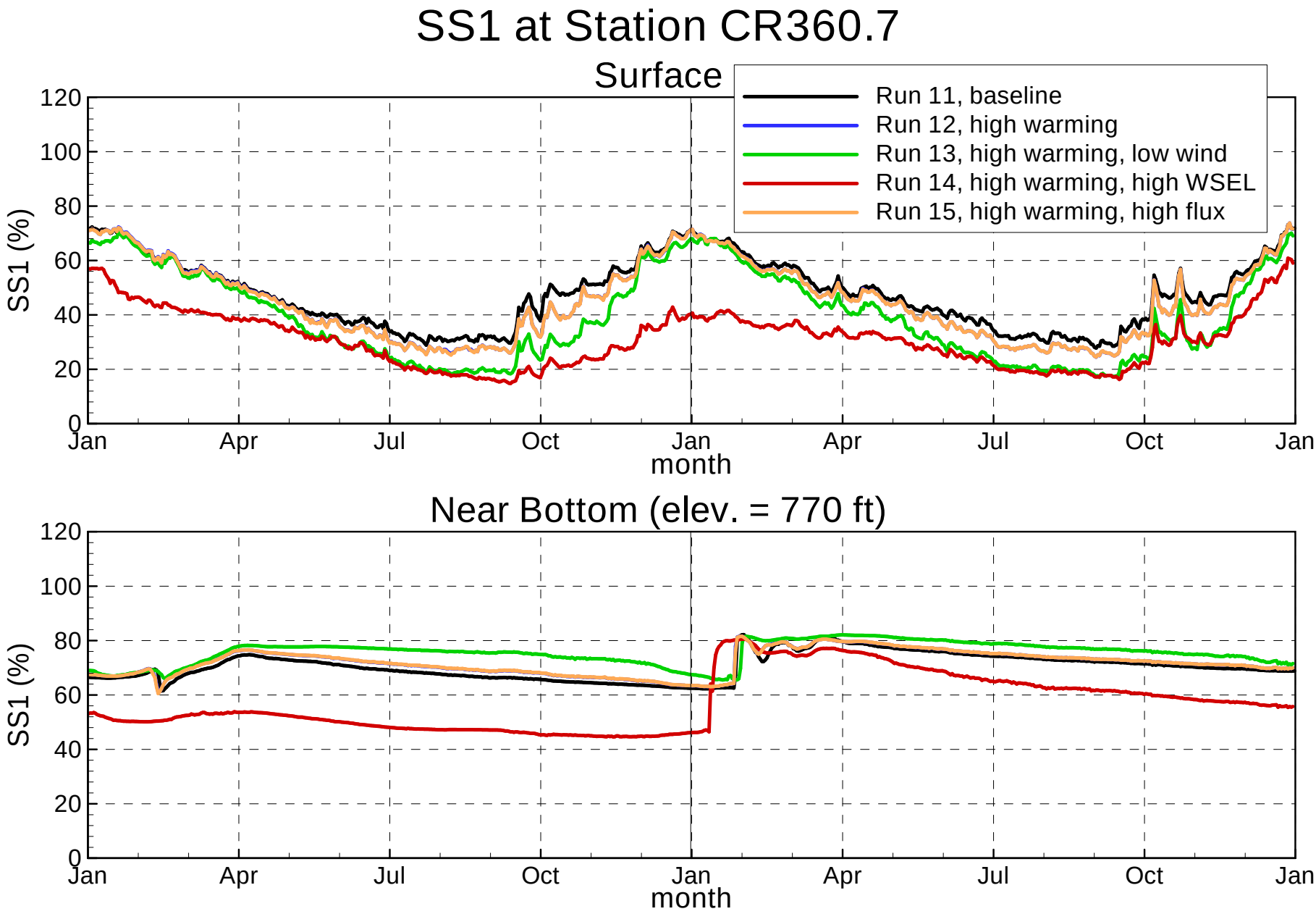
SS1 at Station CR360.7
Surface
Run 11, baseline
Run 12, high warming
Run 13, high warming, low wind
Run 14, high warming, high WSEL
Run 15, high warming, high flux
SS1 (%)
120
100
80
60
40
20
0
Jan
Apr
Jul
Oct
Jan
Apr
Jul
Oct
Jan
month
Near Bottom (elev. = 770 ft)
SS1 (%)
120
100
80
60
40
20
0
Jan
Apr
Jul
Oct
Jan
Apr
Jul
Oct
Jan
month

Figure A.188

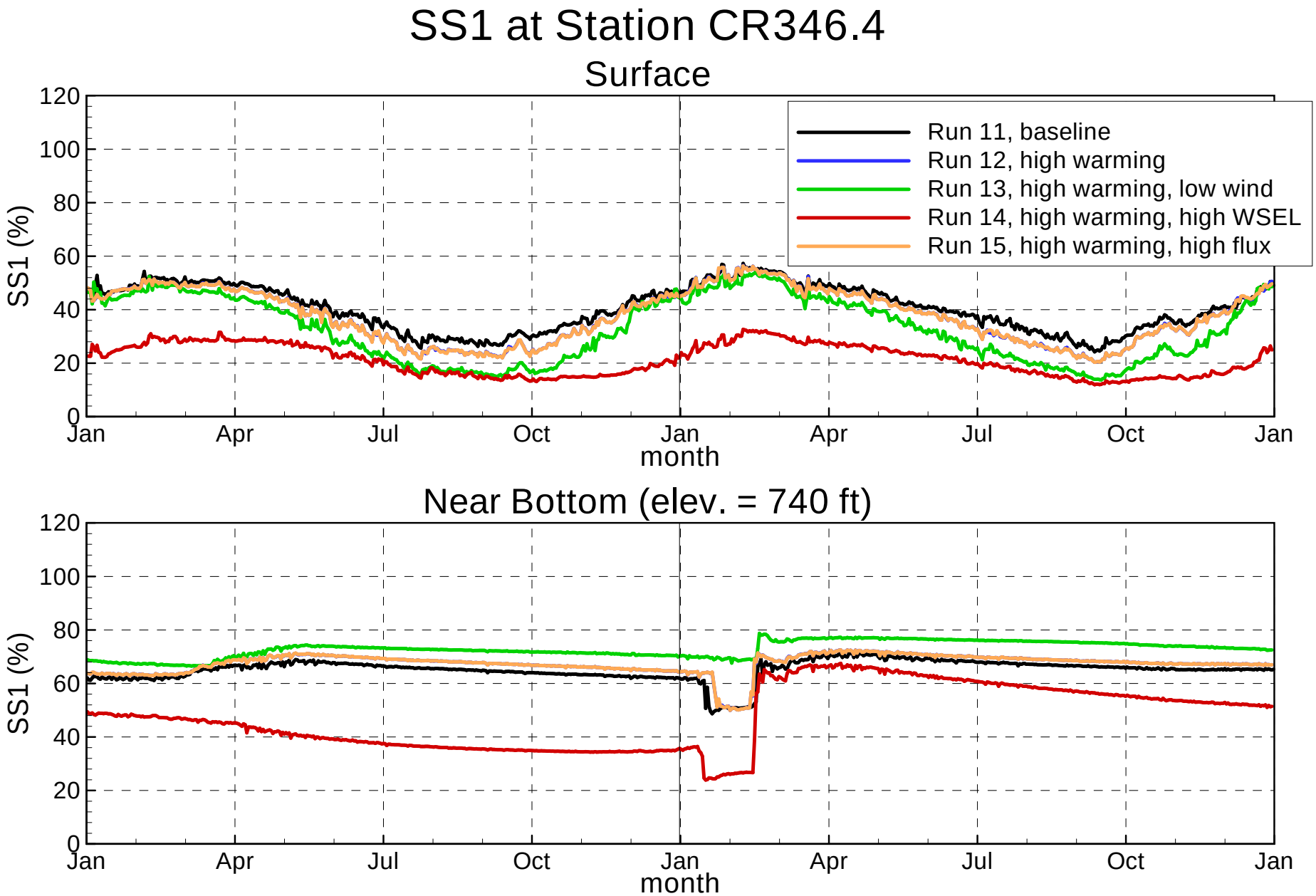
SS1 at Station CR346.4
Surface
Run 11, baseline
Run 12, high warming
Run 13, high warming, low wind
Run 14, high warming, high WSEL
Run 15, high warming, high flux
SS1 (%)
120
100
80
60
40
20
0
Jan
Apr
Jul
Oct
Jan
Apr
Jul
Oct
Jan
month
Near Bottom (elev. = 740 ft)
SS1 (%)
120
100
80
60
40
20
0
Jan
Apr
Jul
Oct
Jan
Apr
Jul
Oct
Jan
month

Figure A.189

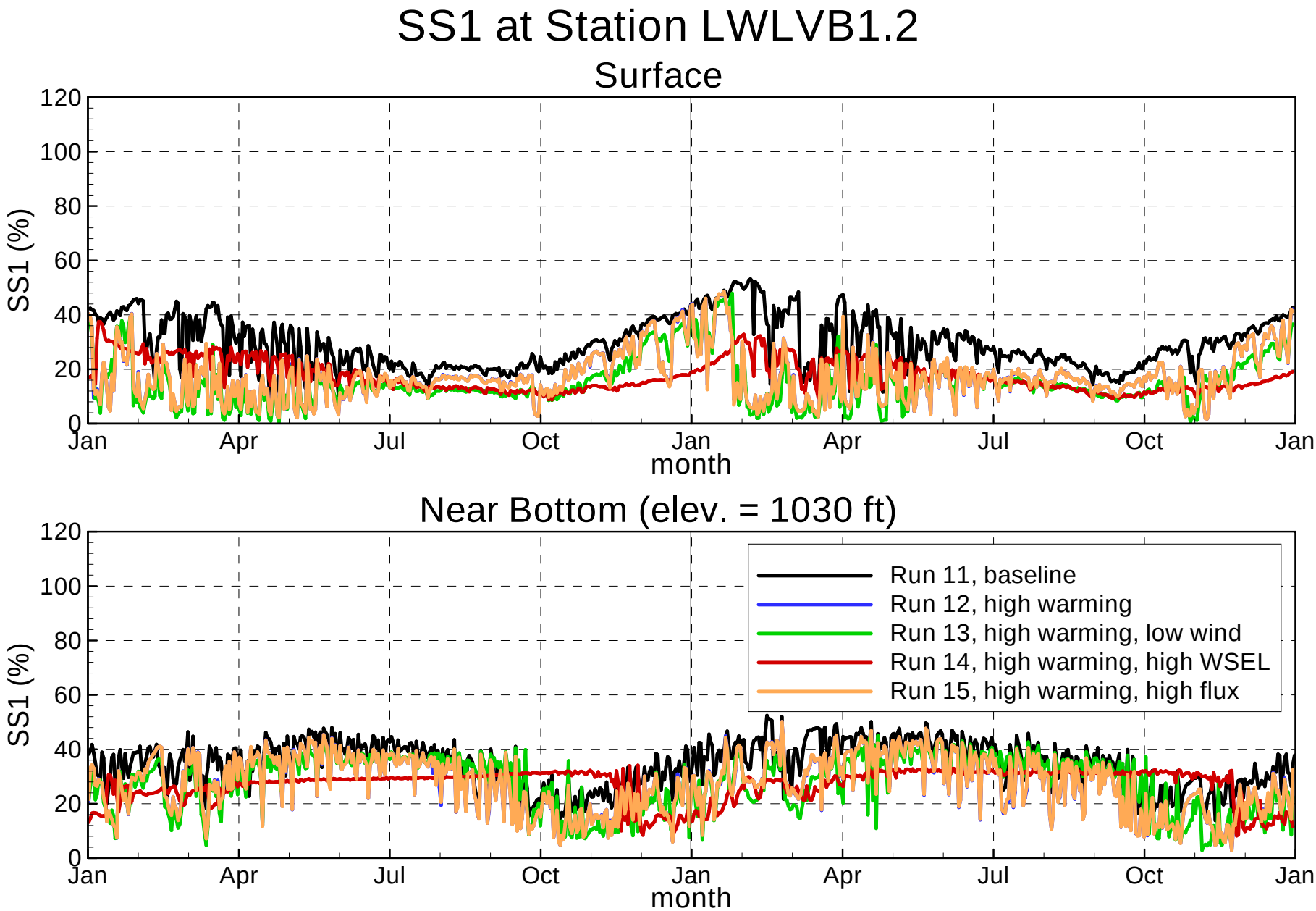
SS1 at Station LWLVB1.2
Surface
SS1 (%)
120
100
80
60
40
20
0
Jan
Apr
Jul
Oct
Jan
Apr
Jul
Oct
Jan
month
Near Bottom (elev. = 1030 ft)
SS1 (%)
Run 11, baseline
Run 12, high warming
Run 13, high warming, low wind
Run 14, high warming, high WSEL
Run 15, high warming, high flux
month

Figure A.190

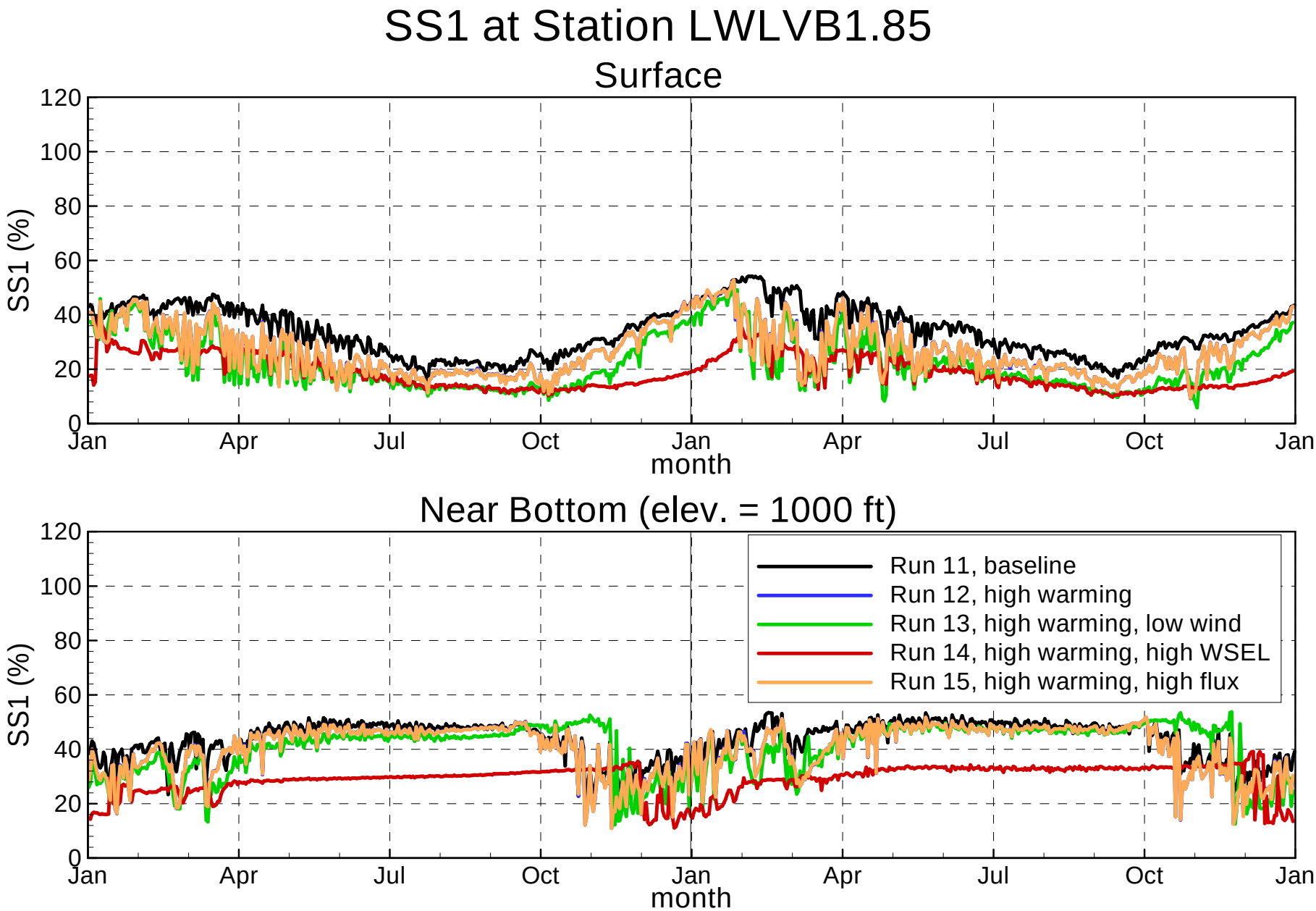
SS1 at Station LWLVB1.85
Surface
SS1 (%)
120
100
80
60
40
20
0
Jan
Apr
Jul
Oct
Jan
Apr
Jul
Oct
Jan
month
Near Bottom (elev. = 1000 ft)
SS1 (%)
Run 11, baseline
Run 12, high warming
Run 13, high warming, low wind
Run 14, high warming, high WSEL
Run 15, high warming, high flux
month

Figure A.191

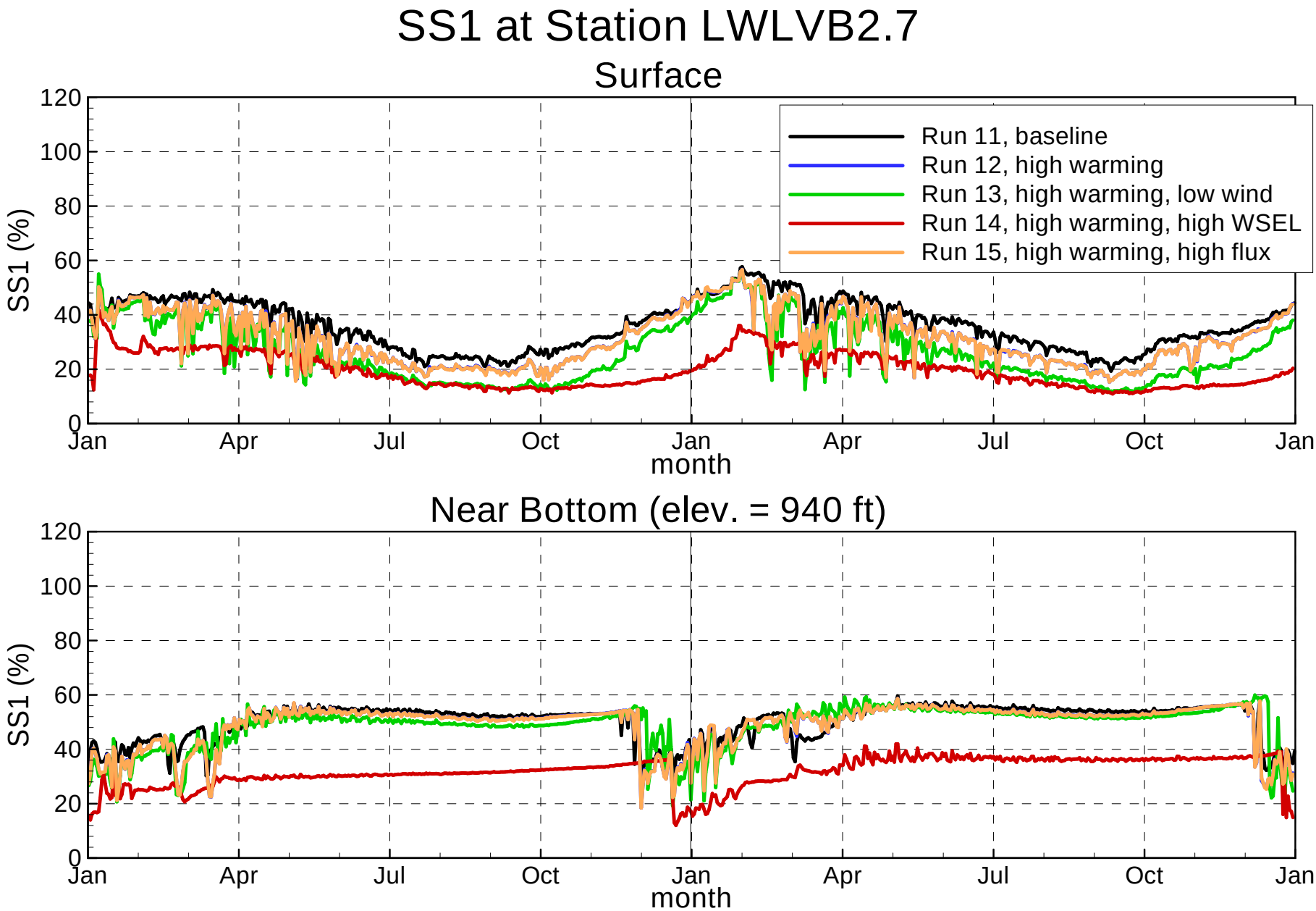
SS1 at Station LWLVB2.7
Surface
Run 11, baseline
Run 12, high warming
Run 13, high warming, low wind
Run 14, high warming, high WSEL
Run 15, high warming, high flux
SS1 (%)
120
100
80
60
40
20
0
Jan
Apr
Jul
Oct
Jan
Apr
Jul
Oct
Jan
month
Near Bottom (elev. = 940 ft)
SS1 (%)
120
100
80
60
40
20
0
Jan
Apr
Jul
Oct
Jan
Apr
Jul
Oct
Jan
month

Figure A.192

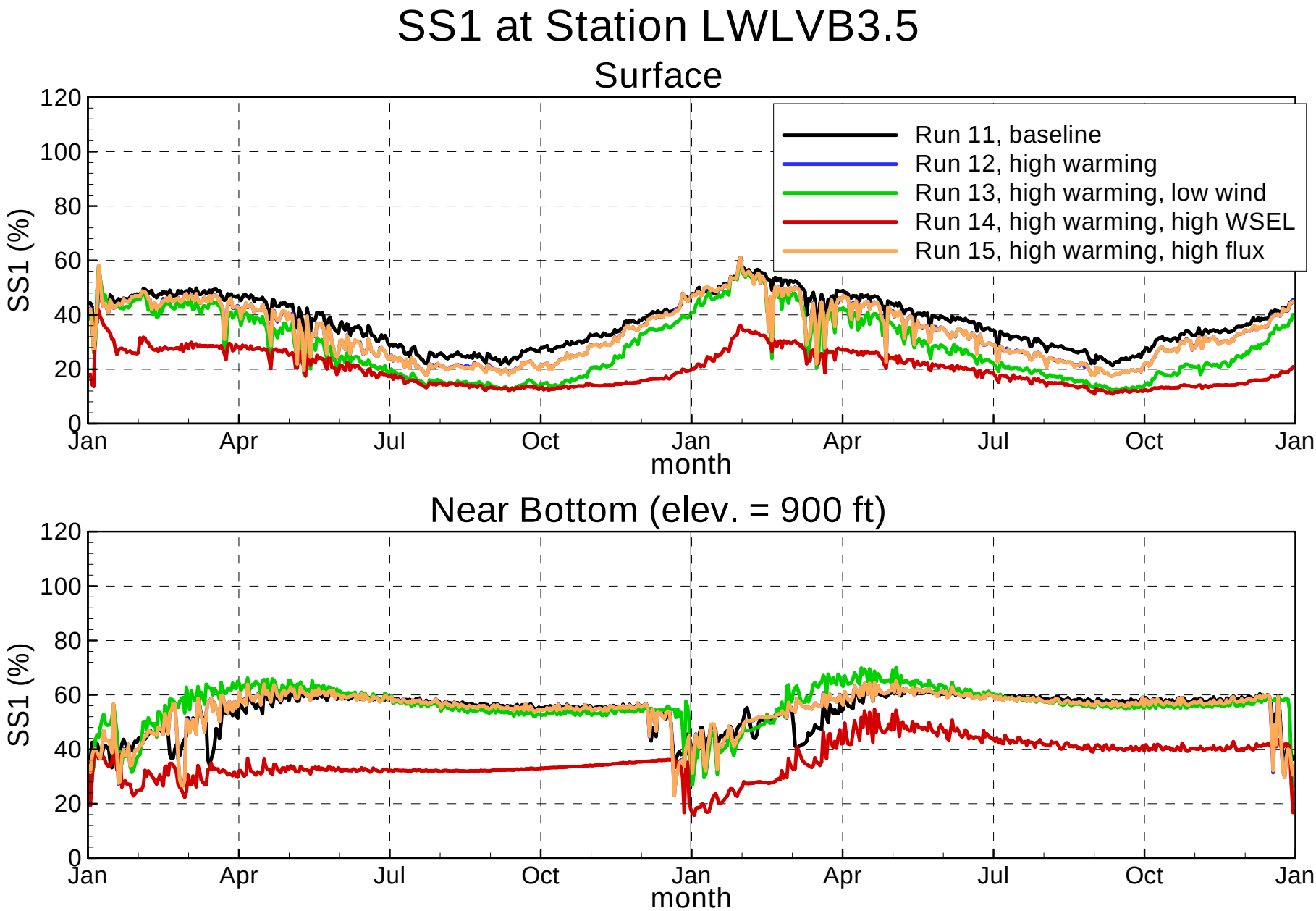
SS1 at Station LWLVB3.5
Surface
Run 11, baseline
Run 12, high warming
Run 13, high warming, low wind
Run 14, high warming, high WSEL
Run 15, high warming, high flux
SS1 (%)
0
20
40
60
80
100
120
Jan
Apr
Jul
Oct
Jan
Apr
Jul
Oct
Jan
month
Near Bottom (elev. = 900 ft)
SS1 (%)
0
20
40
60
80
100
120
Jan
Apr
Jul
Oct
Jan
Apr
Jul
Oct
Jan
month

Figure A.193

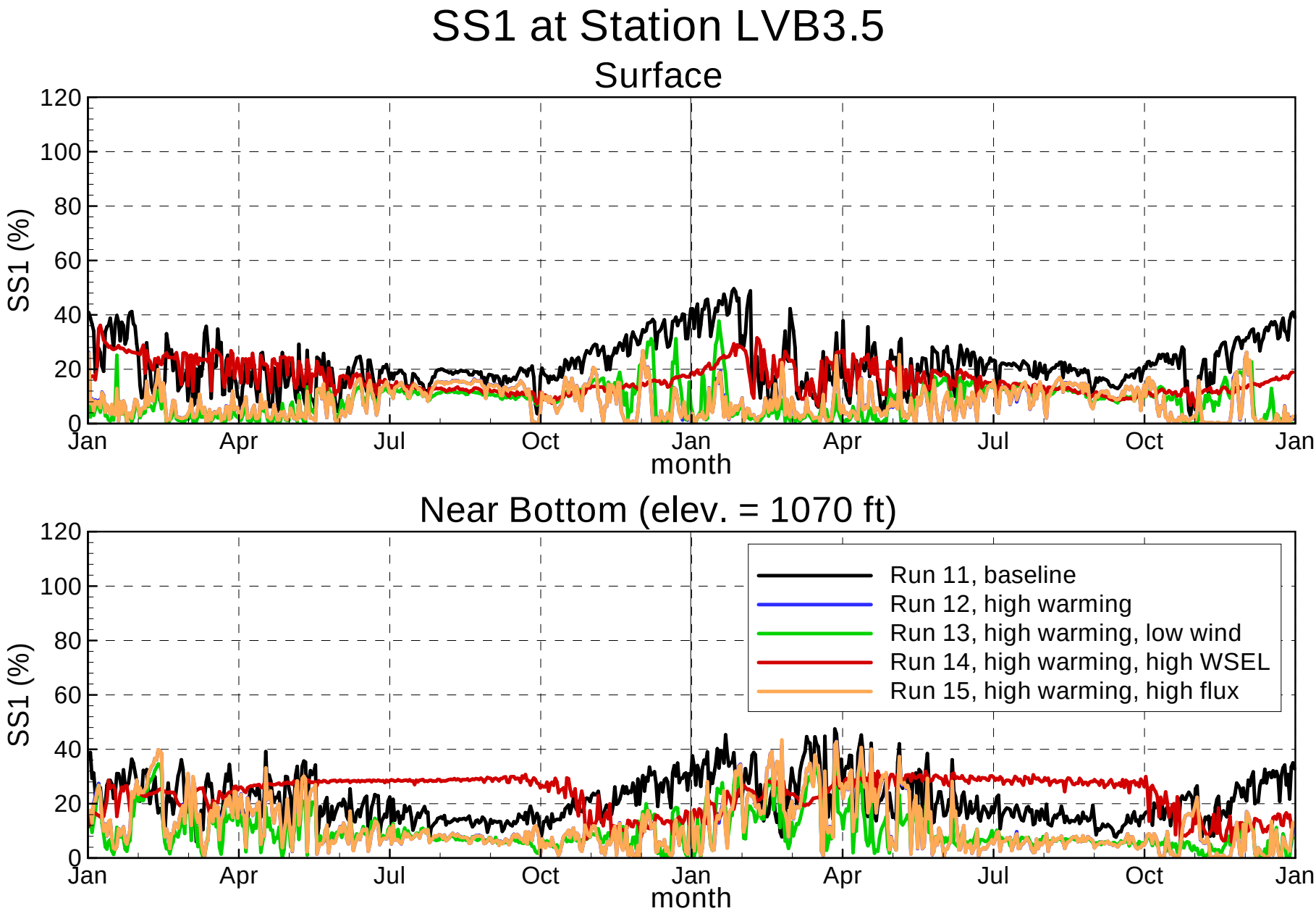
SS1 at Station LVB3.5
Surface
SS1 (%)
120
100
80
60
40
20
0
Jan
Apr
Jul
Oct
Jan
Apr
Jul
Oct
Jan
month
Near Bottom (elev. = 1070 ft)
SS1 (%)
Run 11, baseline
Run 12, high warming
Run 13, high warming, low wind
Run 14, high warming, high WSEL
Run 15, high warming, high flux
month

Figure A.194

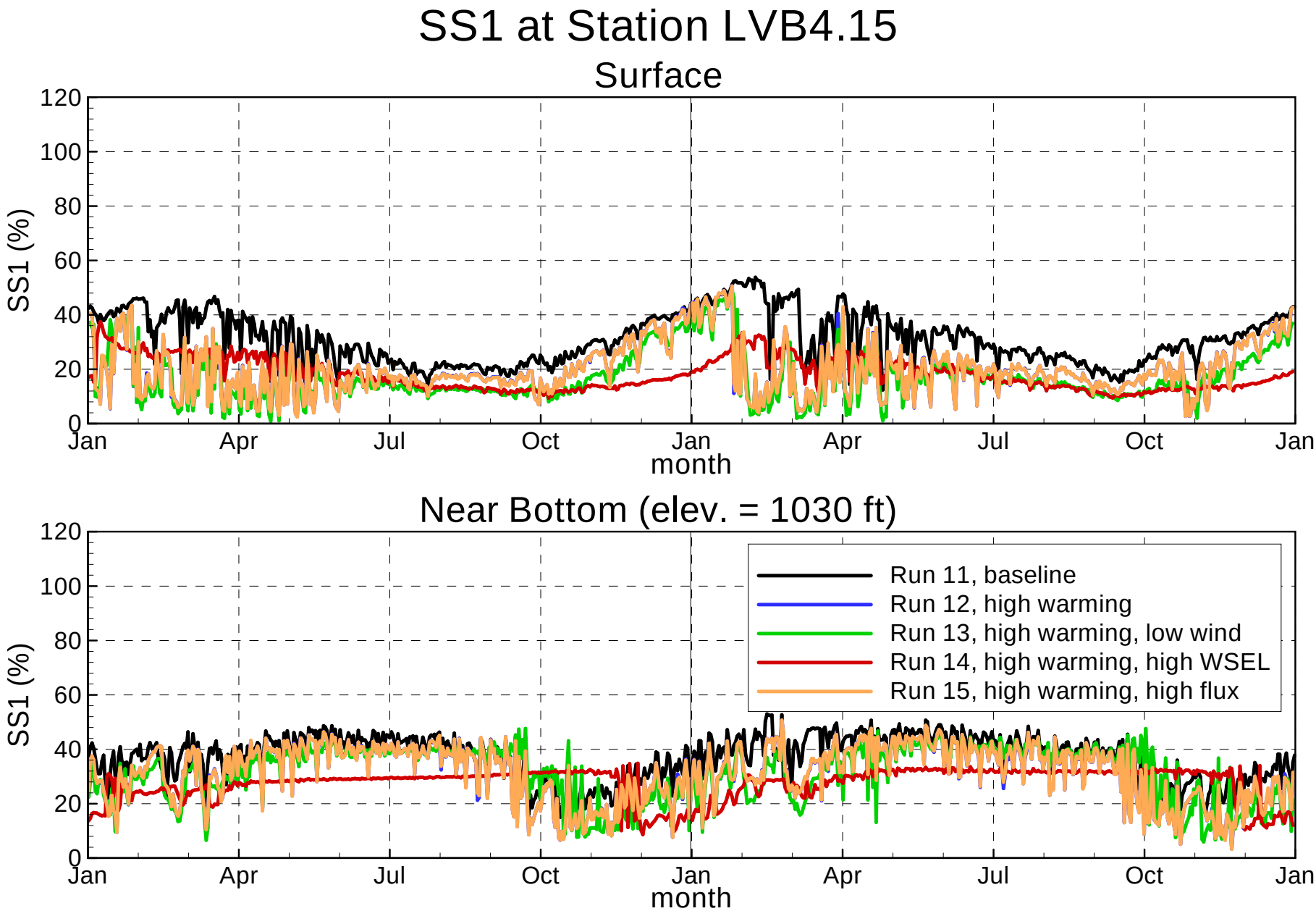
SS1 at Station LVB4.15
Surface
SS1 (%)
120
100
80
60
40
20
0
Jan
Apr
Jul
Oct
Jan
Apr
Jul
Oct
Jan
month
Near Bottom (elev. = 1030 ft)
SS1 (%)
Run 11, baseline
Run 12, high warming
Run 13, high warming, low wind
Run 14, high warming, high WSEL
Run 15, high warming, high flux
month

Figure A.195

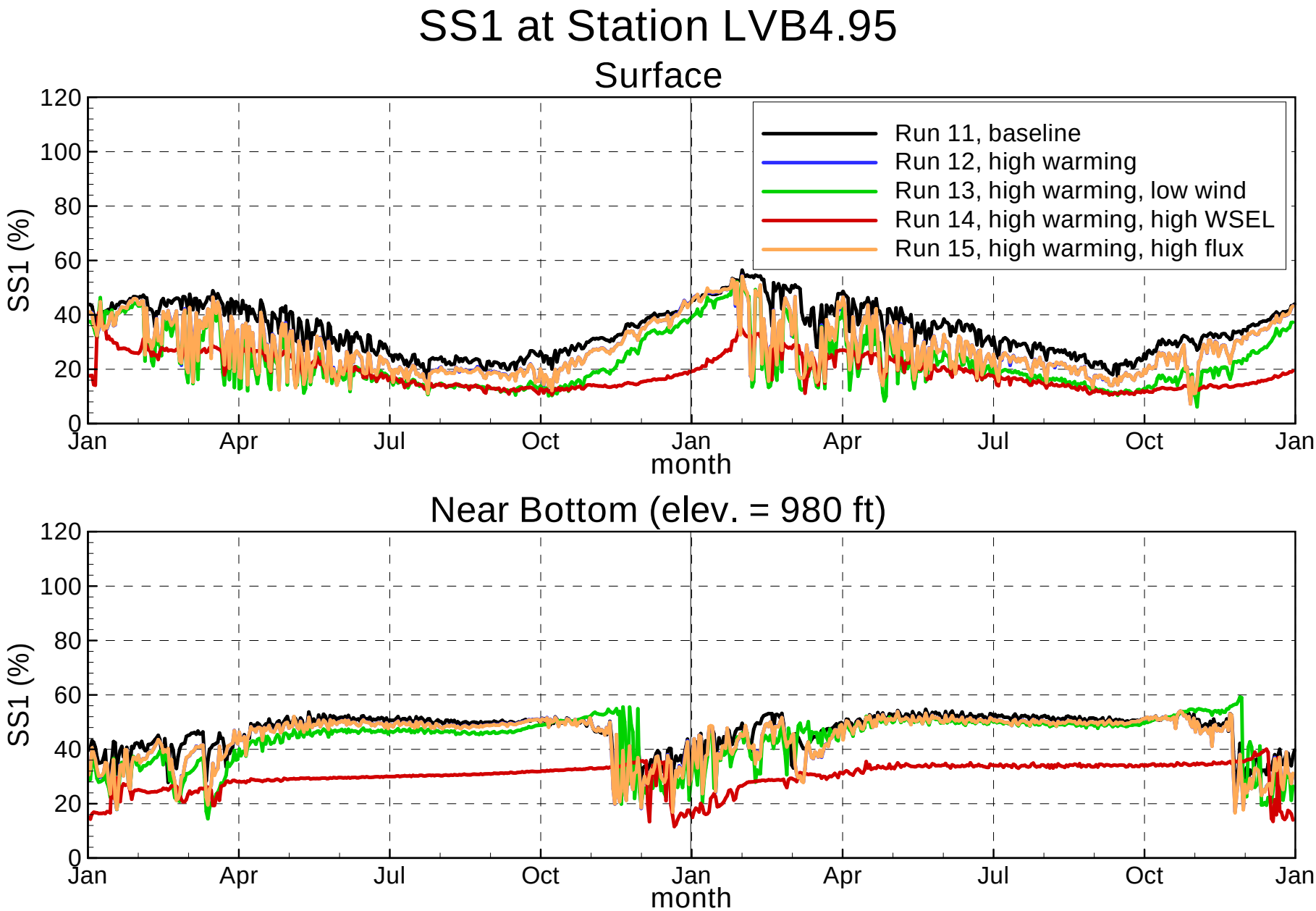
SS1 at Station LVB4.95
Surface
Run 11, baseline
Run 12, high warming
Run 13, high warming, low wind
Run 14, high warming, high WSEL
Run 15, high warming, high flux
SS1 (%)
120
100
80
60
40
20
0
Jan
Apr
Jul
Oct
Jan
Apr
Jul
Oct
Jan
month
Near Bottom (elev. = 980 ft)
SS1 (%)
120
100
80
60
40
20
0
Jan
Apr
Jul
Oct
Jan
Apr
Jul
Oct
Jan
month

Figure A.196

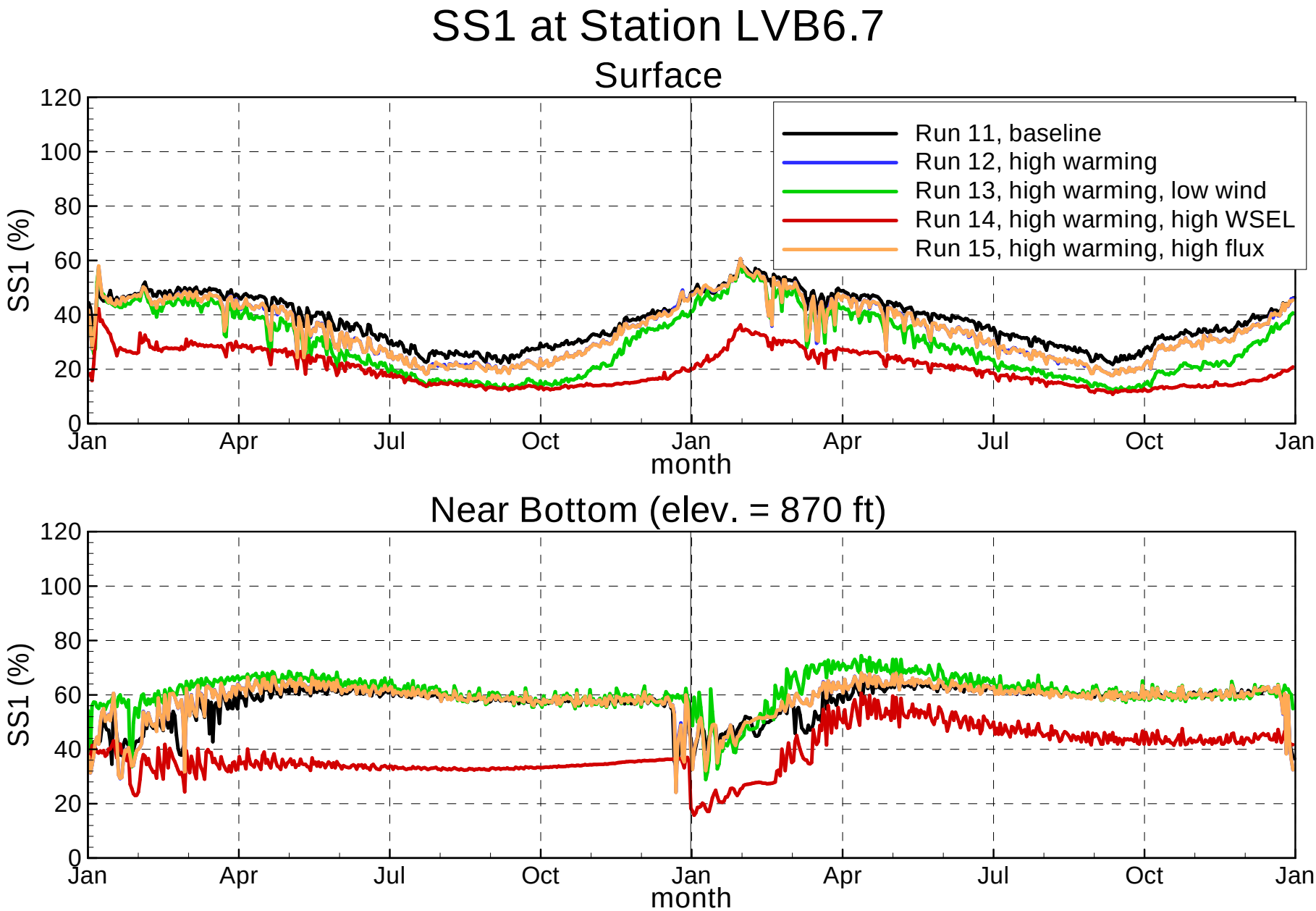
SS1 at Station LVB6.7
Surface
Run 11, baseline
Run 12, high warming
Run 13, high warming, low wind
Run 14, high warming, high WSEL
Run 15, high warming, high flux
SS1 (%)
120
100
80
60
40
20
0
Jan
Apr
Jul
Oct
Jan
Apr
Jul
Oct
Jan
month
Near Bottom (elev. = 870 ft)
SS1 (%)
120
100
80
60
40
20
0
Jan
Apr
Jul
Oct
Jan
Apr
Jul
Oct
Jan
month

Figure A.197

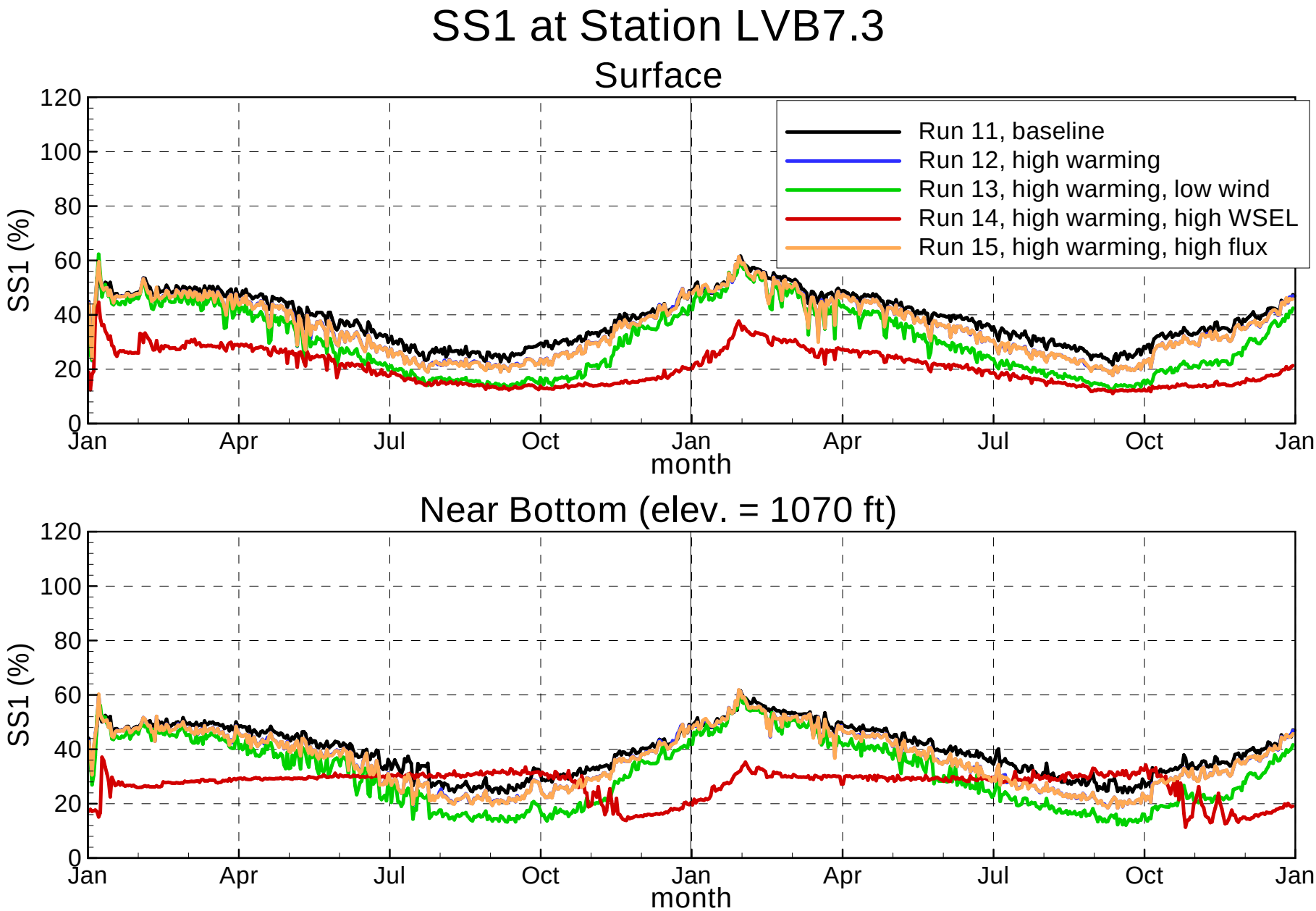
SS1 at Station LVB7.3
Surface
Run 11, baseline
Run 12, high warming
Run 13, high warming, low wind
Run 14, high warming, high WSEL
Run 15, high warming, high flux
SS1 (%)
120
100
80
60
40
20
0
Jan
Apr
Jul
Oct
Jan
Apr
Jul
Oct
Jan
month
Near Bottom (elev. = 1070 ft)
SS1 (%)
120
100
80
60
40
20
0
Jan
Apr
Jul
Oct
Jan
Apr
Jul
Oct
Jan
month

Figure A.198

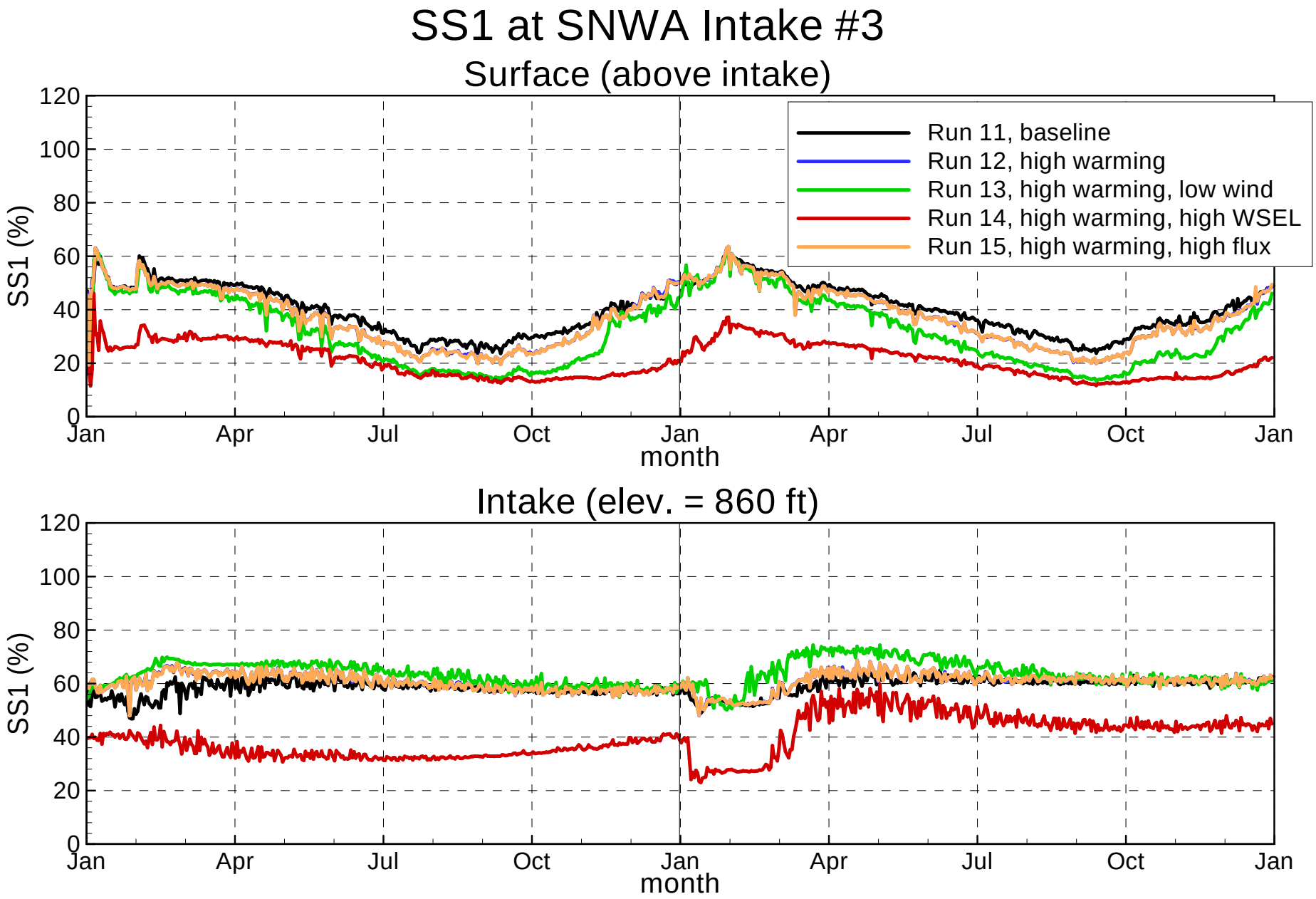
SS1 at SNWA Intake #3
Surface (above intake)
Intake (elev. = 860 ft)
SS1 (%)
month
Jan
Apr
Jul
Oct
0
20
40
60
80
100
120
Run 11, baseline
Run 12, high warming
Run 13, high warming, low wind
Run 14, high warming, high WSEL
Run 15, high warming, high flux

Figure A.199

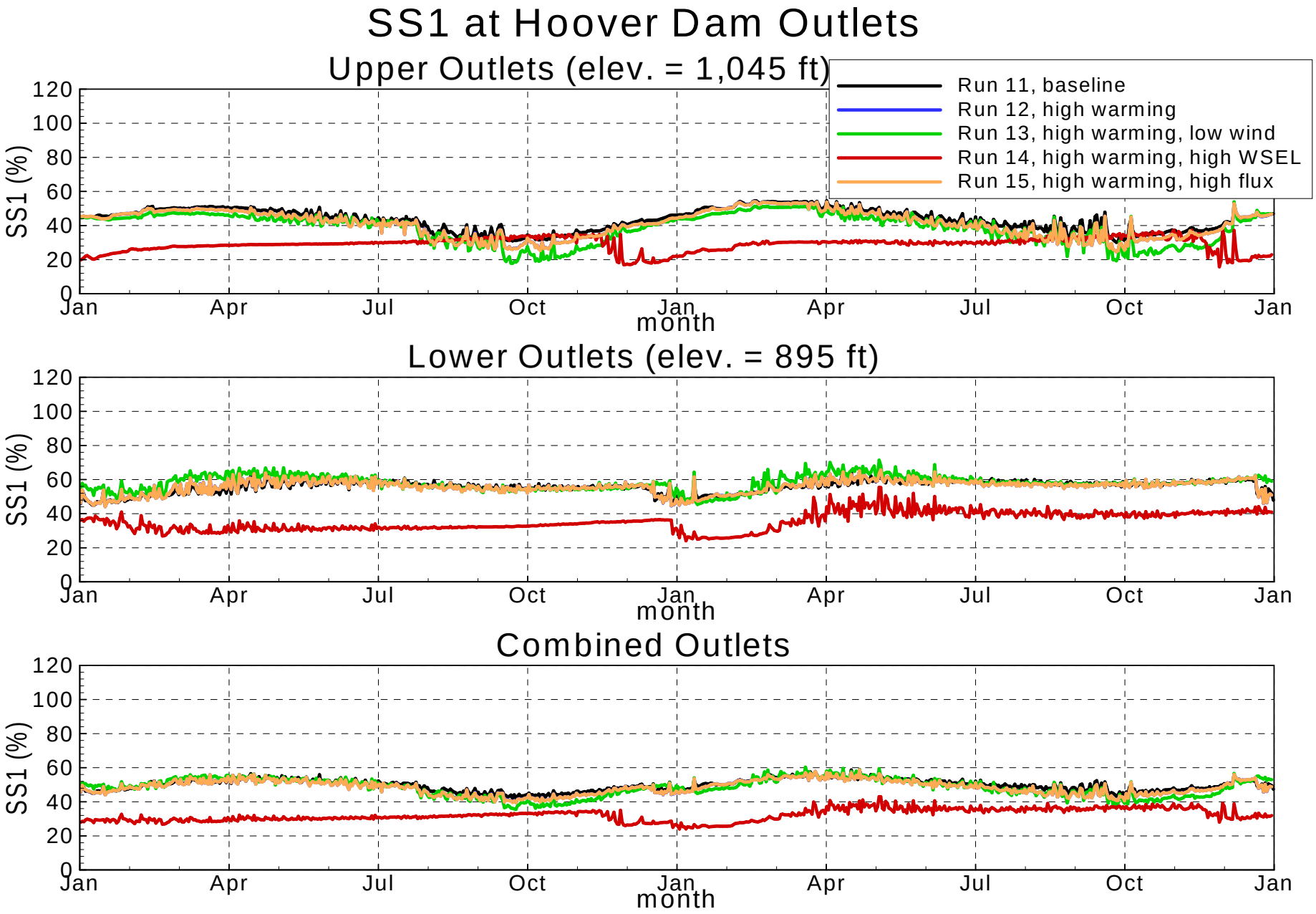

Figure A.200

FLOW SCIENCE

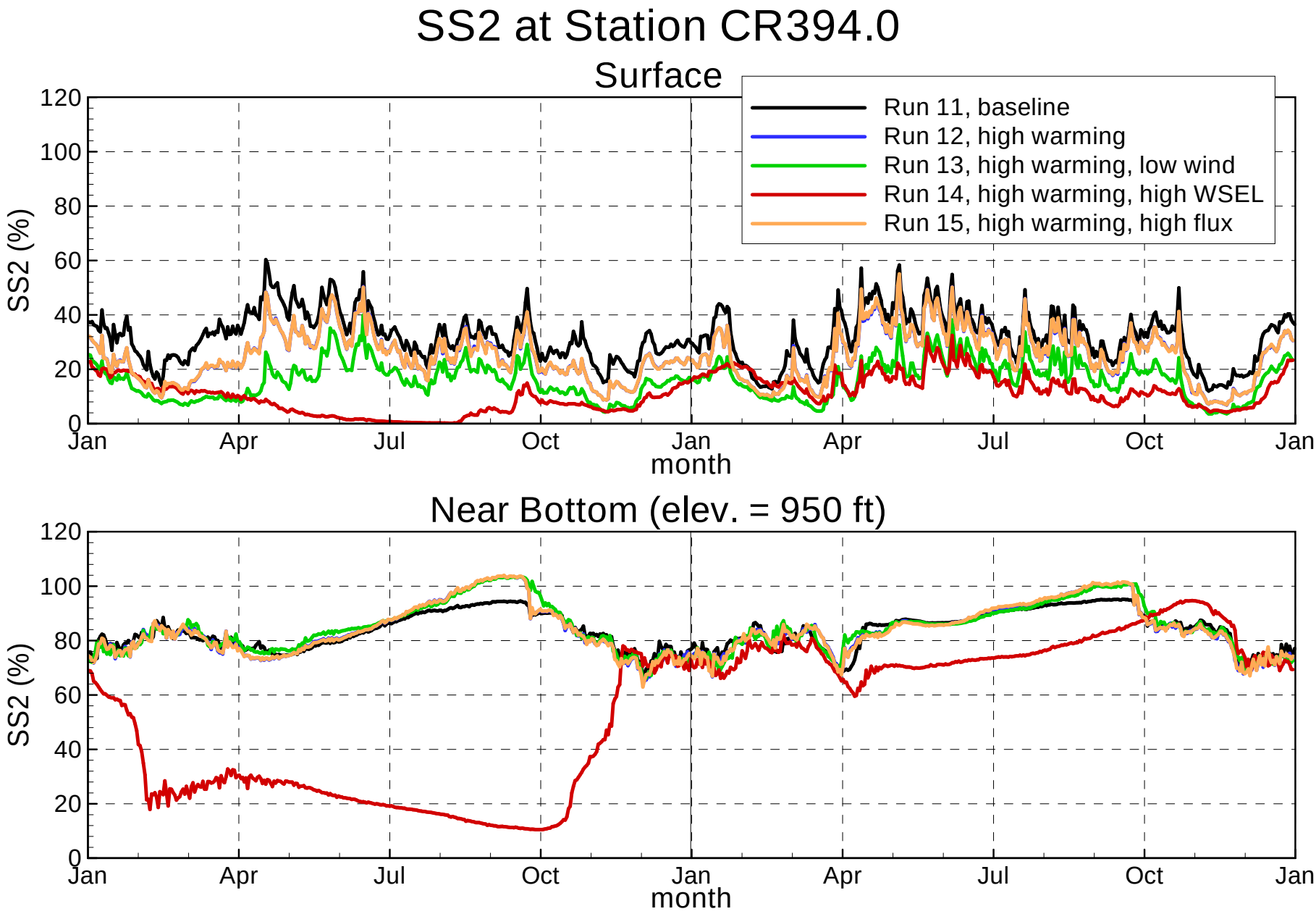
SS2 at Station CR394.0
Surface
Run 11, baseline
Run 12, high warming
Run 13, high warming, low wind
Run 14, high warming, high WSEL
Run 15, high warming, high flux
SS2 (%)
120
100
80
60
40
20
0
Jan
Apr
Jul
Oct
Jan
Apr
Jul
Oct
Jan
month
Near Bottom (elev. = 950 ft)
SS2 (%)
120
100
80
60
40
20
0
Jan
Apr
Jul
Oct
Jan
Apr
Jul
Oct
Jan
month

Figure A.201

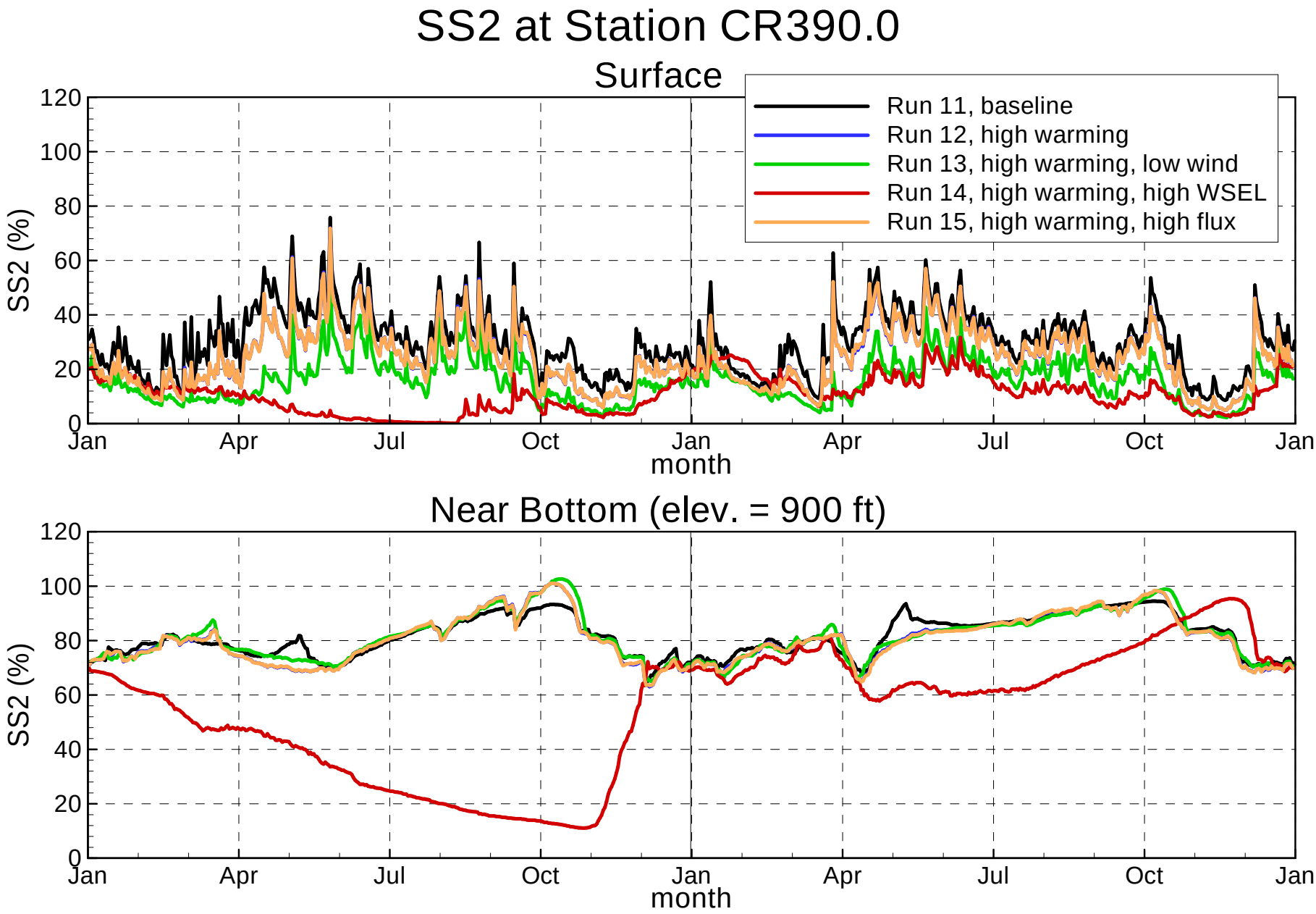
SS2 at Station CR390.0
Surface
Run 11, baseline
Run 12, high warming
Run 13, high warming, low wind
Run 14, high warming, high WSEL
Run 15, high warming, high flux
SS2 (%)
120
100
80
60
40
20
0
Jan
Apr
Jul
Oct
Jan
Apr
Jul
Oct
Jan
month
Near Bottom (elev. = 900 ft)
SS2 (%)
120
100
80
60
40
20
0
Jan
Apr
Jul
Oct
Jan
Apr
Jul
Oct
Jan
month

Figure A.202

SS2 at Station CR380.0

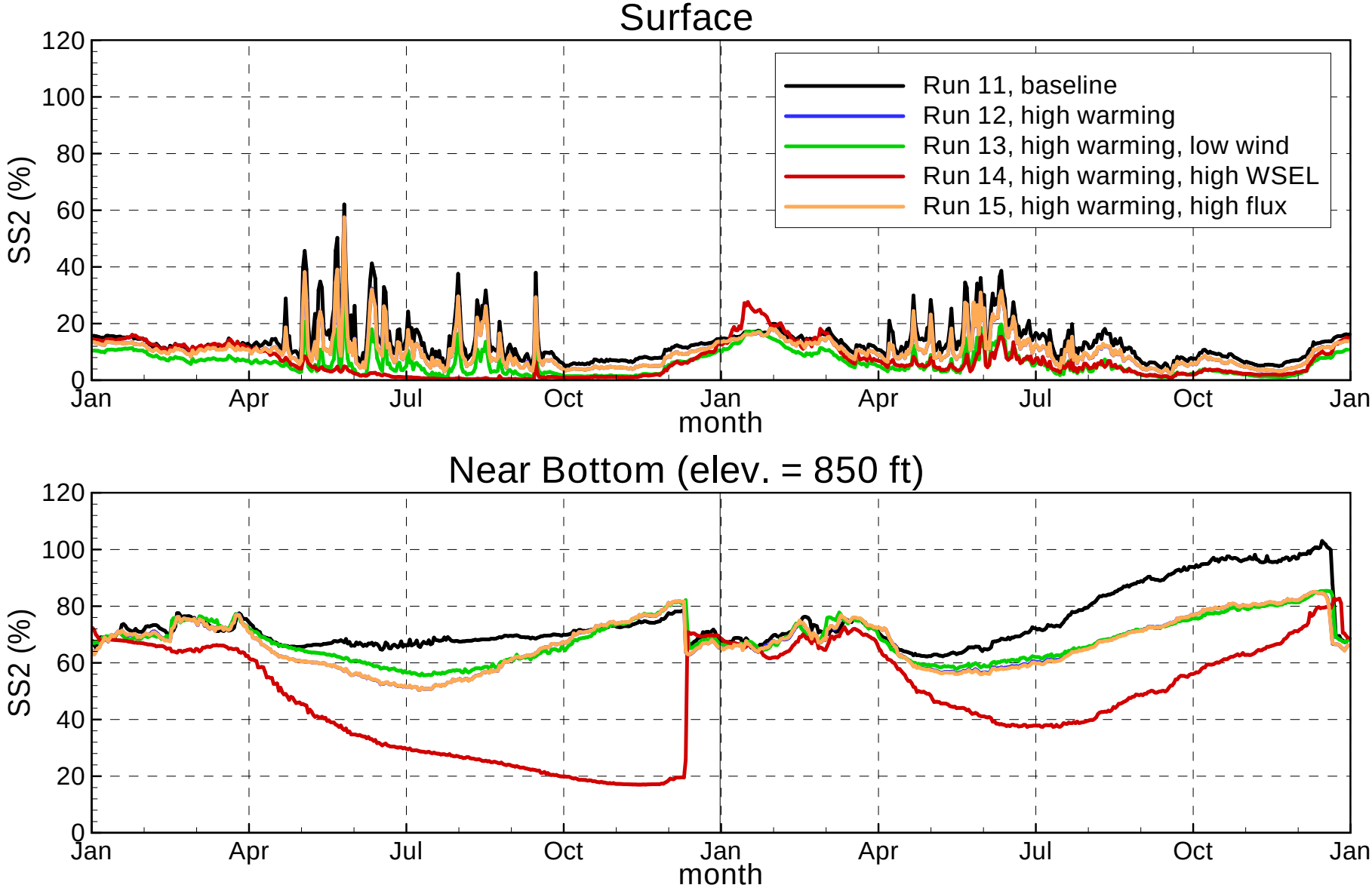

Figure A.203

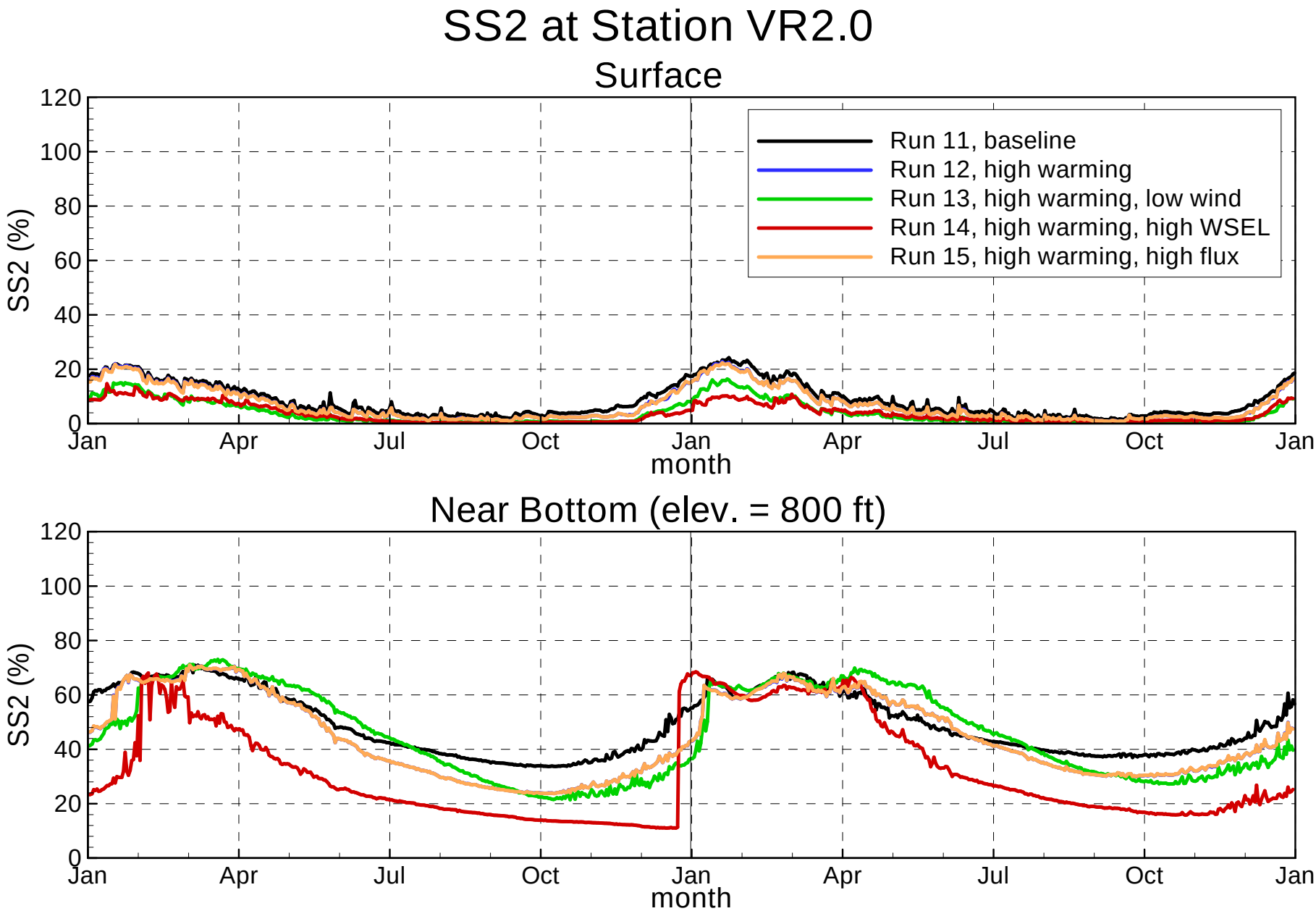
SS2 at Station VR2.0
Surface
SS2 (%)
120
100
80
60
40
20
0
Jan
Apr
Jul
Oct
Jan
Apr
Jul
Oct
Jan
month
Run 11, baseline
Run 12, high warming
Run 13, high warming, low wind
Run 14, high warming, high WSEL
Run 15, high warming, high flux
Near Bottom (elev. = 800 ft)
SS2 (%)
120
100
80
60
40
20
0
Jan
Apr
Jul
Oct
Jan
Apr
Jul
Oct
Jan
month

Figure A.204

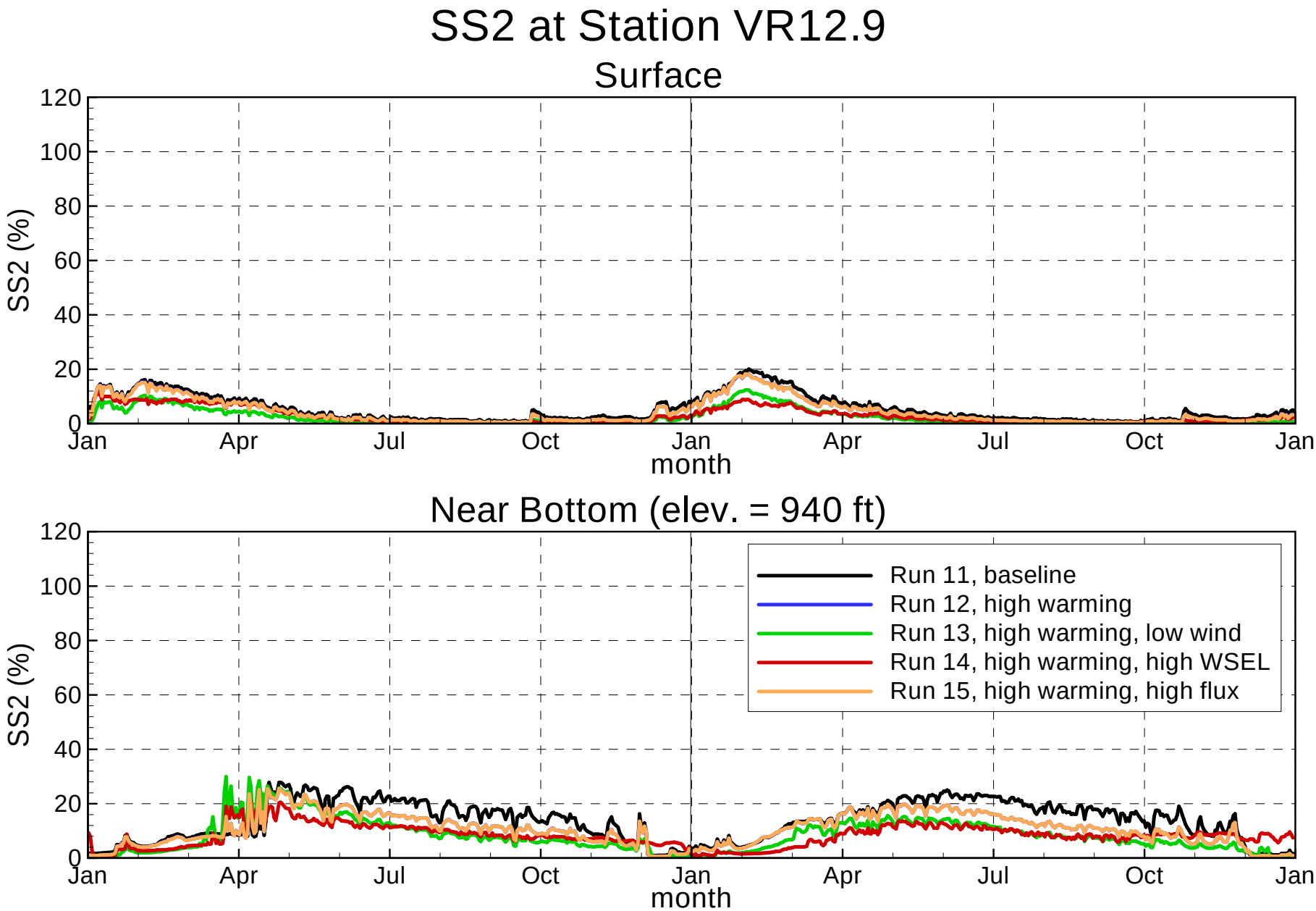
SS2 at Station VR12.9
Surface
SS2 (%)
120
100
80
60
40
20
0
Jan
Apr
Jul
Oct
Jan
Apr
Jul
Oct
Jan
month
Near Bottom (elev. = 940 ft)
SS2 (%)
Run 11, baseline
Run 12, high warming
Run 13, high warming, low wind
Run 14, high warming, high WSEL
Run 15, high warming, high flux
month

Figure A.205

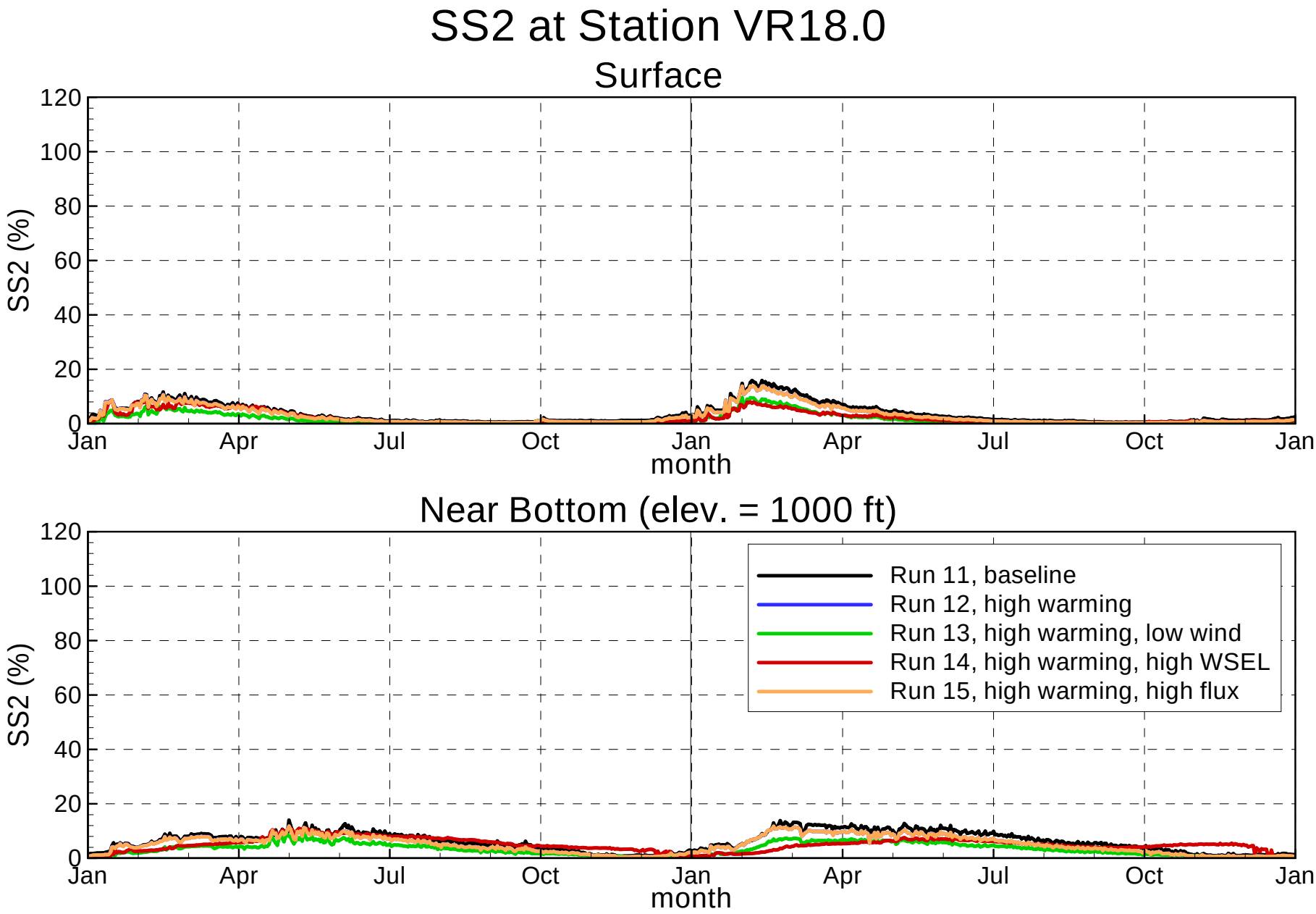
SS2 at Station VR18.0
Surface
SS2 (%)
120
100
80
60
40
20
0
Jan
Apr
Jul
Oct
Jan
Apr
Jul
Oct
Jan
month
Near Bottom (elev. = 1000 ft)
SS2 (%)
Run 11, baseline
Run 12, high warming
Run 13, high warming, low wind
Run 14, high warming, high WSEL
Run 15, high warming, high flux
month

Figure A.206

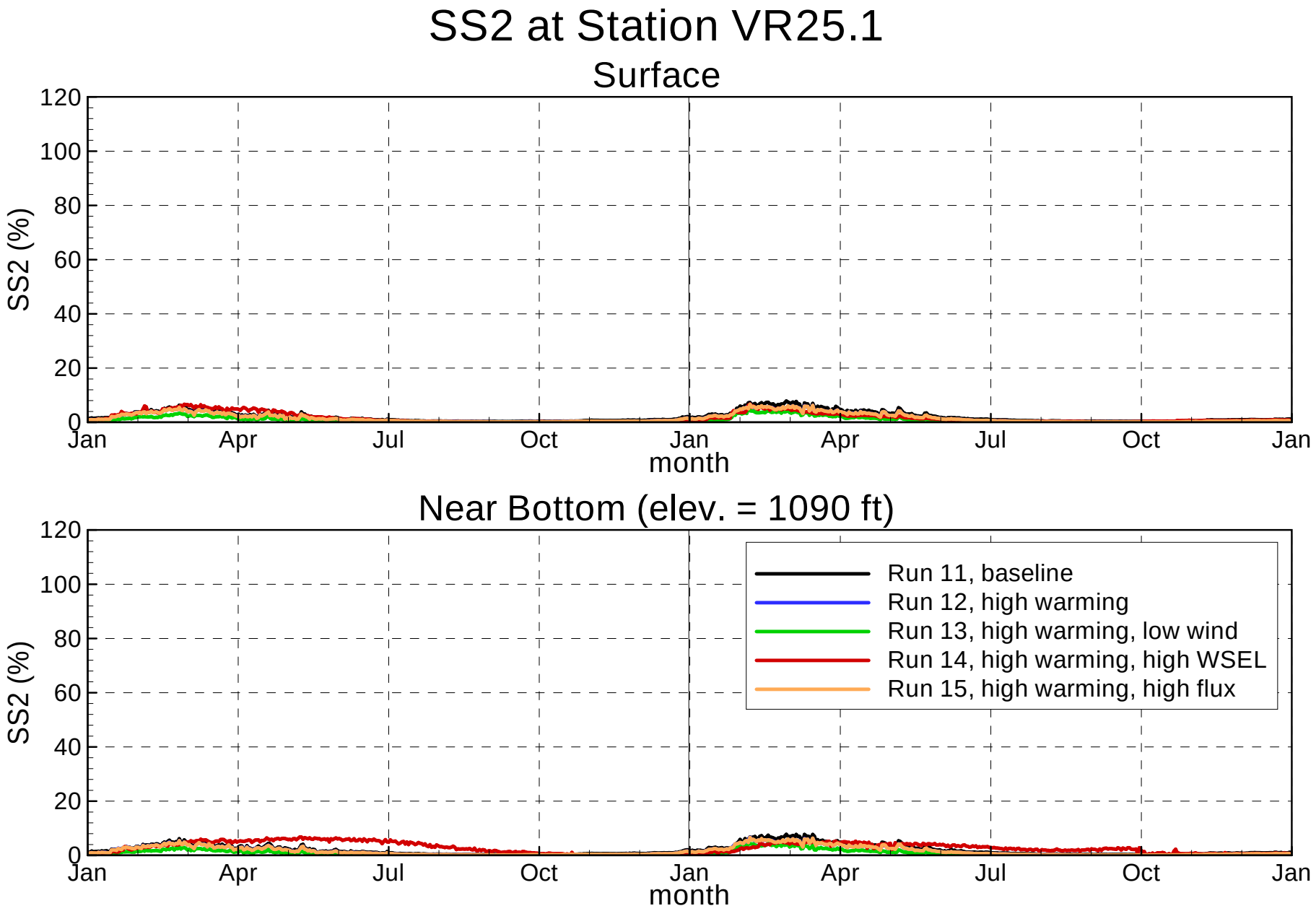
SS2 at Station VR25.1
Surface
SS2 (%)
120
100
80
60
40
20
0
Jan
Apr
Jul
Oct
Jan
Apr
Jul
Oct
Jan
month
Near Bottom (elev. = 1090 ft)
SS2 (%)
Run 11, baseline
Run 12, high warming
Run 13, high warming, low wind
Run 14, high warming, high WSEL
Run 15, high warming, high flux
month

Figure A.207

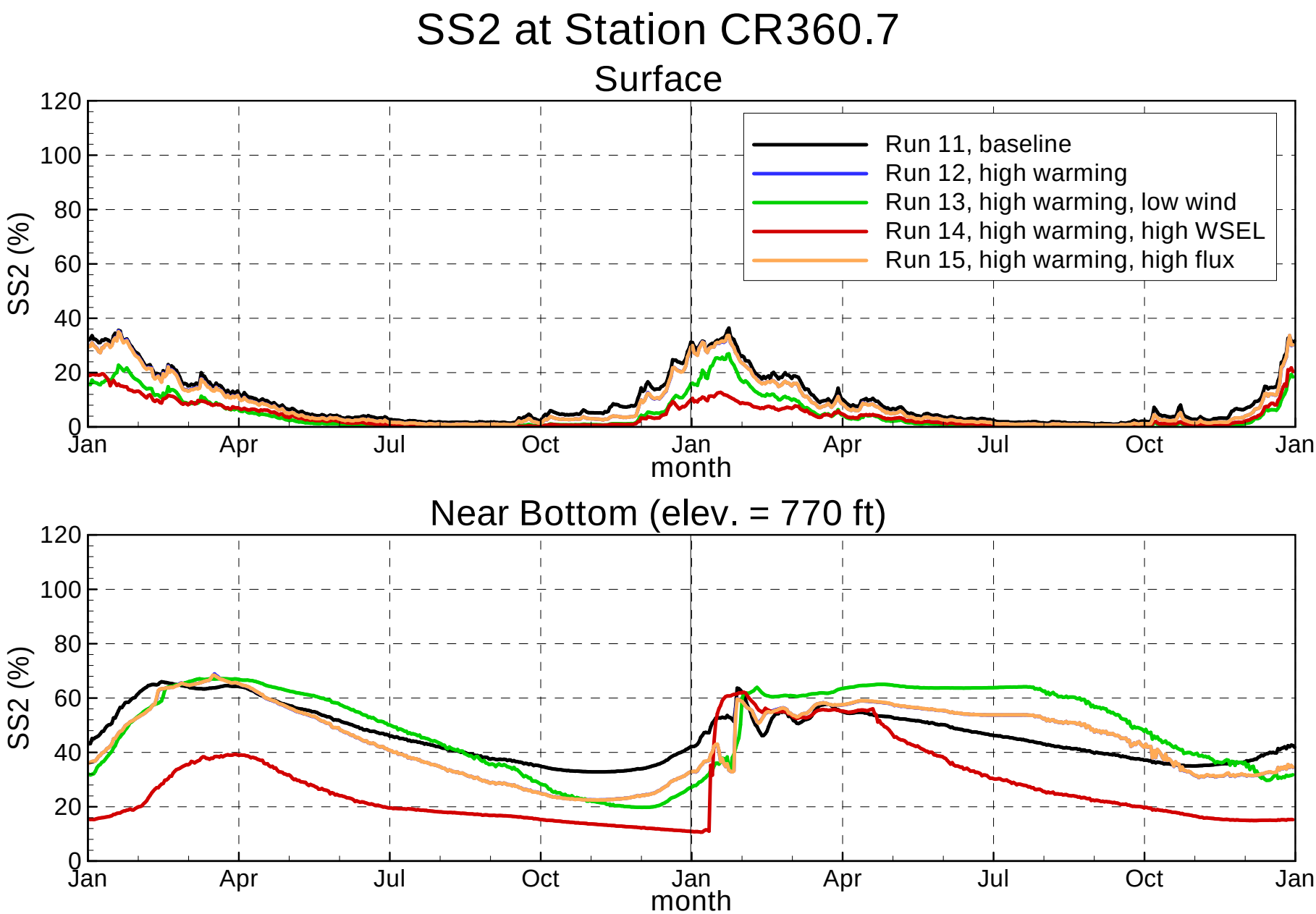
SS2 at Station CR360.7
Surface
Run 11, baseline
Run 12, high warming
Run 13, high warming, low wind
Run 14, high warming, high WSEL
Run 15, high warming, high flux
SS2 (%)
120
100
80
60
40
20
0
Jan
Apr
Jul
Oct
Jan
Apr
Jul
Oct
Jan
month
Near Bottom (elev. = 770 ft)
SS2 (%)
120
100
80
60
40
20
0
Jan
Apr
Jul
Oct
Jan
Apr
Jul
Oct
Jan
month

Figure A.208

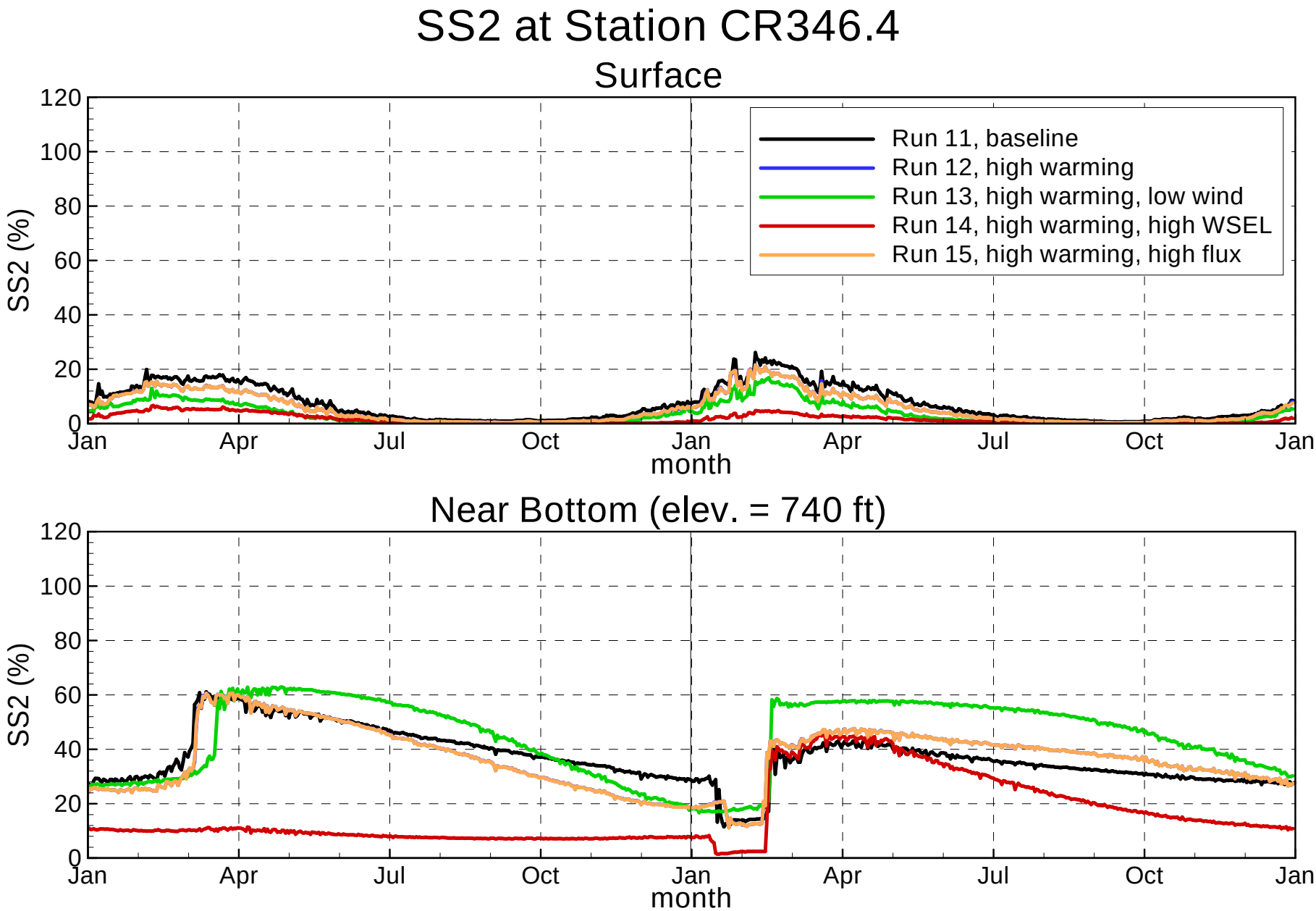
SS2 at Station CR346.4
Surface
Run 11, baseline
Run 12, high warming
Run 13, high warming, low wind
Run 14, high warming, high WSEL
Run 15, high warming, high flux
SS2 (%)
120
100
80
60
40
20
0
Jan
Apr
Jul
Oct
Jan
Apr
Jul
Oct
Jan
month
Near Bottom (elev. = 740 ft)
SS2 (%)
120
100
80
60
40
20
0
Jan
Apr
Jul
Oct
Jan
Apr
Jul
Oct
Jan
month

Figure A.209

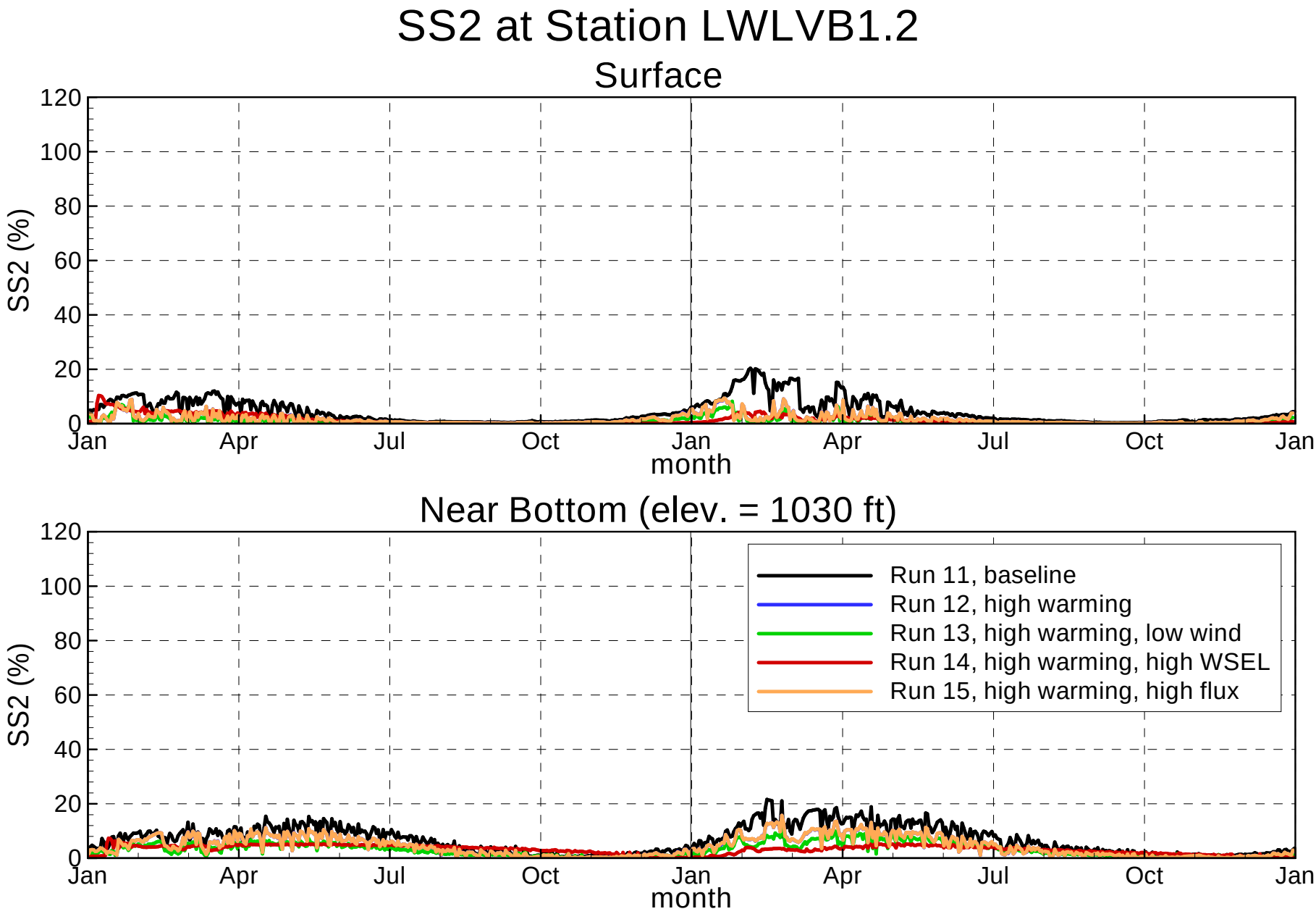
SS2 at Station LWLVB1.2
Surface
SS2 (%)
120
100
80
60
40
20
0
Jan
Apr
Jul
Oct
Jan
Apr
Jul
Oct
Jan
month
Near Bottom (elev. = 1030 ft)
SS2 (%)
Run 11, baseline
Run 12, high warming
Run 13, high warming, low wind
Run 14, high warming, high WSEL
Run 15, high warming, high flux
month

Figure A.210

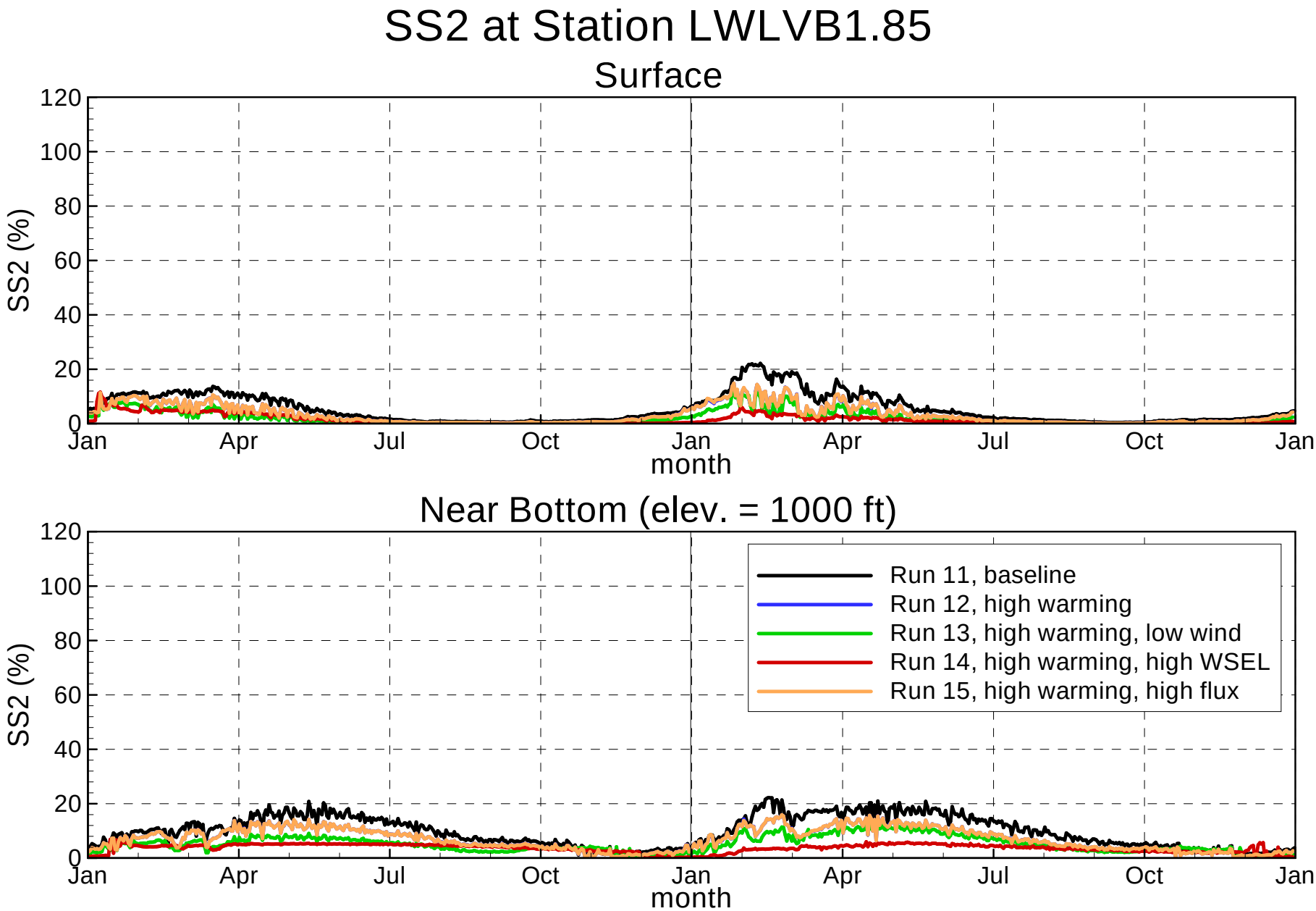
SS2 at Station LWLVB1.85
Surface
SS2 (%)
120
100
80
60
40
20
0
Jan
Apr
Jul
Oct
Jan
Apr
Jul
Oct
Jan
month
Near Bottom (elev. = 1000 ft)
SS2 (%)
Run 11, baseline
Run 12, high warming
Run 13, high warming, low wind
Run 14, high warming, high WSEL
Run 15, high warming, high flux
month

Figure A.211

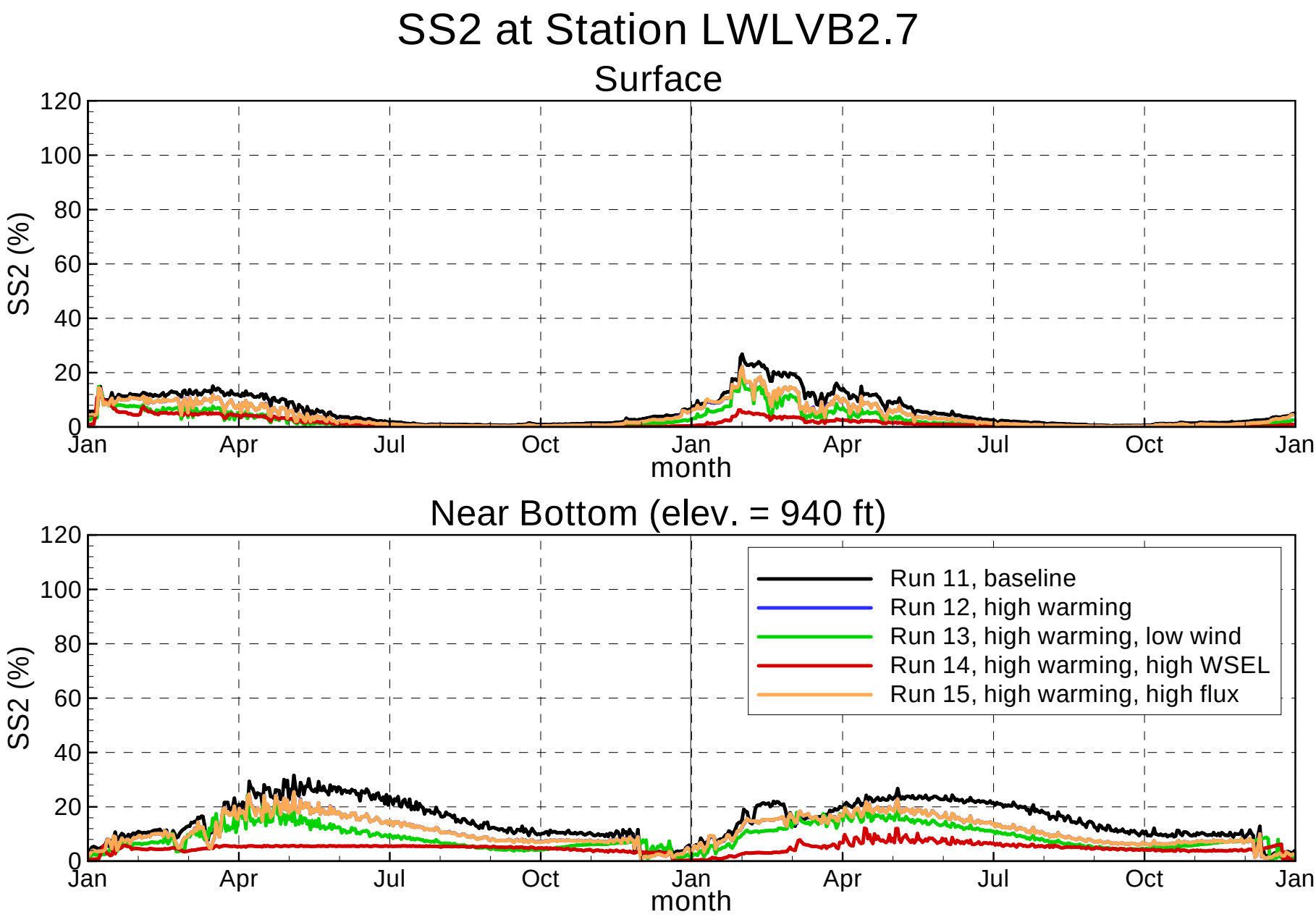
SS2 at Station LWLVB2.7
Surface
SS2 (%)
120
100
80
60
40
20
0
Jan
Apr
Jul
Oct
Jan
Apr
Jul
Oct
Jan
month
Near Bottom (elev. = 940 ft)
SS2 (%)
Run 11, baseline
Run 12, high warming
Run 13, high warming, low wind
Run 14, high warming, high WSEL
Run 15, high warming, high flux
month

Figure A.212

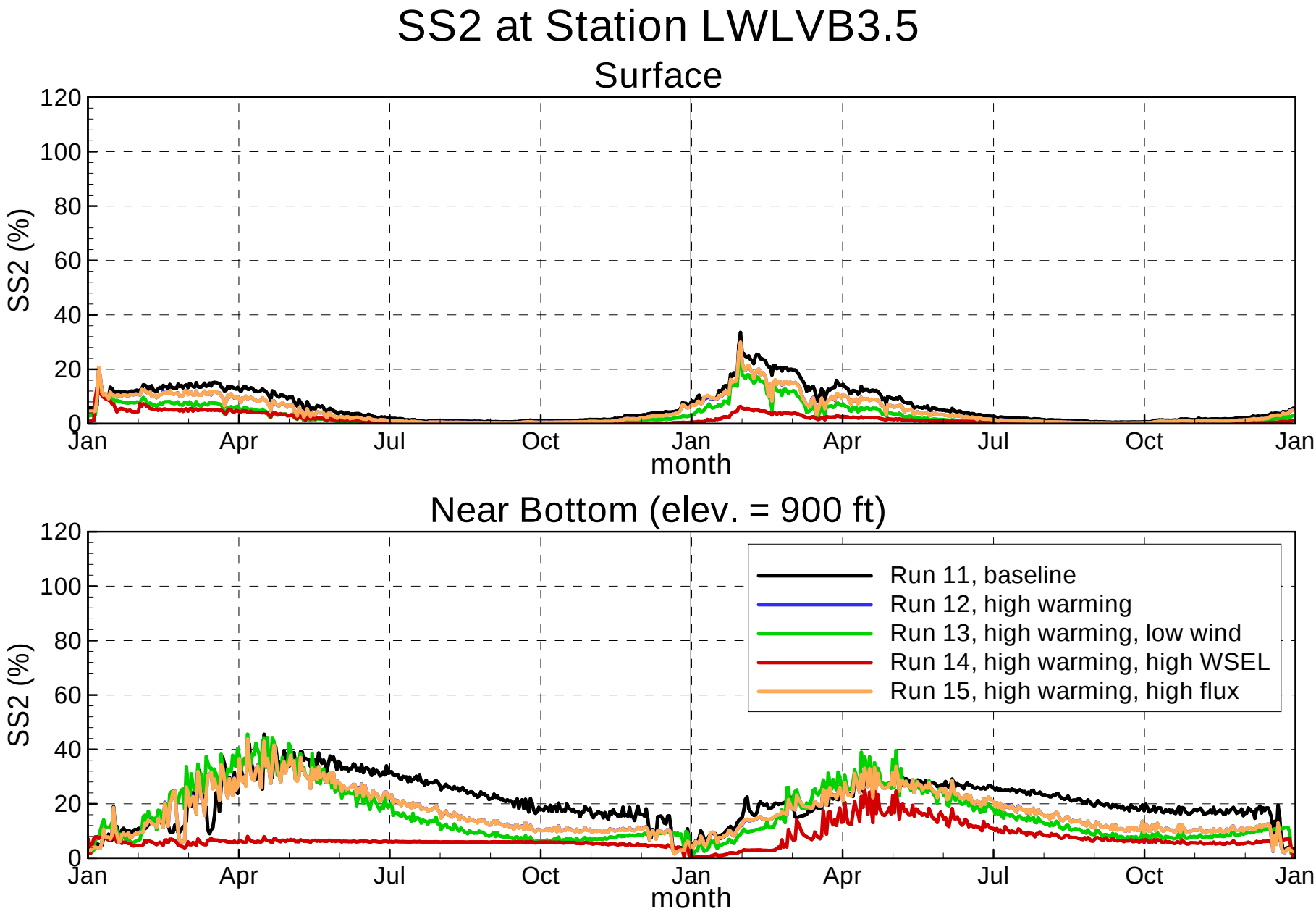
SS2 at Station LWLVB3.5
Surface
SS2 (%)
120
100
80
60
40
20
0
Jan
Apr
Jul
Oct
Jan
Apr
Jul
Oct
Jan
month
Near Bottom (elev. = 900 ft)
SS2 (%)
Run 11, baseline
Run 12, high warming
Run 13, high warming, low wind
Run 14, high warming, high WSEL
Run 15, high warming, high flux
month

Figure A.213

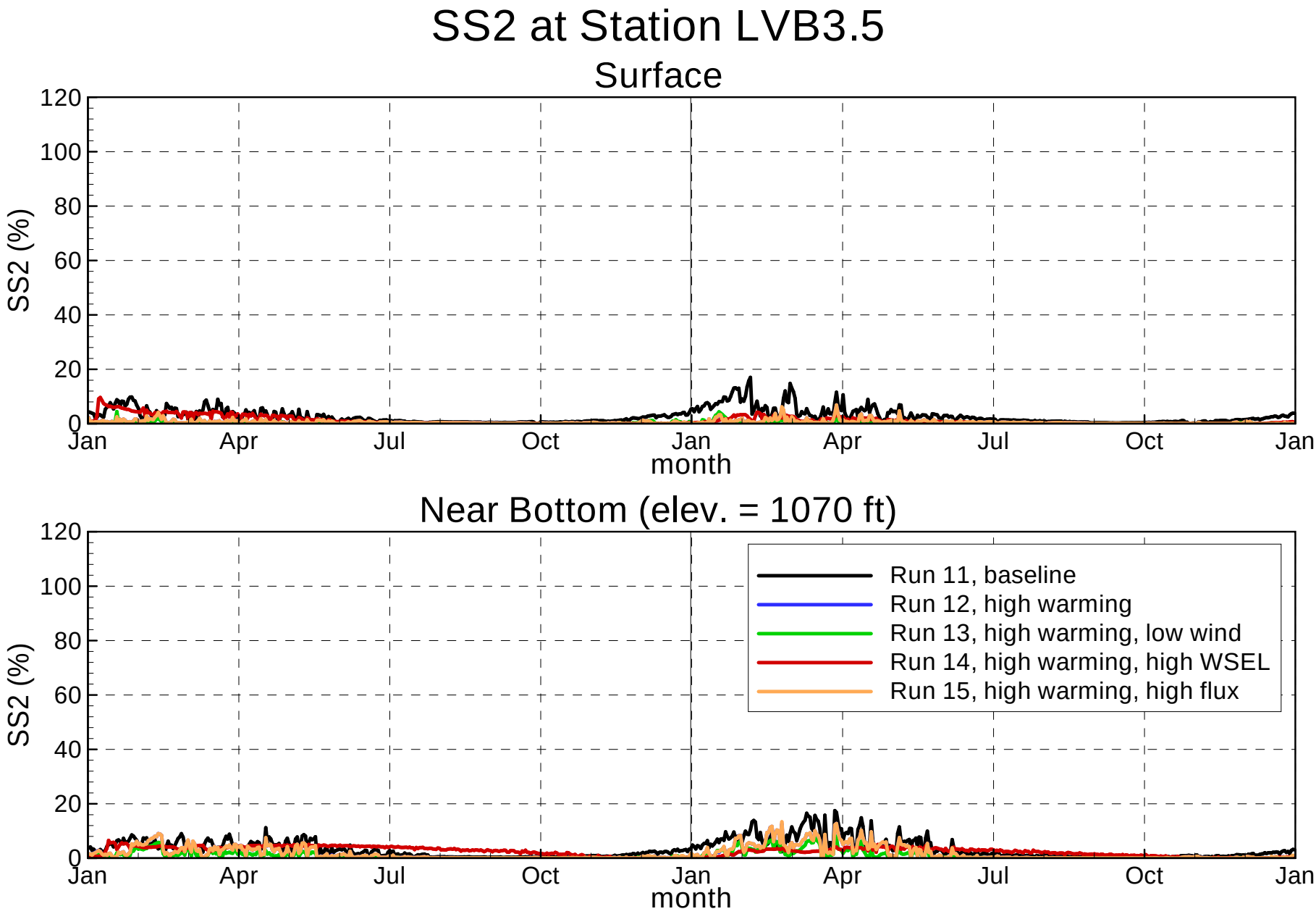
SS2 at Station LVB3.5
Surface
SS2 (%)
120
100
80
60
40
20
0
Jan
Apr
Jul
Oct
Jan
Apr
Jul
Oct
Jan
month
Near Bottom (elev. = 1070 ft)
SS2 (%)
Run 11, baseline
Run 12, high warming
Run 13, high warming, low wind
Run 14, high warming, high WSEL
Run 15, high warming, high flux
month

Figure A.214

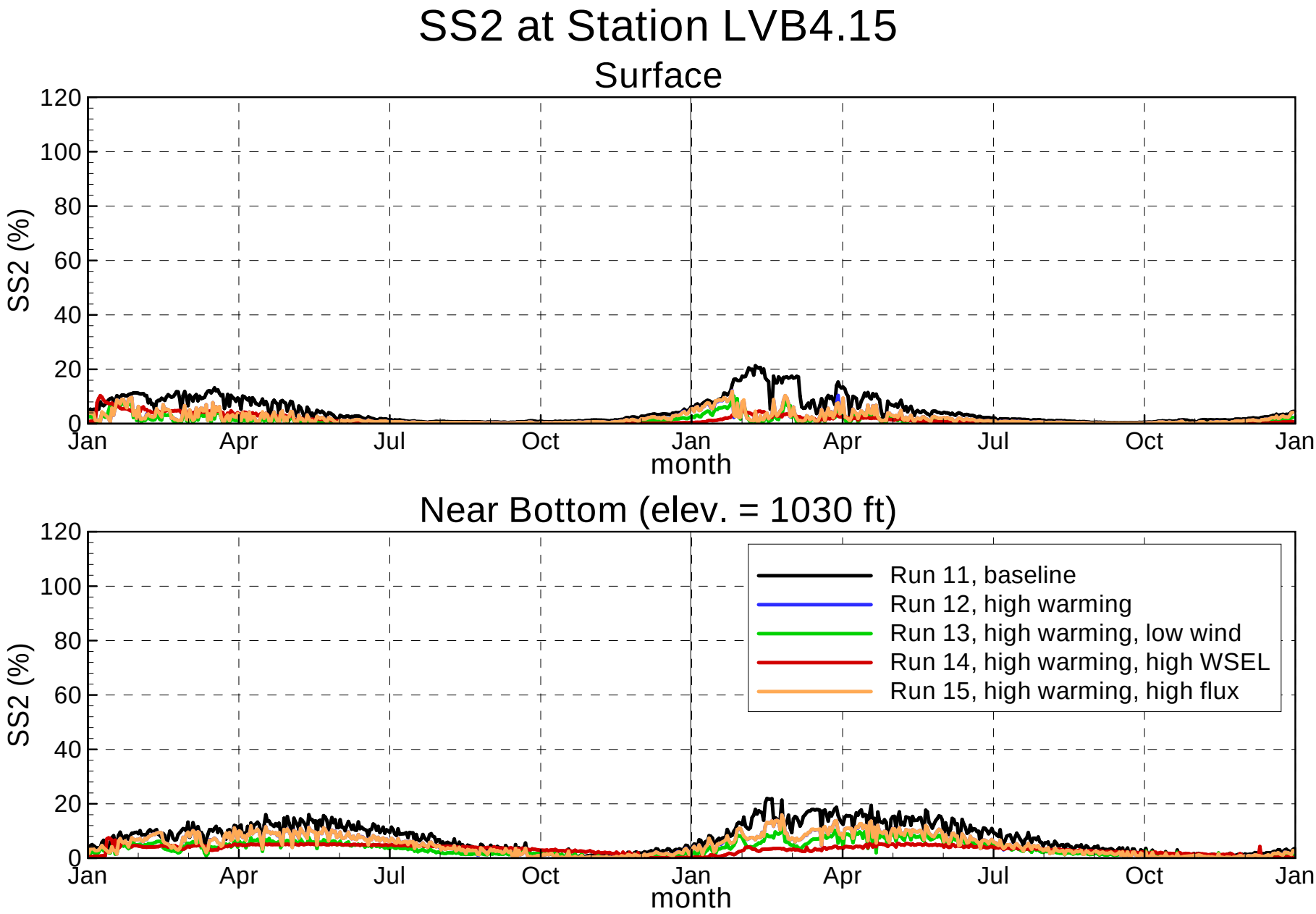
SS2 at Station LVB4.15
Surface
SS2 (%)
120
100
80
60
40
20
0
Jan
Apr
Jul
Oct
Jan
Apr
Jul
Oct
Jan
month
Near Bottom (elev. = 1030 ft)
SS2 (%)
Run 11, baseline
Run 12, high warming
Run 13, high warming, low wind
Run 14, high warming, high WSEL
Run 15, high warming, high flux
month

Figure A.215

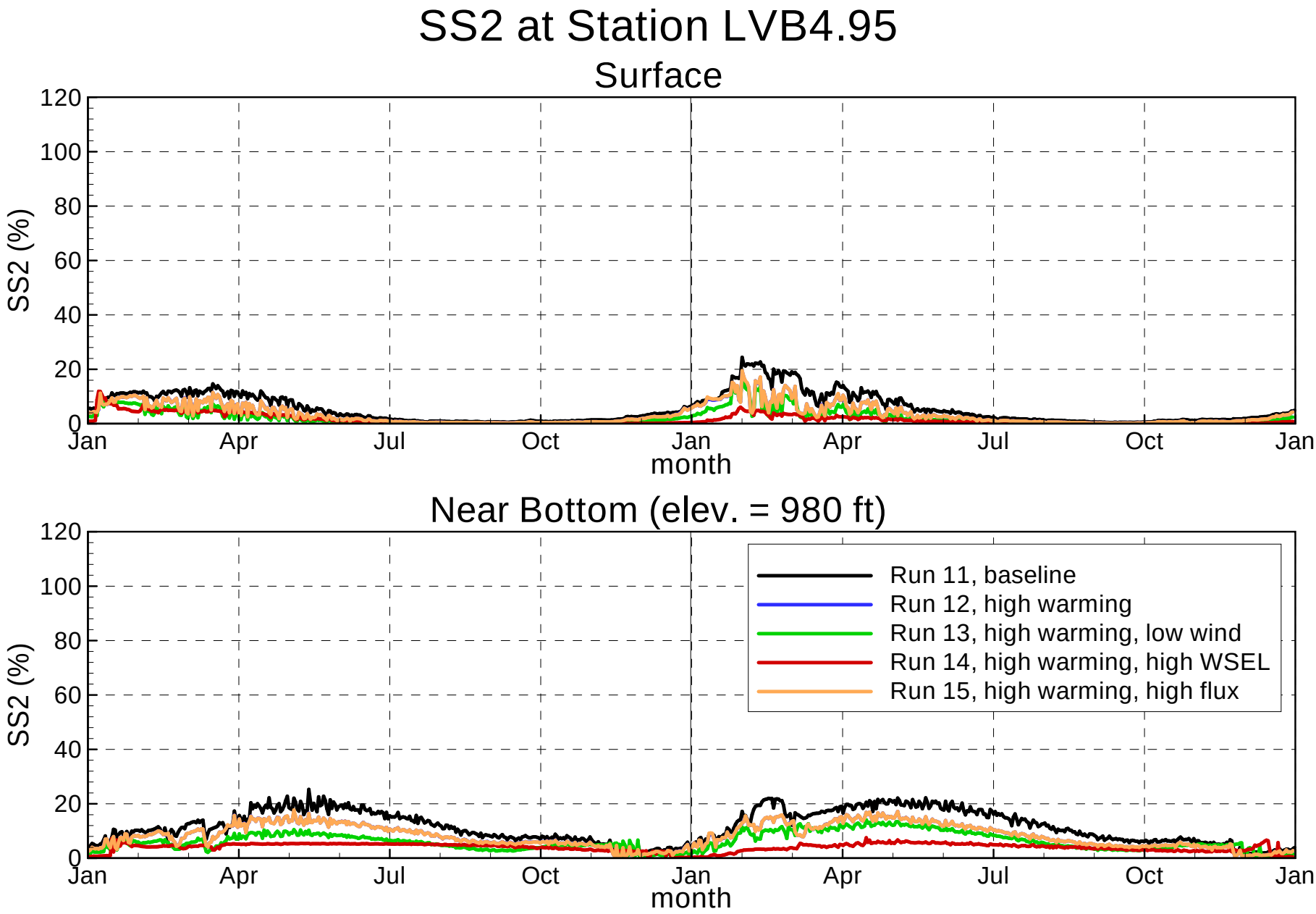
SS2 at Station LVB4.95
Surface
SS2 (%)
120
100
80
60
40
20
0
Jan
Apr
Jul
Oct
Jan
Apr
Jul
Oct
Jan
month
Near Bottom (elev. = 980 ft)
SS2 (%)
Run 11, baseline
Run 12, high warming
Run 13, high warming, low wind
Run 14, high warming, high WSEL
Run 15, high warming, high flux
month

Figure A.216

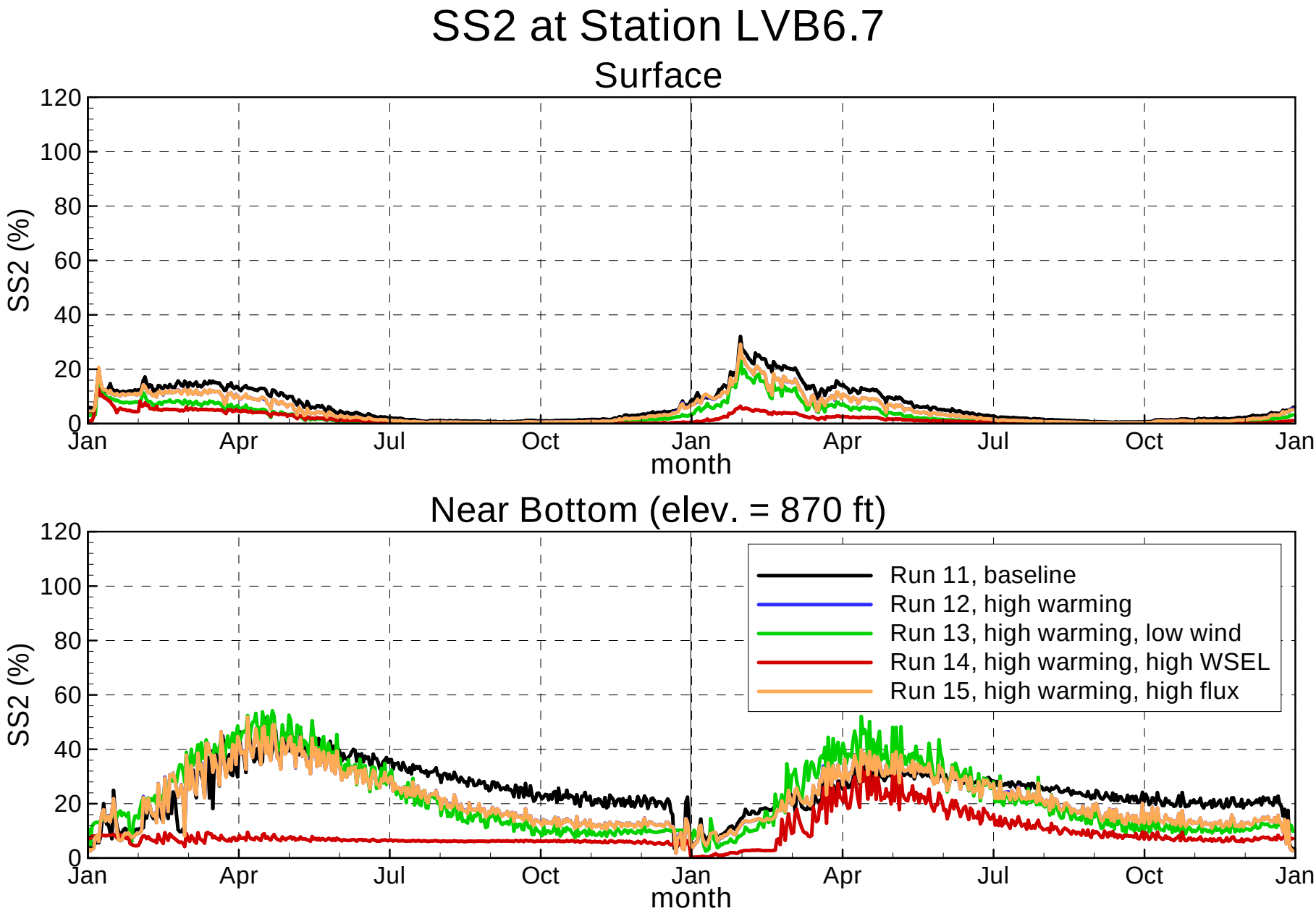
SS2 at Station LVB6.7
Surface
SS2 (%)
120
100
80
60
40
20
0
Jan
Apr
Jul
Oct
Jan
Apr
Jul
Oct
Jan
month
Near Bottom (elev. = 870 ft)
SS2 (%)
Run 11, baseline
Run 12, high warming
Run 13, high warming, low wind
Run 14, high warming, high WSEL
Run 15, high warming, high flux
month

Figure A.217

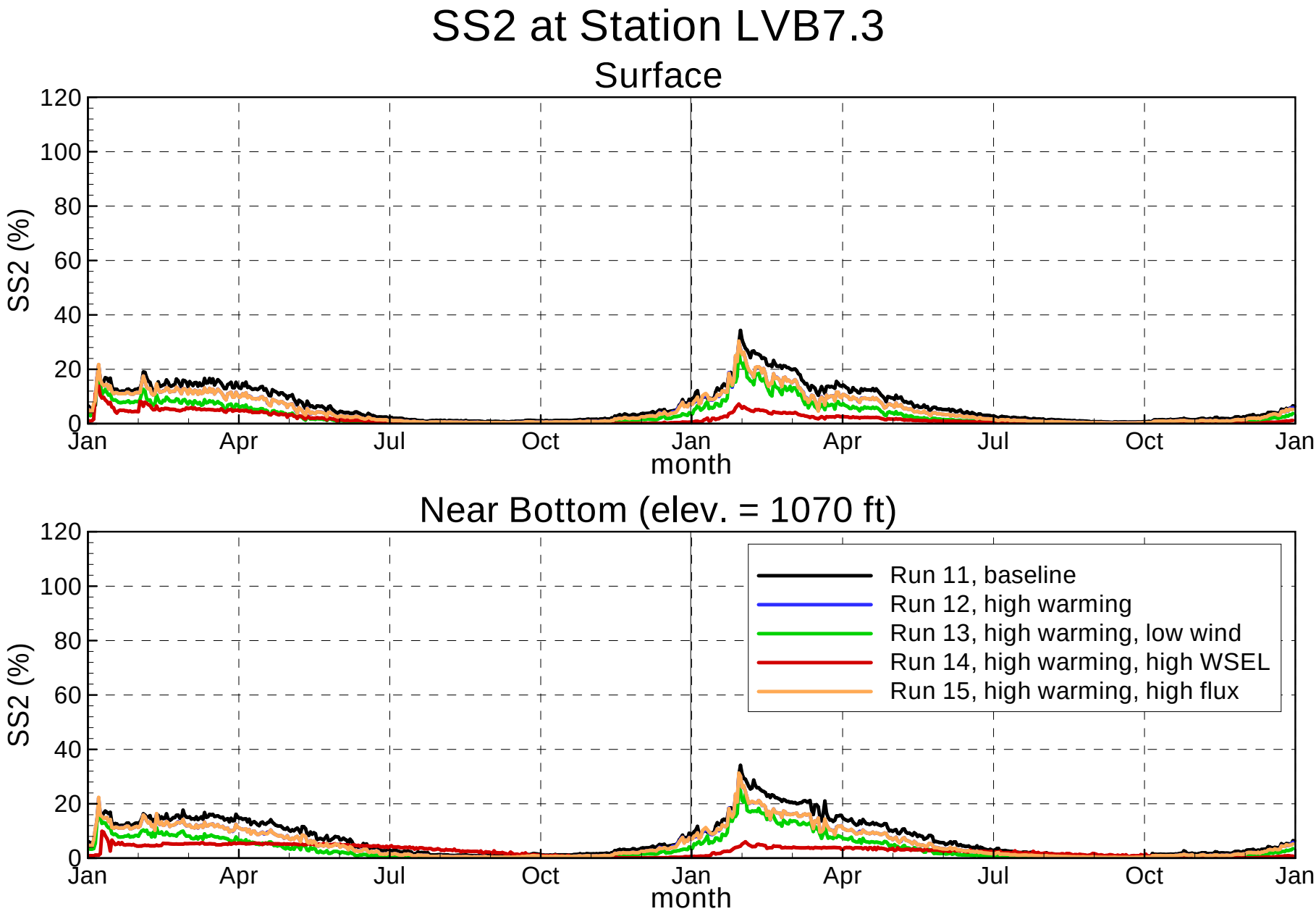
SS2 at Station LVB7.3
Surface
SS2 (%)
120
100
80
60
40
20
0
Jan
Apr
Jul
Oct
Jan
Apr
Jul
Oct
Jan
month
Near Bottom (elev. = 1070 ft)
SS2 (%)
Run 11, baseline
Run 12, high warming
Run 13, high warming, low wind
Run 14, high warming, high WSEL
Run 15, high warming, high flux
month

Figure A.218

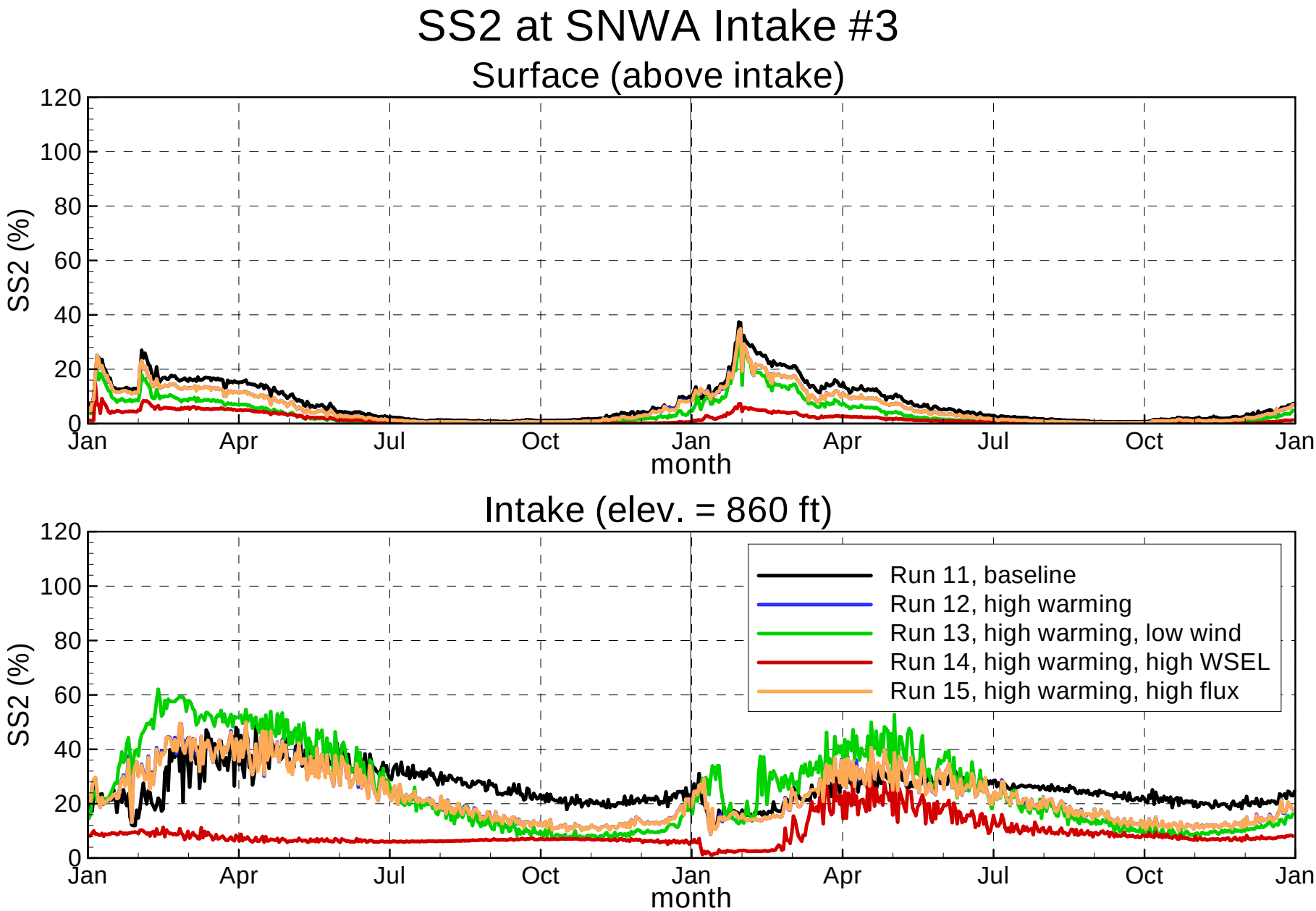
SS2 at SNWA Intake #3
Surface (above intake)
SS2 (%)
120
100
80
60
40
20
0
Jan
Apr
Jul
Oct
Jan
Apr
Jul
Oct
Jan
month
Intake (elev. = 860 ft)
SS2 (%)
Run 11, baseline
Run 12, high warming
Run 13, high warming, low wind
Run 14, high warming, high WSEL
Run 15, high warming, high flux
month

Figure A.219

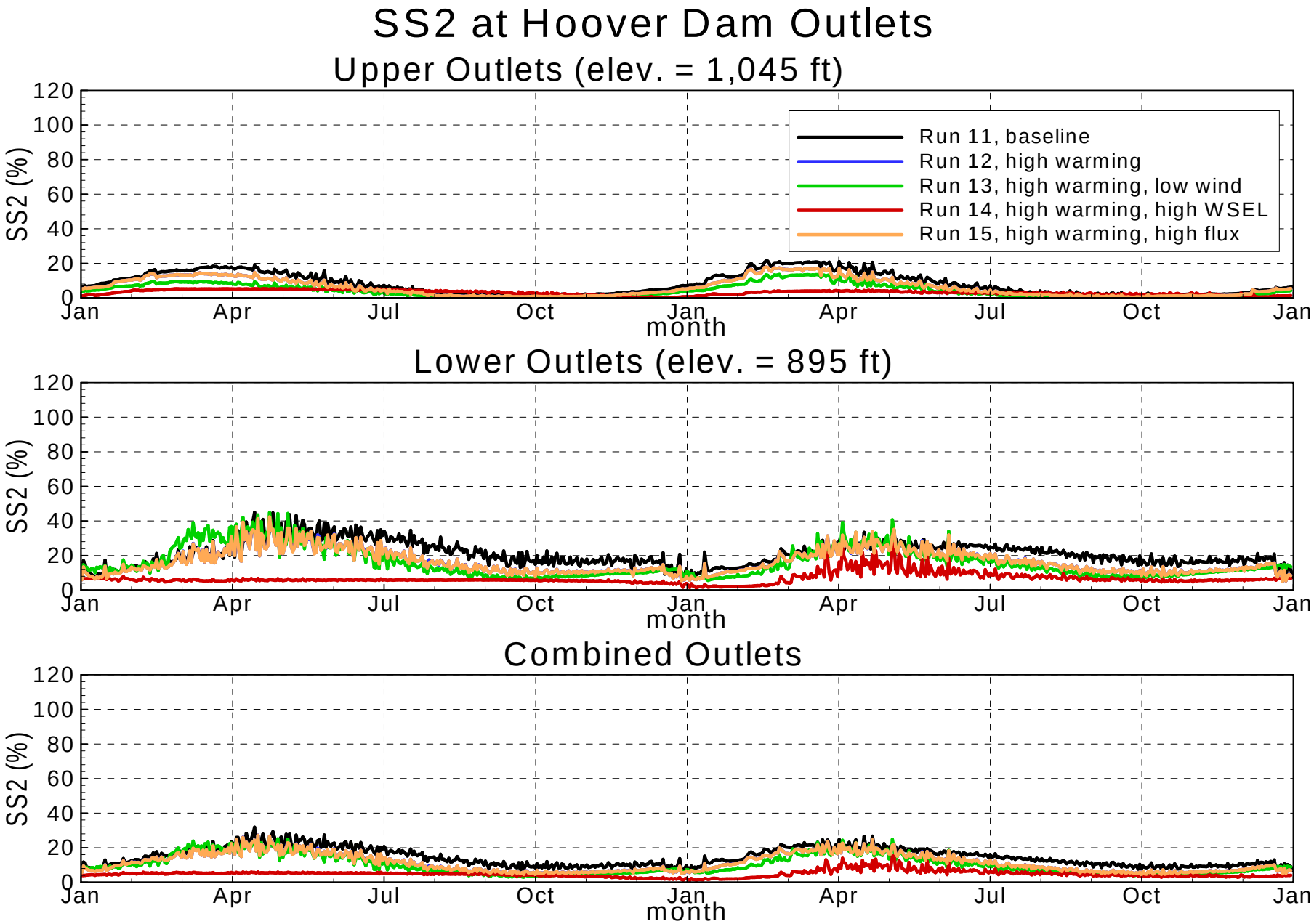

Figure A.220

FLOW SCIENCE

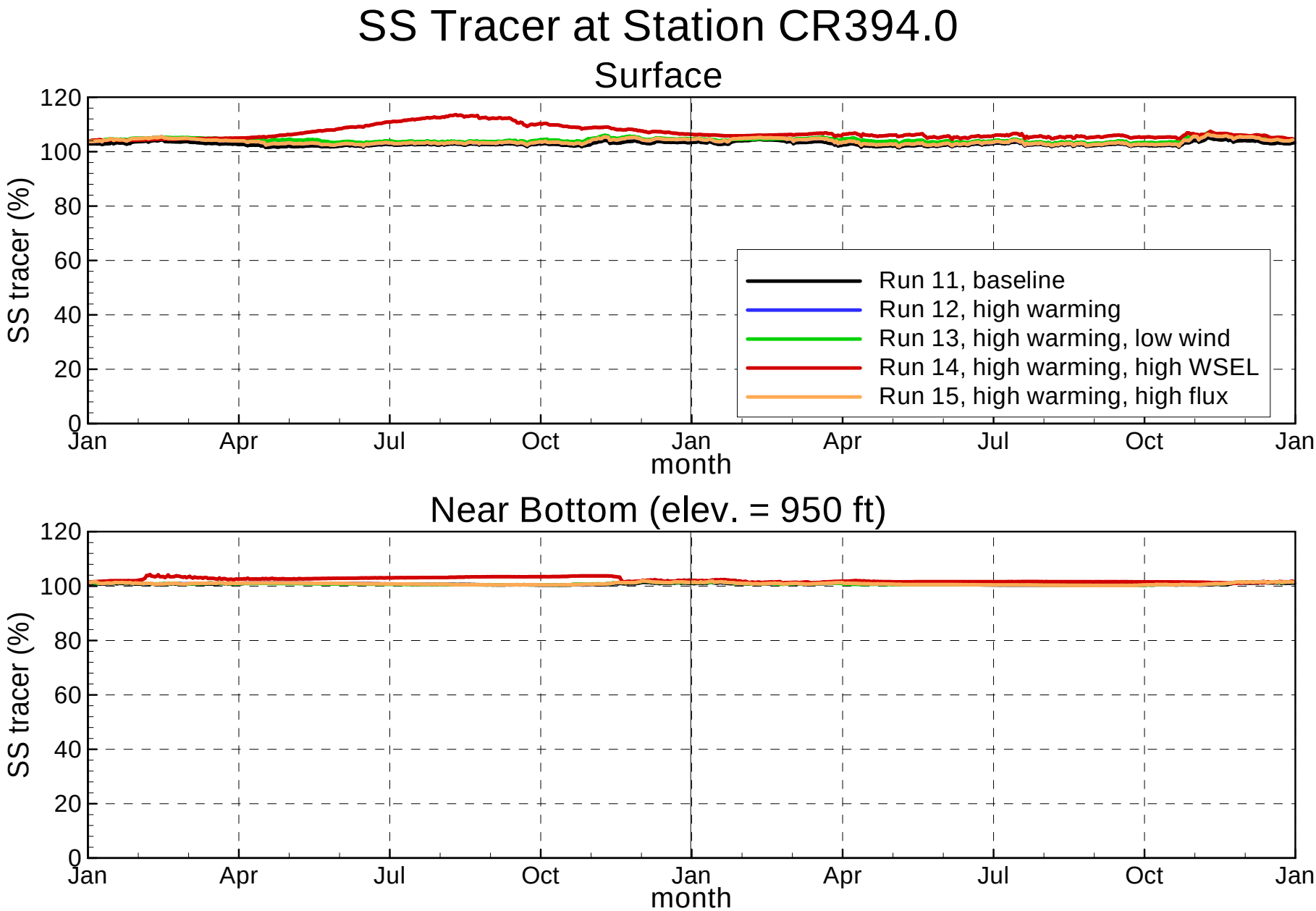
SS Tracer at Station CR394.0
Surface
SS tracer (%)
120
100
80
60
40
20
0
Jan
Apr
Jul
Oct
Jan
Apr
Jul
Oct
Jan
month
Run 11, baseline
Run 12, high warming
Run 13, high warming, low wind
Run 14, high warming, high WSEL
Run 15, high warming, high flux
Near Bottom (elev. = 950 ft)
SS tracer (%)
120
100
80
60
40
20
0
Jan
Apr
Jul
Oct
Jan
Apr
Jul
Oct
Jan
month

Figure A.221

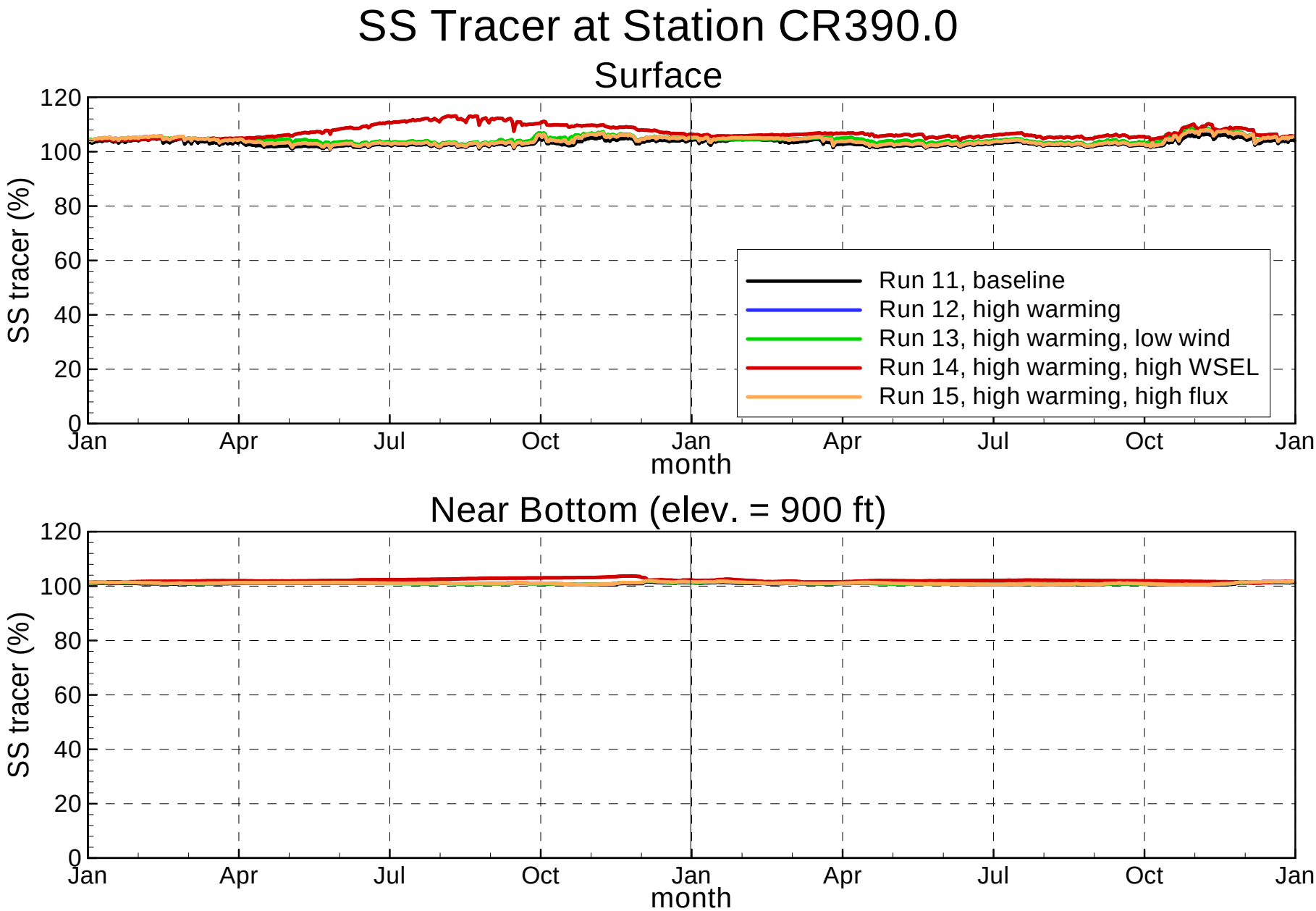
SS Tracer at Station CR390.0
Surface
SS tracer (%)
120
100
80
60
40
20
0
Jan
Apr
Jul
Oct
Jan
Apr
Jul
Oct
Jan
month
Run 11, baseline
Run 12, high warming
Run 13, high warming, low wind
Run 14, high warming, high WSEL
Run 15, high warming, high flux
Near Bottom (elev. = 900 ft)
SS tracer (%)
120
100
80
60
40
20
0
Jan
Apr
Jul
Oct
Jan
Apr
Jul
Oct
Jan
month

Figure A.222

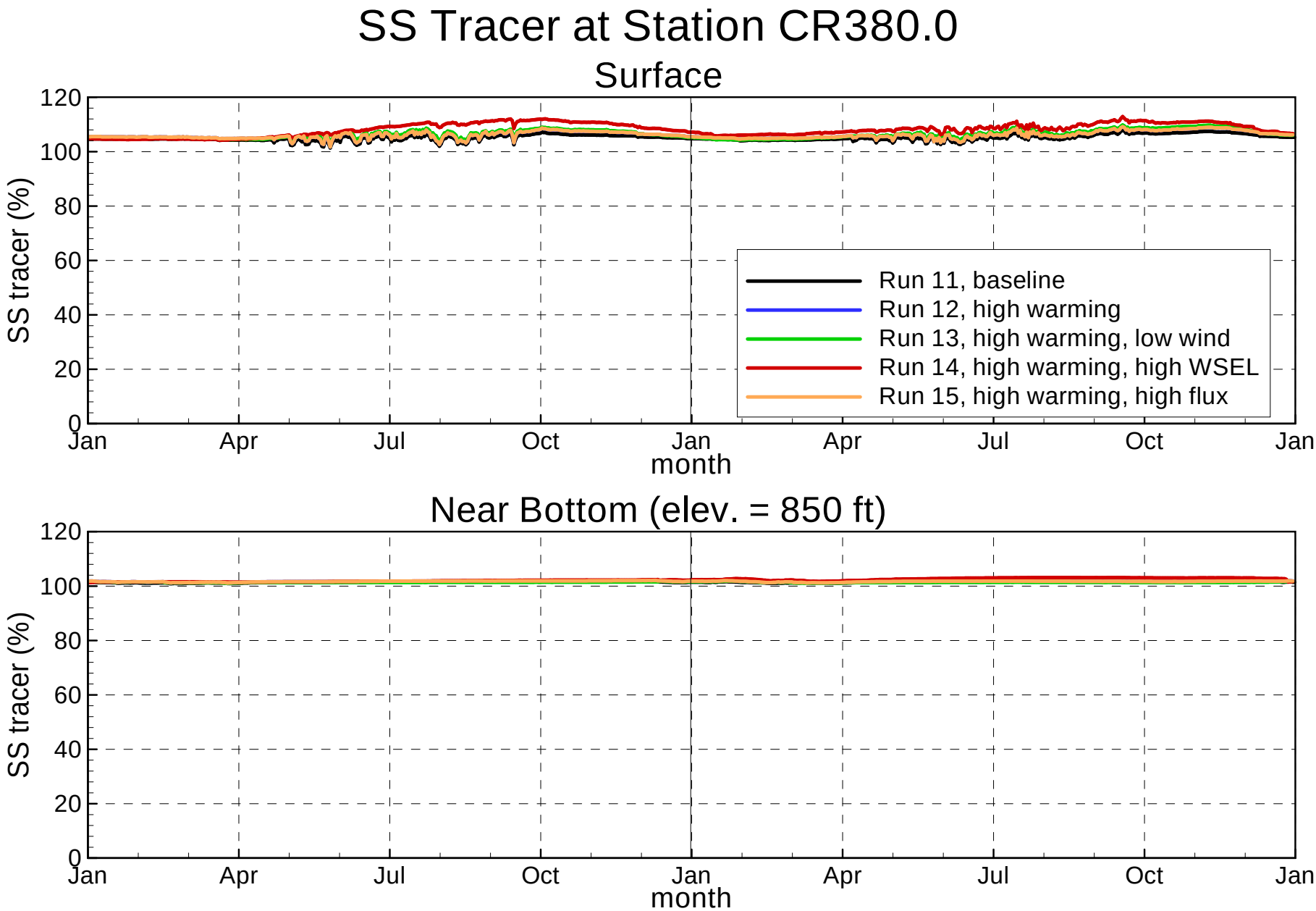
SS Tracer at Station CR380.0
Surface
SS tracer (%)
120
100
80
60
40
20
0
Jan
Apr
Jul
Oct
Jan
Apr
Jul
Oct
Jan
month
Run 11, baseline
Run 12, high warming
Run 13, high warming, low wind
Run 14, high warming, high WSEL
Run 15, high warming, high flux
Near Bottom (elev. = 850 ft)
SS tracer (%)
120
100
80
60
40
20
0
Jan
Apr
Jul
Oct
Jan
Apr
Jul
Oct
Jan
month

Figure A.223

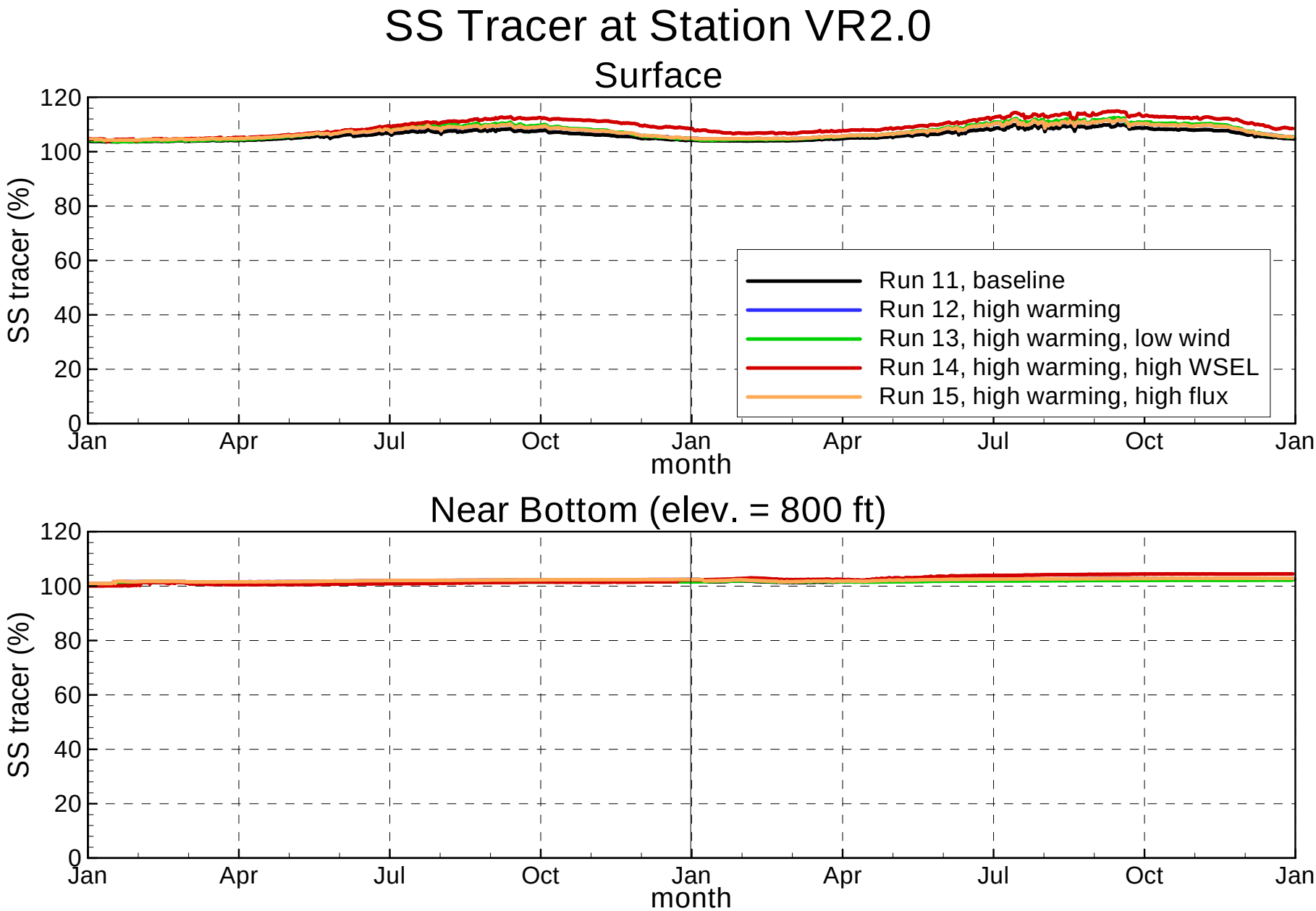
SS Tracer at Station VR2.0
Surface
SS tracer (%)
120
100
80
60
40
20
0
Jan
Apr
Jul
Oct
Jan
Apr
Jul
Oct
Jan
month
Run 11, baseline
Run 12, high warming
Run 13, high warming, low wind
Run 14, high warming, high WSEL
Run 15, high warming, high flux
Near Bottom (elev. = 800 ft)
SS tracer (%)
120
100
80
60
40
20
0
Jan
Apr
Jul
Oct
Jan
Apr
Jul
Oct
Jan
month

Figure A.224

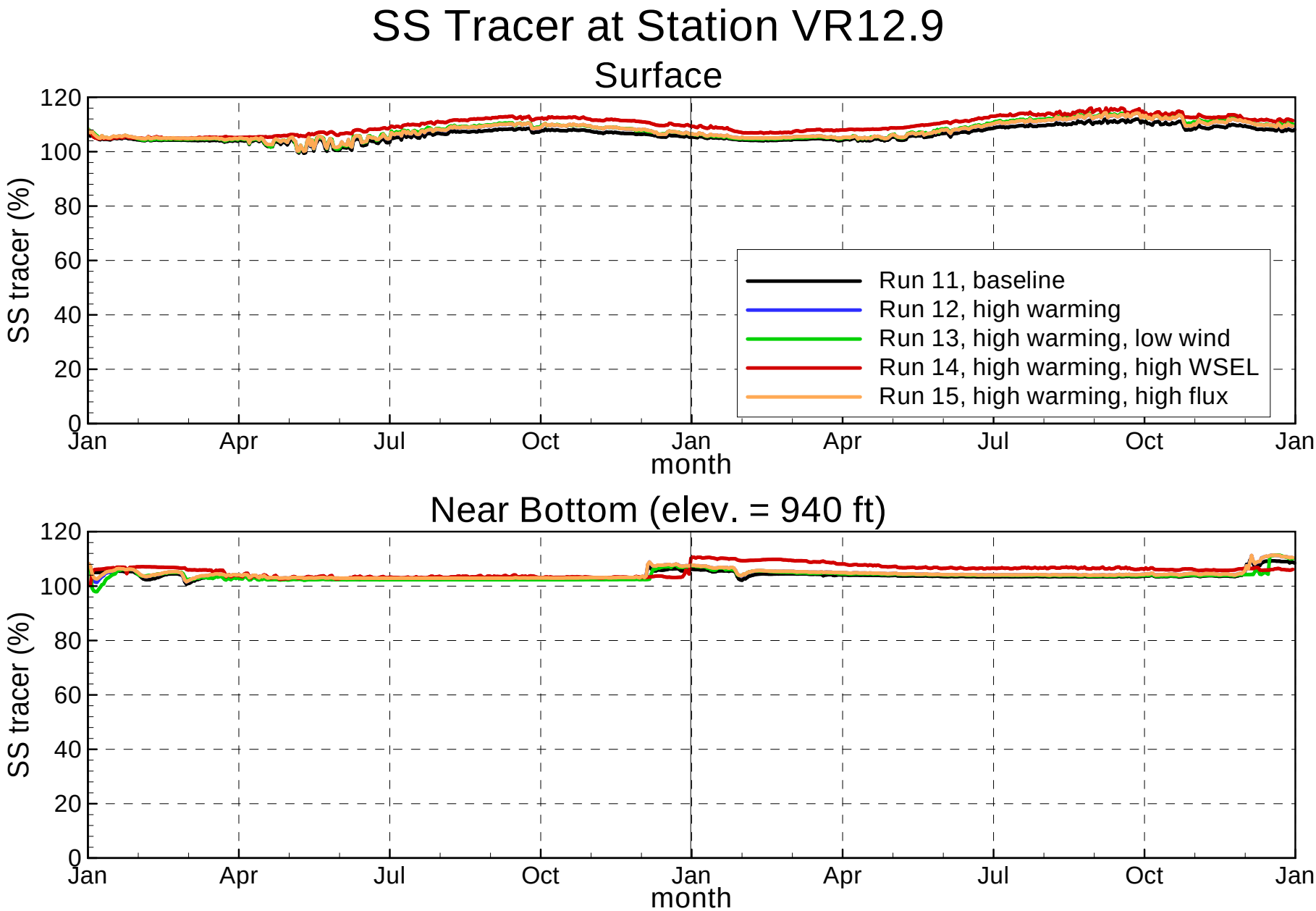
SS Tracer at Station VR12.9
Surface
SS tracer (%)
120
100
80
60
40
20
0
Jan
Apr
Jul
Oct
Jan
Apr
Jul
Oct
Jan
month
Run 11, baseline
Run 12, high warming
Run 13, high warming, low wind
Run 14, high warming, high WSEL
Run 15, high warming, high flux
Near Bottom (elev. = 940 ft)
SS tracer (%)
120
100
80
60
40
20
0
Jan
Apr
Jul
Oct
Jan
Apr
Jul
Oct
Jan
month

Figure A.225

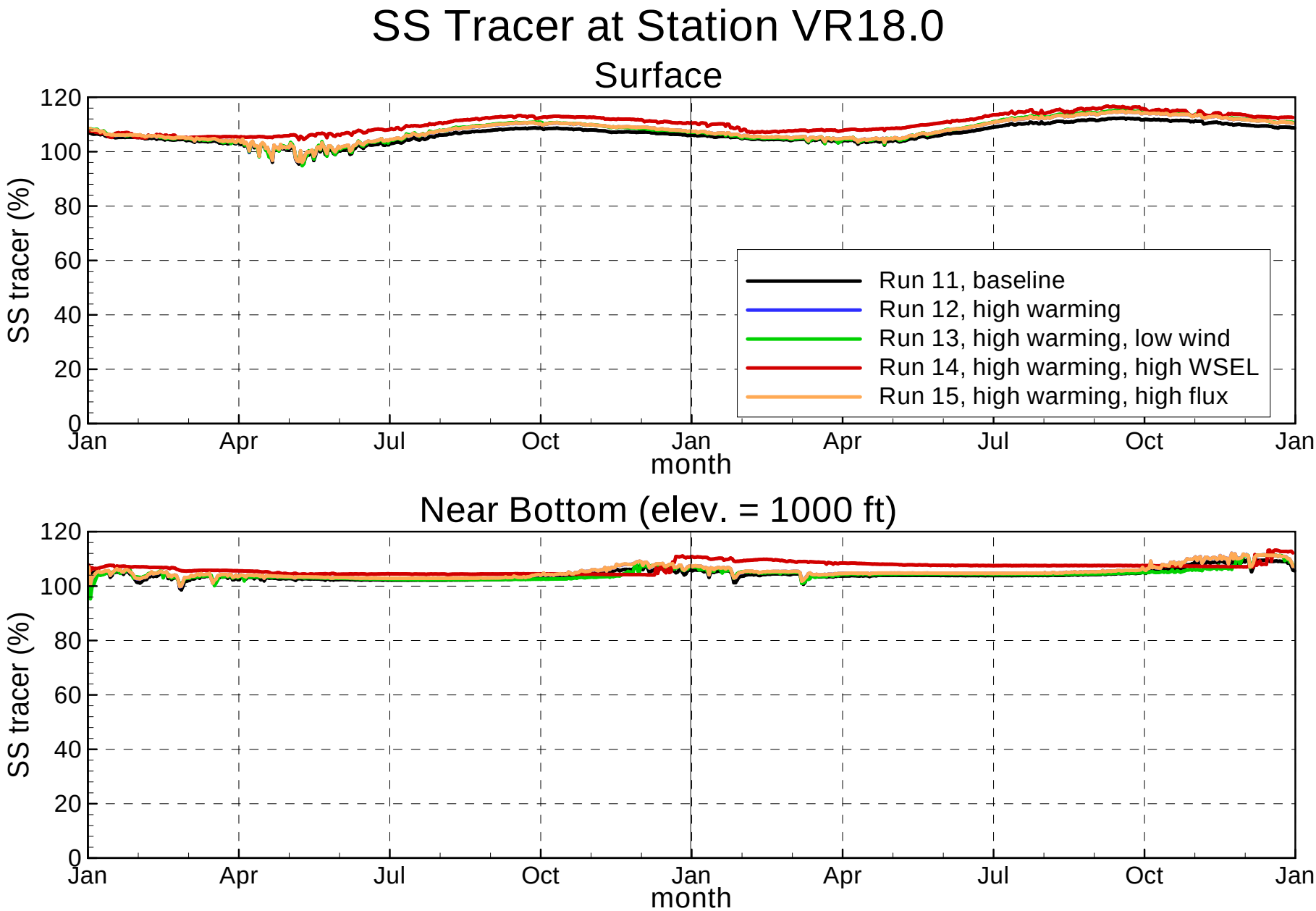
SS Tracer at Station VR18.0
Surface
SS tracer (%)
120
100
80
60
40
20
0
Jan
Apr
Jul
Oct
Jan
Apr
Jul
Oct
Jan
month
Run 11, baseline
Run 12, high warming
Run 13, high warming, low wind
Run 14, high warming, high WSEL
Run 15, high warming, high flux
Near Bottom (elev. = 1000 ft)
SS tracer (%)
120
100
80
60
40
20
0
Jan
Apr
Jul
Oct
Jan
Apr
Jul
Oct
Jan
month

Figure A.226

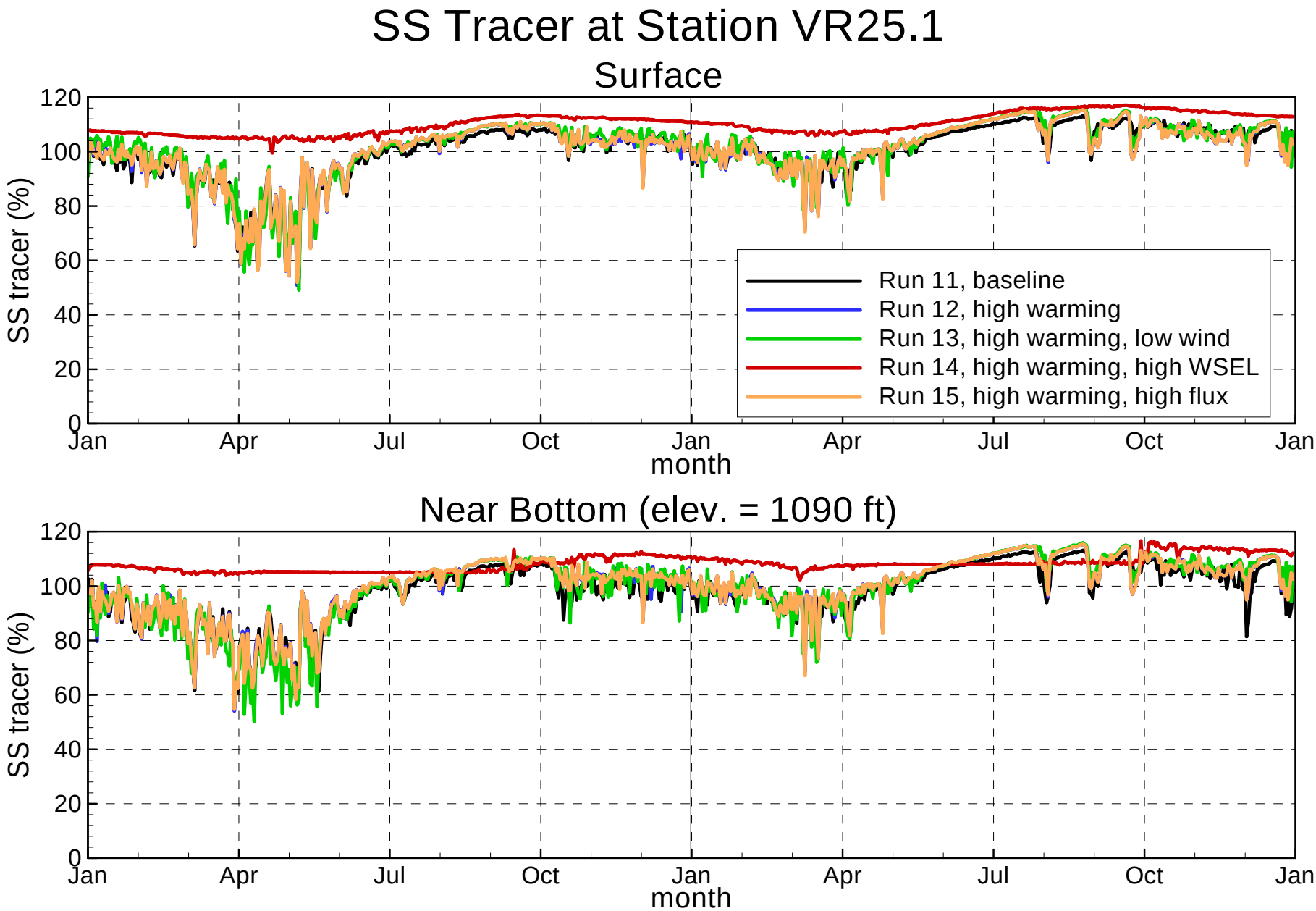
SS Tracer at Station VR25.1
Surface
SS tracer (%)
120
100
80
60
40
20
0
Jan
Apr
Jul
Oct
Jan
Apr
Jul
Oct
Jan
month
Run 11, baseline
Run 12, high warming
Run 13, high warming, low wind
Run 14, high warming, high WSEL
Run 15, high warming, high flux
Near Bottom (elev. = 1090 ft)
SS tracer (%)
120
100
80
60
40
20
0
Jan
Apr
Jul
Oct
Jan
Apr
Jul
Oct
Jan
month

Figure A.227

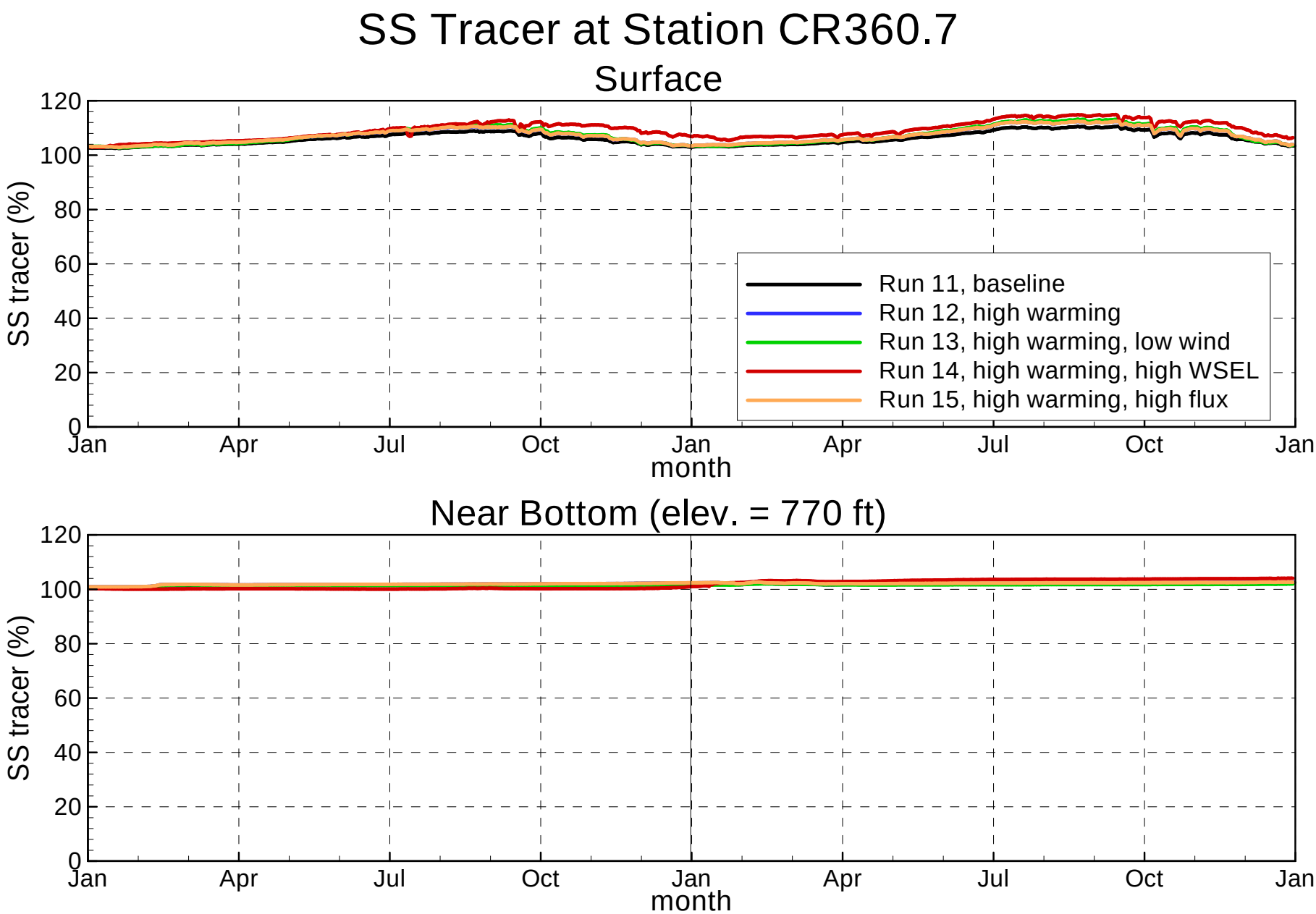
SS Tracer at Station CR360.7
Surface
SS tracer (%)
120
100
80
60
40
20
0
Jan
Apr
Jul
Oct
Jan
Apr
Jul
Oct
Jan
month
Run 11, baseline
Run 12, high warming
Run 13, high warming, low wind
Run 14, high warming, high WSEL
Run 15, high warming, high flux
Near Bottom (elev. = 770 ft)
SS tracer (%)
120
100
80
60
40
20
0
Jan
Apr
Jul
Oct
Jan
Apr
Jul
Oct
Jan
month

Figure A.228

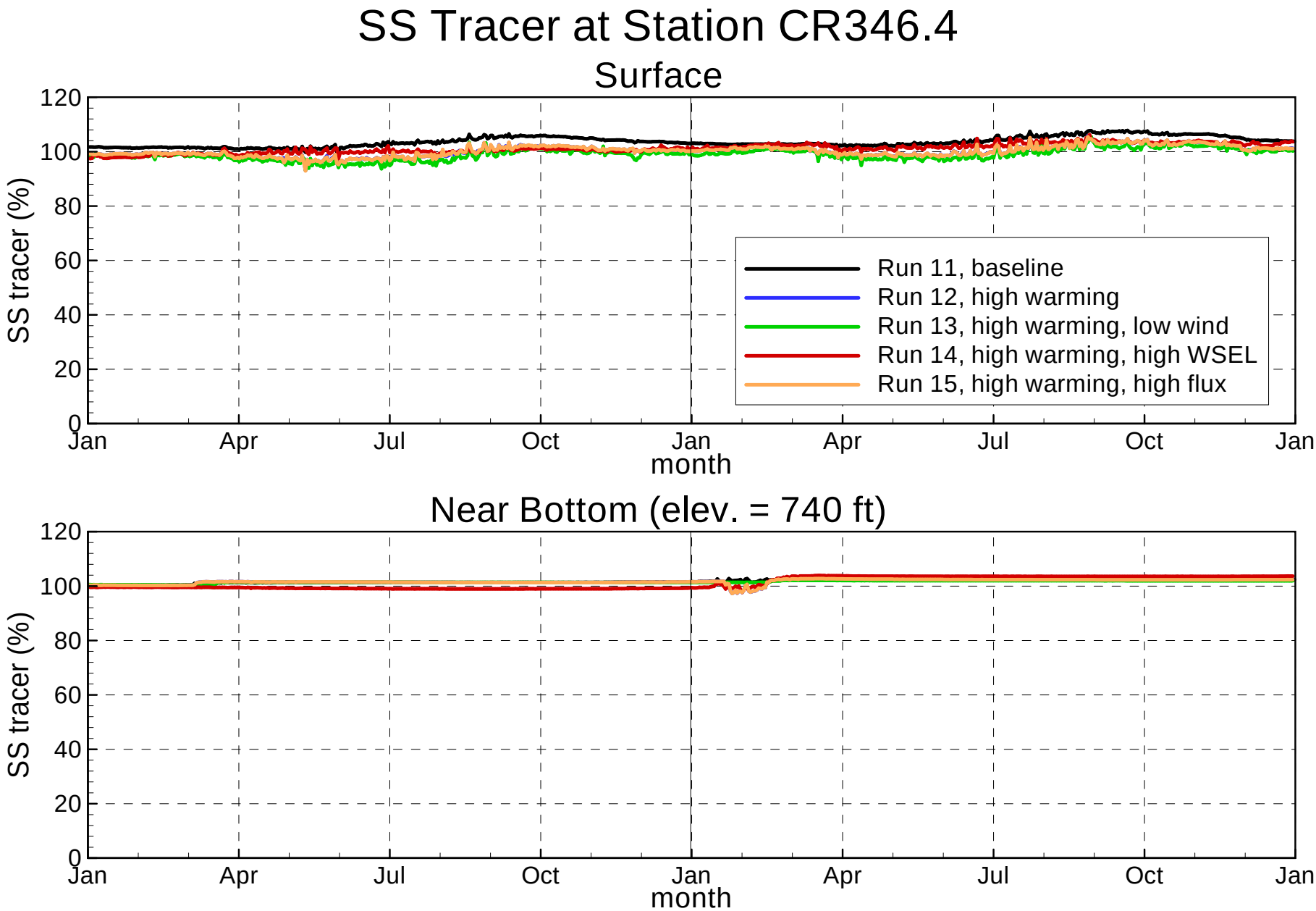
SS Tracer at Station CR346.4
Surface
SS tracer (%)
120
100
80
60
40
20
0
Jan
Apr
Jul
Oct
Jan
Apr
Jul
Oct
Jan
month
Run 11, baseline
Run 12, high warming
Run 13, high warming, low wind
Run 14, high warming, high WSEL
Run 15, high warming, high flux
Near Bottom (elev. = 740 ft)
SS tracer (%)
120
100
80
60
40
20
0
Jan
Apr
Jul
Oct
Jan
Apr
Jul
Oct
Jan
month

Figure A.229

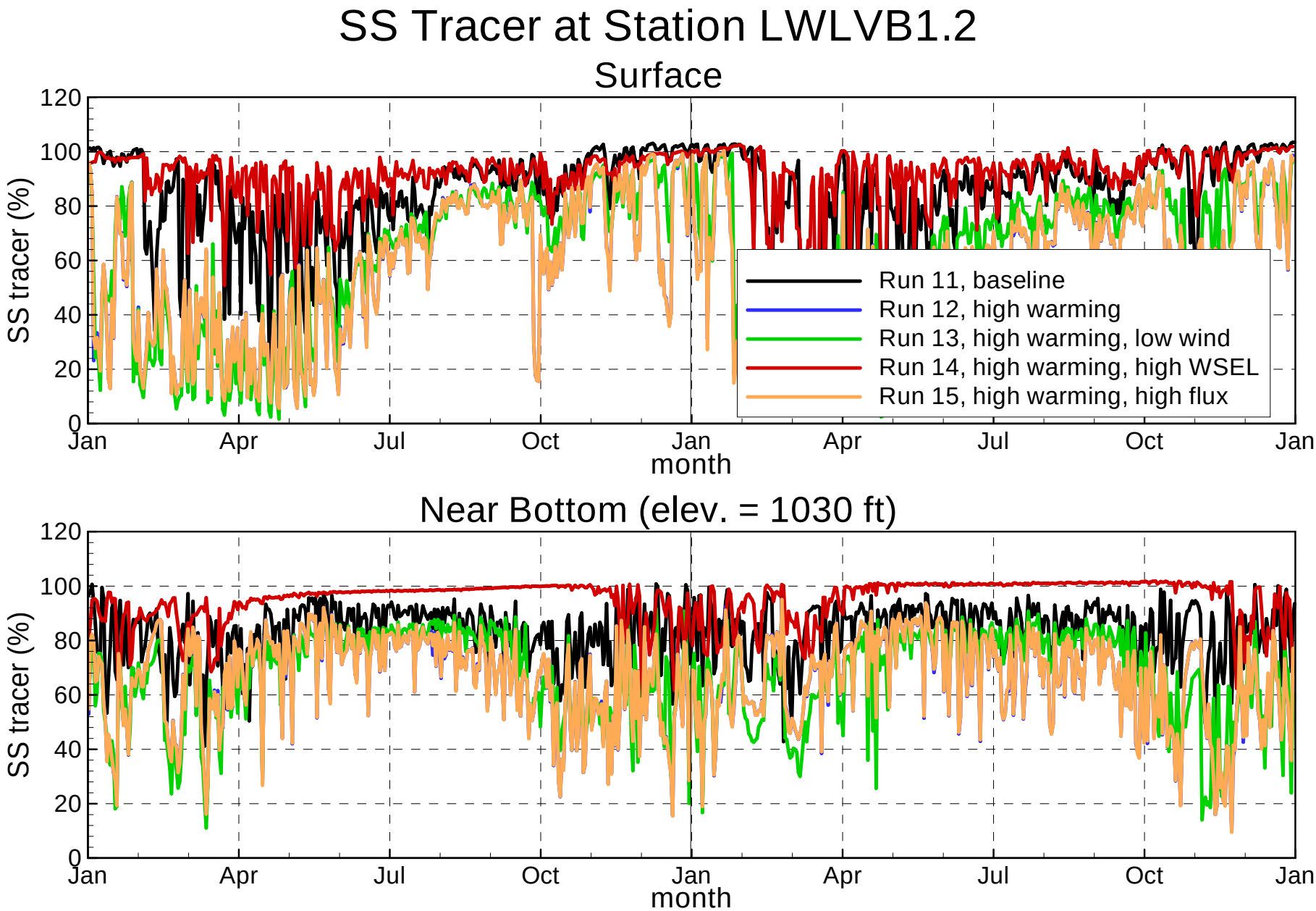
SS Tracer at Station LWLVB1.2
Surface
SS tracer (%)
120
100
80
60
40
20
0
Jan
Apr
Jul
Oct
Jan
Apr
Jul
Oct
Jan
month
Run 11, baseline
Run 12, high warming
Run 13, high warming, low wind
Run 14, high warming, high WSEL
Run 15, high warming, high flux
Near Bottom (elev. = 1030 ft)
SS tracer (%)
120
100
80
60
40
20
0
Jan
Apr
Jul
Oct
Jan
Apr
Jul
Oct
Jan
month

Figure A.230

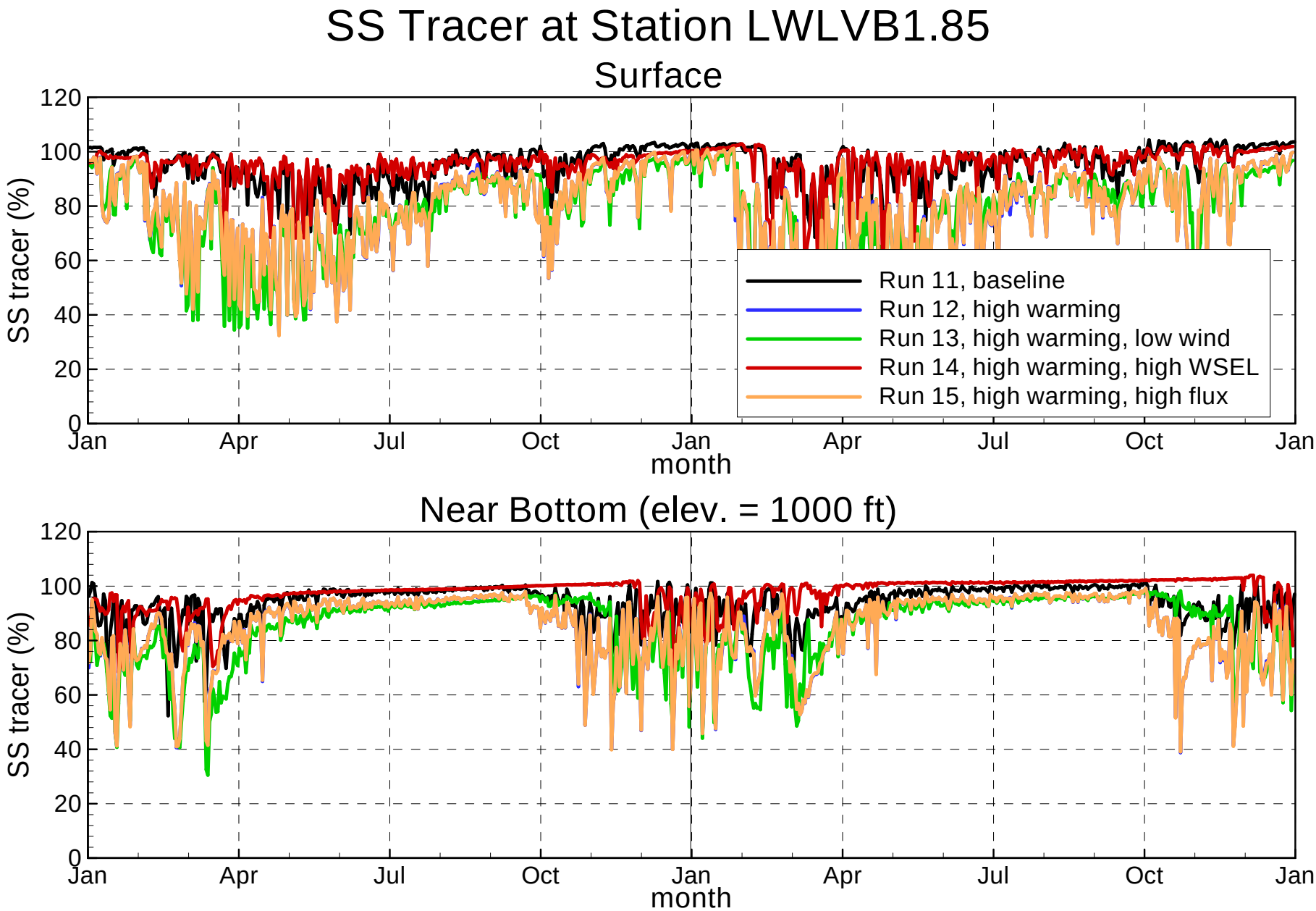
SS Tracer at Station LWLVB1.85
Surface
SS tracer (%)
120
100
80
60
40
20
0
Jan
Apr
Jul
Oct
Jan
Apr
Jul
Oct
Jan
month
Run 11, baseline
Run 12, high warming
Run 13, high warming, low wind
Run 14, high warming, high WSEL
Run 15, high warming, high flux
Near Bottom (elev. = 1000 ft)
SS tracer (%)
120
100
80
60
40
20
0
Jan
Apr
Jul
Oct
Jan
Apr
Jul
Oct
Jan
month

Figure A.231

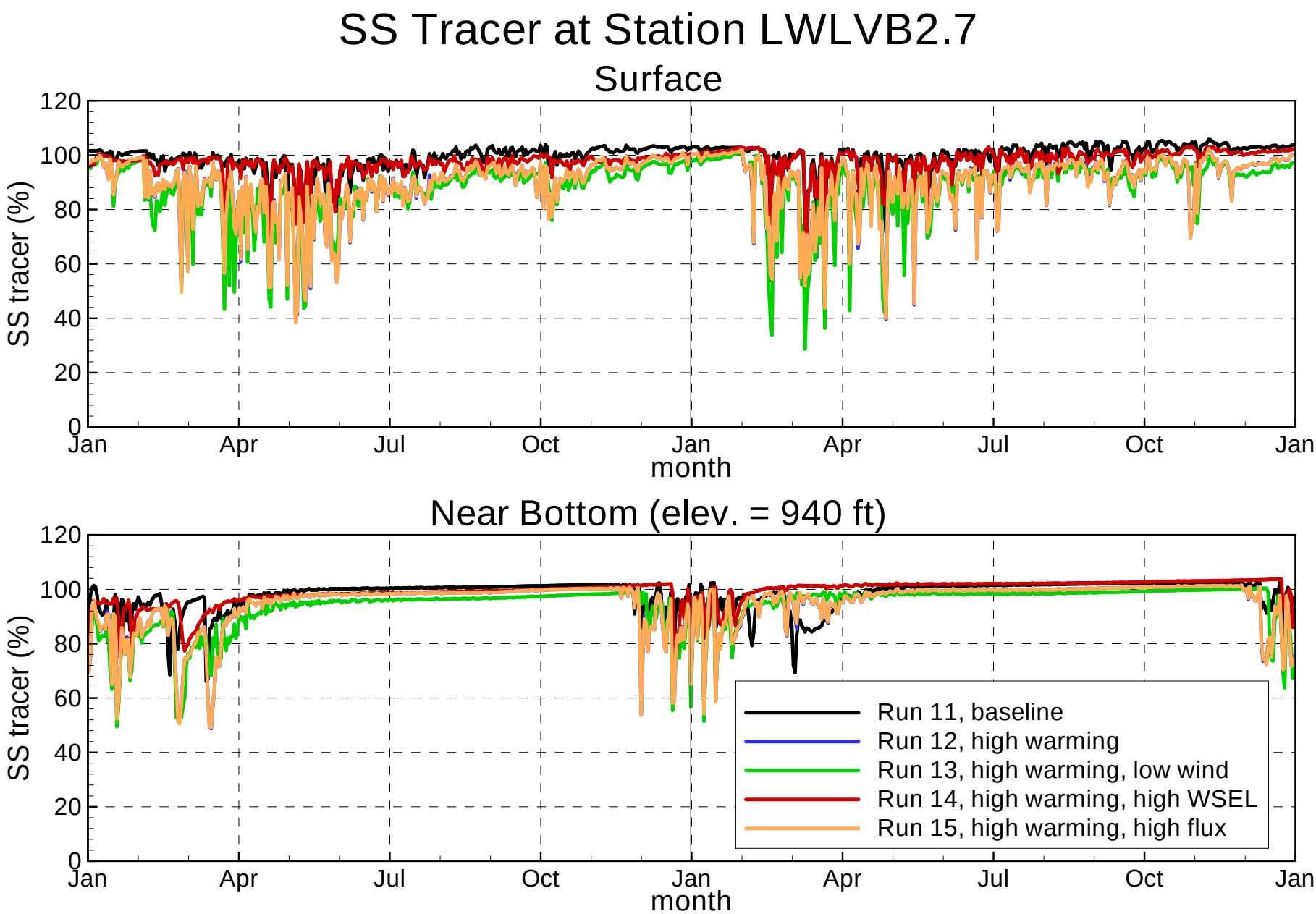

Figure A.232

FLOW SCIENCE

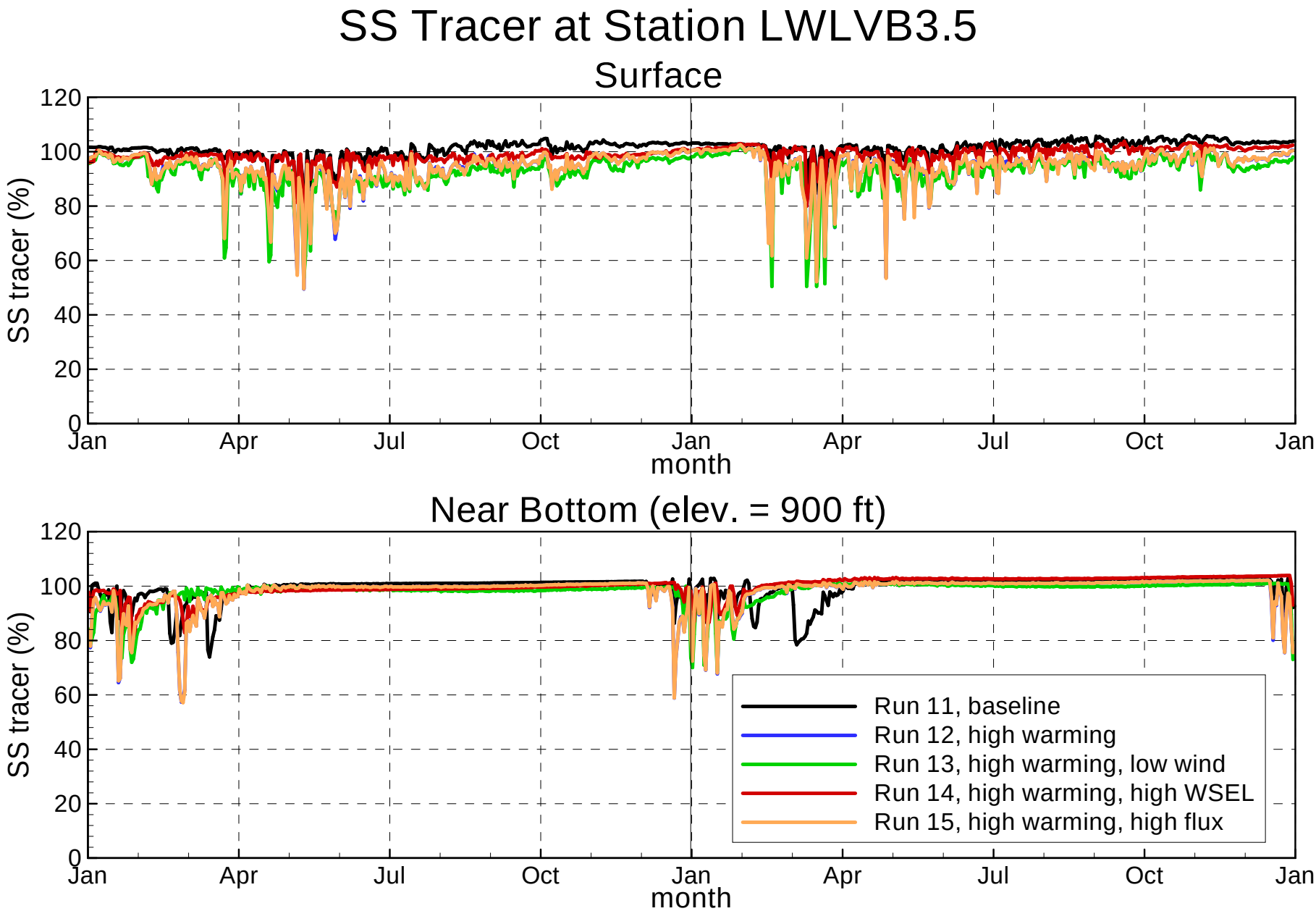
SS Tracer at Station LWLVB3.5
Surface
SS tracer (%)
120
100
80
60
40
20
0
Jan
Apr
Jul
Oct
Jan
Apr
Jul
Oct
Jan
month
Near Bottom (elev. = 900 ft)
SS tracer (%)
Run 11, baseline
Run 12, high warming
Run 13, high warming, low wind
Run 14, high warming, high WSEL
Run 15, high warming, high flux
month

Figure A.233

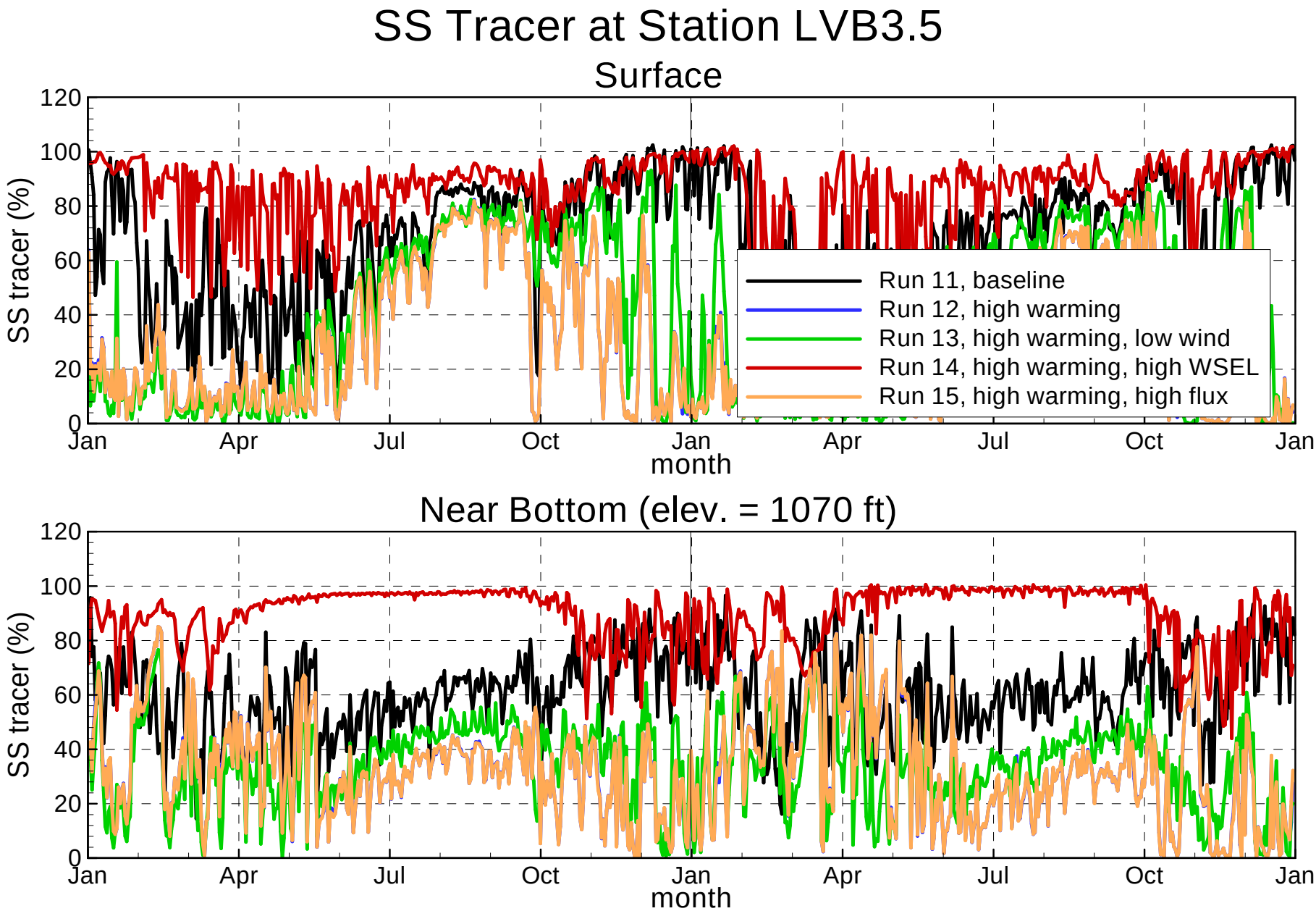
SS Tracer at Station LVB3.5
Surface
SS tracer (%)
120
100
80
60
40
20
0
Jan
Apr
Jul
Oct
Jan
Apr
Jul
Oct
Jan
month
Run 11, baseline
Run 12, high warming
Run 13, high warming, low wind
Run 14, high warming, high WSEL
Run 15, high warming, high flux
Near Bottom (elev. = 1070 ft)
SS tracer (%)
120
100
80
60
40
20
0
Jan
Apr
Jul
Oct
Jan
Apr
Jul
Oct
Jan
month

Figure A.234

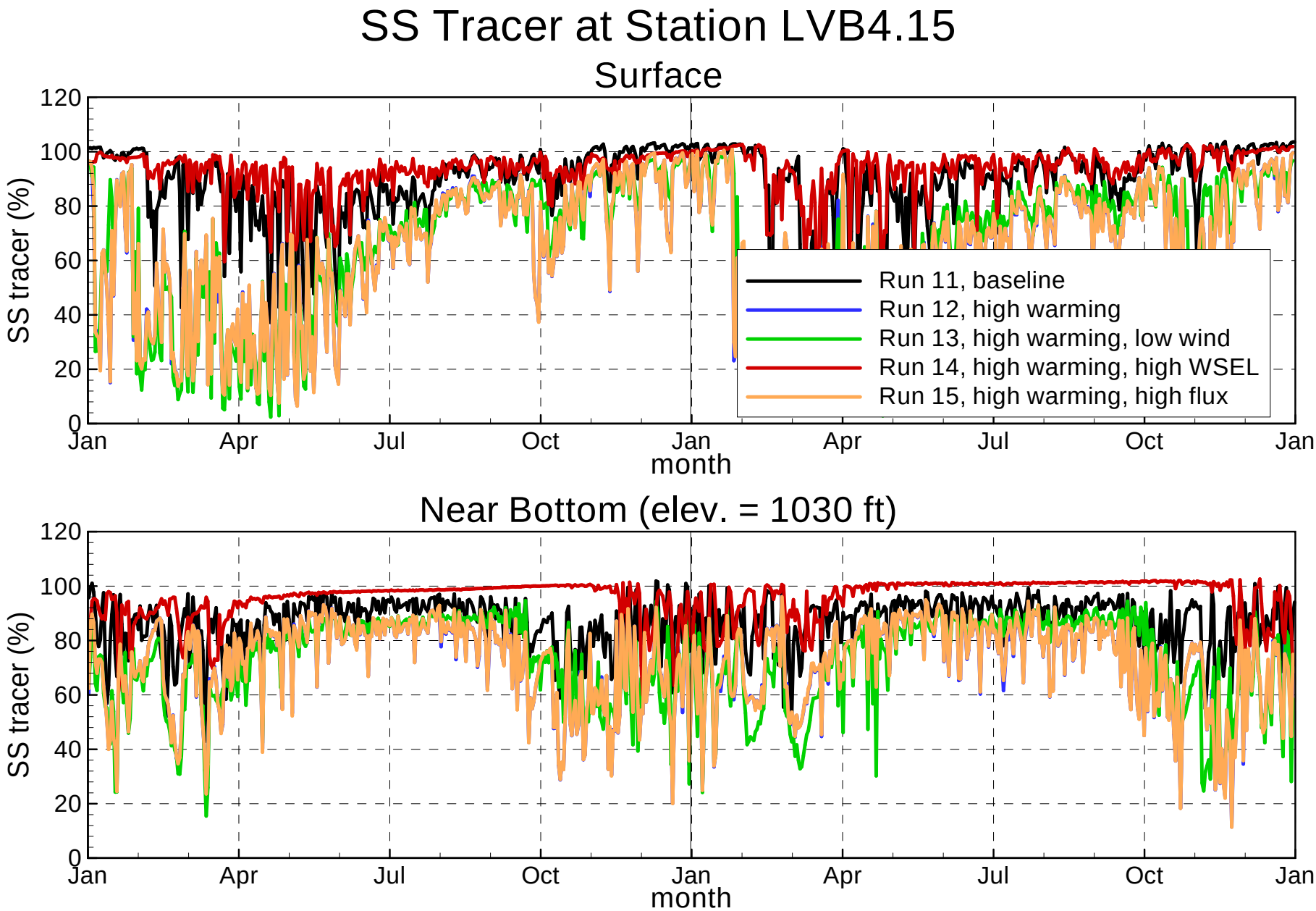
SS Tracer at Station LVB4.15
Surface
SS tracer (%)
120
100
80
60
40
20
0
Jan
Apr
Jul
Oct
Jan
Apr
Jul
Oct
Jan
month
Run 11, baseline
Run 12, high warming
Run 13, high warming, low wind
Run 14, high warming, high WSEL
Run 15, high warming, high flux
Near Bottom (elev. = 1030 ft)
SS tracer (%)
120
100
80
60
40
20
0
Jan
Apr
Jul
Oct
Jan
Apr
Jul
Oct
Jan
month

Figure A.235

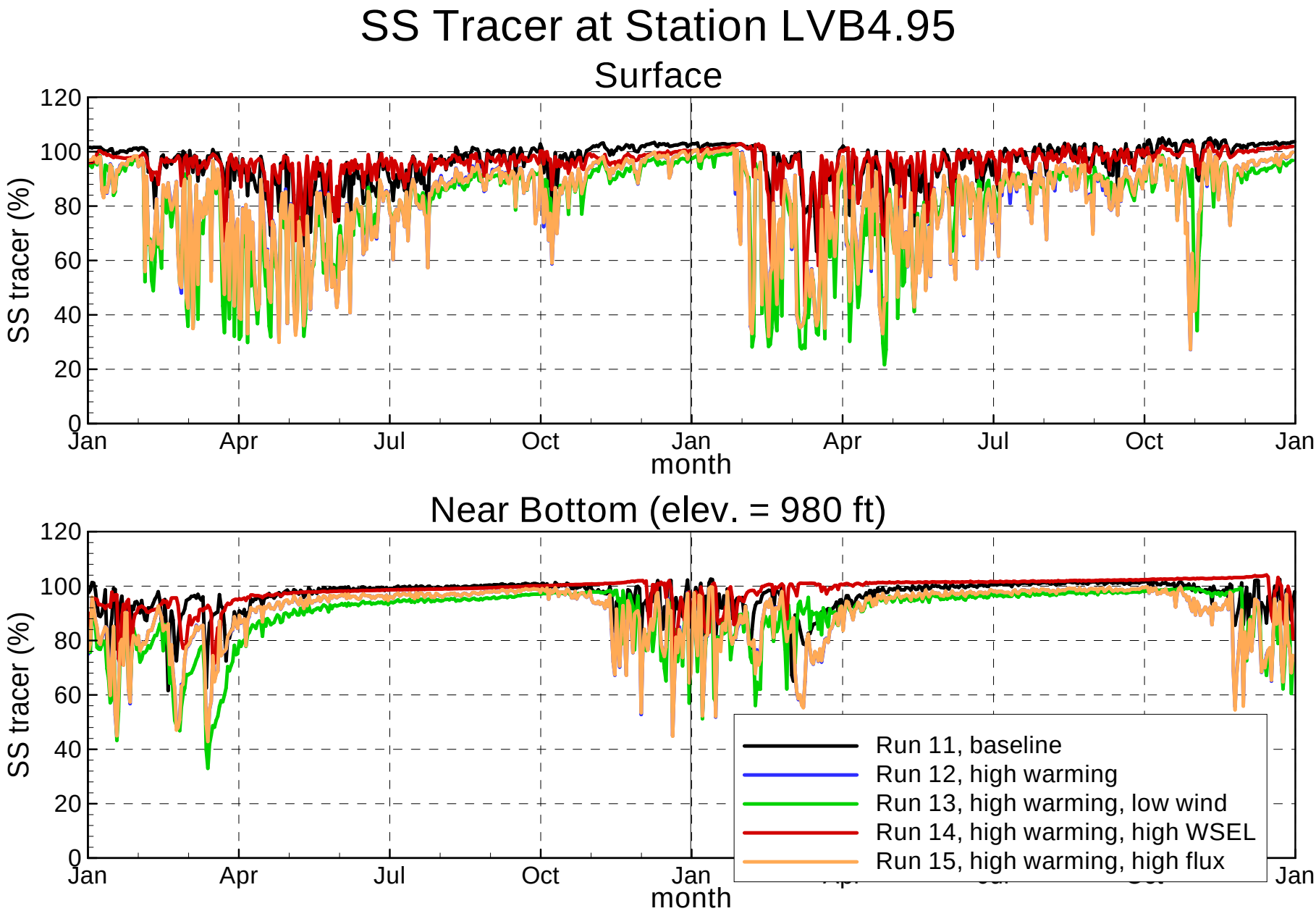
SS Tracer at Station LVB4.95
Surface
SS tracer (%)
120
100
80
60
40
20
0
Jan
Apr
Jul
Oct
Jan
Apr
Jul
Oct
Jan
month
Near Bottom (elev. = 980 ft)
SS tracer (%)
Run 11, baseline
Run 12, high warming
Run 13, high warming, low wind
Run 14, high warming, high WSEL
Run 15, high warming, high flux

Figure A.236

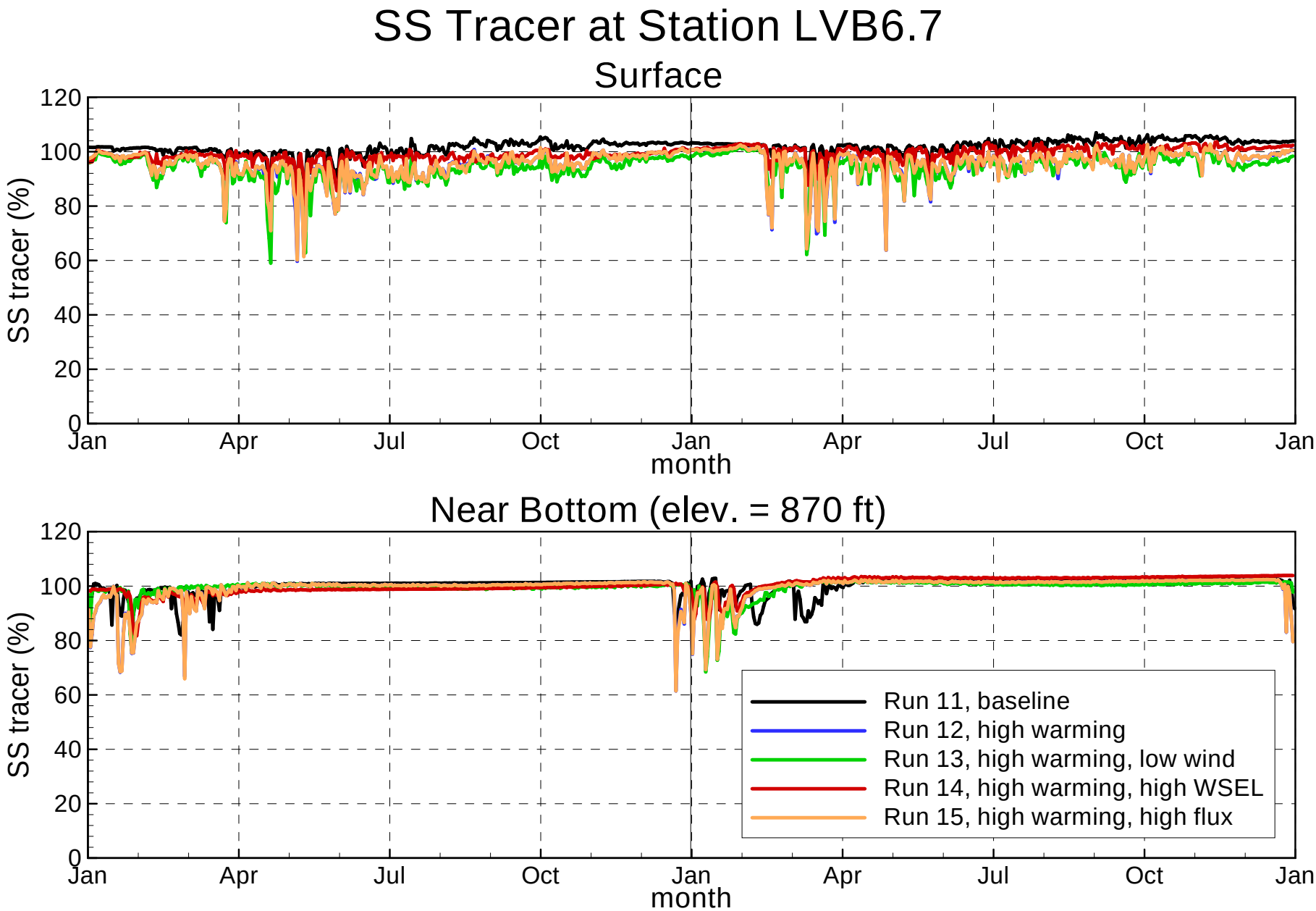
SS Tracer at Station LVB6.7
Surface
SS tracer (%)
120
100
80
60
40
20
0
Jan
Apr
Jul
Oct
Jan
Apr
Jul
Oct
Jan
month
Near Bottom (elev. = 870 ft)
SS tracer (%)
Run 11, baseline
Run 12, high warming
Run 13, high warming, low wind
Run 14, high warming, high WSEL
Run 15, high warming, high flux
month

Figure A.237

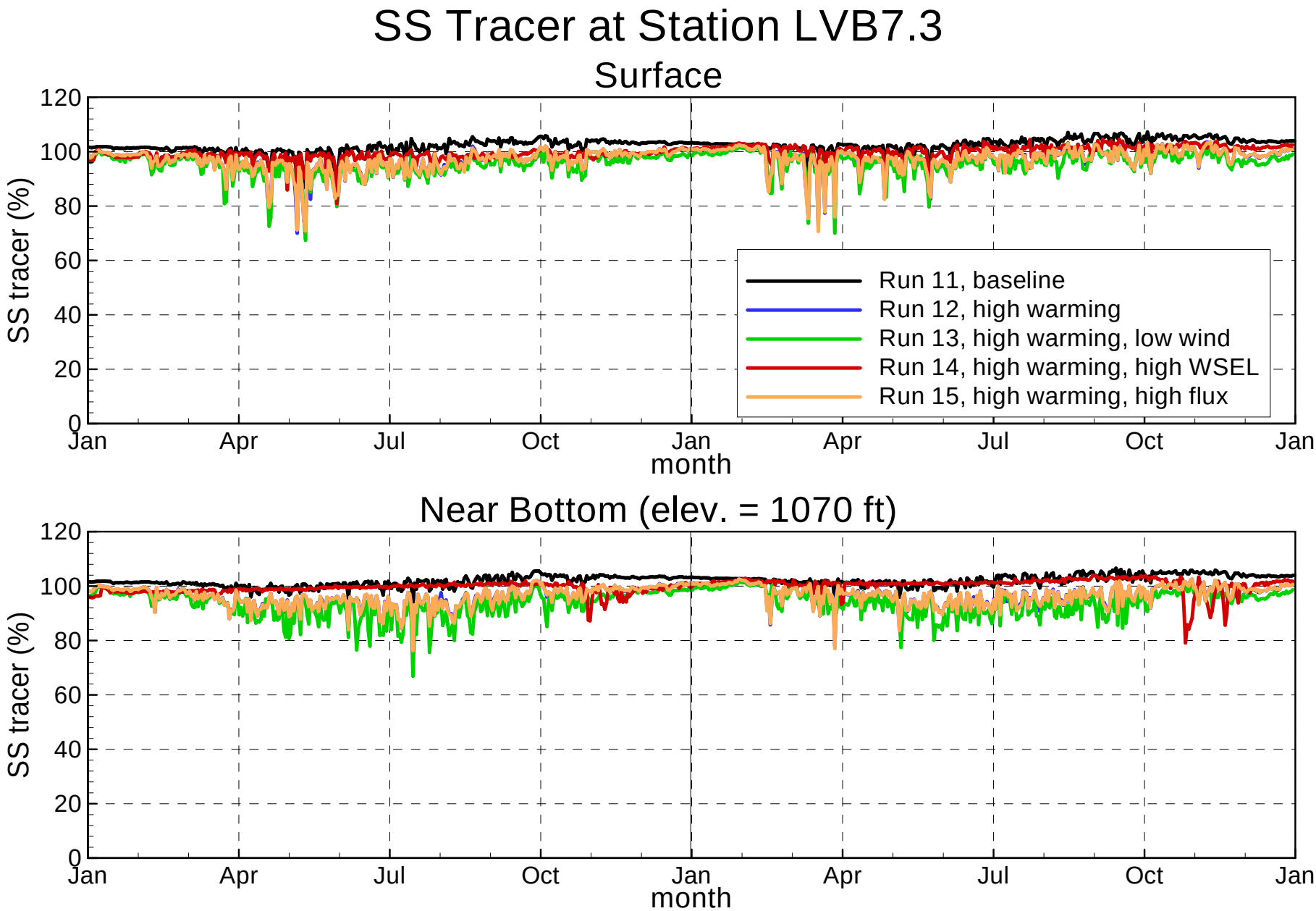
SS Tracer at Station LVB7.3
Surface
SS tracer (%)
120
100
80
60
40
20
0
Jan
Apr
Jul
Oct
Jan
Apr
Jul
Oct
Jan
month
Run 11, baseline
Run 12, high warming
Run 13, high warming, low wind
Run 14, high warming, high WSEL
Run 15, high warming, high flux
Near Bottom (elev. = 1070 ft)
SS tracer (%)
120
100
80
60
40
20
0
Jan
Apr
Jul
Oct
Jan
Apr
Jul
Oct
Jan
month

Figure A.238

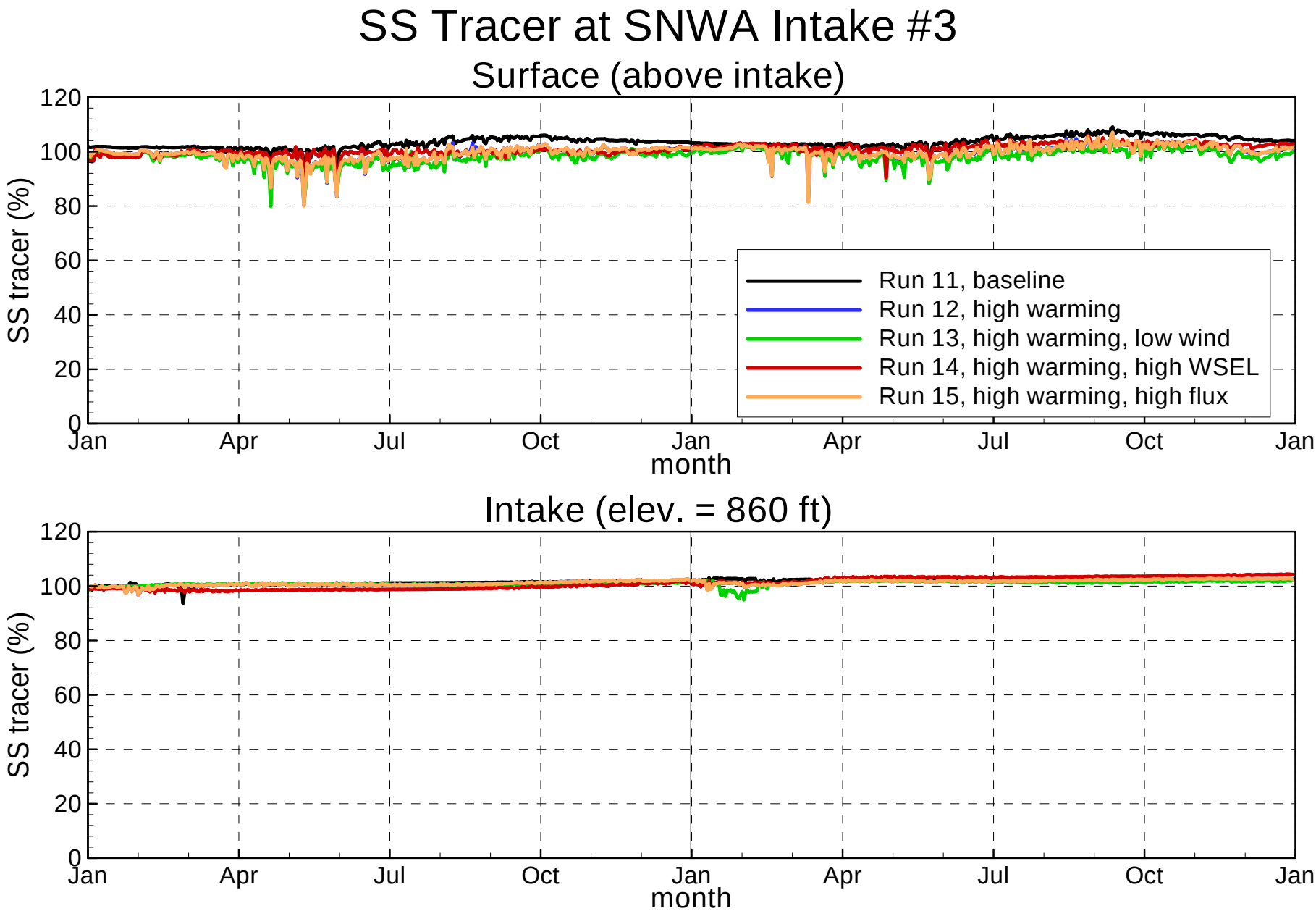
SS Tracer at SNWA Intake #3
Surface (above intake)
SS tracer (%)
120
100
80
60
40
20
0
Jan
Apr
Jul
Oct
Jan
Apr
Jul
Oct
Jan
month
Run 11, baseline
Run 12, high warming
Run 13, high warming, low wind
Run 14, high warming, high WSEL
Run 15, high warming, high flux
Intake (elev. = 860 ft)
SS tracer (%)
120
100
80
60
40
20
0
Jan
Apr
Jul
Oct
Jan
Apr
Jul
Oct
Jan
month

Figure A.239

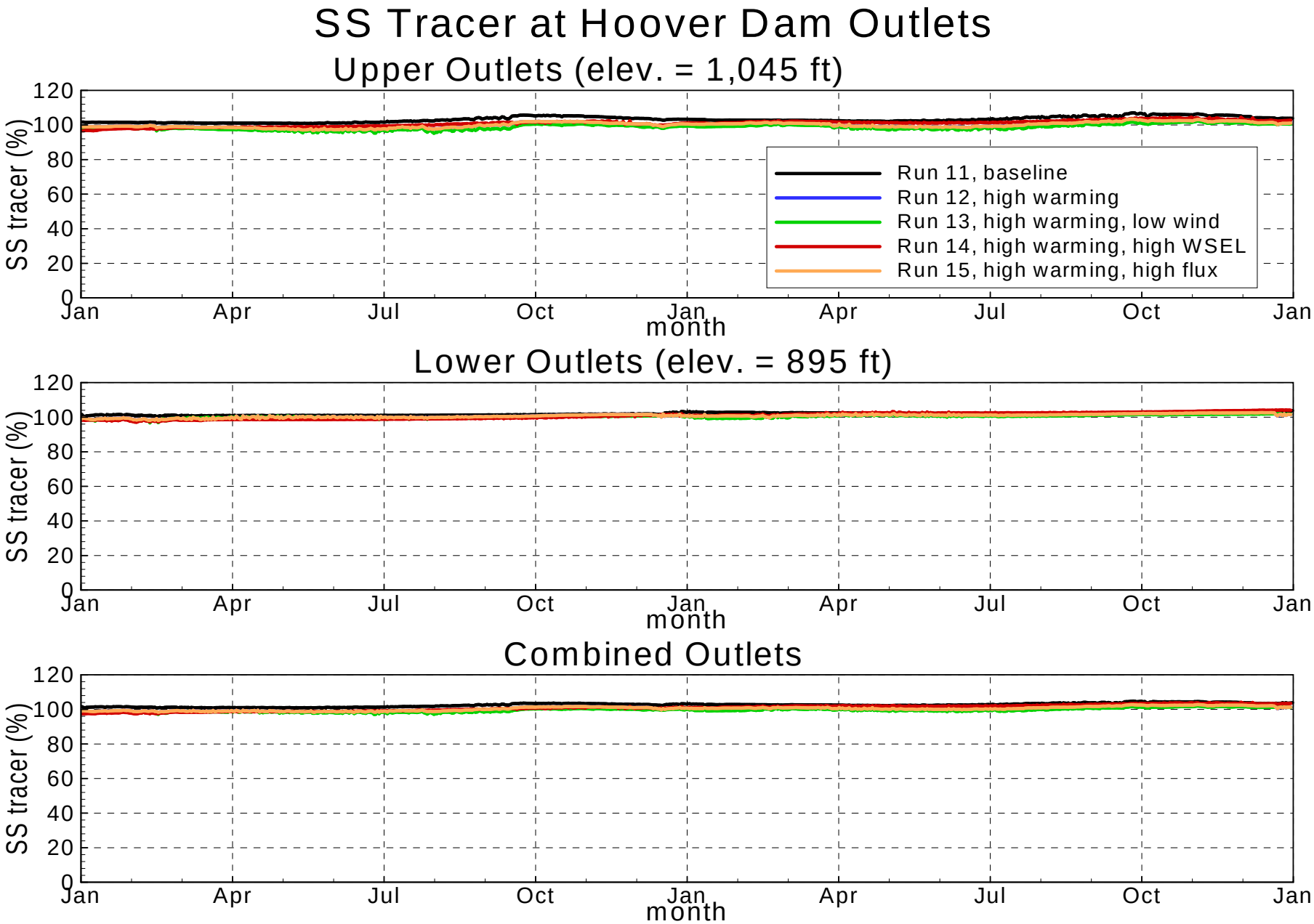
SS Tracer at Hoover Dam Outlets
Upper Outlets (elev. = 1,045 ft)
SS tracer (%)
120
100
80
60
40
20
0
Jan
Apr
Jul
Oct
Jan
Apr
Jul
Oct
Jan
month
Run 11, baseline
Run 12, high warming
Run 13, high warming, low wind
Run 14, high warming, high WSEL
Run 15, high warming, high flux
Lower Outlets (elev. = 895 ft)
Combined Outlets

Figure A.240

Total Organic Carbon at Station CR394.0

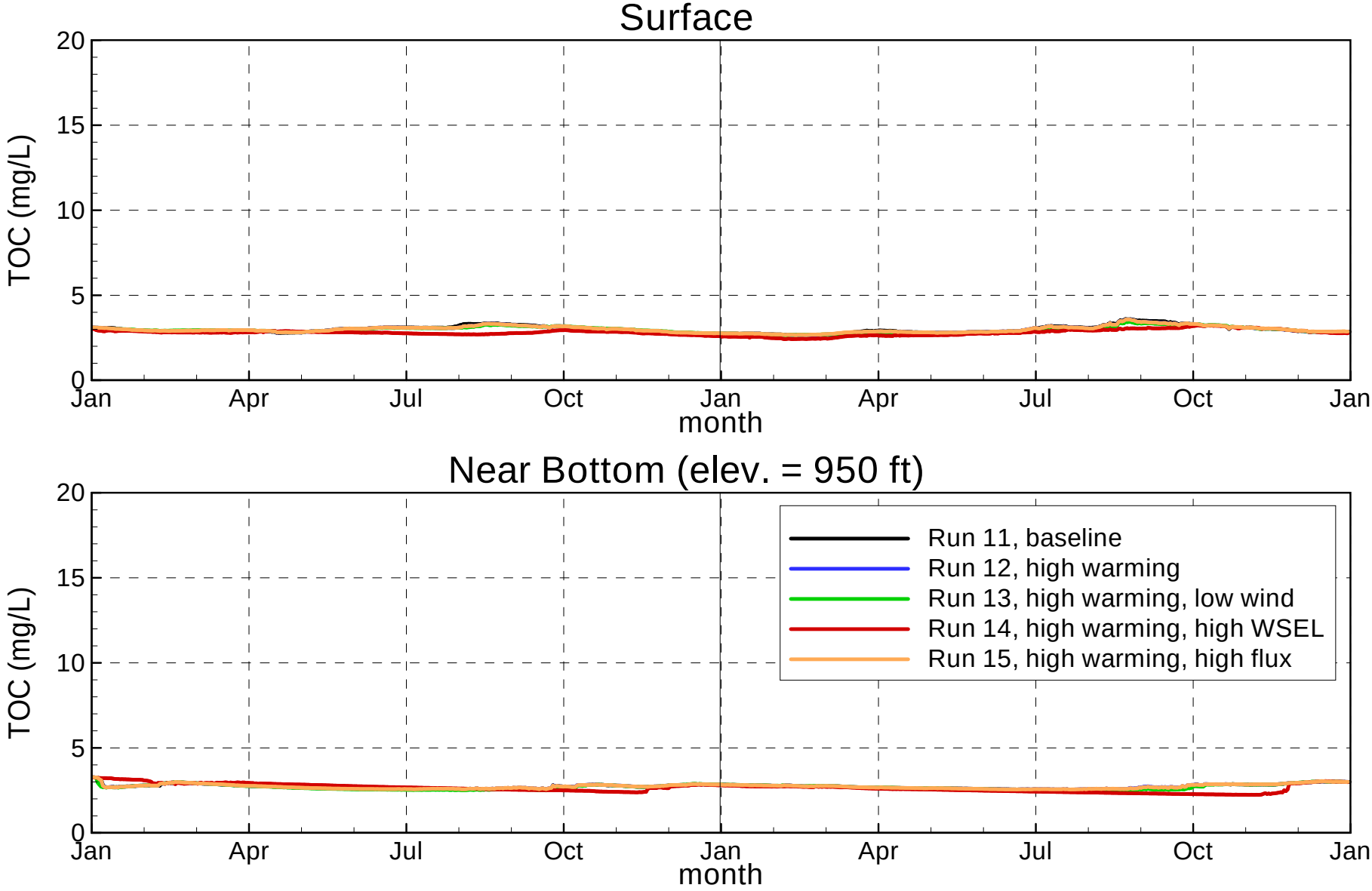

Figure A.241

Total Organic Carbon at Station CR390.0

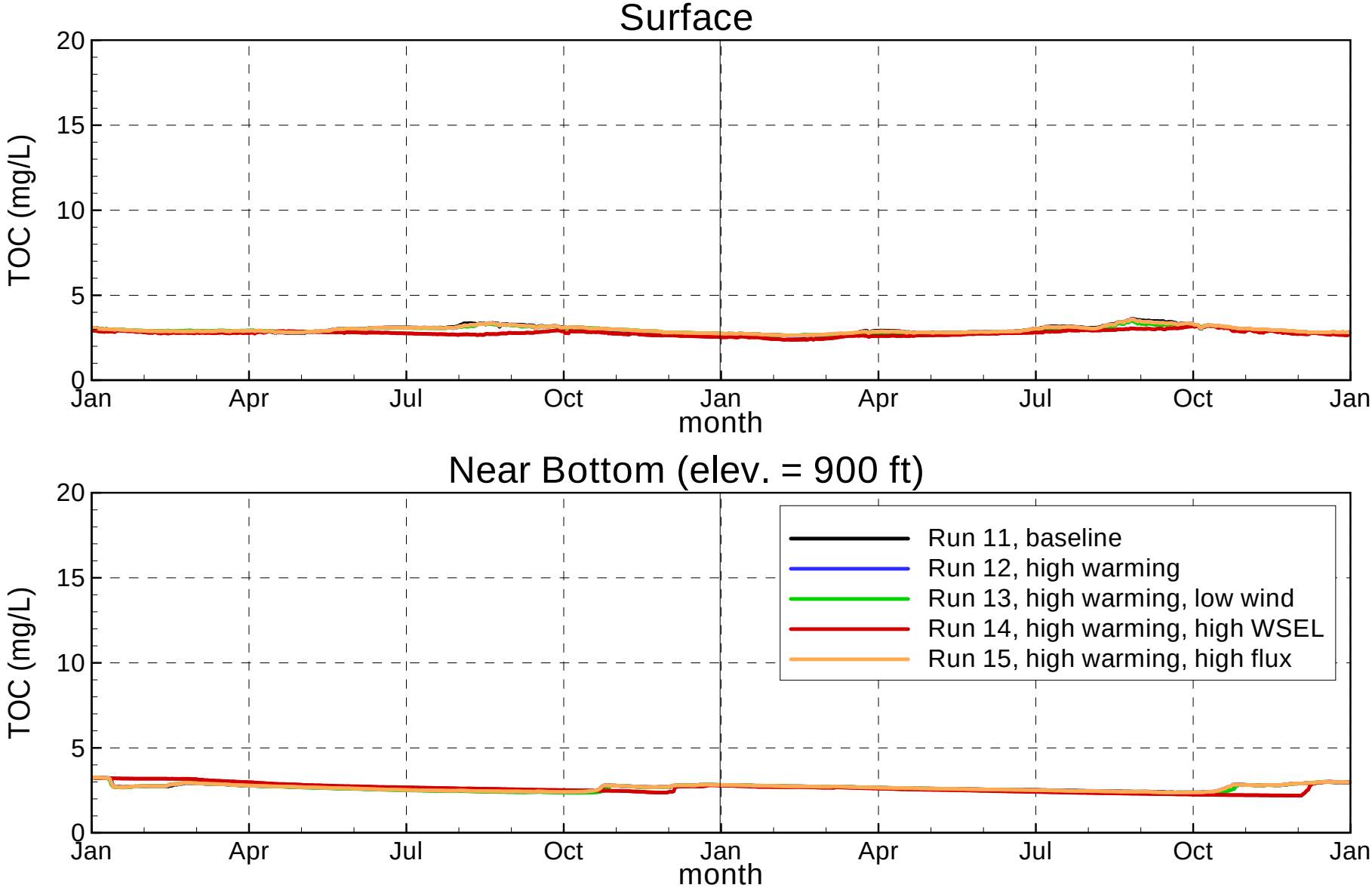

Figure A.242

Total Organic Carbon at Station CR380.0

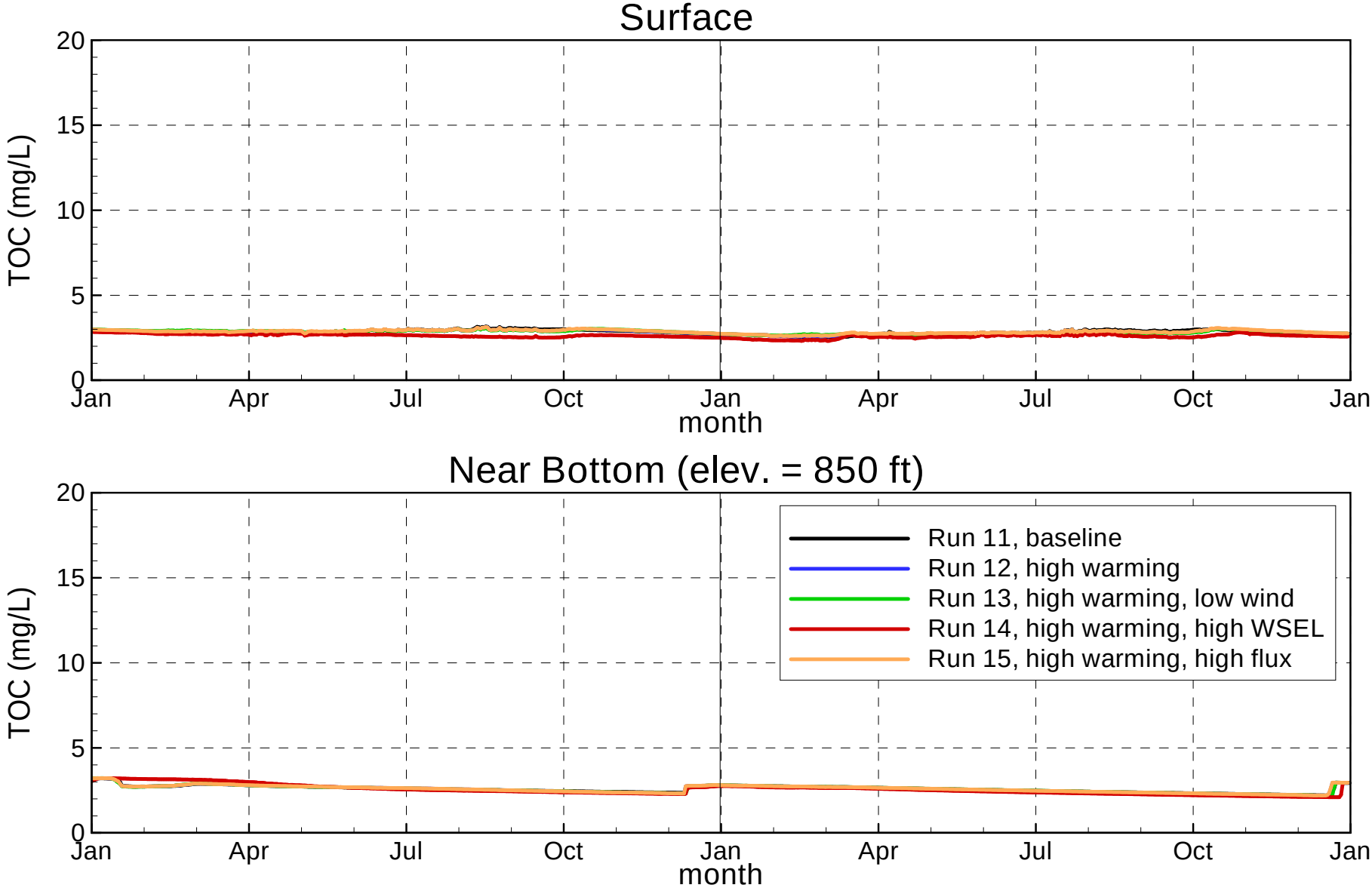

Figure A.243

Total Organic Carbon at Station VR2.0

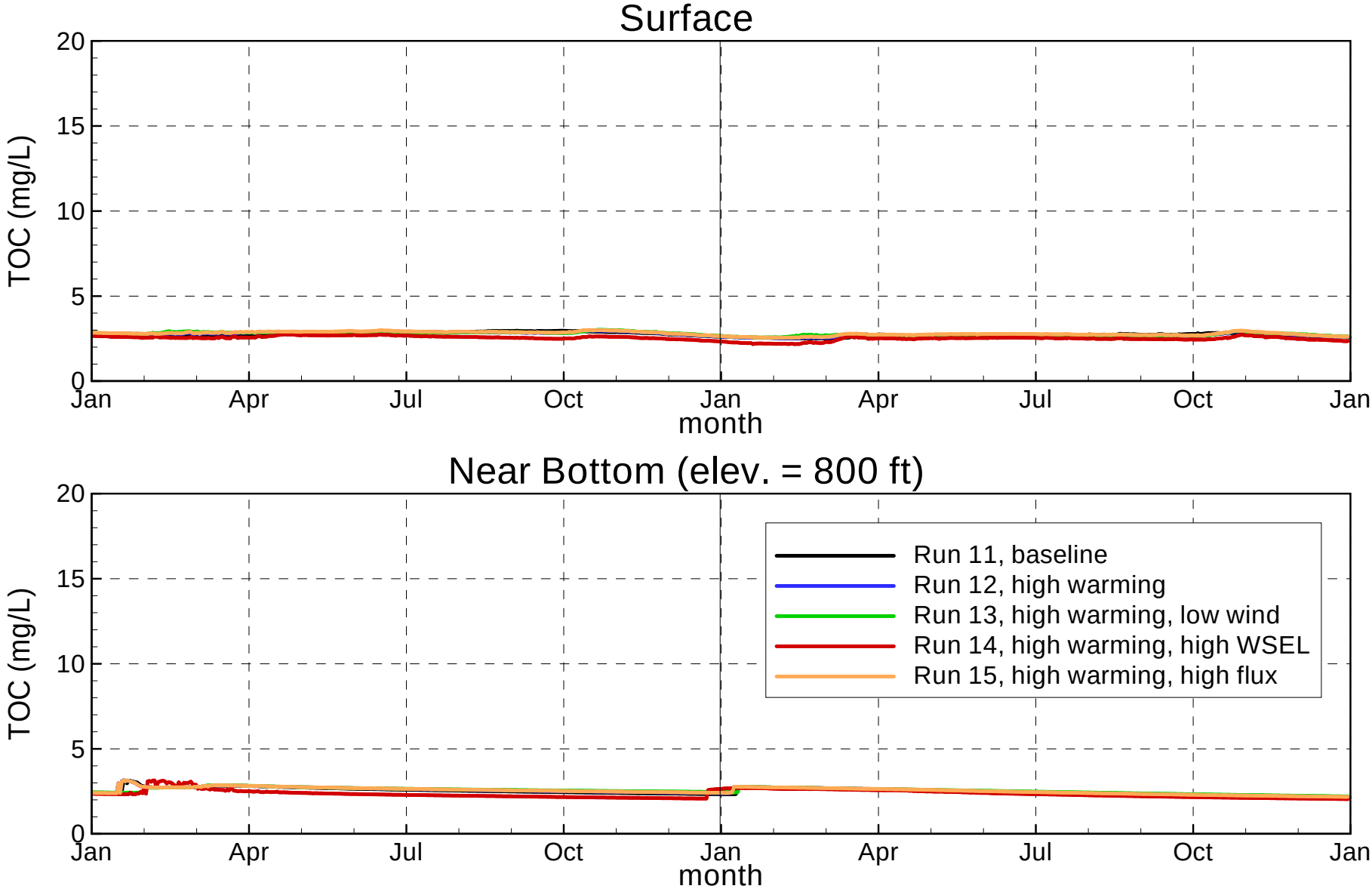

Figure A.244

Total Organic Carbon at Station VR12.9

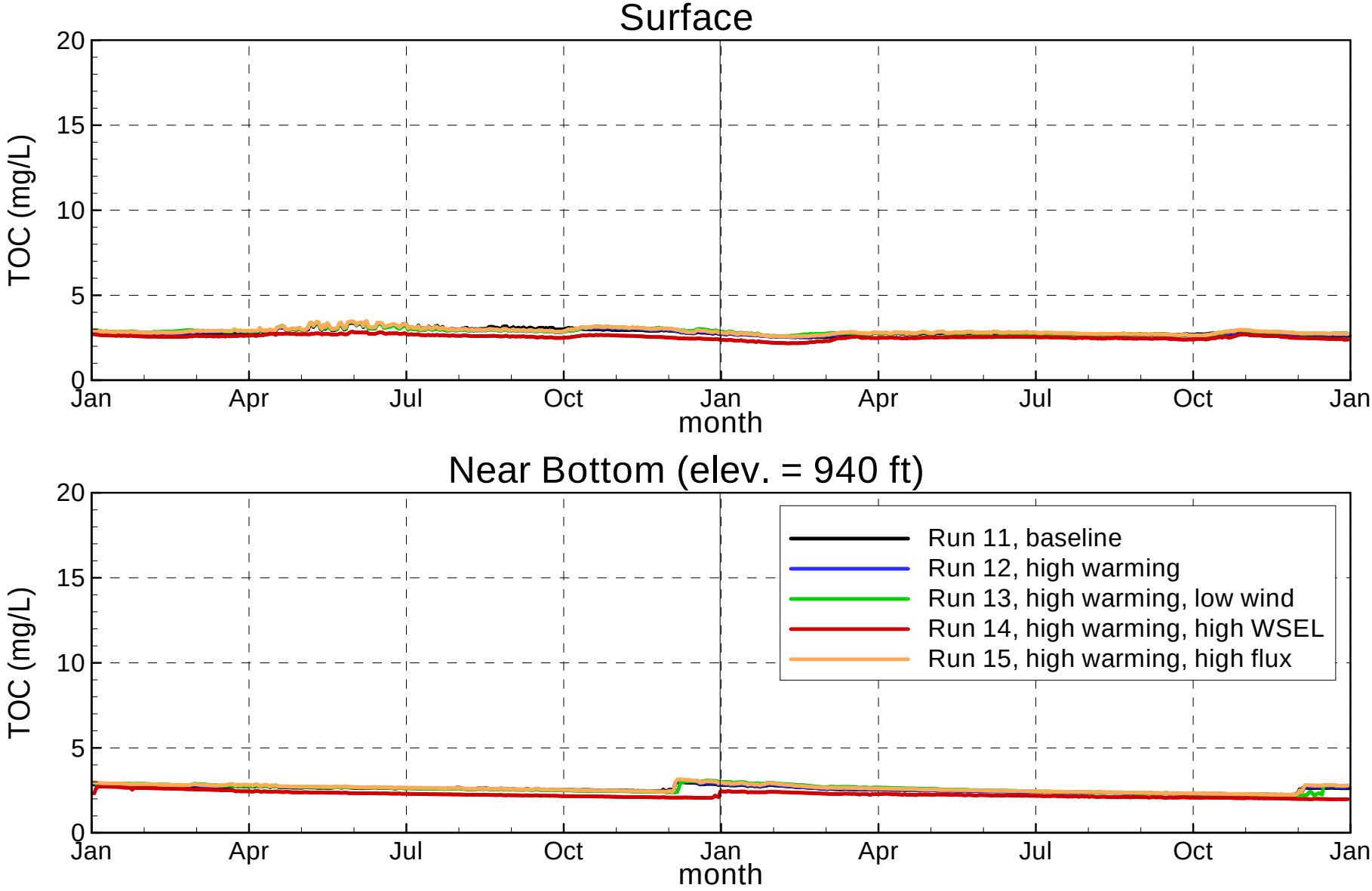

Figure A.245

Total Organic Carbon at Station VR18.0

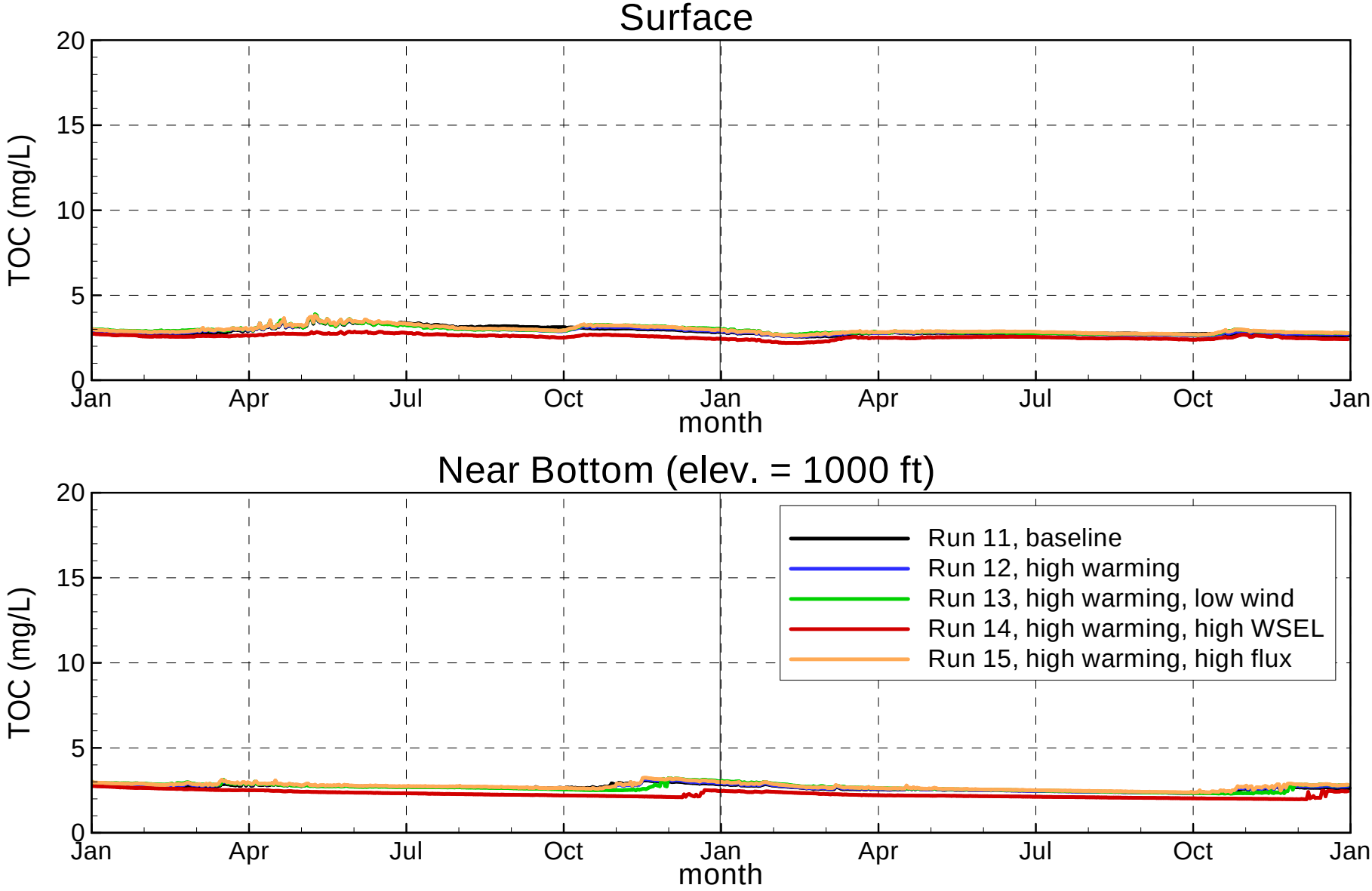

Figure A.246

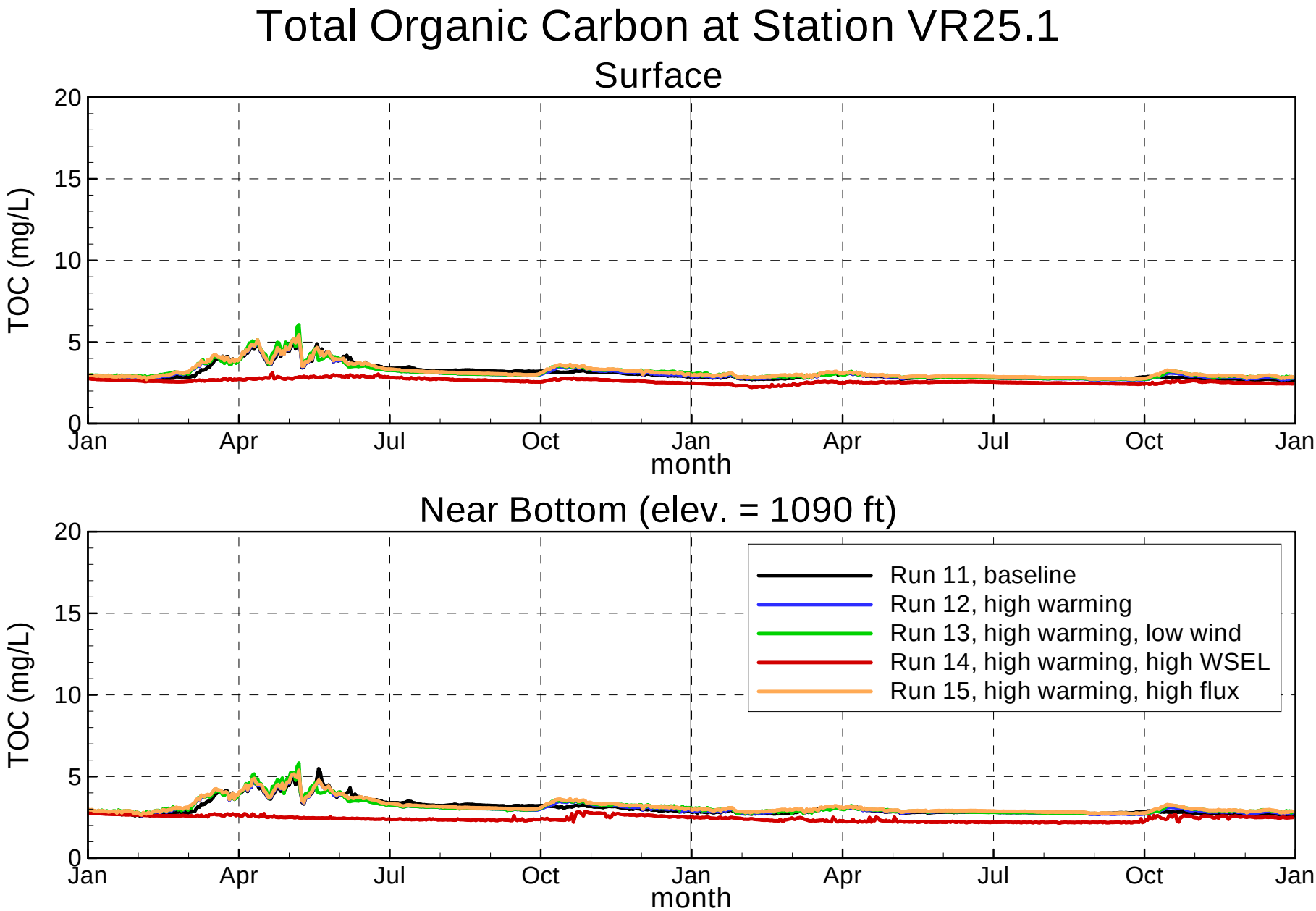
Total Organic Carbon at Station VR25.1
Surface
TOC (mg/L)
20
15
10
5
0
Jan
Apr
Jul
Oct
Jan
Apr
Jul
Oct
Jan
month
Near Bottom (elev. = 1090 ft)
TOC (mg/L)
Run 11, baseline
Run 12, high warming
Run 13, high warming, low wind
Run 14, high warming, high WSEL
Run 15, high warming, high flux
month

Figure A.247

Total Organic Carbon at Station CR360.7

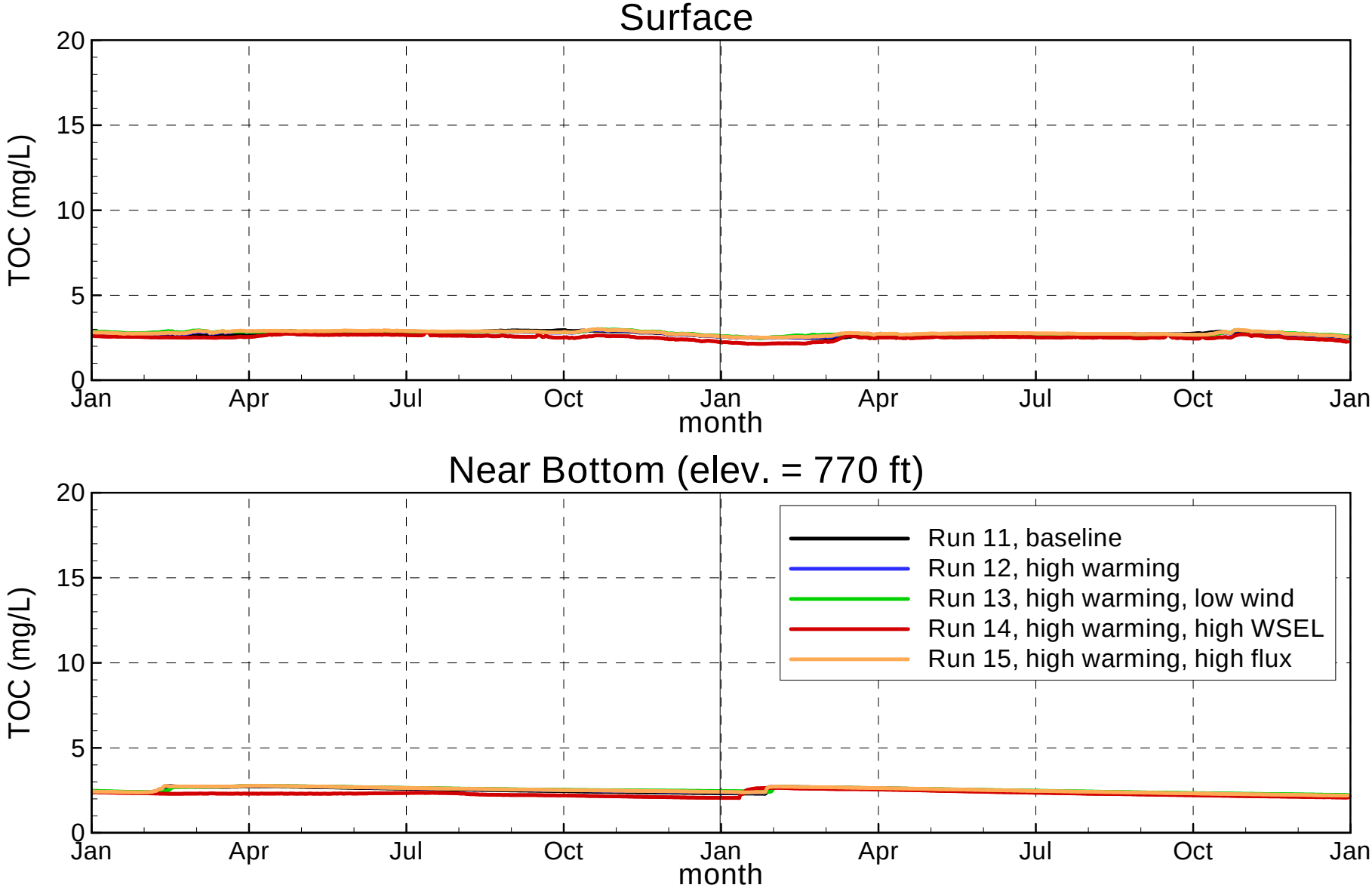

Figure A.248

Total Organic Carbon at Station CR346.4

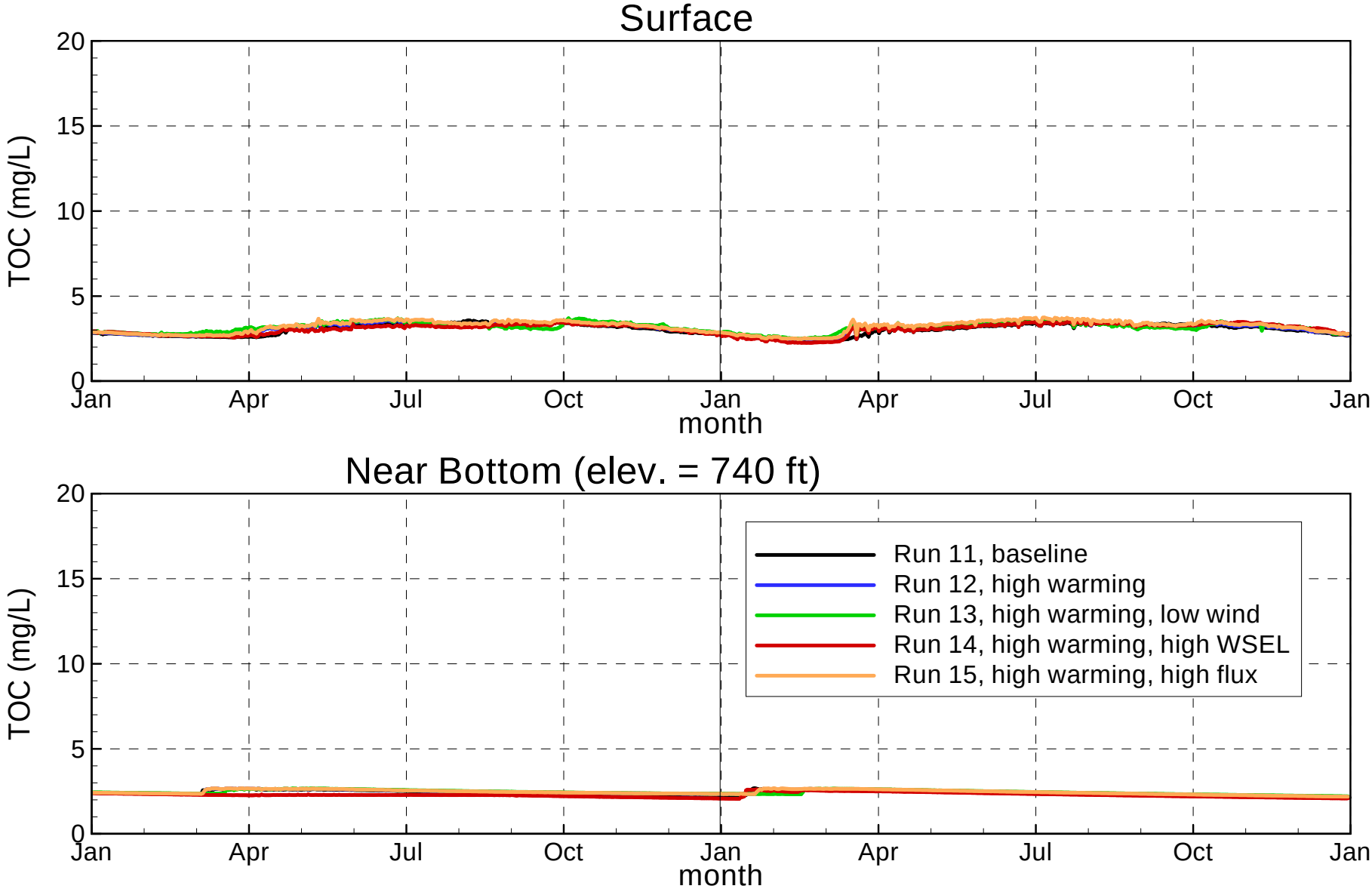

Figure A.249

Total Organic Carbon at Station LWLVB1.2

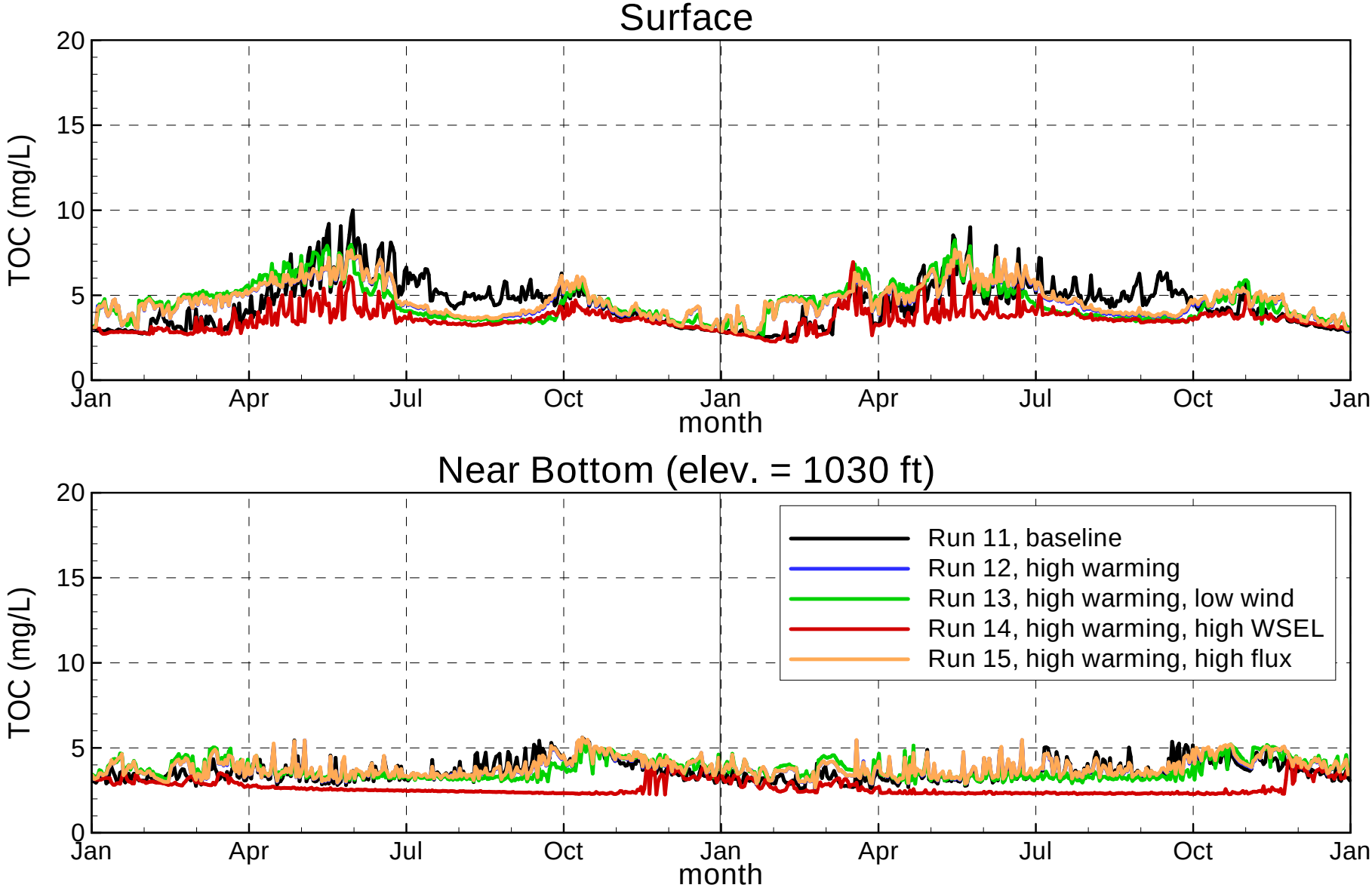

Figure A.250

Total Organic Carbon at Station LWLVB1.85

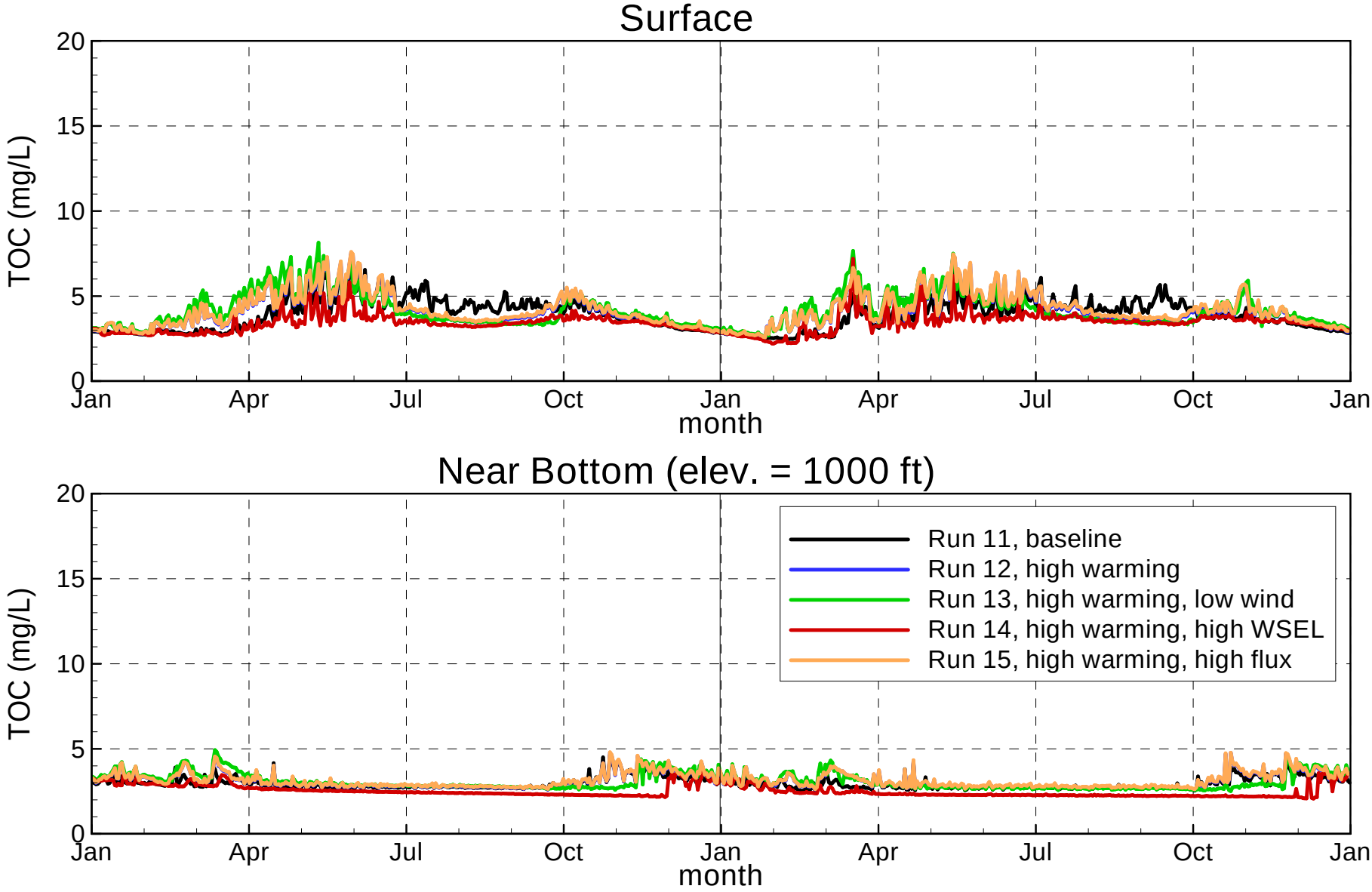

Figure A.251

Total Organic Carbon at Station LWLVB2.7

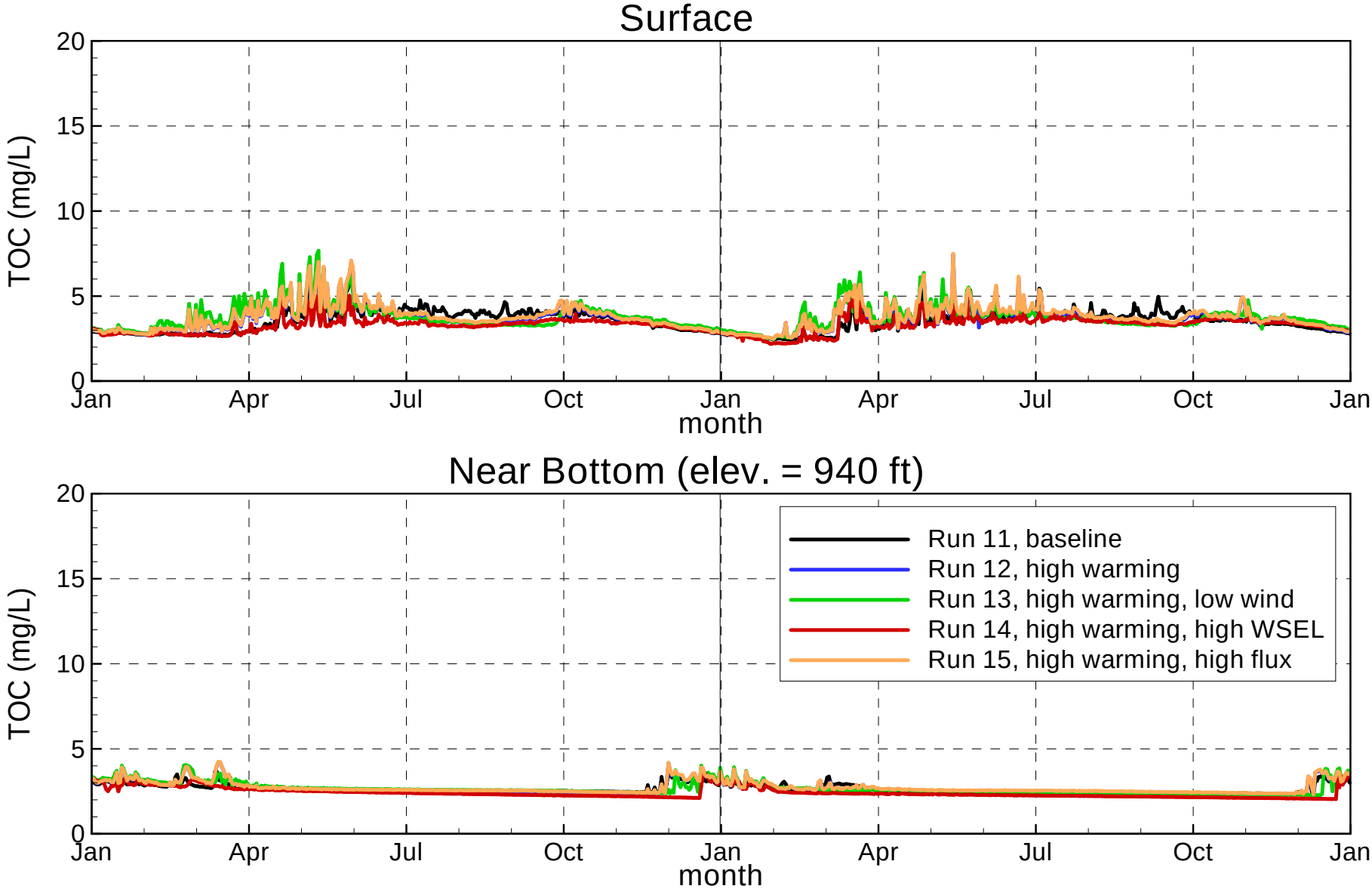

Figure A.252

Total Organic Carbon at Station LWLVB3.5

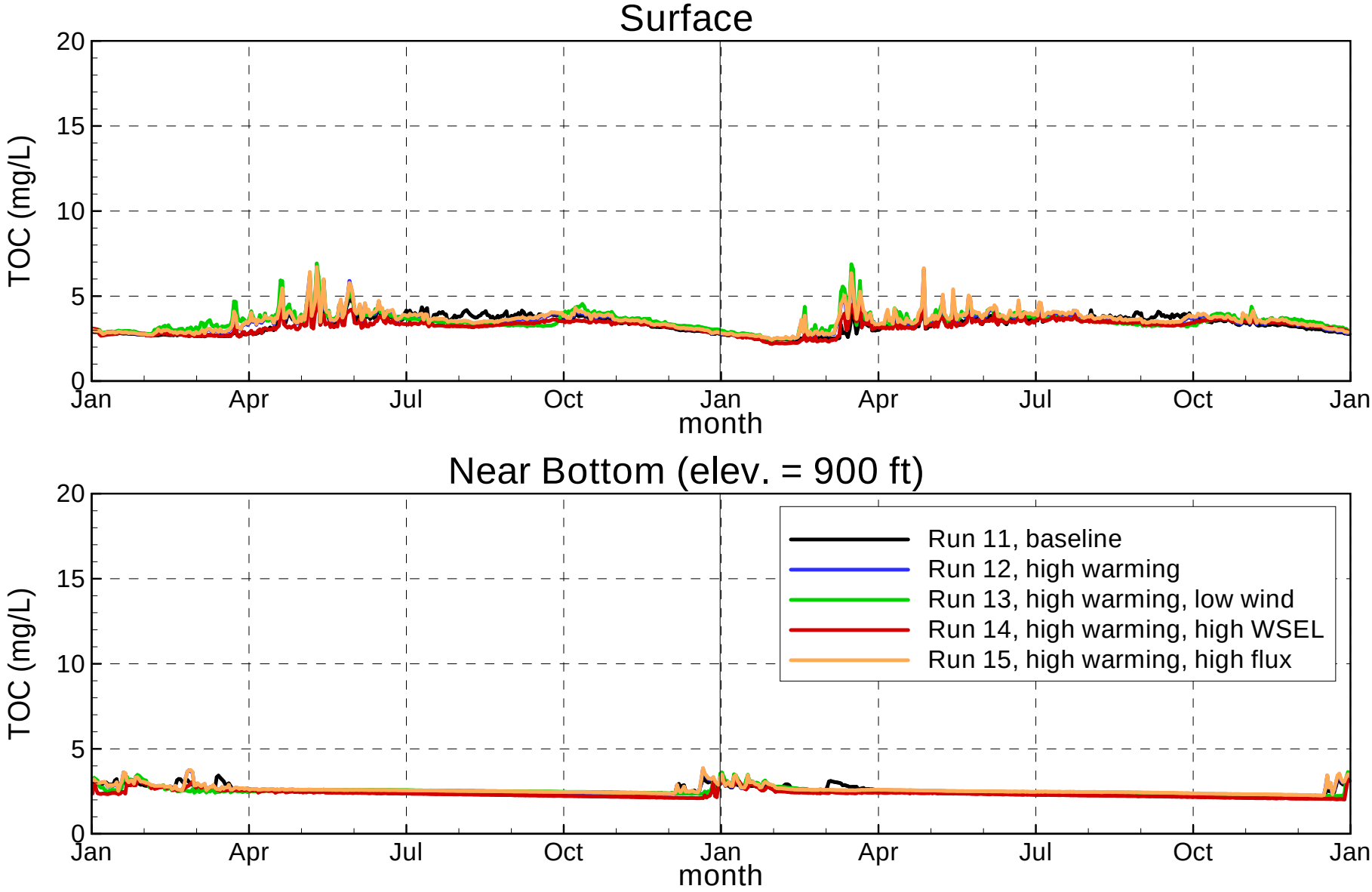

Figure A.253

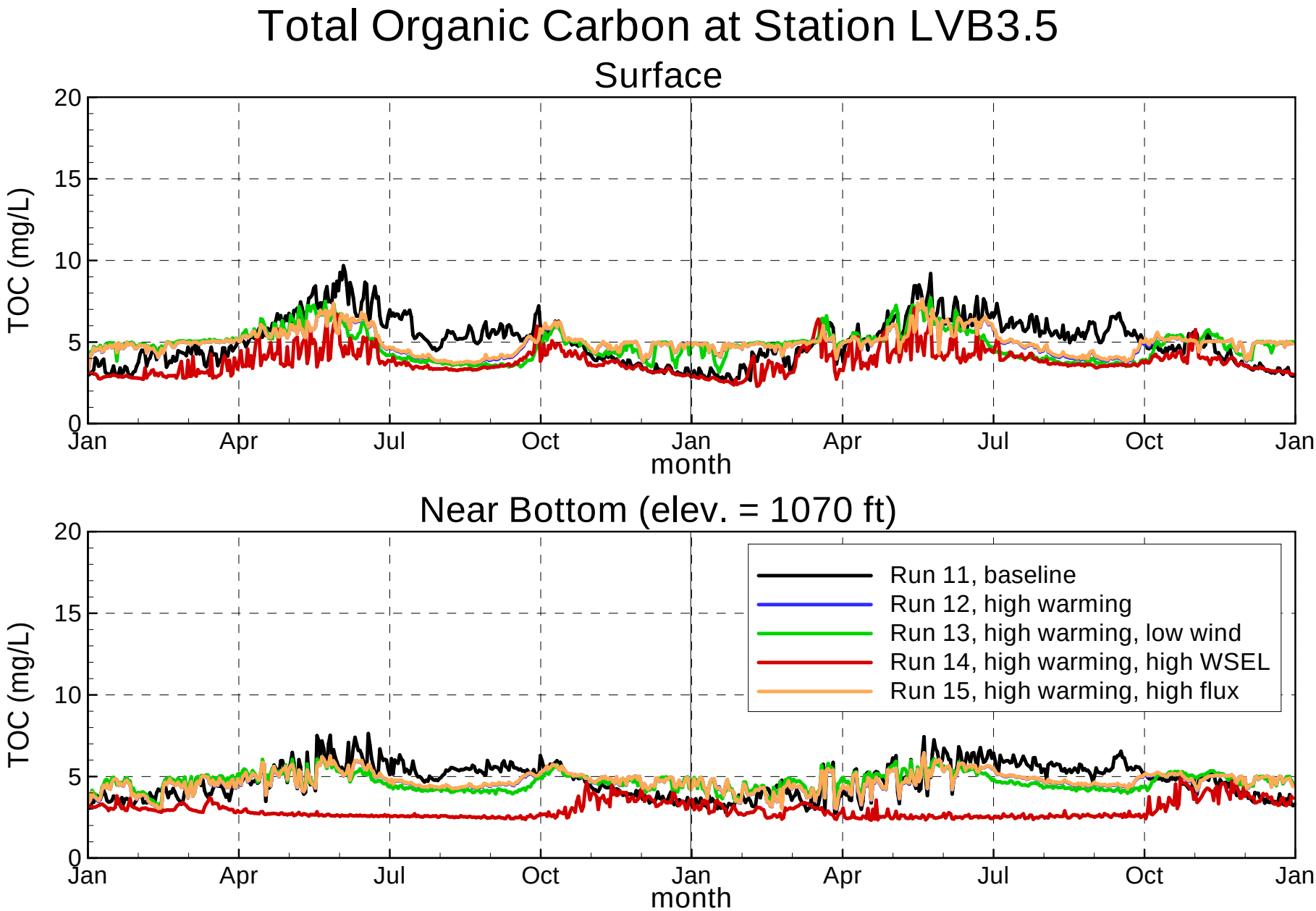
Total Organic Carbon at Station LVB3.5
Surface
TOC (mg/L)
20
15
10
5
0
Jan
Apr
Jul
Oct
Jan
Apr
Jul
Oct
Jan
month
Near Bottom (elev. = 1070 ft)
TOC (mg/L)
Run 11, baseline
Run 12, high warming
Run 13, high warming, low wind
Run 14, high warming, high WSEL
Run 15, high warming, high flux
month

Figure A.254

Total Organic Carbon at Station LVB4.15

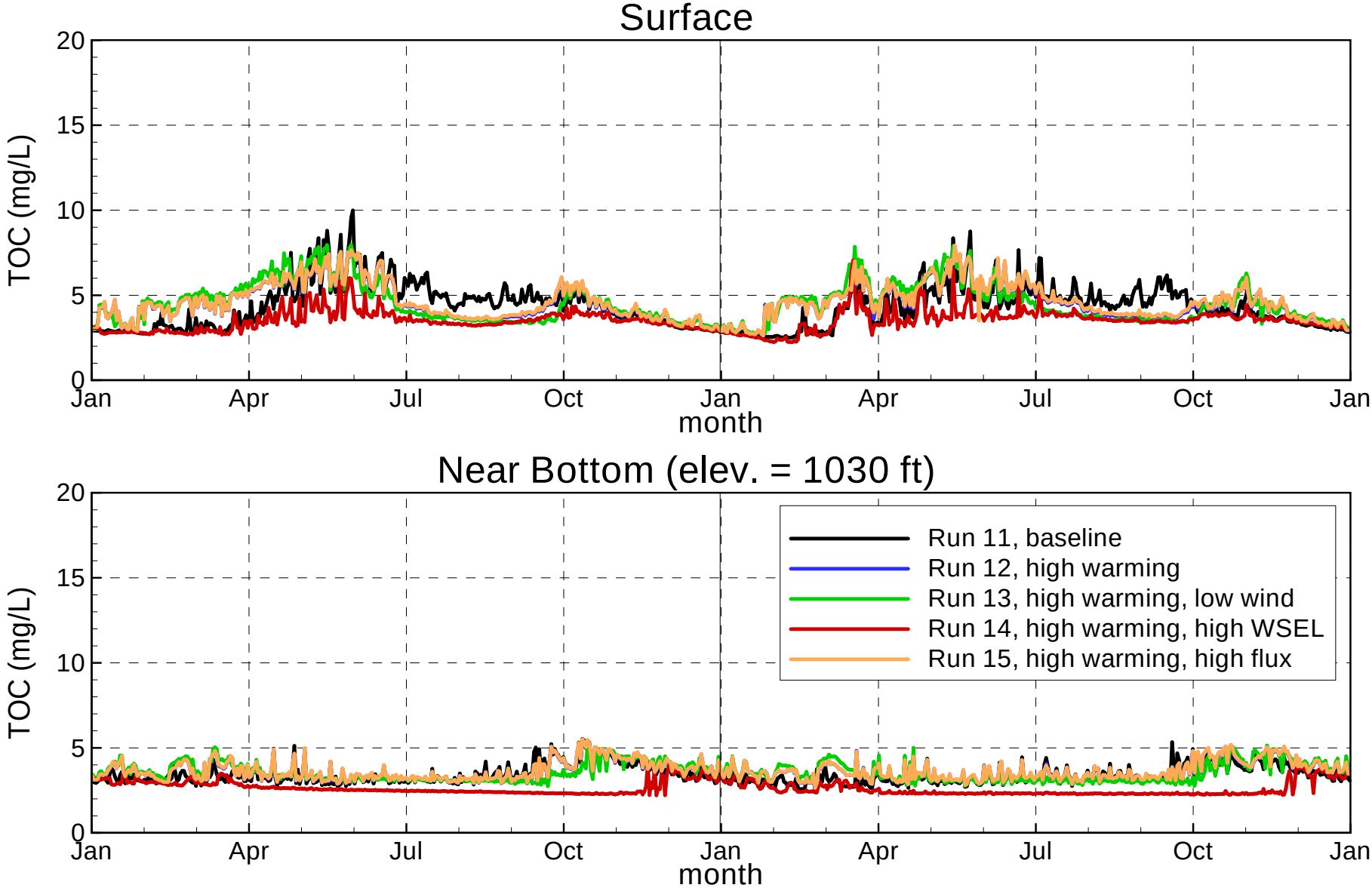

Figure A.255

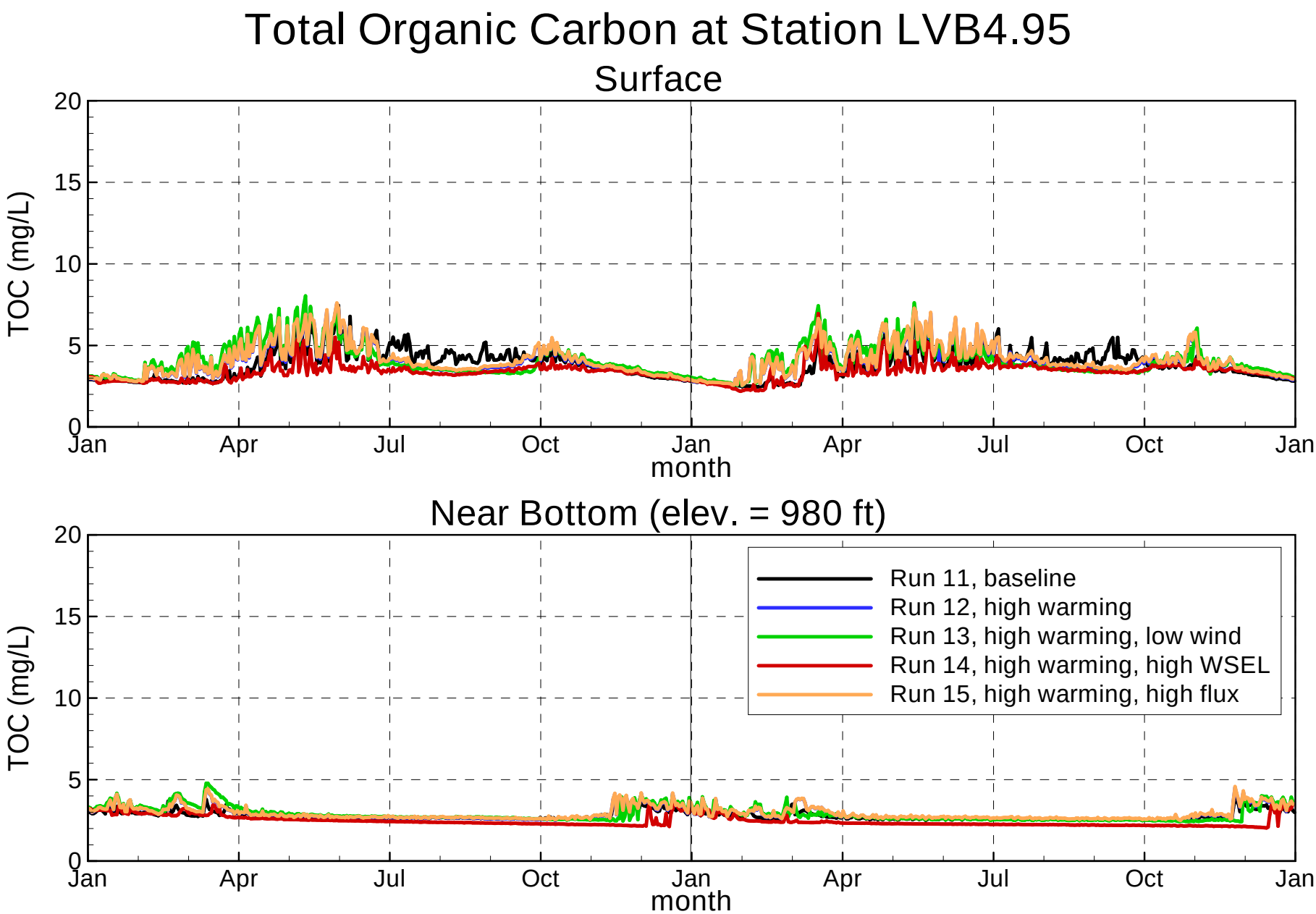
Total Organic Carbon at Station LVB4.95
Surface
TOC (mg/L)
20
15
10
5
0
Jan
Apr
Jul
Oct
Jan
Apr
Jul
Oct
Jan
month
Near Bottom (elev. = 980 ft)
TOC (mg/L)
Run 11, baseline
Run 12, high warming
Run 13, high warming, low wind
Run 14, high warming, high WSEL
Run 15, high warming, high flux
month

Figure A.256

Total Organic Carbon at Station LVB6.7

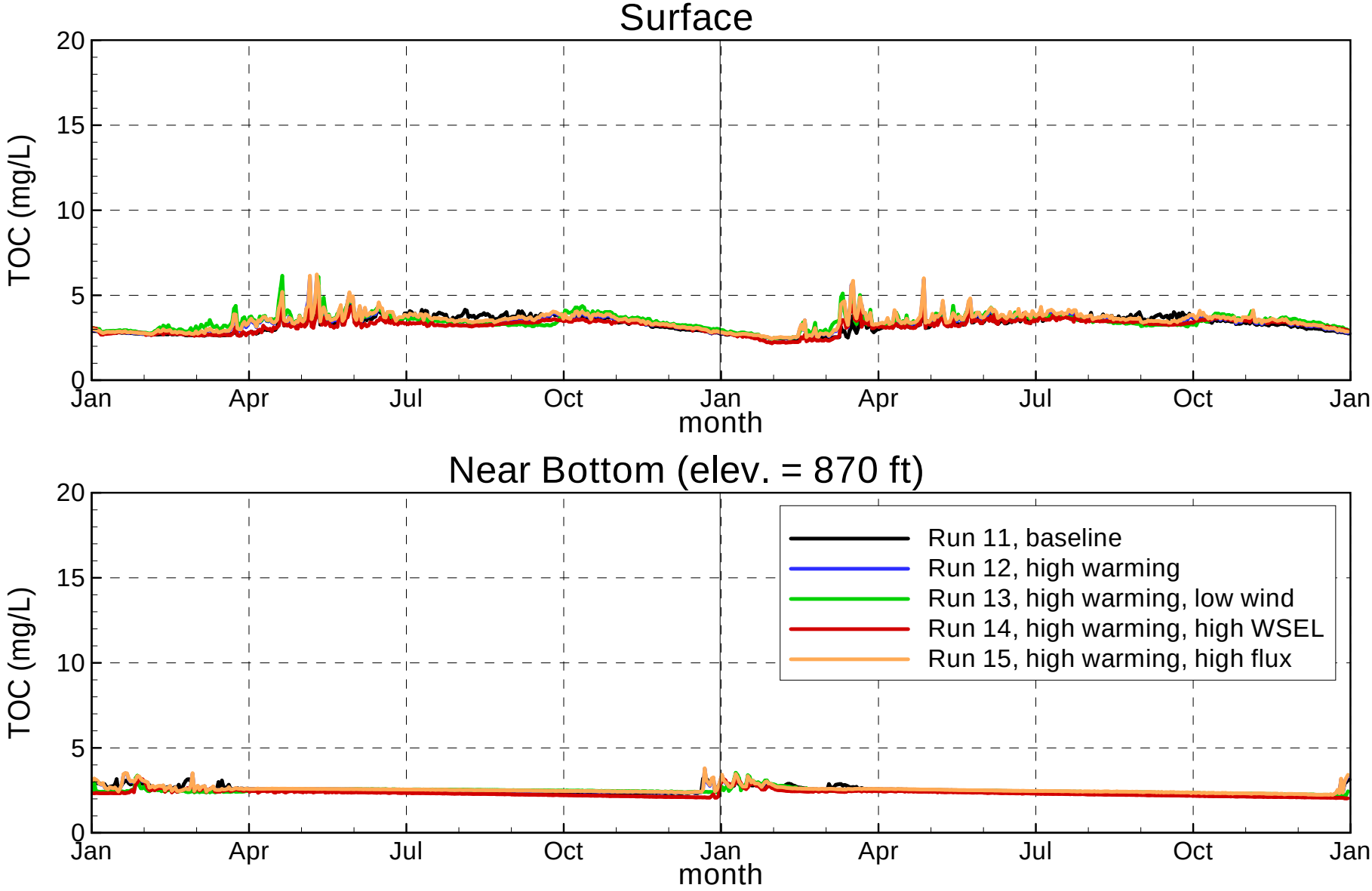

Figure A.257

Total Organic Carbon at Station LVB7.3

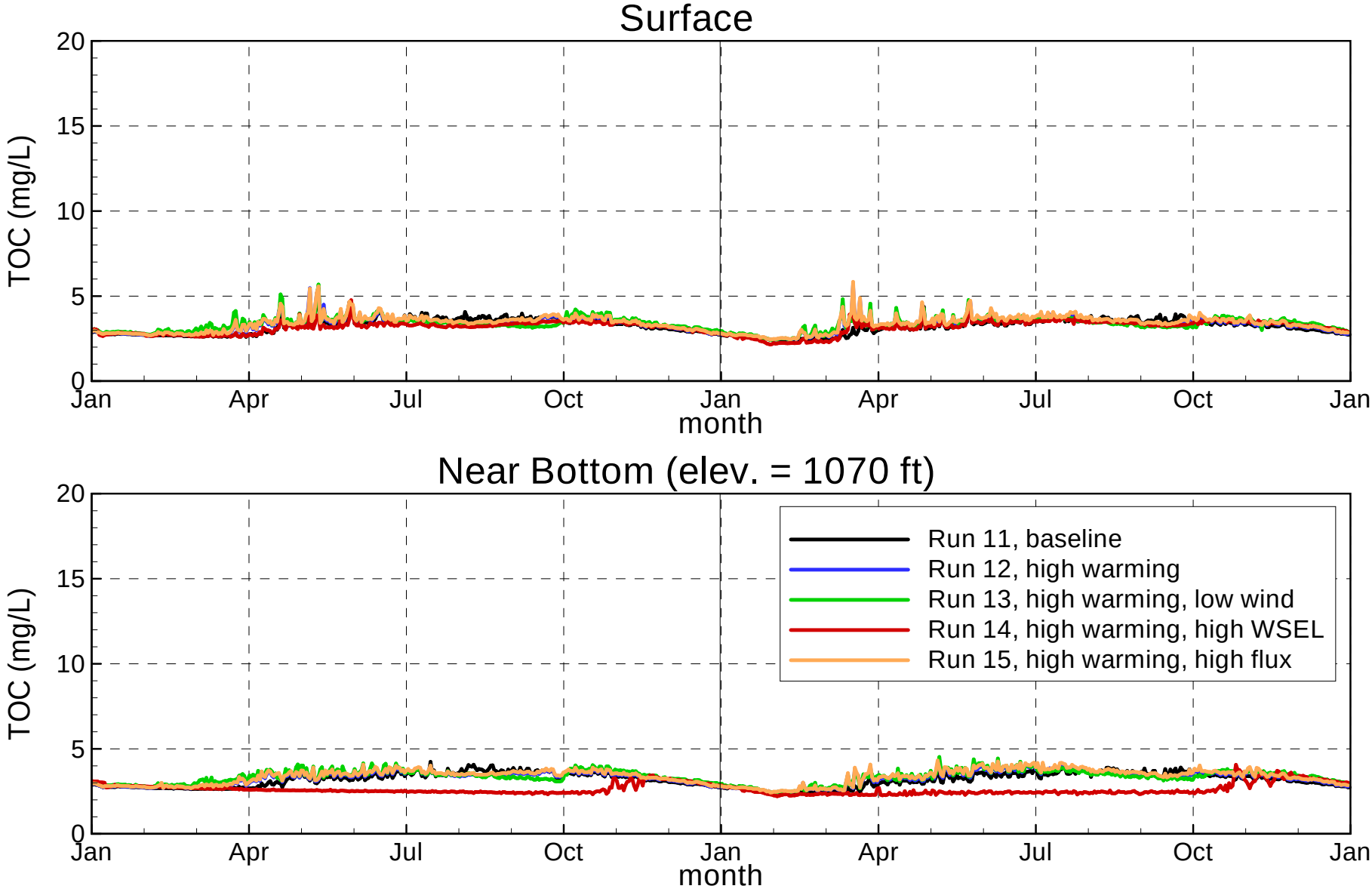

Figure A.258

Total Organic Carbon at SNWA Intake #3

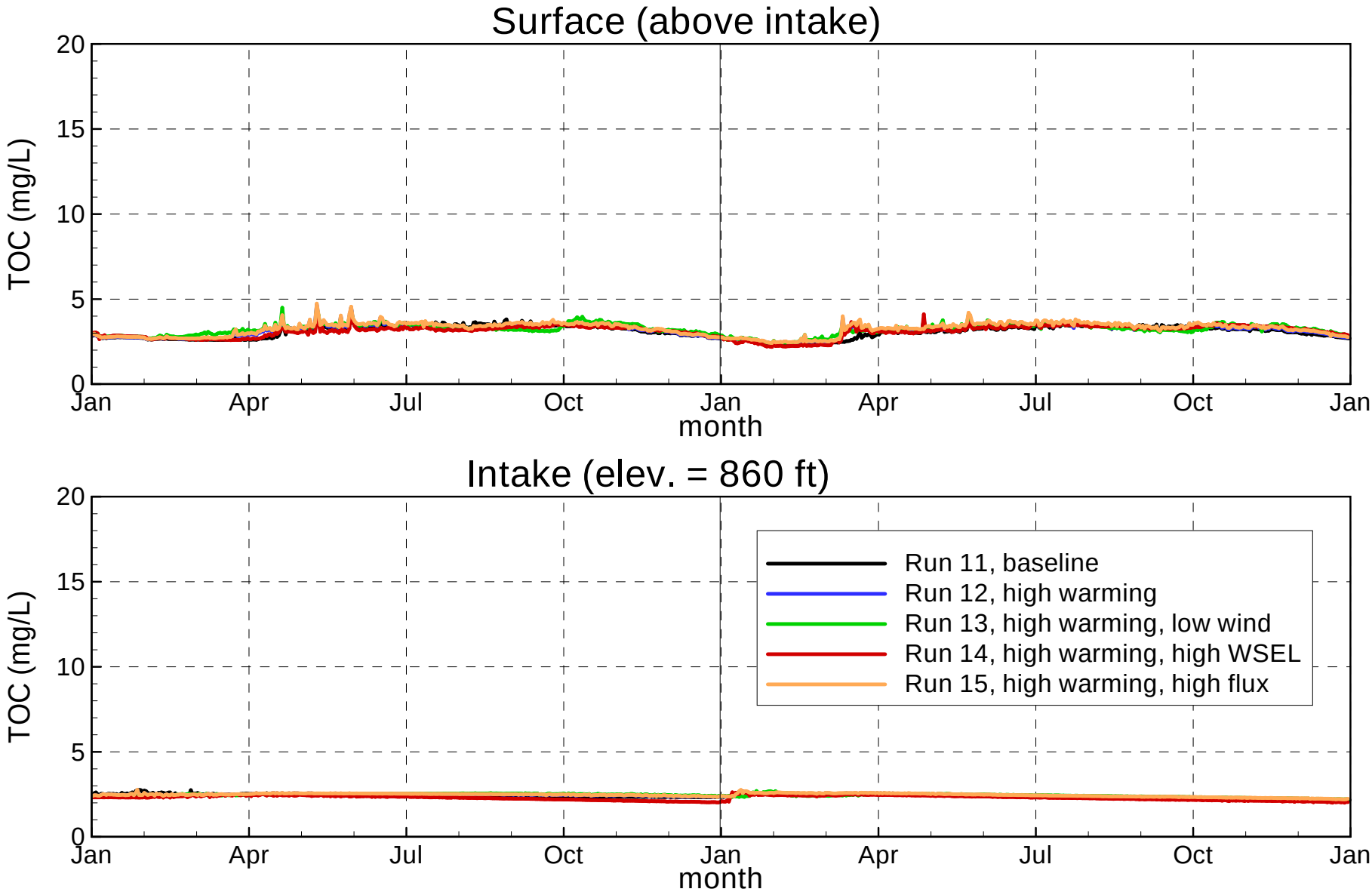

Figure A.259

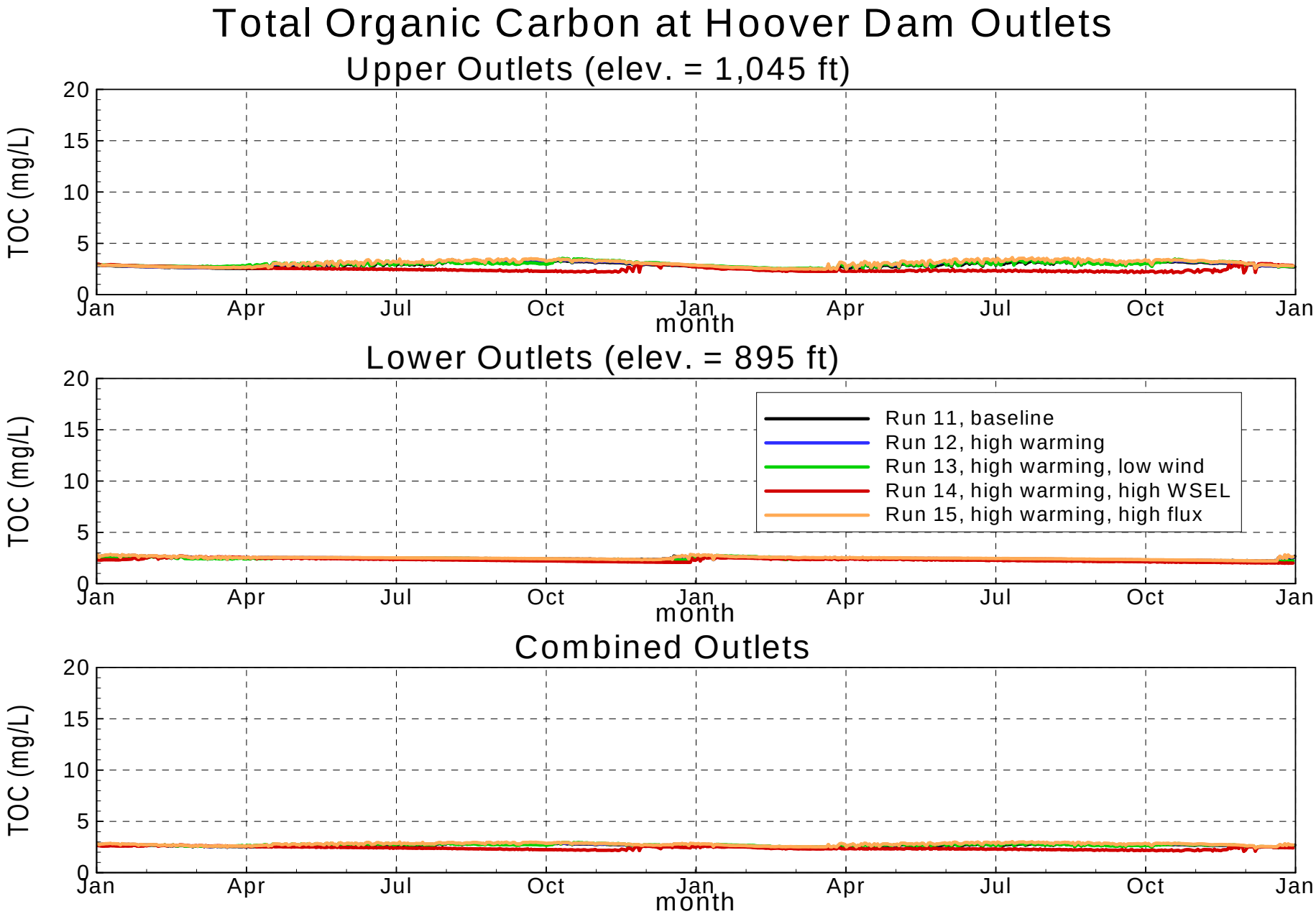
Total Organic Carbon at Hoover Dam Outlets
Upper Outlets (elev. = 1,045 ft)
Lower Outlets (elev. = 895 ft)
Combined Outlets
TOC (mg/L)
0
5
10
15
20
Jan
Apr
Jul
Oct
Jan
Apr
Jul
Oct
Jan
month
Run 11, baseline
Run 12, high warming
Run 13, high warming, low wind
Run 14, high warming, high WSEL
Run 15, high warming, high flux

Figure A.260

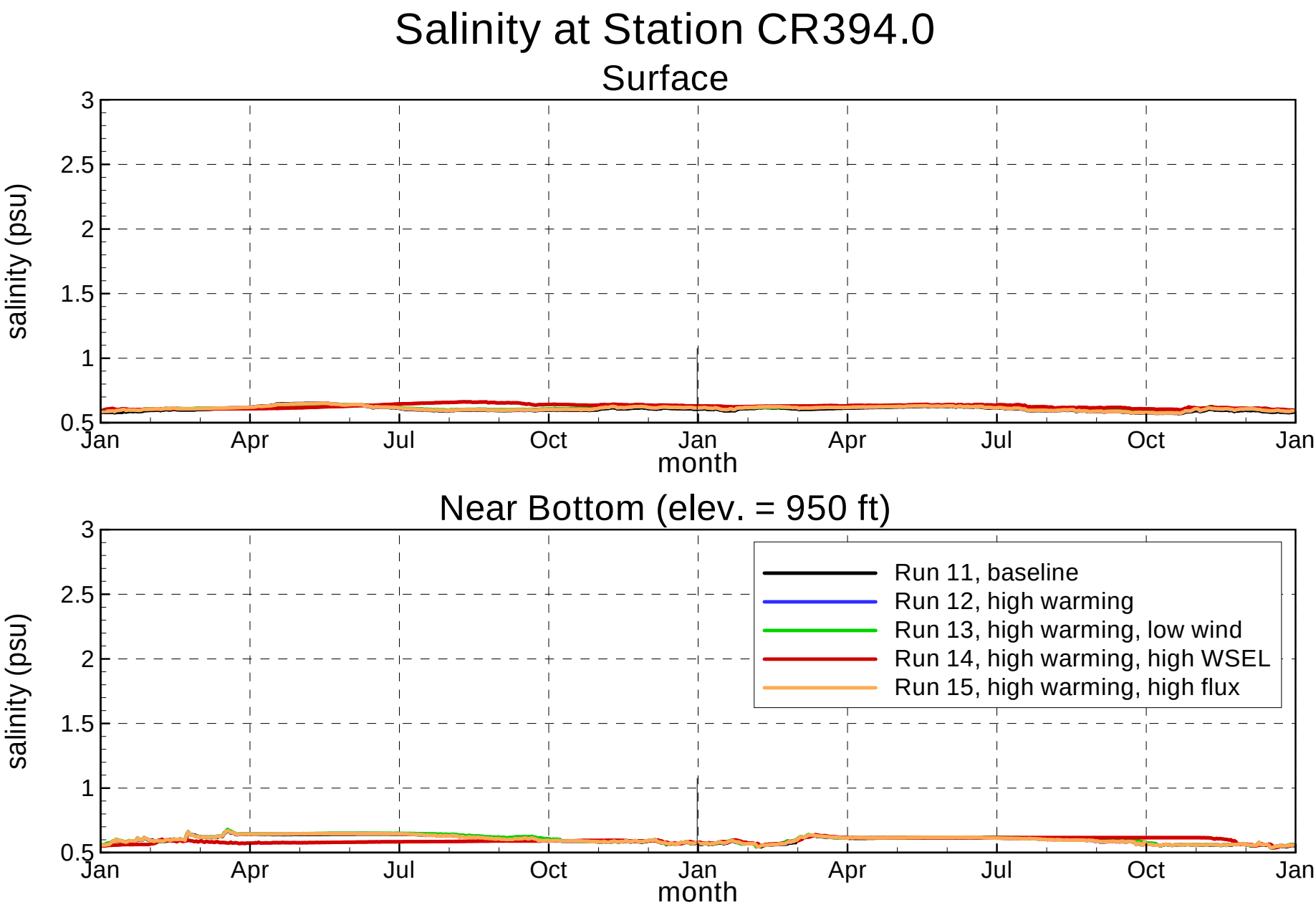
Salinity at Station CR394.0
Surface
salinity (psu)
3
2.5
2
1.5
1
0.5
Jan
Apr
Jul
Oct
Jan
Apr
Jul
Oct
Jan
month
Near Bottom (elev. = 950 ft)
salinity (psu)
3
2.5
2
1.5
1
0.5
Jan
Apr
Jul
Oct
Jan
Apr
Jul
Oct
Jan
month
Run 11, baseline
Run 12, high warming
Run 13, high warming, low wind
Run 14, high warming, high WSEL
Run 15, high warming, high flux

Figure A.261

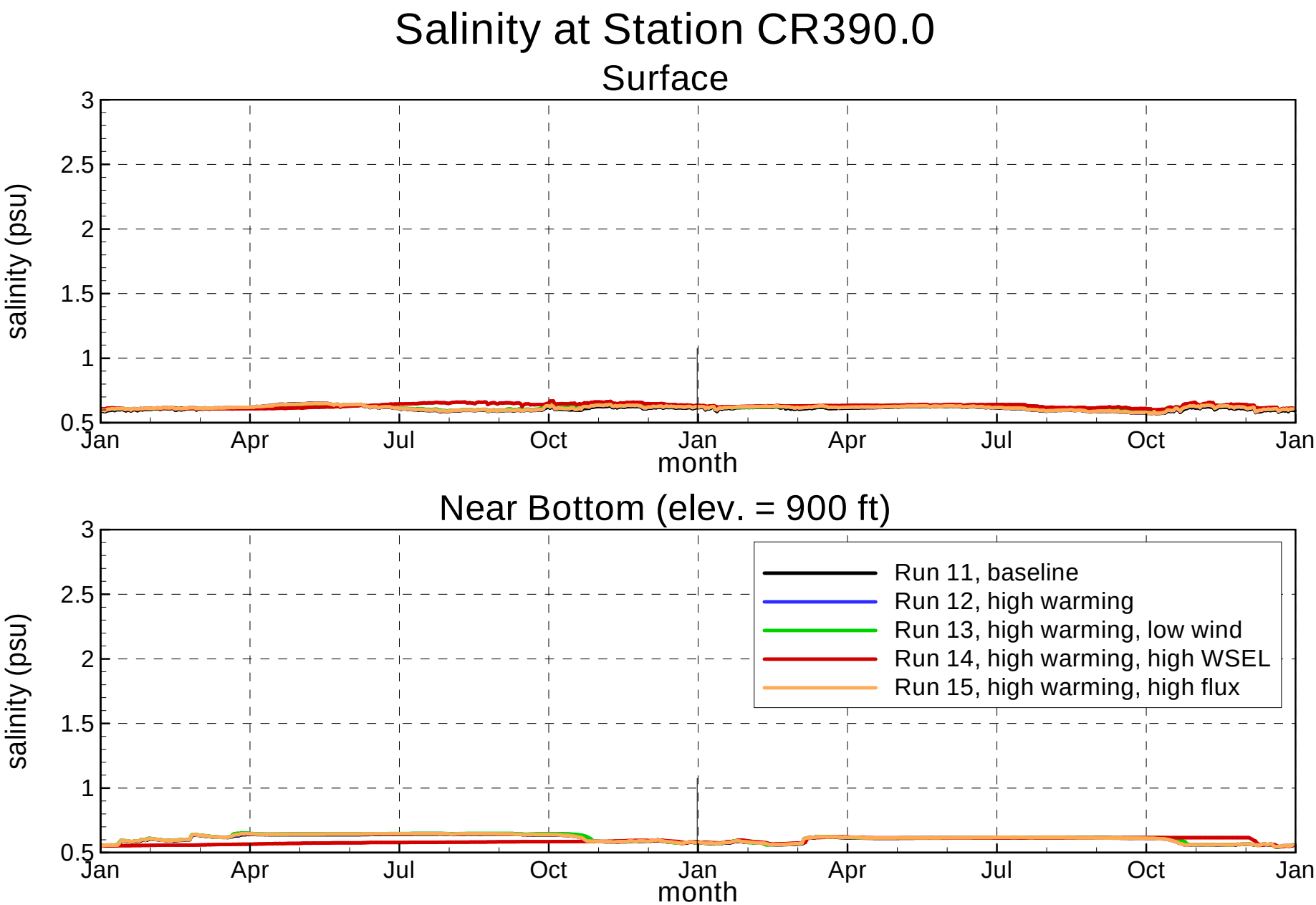
Salinity at Station CR390.0
Surface
salinity (psu)
3
2.5
2
1.5
1
0.5
Jan
Apr
Jul
Oct
Jan
Apr
Jul
Oct
Jan
month
Near Bottom (elev. = 900 ft)
salinity (psu)
3
2.5
2
1.5
1
0.5
Jan
Apr
Jul
Oct
Jan
Apr
Jul
Oct
Jan
month
Run 11, baseline
Run 12, high warming
Run 13, high warming, low wind
Run 14, high warming, high WSEL
Run 15, high warming, high flux

Figure A.262

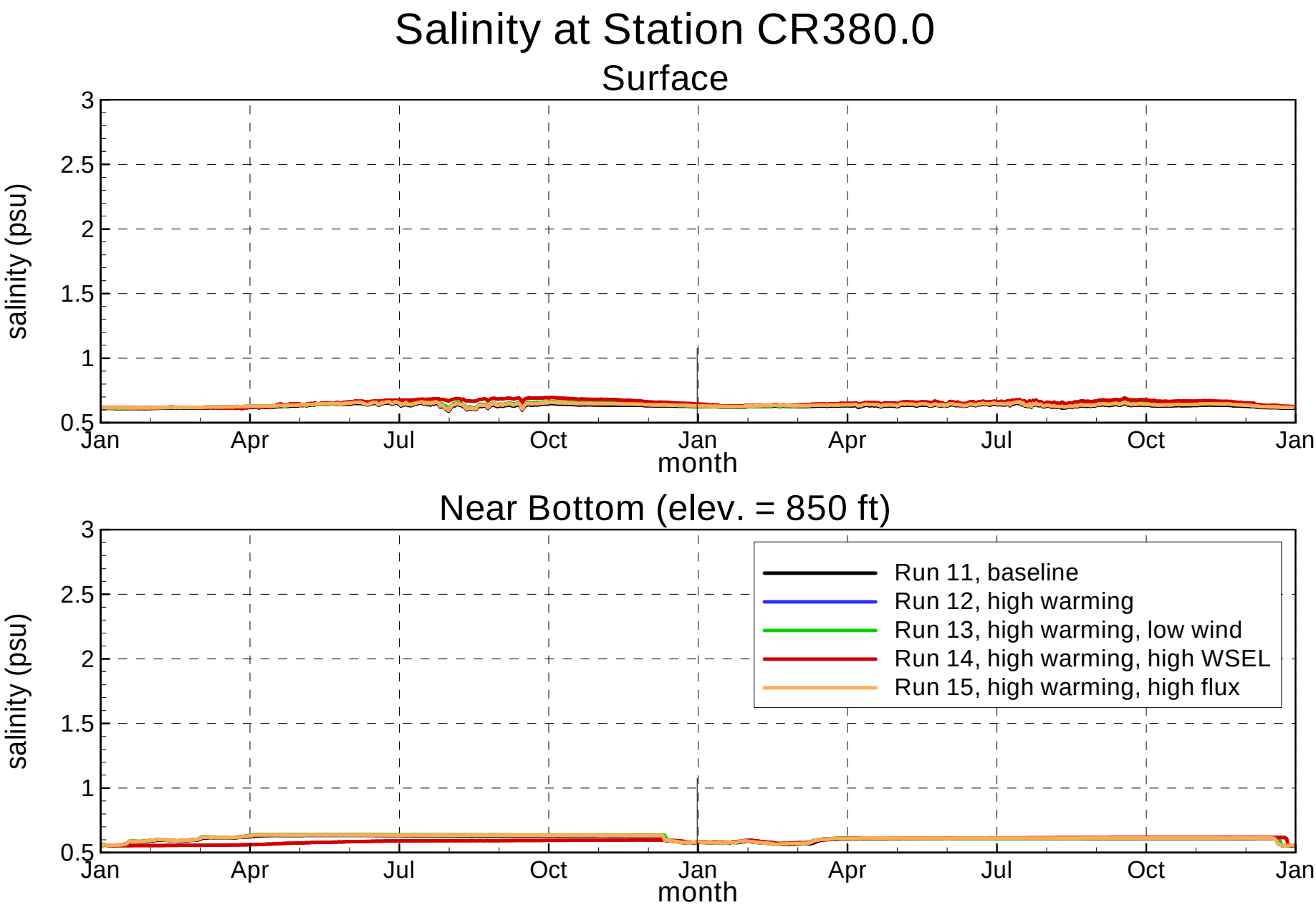
Salinity at Station CR380.0
Surface
salinity (psu)
3
2.5
2
1.5
1
0.5
Jan
Apr
Jul
Oct
Jan
Apr
Jul
Oct
Jan
month
Near Bottom (elev. = 850 ft)
salinity (psu)
3
2.5
2
1.5
1
0.5
Jan
Apr
Jul
Oct
Jan
Apr
Jul
Oct
Jan
month
Run 11, baseline
Run 12, high warming
Run 13, high warming, low wind
Run 14, high warming, high WSEL
Run 15, high warming, high flux

Figure A.263

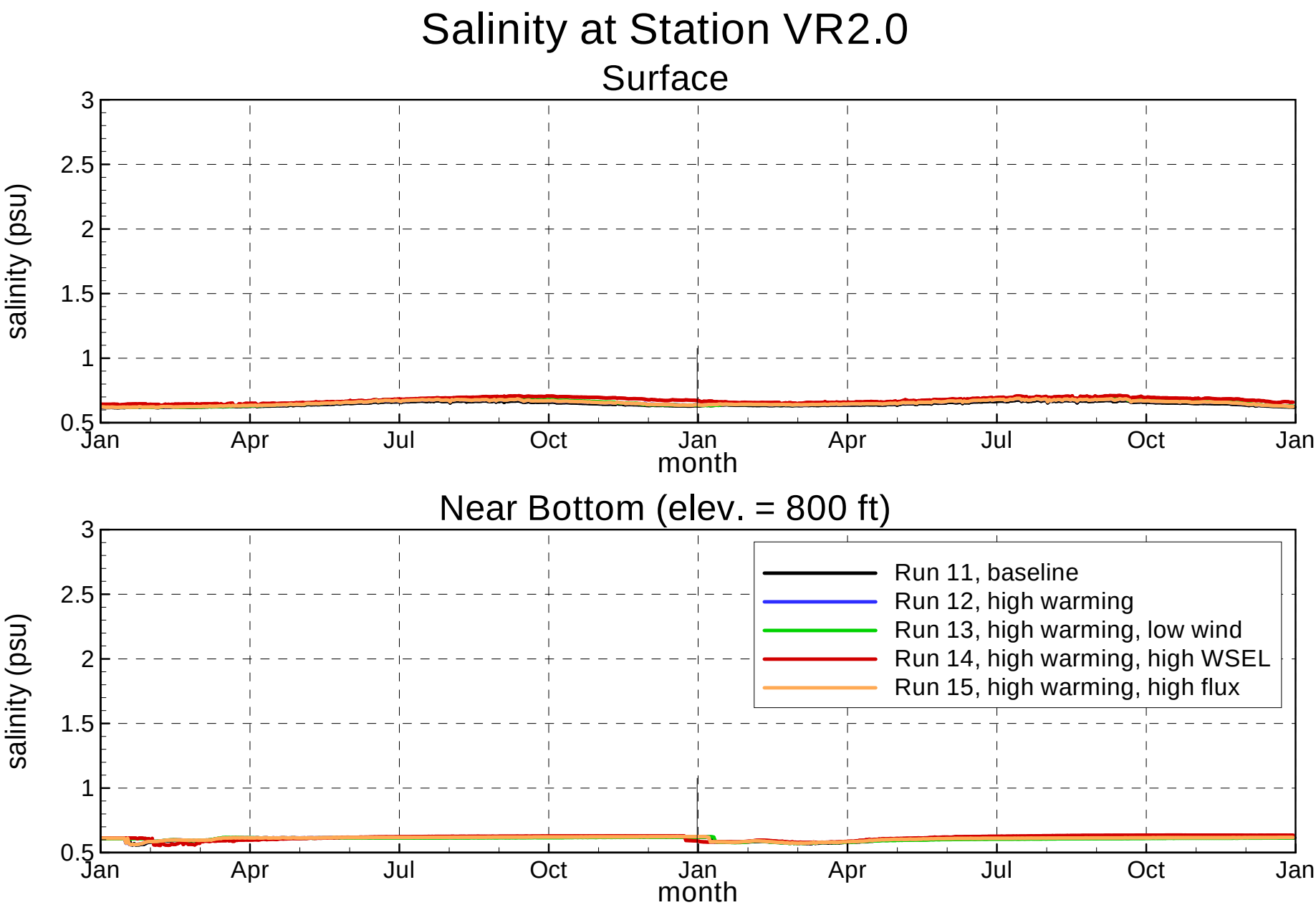
Salinity at Station VR2.0
Surface
salinity (psu)
3
2.5
2
1.5
1
0.5
Jan
Apr
Jul
Oct
Jan
Apr
Jul
Oct
Jan
month
Near Bottom (elev. = 800 ft)
salinity (psu)
3
2.5
2
1.5
1
0.5
Jan
Apr
Jul
Oct
Jan
Apr
Jul
Oct
Jan
month
Run 11, baseline
Run 12, high warming
Run 13, high warming, low wind
Run 14, high warming, high WSEL
Run 15, high warming, high flux

Figure A.264

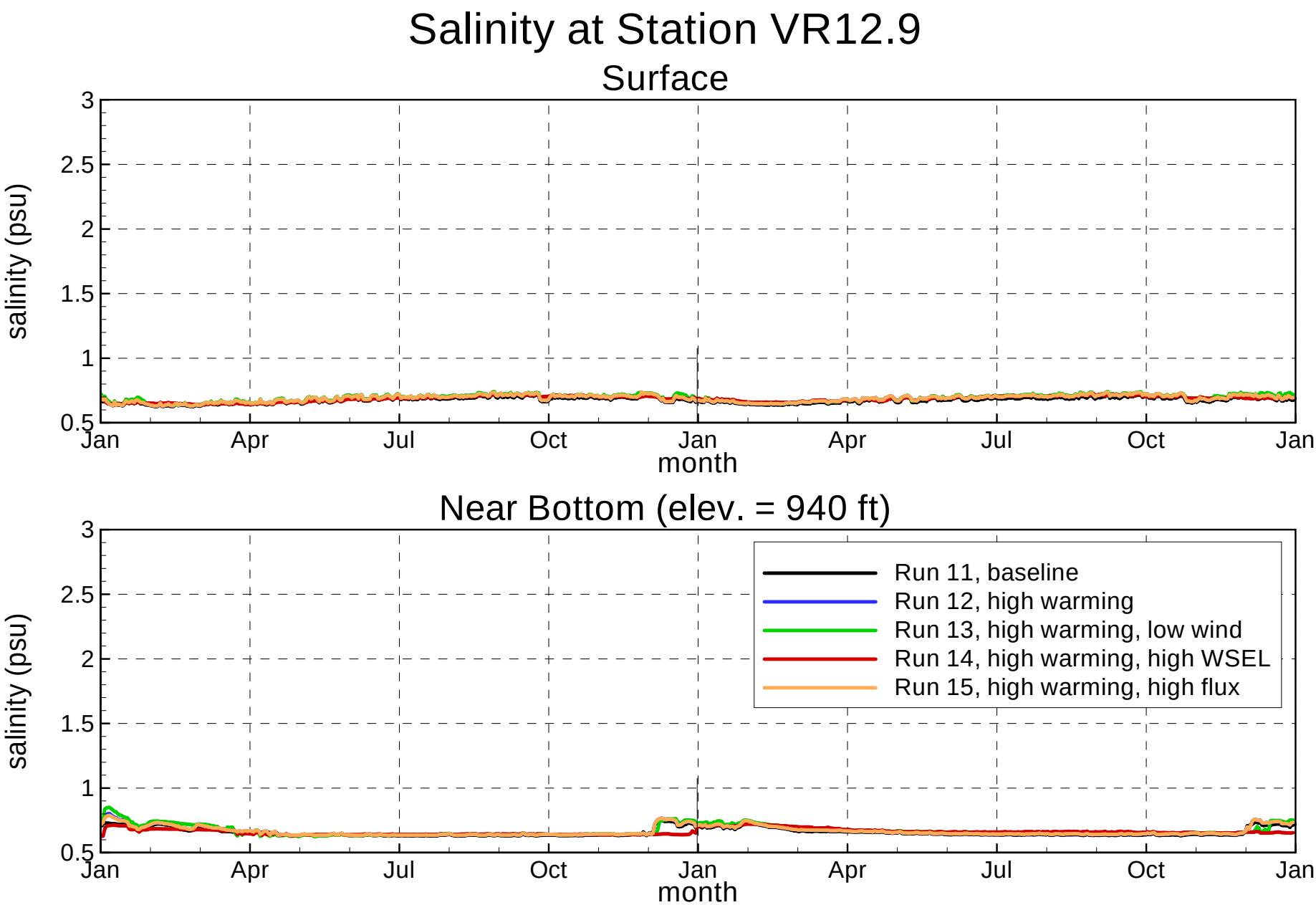
Salinity at Station VR12.9
Surface
salinity (psu)
3
2.5
2
1.5
1
0.5
Jan
Apr
Jul
Oct
Jan
Apr
Jul
Oct
Jan
month
Near Bottom (elev. = 940 ft)
salinity (psu)
Run 11, baseline
Run 12, high warming
Run 13, high warming, low wind
Run 14, high warming, high WSEL
Run 15, high warming, high flux
month

Figure A.265

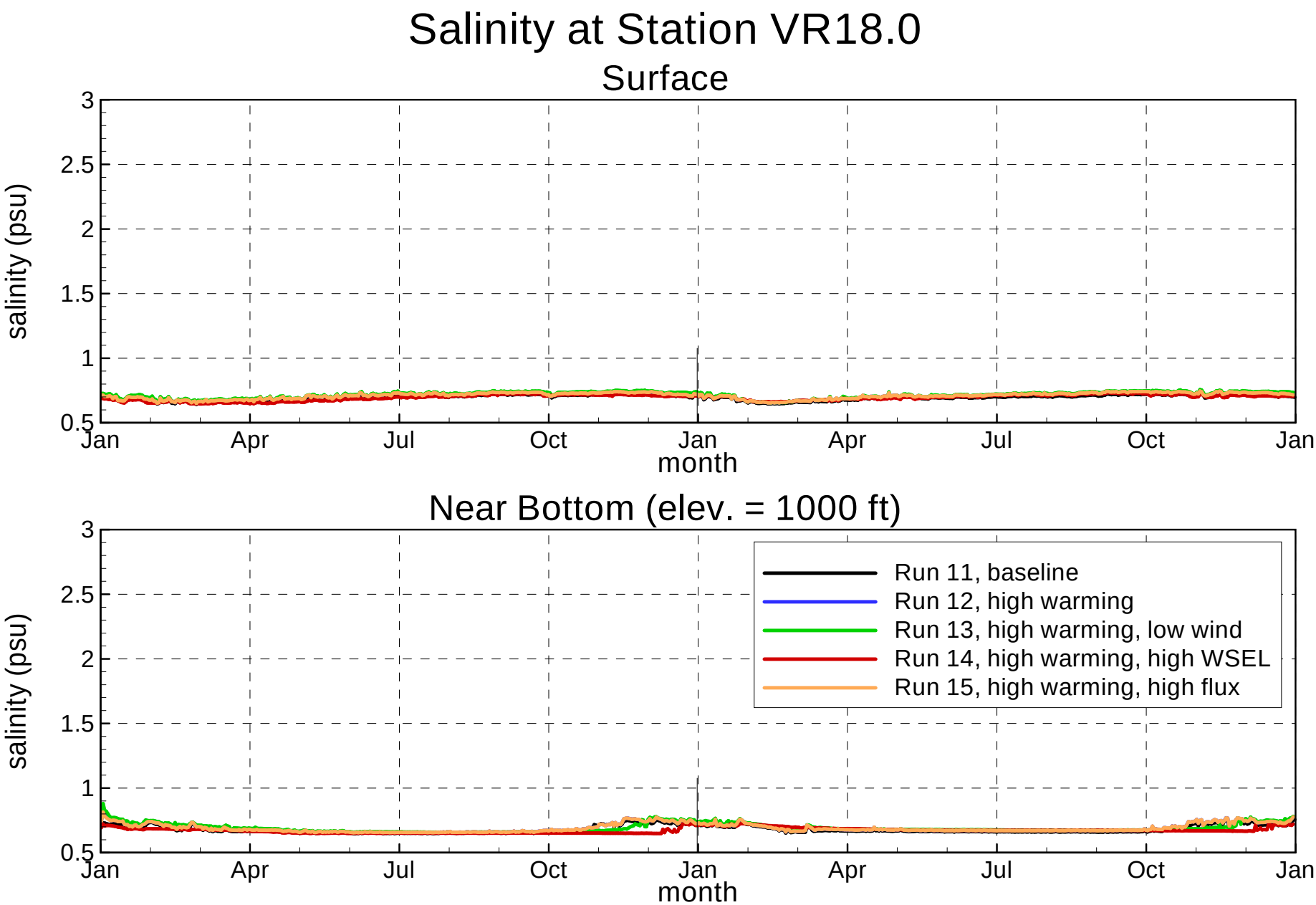
Salinity at Station VR18.0
Surface
salinity (psu)
3
2.5
2
1.5
1
0.5
Jan
Apr
Jul
Oct
Jan
Apr
Jul
Oct
Jan
month
Near Bottom (elev. = 1000 ft)
salinity (psu)
Run 11, baseline
Run 12, high warming
Run 13, high warming, low wind
Run 14, high warming, high WSEL
Run 15, high warming, high flux
month

Figure A.266

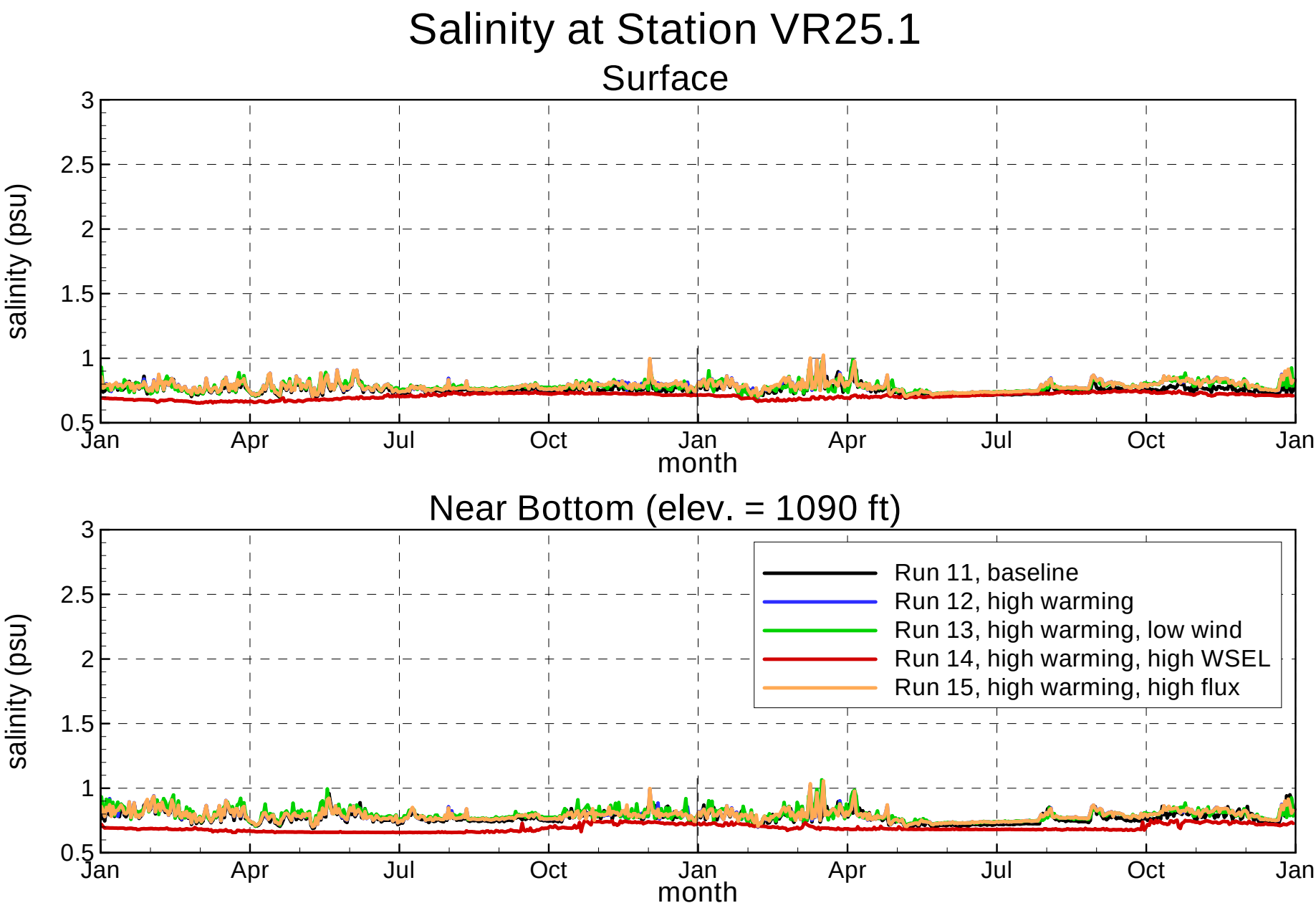
Salinity at Station VR25.1
Surface
salinity (psu)
3
2.5
2
1.5
1
0.5
Jan
Apr
Jul
Oct
Jan
Apr
Jul
Oct
Jan
month
Near Bottom (elev. = 1090 ft)
salinity (psu)
Run 11, baseline
Run 12, high warming
Run 13, high warming, low wind
Run 14, high warming, high WSEL
Run 15, high warming, high flux
month

Figure A.267

Salinity at Station CR360.7

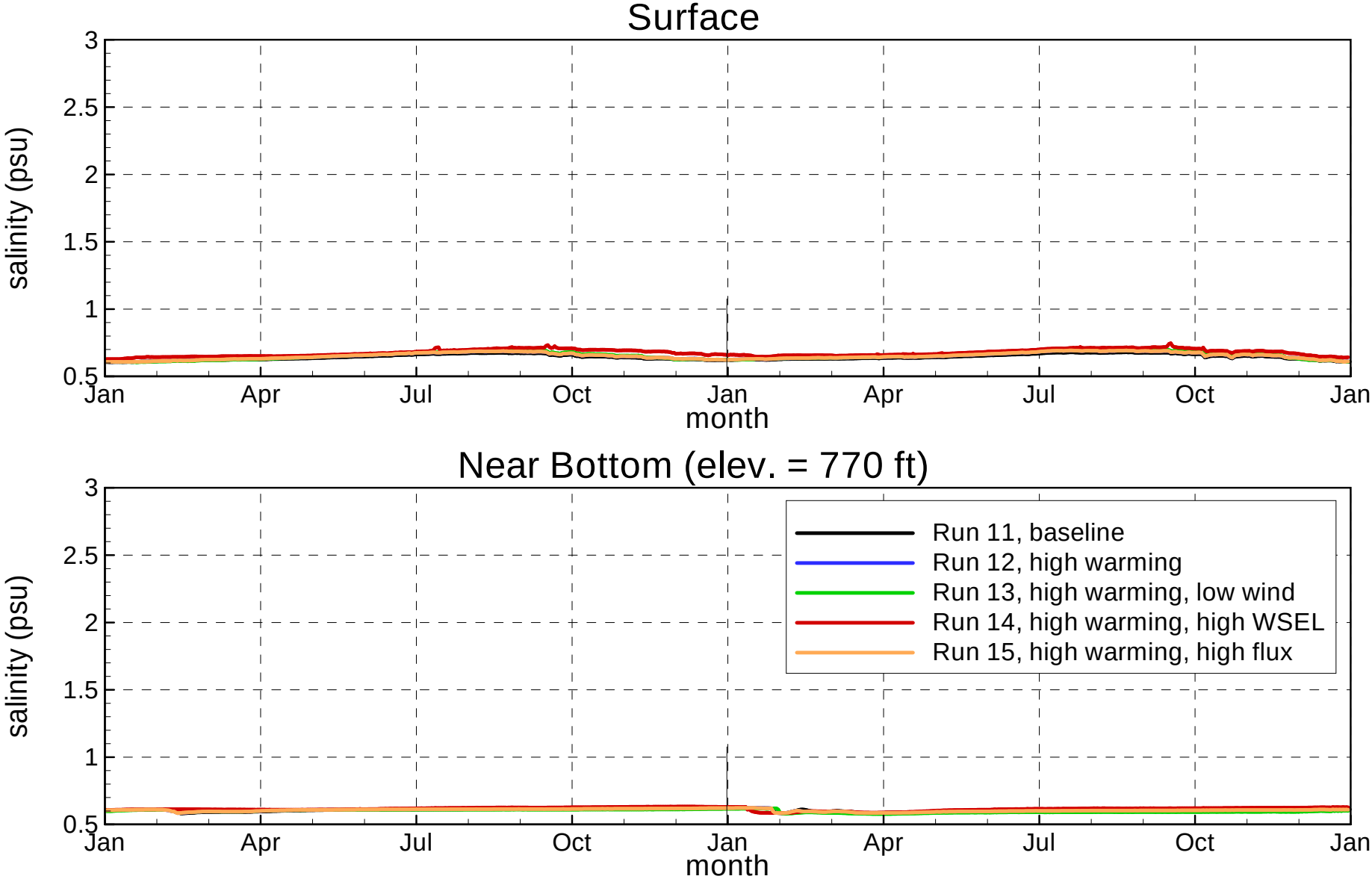

Figure A.268

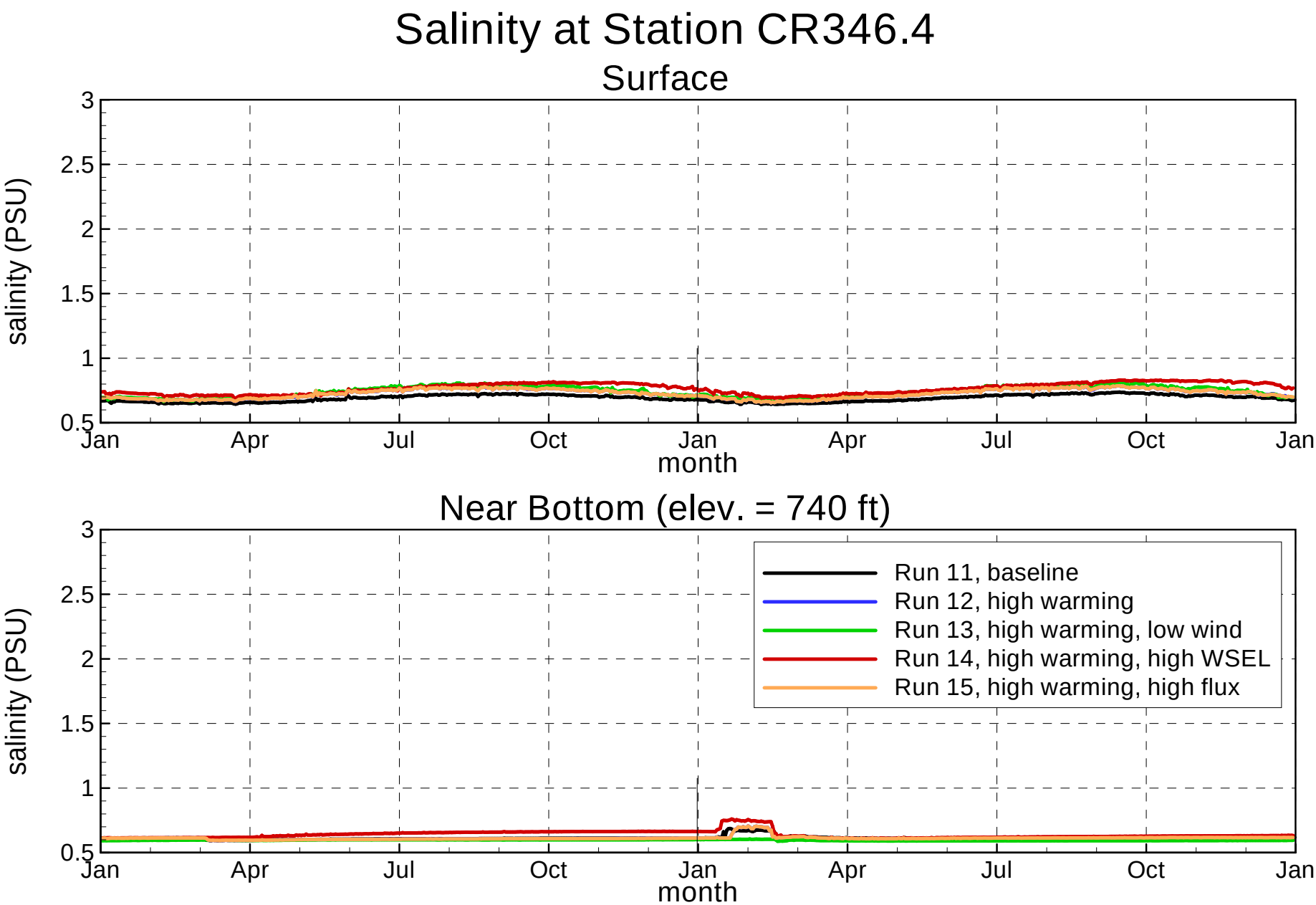
Salinity at Station CR346.4
Surface
salinity (PSU)
3
2.5
2
1.5
1
0.5
Jan
Apr
Jul
Oct
Jan
Apr
Jul
Oct
Jan
month
Near Bottom (elev. = 740 ft)
salinity (PSU)
3
2.5
2
1.5
1
0.5
Jan
Apr
Jul
Oct
Jan
Apr
Jul
Oct
Jan
month
Run 11, baseline
Run 12, high warming
Run 13, high warming, low wind
Run 14, high warming, high WSEL
Run 15, high warming, high flux

Figure A.269

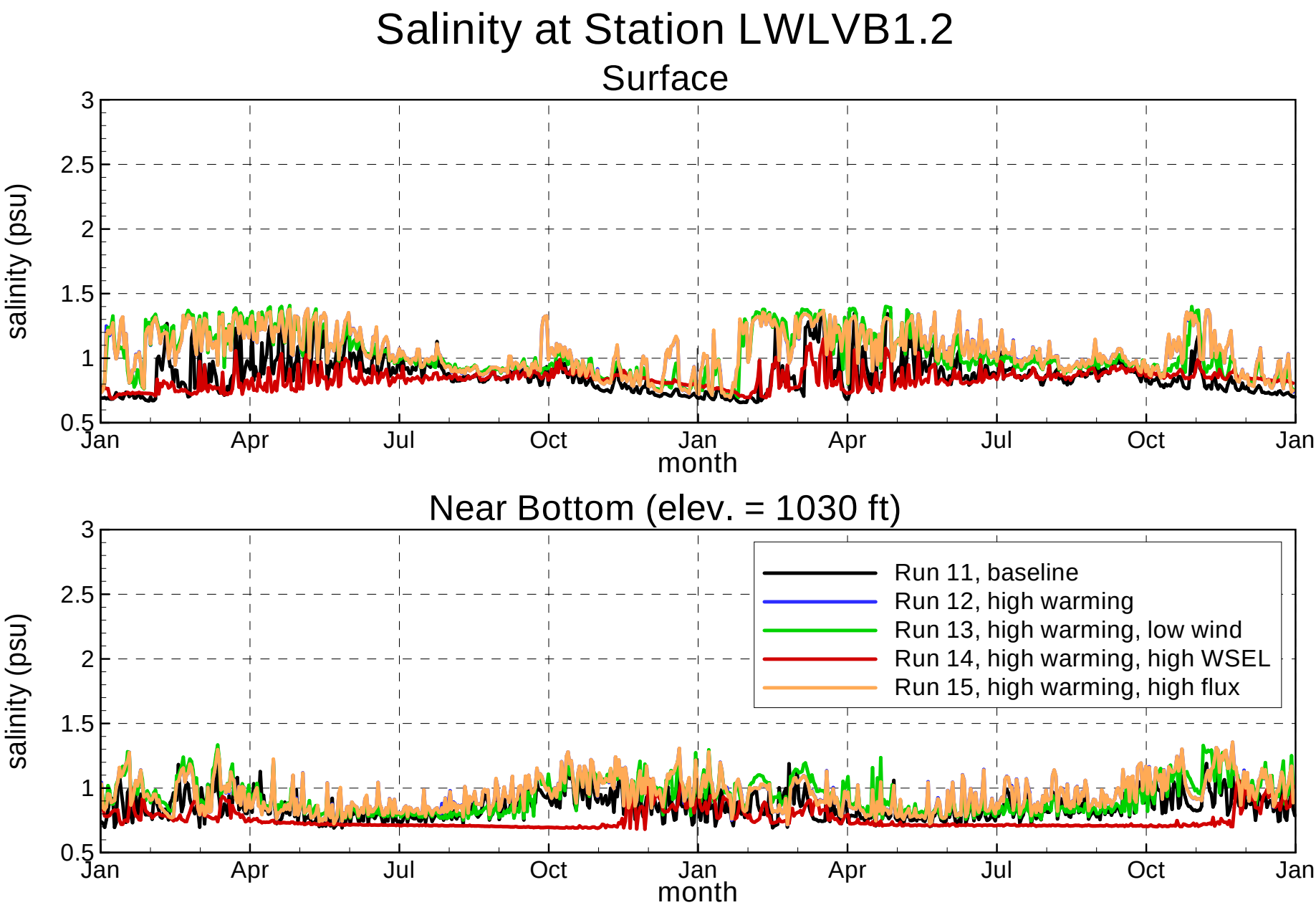
Salinity at Station LWLVB1.2
Surface
salinity (psu)
3
2.5
2
1.5
1
0.5
Jan
Apr
Jul
Oct
Jan
Apr
Jul
Oct
Jan
month
Near Bottom (elev. = 1030 ft)
salinity (psu)
Run 11, baseline
Run 12, high warming
Run 13, high warming, low wind
Run 14, high warming, high WSEL
Run 15, high warming, high flux
month

Figure A.270

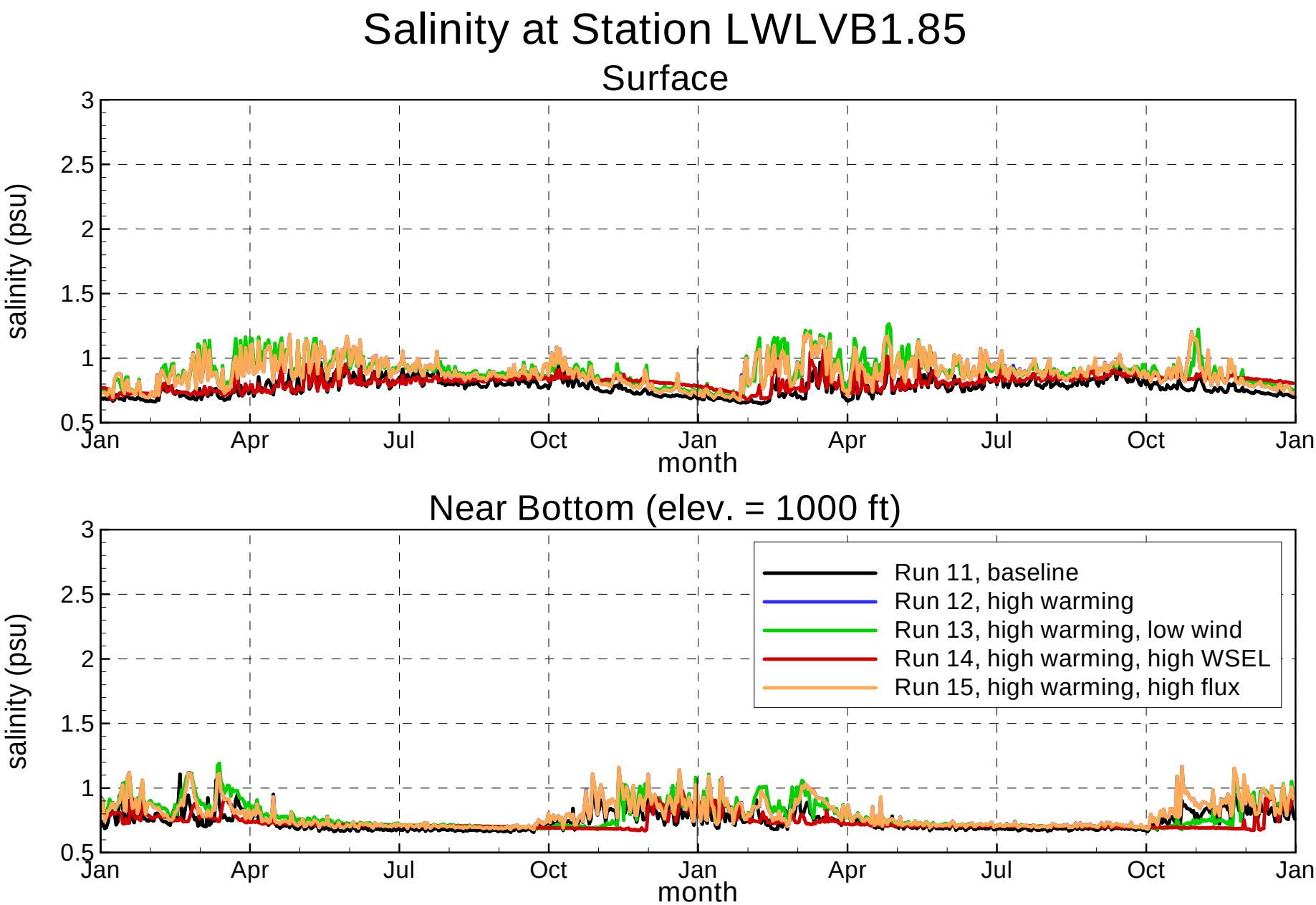
Salinity at Station LWLVB1.85
Surface
salinity (psu)
3
2.5
2
1.5
1
0.5
Jan
Apr
Jul
Oct
Jan
Apr
Jul
Oct
Jan
month
Near Bottom (elev. = 1000 ft)
salinity (psu)
Run 11, baseline
Run 12, high warming
Run 13, high warming, low wind
Run 14, high warming, high WSEL
Run 15, high warming, high flux
month

Figure A.271

Salinity at Station LWLVB2.7

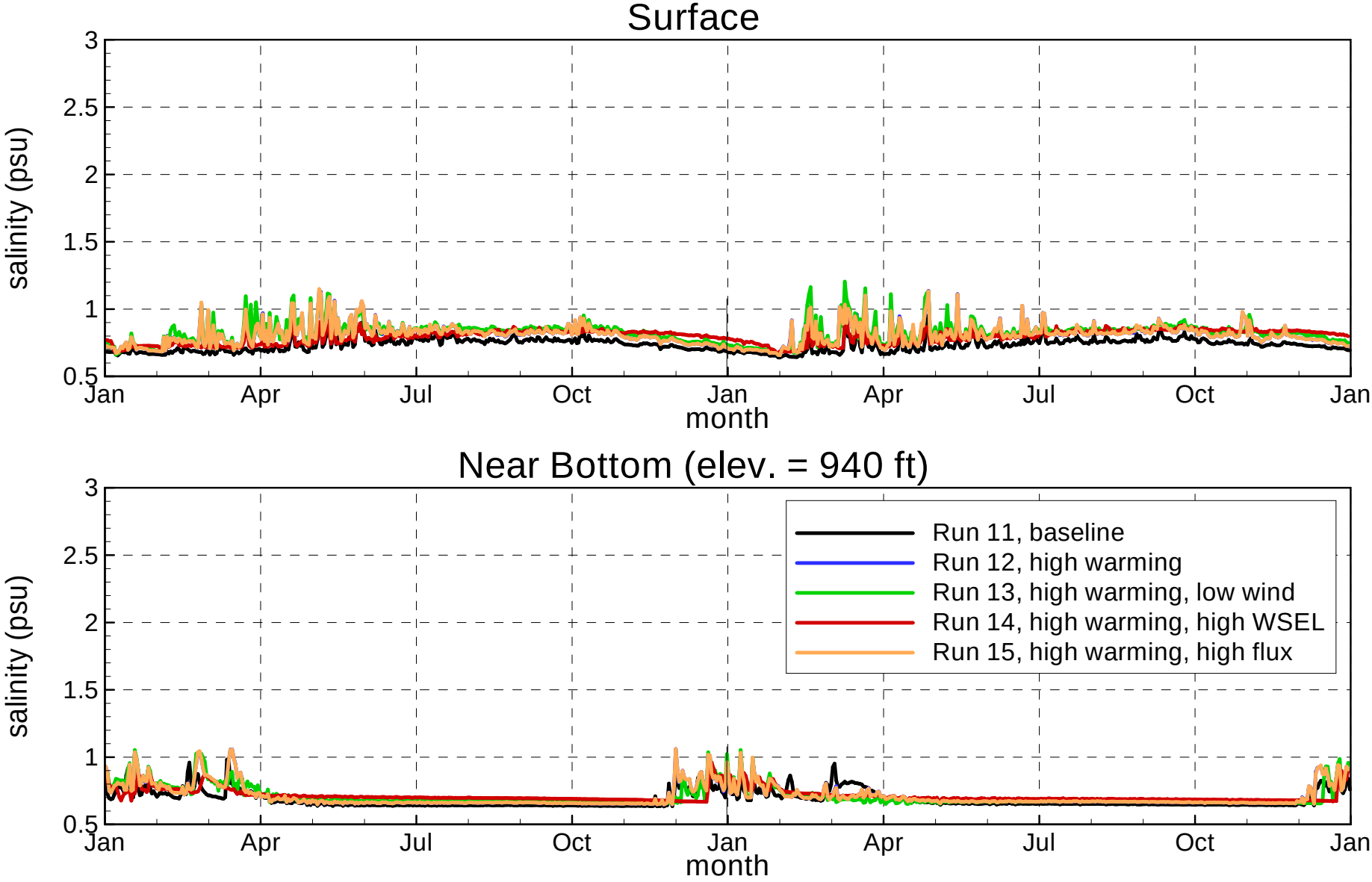

Figure A.272

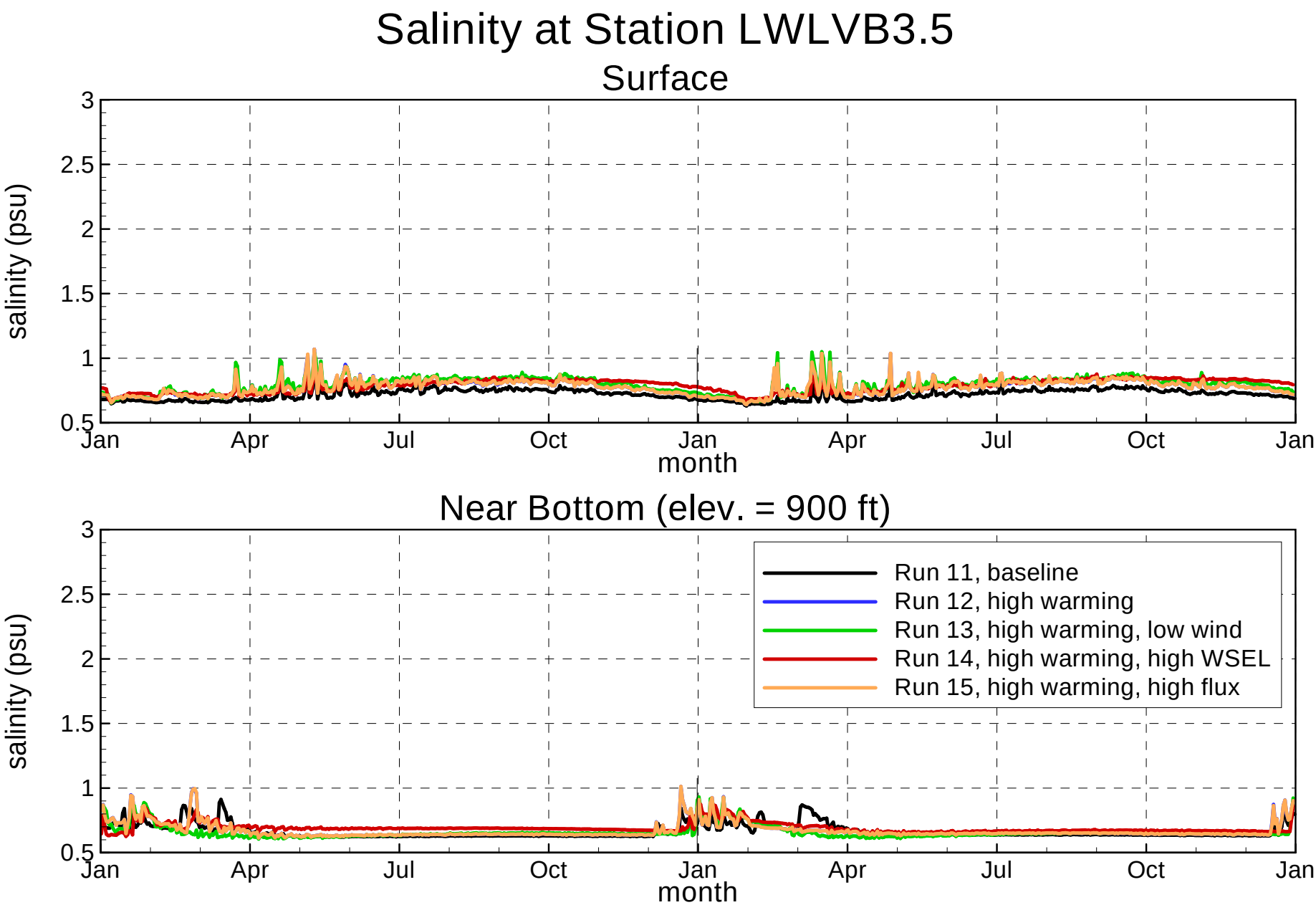
Salinity at Station LWLVB3.5
Surface
salinity (psu)
3
2.5
2
1.5
1
0.5
Jan
Apr
Jul
Oct
Jan
Apr
Jul
Oct
Jan
month
Near Bottom (elev. = 900 ft)
salinity (psu)
Run 11, baseline
Run 12, high warming
Run 13, high warming, low wind
Run 14, high warming, high WSEL
Run 15, high warming, high flux
month

Figure A.273

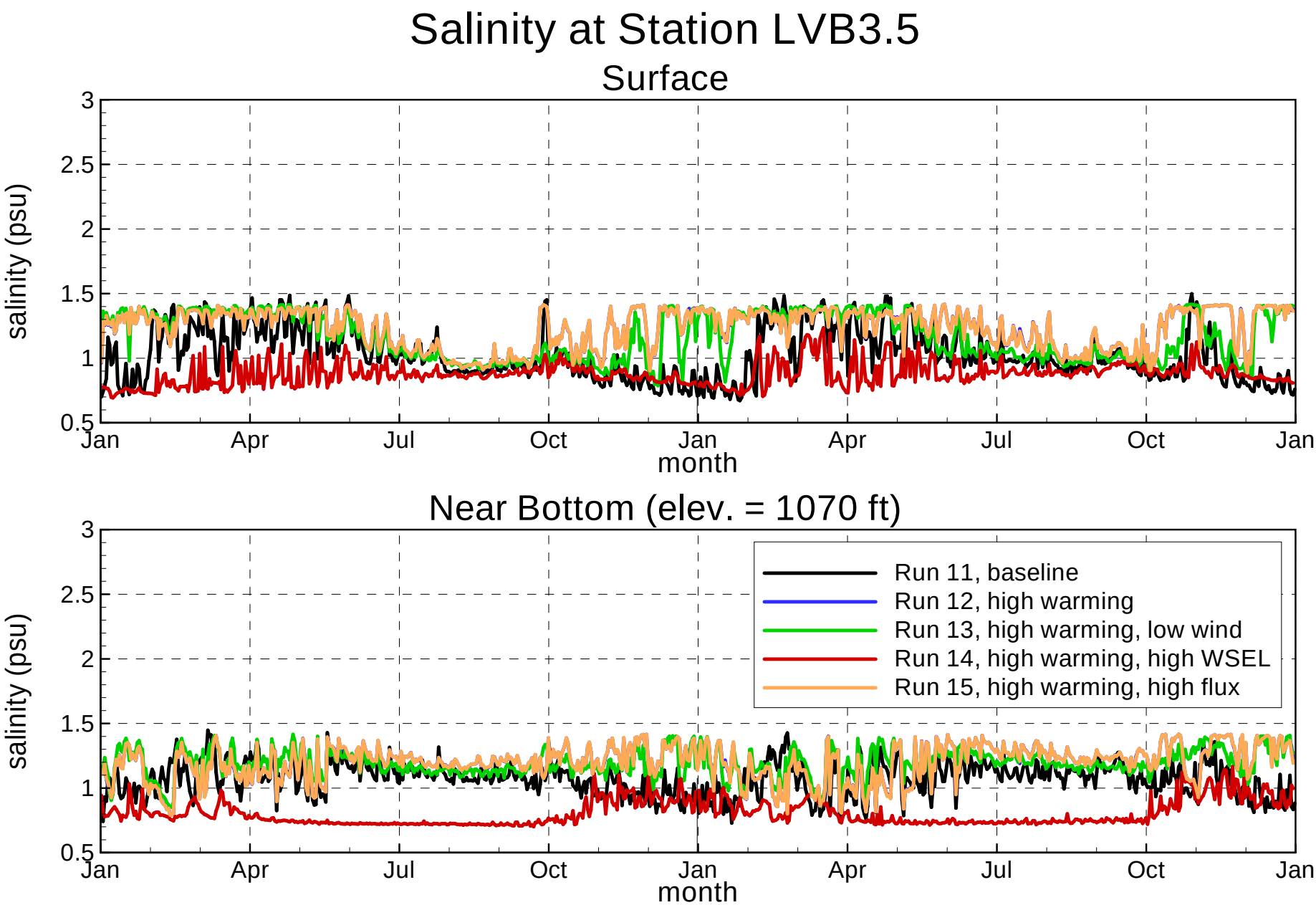
Salinity at Station LVB3.5
Surface
salinity (psu)
3
2.5
2
1.5
1
0.5
Jan
Apr
Jul
Oct
Jan
Apr
Jul
Oct
Jan
month
Near Bottom (elev. = 1070 ft)
salinity (psu)
Run 11, baseline
Run 12, high warming
Run 13, high warming, low wind
Run 14, high warming, high WSEL
Run 15, high warming, high flux
month

Figure A.274

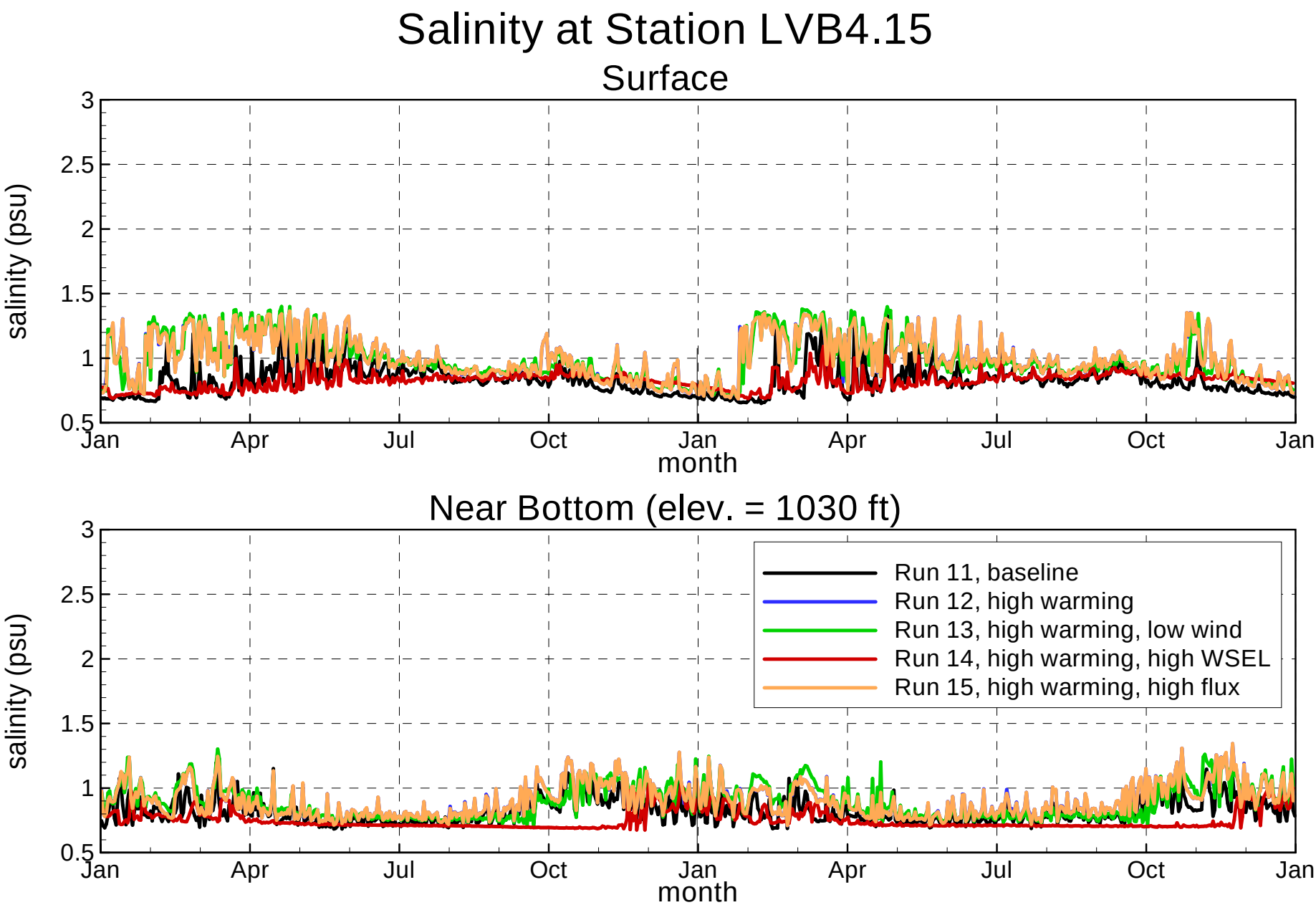
Salinity at Station LVB4.15
Surface
salinity (psu)
3
2.5
2
1.5
1
0.5
Jan
Apr
Jul
Oct
Jan
Apr
Jul
Oct
Jan
month
Near Bottom (elev. = 1030 ft)
salinity (psu)
Run 11, baseline
Run 12, high warming
Run 13, high warming, low wind
Run 14, high warming, high WSEL
Run 15, high warming, high flux
month

Figure A.275

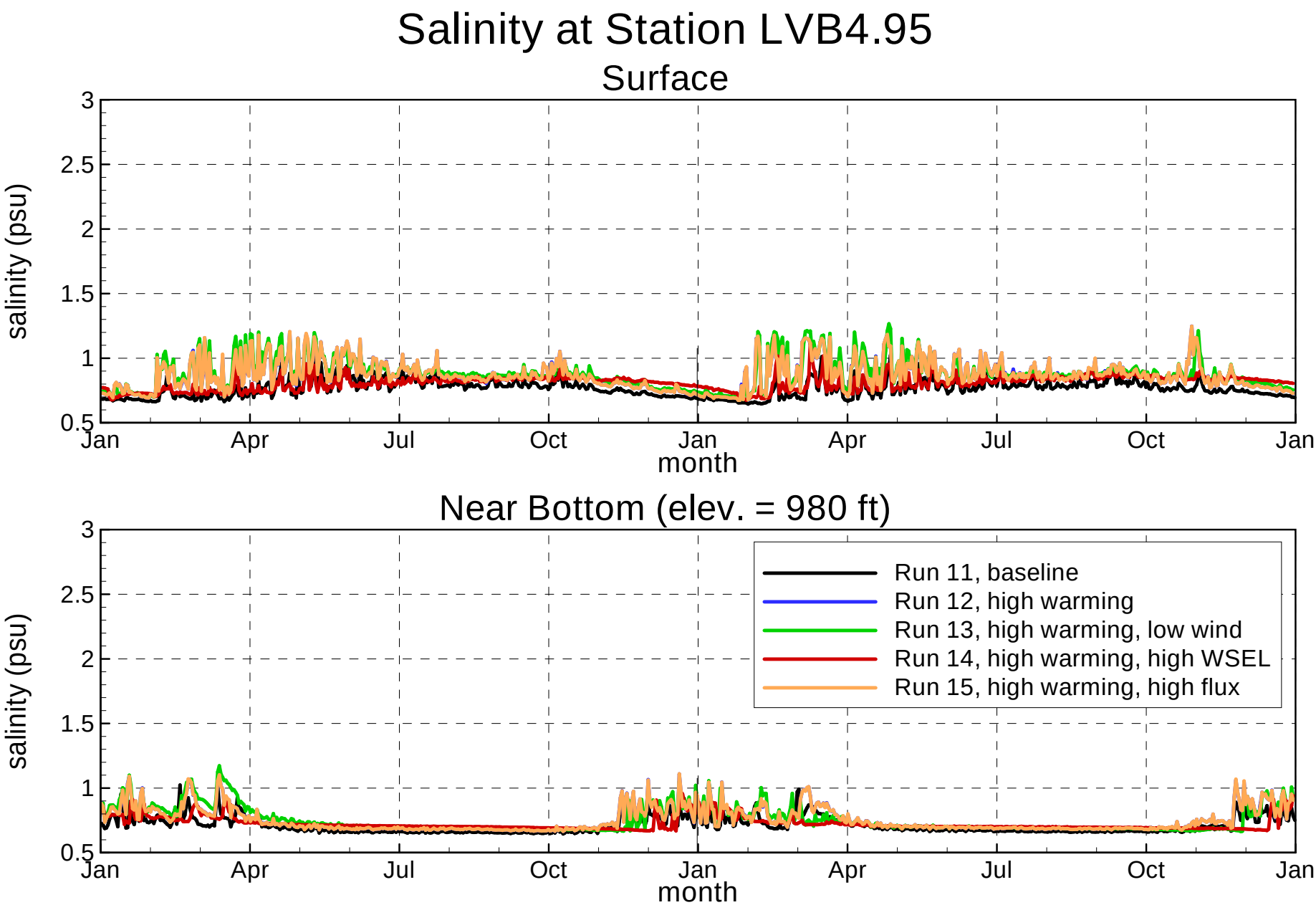
Salinity at Station LVB4.95
Surface
salinity (psu)
3
2.5
2
1.5
1
0.5
Jan
Apr
Jul
Oct
Jan
Apr
Jul
Oct
Jan
month
Near Bottom (elev. = 980 ft)
salinity (psu)
Run 11, baseline
Run 12, high warming
Run 13, high warming, low wind
Run 14, high warming, high WSEL
Run 15, high warming, high flux
month

Figure A.276

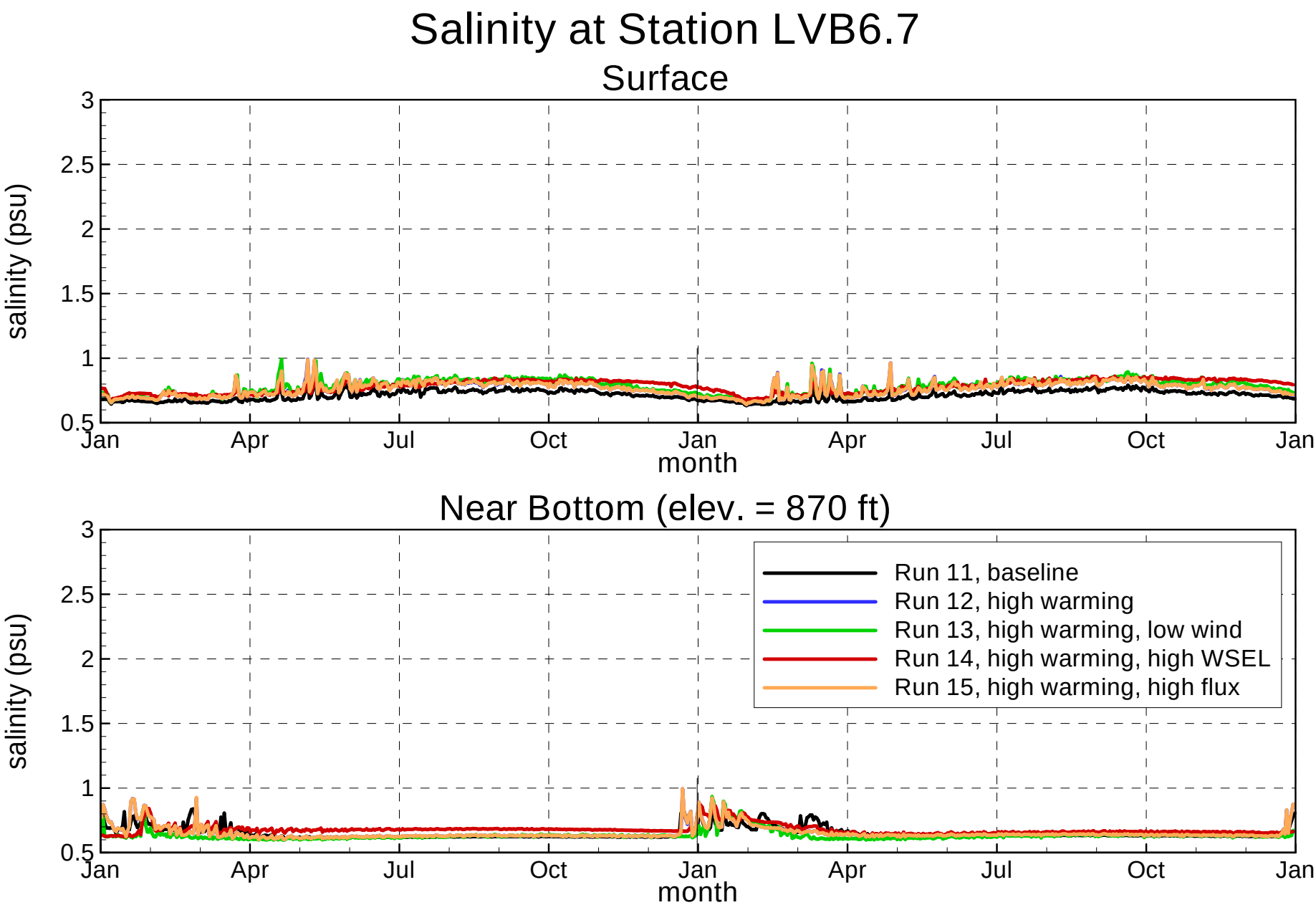
Salinity at Station LVB6.7
Surface
salinity (psu)
3
2.5
2
1.5
1
0.5
Jan
Apr
Jul
Oct
Jan
Apr
Jul
Oct
Jan
month
Near Bottom (elev. = 870 ft)
salinity (psu)
Run 11, baseline
Run 12, high warming
Run 13, high warming, low wind
Run 14, high warming, high WSEL
Run 15, high warming, high flux
month

Figure A.277

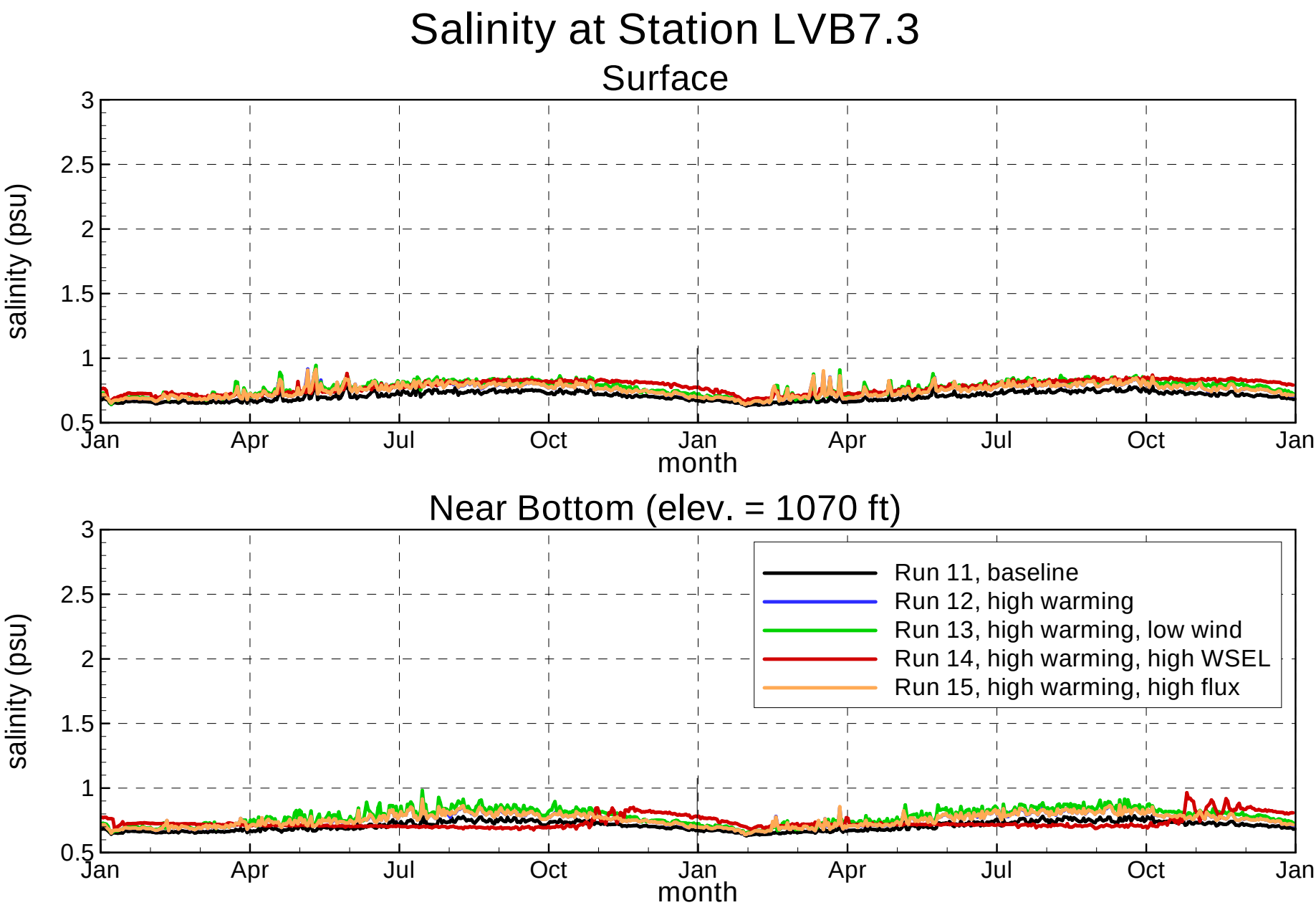
Salinity at Station LVB7.3
Surface
salinity (psu)
3
2.5
2
1.5
1
0.5
Jan
Apr
Jul
Oct
Jan
Apr
Jul
Oct
Jan
month
Near Bottom (elev. = 1070 ft)
salinity (psu)
Run 11, baseline
Run 12, high warming
Run 13, high warming, low wind
Run 14, high warming, high WSEL
Run 15, high warming, high flux
month

Figure A.278

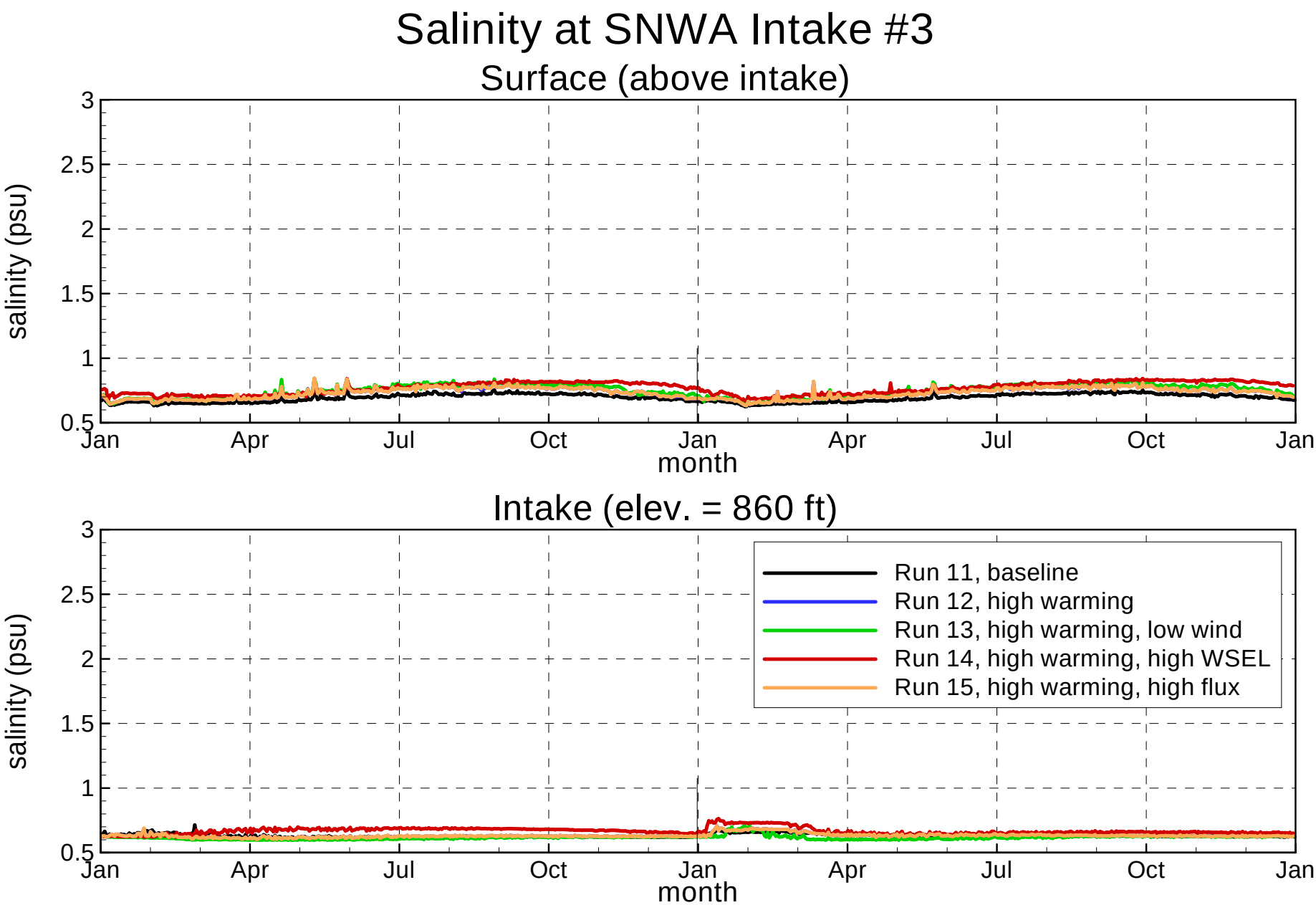
Salinity at SNWA Intake #3
Surface (above intake)
salinity (psu)
3
2.5
2
1.5
1
0.5
Jan
Apr
Jul
Oct
Jan
Apr
Jul
Oct
Jan
month
Intake (elev. = 860 ft)
salinity (psu)
3
2.5
2
1.5
1
0.5
Jan
Apr
Jul
Oct
Jan
Apr
Jul
Oct
Jan
month
Run 11, baseline
Run 12, high warming
Run 13, high warming, low wind
Run 14, high warming, high WSEL
Run 15, high warming, high flux

Figure A.279

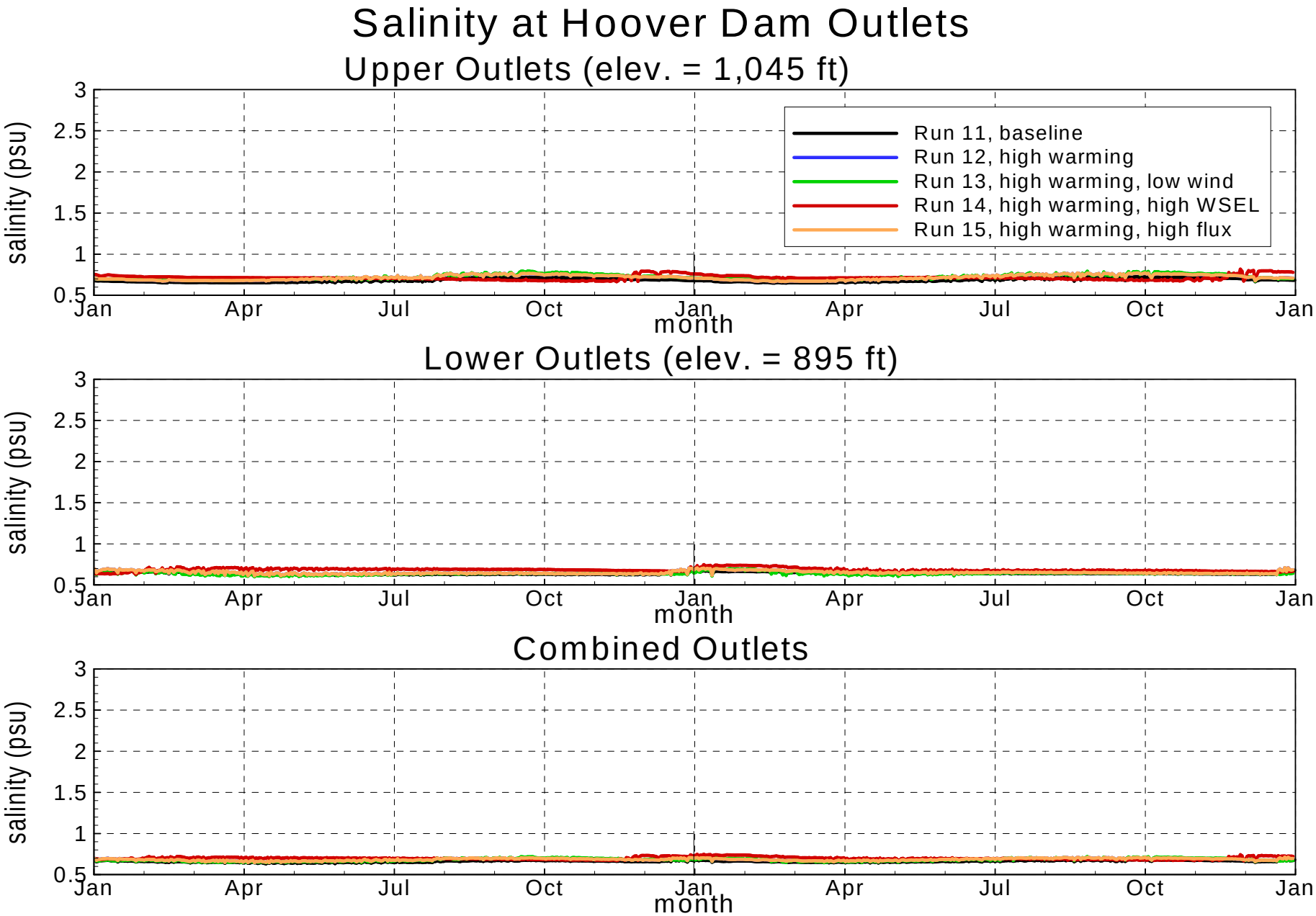
Salinity at Hoover Dam Outlets
Upper Outlets (elev. = 1,045 ft)
Lower Outlets (elev. = 895 ft)
Combined Outlets
salinity (psu)
3
2.5
2
1.5
1
0.5
Jan
Apr
Jul
Oct
Jan
Apr
Jul
Oct
Jan
month
Run 11, baseline
Run 12, high warming
Run 13, high warming, low wind
Run 14, high warming, high WSEL
Run 15, high warming, high flux

Figure A.280

Conductivity at Station CR394.0

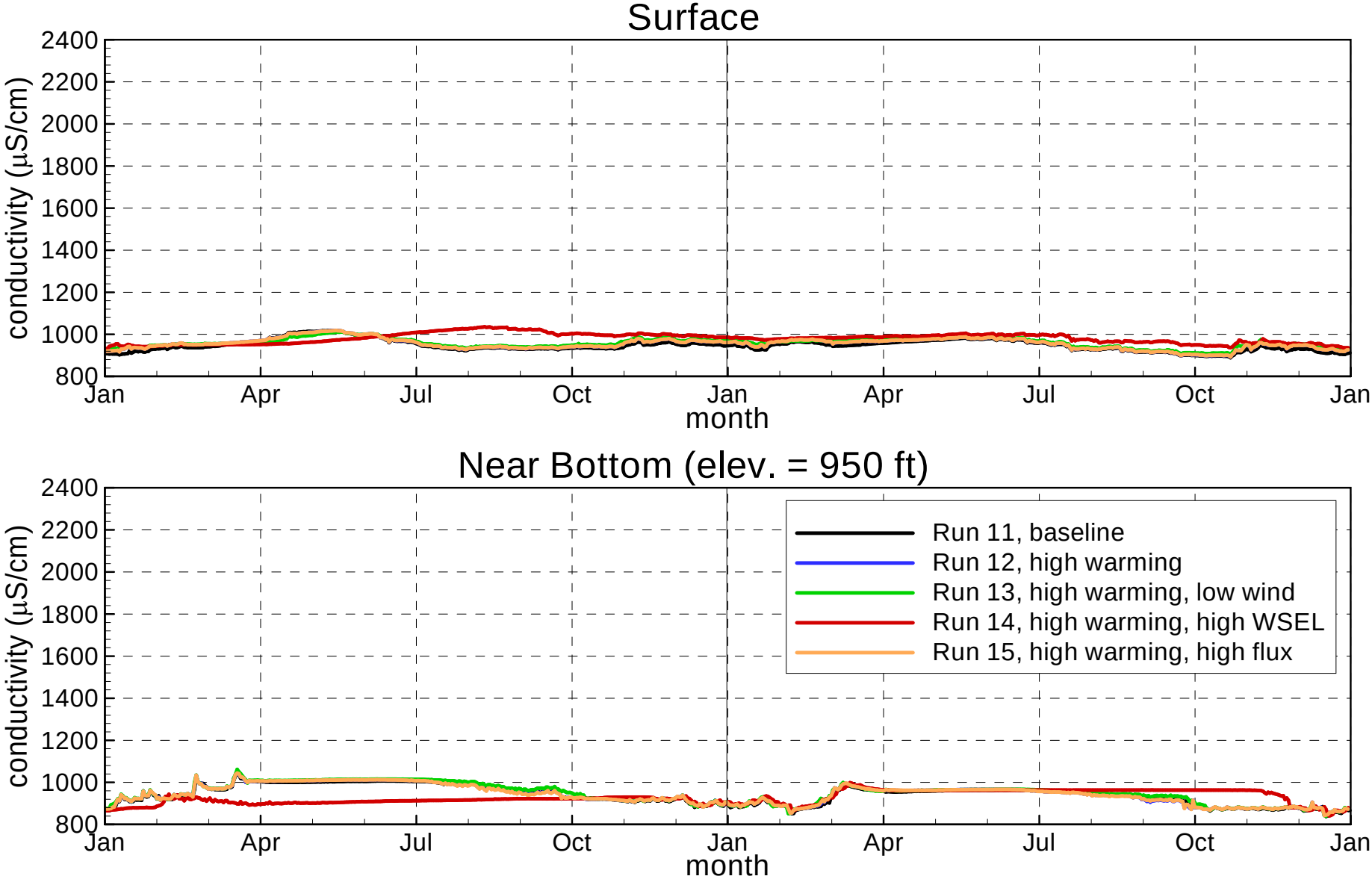

Figure A.281

Conductivity at Station CR390.0

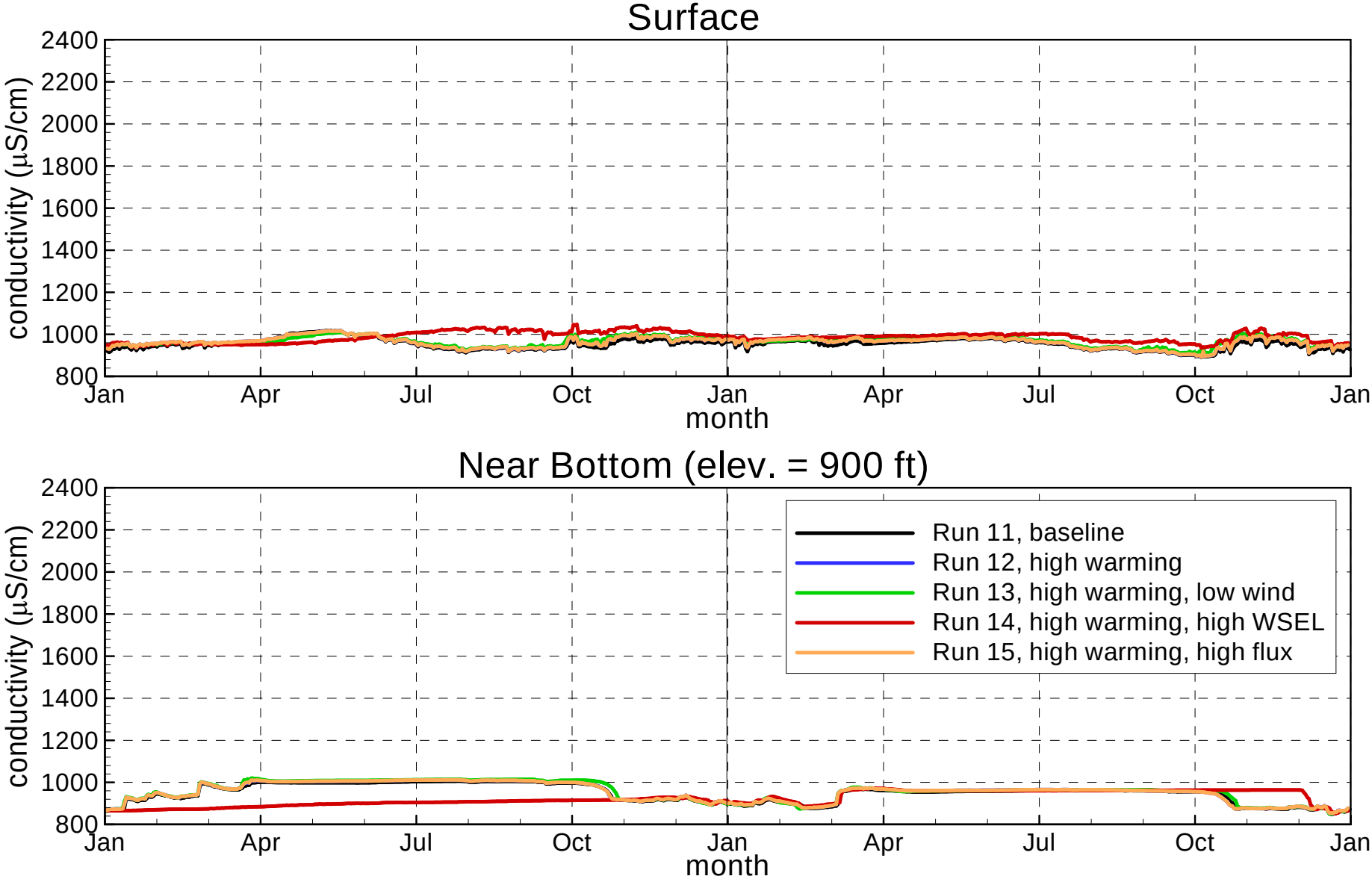

Figure A.282

FLOW SCIENCE

Conductivity at Station CR380.0

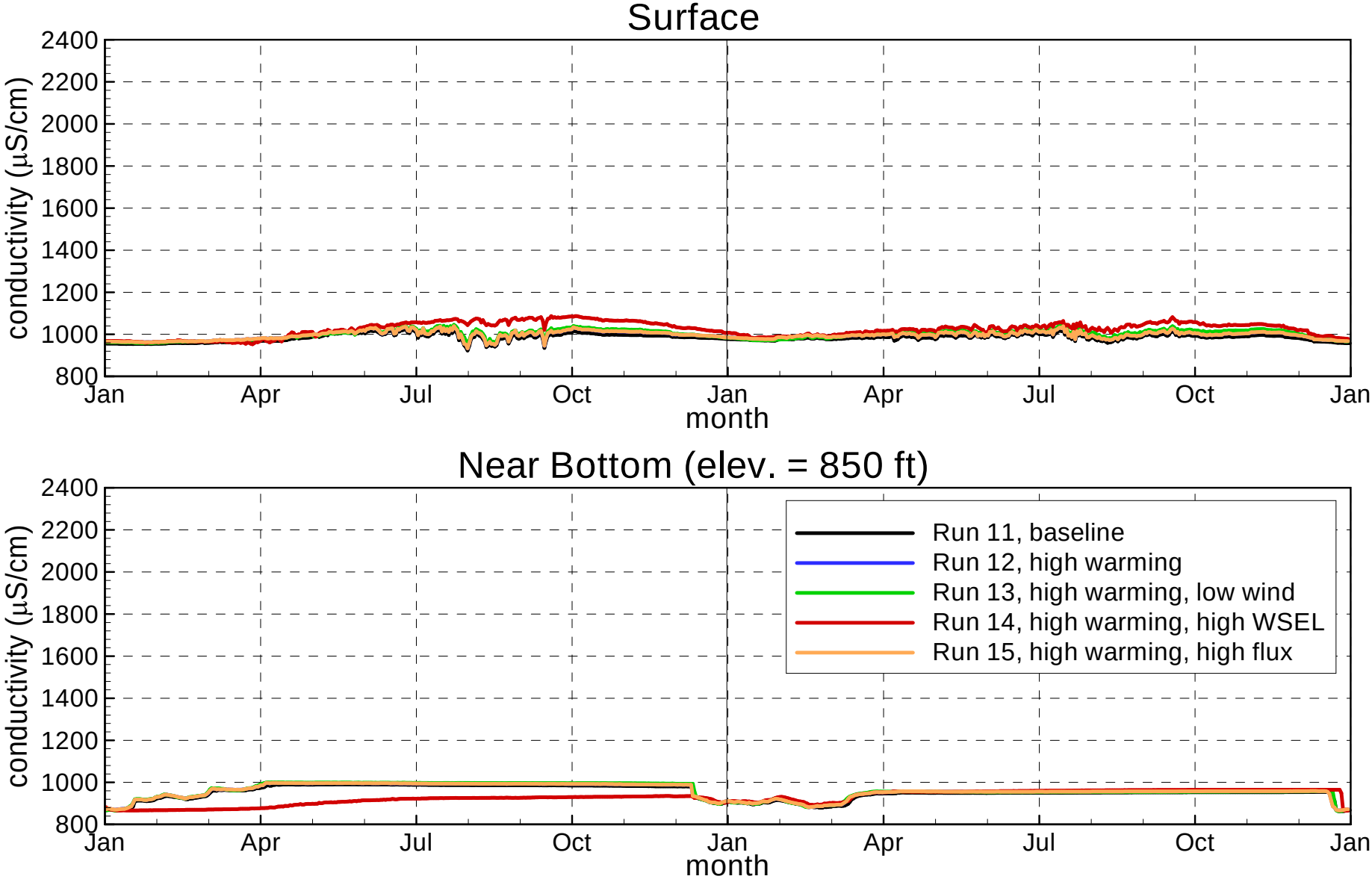

Figure A.283

FLOW SCIENCE

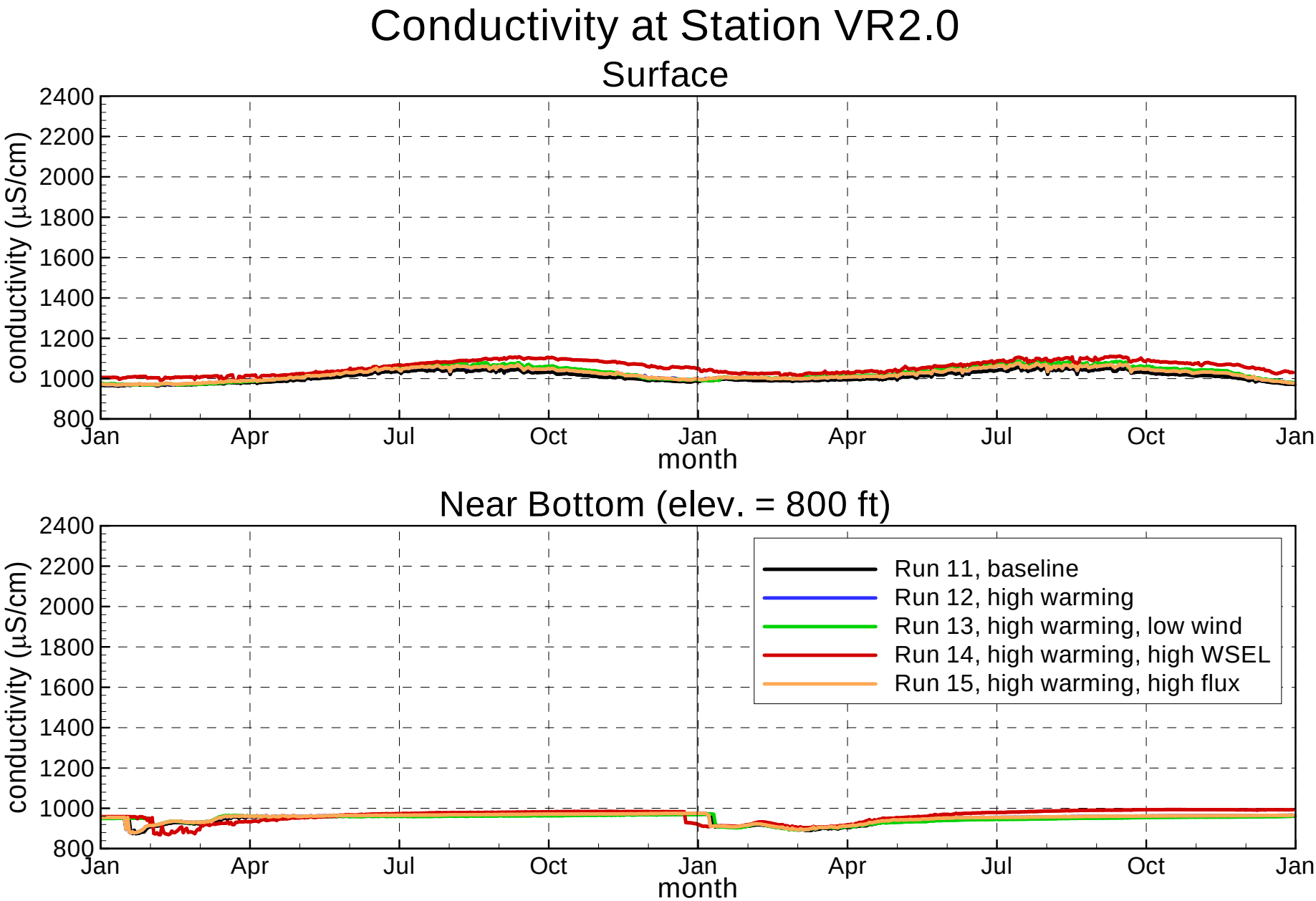
Conductivity at Station VR2.0
Surface
conductivity (µS/cm)
2400
2200
2000
1800
1600
1400
1200
1000
800
Jan
Apr
Jul
Oct
Jan
Apr
Jul
Oct
Jan
month
Near Bottom (elev. = 800 ft)
Run 11, baseline
Run 12, high warming
Run 13, high warming, low wind
Run 14, high warming, high WSEL
Run 15, high warming, high flux

Figure A.284

Conductivity at Station VR12.9

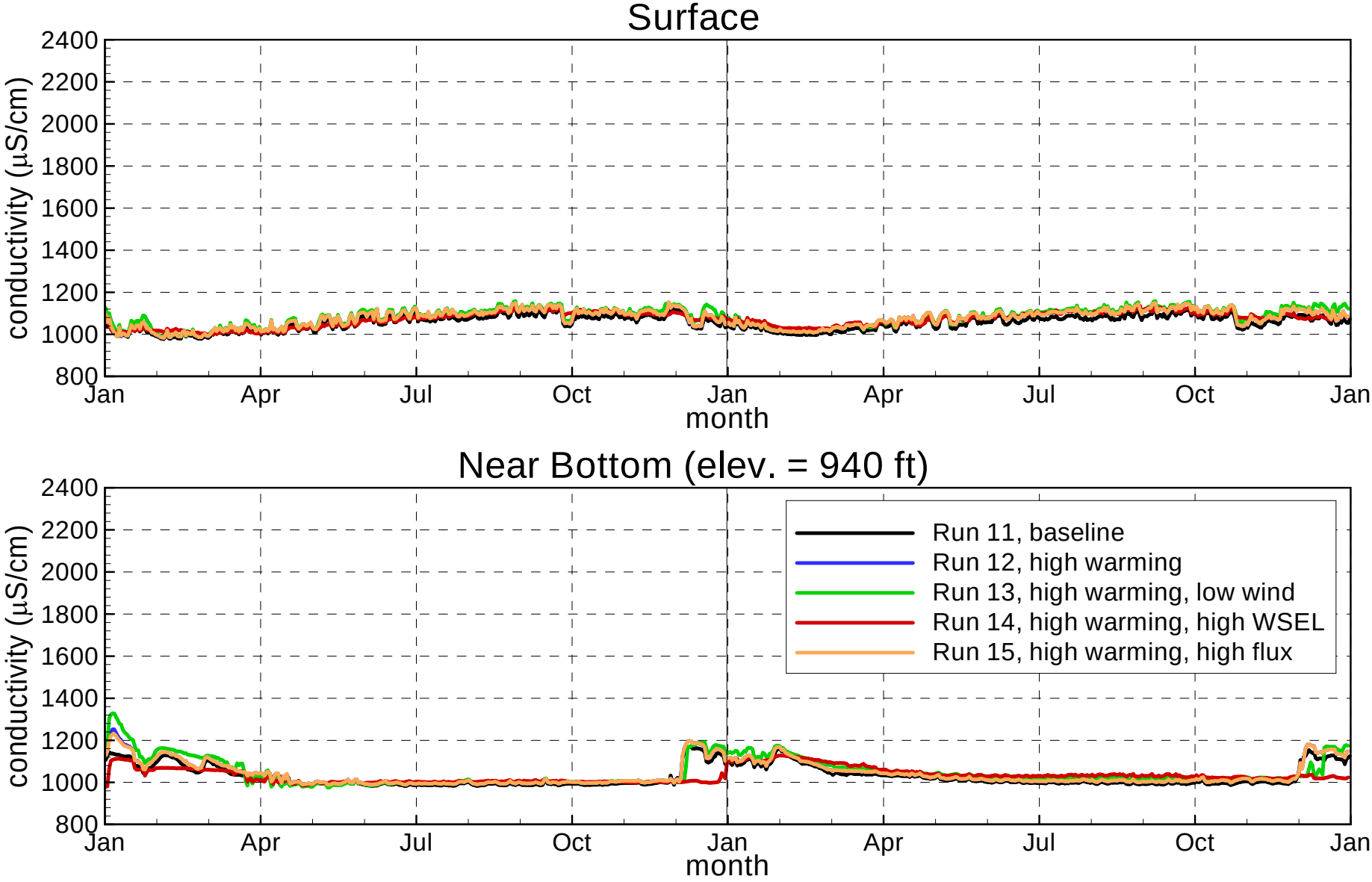

Figure A.285

Conductivity at Station VR18.0

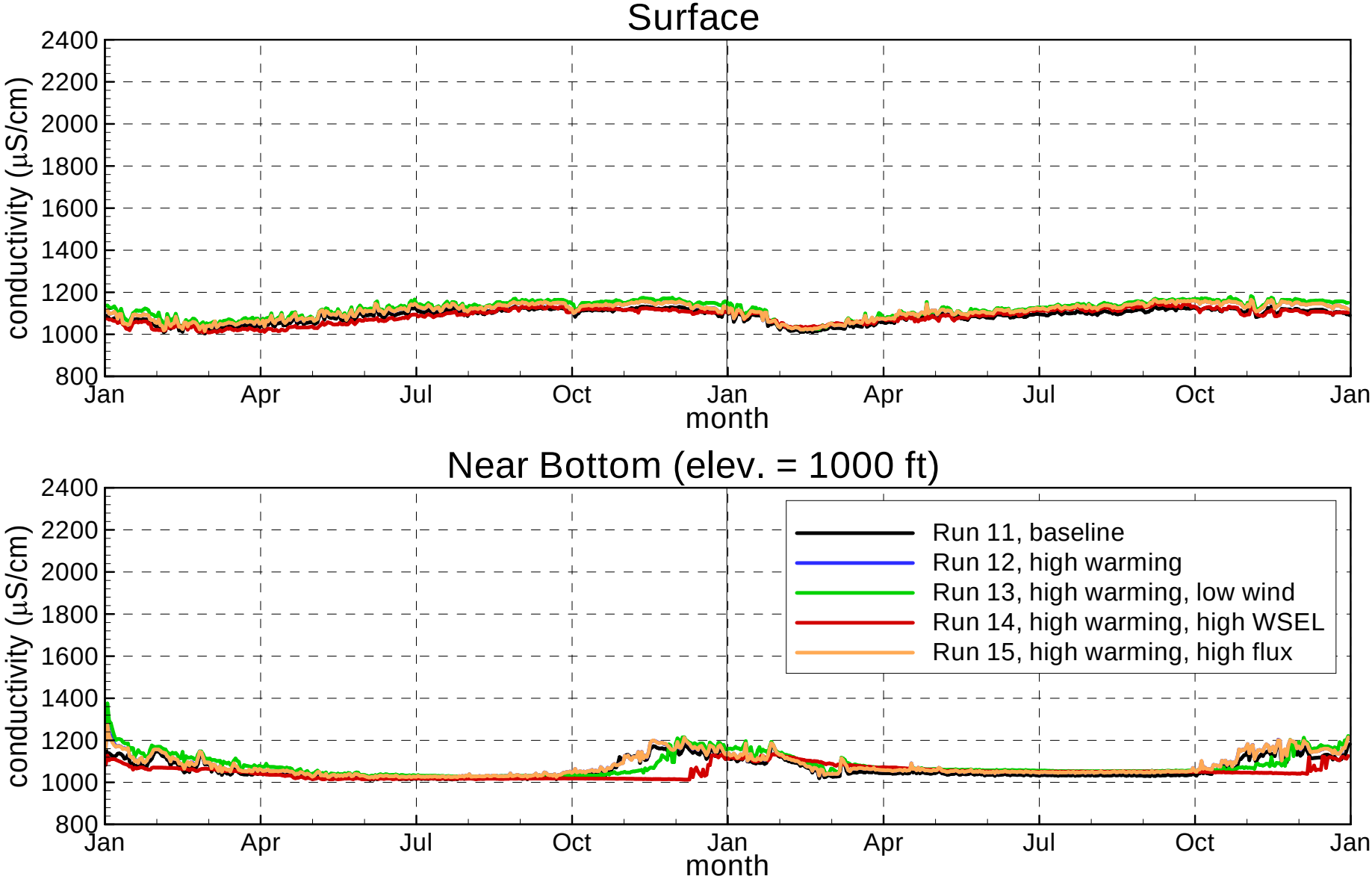

Figure A.286

Conductivity at Station VR25.1

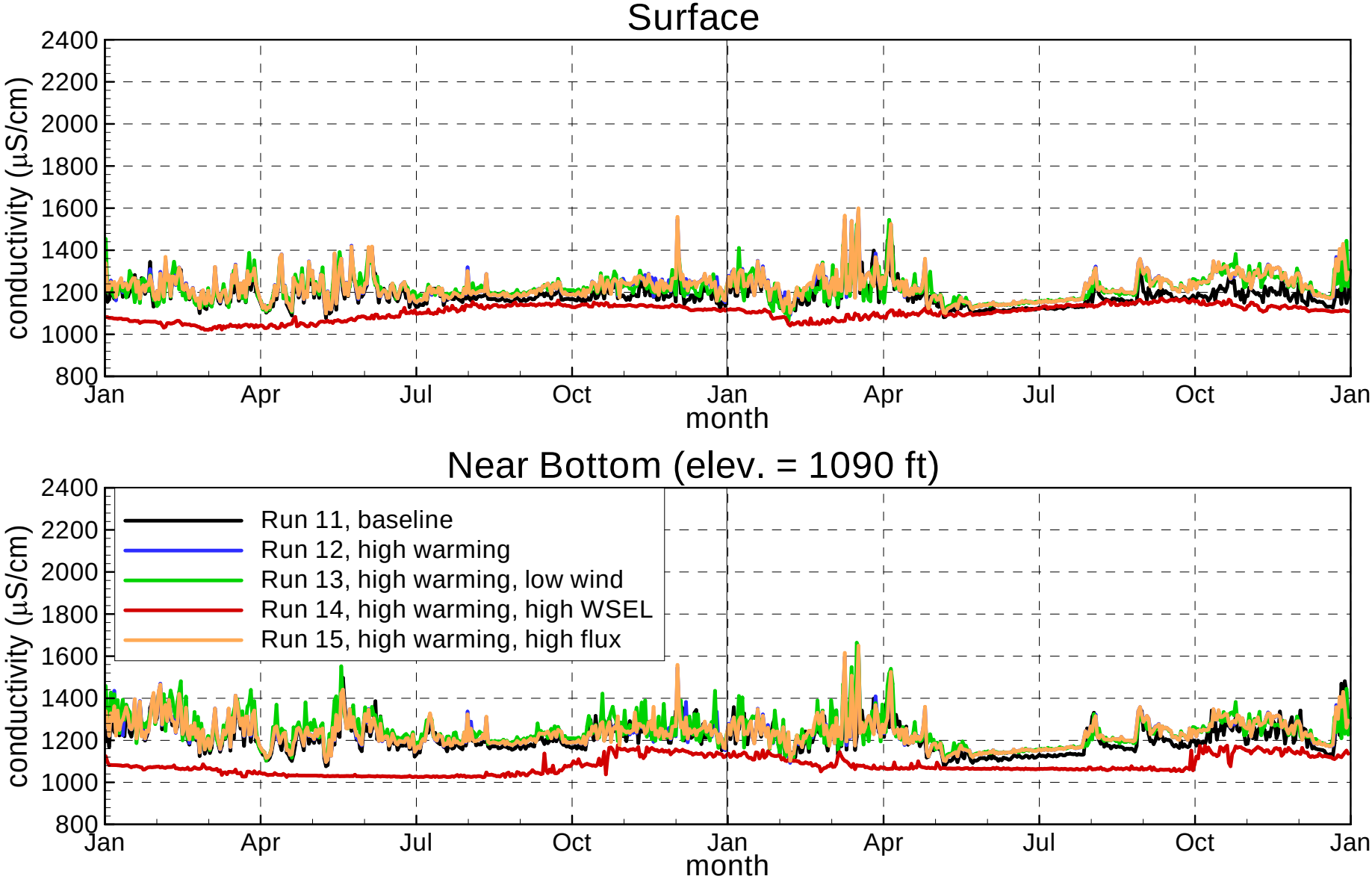

Figure A.287

Conductivity at Station CR360.7

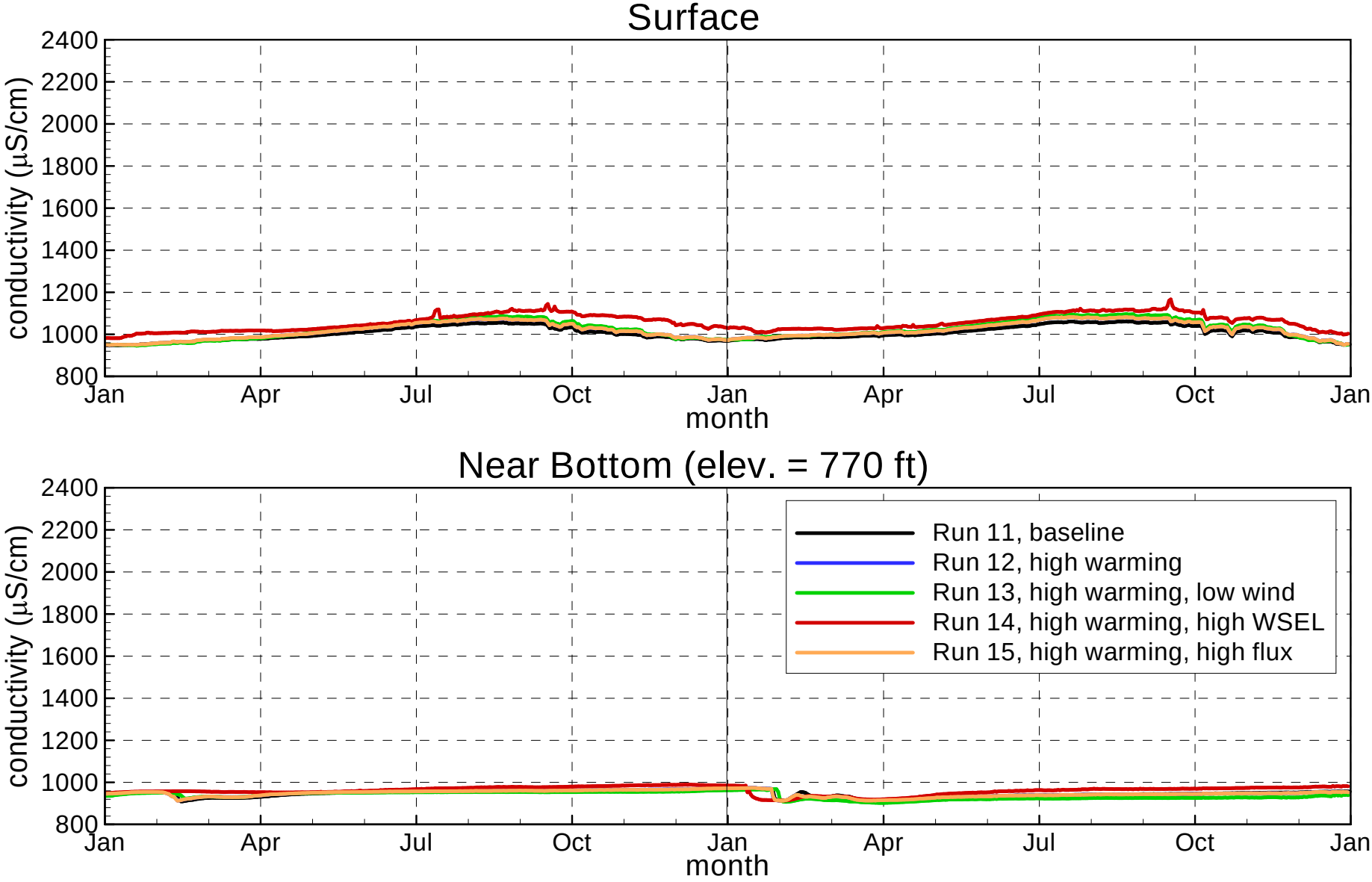

Figure A.288

Conductivity at Station CR346.4

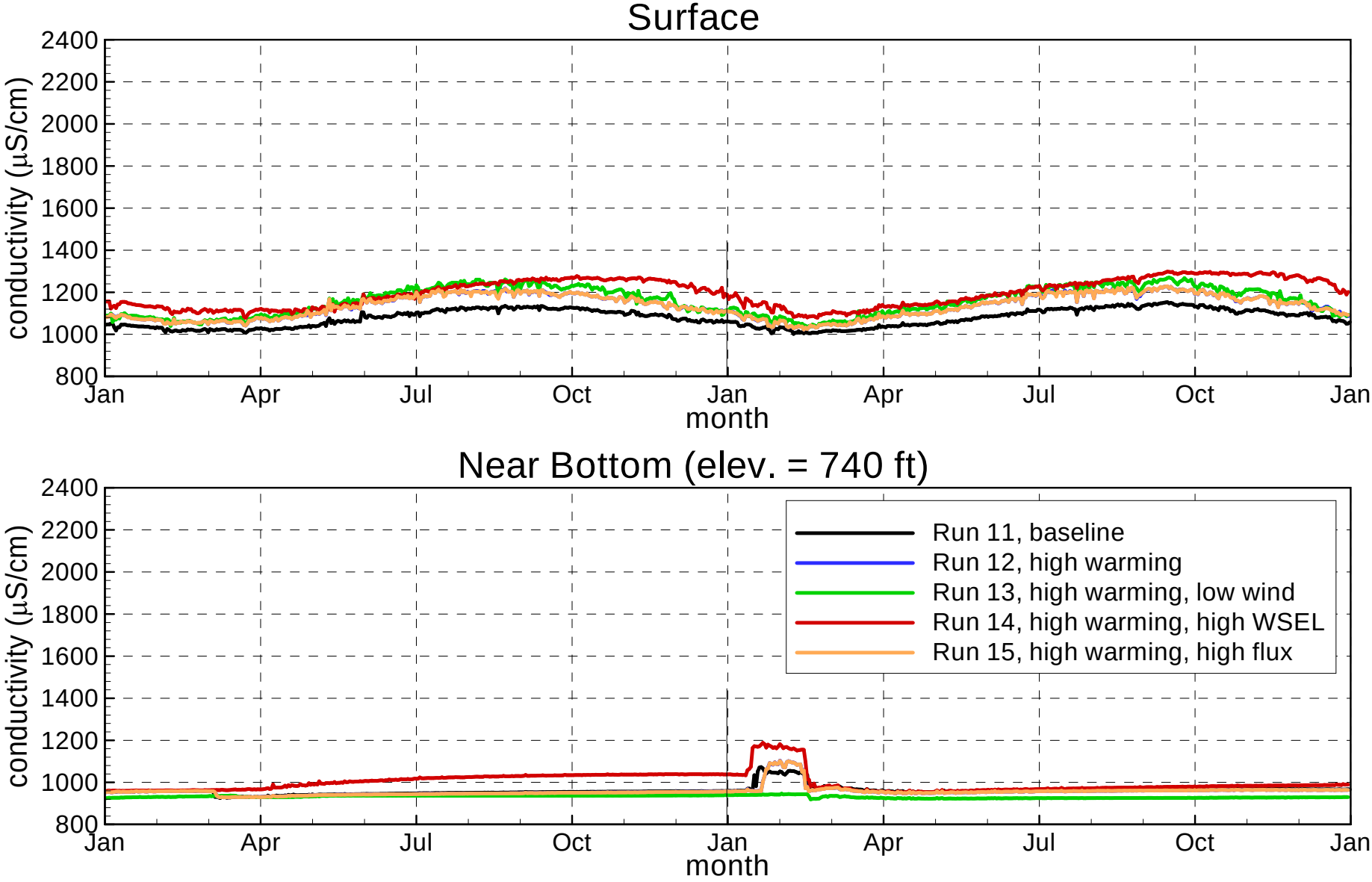

Figure A.289

Conductivity at Station LWLVB1.2

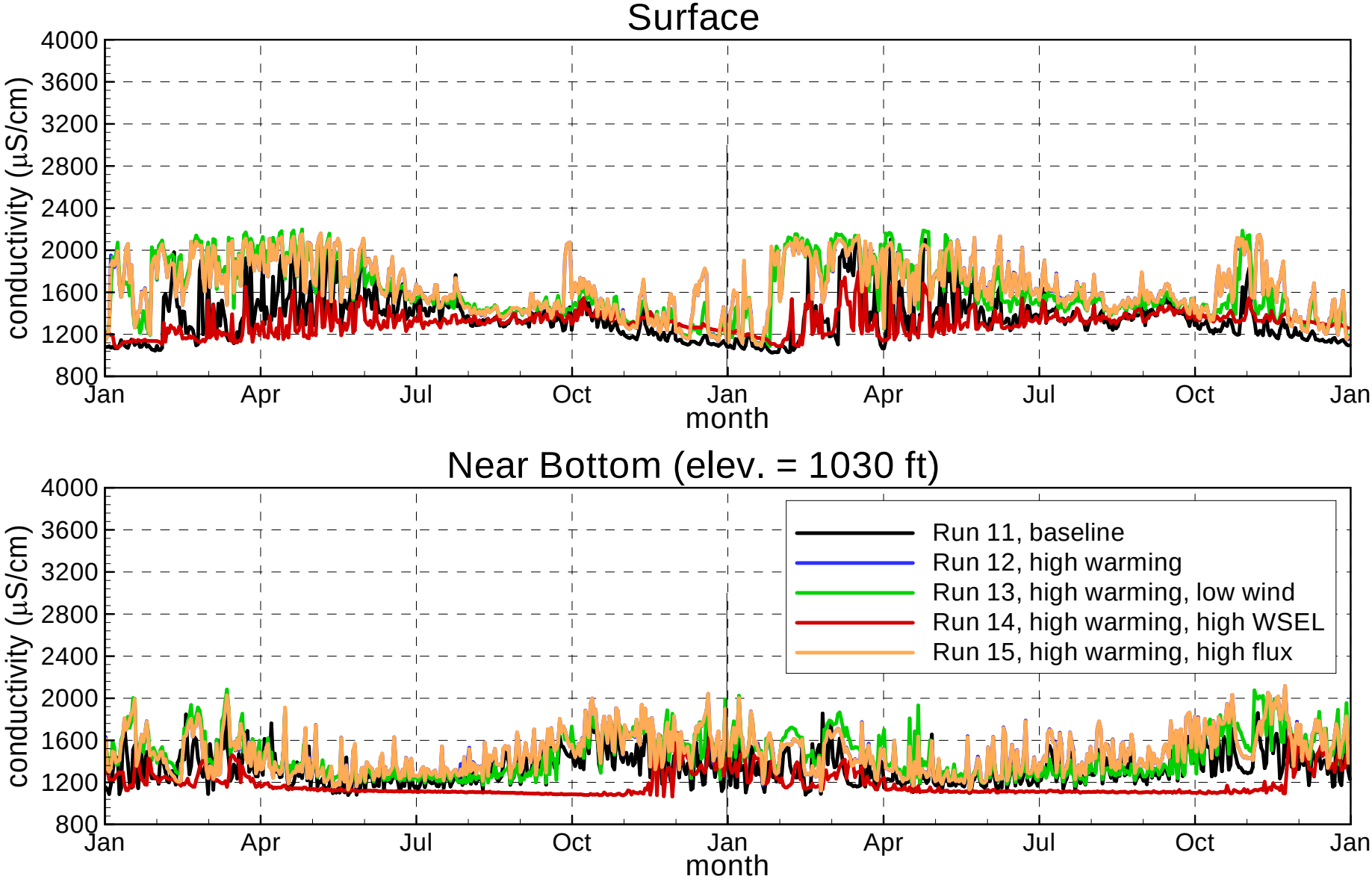

Figure A.290

FLOW SCIENCE

Conductivity at Station LWLVB1.85

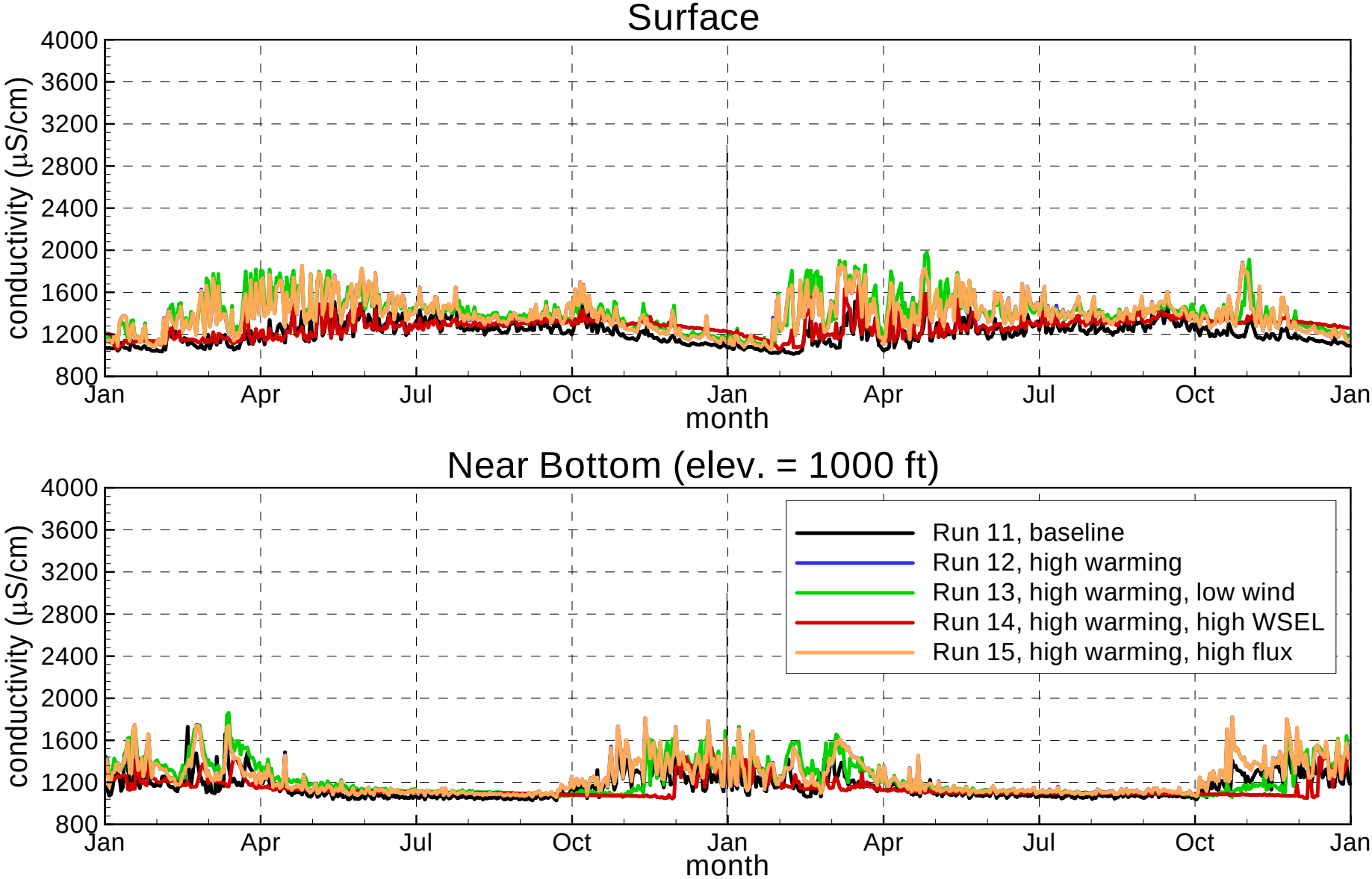

Figure A.291

Conductivity at Station LWLVB2.7

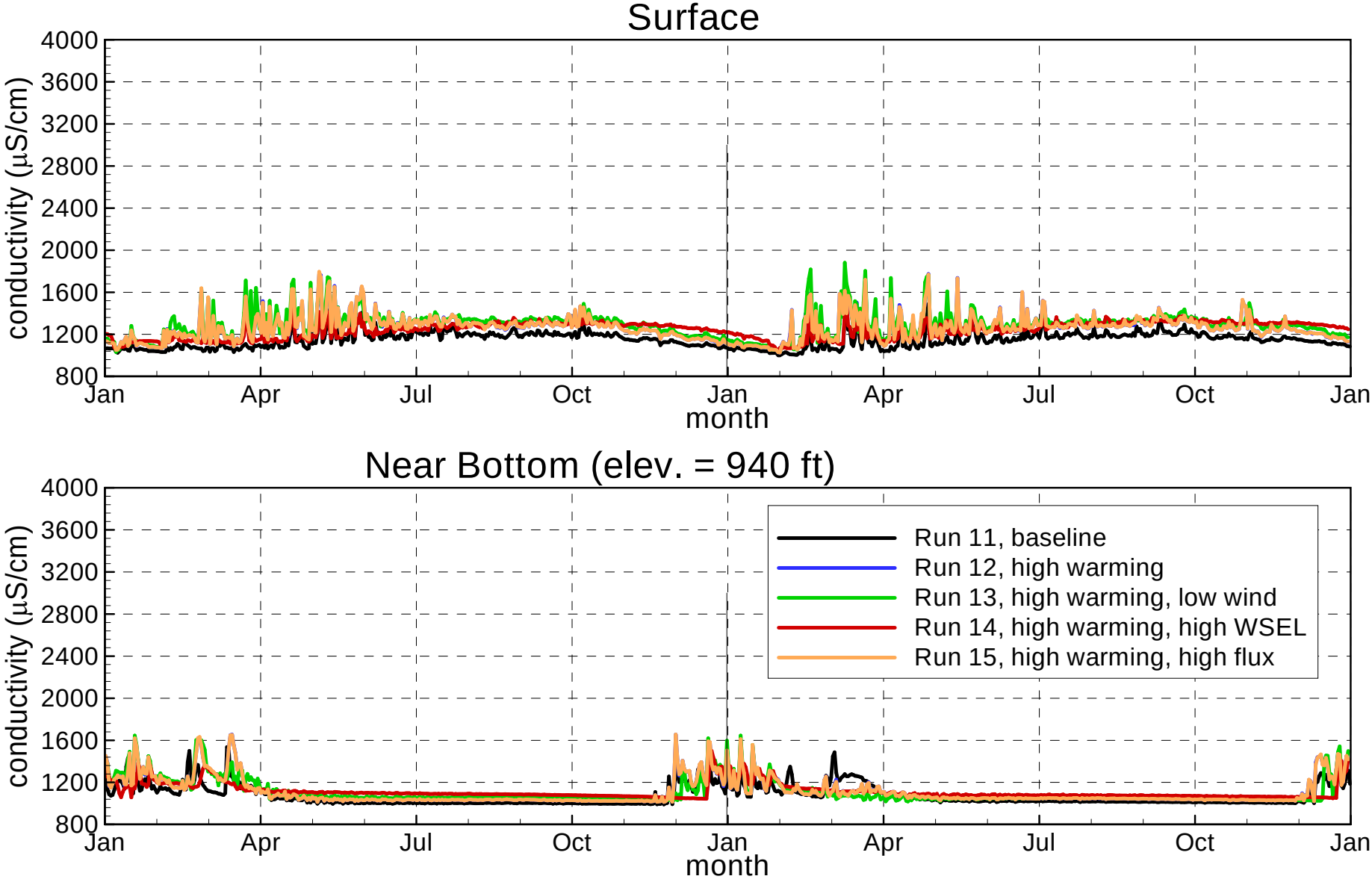

Figure A.292

Conductivity at Station LWLVB3.5

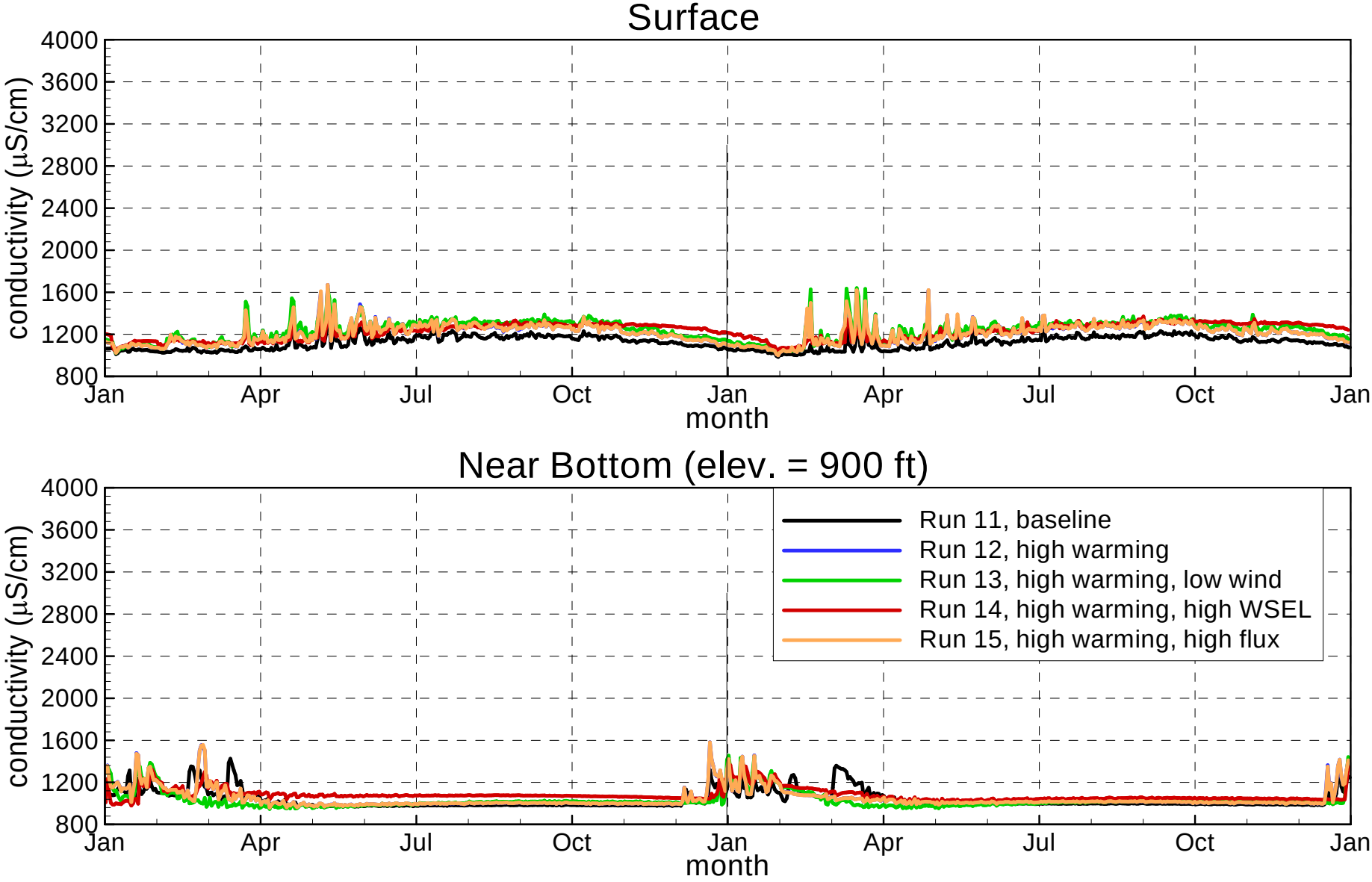

Figure A.293

FLOW SCIENCE

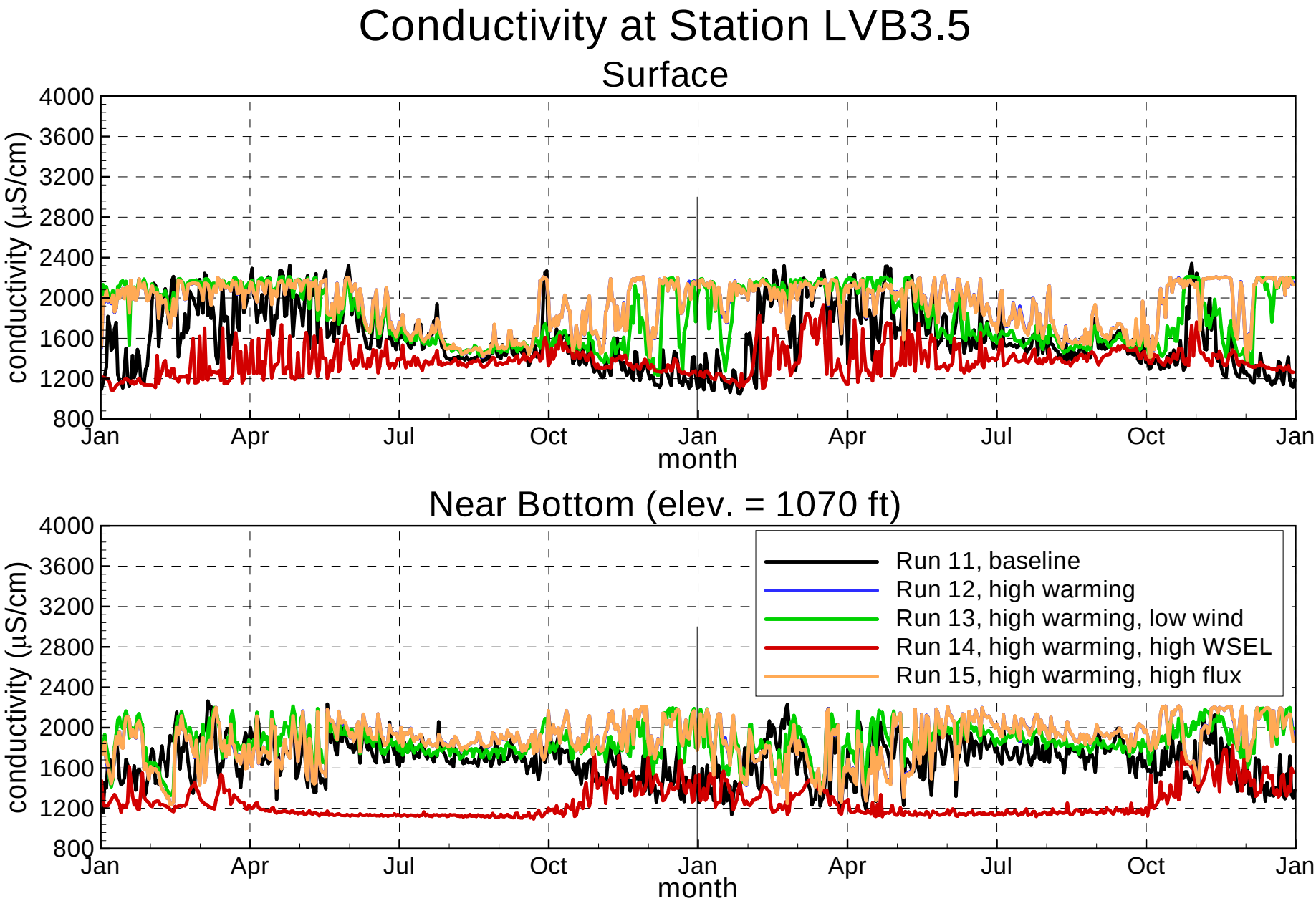
Conductivity at Station LVB3.5
Surface
conductivity (µS/cm)
4000
3600
3200
2800
2400
2000
1600
1200
800
Jan
Apr
Jul
Oct
Jan
Apr
Jul
Oct
Jan
month
Near Bottom (elev. = 1070 ft)
Run 11, baseline
Run 12, high warming
Run 13, high warming, low wind
Run 14, high warming, high WSEL
Run 15, high warming, high flux

Figure A.294

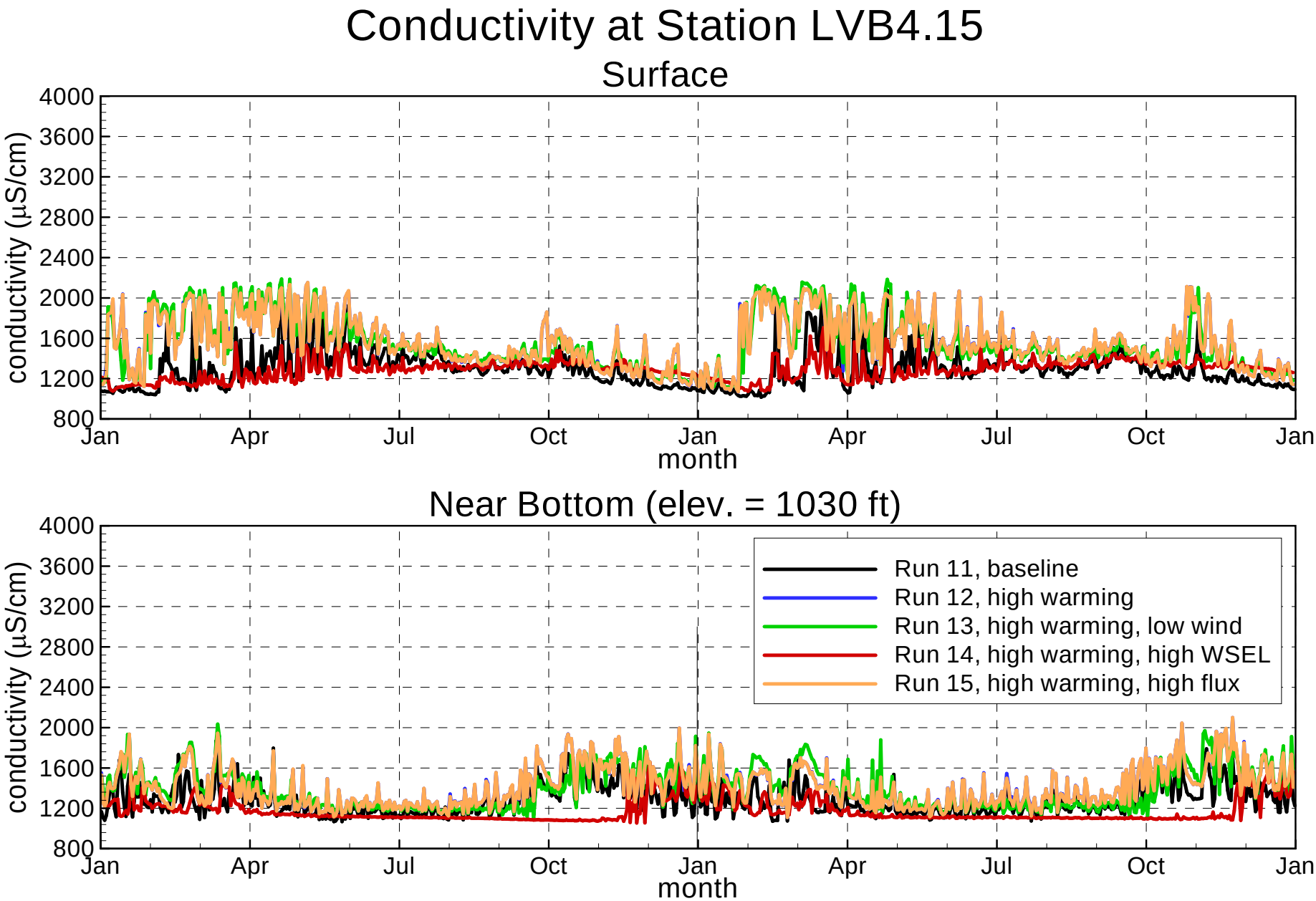
Conductivity at Station LVB4.15
Surface
conductivity (µS/cm)
4000
3600
3200
2800
2400
2000
1600
1200
800
Jan
Apr
Jul
Oct
Jan
Apr
Jul
Oct
Jan
month
Near Bottom (elev. = 1030 ft)
Run 11, baseline
Run 12, high warming
Run 13, high warming, low wind
Run 14, high warming, high WSEL
Run 15, high warming, high flux

Figure A.295

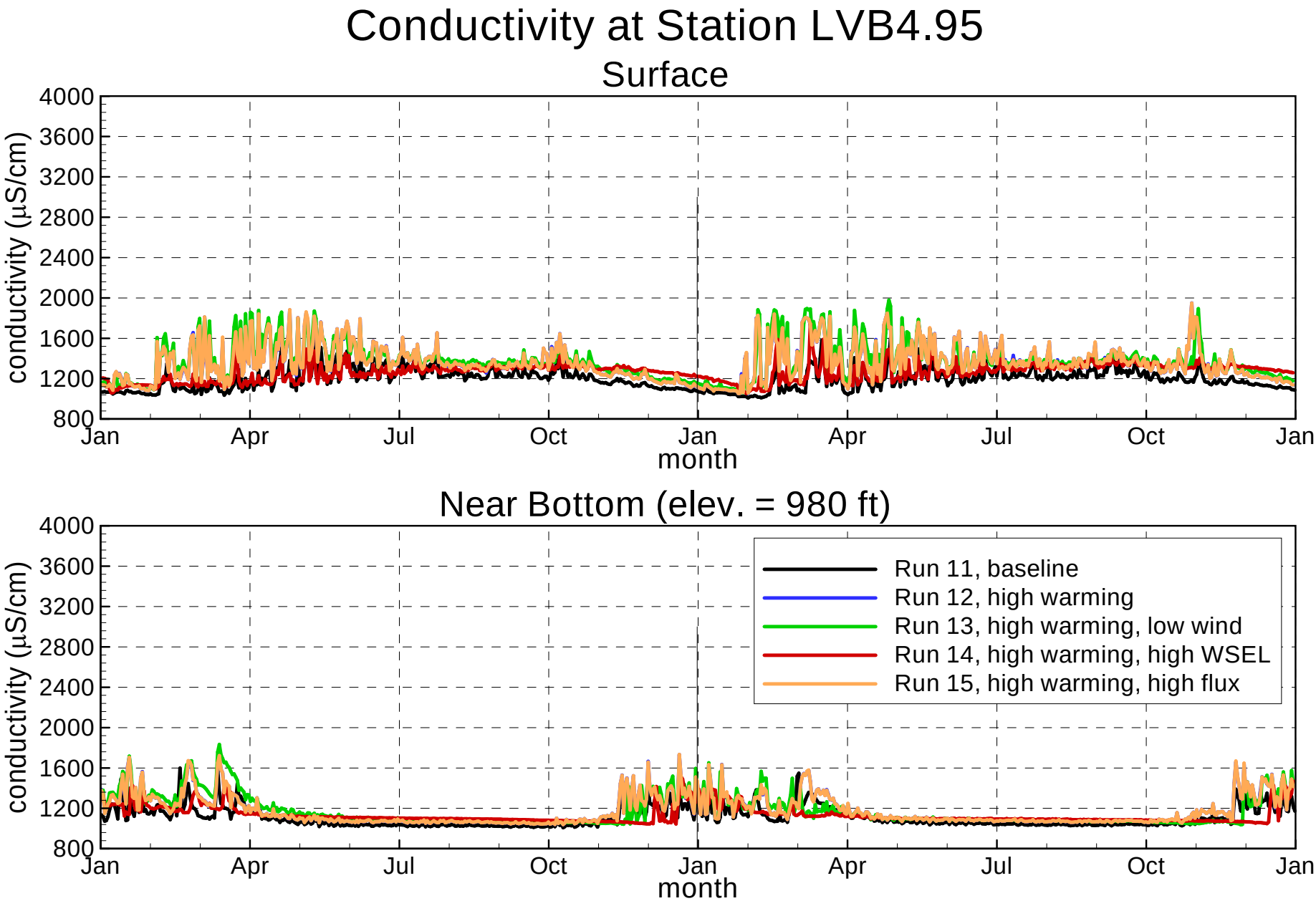

Figure A.296

FLOW SCIENCE

Conductivity at Station LVB6.7

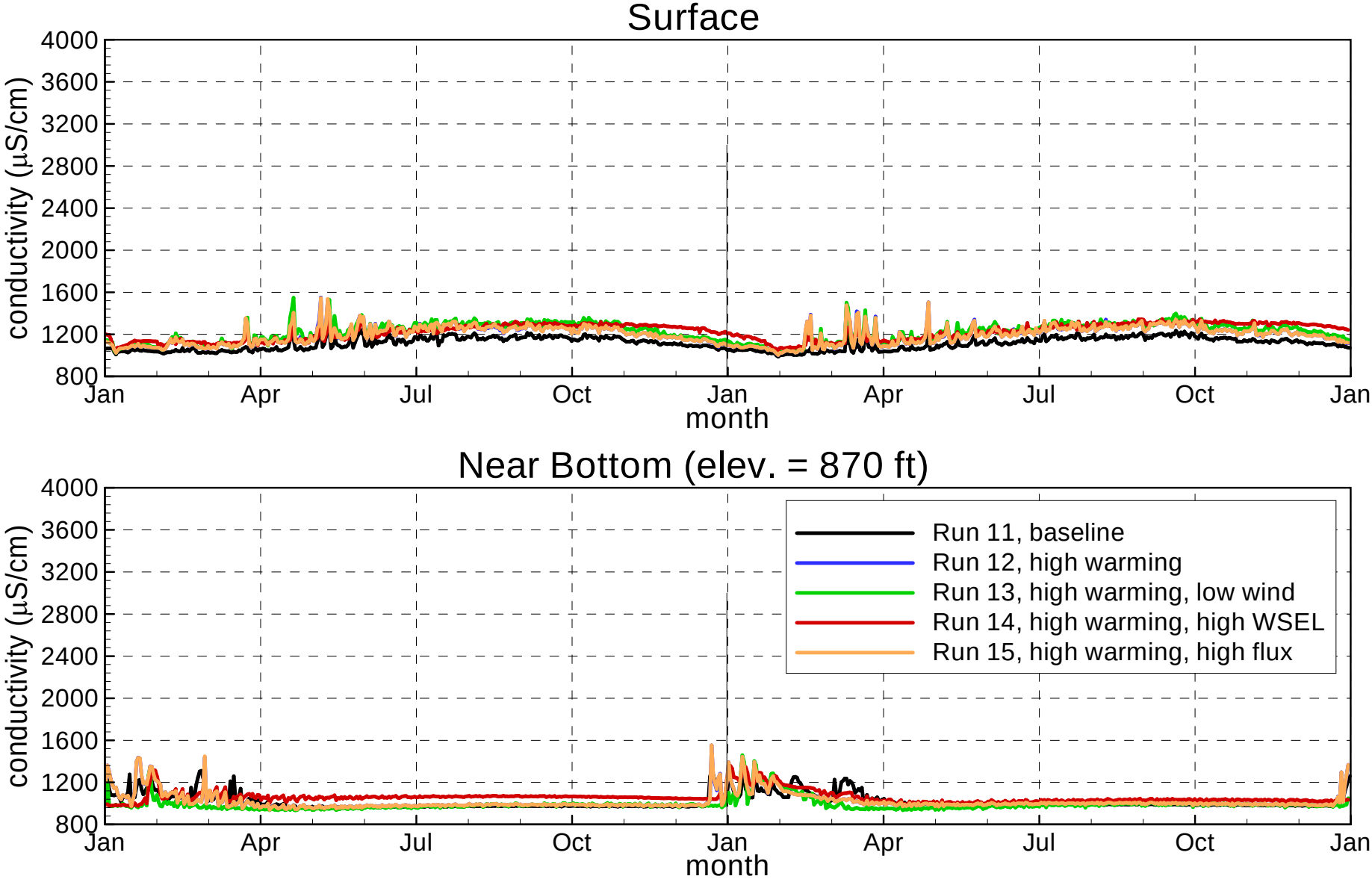

Figure A.297

Conductivity at Station LVB7.3

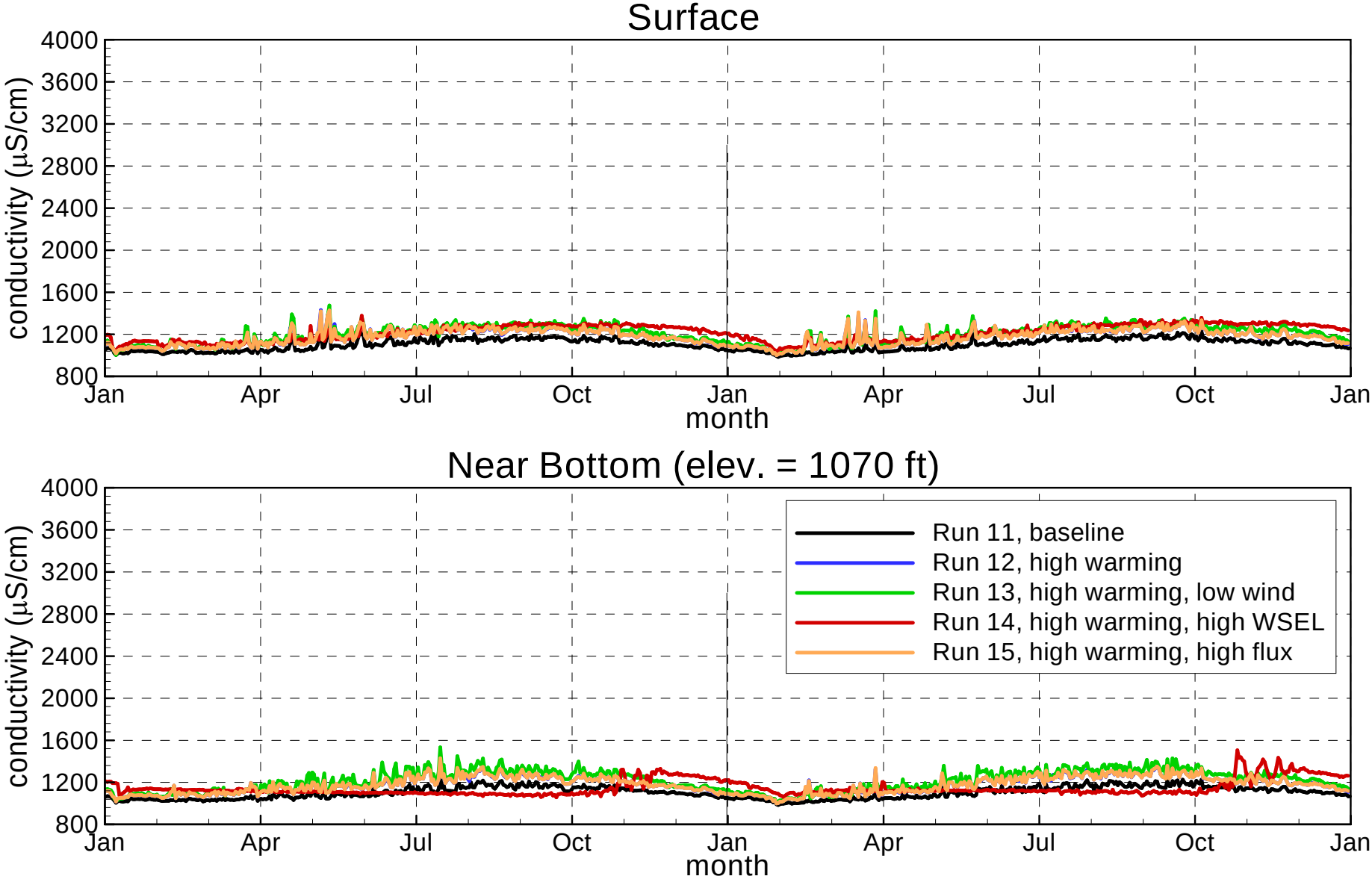

Figure A.298

Conductivity at SNWA Intake #3

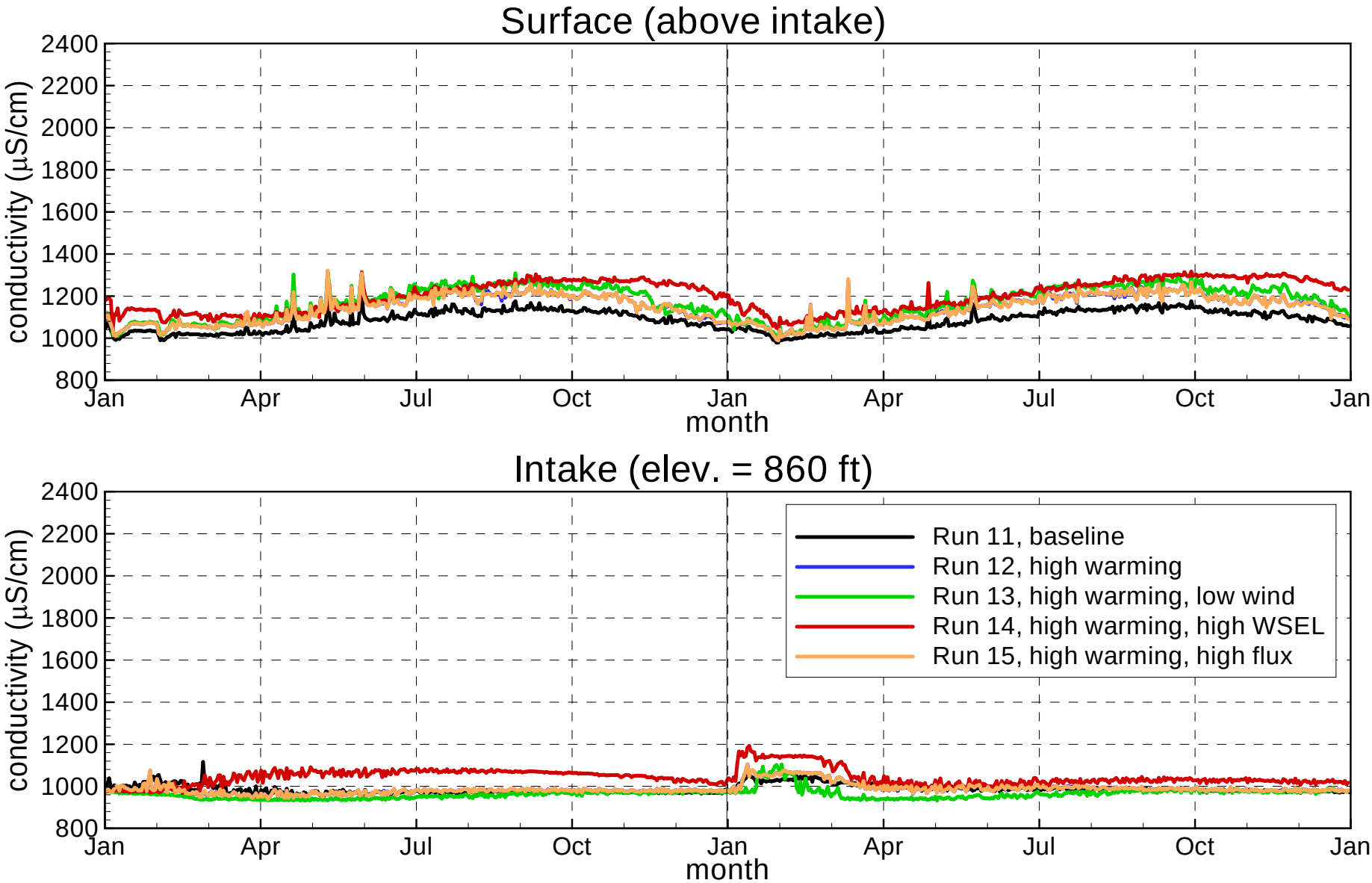

Figure A.299

FLOW SCIENCE

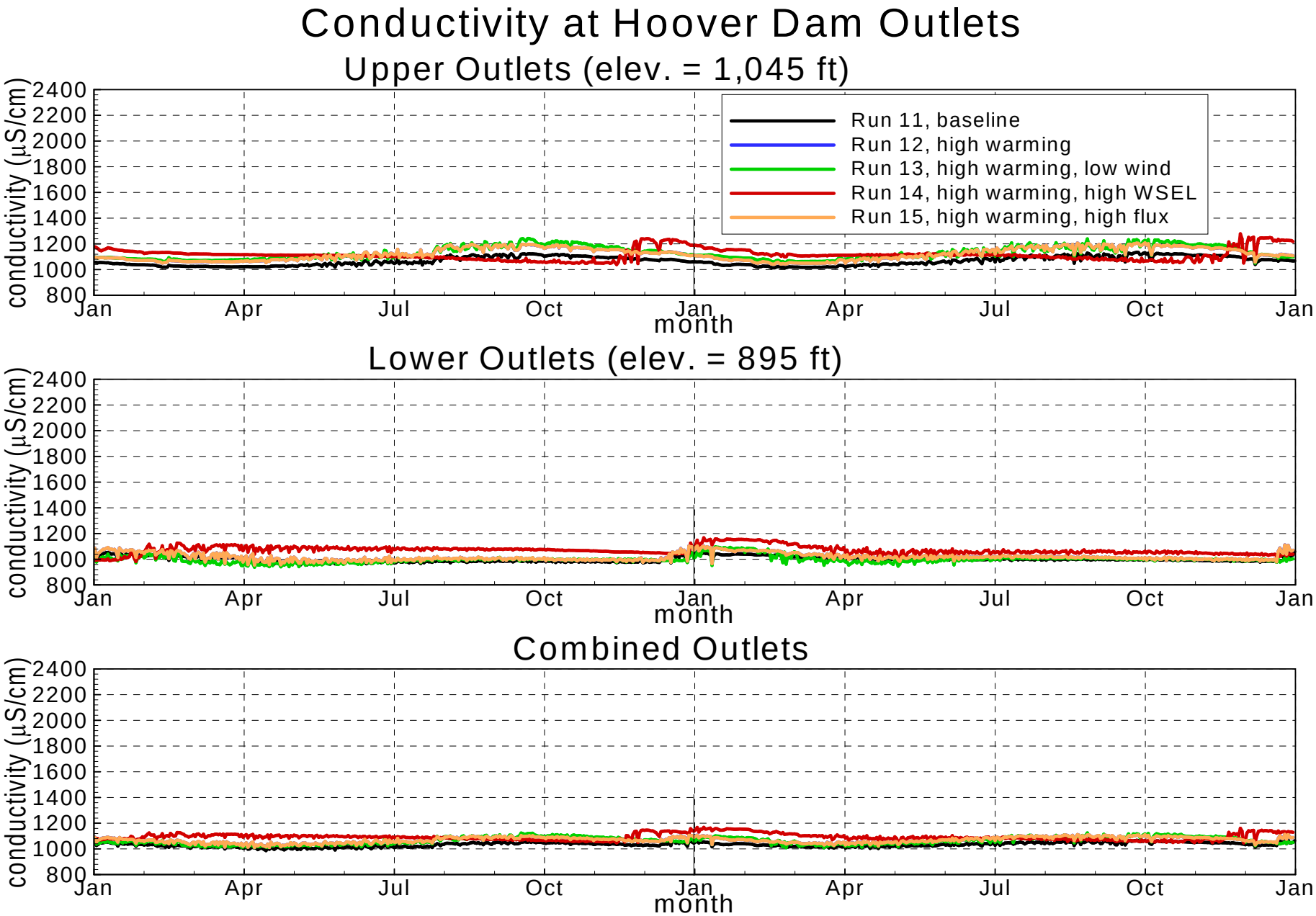

Figure A.300

FLOW SCIENCE

Bromide at Station CR394.0

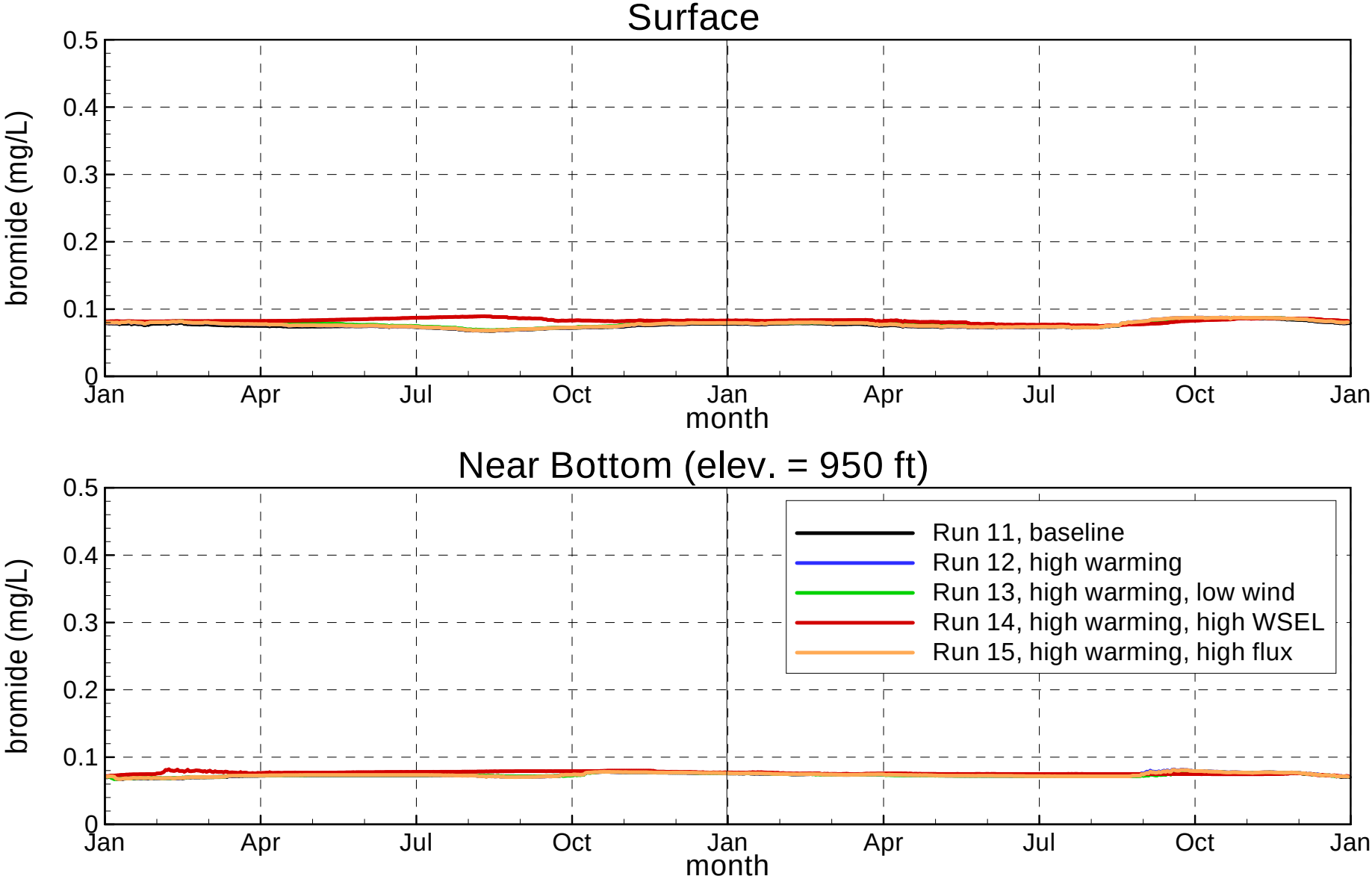

Figure A.301

FLOW SCIENCE

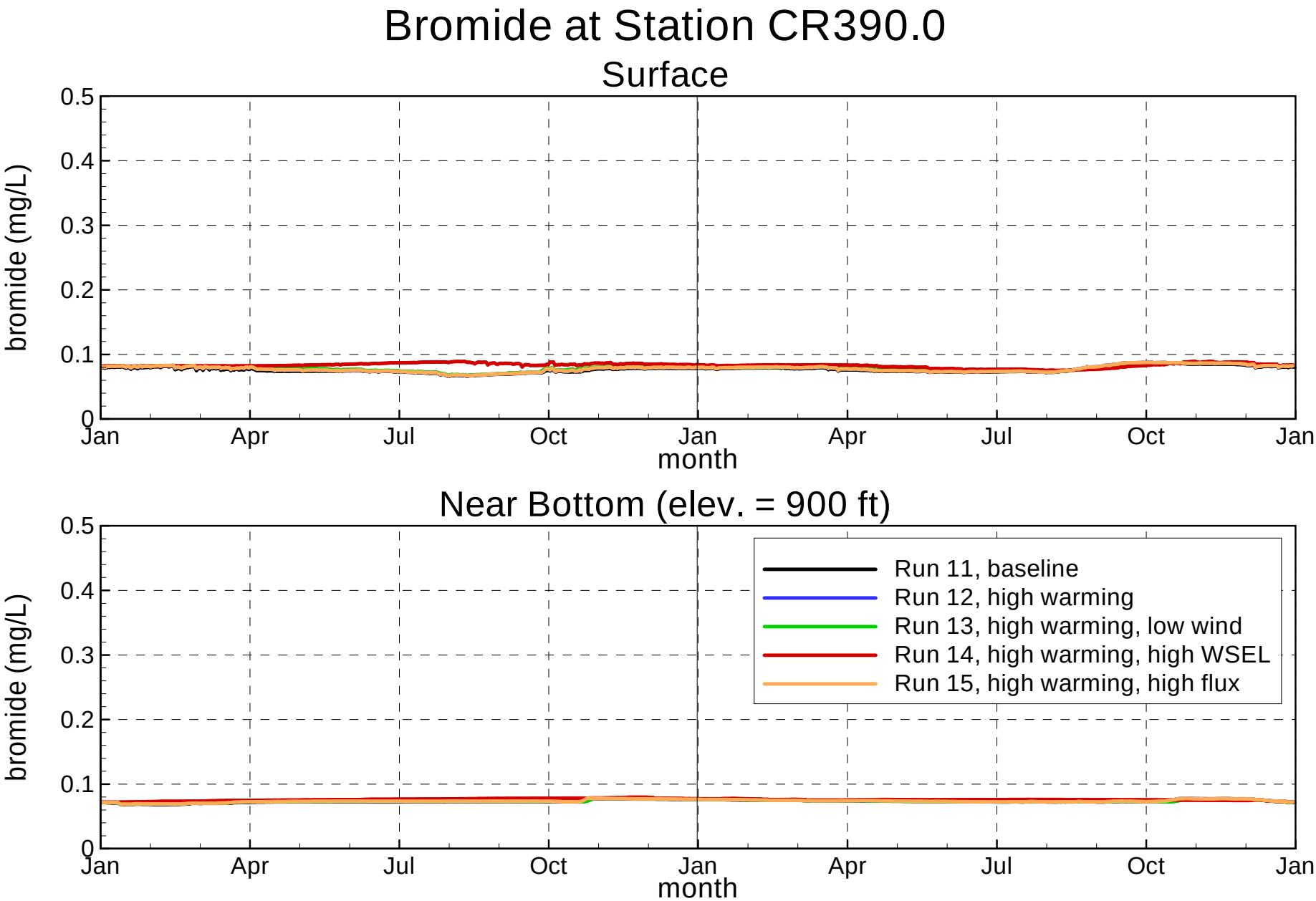
Bromide at Station CR390.0
Surface
bromide (mg/L)
0.5
0.4
0.3
0.2
0.1
0
Jan
Apr
Jul
Oct
Jan
Apr
Jul
Oct
Jan
month
Near Bottom (elev. = 900 ft)
bromide (mg/L)
0.5
0.4
0.3
0.2
0.1
0
Jan
Apr
Jul
Oct
Jan
Apr
Jul
Oct
Jan
month
Run 11, baseline
Run 12, high warming
Run 13, high warming, low wind
Run 14, high warming, high WSEL
Run 15, high warming, high flux

Figure A.302

Bromide at Station CR380.0

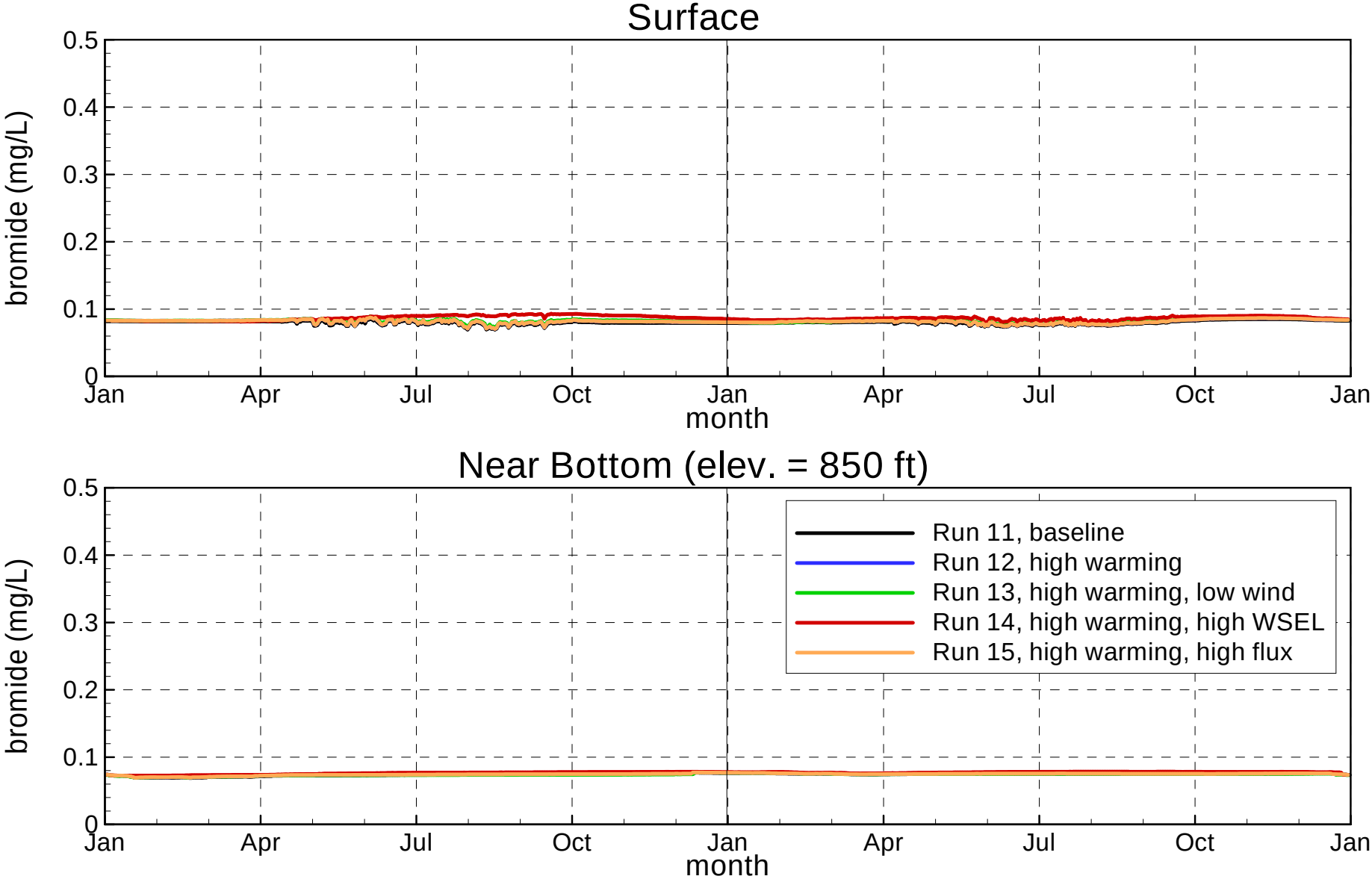

Figure A.303

Bromide at Station VR2.0

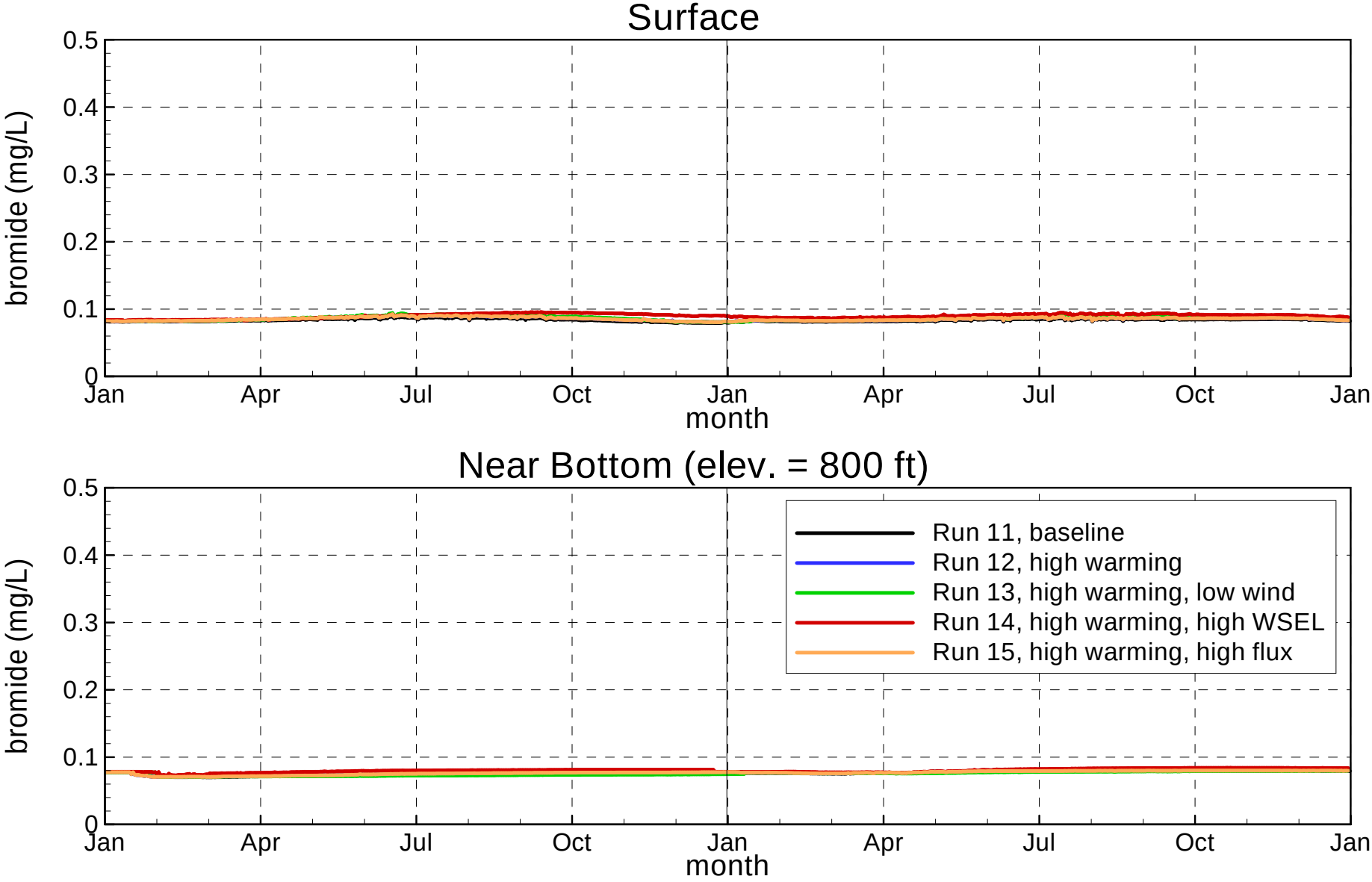

Figure A.304

Bromide at Station VR12.9

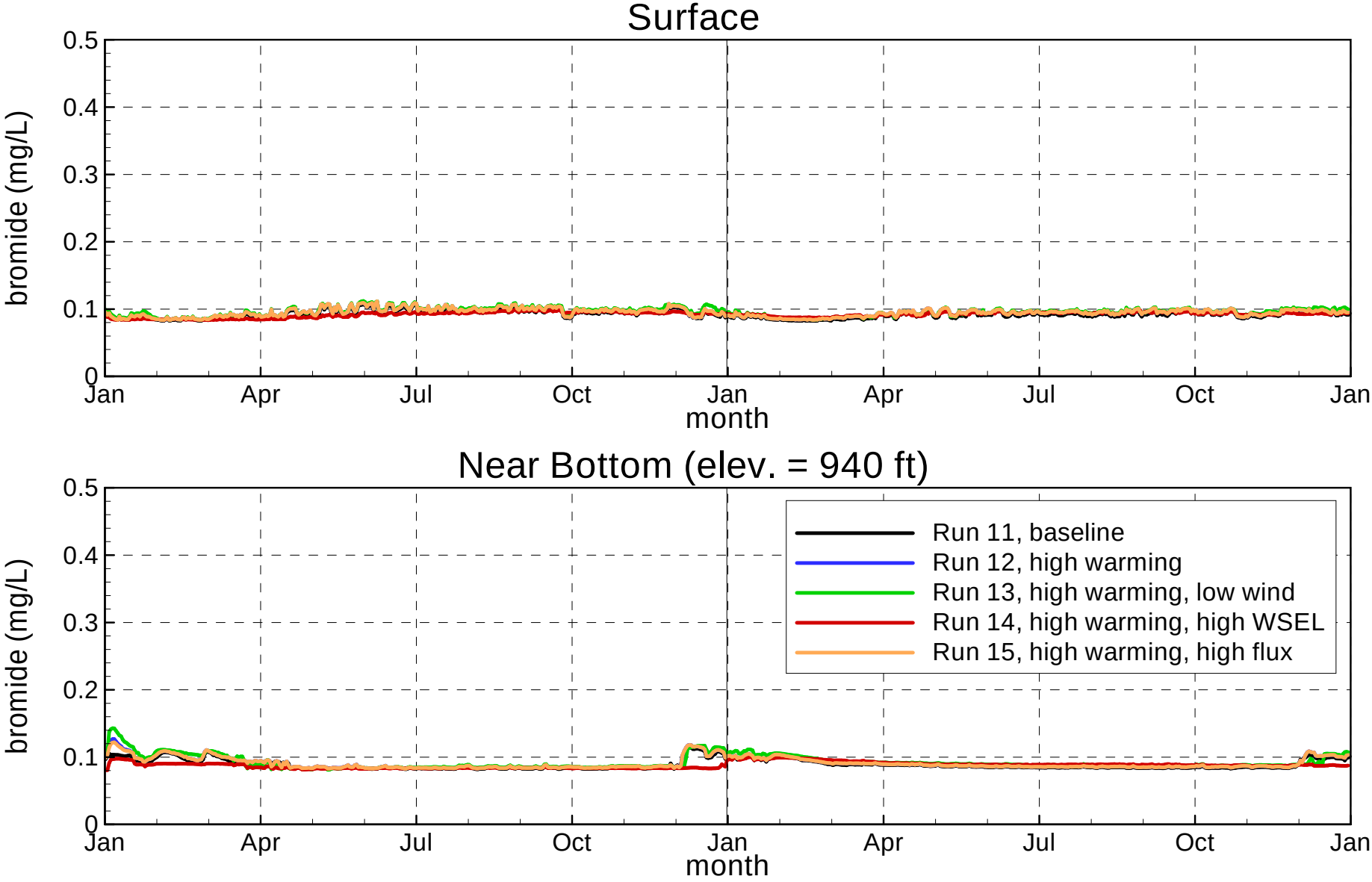

Figure A.305

FLOW SCIENCE

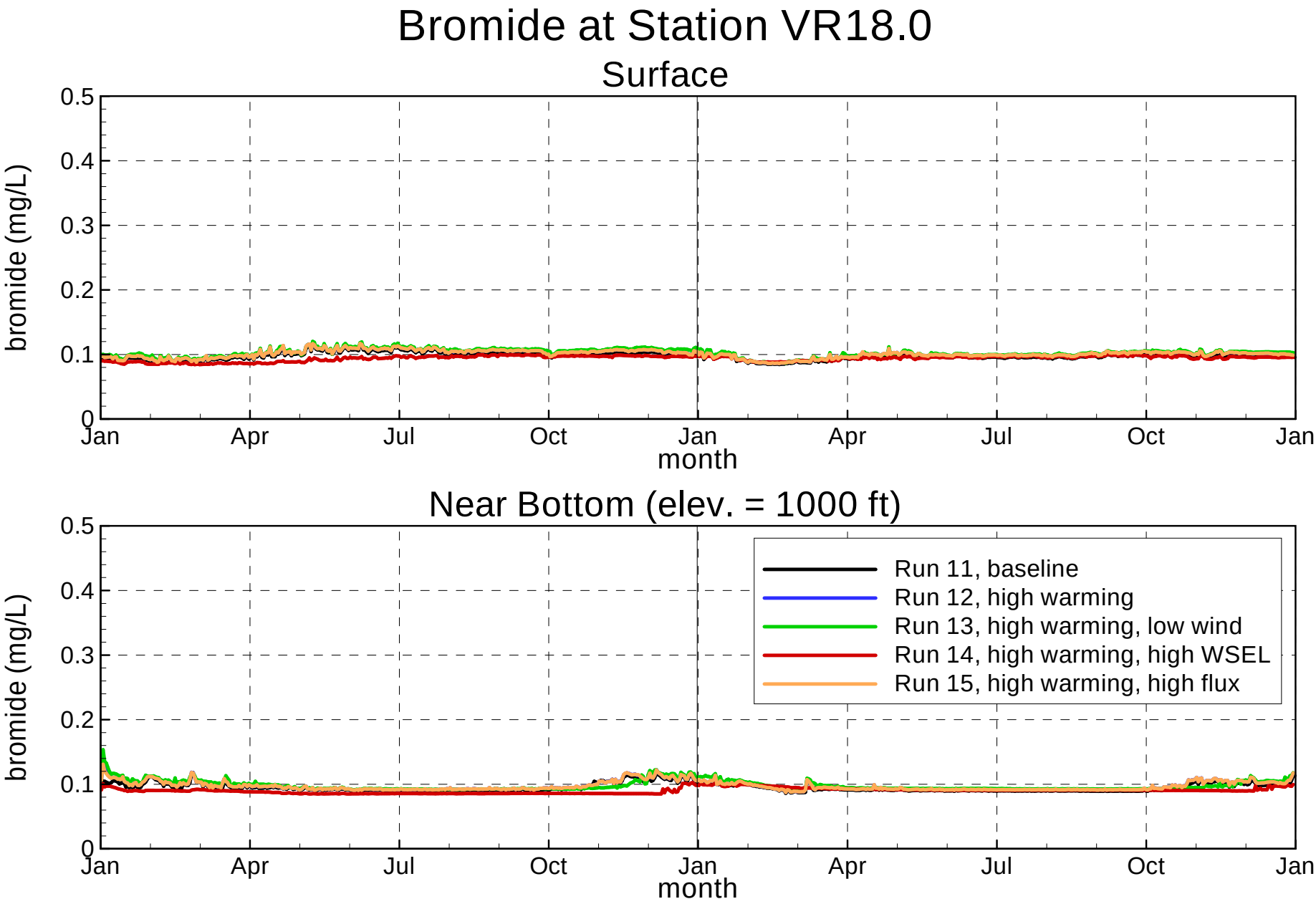
Bromide at Station VR18.0
Surface
bromide (mg/L)
0.5
0.4
0.3
0.2
0.1
0
Jan
Apr
Jul
Oct
Jan
Apr
Jul
Oct
Jan
month
Near Bottom (elev. = 1000 ft)
bromide (mg/L)
0.5
0.4
0.3
0.2
0.1
0
Jan
Apr
Jul
Oct
Jan
Apr
Jul
Oct
Jan
month
Run 11, baseline
Run 12, high warming
Run 13, high warming, low wind
Run 14, high warming, high WSEL
Run 15, high warming, high flux

Figure A.306

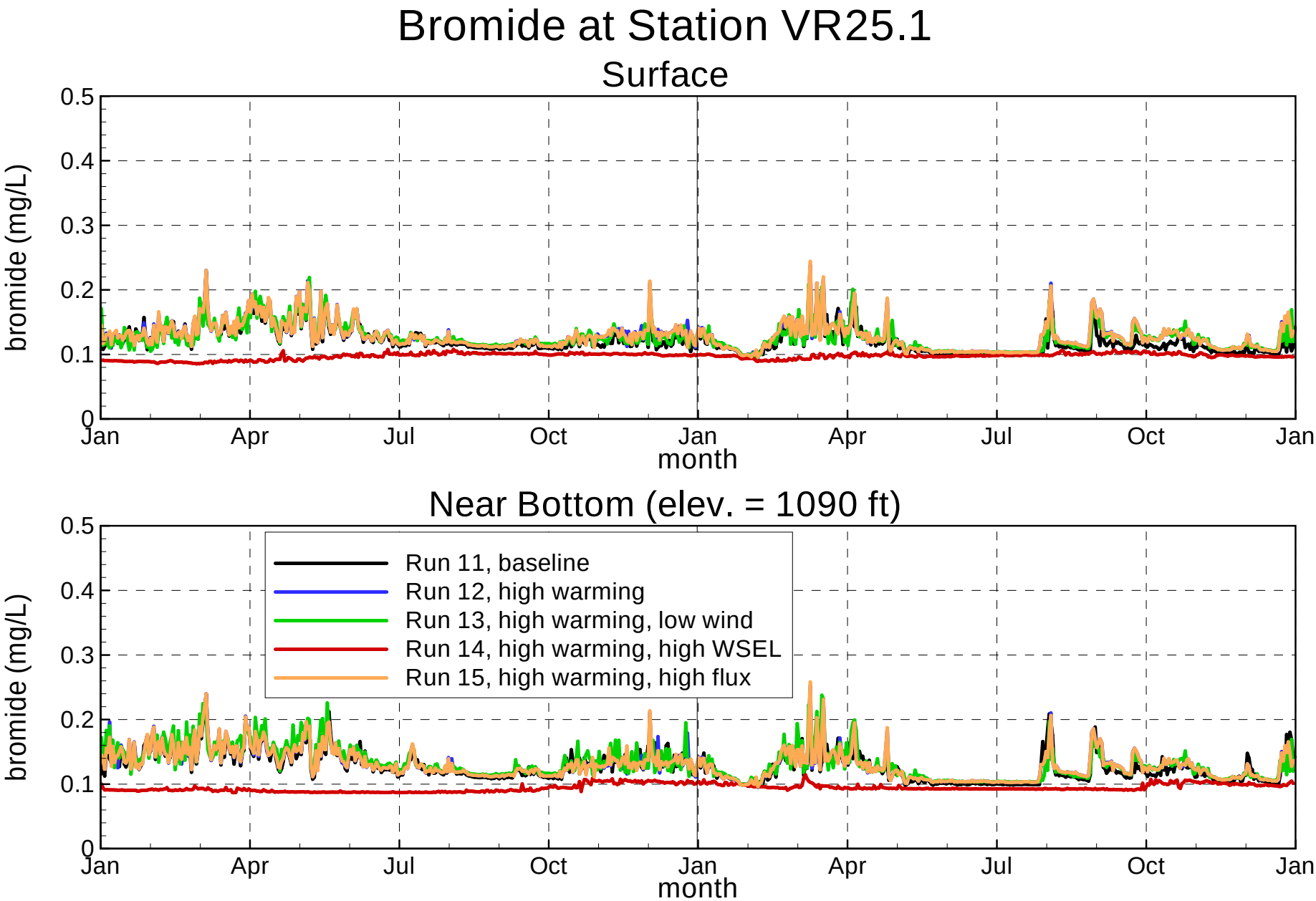
Bromide at Station VR25.1
Surface
bromide (mg/L)
0.5
0.4
0.3
0.2
0.1
0
Jan
Apr
Jul
Oct
Jan
Apr
Jul
Oct
Jan
month
Near Bottom (elev. = 1090 ft)
Run 11, baseline
Run 12, high warming
Run 13, high warming, low wind
Run 14, high warming, high WSEL
Run 15, high warming, high flux

Figure A.307

Bromide at Station CR360.7

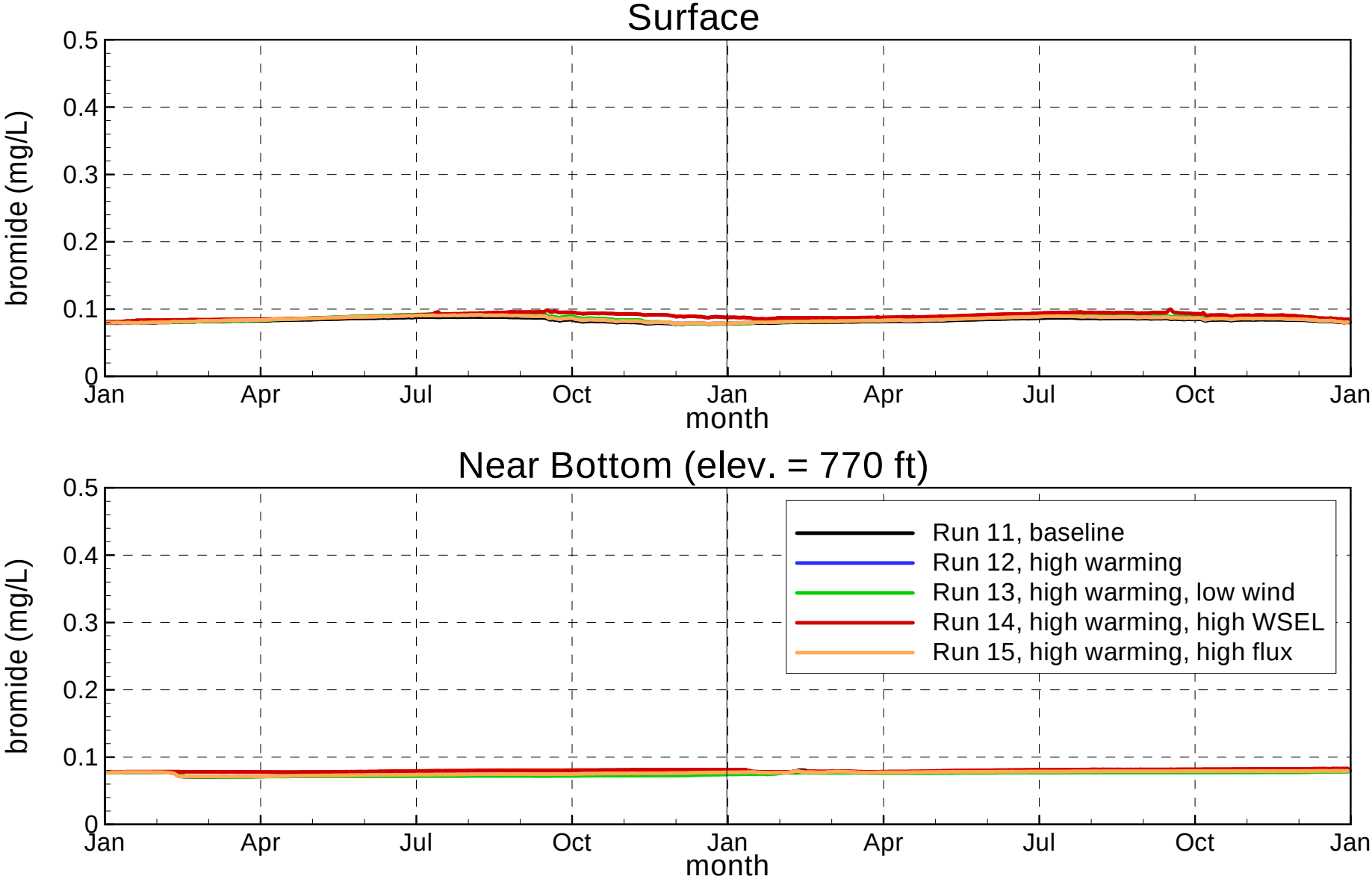

Figure A.308

Bromide at Station CR346.4

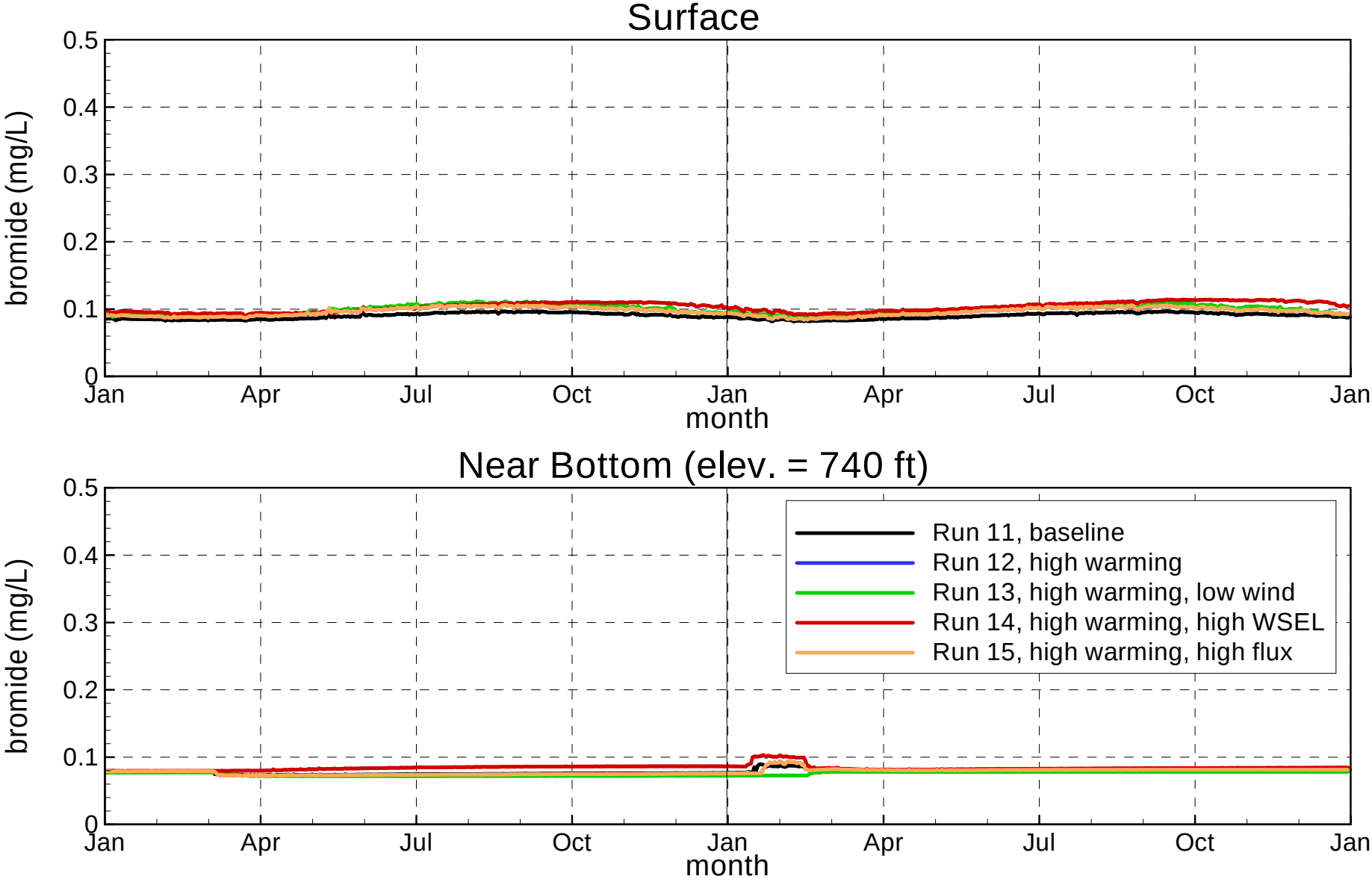

Figure A.309

FLOW SCIENCE

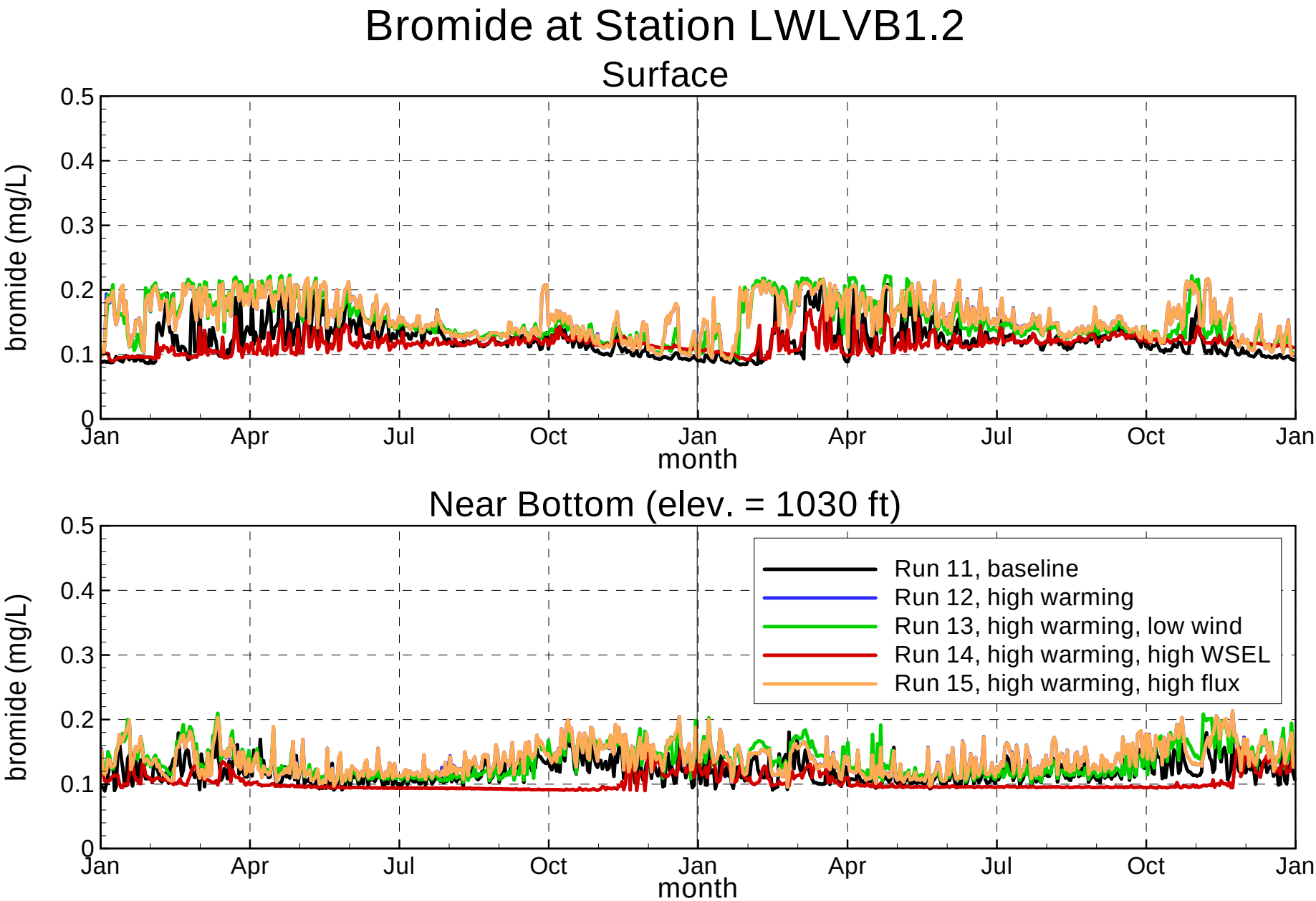
Bromide at Station LWLVB1.2
Surface
bromide (mg/L)
0.5
0.4
0.3
0.2
0.1
0
Jan
Apr
Jul
Oct
Jan
Apr
Jul
Oct
Jan
month
Near Bottom (elev. = 1030 ft)
bromide (mg/L)
0.5
0.4
0.3
0.2
0.1
0
Jan
Apr
Jul
Oct
Jan
Apr
Jul
Oct
Jan
month
Run 11, baseline
Run 12, high warming
Run 13, high warming, low wind
Run 14, high warming, high WSEL
Run 15, high warming, high flux

Figure A.310

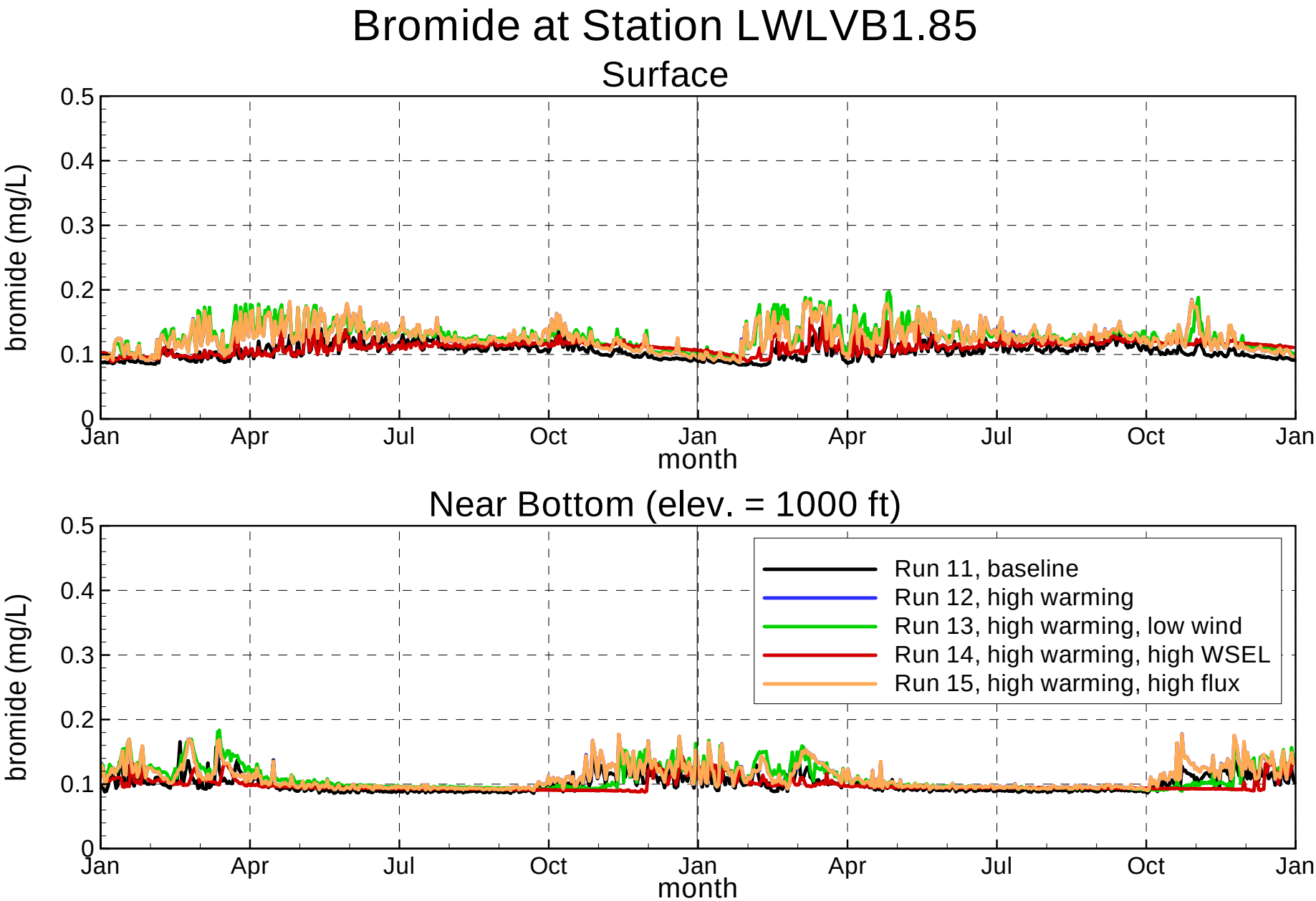
Bromide at Station LWLVB1.85
Surface
bromide (mg/L)
0.5
0.4
0.3
0.2
0.1
0
Jan
Apr
Jul
Oct
Jan
Apr
Jul
Oct
Jan
month
Near Bottom (elev. = 1000 ft)
bromide (mg/L)
0.5
0.4
0.3
0.2
0.1
0
Jan
Apr
Jul
Oct
Jan
Apr
Jul
Oct
Jan
month
Run 11, baseline
Run 12, high warming
Run 13, high warming, low wind
Run 14, high warming, high WSEL
Run 15, high warming, high flux

Figure A.311

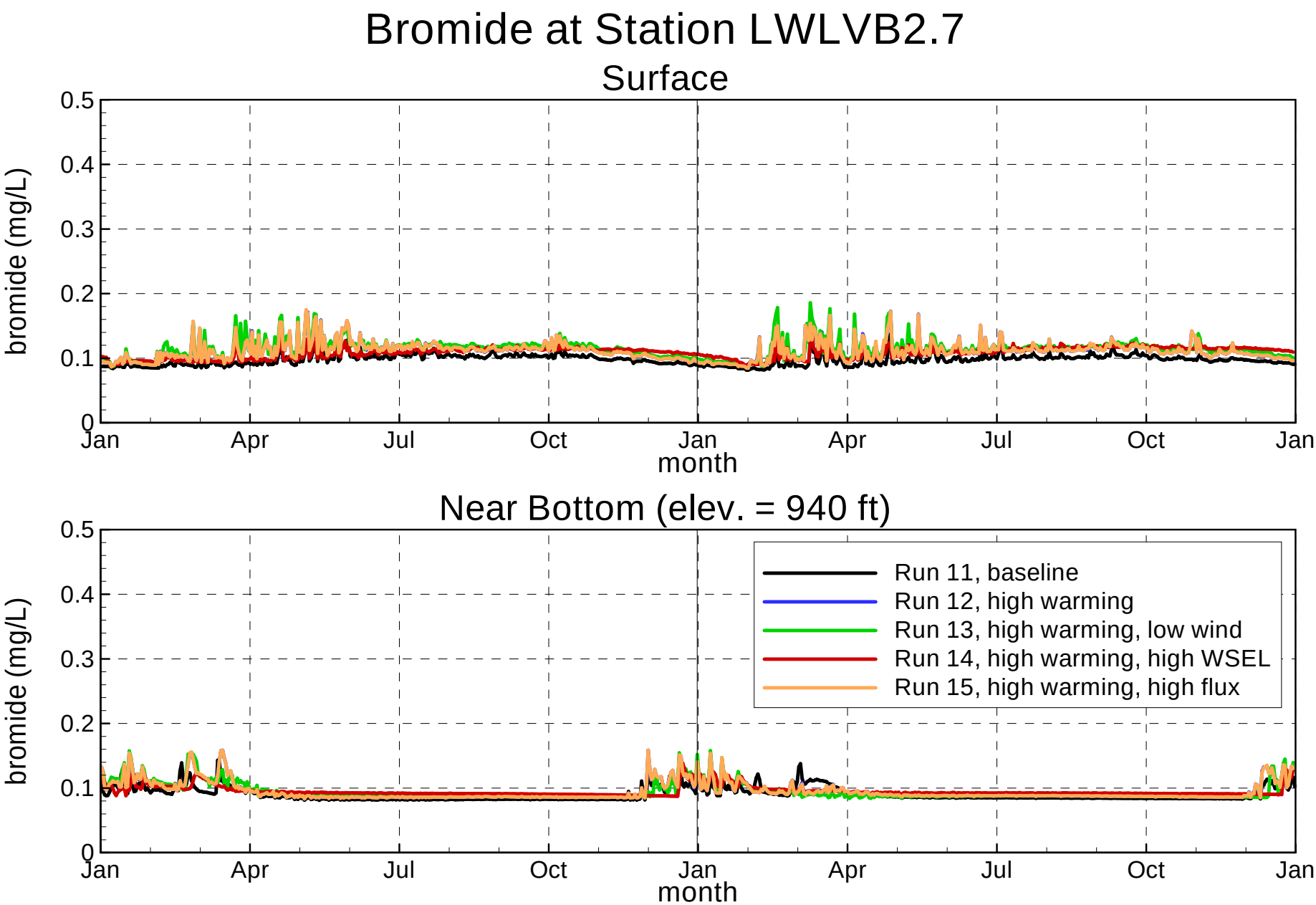
Bromide at Station LWLVB2.7
Surface
bromide (mg/L)
0.5
0.4
0.3
0.2
0.1
0
Jan
Apr
Jul
Oct
Jan
Apr
Jul
Oct
Jan
month
Near Bottom (elev. = 940 ft)
bromide (mg/L)
0.5
0.4
0.3
0.2
0.1
0
Jan
Apr
Jul
Oct
Jan
Apr
Jul
Oct
Jan
month
Run 11, baseline
Run 12, high warming
Run 13, high warming, low wind
Run 14, high warming, high WSEL
Run 15, high warming, high flux

Figure A.312

Bromide at Station LWLVB3.5

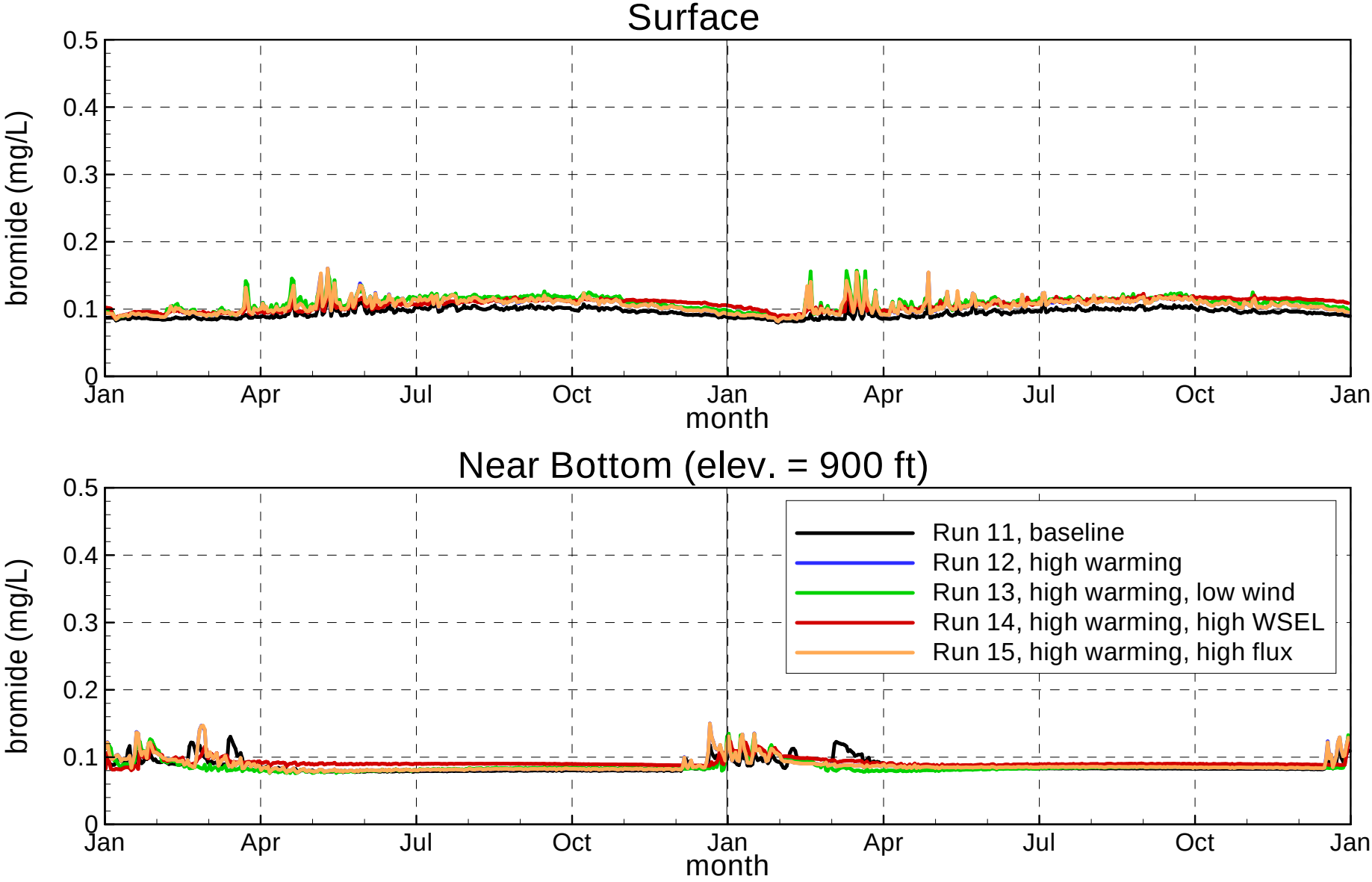

Figure A.313

FLOW SCIENCE

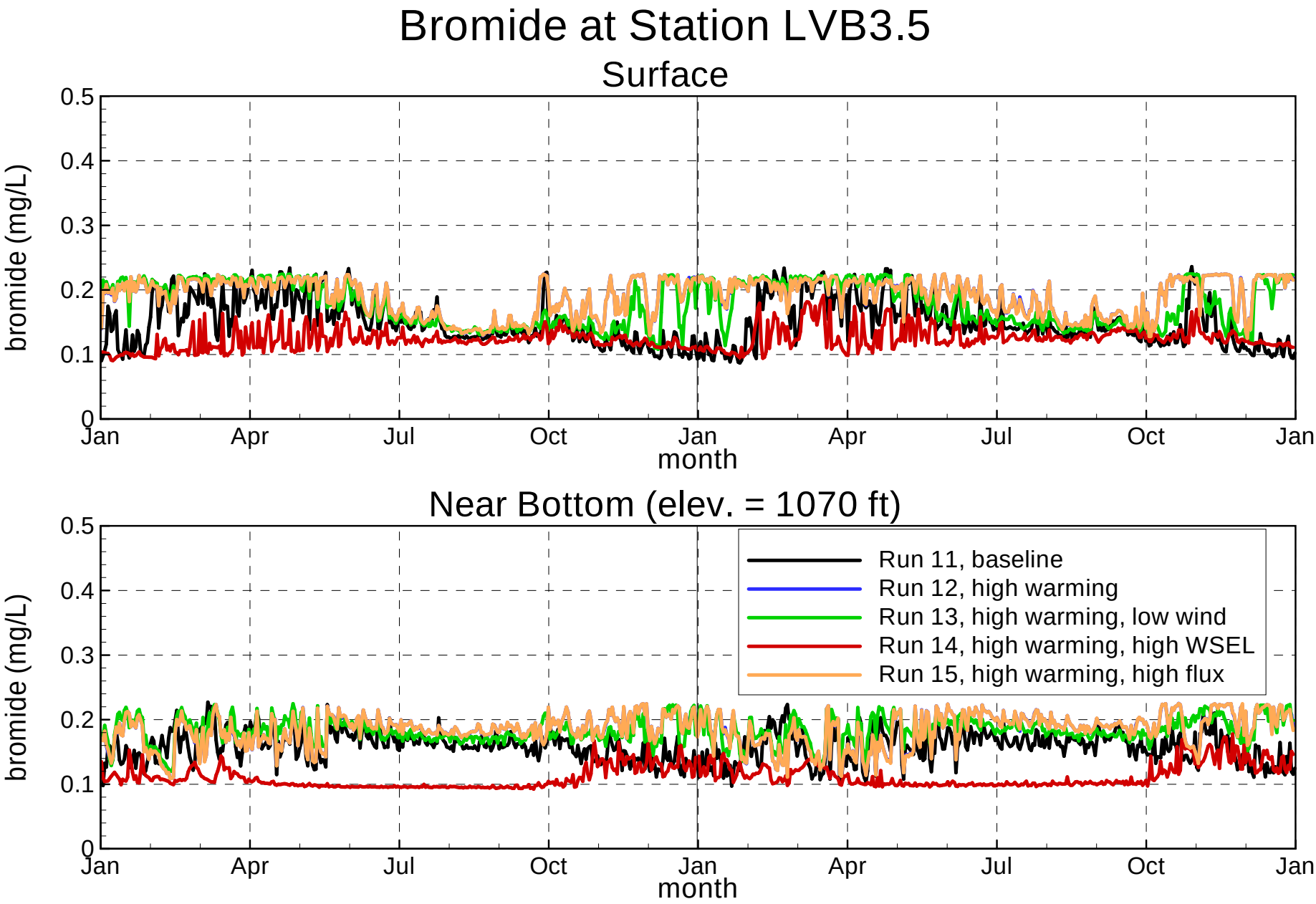
Bromide at Station LVB3.5
Surface
bromide (mg/L)
0.5
0.4
0.3
0.2
0.1
0
Jan
Apr
Jul
Oct
Jan
Apr
Jul
Oct
Jan
month
Near Bottom (elev. = 1070 ft)
bromide (mg/L)
0.5
0.4
0.3
0.2
0.1
0
Jan
Apr
Jul
Oct
Jan
Apr
Jul
Oct
Jan
month
Run 11, baseline
Run 12, high warming
Run 13, high warming, low wind
Run 14, high warming, high WSEL
Run 15, high warming, high flux

Figure A.314

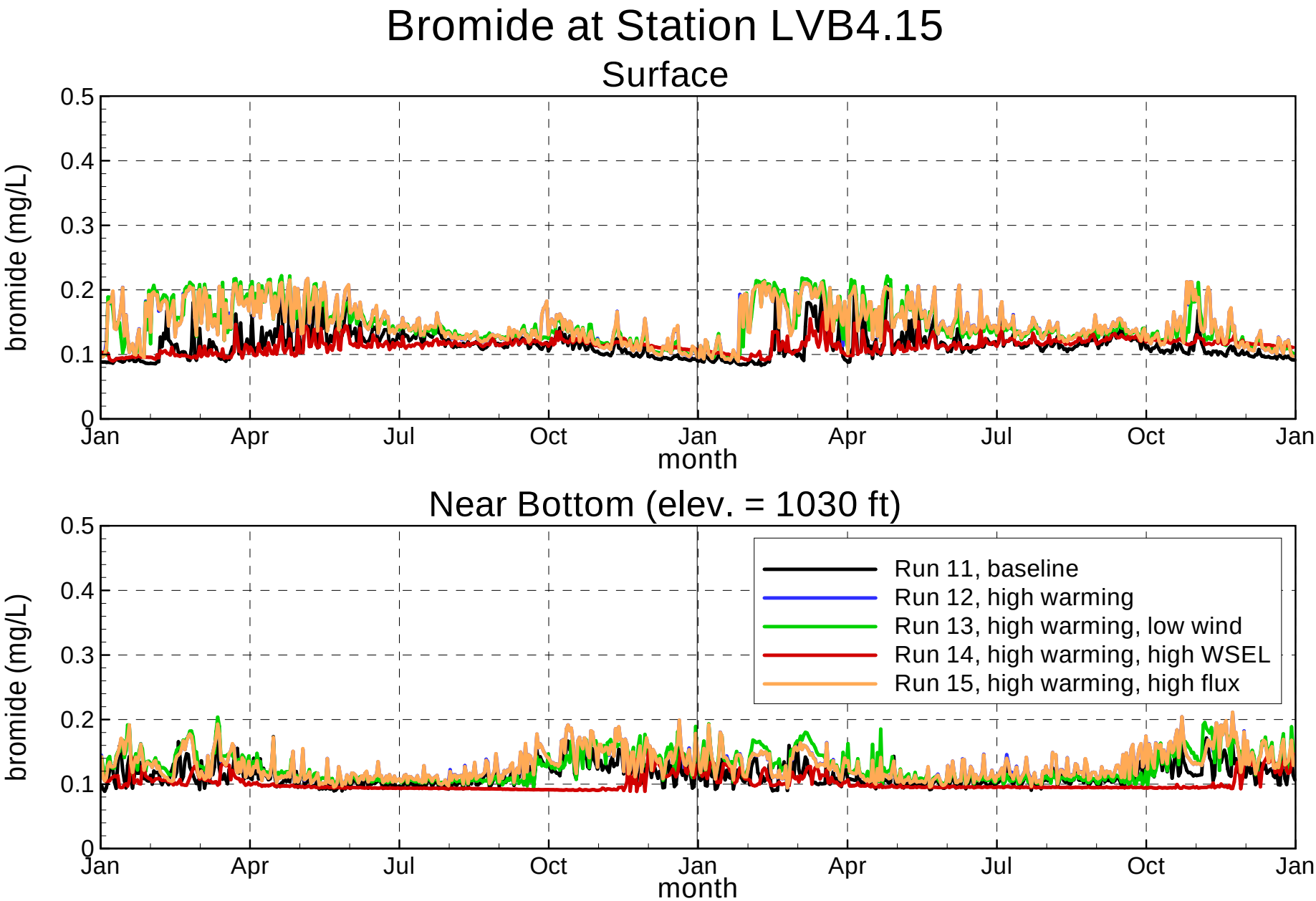
Bromide at Station LVB4.15
Surface
bromide (mg/L)
0.5
0.4
0.3
0.2
0.1
0
Jan
Apr
Jul
Oct
Jan
Apr
Jul
Oct
Jan
month
Near Bottom (elev. = 1030 ft)
bromide (mg/L)
0.5
0.4
0.3
0.2
0.1
0
Jan
Apr
Jul
Oct
Jan
Apr
Jul
Oct
Jan
month
Run 11, baseline
Run 12, high warming
Run 13, high warming, low wind
Run 14, high warming, high WSEL
Run 15, high warming, high flux

Figure A.315

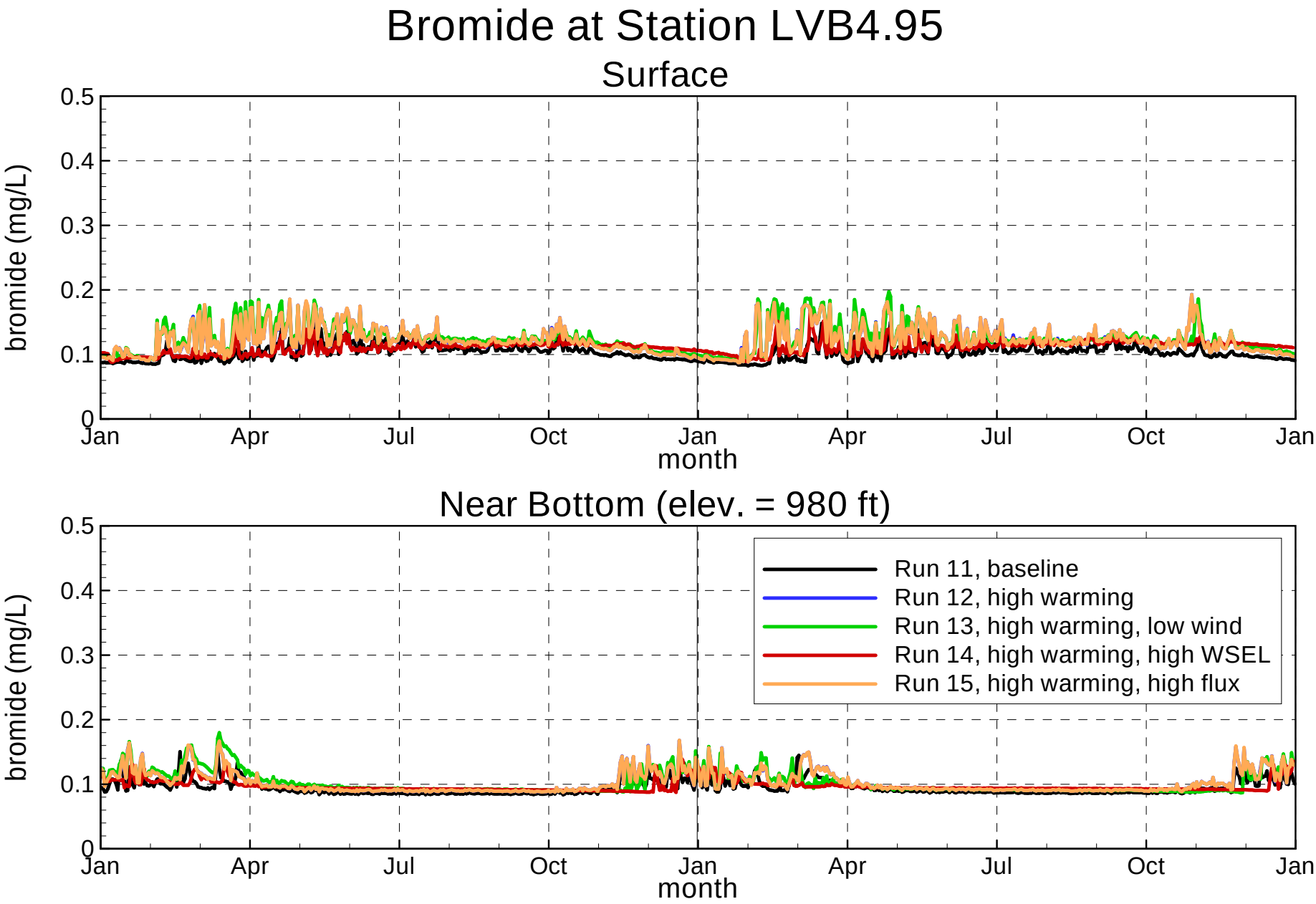
Bromide at Station LVB4.95
Surface
bromide (mg/L)
0.5
0.4
0.3
0.2
0.1
0
Jan
Apr
Jul
Oct
Jan
Apr
Jul
Oct
Jan
month
Near Bottom (elev. = 980 ft)
bromide (mg/L)
0.5
0.4
0.3
0.2
0.1
0
Jan
Apr
Jul
Oct
Jan
Apr
Jul
Oct
Jan
month
Run 11, baseline
Run 12, high warming
Run 13, high warming, low wind
Run 14, high warming, high WSEL
Run 15, high warming, high flux

Figure A.316

Bromide at Station LVB6.7

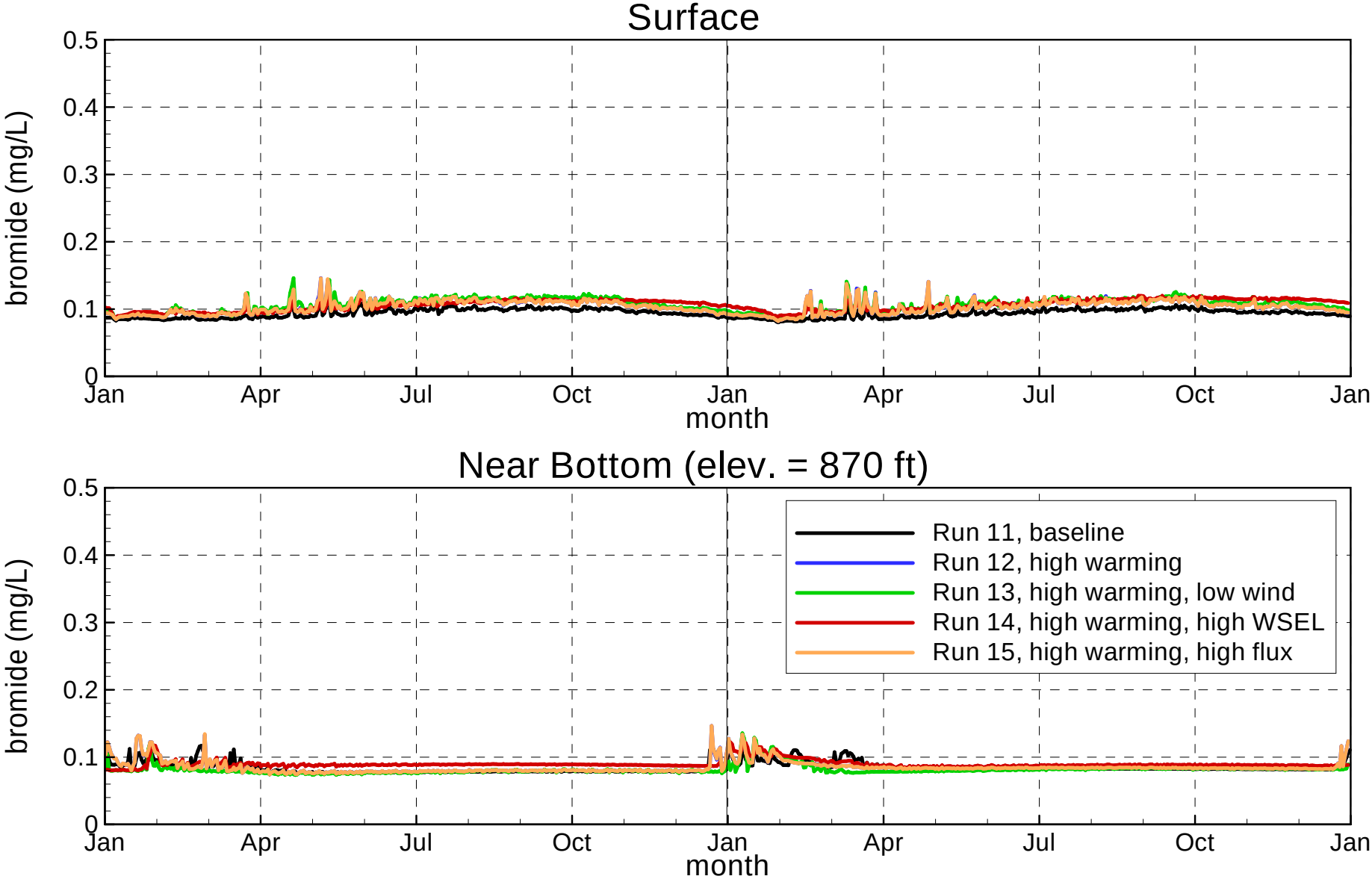

Figure A.317

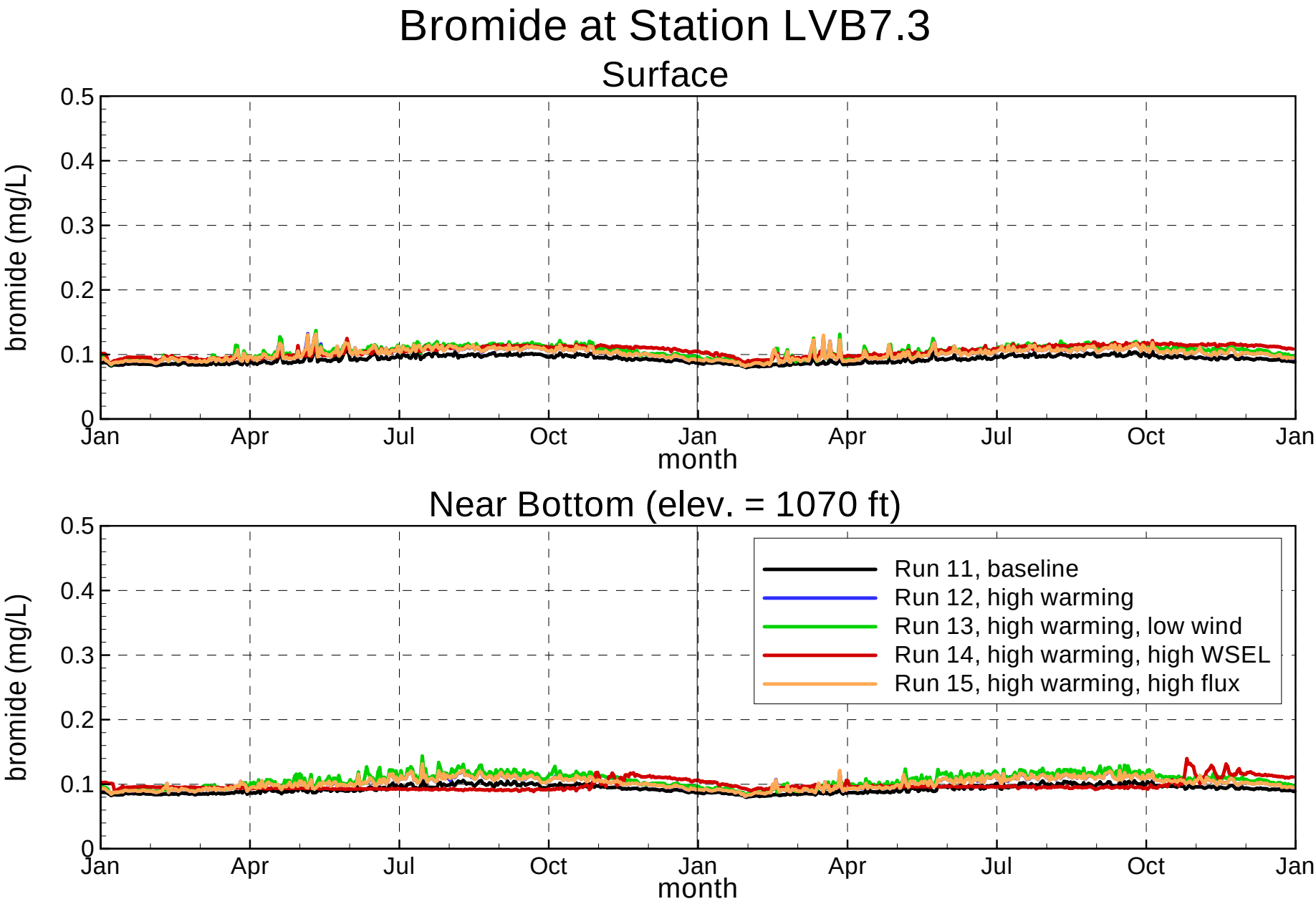
Bromide at Station LVB7.3
Surface
bromide (mg/L)
0.5
0.4
0.3
0.2
0.1
0
Jan
Apr
Jul
Oct
Jan
Apr
Jul
Oct
Jan
month
Near Bottom (elev. = 1070 ft)
bromide (mg/L)
0.5
0.4
0.3
0.2
0.1
0
Jan
Apr
Jul
Oct
Jan
Apr
Jul
Oct
Jan
month
Run 11, baseline
Run 12, high warming
Run 13, high warming, low wind
Run 14, high warming, high WSEL
Run 15, high warming, high flux

Figure A.318

Bromide at SNWA Intake #3

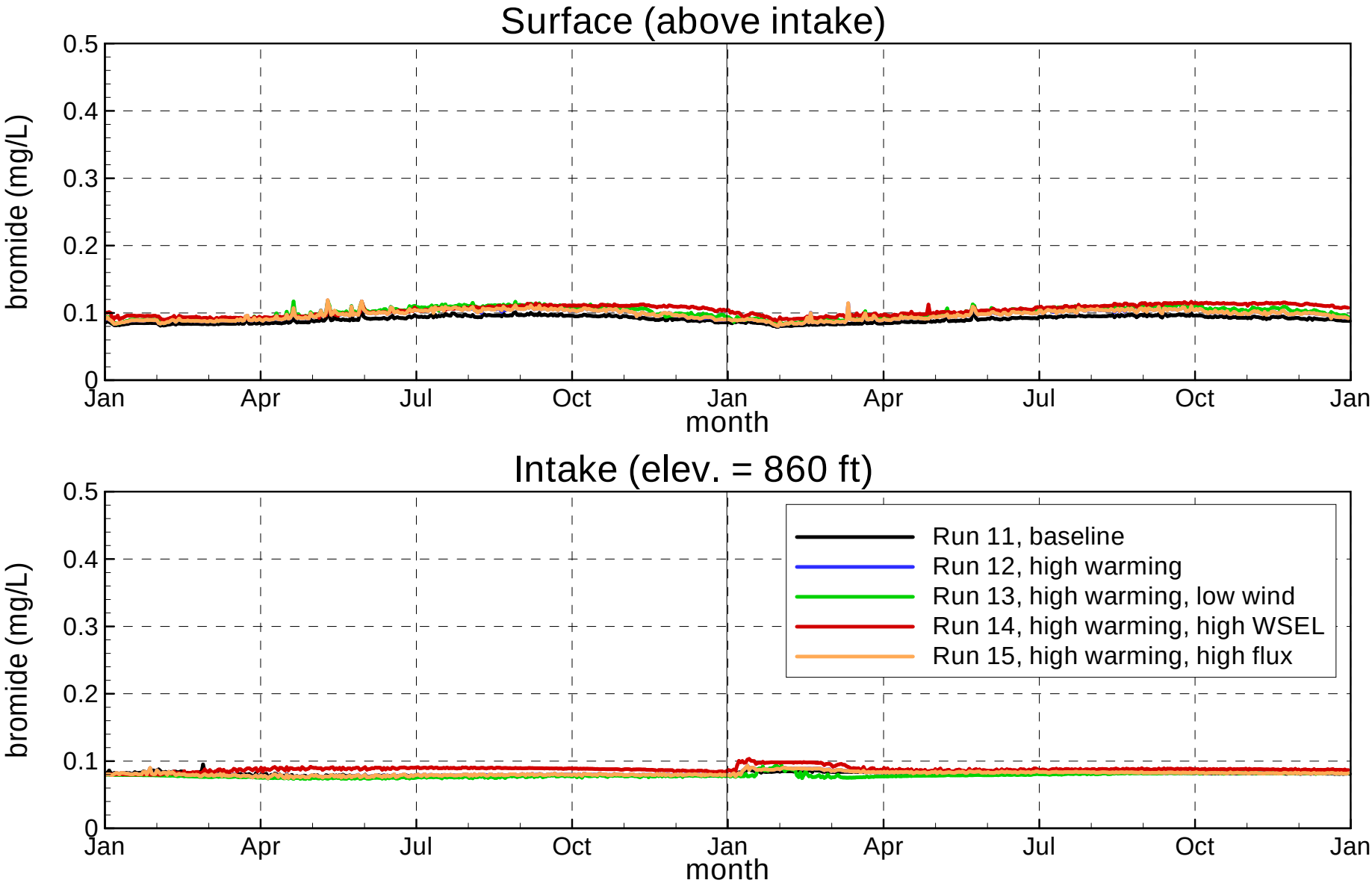

Figure A.319

FLOW SCIENCE

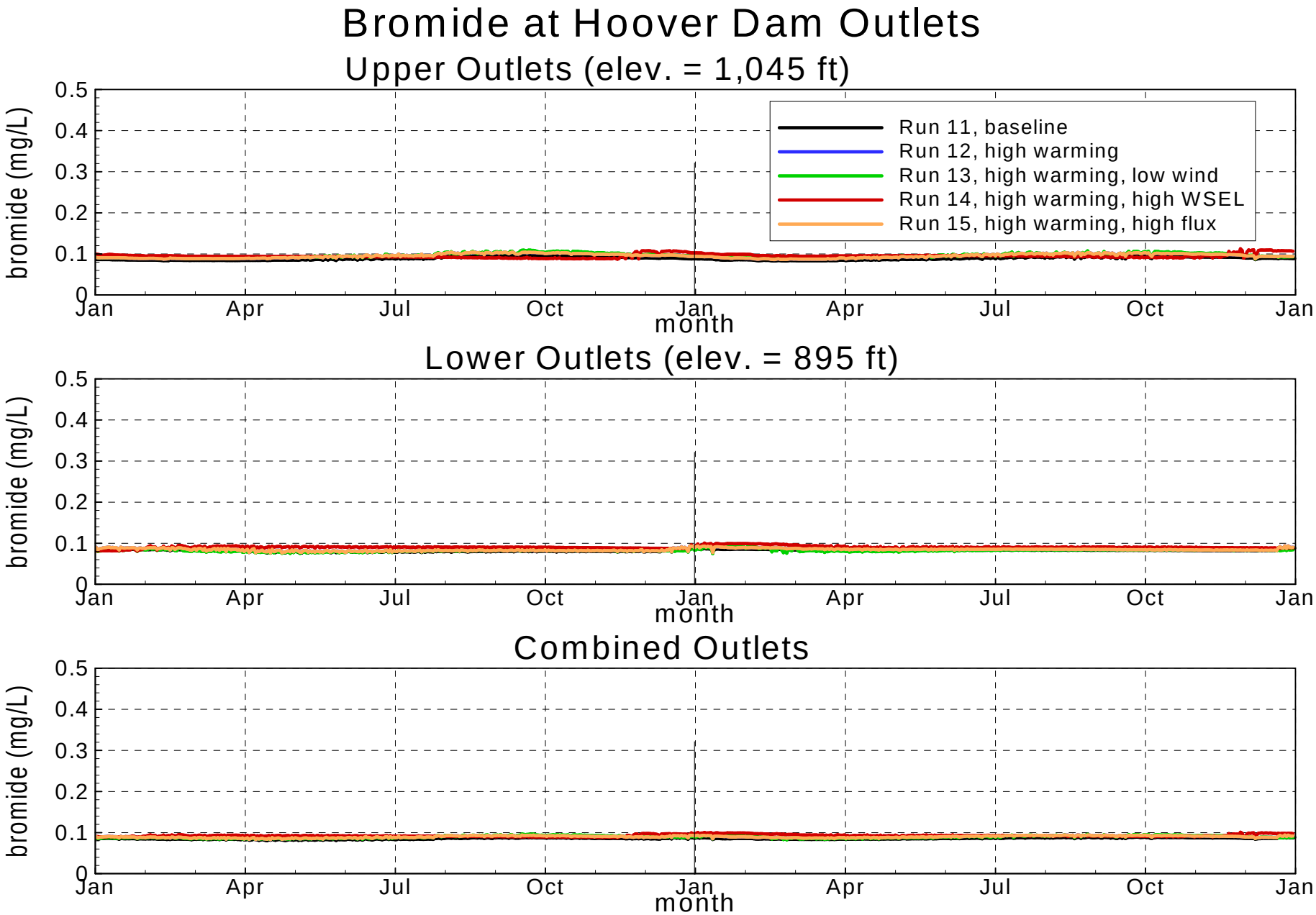

Figure A.320

FLOW SCIENCE

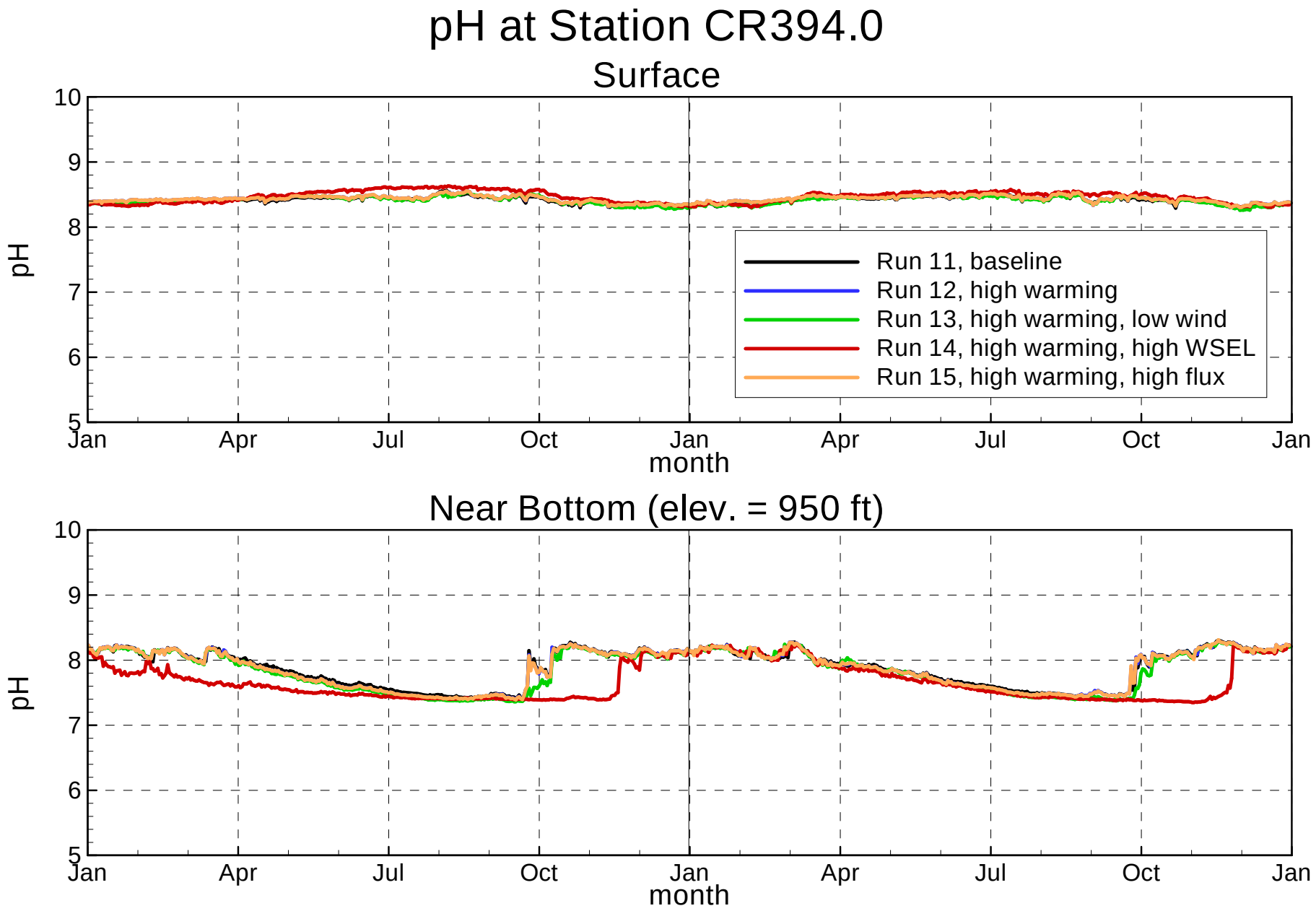
pH at Station CR394.0
Surface
Near Bottom (elev. = 950 ft)
pH
month
Jan
Apr
Jul
Oct
Jan
Apr
Jul
Oct
Jan
10
9
8
7
6
5
Run 11, baseline
Run 12, high warming
Run 13, high warming, low wind
Run 14, high warming, high WSEL
Run 15, high warming, high flux

Figure A.321

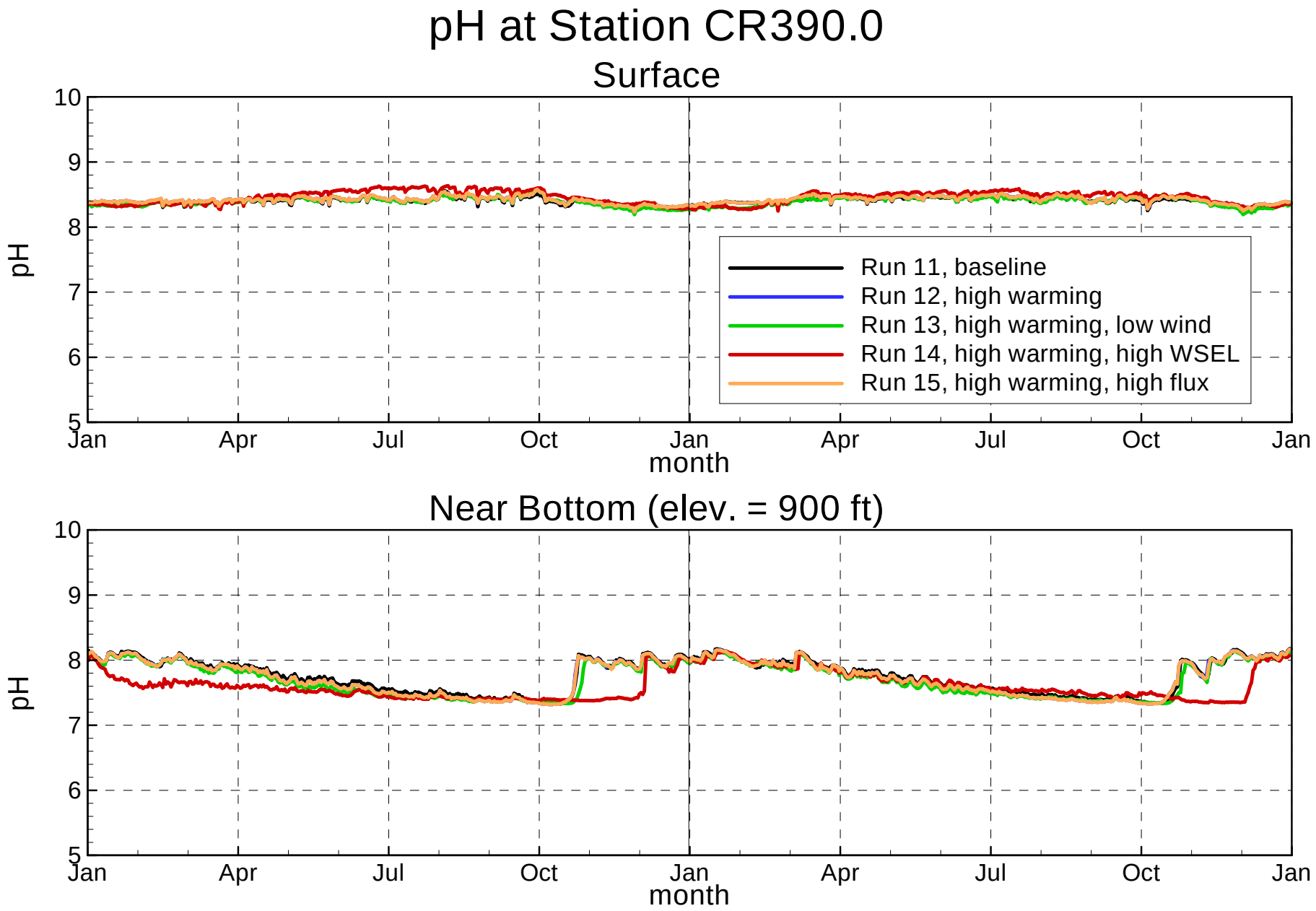
pH at Station CR390.0
Surface
Near Bottom (elev. = 900 ft)
pH
month
Jan
Apr
Jul
Oct
Run 11, baseline
Run 12, high warming
Run 13, high warming, low wind
Run 14, high warming, high WSEL
Run 15, high warming, high flux

Figure A.322

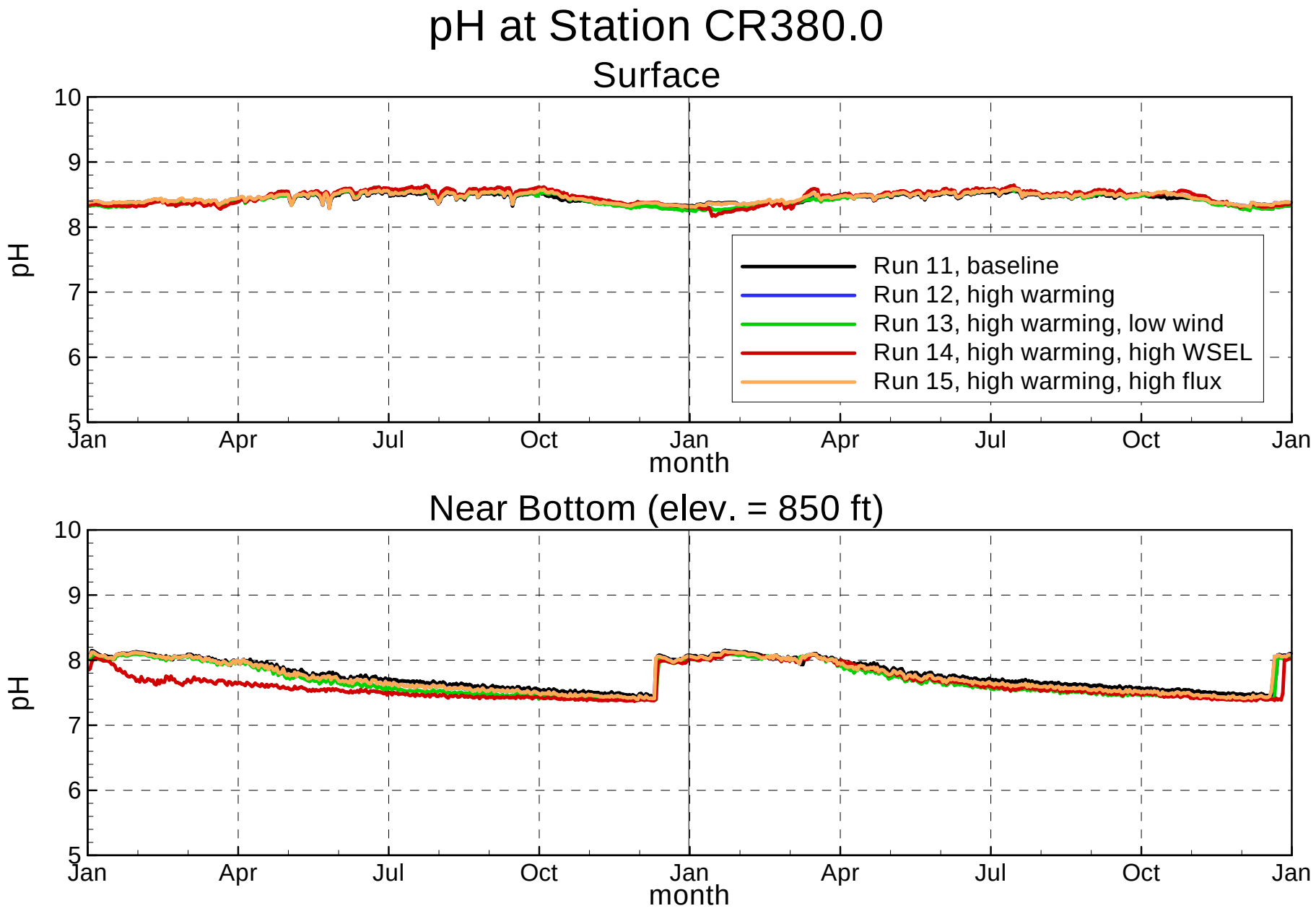
pH at Station CR380.0
Surface
Near Bottom (elev. = 850 ft)
pH
month
Jan
Apr
Jul
Oct
Jan
Apr
Jul
Oct
Jan
10
9
8
7
6
5
Run 11, baseline
Run 12, high warming
Run 13, high warming, low wind
Run 14, high warming, high WSEL
Run 15, high warming, high flux

Figure A.323

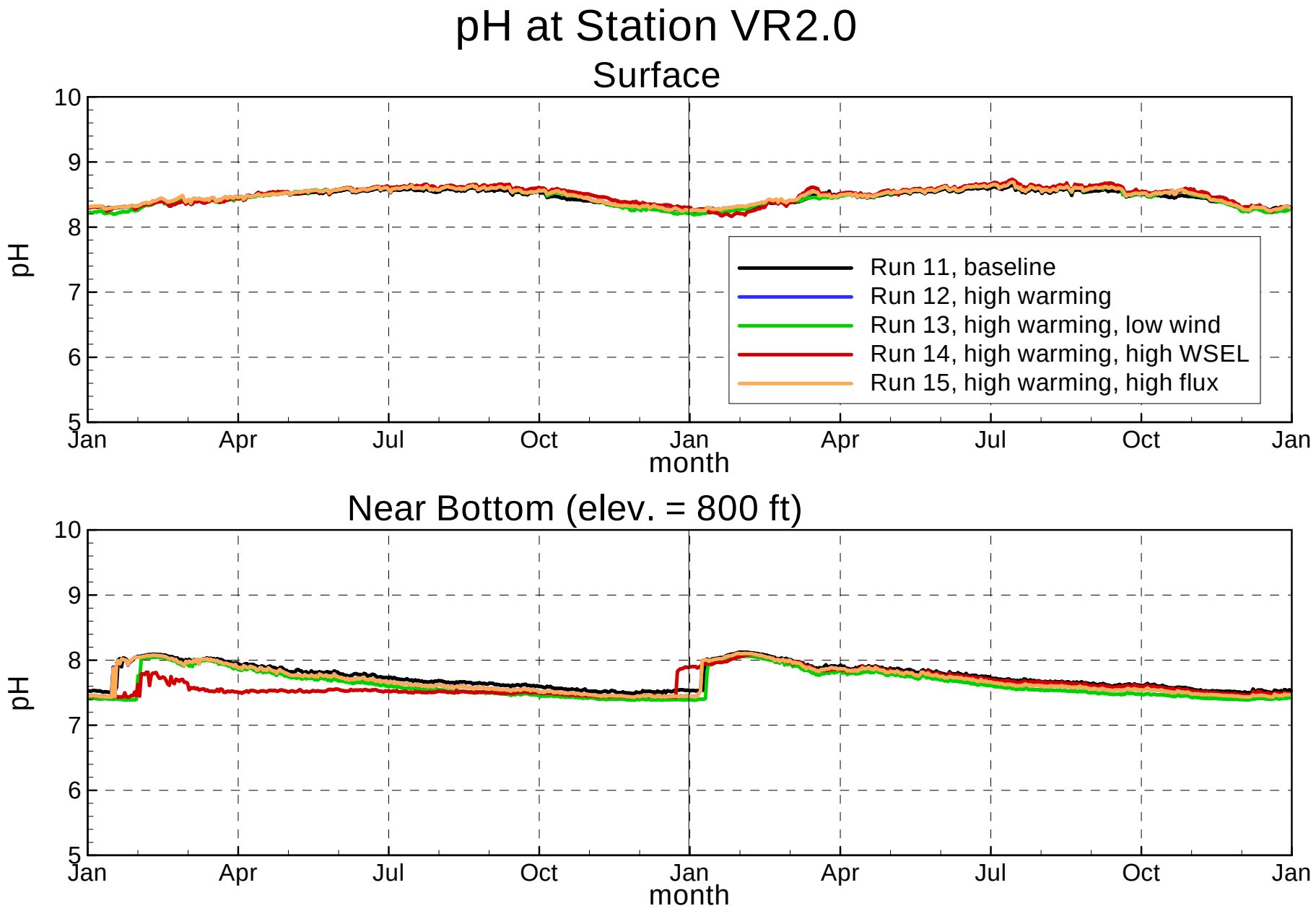
pH at Station VR2.0
Surface
Near Bottom (elev. = 800 ft)
pH
month
Jan
Apr
Jul
Oct
Jan
Apr
Jul
Oct
Jan
10
9
8
7
6
5
Run 11, baseline
Run 12, high warming
Run 13, high warming, low wind
Run 14, high warming, high WSEL
Run 15, high warming, high flux

Figure A.324

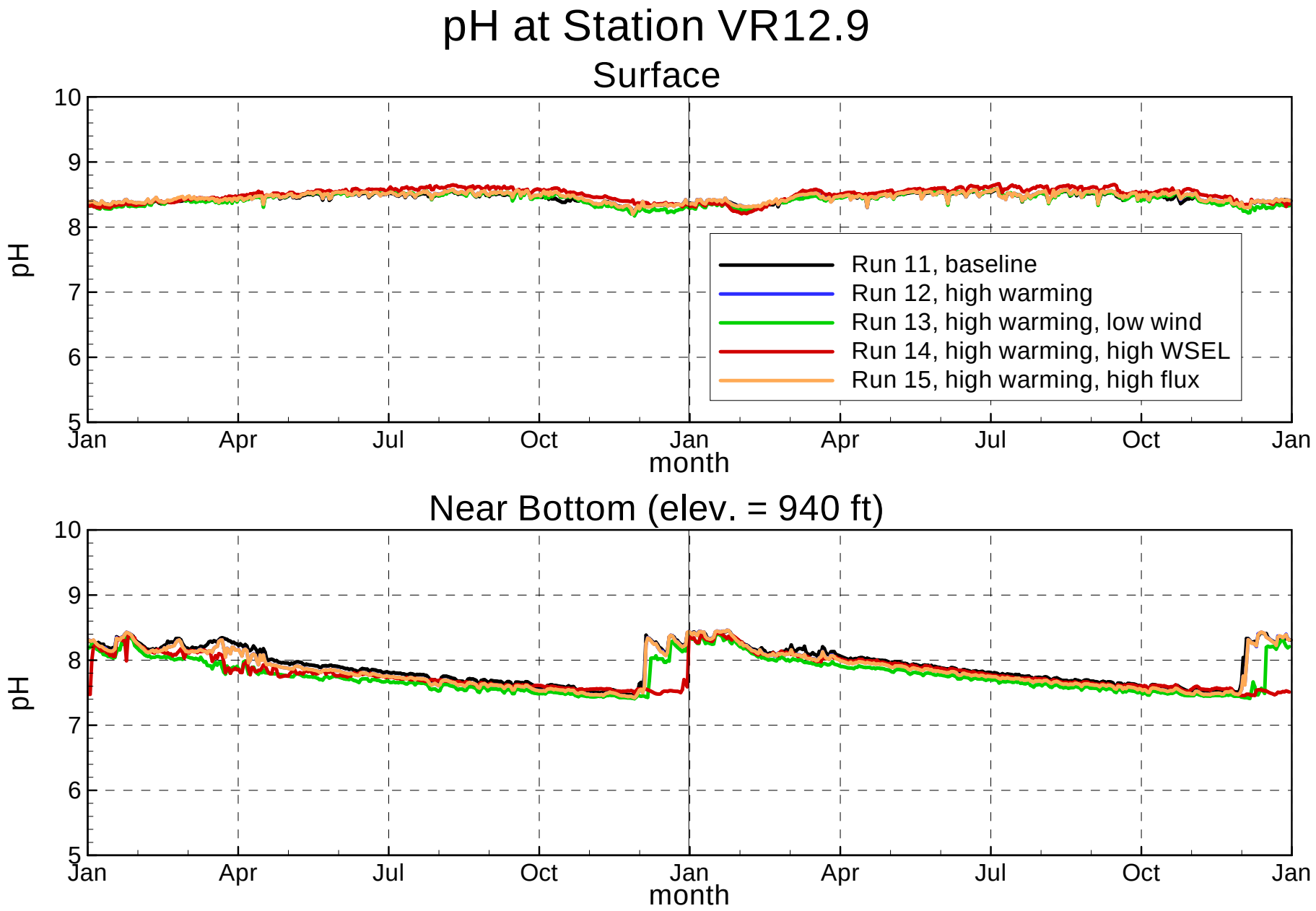
pH at Station VR12.9
Surface
10
9
8
7
6
5
pH
Jan
Apr
Jul
Oct
Jan
Apr
Jul
Oct
Jan
month
Run 11, baseline
Run 12, high warming
Run 13, high warming, low wind
Run 14, high warming, high WSEL
Run 15, high warming, high flux
Near Bottom (elev. = 940 ft)
10
9
8
7
6
5
pH
Jan
Apr
Jul
Oct
Jan
Apr
Jul
Oct
Jan
month

Figure A.325

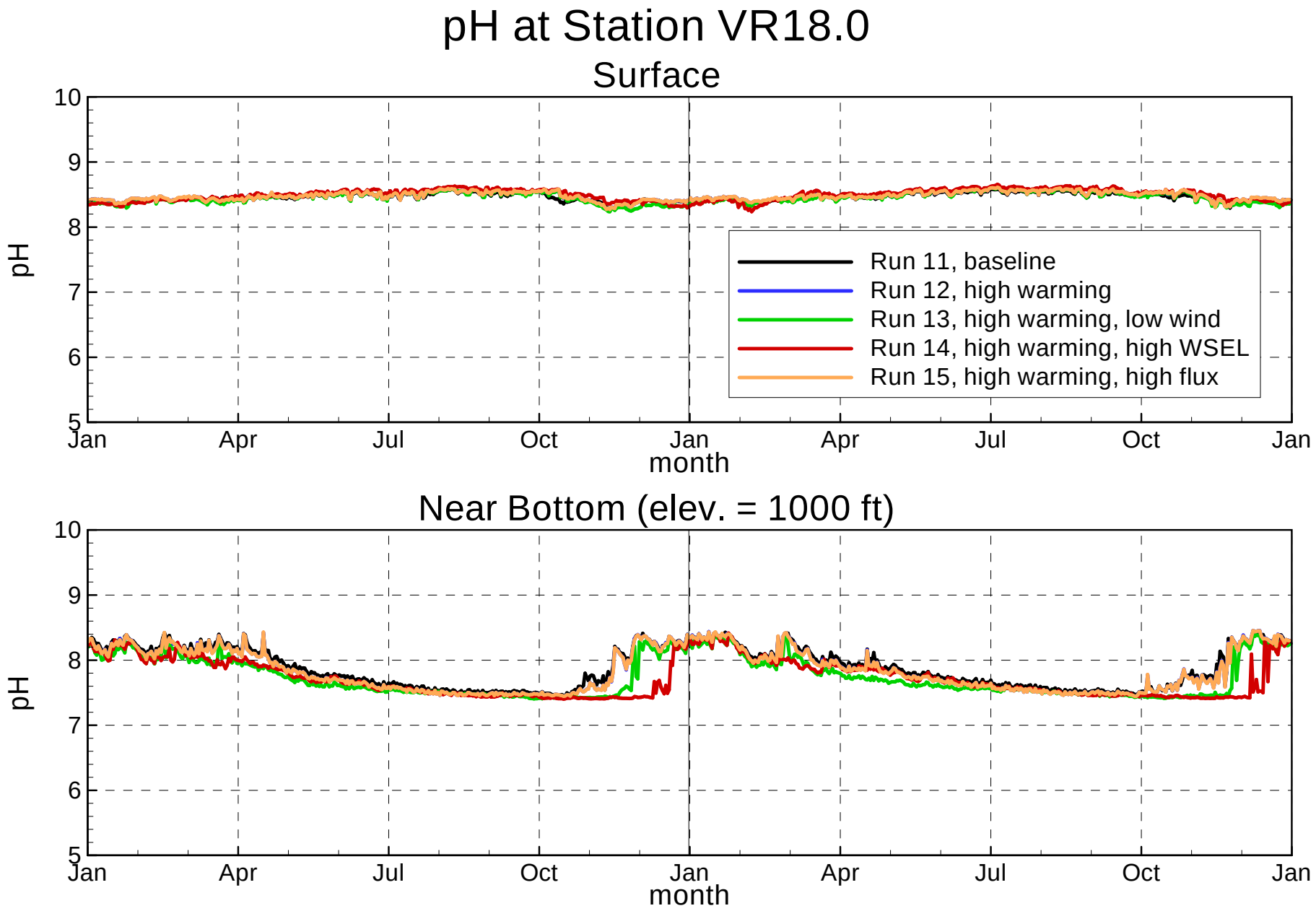
pH at Station VR18.0
Surface
10
9
8
7
6
5
pH
Jan
Apr
Jul
Oct
Jan
Apr
Jul
Oct
Jan
month
Run 11, baseline
Run 12, high warming
Run 13, high warming, low wind
Run 14, high warming, high WSEL
Run 15, high warming, high flux
Near Bottom (elev. = 1000 ft)
10
9
8
7
6
5
pH
Jan
Apr
Jul
Oct
Jan
Apr
Jul
Oct
Jan
month

Figure A.326

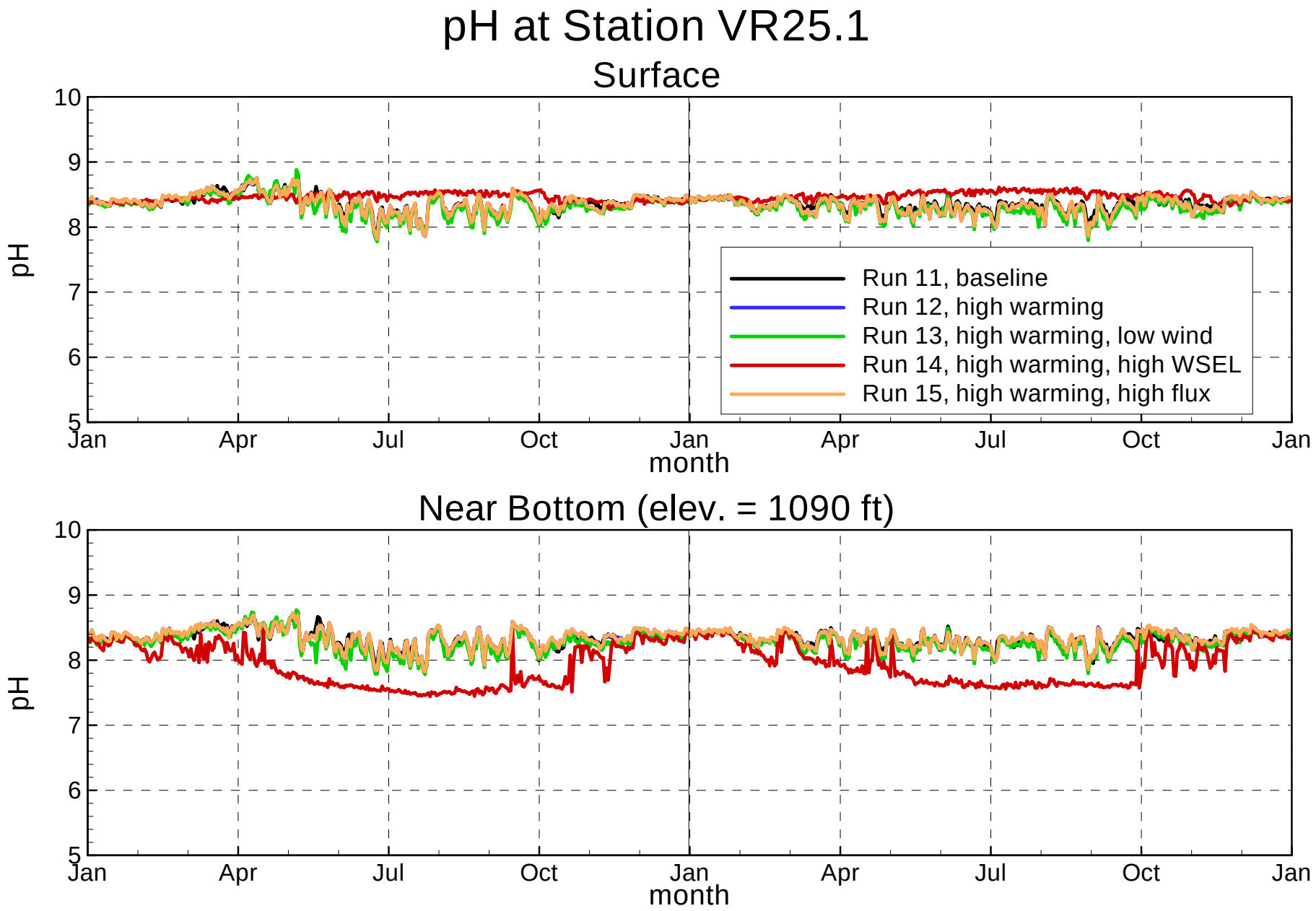
pH at Station VR25.1
Surface
Near Bottom (elev. = 1090 ft)
pH
month
Jan
Apr
Jul
Oct
Run 11, baseline
Run 12, high warming
Run 13, high warming, low wind
Run 14, high warming, high WSEL
Run 15, high warming, high flux

Figure A.327

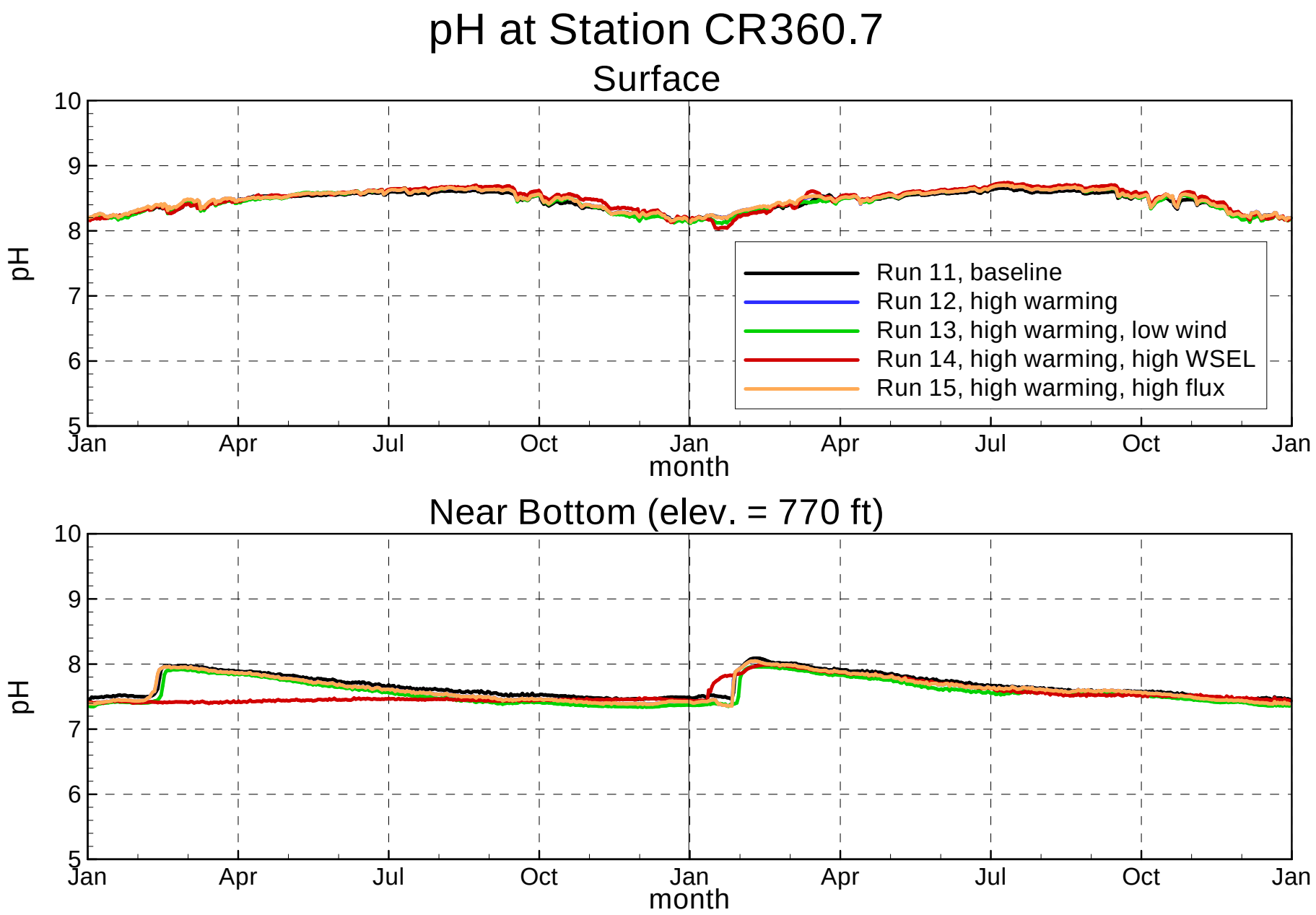
pH at Station CR360.7
Surface
Near Bottom (elev. = 770 ft)
pH
month
Jan
Apr
Jul
Oct
Run 11, baseline
Run 12, high warming
Run 13, high warming, low wind
Run 14, high warming, high WSEL
Run 15, high warming, high flux

Figure A.328

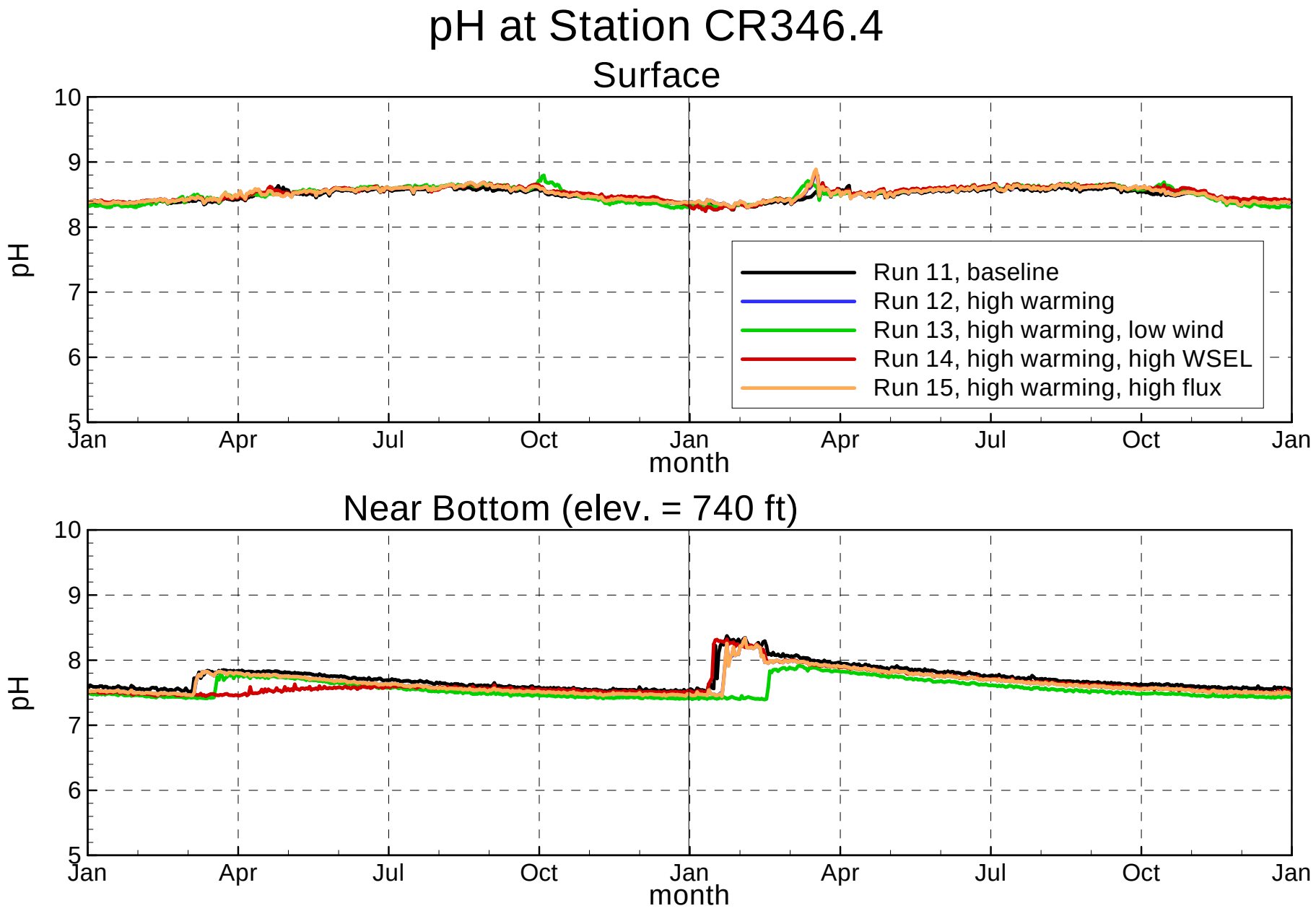
pH at Station CR346.4
Surface
Near Bottom (elev. = 740 ft)
pH
month
Jan
Apr
Jul
Oct
Jan
Apr
Jul
Oct
Jan
10
9
8
7
6
5
Run 11, baseline
Run 12, high warming
Run 13, high warming, low wind
Run 14, high warming, high WSEL
Run 15, high warming, high flux

Figure A.329

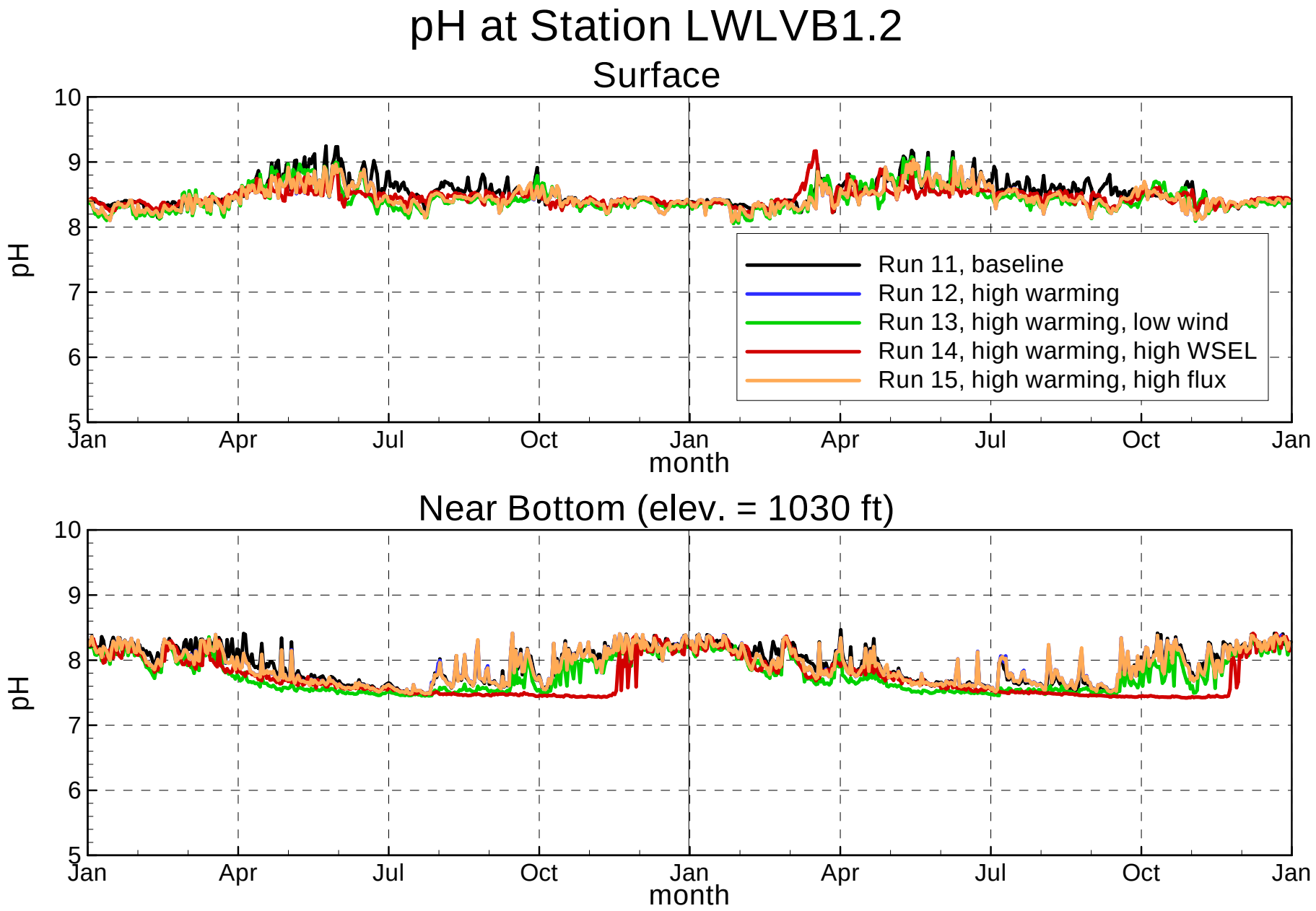
pH at Station LWLVB1.2
Surface
Near Bottom (elev. = 1030 ft)
pH
month
Jan
Apr
Jul
Oct
Run 11, baseline
Run 12, high warming
Run 13, high warming, low wind
Run 14, high warming, high WSEL
Run 15, high warming, high flux

Figure A.330

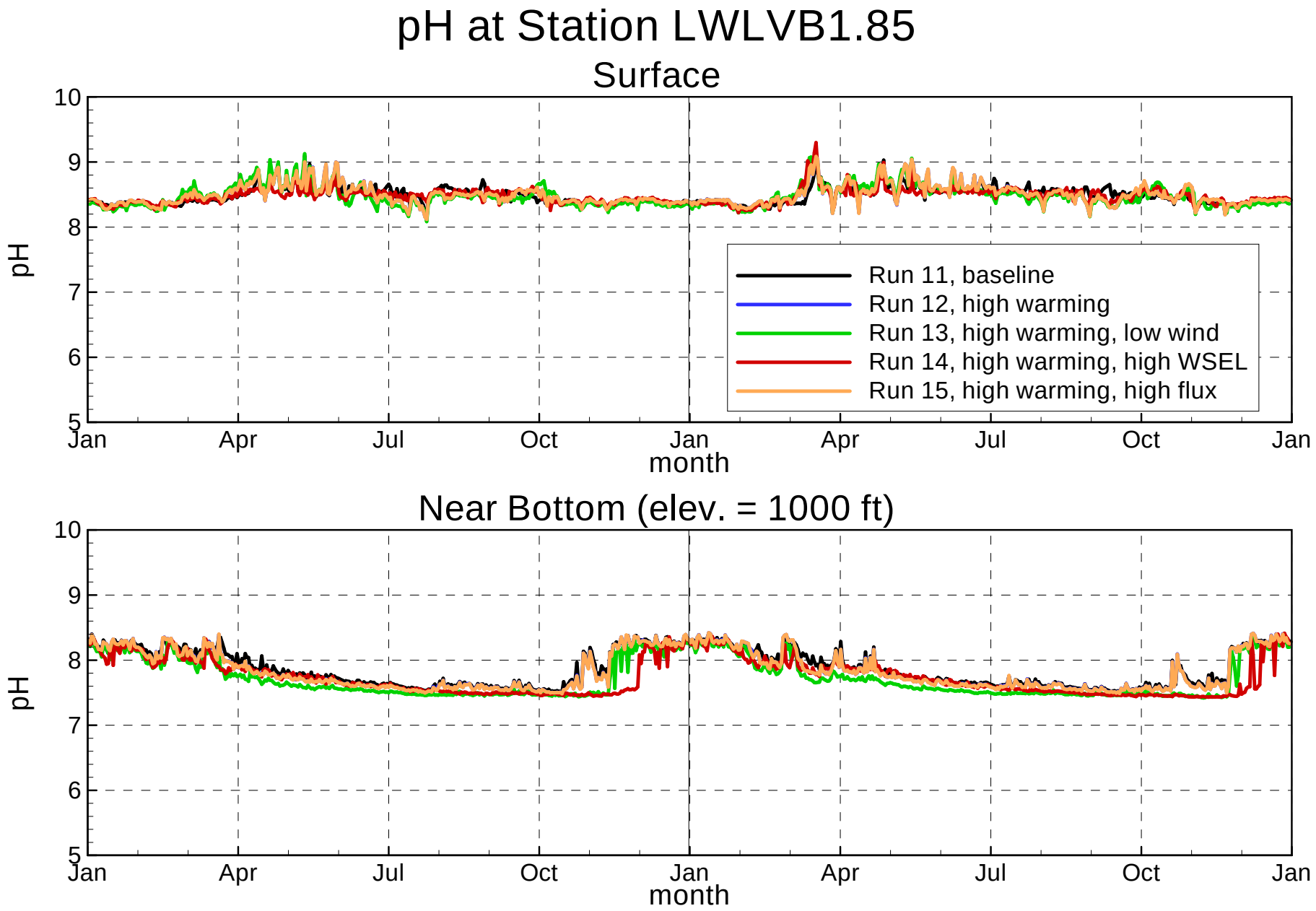
pH at Station LWLVB1.85
Surface
Near Bottom (elev. = 1000 ft)
pH
month
Jan
Apr
Jul
Oct
Jan
Apr
Jul
Oct
Jan
10
9
8
7
6
5
Run 11, baseline
Run 12, high warming
Run 13, high warming, low wind
Run 14, high warming, high WSEL
Run 15, high warming, high flux

Figure A.331

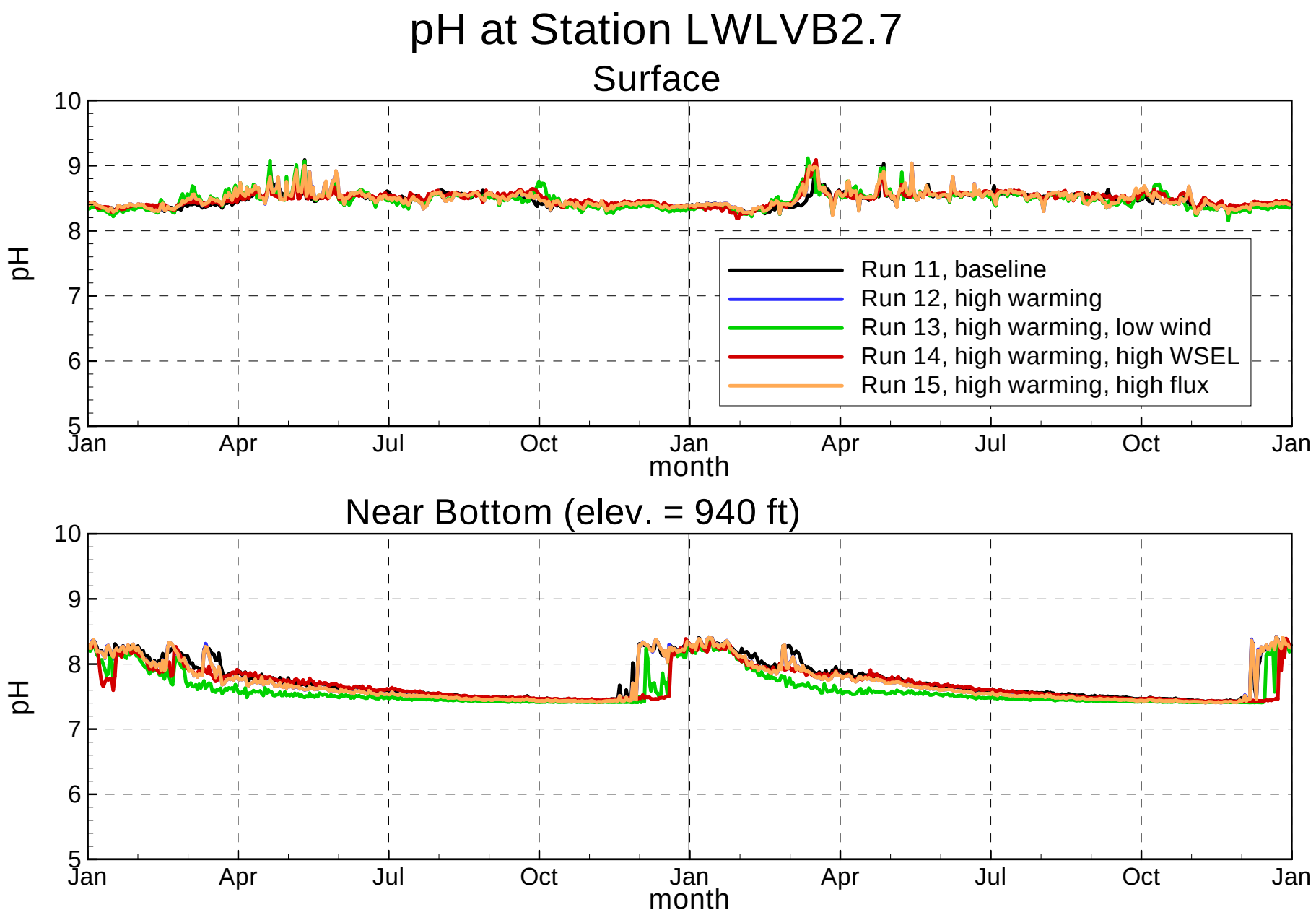
pH at Station LWLVB2.7
Surface
Near Bottom (elev. = 940 ft)
pH
month
Jan
Apr
Jul
Oct
Run 11, baseline
Run 12, high warming
Run 13, high warming, low wind
Run 14, high warming, high WSEL
Run 15, high warming, high flux

Figure A.332

pH at Station LWLVB3.5

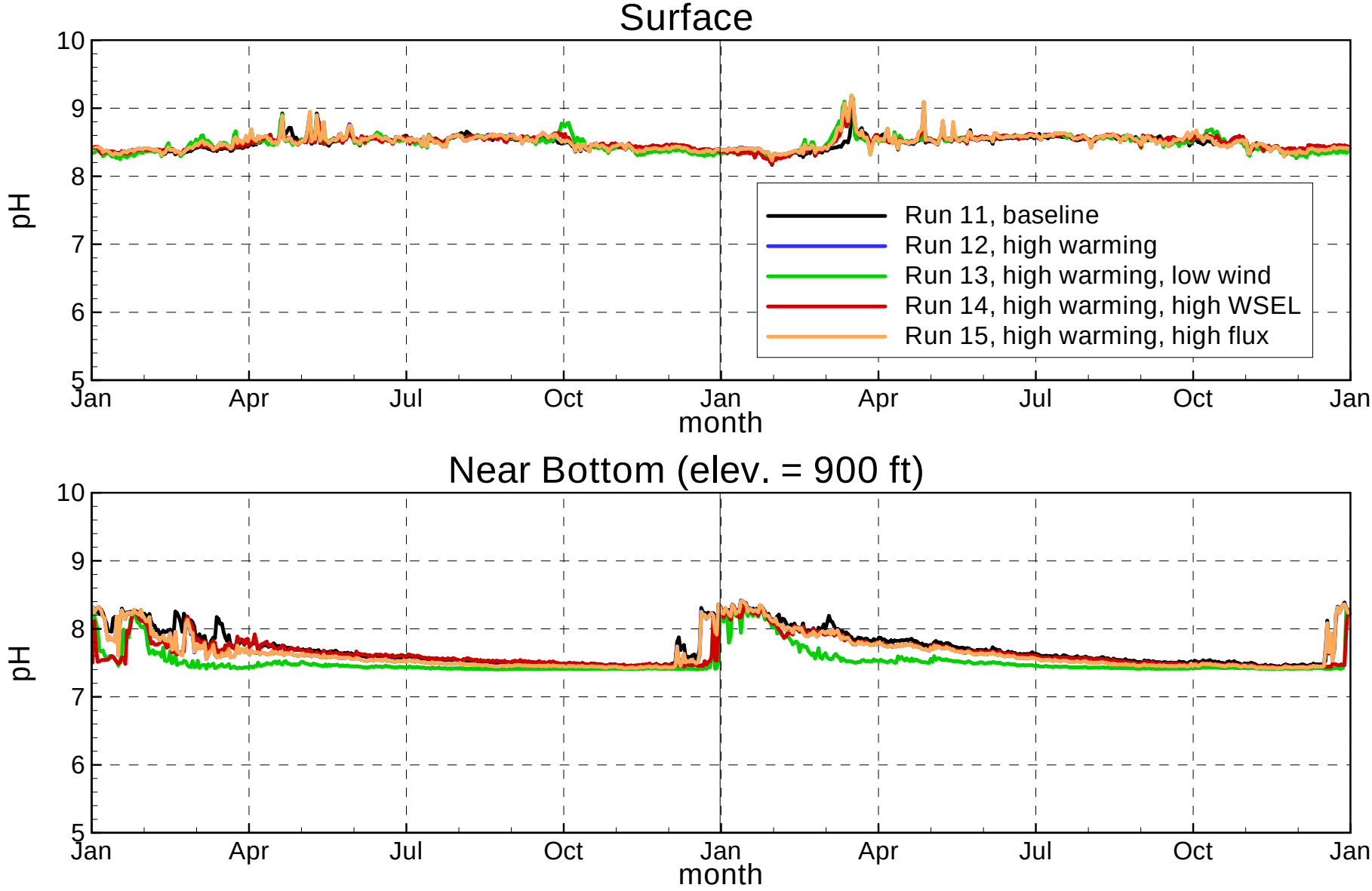

Figure A.333

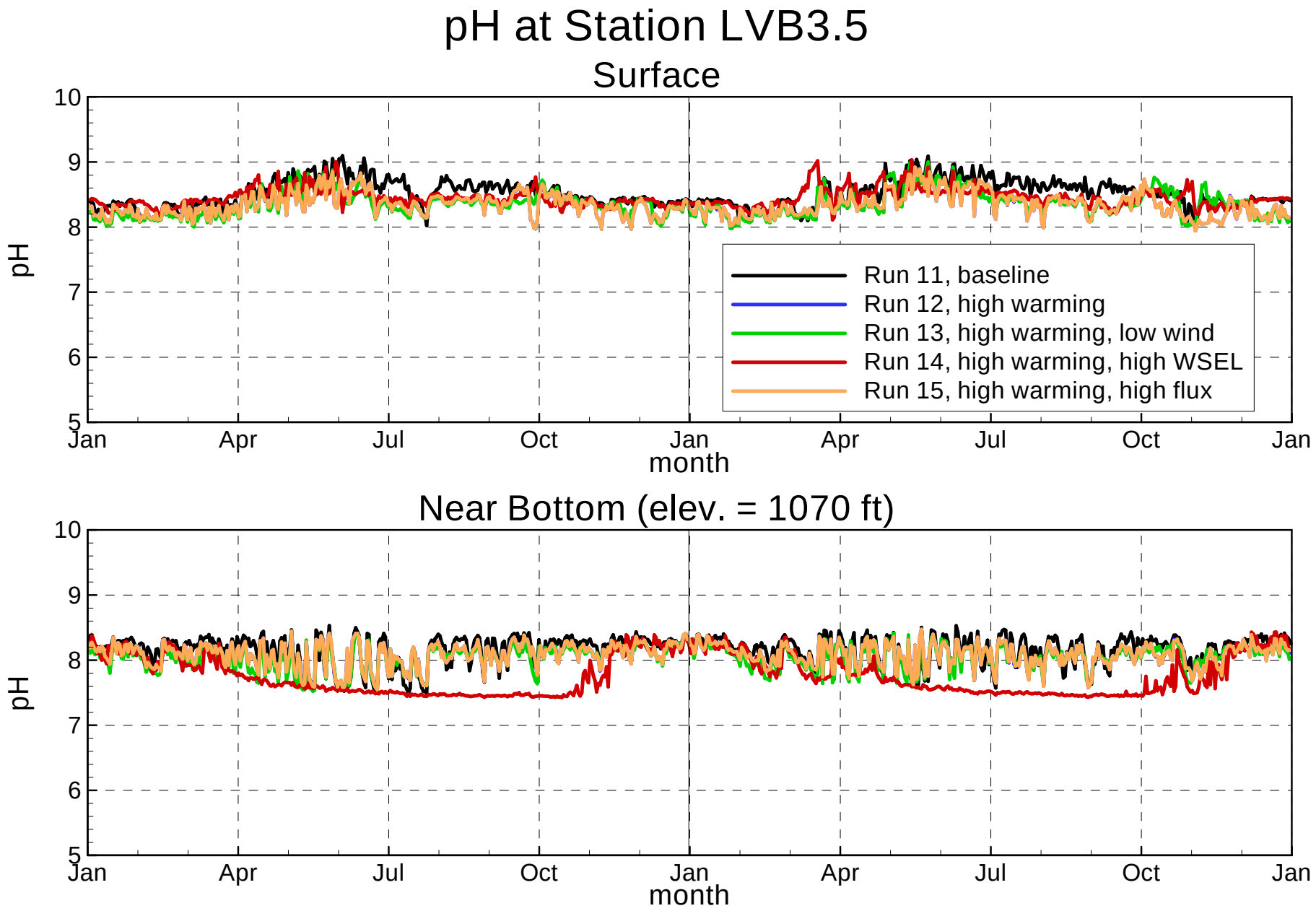
pH at Station LVB3.5
Surface
Near Bottom (elev. = 1070 ft)
pH
month
Jan
Apr
Jul
Oct
Run 11, baseline
Run 12, high warming
Run 13, high warming, low wind
Run 14, high warming, high WSEL
Run 15, high warming, high flux

Figure A.334

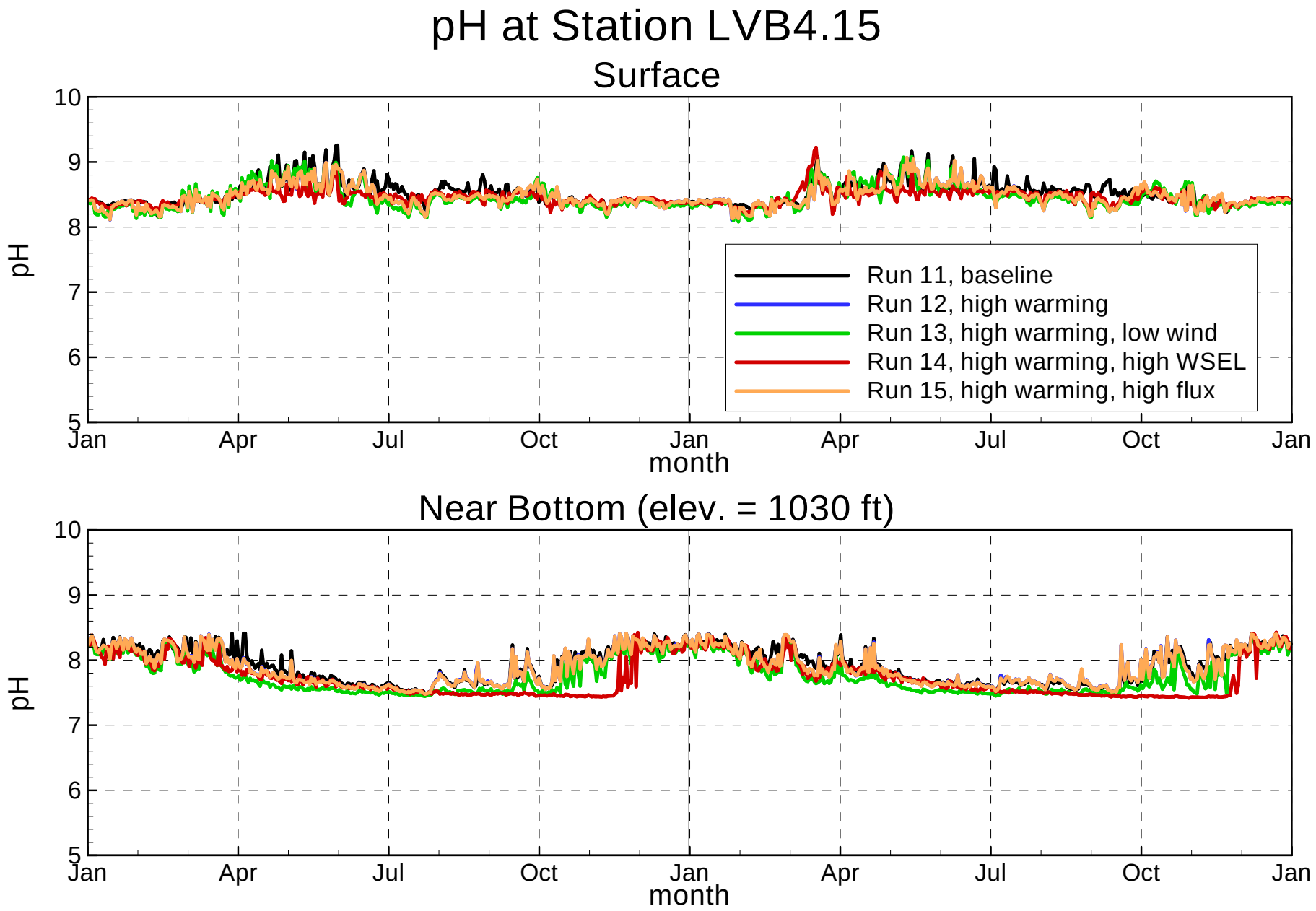
pH at Station LVB4.15
Surface
Near Bottom (elev. = 1030 ft)
pH
month
Jan
Apr
Jul
Oct
Run 11, baseline
Run 12, high warming
Run 13, high warming, low wind
Run 14, high warming, high WSEL
Run 15, high warming, high flux

Figure A.335

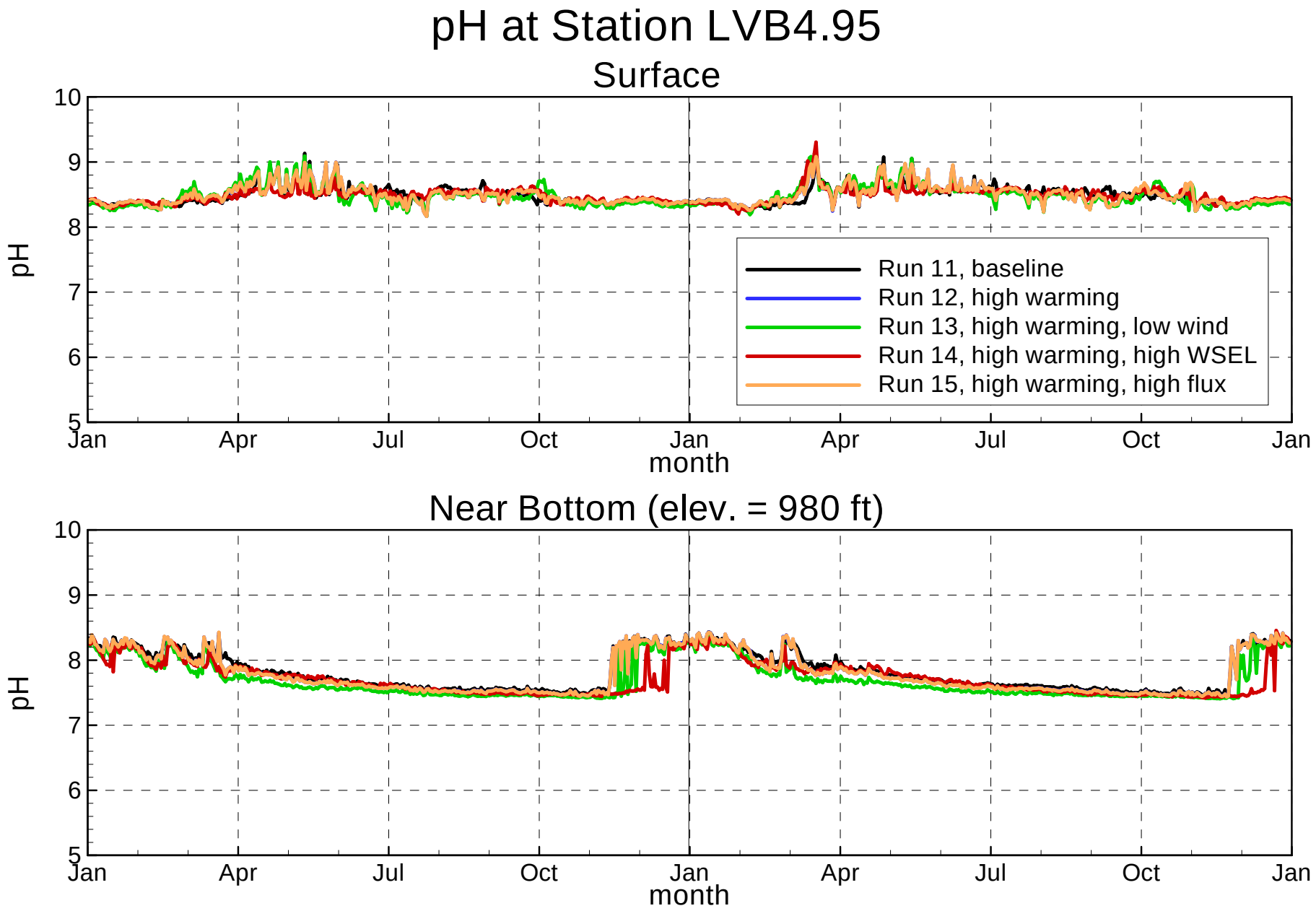
pH at Station LVB4.95
Surface
Near Bottom (elev. = 980 ft)
pH
month
Jan
Apr
Jul
Oct
Run 11, baseline
Run 12, high warming
Run 13, high warming, low wind
Run 14, high warming, high WSEL
Run 15, high warming, high flux

Figure A.336

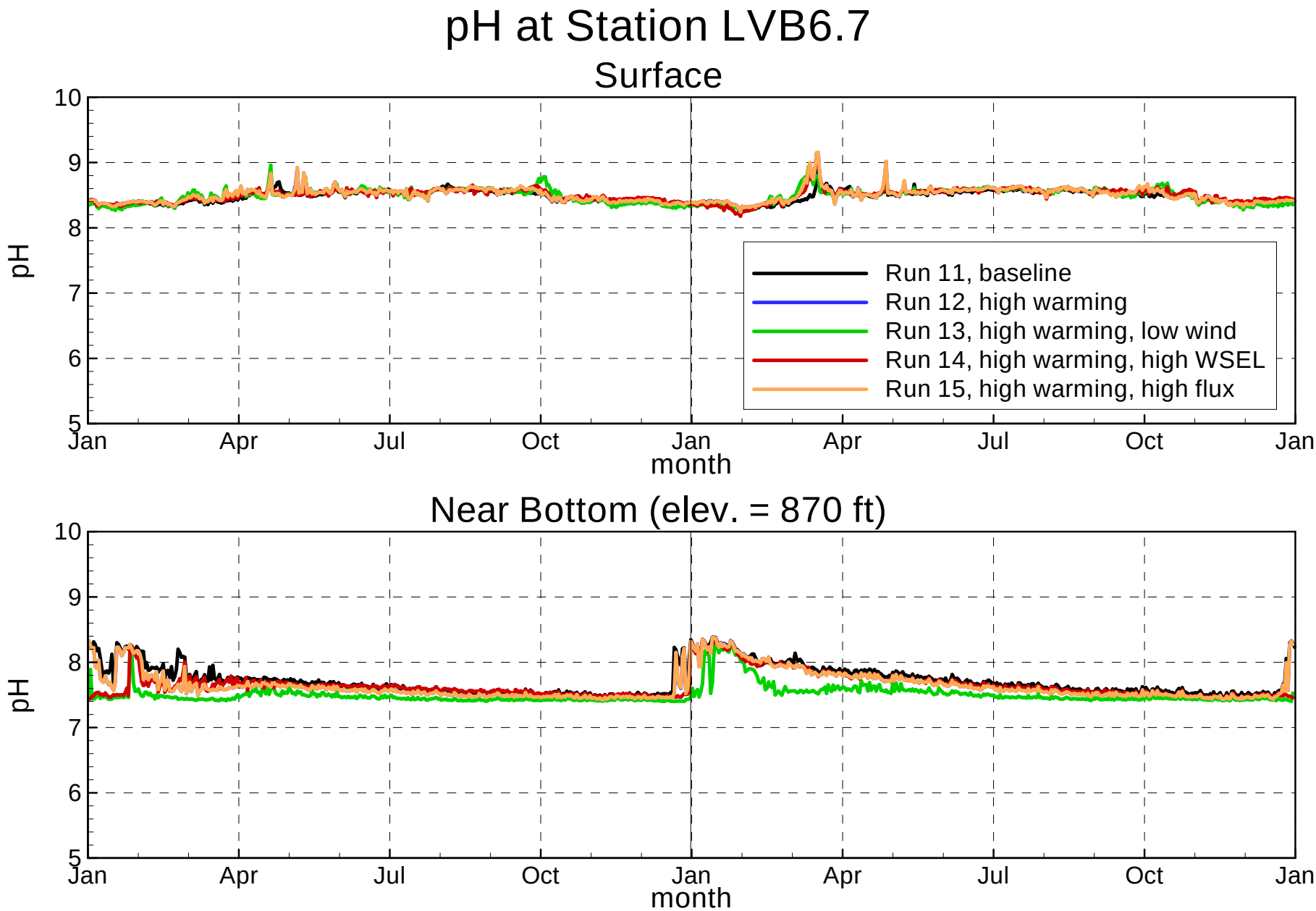
pH at Station LVB6.7
Surface
10
9
8
7
6
5
pH
Jan
Apr
Jul
Oct
Jan
Apr
Jul
Oct
Jan
month
Run 11, baseline
Run 12, high warming
Run 13, high warming, low wind
Run 14, high warming, high WSEL
Run 15, high warming, high flux
Near Bottom (elev. = 870 ft)
10
9
8
7
6
5
pH
Jan
Apr
Jul
Oct
Jan
Apr
Jul
Oct
Jan
month

Figure A.337

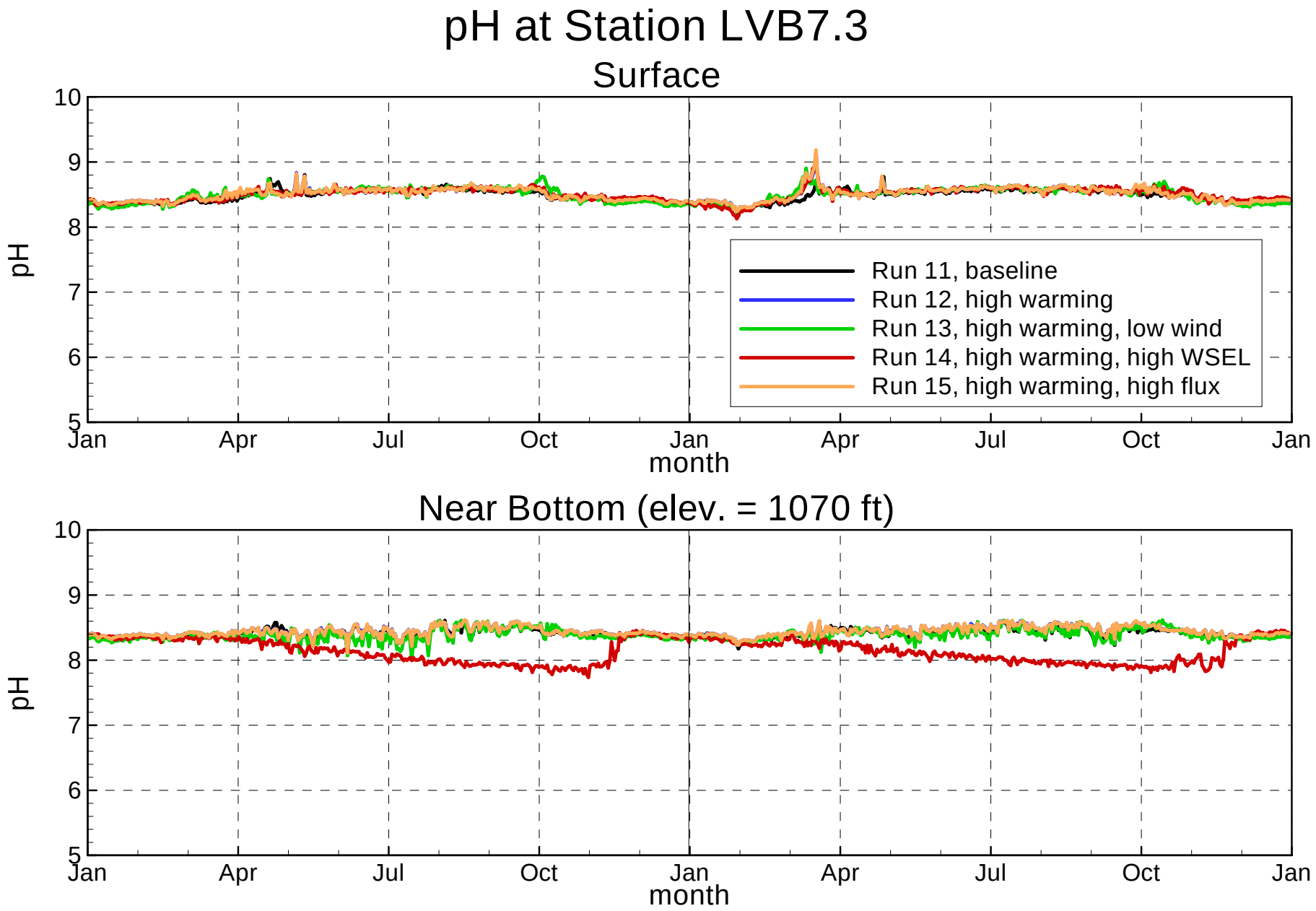
pH at Station LVB7.3
Surface
Near Bottom (elev. = 1070 ft)
pH
month
Jan
Apr
Jul
Oct
Run 11, baseline
Run 12, high warming
Run 13, high warming, low wind
Run 14, high warming, high WSEL
Run 15, high warming, high flux

Figure A.338

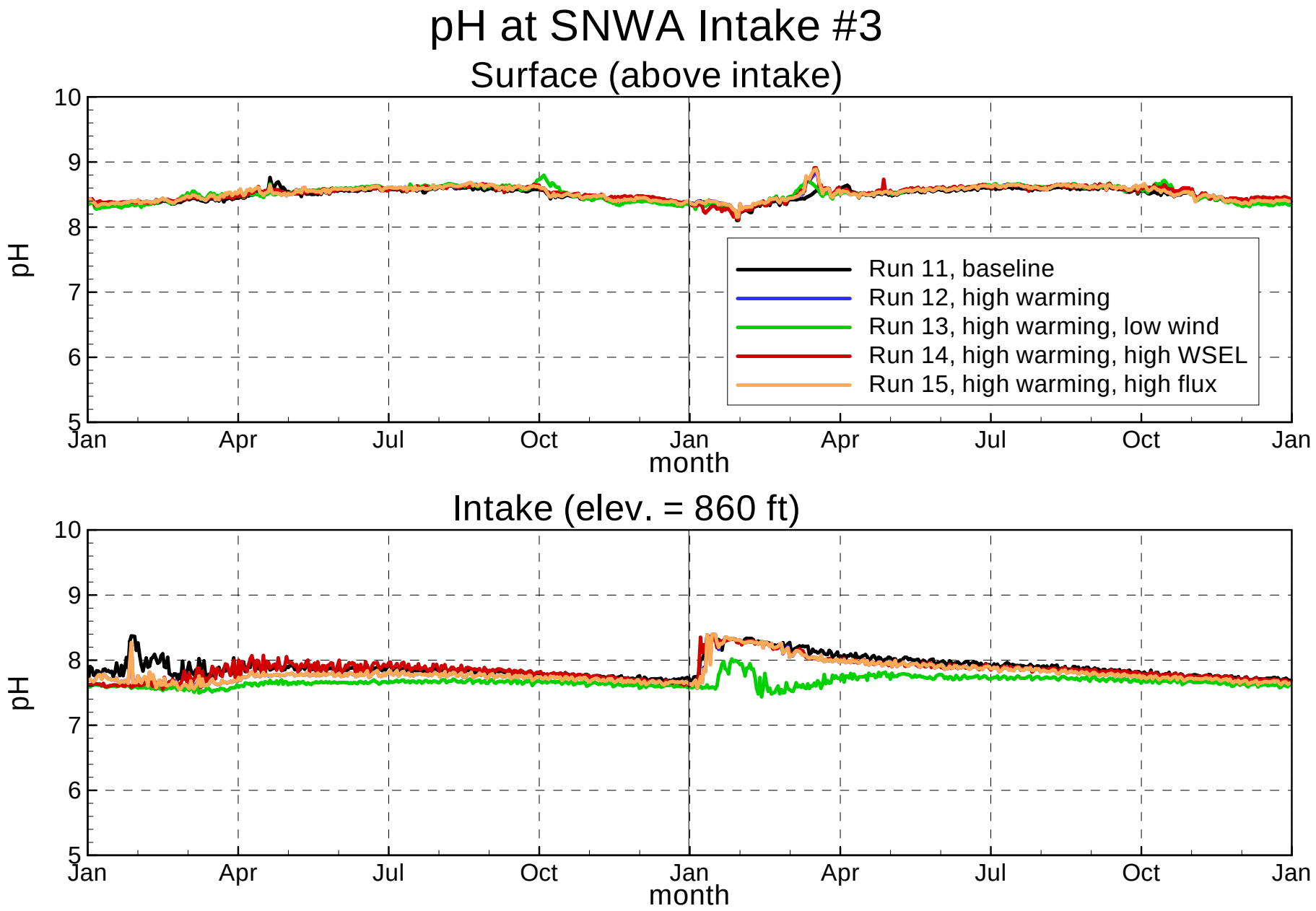
pH at SNWA Intake #3
Surface (above intake)
Intake (elev. = 860 ft)
pH
month
Jan
Apr
Jul
Oct
Run 11, baseline
Run 12, high warming
Run 13, high warming, low wind
Run 14, high warming, high WSEL
Run 15, high warming, high flux

Figure A.339

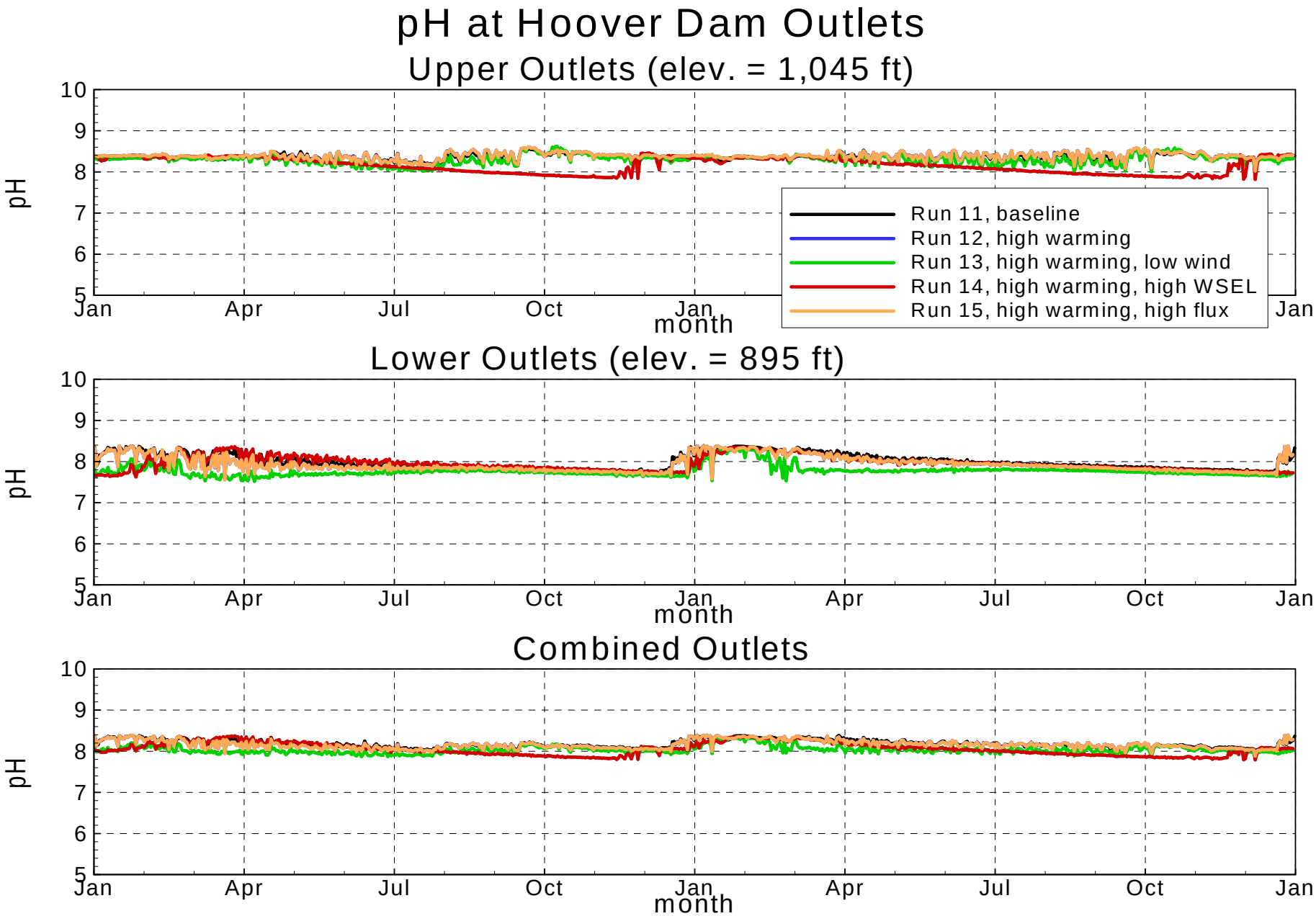
pH at Hoover Dam Outlets
Upper Outlets (elev. = 1,045 ft)
Lower Outlets (elev. = 895 ft)
Combined Outlets
pH
10
9
8
7
6
5
Jan
Apr
Jul
Oct
Jan
month
Run 11, baseline
Run 12, high warming
Run 13, high warming, low wind
Run 14, high warming, high WSEL
Run 15, high warming, high flux

Figure A.340

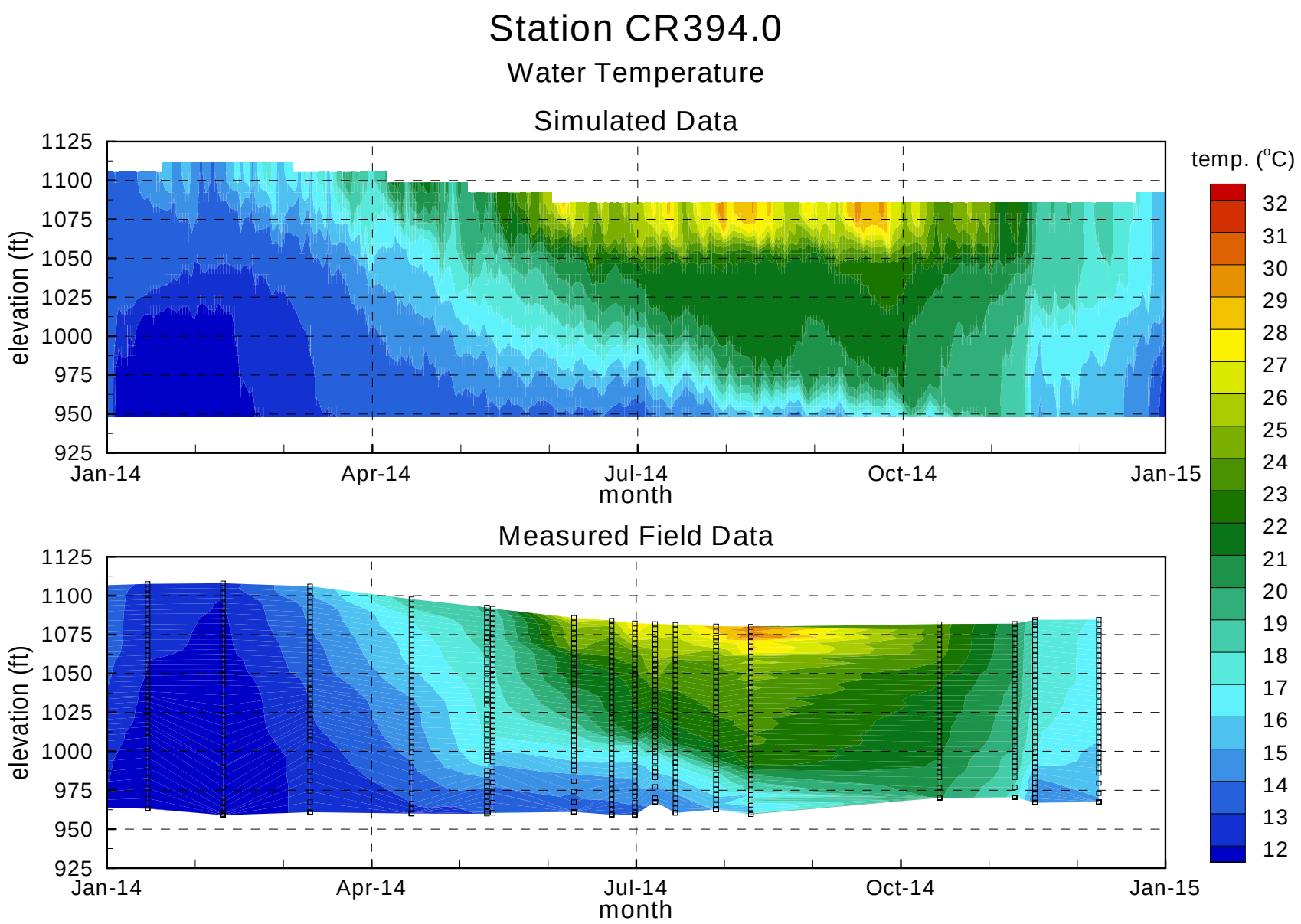

Figure B.1

FLOW SCIENCE

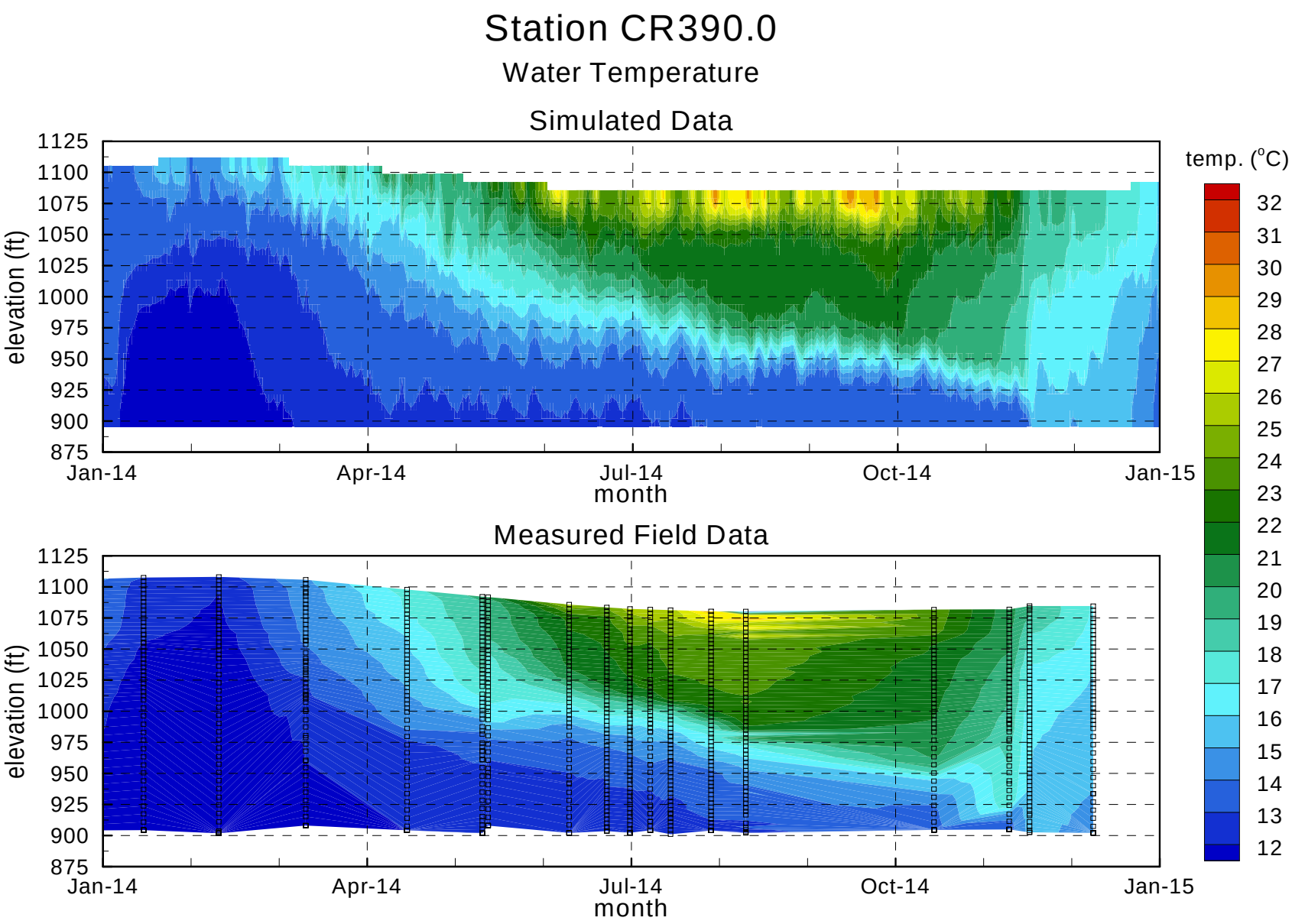
Station CR390.0
Water Temperature
Simulated Data
Measured Field Data
elevation (ft)
1125
1100
1075
1050
1025
1000
975
950
925
900
875
Jan-14
Apr-14
Jul-14
Oct-14
Jan-15
month
temp. (°C)
32
31
30
29
28
27
26
25
24
23
22
21
20
19
18
17
16
15
14
13
12

Figure B.2

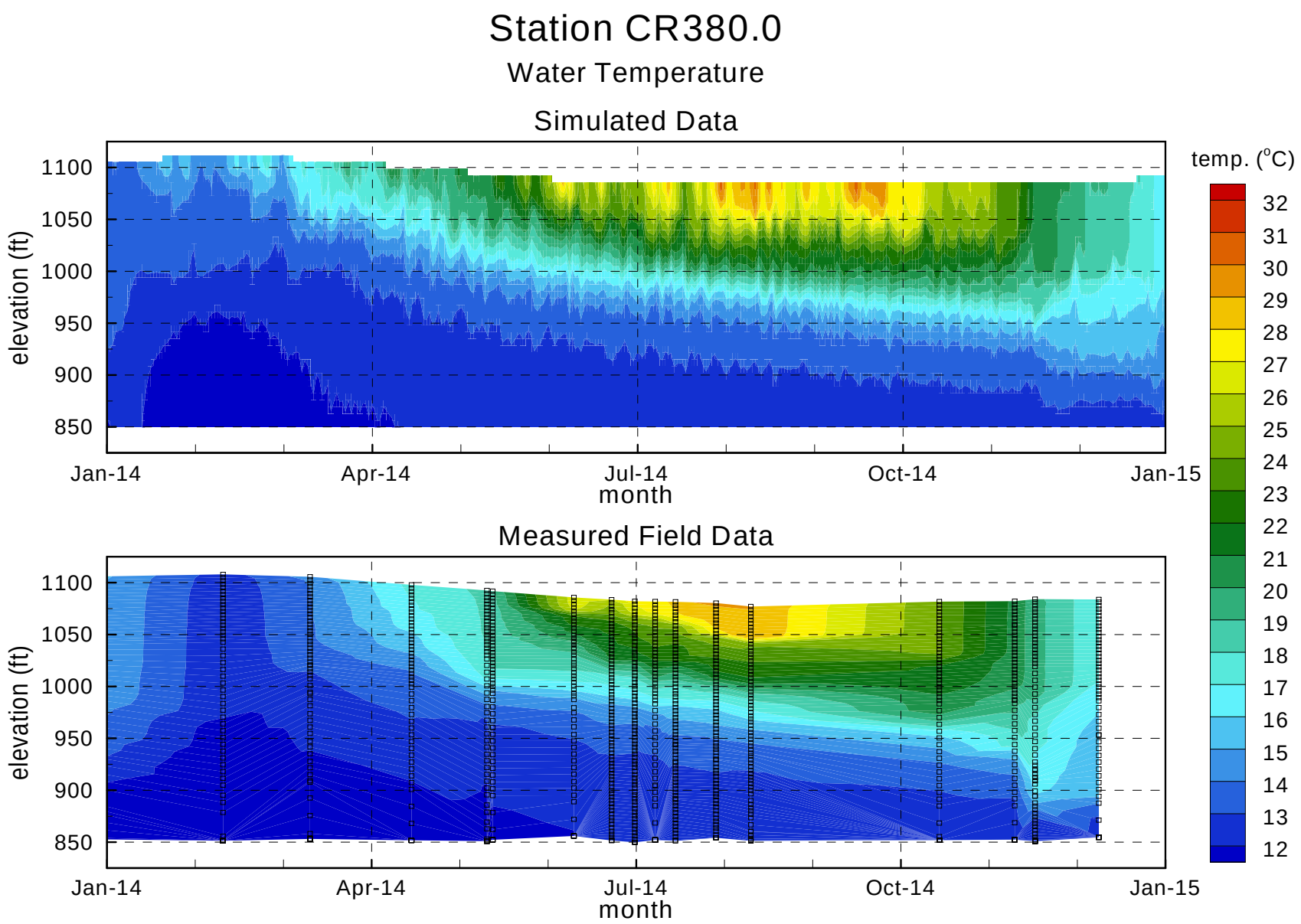
Station CR380.0
Water Temperature
Simulated Data
Measured Field Data
elevation (ft)
1100
1050
1000
950
900
850
Jan-14
Apr-14
Jul-14
Oct-14
Jan-15
month
temp. (°C)
32
31
30
29
28
27
26
25
24
23
22
21
20
19
18
17
16
15
14
13
12

Figure B.3

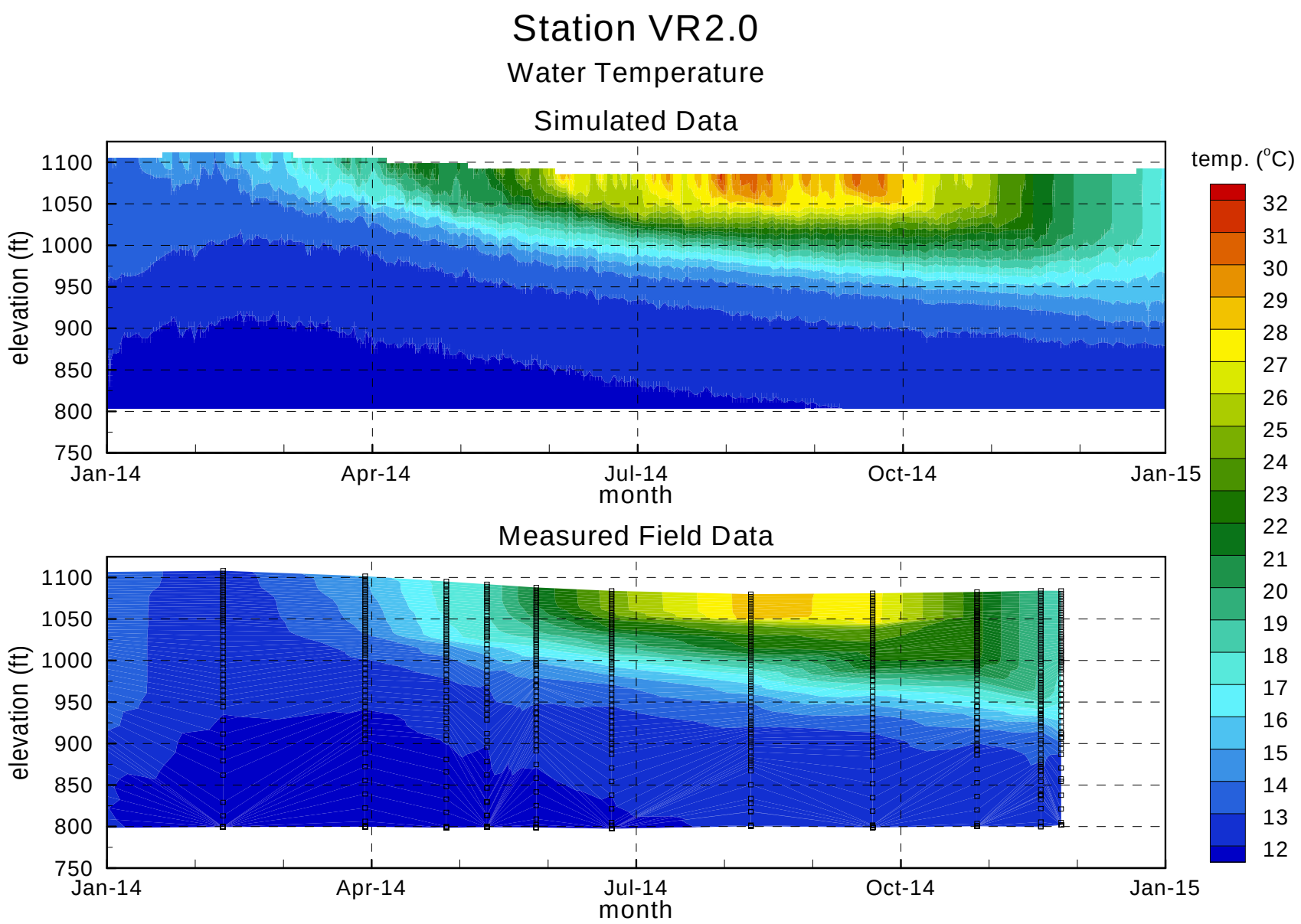
Station VR2.0
Water Temperature
Simulated Data
Measured Field Data
elevation (ft)
1100
1050
1000
950
900
850
800
750
Jan-14
Apr-14
Jul-14
Oct-14
Jan-15
month
temp. (°C)
32
31
30
29
28
27
26
25
24
23
22
21
20
19
18
17
16
15
14
13
12

Figure B.4

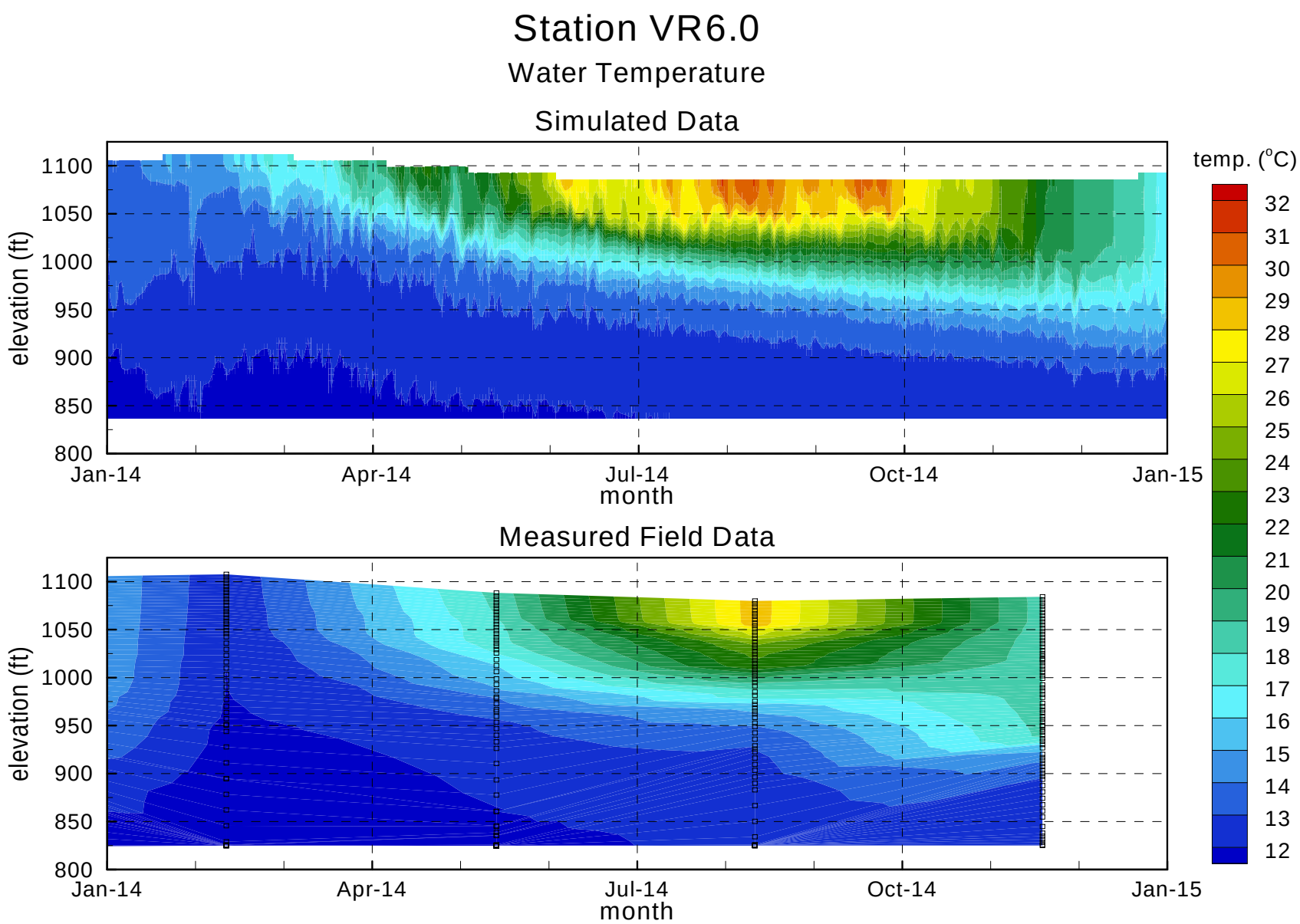
Station VR6.0
Water Temperature
Simulated Data
Measured Field Data
elevation (ft)
1100
1050
1000
950
900
850
800
Jan-14
Apr-14
Jul-14
Oct-14
Jan-15
month
temp. (°C)
32
31
30
29
28
27
26
25
24
23
22
21
20
19
18
17
16
15
14
13
12

Figure B.5

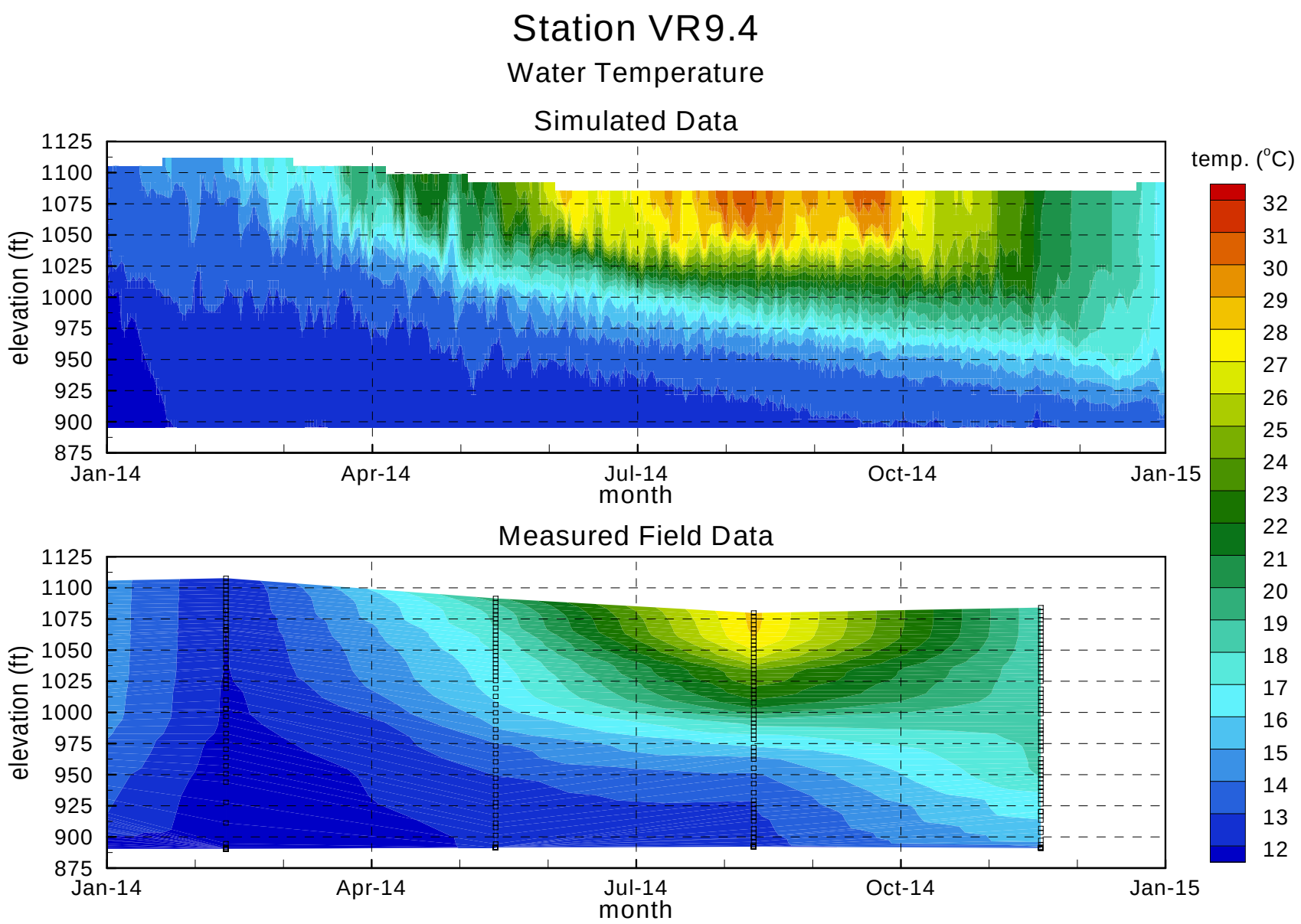
Station VR9.4
Water Temperature
Simulated Data
Measured Field Data
elevation (ft)
1125
1100
1075
1050
1025
1000
975
950
925
900
875
Jan-14
Apr-14
Jul-14
Oct-14
Jan-15
month
temp. (°C)
32
31
30
29
28
27
26
25
24
23
22
21
20
19
18
17
16
15
14
13
12

Figure B.6

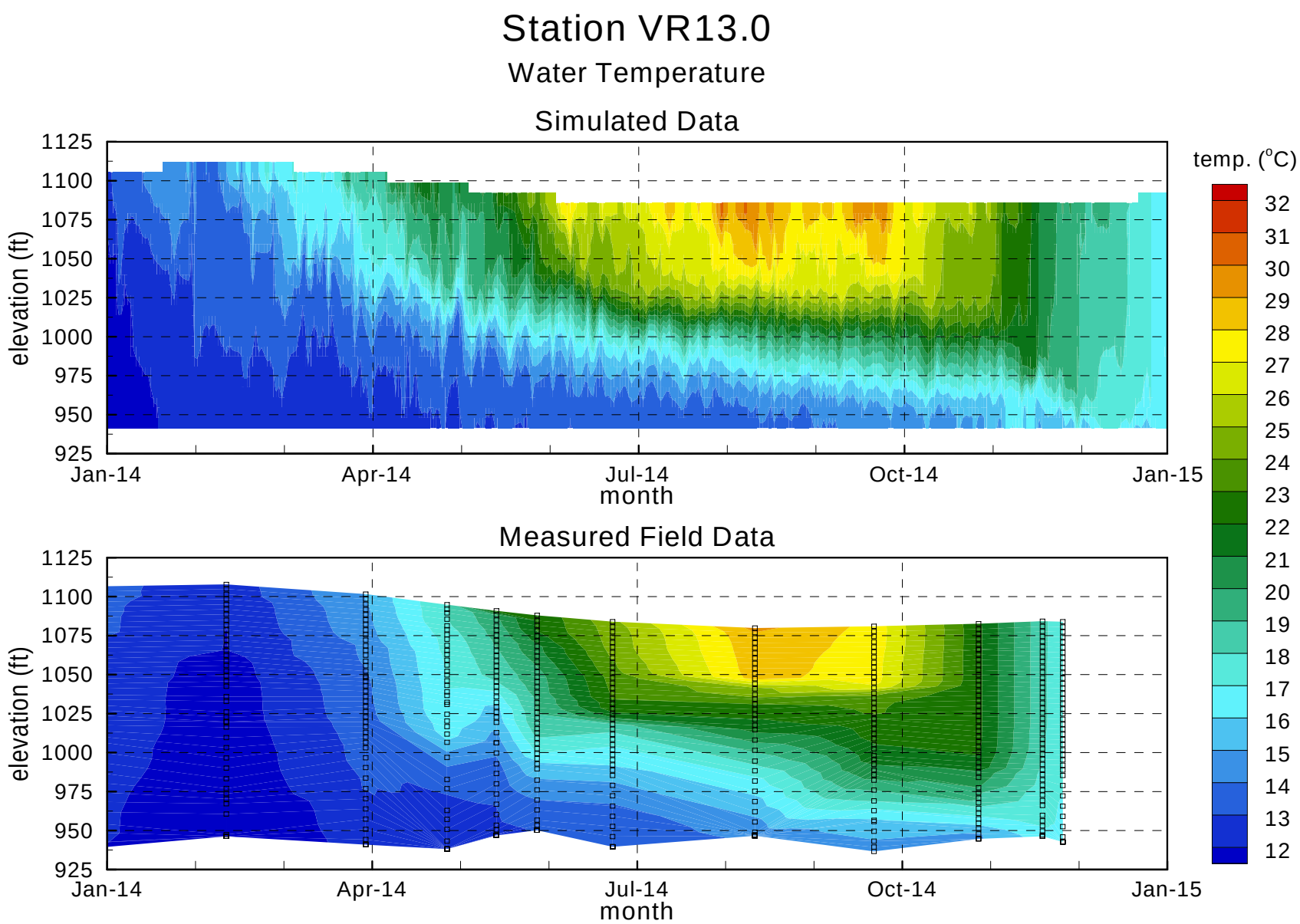
Station VR13.0
Water Temperature
Simulated Data
Measured Field Data
elevation (ft)
1125
1100
1075
1050
1025
1000
975
950
925
Jan-14
Apr-14
Jul-14
Oct-14
Jan-15
month
temp. (°C)
32
31
30
29
28
27
26
25
24
23
22
21
20
19
18
17
16
15
14
13
12

Figure B.7

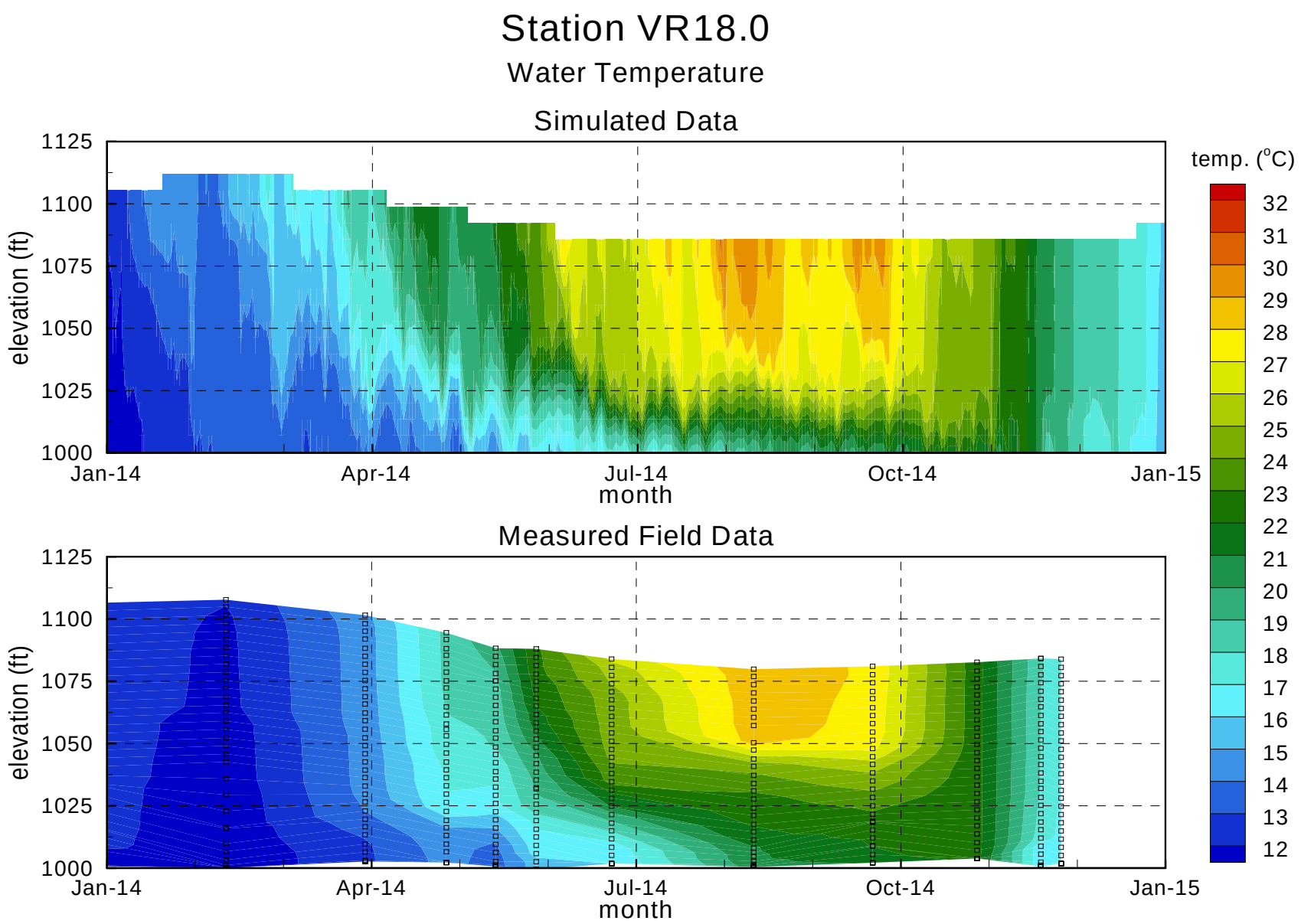
Station VR18.0
Water Temperature
Simulated Data
Measured Field Data
elevation (ft)
1125
1100
1075
1050
1025
1000
Jan-14
Apr-14
Jul-14
Oct-14
Jan-15
month
temp. (°C)
32
31
30
29
28
27
26
25
24
23
22
21
20
19
18
17
16
15
14
13
12

Figure B.8

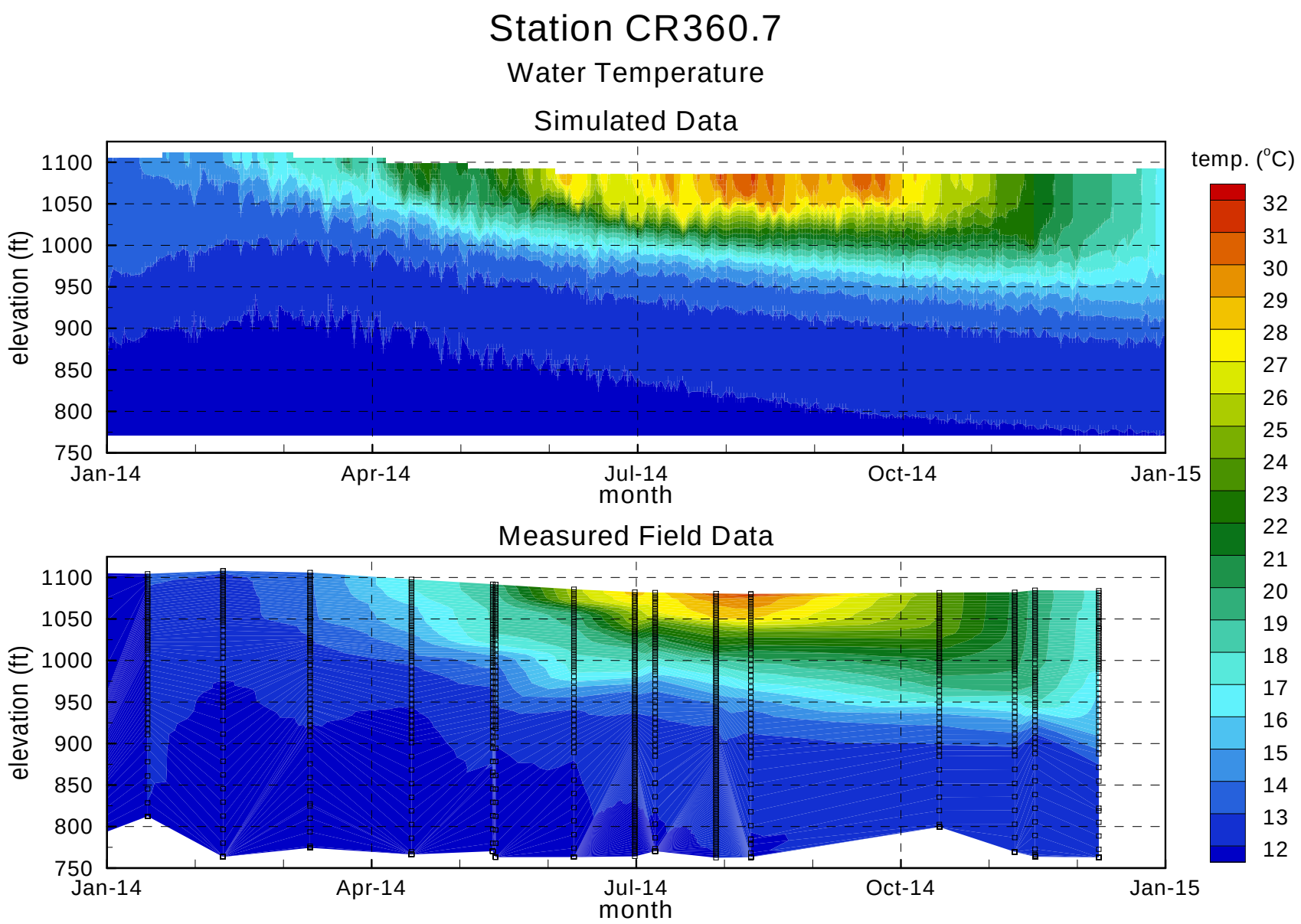

Figure B.9

FLOW SCIENCE

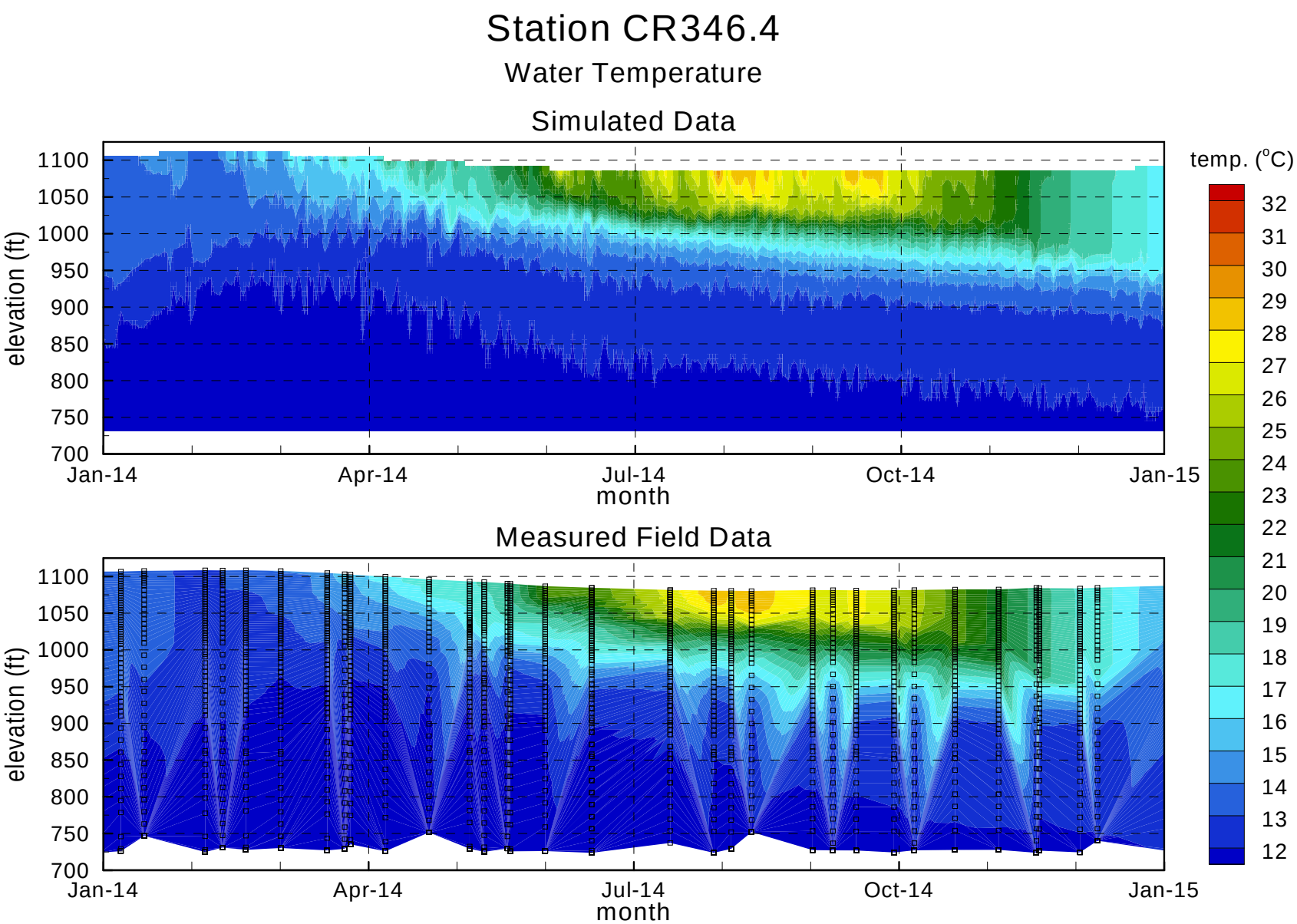
Station CR346.4
Water Temperature
Simulated Data
Measured Field Data
elevation (ft)
1100
1050
1000
950
900
850
800
750
700
Jan-14
Apr-14
Jul-14
Oct-14
Jan-15
month
temp. (°C)
32
31
30
29
28
27
26
25
24
23
22
21
20
19
18
17
16
15
14
13
12

Figure B.10

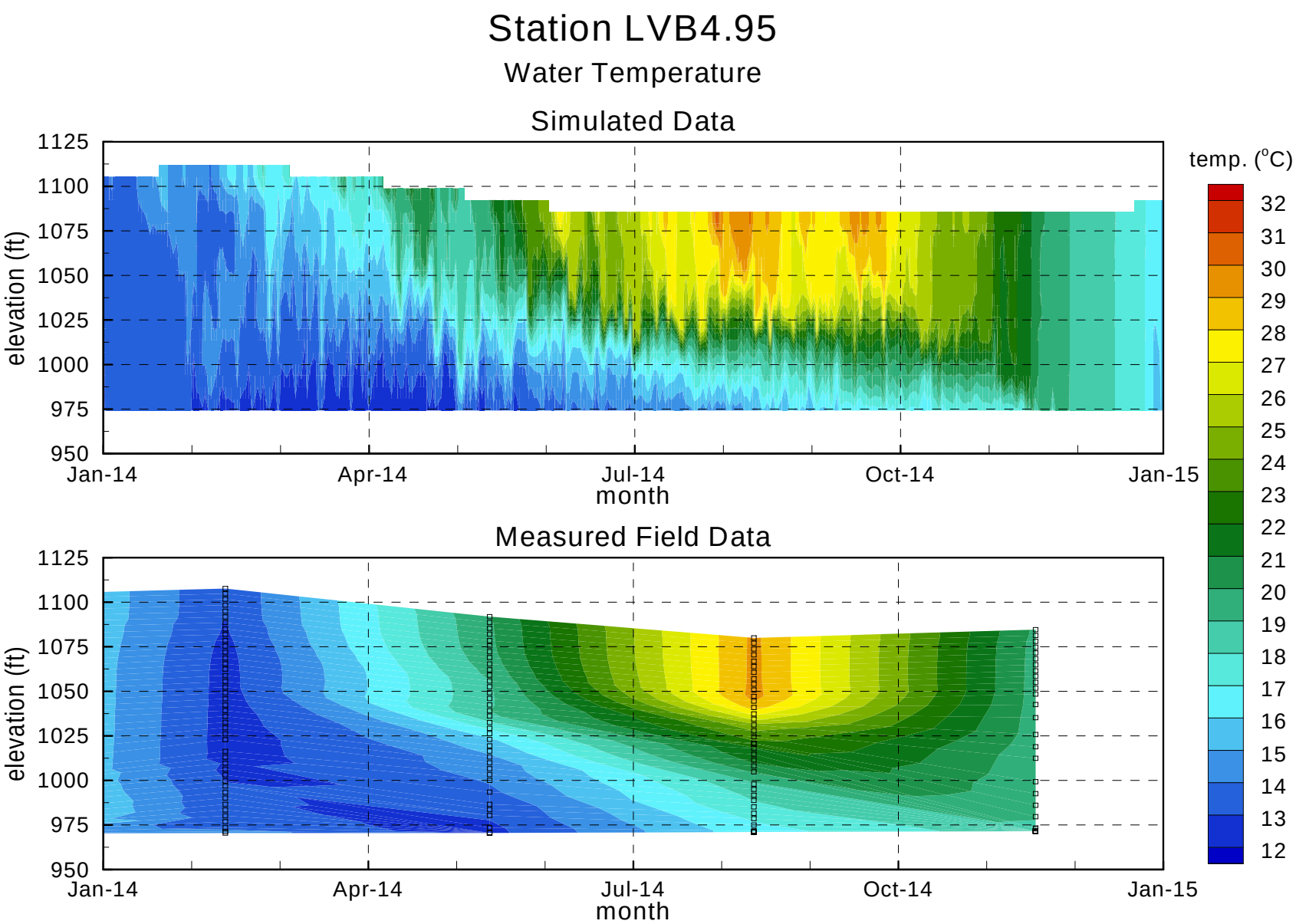

Figure B.11

FLOW SCIENCE

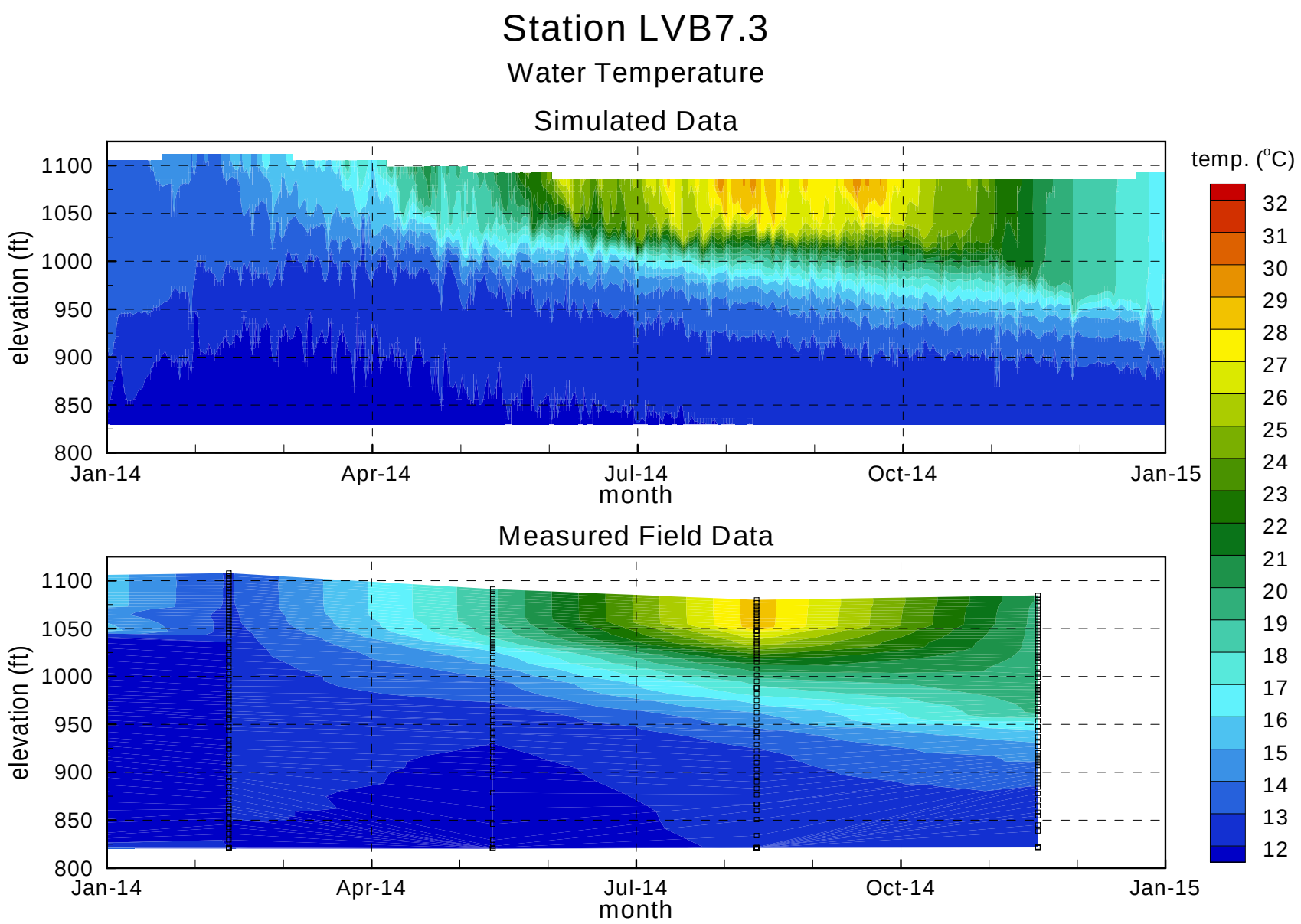
Station LVB7.3
Water Temperature
Simulated Data
Measured Field Data
elevation (ft)
1100
1050
1000
950
900
850
800
Jan-14
Apr-14
Jul-14
Oct-14
Jan-15
month
temp. (°C)
32
31
30
29
28
27
26
25
24
23
22
21
20
19
18
17
16
15
14
13
12

Figure B.12

Colorado River Profile

January, Water Temperature

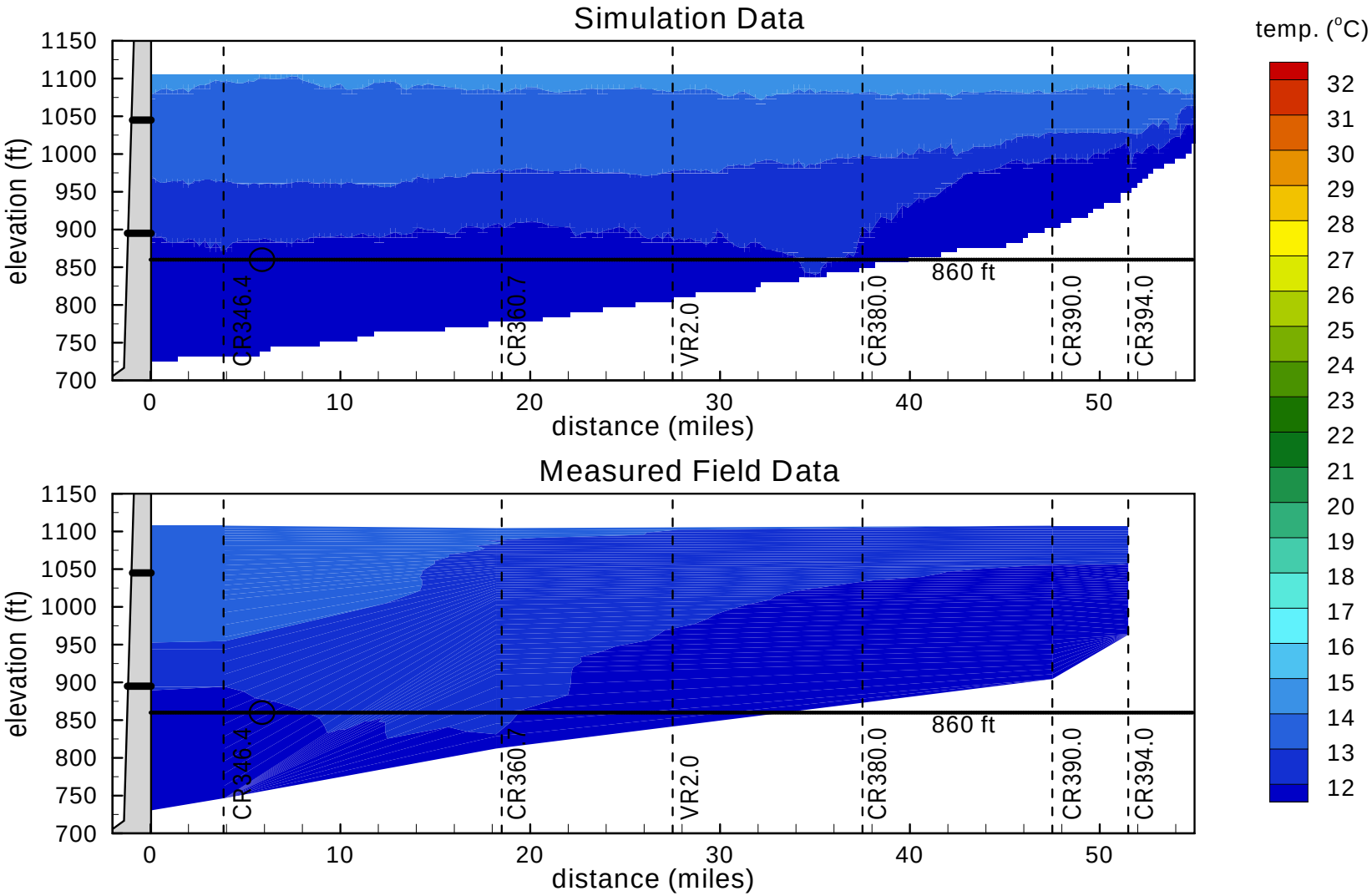

Figure B.13

FLOW SCIENCE

Colorado River Profile

February, Water Temperature

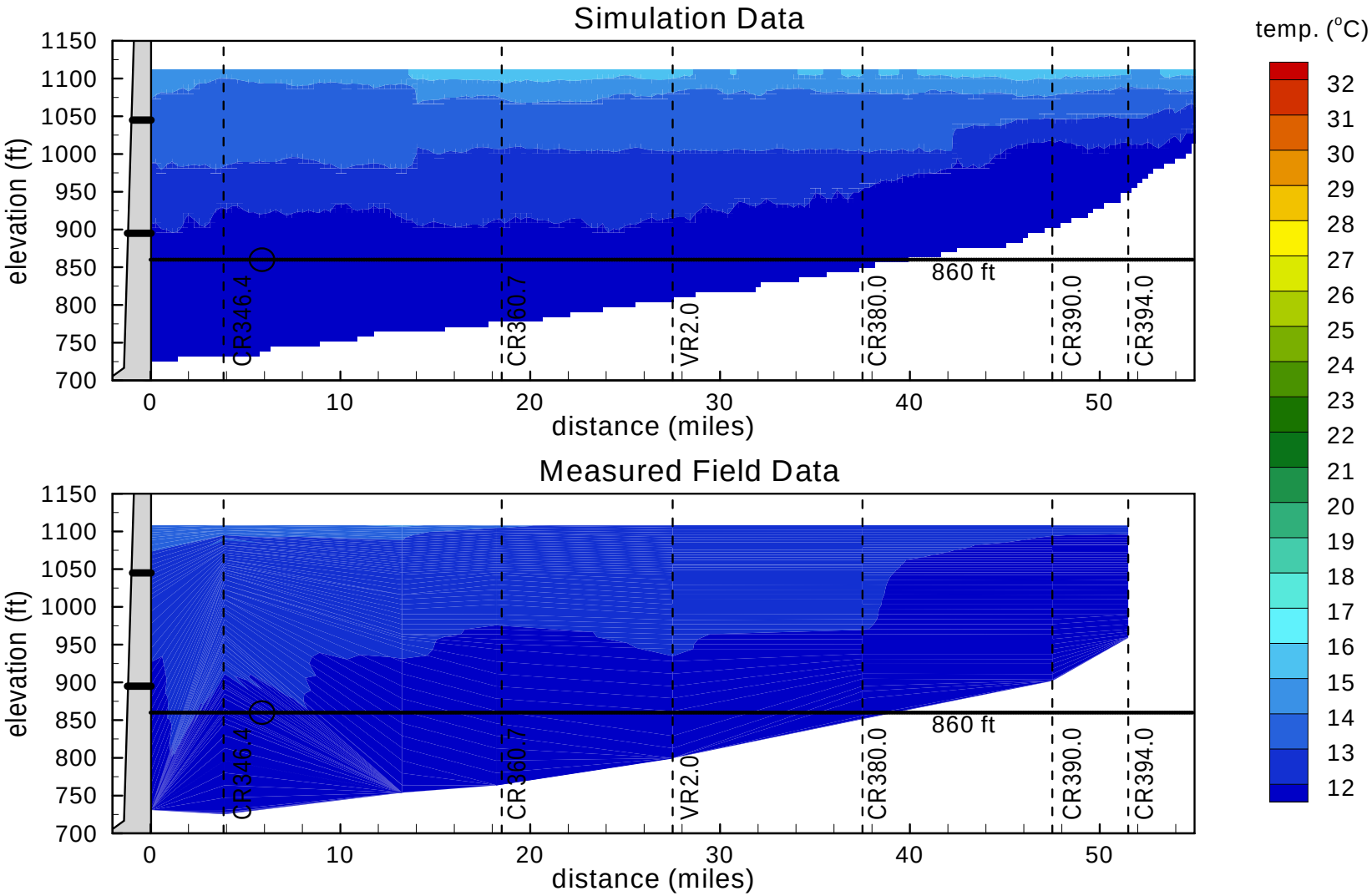

Figure B.14

FLOW SCIENCE

Colorado River Profile

March, Water Temperature

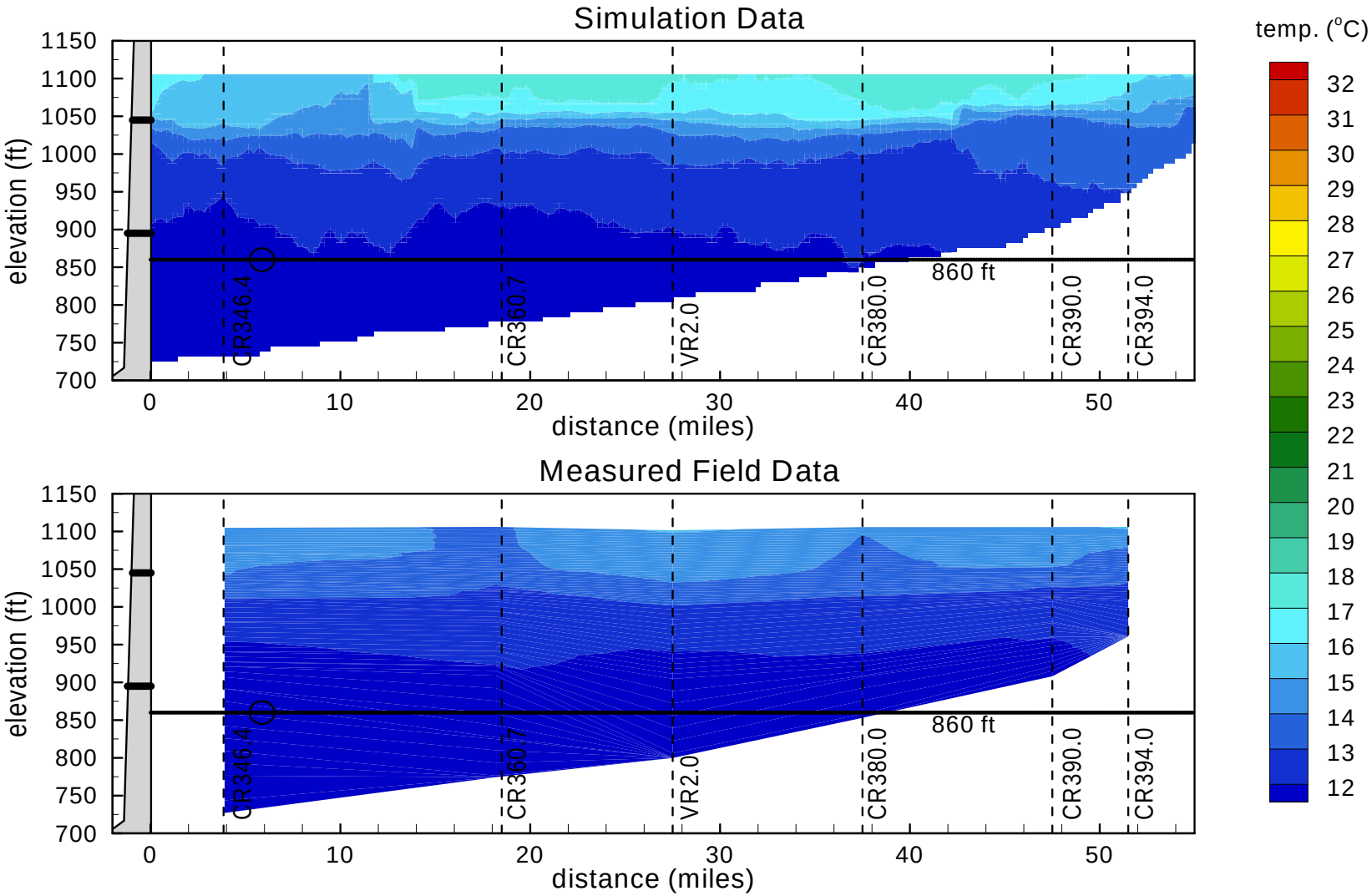

Figure B.15

Colorado River Profile

April, Water Temperature

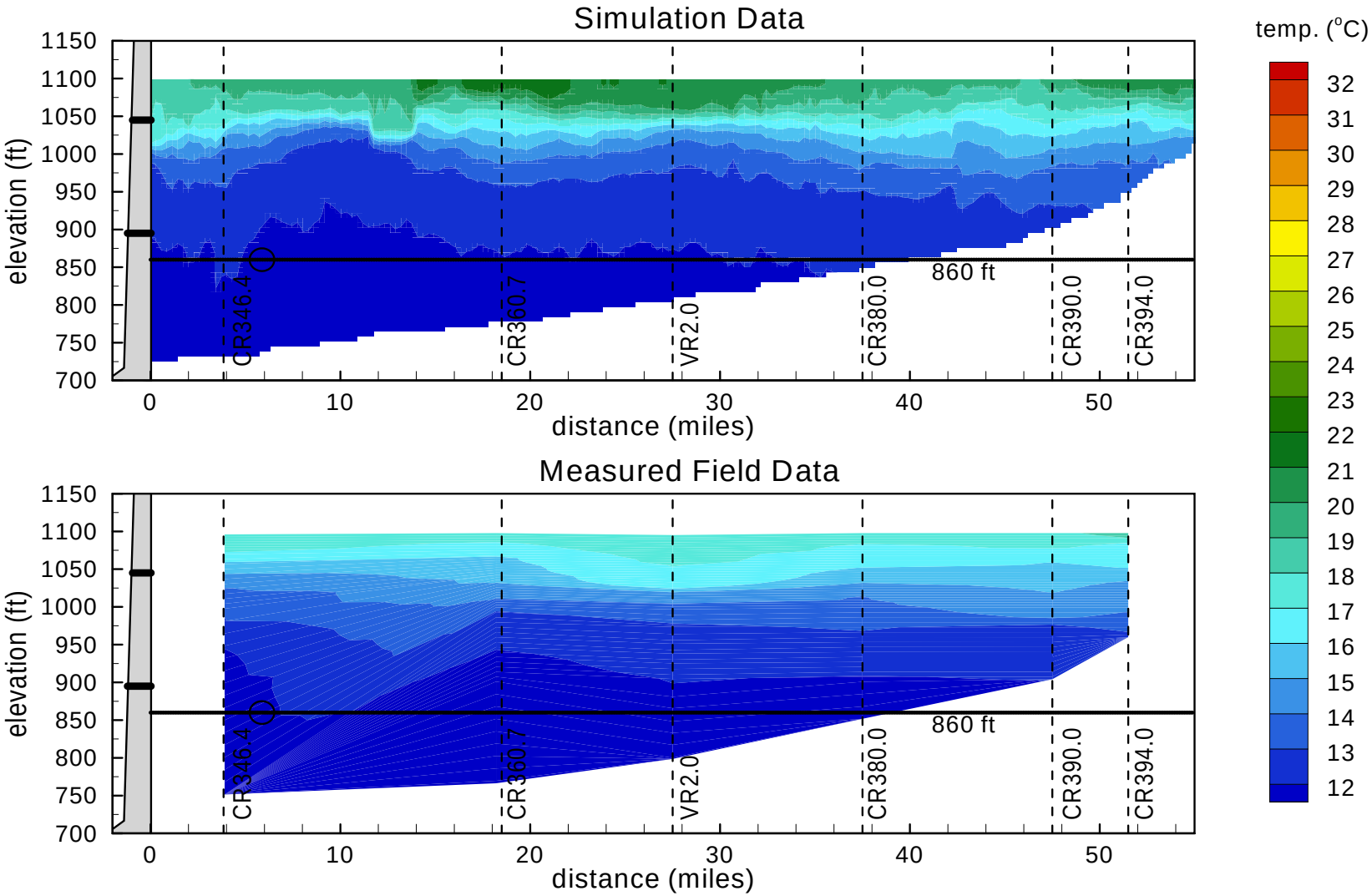

Figure B.16

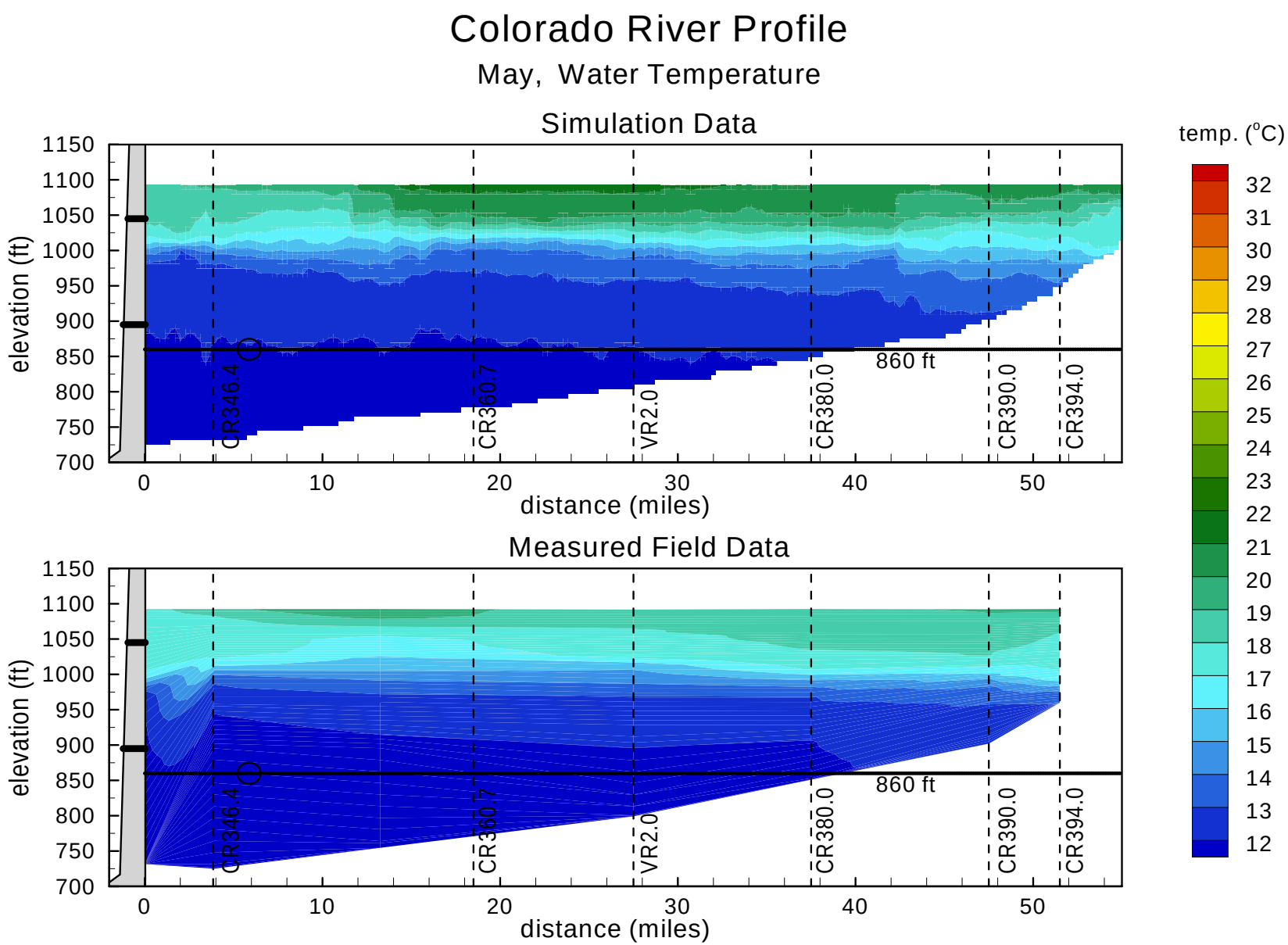

Figure B.17

FLOW SCIENCE

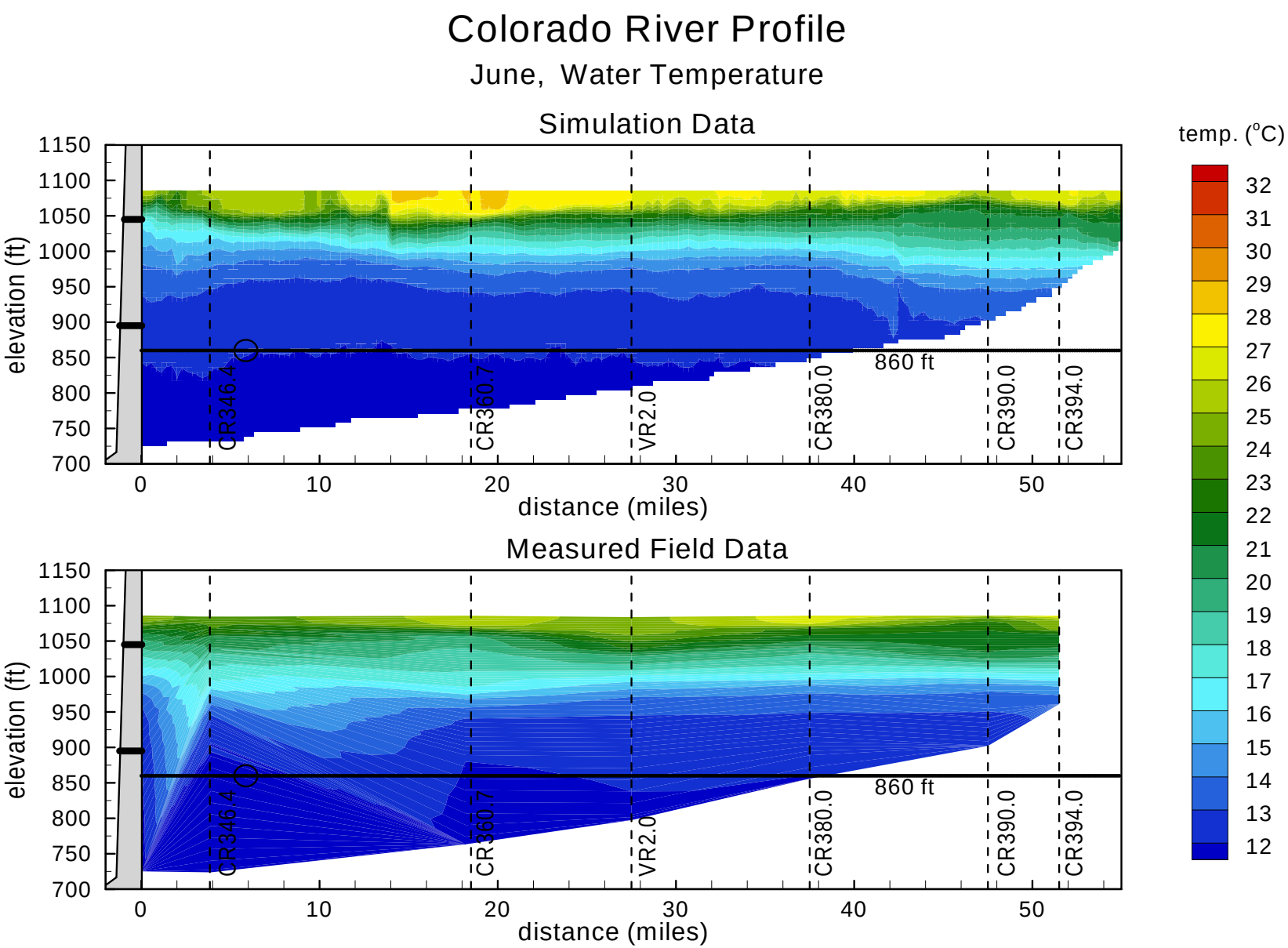
Colorado River Profile
June, Water Temperature
Simulation Data
Measured Field Data
elevation (ft)
distance (miles)
860 ft
CR346.4
CR360.7
VR2.0
CR380.0
CR390.0
CR394.0
temp. (°C)
32
31
30
29
28
27
26
25
24
23
22
21
20
19
18
17
16
15
14
13
12

Figure B.18

Colorado River Profile

July, Water Temperature

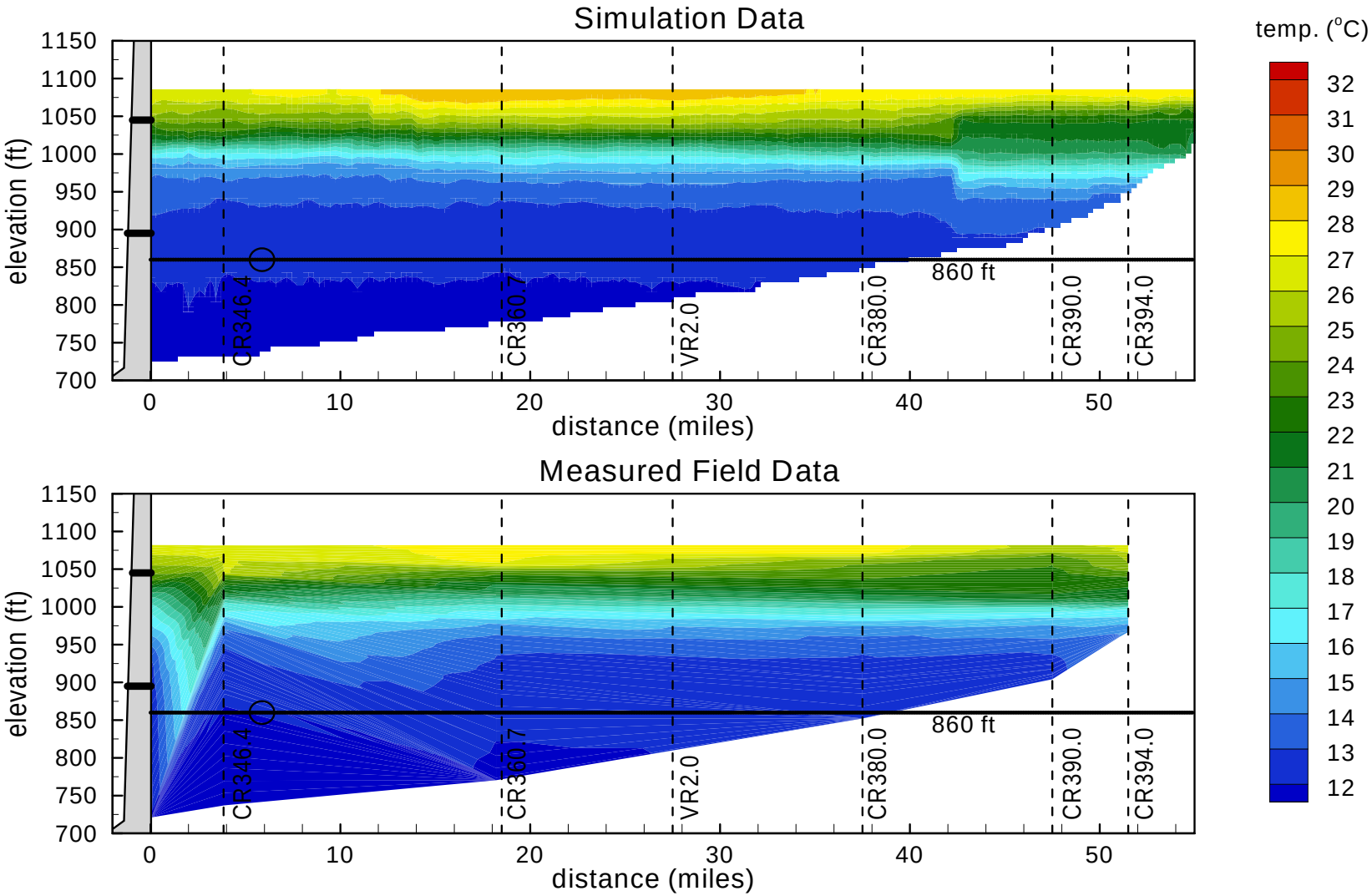

Figure B.19

FLOW SCIENCE

Colorado River Profile

August, Water Temperature

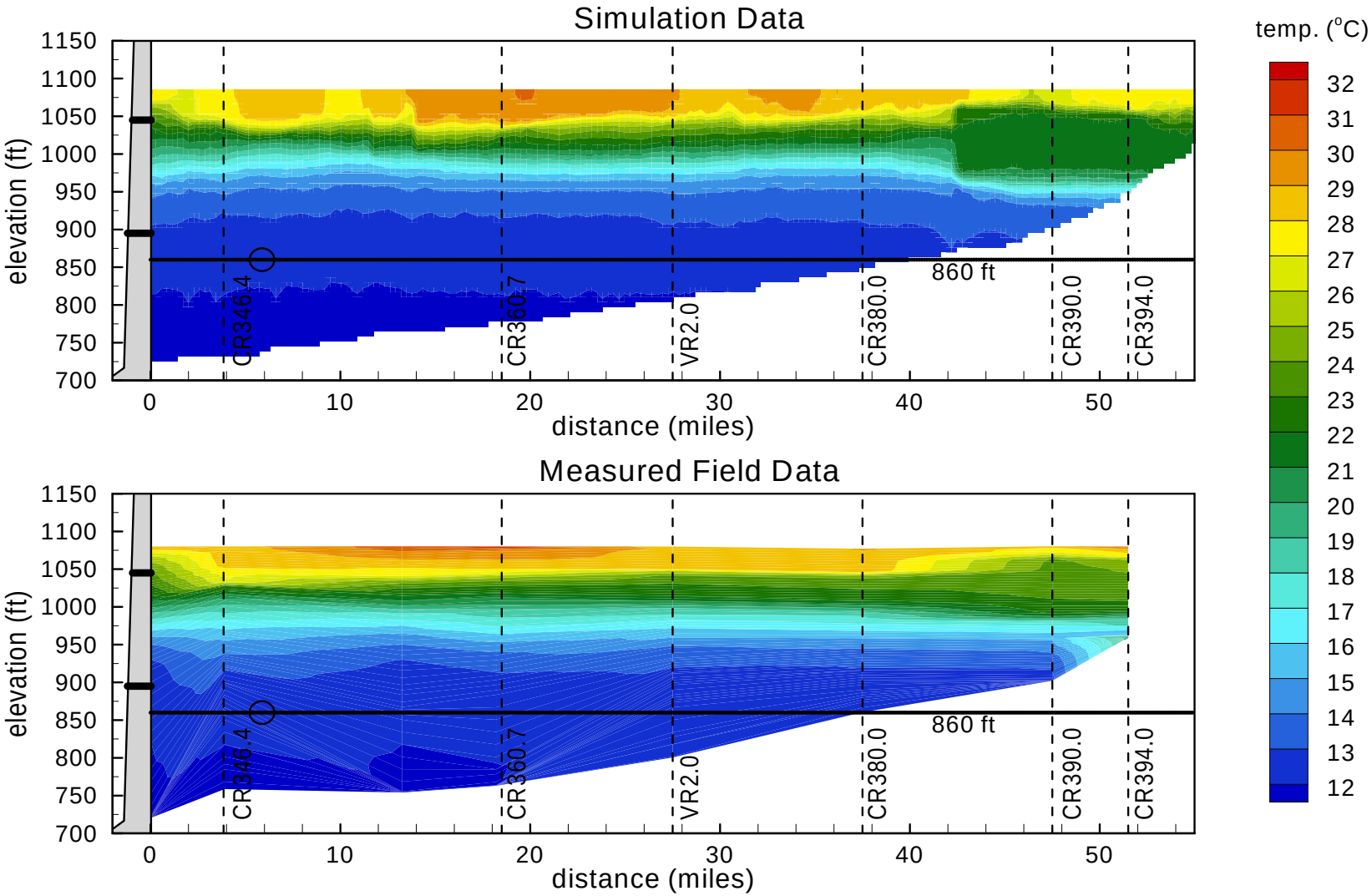

Figure B.20

FLOW SCIENCE

Colorado River Profile

October, Water Temperature

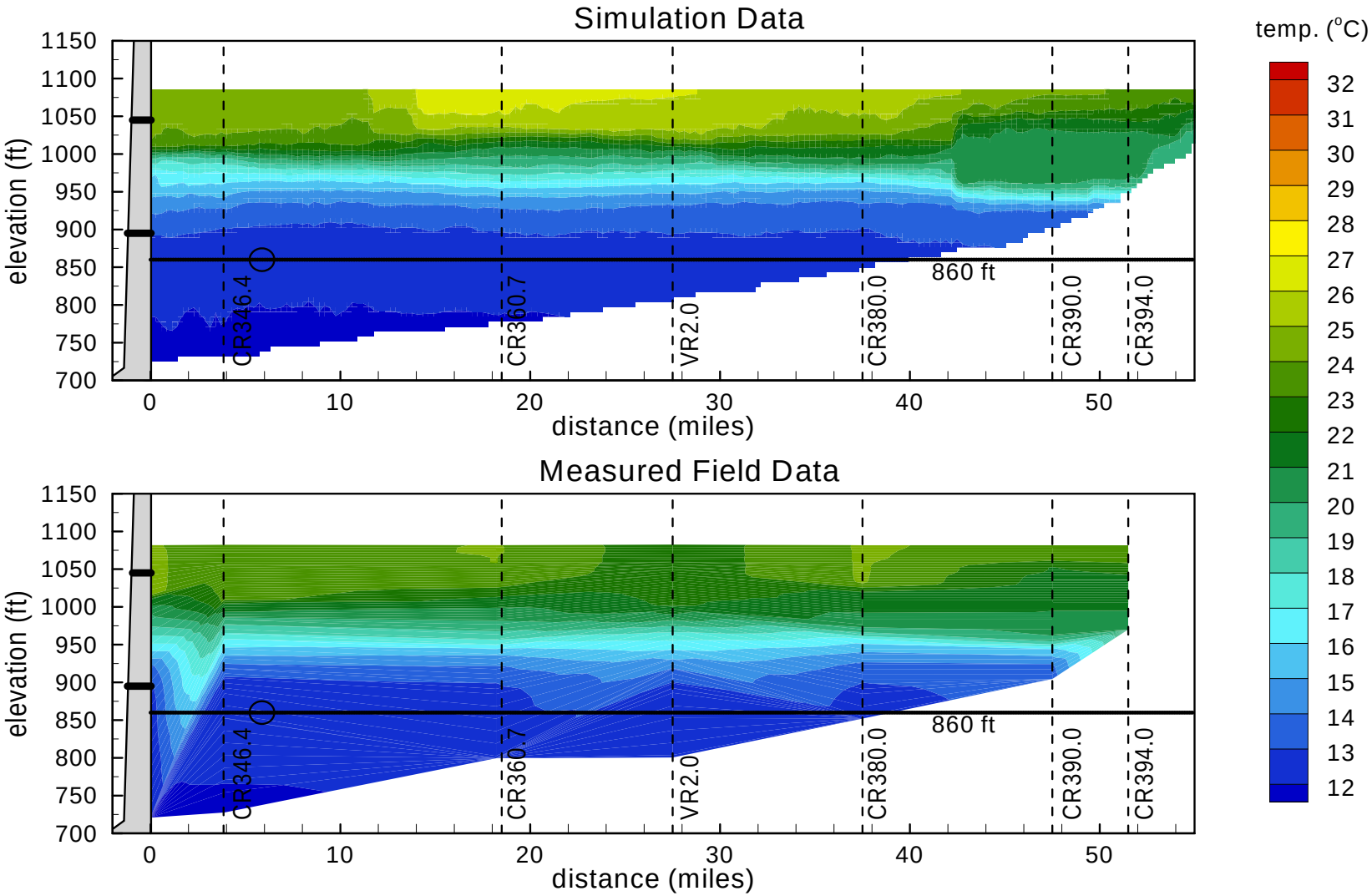

Figure B.21

FLOW SCIENCE

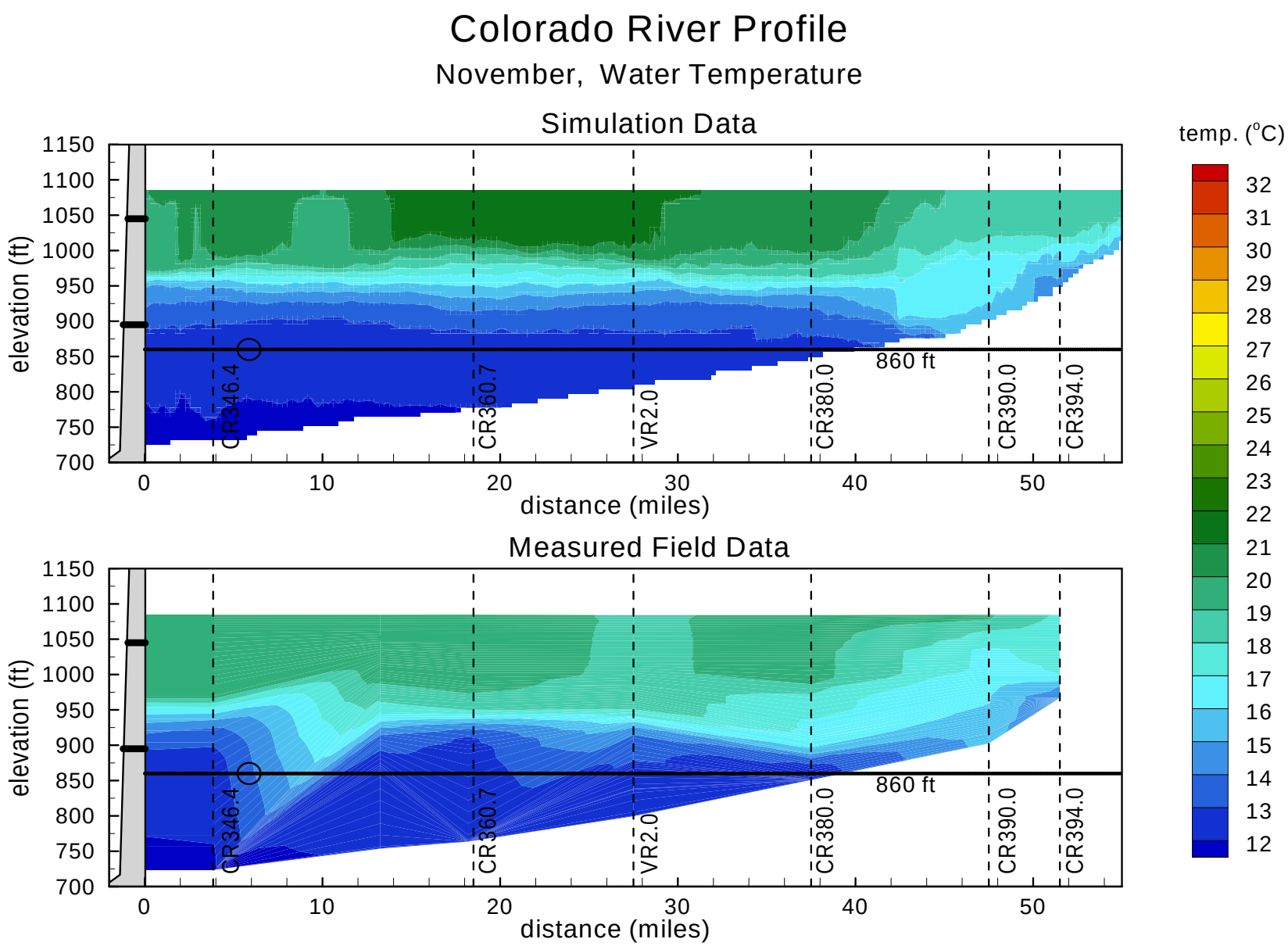
Colorado River Profile
November, Water Temperature
Simulation Data
Measured Field Data
elevation (ft)
distance (miles)
860 ft
CR346.4
CR360.7
VR2.0
CR380.0
CR390.0
CR394.0
temp. (°C)
32
31
30
29
28
27
26
25
24
23
22
21
20
19
18
17
16
15
14
13
12

Figure B.22

Colorado River Profile

December, Water Temperature

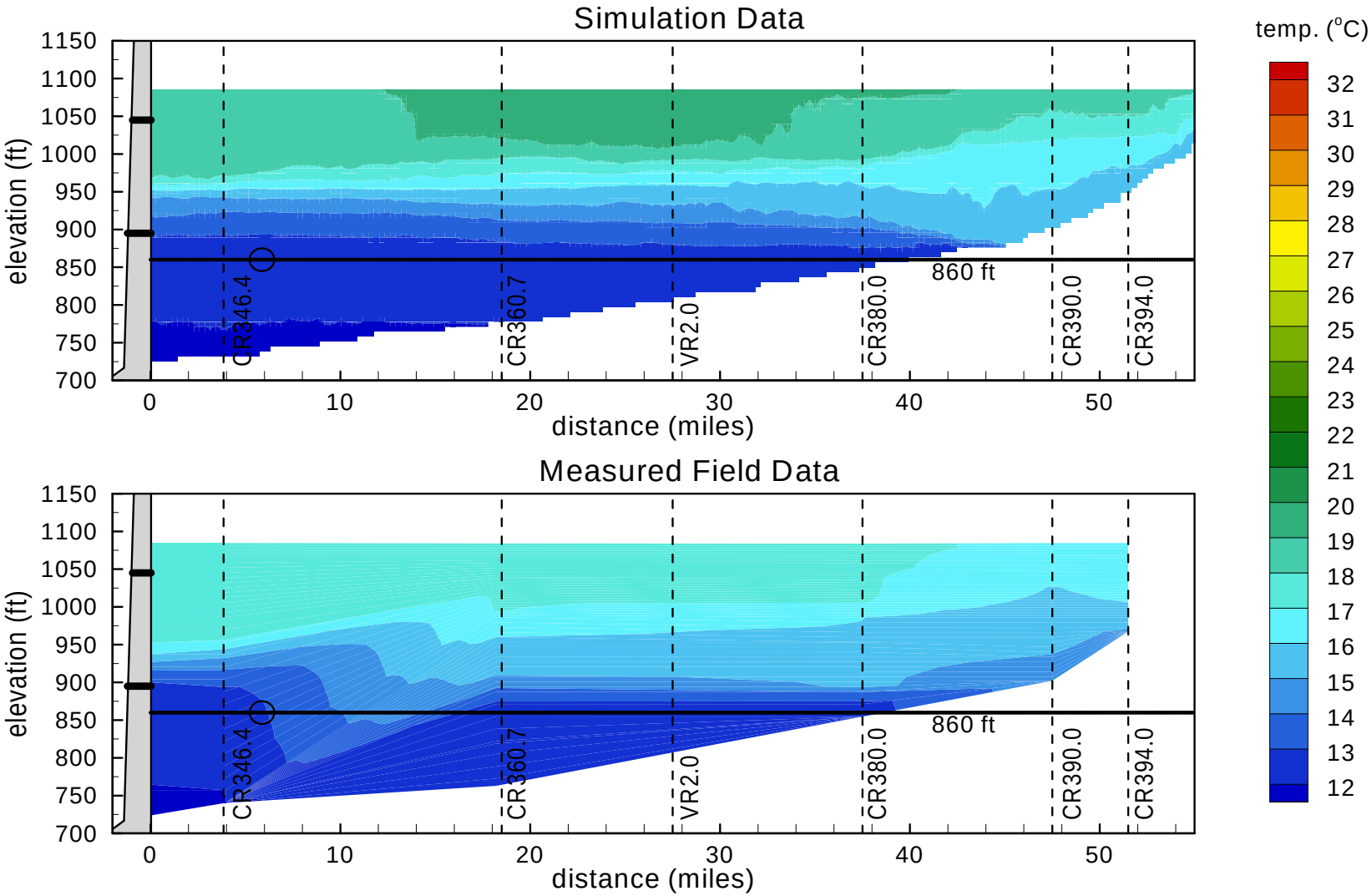

Figure B.23

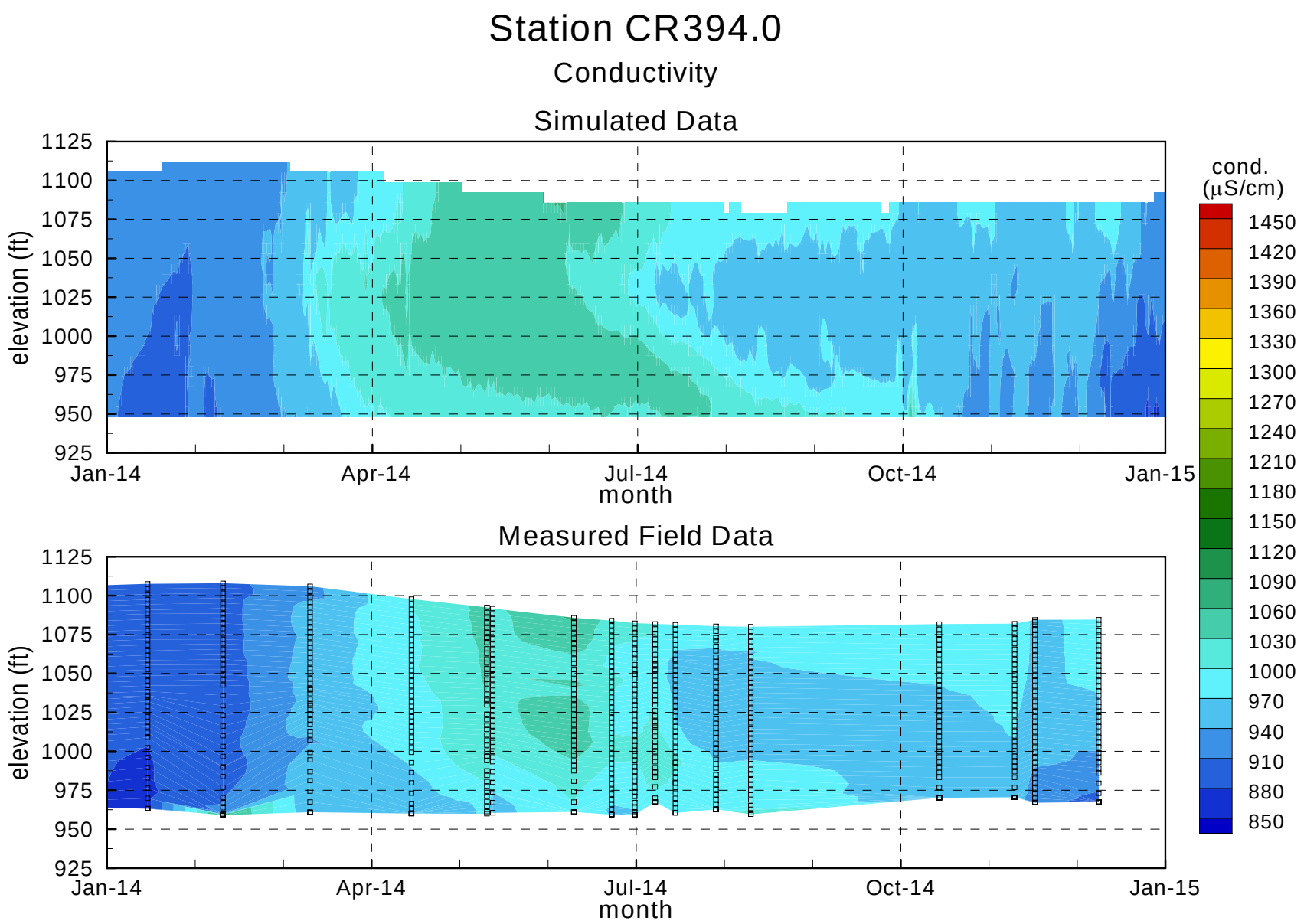
Station CR394.0
Conductivity
Simulated Data
Measured Field Data
elevation (ft)
1125
1100
1075
1050
1025
1000
975
950
925
Jan-14
Apr-14
Jul-14
Oct-14
Jan-15
month
cond.
(µS/cm)
1450
1420
1390
1360
1330
1300
1270
1240
1210
1180
1150
1120
1090
1060
1030
1000
970
940
910
880
850

Figure B.24

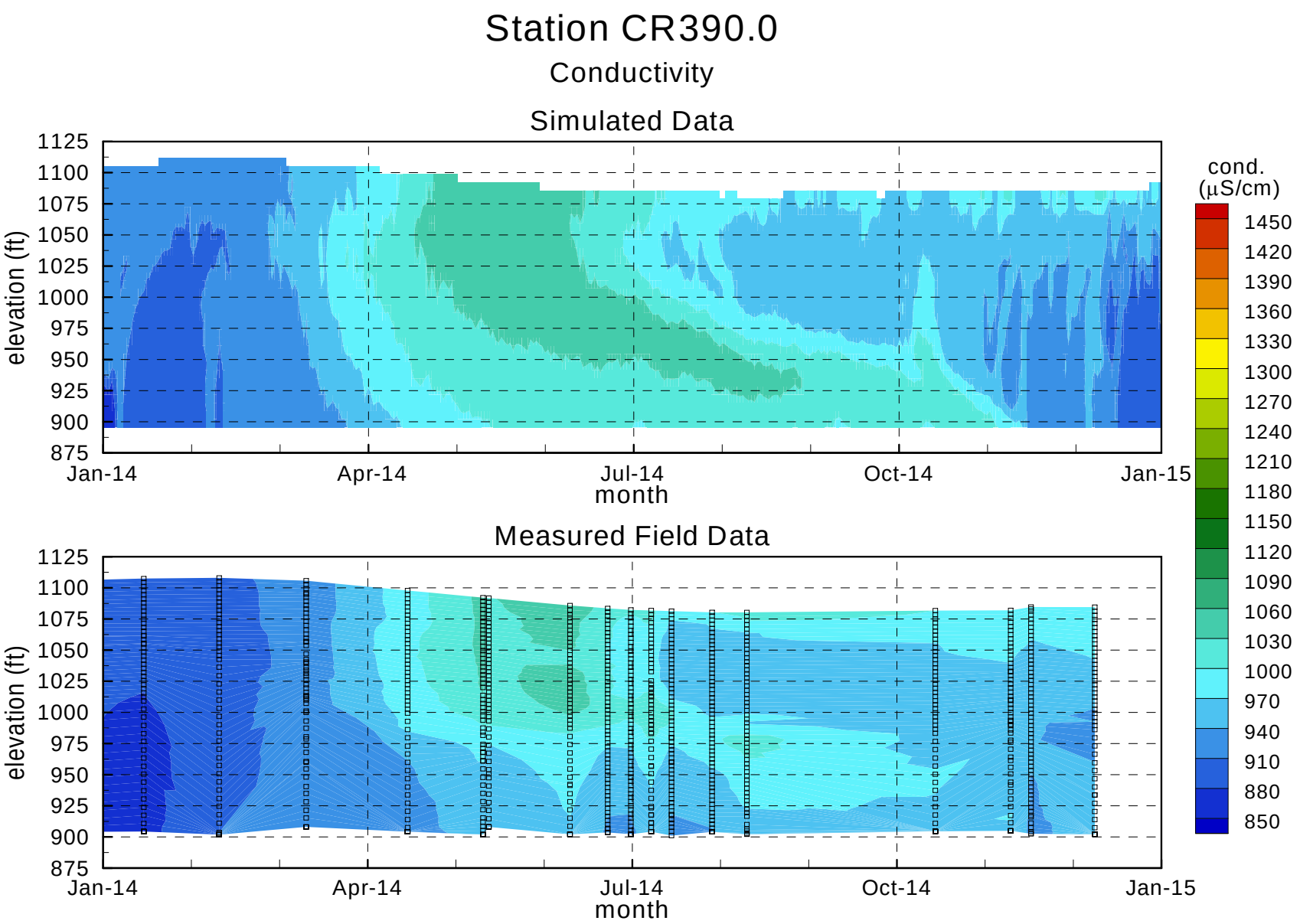

Figure B.25

FLOW SCIENCE

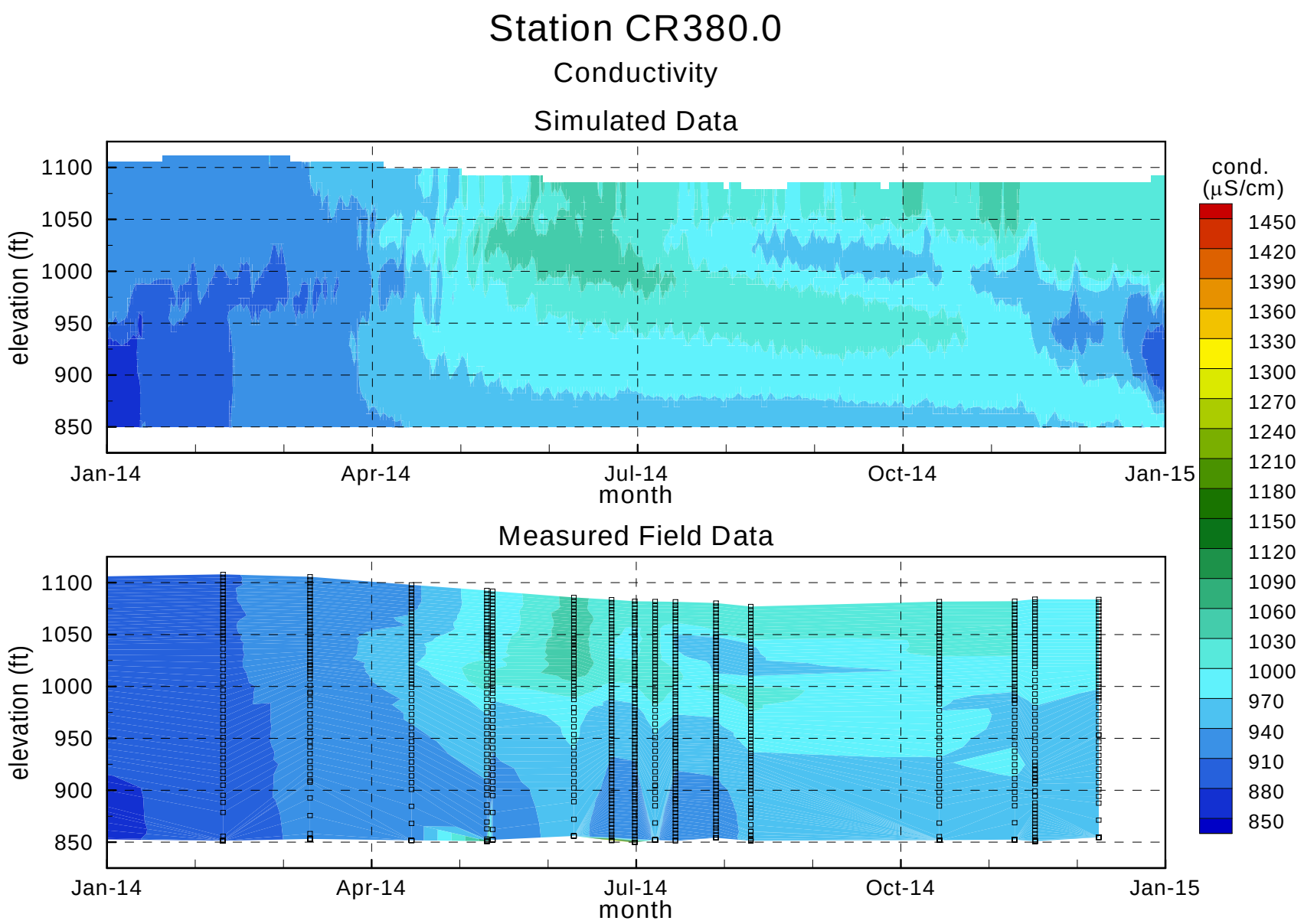
Station CR380.0
Conductivity
Simulated Data
Measured Field Data
elevation (ft)
1100
1050
1000
950
900
850
Jan-14
Apr-14
Jul-14
Oct-14
Jan-15
month
cond.
(µS/cm)
1450
1420
1390
1360
1330
1300
1270
1240
1210
1180
1150
1120
1090
1060
1030
1000
970
940
910
880
850

Figure B.26

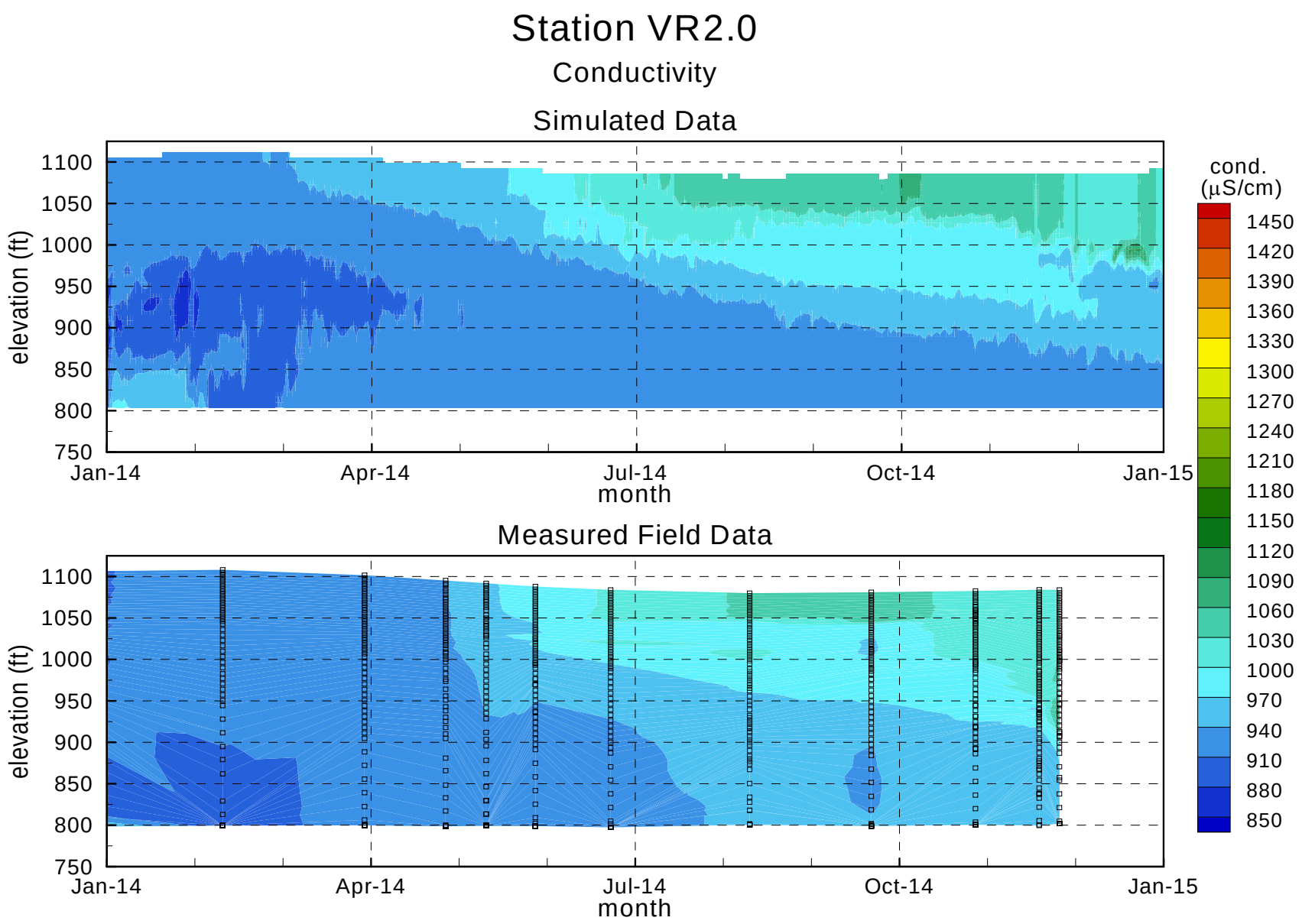

Figure B.27

FLOW SCIENCE

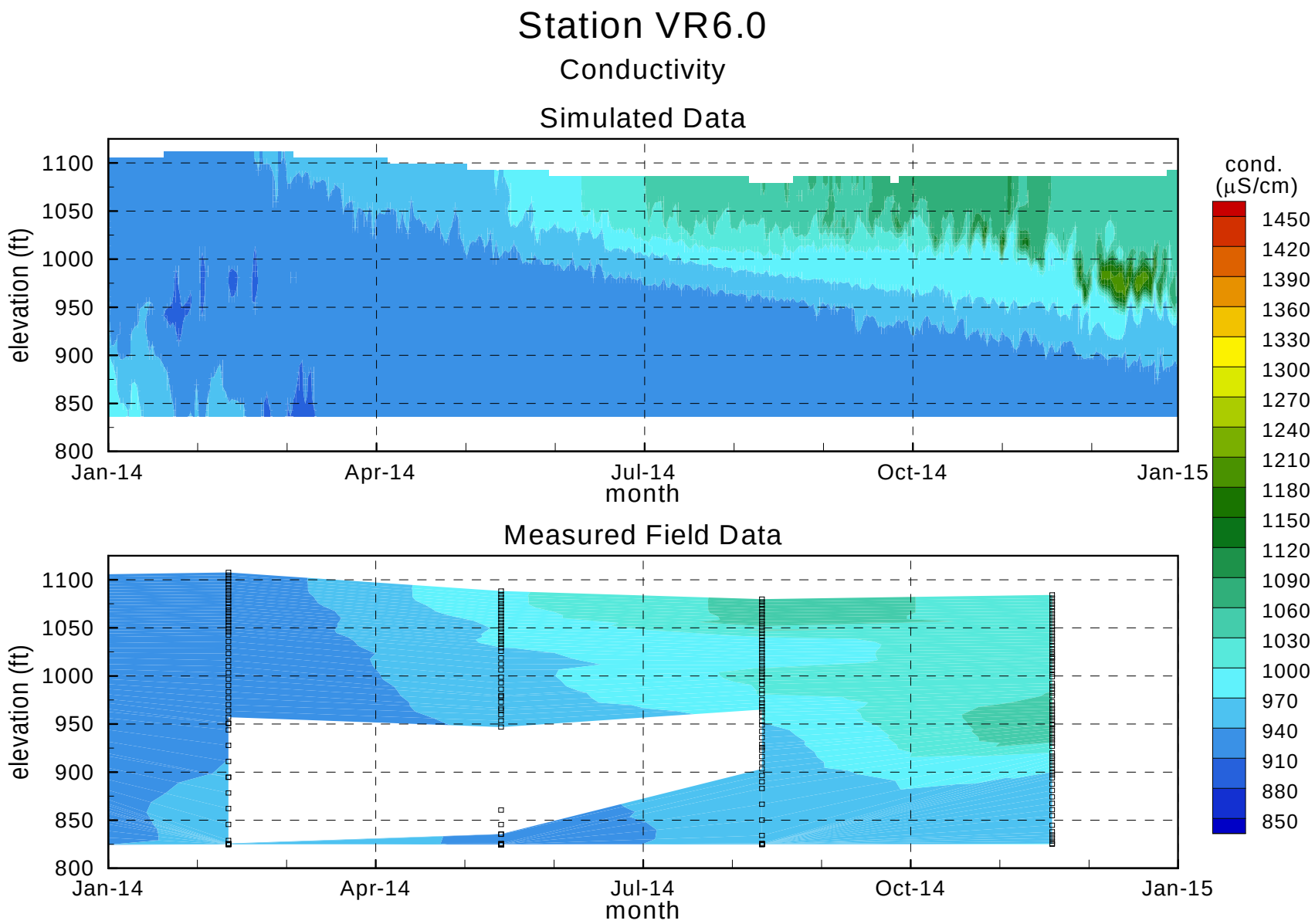

Figure B.28

FLOW SCIENCE

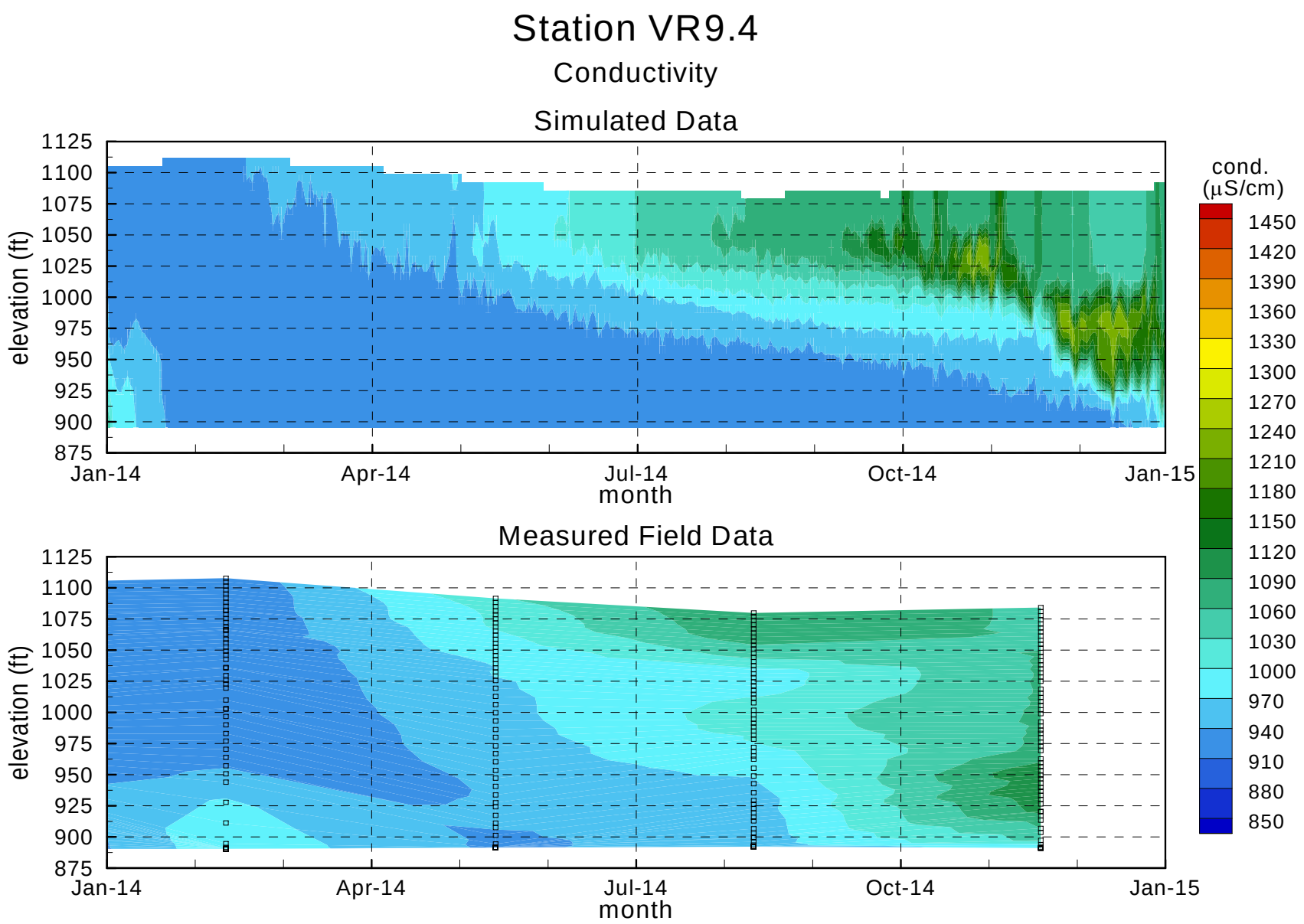
Station VR9.4
Conductivity
Simulated Data
Measured Field Data
elevation (ft)
1125
1100
1075
1050
1025
1000
975
950
925
900
875
Jan-14
Apr-14
Jul-14
Oct-14
Jan-15
month
cond.
(µS/cm)
1450
1420
1390
1360
1330
1300
1270
1240
1210
1180
1150
1120
1090
1060
1030
1000
970
940
910
880
850

Figure B.29

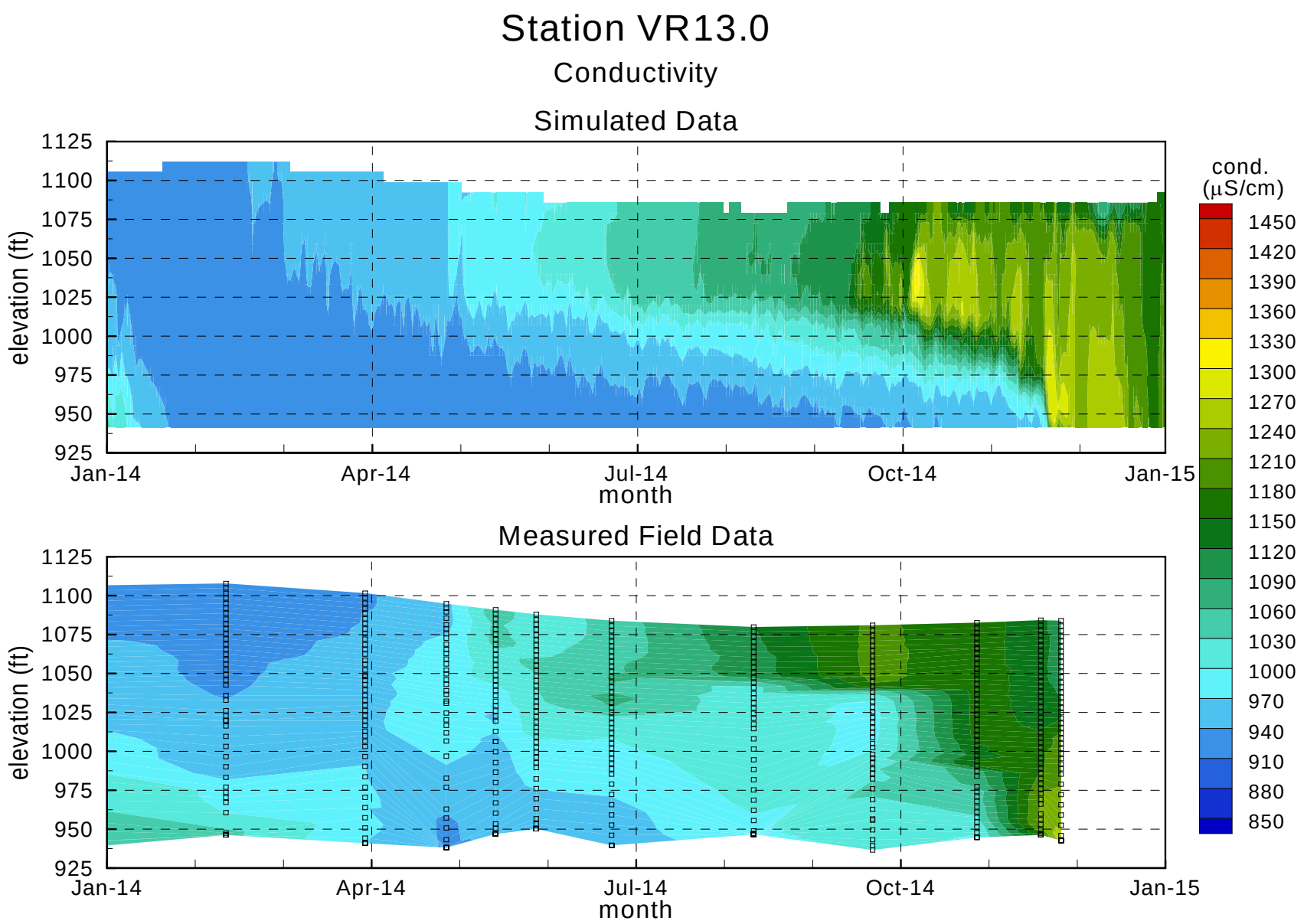
Station VR13.0
Conductivity
Simulated Data
Measured Field Data
elevation (ft)
1125
1100
1075
1050
1025
1000
975
950
925
Jan-14
Apr-14
Jul-14
Oct-14
Jan-15
month
cond.
(µS/cm)
1450
1420
1390
1360
1330
1300
1270
1240
1210
1180
1150
1120
1090
1060
1030
1000
970
940
910
880
850

Figure B.30

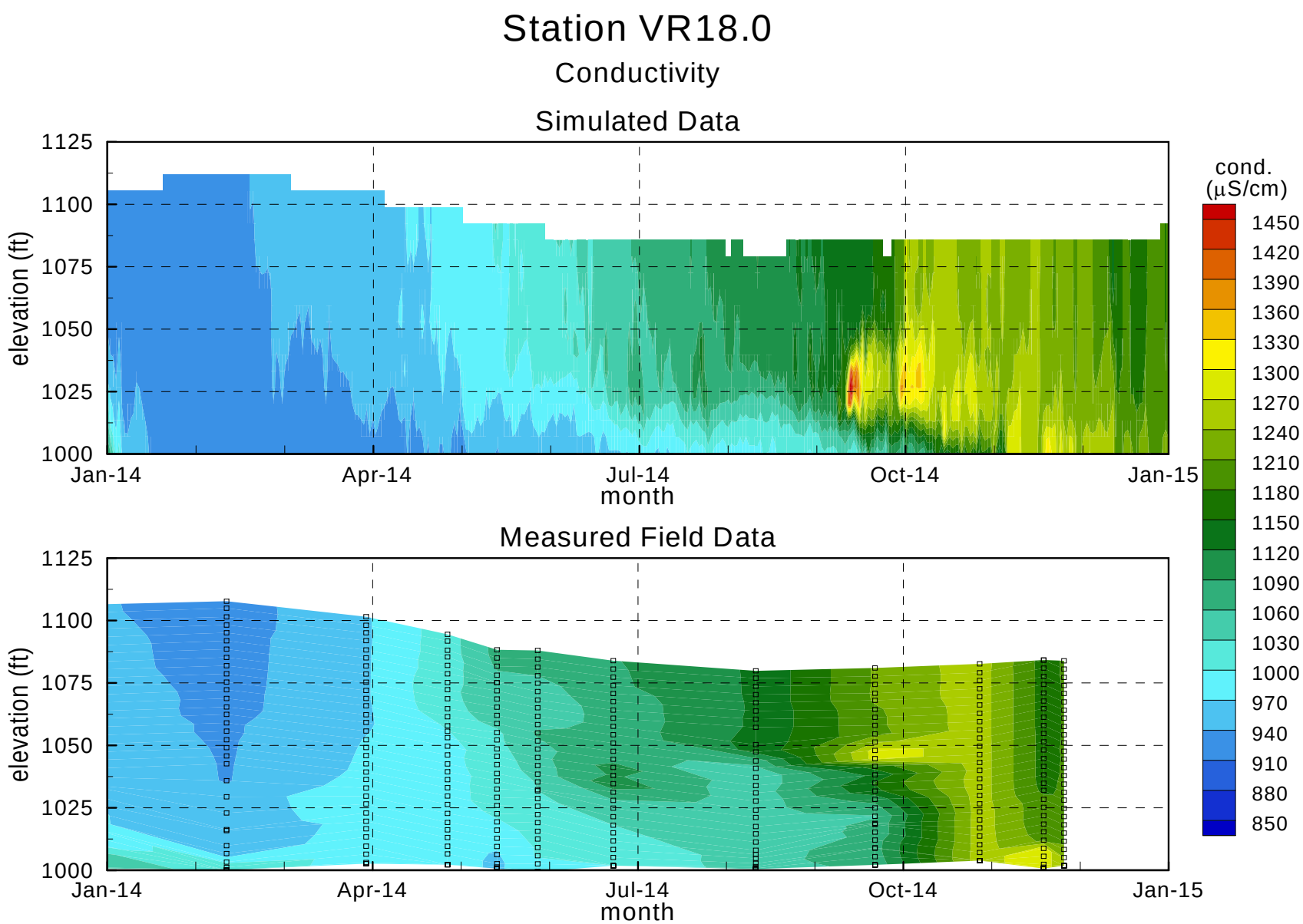

Figure B.31

FLOW SCIENCE

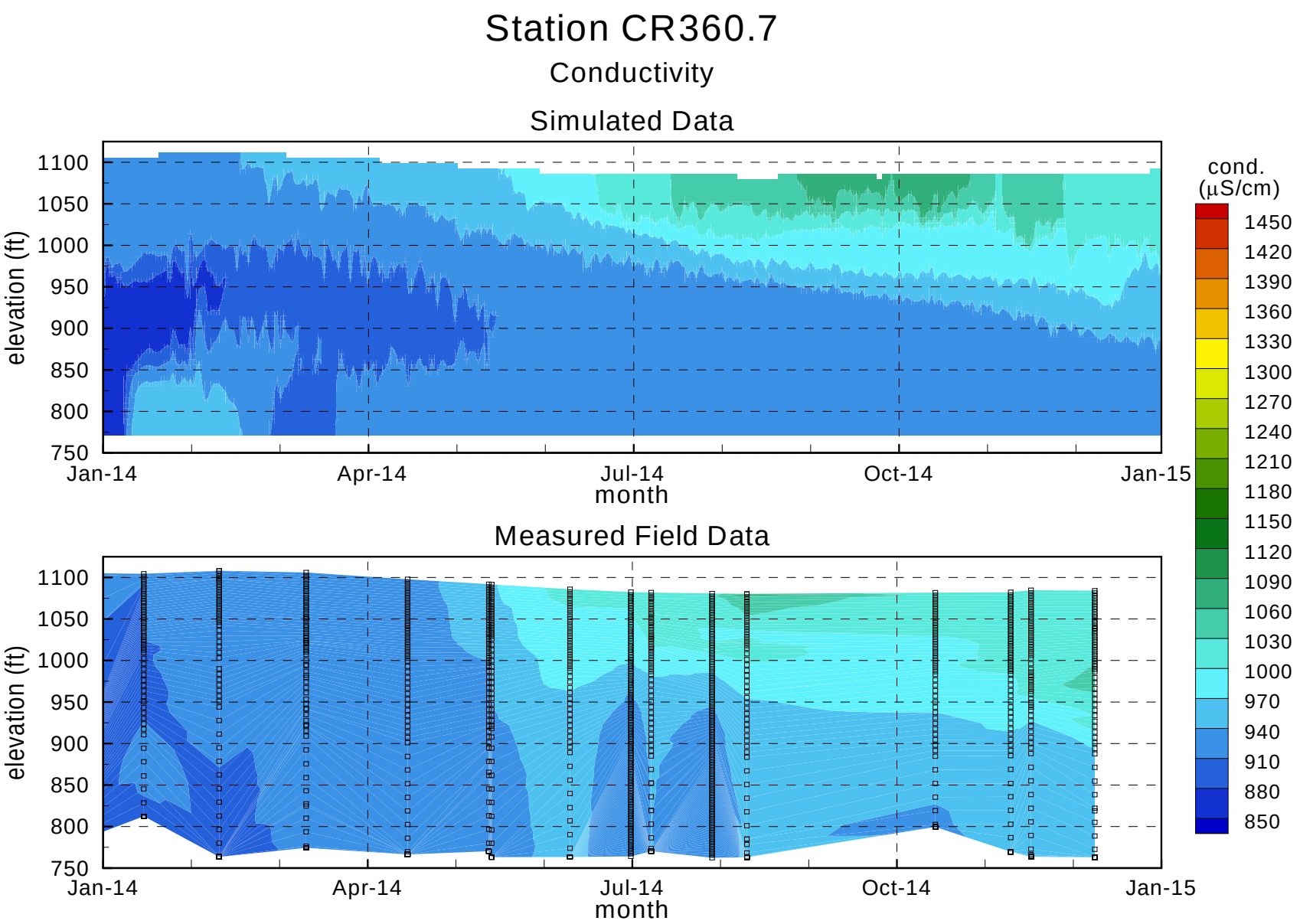
Station CR360.7
Conductivity
Simulated Data
Measured Field Data
elevation (ft)
1100
1050
1000
950
900
850
800
750
Jan-14
Apr-14
Jul-14
Oct-14
Jan-15
month
cond.
(µS/cm)
1450
1420
1390
1360
1330
1300
1270
1240
1210
1180
1150
1120
1090
1060
1030
1000
970
940
910
880
850

Figure B.32

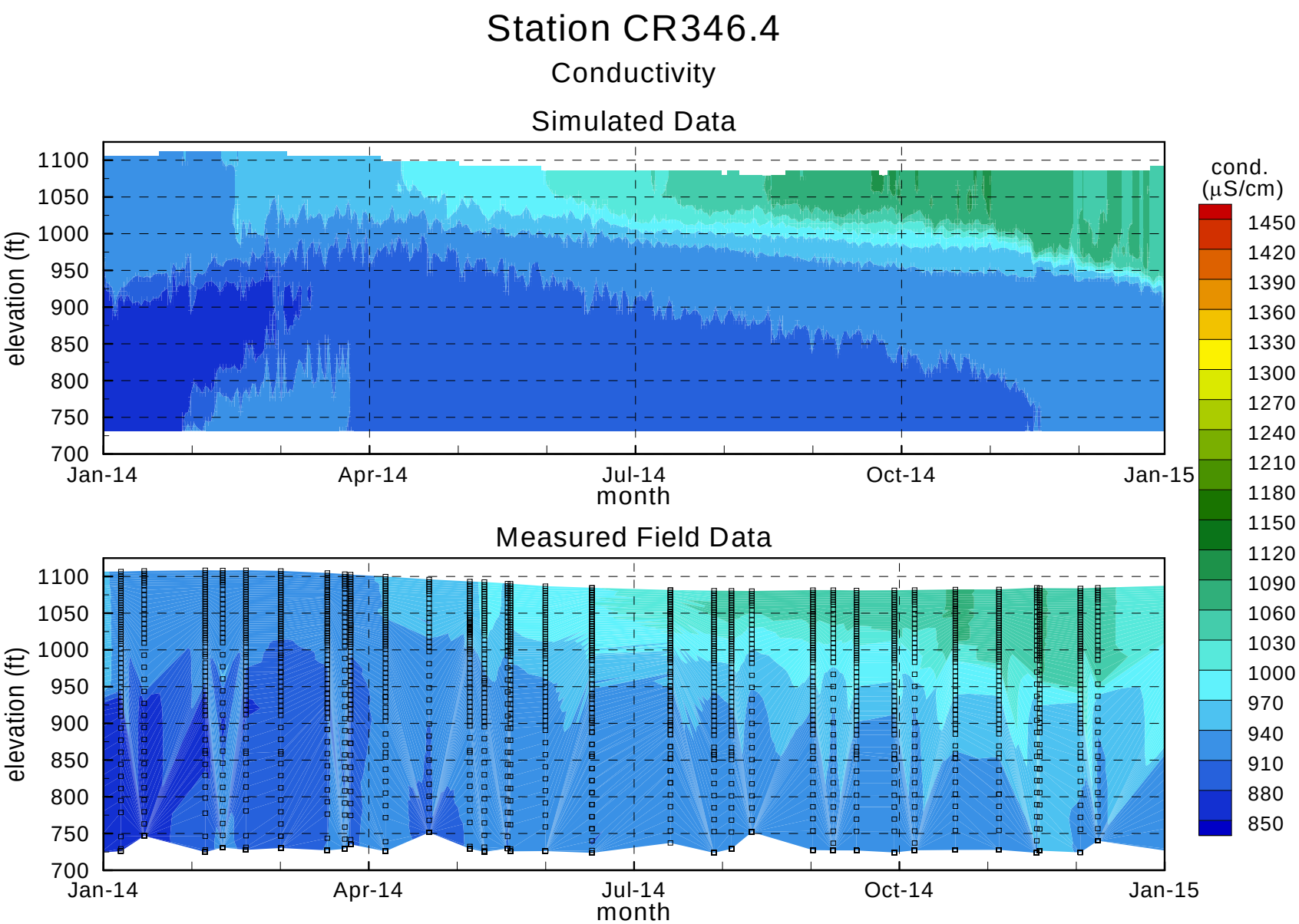

Figure B.33

FLOW SCIENCE

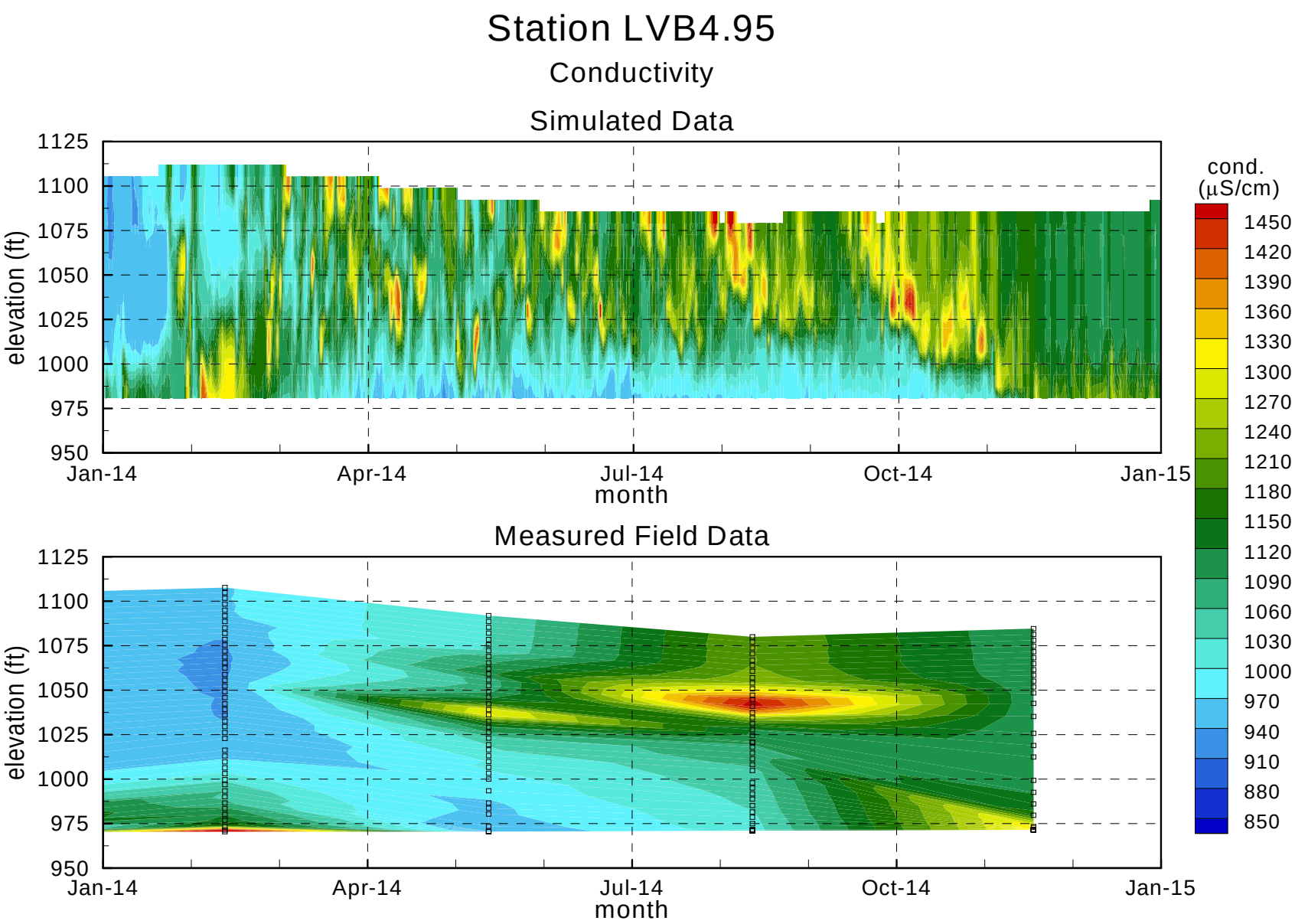

Figure B.34

FLOW SCIENCE

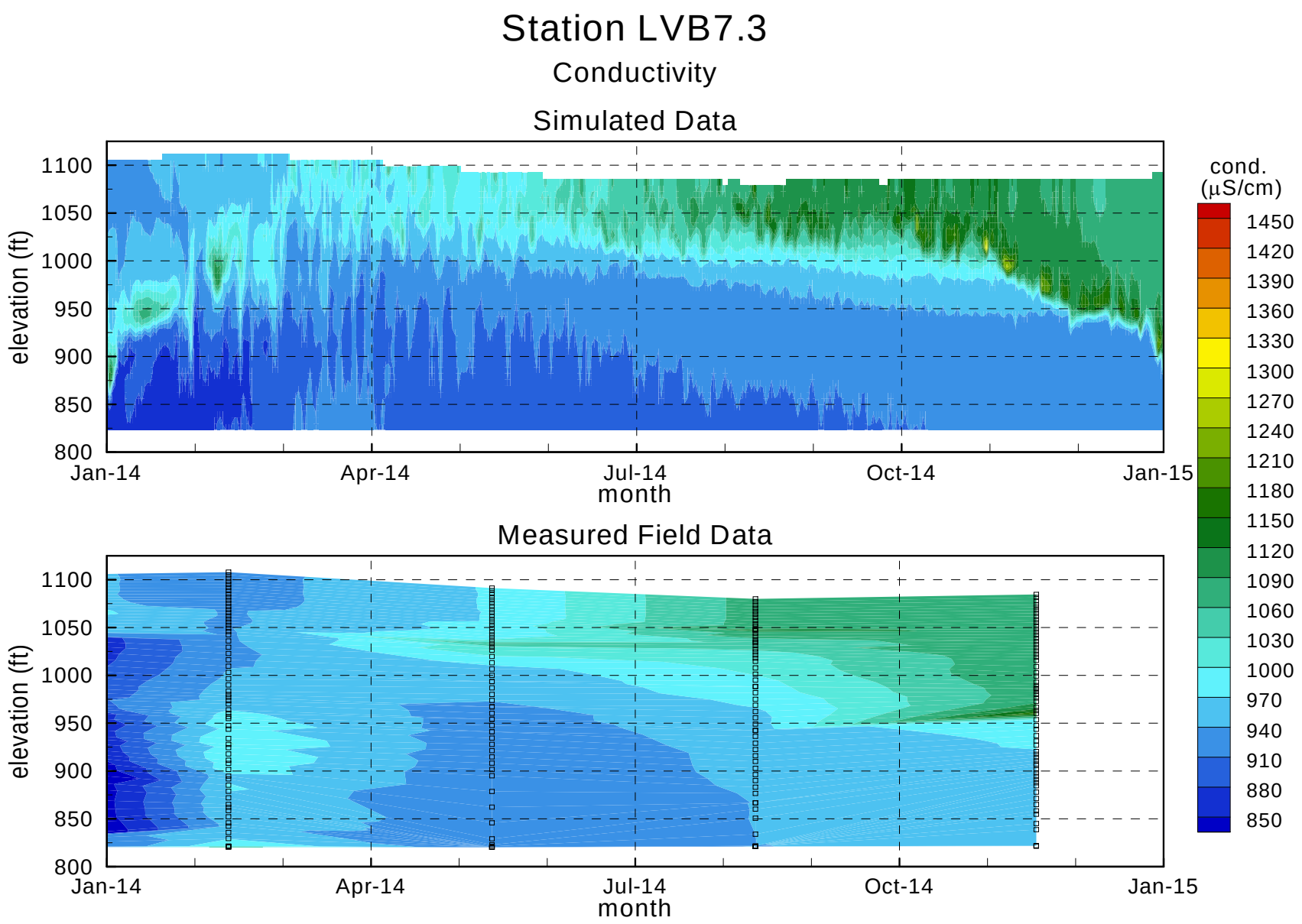
Station LVB7.3
Conductivity
Simulated Data
elevation (ft)
1100
1050
1000
950
900
850
800
Jan-14
Apr-14
Jul-14
Oct-14
Jan-15
month
Measured Field Data
cond.
(µS/cm)
1450
1420
1390
1360
1330
1300
1270
1240
1210
1180
1150
1120
1090
1060
1030
1000
970
940
910
880
850

Figure B.35

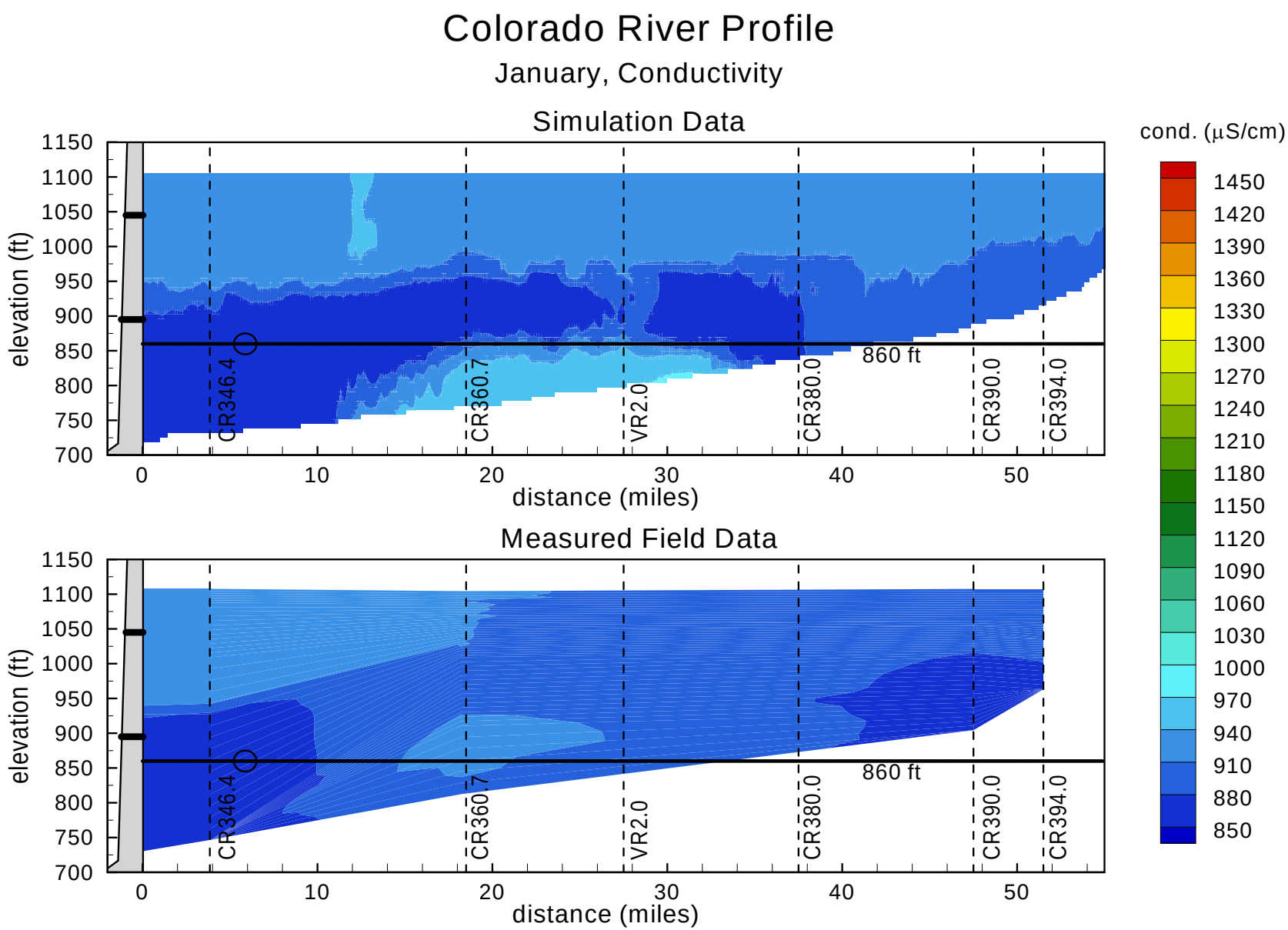

Figure B.36

FLOW SCIENCE

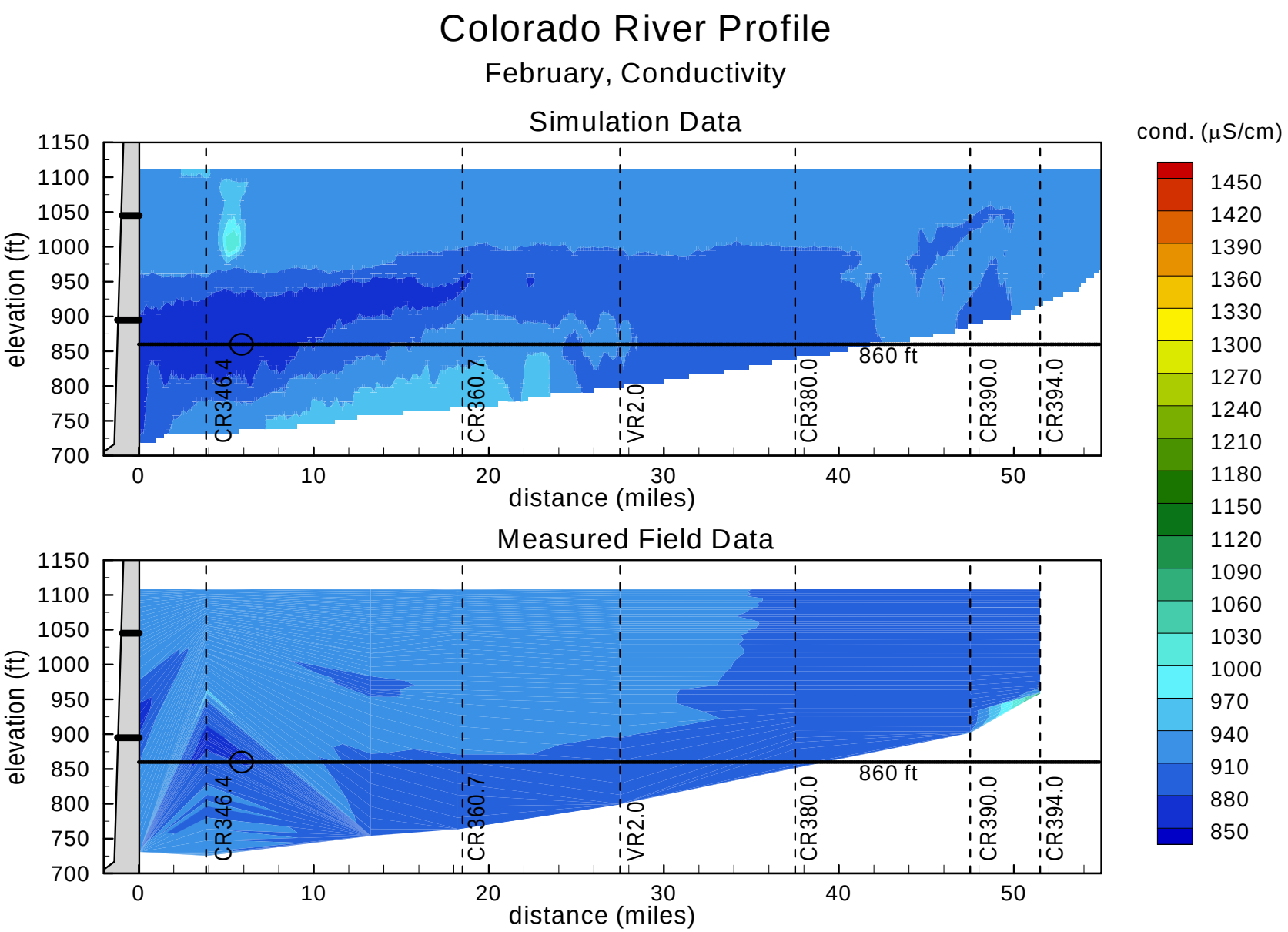

Figure B.37

FLOW SCIENCE

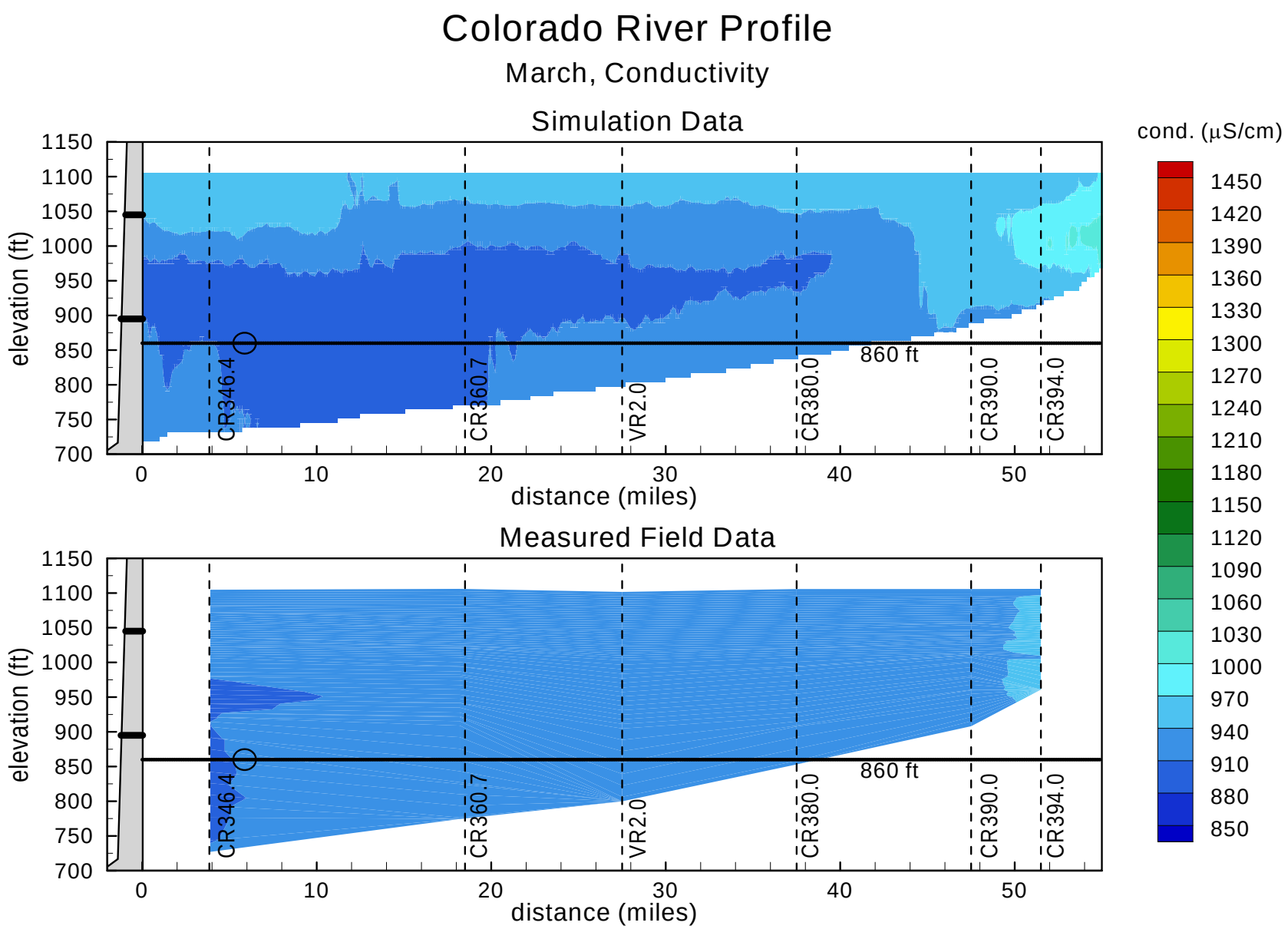
Colorado River Profile
March, Conductivity
Simulation Data
Measured Field Data
elevation (ft)
distance (miles)
860 ft
CR346.4
CR360.7
VR2.0
CR380.0
CR390.0
CR394.0
cond. (µS/cm)
1450
1420
1390
1360
1330
1300
1270
1240
1210
1180
1150
1120
1090
1060
1030
1000
970
940
910
880
850

Figure B.38

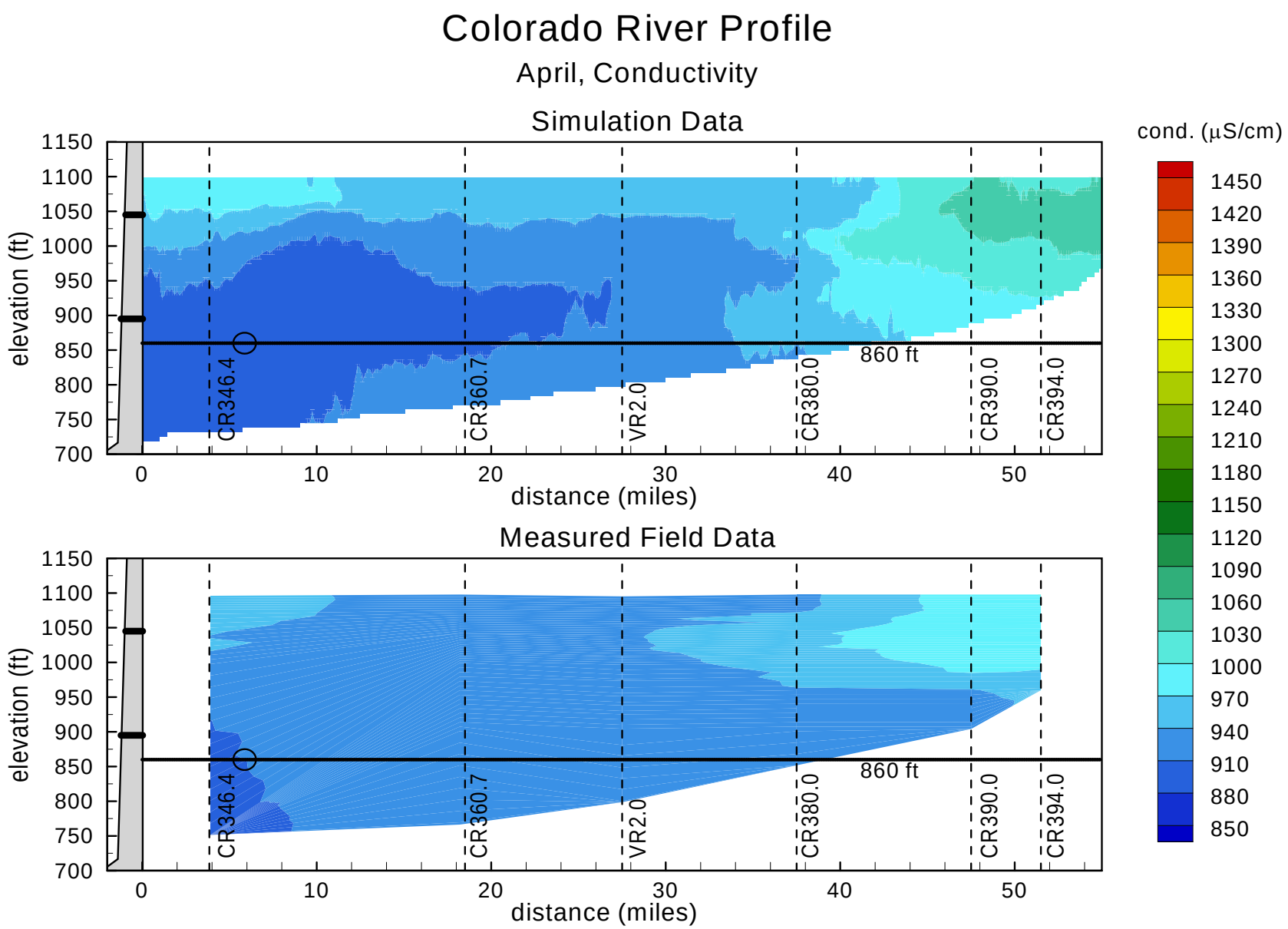
Colorado River Profile
April, Conductivity
Simulation Data
Measured Field Data
elevation (ft)
distance (miles)
860 ft
CR346.4
CR360.7
VR2.0
CR380.0
CR390.0
CR394.0
cond. (µS/cm)
1450
1420
1390
1360
1330
1300
1270
1240
1210
1180
1150
1120
1090
1060
1030
1000
970
940
910
880
850

Figure B.39

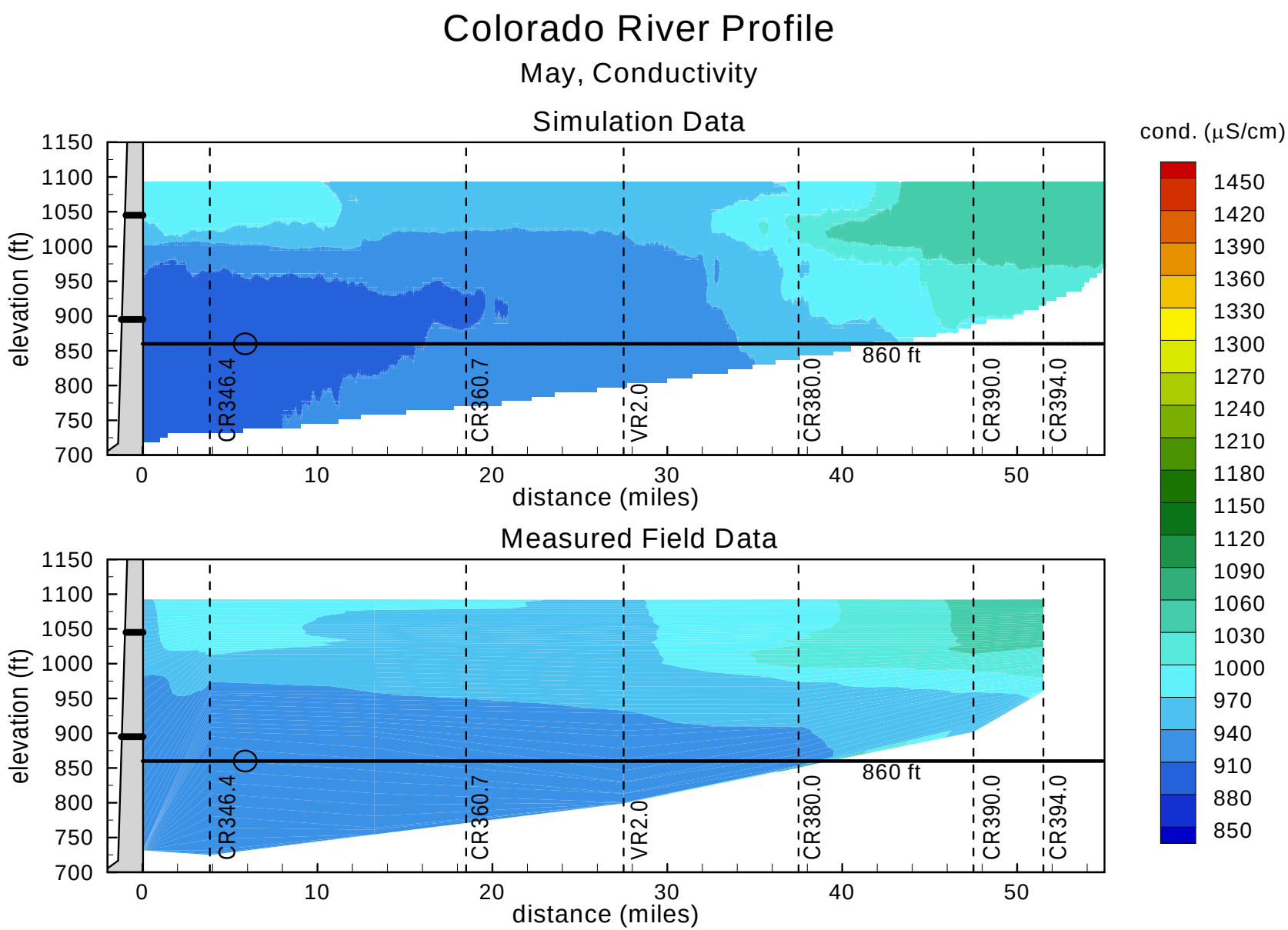
Colorado River Profile
May, Conductivity
Simulation Data
Measured Field Data
elevation (ft)
distance (miles)
860 ft
CR346.4
CR360.7
VR2.0
CR380.0
CR390.0
CR394.0
cond. (µS/cm)
1450
1420
1390
1360
1330
1300
1270
1240
1210
1180
1150
1120
1090
1060
1030
1000
970
940
910
880
850

Figure B.40

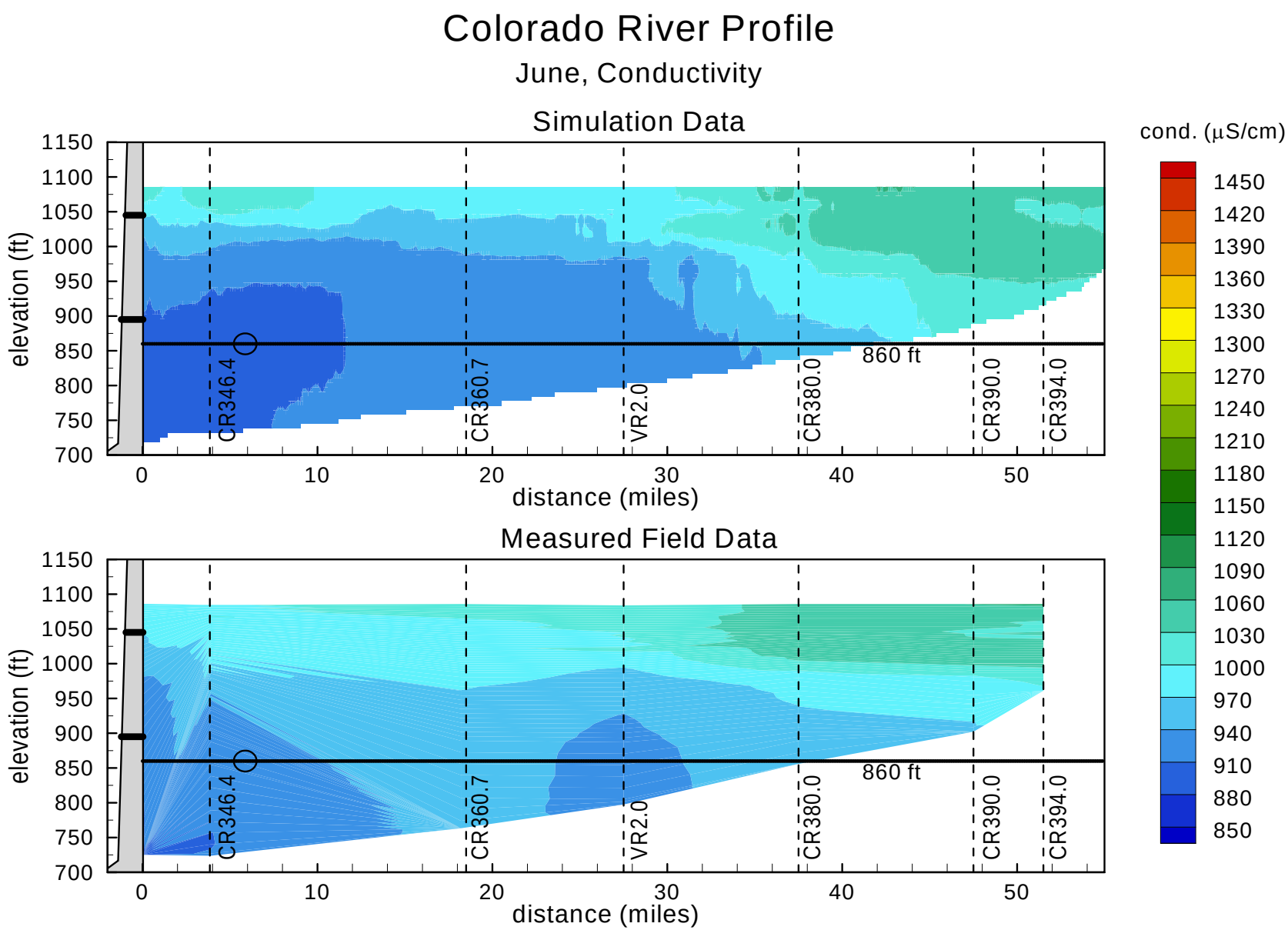

Figure B.41

FLOW SCIENCE

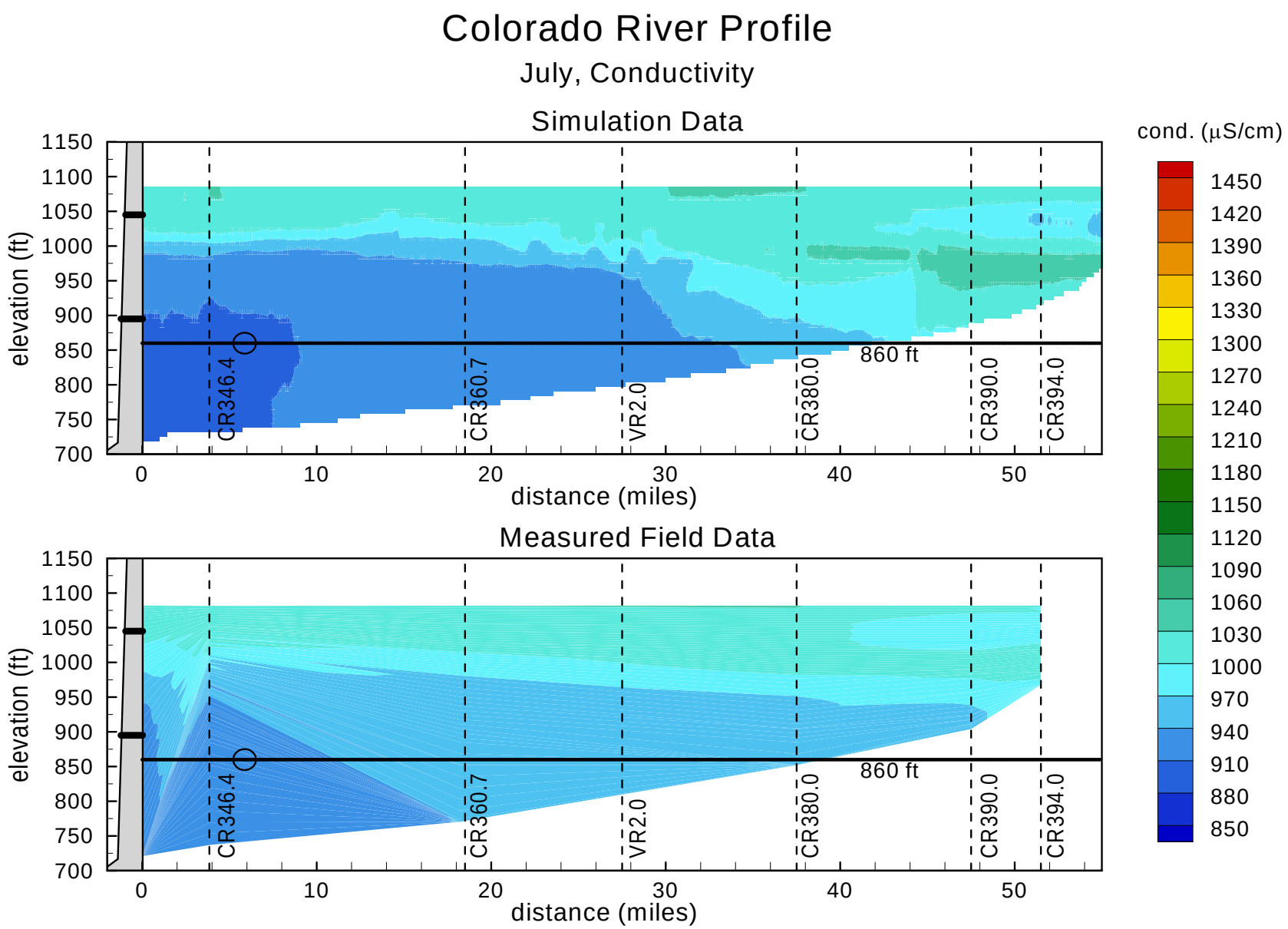

Figure B.42

FLOW SCIENCE

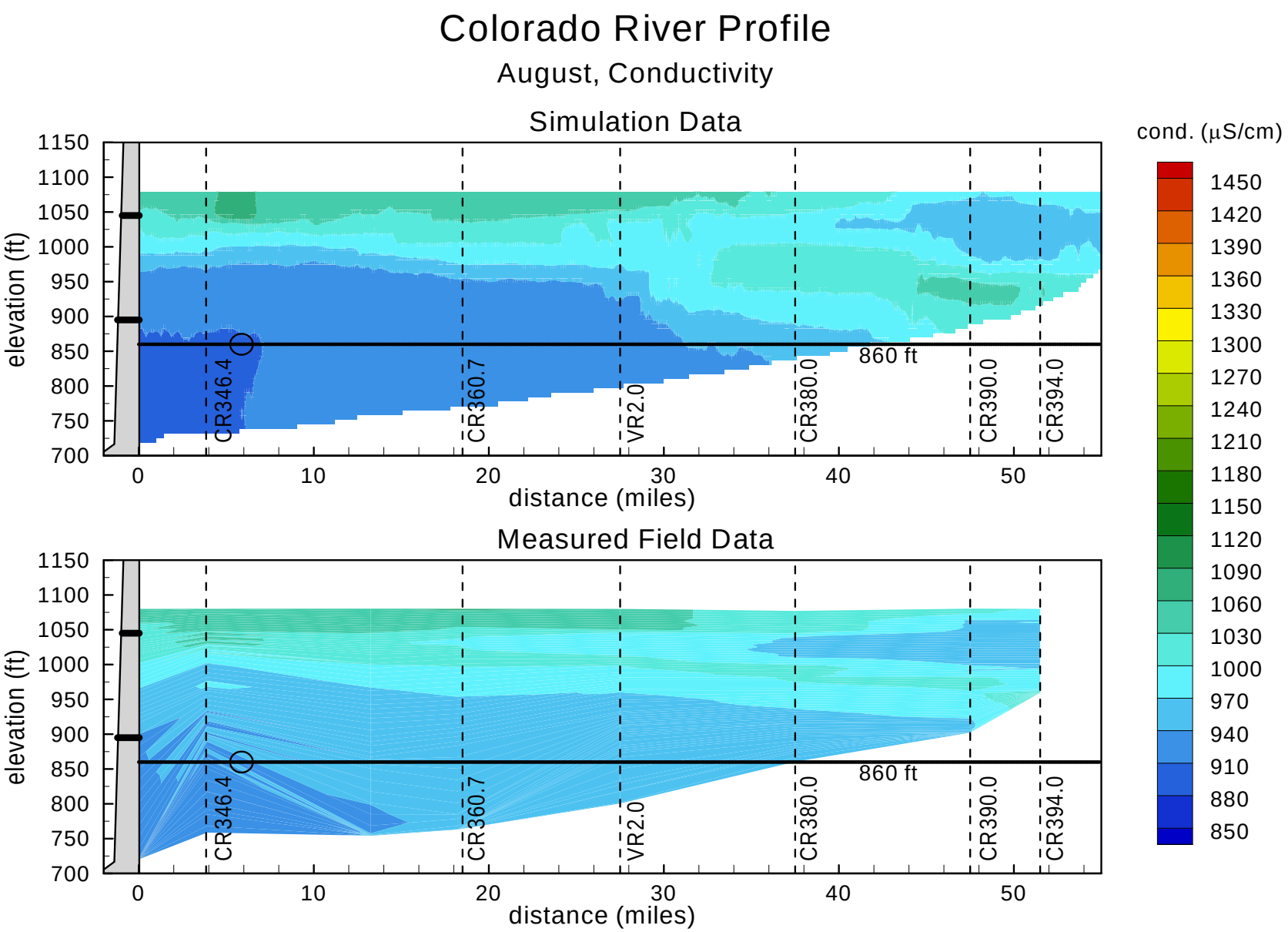
Colorado River Profile
August, Conductivity
Simulation Data
Measured Field Data
elevation (ft)
distance (miles)
860 ft
CR346.4
CR360.7
VR2.0
CR380.0
CR390.0
CR394.0
cond. (µS/cm)
1450
1420
1390
1360
1330
1300
1270
1240
1210
1180
1150
1120
1090
1060
1030
1000
970
940
910
880
850

Figure B.43

Colorado River Profile

October, Conductivity

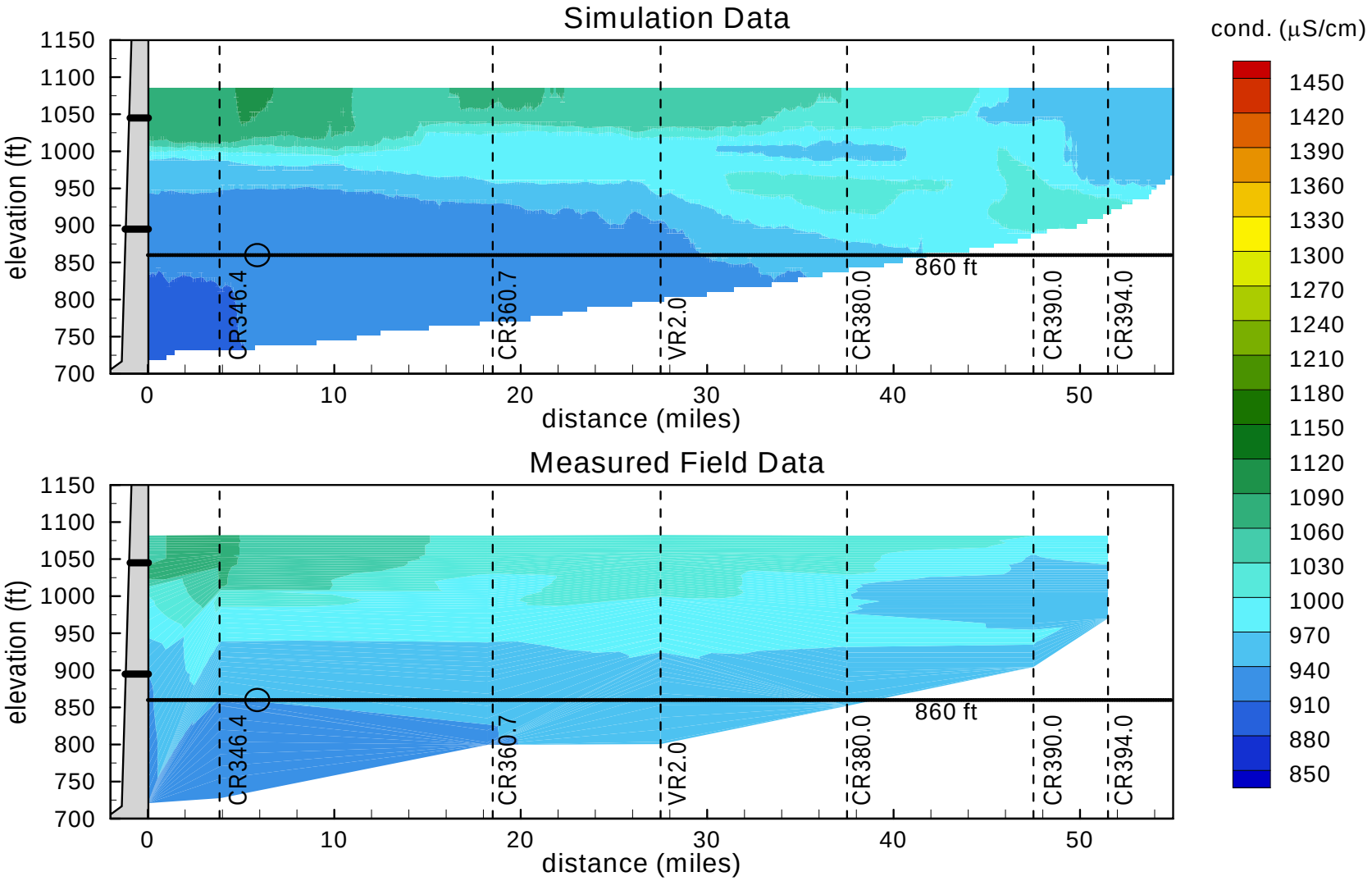

Figure B.44

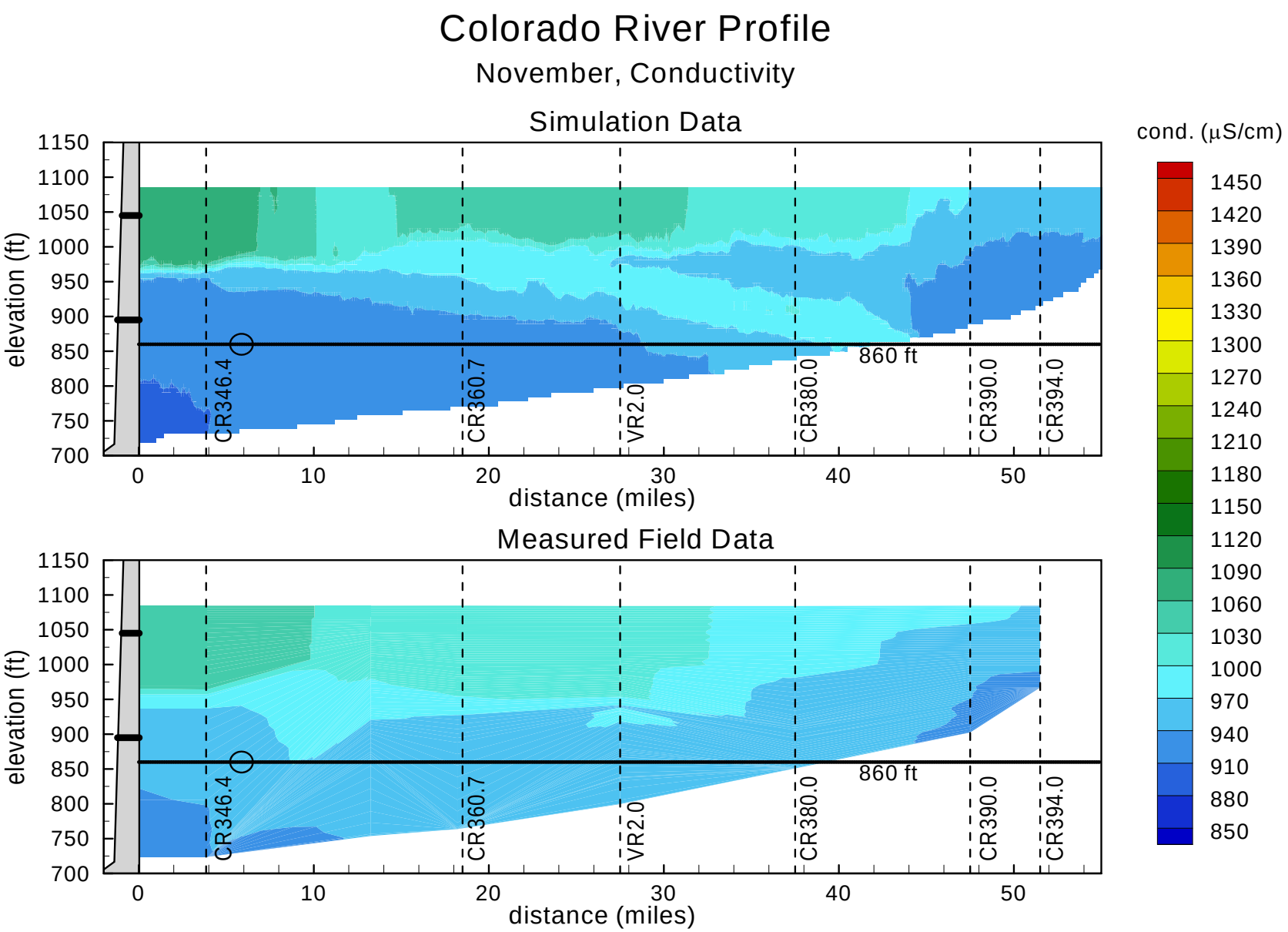
Colorado River Profile
November, Conductivity
Simulation Data
Measured Field Data
elevation (ft)
distance (miles)
860 ft
CR346.4
CR360.7
VR2.0
CR380.0
CR390.0
CR394.0
cond. (µS/cm)
1450
1420
1390
1360
1330
1300
1270
1240
1210
1180
1150
1120
1090
1060
1030
1000
970
940
910
880
850

Figure B.45

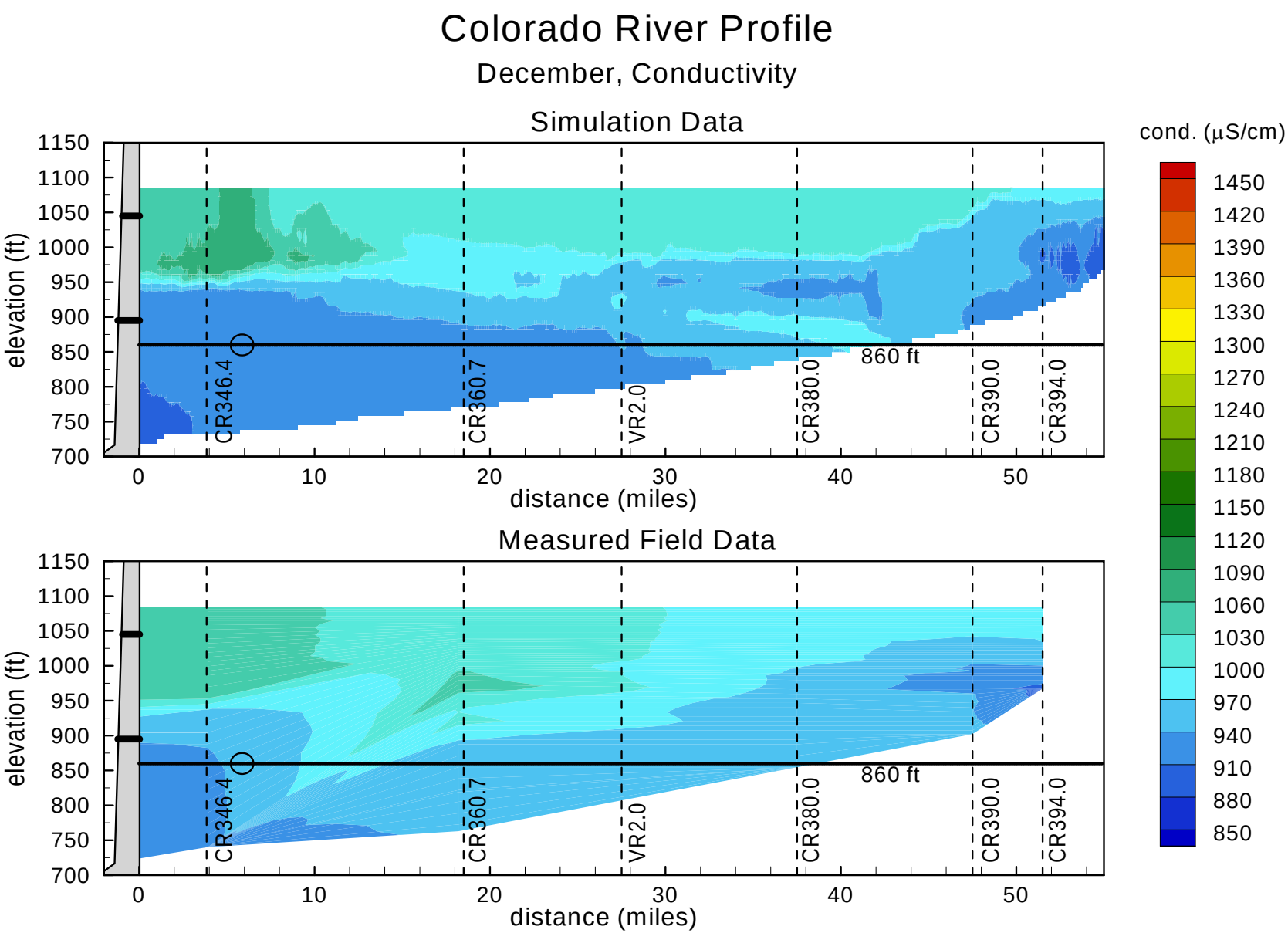

Figure B.46

FLOW SCIENCE

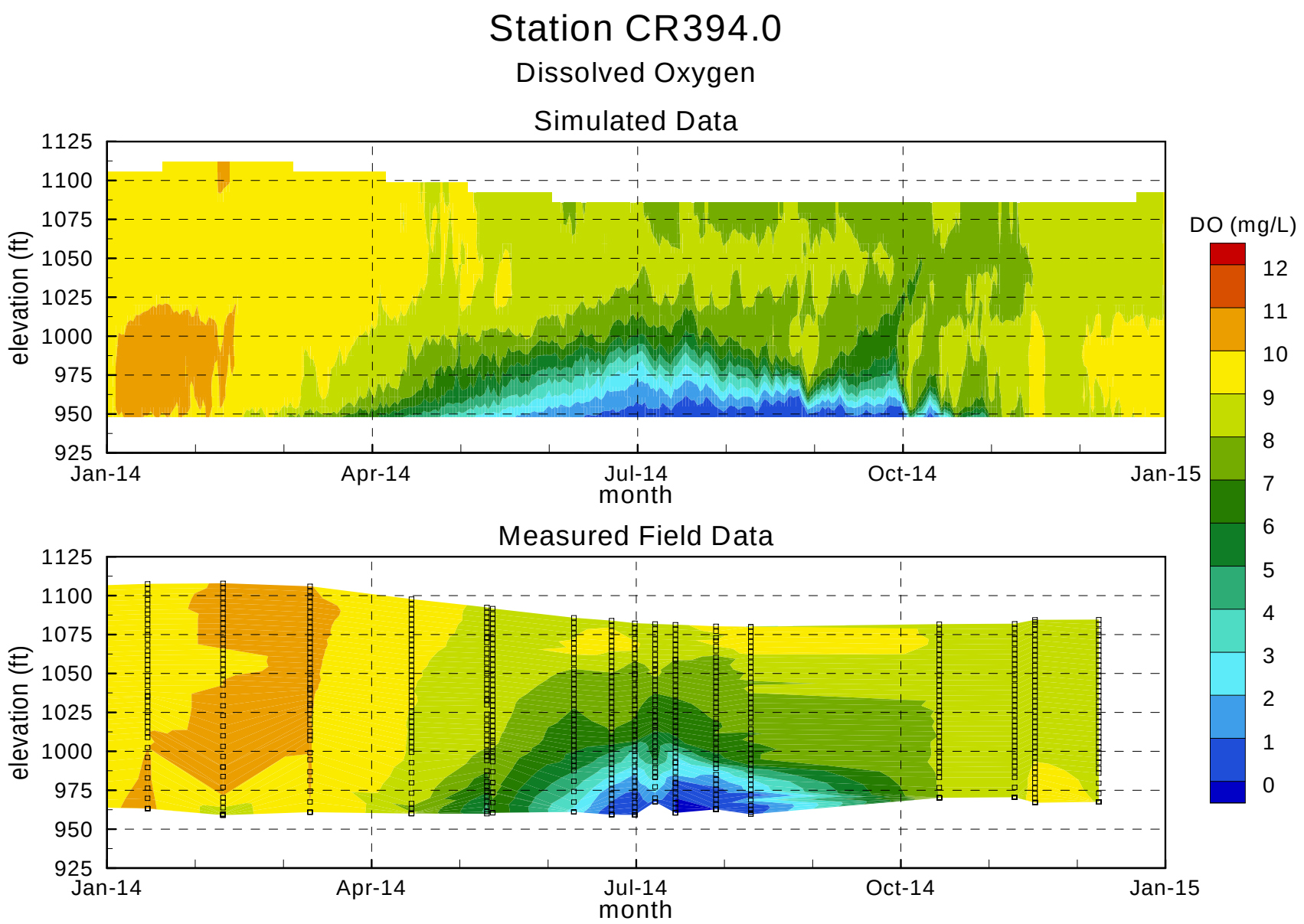

Figure B.47

FLOW SCIENCE

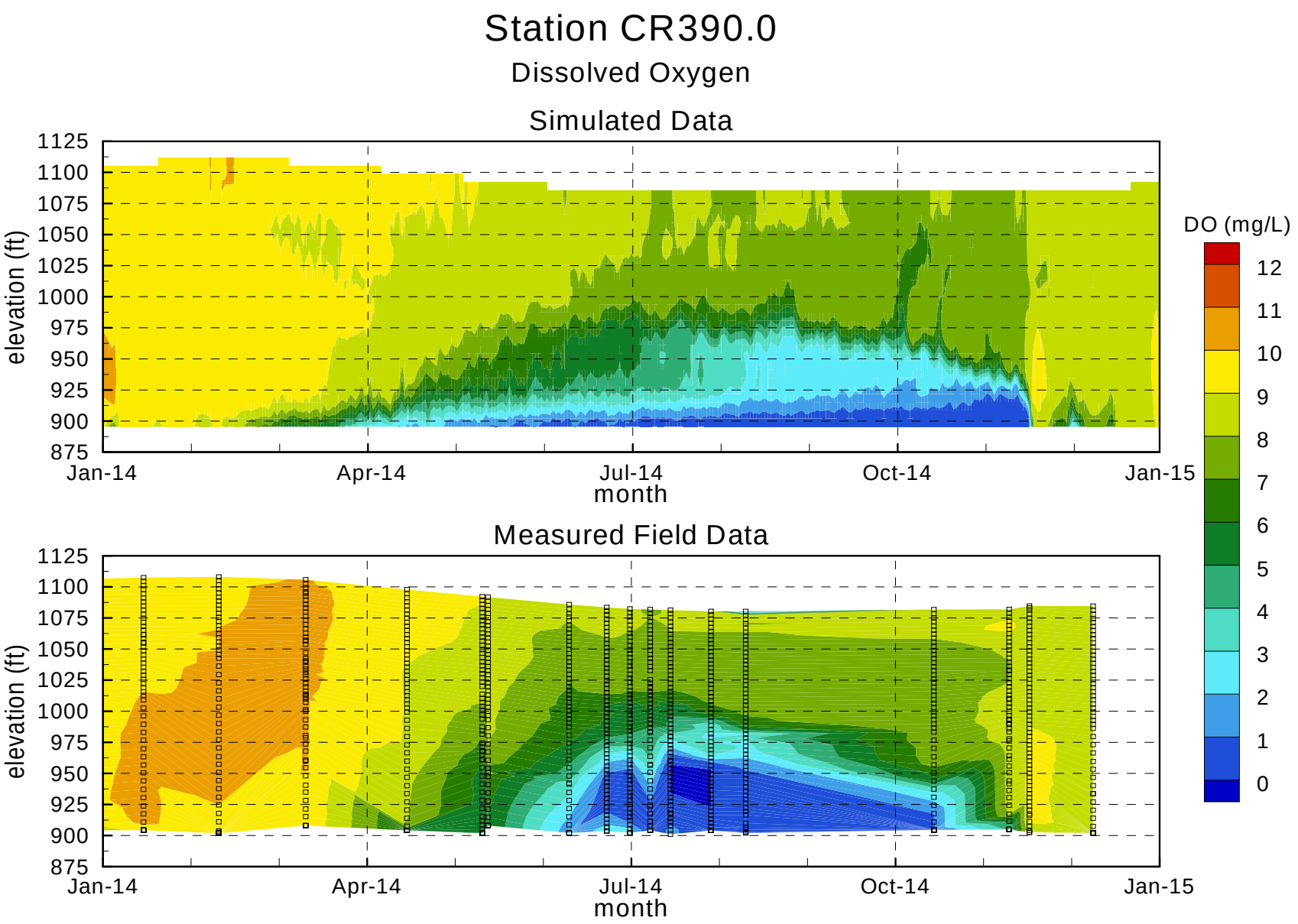
Station CR390.0
Dissolved Oxygen
Simulated Data
Measured Field Data
elevation (ft)
1125
1100
1075
1050
1025
1000
975
950
925
900
875
Jan-14
Apr-14
Jul-14
Oct-14
Jan-15
month
DO (mg/L)
12
11
10
9
8
7
6
5
4
3
2
1
0

Figure B.48

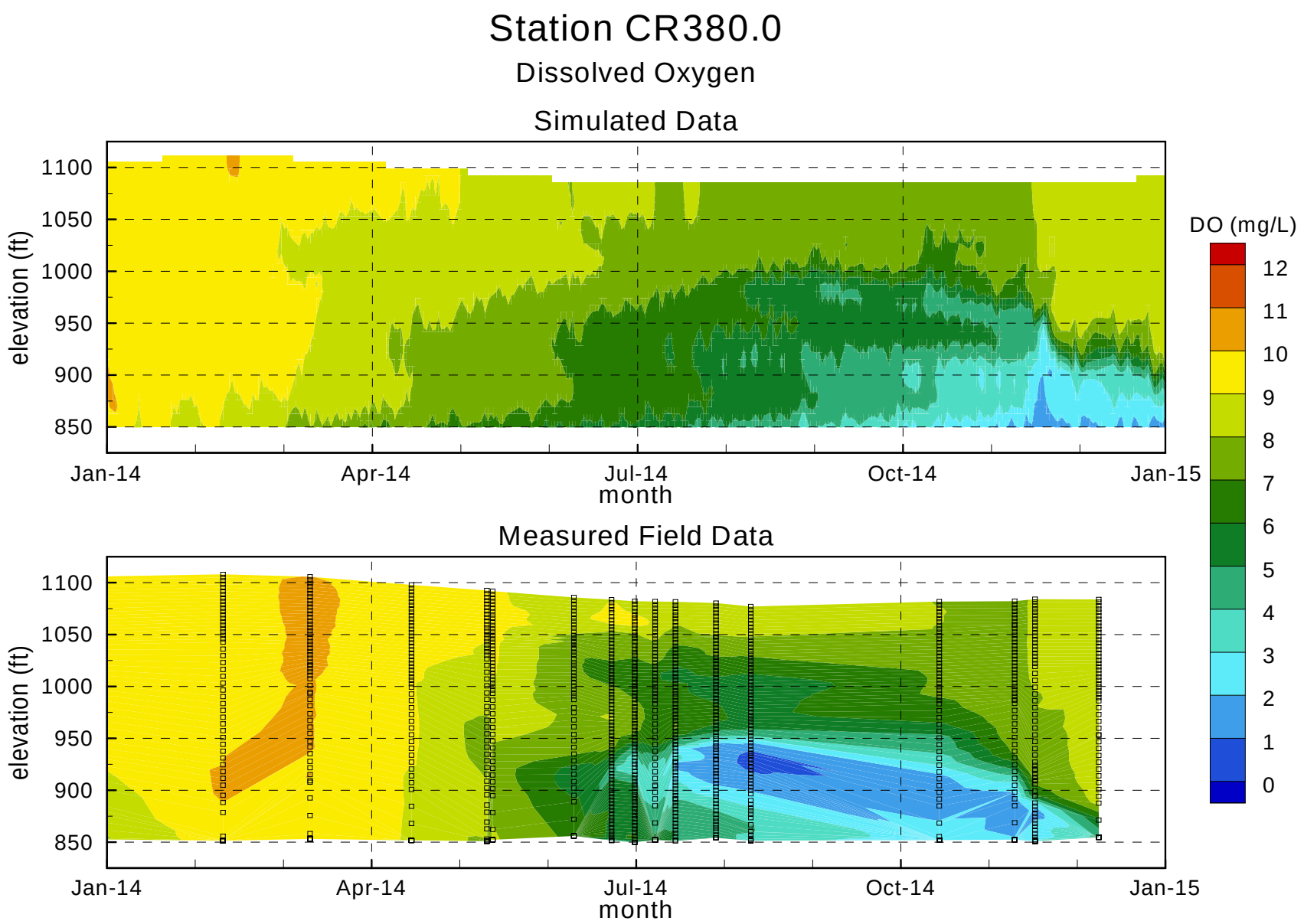

Figure B.49

FLOW SCIENCE

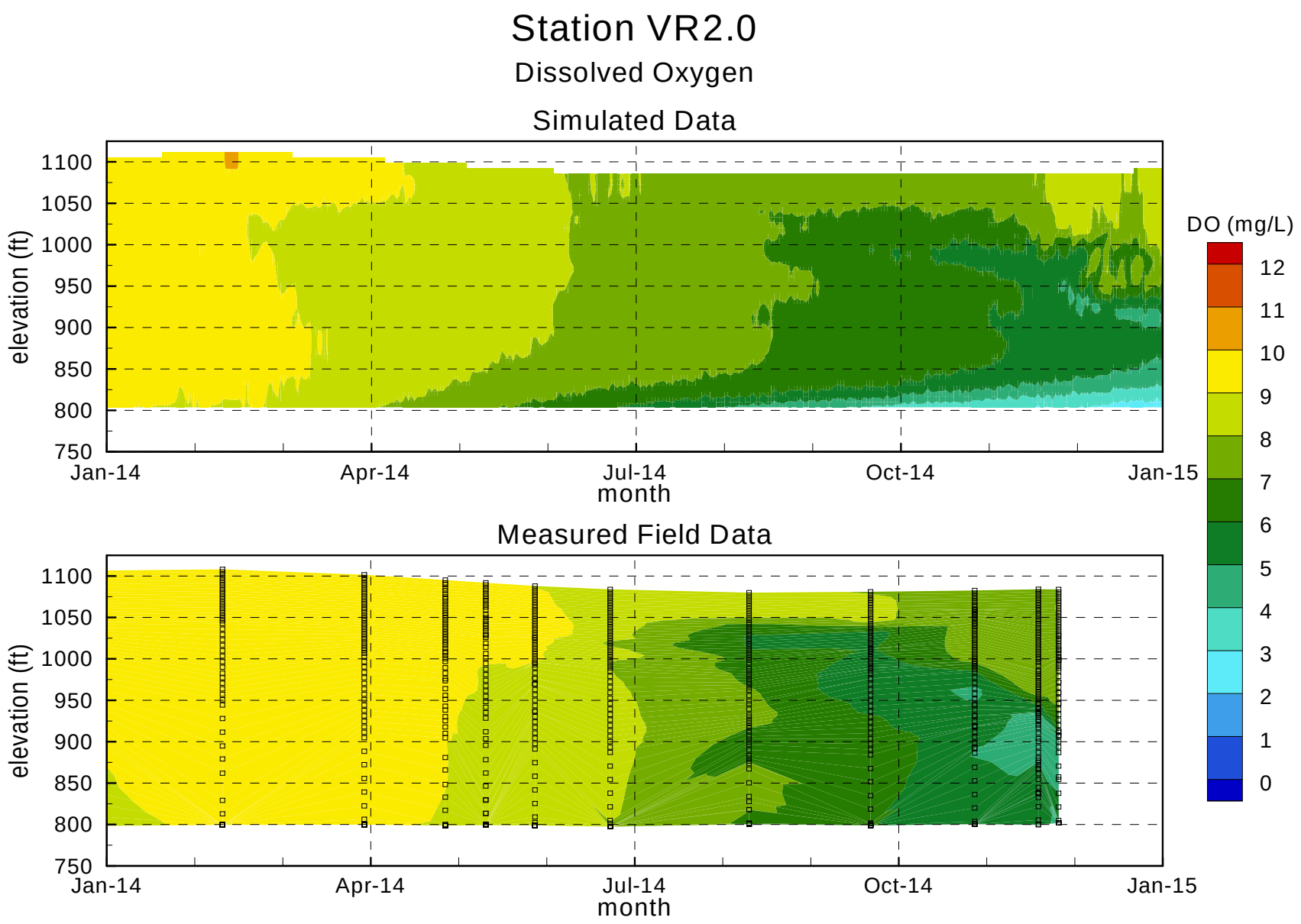
Station VR2.0
Dissolved Oxygen
Simulated Data
Measured Field Data
elevation (ft)
1100
1050
1000
950
900
850
800
750
Jan-14
Apr-14
Jul-14
Oct-14
Jan-15
month
DO (mg/L)
12
11
10
9
8
7
6
5
4
3
2
1
0

Figure B.50

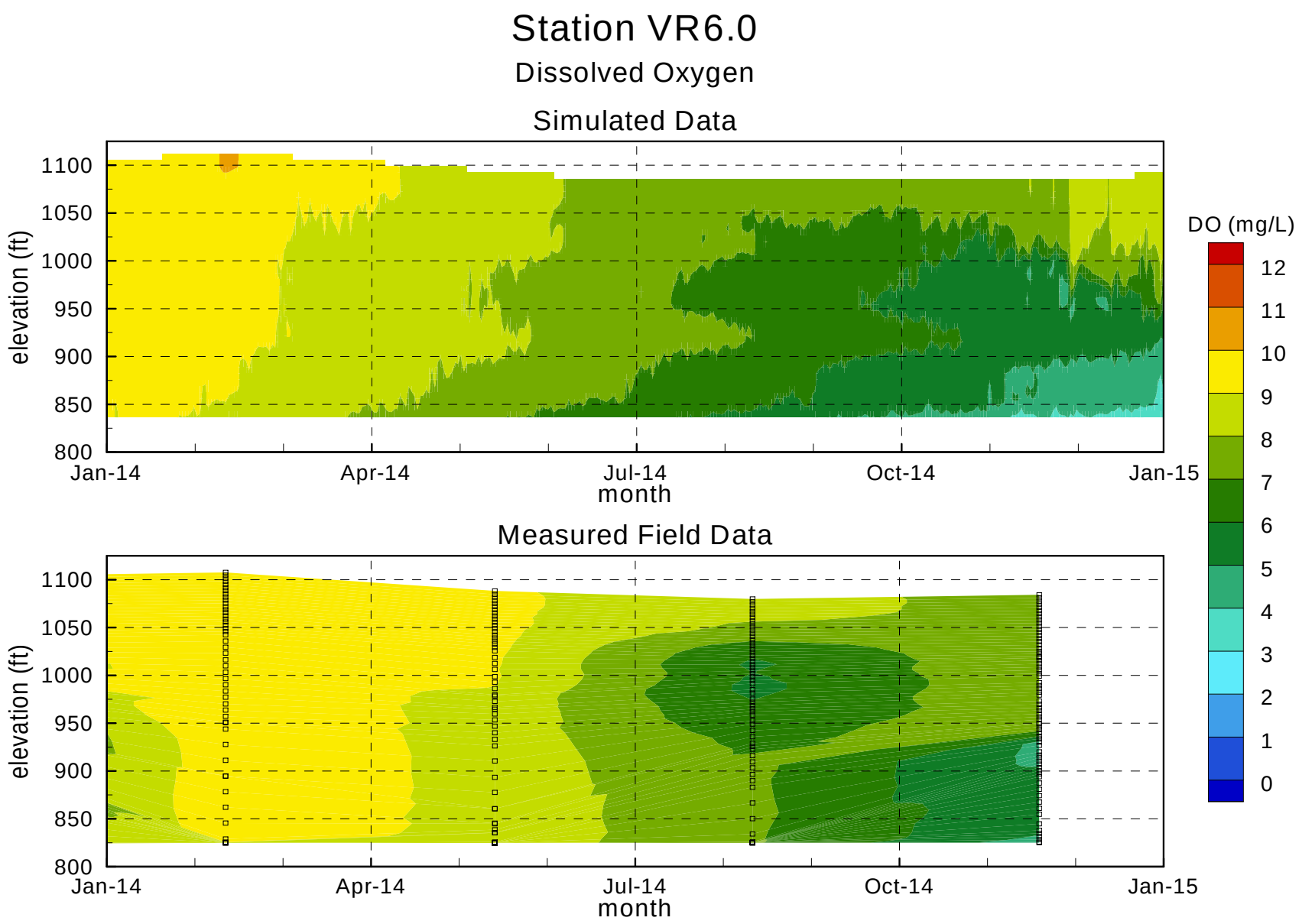
Station VR6.0
Dissolved Oxygen
Simulated Data
Measured Field Data
elevation (ft)
1100
1050
1000
950
900
850
800
Jan-14
Apr-14
Jul-14
Oct-14
Jan-15
month
DO (mg/L)
12
11
10
9
8
7
6
5
4
3
2
1
0

Figure B.51

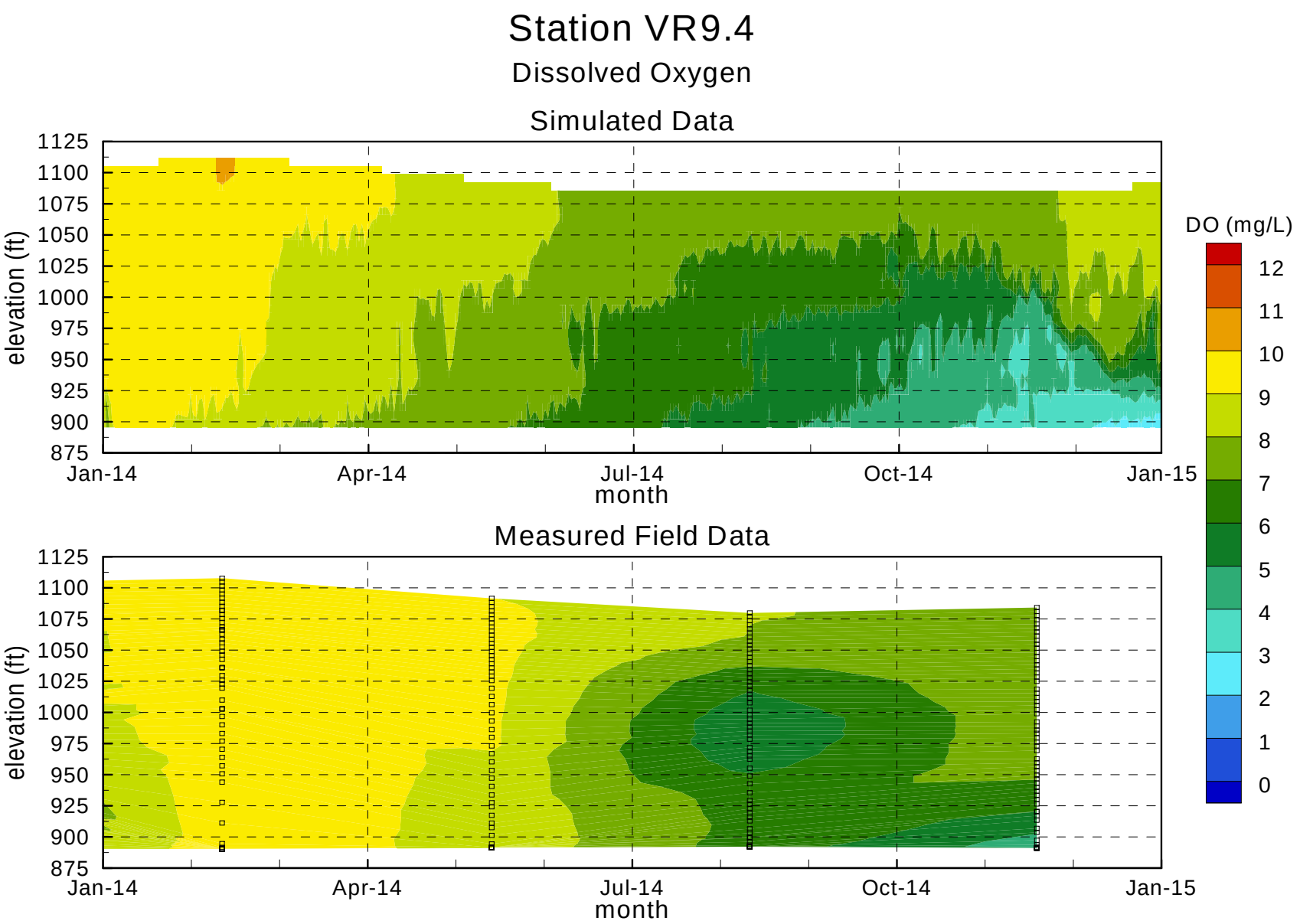
Station VR9.4
Dissolved Oxygen
Simulated Data
Measured Field Data
elevation (ft)
1125
1100
1075
1050
1025
1000
975
950
925
900
875
Jan-14
Apr-14
Jul-14
Oct-14
Jan-15
month
DO (mg/L)
12
11
10
9
8
7
6
5
4
3
2
1
0

Figure B.52

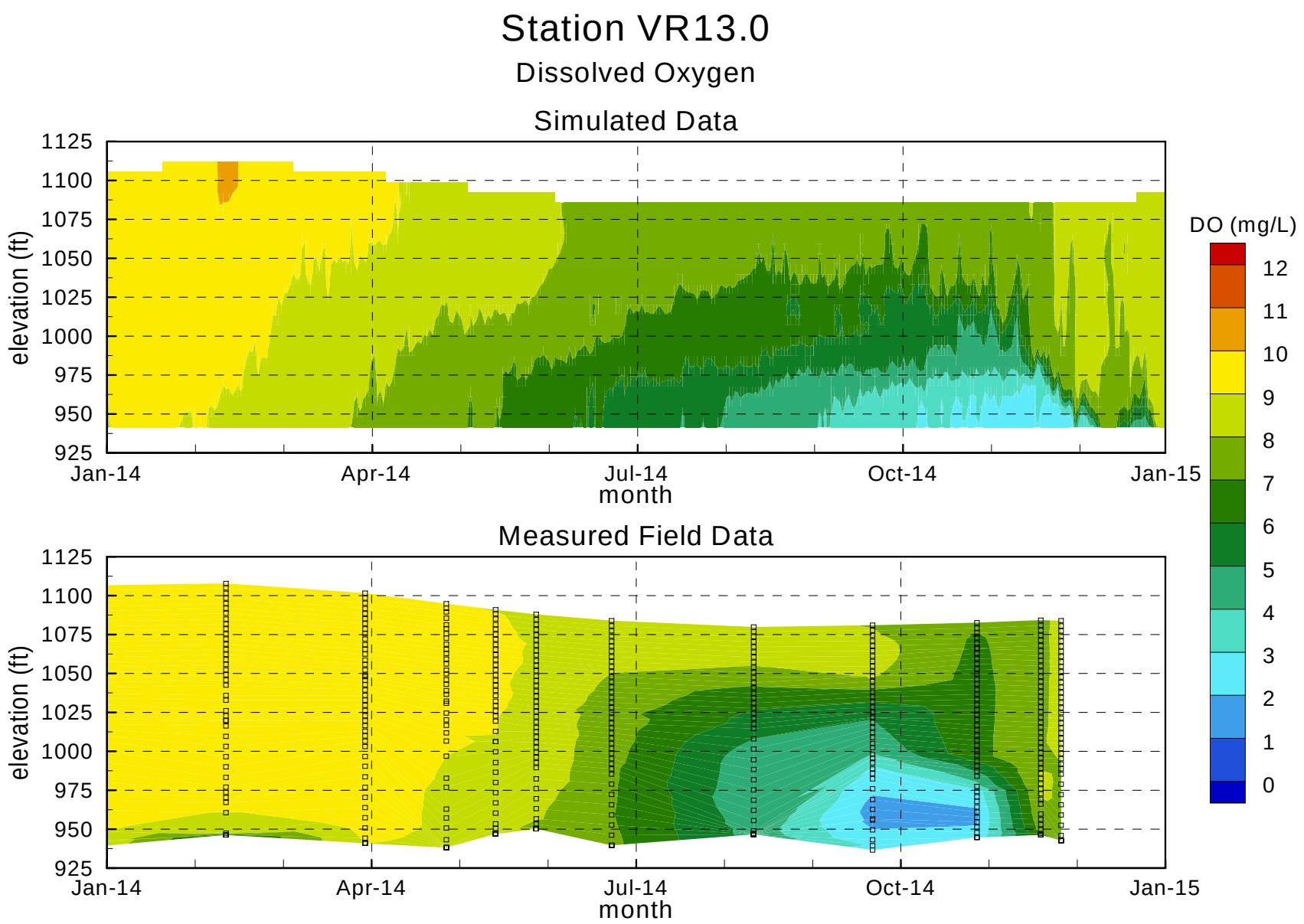
Station VR13.0
Dissolved Oxygen
Simulated Data
Measured Field Data
elevation (ft)
1125
1100
1075
1050
1025
1000
975
950
925
Jan-14
Apr-14
Jul-14
Oct-14
Jan-15
month
DO (mg/L)
12
11
10
9
8
7
6
5
4
3
2
1
0

Figure B.53

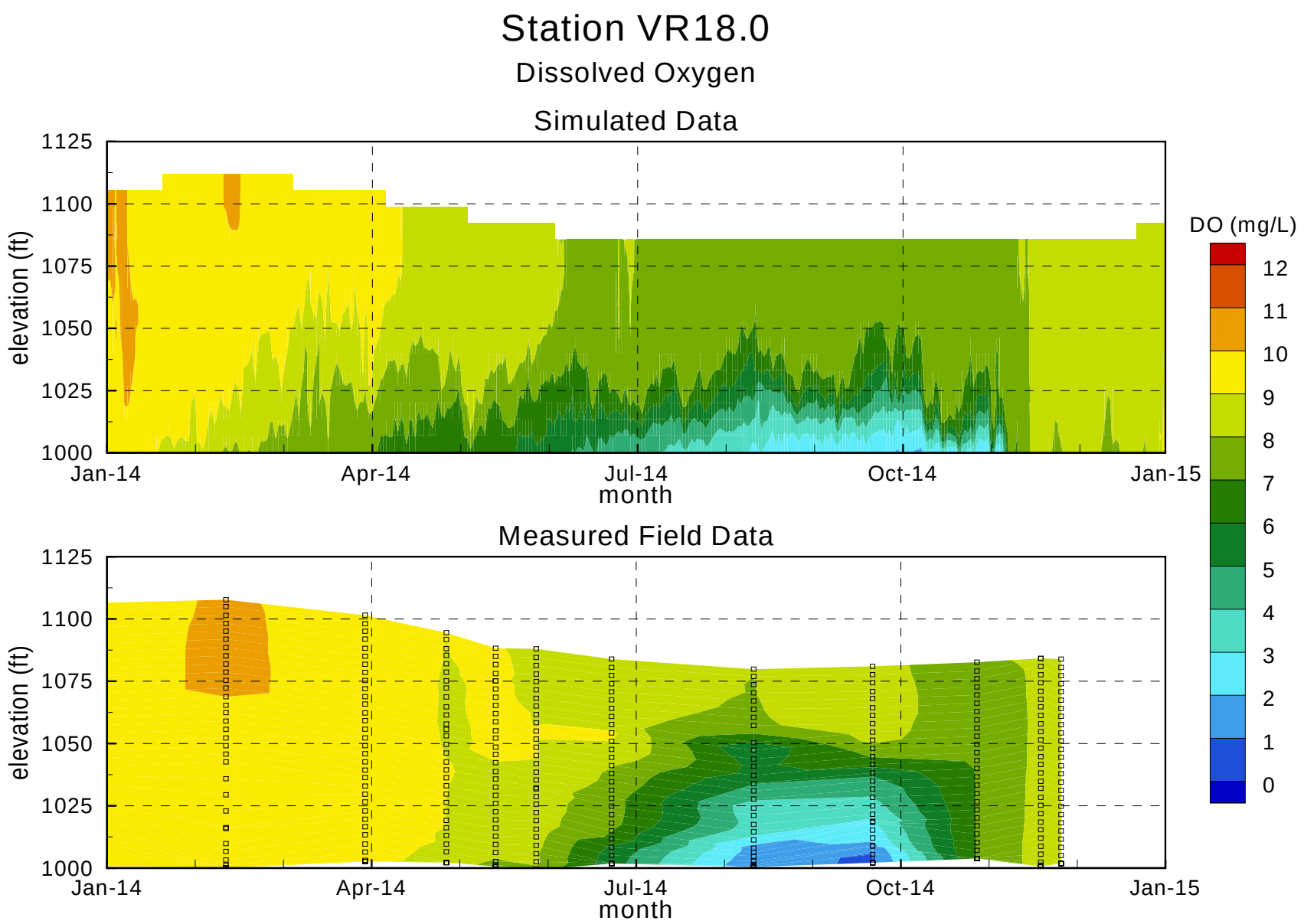
Station VR18.0
Dissolved Oxygen
Simulated Data
Measured Field Data
elevation (ft)
1125
1100
1075
1050
1025
1000
Jan-14
Apr-14
Jul-14
Oct-14
Jan-15
month
DO (mg/L)
12
11
10
9
8
7
6
5
4
3
2
1
0

Figure B.54

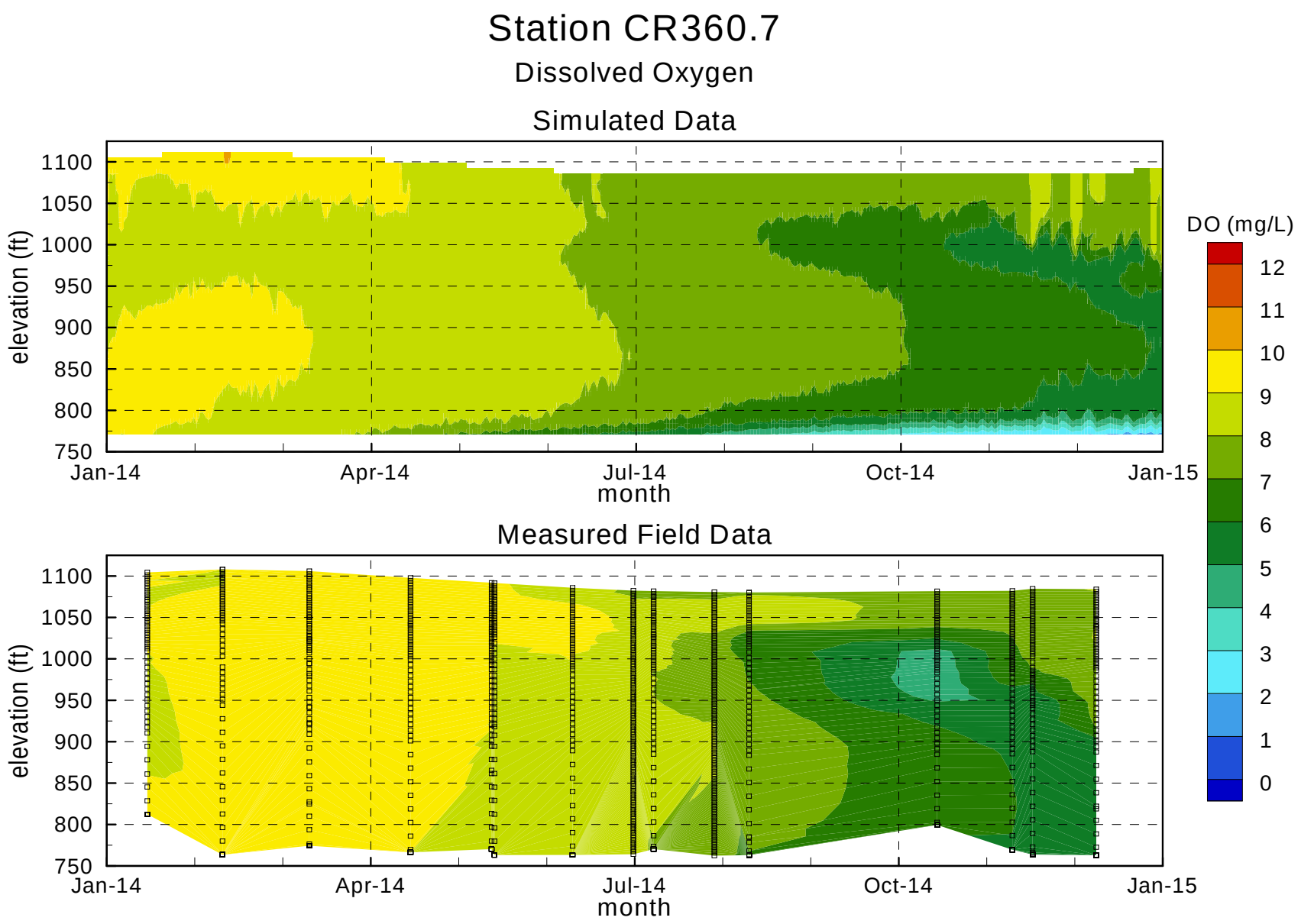

Figure B.55

FLOW SCIENCE

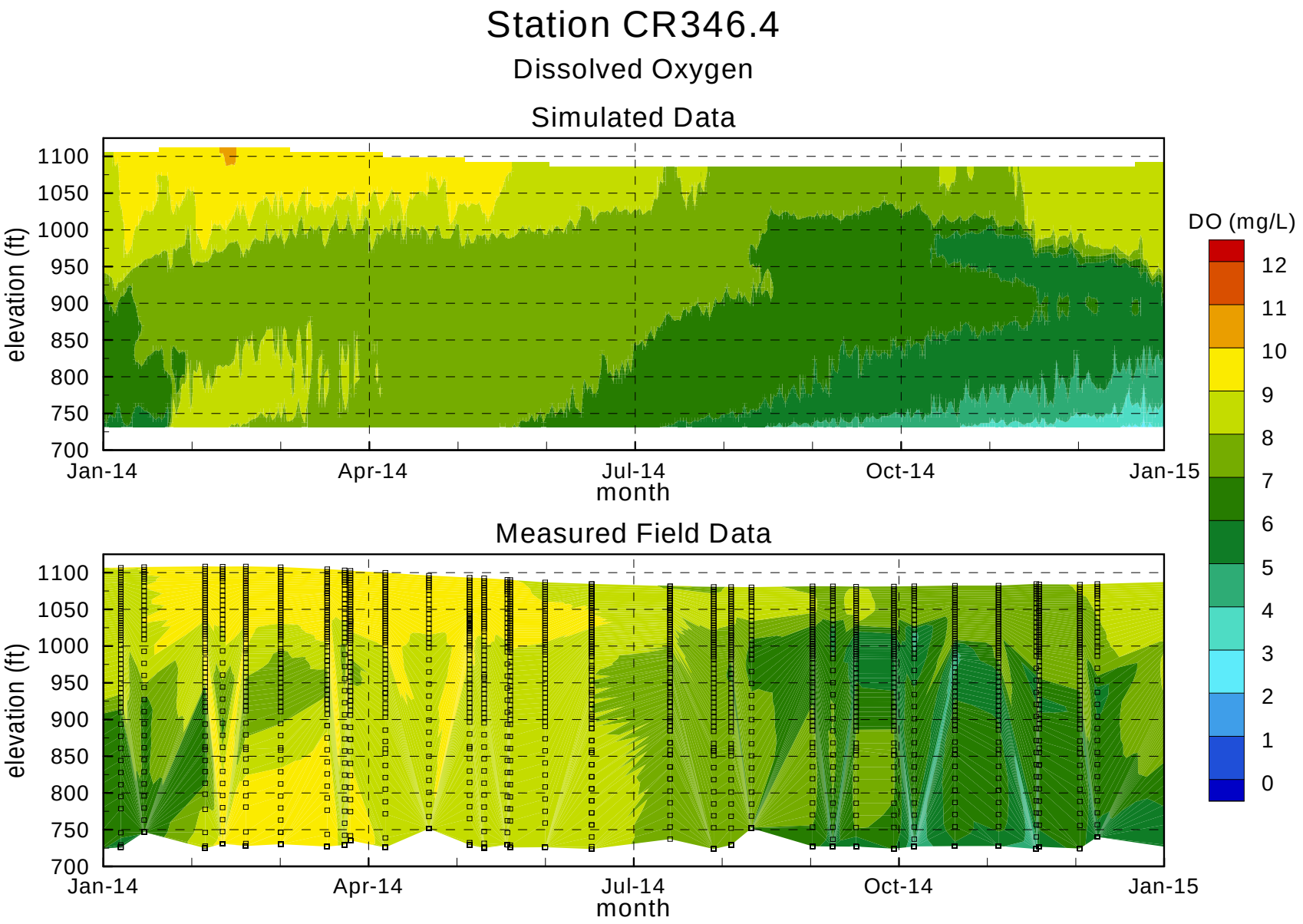

Figure B.56

FLOW SCIENCE

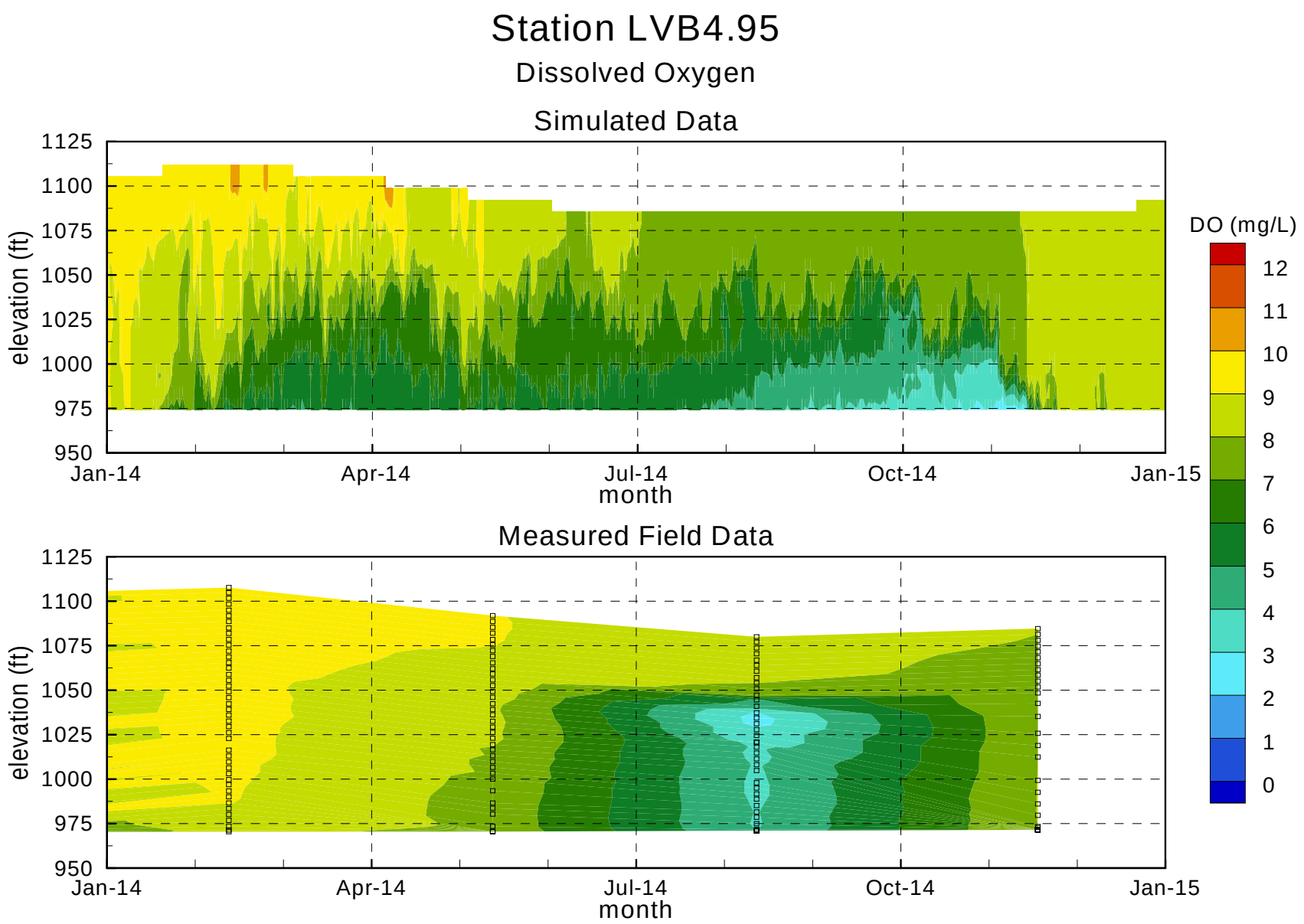
Station LVB4.95
Dissolved Oxygen
Simulated Data
Measured Field Data
elevation (ft)
1125
1100
1075
1050
1025
1000
975
950
Jan-14
Apr-14
Jul-14
Oct-14
Jan-15
month
DO (mg/L)
12
11
10
9
8
7
6
5
4
3
2
1
0

Figure B.57

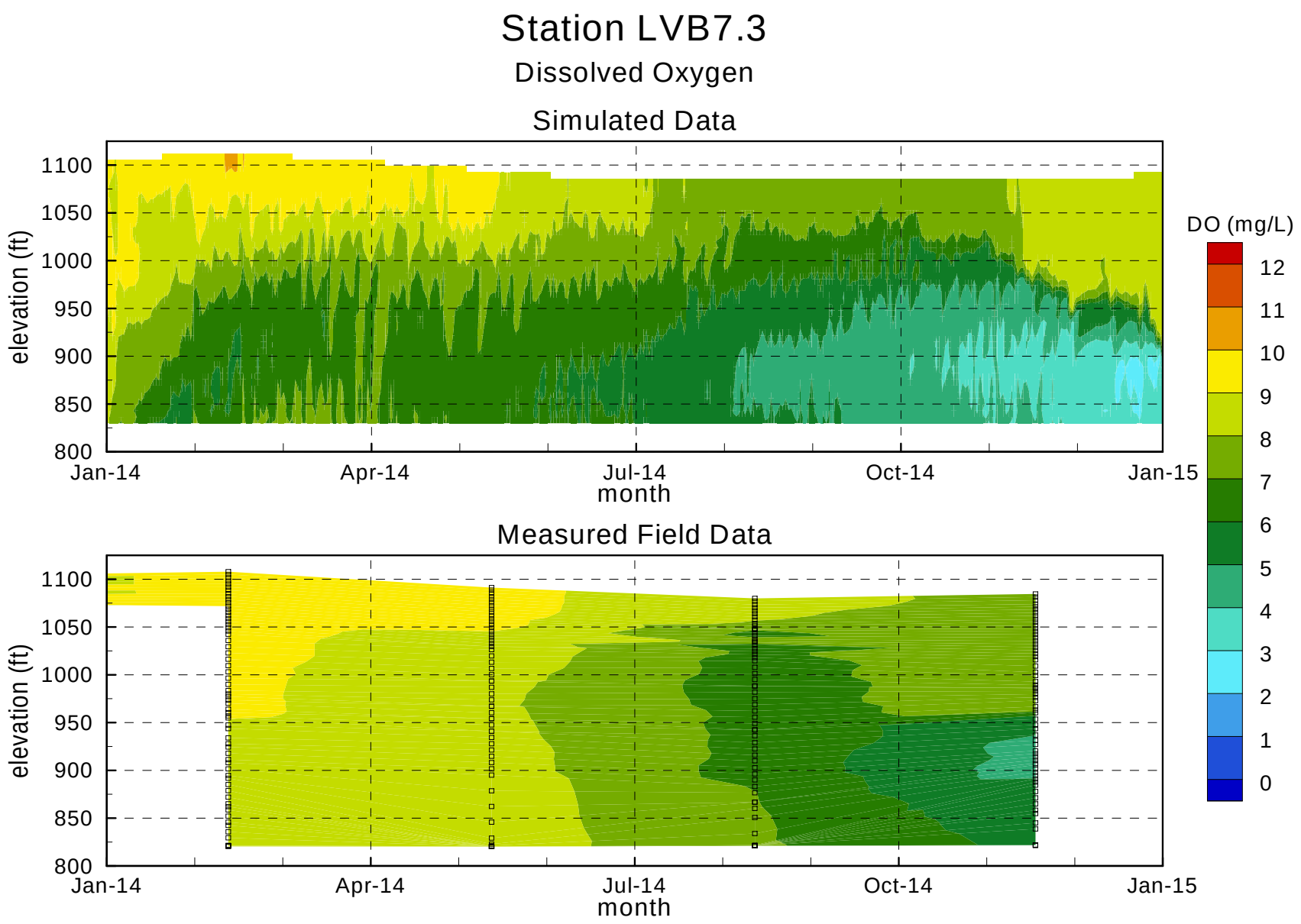
Station LVB7.3
Dissolved Oxygen
Simulated Data
elevation (ft)
1100
1050
1000
950
900
850
800
Jan-14
Apr-14
Jul-14
Oct-14
Jan-15
month
Measured Field Data
elevation (ft)
1100
1050
1000
950
900
850
800
Jan-14
Apr-14
Jul-14
Oct-14
Jan-15
month
DO (mg/L)
12
11
10
9
8
7
6
5
4
3
2
1
0

Figure B.58

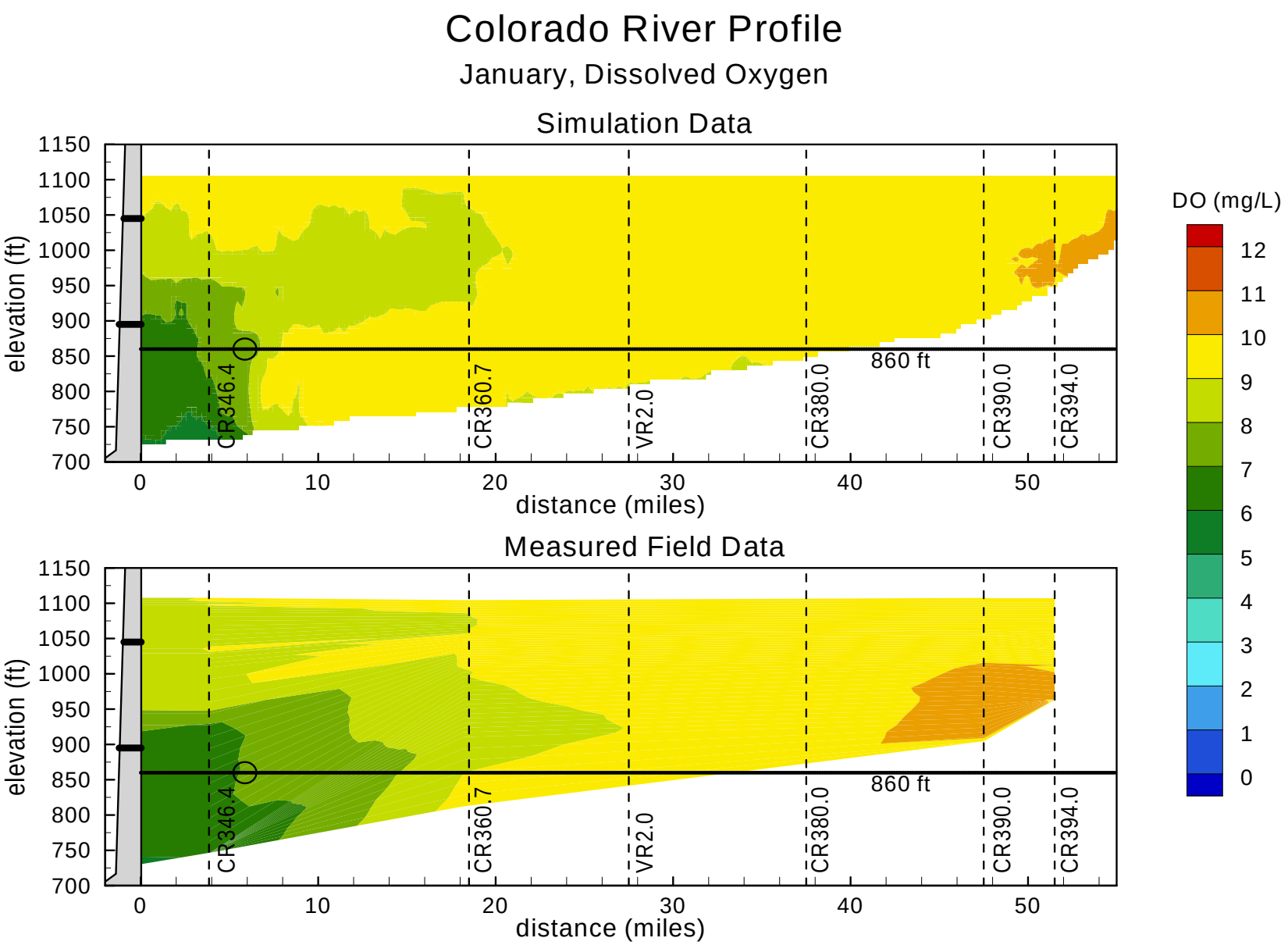
Colorado River Profile
January, Dissolved Oxygen
Simulation Data
Measured Field Data
elevation (ft)
distance (miles)
860 ft
CR346.4
CR360.7
VR2.0
CR380.0
CR390.0
CR394.0
DO (mg/L)
0
1
2
3
4
5
6
7
8
9
10
11
12

Figure B.59

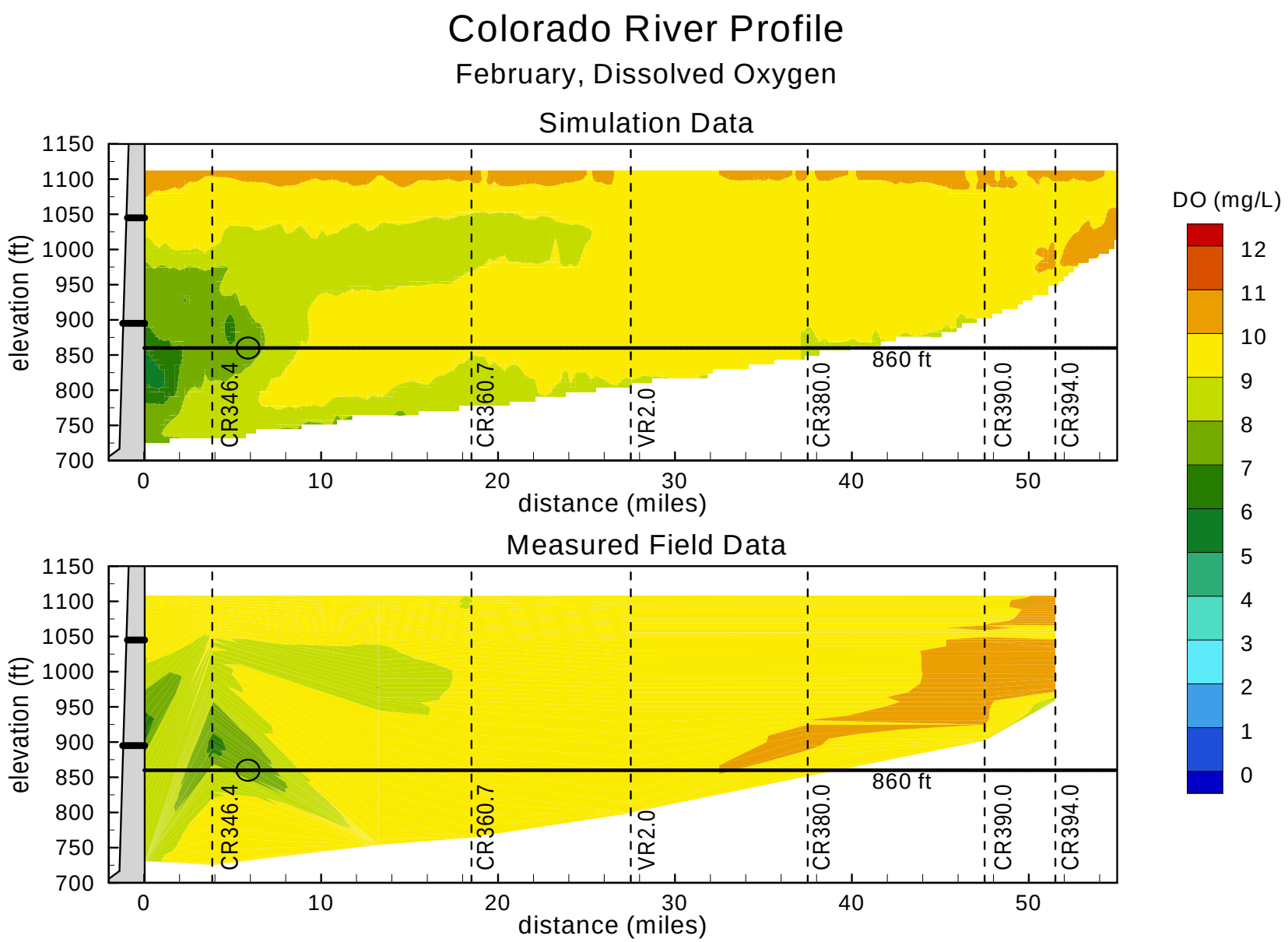
Colorado River Profile
February, Dissolved Oxygen
Simulation Data
Measured Field Data
elevation (ft)
distance (miles)
860 ft
CR346.4
CR360.7
VR2.0
CR380.0
CR390.0
CR394.0
DO (mg/L)
0
1
2
3
4
5
6
7
8
9
10
11
12

Figure B.60

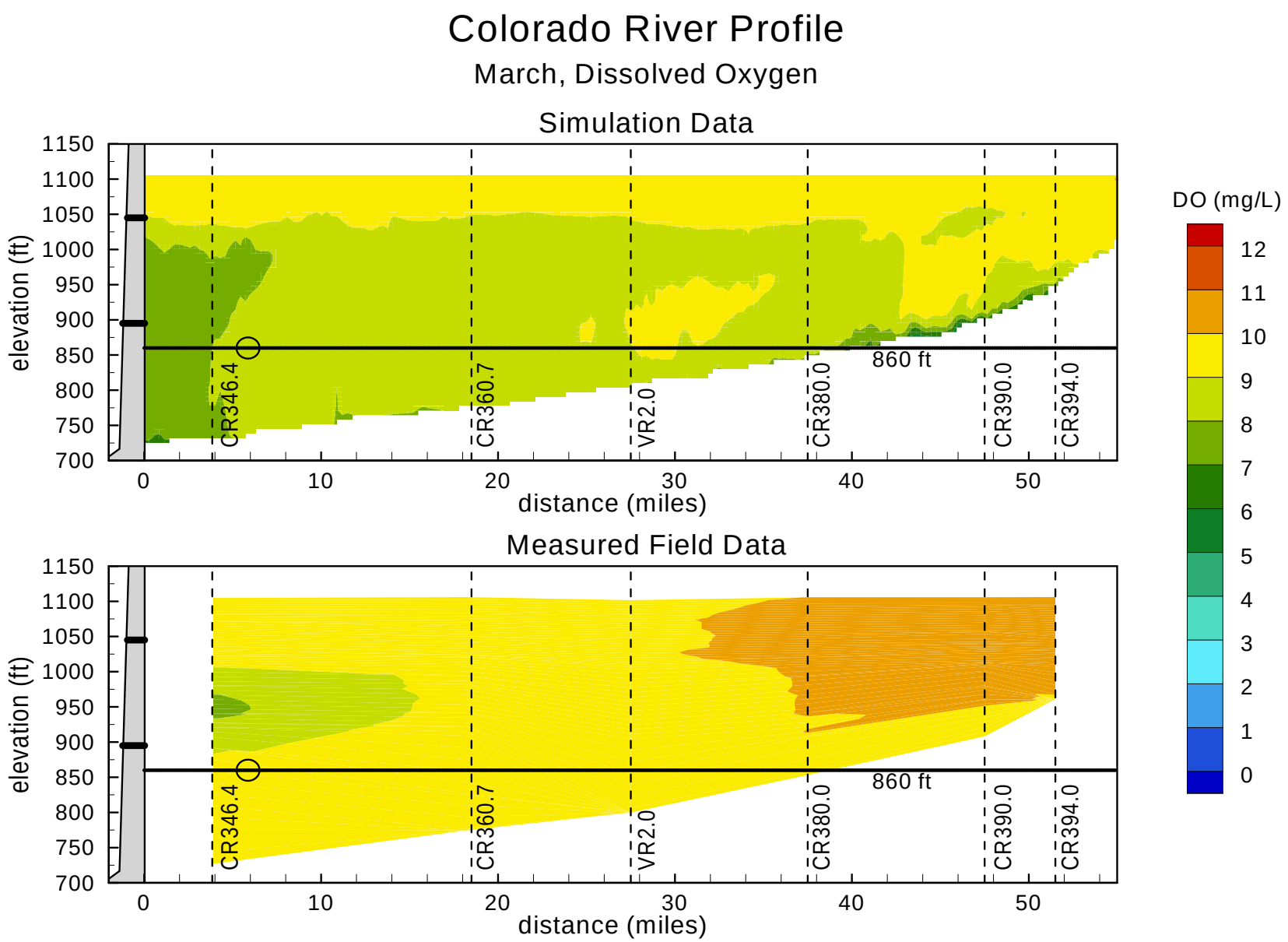
Colorado River Profile
March, Dissolved Oxygen
Simulation Data
Measured Field Data
elevation (ft)
distance (miles)
860 ft
CR346.4
CR360.7
VR2.0
CR380.0
CR390.0
CR394.0
DO (mg/L)
12
11
10
9
8
7
6
5
4
3
2
1
0

Figure B.61

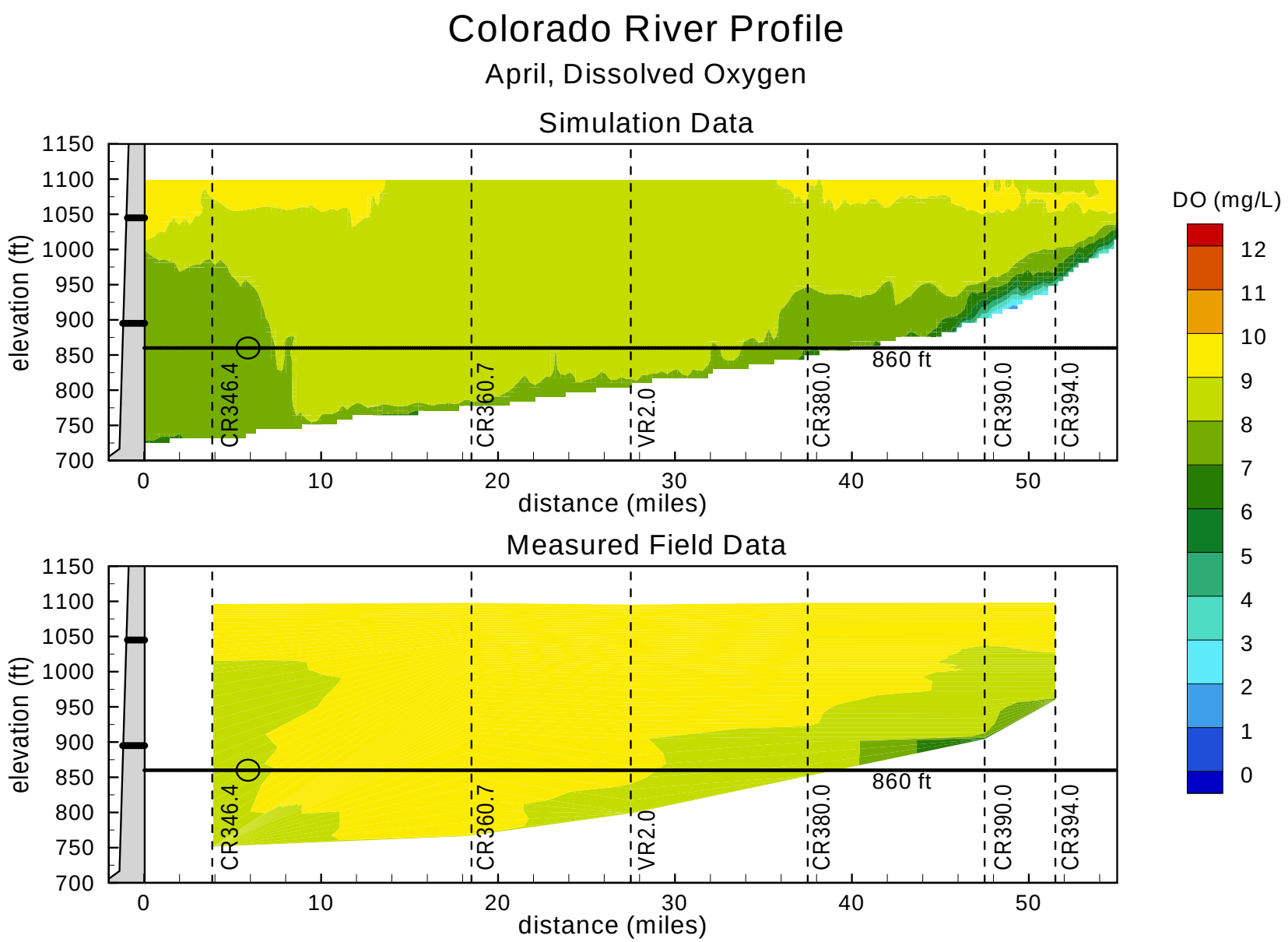

Figure B.62

FLOW SCIENCE

Colorado River Profile

May, Dissolved Oxygen

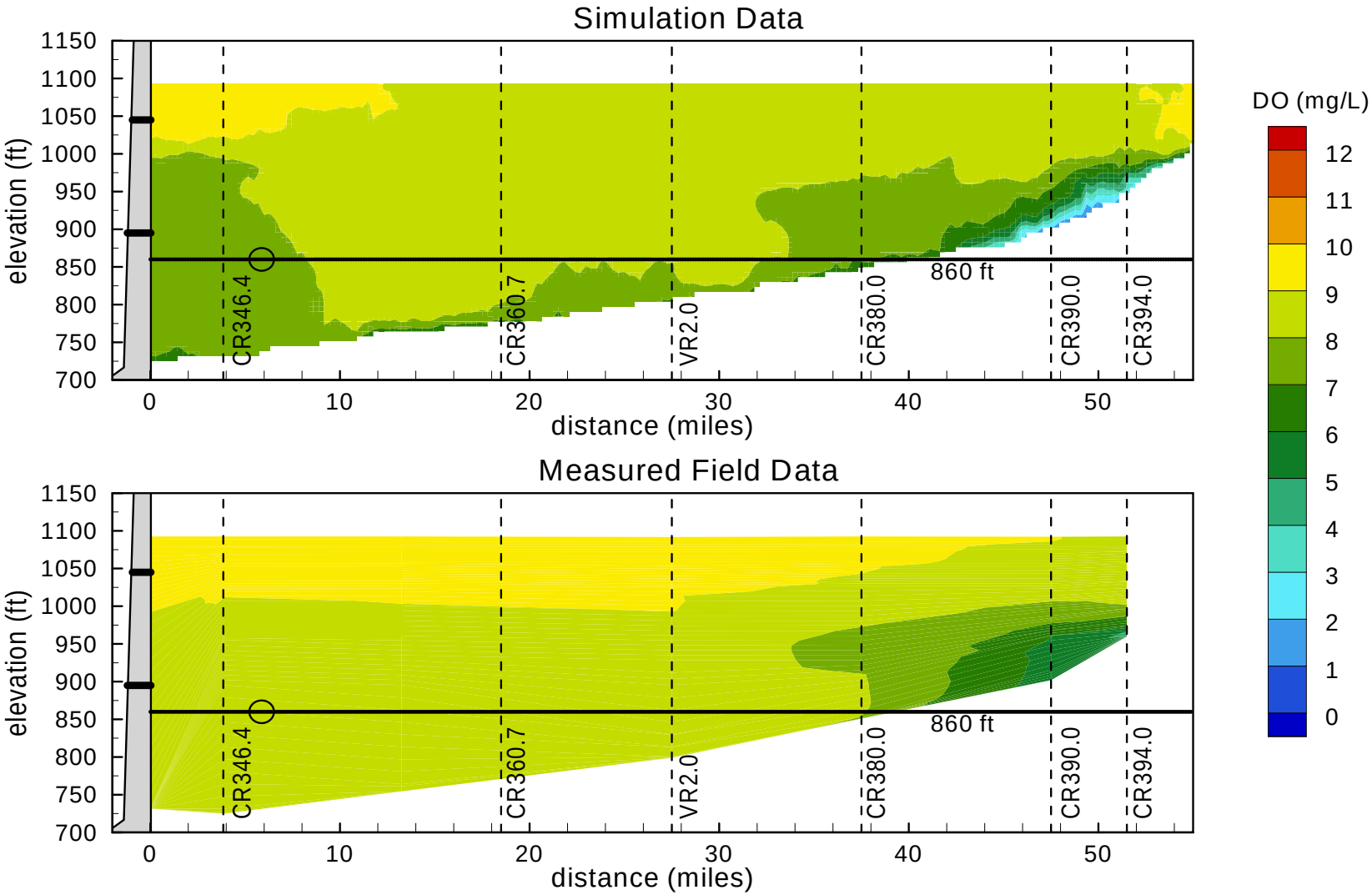

Figure B.63

FLOW SCIENCE

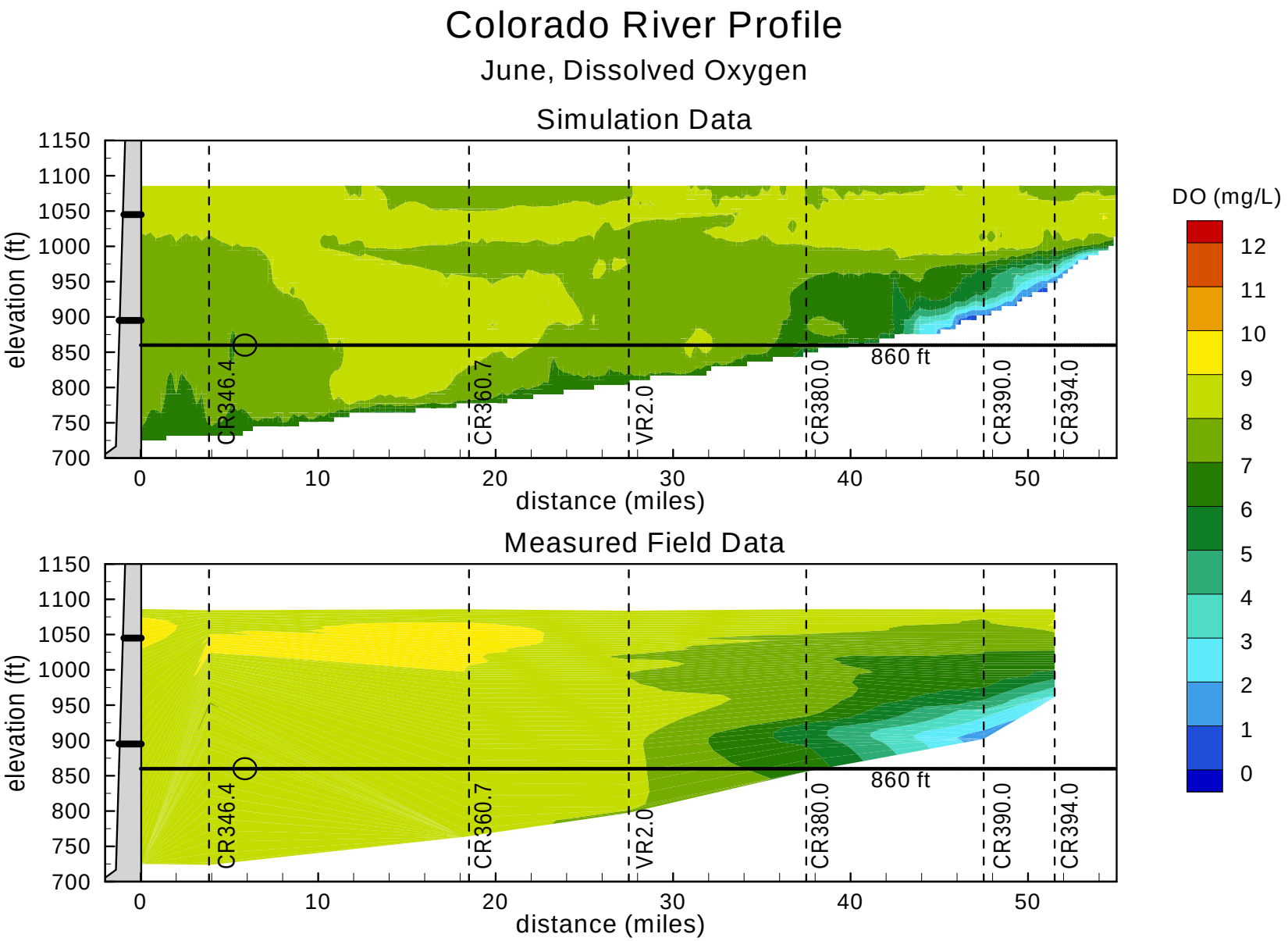
Colorado River Profile
June, Dissolved Oxygen
Simulation Data
Measured Field Data
elevation (ft)
distance (miles)
860 ft
CR346.4
CR360.7
VR2.0
CR380.0
CR390.0
CR394.0
DO (mg/L)
12
11
10
9
8
7
6
5
4
3
2
1
0

Figure B.64

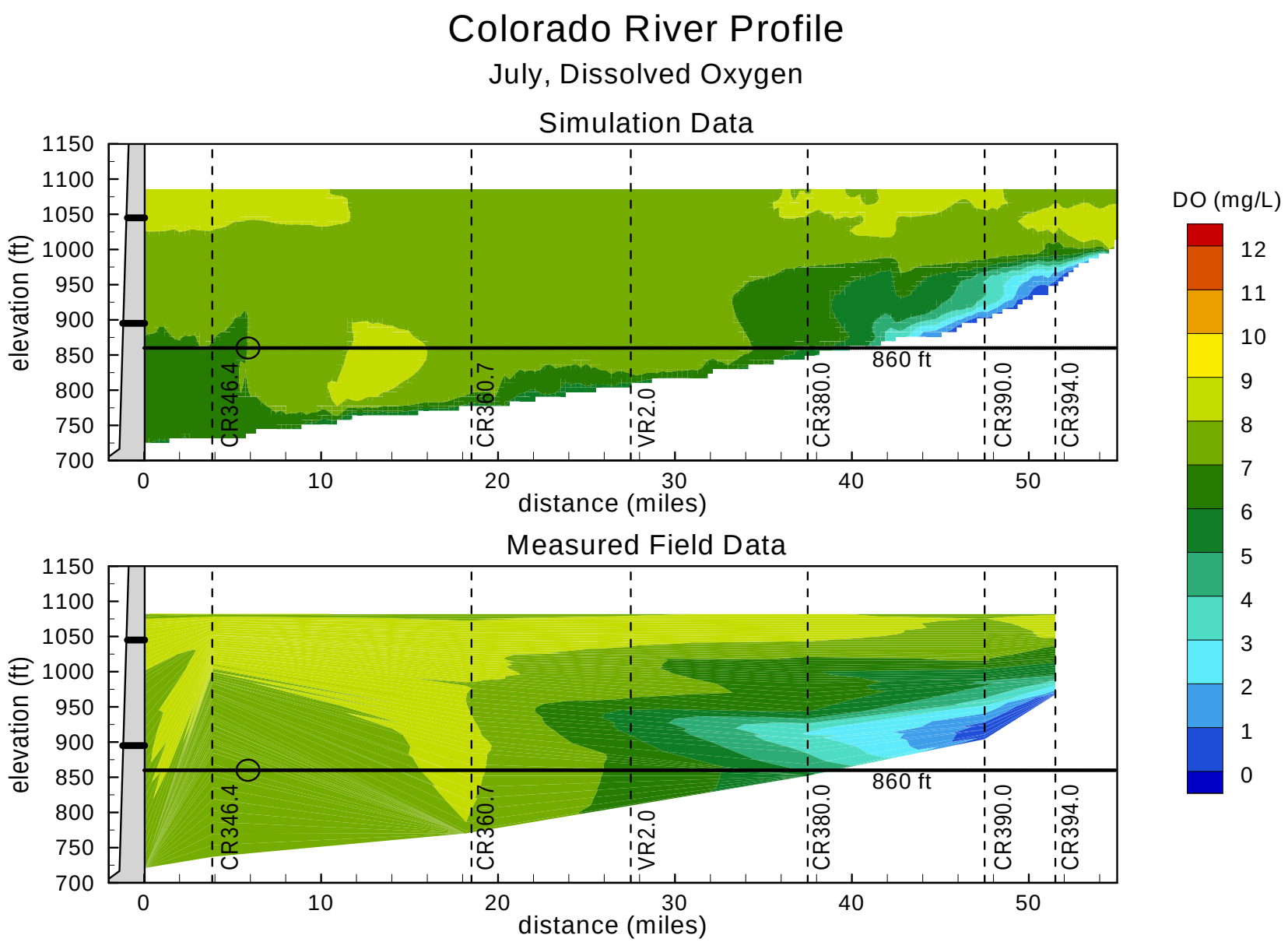
Colorado River Profile
July, Dissolved Oxygen
Simulation Data
Measured Field Data
elevation (ft)
distance (miles)
860 ft
CR346.4
CR360.7
VR2.0
CR380.0
CR390.0
CR394.0
DO (mg/L)
0
1
2
3
4
5
6
7
8
9
10
11
12

Figure B.65

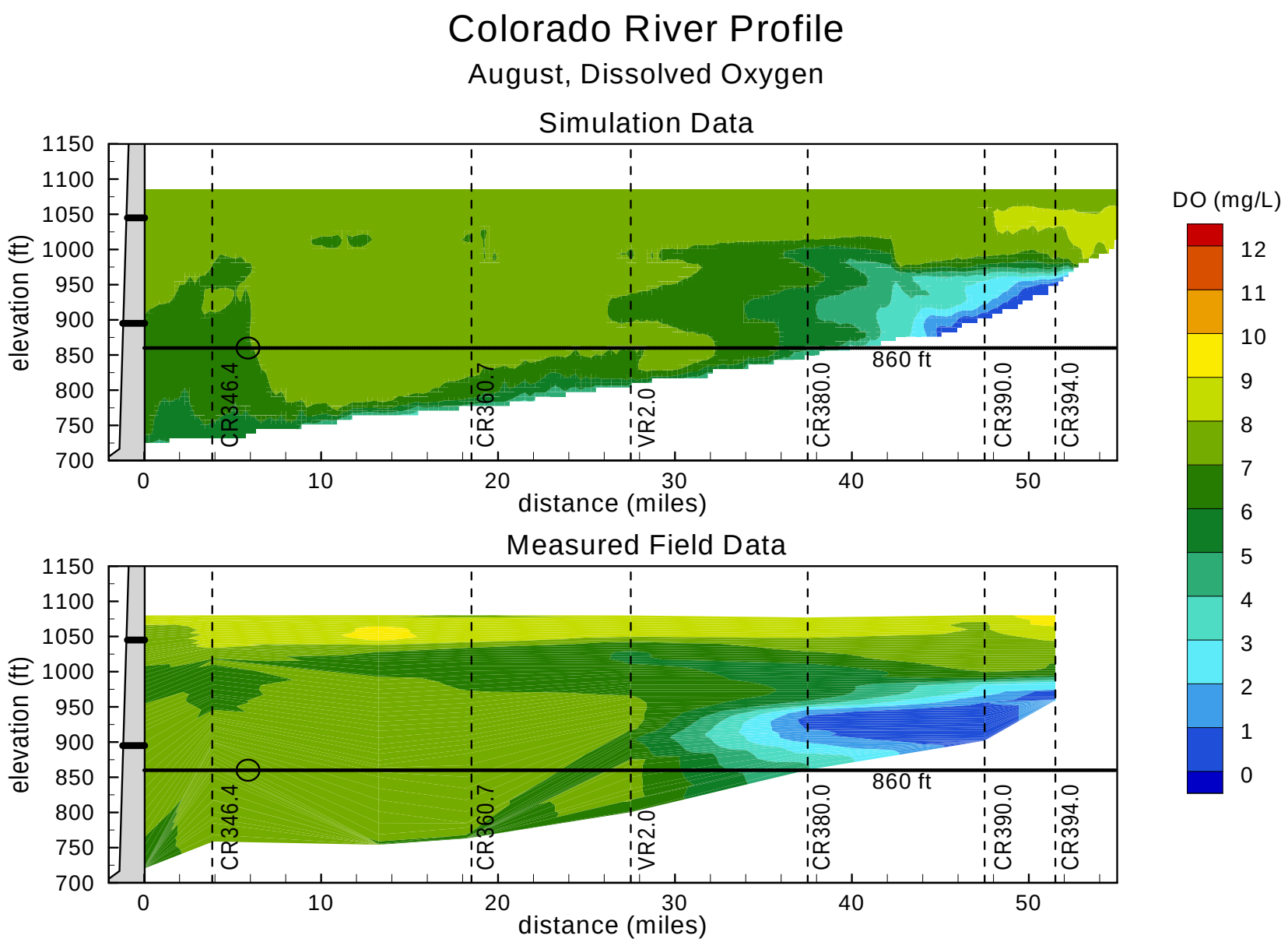
Colorado River Profile
August, Dissolved Oxygen
Simulation Data
Measured Field Data
elevation (ft)
distance (miles)
860 ft
CR346.4
CR360.7
VR2.0
CR380.0
CR390.0
CR394.0
DO (mg/L)
12
11
10
9
8
7
6
5
4
3
2
1
0

Figure B.66

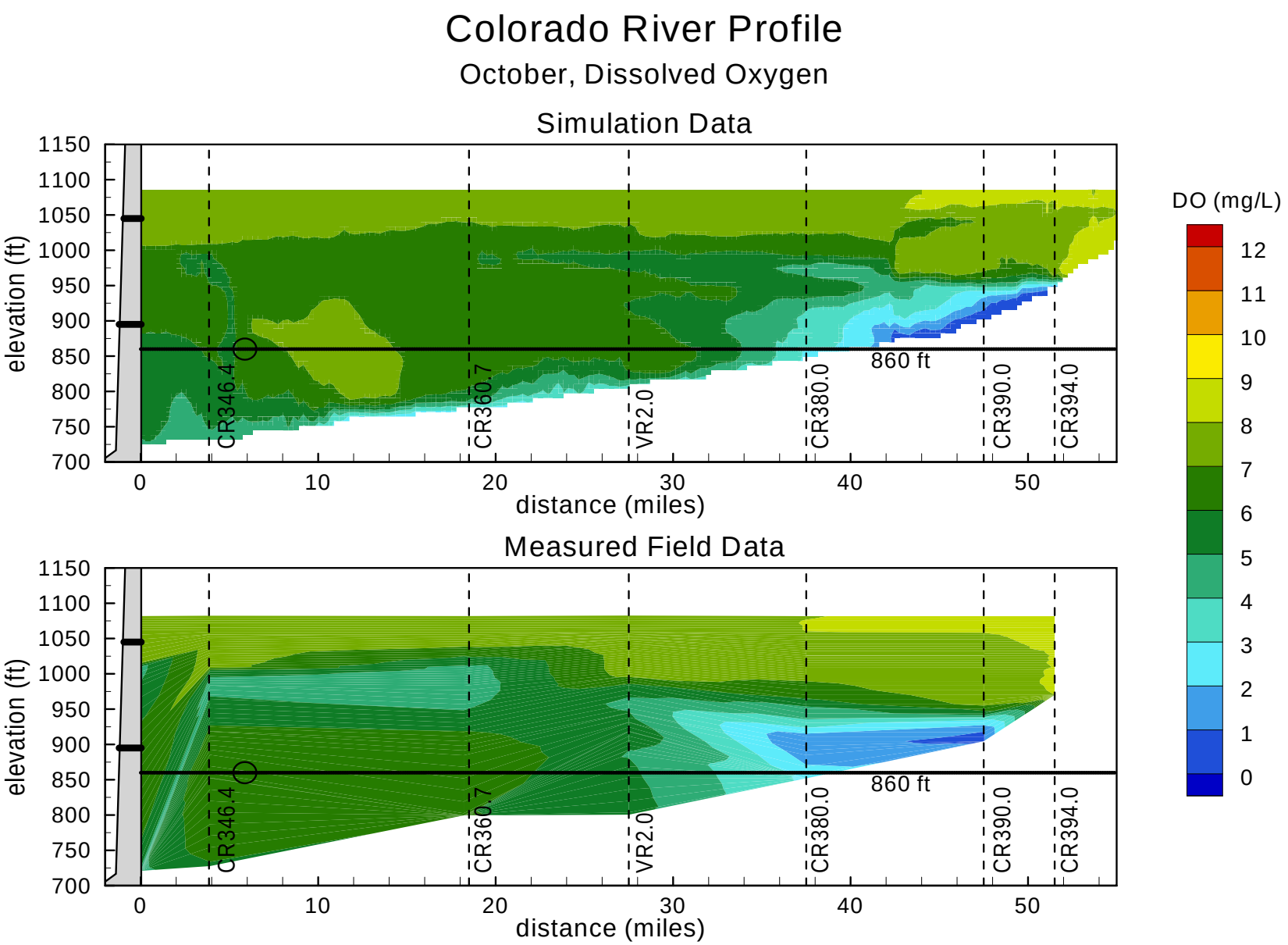

Figure B.67

FLOW SCIENCE

Colorado River Profile

November, Dissolved Oxygen

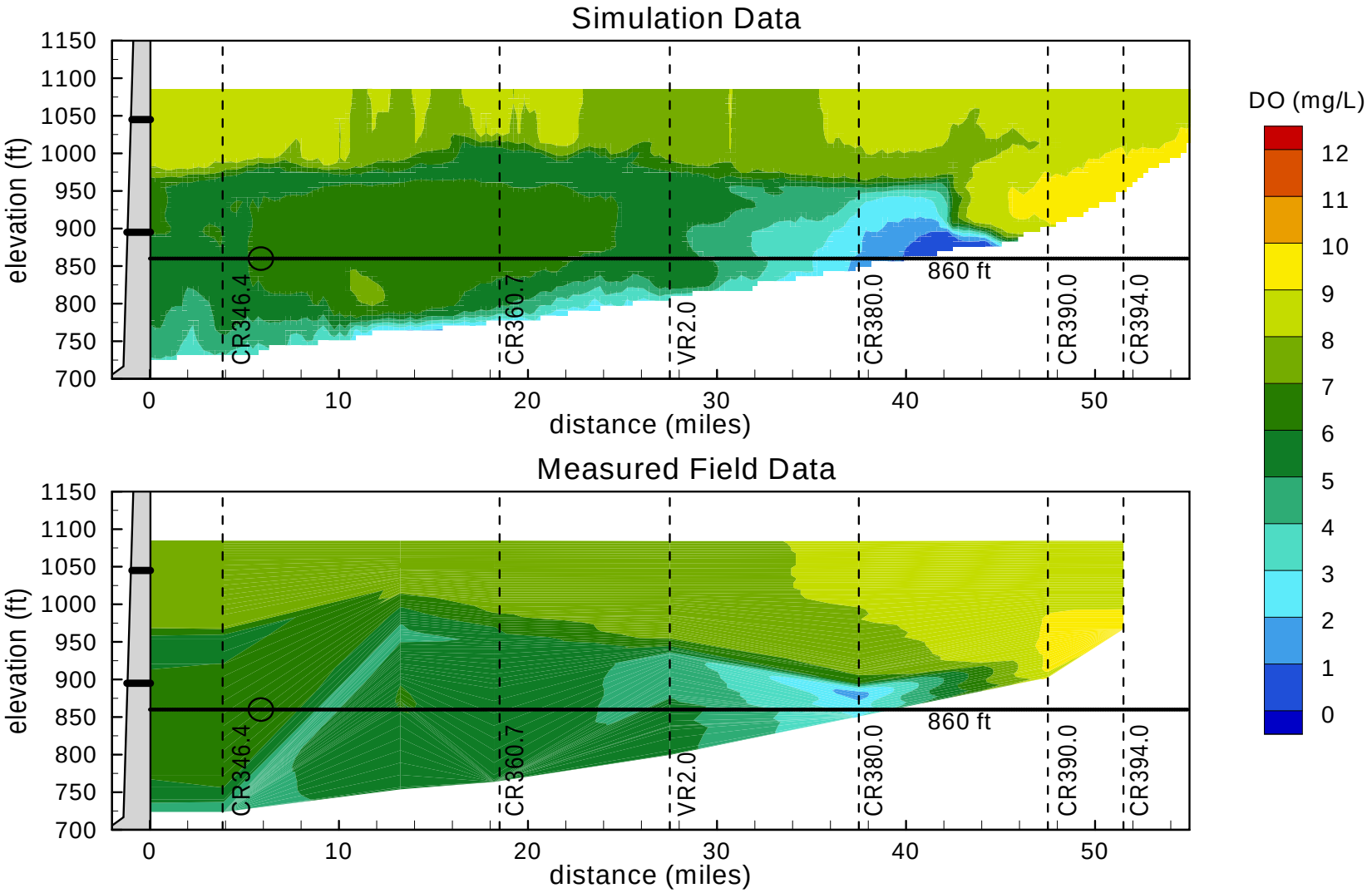

Figure B.68

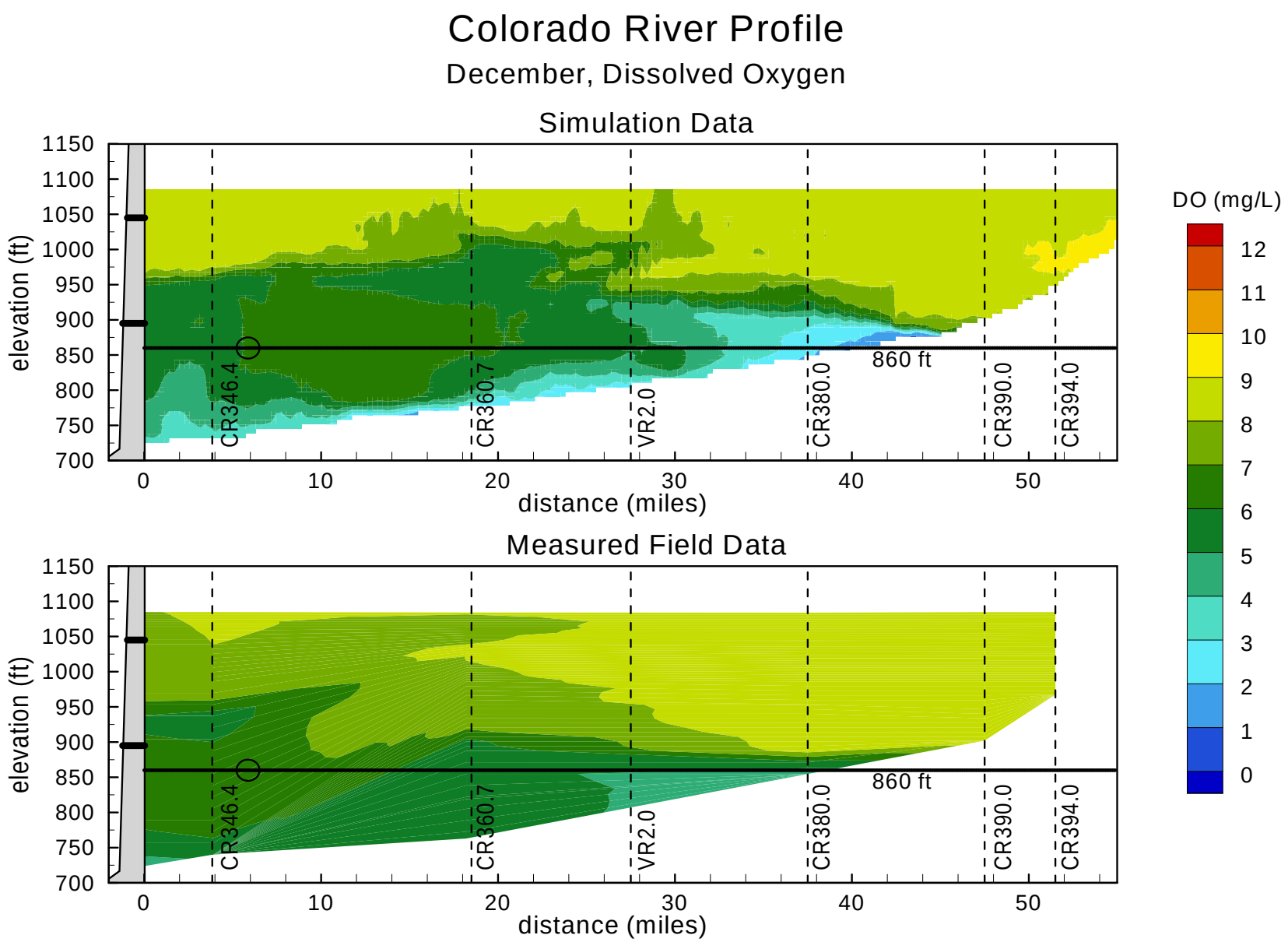

Figure B.69

FLOW SCIENCE

Filterable Reactive Phosphorus at Station CR394.0

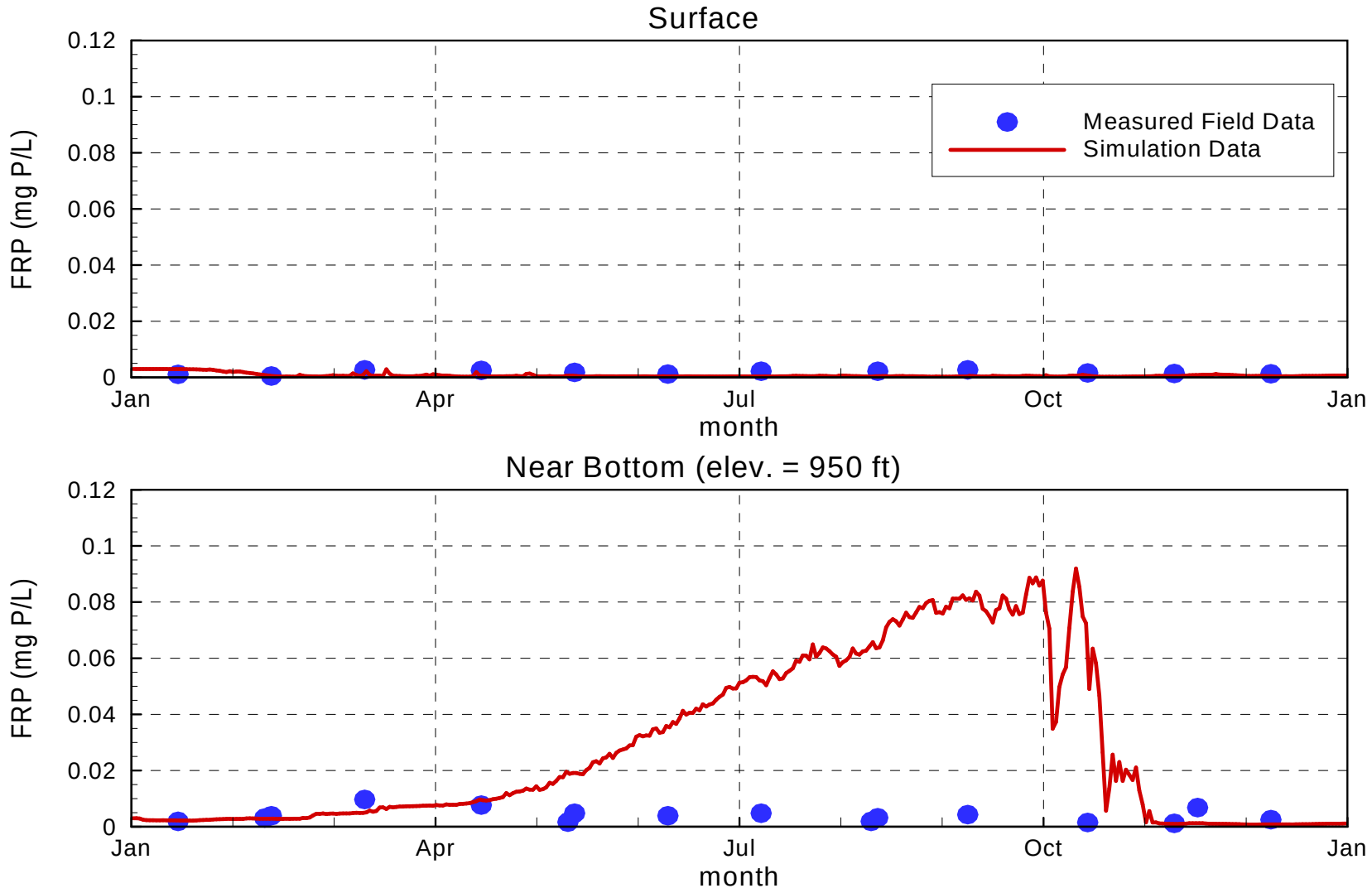

Figure B.70

Filterable Reactive Phosphorus at Station CR390.0

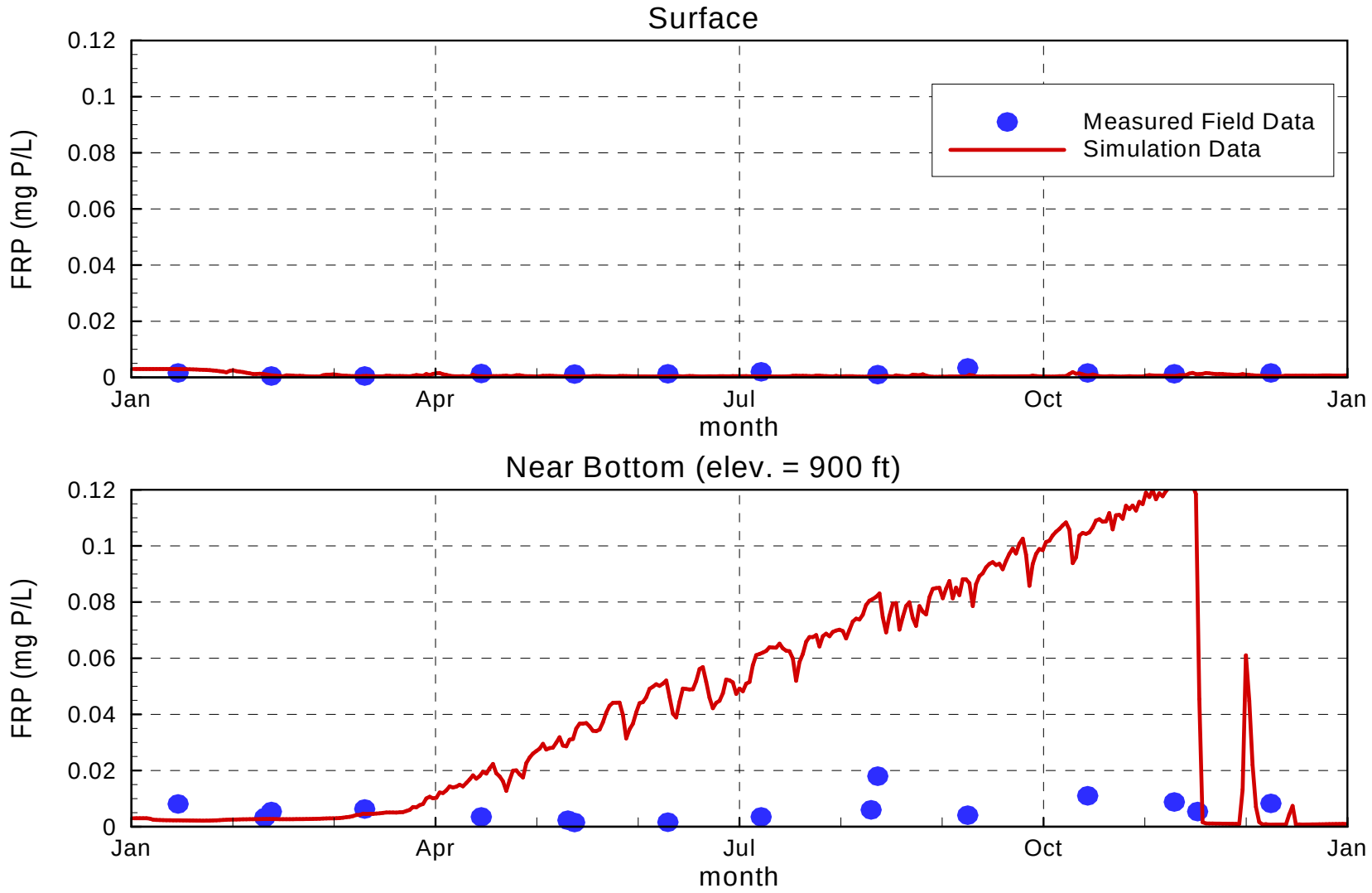

Figure B.71

FLOW SCIENCE

Filterable Reactive Phosphorus at Station CR380.0

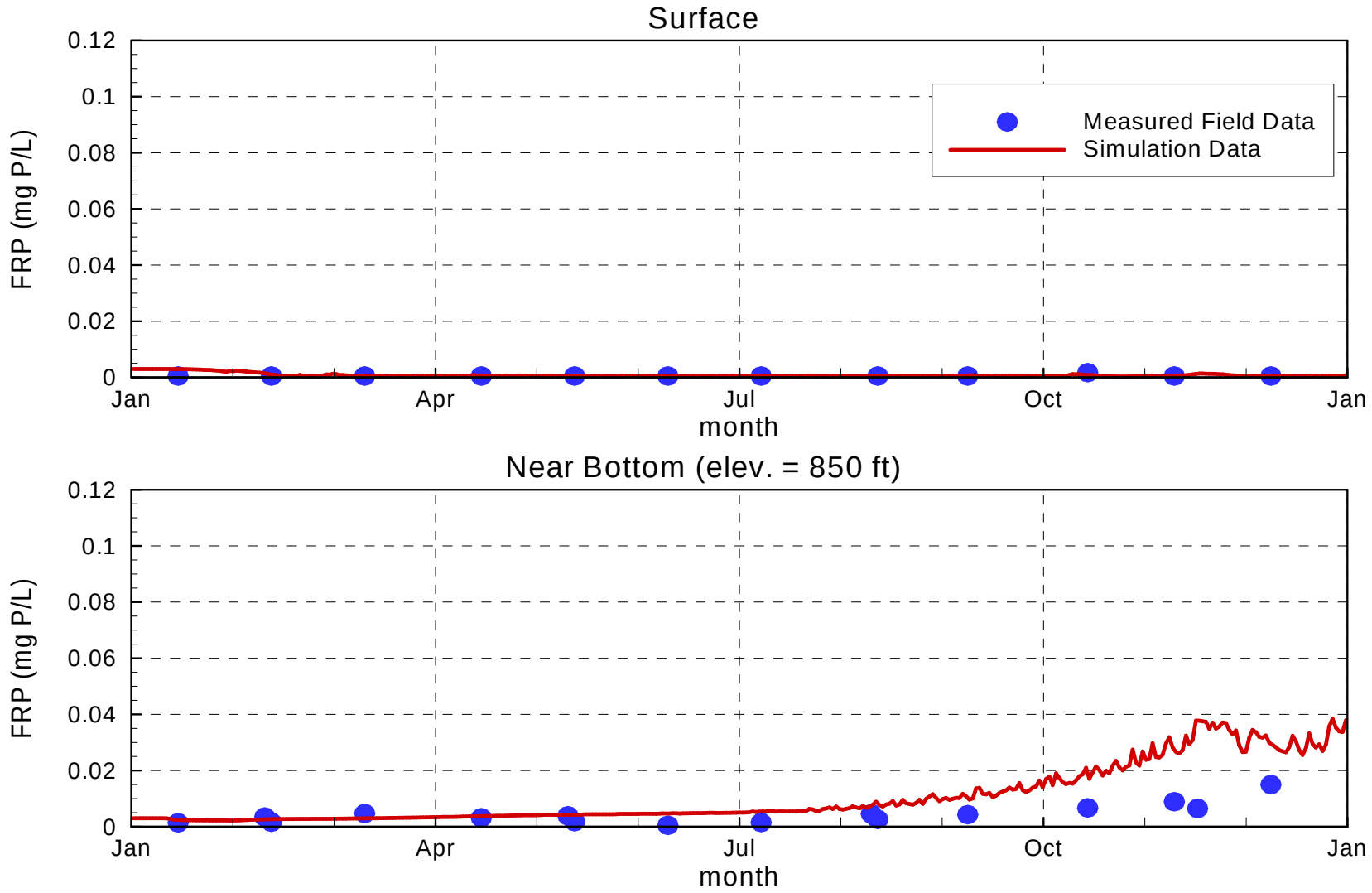

Figure B.72

Filterable Reactive Phosphorus at Station VR2.0

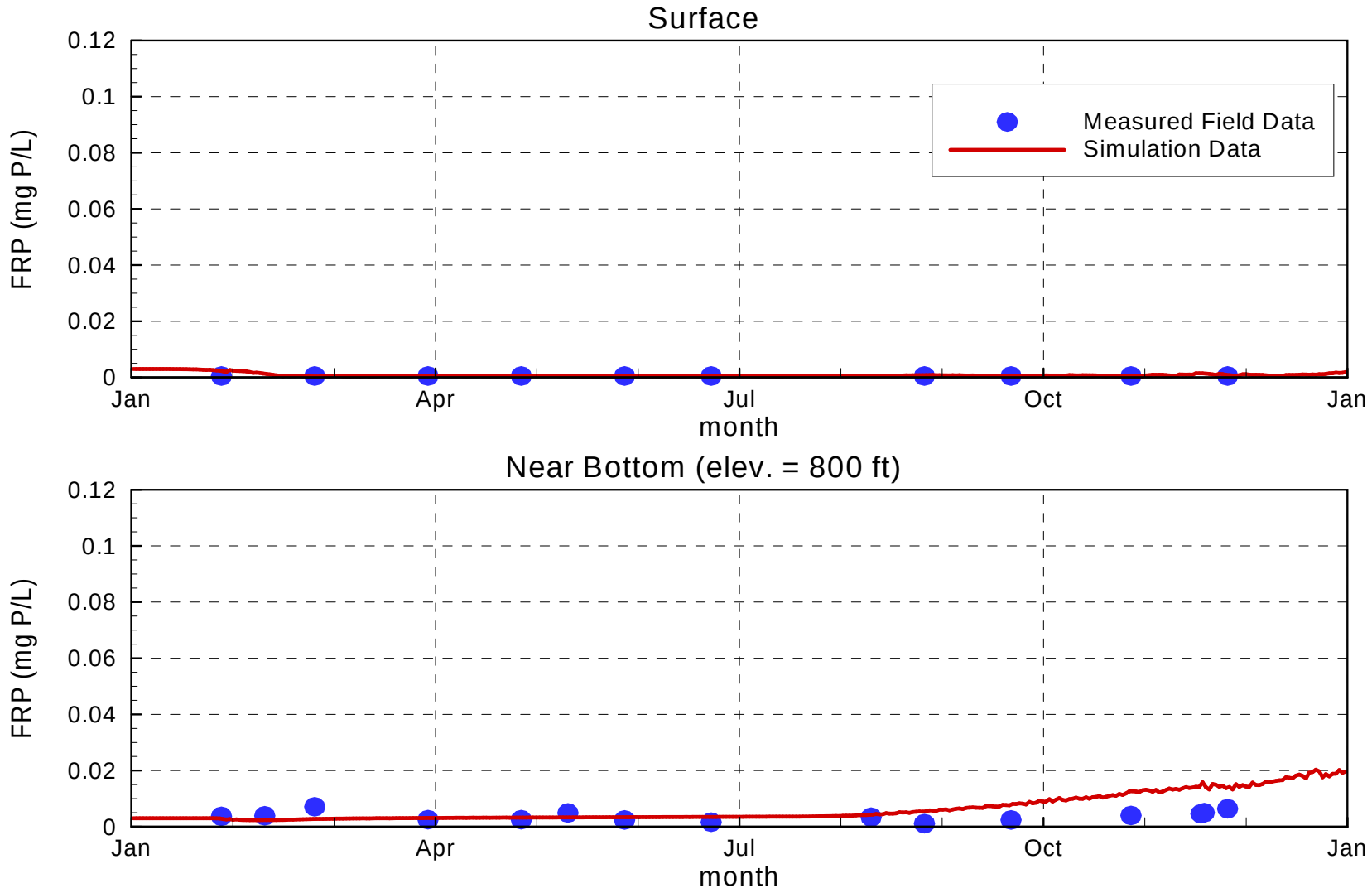

Figure B.73

FLOW SCIENCE

Filterable Reactive Phosphorus at Station VR6.0

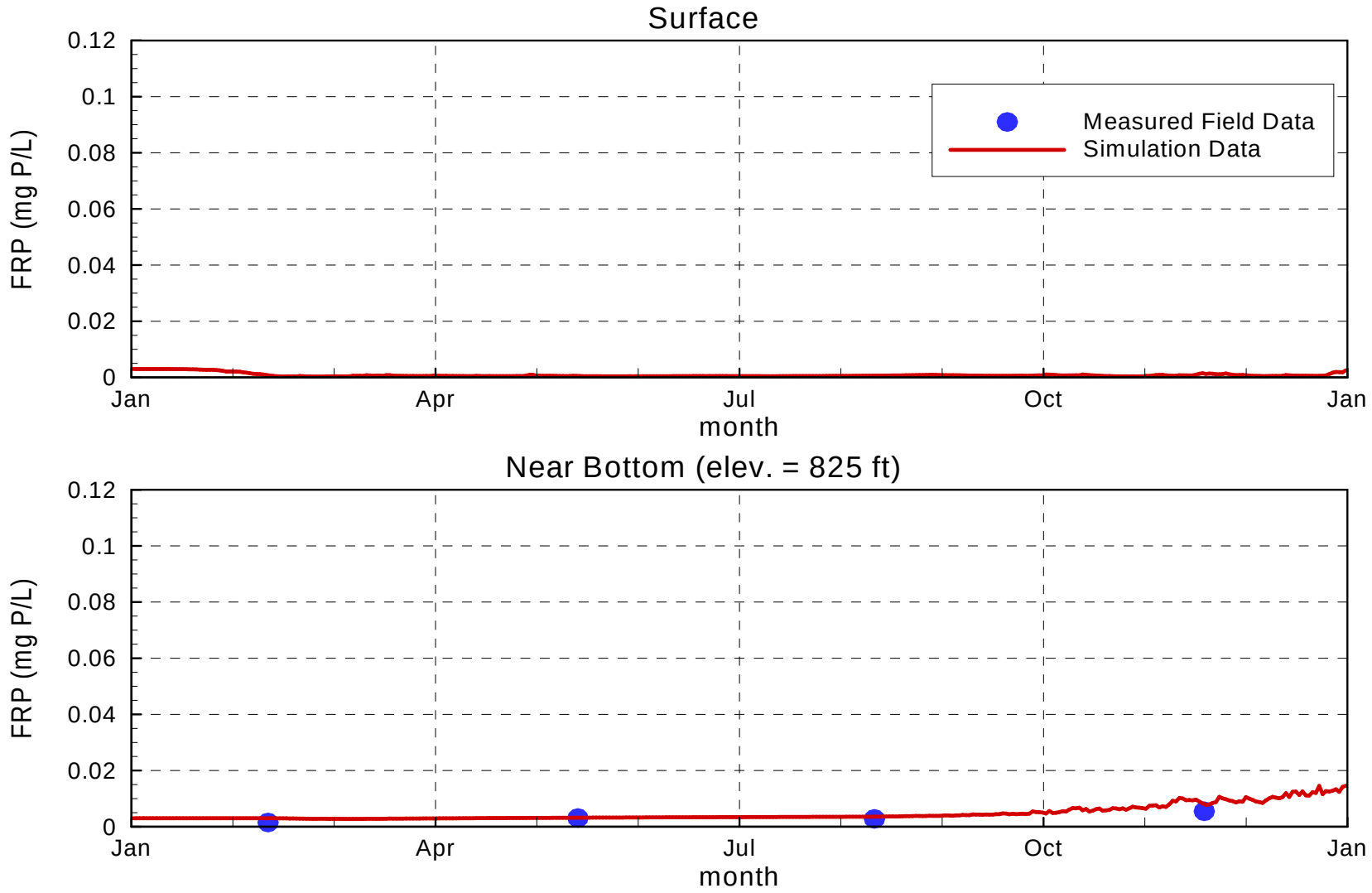

Figure B.74

Filterable Reactive Phosphorus at Station VR9.4

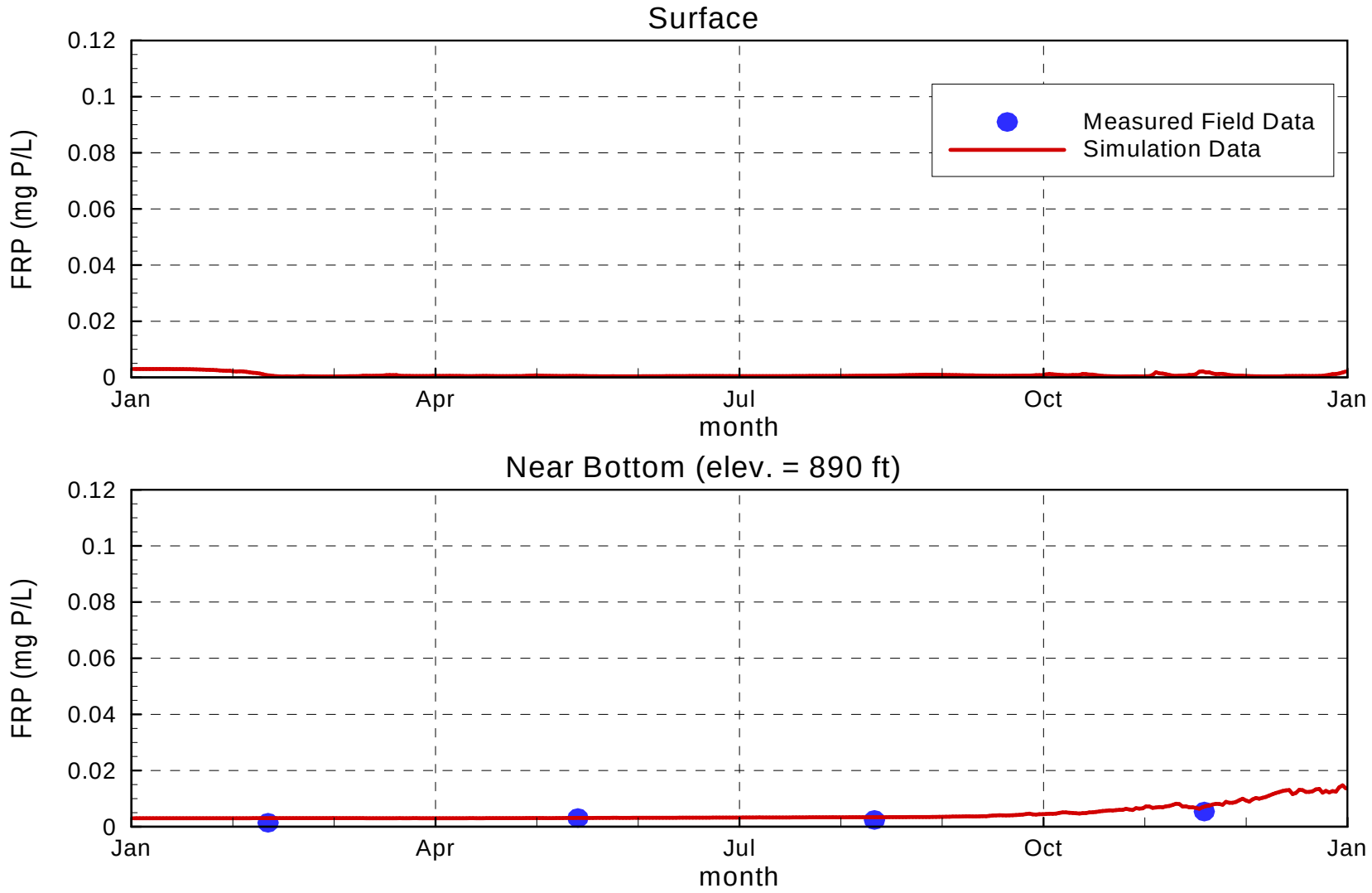

Figure B.75

Filterable Reactive Phosphorus at Station VR13.0

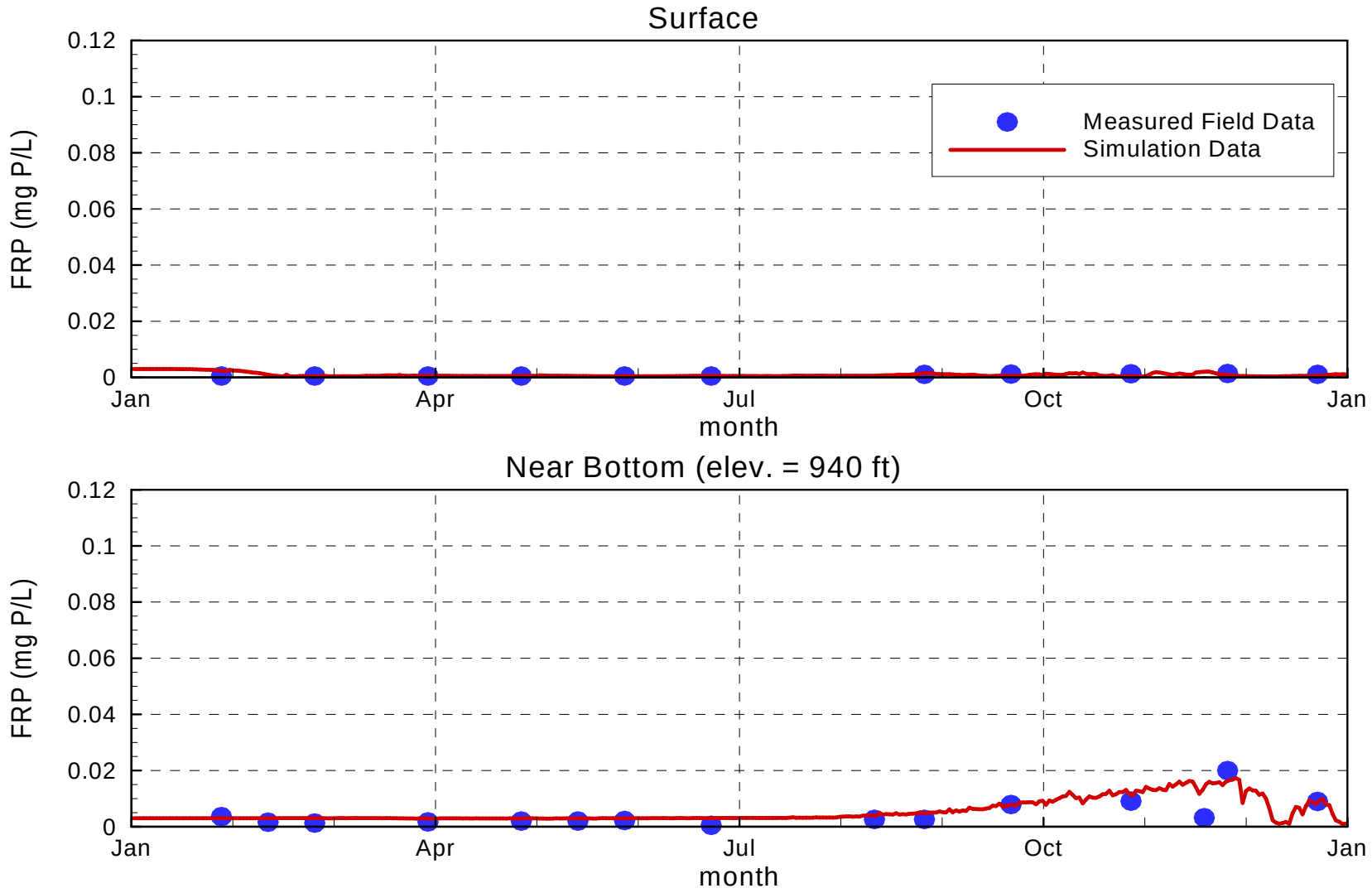

Figure B.76

Filterable Reactive Phosphorus at Station VR18.0

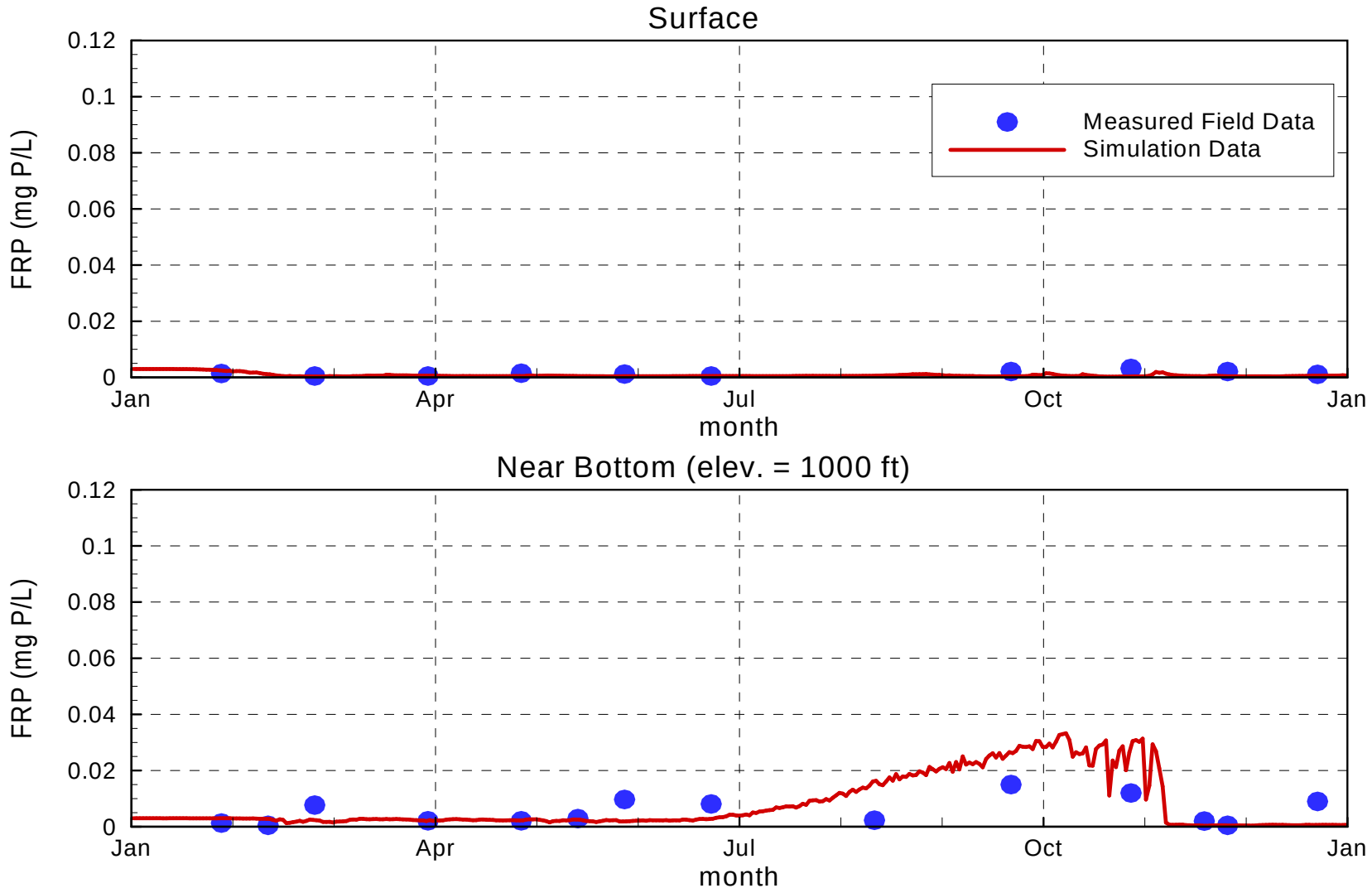

Figure B.77

Filterable Reactive Phosphorus at Station CR360.7

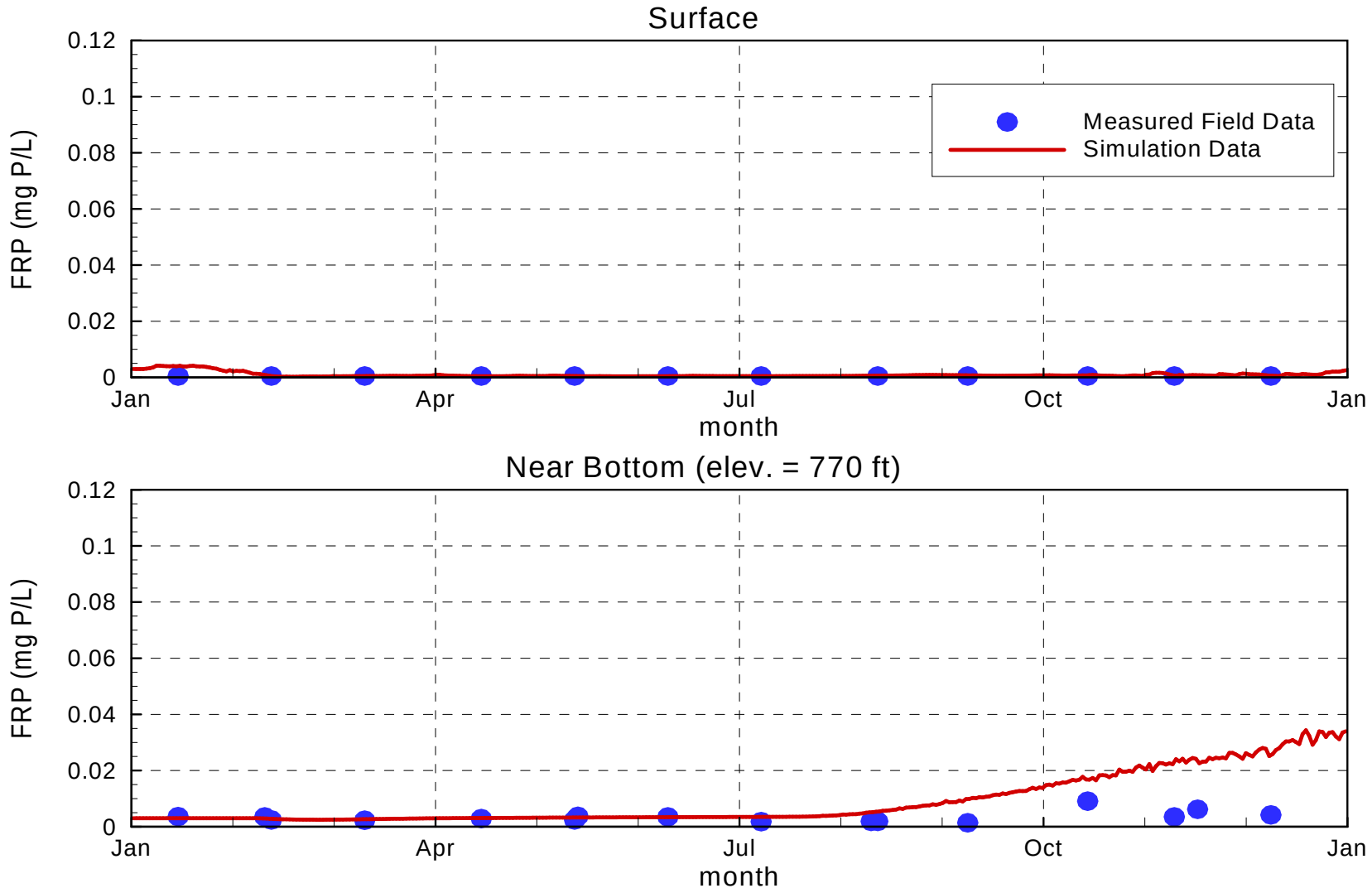

Figure B.78

Filterable Reactive Phosphorus at Station CR346.4

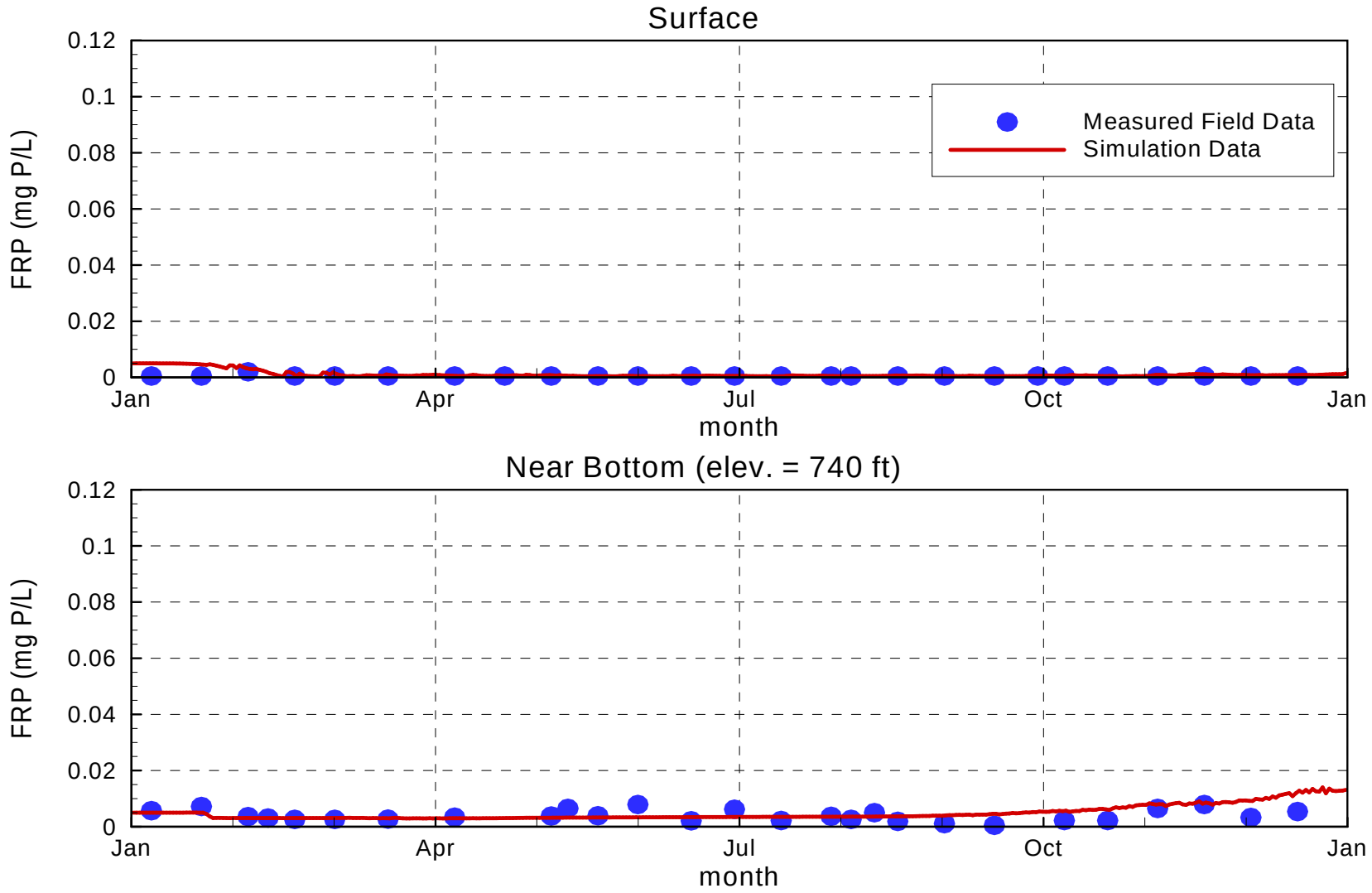

Figure B.79

Filterable Reactive Phosphorus at Station LVB4.95

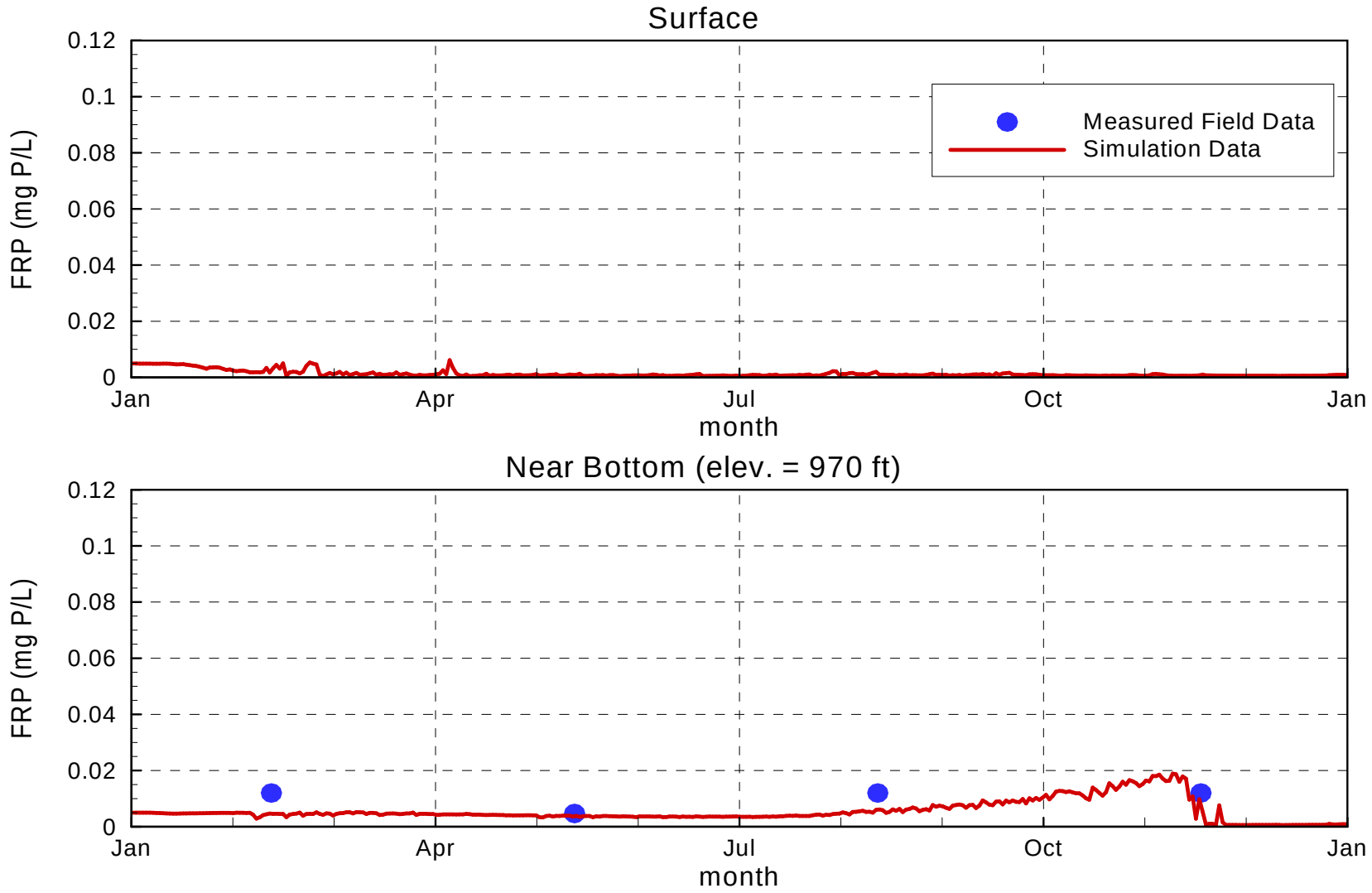

Figure B.80

FLOW SCIENCE

Filterable Reactive Phosphorus at Station LVB7.3

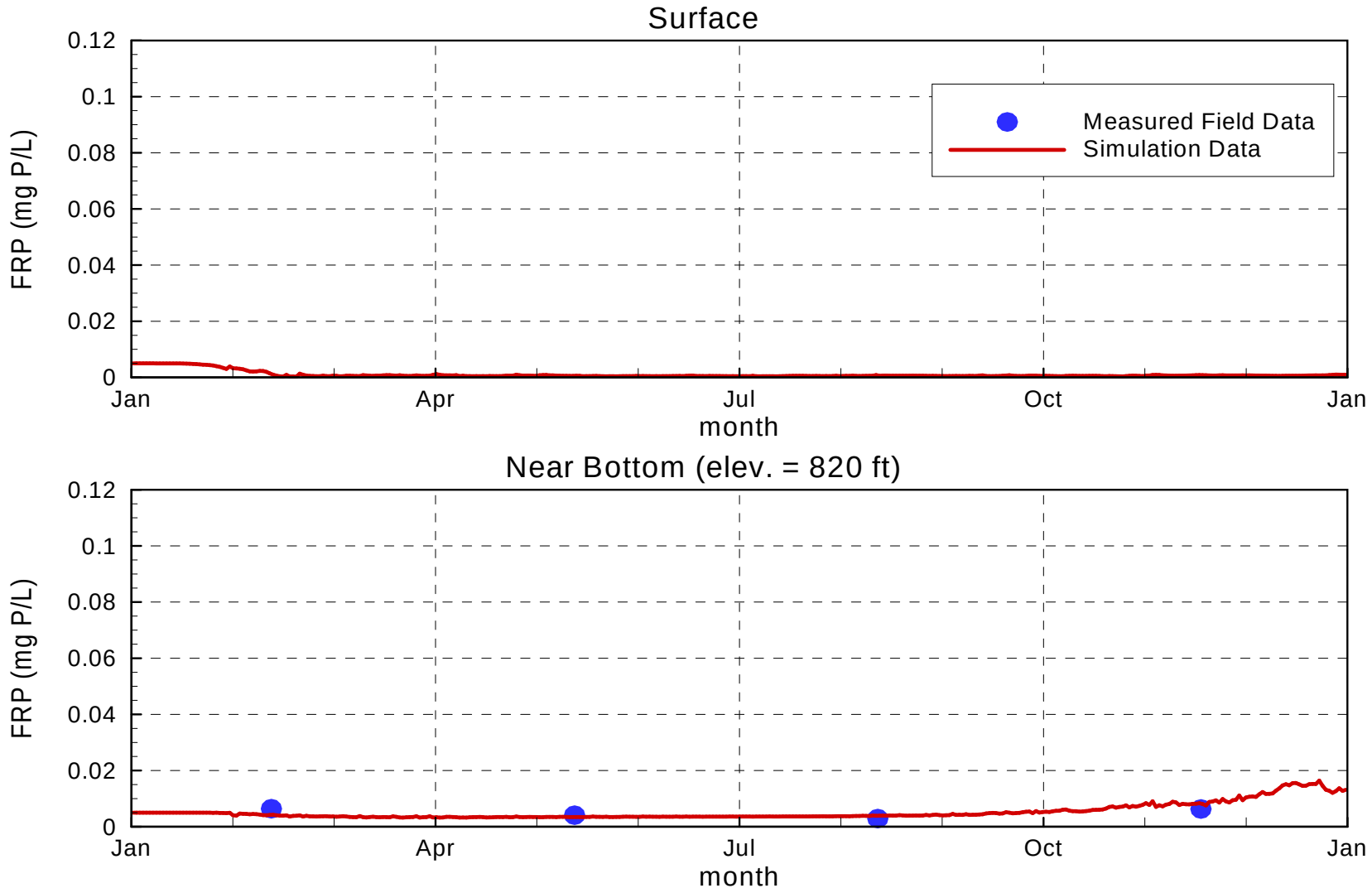

Figure B.81

Total Phosphorus at Station CR394.0

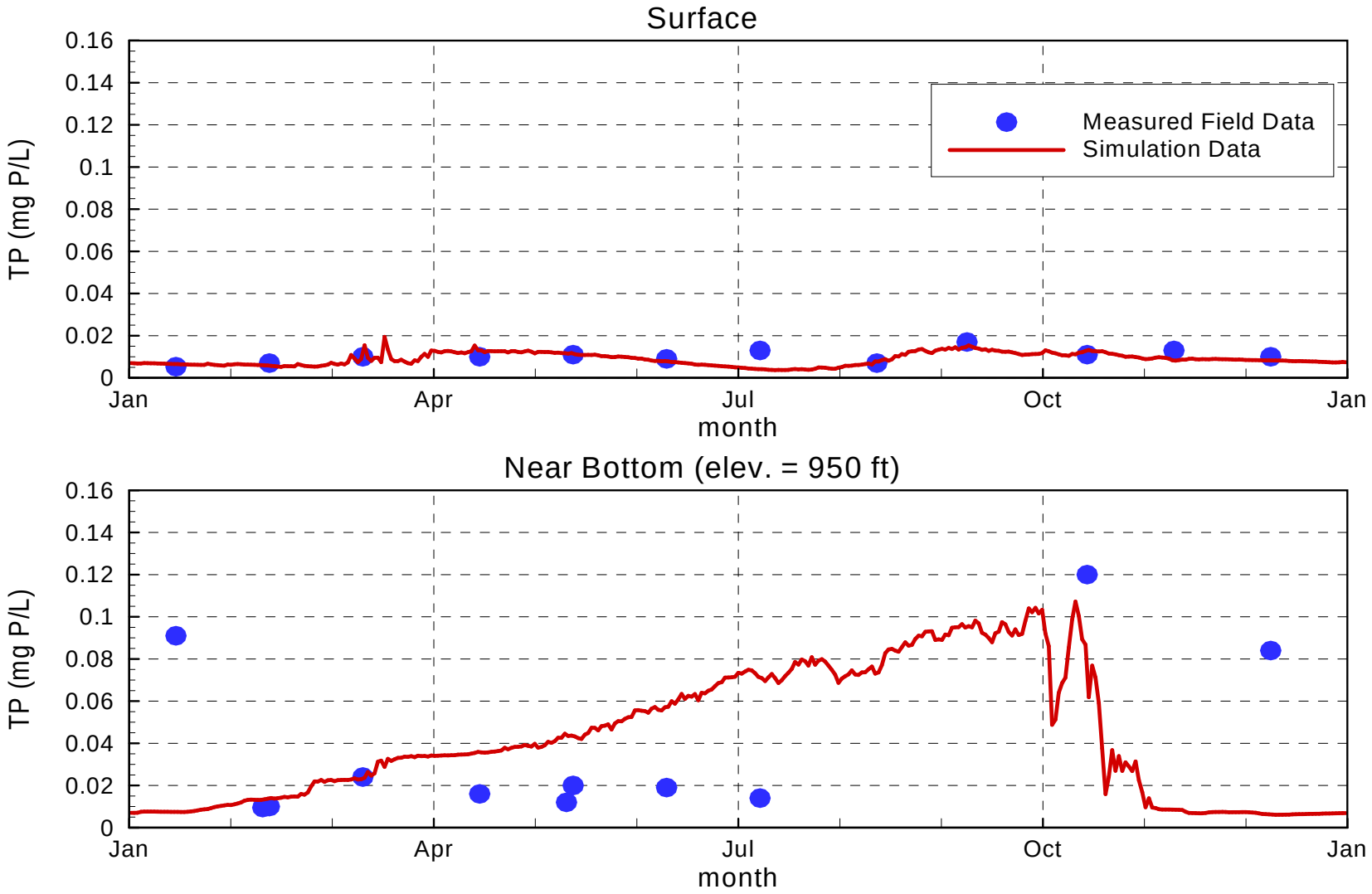

Figure B.82

Total Phosphorus at Station CR390.0

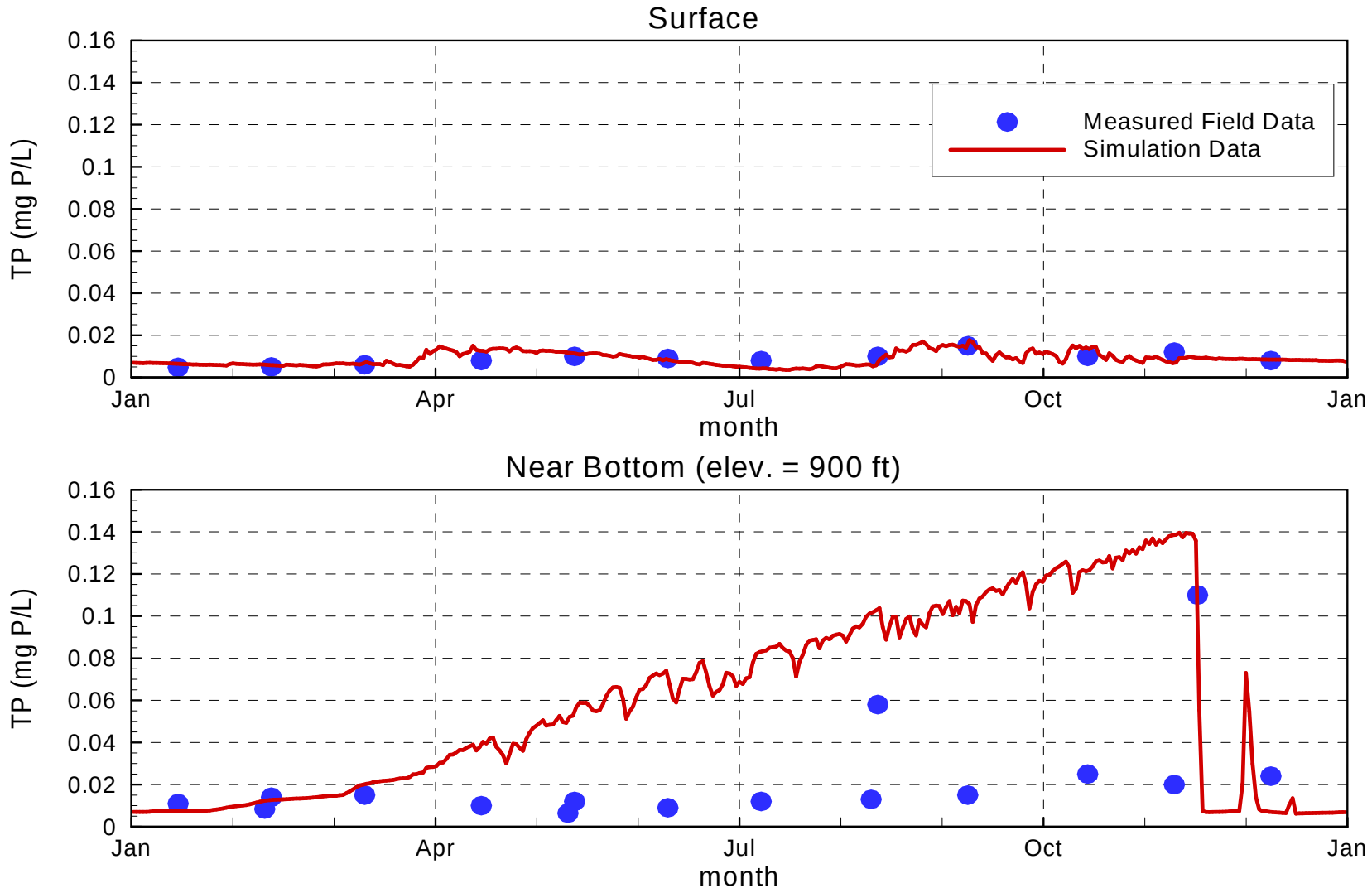

Figure B.83

Total Phosphorus at Station CR380.0

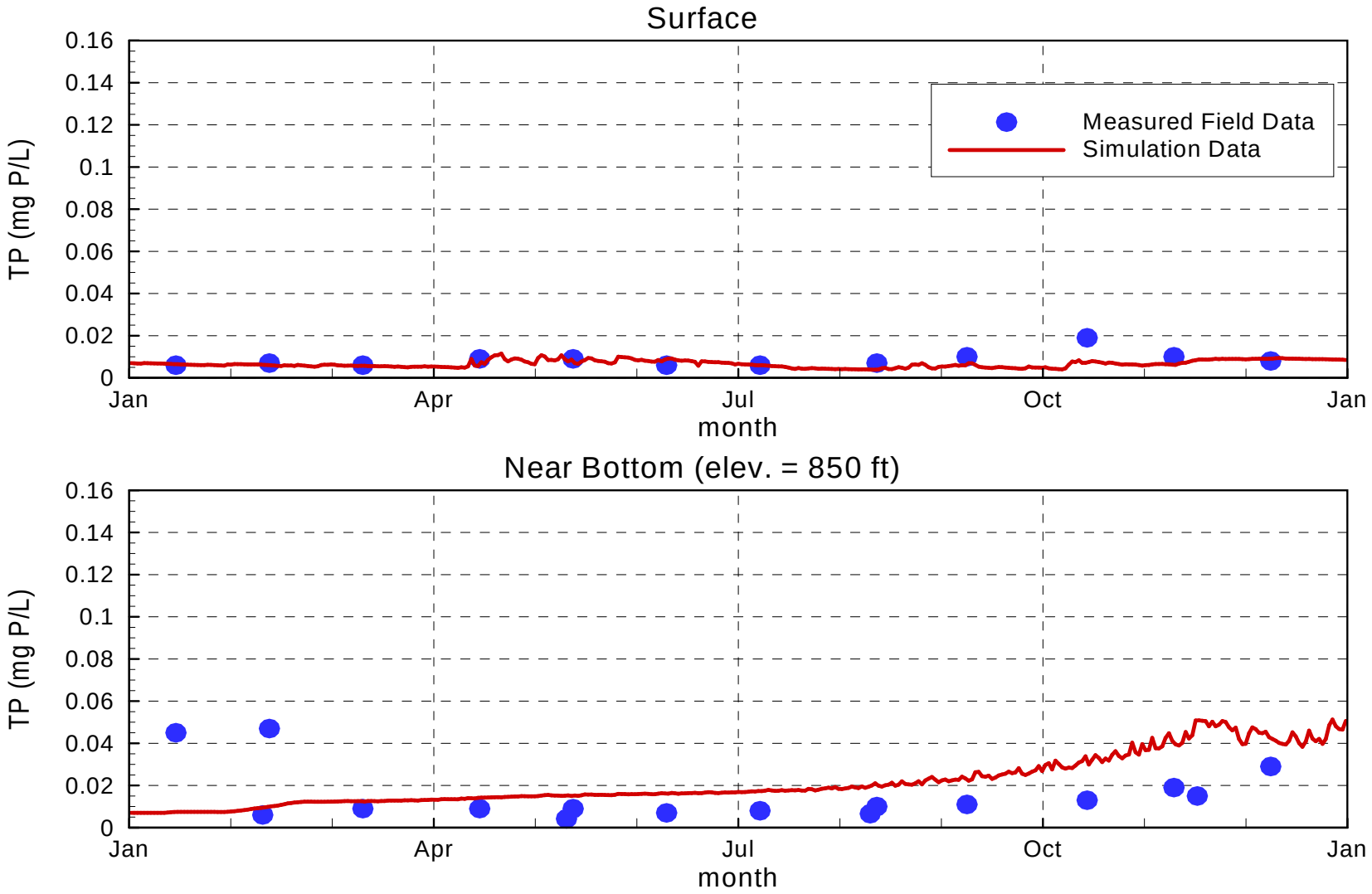

Figure B.84

Total Phosphorus at Station VR2.0

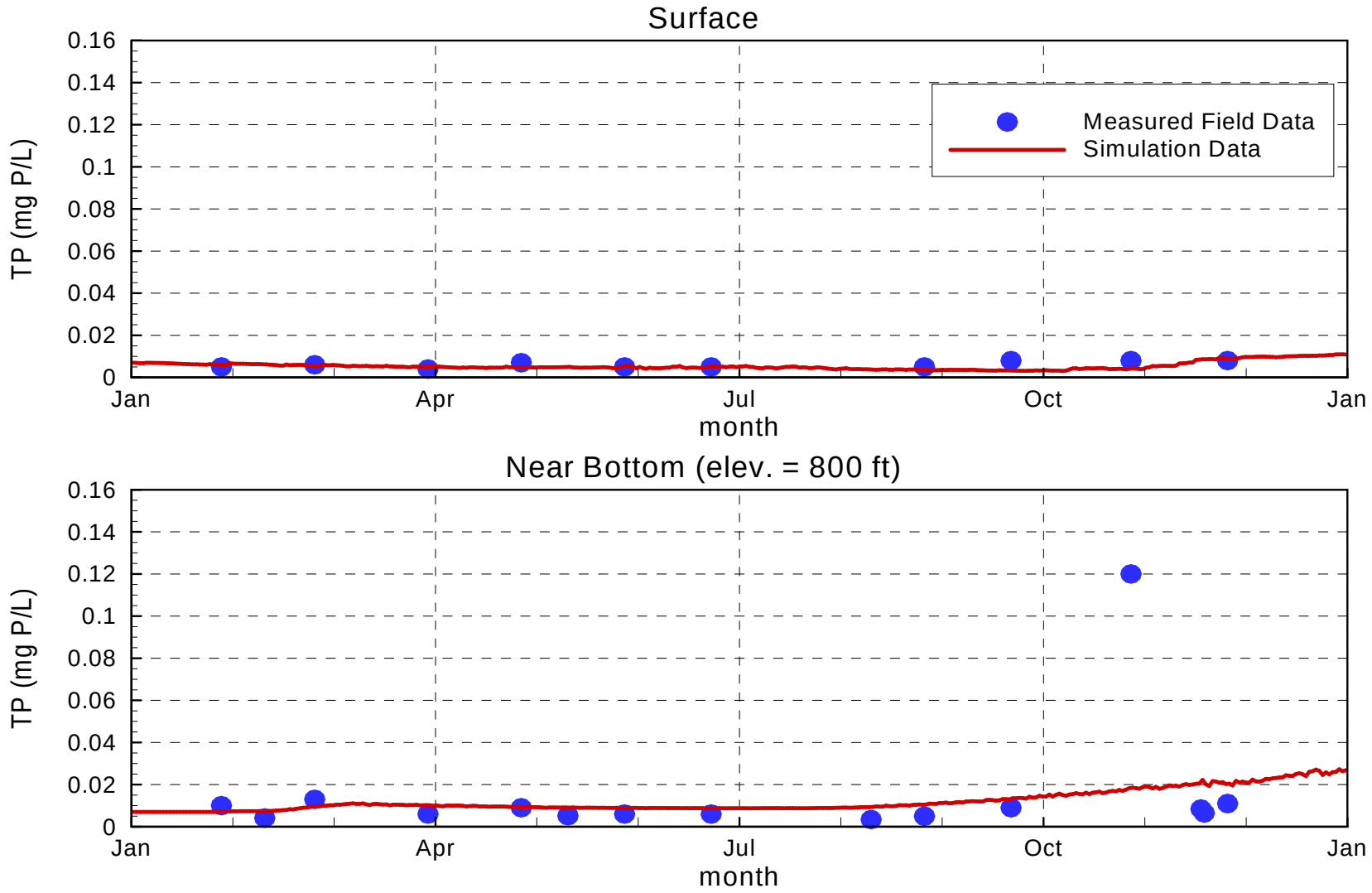

Figure B.85

Total Phosphorus at Station VR6.0

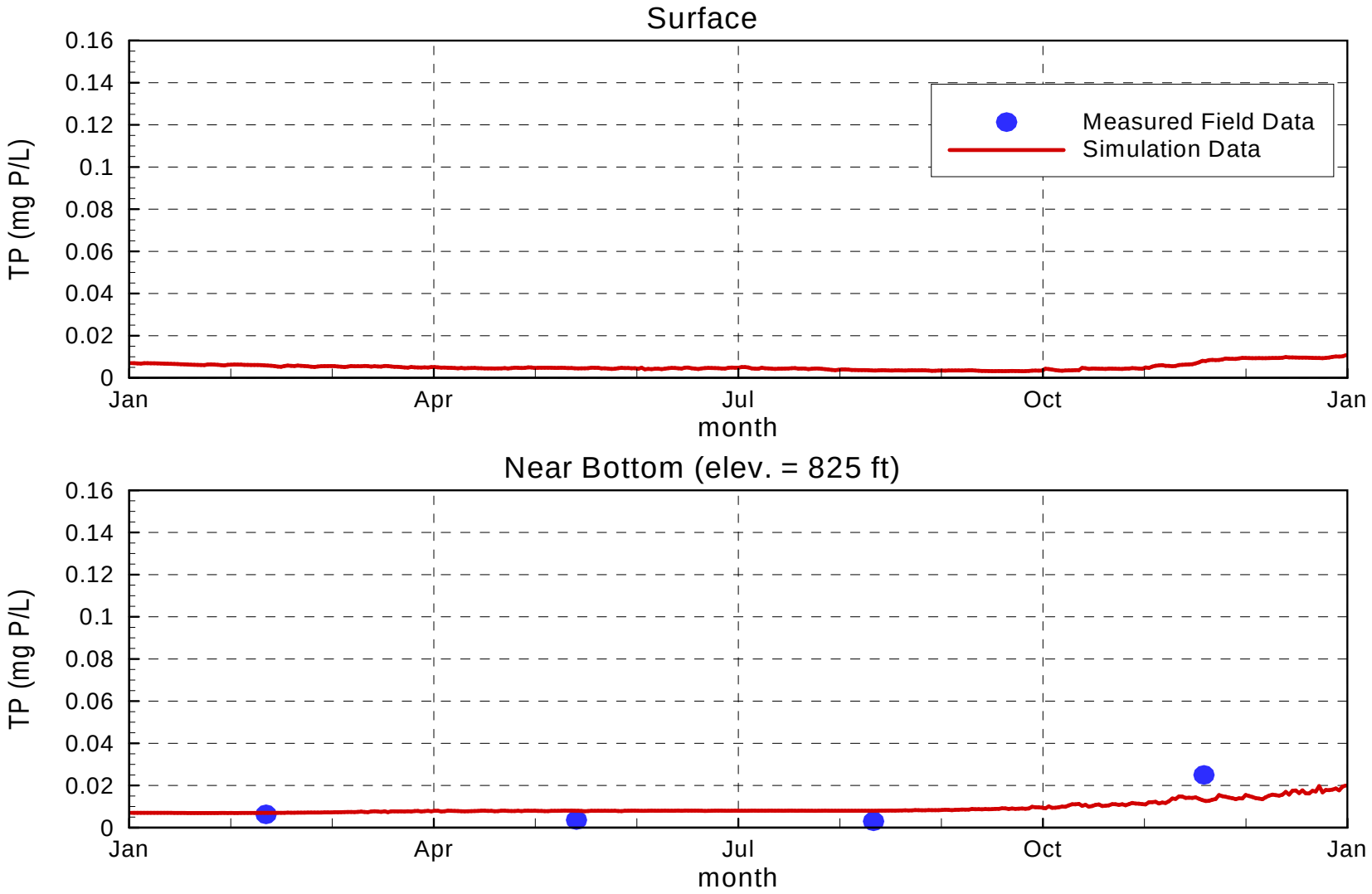

Figure B.86

Total Phosphorus at Station VR9.4

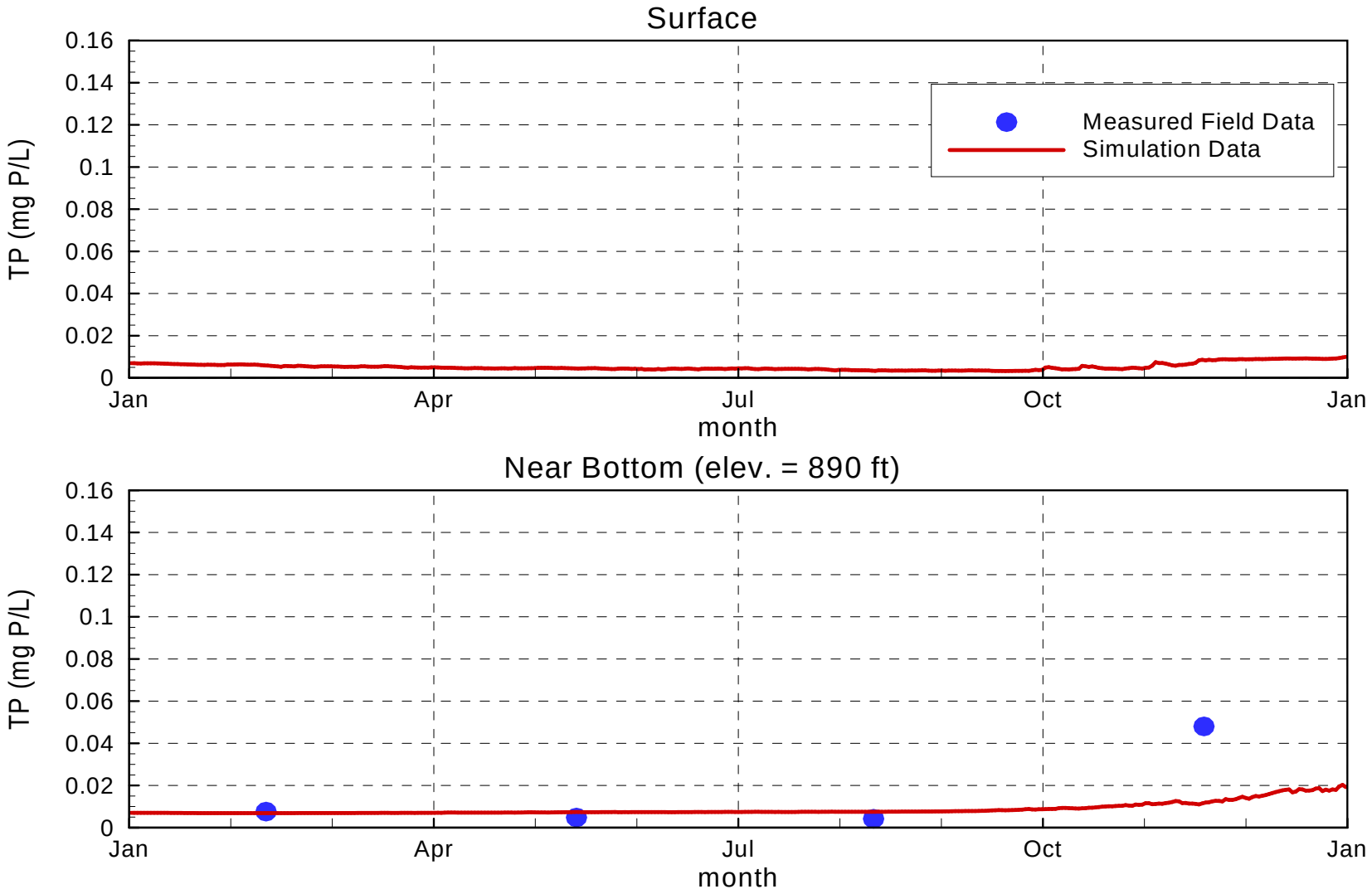

Figure B.87

Total Phosphorus at Station VR13.0

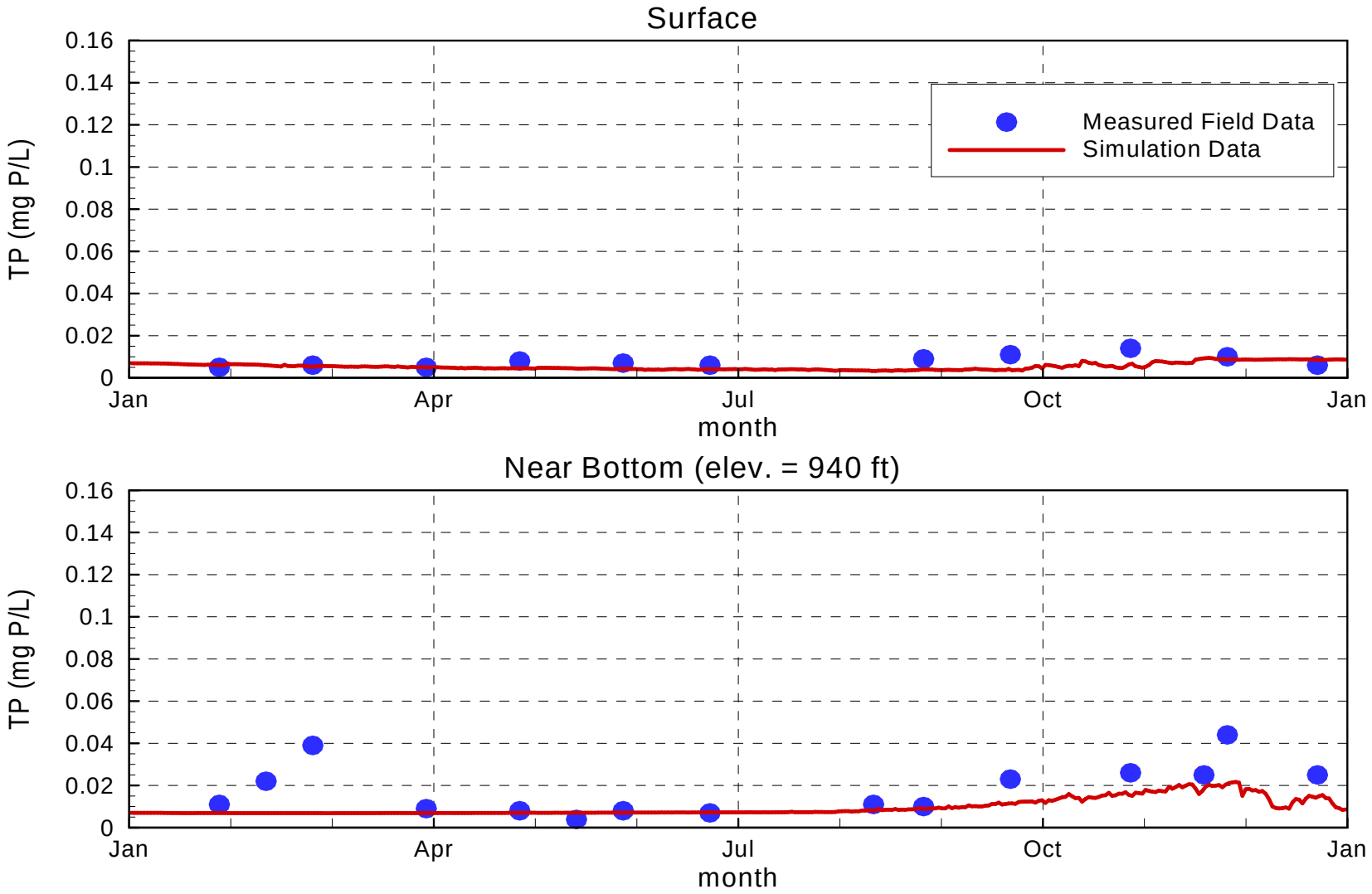

Figure B.88

Total Phosphorus at Station VR18.0

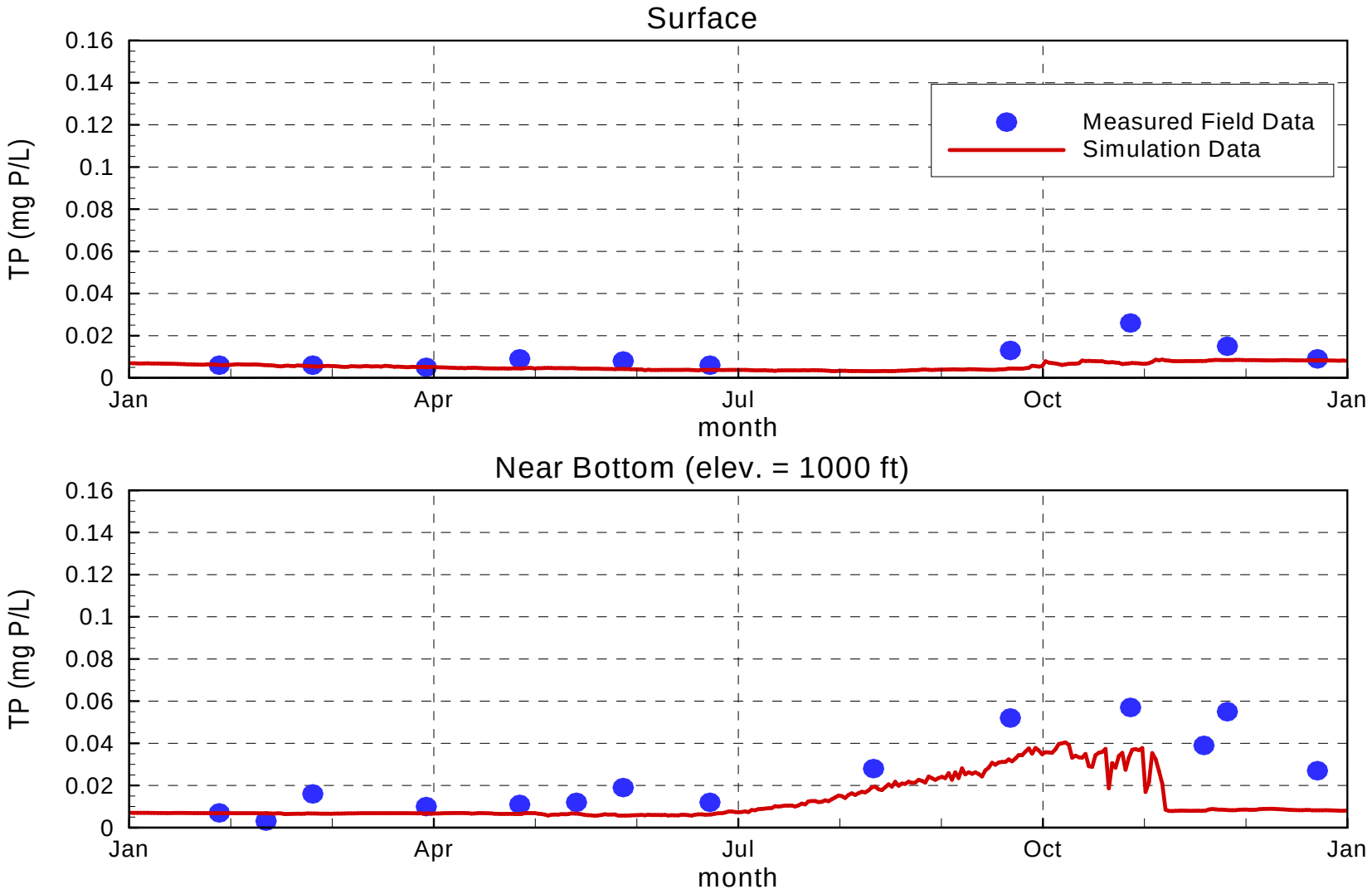

Figure B.89

Total Phosphorus at Station CR360.7

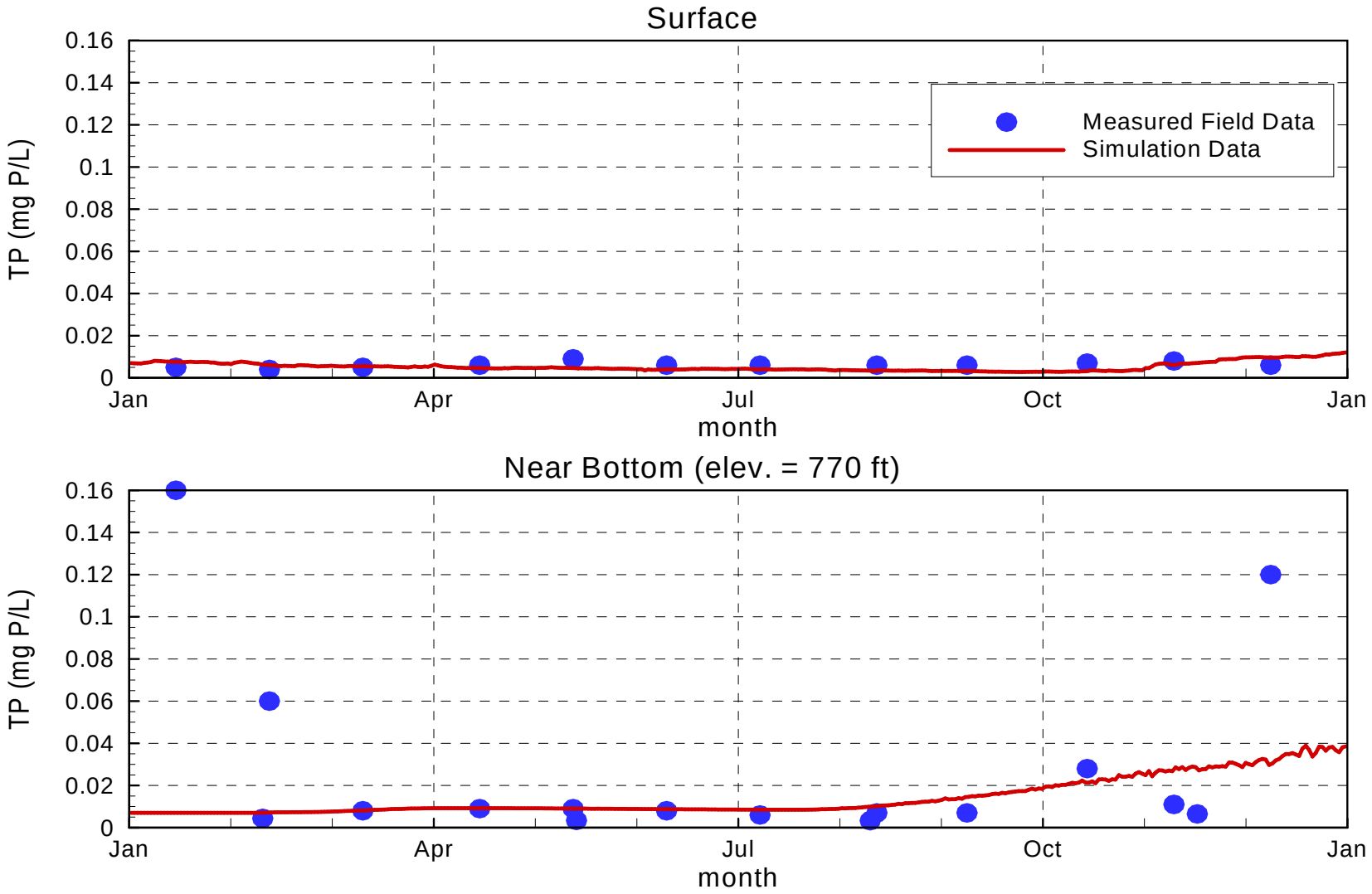

Figure B.90

Total Phosphorus at Station CR346.4

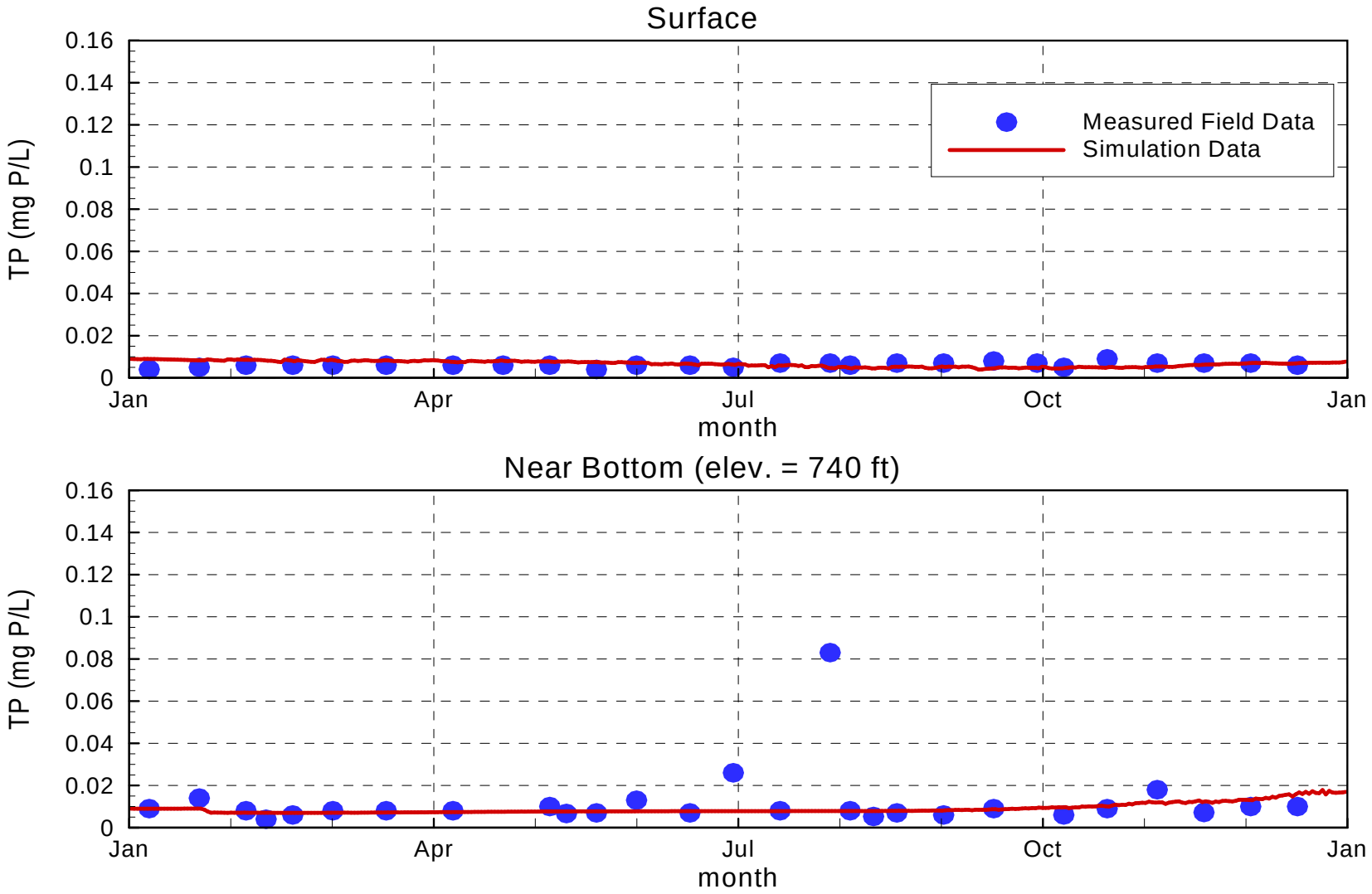

Figure B.91

Total Phosphorus at Station LVB4.95

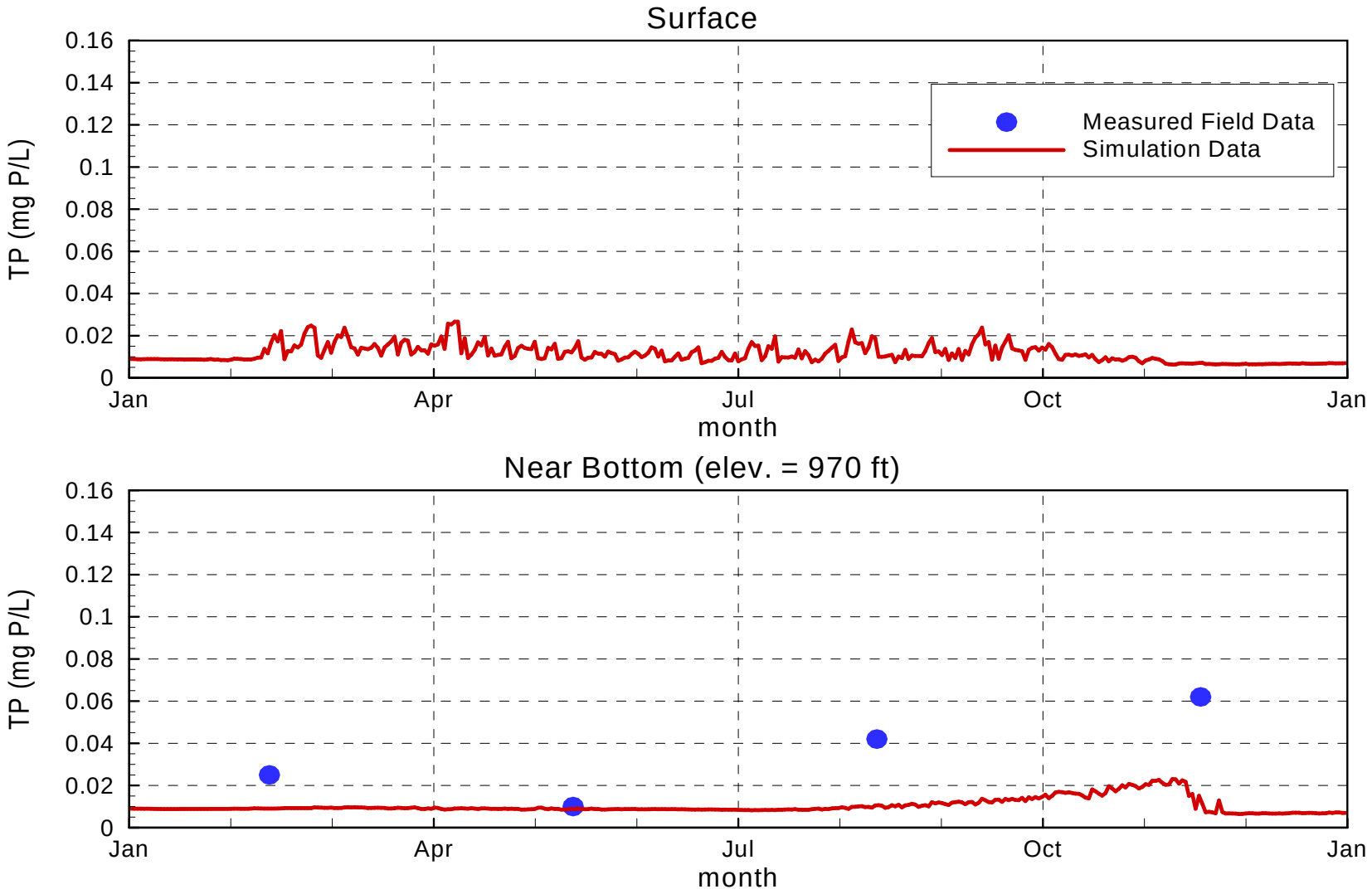

Figure B.92

Total Phosphorus at Station LVB7.3

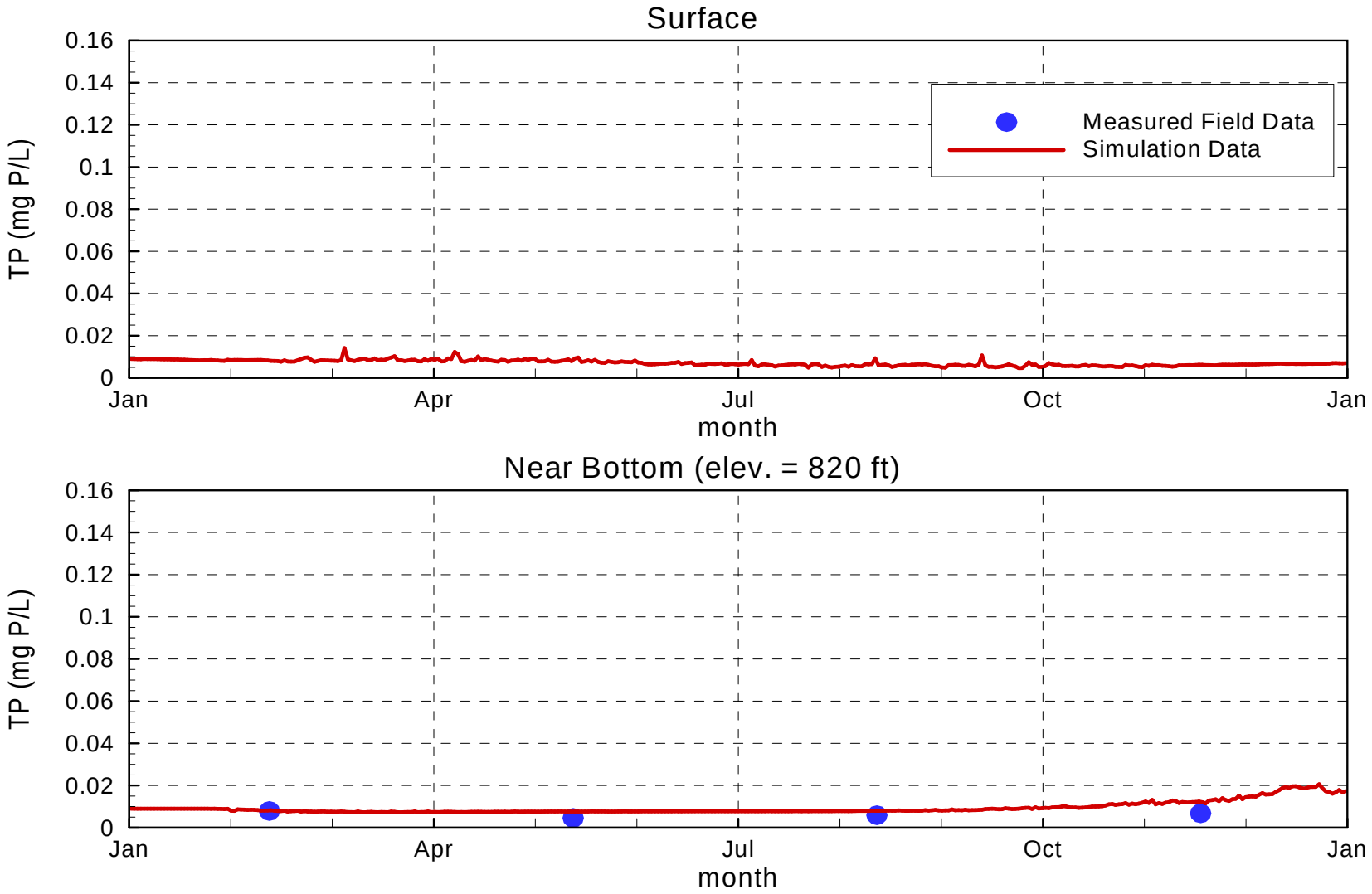

Figure B.93